Class Revisit Oil Recovery Projects
Table of Contents

Ensign Operating Co./Ensign Oil & Gas, Inc. (DE-FC26-00BC15120)
Final Report – (February 29, 2000-July 31, 2001)
"Advanced Reservoir Characterization and Development through High-Resolution 3C3D Seismic and Horizontal Drilling: Eva South Morrow Sand Unit, Texas County, Oklahoma – Class Revisit"

Binger Operations. (DE-FC26-00BC15121)
Fact Sheet
"Improved Miscible Nitrogen Flood Performance Utilizing Advanced Reservoir Characterization – Class Revisit"

Michigan Technological University (DE-FC26-00BC15122)
Annual Report – (April 1, 2003-March 31, 2004)
"Using Recent Advances in 2D Seismic Technology and Surface Geochemistry to Economically Redevelop a Shallow Shelf Carbonate Reservoir: Vernon Field, Isabella County, MI – Class Revisit"

Luff Exploration Company (DE-FC26-00BC15123)
Final Report – (November 12, 2003)
"Intelligent Computing System for Reservoir Analysis and Risk Assessment of the Red River Formation – Class Revisit"

University of Kansas Center for Research, Inc. (DE-FC26-00BC15124)
Budget Period I Report – (January 28, 2004)
"Field Demonstration of Carbon Dioxide Miscible Flooding in the Lansing Kansas City Formation, Central Kansas – Class Revisit"

University of Tulsa (DE-FC26-00NT15125)
Annual Report – (October 1, 2002-September 30, 2003)
"Exploitation and Optimization of Reservoir Performance in Hunton Formation, Oklahoma – Class Revisit"

Venoco, Inc.. (DE-AC26-00BC15127)
Fact Sheet
"An Advanced Fracture Characterization and Well Path Navigation System for Effective Re-Development and Enhancement of Ultimate Recovery from the Complex Monterey Reservoir of the South Ellwood Field, Offshore California – Class Revisit"

Utah Geological Survey (DE-FC26-00BC15128)
Semi-Annual Report – (April 6, 2003-October 5, 2003)
"Heterogeneous Shallow-Shelf Carbonate Buildups in the Paradox Basin, Utah and Colorado: Targets for Increased Oil Production and Reserves Using Horizontal Drilling Techniques – Class Revisit"

University of Alabama (DE-FC26-00BC15129)
Annual Report – (May 1, 2001-April 30, 2002)
"Improved Oil Recovery from Upper Jurassic Smackover Carbonates through the Application of Advanced Technologies at Womack Hill Oil Field, Choctaw and Clarke Counties, Eastern Gulf Coastal Plain – Class Revisit"

Advanced Reservoir Characterization and Development through High-Resolution 3C3D Seismic and Horizontal Drilling: Eva South Morrow Sand Unit, Texas County, Oklahoma

Final Report

Reporting Period Start Date:	February 29, 2000
Reporting Period End Date:	July 31, 2001
Principal Authors:	David M. Wheeler, Project Director Senior Staff Geologist, Ensign Oil & Gas, Inc.
	William A. Miller Geophysicist/President, Miller Consulting Services
	Travis C. Wilson Graduate Student, Department of Geophysics Colorado School of Mines
Report Issue Date:	February, 2002
DOE Award Number:	DE-FC26-00BC15120
Submitting Organization:	Ensign Operating Co./Ensign Oil & Gas, Inc. 1225 17th Street, Suite 1900 Denver CO 80202
Key Subcontractors:	Miller Consulting Services 1641 California Street, Suite 300 Denver, CO 80202
	WesternGeco 1625 Broadway, Suite 1300 Denver, CO 80202
	Sterling Seismic Services, LTD. 8122 Southpark Lane, Suite 207 Littleton, CO 80120
	Colorado School of Mines Golden, CO 80401

DISCLAIMER

This report was prepared as an account of work sponsored by an agency of the United States Government. Neither the United States Government nor any agency thereof, nor any of their employees, makes any warranty, express or implied, or assumes any legal liability or responsibility for the accuracy, completeness, or usefulness of any information, apparatus, product, or process disclosed, or represents that its use would not infringe privately owned rights. Reference herein to any specific commercial product, process, or service by trade name, trademark, manufacturer, or otherwise does not necessarily constitute or imply its endorsement, recommendation, or favoring by the United States Government or any agency thereof. The views and opinions of authors expressed herein do not necessarily state or reflect those of the United States Government or any agency thereof.

ACKNOWLEDGEMENTS

Ensign Operating Co. would like to express sincere thanks to the organizations and people that made this project possible: The U.S. Department of Energy and the National Petroleum Technology Office provided a significant part of the funding for this project. Dan Ferguson was the DOE Project Officer and provided great assistance throughout the duration of the project. WesternGeco provided the acquisition of the shear-wave data at no additional cost. Mark Sterling of Sterling Geophysical Services provided the final P-wave processing at no cost. Travis Wilson, a graduate student at the Colorado School of Mines worked on the data for his M.S. thesis and made many significant contributions to the project. Terry Donze acted as the field supervisor during seismic acquisition and did a superior job. Finally, William Miller, Miller Consulting Services, did an outstanding job as the chief geophysicist on the project. All of these organizations and people deserve recognition for their dedication to the advancement of technologies for improvements in exploration and development.

ABSTRACT

The Eva South Morrow Sand Unit is located in western Texas County, Oklahoma. The field produces from an upper Morrow sandstone, termed the Eva sandstone, deposited in a transgressive valley-fill sequence. The field is defined as a combination structural-stratigraphic trap; the reservoir lies in a convex up-dip bend in the valley and is truncated on the west side by the Teepee Creek fault. Although the field has been a successful waterflood since 1993, reservoir heterogeneity and compartmentalization has impeded overall sweep efficiency. A 4.25 square mile high-resolution, three-component three-dimensional (3C3D) seismic survey was acquired in order to improve reservoir characterization and pinpoint the optimal location of a new horizontal producing well, the ESU 13-H.

Extensive modeling was conducted prior to seismic acquisition to predict the seismic response and define acquisition parameters. Although the seismic did not define any new undeveloped reservoir compartments, the P-wave data was successful in providing excellent detail of the structural configuration of the field and adequate resolution of reservoir extents and geometry. The PSV converted-wave data appears to have defined reservoir extents and geometry, although with a probable overprint from acquisition geometry and principle stress fields. In general, the P-wave data proved to be a valuable exploration and development tool, though not capable of defining all reservoir complexities for detailed reservoir engineering. The PSV converted-wave data showed promise for future applications of this evolving technology.

The seismic data were utilized to locate the ESU 13-H horizontal well parallel to, and within 200 feet of the Teepee Creek fault in an area thought to contain additional reserves. The reservoir development was as expected, although only approximately 1000 feet of the planned 2800 feet of horizontal drilling was achieved prior to the well becoming permanently stuck. Despite this setback, the well was successful in adding 122 MBO of incremental reserves, representing 1.7% of the original oil in place (OOIP) in the field; targeted incremental reserves were 150 MBO, or 2.0% of the OOIP.

Conclusions are that high-resolution 3C3D seismic and horizontal wells are effective tools for improving reservoir characterization and sweep efficiency in Morrow and other (DOE) Class 1 reservoirs.

TABLE OF CONTENTS

		Page
1.0	**INTRODUCTION**	1
1.1	Location and Geological Setting	1
1.2	Field History	2
1.3	Regional Geology	4
1.4	Eva South Geology (Pre Seismic)	5
1.5	Reservoir Compartmentalization and Heterogeneity	10
1.6	Reservoir Engineering	12
1.7	Project Objectives	12
2.0	**EXECUTIVE SUMMARY**	13
3.0	**EXPERIMENTAL**	15
3.1	3C3D Seismic	15
3.1.1	*PSV Converted-Wave Conventions and Definitions*	16
3.1.2	*Seismic Modeling*	19
	ESU 10 Synthetic	19
	P-wave Seismic Cross Section and Model	20
	AVO and PSV-wave Seismic Model Studies	22
	AVO Seismic Model	23
	PSV Converted-wave Seismic Model	24
3.1.3	*3C3D Seismic Design and Acquisition Parameters*	25
3.1.4	*3C3D Seismic Processing Parameters*	31
	P-wave	31
	PSV Converted Wave	31
3.2	Horizontal Drilling	32
4.0	**RESULTS and DISCUSSION**	33
4.1	3C3D Seismic	33
4.1.1	*P-wave Interpretations*	33
	Synthetic Tie and Event Correlations	33
	Structural Interpretation	34
	Stratigraphic Interpretation	37
	Seismic Tuning Considerations	43
	Reservoir Compartment Interpretation	46
	Source to Receiver Offset Analysis	49
4.1.2	*PSV Converted-Wave Interpretation*	55
	P-wave Tie and Event Correlations	55
	Structural Interpretation	56
	Stratigraphic Interpretation	57
	Acquisition Geometry Effects on Stratigraphic Interpretation	59
	Evaluation of S-wave Splitting	62
	Anisotropy Analysis	69
	Vp/Vs Analysis	71

4.1.3 Integrated P-wave Interpretation 72
Reservoir Interpretation 73
Exploration Application 76
4.2 Horizontal Drilling 78
4.2.1 ESU 13-H Drilling and Completion 78
4.2.2 Eva South Production History 81
ESU 13-H Incremental Reserves 82
Comparison of Actual vs. Predicted Performance 84

5.0 CONCLUSIONS and RECOMMENDATIONS 84
5.1 3C3D Seismic 84
5.2 Horizontal Drilling 87

REFERENCES/BIBLIOGRAPHY 89

LIST of ACRONYMS and ABBREVIATIONS 91

LIST OF TABLES AND FIGURES

Table		**Page**
1.6a.	Eva South Reservoir Properties	12

Figure		
1.1a	Location map of Eva South	1
1.1b	Stratigraphic column	2
1.2a	Eva South base map	3
1.3a	Morrow transgressive valley-fill model	4
1.3b	Fluvial-estuarine depositional model	5
1.4a	Morrow structure map from well control	6
1.4b	Stratigraphic cross section A-A'	7
1.4c	Stratigraphic cross section B-B'	8
1.4d	Net Eva sandstone Isopach	9
1.4e	Structure on Eva sandstone	10
1.5a	Eva South reservoir compartments	11
3.1.1a	Diagram of S-wave and PSV conventions	17
3.1.1b	Characteristics of PSV converted waves	18
3.1.2a	ESU 10 synthetic seismogram	20
3.1.2b	Seismic model cross section	21
3.1.2c	Plot of reflection coefficient vs. angle of incidence	23
3.1.2d	Eva sandstone AVO model	23
3.1.2e	Eva sandstone PSV converted-wave model	24
3.1.3a	Photograph of vibroseis trucks	26
3.1.3b	Photograph of three-component geophones	27
3.1.3c	Photograph of three-component geophones in place	28
3.1.3d	Map of 3D survey source and receiver layout	30
4.1.1a	ESU 10 synthetic tie to data	34
4.1.1b	Arbitrary seismic line, P-wave data	35
4.1.1c	Morrow shale time structure map, P-wave data	36
4.1.1d	Integrated Morrow structure map, P-wave data	37
4.1.1e	Arbitrary line, structural and flattened, P-wave data	38
4.1.1f	P-wave amplitude map of Eva sandstone	39
4.1.1g	Plot of net Eva sandstone vs. amplitude	40
4.1.1h	Amplitude extractions, 18-22 ms below Morrow shale and 4-8 ms above Valley event, P-wave data	41
4.1.1i	Plots of Net Eva sandstone vs. amplitude for extractions	42
4.1.1j	Isochron map, Morrow shale to Valley pick, P-wave data	43
4.1.1k	Tuning plot	44
4.1.1l	Eva Sandstone amplitude maps at 90- and 70-hertz, P-wave data	46
4.1.1m	Map of compartmentalization and heterogeneity elements, P-wave data	48
4.1.1n	Eva Sandstone amplitude maps, near and far offset volumes, P-wave data	50
4.1.1o	Plots of net Eva sandstone vs. seismic amplitude, near and far offsets, P-wave data	51

4.1.1p	Eva sandstone amplitude map and plot of net Eva sandstone vs. amplitude, far offset minus near offset volume, P-wave data	53
4.1.1q	Comparison of CDP fold, near vs. far offsets, P-wave data	54
4.1.2a	Arbitrary line comparing P-wave filtered to 45-hertz with PSV-wave data	56
4.1.2b	Morrow time-structure, PSV-wave data	57
4.1.2c	Eva sandstone amplitude map, PSV-wave data	58
4.1.2d	Plot of net Eva sandstone vs. PSV-wave amplitude	59
4.1.2e	Map of CCP fold at Morrow horizon, PSV-wave data	60
4.1.2f	Comparison of amplitude maps for Eva sandstone and Atoka event, PSV-wave data	61
4.1.2g	CCP radial-component supergather, PSV-wave data	63
4.1.2h	Comparison of radial vs. transverse components, PSV-wave data	64
4.1.2i	Comparison of Eva sandstone amplitude for 220-degree and 130-degree azimuths, PSV-wave data	66
4.1.2j	Comparison of Eva sandstone time-structure for 220-degree and 130-degree azimuths, PSV-wave data	67
4.1.2k	Time-structure difference of 130-degree minus 220-degree azimuths, PSV-wave data	68
4.1.2l	Seismic anisotropy for Morrow to Mississippian interval, PSV-wave data	70
4.1.2m	Map of Vp/Vs for the upper Morrow interval	72
4.1.3a	Interpreted Eva net sandstone isopach, linear relationship, P-wave data	73
4.1.3b	Interpreted Eva net sandstone isopach, tuning factor, P-wave data	75
4.1.3c	Bubble map of Eva South primary production	76
4.1.3d	Integrated Morrow structure contours overlain on color grid of interpreted Eva net sandstone, P-wave data	77
4.2.1a	Seismic map and cross section of ESU 13-H horizontal well	79
4.2.1b	Photograph of MWD tool	81
4.2.2a	Plot of Eva South production history	82
4.2.2b	Plot of incremental reserves for ESU 13-H horizontal well	83

1.0 INTRODUCTION

1.1 Location and Geological Setting

The Eva South Morrow Sand Unit (ESU) is located in western Texas County, Oklahoma, in parts of Sections 5-8, T3N-R11 ECM (Fig. 1.1a). Geologically, it is situated on the southwest margin of the Hugoton Embayment. The field produces from sandstone in the upper portion of the Morrow Formation, here termed the Eva sandstone (Fig. 1.1b).

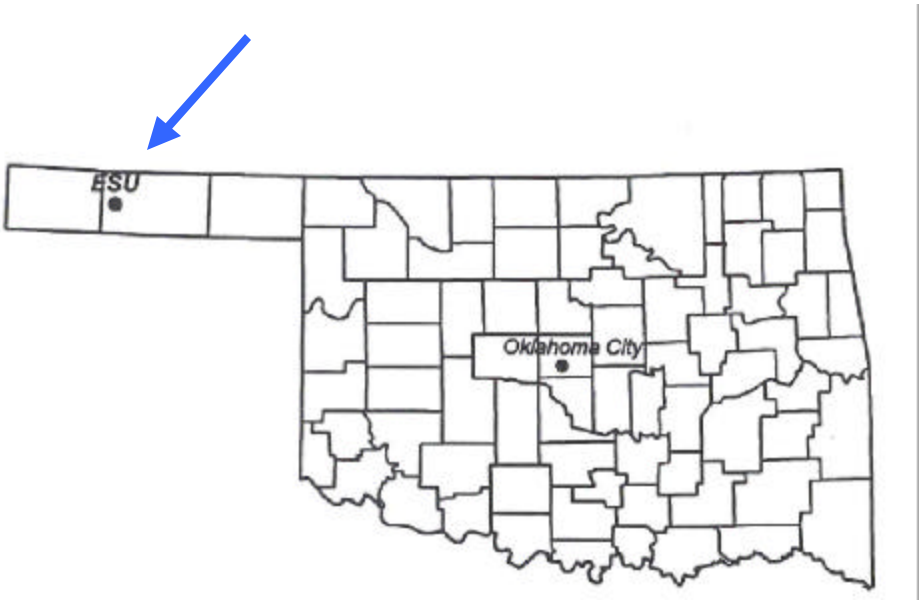

Figure 1.1a. Map showing the location of the Eva South Morrow Sand Unit (ESU) relative to the state of Oklahoma. The Eva South Unit is located in T3N-R11ECM, Texas County, Oklahoma.

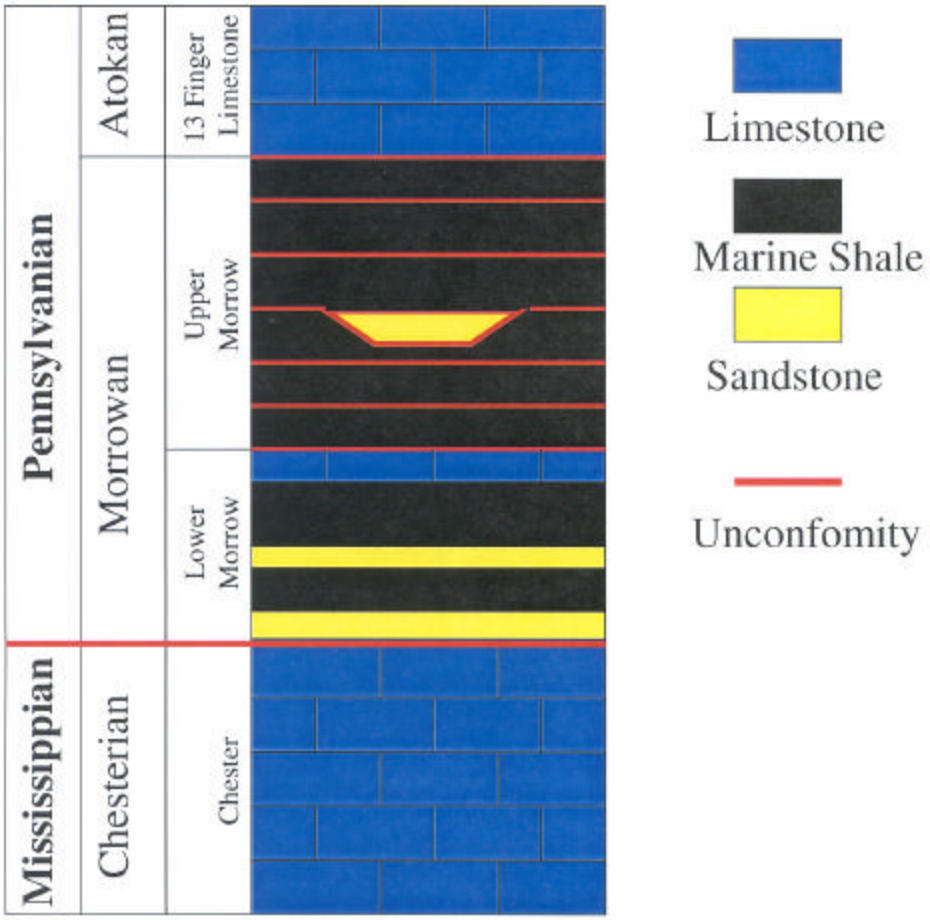

Figure 1.1b. Stratigraphic column for the area of Eva South (Wilson, 2002). The relative position of the Eva sandstone is schematically represented in the upper Morrow.

1.2 Field History

Eva South was discovered in 1961 and was developed on 80-acre spacing. The last productive lease was added in 1966. In 1988, a spacing exception was granted for an increased density well (ESU 5) in NE NE Sec. 7 (Fig. 1.2a). That well encountered a depleted reservoir and was completed for only 20 BOPD. The field was acquired by Ensign Oil & Gas, Inc. in 1992 and is operated by its subsidiary, Ensign Operating Co. (EOC).

Through production plot analysis, ultimate primary production was determined to be 1,288 MSTBO. A waterflood feasibility study conducted by EOC in 1992 determined the original oil in place (OOIP) to be 7,225 MSTBO, indicating a primary recovery factor of 17.8%. The feasibility study also revealed that two wells are separated from the main reservoir body and were excluded from the waterflood unit (Fig. 1.2.a). The Webb C-2 (NW NE Sec. 7) was found to be fault separated from the rest of the field. Production tests on the Weede Trust No. 1 (NW SE Sec. 7) recovered significant amounts of formation water even though the base of the sandstone is above the oil/water contact

for the rest of the field. Additional production data confirmed that the Weede Trust No. 1 is in a separate reservoir from the rest of the field.

In 1993, EOC installed the waterflood facilities at Eva South. This comprised the drilling of the water supply well, conversion of four wells to injection and installation of the injection and production facilities. Wells were reassigned unit numbers as shown on Figure 1.2.a, which also shows the current status of all wells in the waterflood unit. Injection began in December, 1993 and initial response was observed in September, 1994. The ESU 9 was drilled in December, 1994 to give additional injection support and the ESU 10 and 11 wells were drilled as new producers in May, 1995 and June, 1996, respectively. In March, 1997 the ESU 12 was drilled as a twin to the ESU 6; the ESU 6 experiences periodic mechanical problems, necessitating a second well to keep up with required production volume. As a part of this project, the ESU 13-H horizontal well was drilled in December, 1999. Currently Eva South comprises 6 injection wells, 6 vertical production wells and 1 horizontal production well.

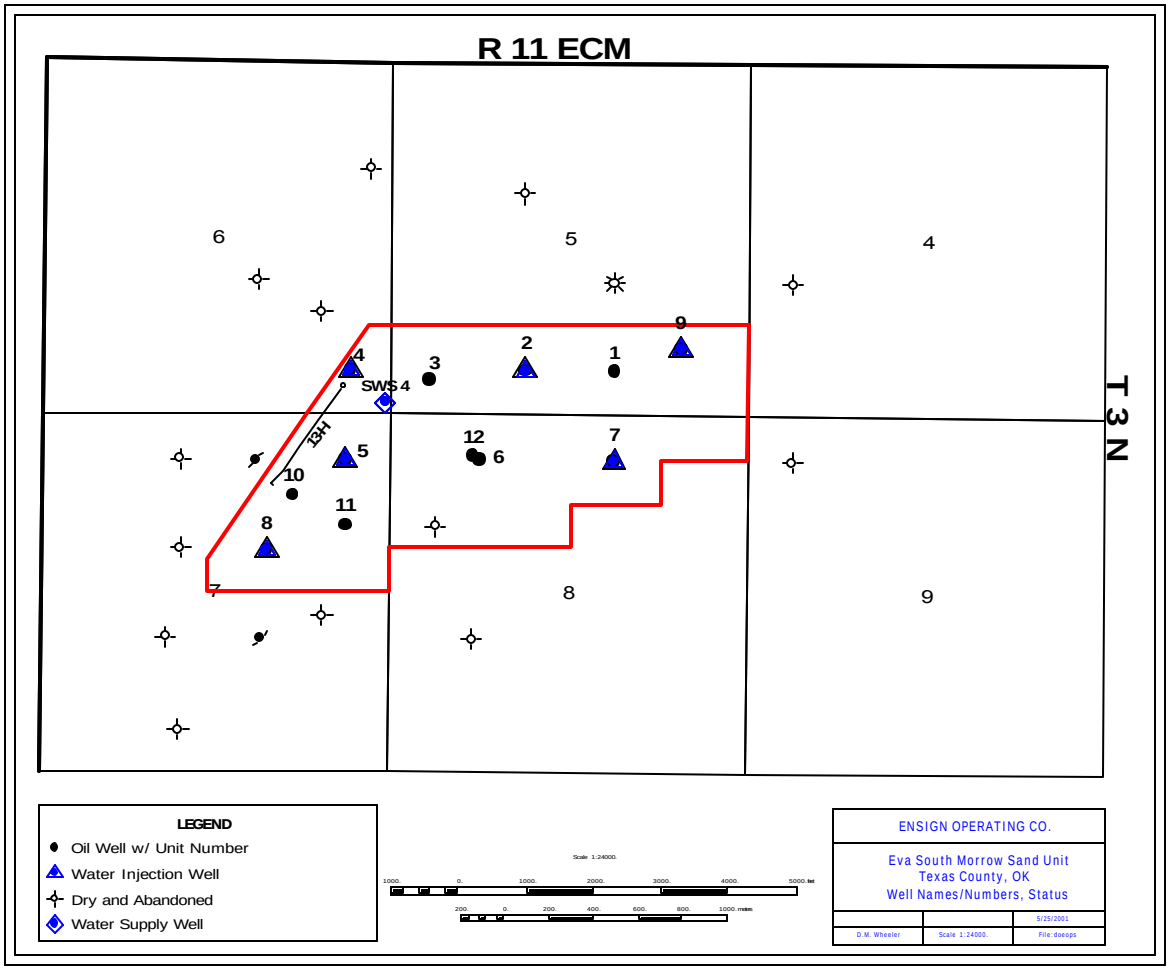

Figure 1.2a. Map of Eva South showing well names and well status as of January, 2002. The ESU 13-H is a horizontal producing well, drilled as a part of this project. The unit outline is shown in red.

1.3 Regional Geology

The Morrow Formation consists predominantly of offshore marine shale with thin limestone interbeds and narrow, elongate sandstone units ranging from 10 to 60 feet in thickness that are developed at various stratigraphic horizons. In the TORIS project the United States Department of Energy (DOE) classified these sandstone units as fluvial-deltaic reservoirs (Class I). The DOE recognized that Class I reservoirs are major contributors to the Nation's petroleum production, commonly have low recovery factors and are at high risk of premature abandonment. Previous detailed stratigraphic analysis of the Morrow Formation by the senior author of this report revealed that Morrow reservoirs are more accurately characterized as transgressive valley-fill sequences (Wheeler et al., 1990) (Fig. 1.3a).

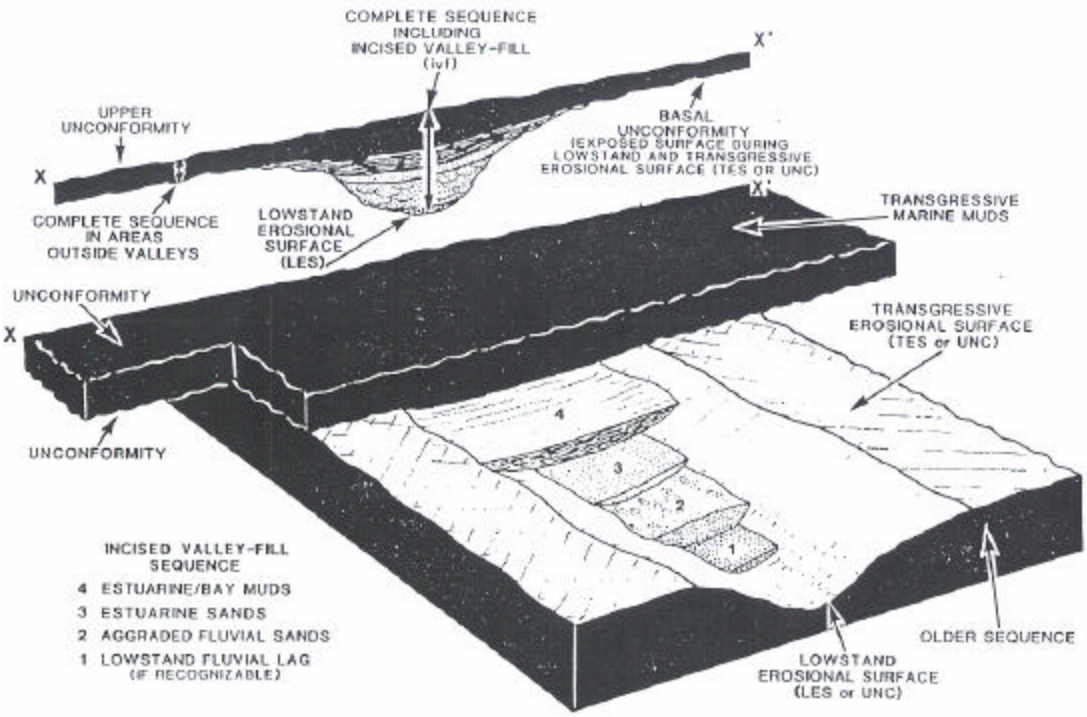

Figure 1.3a. Transgressive valley-fill model for deposition of upper Morrow reservoirs (Wheeler et al., 1990). Upper Morrow reservoirs are dominantly aggraded fluvial and estuarine sandstones (units 2 and 3).

Offshore marine deposition during Morrow time was periodically interrupted by eustatic drops in sea level caused by repeated glacial cycles in the southern hemisphere. This resulted in subaerial exposure of the entire Hugoton Embayment and the establishment of fluvial drainage systems that incised valleys into the underlying marine shale. Sediments shed off the Ancestral Rocky Mountains were transported by these rivers to the deeper portions of the Anadarko Basin. The valleys were backfilled with fluvial-estuarine sediments during the subsequent sea-level rise and transgression. Offshore

marine deposition resumed at the close of each cycle. As a result, porous and permeable fluvial sandstone units of the Morrow Formation are incased in marine shale.

Depositional facies of the fluvial-estuarine component of this system are illustrated in Figure 1.3b. Very important components of this system are abandoned channel-fill deposits (oxbow lakes). Abandoned channels typically fill with mudstone and shale that can result in reservoir heterogeneity and compartmentalization.

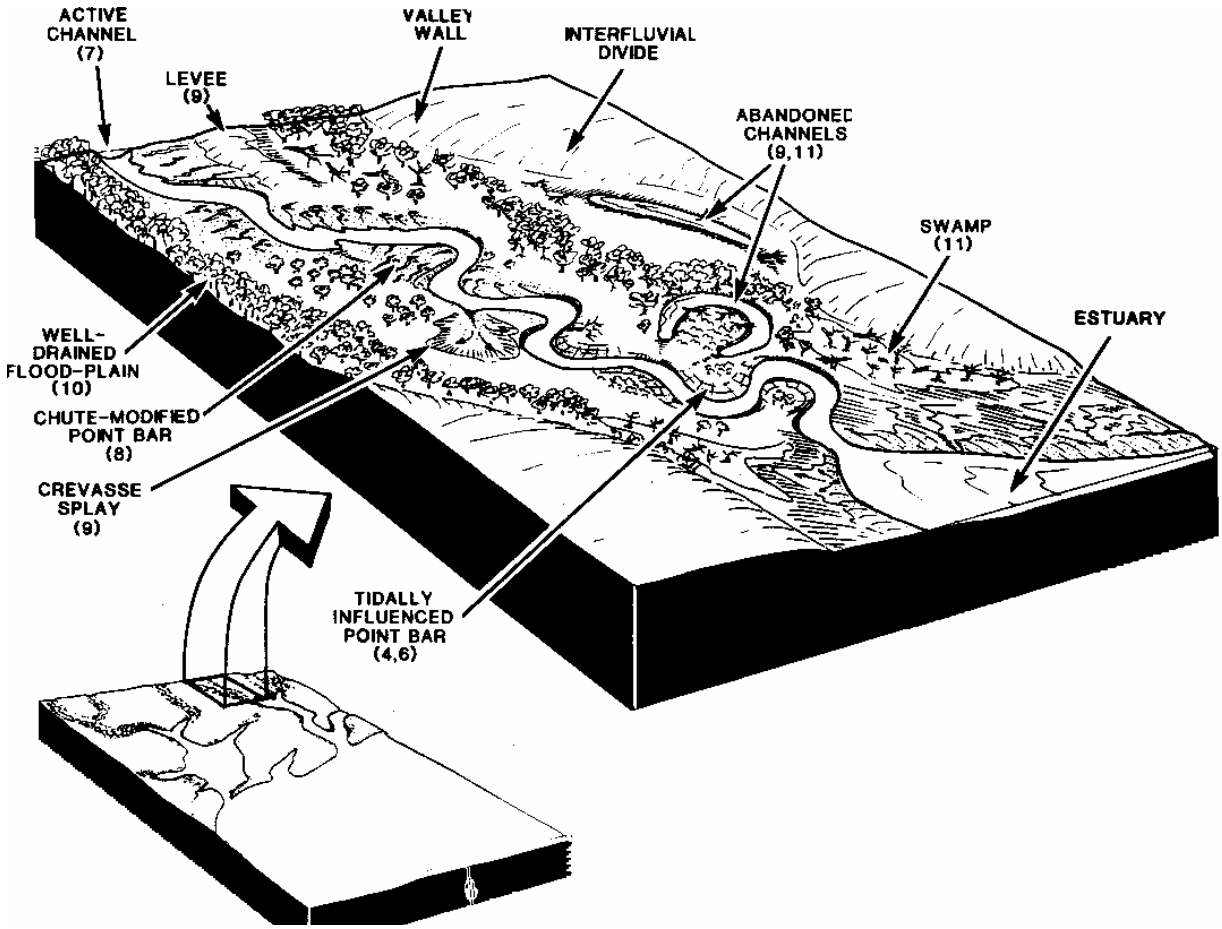

Figure 1.3b. Fluvial-estuarine depositional model for upper Morrow sandstones (Wheeler et al., 1990). Abandoned channels (oxbow lakes) are typically filled with mudstone or shale. They are directly associated with fluvial-estuarine sandstone and can cause reservoir heterogeneity and compartmentalization.

1.4 Eva South Geology (Pre Seismic)

Eva South is a combination structural-stratigraphic trap. The field lies on a northeast-plunging structural nose with a small amount of closure (Fig. 1.4a); much of this structure is believed to be from differential compaction over the reservoir. The Teepee Creek fault dips approximately 58 degrees to the southeast and forms the western boundary of the waterflood unit. Displacement across the fault is documented by

missing section in several wells and ranges from 120 to 50 feet from southwest to northeast. Although structure is a significant factor in the field, stratigraphic relationships complete the trap.

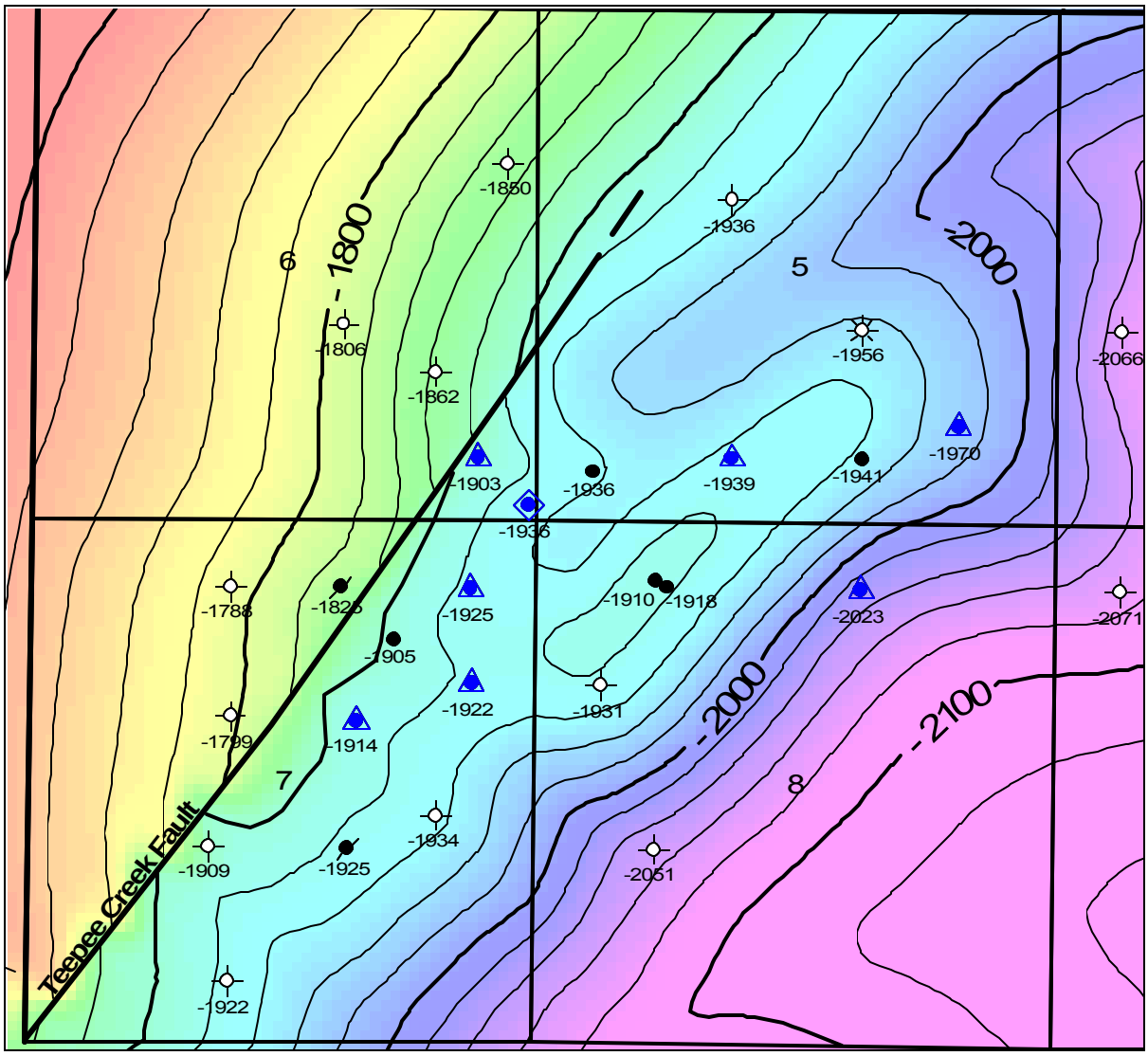

Figure 1.4a. Structure map on the top of the Morrow Formation generated from well control. Contour interval is 20 feet. (Status as of December, 1999, prior to DOE project inception.)

Stratigraphic cross sections A-A' and B-B' (Figs. 1.4b, c) and the net sandstone isopach map (Fig. 1.4d) illustrate the geometry of the productive upper Morrow sandstone and abandoned channel-fill deposits. The width of the reservoir, approximately 3000 feet, indicates it is an amalgamation of multiple fluvial channel deposits representing a meanderbelt system, rather than point-bar deposits of a single channel. Reservoir heterogeneity is caused by individual abandoned channel-fill (oxbow lake) deposits, as encountered in the ESU SWS 4 well (Fig. 1.4b). Overall, the juxtaposition of porous and permeable fluvial sandstone against impermeable shale and the convex up-dip bend of the meanderbelt forms the trap.

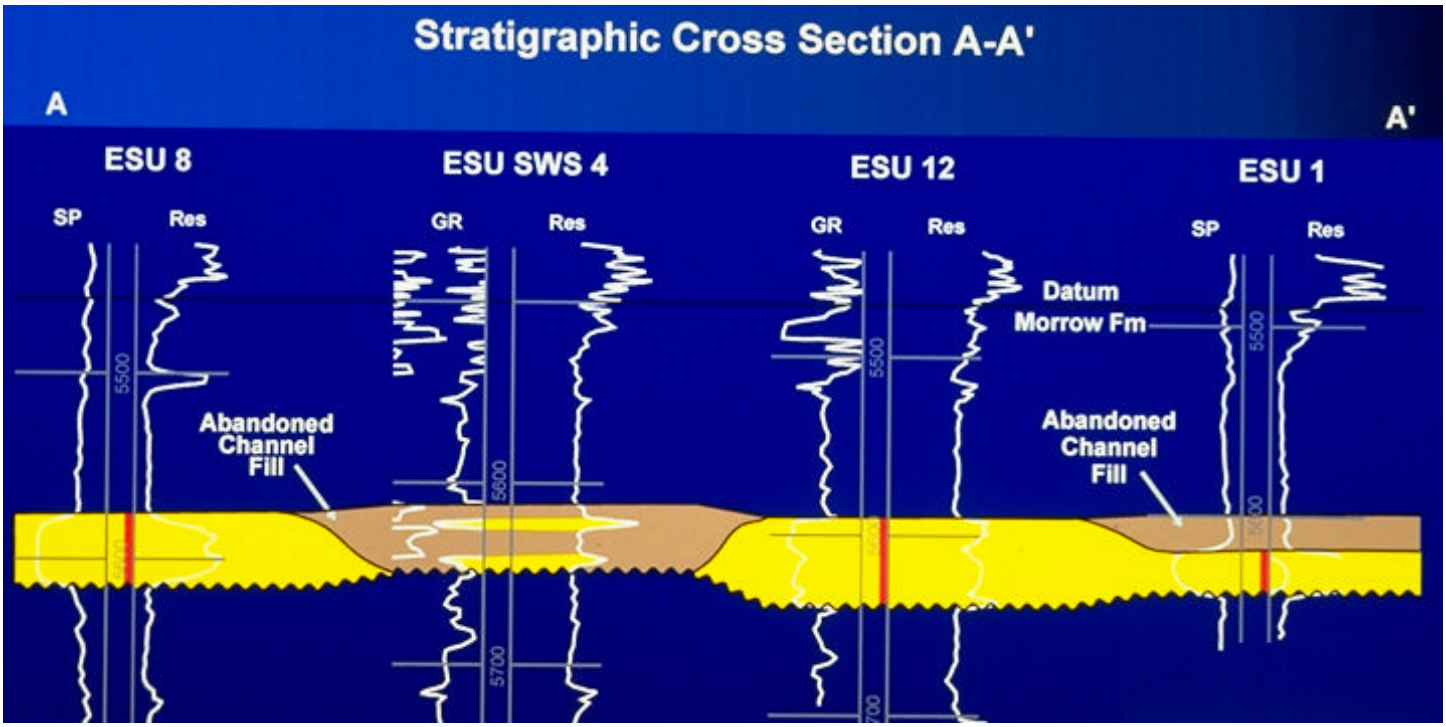

Figure 1.4b. Down-valley, stratigraphic cross section A-A'. Datum is the top of the Morrow Formation. The Eva sandstone reservoir was deposited by active fluvial-estuarine channels (yellow) in an incised valley. The valley is encased is marine shales and limestones (blue). Abandoned channel fill deposits (tan) are primarily mudstone and shale that can act as permeability barriers and compartmentalize the reservoir. Perforations are shown in red. Cross section location is shown in Figure 1.4d.

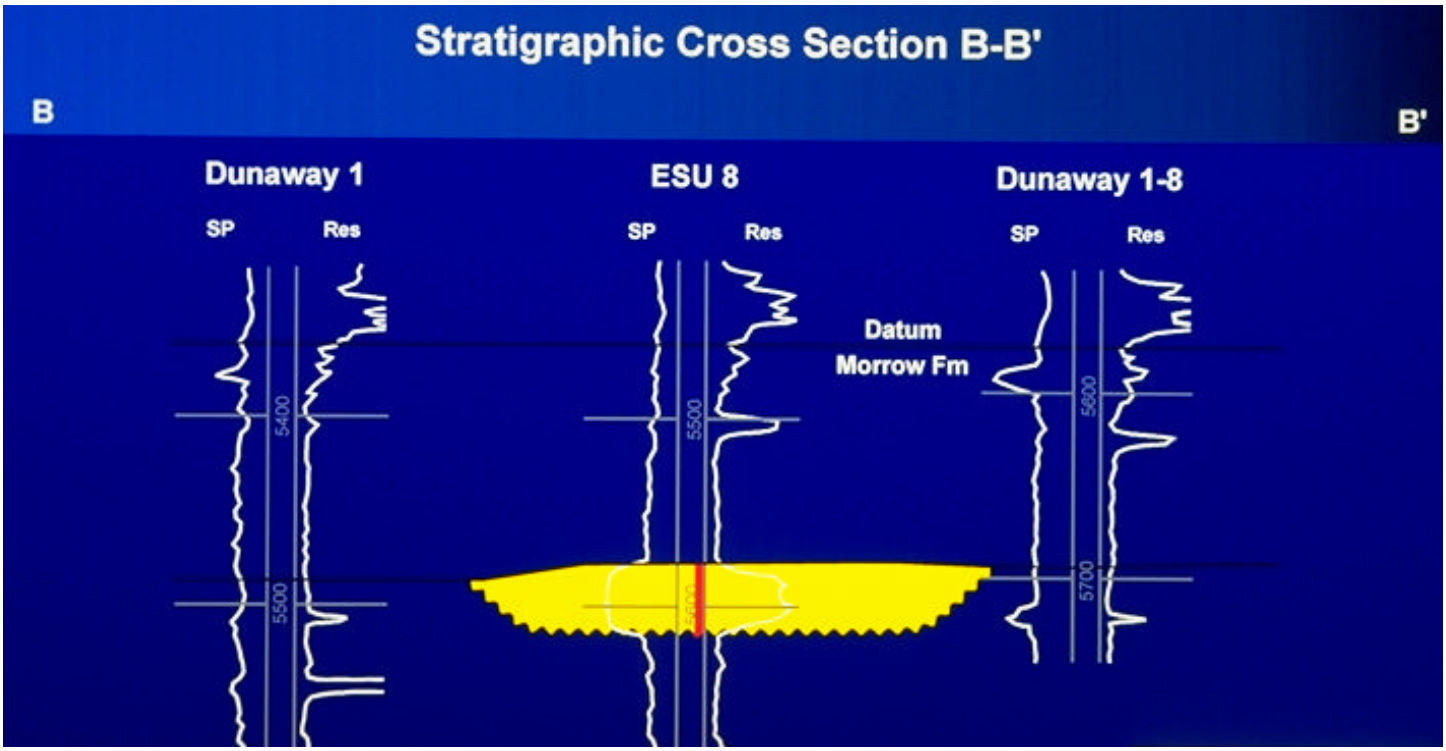

Figure 1.4c. Cross-valley, stratigraphic cross section B-B'. Datum is the top of the Morrow Formation. The upper Morrow section is dominantly marine shale with thin sandstone and limestone interbeds, depicted in blue. The Eva sandstone (yellow) is a transgressive valley-fill deposit that is totally encased in these marine deposits. Perforations are shown in red. Cross section location is shown in Figure 1.4d.

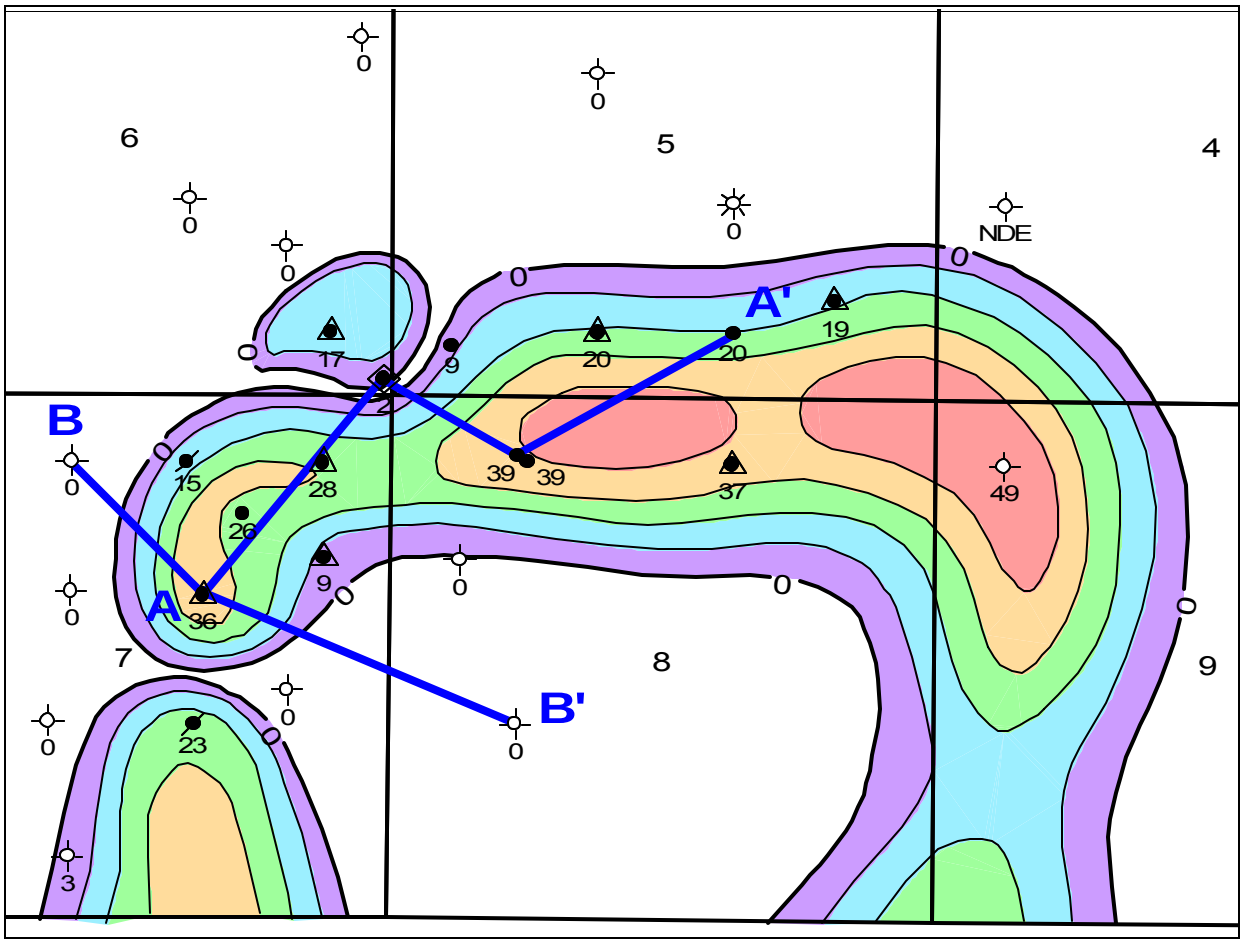

Figure 1.4d. Net (≥ 10% porosity) sandstone isopach of the Eva sandstone mapped from well control. Contour interval is 10 feet. Cross sections are shown in Figures 1.4b,c. (Status as of December, 1999, prior to DOE project inception.)

The trap at Eva South is best illustrated by the structure map on top of the Eva sandstone (Fig. 1.4e). The original oil-water contact was found in the ESU 7 (Norris A-1) well (NW NE Sec. 8) at an elevation of -2126 feet. Oil occurs up-dip from this point and is confined laterally by the margins of the valley. A second oil/water contact, observed in the Weede Trust No. 1 (NW SE Sec. 7), demonstrates that a permeability barrier separates this well from the rest of the field.

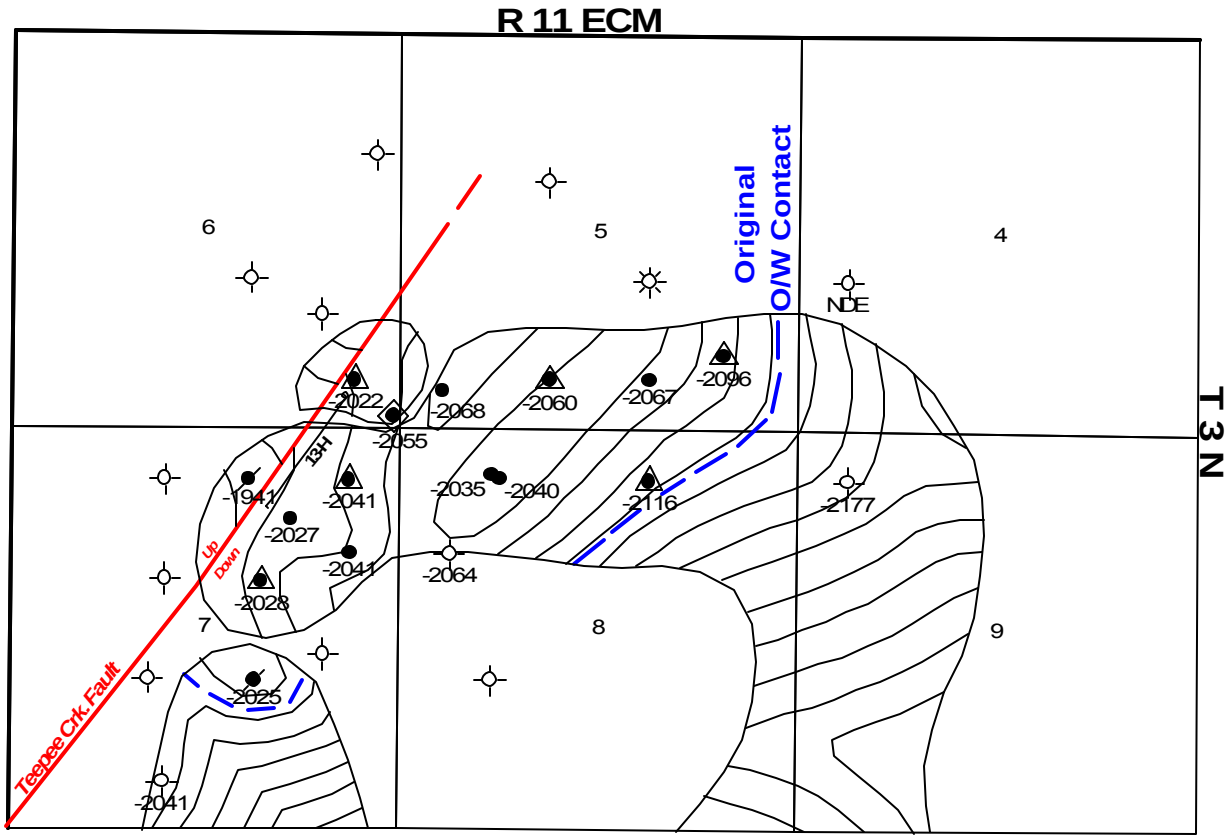

Figure 1.4e. Structure map on the top of the Eva sandstone. Note the two oil/water contacts shown by the dashed lines. (Status as of December, 1999, prior to DOE project inception.)

1.5 Reservoir Compartmentalization and Heterogeneity

EOC identified several reservoir compartments in the Eva South Field (Fig. 1.5a). In the original waterflood feasibility study, subsurface mapping, well testing and production data evaluation identified two wells in compartments that were excluded from the waterflood unit. The Webb C-2 is fault separated from the rest of the field and is not in communication with the wells in the waterflood unit. Production tests on the Weede Trust No. 1 (NW SE Sec. 7) recovered significant amounts of formation water even though the base of the sandstone is above the oil-water contact for the rest of the field. A permeability barrier, interpreted to be an abandoned channel-fill deposit, isolates the Weede Trust No. 1 from the rest of the field.

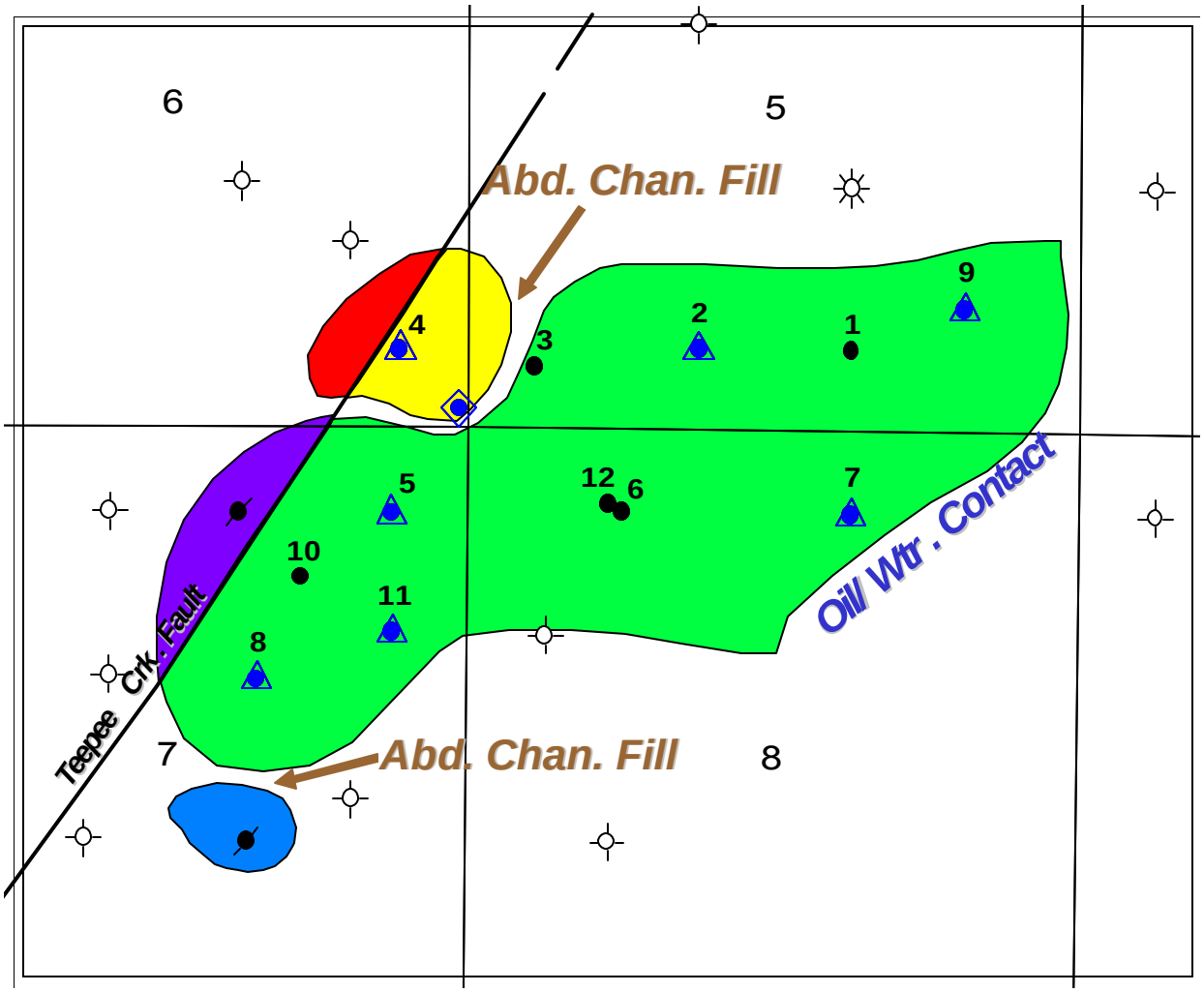

Figure 1.5a. Reservoir compartments in Eva South as defined by engineering and geological data. The diamond symbol around the well in SE SE SE Sec. 6 denotes the water supply well (SWS 4). (Field status as of December, 1999, prior to DOE project inception.)

A third compartmentalized well was found during waterflood operations. The ESU 4 injection well (SE SE SE Sec. 6) encountered high pressures after injecting only 53,456 BW. This well is compartmentalized by the Teepee Creek fault on the west, the edge of the fluvial-estuarine sandstone on the north, and by abandoned channel-fill deposits on the south and east. The abandoned channel-fill deposits are recognizable on logs in the ESU 3 and in the water supply well (SWS 4). The ESU 3 has some reservoir sandstone (active channel-fill) at the base of the deposit, overlain by abandoned channel-fill mudstones. At ESU SWS 4, there is virtually no sandstone in the reservoir interval; rather it is mainly composed of abandoned channel-fill mudstone.

Compartmentalization and heterogeneity caused by abandoned channel-fill deposits and faulting at Eva South have impeded sweep efficiency of the waterflood. One of the primary goals of this project was to resolve the geometry of the identified compartments

and permeability barriers and to locate any that were not identified prior to drilling additional wells.

1.6 Reservoir Engineering

Eva South reservoir properties were defined in the 1992 waterflood feasibility study by EOC. These properties, summarized in Table 1.6a, were derived from log analysis, core analysis and production testing.

Table 1.6a

Average Porosity	17.0%
Average Water Saturation	23.0%
Average Net Thickness	24 Ft.
Average Permeability	50.3 md
Oil Gravity	36 API
Original GOR	372
Original BHP	1625 psig
Saturation Pressure	1340 psig
Original Formation Volume Factor	1.18
Reservoir Volume	8395 Acre Feet
Original Oil in Place (OOIP)	7,224,833 STBO
Primary Recovery	1,288,300 STBO
Primary Recovery Factor	17.8%

Prior to inception of this project, ultimate secondary recovery was projected to be 961 MBO, representing 13.3% of the original oil in place (OOIP). Total ultimate recovery of the field was projected to be 2249 MBO, representing a 31.1% recovery factor. (Note: The above figures have been revised, based on actual well performance, since the estimates were made in the original project proposal.)

1.7 Project Objectives

Project objectives were twofold; promote the use of the advanced technologies of high-resolution multicomponent seismology and horizontal drilling, and improve ultimate recovery and economics. Specific goals are outlined below.

High-resolution 3C3D Seismic:

1) *Improve reservoir characterization and definition through:*
   a. *Enhanced mapping of structure, especially faulting.*
   b. *Enhanced mapping of reservoir thickness and limits.*
   c. *Definition of reservoir compartmentalization.*

2) *Define optimal in-fill drilling locations.*

Horizontal Drilling:

1) *Improve waterflood sweep efficiency and ultimate recovery, thereby improving economics.*

2.0 EXECUTIVE SUMMARY

This project entailed the use of high-resolution, three-component, three-dimensional seismic data (3C3D) to improve reservoir characterization at Eva South. These data were utilized to identify the optimal location for a new horizontal well.

The first phase of the project involved extensive seismic modeling utilizing existing well-data as well as the actual seismic data as it was acquired. Sonic and density logs from the ESU 10 well were used to generate a synthetic seismogram in order to analyze the seismic response of the Eva sandstone. The seismic response of the Eva sandstone was also modeled in a P-wave, seismic cross section using wells that are both in and out of the valley-fill reservoir. These models indicated a good response could be expected and also provided ties from the well control to the actual P-wave seismic data.

Low-frequency amplitude-versus-offset (AVO) and PSV converted-wave models were generated in order to predict the PSV converted-wave response of the Eva sandstone. These models indicated that the actual seismic data should produce a mappable event for the Eva sandstone.

Based on the strength of the modeling, the seismic survey was designed to maximize the acquisition of high-quality, high-resolution P-wave data. Although PSV converted waves would also be recorded, the design parameters for the P-wave data were not compromised.

The survey was acquired in the spring of 1999. The design resulted in a 4.25 square mile survey with 29-fold at the Morrow horizon and a density of 271 receivers and 193 sources per square mile. Adjacent receiver lines were staggered creating a 82.5 foot bin-size that could be fractionated and interpolated to 41.25 feet. It was later determined that the larger bin-size (82.5 feet) provided the best resolution.

Initial P-wave processing was done by WesternGeco and employed migration and dip moveout (DMO). A second, and final phase of processing was done by Sterling Seismic Services and generated several volumes, including both near and far offset volumes and two azimuthal volumes.

All of the PSV converted-wave processing was done by WesternGeco. This is an evolving process that continues to improve with each new survey. Critical steps included: accurate sorting of the geophone components and accounting of all source to receiver azimuths for each source point; derivation of the radial component of the PSV converted-wave energy; and, accounting for polarity differences between radial and transverse components recorded at receivers 180 degrees opposed along an azimuth

from a common source. A final crucial component was the determination of the common conversion point (CCP) for accurate binning of the data.

The P-wave data proved to be very beneficial in defining the structural framework of Eva South, including the recognition to two previously unknown faults. General valley geometry and extents also appeared to be accurately derived from the data. The seismic data also resolved several of the known compartments but did not delineate any new compartments. Similarly, the data appeared to reflect general reservoir distribution as known from well control, but did not define any new areas of reservoir heterogeneity. This may reflect good continuity of the reservoir as much as a failure to image additional detail.

The reservoir creates a discrete and unique seismic event at the frequencies available (90 hertz). Amplitude maps of the actual sandstone event proved most useful, but an approach using time window amplitude extractions referenced from more regional and less interpretive seismic horizons also produced a good description of the reservoir. There was good agreement with know reservoir compartments but the data did not suggest the existence of any undeveloped compartments. Though the extents and overall geometry of the reservoir can be defined by amplitude maps, plots of amplitude versus net sandstone did not yield a strictly linear relationship. This was determined to be the result of tuning effects which caused a decrease in amplitude above 30 feet of net sandstone. As a result, an interpretive approach was required in making the final reservoir map. Offset dependency on the P-wave seismic amplitudes was analyzed, but did not provide any additional insight.

The PSV converted-wave data showed a good correlation of amplitude to net sandstone, but did not reveal any additional details about reservoir extents or geometry. Analysis of common conversion point (CCP) fold suggests the possibility of an acquisition geometry overprint. A CCP supergather from the center of the PSV converted-wave radial-component volume sorted by azimuth indicated a measure of shear-wave splitting, confirmed by seismic reflection energy in the transverse component. The supergather suggested a fast direction oriented along 130 degrees azimuth and a slow direction oriented along 220 degrees azimuth. The PSV-wave volume was rotated into these two azimuths and final stack volumes created to analyze this splitting; amplitudes of the Eva sandstone were much stronger on the 130 degree volume, though the fault framework is more apparent in the 220 degree volume. Two-way travel times to the Eva sandstone revealed that the area outside the fault framework displayed a fast direction at 130 degrees azimuth. While this is generally acknowledged as the principle stress direction in the area, it is perpendicular to the fault system. Within the fault system, the apparent fast direction changes radically. Similarly, apparent seismic anisotropy from the two PSV-wave azimuthal volumes showed a high degree of variability. A possible explanation is that differential strike-slip movement on the faults created internal rotation on the blocks bounded by the faults that changed the direction of stress and fracturing between the faults.

Calculations of Vp/Vs showed some contribution to the PSV-seismic response from the Eva sandstone. That observation coupled with the amplitude map of the Eva sandstone seismic event offers encouragement for the continued application of PSV-wave data to map upper Morrow and other (DOE) Class 1 reservoirs.

Although the 3C3D seismic study did not result in the identification of any additional undeveloped compartments in Eva South, it did provide excellent detail on the structure of the field and defined areas of good reservoir continuity. Based on a combination of geological, geophysical and engineering analyses it was determined that the best location for a horizontal well was parallel to the Teepee Creek fault. Specific factors that determined the location of the ESU 13-H horizontal well were: 1) The 3D seismic provided excellent structural control, especially in locating the position of the Teepee Creek fault; 2) The seismic indicated good reservoir continuity along a trend parallel to the fault; 3) Although adequate, sweep efficiency in the western portion of the field was not as high as to the east; and, 4) A theory that oil may have been banked up against the fault.

The drilling plan for the ESU 13-H called for the well to be drilled parallel to, and within 200 feet of, the Teepee Creek fault. Total lateral displacement in the Eva sandstone was planned to be 2800 feet. The well entered the Eva sandstone within three feet of the targeted elevation as defined by seismic. Approximately 1000 feet of reservoir was drilled horizontally before the drilling assembly became permanently stuck. Despite the disappointment of only attaining approximately one third of the planned horizontal displacement, the well was successful in adding 122 MBO of incremental reserves to the field, representing 1.7% of the original oil in place (OOIP). This compares favorably with the objective of adding 2% (150 MBO) of the OOIP per well and indicates that horizontal wells can be very effective in improving sweep efficiency in a Morrow waterflood. It is concluded that horizontal wells should have widespread application in (DOE) Class 1 reservoirs.

3.0 EXPERIMENTAL

Neither of the advanced technologies applied in this project, 3C3D seismic nor horizontal drilling, could be considered as new or experimental. However, the applications described herein are certainly new and emerging. Numerous references for these technologies are supplied in the bibliography and particularly noteworthy publications are noted in the text.

3.1 3C3D Seismic

The onshore application of three-component, three-dimensional seismic (3C3D) is an emerging technology in the oil and gas industry. Converted-wave seismic was developed out of necessity for offshore applications where shear waves can not be generated from a direct source. This technology allows for the recording of shear-wave

(S-wave) data in addition to compressional (P-wave) data from only a compressional wave source (see Tatham and McCormack, 1991); it is now being tested as a cost effective alternative to shear-wave sourced seismic for onshore applications. Publications specific to this project include Miller and Wheeler (2000), Van Dock and Gaiser (2001) and Wilson et al. (2001).

As explained by Hardage (1996), among other things, shear-wave data can aid in the differentiation of sandstone versus shale in clastic environments. The advent of onshore P-S (PSV) converted-wave seismic provides a cost effective means of acquiring these data.

3.1.1 PSV Converted-Wave Conventions and Definitions

Figure 3.1.1a illustrates how conventions used in defining the SV (shear in the vertical plane) and SH (shear in the horizontal plane) directions differ between 2D and 3D seismic acquisition. In 2D seismic acquisition, the sources and receivers are typically in the same surface line, and reflecting events in a flat layered earth would be contained in the vertical plane under the surface line of sources and receivers. Horizontal particle motion parallel to the receiver line orientation is defined as the SV direction, and particle motion perpendicular, or transverse, to the receiver line orientation is defined as the SH direction. The 3-component geophones used in the recording of S-wave information are deployed such that the horizontal elements are aligned with the SV and SH directions as shown by the red receiver locations in Figure 3.1.1a. PSV converted waves are only generated in the SV direction.

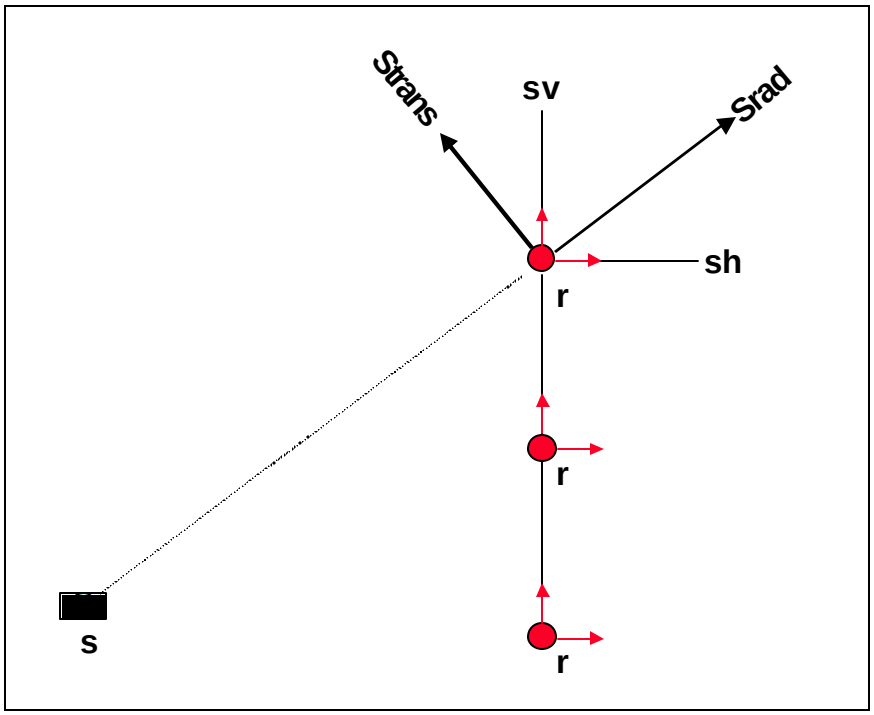

Figure 3.1.1a. Conventions used in S-wave and PSV converted-wave recording and processing. S = source; r = receiver; Strans = transverse shear component; Srad = radial shear component; SV = particle motion parallel to receiver line; SH = particle motion perpendicular to receiver line.

In 3D acquisition, receivers are deployed in a series of parallel lines across the survey area and the 3-component geophones are aligned relative to the receiver line azimuth as in 2D acquisition. The source locations typically are grouped in lines at some angle (usually 90 degrees) across the receiver lines. A number of receiver lines may be actively recording for any particular source location. As shown in Figure 3.1.1a, the source location may be at some angle to the receiver lines, hence the 3-component geophone orientation. PSV converted waves are generated in the plane containing the source and receiver. In 3D applications the source to receiver azimuth is termed the radial component and the direction perpendicular to the source to receiver azimuth is termed the transverse component. The SV and SH elements of the 3-component geophones each record some vector component of the true radial and transverse particle motions relative to the source location and the true radial and transverse particle motions are recovered in processing by vector math. Both the radial and transverse motions can be processed individually. While the radial component typically contains the majority of the PSV converted-wave response, a thorough analysis of S-wave splitting requires analyzing both the radial and transverse components.

Figure 3.1.1b illustrates the ray-path geometry of PSV converted waves and summarizes some of the characteristics which have an impact on the recording and processing of this type of data. The down-going energy is generated from a P-wave source and hence travels at the P-wave velocity of the geologic section from the source location to the reflecting interface in the subsurface. At angles of incidence as small as

15 degrees, the "push-pull" particle motion of the P-wave converts to a component of horizontal S-wave motion at the reflection point. This horizontal particle motion is back and forth in the vertical plane containing the source and receiver and this reflected energy travels upward at the S-wave velocity of the geologic section. Note that the angle of the emerging ray-path is more vertical than the down-going ray-path and the reflecting point is not at the midpoint between the source and receiver, as is the case in typical P-wave acquisition or in S-wave recording using an S-wave source. This has great implications in the processing of PSV converted-wave data and in determining the source to receiver offset requirements of the acquisition design.

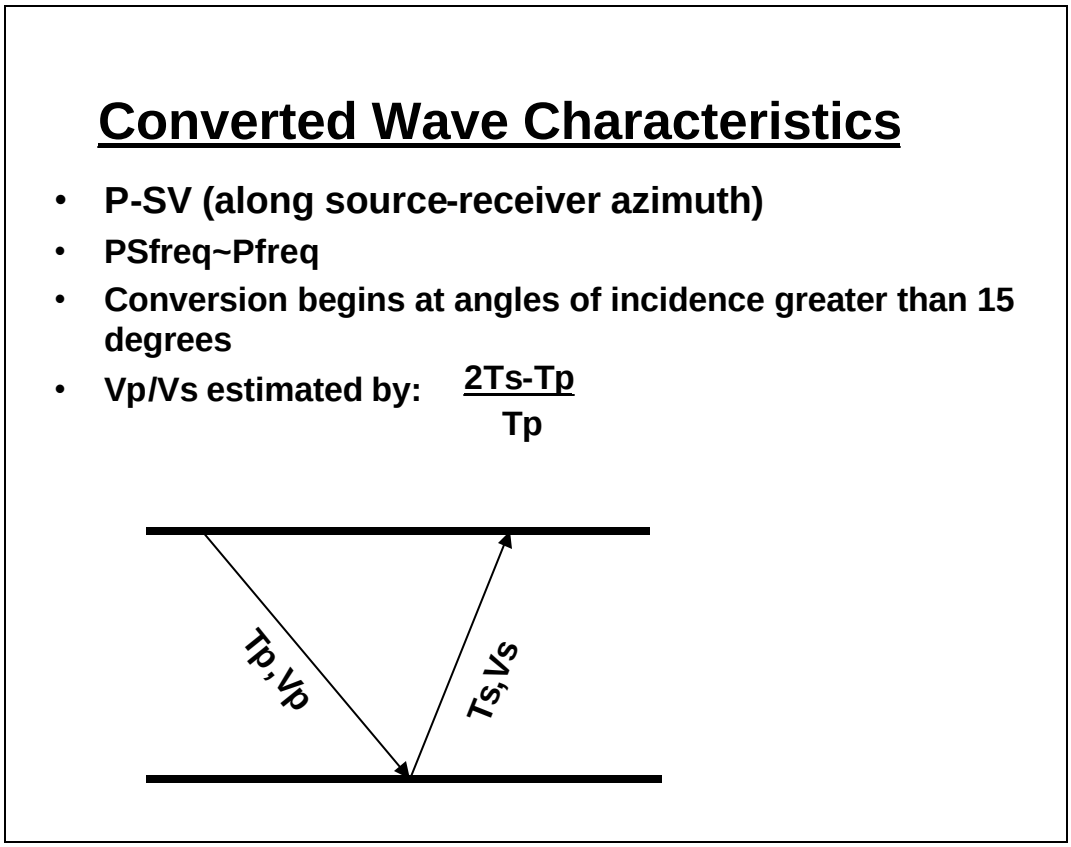

Figure 3.1.1b. Characteristics of PSV converted waves. Note that the reflection point PSV-waves is not the mid point between source and receiver. Tp = P-wave travel time; Ts = S-wave travel time; Vp = P-wave velocity, Vs = S-wave velocity.

Another important consideration in the acquisition of PSV converted waves, especially using a vibroseis source, is that the frequency of the PSV converted wave is approximately equal to the P-wave frequency at the reflection point. If the earth response of an area yields relatively low frequency S-wave data, then the P-wave source must contain enough low-frequency information to generate PSV converted waves of sufficient bandwidth to have a robust seismic signature. This has an impact on the choice of start frequency for a vibroseis source, but may not be as critical of a

consideration for dynamite data recorded with 24-bit instruments as the low-cut filters are usually at very low frequencies.

The 2-way travel time of a PSV converted-wave reflection event is the sum of the travel time of the down-going P-wave to the depth of the reflecting horizon and the travel time of the emerging S-wave from the reflecting horizon depth back to the surface. Since P-wave velocities are typically much faster than S-wave velocities, the down-going travel time is much shorter than the emerging travel time. This must be taken into consideration when correlating reflecting events on PSV converted-wave data to reflecting events on P-wave data. If the P-wave to S-wave velocity ratio (Vp/Vs) is 2 to 1, then a common reflection event on a PSV converted wave section should have a travel time of approximately 1.5 times that of the travel time of the corresponding reflection on a P-wave section. Likewise, if event correlations have been firmly established between P-wave and PSV converted-wave sections, then Vp/Vs can be estimated using either the travel times or interval times by the simple equation shown in Figure 3.1.1b. This can be an important interpretation tool as Poisson's ratio is directly related to Vp/Vs and can be used to help determine lithology.

3.1.2 Seismic Modeling

The initial phase of the project was an extensive modeling study to determine the feasibility of utilizing 3D seismic data to improve characterization of the reservoir at Eva South. This phase of the project involved the generation of synthetic seismograms from well-logs, construction of P-wave seismic cross sections and models, analysis of amplitude versus offset (AVO) and converted-wave (PSV) response and the generation of AVO and PSV models.

In order to investigate the feasibility of using seismic data at Eva South, it was important to model the seismic response of the reservoir interval using existing borehole information. The majority of the wells in Eva South have sonic logs as the principle porosity device. This allowed for seismic model studies to be performed on the actual field geology and not an idealized model. Most of the sonic logs are 1960s vintage uncompensated logs, which required some editing for borehole conditions. Many of the wells only penetrated a short depth below the base of the reservoir. These were combined with deeper logs for the purpose of modeling to minimize any misleading results which might occur by not including information within a full seismic wavelength of the target reservoir. Modern logs, including both a compensated sonic log and a density log were available for the ESU 10 well.

<u>ESU 10 Synthetic</u>

The ESU 10, drilled in 1995 by EOC, is the only well which has a modern vintage compensated sonic log run from base of casing to total depth. A density log was also acquired for this well. As a result, the ESU 10 serves as a key well for generating a synthetic seismogram to correlate seismic data and for analyzing the seismic response of the Eva sandstone reservoir.

A synthetic seismogram constructed with a 90 hertz, zero-phase wavelet shows the top of the Morrow shale (top Morrow Fm.) to generate a strong trough (left deflecting) seismic event (Fig. 3.1.2a). The top of the Eva sandstone appears as a weak peak (right deflecting) seismic event followed by a stronger trough. It was observed on the actual 3D seismic data at Eva South that most of the useful seismic stratigraphic information in terms of amplitude and continuity is contained within the trough event.

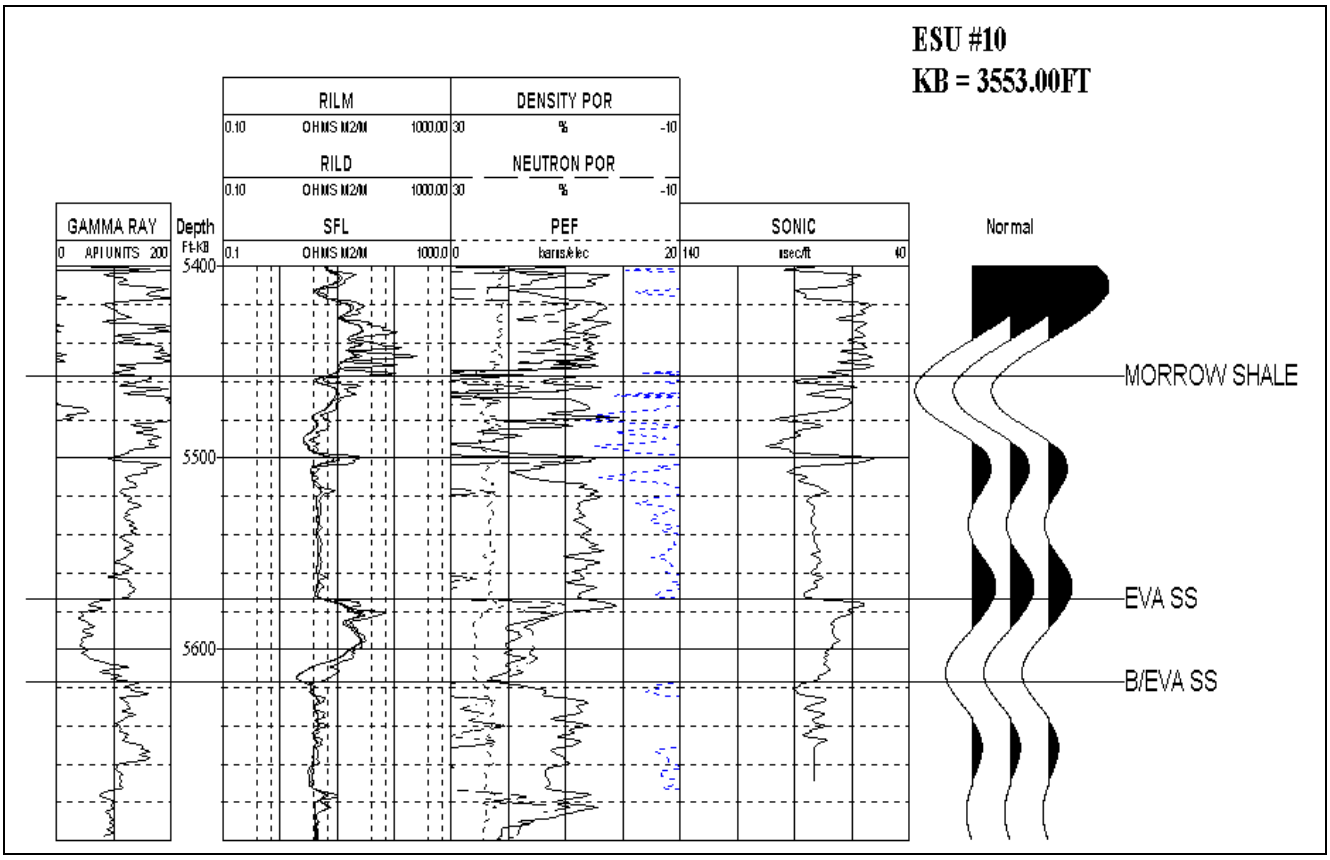

Figure 3.1.2a. Synthetic seismogram generated from the sonic and density logs in the ESU 10 well showing the response of the top of Morrow shale and Eva sandstone interval. Morrow shale seismic-event represents the top of the Morrow Formation.

P-wave Seismic Cross-section and Model

A P-wave seismic model constructed through wells in Eva South investigated the seismic response of varying stratigraphy of the producing Eva sandstone observed across the field. The following wells were put into cross section and have varying interval lithology as noted:

Ivie 1: marine shale; no valley fill, no Eva sandstone.

ESU 6 (Dunaway Trust #1): 43 feet of valley-fill, dominantly active channel-fill sandstone.

ESU 2 (C.F. Webb #1): 37 feet of valley-fill, approximately half abandoned channel-fill mudstone and half active channel-fill sandstone.

Eggers 1: marine shale; no valley-fill, no Eva sandstone.

This cross section (Fig. 3.1.2b) serves as the input into construction of the seismic model.

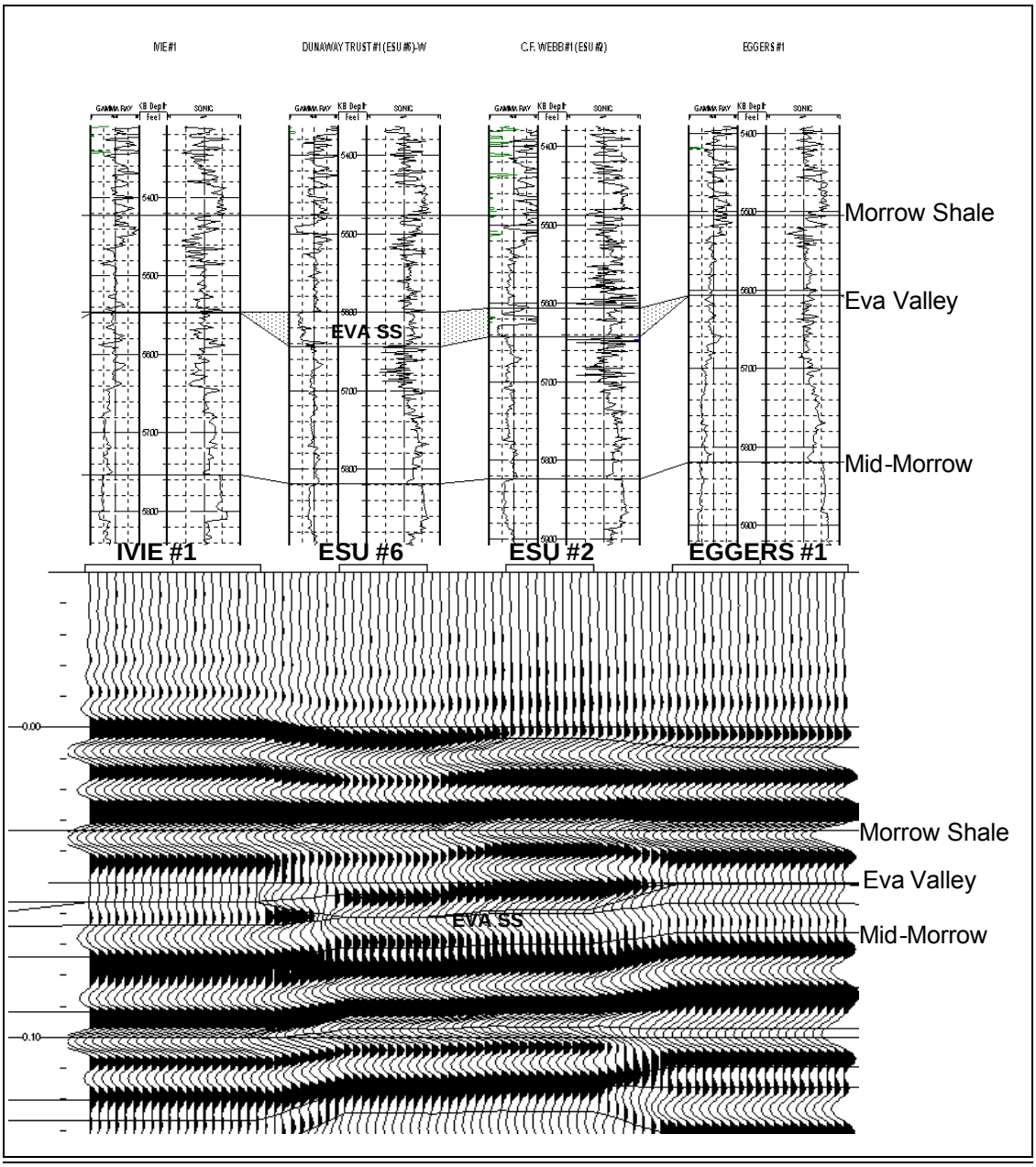

Figure 3.1.2b. Seismic-model input cross-section (top) through wells in Eva South showing varying Morrow stratigraphy in the reservoir sequence and the corresponding P-wave seismic-model response (bottom). The Eva sandstone models as a trough event, as labeled.

The sonic logs of the input cross section were interpolated, integrated, and convolved with a 90 hertz, zero-phase seismic wavelet to create the seismic trace model. No density logs are available for the wells in this model. The model response showed the Eva sandstone interval in the ESU 6 and ESU 2 wells to have a distinct seismic event consisting of a peak followed by a strong trough consistent with the ESU 10 synthetic seismogram. The Ivie 1 and Eggers 1 wells, located out of the valley-fill, showed no seismic event in the corresponding interval. This model indicated that the valley-fill sequence, including the Eva sandstone, generates a mappable seismic event distinct from areas outside the valley.

Of particular interest was whether active channel-fill sandstone (reservoir) could be distinguished from abandoned channel-fill mudstone (non-reservoir) within the valley-fill. Contrasting the ESU 6 and ESU 2 responses suggests that an increase in abandoned channel-fill at the top of the valley creates an increase in the top peak event. However, the trough event shows little difference between these wells across the lower portion of the valley, an interval occupied by active channel-fill sandstone in both wells.

The seismic model suggested that the onset of the Eva sandstone is a strong peak event, yet both the actual seismic data and the ESU 10 synthetic seismogram show that this peak is not a particularly high-amplitude event. From a model perspective, this is primarily a function of not having density information to use with the older sonic logs. It is believed that low-density of high-porosity active channel-fill sandstone attenuates the peak-event on actual seismic data; the seismic reflectivity of a geologic boundary is a function of the contrast of both the velocity and density of the lithology across the boundary.

AVO and PSV-wave Seismic Model Studies

In support of interpreting the PSV-wave data, the amplitude versus offset (AVO) response of the Eva sandstone for low-frequency P-wave and PSV-wave data was investigated. The modeled seismic response versus sandstone thickness was also investigated for the PSV converted-wave response.

The offset dependent reflectivity of the Eva sandstone for a 30 hertz Ricker wavelet was generated using the ESU 10 sonic log and is shown in Figure 3.1.2c, a plot of the reflection coefficient versus angle of incidence. This plot shows the zero offset response to be a weak peak-event that shows a phase reversal to a trough-event of increasing amplitude with increasing angle of incidence (offset) and is characterized as a Class II AVO response (Castagna and Backus, 1993).

The generation of PSV waves occurs when a down-going P-wave impinging on a reflecting interface at increasing angles of incidence creates a conversion to reflected S-wave energy. In theory, this conversion takes place at angles as low as 15 degrees. The predicted PSV-wave reflection strength with increasing angle of incidence for the Eva sandstone in the ESU 10 (Fig. 3.1.2c) suggested that the optimal offset range for

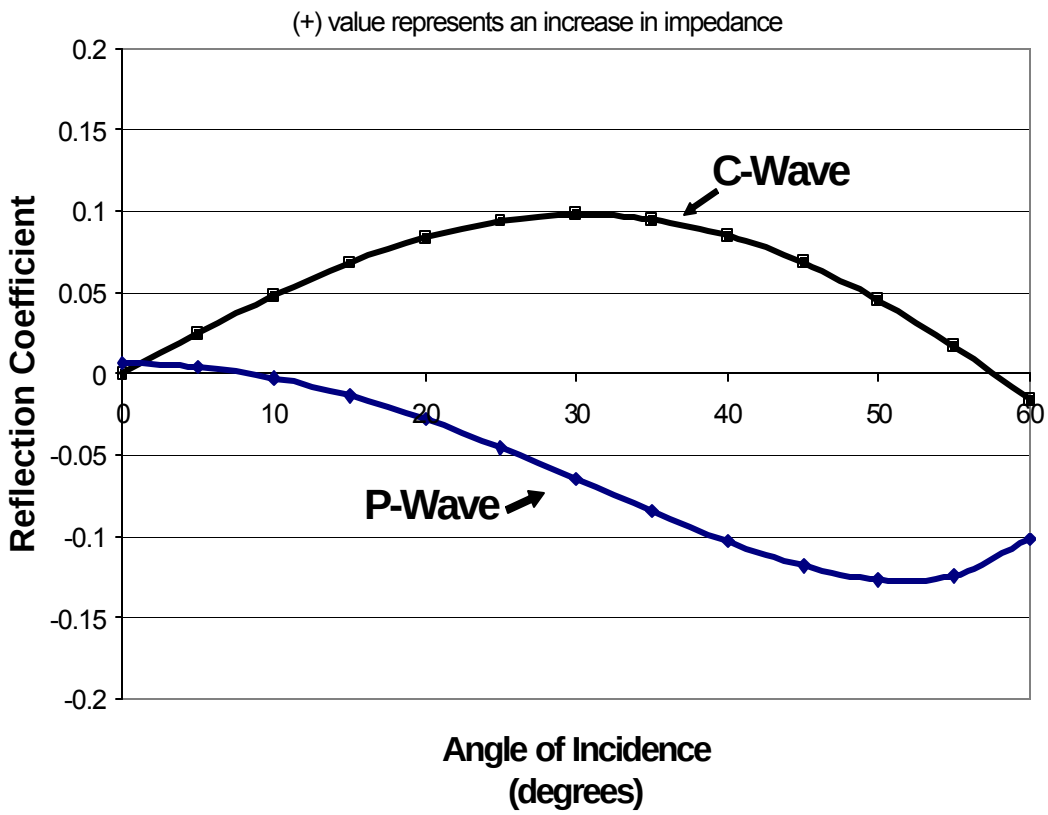

the PSV-wave reflection is at angles of incidence between 15 to 45 degrees, with a maximum response at 30 degrees.

Figure 3.1.2c. Plot of reflection coefficient versus angle of incidence for the Eva sandstone event in the ESU 10 for both a PSV converted-wave and 30 hertz P-wave (Wilson, 2002).

AVO Seismic Model

The AVO response of the Eva sandstone encountered in the ESU 10 was generated for a 30 hertz Ricker wavelet and contrasted with the response from a similar interval with the sandstone removed (Fig. 3.1.2d). The peak-event corresponding to the Eva sandstone is observed to diminish in amplitude with increasing offset. In the zero sandstone case, there is no observable change in amplitude with increasing offset of the peak occupying the relative stratigraphic position of the Eva sandstone.

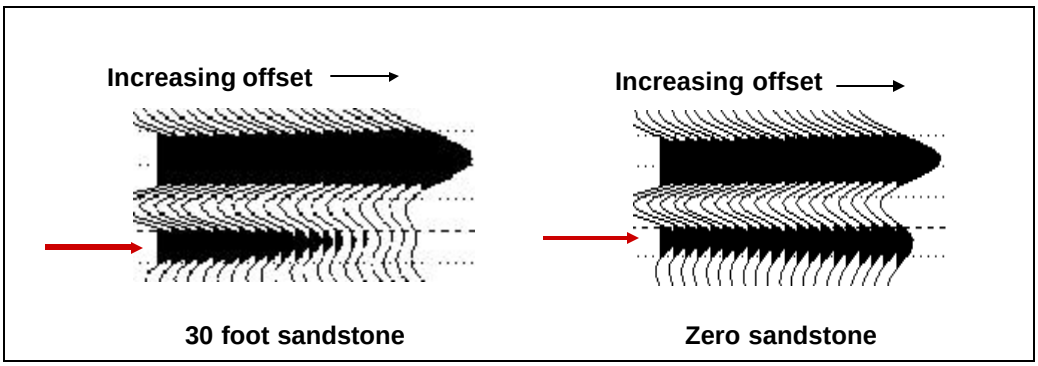

Figure 3.1.2d. Amplitude versus offset (AVO) response for the Eva sandstone encountered in the ESU 10 contrasted with a similar section with no sandstone. Offset increases left to right. The traces were generated using a 30 hertz Ricker wavelet. The red arrows indicate the position of the Eva sandstone. (Wilson, 2002)

It should be stressed that at the 30-hertz frequency, the event corresponding to the Eva sandstone interval is interfering with the peak side-lobe from the stronger Morrow shale trough event immediately above. When the sandstone is present, there is interference with this event creating the amplitude change with increasing offset. Notice that at zero offset (first trace on the left) the amplitude of this peak is higher in the presence of a 30-foot sandstone than for the case with zero sandstone suggesting some measure of constructive interference between the sandstone event and the trough sidelobe. The interference becomes destructive with increasing offset as the sandstone-event phase begins to change as suggested by Figure 3.1.2c. In the zero sandstone case, the peak is solely due to the Morrow shale trough-event sidelobe and displays no change with increasing offset.

The intent of the low frequency AVO modeling was to assist in predicting whether or not to expect a PSV converted-wave response in the presence of Eva sandstone. The low-frequency model response varies markedly from the 90 hertz response previously modeled.

PSV Converted-wave Seismic Model

In order to predict the PSV converted-wave response of Eva sandstone a wedge model of increasing sandstone thickness was generated (Fig. 3.1.2e). The model shows an increase in amplitude with increasing sandstone thickness for the event corresponding to the Eva sandstone interval. This indicated that PSV converted-wave data should be useable to identify and map the distribution of the Eva sandstone reservoir.

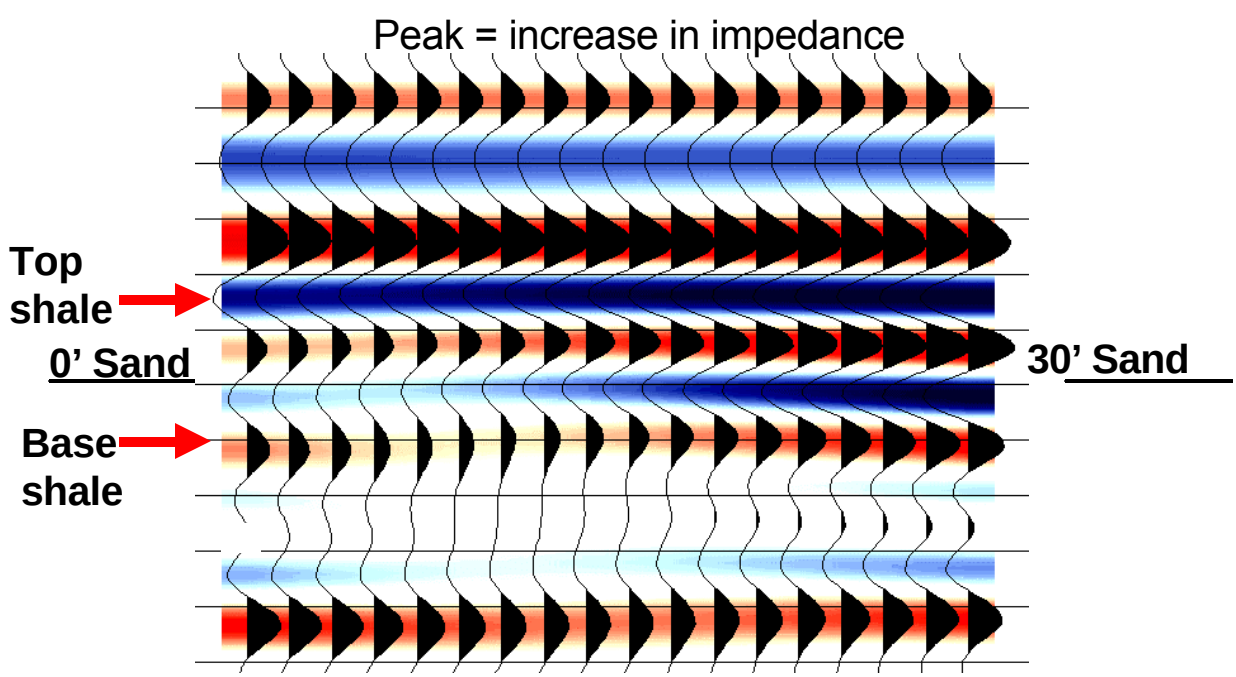

Figure 3.1.2e. PSV converted-wave seismic model response to Eva sandstone of increasing thickness (Wilson, 2002). Note the increase in amplitude from zero to 30 feet of sandstone.

This model was generated by Travis Wilson, a graduate student at the Colorado School of Mines, Golden, Colorado, who investigated PSV converted-wave response in the Kansas/Oklahoma area around the Eva South project and has written an application to predict the PSV converted-wave response using P-wave and S-wave velocity information as well as density information (Wilson, 2001). Key to this model creation was the conversion of P-wave velocities to an estimate of S-wave velocities based on regional knowledge of the P-wave to S-wave velocity ratios for the geologic section in this area. This is important as only P-wave velocity information is available at Eva South. The predicted PSV converted-wave travel times were generated as well as the PSV converted-wave reflectivity based on an angle of incidence of 20 degrees. Once the PSV converted-wave velocity section was established, the interval thickness of the Eva sandstone was manipulated to generate the seismic model response to increasing sandstone thickness. The input wavelet used in the generation of the model was 25 hertz, typical for PSV converted-wave data in the Eva South area.

3.1.3 3C3D Seismic Design and Acquisition Parameters

One of the primary goals of this project was to utilize high-resolution P-wave seismic data to image the Eva sandstone reservoir in support of a proposed infill drilling program. Of particular interest was the identification of potential reservoir compartments not currently being efficiently produced or swept by the waterflood. These compartments may be related to areas of abandoned channel-fill, or to subtle faults within the field linked to the major Teepee Creek fault which bounds the west side of the unit.

Results of the P-wave seismic modeling suggest that the Eva sandstone is mappable with high quality, high resolution P-wave seismic data having frequency content in upwards of 90 hertz. Based on the favorable results of the seismic modeling, a 4.25 square mile 3D seismic survey was designed and acquired over Eva South.

Discussions about survey design and acquisition parameters with WesternGeco led to the proposal of using three-component geophones to record PSV converted-waves generated by a standard P-wave vibroseis source (Fig's. 3.1.3a,b,c). This was part of an effort by WesternGeco to promote the use of PSV converted-waves in oil and gas exploration. The use of PSV converted-waves to acquire S-wave information is inherently less expensive than using a specialized S-wave source in that it greatly reduces the acquisition effort in the field. In theory, PSV-wave seismic can record both P-wave and S-wave datasets from a common P-wave source rather than duplicating the recording for each separate source. The combination of P-wave and S-wave information allows for additional analyses to be made into such parameters as the Poisson's ratio characteristics of the subsurface lithology as well as a more comprehensive fracture analysis than can be made from P-wave data alone.

Figure 3.1.3a. Vibroseis trucks lining up to begin the survey at Eva South. These are conventional vibroseis trucks that generate standard P-waves.

Figure 3.1.3b. Photograph of three-component geophones. These phones record both P- and PSV-waves and are the critical component to 3C3D seismic acquisition. Note the arrows on top for orientation.

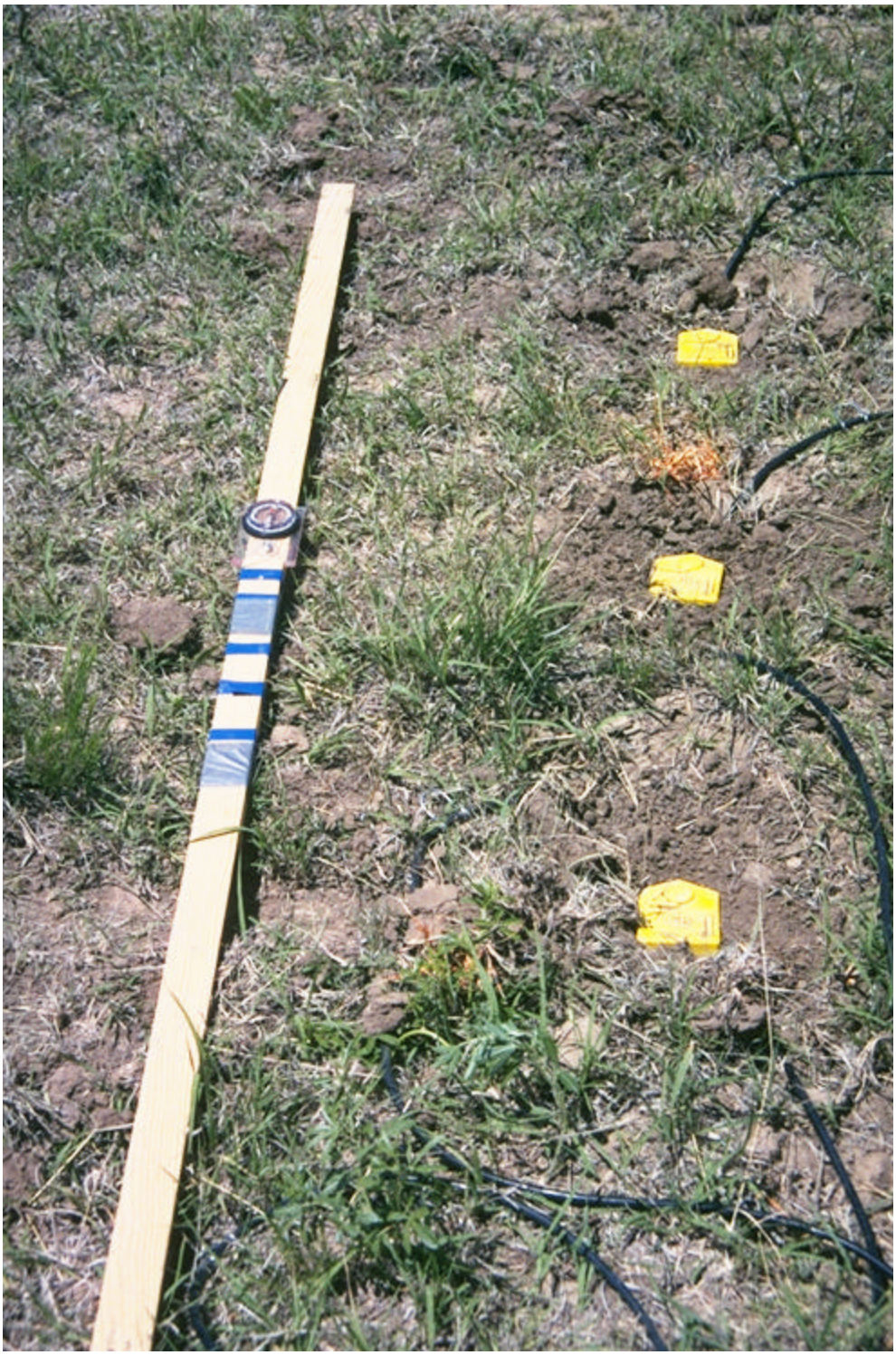

Figure 3.1.3c. Photograph of three-component geophones in place. A compass was used to orient the phones to within 10 degrees tolerance.

The design for the Eva South 3D used the following parameters:

- ? Receiver line spacing of 660 feet
- ? Receiver interval of 165 feet
- ? Source line spacing of 990 feet
- ? Source interval of 165 feet
- ? Vibroseis source, 14-128 hertz non-linear sweep

This design resulted in:

- ? Bin Size, 82.5 X 82.5 feet
- ? 271 Receivers per square mile
- ? 193 sources per square mile
- ? 29-Fold at Morrow horizon

The source lines are in a brick pattern and the source line and receiver line geometry is shown in the layout map of Figure 3.1.3d. This brick pattern is disrupted in the south half of Section 5 due to a permit restriction which made it necessary to deploy the sources in straight lines to minimize track damage. Because of the infrastructure of production and injection flow-lines at Eva South, some shot locations were moved off pattern to accommodate a safe distance from these lines and minimize the potential for damage from the vibratory sources.

Adjacent receiver lines were staggered by 82.5 feet to permit the fractionation of the survey data to a bin size of 41.25 by 41.25 feet if desired. Fractionation increases the lateral resolution of the survey in the receiver line direction at the expense of the fold of the data. The receiver lines were deployed in a north-south direction, perpendicular to the axis of the Eva sandstone reservoir. The source lines were deployed in an east-west direction as shown in Figure 3.1.3d.

As previously noted, in order to record PSV converted waves, three-component geophones were used as receivers for the Eva South 3D instead of traditional vertical component geophones which record only P-waves. Three-component geophones have three geophone elements: one oriented in a vertical direction; one in a horizontal direction parallel to the receiver line azimuth; and the third oriented in a horizontal direction perpendicular to the receiver line azimuth. This allows for the recording of ground particle motion in all three directions. P-wave particle motion is in the vertical direction and S-wave particle motion is in the horizontal direction.

The original P-wave parameters planned on using a 20- to 128-hertz non-linear vibroseis sweep. The choice of a 20-hertz start frequency was based on experience in the area and the observation that ground roll is generated at lower frequencies towards 10-hertz, but is greatly attenuated at higher frequencies. Ground roll is a series of surface seismic waves which adversely interfere with the recording of reflected seismic data. However, the inherently low-frequency nature of the PSV converted-waves required lower input frequencies in order to maintain enough frequency bandwidth to reconstruct a useful seismic signal. During field testing, it was observed by Ensign's field representative that the original 20-hertz start frequency should be lowered as much

as practical to more efficiently generate PSV converted waves. After a series of sweep tests it was determined that a 14-hertz start frequency was the best compromise between having a lower frequency input for PSV converted-wave generation and keeping ground roll generation to a level which did not adversely impact the quality of P-wave recording to a level that could not be corrected in data processing.

Data acquisition was performed by WesternGeco with a crew operated out of the Oklahoma City, Oklahoma office. Field supervision and monitoring was performed on Ensign's behalf by Terry Donze of Wheat Ridge, Colorado.

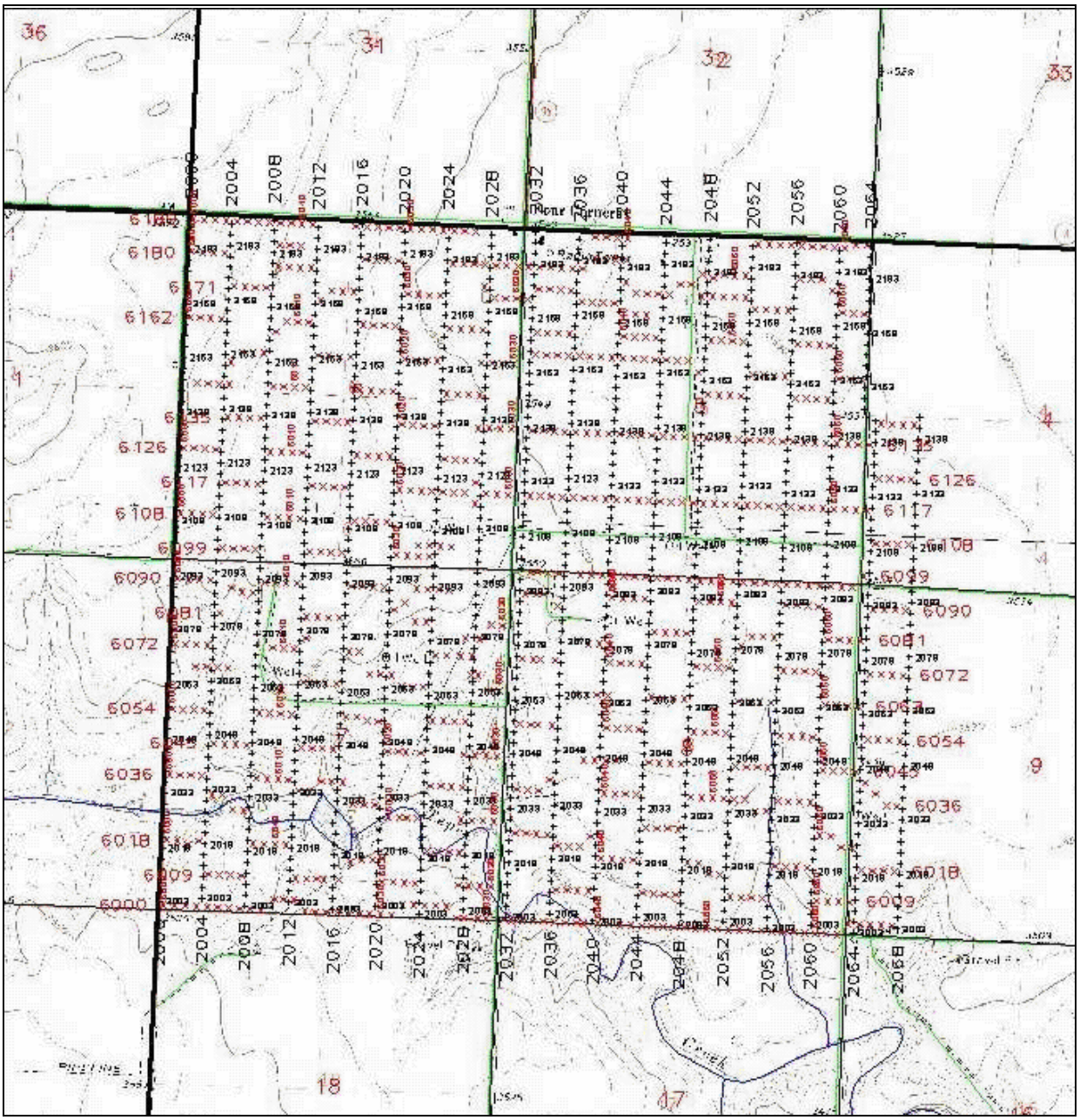

Figure 3.1.3d. Layout of the Eva South 3D survey with receivers shown as "+" in the north-south direction and sources shown as "x" in the east-west direction.

It is important to note that the P-wave acquisition design was not compromised in order to record PSV converted-wave information. As a result, the acquisition survey was not necessarily optimal for PSV converted-wave recording. Various technical aspects of the PSV converted-wave acquisition could be improved upon. These are noted and discussed in the conclusions. Still, the PSV converted-wave data set provided an important opportunity to analyze these issues and form a better understanding of the utility of this type of data in petroleum exploration and development for Morrow and other (DOE) Class 1 reservoirs.

3.1.4 3C3D Seismic Processing Parameters

P-wave

The initial processing of the P-wave data was done by WesternGeco, Denver, Colorado.

Binning of the 3D data was done to both 82.5 by 82.5 feet and fractionated and interpolated to 41.25 by 41.25 feet. Both volumes were migrated and a comparison showed that there was no significant improvement in the resolution of the smaller bin size. If anything, the smaller bin-size volume appears to have too much smoothing introduced into the data. As a result, the final interpretation volume used the larger bin size and was migrated after the application of dip moveout (DMO).

A second, and final, phase of processing of the P-wave volume was performed by Sterling Seismic Services, Littleton, Colorado. This processing flow binned the data to 82.5 feet and was carried through to migration, but without the application of DMO. In addition to the migrated volume, the following additional processed volumes were generated:

- Near-offset migrated volume, only source to receiver offsets less than 3500 feet used
- Far-offset migrated volume, only source to receiver offsets greater than 3500 feet used
- Azimuth-limited migrated volume, only source to receiver combinations falling within 45 degrees of a NW to SE azimuth used
- Azimuth-limited migrated volume, only source to receiver combinations falling within 45 degrees of a NE to SW azimuth used

PSV Converted Wave

The initial processing of the PSV converted-wave data was done by WesternGeco, Denver, Colorado.

While the acquisition of PSV converted-wave data required only minimal changes to a typical P-wave acquisition, there were extreme differences in processing PSV converted-wave data versus P-wave data. Because of the multi-component nature of the data, a critical initial step in the processing of the PSV converted-wave data was an accurate sorting of the recorded geophone components and accounting of all of the

source to receiver azimuths for each source point. Next was the derivation of the radial component of the PSV converted-wave energy which, by definition, is along the source to receiver azimuth. This also involved accounting for a polarity difference between radial components recorded at receivers which are 180 degrees opposed along an azimuth from a common source. Similarly, the transverse component of the PSV converted-wave energy was also derived by these computations.

Figure 3.1.1b illustrates another crucial difference between P-wave and PSV converted-wave processing. Because the down-going P-wave travels at P-wave velocity and the up-going reflected PSV converted-wave travels at S-wave velocity, the ray-path angles are not symmetrical around the reflecting point. As a result, traditional P-wave Common Depth Point (CDP) processing approaches are not applicable in the gathering of data to common reflection points as these approaches assume a reflection point midway between the source and receiver. For the PSV converted-wave data, the Common Conversion Point (CCP) must be determined to accurately gather, or bin, the data traces into their proper spatial location.

PSV converted-wave data is inherently of lower signal to noise ratio than P-wave data which can make velocity and statics determinations difficult. The statics and velocity information from the P-wave processing are used as an important estimate of the S-wave statics and velocities by adjusting them with a knowledge of typical P-wave to S-wave velocity ratios for the area. This could be done more robustly with either dipole sonic or S-wave Vertical Seismic Profile (VSP) information from a nearby borehole, but unfortunately this information was not available at Eva South.

As with the P-wave data, the PSV converted-wave 3D volume was binned to 82.5 by 82.5 feet. The final processing step was a PSV converted-wave migration.

3.2 Horizontal Drilling

Although horizontal drilling is not a particularly new technology, to our knowledge few, if any, horizontal wells have been drilled targeting an upper Morrow sandstone reservoir in a waterflood unit in the Mid Continent region. The objective was to determine the horizontal producing characteristics of the Eva sandstone and to test the effectiveness of improving waterflood sweep efficiency.

Based on interpretation of the geology from well control and seismic data, it was determined that the best location to drill a horizontal well was parallel to, and within 200 feet, of the Teepee Creek fault. The location of this well, the ESU 13-H, is shown in Figure 1.2a. Based on directional and depth requirements provided by EOC, the drilling plan was prepared by Sperry Sun (a division of Halliburton).

4.0 RESULTS and DISCUSSION

4.1 3C3D Seismic

As discussed in Section 3.1.4 (*Seismic Processing Parameters*), multiple 3D seismic volumes were generated. All of these volumes were analyzed and the best quality data were utilized for the interpretations presented herein. For the P-wave data the volumes generated in the second phase of processing, done by Sterling Geophysical Services were utilized; final PSV-wave volumes were generated by WesternGeco.

4.1.1 P-wave Interpretations

Synthetic Tie and Event Correlations

Event correlations and data phase were established by examination of the tie of the seismic data to a synthetic seismogram generated from the ESU 10 sonic log. As discussed in Section 3.1.2, the ESU 10 is the only well in ESU with a modern log suite run from surface casing to total depth (TD). Figure 3.1.2a shows the predicted seismic response of the Morrow section and Eva reservoir based on the ESU 10 synthetic seismogram.

Figure 4.1.1a shows the correlation of seismic events to key geologic formations at the tie of the ESU 10 well to a seismic line from the 3D volume. It was necessary to phase rotate the seismic data 180 degrees, or reverse the polarity, to establish the tie to the synthetic seismogram polarity. At this polarity, the data appear to very closely match the zero-phase wavelet used to construct the synthetic seismogram.

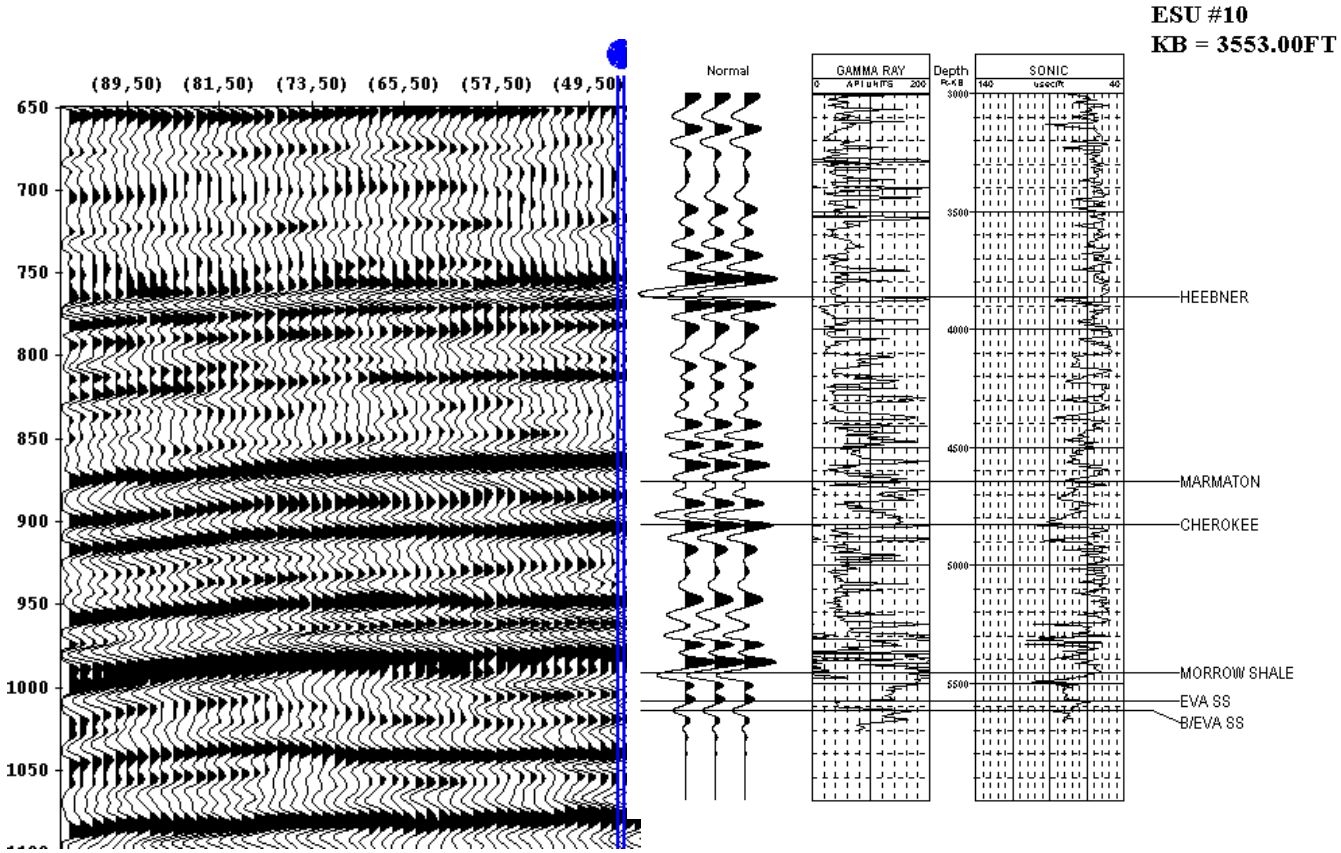

Figure 4.1.1a. Tie of the Eva South 3D P-wave data to the synthetic generated from the ESU 10. Morrow shale is equivalent to the top of the Morrow Formation.

The key horizons chosen for mapping are the Morrow shale (top of Morrow Formation), Eva sandstone (SS), and a middle Morrow event arbitrarily named the Valley event. Based on the synthetic seismogram of Figure 3.1.2a, the Morrow shale event is a trough corresponding to the low-velocity section. However, this event was picked in the 3D seismic data at the zero crossing into the trough event; locally developed sandstones at the top of the Morrow Formation were observed to distort the trough event slightly, making the zero-crossing pick a closer correlation to the actual top of Morrow. The Eva SS event was picked as a trough event in the 3D. The Valley event was picked as a peak below the Eva SS event as shown in Figure 4.1.1a and was correlated in order to determine if there was a relationship to the distribution of the Eva sandstone.

Structural Interpretation

The seismic data provided a significant amount of Morrow structure detail. In particular, the seismic interpretation showed the faulting at Eva South to be more complex than was suggested solely by the well control. Figure 4.1.1b shows an arbitrary seismic line extracted from the 3D seismic volume which trends northwest to southeast (left to right) across the survey through the ESU 5 well. The location of this line is shown on the time-structure map (Fig. 4.1.1c). The Teepee Creek Fault (red) is immediately to the

west of the ESU 5 and is observed to have vertical displacement which decreases upwards. The fault also shows rapid changes in dip along its vertical profile. Additional faults are observed to the west (green) and east (magenta). These faults appear to be deep-seated, but do not extend as high into the shallow section.

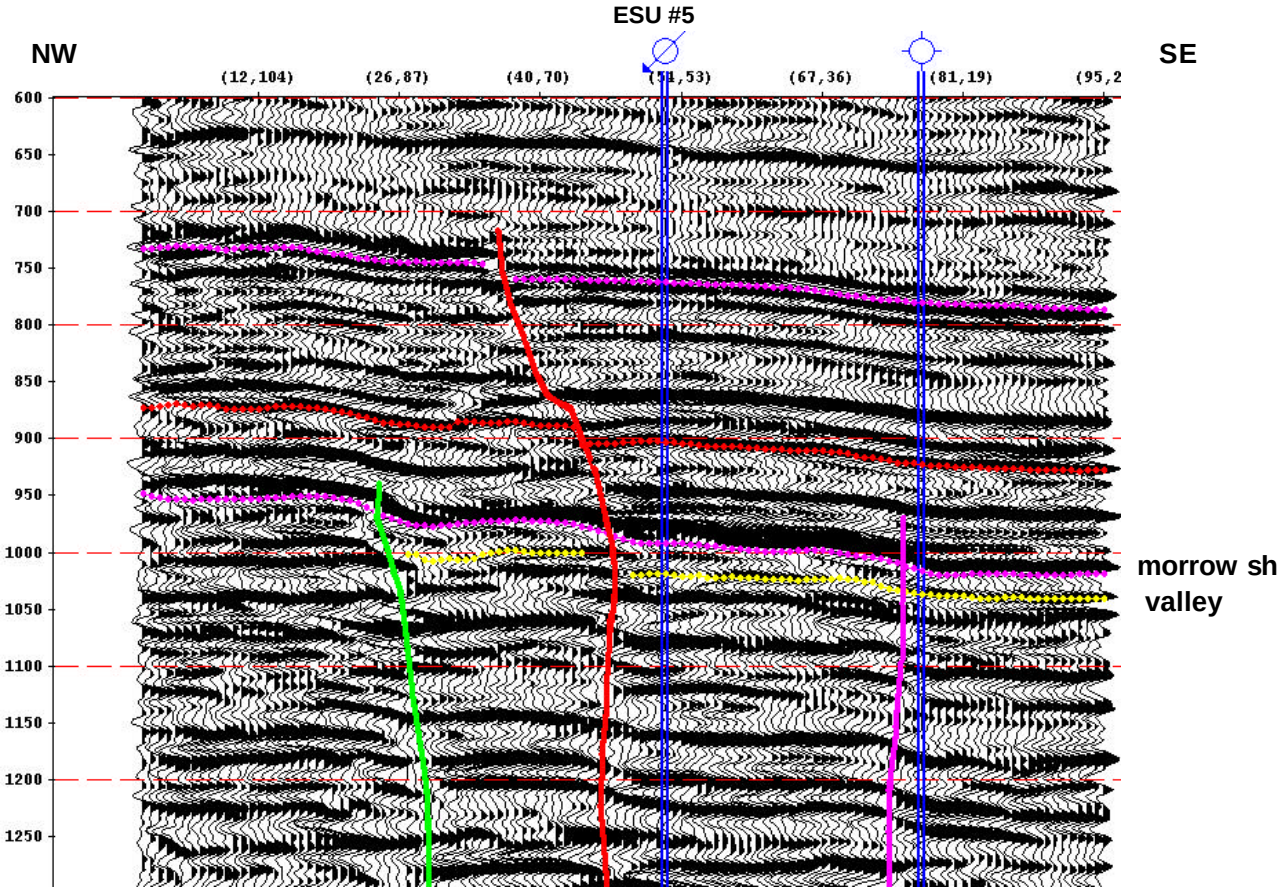

Figure 4.1.1b. Arbitrary seismic line extracted from the Eva South 3D, northwest-southeast (left-right) through the ESU 5. The Morrow shale event is shown as the magenta line. Three separate faults are shown in green, red (Teepee Creek) and magenta. The location of this line is shown on Figure 4.1.1c.

The time structure for the Morrow shale seismic event (top Morrow Fm.) is shown as Figure 4.1.1c. The Teepee Creek Fault is observed to be one of a series of faults. The en echelon pattern of these faults suggests that they are related to a wrench system across the area. The coincidence of the sandstone reservoir geometry to the structural nose, extending from NE NE Section 7 across NW NW Section 8 and into SE SW Section 5, suggests a degree of compaction structure over the reservoir. The time structure was converted to sub-sea depth by calculating the apparent average velocity to the Morrow at the well ties to the seismic data. The resultant Morrow structure map is shown as Figure 4.1.1d; compare the significant improvement in structural resolution in this map as compared to the pre-seismic structure map shown in Figure 1.4a.

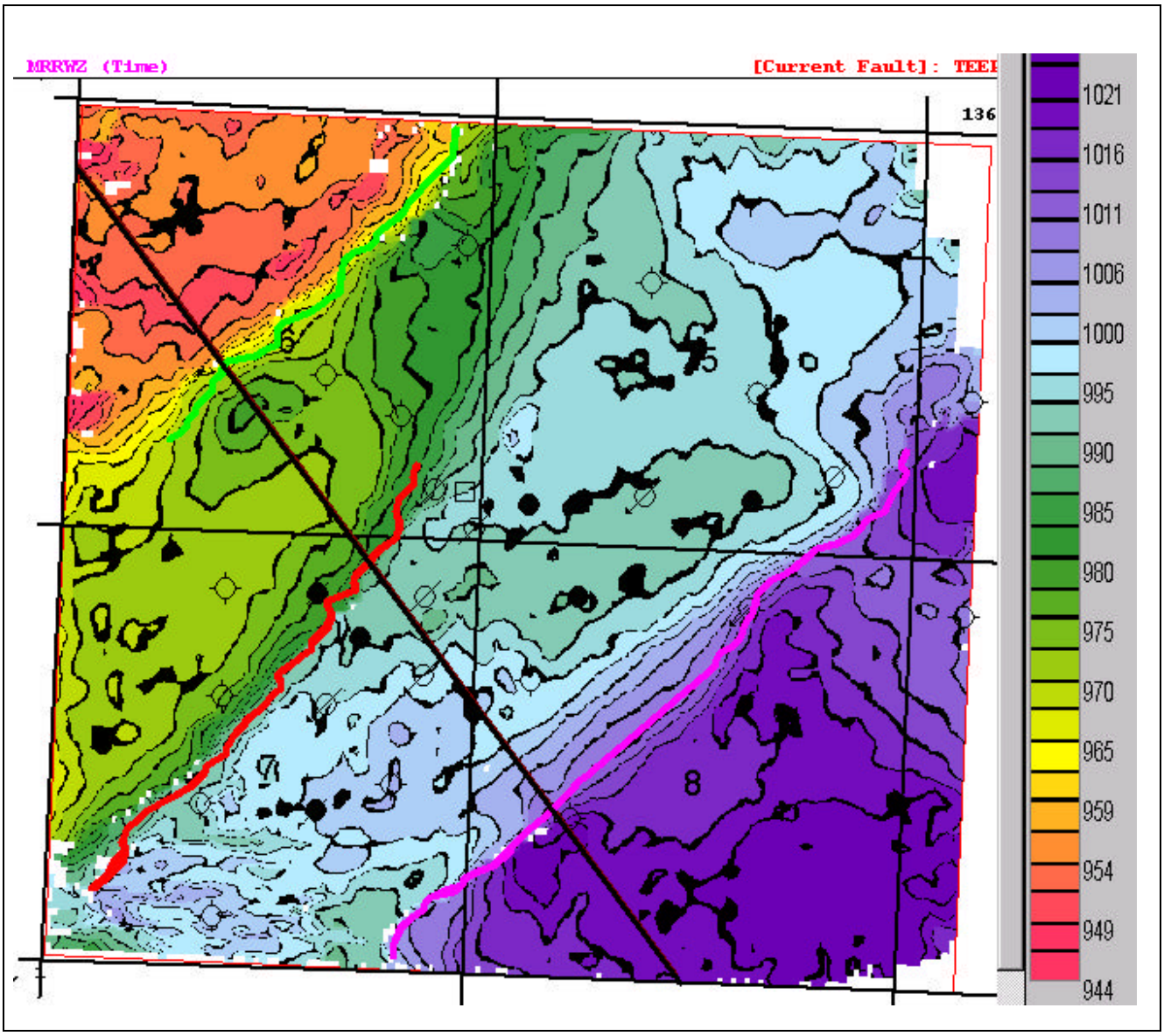

Figure 4.1.1c. Time Structure on the Morrow shale seismic event. The trace of the arbitrary seismic line of Figure 4.1.1b is shown running northwest-southeast, through the ESU 5 in the NE/4 of section 7. The Teepee Creek fault is shown as the red line. Newly recognized faults are shown as green (west) and magenta (east).

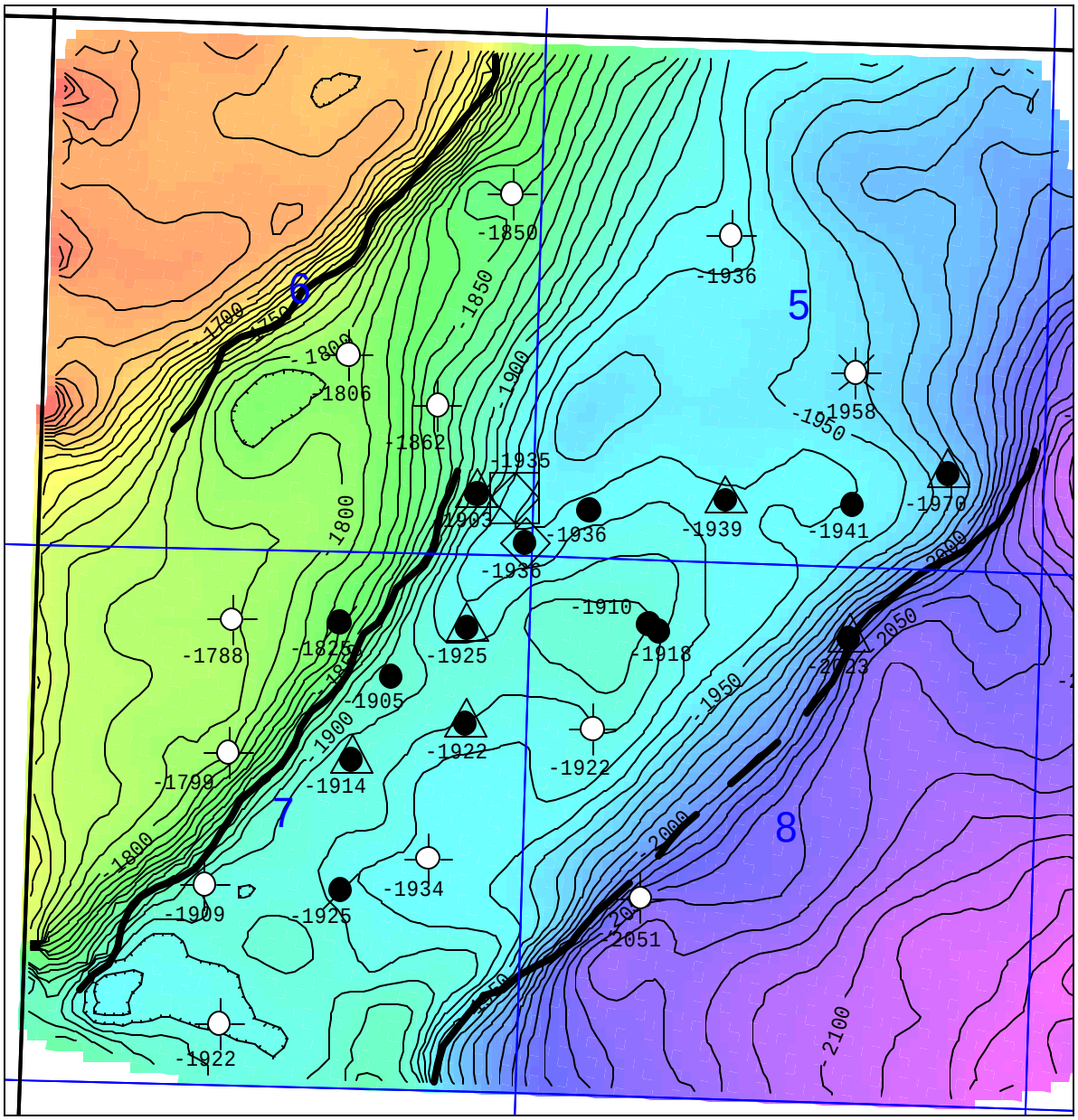

Figure 4.1.1d. Structure on the Morrow shale (top Morrow Formation) from the integration of the 3D seismic (P-wave) data with subsurface well control. Contour interval is 10 feet. Compare the significant improvement in detail versus the pre-seismic structural interpretation shown in Figure 1.4a.

Stratigraphic Interpretation

Figure 4.1.1e displays an arbitrary line extracted from the 3D seismic volume in a north-south direction (right to left) through the ESU 12 and ESU 2 in the main part of the field (see Figure 4.1.1f for location). The top view is the structural representation of the line; the bottom view is flattened on the Morrow shale event (magenta line) to show the stratigraphic detail. The Eva SS seismic event is the trough (primarily green amplitudes) immediately above the Valley peak-event (yellow dotted line). The amplitude of the Eva SS seismic event correlates well on this section to the known

extents of the field. It is present through the producing ESU 12 and 2 wells and is absent in the dry holes to the right (north) and left (south) which define the northern and southern limits of the field. The seismic line suggests that the main portion of the field is also characterized by a thickening of the interval from the Morrow shale to Valley events.

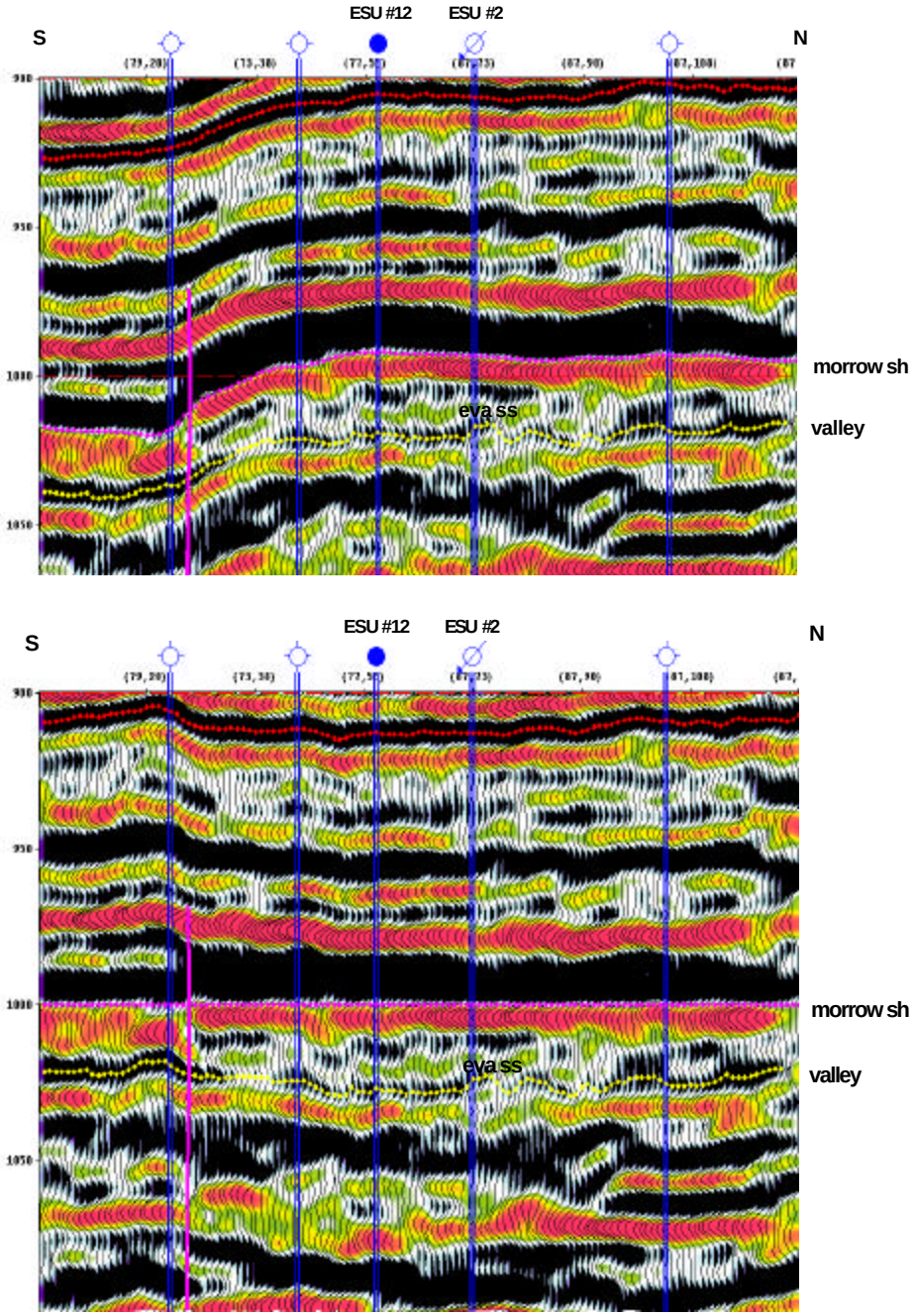

Figure 4.1.1e. Arbitrary line extracted from the Eva South 3D seismic volume through the main portion of the field. The top view is a structural display; the bottom view is flattened on the Morrow shale event (magenta line). The Eva sandstone appears (where present) as the green trough, immediately above the Valley pick (yellow line). The location of this line is shown on Figure 4.1.1f.

Figure 4.1.1f is the amplitude map of the Eva SS seismic event. There is good correlation of the amplitude map of the Eva SS event to the main distribution of the Eva sandstone reservoir. The net Eva sandstone isopach values from well-logs are posted next to the wells in this figure. The amplitudes tend to increase with increasing net sandstone thickness; exceptions are in the vicinity of the ESU 6 and ESU 12 wells in the N/2 NW of Section 8 where the amplitudes are not as strong as the isopach values would suggest. The amplitude map does suggest a separate reservoir compartment in the N/2 SE of Section 7, a compartment known from geological and engineering data (Figure 1.5a), but does not discriminate very well between the producing well and the dry hole in this compartment. A plot of the net sandstone thickness of the Eva sandstone versus the amplitude of the Eva SS seismic event is shown in Figure 4.1.1g. There is a good linear relationship between the seismic amplitude and the net sandstone isopach from 10 to 30 feet of thickness. Below 10 feet of thickness the deviation from this linear trend is due to the inability of the seismic to resolve thin beds. The deviation from the trend at thicknesses above 30 feet is harder to explain, though a probable tuning effect is discussed in more detail in the following section (*Seismic Tuning Considerations*).

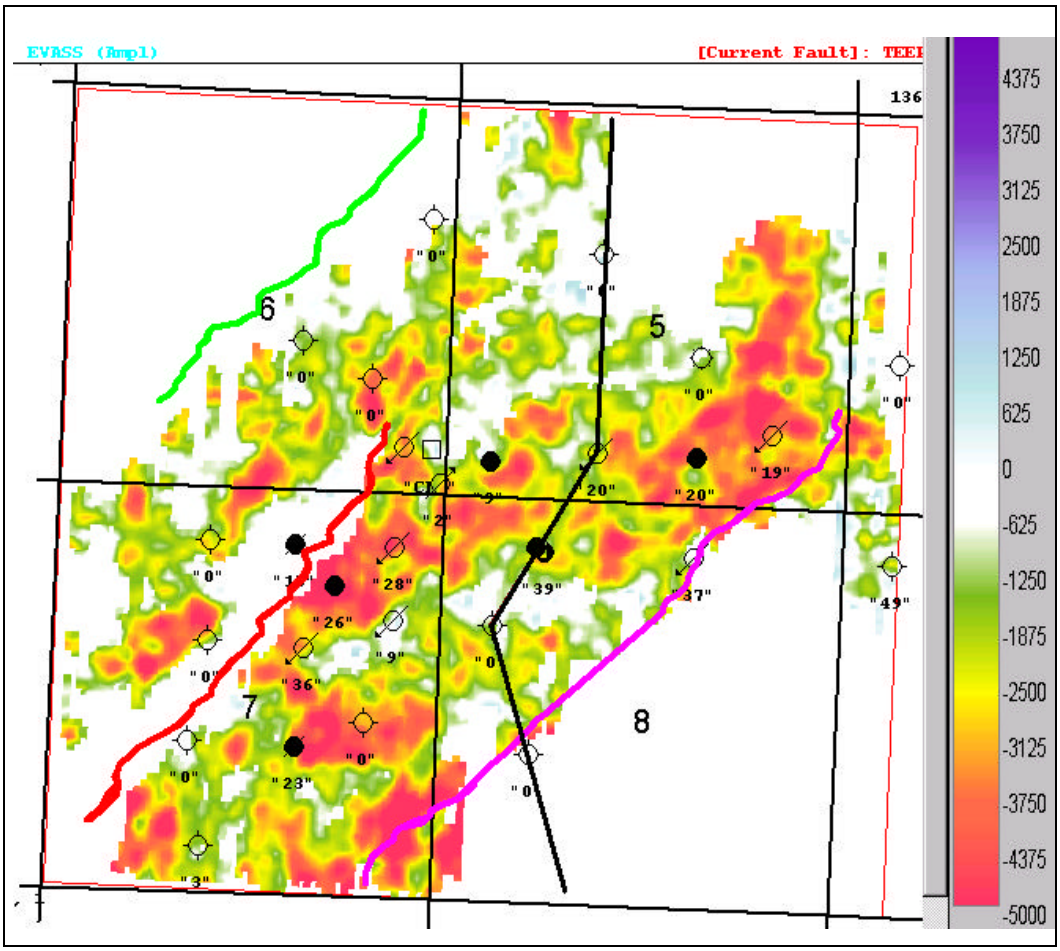

Figure 4.1.1f. Amplitude map of the Eva SS seismic event from the Eva South 3D. The location of the arbitrary 2D seismic line of Figure 4.1.1e is shown. The net Eva sandstone isopach values are posted at the wells.

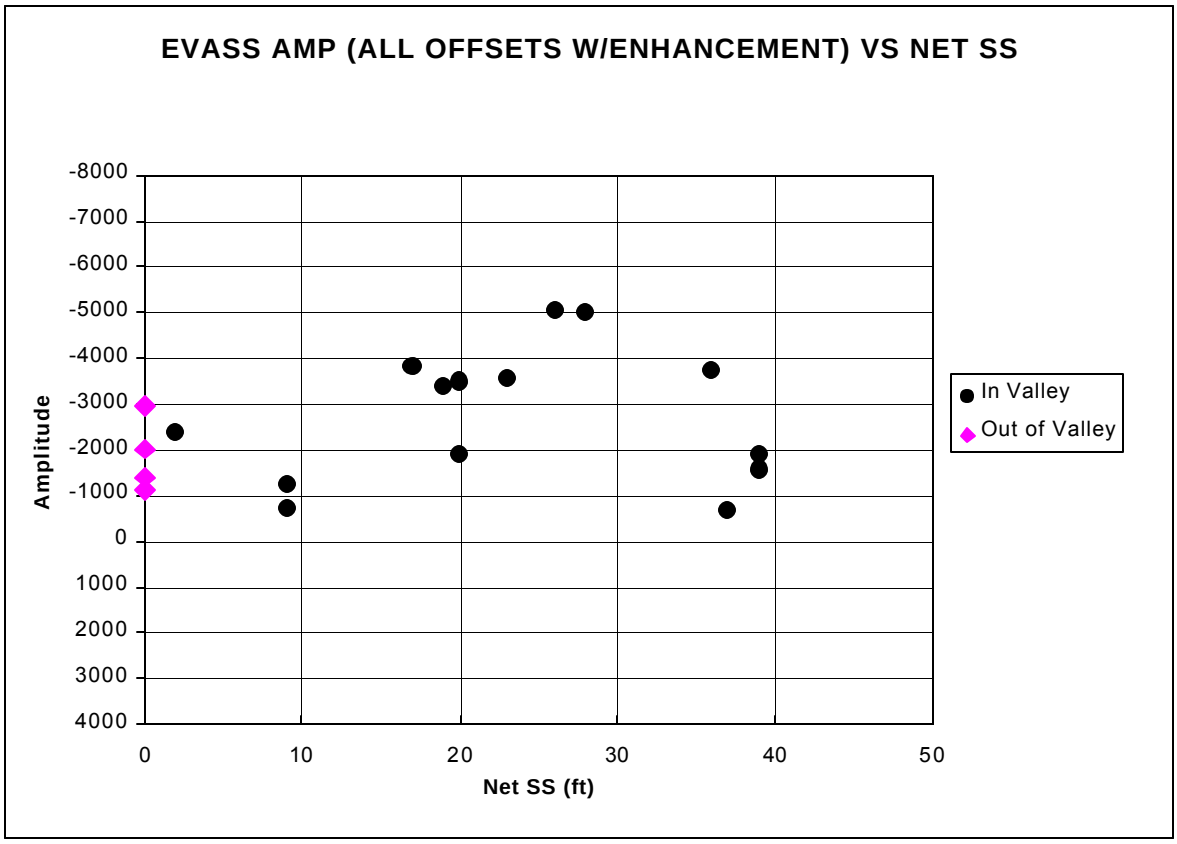

Figure 4.1.1g. Plot of Eva sandstone net thickness versus amplitude of the Eva SS seismic event. The data show a good linear relationship between 10 and 30 feet of sandstone, but significant scatter beyond these limits.

Amplitudes from time windows bracketed by regional seismic events were extracted to test their reliability in delineating the Eva sandstone reservoir. This approach can be useful when interpreting seismic data where there is little well control to help define the reservoir seismic events. Figure 4.1.1h shows the amplitude maps from a time window 18 to 22 milliseconds below the Morrow shale seismic event (top) and from 4 to 8 milliseconds above the Valley event. The window times are chosen to bracket the Eva sandstone interval. Both maps do a good job of describing the general reservoir trend, though the window 4 to 8 milliseconds above the Valley event conforms slightly better to the picked Eva SS event amplitude. From a practical point of view, the Morrow shale event is more of a regional seismic event than the Valley event and it is more likely that windowed amplitude extractions referenced from the Morrow shale event would be used in interpreting exploration seismic data. Figure 4.1.1i compares the plots of the Eva Sandstone net thickness versus the Eva SS seismic event amplitude for the amplitudes extracted from the window 18 to 22 milliseconds below the Morrow shale (top) and the window 4 to 8 milliseconds above the Valley event (bottom). There is a slightly better relationship for the data extracted from the window 4 to 8 milliseconds above the Valley event.

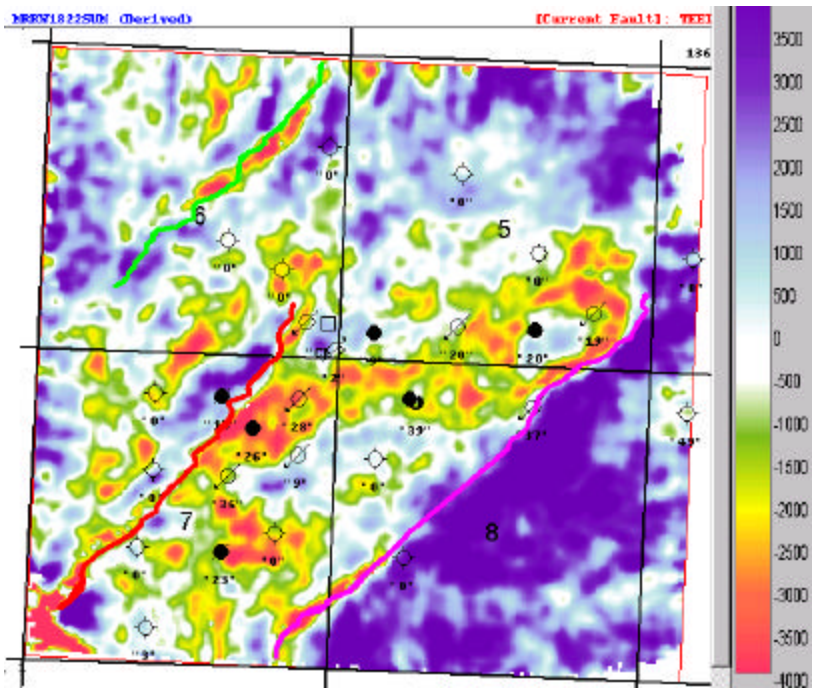

Windowed Amplitude -Morrow + 18-22 msec (P-wave)

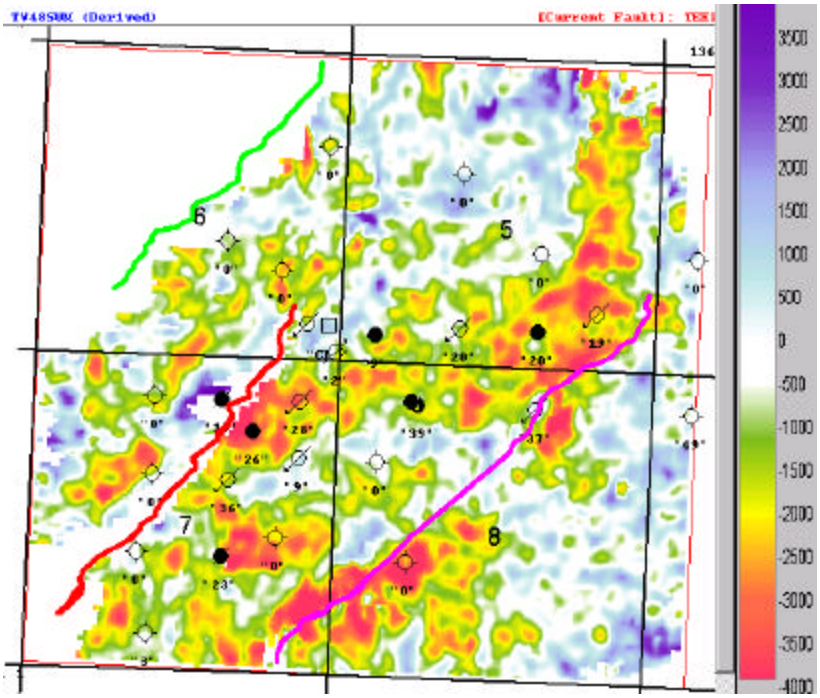

Windowed Amplitude-Valley - 4-8 msec (P-wave)

Figure 4.1.1h. Amplitude extractions from a time window 18 to 22 milliseconds below the Morrow Shale seismic event (top) and from 4 to 8 milliseconds above the Valley seismic event (bottom).

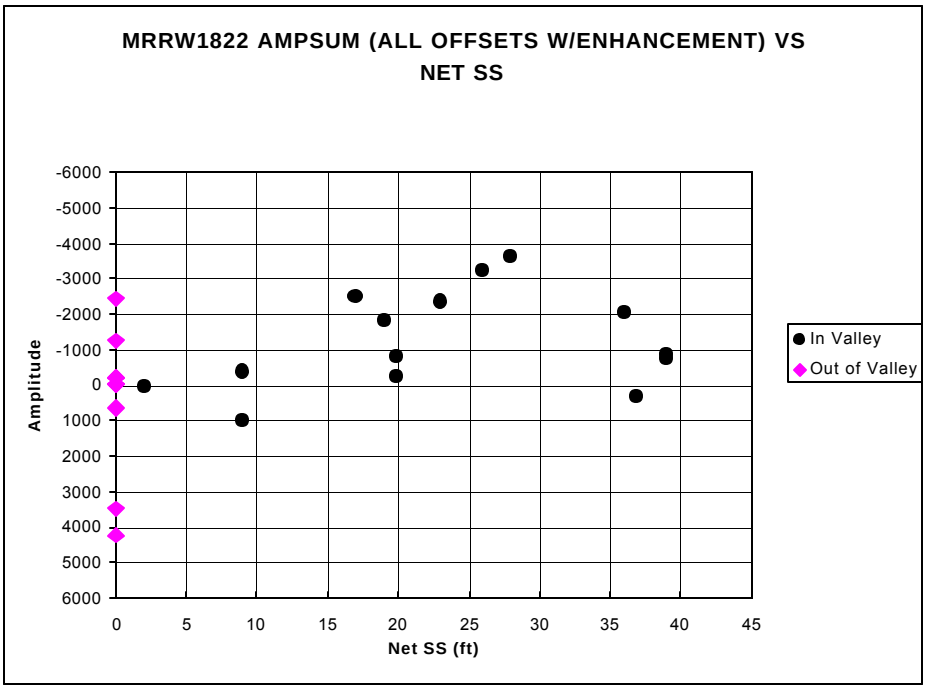

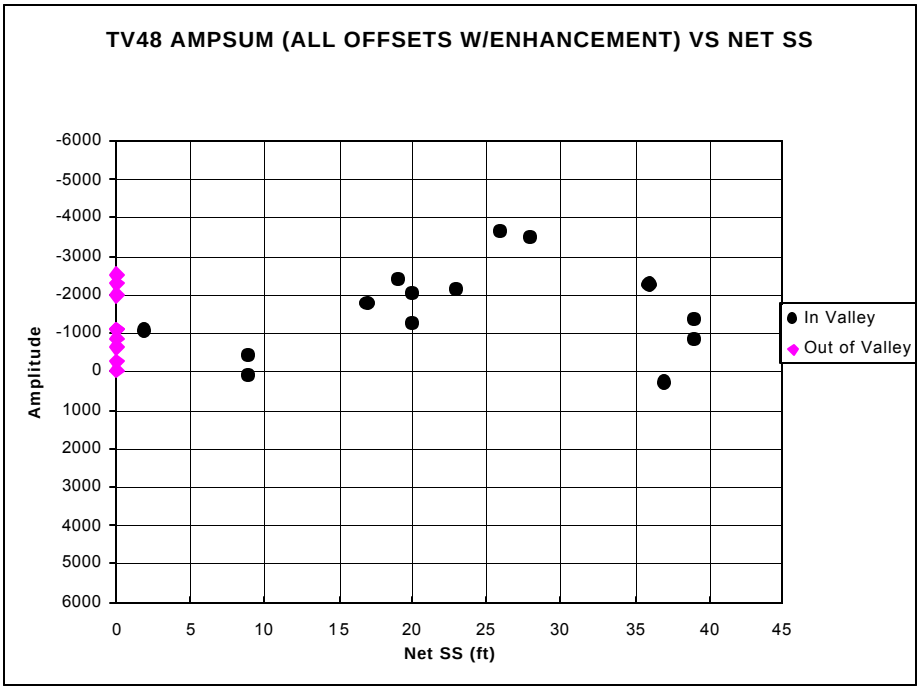

Figure 4.1.1i. Plots of Eva net sandstone thickness versus amplitude for the windowed amplitude extractions 18 to 22 milliseconds below the Morrow seismic event (top) and 4 to 8 milliseconds above the Valley seismic event (bottom). Note the better overall relationship displayed in the lower plot, particularly for wells outside the valley-fill.

Figure 4.1.1j is an isochron map for the interval from the Morrow shale to Valley seismic events. An arcuate isochron thick generally conforms to the trend of productive wells in

the field, consistent with the valley-fill depositional model. A second arcuate trend is also apparent to the north of the field. However, the amplitude does not suggest the presence of reservoir and the few wells that have penetrated this trend are devoid of sandstone.

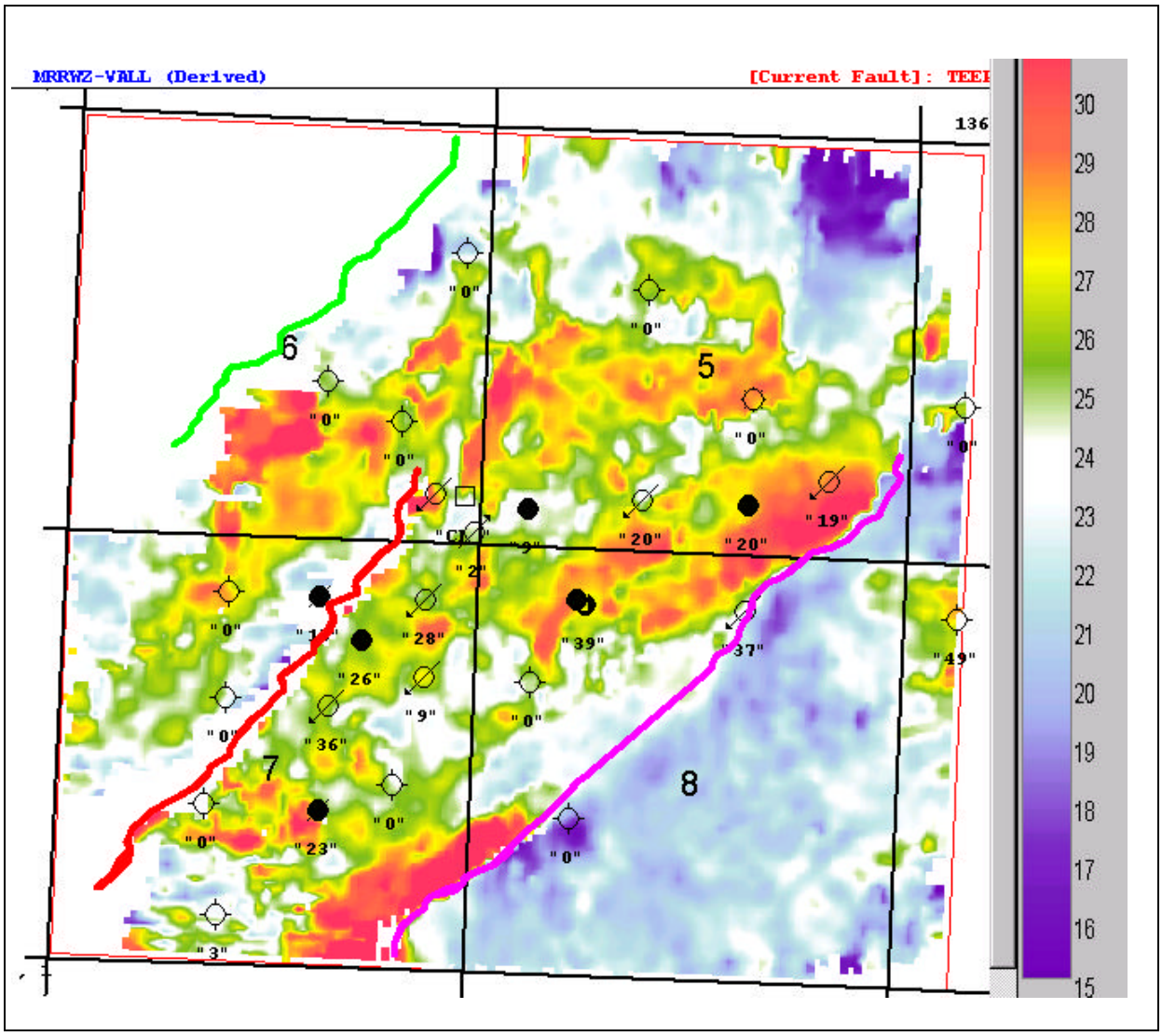

Figure 4.1.1j. Isochron map of the interval from the Morrow Shale to Valley seismic events. Two, parallel trends are apparent. One generally conforms to the productive wells in the field; the second, to the north, does not display amplitudes indicative of reservoir development and the few wells that have penetrated it are devoid of sandstone.

Seismic Tuning Considerations

The plot of Eva sandstone thickness versus amplitude of the Eva seismic event (Fig. 4.1.1g) generally shows an increase in amplitude with increasing sandstone thickness up to 30 feet. At thicknesses above 30 feet, the amplitude decreases. This observation is consistent with a classic tuning-thickness plot of a geologic-wedge model. Amplitude

increases with increasing thickness up to the point where time resolution is reached (the point where the top and bottom of the wedge are identifiable in the seismic waveform); at thicknesses above this point the amplitude is seen to decrease. The point where the thickness versus amplitude plot reaches a maximum and begins to decrease is referred to as the tuning thickness.

In order to test the idea that tuning thickness may have been reached with the Eva South data, a wavelet was extracted from the data and used to construct a tuning plot (Fig. 4.1.1k). A velocity of 10,000 feet per second was used to convert the plot to thickness in feet. The plot suggests a tuning thickness of approximately 40 feet for the seismic frequency of the Eva South data, which is slightly thicker than that suggested by the plot of net sandstone versus amplitude (Fig. 4.1.1g). If tuning is a consideration in the Eva South data, it would suggest that internal amplitude decreases within the overall outline of the amplitude map (Fig. 4.1.1f) could represent sandstone thicknesses above 30 feet. This would explain the low amplitudes around the ESU 6 and ESU 12 wells in the N/2 NW of Section 8 and the ESU 8 well in the SW NE of Section 8, which have sandstone thicknesses of 39 and 36 feet respectively. Unfortunately, a decrease in amplitude could also mean a thinning of the sandstone that could represent a discontinuity in the reservoir due to abandoned channel-fill.

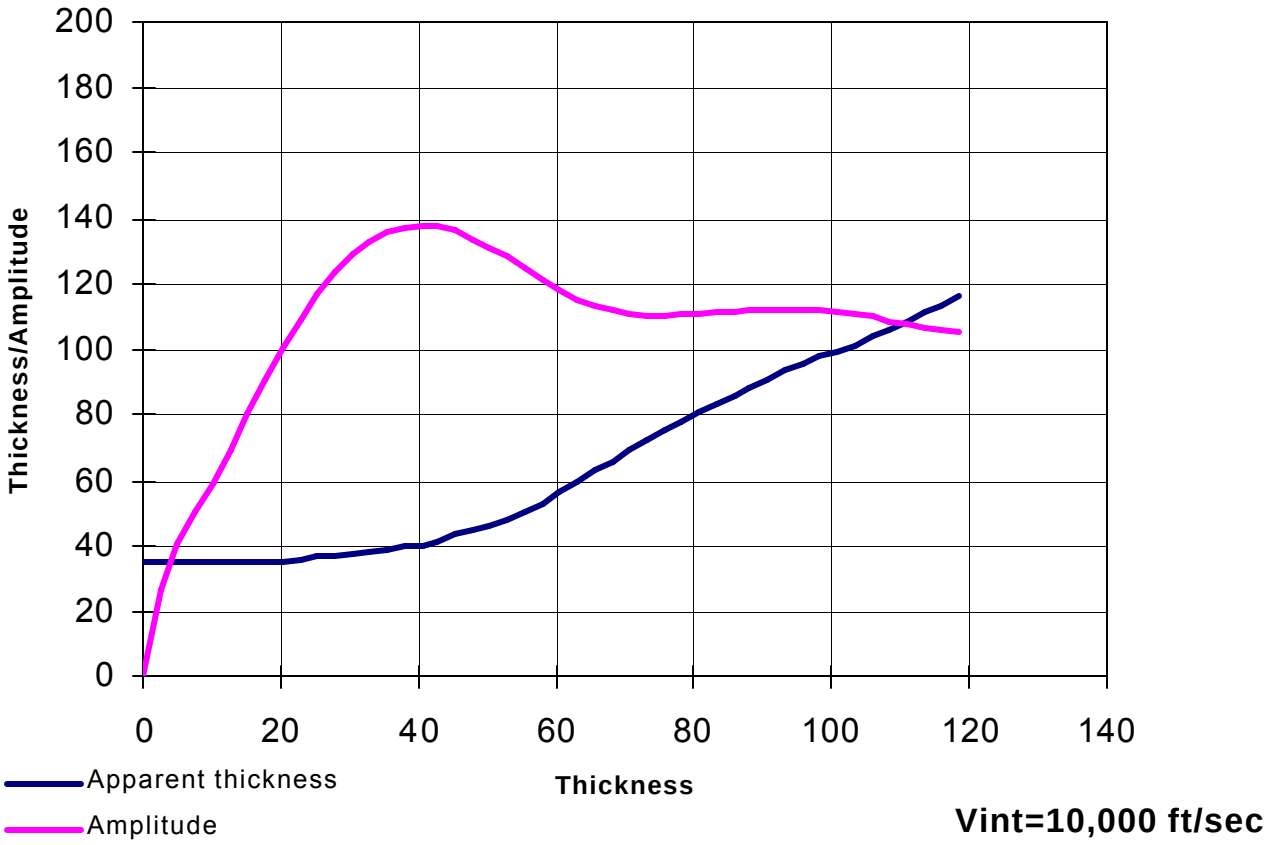

Figure 4.1.1k. Tuning plot for wavelet extracted from Eva South 3D data. The tuning thickness is represented by the peak in amplitude at 40 feet.

Theoretically, the tuning thickness should increase with lower seismic frequency, meaning the linear portion of the thickness versus amplitude curve should extend out to greater thickness for lower frequency data. The Eva South 3D data has an apparent frequency of approximately 90 hertz, so to test this idea the data were filtered to 70 hertz and the amplitude of the Eva sandstone event captured. Figure 4.1.1l shows a comparison of the Eva sandstone event amplitude map at 90 hertz (top) to the amplitude map at 70 hertz (bottom). While the 70-hertz amplitude smoothes out the amplitudes in the central portion of the reservoir body, it does not significantly increase the amplitude around the thicker wells. One problem with trying to improve the thickness to amplitude relationship by lowering the frequency of the seismic data is that at lower frequency the Eva sandstone trough event disappears.

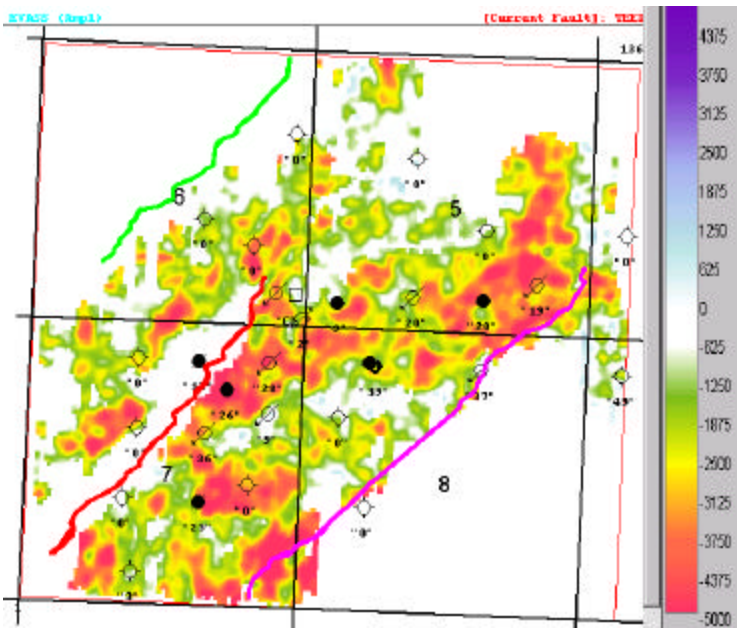

Eva SS Amplitude (P-wave)

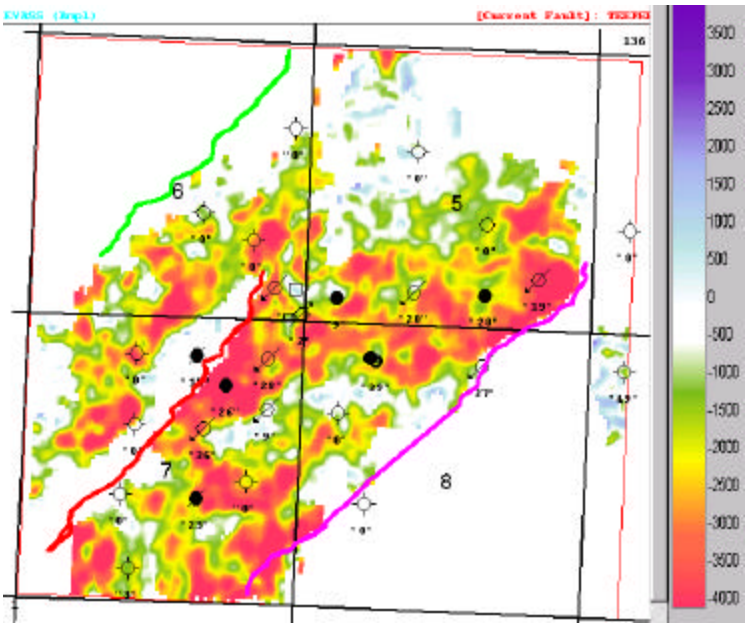

Eva SS Amplitude (P-wave filtered at 70 hz)

Figure 4.1.1l. Eva sandstone seismic event amplitude at 90 hertz (top) and at 70 hertz (bottom).

Reservoir Compartment Interpretation

One goal of the 3D seismic interpretation was to determine the degree of reservoir compartmentalization at Eva South and contrast that with the known reservoir compartments determined from geological and engineering data as shown in Figure 1.5a.

Figure 4.1.1m is a detail view of the Eva sandstone seismic event amplitude (top) and an interpretation of possible causes of reservoir compartmentalization and/or heterogeneity. Engineering data has shown the ESU 4 (SE SE Section 6) and the Weede Trust No.1 (NW SE Section 7) to be in separate reservoir compartments from the rest of the field. The ESU 4 is compartmentalized by abandoned channel-fill deposits, recognized on well-logs that show as low amplitudes to the south and east. The Weede Trust No. 1 is separate from the main reservoir as evidenced by a separate high-amplitude trend bounded by abandoned channel-fill (low-amplitude) and lineaments that might represent minor faults.

The seismic data suggests additional lineaments in the main reservoir body. A north-south lineament is observed immediately to the east of the ESU 2 (SE SW Section 5). A northeast-southwest lineament appears to trend into the ESU 6 and ESU12 wells (N/2 NW Section 8). These lineaments would suggest that the east side of the field could be in a compartment separate from the west side of the field, but there is no conclusive engineering data to support this. However, there are some interesting production differences between the ESU 6 and ESU 12 wells which support the existence of a lineament between the wells. Although the ESU 12 is a twin to the ESU 6, and the two wells have the same appearance on well-logs, they have always produced at significantly different water cuts. This lineament does not appear to create a significant reservoir compartment between the wells which affects secondary recovery performance, but it may be the cause of the different production characteristics.

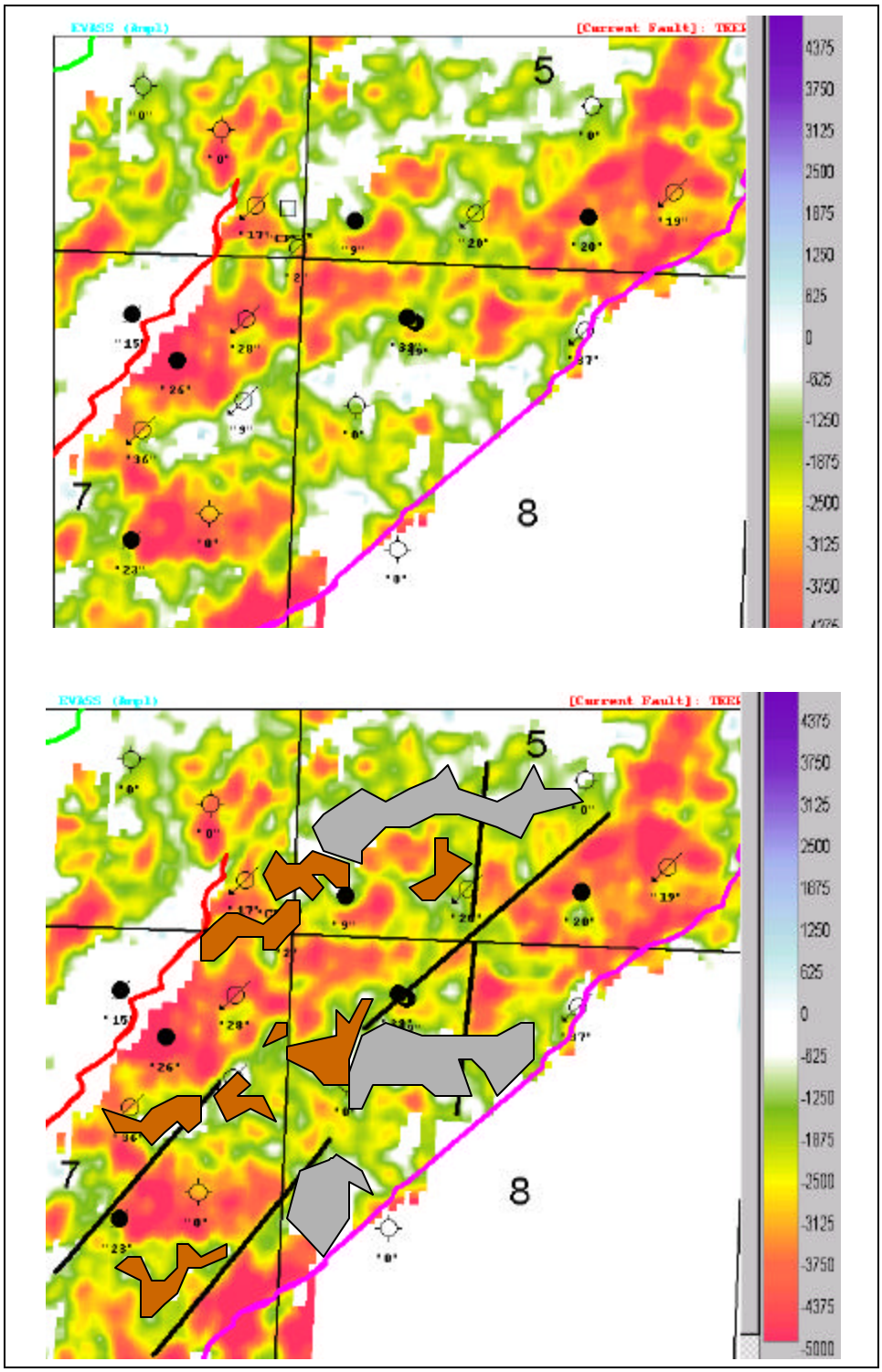

Figure 4.1.1m. Eva SS amplitude map, un-interpreted (top) and interpreted (bottom) with potential compartmentalization/heterogeneity elements. Areas of abandoned channel-fill (brown) and flood-plain (gray) mudstones are shown. Abandoned channel-fill deposits appear to be the main cause of compartmentalization in the ESU 4 (SE SE Sec. 6) and Weede Trust No. 1 (NW SE Sec. 7) wells. Also shown are lineaments (black lines), possibly representing minor faults.

Source to Receiver Offset Analysis

In order to investigate the impact of source to receiver offset on the seismic response of the Eva sandstone, two additional 3D volumes were created for the P-wave data. The near-offset volume is a stacked and migrated volume using only source to receiver offsets from 0 to 3300 feet. The far-offset volume is a stacked and migrated volume using only source to receiver offsets from 3,300 to 12,000 feet.

The Eva sandstone event was picked on both volumes and the amplitudes captured to analyze whether or not amplitude versus offset (AVO) effects are present in the data. The low-frequency offset-modeling (see section 3.1.2, Seismic Modeling, *AVO Seismic Model*) suggests that there is a decrease in amplitude with increasing offset for a 30 foot Eva sandstone event. As shown in Figure 3.1.2d, the equivalent seismic event where no sandstone is present does not show any amplitude change with offset. While these models were created for the low-frequency case to evaluate possible converted wave response, it is reasonable to assume that there might be some AVO effects at the higher frequencies interpreted in the P-wave volumes.

An analysis of offset-limited 3D seismic volumes for AVO effects is not as rigorous as true AVO processing, but it is a cost effective means to evaluate whether or not AVO is an issue with the interpretation. Figure 4.1.1n shows the amplitude maps for the Eva SS seismic event extracted from the near-offset volume (top) and the far-offset volume (bottom). The Eva net sandstone isopach values are posted at the wells. Plots of the Eva net sandstone thickness against the Eva SS seismic event amplitude are shown in Figure 4.1.1o. Visually the far-offset amplitude map appears more continuous through the main portion of the field than the near-offset amplitude map. However, the plot of net sandstone thickness versus amplitude for the far-offset data shows more scatter than the near-offset data and the out-of-valley-wells with no sandstone plot closer to zero amplitude on the near-offset data than the far-offset data. Neither dataset does a better job of describing the thickest sandstones than the full offset data.

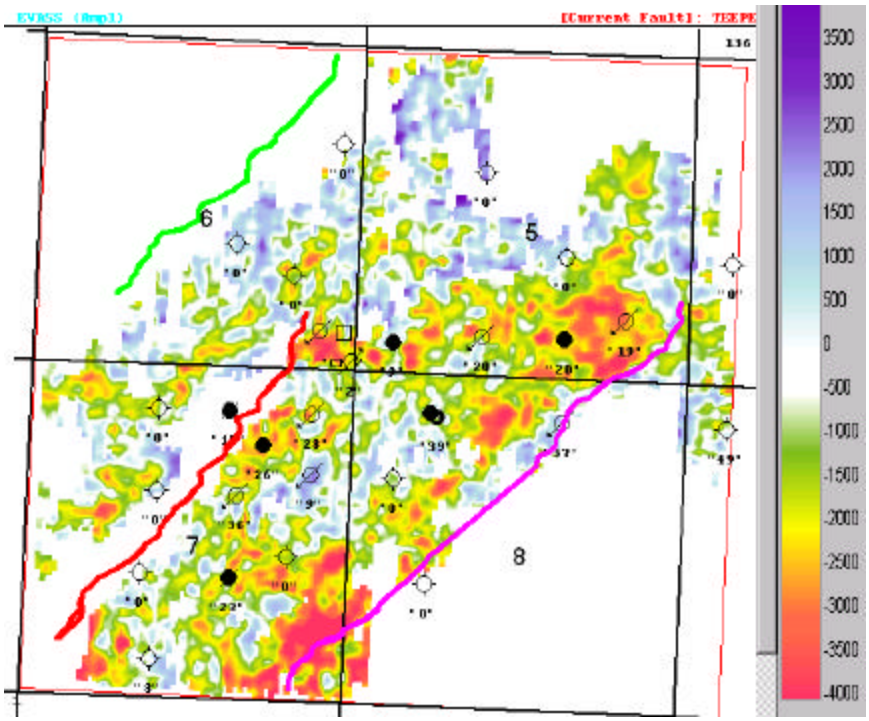

Eva SS Amplitude (P-wave)-Near Offset Volume

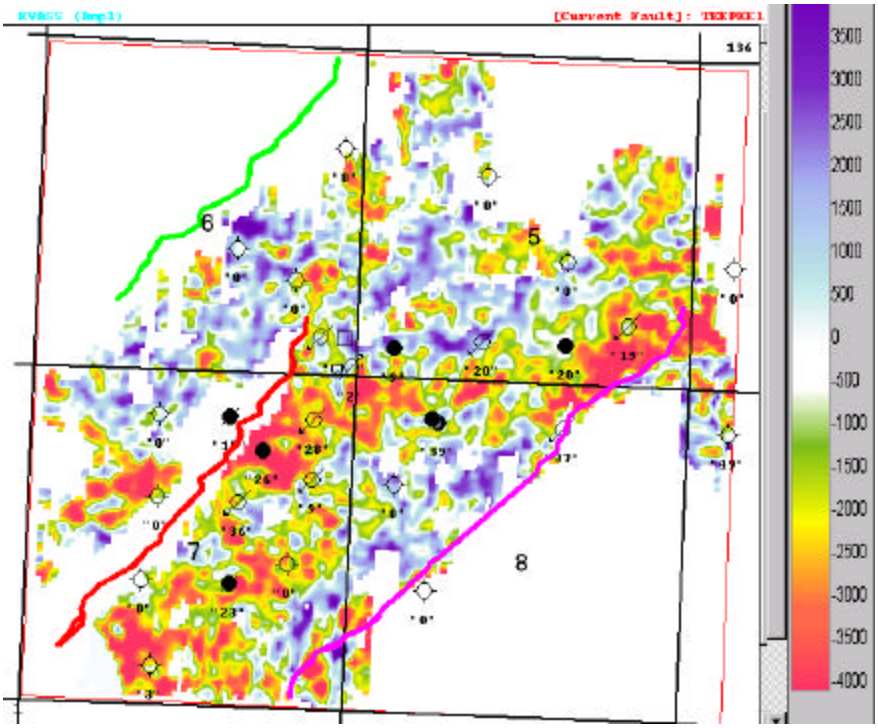

Eva SS Amplitude (P-wave)-Far Offset Volume

Figure 4.1.1n. Eva sandstone seismic event amplitude maps for the near-offset volume (top) and far-offset volume (bottom). The far offset map appears to have better conformance to the known reservoir geometry from well control.

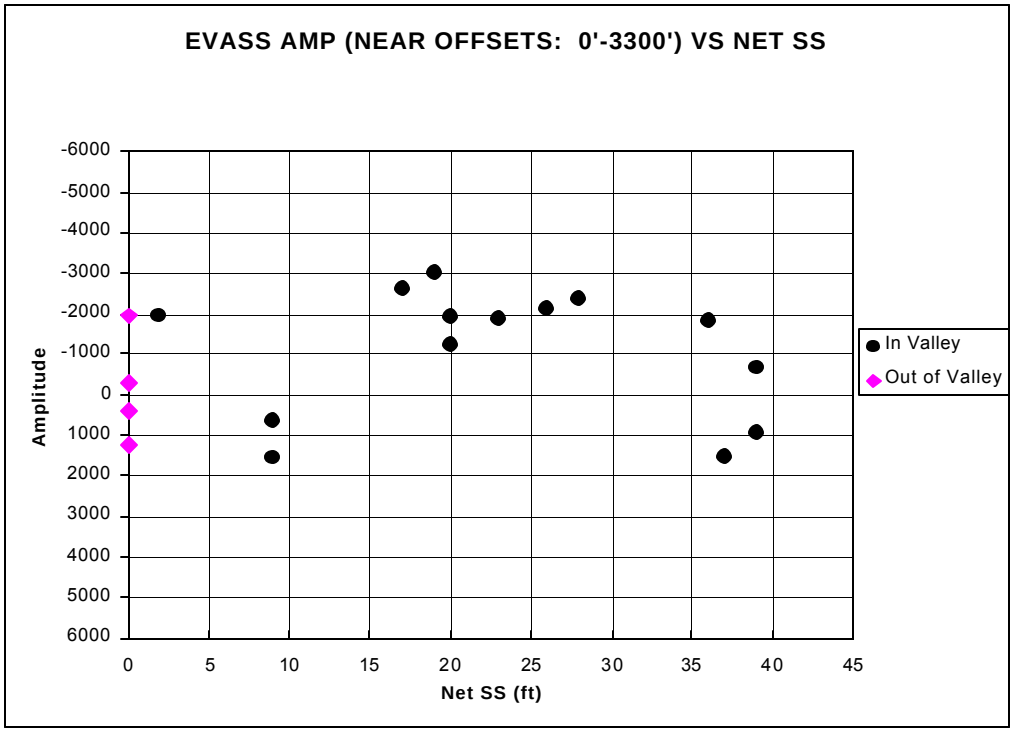

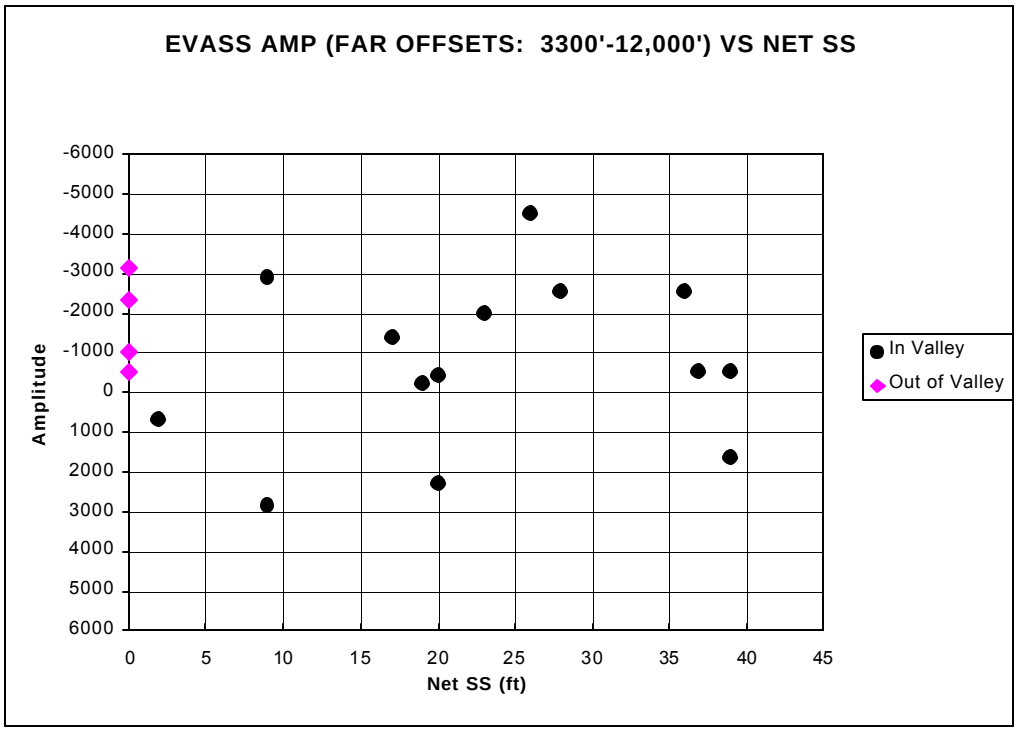

Figure 4.1.1o. Plots of Eva net sandstone thickness versus seismic amplitude of the Eva sandstone event for the near-offset volume (top) and far-offset volume (bottom). Although the far offset map (Fig. 4.1.1n) looked better, the plot shows more scatter than the near offsets.

An offset difference dataset was generated by subtracting the far-offset amplitude from the near-offset amplitude. The resultant amplitude map is shown as Figure 4.1.1p along with a plot of the amplitude difference versus net Eva sandstone from well data. The map and plot show that the difference amplitudes are positive for the thinner sandstones and decrease in amplitude with increasing net sandstone thickness. At greater thicknesses the amplitudes become negative. While the plot shows a fairly linear trend, wells with no sandstone plot into the thicker sandstone amplitude range. The map also does not display a visual pattern that separates thicker sandstone wells from the wells outside the valley-fill.

Figure 4.1.1q compares the CDP fold at the Morrow level for the near-offset volume (top) and the far-offset volume (bottom). There does not appear to be any substantial disruptions in the fold continuity of either volume that would create the patterns of amplitude mapped for the Eva SS event. This was investigated because non-regular or non-symmetrical acquisition patterns can result in irregular offset distributions into each CDP that could create amplitude artifacts in the data.

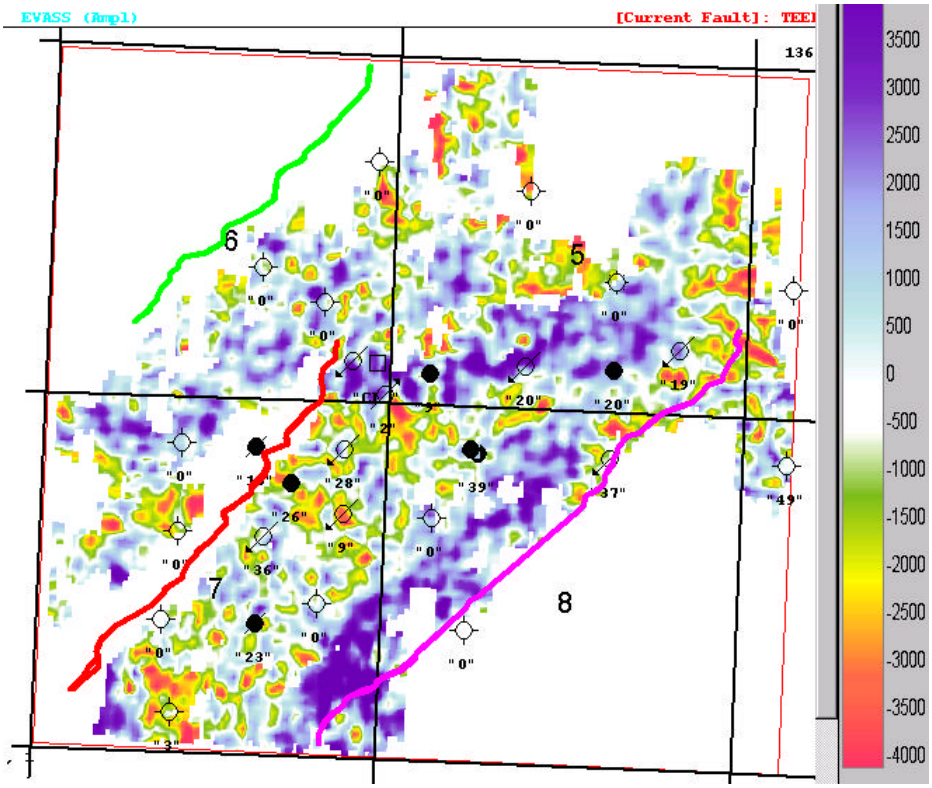

Eva SS Amplitude (P-wave)-Near-Far Offset Difference Volume

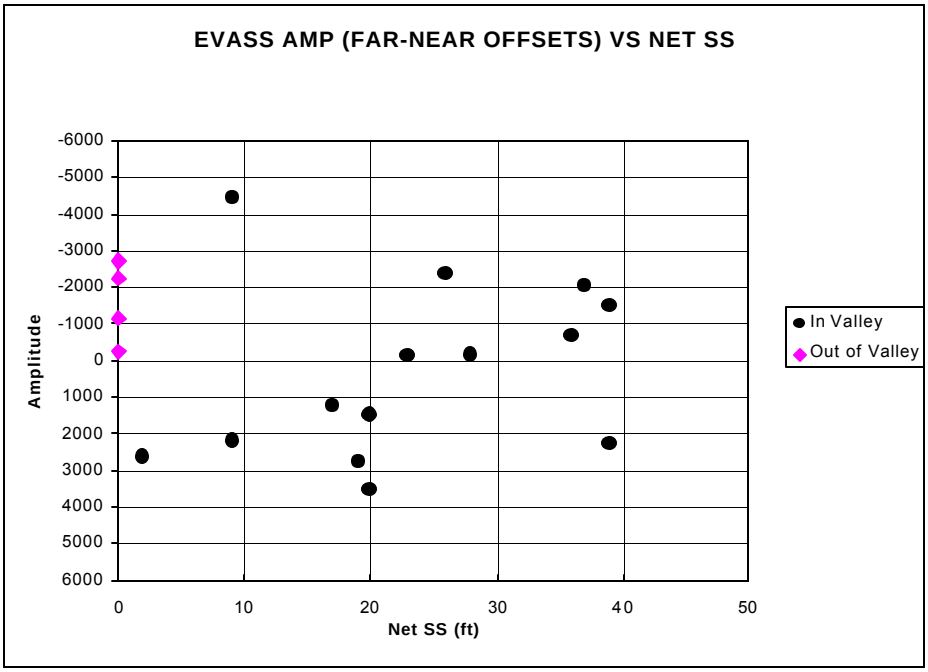

Figure 4.1.1p. Eva sandstone seismic event amplitude map (top) and plot of Eva net sandstone thickness versus amplitude generated from the far-offset minus near-offset difference volume.

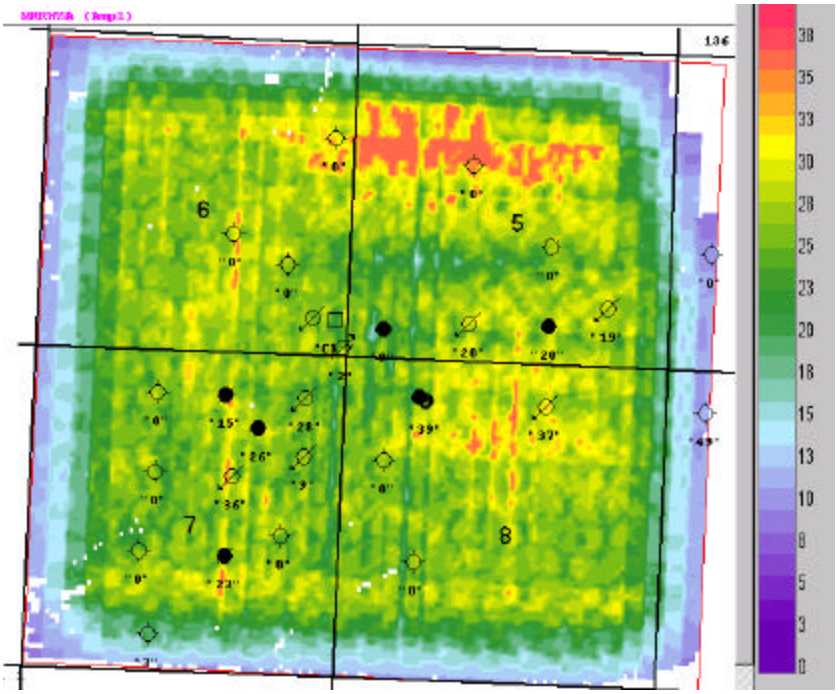

Fold at Morrow (0'-3300' offset range)

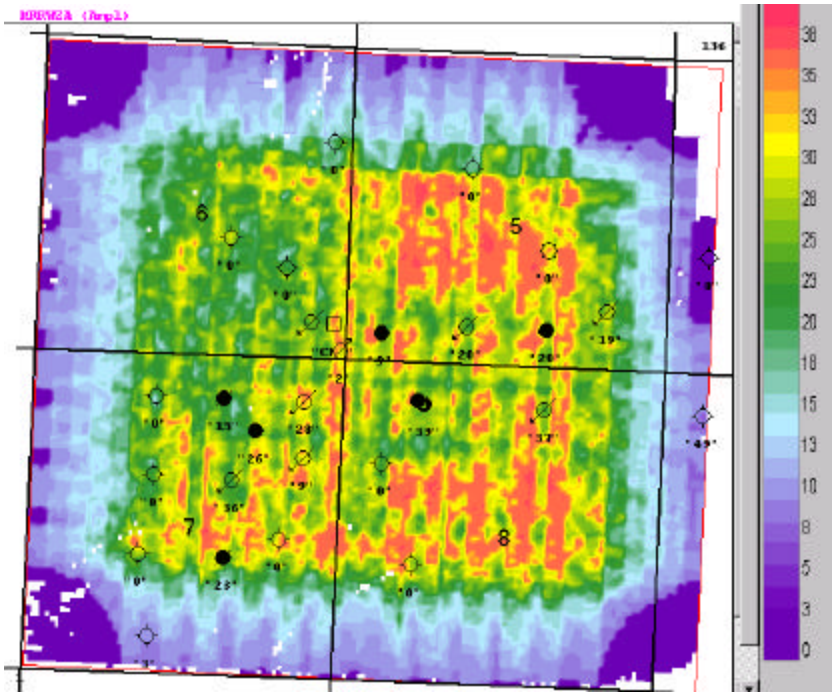

Fold at Morrow (3300'-12000' offset range)

Figure 4.1.1q. Comparison of CDP fold at the Morrow for the near-offset volume (top) and the far-offset volume (bottom).

4.1.2 PSV Converted-wave Interpretation

<u>P-wave Tie and Event Correlations</u>

To establish the event correlations between the P-wave and PSV-wave data, the longer travel time due to slower S-wave velocities must be accounted for as well as matching the frequency of the data. As discussed in Section 3.1.1, the PSV-wave data travels downward at the P-wave velocity and upward at the S-wave velocity. For a Vp/Vs ratio of 2, the travel time to a common reflecting event is 1.5 times more on the PSV-wave data as compared to the P-wave data. After accounting for the travel time difference by adjusting the appropriate time scales, the best match between the P-wave and PSV-wave data was obtained by filtering the P-wave data to 45 hertz.

Figure 4.1.2a shows the comparison of the filtered P-wave data to the PSV-wave data in the vicinity of the Teepee Creek fault. The correlation of events between the datasets was aided by the nature of the faulting; changes in displacement with depth provided ties between the data sets. This and the character tie of the reflectivity of the data provided a measure of confidence in the event identification on the PSV-wave data. A more direct approach would require a multi-component Vertical Seismic Profile (VSP) or dipole-sonic log, data not available at Eva South. The Morrow shale event (top Morrow Fm.) is the blue line at the zero crossing as shown. At this frequency, the Eva SS seismic event is contained in the first peak below the Morrow, consistent with the low-frequency model (Fig. 3.1.2e).

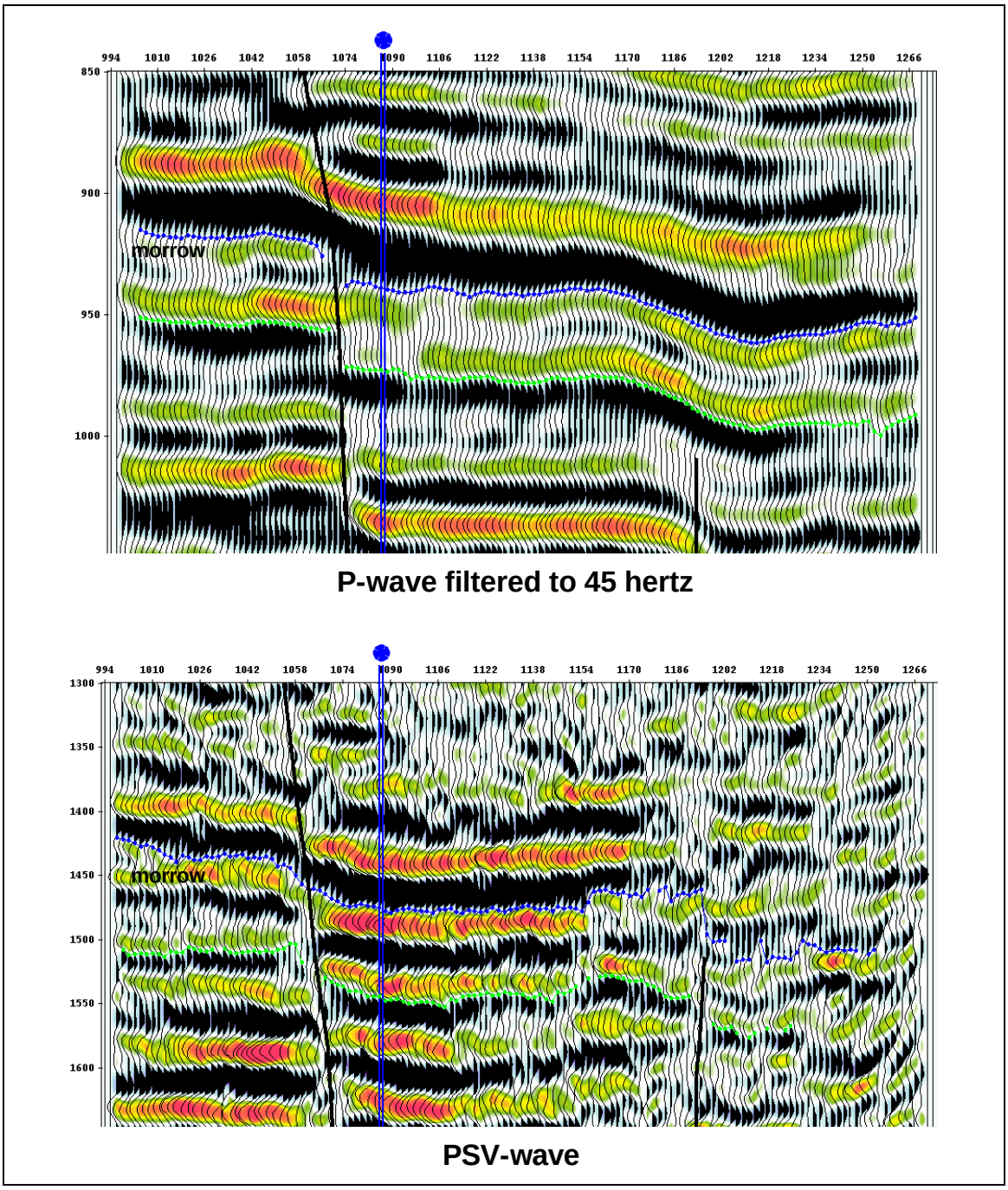

Figure 4.1.2a. Comparison of P-wave filtered to 45 hertz (top) with the PSV-wave data. The Morrow shale (top of the Morrow Formation) is shown in blue on both lines. The Teepee Creek fault is shown in black, left of the well.

Structural Interpretation

The time structure map of the Morrow shale seismic event (top Morrow Fm.) interpreted from the PSV-wave volume is shown in Figure 4.1.2b with the fault interpretation from the P-wave data overlain for comparison. The map generally conforms to the P-wave

Morrow shale time structure (Fig. 4.1.1c) but lacks significant detail; the compaction structure over the reservoir observed on the P-wave data is not apparent. Also, the Teepee Creek fault is imaged but the eastern fault (magenta) is not as apparent. Overall, the PSV-wave data does not have the precision of the P-wave data in resolving time structure.

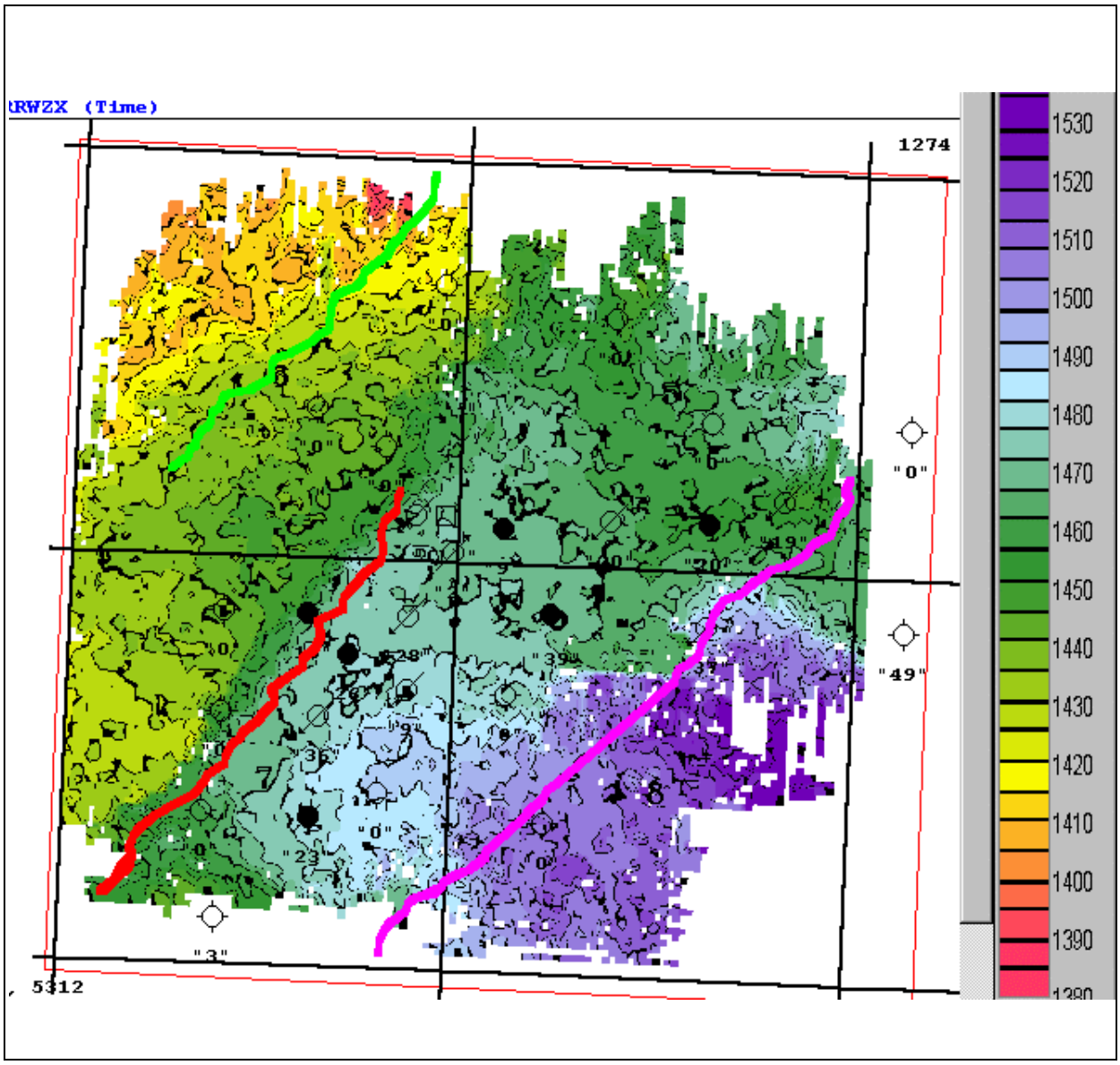

Figure 4.1.2b. Morrow shale seismic-event time-structure from the PSV-wave 3D volume. Fault interpretation is from the P-wave 3D volume. Note the lack of detail as compared to the P-wave time-structure (Fig. 4.1.1c).

Stratigraphic Interpretation

The PSV-wave amplitude of the Eva SS seismic event is shown in Figure 4.1.2c with the P-wave fault interpretation overlain for reference. Visually, this map conforms very

well to the main body of the Eva South reservoir and known limits of the field and the highest amplitude appears to be in the main body of the reservoir. The plot of amplitude versus net sandstone (Fig. 4.1.2d) revealed two parallel trends. The lower amplitude trend projects back into the grouping of wells that do not have any net sandstone. The higher amplitude trend is generally parallel to the lower amplitude trend and is composed of wells that fall consistently along the northern portion of the reservoir. The observation that the two trends correspond to a spatial relationship suggests the potential for some type of amplitude overprint, perhaps due to data acquisition geometry or an azimuthal effect on the PSV-wave data.

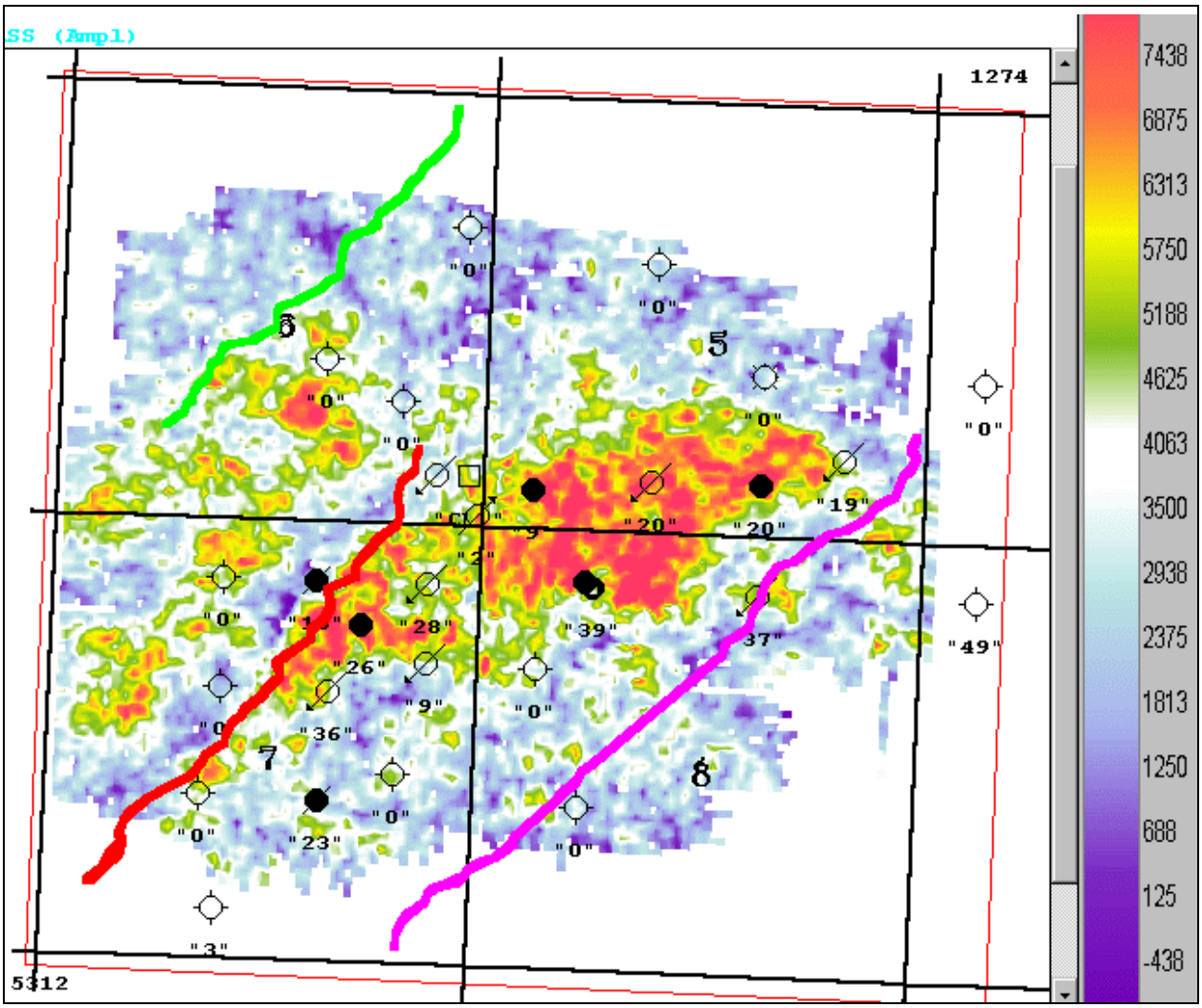

Figure 4.1.2c. Eva sandstone seismic event amplitude map extracted from the PSV-wave 3D volume. The Eva net sandstone isopach values are posted at the wells. The P-wave fault interpretation is overlain for reference. Note the general conformance to known reservoir development from well control.

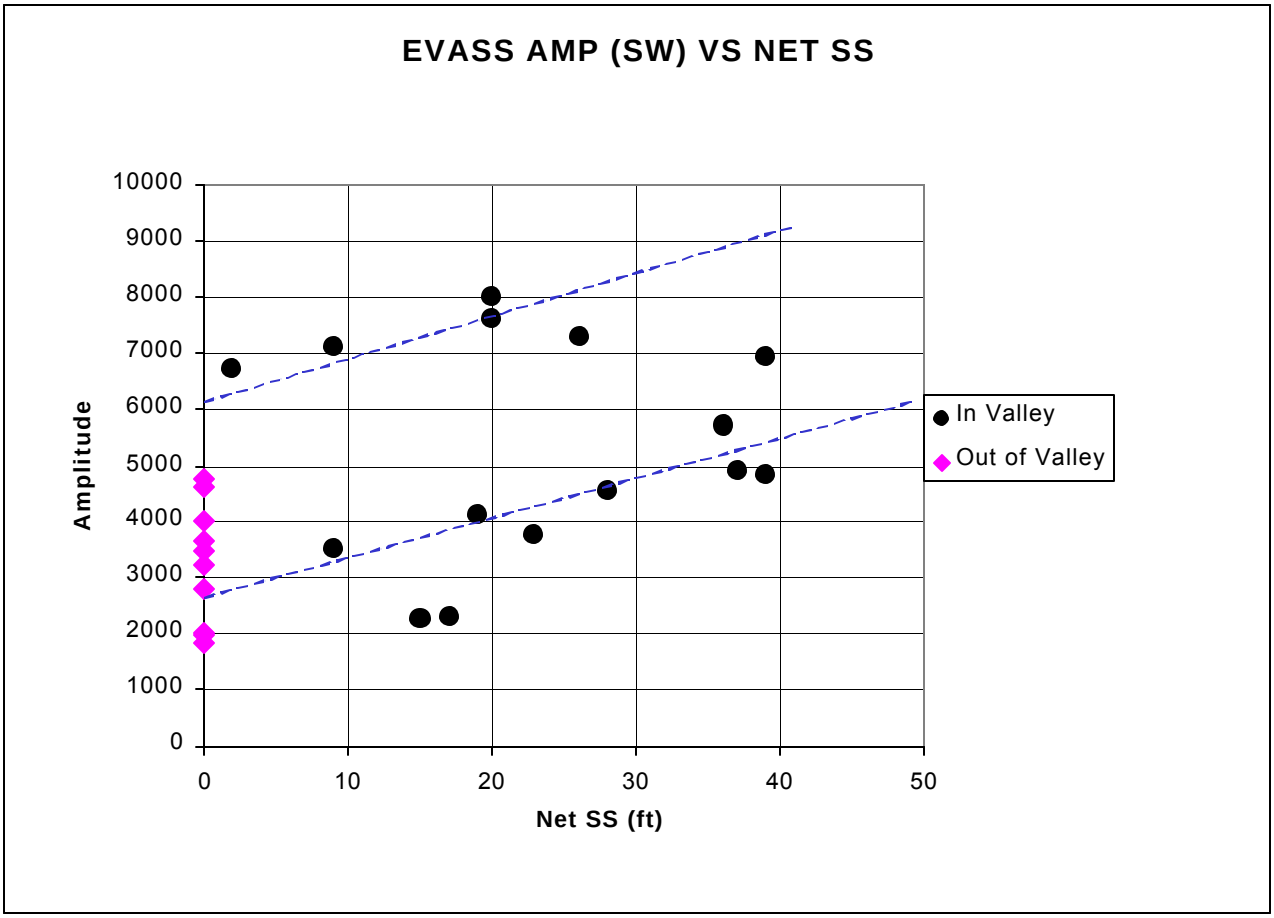

Figure 4.1.2d. Plot of the Eva net sandstone thickness versus the Eva seismic event amplitude extracted from the PSV-wave 3D volume. Two parallel trends are apparent.

Acquisition Geometry Effects on Stratigraphic Interpretation

As discussed in Section 3.1.1, the conversion of P-wave energy to S-wave energy is an offset dependent phenomenon beginning at angles of incidence of at least 15 degrees at the reflecting horizon. At Eva South, the reservoir is found at a depth of 5600 feet, and the generation of converted waves should occur at source to receiver offsets of 3000 feet. The acquisition geometry of the 3D survey determines the distribution of offsets available at the reflecting event and hence the quality of PSV-wave data. Any interpretation that relies on event amplitudes should take into consideration any potential effects of acquisition geometry on the amplitudes.

Figure 4.1.2e is a map of the effective fold of PSV-wave data at the Morrow level (travel time of 1.500 sec) calculated from the acquisition design (Figure 3.1.3d). Only offsets of 3,000 to 10,000 feet are used in the calculation. The fold builds up symmetrically into the center of the survey and usable data above 20-fold comprises approximately 57% of the survey. What needs to be scrutinized is the similarity between the PSV-wave amplitude map of the Eva SS event (Fig. 4.1.2c) and the fold map (Fig. 4.1.2e). While the amplitude map does appear to conform to the fold map, the survey was acquired by

intention in a symmetric geometry over the known reservoir extents that the amplitude map also appears to conform to.

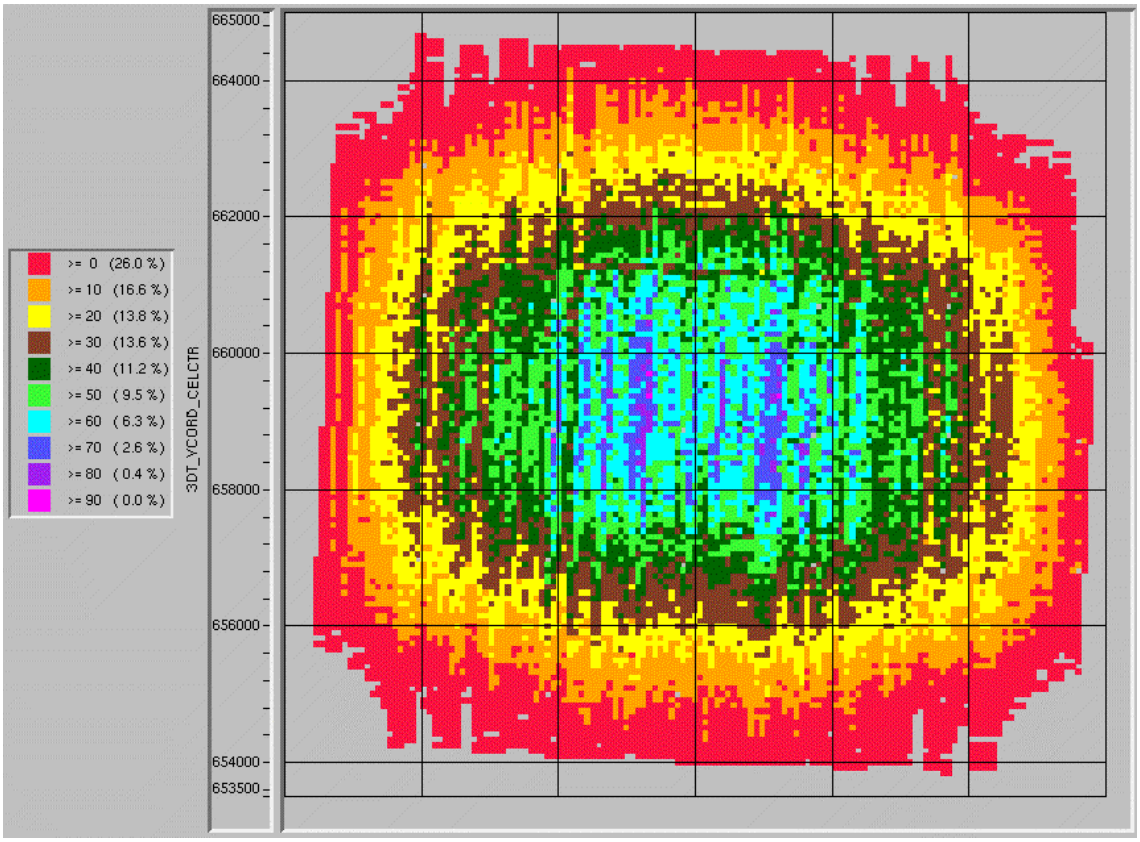

Eva South 3D-Effective PSV Fold at 1500ms (3000'-10000' offset range)

Figure 4.1.2e. CCP fold at the Morrow level from the PSV-wave 3D volume.

To investigate this further, an amplitude map on an overlying carbonate zone, the Atoka limestone, was generated and compared to the Eva SS amplitude map (Fig. 4.1.2f). The Atoka limestone is known to be uniform in thickness and lithology across the survey area. The amplitude of the Atoka event is more widespread but there does appear to be a correlation of the overall amplitude to fold. However, there are some significant differences between the Atoka and Eva SS amplitudes; the amplitude of the Eva SS event aligns along an axis closely parallel to the axis of the main reservoir body while the amplitude of the Atoka event aligns along an axis closer to the orientation of the fault trends. Also, the highest Atoka amplitude is generally over wells along the northern limit of the field that make up the trend of higher amplitude in the plot of Figure 4.1.2d, discussed in the previous section (*Structural Interpretation)*. It could be concluded that there is a contribution from the reservoir in the amplitude of the Eva SS event and that there is a contribution from the fault geometry in the Atoka amplitude, suggesting some azimuthal effect on the data. The overprint of amplitude into the Eva

SS event suggests that an azimuthal effect could be present in that map as well. In either case, there is a marked decrease in amplitude with decreasing fold towards the edge of the survey, so the observations are clouded by an acquisition geometry effect.

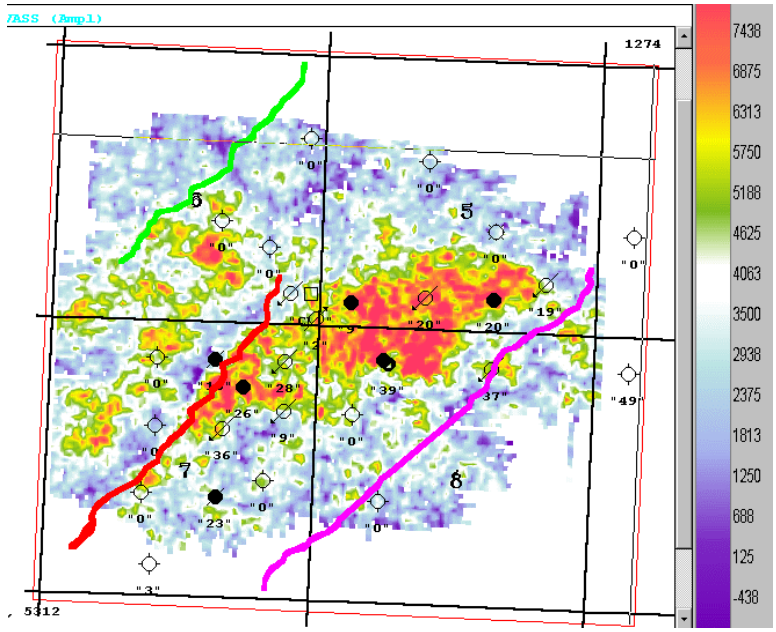

Eva SS amplitude (PSV-wave)

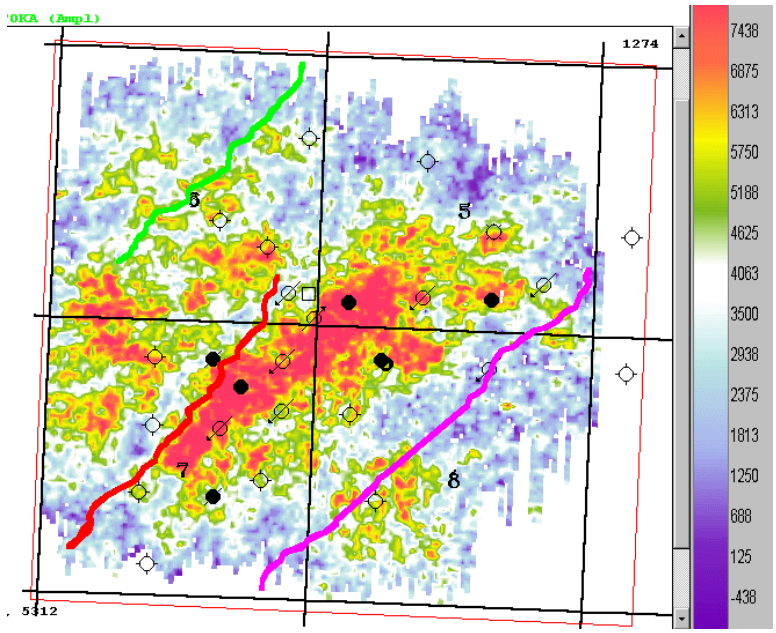

Atoka amplitude (PSV-wave)

Figure 4.1.2f. Comparison of amplitude maps for the Eva sandstone seismic event (top) and the Atoka seismic event (bottom) extracted from the PSV-wave 3D volume. P-wave fault interpretation is overlain.

Evaluation of S-wave Splitting

It has been well documented that the horizontal motion of S-waves will align in directions both parallel to a fracture system as well as perpendicular to it. The velocity of S-waves in the direction parallel to fractures is generally faster than the velocity of the S-waves perpendicular to the fractures. The fast direction is referred to as S1 and the slow direction S2. The alignment of S-wave energy in this manner is termed S-wave birefringence, or S-wave splitting. S-waves are also known to align on regional stress directions. The discussions on the PSV-wave data have alluded to an azimuthal influence on the data suggesting the possibility of S-wave splitting.

A common conversion point (CCP) supergather from the radial component of the PSV-data is shown in Figure 4.1.2g. This was constructed by gathering together traces in the vicinity of the CCP and sorting them on the basis of source to receiver azimuth. Traces are displayed in 10 degree increments. The most obvious observation is the increase in amplitude at the Morrow level at azimuths of 130 and 310 degrees that is a common azimuth along N50W. The data amplitude decreases along the perpendicular azimuth of 220-degrees, or N40E. Contained in the data, but not as obvious, is a shorter travel time to the Morrow at 130-degrees versus 220-degrees at this CCP, suggesting that the fast S1 direction is 130-degrees. This direction is opposite of what would be expected if the major faults at Eva South represent the primary fracture direction.

Further evidence of S-wave splitting can be seen in a comparison of processed data from the radial component versus the transverse component. The radial and transverse components are compared for two cross-lines in the survey (Fig. 4.1.2h). If all of the PSV conversion had taken place with no external influence, then theoretically all the energy should be contained in the radial component. While the strongest reflection energy is in the radial component, there is still a significant amount of reflection energy in the transverse component suggesting some measure of S-wave splitting has occurred.

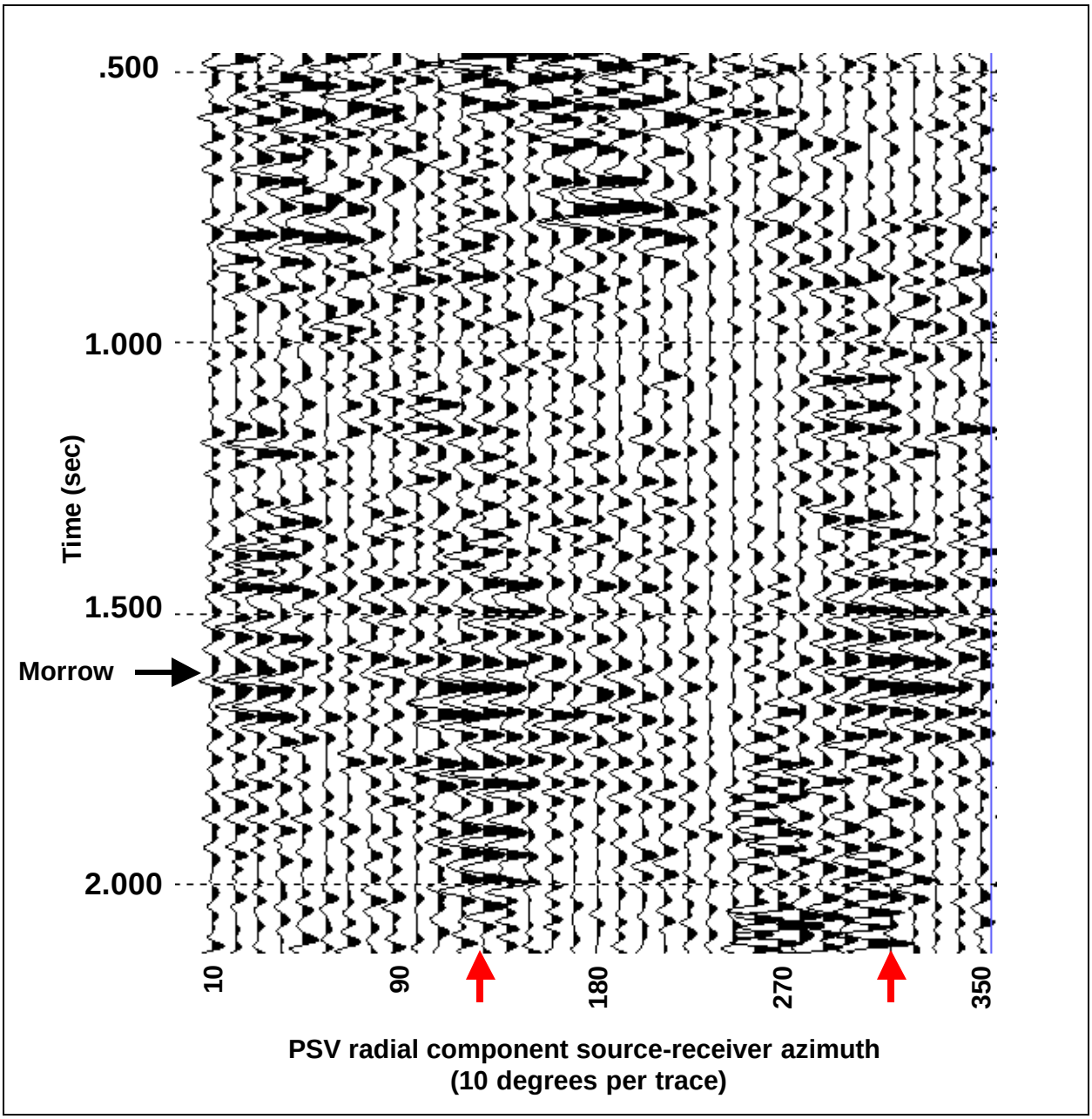

Figure 4.1.2g. CCP supergather of the radial component from the center of the Eva South PSV-wave 3D volume sorted by source-receiver azimuth in 10 degree increments per trace. Note the increase in amplitude at the Morrow horizon at 130- and 310-degrees (red arrows).

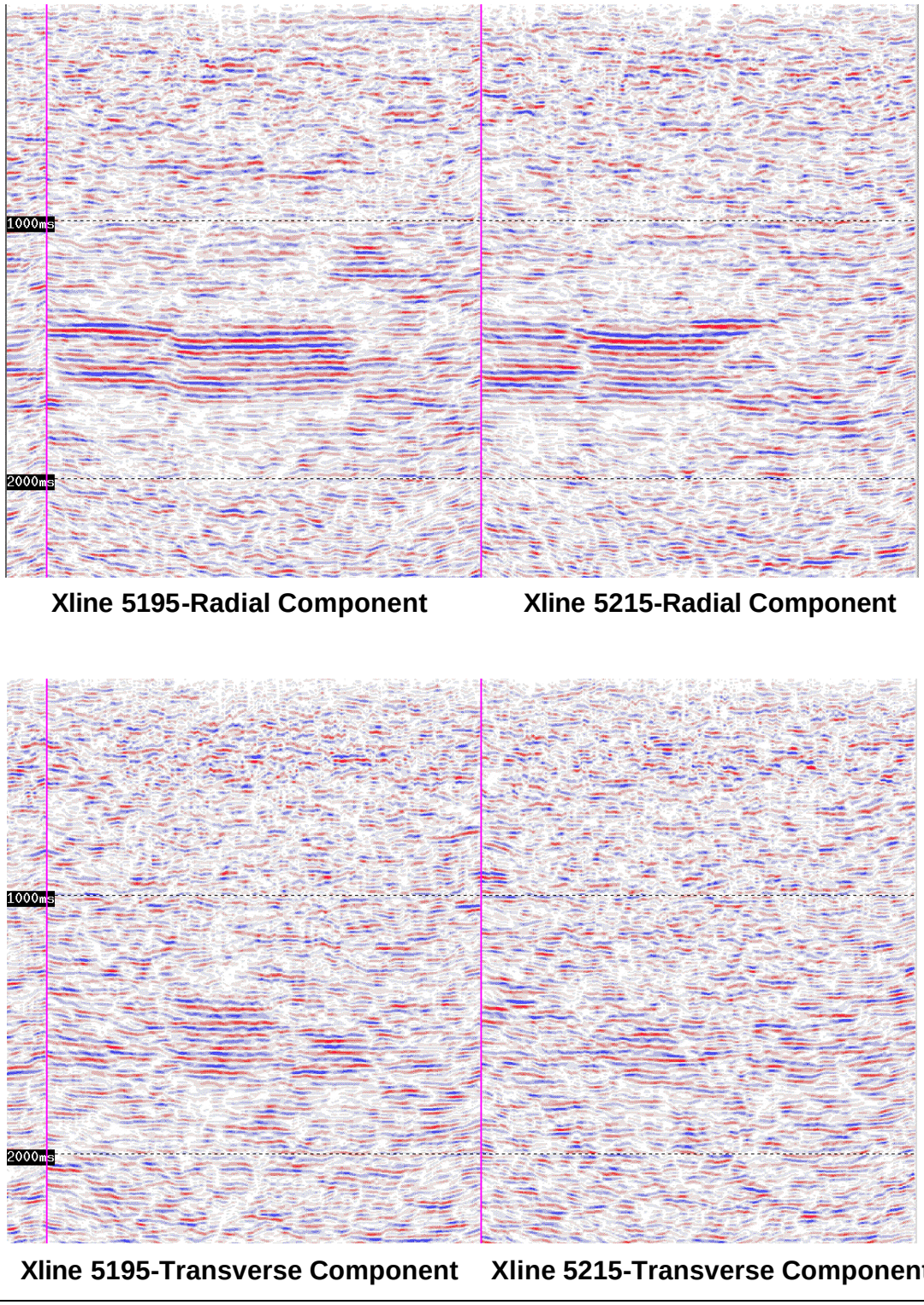

Figure 4.1.2h. Comparison of the radial and transverse components for cross-lines extracted from the Eva South PSV-wave 3D volume. Most of the reflection energy is in the radial component, though some is apparent in the transverse component, indicating S-wave splitting has occurred.

Figure 4.1.2g illustrated an increase in amplitude at the Morrow level along a 130-degrees azimuth. In order to investigate this azimuthal phenomenon further, the PSV-wave data were rotated into fixed azimuths of 130-degrees and the 220-degrees conjugate and re-stacked as separate volumes. Unfortunately the data were not enhanced or migrated due to time and budget constraints. Figure 4.1.2i compares the Eva SS PSV-wave amplitude at the 130-degrees and 220-degrees azimuths. The P-wave fault interpretation is overlain for reference. There is a noticeable increase in amplitude of the Eva SS event over the central portion of the reservoir at the 130-degrees azimuth. This is consistent with the CCP supergather of Figure 4.1.2g; not surprising considering the supergather comes from the center of the survey. The 220-degrees azimuth amplitude does not show as good of correlation to the reservoir, but there are more noticeable amplitude changes across the fault system at this azimuth, particularly across the main Teepee Creek fault at the west edge of the field. The data quality can be seen to degrade rapidly towards the edges of the survey which is to be expected on the non-enhanced, un-migrated volumes and any analysis is only considered valid in the central portion of the survey.

The two-wave travel time (time structure) to the Eva SS seismic event is shown in Figure 4.1.2j, as extracted from the 130 degrees volume (bottom) and the 220-degrees volume (top). The P-wave fault interpretation is overlain for reference. A comparison of the travel times shows that there is not a consistency to the fast velocity direction across the survey.

To show the differences in the travel times as a function of azimuth more clearly, the 130-degrees azimuth travel times are subtracted from the 220-degrees travel times, and this difference calculation is shown in Figure 4.1.2k. The P-wave fault interpretation is again overlain for reference. Red areas of the map correspond to where the 130-degrees azimuth travel-times are faster than the 220-degrees azimuth. Areas where the 220-degrees azimuth is faster are shown as blue, and the velocities are approximately equal in the white areas of the map. The regional areas outside the fault system tend to show the 130-degrees azimuth to be the fast direction. Other S-wave studies conducted in the Mid-Continent and Rocky Mountain Regions have suggested that this direction is the approximate orientation of a persistent regional stress field. The most radical deviations from the 130-degrees direction occur in the regions between the faults across Eva South. The velocities show the smallest difference over the know portion of the reservoir. There is the suggestion of a north-south discontinuity of the reservoir as shown by the green area along the west line of the NW/4 of Section 8, but reservoir performance data does not support the idea of such a discontinuity.

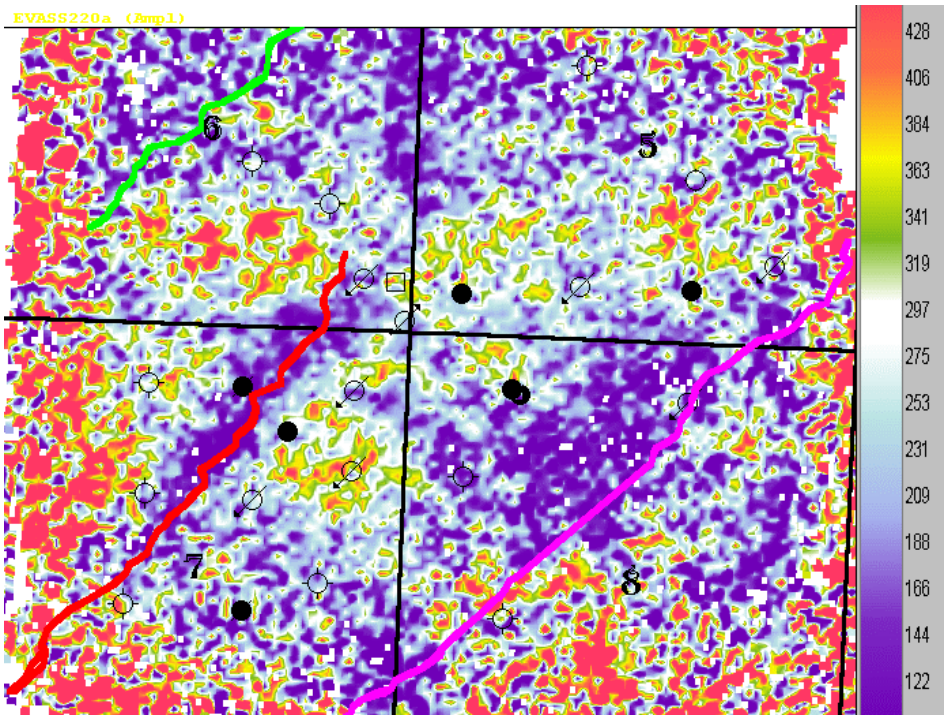

Eva SS amplitude-PSV 220 degree azimuth volume

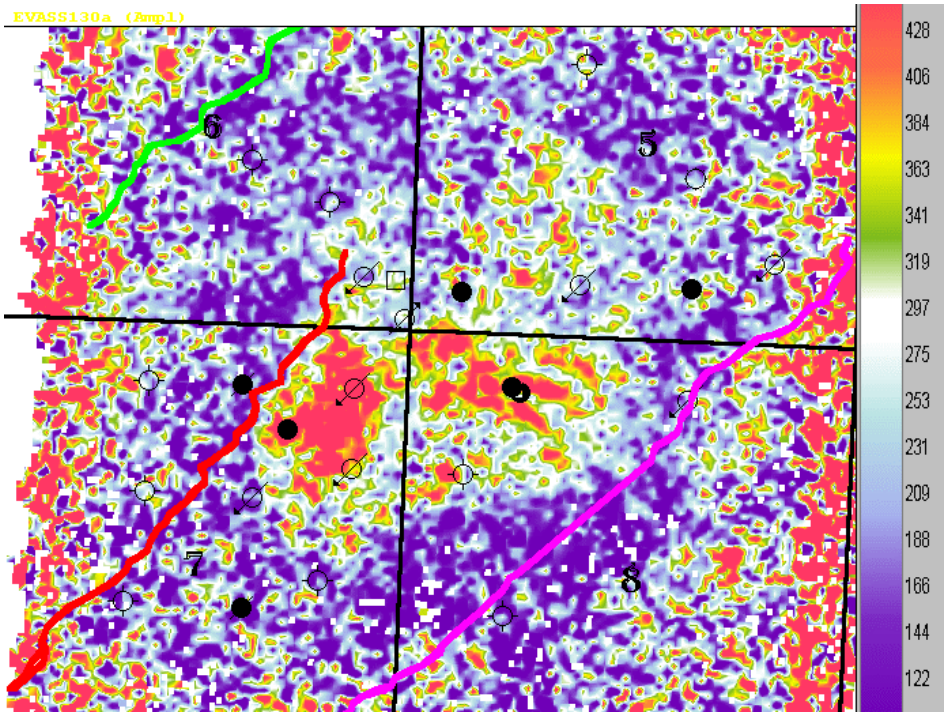

Eva SS amplitude-PSV 130 degree azimuth volume

Figure 4.1.2i. Detail views of the comparison of the Eva sandstone seismic event amplitude extracted from the PSV-wave 220-degrees azimuth volume (top) and PSV-wave 130-degrees azimuth volume (bottom). P-wave fault interpretation is overlain for reference.

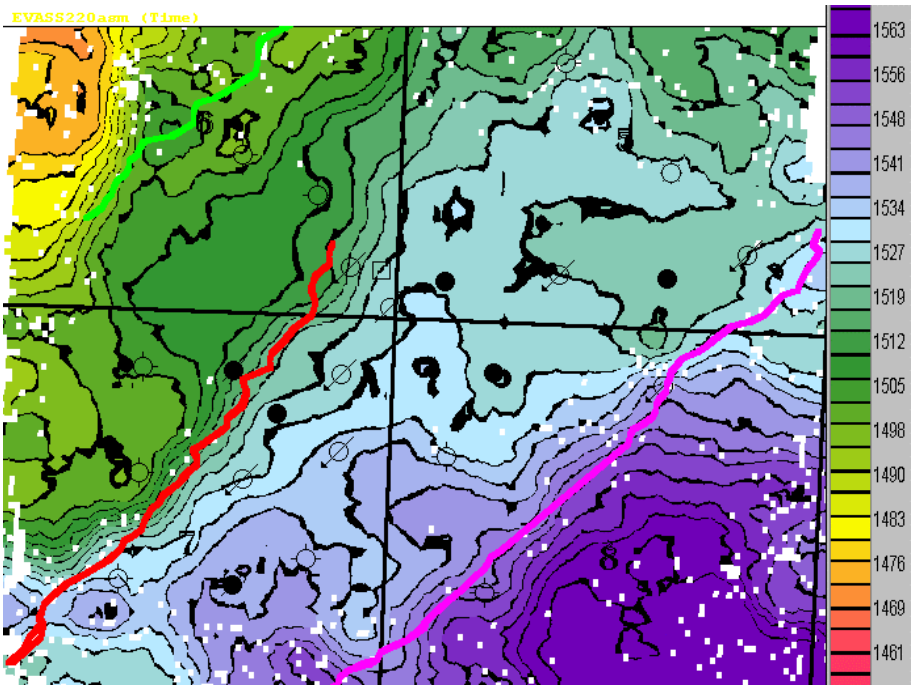

Eva SS time-PSV 220 degree azimuth

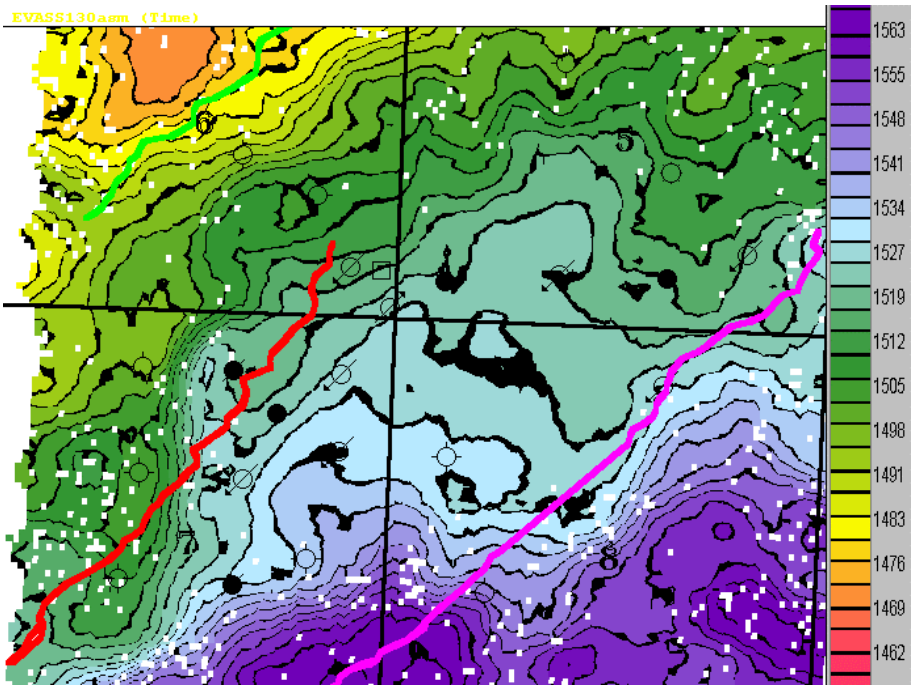

Eva SS time-PSV 130 degree azimuth

Figure 4.1.2j. Detail views of the comparison of the Eva sandstone seismic event time structure extracted from the PSV-wave 220-degrees azimuth volume (top) and the PSV-

wave 130-degrees azimuth volume (bottom). P-wave fault interpretation is overlain for reference.

The observation that the greatest deviations from a regional 130-degrees fast velocity direction occur between the faults suggests that there may be mechanisms in the inter-fault area that change the stress characteristics of the field. It is believed that the fault systems have a component of strike-slip offset along their traverse as part of a regional wrench system. If so, it is quite possible that differential strike-slip motion along the fault planes could create inter-fault rotation of the bounded blocks. This mechanism could change the orientation of stress and/or fractures in the inter-fault blocks from the dominant regional direction, resulting in the pattern of velocity differences shown in Figure 4.1.2k. If the fast-velocity direction across the survey is changing, then correcting for azimuthally-dependent amplitude changes cannot be accomplished by a single rotation assumption. The direct correlation of PSV-wave amplitude to a petrophysical property would be likewise compromised and a great deal of ambiguity introduced.

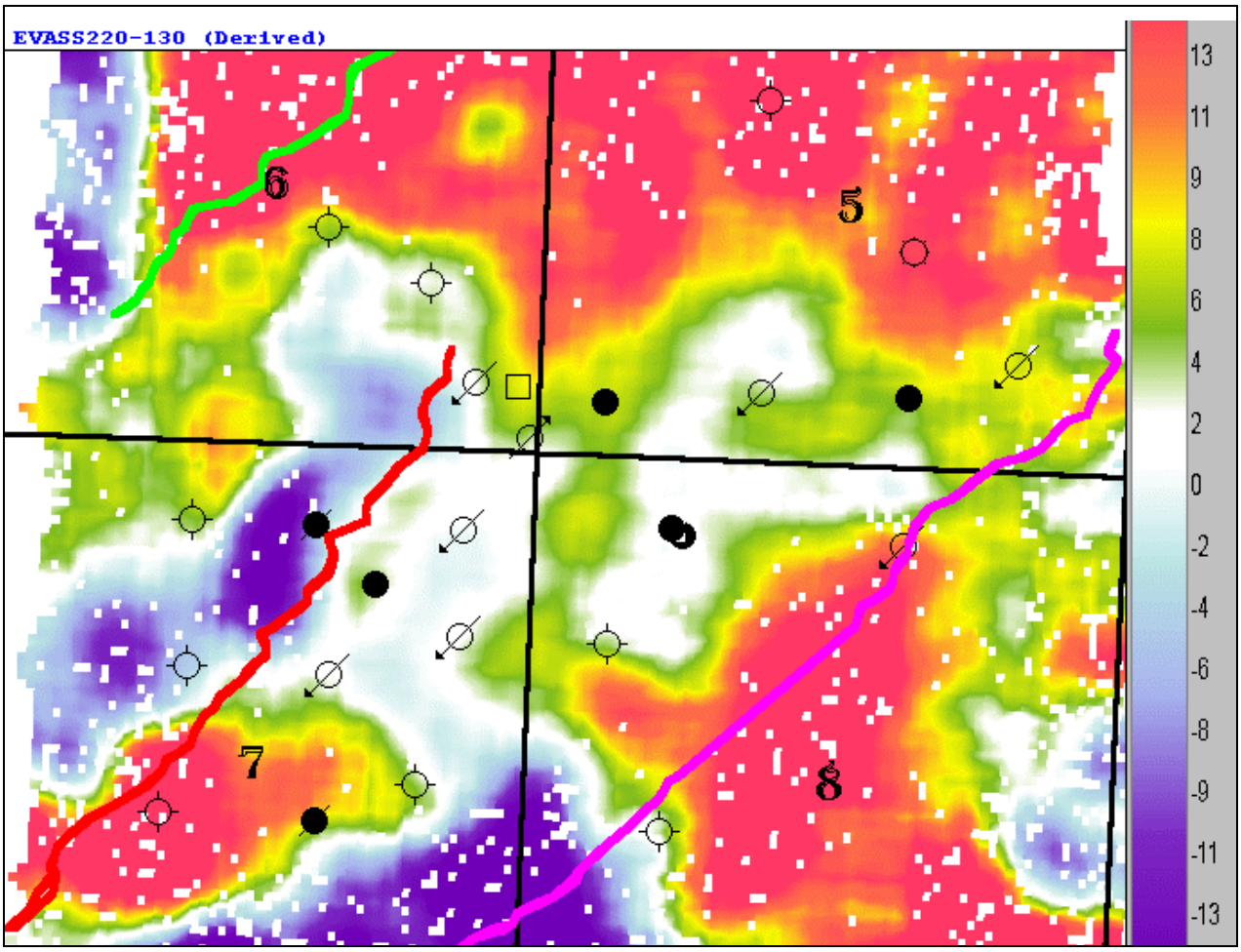

Figure 4.1.2k. Detail view of the time structure difference of the PSV-wave 130-degrees azimuth volume subtracted from the PSV-wave 220-degrees azimuth volume. Red areas

indicate where the travel times in the 220-degrees azimuth direction are slower than in the 130-degrees direction. P-wave fault interpretation is overlain for reference.

Anisotropy Analysis

Seismic interval anisotropy measurements can provide information about the distribution and intensity of shear stresses and the orientation of their polarization. Pre-stack azimuthal analyses at the middle of the survey showed both fast and slow S-wave polarizations (Fig. 4.1.2g). The fast azimuth was determined to be 130-degrees (N50W) and the slow azimuth was determined to be 220-degrees (N40E). The PSV-wave data was rotated to these principle azimuths throughout the survey area.

The orientations suggested by the azimuthal analyses were somewhat surprising. The NE-SW orientation of the three major faults suggests that the principal stress direction (S1) would be parallel to the faults. The opposite orientation was observed in the converted-wave data. The faults lose any sense of vertical displacement at a depth of about 3000 feet and travel time delays between the fast and the slow PSV-wave directions are observed at this depth as well. This suggests that the onset of azimuthal anisotropy and S-wave polarization likely occurs somewhere in the shallower section above the faults. If this is the case, then layer stripping rotations need to be applied to the PSV-wave data to account for azimuthal anisotropy variations with depth.

Interval anisotropy measurements can assess the intensity of anisotropy and whether the original rotation azimuth was correct. The absolute values of interval anisotropy are related to the amount of anisotropy within the interval. For example, areas of high fracture intensity often produce areas of high seismic-anisotropy. Negative (-) values of anisotropy suggest that the original rotation azimuth was incorrect, and may actually be 90-degrees off.

Anisotropy measurements for the Morrow interval were calculated from the 130-degrees and 220-degrees PSV-wave volumes. Since the Valley reflection on these two volumes is rather noisy, the interval used in anisotropy calculations was from the Morrow shale (top of Morrow Formation) reflection to the Mississippian reflection. This interval contains a somewhat greater section than the upper Morrow alone, yet azimuthal anisotropy effects of the upper Morrow should still contribute to the anisotropy of this larger interval.

Interval anisotropy measurements are calculated by taking the difference between the slow and fast PSV-wave interval isochrons, and then normalizing by the fast interval isochron.

%Anisotropy=100*(S2 isochron–S1 isochron)/S1 isochron

Where the S1 isochron is derived from the 130-degrees volume and the S2 isochron is derived from the 220-degrees volume.

Figure 4.1.2l shows the Morrow to Mississippian interval anisotropy map. A black marker separates the positive anisotropy values from the negative values. Values generally range from –10% to 10%. The PSV-wave volumes are rather noisy and the accuracy of these measurements is questionable. If these measurements are valid, some very interesting details can be inferred.

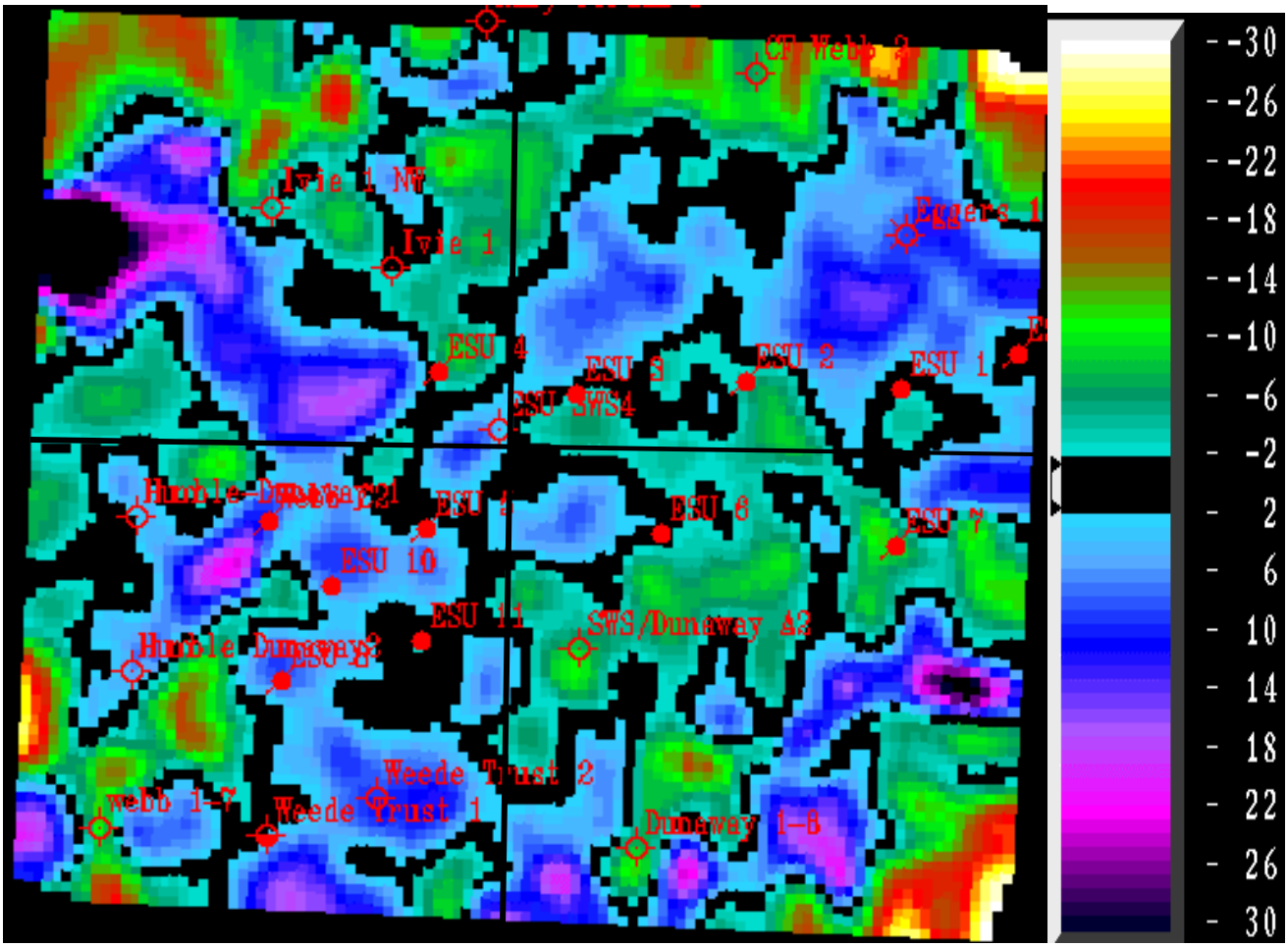

Figure 4.1.2l. Apparent seismic anisotropy calculated from the PSV-wave azimuth limited 3D volumes for the Morrow to Mississippian interval (Wilson, 2002). Green indicates negative anisotropy.

As suggested by the travel-time differences previously discussed (*Evaluation of S-wave Splitting*), the large variation of anisotropy throughout the survey suggests that the principal S-wave polarization azimuth and the intensity of anisotropy is not laterally consistent. Negative values (green) may mean that the 130-degrees principal stress azimuth, to which the PSV-wave data was originally rotated, is actually 90-degrees off within the Morrow interval. The quality of the non-enhanced, unmigrated PSV-wave data is rather low. Therefore the interval anisotropy calculations may be questionable. However, the laterally varying values and signs (positive or negative) of the anisotropy measurements, as well as the discrepancies between the fast and slow PSV-wave Morrow sandstone amplitudes, strongly suggest the need for more accurate rotation

analysis of the PSV-wave data. In the Eva South survey, azimuthal analysis was only performed on a single supergather at the center of the survey. In future surveys, it is recommended that layer stripping and laterally varying azimuthal analysis be conducted to achieve proper rotation angle throughout the survey. This process is very time consuming and expensive, and was not a viable option in this study.

Vp/Vs Analysis

One of the traditional expectations of multi-component seismic data is the ability to calculate changes in the apparent P-wave velocity (Vp) to S-wave velocity (Vs) ratio. The Vp/Vs ratio is directly related to Poisson's ratio and can be a valuable measure of lithologic changes; there is a large difference in Poisson's ratio between sandstone and shale. For analyzing seismic data, a relatively low Vp/Vs ratio is consistent with sandstone; conversely, a relatively high Vp/Vs ratio is consistent with shale.

Vp/Vs values are estimated by comparing the same geologic interval isochrons from both the P-wave and PSV-wave data. The focus of this study was the upper Morrow interval inclusive of the Eva sandstone as defined by the Morrow shale to Valley isochron. Only upper Morrow Vp/Vs interpretations are discussed here. The Upper Morrow isochrons were calculated from the migrated P-wave data (Fig. 4.1.1j) and from the radial, full-azimuth PSV-wave data. The radial volume was used because the Valley reflection is much more consistent on this higher-fold volume than the limited azimuth volume.

The formula for calculating Vp/Vs from PSV-wave data is as follows:

Vp/Vs=(2*PSV-wave isochron–P-wave isochron)/P-wave isochron

(Margrave, 1998)

This ratio was calculated for the upper Morrow interval and then multiplied by 100 for display purposes.

Figure 4.1.2m is the Upper Morrow Vp/Vs X 100 map. An area of low Vp/Vs, consistent with a sandstone lithology, is located over much of the known reservoir. Vp/Vs calculations are very sensitive to errors or discrepancies in picking the P-wave isochron. The higher resolution of the P-wave isochron has a significant effect on the resulting Vp/Vs calculations. Additionally, values calculated for Vp/Vs are only relative, as the absolute Vp/Vs that is computed is strongly affected by the different resolutions of the P-wave and PSV-wave data. This is why the Vp/Vs values from the seismic data are much higher (around 4.0) than would be calculated from more precise measurements from well-logs (around 2.0). Regardless, Vp/Vs calculations for the upper Morrow interval provide a relative assessment of sandstone versus shale and generally coincide with known values from well control.

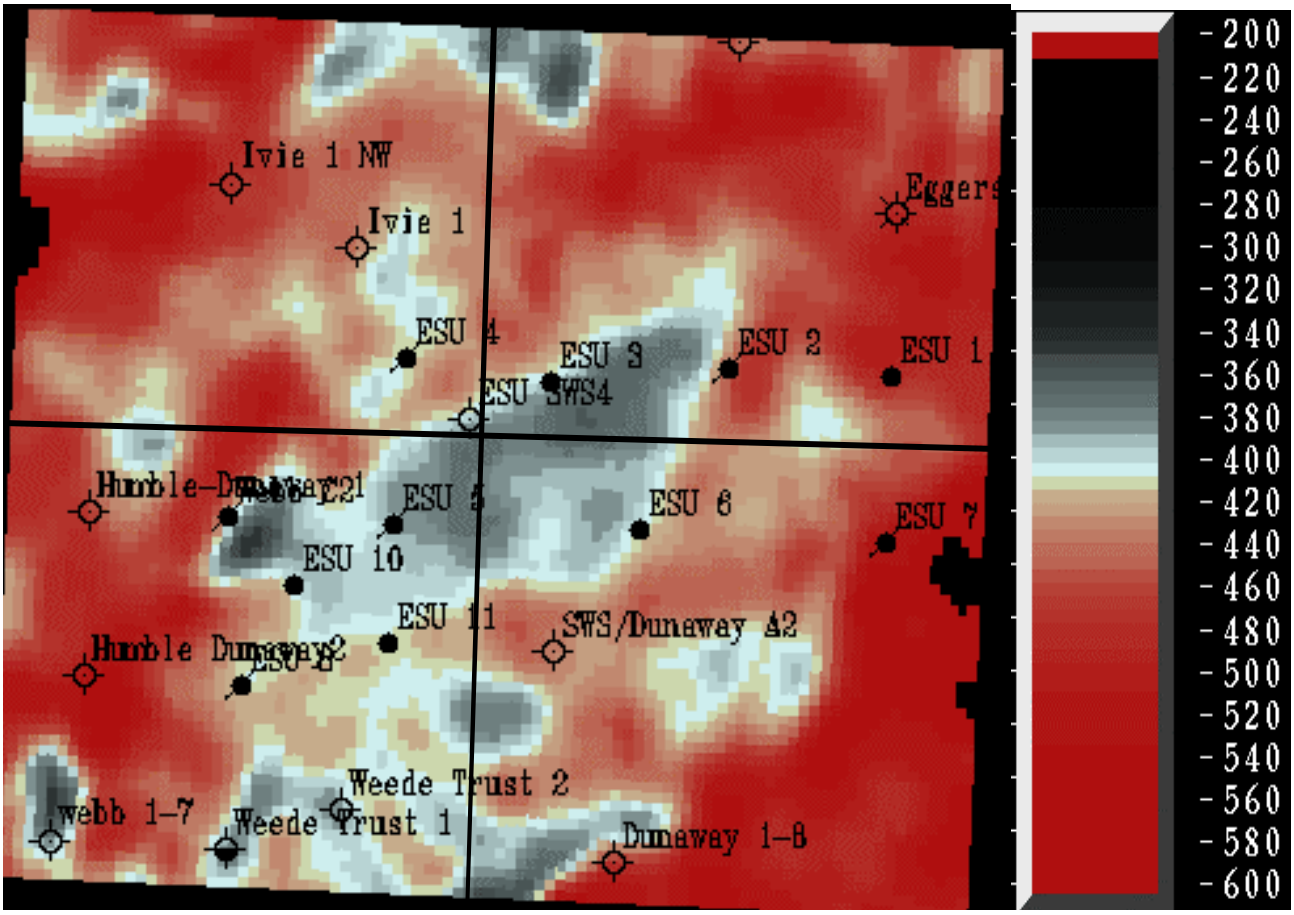

Figure 4.1.2m. Vp/Vs ratio multiplied by 100, calculated by comparing interval times between the P-wave and PSV-wave 3D volumes at Eva South (Wilson, 2002). Grey to black areas have lower Vp/Vs ratios and are consistent with a sandstone lithology. Note the general coincidence with known sandstone from well control, especially in the central portion of the survey.

4.1.3 Integrated P-wave Interpretation

The P-wave data was determined to be more useful in defining detailed structure and reservoir geometry at Eva South than the PSV-wave data as it correlates more closely with the well control. A detailed interpretation that integrated the P-wave seismic data and geologic well information was constructed to provide a set of maps that characterize the Eva South reservoir and production. The determination of structure was done by converting the time structure to elevation by the application of a contoured velocity field generated by ties to well control and is a direct numerical computation. The sandstone isopach maps were generated by interpretive contouring of the well-data in a manner that conforms to the seismic amplitude maps. Numerical conversions of seismic amplitude to sandstone thickness were not considered robust, necessitating this interpretative approach.

Reservoir Interpretation

Detailed Eva net sandstone isopachs maps were generated by contouring the well-data in a manner that conforms to the Eva SS seismic event amplitudes. Figure 4.1.3a is the resultant net sandstone isopach that conforms to the seismic amplitude map (Fig. 4.1.1f) and assumes a linear relationship between seismic amplitude and net sandstone thickness across the entire field. The map is problematic in the area of the ESU 6 and ESU 12 in the N/2 NW of Section 8; honoring the decrease in seismic amplitude in the area of these wells creates the appearance of a disrupted and thin portion of the reservoir despite the fact that the ESU 6 and ESU 12 have the thickest net sandstone in the field.

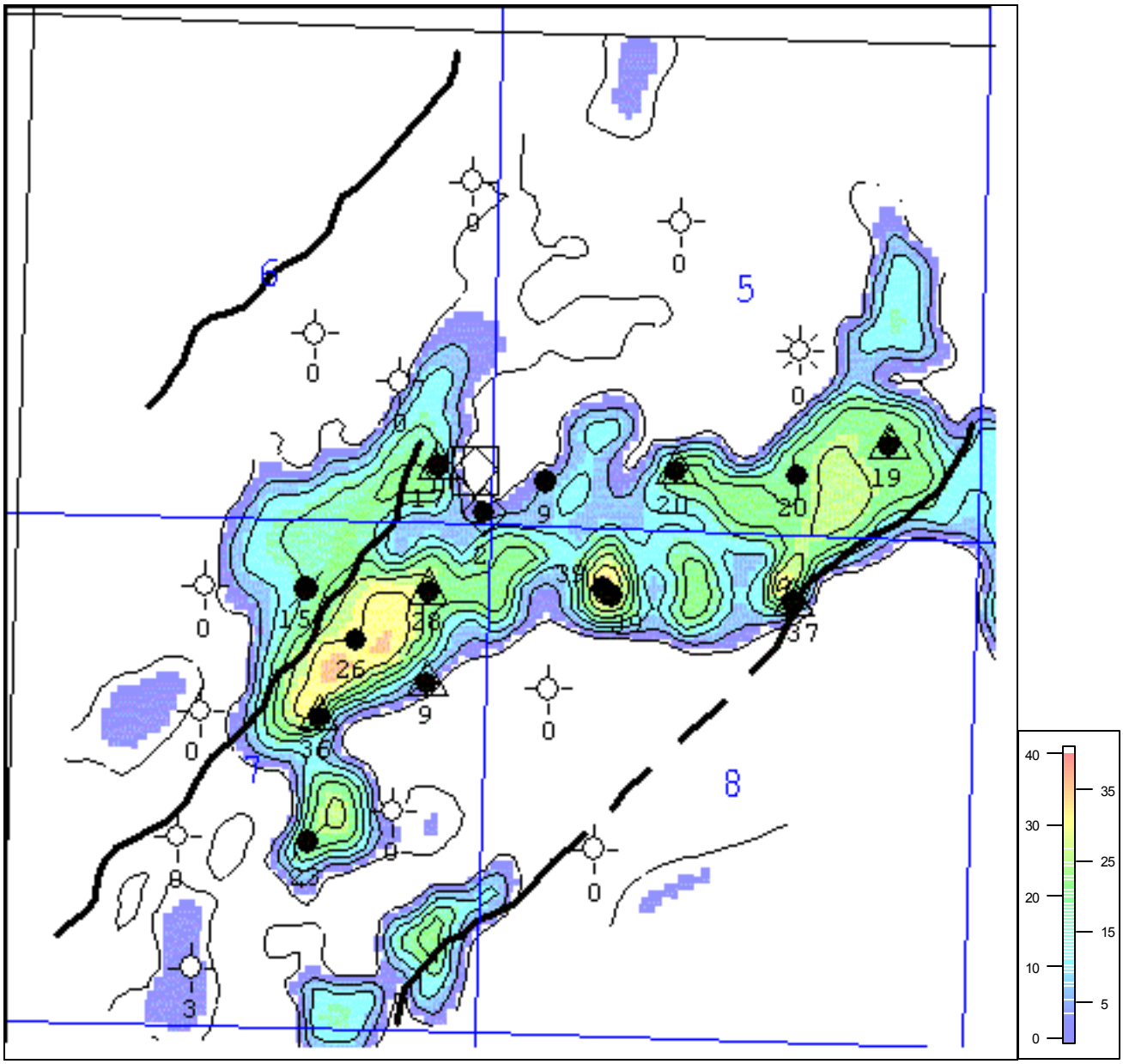

Figure 4.1.3a. Interpreted Eva net sandstone isopach assuming a linear relationship between seismic amplitude and thickness. Contour interval is 5 feet.

A different and more interpretive approach was taken to generate the Eva net sandstone isopach of Figure 4.1.3b. The area around the ESU 6 and ESU 12 wells was contoured with less value given to the seismic amplitude map and more weight on the well data. The justification for this approach is the possibility of a seismic tuning phenomenon as previously discussed (*Seismic Tuning Considerations*) that would cause nonlinearity in the seismic amplitude to sandstone-thickness relationship. The Eva sandstone reservoir is represented as more continuous in Figure 4.1.3b than in Figure 4.1.3a. An inspection of primary recovery, as shown in the bubble map (Fig. 4.1.3c), shows that the ESU 6 has been a very high-volume oil producer. Secondary production performance by waterflood has also shown the ESU 6 to be well communicated to the rest of the field making it highly unlikely that the discontinuous appearance suggested by Figure 4.1.3a is a valid interpretation. Therefore, the net sandstone map of Figure 4.1.3b is a better representation of the reservoir.

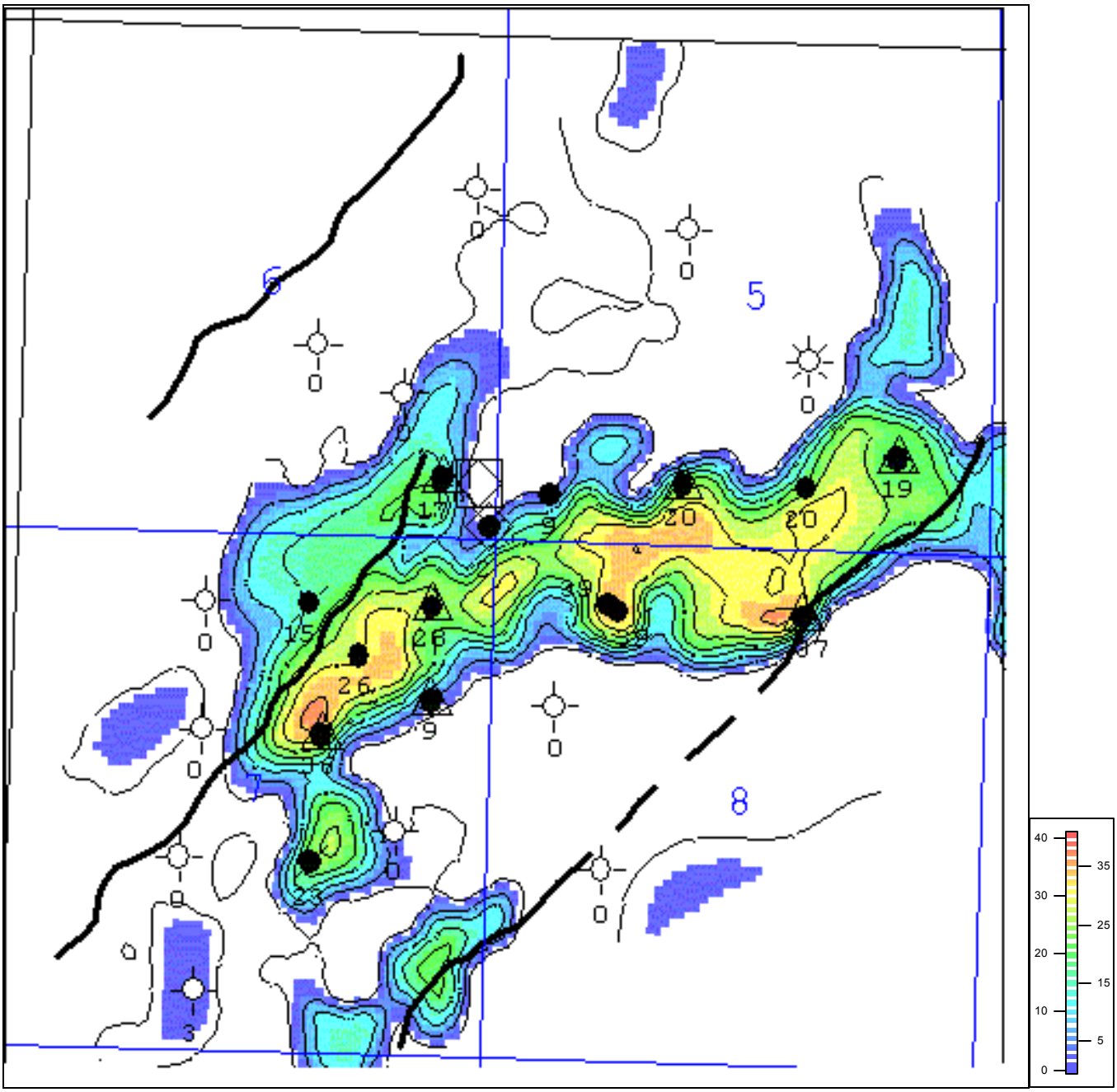

Figure 4.1.3b. Interpreted Eva net sandstone isopach assuming seismic tuning is a factor in the known thickest portion of the reservoir. Porosity cut-off for posted well data is ≥10%. Contour interval is 5 feet.

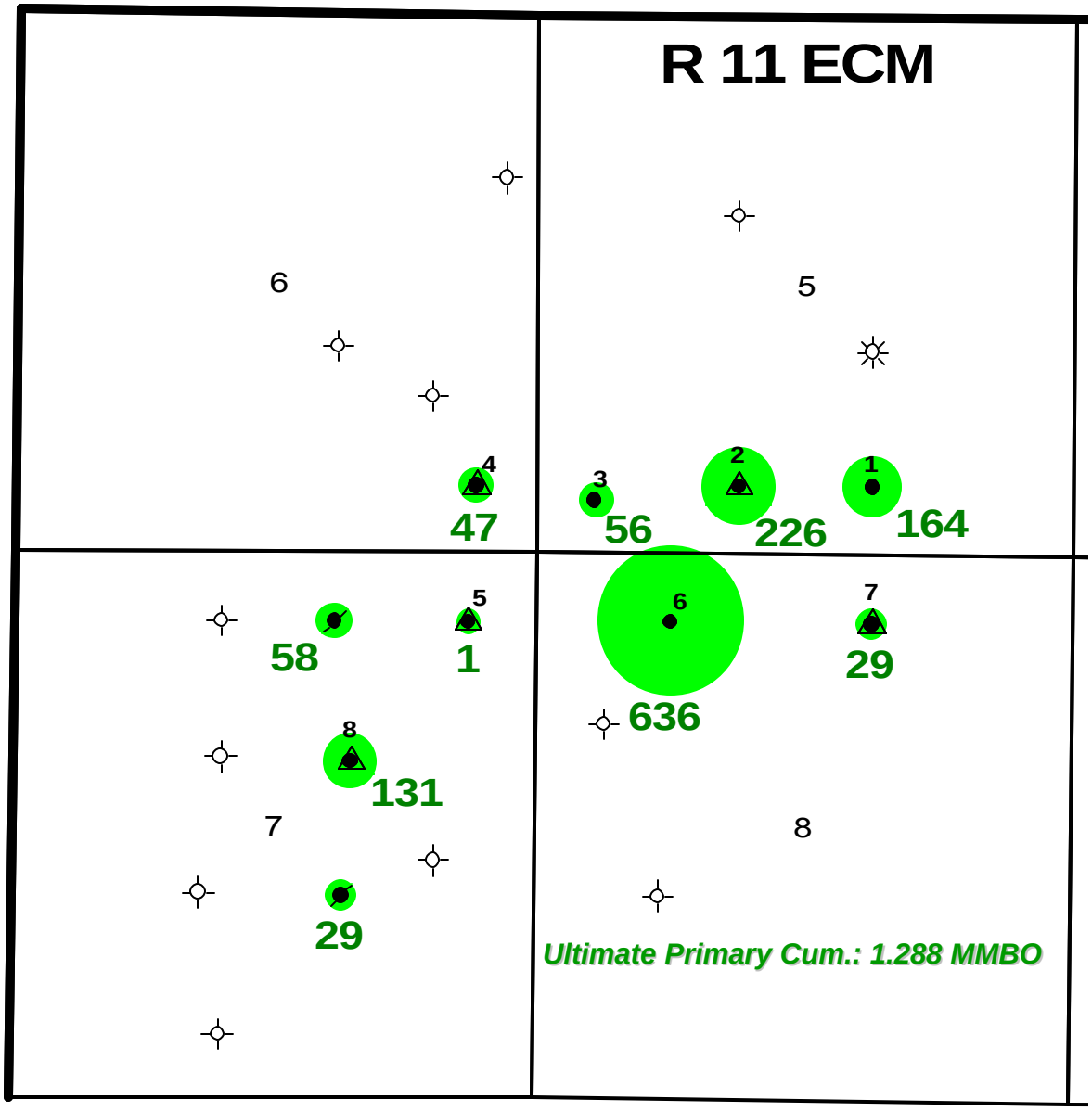

Figure 4.1.3c. Bubble map showing the primary production (MBO) per well in Eva South. Note the outstanding production from the ESU 6, indicating good reservoir continuity around this well. Poor production in some wells is due to: isolation in small compartments (Fig. 1.5a) in the ESU 4, Webb C-2 (NW NE Sec. 7) and Weede Trust No.1 (NW SE Sec. 7); a thin oil column above the oil/water contact in the ESU 7; thin reservoir due to abandoned channel-fill in the ESU 3; and depletion in the ESU 5.

Exploration Application

The study of the Eva South 3D seismic data illustrates the practical applications and limits of seismic data in exploring for and exploiting the type of reservoirs productive in the field. The data do a very good job of defining structure and fault geometries over the field and a good job of identifying gross reservoir geometry. In this sense, the data

would appear to be very useful in exploring for these reservoirs on a regional basis and for developing a new discovery.

Figure 4.1.3d is a composite map of Morrow structure contours (Fig. 4.1.1d) overlain on a color net sandstone grid from interpreted net, Eva sandstone map (Fig. 4.1.3b). It was noted that the Morrow structure at Eva South generally conforms to the outline of the reservoir sandstone. This element of differential compaction is apparent in this overlay and forms the basis for an exploration model for upper Morrow valley-fill reservoirs that can be used in other areas; the coincidence of differential structure and high seismic-amplitudes can be used to define exploration targets.

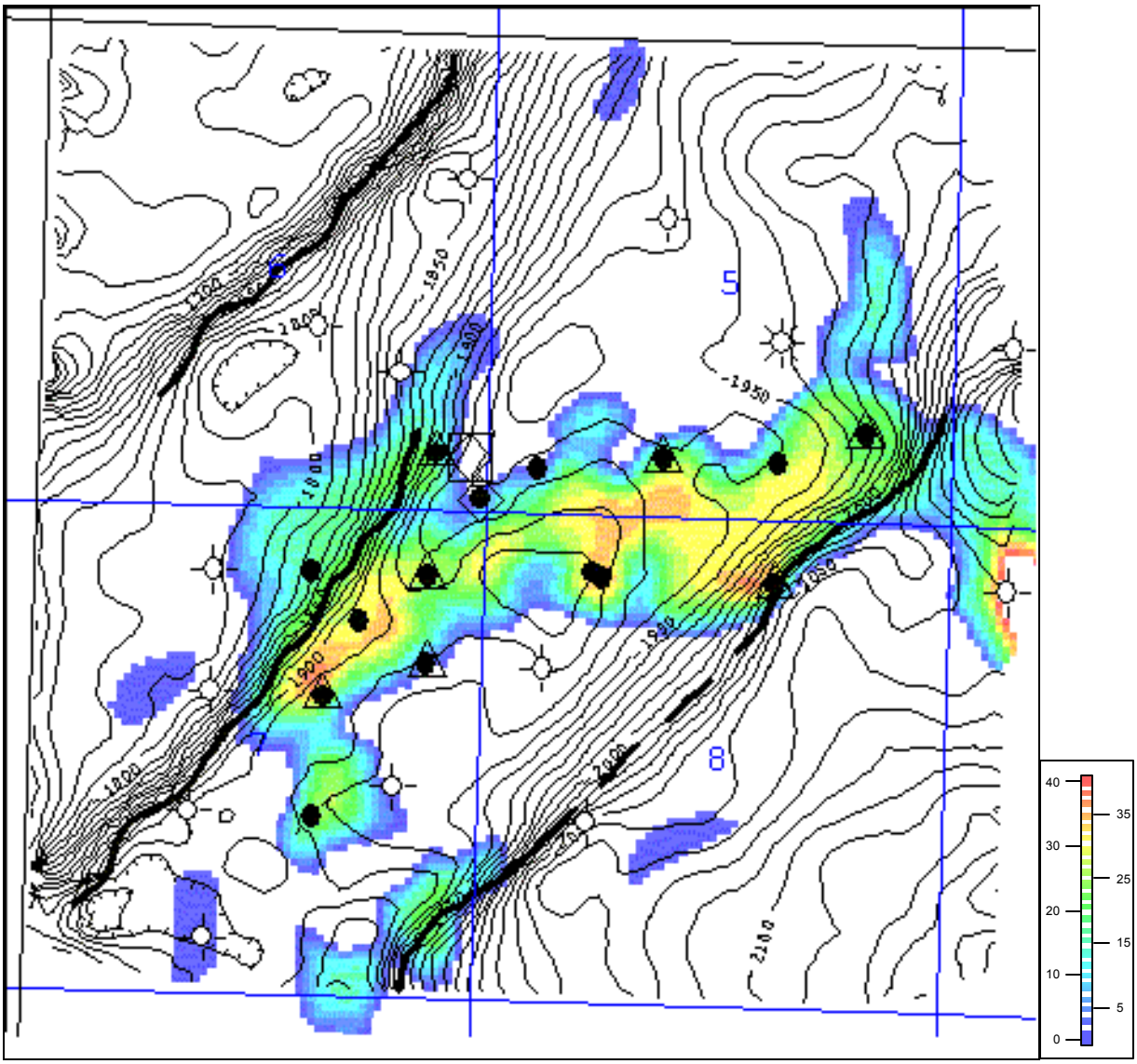

Figure 4.1.3d. Morrow structure contours and faults (from Figure 4.1.1d) overlain on a color grid of Eva net sandstone amplitude. The maps are derived by the integration of the well control with the Eva South 3D seismic data. Structure contour interval is 10 feet. This composite map defines an exploration model for upper Morrow reservoirs. Color bar shows thickness of net sandstone.

The composite map of Figure 4.1.3d was constructed with the benefit of abundant well control. A more practical set of maps to use in an exploration, without the benefit of well control, might be the Morrow time structure (Fig. 4.1.1c) and an upper Morrow amplitude map such as the Eva SS seismic event amplitude (Fig. 4.1.1f) or a windowed amplitude map in the upper Morrow (Fig. 4.1.1h). The amplitude maps based on a time window from the Morrow shale event are probably a more practical approach as they are less interpretative and require only that the regional Morrow shale event be identified and mapped.

If only one Eva South producing well was known and the composite map of Figure 4.1.3d was available to define development locations, the use of the 3D seismic would have resulted in a very high development drilling success rate for the field.

4.2 Horizontal Drilling

4.2.1 ESU 13-H Drilling and Completion

The final location of the ESU 13-H horizontal well (Fig. 4.2.1a) was based on several factors: 1) The 3D seismic provided excellent structural control, especially in locating the position of the Teepee Creek fault; 2) The 3D seismic indicated good reservoir continuity along a trend parallel to the fault (Fig. 4.2.1a); 3) Although adequate, sweep efficiency in the western portion of the unit was not as high as to the east; and 4) The theory that oil may have been banked up against the fault.

It was decided to drill the ESU 13-H parallel to the Teepee Creek fault, along the western margin of the unit. With the excellent seismic control the well was positioned no more than 200 feet from the fault plane. The goal was to establish a line of continuous withdrawal across the entire western (up-dip) margin of the unit. As performance dictated, other wells in the unit could be converted to injectors to sweep oil to this well.

The drilling plan called for a total lateral displacement of 3,285 feet with approximately 2,800 feet in the Eva sandstone reservoir. A complete open-hole log suite (gamma ray, spontaneous potential, resistivity, micro-resistivity, neutron/density and sonic) was planned in order to evaluate porosity, permeability and water saturation in this transect across the unit. The logging tools were to be conveyed via coiled tubing. Completion plans called for the use of an innovative, sliding-sleeve production liner that would allow portions of the well to be open or closed (alternatively) to fluid entry depending on water saturation established from the open-hole logs and production testing.

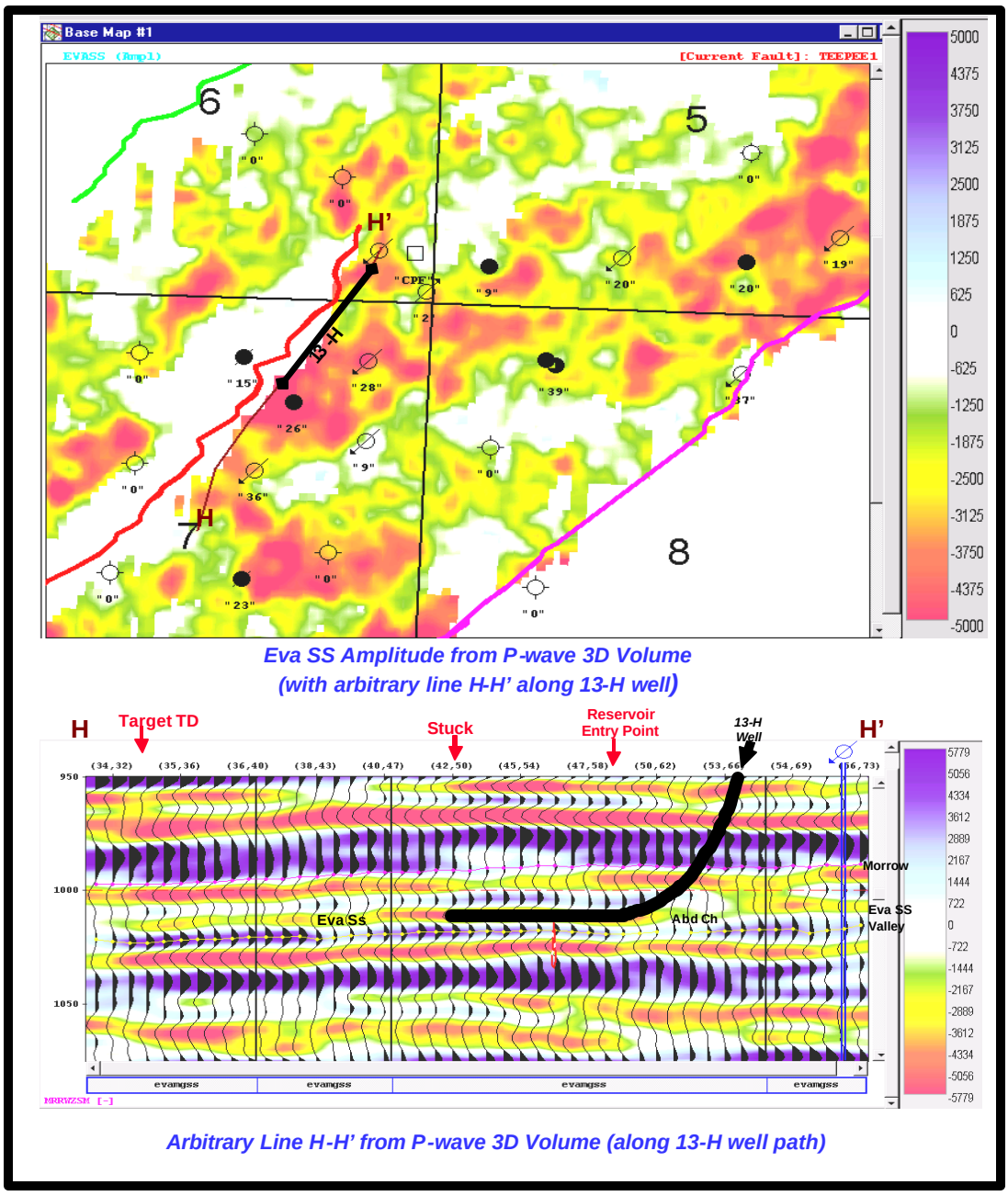

Figure 4.2.1a. Map and cross section showing the targeted path of the ESU 13-H along seismic line H-H'. Black lines show actual length drilled. In the cross section view the seismic response of the Eva sandstone is imaged as a trough (left deflecting wavelets) and is labeled (Eva Ss). The brighter colors, yellow to red, denote good reservoir development. The well was planned to extend to the point labeled (Target TD), just short of where the amplitude begins to fade, indicating the edge of the reservoir.

Drilling problems precluded the well from attaining the targeted depth and the planned completion procedure had to be dramatically altered. Figure 4.2.1a (top) shows the

location of the proposed ESU 13-H well path and the section that was successfully drilled.

The well was spud on November 11, 1999. The kick-off-point for building the turn to horizontal was reached on November 28. Drilling of the build section was completed on December 1 and preparations made to set 7 inch casing to a point just short of entering the Eva sandstone; drilling into the reservoir without casing was to be avoided because of high reservoir pressure from the waterflood and the potential for uncontrolled flow or a down-hole blow-out. At this time the well began experiencing lost circulation problems, believed to be in the Cherokee or Atoka section from 4,500 to 5,300 feet. This was compounded by mechanical problems with the rig which caused further delay. When circulation was eventually reestablished the casing was set on December 6. The casing then became stuck and would not circulate and could not be cemented. From December 9 through December 21 it took several trips in and out of the hole, including becoming stuck in the casing several times, to clean shale out of the casing; the combination of the horizontal orientation of the well-bore, decrease in mud weight due to lost circulation and prolonged exposure to drilling fluids had caused the upper Morrow shale to begin sloughing and caving. Eventually the hole was cleaned and horizontal drilling, albeit slow, began on December 22.

The Eva sandstone was encountered on December 26 at a measured depth of 6,052 feet (5,607 true vertical depth). The reservoir entry point was within three feet as defined by the seismic data. From December 26 through December 29 the well drilled continuous, oil saturated, Eva sandstone. The well intermittently flowed oil if mud weight fell below 13.2 pounds per gallon, indicating a reservoir pressure in excess of 3,800 PSI. On December 30 the drill pipe became stuck at a measured depth of 7,063 feet. Several unsuccessful attempts were made to free the pipe. At this point the decision was made to leave the drill pipe and drilling assembly in the hole and complete the well rather than risk losing the well-bore (Fig. 4.2.1b). Of the 2,800 feet of horizontal section planned, only 1,011 feet were drilled. Despite this setback, the well showed promise as a producer.

Figure 4.2.1b. Photograph of a technician preparing the MWD (measurement while drilling) tool prior to horizontal drilling. This tool, along with the rest of the drilling assembly and drill pipe became permanently stuck in the hole.

Tests were conducted and it was determined that perforation guns could adequately penetrate the drill pipe. Eventually, a four foot interval in the middle of each section of drill pipe was perforated. Due to the high pressure in the field from water injection the well was initially capable of flowing approximately 65 BOPD and 800 BWPD. In March of 2000 the ESU 13-H was equipped with an electronic, submersible pump. This increased daily production to approximately 250 BOPD and 1700 BWPD.

4.2.2 Eva South Production History

Figure 4.2.2a shows the production history of Eva South. Significant events are noted, particularly the completion of the ESU 13-H.

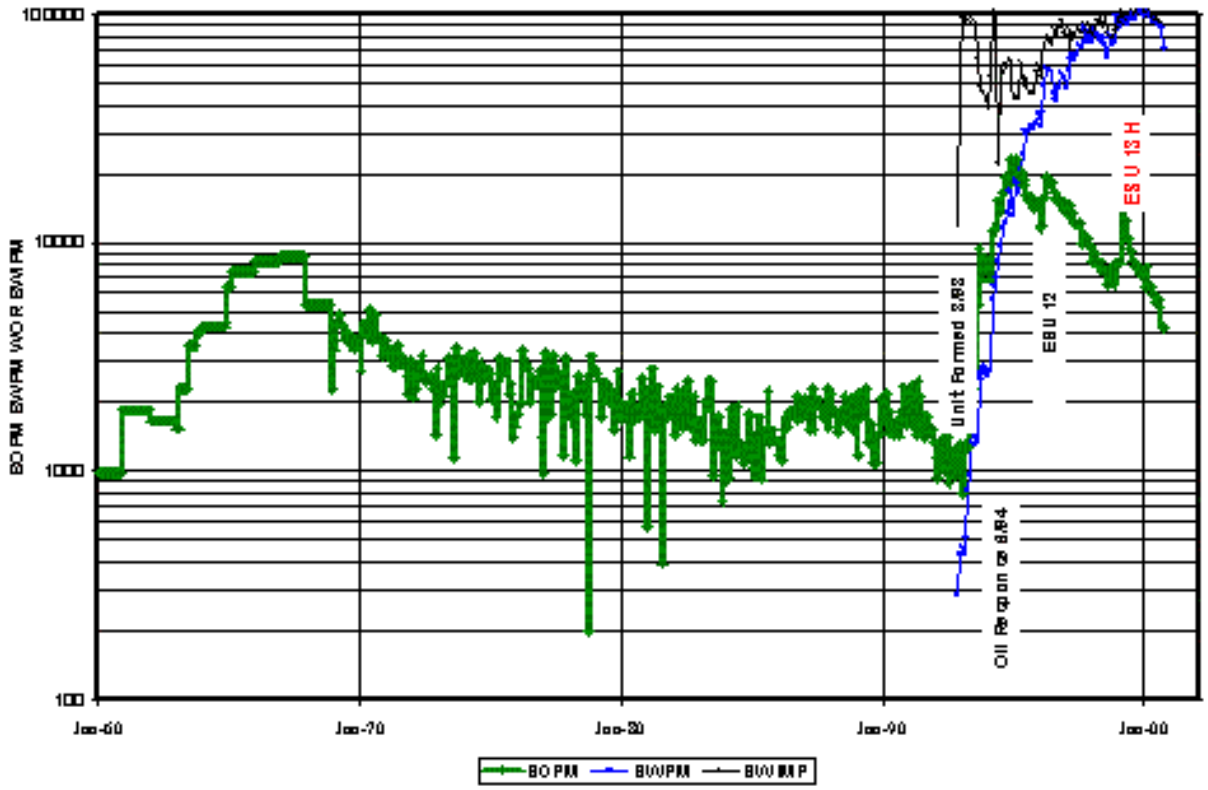

Figure 4.2.2a. Production history of Eva South from discovery to November 2001. Notable features include the rapid and pronounced response to the waterflood and the spikes in production due to completion of the ESU 12 and 13-H wells.

As evident from the graph, the waterflood at Eva South was very successful. Primary recovery from field discovery until the unit was formed (8/1993) was 1,106 MBO with an estimated ultimate primary recovery of 1,228 MBO. The field quickly responded to water injection with a peak production rate of well over 20 MBO per month. Prior to completion of the ESU 13-H, secondary recovery (9/1993-1/2000) was 851 MBO with estimated ultimate secondary recovery projected at 961 MBO.

<u>ESU 13-H Incremental Reserves</u>

The effect of adding the ESU 13-H to the unit is documented in Figure 4.2.2b.

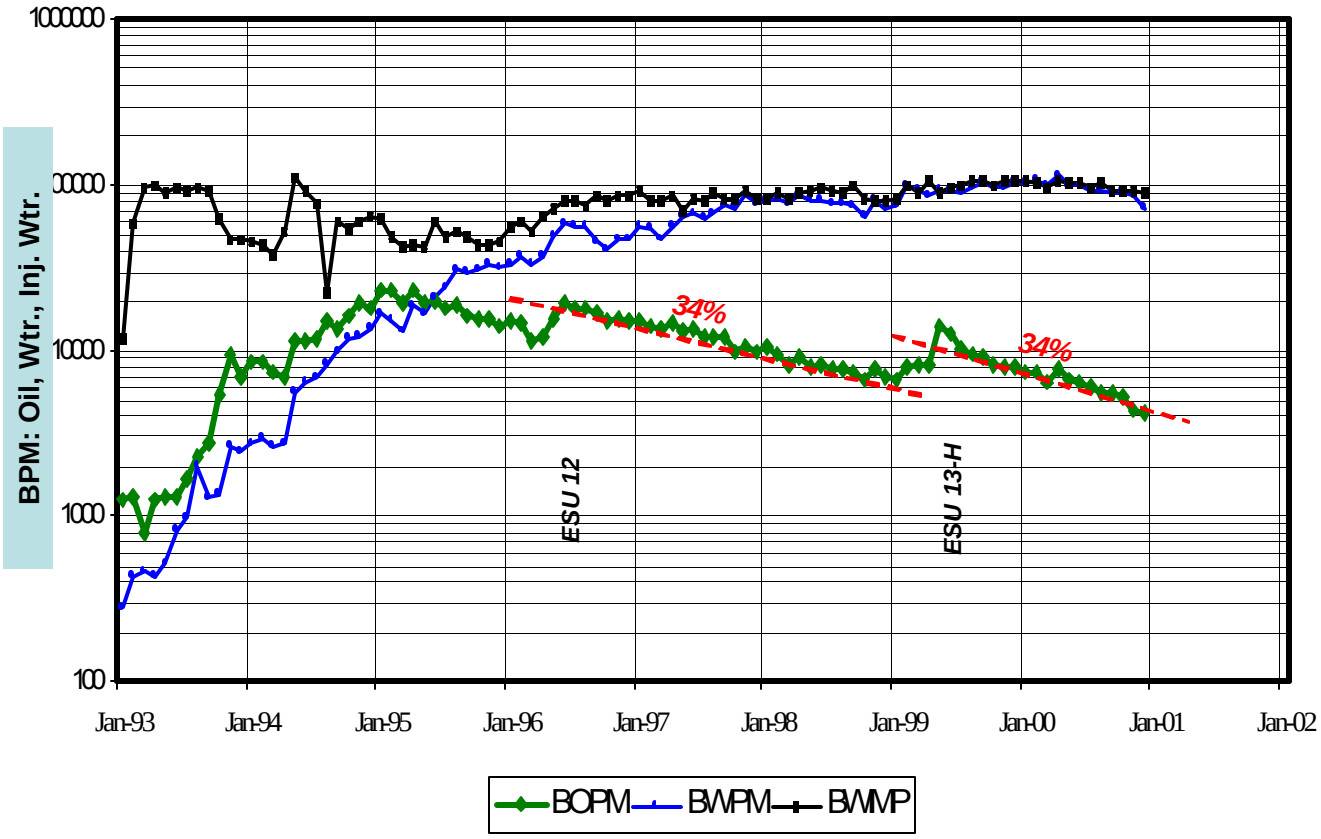

Figure 4.2.2b. Detail of Eva South production history showing the results of adding the ESU 13-H. Prior to drilling the 13-H the field had a steady decline of 34%. After completion of the 13-H the field returned to the same rate of decline. Incremental reserves are the difference between projecting the ultimate recovery with and without the ESU 13-H and represent approximately 122 MBO.

With the ESU 13-H the estimated ultimate secondary recovery for the field is now projected to be 1,083 MBO. Therefore, incremental reserves added by the ESU 13-H are 122 MBO (1,083 – 961 = 122). These additional reserves are a result of the improved sweep efficiency provided by the horizontal well.

Unfortunately, the success in gaining the incremental reserves from the ESU 13-H was offset by the high cost of the well. Due to the severe drilling problems experienced in this well, and the fact that expensive drill pipe and directional drilling equipment had to be left in the hole, the total cost of drilling and completion was approximately $1,473,000. Consequently, overall economics of the well are marginal. Nevertheless, recalling that the well only attained approximately one third of the targeted horizontal displacement in the reservoir is promising. If the full length had been drilled at or near the expected cost (approximately $745,000), incremental reserves could have easily been doubled, resulting in very favorable economics.

Comparison of Actual vs. Predicted Performance

Based on production data up to the time the project proposal was written (5/1999) ultimate secondary recovery, without any additional development, was estimated at 1,164 MBO. As actual production figures were collected during the project this number was revised to 961 MBO. The estimated ultimate secondary combined with the 1,228 MBO of primary production yields a total recovery for the field of 2,067 MBO. Total recovery divided by the original oil in place (7,225 MBO) yields a recovery factor of 28.6% (revised from 33.9% estimated in the proposal).

In the project proposal it was hoped that an additional 6% of the original oil in place could be recovered through the drilling and completion of three new horizontal wells; 2% additional recovery for each well, representing approximately 150 MBO of incremental reserves per well. Although only one new horizontal well was drilled, the ESU 13-H added incremental reserves of 122 MBO. This represented 1.7% of the original oil in place. Had the well been drilled to the full extent planned the ultimate recovery would have certainly been higher. Therefore it is fair to conclude that the one horizontal well drilled did perform to expectations and demonstrates the ability of horizontal wells to substantially improve sweep efficiency in a Morrow sandstone waterflood.

5.0 CONCLUSIONS and RECOMMENDATIONS

5.1 3C3D Seismic

The Eva South 3D seismic survey yields a great deal of useful information about the geology of the field and at the same time illustrates some of the limitations in using this type of seismic data.

The most practical information about the field was obtained from the P-wave seismic data. While the potential value in using PSV-wave data in this type of geologic setting was demonstrated, there is no denying that the P-wave data is of more immediate use in seismically characterizing Eva South. The greatest value in the type of 3D seismic information gathered at Eva South may be in exploration and early development drilling. There is not as much confidence in the ability of the seismic data to resolve reservoir detail at a high level of precision. Still, a good picture of the Eva South reservoir emerged and it would suggest that the field has been exploited in an efficient manner and that no appreciable accumulations have been by-passed by the current secondary recovery program.

The P-wave seismic data revealed that the Teepee Creek fault which bounds the west side of the Eva South is one of a series of faults most likely related to a wrench fault system.

The sandstone reservoir geometry was delineated reasonably well by P-wave seismic event amplitudes. The reservoir creates a discrete and unique seismic event at the seismic frequencies available in the P-wave data (approximately 90 hertz). Amplitude

maps of the actual event are most useful, but an approach using time window amplitude extractions referenced from more regional, and less interpretive, seismic horizons also yields a good description of the reservoir geometry. Though the existence and overall geometry of the reservoir sandstone can be defined by these amplitude maps, plots of seismic amplitude versus net sandstone thickness do not yield strictly linear relationships. As a result, an interpretative approach to making a final reservoir isopach map was of greater practical use than one based on numerical computation.

The relationship of P-wave seismic amplitude to net sandstone was found to be linear from 10 to 30 feet in thickness. Below 10 feet the relationship breaks down due to the inability of the seismic data to detect the thinnest sandstones; above 30 feet the seismic amplitudes decreases due to tuning effects. No significant improvement upon the relationship was gained by filtering the seismic data to lower frequency.

The P-wave amplitude maps are generally in good agreement with known reservoir compartments; known abandoned channel-fill deposits were imaged as low-amplitude discontinuities. No additional, previously unknown, compartments were identified. Indications of additional, subtle intra-reservoir discontinuities in the form of lineaments that may represent minor faults are not supported by the engineering data. While these subtle seismic discontinuities may be describing real geologic changes, they do not appear to influence reservoir production performance.

Offset dependency on the P-wave seismic amplitudes was analyzed by re-stacking the 3D volume within ranges of 0-3300 feet (near-offset) and 3300-12000 feet (far-offset). While the amplitude maps of the Eva SS seismic event for the near-offsets and far-offsets show differences, they do not provide any additional detail or information beyond the full-offset volume. A difference volume created by subtracting the near-offset volume from the far-offset volume likewise did not provide any additional information. The analysis of the offset volumes does not provide any additional insight into why the thickest sandstones at Eva South show a decrease in seismic event amplitude in the full offset P-wave volume.

An interpretation of the radial component of the PSV-wave data shows a good correlation of the Eva SS seismic event amplitude to the Eva sandstone thickness. A plot of the amplitudes versus net sandstone thickness showed two parallel trends which correlate into specific areas of the field. The distribution of amplitude does conform generally to the CCP fold of the PSV-wave data at the Morrow interval suggesting the possibility of an acquisition geometry overprint. A comparison of the amplitude of an overlying carbonate seismic event from what should be a uniform geologic horizon again shows amplitude that focuses in the center of the survey. However, the apparent axis of the amplitude trend of the Eva SS seismic event aligns along the known axis of the reservoir; the apparent axis of the overlying carbonate amplitude trend aligns more closely to the orientation of the fault system at. The area of the field where the amplitude trends coincide most closely is the same area where the plot of Eva SS seismic event amplitude versus net sandstone thickness shows a second but higher amplitude trend. The alignment of the Eva SS seismic event amplitude suggests some

measure of correlation to the Eva sandstone, while the alignment of the overlying carbonate amplitude to the fault system may suggest a fracture influence on the trend.

A CCP supergather from the center of the PSV-wave radial-component volume sorted by azimuth shows a distinct azimuthal influence on the data suggesting a measure of S-wave splitting. This is confirmed by the appearance of the seismic reflection energy in the PSV-wave transverse component. The supergather from the center of the survey suggests that a fast direction is along 130-degrees azimuth, and a slow direction at 220-degrees azimuth. The PSV-wave data were rotated into these two azimuths and final stack volumes created to analyze the apparent S-wave splitting. Amplitudes of the Eva SS seismic event are much stronger on the 130-degrees volume, though the fault framework is more apparent in amplitude on the 220-degrees volume. The two-way travel times to the Eva SS seismic event show that the regional area outside the fault frameworks displays a fast direction at 130-degrees, generally acknowledged as the principle stress direction in the area. Within the fault system, the apparent fast direction changes radically.

A calculation of apparent seismic anisotropy from the two PSV-wave azimuth volumes likewise shows a high degree of variability. Negative anisotropy values suggest that the fast-velocity direction deviates greatly from the 130-degrees direction suggested by the supergather in the center of the survey. All of the analyses of the azimuth volumes revealed a complicated pattern of varying anisotropy and apparent fracture orientation that deviates from a direction suggested by fault orientations. One possible explanation for this is that differential strike-slip movement on the faults created internal rotation of that changed the direction of stress and fracturing. This might explain why outside the fault areas the apparent fast direction more closely aligns to the regional principle-stress orientation. Since the vertical displacement of the faults is observed to die out into the shallow section, it is likely that there are vertical changes in anisotropy and stress as well. The only way to accurately construct a horizon specific analysis may be to remove the overlying effects by a layer-stripping approach. It is also apparent that a singular assumption of rotating to one fast-azimuth is not valid.

The Vp/Vs calculations showed some contribution on the PSV-seismic response from the Eva sandstone reservoir. That observation coupled with the amplitude map of the Eva SS seismic event offers encouragement in the application potential of PSV-wave data to map upper Morrow reservoirs. But while it appears that the PSV-wave Eva SS seismic-event amplitudes contain a contribution of reflection energy from the Eva sandstone, it is also apparent that there are azimuthal effects on the amplitude as well as some influence from the acquisition geometry. If the PSV-wave response of the Eva sandstone is to be isolated to a degree high enough to be used in detailed reservoir interpretations, it will be necessary to analyze and remove vertical anisotropy variations by layer stripping as well as investigate rotation directions at a much more robust level than was possible in this data analysis.

Though there is some disappointment in the level of precision that could be achieved in an interpretation of the PSV-wave data, it should not be left unstated that the data

revealed a great deal of information about potential stress and fracture mechanisms in the fault system at Eva South. This information may not be critical to the production at Eva South, but the ability of the PSV-wave data to evaluate these types of systems may be of great benefit in other geologic settings and warrants further study and attention.

For future applications, it can be concluded that high frequency P-wave data is a good tool for exploration and development of upper Morrow reservoirs. An exploration model was developed based on the coincidence of differential compaction-structure with anomalous upper Morrow amplitudes.

It must be reiterated that the original objective of the Eva South 3D seismic survey was weighed heavily towards high-quality P-wave data, and that extraordinary attempts to maximize the PSV-wave data were not undertaken. For future PSV-wave surveys, the acquisition lessons learned at Eva South would suggest the following:

- Greater attention should be given to the offset requirements for optimal PSV-wave generation from a P-wave source. Recording longer source to receiver offsets at Eva South could have improved the quality of the PSV-wave data.
- A source frequency much lower than typical P-wave data should be considered to achieve good bandwidth of the PSV-wave data that by nature is much lower than P-wave data. For vibroseis applications it might be appropriate to consider a separate sweep for the high frequency P-wave data and a separate lower frequency sweep for the PSV-wave data at the same source point. This will increase the acquisition time but help maximize the quality of both datasets. A more practical approach may be to use a dynamite source and a 24-bit recording system with no low-cut filter to capture the broadest spectral range of data possible.

The processing of PSV-wave data is and will continue to be a demanding undertaking requiring great attention to detail and extraordinarily high degrees of iteration. Improvements in all facets of PSV-wave processing are continually occurring. Some examples are improvements in handling asymptotic binning issues, a better understanding of the variability in Vp/Vs ratios especially in the shallow section, more robust approaches to rotation analysis and application, and more computationally efficient ways to evaluate and correct for vertically varying anisotropy effects by layer stripping applications.

5.2 Horizontal Drilling

The project proposal called for the drilling of a minimum of one and maximum of three horizontal wells. If three horizontal wells could have been drilled, it was predicted that an additional 6% of the OOIP could be recovered. This represented total incremental reserves of 450 MBO, or 150 MBO per well (2% of the OOIP per well). Feasibility

studies based on seismic and engineering data indicated that only one well, the ESU 13-H was justified. As noted, this well experienced severe drilling problems that greatly escalated the cost and ultimately cut the planned horizontal displacement by nearly two thirds. Despite these setbacks, the well was successful in adding incremental reserves of 122 MBO, representing 1.7% of the OOIP. These results indicate that horizontal wells can significantly increase sweep efficiency and ultimate recovery in Morrow waterfloods. It is expected that horizontal wells would be equally effective in similar Class I reservoirs and should be considered for widespread application.

The drilling problems encountered in the ESU 13-H could be avoided by careful advance planning. It is recommended that operators review the drilling records of all wells in a particular area for any indications of lost circulation problems. If present, the well-bore should be protected with intermediate casing prior to any directional drilling. In the case of the ESU 13-H, it is believed that the lost circulation originated in the Cherokee or Atoka section between 4,500 and 5,300 feet.

A second drilling problem encountered in the ESU 13-H was sloughing or caving shale in the upper Morrow, above the Eva sandstone. These problems were compounded by the high-angle to horizontal orientation of the well and the mechanical problems that delayed the setting of casing. It is recommended that horizontal wells in the Morrow be drilled until a few feet of the reservoir has been encountered. Casing should then be set immediately to minimize the potential for sloughing or caving of the shale. Once the Morrow shale is behind casing the drilling of reservoir sandstone should be routine.

REFERENCES/BIBLIOGRAPHY

Andrews, R.D., R.M. Knapp and Z. Bhatti, 1995, Fluvial-dominated deltaic (FDD) oil reservoirs in Oklahoma – the Morrow play: Special Publication 95-1, Oklahoma Geological Survey, 67 p.

Blott, J.E., 1997, Morrow valley-fill sandstone reservoir characterization with 3-D 3-C seismology, Sorrento Field, Colorado: PhD Thesis, Colorado School of Mines, T-5006, 223p.

Blott, J.E., T. L. Davis, and R.D. Benson, 1999, Morrow sandstone reservoir characterization – A 3-D multicomponent seismic success: The Leading Edge, March, Vol. 18, No. 3, p. 394-397.

Castagna, J.P. and M.M. Backus (*eds.*), 1993, Offset dependent reflectivity – Theory and practice of AVO analysis: Society of Exploration Geophysicists.

Englemark, F., 2000, Using shear waves to image reservoirs with low-impedance contrast: The Leading Edge, June, Vol. 19, No. 6, p. 600-603.

Garotta, R., 2000, Shear waves from acquisition to interpretation: Society of Exploration Geophysicists, Distinguished Instructor Series No. 3.

Hardage, B.A., 1996, Combining P-wave and S-wave seismic data to improve prospect evaluation: Report of Investigations No. 237, Texas Bureau of Economic Geology, 47 p.

Margrave, G., D. Lawton, and R. Stewart, 1998, Interpreting channel sands with 3C-3D seismic data: The Leading Edge, April, Vol. 17, No. 4 p. 509-513.

Miller, W.A. and D.M. Wheeler, 2000, 3C3D seismic characterization of the Eva South Morrow Sand Unit, Texas County, Oklahoma: 6th Annual 3-D Seismic Symposium, Rocky Mountain Association of Geologists.

Peyton, L., R. Bottjer and G. Partyka, 1998, Interpretation of incised valleys using new 3-D seismic techniques – A case history using spectral decomposition and coherency: The Leading Edge, September, Vol. 17, No. 9, p. 1294-1298.

Rampton, D.C., 1995, The shear difference – Improved characterization of a Morrow fluvial sandstone using the shear seismic response, Sorrento Field, southeast Colorado: Masters Thesis, Colorado School of Mines, T-4759, 146p.

Stewart, R.R. and J.E. Gaiser *eds*., 2000, Application and interpretation of converted waves: Society of Exploration Geophysicists, Continuing Education Short Course Notes, 382 p.

Tatham, R.H. and M.D. McCormack, 1991, Multicomponent seismology in petroleum exploration: Society of Exploration Geophysicists, Investigations in Geophysics, No. 6, 248 p.

Van Dock, R. and J. Gaiser, 2001, Stratigraphic description of the Morrow Formation using mode-converted shear waves - Interpretation tools and techniques for three land surveys: The Leading Edge, September, Vol. 20, No. 9, p. 1042-1047.

Wheeler, D.M., A.J. Scott, V.J. Coringrato and P.E. Devine, 1990, Stratigraphy and depositional history of the Morrow Formation, southeast Colorado and Western Kansas, *in* S.A. Sonnenberg, L.T. Shannon, K.R. Rader, W. F. Von Drehle and G.W. Martin eds., Morrow Sandstones of Southeast Colorado and adjacent Areas: 1990 Rocky Mountain Association of Geologists Guidebook, Denver, Co., p. 9-37.

Wilson, T.C., T.L. Davis, D.M. Wheeler, W.A. Miller and M. Sterling, 2001, Using converted waves to detect a Morrow sandstone reservoir: 71st Annual International Meeting, Society of Exploration Geophysicists, Expanded Abstracts, p. x-x.

Wilson, T.A., 2001, Creating a converted wave synthetic: *in* M. Terrell ed., Spring 2001 Sponsor Meeting Notes, Reservoir Characterization Project, Colorado School of Mines, p. 21-22.

Wilson, T.A., in prep, Detecting a Morrow sandstone reservoir with converted wave at the Eva South Field, Texas County, Oklahoma: Masters Thesis, Colorado School of Mines.

LIST of ACRONYMS and ABBREVIATIONS

AMP	Amplitude
API	American Petroleum Institute, Gravity of Oil in Degrees
AVO	Amplitude Versus Offset
BO	Barrels of Oil
BOPD	Barrels of Oil per Day
BW	Barrels of Water
BWPD	Barrels of Water per Day
CDP	Common Depth Point
CCP	Common Conversion Point
DMO	Dip Moveout
DOE	United States Department of Energy
EOC	Ensign Operating Company
ESU	Eva South (Morrow) Sand Unit
Fm	Formation
Ft	Feet
MBO	Thousand Barrels of Oil (stock tank)
MBW	Thousand Barrels of Water
Md	millidarcys
ms (msec)	milliseconds
OOIP	Original Oil in Place (stock tan
P (wave)	Compressional seismic wave
PSI(G)	Pounds per Square Inch (Gravity)
PSV	P to S converted seismic wave
SEC	Seconds
S (wave)	Shear seismic wave
S1	Maximum Horizontal Stress Direction
S2	Minimum Horizontal Stress Direction
SH	Shear in the horizontal plane
SS	Sandstone
STBO	Stock Tank Barrels of Oil
SV	Shear in the vertical plan
TD	Total Depth
Vp	Velocity of P-wave
Vs	Velocity of S-wave
2D	Two-Dimensional Seismic
3D	Three- Dimensional Seismic
3C3D	Three-component, Three-dimensional Seismic

Quarter Section Abbreviations:

NW	Northwest
NE	Northeast
SW	Southwest
SE	Southeast

Improved Miscible Nitrogen Flood Performance Utilizing Advanced Reservoir Characterization

DE-FC26-00BC15121

Program

This project was in response to DOE's solicitation DE-PS26-99BC15144, Reservoir Class Field Demonstration Program – Class Revisit. The goal of the Class Program was to extend the economic production of domestic fields, by slowing the rate of well abandonments and preserving industry infrastructure, and to increase ultimate recovery using improved reservoir characterization and advanced technologies.

Project Goal

The goal was to increase production at the East Binger unit of Binger Field by use of improved nitrogen injection technology, and explore the use of horizontal wells. The project was to determine if widely available N_2 is cost-effective for a miscible flood and if horizontal wells can reduce gas break-through and cycling. It is expected that the demonstration will lead to implementation of nitrogen (N_2) injection projects in areas without readily available carbon dioxide sources. Technology transfer will occur throughout the project.

The objectives are to demonstrate that nitrogen is a widely available, cost-effective and environmentally superior injectant for miscible floods, and explore the use of horizontal wellbores for N_2 floods.

Performer

Binger Operations, LLC, Cody, WY

Project Results

The project has successfully demonstrated technologies for N_2 flooding of fluvial-dominated deltaic reservoirs.

Benefits

The most obvious benefit of N_2 injection is its availability in areas where CO_2 is not available for EOR. Nitrogen is more "portable" and can be utilized anywhere a nitrogen plant or air separator can be built. It does not necessitate having a source nearby or a pipeline infrastructure in order to bring distant injection gas to the field. Binger Operations bought the local N_2 generation plant and is able to produce N_2 at $0.35 per MCF, making it a very cost-effective injectant. In addition N_2 is environmentally superior to CO_2 for injection and handling and is less corrosive, but requires much higher pressure to achieve miscibility with oil. Identification of channeling and improved N_2 injection techniques coupled with horizontal injection have significantly reduced gas breakthrough and loss of miscible pressure. In FY03 production from the EBU increased 30% due to improved N_2 injection.

Chiller in an air separation/compression unit.

Background

The East Binger Unit (EBU) located in the Anadarko Basin of Caddo County, Oklahoma produces from the Pennsylvanian Upper Marchand sand, Class I Fluvial Dominated Deltaic reservoir located at a depth of 9,000 to 10,100 ft. The Marchand reservoir covers 13,000 acres at EBU. Production from 5,300 acres on Indian lease lands will benefit the Caddo Tribe.

Original oil in place for the reservoir is estimated at 115 MMbbl. To date approximately 20 MMbbl have been recovered; primary recovery processes produced 3 MMbbl, enhanced oil recovery (EOR) processes recovered the additional 17 MMbbls. Phillips Petroleum started enhanced oil recovery experimenting with flue gas (80% N_2, 20% CO_2) injection in the 1970s, but experienced immediate gas break through. In 1986 a change was made to N_2 injection. By 1998 when Binger Operations took over the field, oil recovery was declining due to gas injection problems involving early breakthrough and loss of miscible pressure caused by gas channeling in the Marchand sand.

Binger's project reassessed EOR technologies. CO_2 was ruled out because there was no close source and transportation costs make its use prohibitive. Nitrogen was selected because it has the advantages of being widely available, cost-effective, and as an injectant for miscible floods. Binger purchased facilities in 2001 for nitrogen injection, making the project more cost-effective.

Project Summary

- Drilled and completed a horizontal well
- Gathered all pre-drilling reservoir data # pressure surveys on 13 wells, injection profiles on 4 wells, production profiles on 2 wells, and gas compositions on 50 of the

Air separation and compression facility for N_2 injection plant at East Binger Unit, Caddo County, OK.

Air separation plant, East Binger Unit, Caddo County, OK.

Unit's 55 producing wells (the other 5 wells are in fringe areas unlikely to be impacted by the project or have been shut-in for an extended period due to a high nitrogen content in produced gas)

- Built web site for technology transfer and updated with company information, field history, project description, and quarterly reports
- Updated full-field model with production data through April 2000 and re-run history match
- Built pilot area model; history match of same is nearing completion, and
- The horizontal well was hydraulically fractured in early November 2003, following repeated attempts to improve production by other means. Early production performance has been positive. The well was originally intended for N_2 injection, but was changed to production to learn as much as possible about horizontal performance with one horizontal well.

This project is intended to improve the performance and efficiency of the EBU's miscible N_2 flood through the use of improved nitrogen injection techniques combined with horizontal wellbores. Recent drilling results are validating a new understanding of the sweep mechanisms in this miscible N_2 flood. Two wells drilled in early 2004, EBU 44-3 and EBU 46-3, are producing at > 200 bbl/d combined, at near solution gas-to-oil ratio (GOR) and with very little N_2. These wells were both drilled in areas previously suspected of being swept by the nitrogen injectant.

When this project was proposed and initiated in 2000, Binger Operations believed that the primary mechanism of N_2 cycling in the reservoir was gravity segregation, with N_2 overriding the oil. In other words, the problem appeared to be poor vertical sweep. The proposed solution was placing horizontal producing wells near the base of the producing interval. By late 2003, three horizontal wells and one vertical well had been drilled. Oil production combined with additional study of the reservoir, have led to a significantly different understanding of the flow mechanisms in the reservoir.

All indicators now suggest that the problem is one of areal sweep. The first indication that gravity segregation might not be a major problem came with the completion of the first horizontal well, EBU 37-3H, drilled in 2001. Because of the concern of gravity segregation, Binger Operations intended to complete this well without a hydraulic fracture treatment, as it was expected that such a treatment would connect with overriding N_2 at the top of the reservoir. However, after a number of unsuccessful attempts to stimulate production in the well, a hydraulic fracture treatment was pumped. Unexpectedly, the N_2 content of produced gas actually decreased!

Over the next two years, two additional horizontal wells were drilled and hydraulically fractured. In both cases, the N_2 content in the produced gas stayed level or dropped after the treatment. Over the same time period, the production and injection data from individual wells was further studied. Combining the results of the horizontal wells and new data led to a new understanding: the primary mechanism of N_2 flow and cycling appears to be fractures – either natural or hydraulic – aligned in a predominantly east-west direction. Armed with this new understanding, Binger Operations drilled two new vertical wells in areas previously thought to have been swept by nitrogen. Both wells came on at near solution GOR, with less than 3% N_2 in the produced gas.

These results indicate the importance of continually studying the reservoir, as well as understanding the implications of how wells are drilled and completed. Binger Operations is testing this new hypothesis with additional drilling.

Current Status

Oil production and monitoring of N_2 flow continues. An evaluation of the value of horizontal wells at EBU is underway.

Project Start: April 11, 2000
Project End: April 10, 2005

Contact Information:
NETL – Gary Walker (gary.walker@netl.doe.gov or 918-699-2083)
Binger Operations – Joe Sinner (binger@180com.net or 307-527-2869)
1401 Sheridan Ave., Ste. 205, P.O. Box 2850, Cody, WY 82414

USING RECENT ADVANCES IN 2D SEISMIC TECHNOLOGY AND SURFACE GEOCHEMISTRY TO ECONOMICALLY REDEVELOP A SHALLOW SHELF CARBONATE RESERVOIR: VERNON FIELD, ISABELLA COUNTY, MI.

TYPE OF REPORT: ANNUAL

REPORTING PERIOD START DATE: APRIL 1, 2003

REPORTING PERIOD END DATE: MARCH 31, 2004

PRINCIPAL AUTHORS:

JAMES R. WOOD, MICHIGAN TECHNOLOGICAL UNIVERSITY, HOUGHTON, MI
A. WYLIE, MICHIGAN TECHNOLOGICAL UNIVERSITY, HOUGHTON, MI
W. QUINLAN, JORDAN EXPLORATION COMPANY LLC, TRAVERSE CITY, MI.

DATE REPORT WAS ISSUED: APRIL, 2004

DOE AWARD NUMBER: DE-FC26-00BC15122

NAME AND ADDRESS OF SUBMITTING ORGANIZATION:

MICHIGAN TECHNOLOGICAL UNIVERSITY
1400 TOWNSEND DRIVE
HOUGHTON, MI. 49931

DISCLAIMER

This report was prepared as an account of work sponsored by an agency of the United States Government. Neither the United States Government nor any agency thereof, nor any of their employees, makes any warranty, express or implied, or assumes any legal liability or responsibility for the accuracy, completeness, or usefulness of any information, apparatus, product or process disclosed, or represents that its use would not infringe on any privately owned rights. Reference herein to any specific commercial product, process, or service by trade name, trademark, manufacturer, or otherwise, does not necessarily constitute or imply its endorsement, recommendation or favoring by the United States Government nor any agency thereof. The views and opinions of authors expressed herein do not necessarily state or reflect those of the United States Government.

ABSTRACT

One of the main objectives of this demonstration project is to test surface geochemical techniques for detecting trace amounts of light hydrocarbons in pore gases as a means of reducing risk in hydrocarbon exploration and production. As part of the project, several field demonstrations were undertaken to assess the validity and usefulness of the microbial surface geochemical technique. The important observations from each of these field demonstrations are briefly reviewed in this annual report. These demonstrations have been successful in identifying the presence or lack of hydrocarbons in the subsurface and can be summarized as follows:

1. The surface geochemistry data showed a fair-to-good microbial anomaly that may indicate the presence of a fault or stratigraphic facies change across the drilling path of the State Springdale & O'Driscoll #16-16 horizontal demonstration well in Manistee County, Michigan. The well was put on production in December 2003. To date, the well is flowing nearly 100 barrels of liquid hydrocarbons per day plus gas, which is a good well in Michigan. Reserves have not been established yet. Two successful follow-up horizontal wells have also been drilled in the Springdale area. Additional geochemistry data will be collected in the Springdale area in 2004.
2. The surface geochemistry sampling in the Bear Lake demonstration site in Manistee County, Michigan was updated after the prospect was confirmed and production begun; the original subsurface and seismic interpretation used to guide the location of the geochemical survey for the Charlich Fauble re-entry was different than the interpreation used by the operator who ultimately drilled the well. As expected, the anomaly appears to be diminishing as the positive (apical) microbial anomaly is replaced by a negative (edge) anomaly, probably due to the pressure draw-down in the reservoir.
3. The geochemical sampling program over the Vernon Field, Isabella County, Michigan is now interpreted as a large negative anomaly associated with the entire field. The results of the State Smock horizontal well and the Bowers 4-25 well confirmed the lack of additional recoverable hydrocarbons in the Vernon Field.
4. The surface geochemistry data showed a strong anomaly in the Myrtle Beach, Burke County, North Dakota area that would justify drilling by itself and even more so in conjunction with the structural interpretation from the geological and geophysical data; the microbial values here were the highest we have observed. The Myrtle Beach geochemical survey indicated a good to excellent prospect which was confirmed by drilling, however, a pipeline has not yet been completed that would allow the wells to be placed into production.

We also present in this annual report the results of recent efforts to map carbonate facies tracts in the middle Devonian Dundee and Rogers City Limestones using gamma ray, bulk density, and photoelectric effect geophysical well log amplitudes. This work was undertaken to identify fairways for exploration in the Dundee and Rogers City where surface geochemical techniques could then be used to screen potential leads.

TABLE OF CONTENTS

TITLE PAGE 1
DISCLAIMER 2
ABSTRACT 3
LIST OF GRAPHICAL MATERIALS 5

1.0 EXECUTIVE SUMMARY 7

2.0 EXPERIMENTAL 11
- 2.1 Sampling Program 11
- 2.2 Sample collection 11
- 2.3 Analytical Procedures 12
  - 2.3.1 Solid-phase microextraction (SPME) 12
  - 2.3.2 MOST 13
  - 2.3.3 Sorbed Soil gas 13
  - 2.3.4 Surface Iodine 13
  - 2.3.5 Trace Element and Rare Earths - Enzyme Leach Selective Extraction 14
  - 2.3.6 Activated Carbon 14
- 2.4 Geochemistry Sample Collection – Michigan and North Dakota 14
- 2.5 Geochemistry Program in Springdale Area, Manistee County, Michigan 14
- 2.6 Geochemistry Program in Bear Lake Area, Manistee County, Michigan 15
- 2.7 Geochemistry Program in Vernon Field Area, Isabella County, Michigan 15
- 2.8 Geochemistry Program in Myrtle Beach Area, Burke County, North Dakota 15
- 2.9 Subsurface Mapping of Dundee and Rogers City Limestones, Michigan 15

3.0 RESULTS AND DISCUSSION 17
- 3.1 Summary - Springdale Area - Manistee County, Michigan 17
- 3.2 Summary - Bear Lake Area - Manistee County, Michigan 17
- 3.3 Summary - Vernon Area - Isabella County, Michigan 17
- 3.4 Summary - Myrtle Beach Area, Burke County, North Dakota 17
- 3.5 Dundee and Rogers City - Regional Facies Tract Mapping 18
  - 3.5.1 Stratigraphy 18
  - 3.5.2 Well Log Tomography - Gamma Ray, Bulk Density and Photoelectric Effect 20
  - 3.5.3 Depositional Model 23

4.0 CONCLUSIONS 26

5.0 REFERENCES 27

6.0 FIGURES 30

LIST OF GRAPHICAL MATERIALS

Figure 1. Index map showing locations of all geochemical sampling in Michigan and North Dakota.

Figure 2. Generalized Stratigraphic Column for the Michigan Basin.

Figure 3. Generalized Stratigraphic Column for the Williston Basin. Black dots are key productive intervals in the Myrtle Beach area.

Figure 4. Springdale area wells and surface geochemical sample locations. Red well path is St. Springdale & O'Driscoll 16-16 HD1 (Permit 55782). Large red circles are bottom hole locations (bhl) of horizontal wells; pink circles are bottom hole locations of deviated wells.

Figure 5. Microbial contour map of the Springdale Prospect in Manistee County, Michigan. Red well path is St. Springdale & O'Driscoll 16-16 HD1. Large red circles are bottom hole locations (bhl) of horizontal wells; pink circles are bottom hole locations of deviated wells. Green color filled contours indicate high microbial anomalies and yellow color filled contours indicate low anomalies. The change in the microbial anomaly along the path of the St. Springdale and O'Driscoll 16-16 HD1 may represent a fault or stratigraphic facies change.

Figure 6. Microbial sample location map for the Vernon Field and surrounding area in Isabella County, Michigan. Black triangles are microbial sample locations and the dark gray symbols are well locations.

Figure 7. Microbial sample location map and contour map for the Vernon Field and surrounding area in Isabella County, Michigan. Black triangles are the microbial sample locations. Blue color filled contours indicate high microbial anomalies and yellow color filled contours indicate low anomalies. The entire Vernon Field is a large negative anomaly.

Figure 8. Microbial sample and well location map for the Bear Lake area, Manistee County, Michigan.

Figure 9. Microbial sample location and contour map for Bear Lake, Manistee County, Michigan. Blue contours indicate high microbial anomalies and yellow contours indicate low anomalies. Location of Charlich-Fauble sidetrack is shown by pink line.

Figure 10. Microbial sample locations in the Myrtle Beach area. Microbial counts posted in red below sample location. Black outline is location of 3D seismic survey. Blue lines are rivers and lakes, Green lines are roads, subsea Winnipegosis tops for 3 deep wells posted in red. North is toward top of map.

Figure 11. Microbial contour and sample locations in the Myrtle Beach area. Red and Purple color filled contours indicate high microbial anomalies and green indicates low anomalies. Contour interval is 5 microbial counts. The high microbial counts recorded here are the highest recorded in the project to date.

Figure 12. Location map for 2003 Dundee-Rogers City producing wells (black dots) from the Michigan Department of Natural Resources (MDNR) production database. County names are also shown for reference.

Figure 13. (A) Stratigraphy diagram for the Dundee-Rogers City and surrounding Middle Devonian units from west to east across the central Lower Peninsula of Michigan (modified from Catacosinos et al., 1991). (B) Cross-sectional stratigraphy schematic from southwest toward the center of the basin, illustrating that the Bell Shale, Rogers City and Dundee intervals are all absent in portions of southwestern Michigan. Note that the vertical scale is exaggerated.

Figure 14. Outcrop and subcrop locations for the Detroit River Group and the combined Dundee-Rogers City ("Dundee") unit. A dotted line in the southwest region illustrates the absence of the Dundee Limestone due to erosion. Black closed circles represent wells used in the WLT slicing program and orange open circles locate the wells discarded before slicing.

Figure 15. Example digital well log, from the Alber #1-23 well, permit 40215 located in Mecosta County, Michigan. The gamma ray (GR) log curve is located on the left track of the well log with a color-filled amplitude. On the right track are the density (RHOB) log curve (red), neutron (blue) and photoelectric effect (green). The top picks are labeled on the depth scale in the center track. The Reed City is labeled but has no top pick because it is only a Member of the Dundee and is not present throughout the entire basin. The horizontal lines are the location of the amplitude slices shown in Figure 16.

Figure 16. Comparison of four proportional gamma ray, bulk density (rhob) and photoelectric factor (Pef) slices for the Dundee and Rogers City Limestones in the Michigan Basin (refer to Figure 15 for approximate slice locations). Note the subtle North-South trends in the gamma ray and pef slices. The rhob slices show the extent of the Reed City Member (anhydrite). The gamma ray slice data range is 0 to 30 api units and the contour interval for each slice is 3 api units. The rhob slice data range is 2.0 to 3.0 grams per cubic centimeter (g/cc) and the contour interval is 0.07 g/cc. The data range for each Pef slice is 0 to 10 barns per electron (b/e). The contour interval is 0.6 b/e. 300 wells were used in the gamma ray slices, 150 wells were used in the rhob slicing and 121 wells were used in the Pef slicing. Gray lines are county boundaries and gray numbers are county names. North is toward the top of the slices. Large white dots are data control points on each slice. Yellow and black rectangles show the location of the Vernon geochemical survey area.

Figure 17. (A) Slice 19 from the top-down Dundee Limestone results. (B) Taylor's (2001) depositional model for the upper Dundee superimposed onto slice 19 illustrating the similarity between the shelf trend in Taylor's model and the low gamma ray trend from the slicing results.

1.0 EXECUTIVE SUMMARY

New Findings

The project has located hydrocarbons a second demonstration site, the Springdale demonstration area (Figure 1) and the initial wells have begun production. The State Springdale-O'Driscoll #16-16 and the Hebart 12-16 are producing at approximately 100 barrels of oil per day and 100 mcf of gas per day, on average. Production is from the Brown Niagaran (Figure 2) interval. These wells are located on a mild geochemical anomaly (Figure 5). A third follow-up well is planned in the northeast quarter of section 21 early in 2004 and additional wells have been located in Section 16 that may be drilled later in 2004

The preliminary microbial geochemical survey over the new Springdale demonstration site shows an anomaly that suggested the presence of a fault crossing the projected path of the proposed 16-16 horizontal well; the horizontal well bore went from reservoir to non-reservoir rock at approximately this same position.

Lessons Learned

The basic lesson is that geochemical surveys should precede drilling in Michigan prospects. It is difficult to convince companies of the value of conducting surveys, but the results to date have been consistent, only marginal results (e.g. gas/oil) show when the geochemical anomaly is mediocre. Preliminary data from the new Springdale site suggests geochemical surveys may be able to indicate the location of faults or other discontinuities in the subsurface.

However, it appears that geochemical surveys over developed fields have to be interpreted with caution due to the disturbances caused by production (e.g. pressure drawdown) which seem to produce negative or apical anomalies in the vicinity of the well bore extending out at least 1/2 mile. Perseverance and patience are also virtues in this type of exploration, as well as adopting a consistent set of sample procedures.

Should Something Else Have Been Done?

We should have stipulated that all project demonstrations had to have surface geochemistry surveys included in the prospectus, that is, as part of the package used to sell the prospect to investors. This would both educate the gas and oil community as to the value of geochemistry as well as insure that we are notified sufficiently in advance of the drilling to make better sampling plans and have an opportunity to conduct a "fill-in" geochemical survey if the original survey shows gaps and/or holes.

Goals and Results

The goals of this project were to: (1) test the use of multi-lateral wells to recover bypassed hydrocarbons and (2) to access the potential of using surface geochemistry to reduce drilling risk and where possible locate and produce hydrocarbons based upon these surveys.

To date various applications of surface geochemistry have been applied to demonstration areas (Vernon, Myrtle Beach, Bear Lake and Springdale) with good success. The Bear Lake, Springdale and Myrtle Beach surveys indicated good-to-excellent prospects for hydrocarbons which were confirmed by drilling. The Vernon survey indicated poor prospects for hydrocarbons which were also confirmed by drilling.

In the Springdale area of Manistee County two successful horizontal wells have been drilled producing 100 barrels of oil per day (Figure 5). In the Bear Lake area in Manistee County, a successful re-entry lateral (Charlich-Fauble 2-9HD1) was drilled by a Michigan operator and has resulted in a well producing 200 barrels of oil per day. Results from the Bear Lake surface geochemical survey indicated this reef would probably be productive (Figure 9). Two demonstration wells, the State Vernon & Smock 13-23 HD1 and HD1A and the Bowers 4-25 #1, were drilled to test the Dundee formation at Vernon Field for bypassed oil and as predicted by the geochemical survey results, these wells did not find commercial hydrocarbons; several additional geochemical anomalies were discovered in the greater Vernon area that could be further investigated (Figure 7). In the Myrtle Beach area of North Dakota, the two existing wells are still shut-in, waiting on pipeline connections (Figure 11). Surface geochemistry in this area recorded the highest positive microbial anomalies we have obtained so far from our geochemistry sampling program.

Applications

The geochemical program will be focused now on Springdale, probably through the summer and fall of 2004. A wider area will be surveyed and new sampling techniques will be tested.

In the July-September, 2003 reporting period, as well as the October-December, 2003 period, the geochemical sampling program was extended with surveys conducted over three field sites in Michigan: Bear Lake, Springdale and Charlton 6 (Figure 1).

The protocols for the geochemical sampling program have now been established. All site locations are recorded using GPS receivers and duplicate samples are being stored at Michigan Tech. In the future, sampling will focus on using activated charcoal to trap soil gases followed by analysis by gas chromatograph. It appears that a technique that uses a known baseline is best since natural samples contain multiple gases that are difficult to interpret.

The results of the Bear Lake, Vernon, Springdale, and North Dakota geochemical surveys can be applied to other carbonate reservoirs worldwide. In particular, the application of appropriate surface geochemistry surveys seems warranted based on the work done here, as well as the advice to record the surveys at the same grid density as complimentary seismic data. The shallow-shelf and reef carbonates in the Permian Basin, the mid-continent, and Rocky Mountains (e.g. Williston basin) are logical targets for application of these techniques.

Did Data Support Project or Not?

The surface geochemistry data did support the demonstration projects quite well: it predicted that the demonstration wells would likely encounter or not encounter hydrocarbons. In other words, the geochemistry showed strong anomalies (Bear Lake, Springdale and Myrtle Beach) that would justify drilling on the basis of that data alone and even more so in conjunction with the seismic and subsurface well data.

Future Work

More geochemical work will be done in conjunction with further field demonstrations as part of this project in Michigan. New demonstration wells are planned for Michigan to test the Silurian reef play in another area. Preliminary results using both the Site Specific Micro Extraction (SPME) and the microbial techniques show good anomaly patterns for the Silurian Niagaran reefs. Activated carbon appears to hold good potential for detecting hydrocarbon anomalies and will be further evaluated in one or more demonstration areas.

Technology Transfer

A booth was set up at the Midwest PTTC horizontal well conference in Mt. Pleasant, MI in March, 2003 to show operators in the Basin the results of geochemical surveys in the basin. A technical paper on well log tomography was published in the April 2003 issue of the Bulletin of the American Association of Petroleum Geologists. A booth was set up with computer hardware at the Eastern Section Meeting of the American Association of Petroleum Geologist's in Pittsburgh, PA in September, 2003 to show live animations and visualizations of our regional mapping and geochemistry database to basin operators and technical personnel. A seminar was presented at Western Michigan University on well log tomography with examples from the Michigan Basin, including the regional fault interpretations in September, 2003. Computer demonstrations and discussions were held at the PTTC core workshop in Mt. Pleasant, MI in October, 2003.

An article on the Bear Lake geochemistry survey and successful horizontal re-entry was prepared for World Oil but was unable to be published due to confidentiality concerns of our industry partner. We plan to publish this article in the future.

An invited presentation was made at the U. S. Geological Survey in Reston, VA in December, 2003 on our regional mapping and fault delineation work. An article was published in the February 9, 2004 issue of the Oil and Gas Journal that highlighted our regional sample attribute mapping and fault delineation work. The annual planning meeting for our industry partners was held in Tampa, FL in early March 2004. Regional maps were posted for viewing by operators from the basin at the PTTC core workshop on March 19, 2004 in Mt. Pleasant, MI. Regional maps were also posted in a booth at the Michigan Oil and Gas Association's Annual Oil Conference on April 22, 2004 in Gaylord, MI and an oral presentation was made highlighting opportunities for exploration in the Michigan Basin. We participated at the Michigan Geological Society Annual Field Excursion from April 30 to May 2 with a presentation on our basin-scale mapping and by attend-

ing several of the field stops in the Traverse and Dundee carbonates. Presentations were also made at the monthly northern SPE meeting in April, 2004 and at the monthly, MBGS meeting in May, 2004.

Results and presentations from a portion of this technology transfer are available on the internet at http://www.geo.mtu.edu/~aswylie/indxhtml.htm while our main subsurface visualization web page (http://www.geo.mtu.edu/svl/) is being updated and expanded.

2.0 EXPERIMENTAL

The theory behind surface geochemical exploration is that direct hydrocarbon indicators leaking from a subsurface petroleum reservoir can be measured on the surface by geochemical methods. Surface geochemistry has been successfully used as an exploration technique for over 50 years. According to the American Petroleum Institute, new field wildcat success rates in the U.S. over the last 50 years peaked in 1979 with a success rate of 19%, however, wildcat drilling programs based upon surface geochemistry have regularly produced success rates over 50% (Davidson, 1994). Surface geochemistry has had many opponents over the years. The refusal of geologists to accept theories of vertical migration has drastically impeded the serious funding of research, and in turn widespread acceptance of surface geochemical exploration (Davidson, 1994). Smith and Ellis (1963) questioned the basis for surface geochemistry by claiming that ethane and heavier hydrocarbons could have grasses and other vegetation as their source, making surface geochemical methods useless. Horvitz (1972) conclusively demonstrated the error in Smith and Ellis' technique, and that organic matter, grass, and roots in the soil do not produce significant amounts of soil hydrocarbons, especially in the ethane through hexane range. This reveals that significant concentrations of hydrocarbons in the soil must have originated not from near surface organics, but from a much deeper source.

There are several different types of anomalies that stem from hydrocarbon seepage, both microseepage and macroseepage. The usual shapes include apical or focal anomalies, halo or doughnut shaped anomalies, and linear or straight-line anomalies. Direct hydrocarbon indicator techniques such as the SPME method can yield any shape of anomaly, but microbial techniques always yield focal anomalies (Kartsev et al., 1959; Price, 1986).

2.1 Sampling Program

Throughout this project, the field locations were sampled with both the soil gas technique that is being tested with this study, and in one or more locales the Geo-Microbial Technologies' MOST microbial method to compare and contrast against the SPME technique. These techniques have slightly different sampling methodology. Boleneus (1994) suggested that at least six samples need to be taken within the anomaly's vicinity to confirm the anomaly. In order to accurately delineate anomalies associated with Niagaran pinnacle reefs, which have a relatively small areal extent, a sampling grid spacing of 200 meters was chosen.

2.2 Sample collection

Microbial samples were taken according to the instructions of Geo-Microbial Technologies (Ochelata, Oklahoma). These soil samples were taken with a shovel at an average depth of 8 inches and placed into paper bags with roll-down tops that were provided by GMT. The samples consisted of approximately 4 ounces of soil. Immediately after collection the samples were shipped overnight to GMT for analysis of butane-consuming microbes.

SPME Samples were taken at approximately 1-meter depth using a cordless power drill with a 1-inch auger bit to drill down 1 meter. A core was then manually taken using a soil-coring tool with a 4-foot handle. The sample core was then quickly placed into 125 ml glass sample jars with a

septum in the lid and sealed. The sample jars were filled to the point that there was just enough room for the SPME fiber to fit in the headspace during extraction, approximately 2/3 full.

In the Vernon demonstration area, surface iodine, enzyme leach selective extraction, and sorbed soil gas samples were also collected for geochemical analyses. Surface iodine samples were collected from the top one inch of the A-horizon. Enzyme leach selective extraction samples were collected just below the top of the B-horizon. Sorbed soil gas samples were collected from approximately one-meter depth, placed into a metal collection can along with biocide.

The sampling technique for the activated carbon method consists of burying small granules and/or fibers of activated charcoal (~24-30 inches), then retrieving them after 15-20 days. Samples were taken in the Bear Lake area in Manistee County, Michigan and at the Bagley prospect area in Ogemaw County.

2.3 Analytical Procedures

2.3.1 Solid-phase microextraction (SPME)

The soil samples were kept on ice during transportation from the field to the laboratory to reduce the amount of microbial activity within the sample jars. The samples were then brought up to room temperature prior to analysis. The samples were manually shaken very briefly to break up the soil and laid on their side for SPME extraction. The septum on the sample jars was too thick for the blunt SPME needle to puncture without bending and destroying the fiber, so the septum was first pierced with a sharp syringe needle. The analyst then pushed the SPME needle past the septum that seals the sample vial and depressed the plunger, exposing the fiber to the headspace above the sample. The hydrocarbon analytes adsorbed to the coating on the fiber. After 10 minutes of exposure to the headspace gas the fiber is drawn back into the hollow needle, and the needle is removed from the sample vial. Finally, the needle is inserted through the septum in the gas chromatograph injector port. The adsorbed analytes are then thermally desorbed and brought to the gas chromatograph column via the carrier gas.

SPME Analytical Equipment

Analyses were carried out with a SRI 8610c gas chromatograph (GC) equipped with a flame ionization detector (FID) and hydrogen as carrier gas. Air for the FID combustion was supplied via a built-in air compressor on the 8610c. A Varian Chrompack CP7348, 25m long x 0.25mm in diameter, with a Porabond Q fused silica capillary column was used as the stationary phase. Samples were injected via the SPME sampler into a heated injection port held at 250 C. The standard injection port liner was replaced with a narrow bore (0.75mm) injection port sleeve to sharpen the peaks from the SPME techniques. The column oven was programmed to begin holding at 30 C for 5 minutes and then ramp at a rate of 10 C/min until it reached 200 C and was held there for and additional 5 minutes. Analyses were performed in the laboratory to a large extent and in the field to a small extent in order to determine the shelf life of the collected soil samples. In the laboratory the carrier and flame gas was supplied through compressed gas in tanks, in the field, the gas chromatograph was set up in the hotel with a SRI hydrogen generator producing the gas. Data acquisition and analysis were done with SRI's PeakSimple software.

SPME Calibration of Equipment

The laboratory equipment was calibrated using a standardized gas mixture of methane, ethane, propane, N-butane, N-pentane, and N-hexane. In the test gas mixture, each gas was present at 1000 ppm by mole. The test gas mixture was analyzed several times with the SPME fiber to determine the retention time for each individual hydrocarbon gas. The analyte adsorption and desorbtion was then varied to determine the optimum analysis procedures. The temperature program for the gas chromatograph's column oven also needed to be optimized for both speed of analysis and separation of the analytes in question. The test gas was then mixed with air to make mixtures of gases with analyte concentrations less than 1000 ppm. Mixtures with several different concentrations were analyzed with the gas chromatograph to calibrate the instrument so that retention areas could be converted to concentrations in parts per million. The retention areas turned out to be roughly linearly proportional to ppm concentrations. In this project, the actual concentration of hydrocarbons measured is not significant, but the proportion of one to another is very significant. When retention areas are converted over to ppm concentrations, some interpolation is required. In this study, to keep analytical error to a minimum, retention areas are used in the place of concentrations to compare one sample to another.

2.3.2 MOST

After receiving the soil samples, Geo-Microbial Technologies incubates the soil samples for one week in agar gel. Microorganisms tolerant to butanol are then selectively counted. The theory is that butane-consuming or butanol-resistant bacteria indicate hydrocarbon microseepage. As butane (and other hydrocarbons) migrates up through the soil, microorganisms will oxidize it, leaving butanol. In areas of high hydrocarbon seepage, the number of butanol resistant microbes is elevated. The number provided in GMT's laboratory report corresponds to the number of colonies of butane-oxidizing microbes that have grown in the laboratory on a Petri dish after seven days of incubation. Three separate dishes, or plates, are prepared for each soil sample; each is counted and the number reported is the average of the three plates (Schumacher, 2002).

2.3.3 Sorbed Soil gas

The sorbed soil gas method (Horvitz, 1985) involves acid extraction of light hydrocarbon gases that are sorbed onto clays or incorporated into carbonate cements in near-surface soils. The gases accumulate through microseepage from the hydrocarbon reservoir. Geo-Microbial Technologies, Inc. (GMT) determined the sorbed soil gases by flame ionization detector gas chromatography of the scrubbed and liberated gases. Soil samples were collected from approximately one-meter depth, placed into a metal collection can along with biocide (supplied by GMT). The concentration of light hydrocarbons can be used as an indicator of increased hydrocarbon microseepage. The ratios of the hydrocarbons, combined with published empirical soil gas ratios (Jones and Drozd, 1983) can be used to establish whether a prospect is in an oil, gas, or mixed prone region.

2.3.4 Surface Iodine

Iodine in surface soil samples has been demonstrated in the literature as an effective pathfinder for oil and gas in the subsurface (Gallagher, 1995). High concentrations of iodine are documented

elsewhere around the perimeter of subsurface oil and gas accumulations, "classic" halo anomaly, and directly above the accumulation, apical anomaly. The halo effect is interpreted as the surface expression of a reduction pipe above the oil and gas accumulation. Soil was collected from the top one inch of the A-horizon for surface iodine analysis. Data and interpretations for this survey are discussed in the geochemical conclusions.

2.3.5 Trace Element and Rare Earths - Enzyme Leach Selective Extraction

The enzyme leach selective extraction method is based on selective extraction of elements trapped on amorphous MnO_2 (Tompkins et al., 2000). Amorphous MnO_2 is a very effective trap for migrating cations, anions, and polar molecules. Oxidation anomalies are predicted over reduced bodies in the subsurface for a suite of elements including Cl, Br, I, As, Sb, Mo, W, Re, Se, Te, V, U, and Th (oxidation suite). Rare-earth elements often follow the same pattern as the oxidation suite. Base metals can be anomalous, but with lower contrast with the background. According to Clark, the most common form of oxidation anomalies is as a halo with a central low over the reduced body in the subsurface. These anomalies may be symmetric, asymmetric, or partial around the buried reduced bodies. Clark provides an electrochemical interpretation for halo oxidation anomalies. Apical anomalies are most often interpreted as related to faults. Since enzyme leach anomalies take 100's of years to develop, they will exist long after oil has been extracted from a reservoir. Soil samples for this technique are collected from just below the top of the B-horizon.

2.3.6 Activated Carbon

Activated charcoal samples were collected in the Bear Lake and Bagley prospect areas in Manistee and Ogemaw Counties, Michigan. This technique consists of burying small granules and/or fibers of activated charcoal (~24-30 inches), then retrieving them after 15-20 days and analyzing them in the Gas Chromatograph. This is a proven technique that has the advantage of looking at changes in a known sample and relating them directly to the sample environment. The disadvantage is that the samples have to be retrieved, necessitating two trips to the site. However, given the problems inherent in sampling material from the site itself, this technique seems to offer the most promise, both in terms of reliability and accuracy. It will be further tested, using substrates other than activate charcoal, over a variety of sites.

2.4 Geochemistry Sample Collection – Michigan and North Dakota

All geochemical data collected to date (1100+ samples) has been archived in a MS Access database. This database will be placed online along with interpretive text in the future.

2.5 Geochemistry Program in Springdale Area, Manistee County, Michigan

A surface geochemistry program was undertaken in the Springdale area, Manistee County, Michigan to determine if geochemical anomalies could discern the limits of the newly discovered Niagaran reservoir (Figures 1 and 5). The survey was designed to examine the microbial geochemical technique using activated charcoal as the collection media.

2.6 Geochemistry Program in Bear Lake Area, Manistee County, Michigan

A surface geochemistry program was undertaken in the Bear Lake area in order to discover if geochemical anomalies were associated with the Niagaran production in the area (Figure 1 shows the location of this survey relative to similar Class Revisit geochemical sampling programs in the basin; Figures 8 and 9 show the Bear Lake survey area and sample locations) (Seaman, 2003). The survey was designed to examine two different geochemical techniques: solid-phase microextraction (SPME) that measures the concentration of C1-C6 hydrocarbons in the headspace gas of near-surface soil, and microbial oil surveying technique (MOST) that measures the hydrocarbon gases or hydrocarbon indicators at the ground surface.

2.7 Geochemistry Program in Vernon Field Area, Isabella County, Michigan

A surface geochemistry program was initiated at Vernon Field in order to discover if geochemical anomalies were associated with the field. The surveys were designed to examine four different geochemical techniques based on a literature review and discussions with vendors. The four geochemical techniques to be evaluated were: surface iodine, microbial, enzyme leach, and soil-gas. These are established techniques with a supportive literature and a number of service companies willing to conduct the surveys and/or do the analyses. In this study, project personnel collected all samples and interpreted the data. Commercial service companies conducted the analyses.

2.8 Geochemistry Program in Myrtle Beach Area, Burke County, North Dakota

A surface geochemistry program was initiated in the Myrtle Beach Prospect area in Burke County, North Dakota, taking samples for microbial. It is apparent from the elevated microbial values that we need to go back and sample a larger area to try to obtain samples with lower microbial values off the prospect. In this area, project personnel collected all samples and interpreted the data.

2.9 Subsurface Mapping of Dundee and Rogers City Limestones, Michigan

More than 900 digital well logs within the Lower Peninsula were reviewed from the Spatial Subsurface Visualization Laboratory database at MTU. The final 295 wells used for well log tomography were selected based upon two primary criteria. Most importantly, the wells had to contain a gamma ray curve throughout the entire Dundee and Rogers City interval. Incomplete or missing gamma ray curves accounted for twenty percent of those wells needing to be discarded. Secondly, groupings of wells within close proximity to one another were eliminated in order to obtain a uniform distribution over the basin. For example, after reviewing each well from an oil field or cluster within a county, only one or two representative wells were chosen instead of keeping every well that met the first criterion. This eliminated seventy-five percent of the LAS files. The remaining five percent of excluded LAS files were removed based on duplicate or triplicate files, deviated well, digitizing errors, outliers, or wells that appeared questionable. Roughly half the selected wells also have bulk density and photoelectric effect curves. Formation tops for the 295

wells were then picked including the Rogers City, Dundee, Detroit River and Detroit River Bentonite to use as chronostratigraphic surfaces for the various slicing techniques.

3.0 RESULTS AND DISCUSSION

3.1 Summary - Springdale Area - Manistee County, Michigan

Analysis of the geology of the Springdale prospect will continue following the successful wells there. The focus will be on collecting additional geochemical data and identifying the controls on this play and the role of surface geochemistry. We hope to produce a detailed geological model for this field and integrate the geochemical data into it. Additional microbial data will be collected in 2004 over an expanded area in sections 15, 16, 21 and 22 (refer to Figure 5).

3.2 Summary - Bear Lake Area - Manistee County, Michigan

Federated Oil and Gas re-entered the Charlich-Fauble well in Section 9 and drilled a horizontal lateral approximately 550 feet toward the southwest after the geochemical survey had been recorded. The target reservoir was a Niagaran reef that had been delineated using seismic and sub-surface data without input or knowledge of the results of the geochemical survey. The solid phase microextraction geochemical survey results indicate anomalies in the vicinity of the path of this lateral well. The well was successful and is flowing oil from the target Niagaran reef at the rate of 75 to 100 barrels of oil per day 15 months after the initial recompletion; the recompleted well has made more than 62,000 barrels of oil. We will monitor the positive results from this well in subsequent quarters. (Figure 9, Refer to Technical Quarterly Reports #15122R14, January-March 2003 and #15122R17, July-September 2003).

3.3 Summary - Vernon Area - Isabella County, Michigan

The major findings are that the large-scale survey at Vernon Field, conducted early on in this project, appears now to be best interpreted as a halo anomaly over a depleted field (Figure 7, refer to Technical Quarterly Report #15122R13, October-December 2002).

3.4 Summary - Myrtle Beach Area, Burke County, North Dakota

A surface geochemistry program in the Myrtle Beach Prospect area in Burke County, North Dakota, collected more than 40 samples for microbial analysis (Figure 11). The microbial results from the 40+ samples were extremely high; higher than any microbial analysis from our Michigan data set.

Well details for the Lawrence 10-21 and Holte 6-21 wells were presented in the Quarterly Technical Report for period ending June 30, 2003 (refer to Technical Annual Report #15122R16, April-June 2003). Negotiations are continuing by our industry partner in a effort to reach agreement on constructing a pipeline to these wells so they may go on production.

3.5 Dundee and Rogers City - Regional Facies Tract Mapping

Gamma ray, bulk density and photoelectric effect log curves for the Dundee and Rogers City Limestones were digitized from vertical wells distributed over the Lower Peninsula of Michigan, converted to Log ASCII Standard files, and input into the well log tomography program. The "slicing" contour results indicate that during the formation of the Dundee and Rogers City Limestone units, carbonates and evaporites with low natural radioactive signatures on gamma ray logs were deposited and clastic input was minimal to non-existent. A subtle north-south, low natural radioactive trend in the center of the basin correlates with a similar Pef trend and these trends may correlate with previously published Dundee facies tracts. High bulk density trends in the western Michigan Basin correlate with the limits of the Reed City Member (anhydrite) of the Dundee.

3.5.1 Stratigraphy

Detroit River Group

The upper Detroit River Group directly underlies the Dundee Limestone (Figures 13) and is composed of a cyclic series of shallow-water dolomite, limestone, sandstone, anhydrite and salt units (Lilienthal, 1978). In the Lower Peninsula, the Detroit River Group is present except in the extreme northern and southeastern regions. The contact between the Detroit River Group and the Dundee Limestone is irregularly marked by an erosional unconformity and is difficult to distinguish in the subsurface due to similarity in lithologies and hence well log responses on either side of the contact (Landes, 1951; Baltrusaitis, 1974). Lilienthal (1978) stated that the top Detroit River pick is often placed a few feet below the top of the Detroit River Group at the first anhydrite or is based upon other lithology characteristics when this anhydrite is not present. Gardner (1974) was one of the workers that used the anhydrite to define the contact except in the absence of anhydrite toward the southeast region of the basin, where he instead used a thin potassium-bentonite ash bed as described below.

Kawkawlin Bentonite

The uppermost unit of the Detroit River Group contains a volcanic bentonite ash bed (Figure 13). Baltrusaitis (1974) proposed the name Kawkawlin Bentonite for this chronostratigraphic surface after the type well located in the Kawkawlin oil field, Bay County, Michigan. This bentonite can be regionally correlated to the Tioga Bentonite of southwestern Ontario (Baltrusaitis, 1974) and northern Indiana (Doheny et al., 1975). As shown in Figure 15, the ash-fall bed appears as a "spike" on gamma ray logs. Baltrusaitis (1974) also identified a second ash bed above the Kawkawlin Bentonite, possessing a similar gamma ray signature but having a slightly different composition. This additional bentonite spike is not present in the well shown in Figure 15 but can be observed in other gamma ray log curves throughout the basin.

Dundee Limestone

The Dundee Limestone is present throughout most of the Lower Peninsula. The formation outcrops in the northernmost counties, subcrops beneath the glacial drift in southeastern Michigan

and is absent due to erosion in the southwest Lower Peninsula (Figure 14). The Dundee Limestone is described as a "buff-to-brownish gray, finely to coarsely crystalline limestone" (Lilienthal, 1978; Catacosinos et al., 1991). In the westernmost regions of the basin, the Dundee is typically dolomite whereas both limestone and dolomite are present in the basin center. Primary and secondary porosity zones within the limestone and dolomite play a significant role in Dundee oil and gas production (Lilienthal, 1978).

The contact between the Dundee Limestone and the overlying Rogers City was originally described as conformable (Ehlers and Radabaugh, 1938; Tinklepaugh, 1957). Radabaugh (1942) made a detailed map of the northern Rogers City outcrop and showed that the limestone thinned from north to south across the basin but could not confirm if the absence of the Rogers City was due to erosion or non-deposition. A more recent publication by Curran and Hurley (1992), in their study of the West Branch oil field in Ogemaw County, stated that this contact is a disconformity, distinguished by a pyritized and bored hardground due to a period of non-deposition coincident with the top of the Dundee.

Reed City Member

The Reed City is a Member within the Dundee Limestone and is only present in the westernmost Michigan Basin (Figure 13) and consequently could not be used as a regionally correlative surface for slicing. Gardner (1974) described the Reed City as a porosity zone containing both laminated anhydrite and massive dolomite deposited during a brief period of Dundee sea regression. This porosity zone is important because it produces both oil and gas (Lilienthal, 1978) and helps define the Dundee depositional environment.

Rogers City Limestone

The initial separation of the Rogers City Limestone from the Dundee Limestone was based on quarry exposures at Rogers City in Presque Isle County in the northeastern lower peninsula (Ehlers and Radabaugh, 1938). Shortly after this initial publication, Addison (1940) described the Rogers City based on subsurface lithology data at Buckeye oil field in Gladwin County. Addison noted that the Rogers City was darker and denser than the Dundee. Similarly, Landes (1944) described the Rogers City to be "waxy" and darker than the Dundee at Porter oil field in Midland County. Within this oil field, distinguishing between the Rogers City and the Dundee had economic importance as oil was produced directly beneath the Dundee-Rogers City contact (Landes, 1944). The Rogers City-Dundee contact is difficult to consistently pick in the subsurface using geophysical log curves due to the similarity in lithology above and below the contact and also because the Rogers City progressively thins and is eroded or laps out in the southern third of the lower peninsula.

The contact between the Rogers City and the overlying Bell Shale is readily apparent in the subsurface on gamma ray, bulk density and pef log curves. This contact was originally described as a disconformity (Ehlers and Radabaugh, 1938) based on removal of 46 feet of Rogers City Limestone at Michigan Limestone and Chemical Company quarry in Presque Isle County. Other workers such as Radabaugh (1942) and Ehlers and Kesling (1970) confirmed this disconformity, but based their interpretations upon data from the margins of the Michigan basin. Addison (1940)

stated that the thickness of the Rogers City did not vary over an anticlinal structure in the Buckeye field of central Michigan. From this observation Addison concluded that the contact between the Bell Shale and the Rogers City appeared to be conformable. Gardner (1974) concluded that an unconformable relationship exists between the Rogers City and the Bell Shale at the basin margin but is conformable in the deeper, central region of the basin.

Bell Shale

The Bell Shale is the basal formation of the Traverse Group and directly overlies the Rogers City Limestone. When the Rogers City is not present, in areas such as western and southern Michigan, the Bell Shale overlies the Dundee Limestone. In 1901, Amadeus W. Grabau first used the term "Bell Shale" when describing bluish colored shale in abandoned clay pits in southeastern Presque Isle County (Ehlers and Kesling, 1970). The Bell Shale Formation studied at quarries and from cores in Presque Isle and Alpena Counties, was deposited on an erosional surface at the top of the Rogers City Limestone.

The lower section of the Bell Shale contains crinoid fragments indicating turbulent water conditions whereas fossils in the upper section depict a calmer, deep-water environment (Ehlers and Kesling, 1970). Bloomer (1969) described a small calcareous unit (lag deposit) at the base of the Bell Shale in the southwest region of the Michigan basin and interpreted the lag to be time transgressive toward the northeast as the result of transgression.

3.5.2 Well Log Tomography - Gamma Ray, Bulk Density and Photoelectric Effect Curves

The well log tomography (WLT) method employs wireline logs. Wireline tools can record and sample geophysical measurements at one-foot intervals or higher resolutions within a borehole. However, as described by Wylie (2002), common practice is to average wireline log curve amplitudes over the interval under analysis when correlating well data. Consequently, Wylie's primary objective for creating the slicing program (WLT) was to analyze well log curves without compromising their vertical resolution (Wylie, 2002; Wylie and Huntoon, 2003). By creating a slice at every foot, the full vertical resolution contained within the log curve data is preserved in each well. The log curve amplitudes for each well are then plotted and contoured in plan-view. In this study we use the gamma ray, bulk density (rhob) and photoelectric effect (Pef) log curves to analyze regional variations in the Dundee and Rogers City Limestones.

Gamma Ray Curve

The gamma ray curve records the natural radioactivity of a formation due to the presence of three radioisotopes, uranium (238U), potassium (40K) and thorium (232Th). As the isotopes of U, K and Th decay, they emit short bursts of electromagnetic energy that can be measured by a gamma ray sensor. The American Petroleum Institute unit (API) is used as a measurement for gamma ray logs and is based on an artificial formation located in Houston, TX containing known values of U, K and Th. A basic gamma ray log records the combined energies from U, K and Th whereas a spectral gamma ray log separates the signal into its three components.

Gamma ray logs are useful for lithology studies because different types of sedimentary rocks exhibit a general range of gamma ray responses. Dewan (1983) stated that generally, pure limestone and anhydrite measure 15-20 API, dolomite and sandstones range between 20-30 API, and shales and volcanic ash (potassium-bentonite) measure high, on average 100 API. In the Dundee and Rogers City formations, anhydrite primarily ranges from 10-14 API, limestone averages 16 API and dolomite covers a broad range, between 10-50 API. The Bell Shale averages approximately 120 API.

Bulk Density Curve

Density logs are used primarily to measure formation porosity but they can also be used to identify evaporite minerals (i.e., the Reed City Member of the Dundee). Density tools work by emitting gamma rays and then these gamma rays collide with electrons of the formation under analysis. Each collision causes any gamma ray to loose some but not all of its energy to the electron and the gamma ray continues with diminished energy and reaches a detector in the bulk density logging tool, at a fixed distance from the source, where it is counted as an indication of formation density. The response of the density tool is related to the electron density of the formation, which is related to bulk density. The density of the rock is a function of its matrix, fluid content, and pore space (Schlumberger, 1986). This study applied WLT to a 150 well subset of the well logs used for the gamma ray mapping that had rhob curves to map basin-scale variations in the bulk density as an indicator of lithology and especially evaporites in the Dundee.

Photoelectric Absorption Curve

Photoelectric absorption measures how many gamma rays reach a low energy level after being scattered by the electrons in the formation (Columbia, 2004). The photoelectric effect index is measured by comparing the counts from a far detector in the high energy region, with those counts in the low energy region, where the count rates depend on both the reactions. The far detector is used because it has a greater depth of investigation. The photoelectric absorption cross section index is measured downhole and is related to the atomic number of the formation and hence to the lithology making the Pef curve a separate indicator of formation lithology. This study applied WLT to approximately 150 wells at the basin-scale to map lithology variations using the Pef curve in the Dundee and Rogers City for comparison with the gamma ray and bulk density WLT mapping.

Borehole Correction

Borehole effects are important to note in this study as they can affect the gamma ray response. Conditions for calibration of the gamma ray tool are defined by Dewan (1983) to include a hole diameter of 8-in, 10-lb drilling mud, and an eccentered logging tool with a 3 5/8-in diameter. A dampened gamma ray response can be attributed to an increase in either the hole diameter or mud weight, or with the use of a centralized logging tool. Conversely, a smaller hole would shift the log curve toward higher gamma ray values (Dewan, 1983).

Charts such as the Schlumberger Por-7, provide correction factors that account for borehole effects using the hole diameter, mud weight and tool position (Schlumberger, 1986). Although the

mud weight was typically recorded in the LAS files and in the header of the original paper logs, neither the hole diameter nor tool position were available in the LAS files or on the paper logs. Consequently, a typical borehole correction could not be performed and is noted as a source of error in the data set.

Casing sizes, ranging from 4 1/2-in to 13 5/8-in, for 217 wells within the "Dundee" interval were available. By mapping the distribution of gamma ray and casing size values for individual wells within the basin, there appeared to be no direct correlation between the casing size and the gamma ray amplitude. The casing sizes were then used as a proxy for borehole diameter and plotted against the gamma ray response for each well to observe possible relationships that could aid in applying a borehole correction. Two cross-plots were used to determine the necessity for a borehole correction: (A) the average gamma ray value for the "Dundee" interval in each well plotted as a function of casing diameter and (B) standard deviation of the gamma ray values for the "Dundee" interval in each well plotted as a function of casing diameter. From these graphs, there is no apparent relationship between the casing size and the gamma ray values. A trend was observed between the distribution of small casing sizes and the standard deviation of the gamma ray values for each well. However, the cause of this relationship in the center of the basin, but not consistently over the entire basin, is unknown.

Normalization

Neinast and Knox (1974) and Hunt et al (1996) stated that more than half of wells studied need to be normalized. Normalization is a correction applied to erroneous well log data to ensure that there is consistency between wells regarding the amplitude of the log curve response. The WLT technique examines amplitude changes rather than absolute amplitude values, but normalization was investigated because different types of errors can alter the amplitude change. "The basic sources of error are tool malfunction, incorrect tool design, inconsistent shop and field calibration, and operator error" (Neinast and Knox, 1974). In addition to these sources, Shier (1997) showed significant variation in gamma ray responses based on a combination of logging contractors, drilling medium, and tool vintages. Hammack and Fertl (1974) described subsurface conditions that cause increased gamma ray amplitudes such as previously perforated intervals with salt present from old drilling fluid, fluid movement behind casing, and the presence of radioactive sandstones and carbonates. Hammack and Fertl also stated that "interpretation of gamma ray logs is straightforward if correctly calibrated and proper time constant and logging speed are used," although, these log constraints are typically unknown for well logs within the Michigan Basin.

The normalization process includes defining a standard curve signature from either one well or a combination of representative wells. This "standard" can be based on a unit of sufficient lateral extent such as a shale layer, a low porosity carbonate or thick sandstone with low porosity. Each well used in the study is then normalized with the standard (Hunt et al., 1996). In this study, a standard formation either above or below the Dundee-Rogers City interval was difficult to identify because of lithology changes across the basin and incomplete digital gamma ray log curve coverage. The Dundee-Rogers City interval was then analyzed to determine if it had a unique log curve signature that could be used as the standard to correct erroneous log amplitudes. This analysis consisted of creating frequency histograms of the gamma ray values within the Dundee-Rogers City interval for individual wells throughout the basin. Consequently, normalization using one

standard for the entire basin could not be performed because the correction was beyond the scope of this study and is noted as a source of error.

As a broad normalization for the 302 wells that were preliminarily sliced, a composite frequency histogram was constructed using the average gamma ray value for the Dundee-Rogers City interval in each well. Of the 302 wells, all but seven wells fell within two standard deviations that equal about 95 percent of the data. Four wells were within the third standard deviation (99.7 percent of data) and three wells were far beyond the mean value. All seven wells were further analyzed and excluded from the final slicing.

Formation Tops Data

The WLT technique slices log curve data between two correlative surfaces. Wylie and Huntoon (2003) stated that if these bounding surfaces can be defined as unconformities, sequence boundaries, parasequence boundaries, flooding surfaces, condensed sections or ash beds, then the slicing image results would be chronostratigraphically significant. An example of a chronostratigraphic surface would be the images that a satellite captures of the modern depositional surface.

Originally, the Dundee and Rogers City Limestones were not separated in this study because the location of their contact, based on previous publications, could not be identified with a high level of certainty using gamma ray logs. The top of the combined "Dundee" limestone was picked at the inflection point on the gamma ray log curve between the Bell Shale and the "Dundee" for every well (Figure 15). The inflection point was chosen as the contact because the complete change from shale to limestone on the logs was typically within the 3-4 ft vertical resolution range for the gamma ray data (Dewan, 1983). In general, the top of the "Dundee" was easier to identify in the center of the basin than in the southwest where the Bell Shale unit pinches or laps out. Most of these picks are equivalent to the top values within the Michigan Department of Environmental Quality Oil and Gas Database (DNR).

The base of the "Dundee" was defined at the first anhydrite within the Detroit River Group. This pick was most consistently picked when the density log curve was available (Figure 15) and became more difficult to pick in the southeastern part of the basin where log signatures for both units become exceedingly similar. These top picks were fairly consistent with the DNR database.

The top boundary of the "Dundee" is marked by an abrupt lithology change as well as an unconformity at the basin margins (Gardner, 1974). This correlative surface may be chronostratigraphically significant although Bloomer (1969) stated that, "the Dundee [including Rogers City] is not time equivalent" due to varying rates of deposition, such that increased distance from this surface would decrease the time significance of a given slice. Similarly, slices from the base of the "Dundee" only illustrate approximate time surfaces.

3.5.3 Depositional Model

The Michigan Basin's paleogeography during Dundee-Rogers City time (376-380 Ma) was approximately 20°S and modeling of the tropical paleoclimate illustrates that the mean tempera-

ture would have averaged 75° Fahrenheit (24° Celsius) (Golonka et al., 1994). Gardner (1974) presented a comprehensive interpretation for this Middle Devonian depositional environment using well cuttings, cores, driller's logs and gamma ray-neutron wireline log curves. In his conceptual model, the basin was divided into three zones, where sediments in the western region of the basin indicate a sabkha-lagoon environment, separated from an eastern open marine environment by a north-south trending shell bank (Figure 17B). A westward transgressing sea and an intermediate regression during Reed City deposition controlled this environmental differentiation (Gardner, 1974).

Many workers applied the Rogers City-Dundee depositional model proposed by Gardner (1974) to their own studies (Lilienthal, 1978; Bush, 1983; Fisher et al., 1988; Catacosinos et al., 1991; Howell and van der Pluijm, 1999). Prior to Gardner's (1974) division of the Michigan Basin, Cohee and Underwood (1945) illustrated a similar north-south separation based on Dundee and Rogers City oil production. Wells west of Gladwin and Midland counties produced primarily from the Rogers City whereas, wells east of this divide produced primarily from the Dundee. Montgomery (1986) and Curran and Hurley (1992) separated the Rogers City and Dundee depositional environments in the center of the basin. The Rogers City Limestone was described as open-marine, and the Dundee Limestone as composed of mostly patch reefs (Montgomery, 1986) in a shallow platform environment (Curran and Hurley, 1992).

The most recent interpretation of the middle to late Dundee depositional environment was presented by Taylor (2001) and closely resembles Gardner's model (Figure 17B). Taylor used a high density of well log curves (more than 1500 well logs) to separate the sabkha from the lagoon environment and identify smaller scale features such as tidal channels, barrier islands and patch reefs. The drawback to typical models such as those shown in Figure 17B is that they only provide one generalized representation of the depositional environment whereas the WLT technique attempts to depict the evolution of depositional patterns.

A subtle similarity exists between the depositional environment proposed by both Gardner (1974) and Taylor (2001) and the trends observed in the proportional slicing shown in Figure 16 as well as in the top-down and bottom-up slicing that is not shown. The location of the shell banks (Gardner, 1974) and inner shelf region (Taylor, 2001) appears as a low gamma ray trend running north-south through the center of the basin in slices through the mid- and upper-Dundee and to a lesser extent through the slice of the Rogers City (dark blues, left most slices, Figure 13). The photoelectric effect slices (right most slices, Figure 13) show similar north-south trends and indicate that the shell banks or inner shelf region is predominantly composed of dolomite. The gamma ray slices also illustrate a consistently higher naturally radioactive region in the southeast basin, described by previous workers as a shallow marine environment area (Gardner, 1974; Taylor, 2001).

Figure 17 superimposes Taylor's (2001) map onto slice 19 from the top-down slicing (upper Dundee). An interpretation of this figure suggests that beyond Taylor's study region, the low natural radioactive trend appears to expand in the northern part of the basin. The occurrence of low naturally radioactive sediments could be attributed to reworking of carbonate material through wave action. The high bulk density (rhob) amplitudes in the slices (oranges and yellows in the middle column of slices in Figure 13) clearly show that evaporite (anhydrite, Reed City Member) deposition dominated in the western one third of the Michigan basin during lower to upper

Dundee time. Comparison of the gamma ray, bulk density, evaporites and carbonates that can be observed regionally using the gamma ray, bulk density and pef log curves.

In a publication on the identification of depositional environments using gamma ray logs, Rider (1990) stated that too many complications and variations exist to base interpretations solely on one log curve. This is evident in slicing the Dundee and Rogers City Limestones as the gamma ray curve does not identify all lithofacies changes. Lilienthal (1978) stated that porosity zones could be traced in the Dundee-Rogers City interval across the basin using the neutron log. Applying WLT to the neutron curve could highlight important porosity trends. The density log was useful for identifying anhydrite and slicing this curve allowed the delineation of the extent of the Reed City Member. If digital lithology or facies data could be assigned amplitude values and input into the WLT slicing program, the resulting trends could improve both the Rogers City and Dundee depositional environment models.

4.0 CONCLUSIONS

The positive results from the Springdale wells show that hydrocarbons can still be recovered in the Michigan Basin by small companies. We now need to establish the reserves and see if there are any further plays in the area. This work will likely stretch out over at least two years, but it is likely that much can be accomplished this summer, year 4 of this project. Thus, we should have a good case history to write up for the final report. In addition, the Springdale play will be presented at various meetings and symposia, including PTTC workshops in the coming years. The main questions now are: 1. the size of the reserves, 2. the presence of additional fields nearby, and 3. details of the geology, including the type of trap and how to locate them. More data will be collected in an expanded area at Springdale in 2004.

Microbial sampling over the Bear Lake prospect has considerably widened the original microbial and SPME coverage there. It appears that the discovery well is now producing a negative (halo) anomaly due to the pressure draw-down and this is reflected in the microbial data. However several relative highs were picked up in the new survey that bear further investigation, preferably by 2d seismic lines to see if there is any structure associated with them.

In general, the geochemical program is proving a valuable addition to the demonstration program in this project. We have mapped both positive and negative anomalies over the demonstration sites and have been able to correlate these observations with production. In general the negative anomalies correlate with produced fields or with reefs that are currently pumping. Positive anomalies occur over prospects that have not been drilled and where at least shows of hydrocarbons were encountered in the subsequent tests. The extensive geochemical sampling over Vernon Field is now seen in retrospect to have defined a large negative anomaly associated with the entire field, indicating that it was a poor candidate for further development, a result confirmed by the drilling of the Smock 13-23-HD1 test well.

We have also developed a sampling and analysis protocol for surface geochemistry based on retrieval of activated carbon and analysis by gas chromatography. This technique is still being developed, but side-by-side comparisons with the microbial data can be used to compare the efficiency and accuracy (consistency) of the technique. If the activated carbon technique proves accurate, it has the advantage of being lower cost and more adaptable to routine application by small operators. We will emphasize this aspect of the project in our future reports.

The well log tomography technique was successfully applied to the Rogers City and Dundee Limestones in the Michigan Basin. The primary result from the suite of gamma ray, rhob and pef log curves sliced over the Lower Peninsula of Michigan indicated a period of quite carbonate and evaporite deposition occurred during Dundee-Rogers City time. This is in sharp contrast with the previous work on the overlying Traverse Group by Wylie (2002) and Wylie and Huntoon (2003) that identified multiple cycles of gamma ray distributions related to the expansion and contraction of muddy deltas in the eastern Michigan Basin. No comparable delta building activity is apparent in the gamma ray, rhob and pef data for the Dundee and Rogers City Limestones. A subtle north-south gamma ray and pef trend within the Dundee interval was found to correlate with previous interpretations of Dundee facies tracts by Gardner (1974) and Taylor (2001). In addition, the bulk density WLT images show the extent of the Reed City Evaporite Member of the Dundee Lime-

stone. By conducting more detailed mapping of the relationship of the Reed City Member and the north-south Dundee system tract, additional lead areas may be located in the Dundee for surface geochemical surveys.

5.0 REFERENCES

Addison, C. C., 1940, Buckeye oil field, Gladwin County, Michigan: The American Association of Petroleum Geologists (AAPG) Bulletin, v. 24, n. 11, p. 1950-1982.

Baltrusaitis, E. J., 1974, Middle Devonian bentonite in Michigan: AAPG Bulletin, v. 58, n. 7, p. 1323-1330.

Bloomer, A. T., 1969, A regional study of the Middle Devonian Dundee dolomite in the Michigan Basin: M. S. Thesis, Michigan State University, 67 p.

Boleneus, D., 1994, Guidelines for surface geochemical surveying: Oil and Gas Journal, v. 92, no. 23, p. 59-64.

Bush, C. V., 1983, Dundee fields in the central Michigan Basin: M. S. Thesis, Michigan State University, 81 p.

Catacosinos, P. A., P. A. Daniels Jr., and W. B. Harrison III, 1991, Structure, stratigraphy and petroleum geology of the Michigan basin in M. W. Leighton, D. R. Kolata, D. F. Oltz, and J. J. Eidel, eds., Interior cratonic basins: AAPG Memoir 51, p. 561-601.

Cohee, G. V., and L. B. Underwood, 1945, Lithology and thickness of the Dundee Formation and the Rogers City Limestone in the Michigan Basin: U. S. Geological Survey, Oil and Gas Investigations Map, Scale 1:1,000,000.

Cohee, G. V., and Landes, K. K., 1958, Oil in the Michigan Basin, in Weeks, L. G., ed., Habitat in oil: Tulsa, Oklahoma, American Association of Petroleum Geologists, p. 473-493.

Columbia University, ODP Loggin website, 2004, <http://www.ldeo.columbia.edu/BRG/ODP/LOGGING/MANUAL/Pages/hlds.html>, last accessed, June 20, 2004.

Curran, B. C., and N. F. Hurley, 1992, Geology of the Devonian reservoir, West Branch Field, Michigan: The AAPG Bulletin, v. 76, n. 9, p. 1363-1383.

Davidson, M. J., 1994, On the acceptance and rejection of surface geochemical exploration, Oil and Gas Journal, v. 92, no. 23, p. 70-76.

Dewan, J. T., 1983, Essentials of Modern Open-hole Log Interpretation: PennWell Publishing Company, Tulsa, Oklahoma, 361 p.

Doheny, E. J., J. B. Droste and R. H. Shaver, 1975, Stratigraphy of the Detroit River Formation

(Middle Devonian) of northern Indiana: Department of Natural Resources (DNR) Geological Survey Bulletin 53, 85 p.

Ehlers, G. M., and R. V. Kesling, 1970, Devonian strata of Alpena and Presque Isle Counties, Michigan: Michigan Basin Geological Society (MBGS), 130 p.

Ehlers, G. M., and R. E. Radabaugh, 1938, The Rogers City Limestone, A new Middle Devonian Formation in Michigan: Papers of the Michigan Academy of Science, Arts, and Letters (1937), v. 23, p. 441-446.

Fisher, J.H., Barratt, M.W., Droste, J.B., and Shaver, R.H., 1988, Michigan Basin, in L. L. Sloss, ed., Sedimentary cover--North American craton: U.S.: The Geology of North America, v. D-2: GSA, Boulder, Colorado, p. 361-382.

Gardner, W. C., 1974, Middle Devonian stratigraphy and depositional environments in the Michigan Basin: MBGS, Special Paper n. 6, 138 p.

Golonka, J., M. I. Ross, and C. R. Scotese, 1994, Phanerozoic paleogeographic and paleoclimatic modeling maps in A. F. Embry, B. Beauchamp and D. J. Glass, eds., Pangea: Global Environments and Resources: Canadian Society of Petroleum Geologists Memoir 17, p. 1-47.

Hammack, G. W. and W. H. Fertl, 1974, How well logs can be misinterpreted: World Oil, v. 179, n. 7, p. 69-73.

Horvitz, L., 1972, Vegetation and geochemical prospecting for petroleum, American Association of Petroleum Geologists Bulletin, v. 56, no. 5, p. 925-940.

Howell, P. D. and B. A. van der Pluijm, 1999, Structural sequences and styles of subsidence in the Michigan Basin: GSA Bulletin, v. 111, n. 7, p. 974-991.

Hunt, E., A. Aly, and D. Pursell, 1996, Fundamentals of log analysis, Part IV: Normalization of logs with histograms: World Oil, Oct., p. 101-102.

Jones, V. T. and Drozd, R. J., 1983, Predictions of oil or gas potential by near-surface geochemistry: AAPG Bulletin, v. 67, no. 6, p. 932-952.

Kartsev, A. A., Tabarsaranskii, Z. A, Subbota, M. I., and Mogilevskii, G. A., 1959, Geochemical methods of prospecting and exploration for petroleum and natural gas: Berkely, California, University of California Press, 349 p.

Kellum, L. B., 1958, The Dundee Limestone in Manistee County, Michigan: Papers of the Academy of Science, Arts, and Letters, v. 43, p. 39-49.

Landes, K. K., 1944, Porter Oil Field, Midland County, Michigan: AAPG Bulletin, v. 28, n. 2, p.

173-196.

Landes, K. K., 1948, Deep River Oil Field, Arenac County, Michigan, in Howell, J. V., ed., Structure of Typical American Oil Fields: A Symposium on the Relation of Oil Accumulation to Structure- Volume III: AAPG, p. 299-304.

Landes, K. K., 1951, Detroit River Group in the Michigan Basin: US Geological Survey Circular 133, 23 p.

Lilienthal, R. T., 1978, Stratigraphic cross-sections of the Michigan Basin: DNR, Geological Survey Division, Report of Investigation No. 19, 36 p. and 89 plates.

Montgomery, E. L., 1986, Facies development and porosity relationships in the Dundee Limestone of Gladwin County, Michigan: M. S. Thesis, Western Michigan University, 81 p.

Neinast, G. S. and C. C. Knox, 1974, Normalization of well log digitizing: Log Analyst, v. 14, n. 2, p. 18-25.

Newcombe, R. B., 1930, Middle Devonian unconformity in Michigan: GSA Bulletin, v. 41, p. 725-737.

Newcombe, R. B., 1932, Geology of Muskegon Oil Field, Muskegon, Michigan: AAPG Bulletin, v. 16, p. 153-168.

Petroleum Technology Transfer Council (PTTC), Michigan's Oil and Gas News Industry at a Glance, May 2002, Michigan Satellite Office, Western Michigan University [referenced Michigan Oil and Gas Association (MOGA) and Michigan Department of Natural Resources, 1993, Michigan oil and gas fields 1985-1986: MDNR Geological Survey Division OFR 89-01, 310 p.], accessed at <http://wst023.west.wmich.edu/mi_oilgas_sum2002.htm> on March 13, 2004.

Price, L. C., 1986, A critical overview and proposed working model of surface geoochemical exploration, in M. J. Davidson, ed., Unconventional methods in exploration for petroleum and natural gas, IV: Southern Methodist University Press, Dallas, p. 245-309.

Radabaugh, R. E., 1942, The Middle Devonian Rogers City Limestone and its gastropod fauna: Ph.D. Dissertation, University of Michigan, 152 p.

Rider, M. H., 1990, Gamma-ray log shape used as a facies indicator: critical analysis of an oversimplified methodology in A. Hurst, M. A. Lovell and A. C. Morton, eds., Geological Applications of Wireline Logs: Geological Society Special Publication , n. 48, p. 27-37.

Schlumberger, 1986, Log Interpretation Charts: Schlumberger Well Services, 122 p.

Schumacher, D., 2002, personal e-mail communication.

Seaman, C. C., 2003, Application of solid-phase microextraction technology in surface geochemical exploration: M. S. thesis, Michigan Technological University, Houghton, MI, 100 p.

Shier, D. E., 1997, A comparison of log response between logging companies and different vintages of tools: Log Analyst, v. 38, n. 3, p. 47-61.

Smith, G. H., and Ellis, M. M., 1963, Chromatographic analysis of gases from soils and vegetation as related to geochemical prospection of petroleum, American Association of Petroleum Geologists Bulletin, v. 47, p. 1897-1903.

Soli, G., 1957, Microorganisms and geochemical methods of oil prospecting: American Association of Petroleum Geologists Bulletin, v. 41, p. 134-140.

Taylor, E. T., 2001, Stratigraphic distribution of the Rogers City dolomitization across the west-central region of the Michigan Basin (Abstract): AAPG Bulletin, v. 85, no. 8, p. 1539.

Tedesco, S. A., 1995, Surface geochemistry in petroleum exploration: New York, Chapman and Hall, 206 p.

Tinklepaugh, B. M., 1957, A chemical, statistical, and structural analysis of secondary dolomitization in the Rogers City- Dundee Formation of the central Michigan Basin: Ph.D. Thesis, East Lansing, Michigan State University, 125p.

Tompkins, R., Clark, J. R., Ziegler, D., 2000, Enzyme Leach(SM) geochemistry; a significant advancement in hydrocarbon exploration: American Association of Petroleum Geologists 2000 annual meeting, Annual Meeting Expanded Abstracts, p. 148.

Wylie, A. S., 2002, Log curve amplitude slicing- Visualization of well log amplitudes for paleogeographic reconstruction of the Middle Devonian Traverse Group, Michigan: Ph. D. Dissertation, Michigan Technological University, 218 p.

Wylie, A. S. and J. E. Huntoon, 2003, Log-curve amplitude slicing: Visualization of log data and depositional trends in the Middle Devonian Traverse Group, Michigan Basin, United States: AAPG Bulletin, v. 87, no. 4, p. 581-608.

6.0 FIGURES

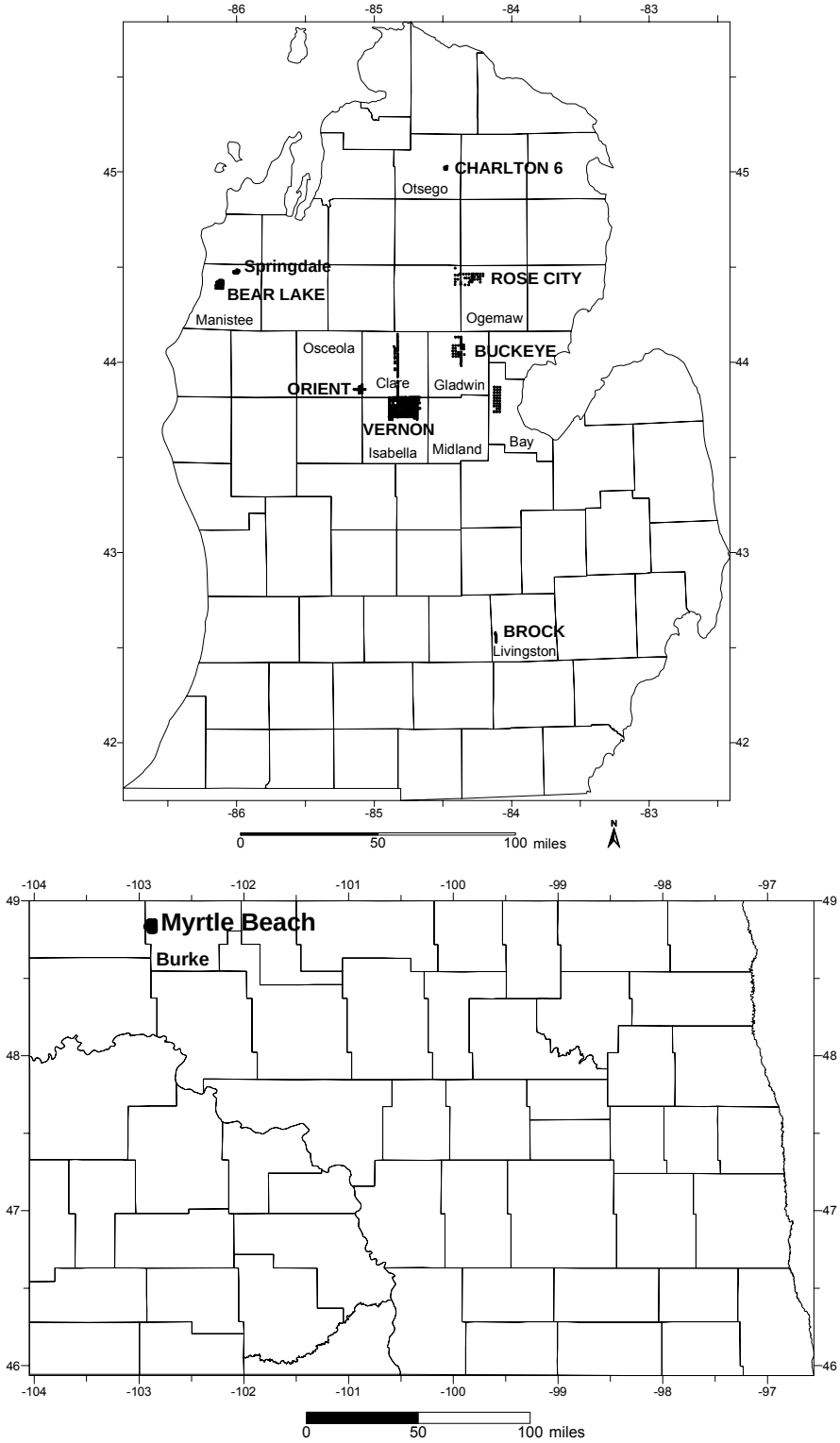

Figure 1. Index map showing locations of all geochemical sampling in Michigan and North Dakota.

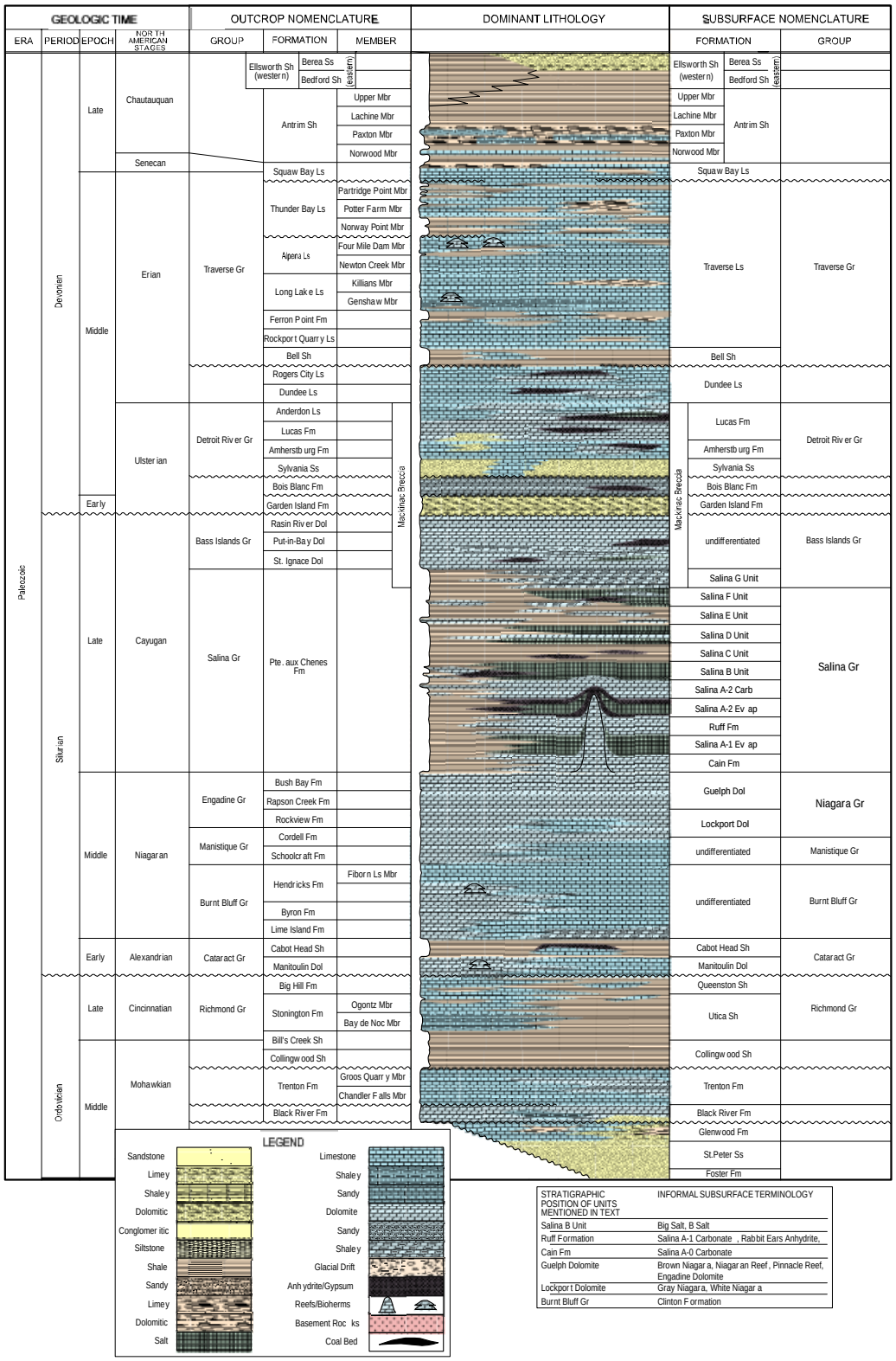

Figure 2. Generalized Stratigraphic Column for the Michigan Basin.

ERA	PERIOD		ROCK UNIT FORMATION	
Cenozoic	Quaternary		Oahe	
	Tertiary		Brule	
			Chadron	
			Golden Valley	
			Sentinel Butte	
			Bullion Creek	
			Slope	
			Cannonball	
			Ludlow	
Mesozoic	Cretaceous		Hell Creek	
			Fox Hills	
			Pierre	
			Niobrara	
			Carlile	
			Greenhorn	
			Belle Fourche	
			Mowry	
			New Castle	
			Skull Creek	
			Inyan Kara	
	Jurassic		Swift	
			Rierdon	
			Piper	
	Triassic		Spearfish	
Paleozoic	Permian		Minnekahta	
			Opeche	
			Broom Creek	
	Carboniferous	Pennsylvanian	Amsden	
			Tyler	
		Mississippian	Otter	
			Kibbey	
			Charles	
			Mission Canyon	
			Lodgepole	
	Devonian		Bakken	
			Three Forks	
			Birdbear	
			Duperow	●
			Souris River	
			Dawson Bay	
			Prairie	
			Winnipegosis	●
			Ashern	
	Silurian		Interlake	
			Stonewall	
	Ordovician		Stony Mountain	
			Red River	●
			Roughlock	
			Icebox	
			Black Island	●
	Cambrian		Deadwood	
PreCambrian				

Figure 3. Generalized Stratigraphic Column for the Williston Basin. Black dots are key productive intervals in the Myrtle Beach area.

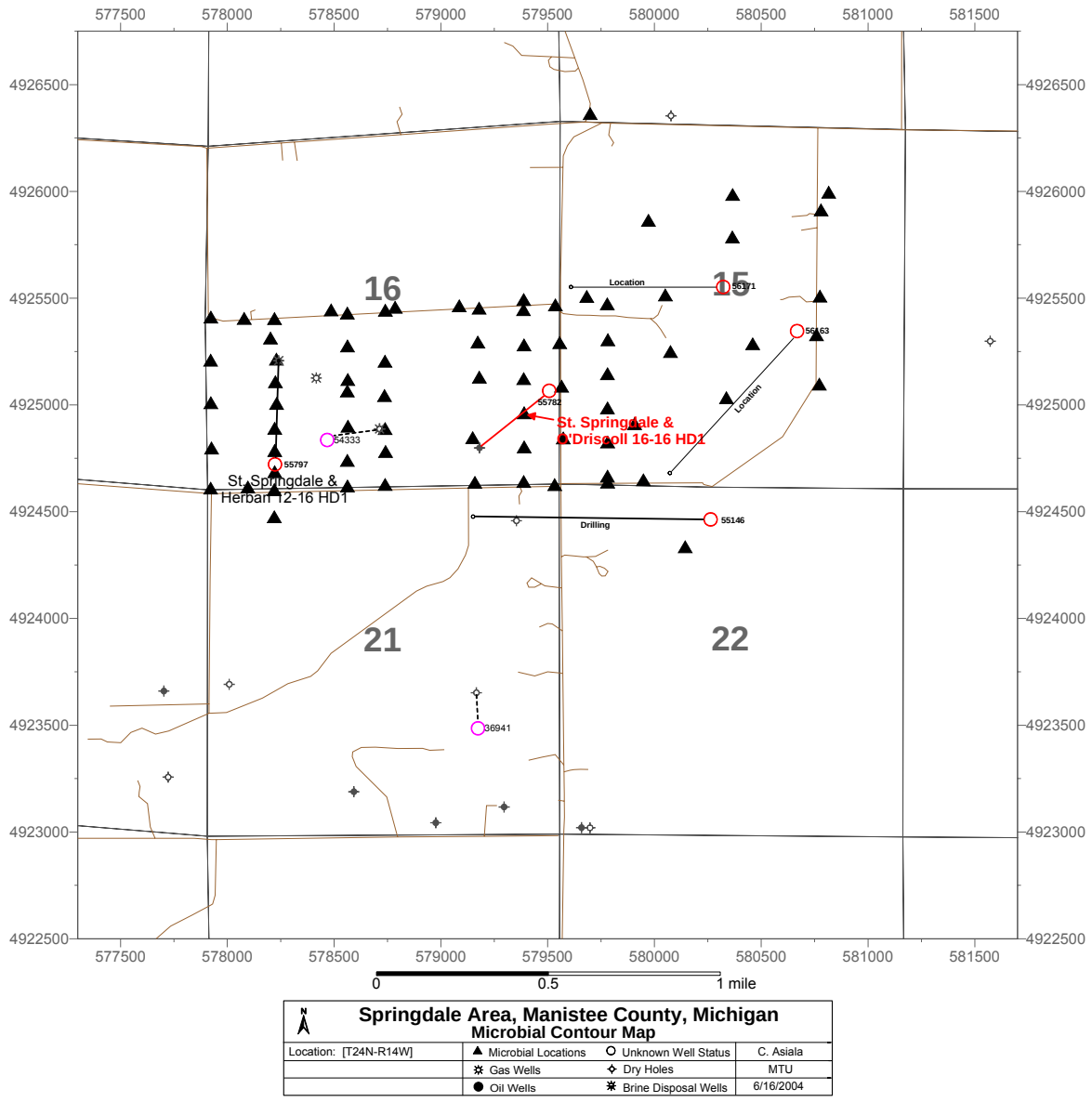

Figure 4. Springdale area wells and surface geochemical sample locations. Red well path is St. Springdale & O'Driscoll 16-16 HD1 (Permit 55782). Large red circles are bottom hole locations (bhl) of horizontal wells; pink circles are bottom hole locations of deviated wells.

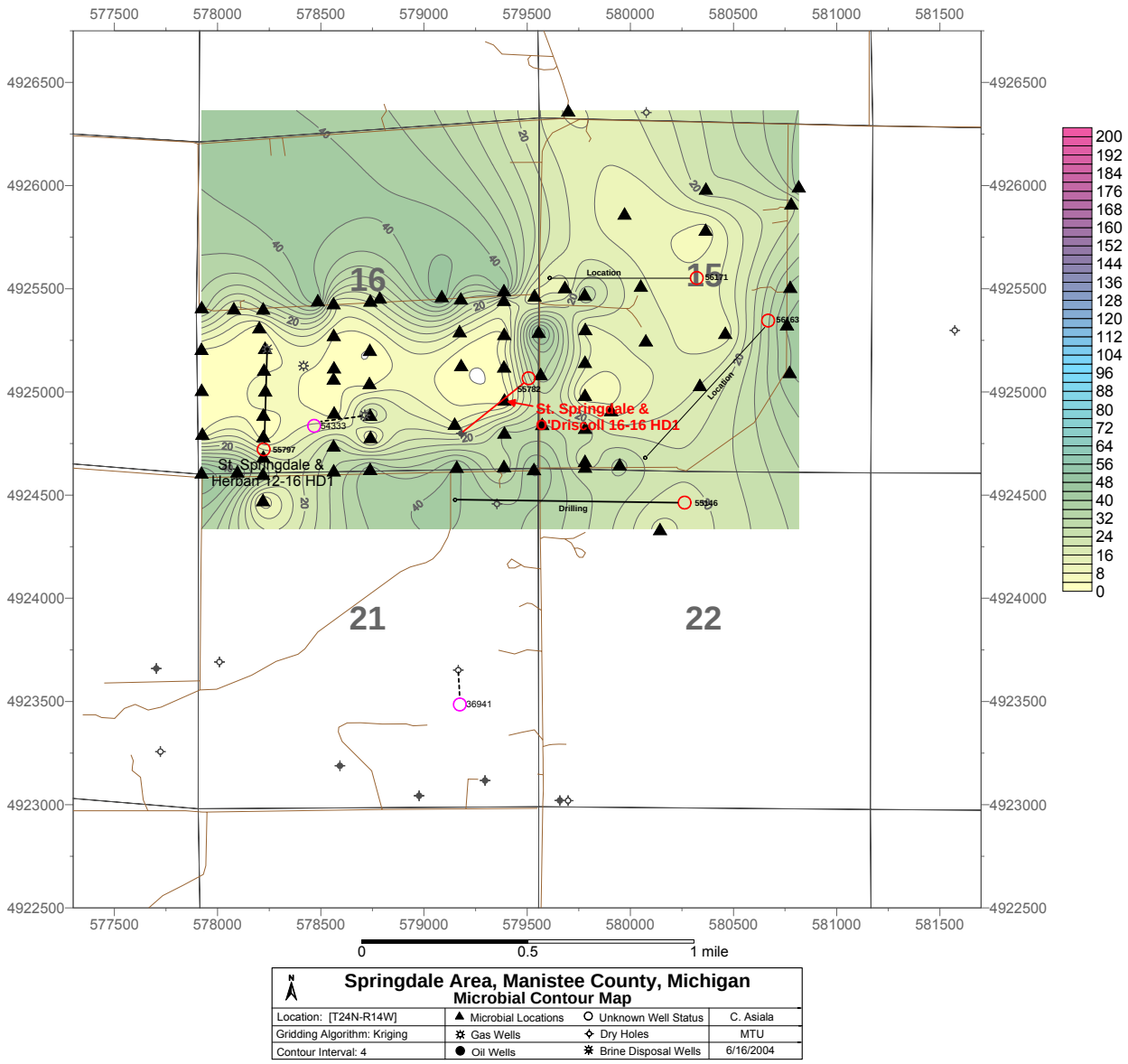

Figure 5. Microbial contour map of the Springdale Prospect in Manistee County, Michigan. Red well path is St. Springdale & O'Driscoll 16-16 HD1. Large red circles are bottom hole locations (bhl) of horizontal wells; pink circles are bottom hole locations of deviated wells. Green color filled contours indicate high microbial anomalies and yellow color filled contours indicate low anomalies. The change in the microbial anomaly along the path of the St. Springdale and O'Driscoll 16-16 HD1 may represent a fault or stratigraphic facies change.

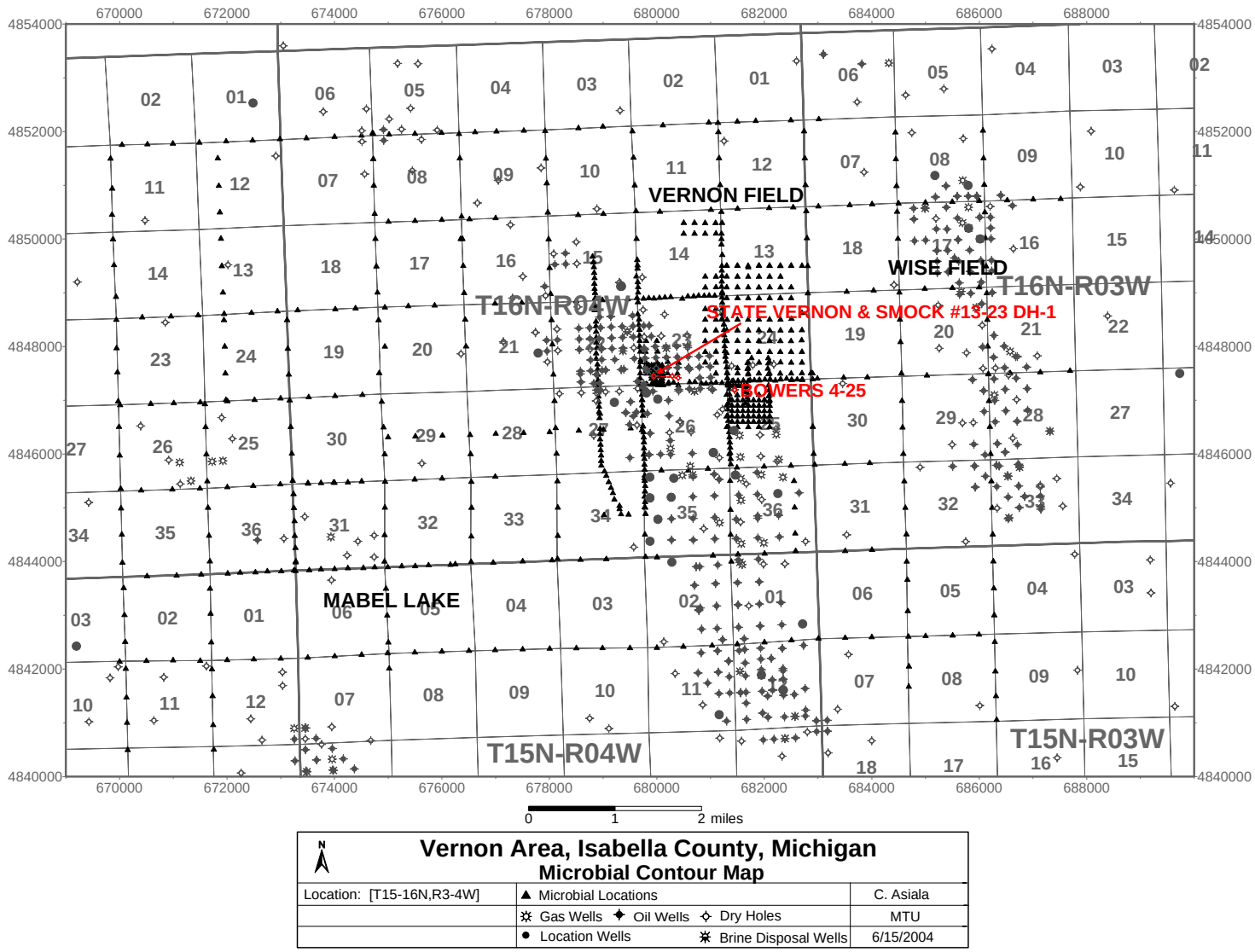

Figure 6. Microbial sample location map for the Vernon Field and surrounding area in Isabella County, Michigan. Black triangles are microbial sample locations and the dark gray symbols are well locations.

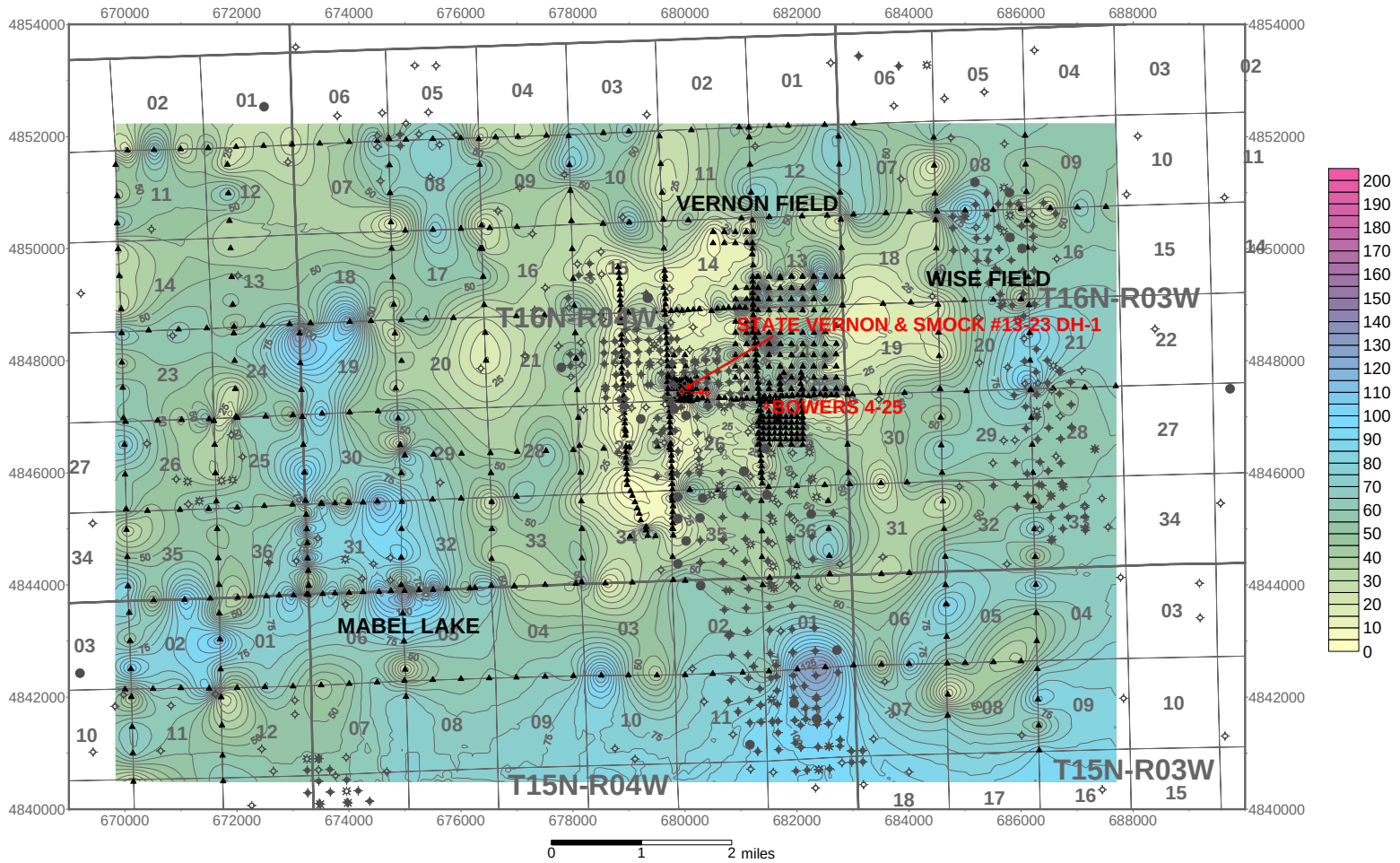

Vernon Area, Isabella County, Michigan
Microbial Contour Map

Location: [T15-16N,R3-4W]	▲ Microbial Locations	C. Asiala
Gridding Algorithm: Kriging	✲ Gas Wells ✦ Oil Wells ✧ Dry Holes	MTU
Contour Interval: 5	● Location Wells ✱ Brine Disposal Wells	6/15/2004

Figure 7. Microbial sample location map and contour map for the Vernon Field and surrounding area in Isabella County, Michigan. Black triangles are the microbial sample locations. Blue color filled contours indicate high microbial anomalies and yellow color filled contours indicate low anomalies. The entire Vernon Field is a large negative anomaly.

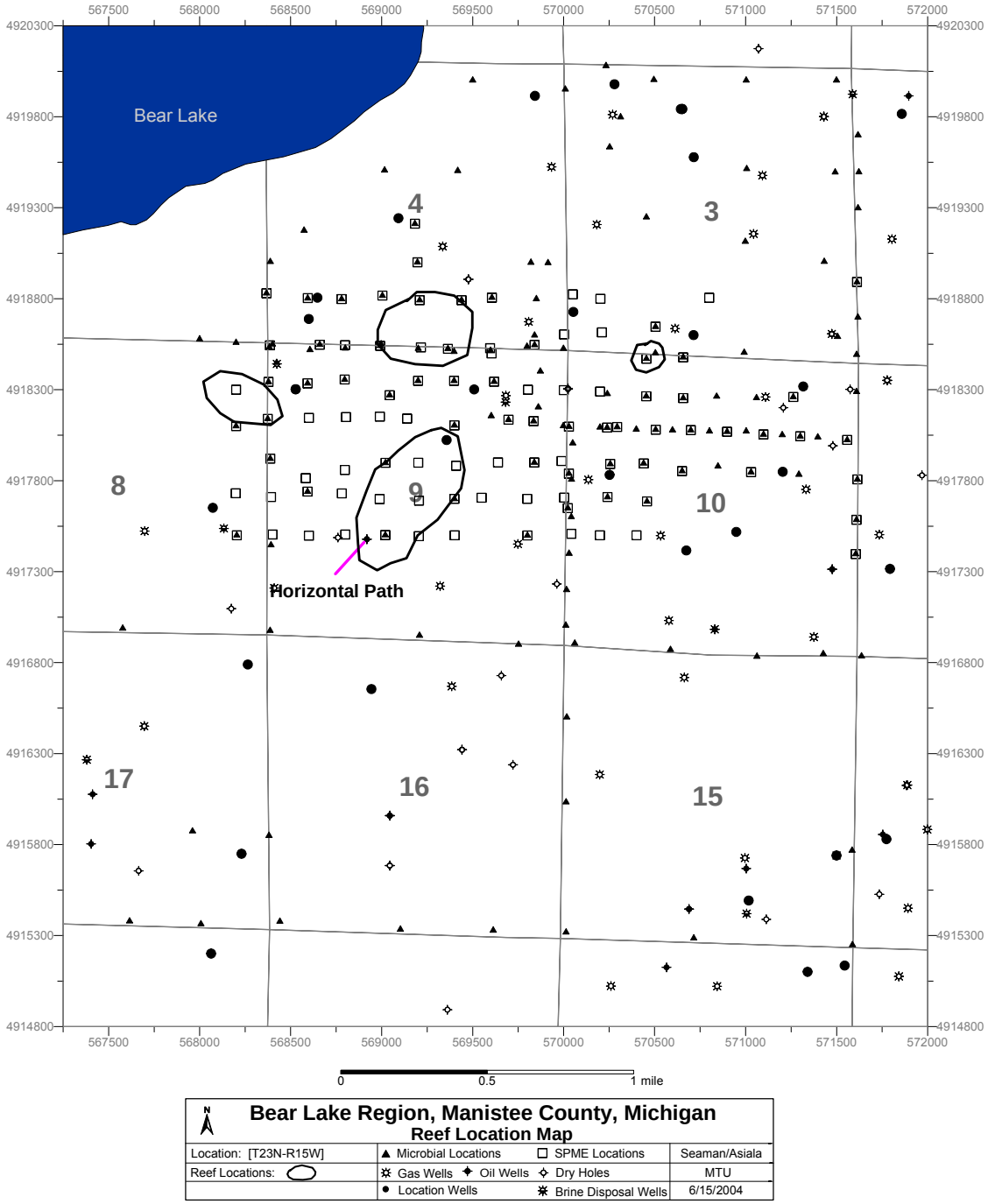

Figure 8. Microbial sample and well location map for the Bear Lake area, Manistee County, Michigan.

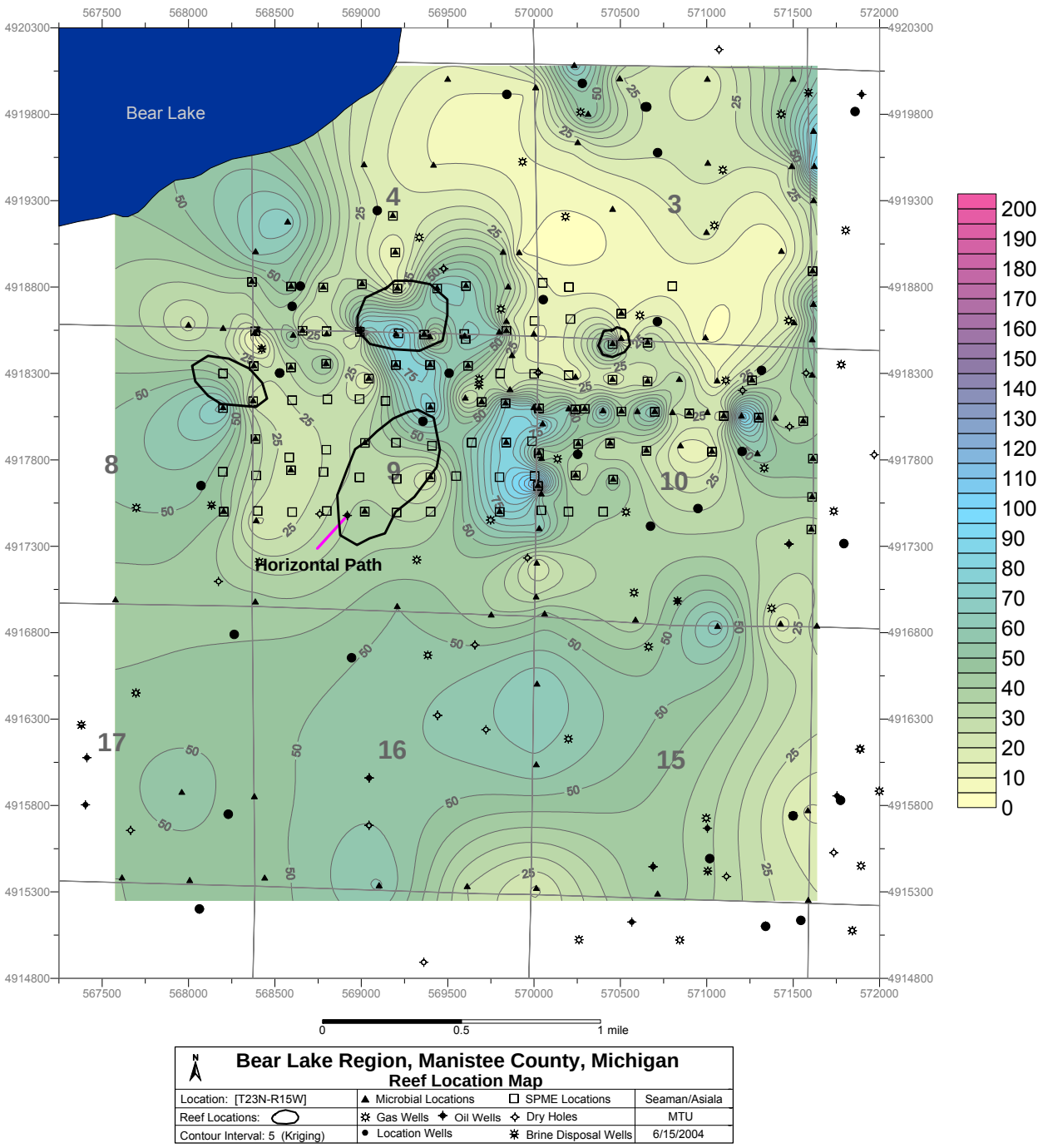

Figure 9. Microbial sample location and contour map for Bear Lake, Manistee County, Michigan. Blue contours indicate high microbial anomalies and yellow contours indicate low anomalies. Location of Charlich-Fauble sidetrack is shown by pink line.

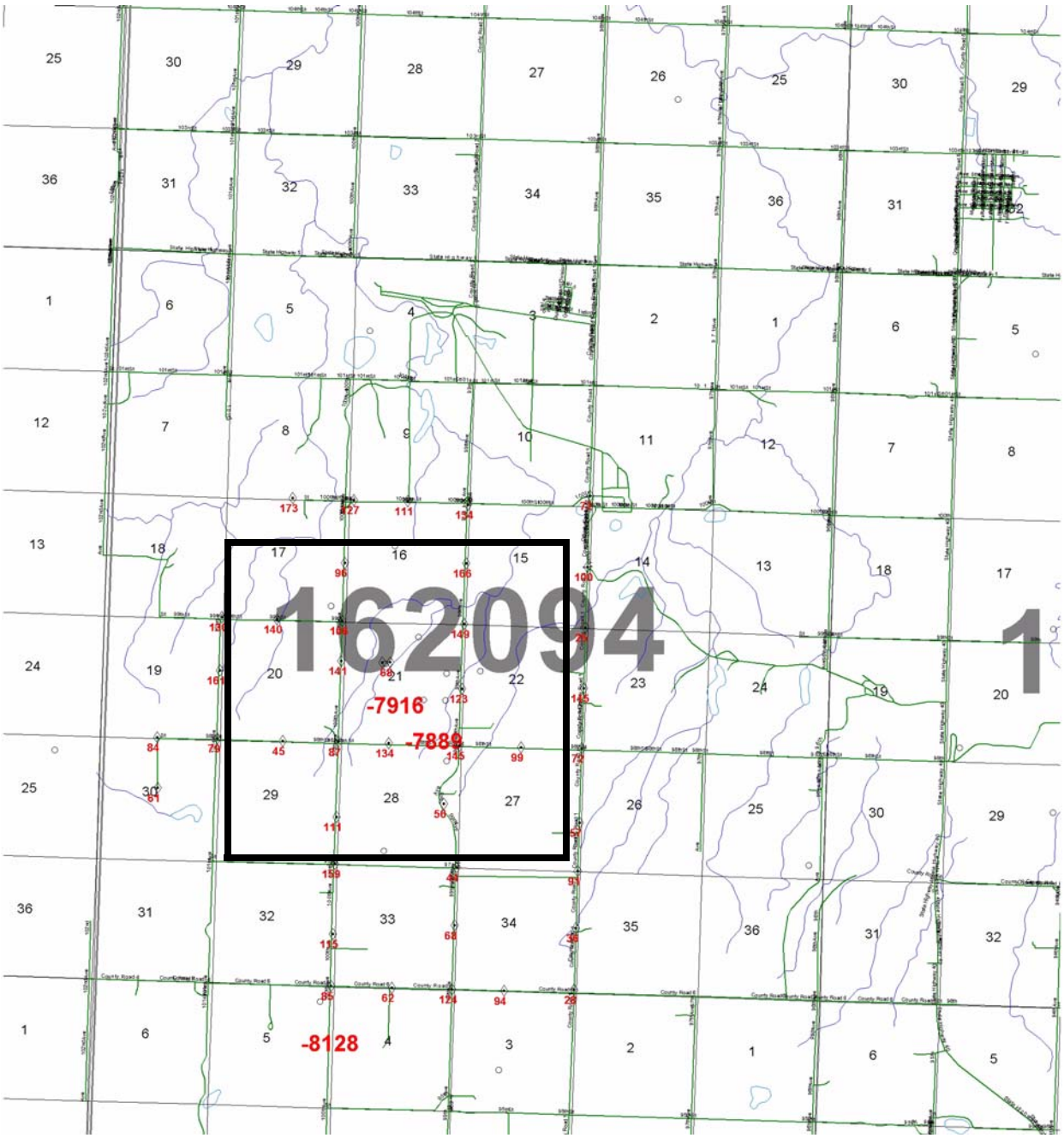

Figure 10. Microbial sample locations in the Myrtle Beach area. Microbial counts posted in red below sample location. Black outline is location of 3D seismic survey. Blue lines are rivers and lakes, Green lines are roads, subsea Winnipegosis tops for 3 deep wells posted in red. North is toward top of map.

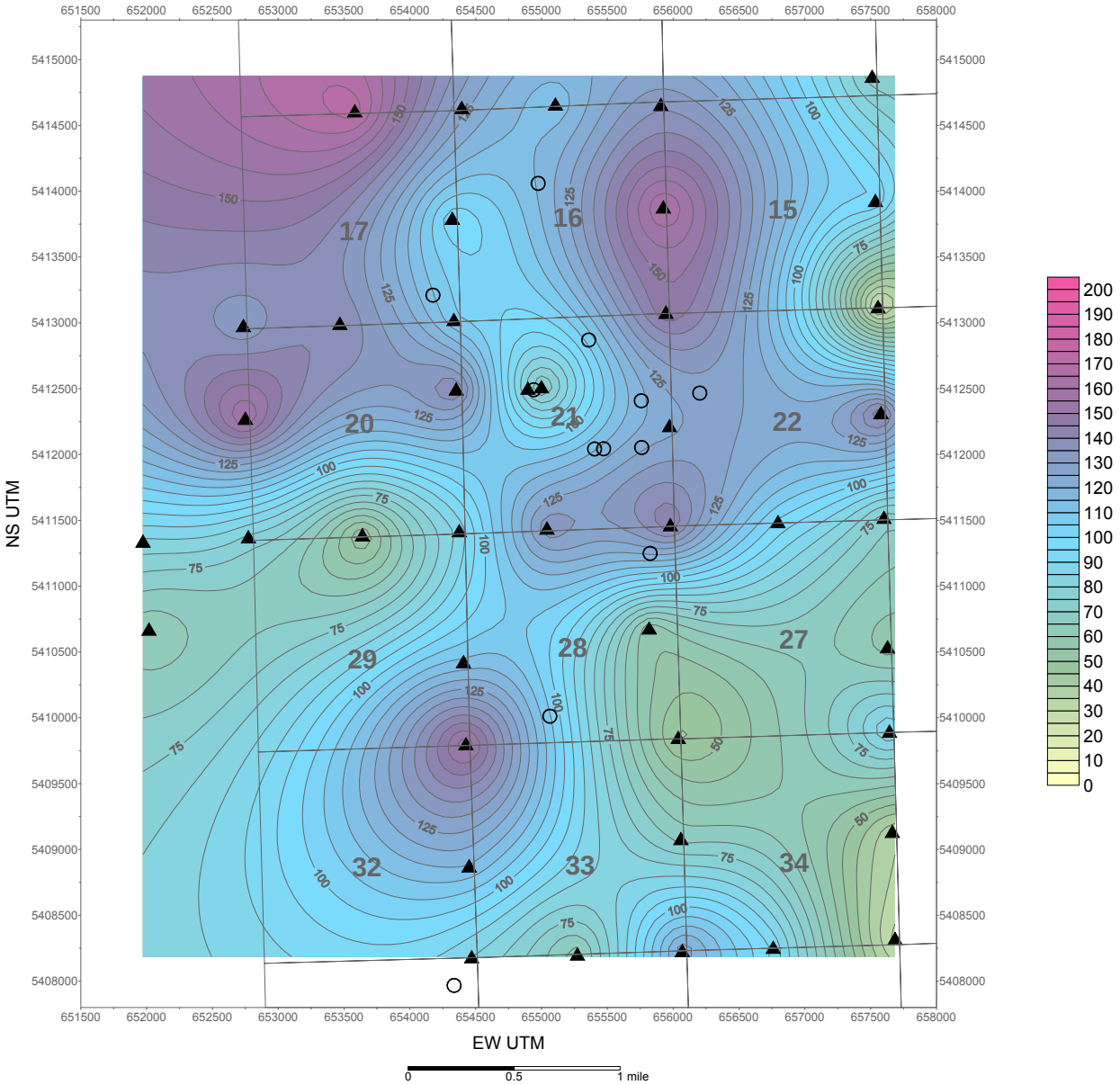

Figure 11. Microbial contour and sample locations in the Myrtle Beach area. Red and Purple color filled contours indicate high microbial anomalies and green indicates low anomalies. Contour interval is 5 microbial counts. The high microbial counts recorded here are the highest recorded in the project to date.

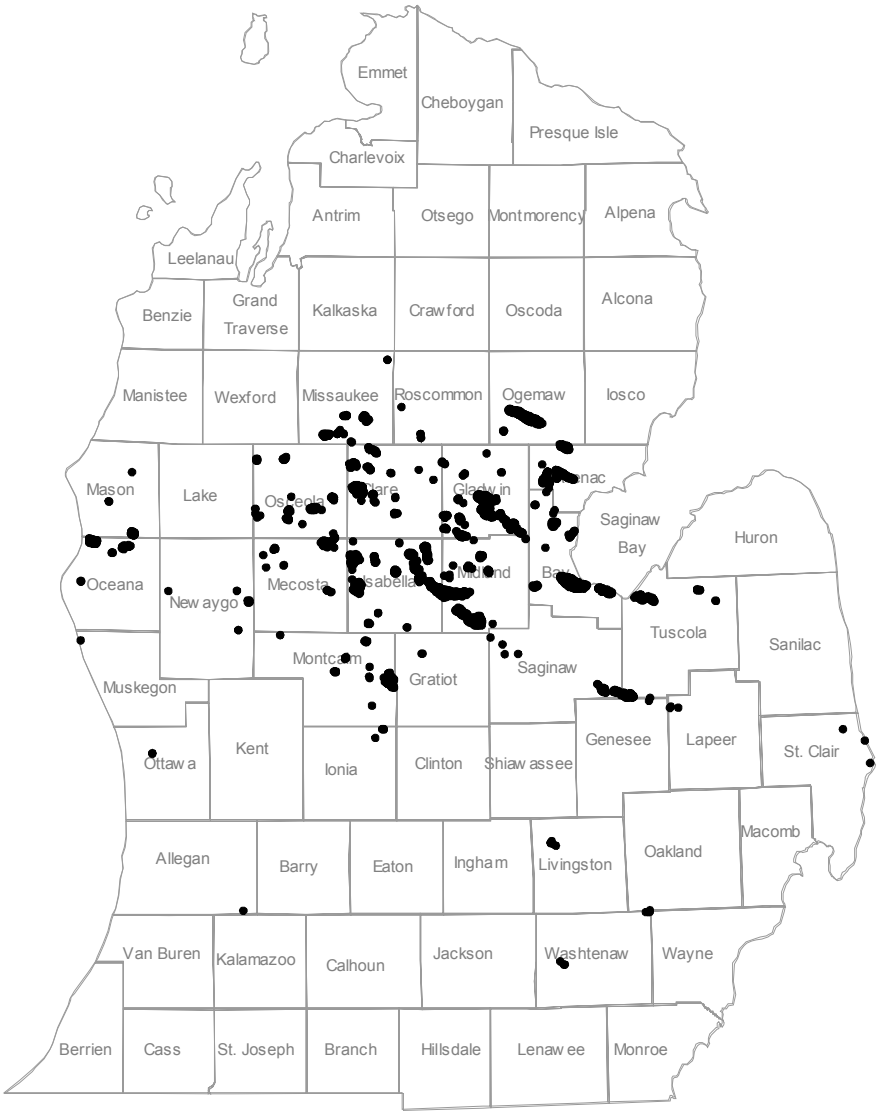

Figure 12. Location map for 2003 Dundee-Rogers City producing wells (black dots) from the Michigan Department of Natural Resources (MDNR) production database. County names are also shown for reference.

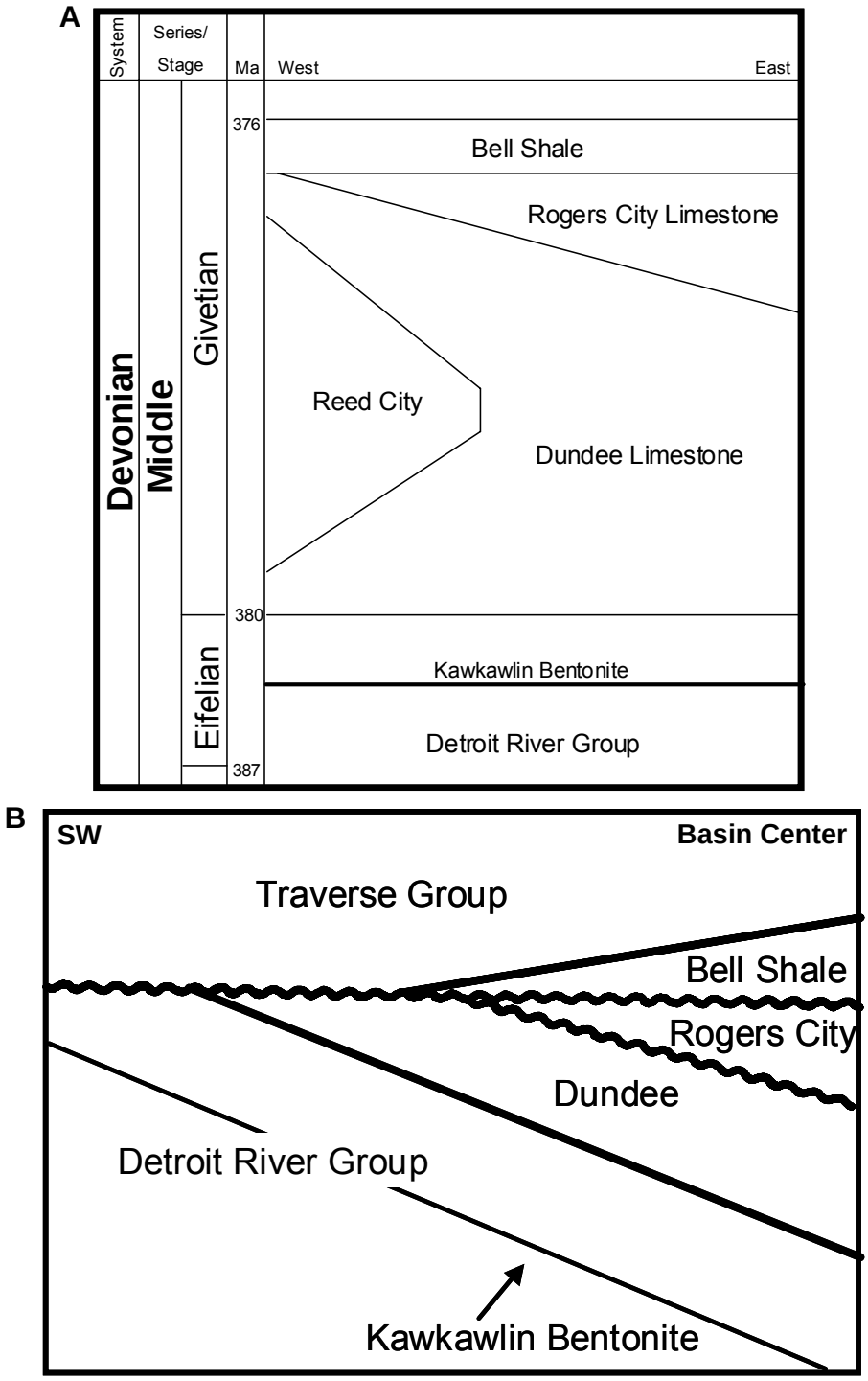

Figure 13. (A) Stratigraphy diagram for the Dundee-Rogers City and surrounding Middle Devonian units from west to east across the central Lower Peninsula of Michigan (modified from Catacosinos et al., 1991). (B) Cross-sectional stratigraphy schematic from southwest toward the center of the basin, illustrating that the Bell Shale, Rogers City and Dundee intervals are all absent in portions of southwestern Michigan. Note that the vertical scale is exaggerated.

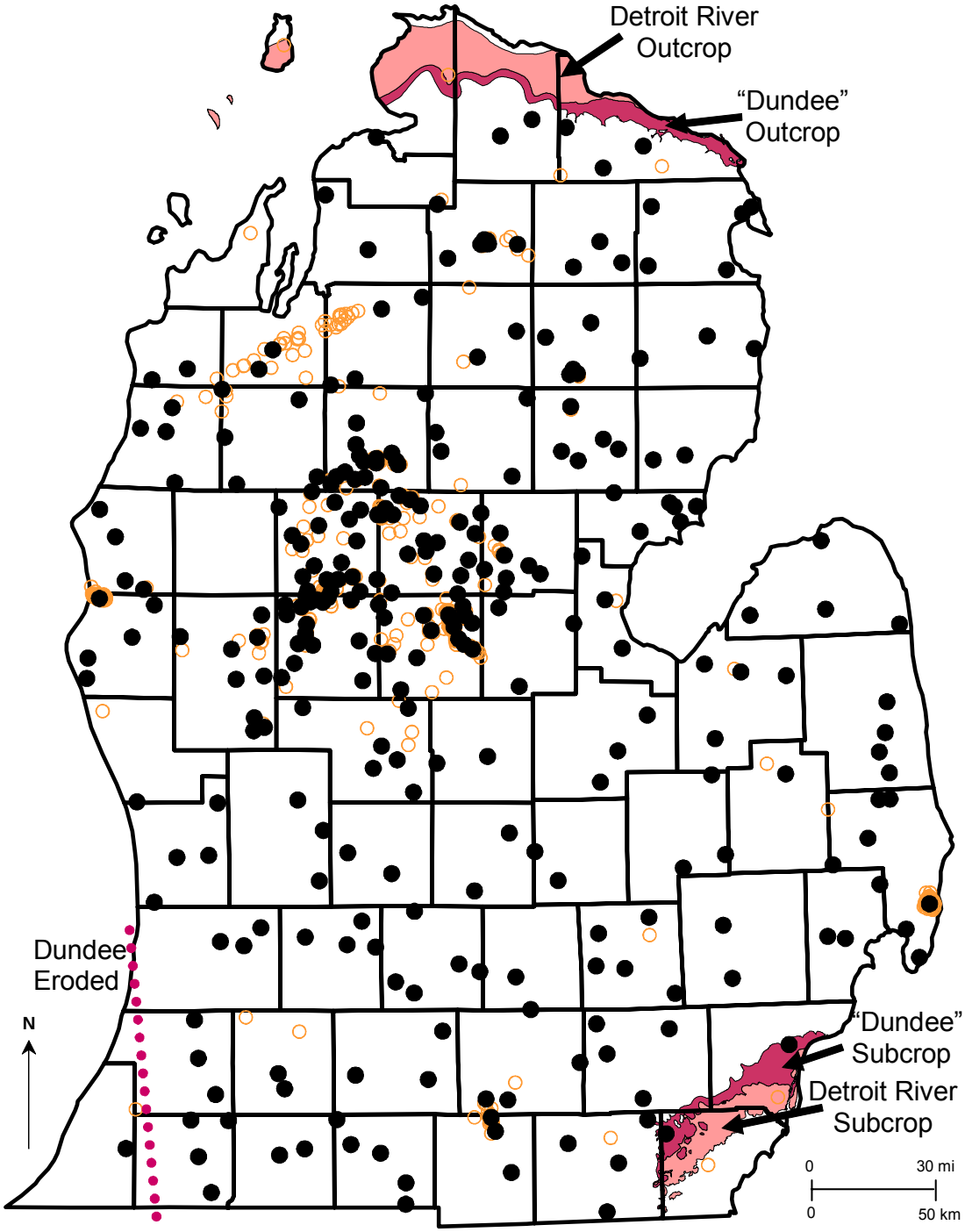

Figure 14. Outcrop and subcrop locations for the Detroit River Group and the combined Dundee-Rogers City ("Dundee") unit. A dotted line in the southwest region illustrates the absence of the Dundee Limestone due to erosion. Black closed circles represent wells used in the WLT slicing program and orange open circles locate the wells discarded before slicing.

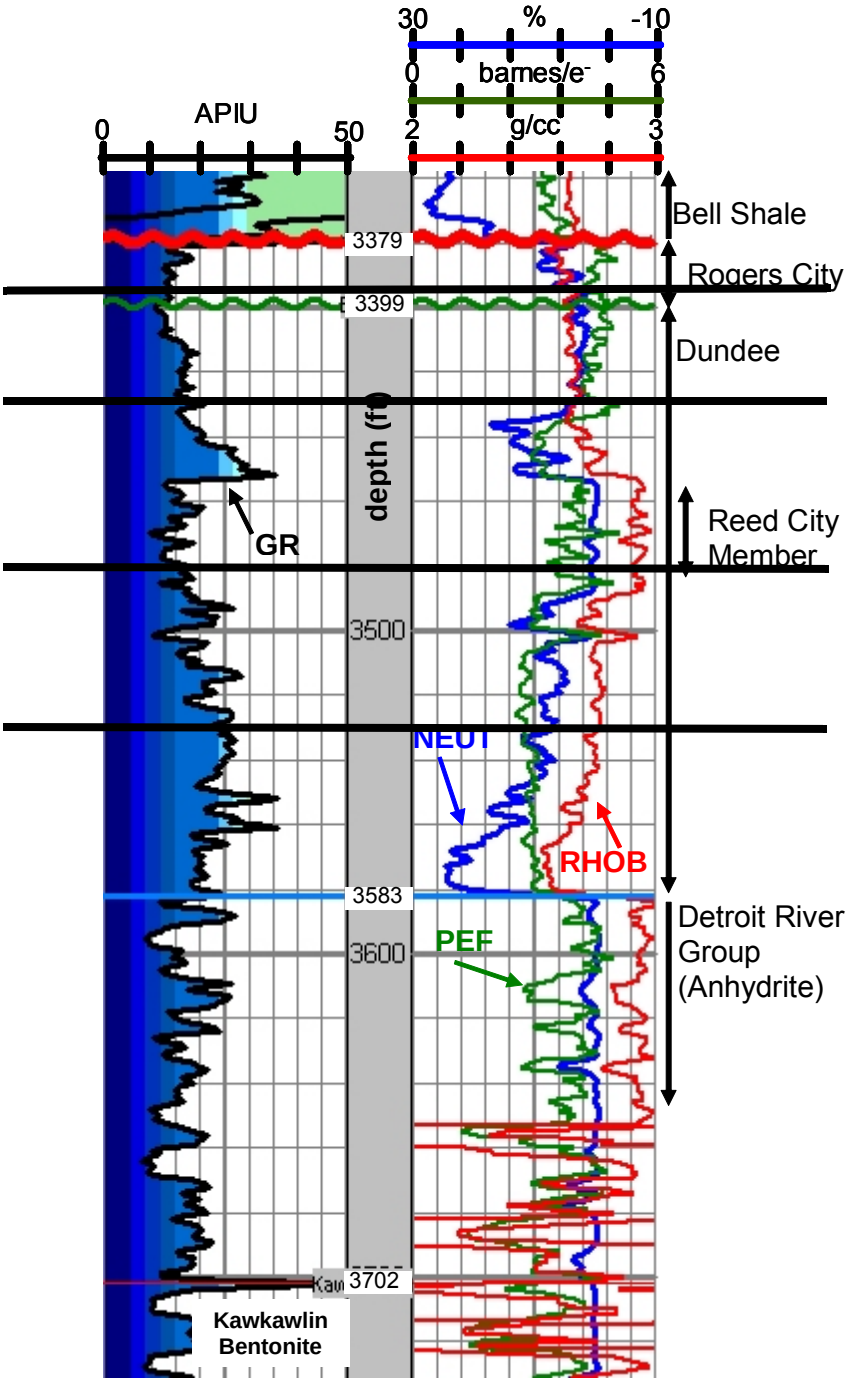

Figure 15. Example digital well log, from the Alber #1-23 well, permit 40215 located in Mecosta County, Michigan. The gamma ray (GR) log curve is located on the left track of the well log with a color-filled amplitude. On the right track are the density (RHOB) log curve (red), neutron (blue) and photoelectric effect (green). The top picks are labeled on the depth scale in the center track. The Reed City is labeled but has no top pick because it is only a Member of the Dundee and is not present throughout the entire basin. The horizontal lines are the location of the amplitude slices shown in Figure 16.

Figure 16. (Next Page) Comparison of four proportional gamma ray, bulk density (rhob) and photoelectric factor (Pef) slices for the Dundee and Rogers City Limestones in the Michigan Basin (refer to Figure 15 for approximate slice locations). Note the subtle North-South trends in the gamma ray and pef slices. The rhob slices show the extent of the Reed City Member (anhydrite). The gamma ray slice data range is 0 to 30 api units and the contour interval for each slice is 3 api units. The rhob slice data range is 2.0 to 3.0 grams per cubic centimeter (g/cc) and the contour interval is 0.07 g/cc. The data range for each Pef slice is 0 to 10 barns per electron (b/e). The contour interval is 0.6 b/e. 300 wells were used in the gamma ray slices, 150 wells were used in the rhob slicing and 121 wells were used in the Pef slicing. Gray lines are county boundaries and gray numbers are county names. North is toward the top of the slices. Large white dots are data control points on each slice. Yellow and black rectangles show the location of the Vernon geochemical survey area.

	Gamma Ray (GR)	Bulk Density (RHOB)	PEF
Rogers City (approximate)	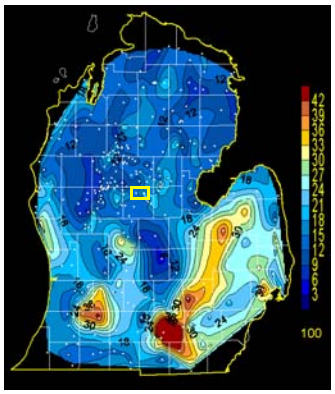	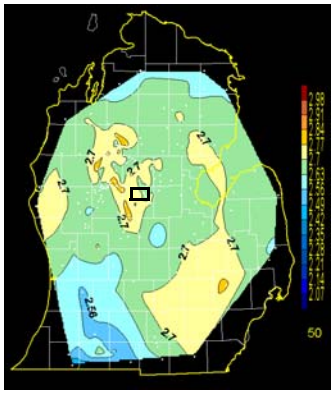	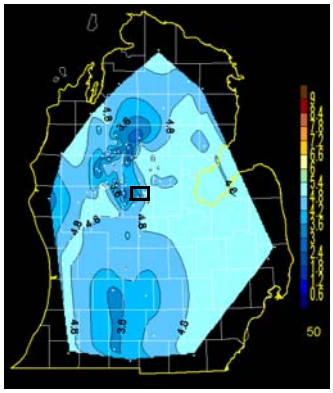
Upper Dundee	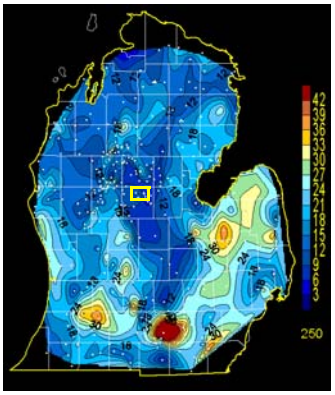	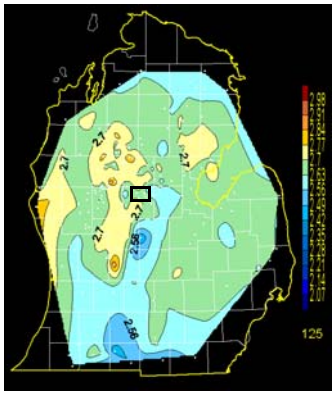	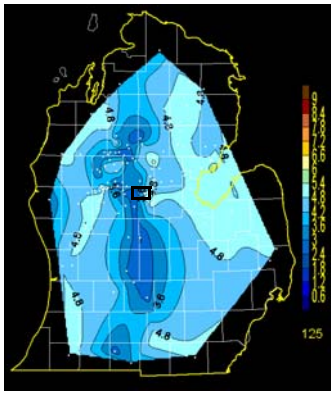
Middle Dundee (Reed City)	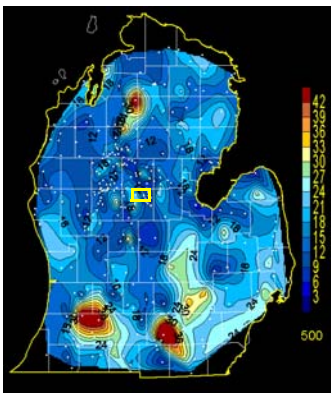	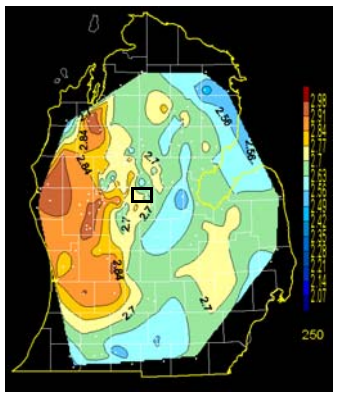	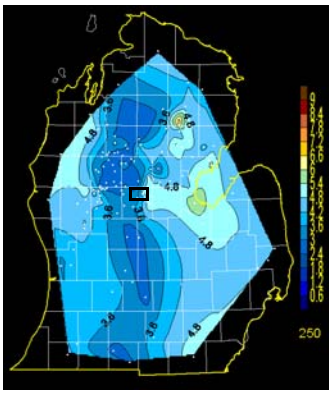
Lower Dundee	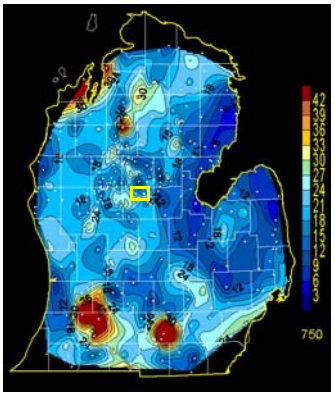	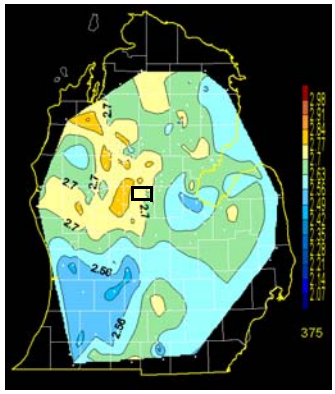	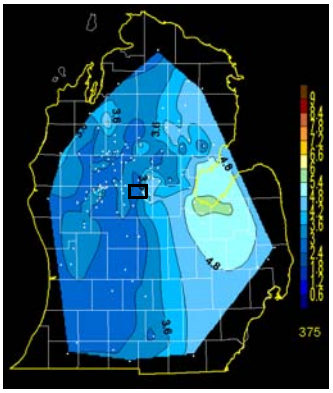
	CI = 3 api	**CI = 0.07 g/cm^3**	**CI = 0.6 b/e**

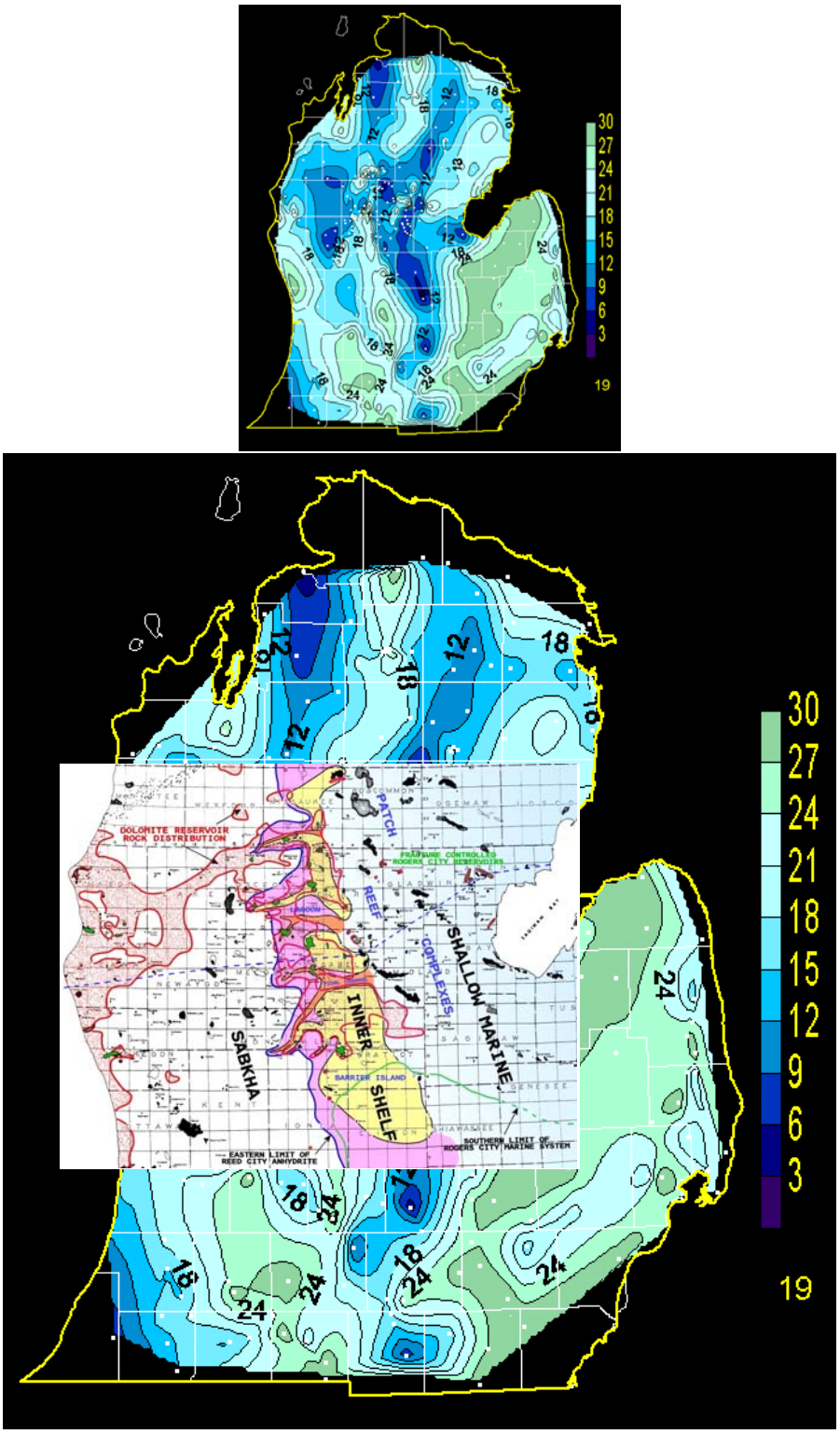

Figure 17. (A) Slice 19 from the top-down Dundee Limestone results. (B) Taylor's (2001) depositional model for the upper Dundee superimposed onto slice 19 illustrating the similarity between the shelf trend in Taylor's model and the low gamma ray trend from the slicing results.

Using Recent Advances in 2-D Seismic Technology and Surface Geochemistry to Economically Redevelop a Shallow Shelf Carbonate Reservoir: Vernon Field, Isabella County, MI

DE-FC26-00BC15122

Program

This project was in response to DOE's solicitation DE-PS26-99BC15144, Reservoir Class Field Demonstration Program – Class Revisit. The goal of the Class Program was to extend economic production of domestic fields, by slowing the rate of well abandonments, preserving industry infrastructure, and to increase ultimate recovery using improved reservoir characterization and advanced technologies.

Project Goal

Develop and execute an economical and environmentally sensitive plan for recovery of hydrocarbons from abandoned shallow-shelf carbonate fields. The project will combine recent advances in 2-D seismic and surface geochemistry with multilateral horizontal drilling, coiled tubing technology and well logging to recover new and bypassed oil in this depositional environment. Five to ten of the more promising locations will be evaluated and characterized as part of this project.

Performers

Michigan Technological University, Houghton, MI
Western Michigan University, Kalamazoo, MI
Jordan Exploration Co, Traverse City, MI

Project Results

The project has demonstrated the success of geochemical sampling (microbial and soil gas analysis) for prediction of drilling locations in carbonate reservoirs.

Benefits

Development of an efficient, reliable surface geochemical sampling technology will allow independent operators to explore for oil and gas reserves in a cost-effective manner. The geochemical survey samples are easy to collect, east to interpret and far less costly than seismic surveys to determine drilling locations in mature oil fields. In general the geochemical program is proving to be a valuable addition to prediction capabilities for locating drilling sites. Increased production from the horizontal wells drilled in Manistee County, Michigan are already providing jobs, tax revenue and royalties.

James Wood and assistant record data from surface geochemical survey. Note the thick lush vegetation in the Michigan Basin demonstration sites.

Background

The resource base at Vernon Field is estimated at over 5-8 MMbbl of oil, with 1.5 MMbbl oil estimated recovery for this project. As much as 900,000 bbls could be produced over the 5 year time period of this project. It is estimated that there are 10 to 20 fields similar to Vernon in the Michigan Basin with comparable possible recoveries (10 to 30 MMbbls. The producing zone in Vernon is the upper Dundee "Rogers City" formation. The Dundee dolomite has good porosity and permeability with abundant vugs and fractures. The "top of porosity" over Vernon coincides with the nearly 100% altered (dolomitized) rock, common in Michigan basin reservoirs.

Producibility problems addressed in the project are: 1) locating remaining oil, 2) characterizing the reservoir architecture (structure, alternation and facies distribution), and 3) efficiently draining remaining hydrocarbons. Economic considerations are paramount: 3D seismic is too expensive, yet the structure and extent of dolomitization needs to be better known prior to drilling. Recent advances in 2D seismic acquisition and interpretation for the first time permit resolution of structure beneath the area's glacial till.

One of the main objectives of DOE's funding of this project is to test surface geochemical techniques for detecting trace amounts of light hydrocarbons as a means of reducing risk in hydrocarbon exploration and production. As part of the project, several field demonstrations were designed to assess the validity and usefulness of the microbial surface geochemical technique. The geochemistry technology demonstrations have been successful in identifying the presence or absence of hydrocarbons in the subsurface.

Project Summary

- Conducted surface geochemistry surveys employing 5 different techniques (surface iodine, microbial, enzyme leaching, soil gas, and subsurface iodine) in Vernon Field.
- Geochemical surveys suggest the best results can be obtained from microbial data and direct measurement of soil gas.
- The project was expanded to include fields in Manistee and Otsego Counties, MI and Burke County, ND to test the validity of the surface geochemical testing.
- In 2003, a 200 bbl/day well drilled at Bear Lake, Manistee County, MI confirmed the use of surface geochemical prediction for drilling on carbonate reef structures.

- Surface geochemistry data showed a good microbial anomaly in the path of a proposed well in the Springdale area Manistee County, MI. In December 2003 the Springdale area well came on line at 100 bbl per day.
- Two follow-up horizontal wells have been drilled in the Springdale area. The 1st is producing 100 bbl/day.
- Detailed mapping of the Central Michigan Basin has revealed for the first time the presence of eleven major faults that control the location of many of the reservoirs in the Michigan Basin. These faults appear to control the location of many of the large anticlinal structures in the Michigan Basin and likely control fluid movements as well.
- 40 microbial samples were collected over a depleted field in Burke County, ND indicating a strong anomaly in the Myrtle Beach field, Burke County, ND.

The geochemical sampling program over the Vernon Field, Isabella County, Michigan is now interpreted as a large negative anomaly associated with the entire field. The results of the two horizontal wells confirmed the lack of additional recoverable hydrocarbons in the Vernon Field. Because of this the research in Michigan has concentrated on the Manistee County, MI demonstration site.

The surface geochemistry sampling in the Bear Lake site in Manistee County, MI was updated after drilling confirmed the presence of oil. The original subsurface and seismic interpretation used to guide the location of the geochemical survey for the a lateral re-entry was different than the interpretation used by the operator who ultimately drilled the well. As expected, the anomaly appears to be diminishing as the positive (apical) microbial anomaly is replaced by a negative (edge) anomaly, probably due to pressure draw-down in the reservoir.

Surface geochemistry data showed a microbial anomaly that indicated the presence of a fault or strata-graphic facies change at the Springdale site in Manistee County, MI. The 100 bbl/day well is considered a good well by Michigan Basin standards. Reserves have not been established; however two successful follow-up horizontal wells have been drilled in the Springdale area.

The Myrtle Beach field, ND produces from Ordovician (Black Island and Red River) and Devonian (Winnipegosis and Duperow) limestones similar to the Dundee and Rogers formations in Michigan. The strong anomaly in the Myrtle Beach, Burke County, ND area would justify drilling by itself and even more so in conjunction with the structural interpretation from geological and geophysical data. The microbial values here were the highest the research team had observed. The Myrtle Beach geochemical survey indicated a good to excellent prospect which was confirmed by drilling, however, a pipeline has not yet been completed that would allow the wells to be placed into production.

Current Status

Additional geochemistry data will be collected in the Springdale area in 2004 to further verify the validity of the geochemical technology. Upon completion of the proposed pipeline in North Dakota additional wells will be drilled at the Myrtle Beach prospect and put on production.

Recent efforts to map carbonate facies tracts in the middle Devonian Dundee and Rogers City Limestones (MI) using gamma ray, bulk density, and photoelectric effect geophysical well log amplitudes will be used identify fairways for exploration where surface geochemical techniques can be used to screen additional potential petroleum prospects for both exploration and infield oil drilling.

Surface samples for geochemical analysis were collected from small, shallow pits. Note the small amount of soil bagged for the soil gas and microbial samples.

Project Start: March 20, 2000
Project End: March 19, 2005

Contact Information:
NETL – Gary Walker (Gary.Walker@netl.doe.gov or 918-699-2083)
Michigan Tech – James Wood (jrw@mtu.edu or 906-487-2894)
1400 Townsend Dr., Houghton, MI 49931

Intelligent Computing System for Reservoir Analysis And Risk Assessment of the Red River Formation

FINAL REPORT

By
Mark A. Sippel, William C. Carrigan, Kenneth D. Luff and Lyn Canter
12 November 2003

Work Performed under Contract No. DE-FC26-00BC15123

Prepared for:

U.S. Department of Energy
Assistant Secretary for Fossil Energy

Paul West
National Petroleum Technology Office
P.O. Box 3628
Tulsa, OK 74101

Prepared by:
Luff Exploration Company
1580 Lincoln Street, Suite 850
Denver, CO 80203

COOPERATIVE AGREEMENT DE- FC26-00BC15123

Disclaimer

This report was prepared as an account of work sponsored by an agency of the United States Government. Neither the United States Government nor any agency thereof, nor their employees, makes any warranty, expressed or implied, or assumes any legal liability or responsibility for the accuracy, completeness, or usefulness of any information, apparatus, product, or process disclosed or represented that its use would not infringe privately owned rights. Reference herein to any specific commercial product, process, or service by trade name, trademark, manufacturer, or otherwise does not necessarily constitute or imply its endorsement, recommendation, or favoring by the United States Government or any agency thereof. The views and opinions of authors expressed herein do not necessarily state or reflect those of the United States Government or any agency thereof.

Intelligent Computing System for Reservoir Characterization and Risk Assessment

Abstract

Integrated software has been written that comprises the tool kit for the Intelligent Computing System (ICS). The software tools in ICS have been developed for characterization of reservoir properties and evaluation of hydrocarbon potential using a combination of inter-disciplinary data sources such as geophysical, geologic and engineering variables. The ICS tools provide a means for logical and consistent reservoir characterization and oil reserve estimates. The tools can be broadly characterized as 1) clustering tools, 2) neural solvers, 3) multiple-linear regression, 4) entrapment-potential calculator and 5) file utility tools. ICS tools are extremely flexible in their approach and use, and applicable to most geologic settings. The tools are primarily designed to correlate relationships between seismic information and engineering and geologic data obtained from wells, and to convert or translate seismic information into engineering and geologic terms or units. It is also possible to apply ICS in a simple framework that may include reservoir characterization using only engineering, seismic, or geologic data in the analysis. ICS tools were developed and tested using geophysical, geologic and engineering data obtained from an exploitation and development project involving the Red River Formation in Bowman County, North Dakota and Harding County, South Dakota. Data obtained from 3D seismic surveys, and 2D seismic lines encompassing nine prospective field areas were used in the analysis. The geologic setting of the Red River Formation in Bowman and Harding counties is that of a shallow-shelf, carbonate system. Present-day depth of the Red River formation is approximately 8000 to 10,000 ft below ground surface. This report summarizes production results from well demonstration activity, results of reservoir characterization of the Red River Formation at demonstration sites, descriptions of ICS tools and strategies for their application.

Executive Summary

This report contains descriptions of software tools for aiding companies and individuals in their efforts to extract the most information from geophysical, geological and engineering data in the pursuit of oil exploration and development. The primary objective of this project is to construct software tools for an integrated system of reservoir characterization and risk assessment. Several reservoir characterization and file utility tools comprise the “Intelligent Computing System” or ICS tool kit. These tools were written in MATLAB™. MATLAB is an integrated programming and visualization environment that uses a proprietary interpreted language designed for easy experimental development of scientific and engineering software. These tools were developed and tested using seismic, geologic and well data from the Red River Play in Bowman County, North Dakota and Harding County, South Dakota. Data was used from 3D seismic surveys covering eight areas and 2D seismic lines covering three areas. The geologic setting for the Red River Formation is shallow-shelf carbonate at a depth from 8000 to 10,000 ft. It is thought that the ICS tools can be used in many geological settings.

The ICS software tools and utilities are delivered both as compiled routines and in native MATLAB™ format. The compiled version will run stand-alone without additional software. To use the software routines in native MATLAB™ format, the user must have purchased a license for the basic MATLAB with Neural Net and Statistic Toolbox add-ins. Other useful software programs for use in conjunction with the ICS tool kit are Microsoft Excel spreadsheet and Golden Software Surfer surface mapping system. The ICS tool kit has been run on Windows 98, 2000 and XP operating systems. A modern computer system with 500 MHz or better processor, 19-inch monitor and high-end graphics are recommended. With large data files of more than 10,000 rows, a 2 GHz computer is recommended.

Predictions were made with ICS for reservoir development and production potential in relatively mature oil fields where there has been production for over 20 years. Wells were drilled or re-drilled with horizontal laterals to test and confirm reservoir characterizations from ICS analysis. Three waterflood units were formed with reservoir characterizations from ICS as a significant role in waterflood design and equity-participation parameters. On average, the production results from horizontal drilling, either new or re-entry, were slightly better than the initial production from vertical wells that were completed 20 to 30 years ago. Over the project term, 25 wells were successfully drilled as new or as re-entry with horizontal laterals in Red River reservoirs. The combined baseline production during 1998 and 1999 averaged 13,121 bbl per month. In 2003, the average production was 46,869 bbl per month. Cumulative incremental oil production was 986,000 bbl through October 2003. Projected incremental ultimate recovery, from primary and secondary, is 5,300,000 bbl. All of these

wells are in fields that have been producing for 20 to 30 years with many wells producing near the economic limit. Some of the wells that were re-entered for horizontal drilling had been plugged and abandoned.

Reservoir characterizations and production metrics from three fields are described in the report. These case studies discuss the application of ICS tools and strategy with 3D and 2D seismic data and integration with production and geologic data from many wells in several fields.

Rock-typing and geologic models were developed for the Red River B and D Zones. Petrographic and analytical studies from cores of the Red River B and D Zones were used for these geologic models. While ICS tools and strategy allow empirical correlation and prediction for reservoir development and production potential, it is best to have a working geologic model, or models, for the depositional system and subsequent diagenisis. Geologic models will aid in interpretation of results from ICS studies and in selection of important training data for cluster and neural network analysis.

During the project, technology transfer was accomplished with an article in the *American Oil and Gas Reporter*, a daylong workshop, a poster session at the 2003 annual meeting of American Association of Petroleum Geologists and a website. The article in the *American Oil and Gas Reporter* entitled “Intelligent Computing Software Allows Independent to Delineate Thin Reservoirs” was published in February 2002. A workshop was hosted by the Rocky Mountain Region of the Petroleum Technology Transfer Council for the Intelligent Computing System that was held at the campus of Colorado School of Mines in November 2002. A presentation was made in December 2002 at Odessa, Texas for a program sponsored by the National Energy Technology Laboratory for Class II Review. A poster session was presented during May 2003 in Salt Lake City at the annual convention of AAPG. The project website, luffdoeproject.com, was active from January 2001 through the remainder of the project term. In the future, the Rocky Mountain Region of the Petroleum Technology Transfer Council will provide Internet access for downloading ICS software though a case studies link at http://www.mines.edu/research/PTTC/.

The website contained an online tutorial for the Intelligent Computing System and provided a means for downloading the ICS software and example data files. Browser activity for the website was monitored and the website provider made tabulation at the end of the project. Shown in the table is a summary of website activity. There were 329 downloads of ICS in Matlab native format and 483 downloads of the compiled version. In addition, there were 825 downloads of the topical report that covered the first budget period. Twenty-nine requests were received for a copy of ICS software on CD-ROM.

Website Activity Sept 2003	Total	2001		2002		2003	
		1st half	2nd half	1st half	2nd half	1st half	2nd half
Sessions	11,913	153	666	714	2,668	4,704	NA
Pageviews	40,568	1,901	NA	3,572	11,750	16,240	NA
Serious (4+ pageviews)	2,515	84	NA	173	532	697	NA
Casual Browser (2 or 3 pageviews)	1,522	8	NA	103	491	690	NA

A manual and guide for the Intelligent Computing System is included in this report. The manual covers all software routines that comprise the ICS tool kit and their application. There are two versions of ICS. One version is compiled and can be used without purchase of any MATLAB products. Users cannot modify the software. The other version of the ICS tool kit is functionally the same as the compiled version but is in native MATLAB script format. Users must have MATLAB with the Neural Net and Statistics Toolboxes to run this version. The script files can be modified.

A CD-ROM accompanies this report. The CD-ROM contains the ICS routines and necessary support files. Instructions for installation are included in the ICS manual and on the CD-ROM. Included on the CD-ROM are appendices for Red River rock-typing sections of the report: Appendix A, B and C. Data from project demonstration sites are also included under the directory Appendix D. Spreadsheets tabulate the data that is included for each demonstration site. General categories for demonstration site data include well logs, core studies, geologic reports from drilling, production and maps from ICS analysis.

Table of Contents

Reservoir Characterization with the Intelligent Computing System 3
Characterization Strategy 3
Data Collection and Organization 4
Understanding Data Error 6
Production Metrics 17
Reservoir Characterization with 3D Seismic at Amor South Red River Unit 25
Historical Background 25
Regional Setting 26
Local Structural Setting 27
Red River D Zone Characterizations 27
Summary for Red River D Zone Characterizations 28
Red River B Zone Characterizations 29
Summary for Red River B Zone Characterizations 31
Reservoir Characterization with 2D Seismic at Amor North Field 50
Historical Background 50
Regional Setting 50
2D Seismic Data 50
Red River D Zone Characterization 52
Red River B Zone Characterization 53
Demonstration Wells 54
Reservoir Characterization at East Harding Springs Area 67
Historical Background 67
Red River B Zone Characterization 67
Production Results 68
Geologic Rock-Typing, Red River B Zone 71
Red River B Zone Lithology and Facies Identification 72
Red River B Zone Depositional Model 73
Application of Depositional Model 75
Amor South Field 77
Cold Turkey Creek Field 79
Grand River Field 79
Conclusions 81
Analytical Rock-Typing, Red River B Zone 111
Analytical Rock-Typing, Red River D Zone 125
Manual and Guide for Intelligent Computing System 133
Data Requirements 134
ICS Front Page 136
Land Grid and Wells 137
File Build Utilities 139
Merge Tool, File Build Utilities 139
Standard-Deviation Normal, File Build Utilities 143
Seismic at Wells, File Build Utilities 147
Build Train or Cluster Files, File Build Utilities 153

Other Utilities 158
Trend Tool, Other Utilities 158
Entrapment Tool, Other Utilities 163
Growth Index Tool, Other Utilities 171
Viewer Tool, Other Utilities 174
MLR STAT, Other Utilities 177
Cluster Rank Combine, Other Utilities 184
ICS Clustering Tools 187
Cluster 1 with Intervals Tool 187
Cluster 2 Non-Intervals Tool 194
Cluster 3 Tool 196
Neural Solvers 199
Overview 199
Neural Solver 1 Tool 199
Neural Solver 2 Tool 206

Intelligent Computing System for Reservoir Characterization and Risk Assessment

Reservoir Characterization with the Intelligent Computing System

Luff Exploration Company has developed software tools and a characterization strategy to better assess reservoir limits, producibility and favorable depositional setting. The Intelligent Computing System (ICS) software uses clustering, artificial neural networks and classical regression methods to combine seismic, geologic and engineering data for predictions of reservoir potential. Output can be used to create characterization maps that directly assess oil-in-place and oil production. The independent nature of the software tools allows the user to develop a characterization strategy for almost any hydrocarbon reservoir. Output from the software is also used for construction of computer reservoir simulation models. Although the software tools were developed to help integrate seismic, borehole and production data, reservoir characterizations can be performed with only well data in situations of fields with many wells.

Luff Exploration Company is applying these tools for analysis of carbonate reservoirs in the Red River Formation of the southern Williston Basin. The integrated software programs are designed to be used by a small team consisting of an engineer, geologist and geophysicist. The software tools can be flexible and robust, allowing application in many environments for hydrocarbon reservoirs. Keystone elements of the software tools include clustering and neural-network techniques. The tools are used to transform seismic attribute data to reservoir characteristics such as storage (phi-h), oilcut with depth, initial oil rate, structural depths and structural growth history. ICS tools and characterization strategy have been tested at nine Red River fields. Luff Exploration Company is using these tools to quantify reservoir parameters for forming waterflood units, targeting drilling locations and orientation of horizontal drill holes.

Characterization Strategy

The reservoir characterization strategy used for Amor South Red River Unit, Bowman County, North Dakota follows the diagram shown in **Figure 1-1**. The final objective was to predict production attributes of oil rate and oilcut for the Red River B Zone and D Zone reservoirs. Further, our objectives were to make these predictions from local well control and also from external control from other 3D seismic survey areas.

The first level of the strategy is to collect basic information about the wells and geology. Included in the first level is understanding the seismic as it relates to variations in reservoir development. The second level integrates the geological and reservoir data with seismic attributes to produce transformed seismic-

reservoir attributes. Transformed seismic-reservoir attributes include depth, thickness, porosity-thickness and entrapment attributes. At the third and last level, the transformed seismic-reservoir attributes are merged with production attributes to make predictions of production potential.

Data Collection and Organization

Application of the Intelligent Computing System requires a database of reservoir and production information. In most instances, seismic information will also be used in transforms to reservoir properties. Data collection and organization should be performed in a manner that is similar to what is required to build a computer reservoir simulation model. General categories for a database are shown in the list below.

Regional structure and depositional setting
Local structure and depositional setting
Thickness, porosity and permeability
Oil, water, and gas production
Seismic attributes

Databases are assembled with spreadsheet software with each row for a well or seismic trace location and each column for an attribute at that location. The first row of the database contains a label for each column. The first two columns are reserved for easting (x) and northing (y) coordinates. Any decimal coordinate system may used but must be consistent. The third column is reserved for a numerical identifier for the location (usually API number for wells). Databases are imported into ICS routines as comma-separated-variable (csv) format. Example file formats are described in detail in the ICS Manual.

Geological Data

A geological model for the reservoir of interest should be created from well log and core data. Sequence boundaries and important cycles within the reservoir and adjacent stratigraphic layers should be cataloged to aid construction of a geological database from well logs. At Amor South Red River Unit, the upper Red River was deposited in a carbonate shelf setting with four major cycles. The cycle boundaries are clearly divided by anhydrite, kerogenite and shale. Reservoir facies and rock-types in the upper Red River vary in a predictable manner with changes in thickness of the depositional cycles. Discussions of upper Red River B and D Zone depositional models, facies and rock-types are found in appendices. **Figure 1-2** shows a porosity type-log for the upper Red River in Bowman County, North Dakota.

Well logs

Well logs are a major source of information for reservoir characterization. Important geological horizons that can be correlated with seismic time markers should be included in the database. In the study area, the geological horizons most frequently used are Cretaceous Eagle, Niobrara, and Greenhorn Formations; Mississippian Mission Canyon; and Ordovician Red River and Winnipeg Formations. At the reservoir level, lithological markers that define sequence boundaries and depositional cycles should be part of the database. In the study of Amor South Red River Unit, geological markers that define the four major depositional cycles of the upper Red River were included in the database. Anhydrite thickness and gross-porosity interval thickness were also included. Digitized well-log data were used to compute porosity-thickness (storage). For other reservoir systems it may be appropriate to include well-log data such as shale volume and water saturation.

Drill-stem Tests

Drill-stem tests can be a rich source of production data for reservoir characterization. Extrapolated production rates, oilcut and transmissibility are included in the database for Amor South Red River Unit studies. In the case of dry holes, the drill-stem test data quantifies the production rate and oilcut beyond the economic reservoir limit.

Production

Ultimately, the goal of reservoir characterization is to allow prediction of production potential. Therefore, production data from wells will be a significant part of the database. Because Red River reservoirs in the study area are oil-water systems, peak oil rate and initial oilcut are included in the database. Also included are cumulative oil and oilcut for the first 24 months for individual wells. In other reservoirs, gas rate, gas-oil ratio and open-flow tests may be appropriate for inclusion in the production database.

Seismic Data

Before interpretation of seismic data can be performed, forward-modeling studies must be undertaken. Synthetic seismograms are frequently generated to correlate seismic events with geological formations. **Figure 1-3** shows a synthetic seismogram for Mission Canyon to Winnipeg in Bowman County, North Dakota. In some cases, vertical-seismic-profile tests are used to accomplish this correlation. At the reservoir level, synthetic logs are generated to cover the spectrum of lithological variation that is identified from geological study. At Amor South Red River Unit, seismic time for events that correlate with Eagle, Niobrara, Greenhorn, Mission Canyon, Red River and Winnipeg were picked using geophysical interpretation software and exported for the seismic database.

Forward-modeling studies of Red River seismic response has helped formulate a consistent seismic interpretation strategy. Forward-modeling studies show that there are two peak-trough amplitude pairs that cover the upper Red River formation. **Figure 1-4** shows a synthetic seismogram for variation of porosity in the upper Red River. Using normal polarity, the two peak-though amplitude pairs have been labeled as Orr P1 peak, Orr T1 trough, Orr P2 peak and Orr T2 trough. This convention is used by us in all 3D and 2D seismic interpretations for the study area. Variation of cycle thickness and porosity cause a change in amplitude and interval time between the peak-trough events. Therefore, these amplitudes and interval times are the seismic attributes that were exported from geophysical interpretation software for inclusion in the seismic-attribute database. In our study of Red River reservoirs in the southwestern Williston Basin, complex seismic attributes and Hilbert transforms did not improve correlation for interval thickness and porosity-thickness. Regardless of the reservoir setting, forward seismic-modeling should be used as a guide for selection of significant seismic attributes to include in the seismic database. For an integrated study database with multiple 3D seismic surveys, it should be noted that the processing parameters must be the same as well as using the same attributes.

After the seismic attributes at reservoir depth are picked and exported to ASCII files, normalization of the seismic attributes must be performed. In our application of ICS tools with seismic attributes, we normalize seismic-reservoir attributes so that each attribute has a mean of zero and a standard deviation of one. This process can be performed with the ICS Standard Deviation Norm Tool. Normalized seismic attributes are captured at well locations for creation of training files with either the ICS Seismic at Wells Tool or ICS Build Train/Cluster File Tool (full discussions of these and other ICS Tools are found in the ICS Manual). The normalized data at wells from multiple 3D seismic surveys can then be used to create a larger control population for ICS seismic-reservoir transforms. Shown in **Figure 1-5** is a map showing five 3D seismic surveys and associated control wells as training to make reservoir and production predictions at a sixth 3D seismic survey.

Understanding Data Error

The Intelligent Computing System toolkit contains neural solver, multiple-linear-regression and clustering tools that allow the user to make transforms from a data set to some objective. The user of the ICS toolkit will invariably discover that the neural solver often does not converge to the default threshold. This does not mean the answer is necessarily a “bad” answer. The neural solver architecture is deliberately structured to be simple. This simple architecture facilitates easy application for the user and attempts to avoid the situation of over-parameterizing. If a problem is over-parameterized, the correlation results are nonsense although the correlation coefficient is very high. Applying principle-component-analysis (PCA) to the data set provides a simple way of reducing the

number of degrees of freedom. The ICS toolkit contains a PCA option for neural solver and multiple-linear-regression tools.

It is prudent to always examine the output results from the perspective of “how good are the input data?” As an example of uncertainty, consider the calculation of reservoir depth from seismic time data. In the Williston Basin and elsewhere, it is a common practice to compute the depth of the formation of interest (here the Red River) by adding a calculated interval thickness (converted from an isochron using local seismic velocity) to the depth of an appropriate “hanging” formation. This calculation is performed to overcome errors produced by areal variation of seismic velocity. In the Bowman-Harding area, a Cretaceous formation marker bed is frequently used as a hanging horizon. Seismic velocity is computed from seismic two-way travel time from the Cretaceous top, such as Niobrara (Kn), to the Ordovician Red River (Orr) and the well-log interval thickness at each well in the seismic survey. A seismic velocity map is contoured from the well control. The seismic isochron (Kn-Orr) is converted to thickness (feet) using the contoured velocity. A transformed isopach of the interval is created. Next, the hanging horizon (Kn) is contoured from the well control. The transformed interval thickness (Kn-Orr ft) is added to the hanging horizon (Kn ft) to produce a depth map of the Red River. Different interpretations of the Red River depth map will result from a different hanging horizon and corresponding interval thickness. There are two main sources of error in the calculation method. These errors result from uncertainty by contouring of the seismic velocity and uncertainty by contouring of the hanging horizon depth. Other uncertainty comes from the surface elevation measurement and exact location of the wellbore at total depth (which may be 200 ft from the surface location). The uncertainty of the computed reservoir depth from seismic should be studied carefully as different constructions may be equally valid.

Shown in **Figure 1-6** is the Red River seismic time from the 3D seismic survey at the Amor South Red River Unit. Vertical well locations are shown with strike points from horizontal wellbores shown with a red “x.” A blind test of conventional depth calculation was performed with two wells removed (identified with a circle and arrow). A graph is shown in **Figure 1-7** for the correlation of Red River subsea depth with Red River seismic time at the Amor South Red River Unit. The graph shows the correlation for measurements at both vertical wells and along horizontal wellbores. The graph shows poor correlation that results from variation of seismic velocity and measurement error along horizontal wellbores. Because of velocity variations, calculations for Red River depth are conventionally based on a contoured hanging horizon, a contoured velocity and seismic interval time.

A computed Red River depth map is shown in **Figure 1-8** from the conventional method using first principles as previously described. From comparison of the Red River time map in **Figure 1-6** and computed Red River depth in **Figure 1-8**, the shift from velocity variation is readily apparent. The original calculation of Red River depth was made from 10 vertical wells with two wells excluded as a blind

test. The two blind-test wells shown in **Figure 1-6** are located less than 500 ft from other wells. The original depth calculation has a perfect correlation with the 10 control wells because the contoured seismic velocity was forced to match the 10-well control. When measured depths at the two blind-test wells are compared to the calculated depth, the correlation coefficient R^2 decreases to 0.825 with an average error of 5.7 ft. As shown in **Figure 1-9**, the correlation coefficient R^2 decreases to 0.589 with an average error of 10 ft when measured depth at all 12 vertical wells and 68 strike points along horizontal wellbores are used for comparison to calculated depth,

In summary, it is possible to produce statististically equal results from different depth construction methods using seismic data. The exercise also indicates that there is an inherent error in depth and seismic velocity calculations. Error statistics suggest that it is not possible to predict Red River depth better than +/- 10 ft with complete confidence from seismic data. A predicted correlation coefficient of 0.65 for predicted and measured depths is probably acceptable.

An important geological attribute for the Red River B Zone reservoir is the thickness of the B Cycle as shown on a type log in **Figure 1-10**. Locally, the B Cycle thickness can vary by 12 ft. Shown in **Figure 1-11** is a graph of predicted B Cycle thickness at one 3D seismic survey with the measured B Cycle thickness from well logs. Predicted values were also captured at four (north-south-east-west) locations surrounding each vertical well location at a distance of 150 ft. While the overall correlation coefficient is very good at R^2 of 0.85, the range of predicted values is a maximum of 3 ft surrounding each vertical well location. This 3-ft variation is 25 percent of the total 12-ft range within the seismic survey. This example shows that while it is possible to measure the B Cycle thickness very closely from well logs, the uncertainty of the actual bottom-hole location of the wellbore produces some additional error in the prediction of reservoir attributes.

Seismic-reservoir transforms are performed on a routine basis by geophysicists for reservoir depth. Despite inherent errors, these seismic-reservoir depth transforms are accepted and used successfully for exploration and development drilling. The seismic-reservoir-production transforms based on ICS tools and methodology that are discussed in this report are empirical and not based on “first principles.” However, reservoir trends and similarity are often as important for reservoir characterization as predictions with high accuracy. Careful screening of data and understanding of error and the sources of those errors will be of benefit for successful application of ICS software tools.

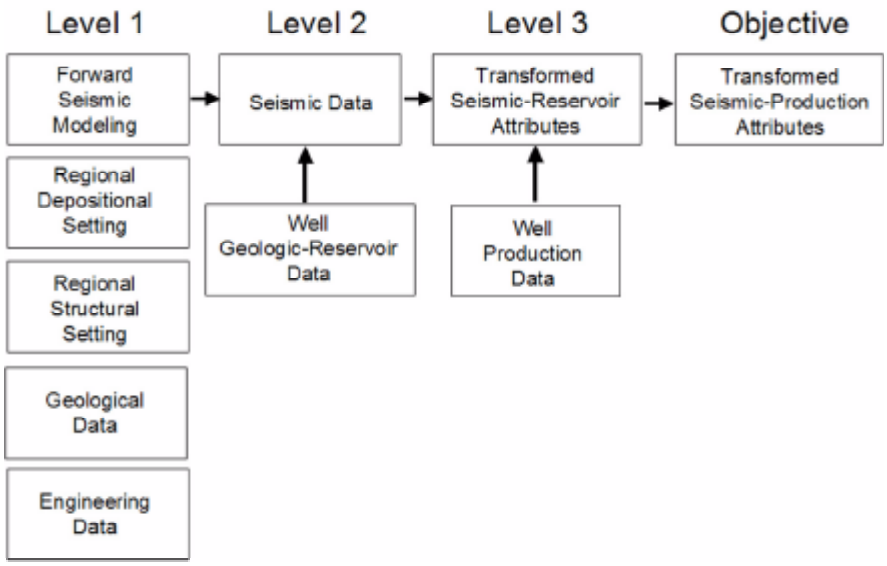

Figure 1-1. Flow diagram for the reservoir characterization strategy used at Amor South Red River Unit and other 3D seismic surveys in the project study area.

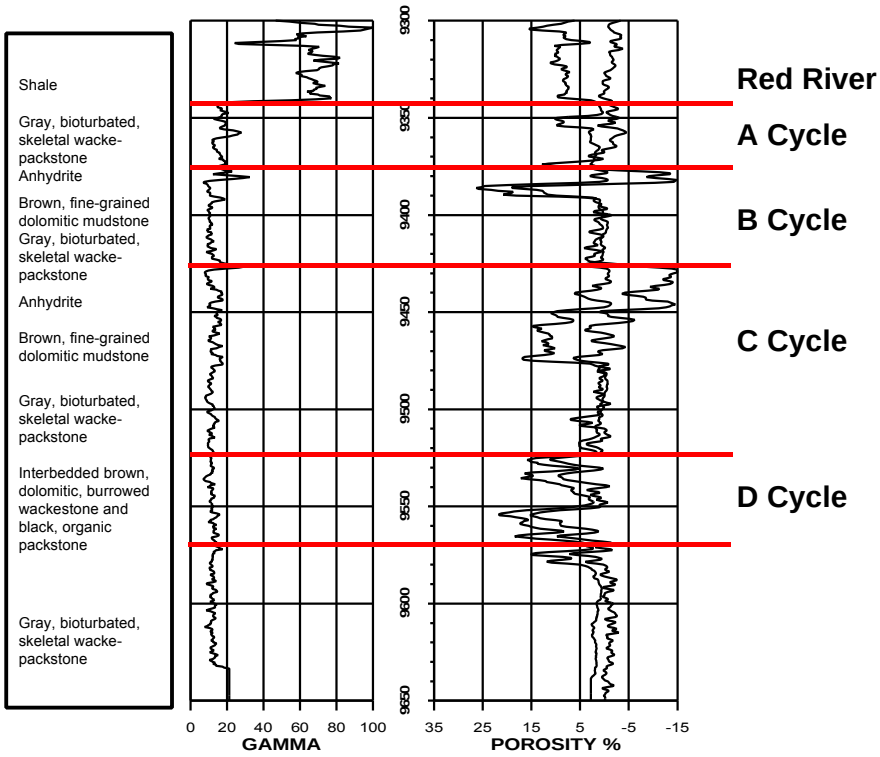

Figure 1-2. Type-log and lithological description of the Upper Red River Formation in Bowman County, North Dakota. The upper Red River contains a series of depositional cycles in a shallow-shelf environment that resulted from changes in sea level. The local water depth and shelf setting affected local rock quality.

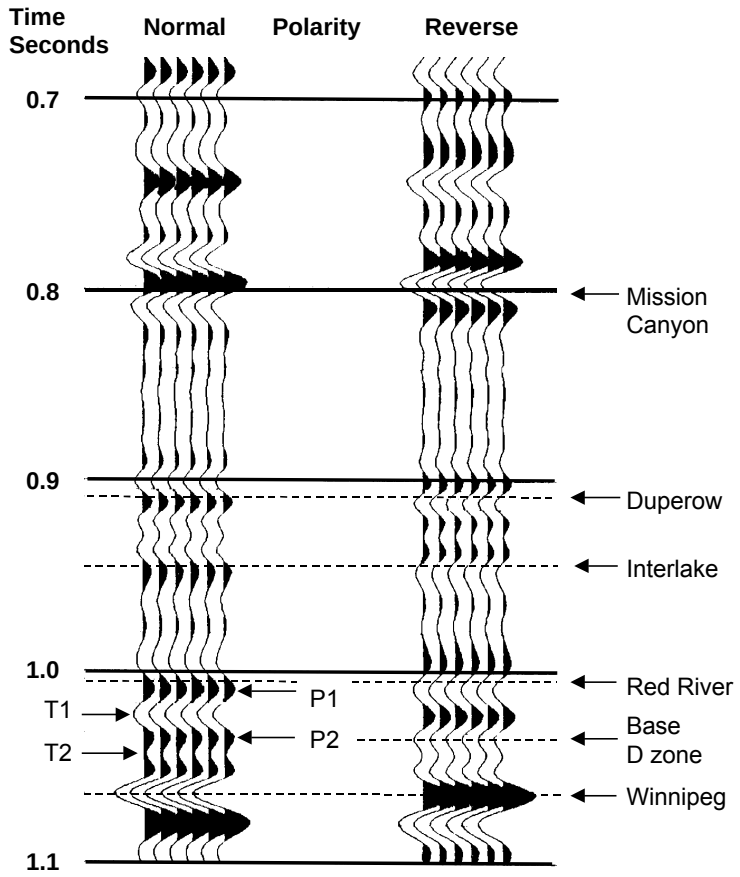

Figure 1-3. Example of forward seismic modeling for the Red River in Bowman County, North Dakota.

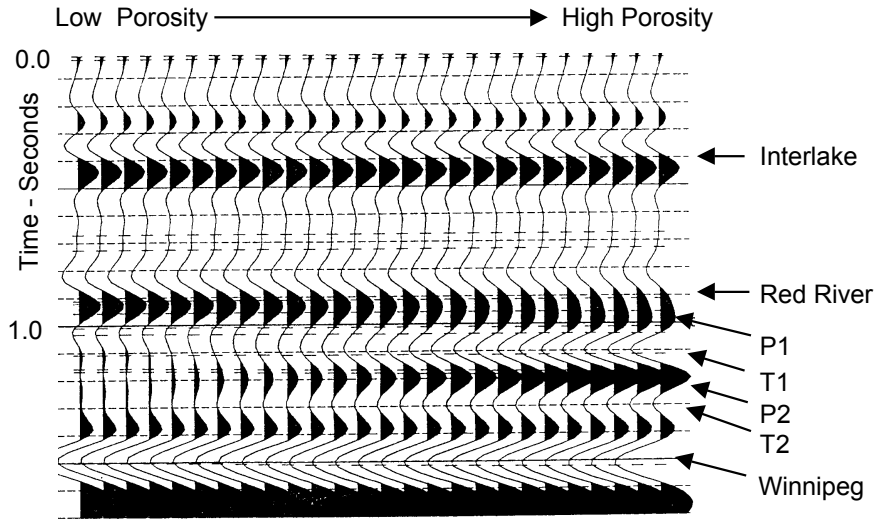

Figure 1-4. Example of forward seismic modeling for the Red River B and D Zones in Bowman County, North Dakota.

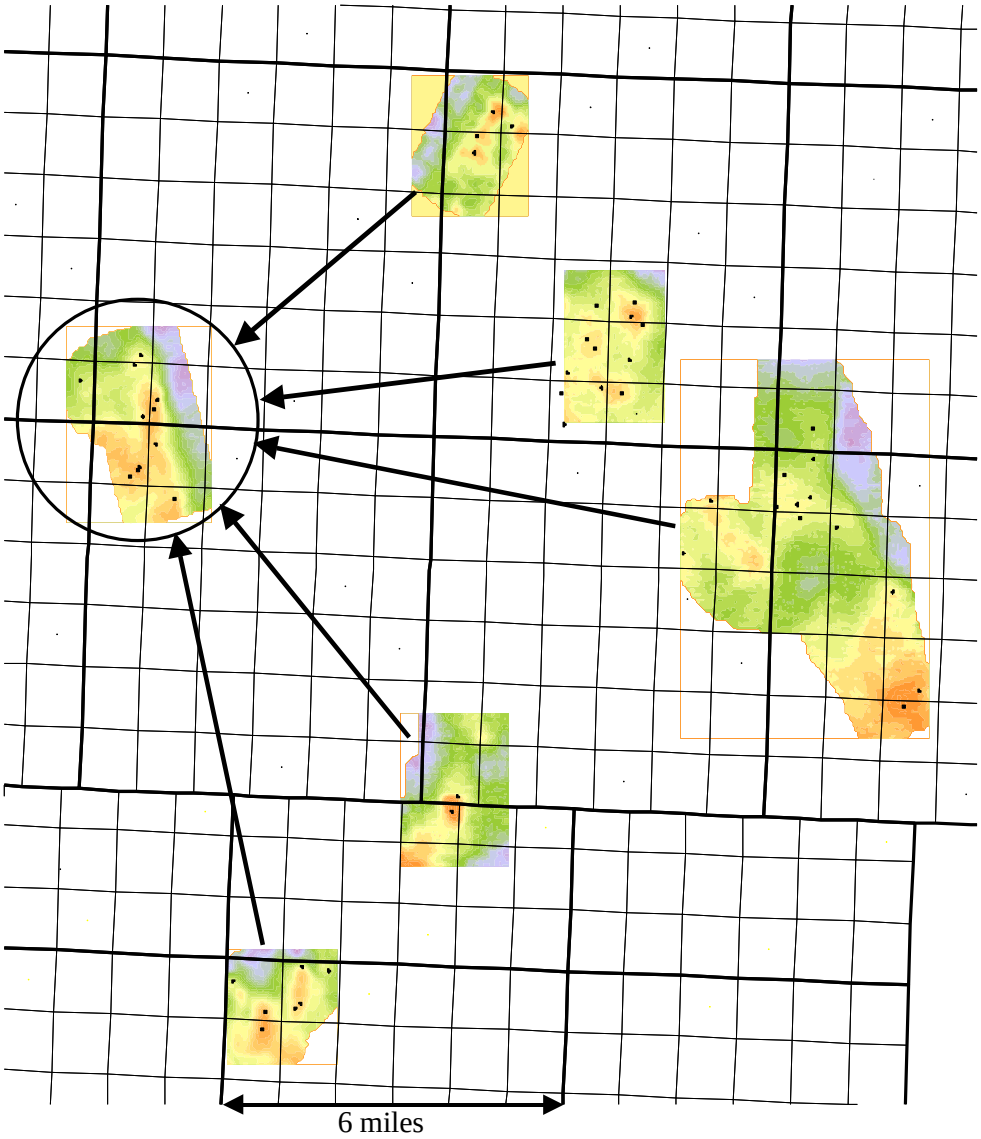

Figure 1-5. Map of five different 3D seismic surveys used as a training source for reservoir characterizations at Amor South Red River Unit.

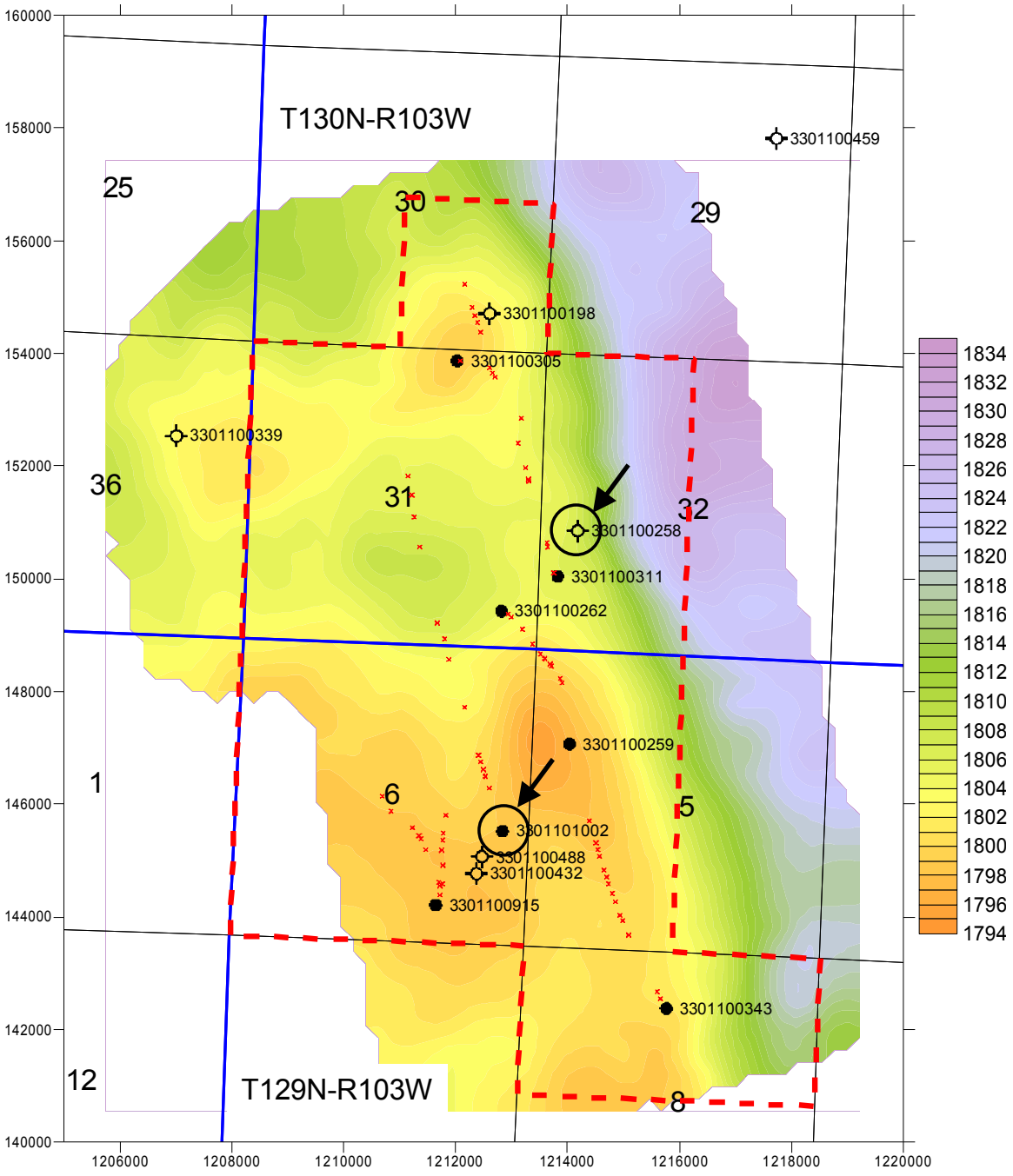

Figure 1-6. Map of the Red River seismic time at the Amor South Red River Unit. Vertical well locations are shown with strike points for horizontal wellbores shown with a red “x.” A blind test of conventional depth calculation was performed with two wells removed (identified with a circle and arrow).

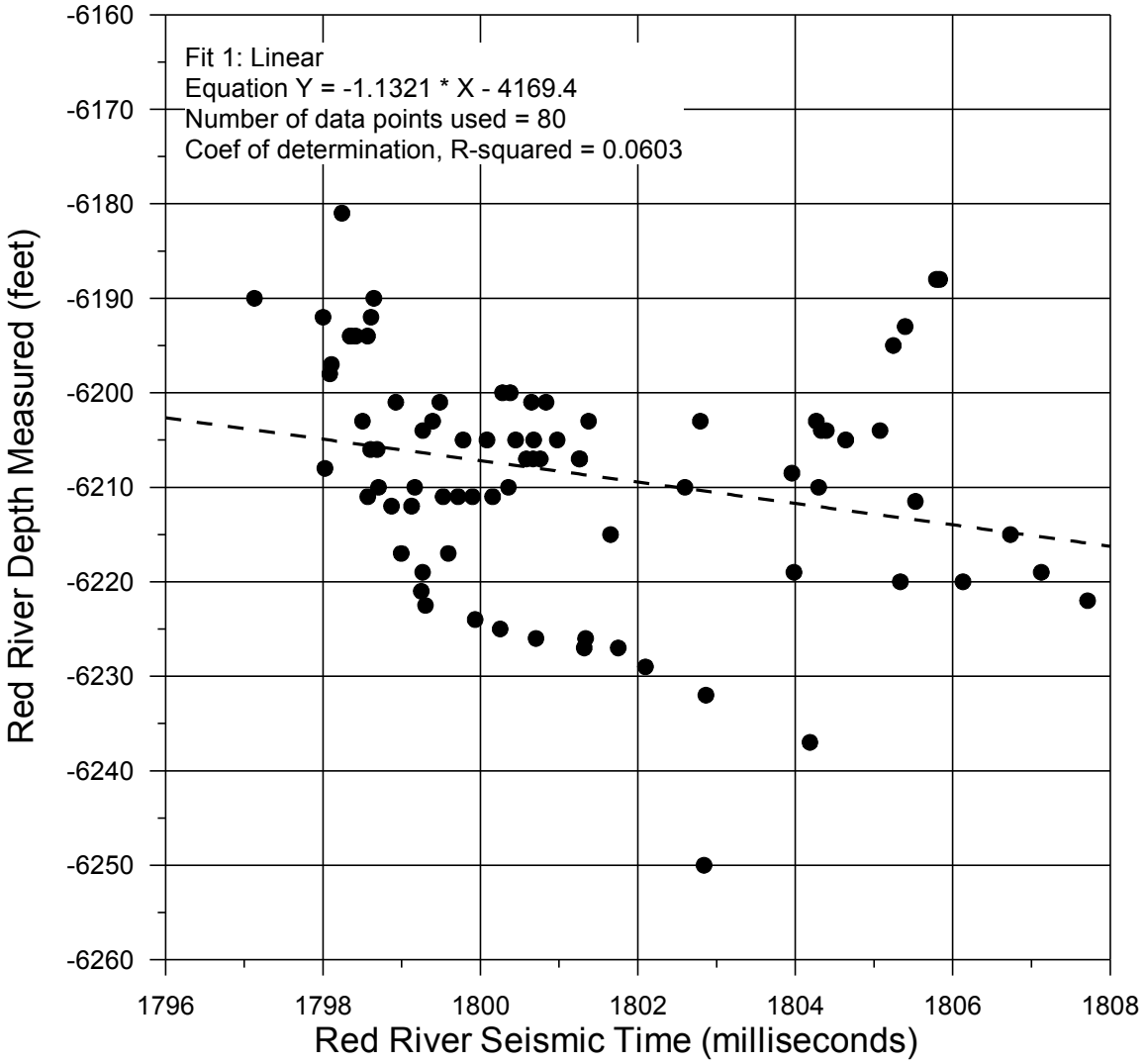

Figure 1-7. Graph for the correlation of Red River subsea depth at both vertical wells and along horizontal wellbores with Red River seismic time. The graph shows the poor correlation that results from variation of seismic velocity and measurement error along horizontal wellbores.

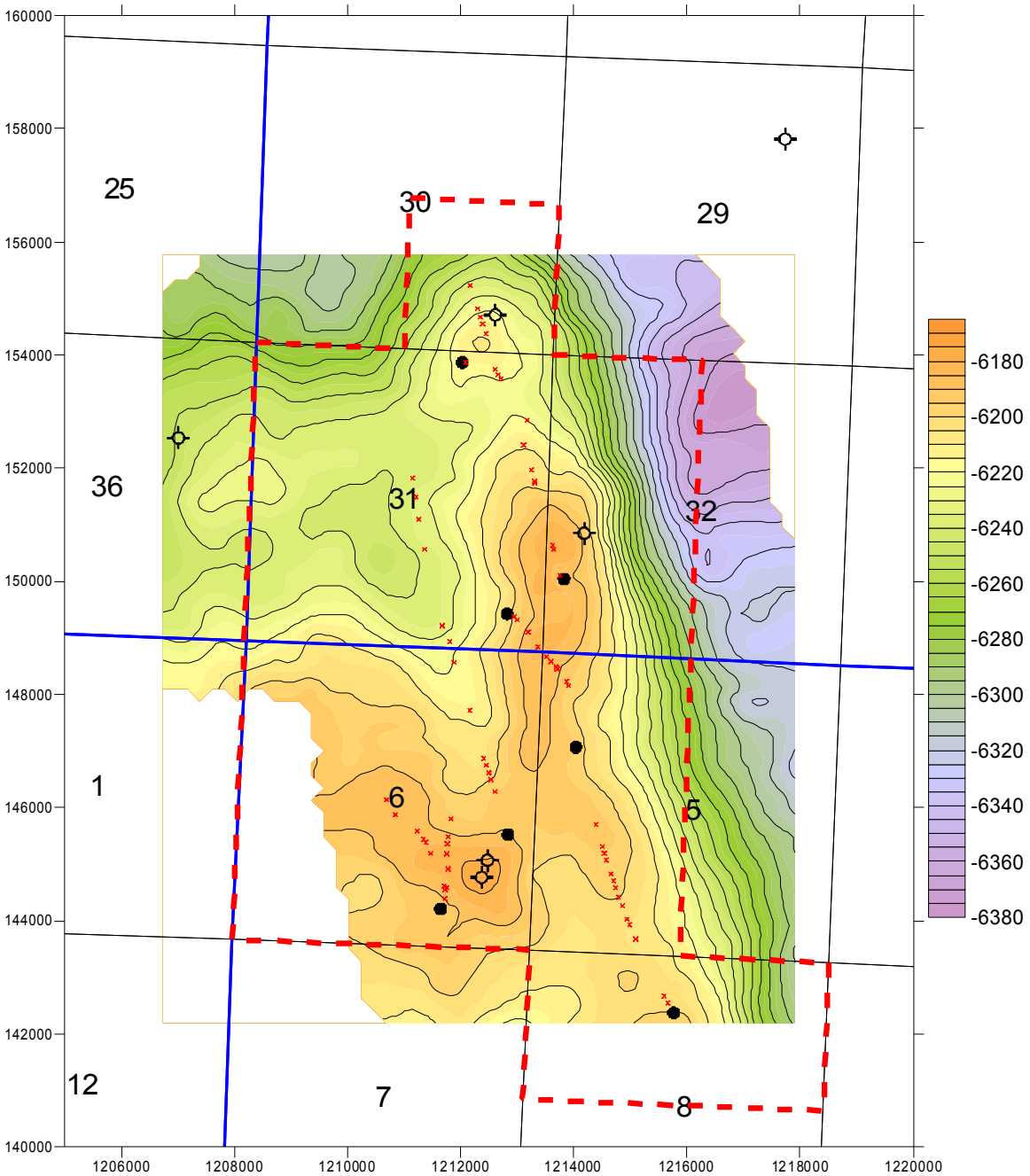

Figure 1-8. Map of computed Red River depth based on Niobrara contoured depth from wells, Niobrara-Red River seismic interval time and contoured Niobrara-Red River velocity from wells.

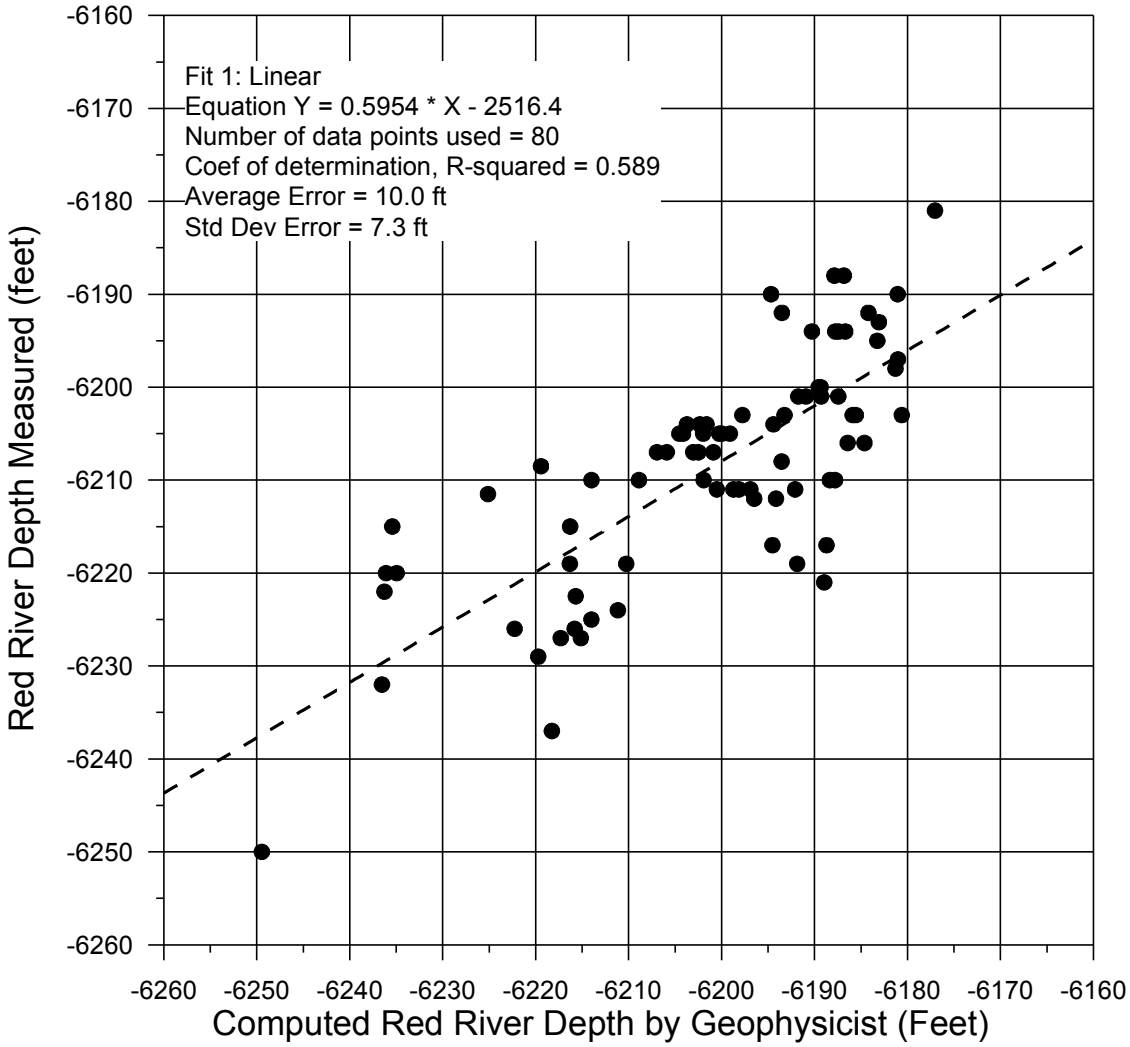

Figure 1-9. Graph of correlation for computed and measured Red River depth from conventional methods of Kn-Orr isotime, velocity and Kn contoured hanging horizon depth from vertical well data. The graph shows all vertical wells and 68 strike points along horizontal wellbores.

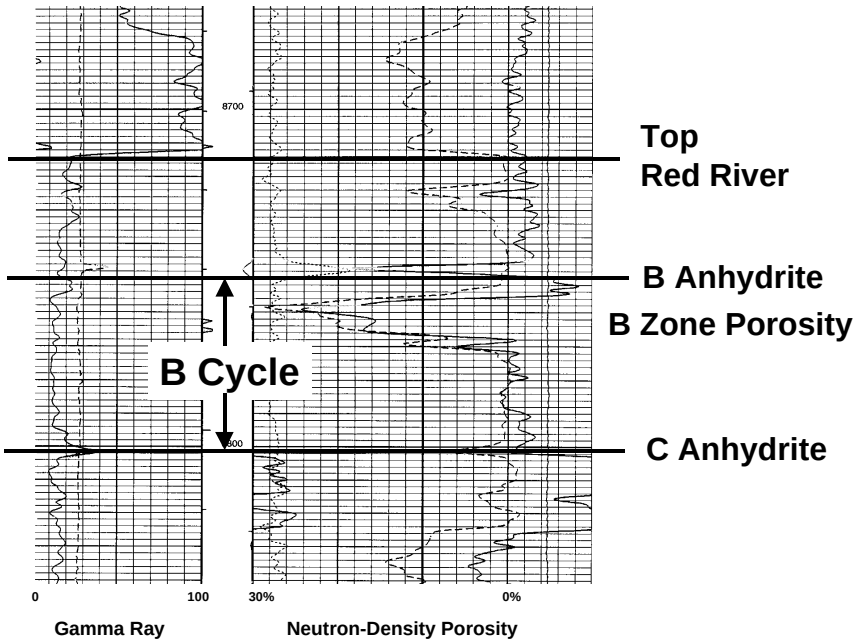

Figure 1-10. Type-log of the upper Red River that covers the B Zone porosity member and the B Cycle.

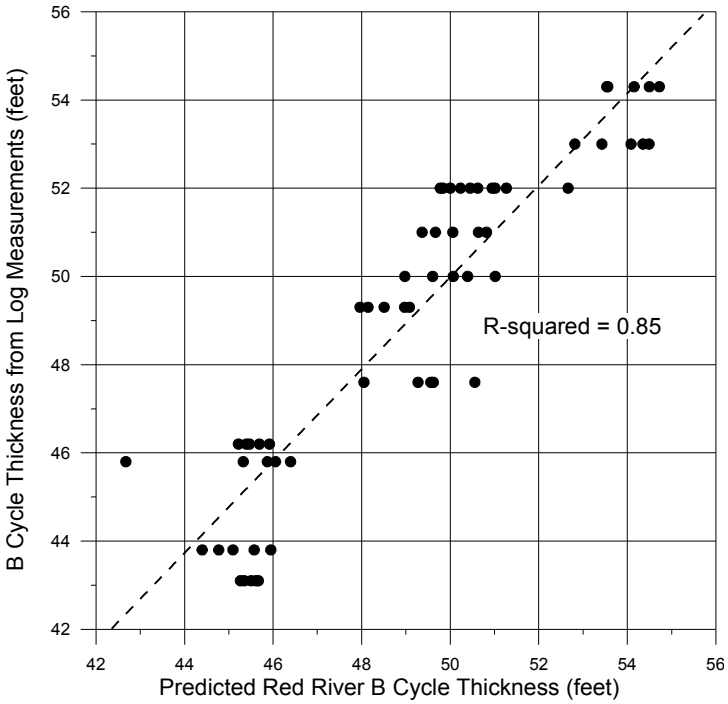

Figure 1-11. Graph for the correlation of predicted B Cycle thickness from seismic attributes using the ICS Neural Solver with the measured thickness at wells at one 3D seismic survey.

Production Metrics

Starting in 2000, Luff Exploration Company began successfully re-developing oilfields producing from the Ordovician Red River in the southwest Williston Basin. Key to this success is better reservoir characterization with horizontal drilling. With large spacing units of 320 acres per vertical well there are generally too few wells at individual reservoir accumulations for detailed reservoir characterization and description of reservoir limits. At reservoir depths that average 9500 ft, drilling costs are prohibitive for defining reservoir limits with dryholes. Seismic records are very good in the area, both for structure and stratigraphy, and are invaluable for exploration and development efforts. With this as a background, Luff Exploration Company joined with the National Petroleum Technology Office of the U.S. Department of Energy in a cooperative project to develop and test computer software tools for reservoir characterization. Application of these software tools for reservoir characterization allowed integration of seismic and well data from many fields. Reservoir characterizations and description of reservoir limits allowed successful targeting of re-entry horizontal laterals. Shown in **Figure 2-1** is a map that identifies the project area in the southwest Williston Basin. Well activity and project demonstration sites are shown in **Figure 2-2**.

Developed reserves and production from activity directly related to the project are shown graphically in **Figure 2-3**. Production from 25 wells that were re-drilled or new is shown on the graph. Baseline production and corresponding trend from 1998 are also shown for reference. From the baseline production trend, an incremental production volume was calculated and shown as incremental cumulative production on the figure. The combined production of these wells during 1998 and 1999 averaged 13,121 bbl per month. In 2003, the average production was 46,869 bbl per month. Cumulative incremental oil production was 986,000 bbl through October 2003. All of these wells are in fields that have been producing for 20 to 30 years with many wells producing at near the economic limit. Some of the wells that were re-entered for horizontal drilling had been plugged and abandoned.

The normalized initial average production for the 25 wells is shown in **Figure 2-4**. The graph was constructed by shifting the production start date for all wells to the same reference time and dividing the total production by the number of active wells. All wells in this population were initially completed vertically and in reservoirs at initial pressure conditions. The average peak rate shown on the graph is 2864 bbl per month per well. After 24 months, the average producing rate is 1382 bbl per month per well.

The normalized average production from horizontal completions is shown in **Figure 2-5**. Production rates after horizontal drilling is normalized to a common reference time and is shown with three years history before re-entry lateral drilling occurred. Before horizontal completion, the production rate averaged 534

bbl per month per well. After horizontal completion the peak production rate is 3364 bbl per month per well. After 24 months of history from the lateral completions, the average producing rate is 1975 bbl per month per well. From these statistics, a six-fold increase has been realized on average for peak rate compared to prior trend. Comparing the production rates of the vertical completions, at original reservoir conditions, with the redevelopment horizontal completions, after 20 or more years of production, indicates average peak and 24-month rates are greater for horizontal completions.

Production results from horizontal completions are similar across the study area. Graphs in **Figure 2-6** through **Figure 2-8** show production results from horizontal completions compared to previous vertical completions in the Red River B Zone at three areas. **Figure 2-9** shows results from the Red River D Zone where vertical completions were replaced with horizontal re-entry laterals. These production graphs show that properly placed horizontal laterals can access significant additional reserves throughout the study area in either the Red River B or D Zone reservoirs.

Incremental reservoirs are estimated to be 5,300,000 bbl from exploitation efforts at 30 wells in the project area. After about two years of production history from relatively mature Red River fields in the project area, it appears that on average enhanced primary reserves from horizontal completions will be equal to the reserves developed by the original vertical wells. Application of reservoir characterization and horizontal completions in old wells has led to the formation of three new waterflood units and identification of several fields with potential for secondary recovery. Additional secondary reserves are being developed in fields where the oilcut and well count are sufficient. Estimates of these secondary reserves are about equal to primary reserves developed by the original vertical wells. In some cases, incremental reserves (primary and secondary) are 200% over that developed with vertical wells some 30 years ago.

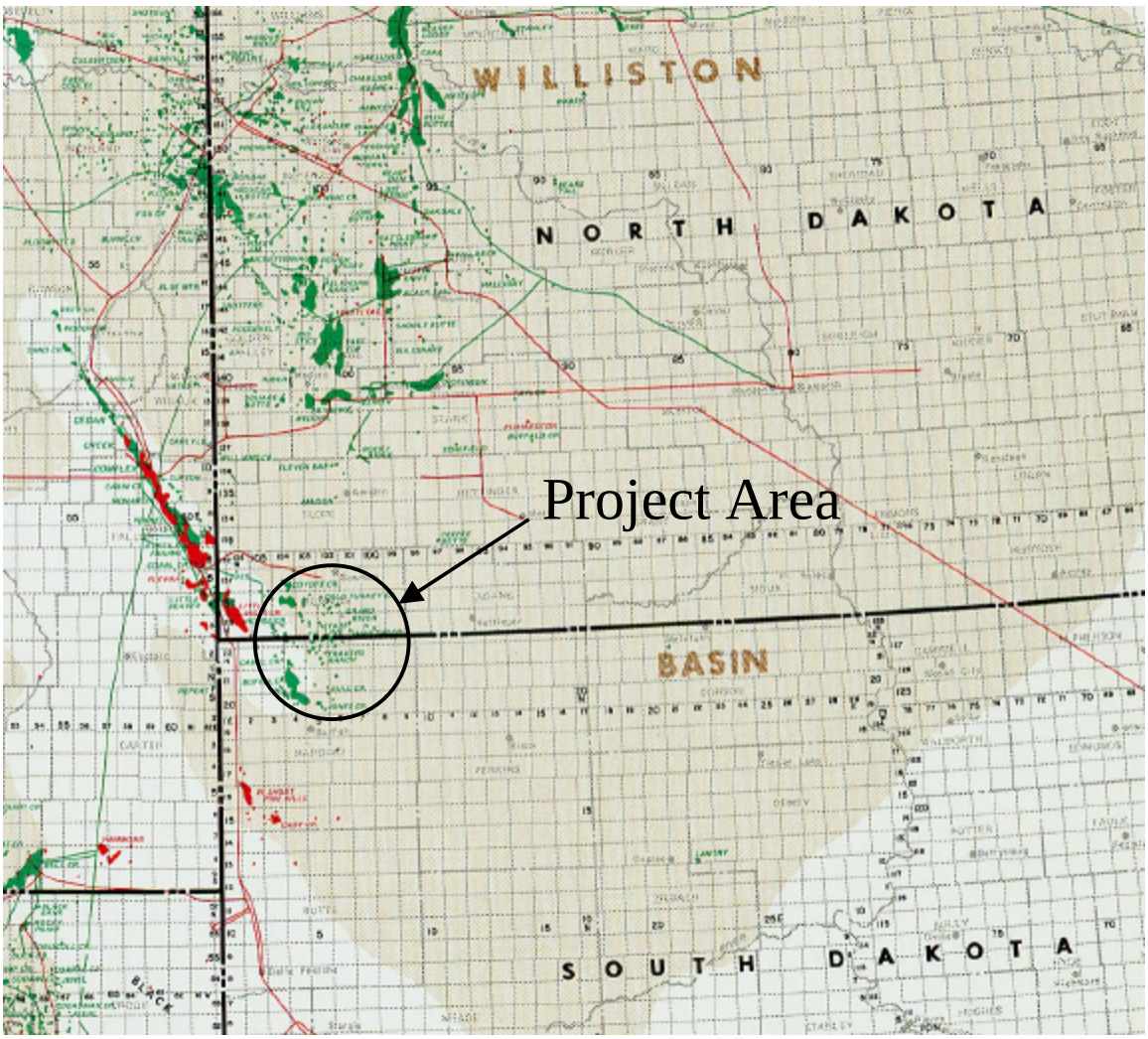

Figure 2-1. A map of the project area in southwest Williston Basin.

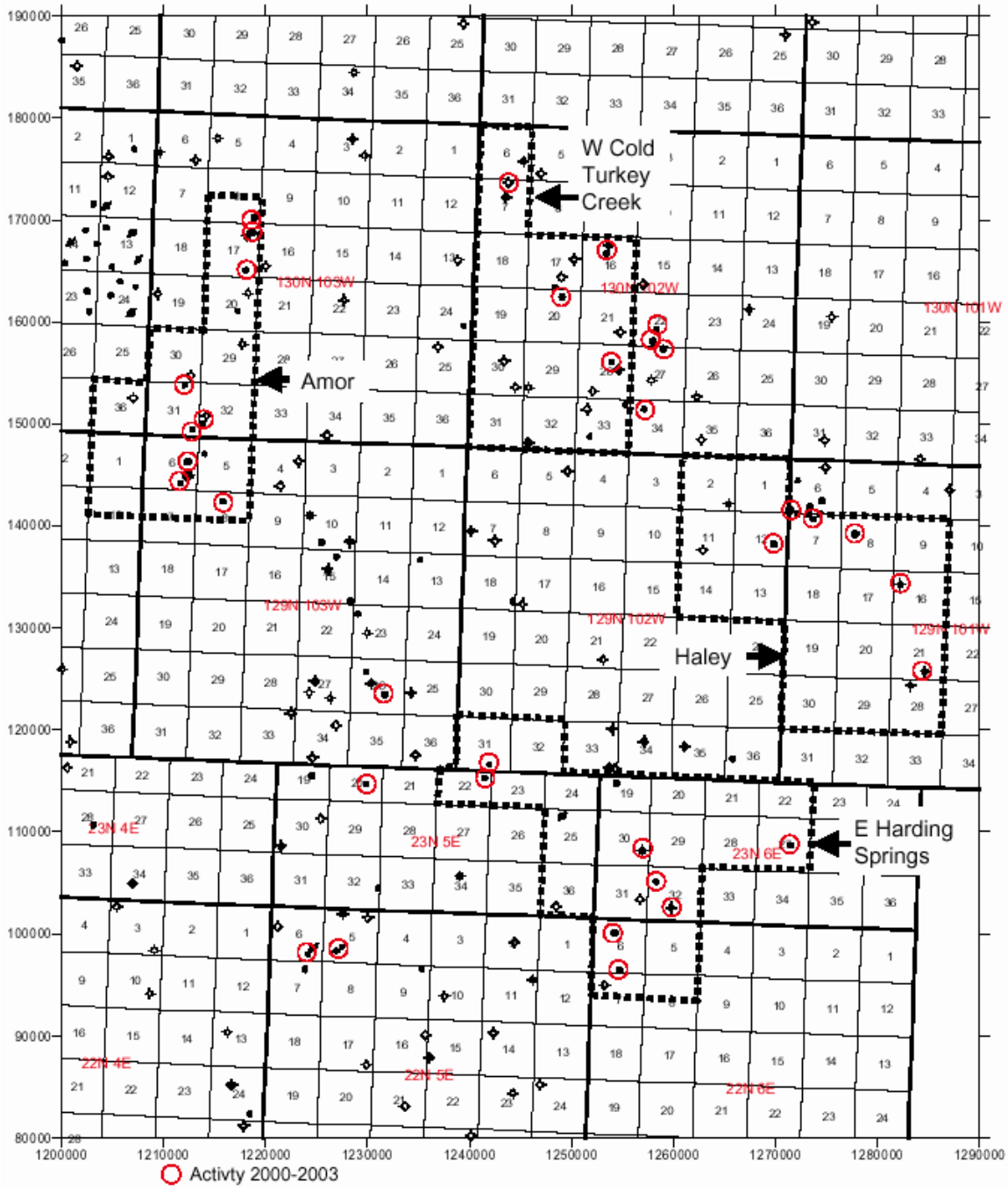

Figure 2-2. A map of project demonstration sites and well activity (direct and indirect) from 2000 through 2003.

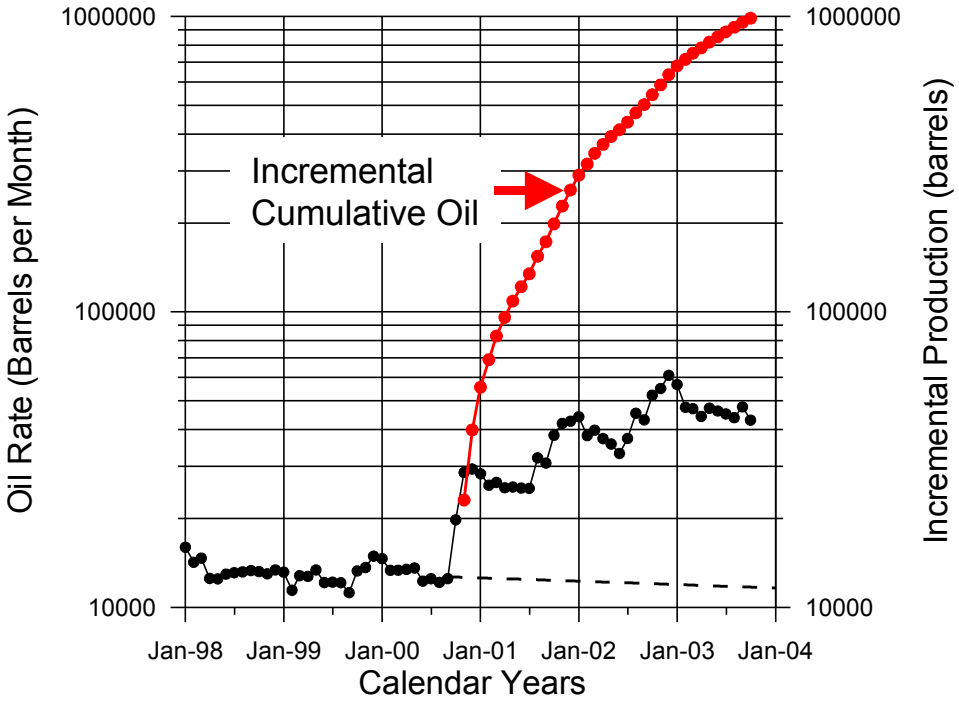

Figure 2-3. Graph shows total monthly production from 25 wells that were re-drilled horizontally.

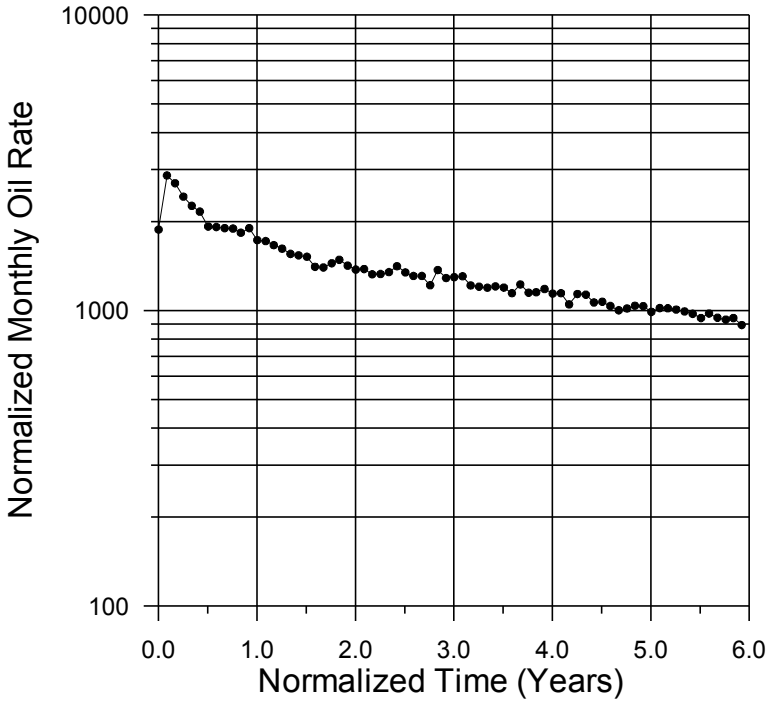

Figure 2-4. A graph of average monthly oil production per well from initial rates of 25 wells completed vertically in the Red River at original reservoir conditions.

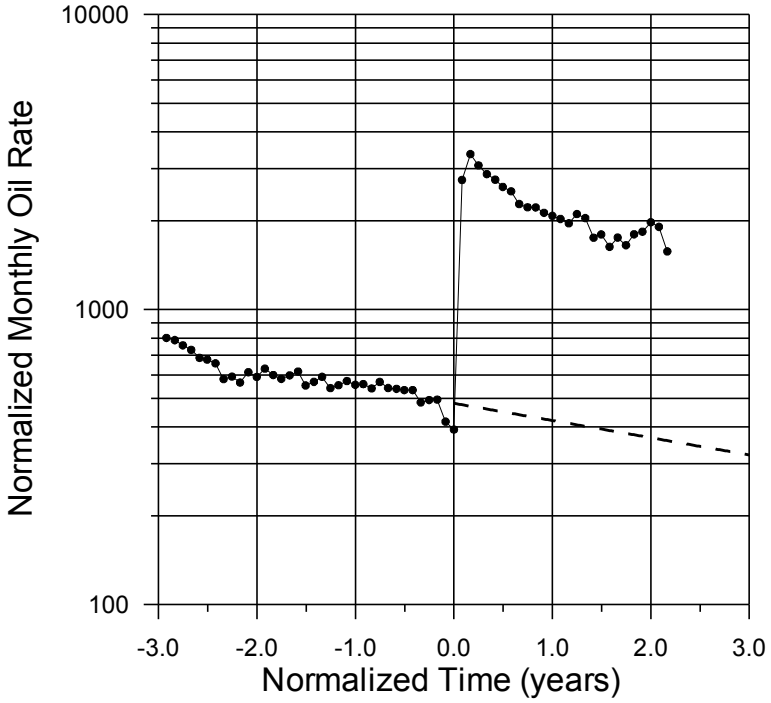

Figure 2-5. A graph of average monthly oil production per well from 25 wells that were re-drilled horizontally in the Red River at near economic limit conditions for the vertical completions.

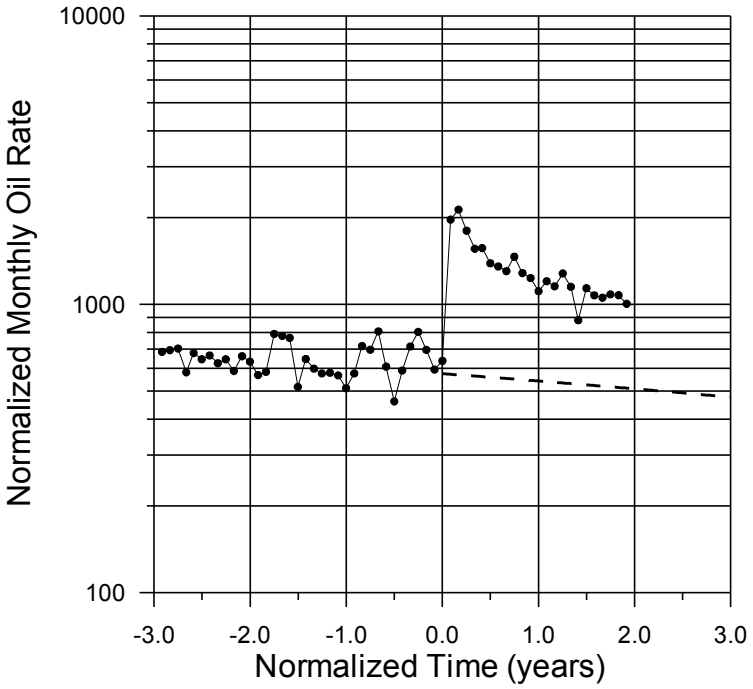

Figure 2-6. A graph of average per well monthly production before and after horizontal re-entry drilling at 3 wells in Cold Turkey Creek Field, Red River B Zone.

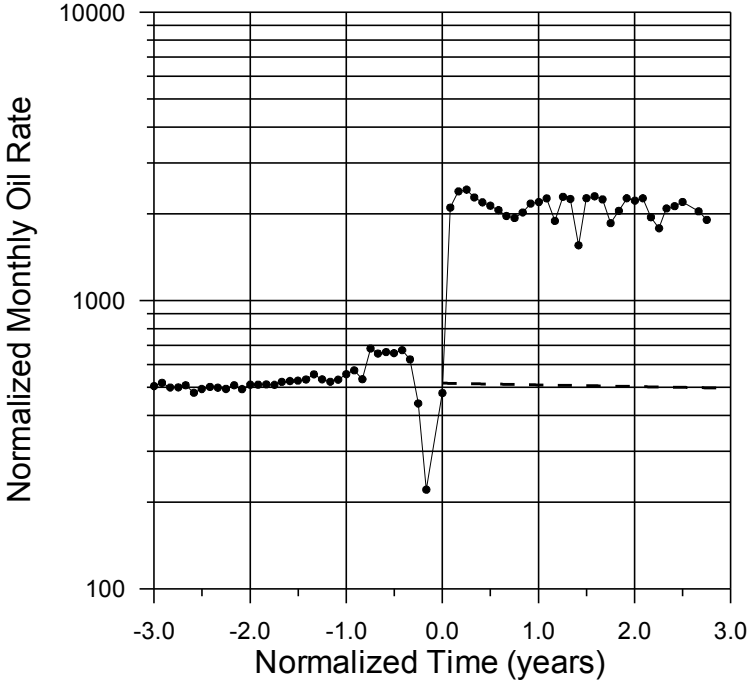

Figure 2-7. A graph of average per well monthly production before and after horizontal re-entry drilling at 2 wells in Buffalo Field, Red River B Zone.

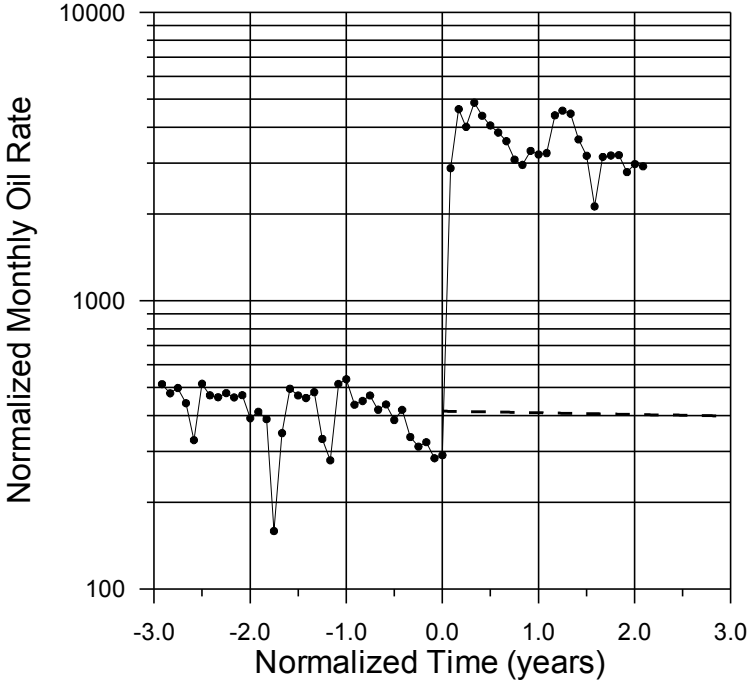

Figure 2-8. A graph of average per well monthly production before and after horizontal drilling at 4 wells in Grand River and Haley Fields, Red River B Zone.

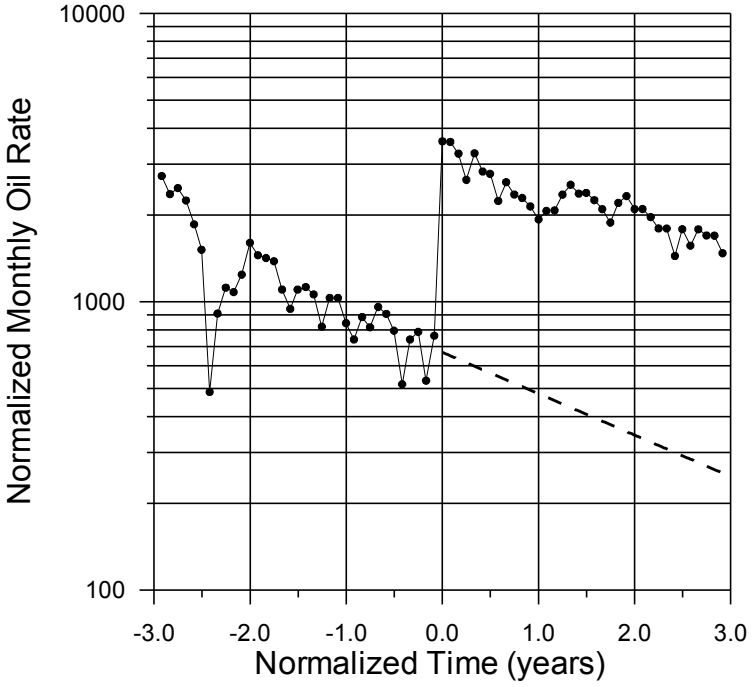

Figure 2-9. A graph of average per well monthly production before and after horizontal drilling at 3 wells in Cold Turkey Creek and Travers Ranch Fields, Red River D Zone.

Reservoir Characterization with 3D Seismic at Amor South Red River Unit

The Amor South Red River Unit (ASRRU) was formed in 2002 as a waterflood secondary recovery project utilizing horizontal wells. Water injection is into the Red River B Zone reservoir at a depth of about 9250 ft. A map of the Amor South Red River Unit outline and wells is shown in **Figure 3-1**. Intelligent Computing Software (ICS) was used in the characterization of Red River reservoirs at the Amor South Red River Unit and those characterization results were used in forming a development plan. Before developing the field with horizontal laterals and commencement of water injection under secondary recovery plans, the field was producing a rate of 120 bbl oil per day. As of October 2003, the Unit was producing at a rate of 650 bbl oil per day with little, if any, re-pressurization of the reservoir from water injection. The ASRRU is an excellent example of the application of ICS tools for reservoir characterization using 3D seismic data with results indicative of more oil production from relatively mature Red River fields. Red River B and D Zone reservoirs are characterized from application of ICS tools and strategy developed during the course of this project. Reservoir and production transforms are shown that allow delineation of reservoir limits and creation of data files that are suitable for reservoir simulation models.

Historical Background

The field area straddles townships T129N-R103W and T130N-R103W in Bowman County, North Dakota and is located two miles southeast from and on regional strike with the Medicine Pole Hills Field. Since Medicine Pole Hills Field is a major Red River oil accumulation in the Bowman County area, it has been described in the literature on several occasions (Kohm and Louden, 1988; Kumar et al, 1995). Exploration drilling began in 1975 (API 33-011-00198) and the first successfully completed well began producing in 1979 (API 33-011-00259). A total of eleven wells were drilled, of which six were completed vertically with commercial production from the Red River. Initial exploration and development efforts were based on a grid of 2D seismic lines that were used for identification of structure at Red River depth. Seismic interpretations of interval time and time structure were used for well placement.

The main producing reservoir at ASRRU is the Red River B Zone. Some wells were perforated also in the Red River C and D Zones, but oil contributions from these intervals are considered minor based on subsequent isolation testing. The exact contribution of the Red River C and D Zones is unknown, however, as all Red River producing intervals were commingled in the wellbore. The average oil rate for the first 24 months of production from the field was 94 bopd per well. Cumulative oil produced by September 2003 was about 1,645,000 bbl. The expected ultimate recovery after secondary recovery by waterflooding is about 3,030,000 bbl.

In 1999, Luff Exploration Company conducted a 3D seismic survey over the field area. Initially, the 3D seismic survey was used for a refined interpretation of Red River structure and seismic amplitude response from the Red River D Zone, the thickest reservoir unit in the upper Red River formation. A well was subsequently drilled to test the new structural interpretation and thick porosity development of the Red River D Zone (API 33-011-00915). Although the new interpretations for structure and D Zone porosity development were correct, the D Zone was tested to be wet. The well was finally completed horizontally in the Red River B Zone, but production results were discouragingly modest at 25 bopd and 50 bwpd after 6 months.

At the time the well API 33-011-00915 was drilled, Luff Exploration Company had just begun to develop software tools for ICS and was experimenting with their application and strategies for prediction of oil production potential. Testing ICS characterizations and strategies at ASRRU have been very successful. The relatively small Red River field and seismic data set have become a good case study for application of ICS. Integrated with well and seismic data from six other 3D seismic surveys, reservoir characterization studies of upper Red River at ASRRU have been successful for predicting reservoir limits and production potential.

Regional Setting

For any reservoir characterization study, it is recommended to begin with an examination of regional structural and depositional setting. The ICS Trend Tool is useful for these studies. Shown in **Figure 3-2** is the regional Red River structural setting for the ASRRU in Bowman County, North Dakota. The Unit area is on regional strike with the Medicine Pole Hills Field at an average Red River depth of 9250 ft. A map of residual structure with regional trend is useful to highlight local relief and setting. Local structural relief that is shallow or low to the regional trend is generally not favorable for significant accumulation of oil in the area. A map of residual structure with regional trend for the ASRRU is shown in **Figure 3-3**. In addition to regional structural setting, it is useful to map various isopachs and residual from trend of major shallow geologic horizons and the reservoir objective. At reservoir depth, regional isopach maps of depositional cycles should be investigated. Shown in **Figure 3-4** is a map of Red River B Cycle thickness for the regional setting around the ASRRU. The Red River B Cycle thickness ranges from 44 to 55 ft. A residual thickness from regional trend can aid in the prediction of areas with favorable facies development. A residual from trend for the Red River B Cycle thickness is shown in **Figure 3-5**. The ASRRU is centered on a subtle thinning of the B Cycle thickness. Regional trend and residual values at wells for reservoir structure and depositional setting were included in a database that was used for creating reservoir-production transforms.

Local Structural Setting

Different isotime maps from shallow horizons to the reservoir objective may be instructional for evaluation of structural genesis. **Figure 3-6** shows an isotime map for the Niobrara-Red River interval and **Figure 3-7** shows the isotime map for the Mission Canyon-Winnipeg interval. Both isotime maps are commonly used for structural interpretation of the Red River. From casual comparison of the two maps, it is readily apparent that they are quite different. Structural growth at Amor South appears to have shifted from north to south with geologic time. A composite structural growth index can be produced with the ICS Growth Index Tool. An example of this growth index map is shown in **Figure 3-8**. The ICS Growth Index Tool computes a score for structure and interval thinning of multiple (generally 3 to 5) seismic horizons. The most common seismic transform is that of reservoir depth as shown in **Figure 3-9** for the top of Red River at ASRRU. Once the local reservoir structure is defined, the ICS Entrapment Tool may be used to calculate an entrapment pressure index. The Entrapment Tool provides an objective manner for ranking structure relief and structure area that can be used across a single field and from field to field. A composite entrapment pressure index for ASRRU is shown in **Figure 3-10**. The two entrapment pressure outputs from the ICS Entrapment Tool were captured at well locations and exported to a master database. These attributes were used with other reservoir characterizations for neural-solver training and creation of reservoir-production transforms.

Red River D Zone Characterizations

The first seismic-reservoir transform for characterization of Red River reservoirs at ASRRU is the gross thickness of the upper Red River. This interval is defined by the base of the overlying Stony Mountain shale and a kerogenite bed at the base of the Red River D Zone. Well-log data and normalized seismic attributes captured at well locations from six 3D seismic surveys were used for training and applied to the same normalized seismic attributes at the Amor South 3D seismic survey. The resulting transform is shown in **Figure 3-11**.

A map is shown in **Figure 3-12** of porosity-feet (storage) for the Red River D Zone that was created by the ICS Neural Solver from seismic attributes and external training. There is sufficient variation of thickness and porosity in the Red River D Zone to produce significant changes in amplitude and other seismic attributes.

A map is shown in **Figure 3-13** of the logarithm of transmissibility as measured from drill-stem tests in the Red River D Zone. This seismic-reservoir transform was generated with the same database and training file used for the porosity-thickness transform. While the seismic data are not influenced by reservoir permeability, inherent in the seismic attributes are responses to thickness and

porosity. For the Red River D Zone, correlation of drill-stem test transmissibility (kh/uB) and log-derived porosity-thickness (phi-h) are very good.

Prediction of production attributes can be made after creating structural and reservoir transforms. From a database that contains D Zone production information at wells and corresponding structural and reservoir information, a training file is created for the ICS Neural Solver. The training file is applied to the same structural and reservoir transforms at the Amor South 3D seismic survey and reservoir-production transform attributes are predicted. From a training file of 50 Red River D Zone producers and dryholes, map of initial oilcut was created and is shown in **Figure 3-14**. Similarly, a direct prediction of initial oil rate was made and is shown in **Figure 3-15**.

Since predictions were also made for initial oilcut and transmissibility for the Red River D Zone, these transforms can be used to make a calculation for oil rate for a given assumption for drawdown pressure at a vertical well. At original pressure conditions and full-drawdown a calculated initial oil rate map is shown in **Figure 3-15** for the Red River D Zone. The productive area and range are very similar to that from the direct oil-rate transform shown in **Figure 3-14**. A graph comparing results from those shown in **Figure 3-14** and **Figure 3-15** is displayed in **Figure 3-16**. The average predicted values for initial oil rate are within about 5 bopd for the two methods.

Volumetric estimates of oil-in-place for the Red River D Zone can be made from the seismic-reservoir and production transforms. The neural solver prediction of oilcut and storage (phi-h) are used. An oil-water relative permeability curve is used with the oilcut prediction to make a calculation of oil saturation. The resulting oil saturation is applied to the phi-h transform to produce a calculation of oil saturated pore volume. As shown in **Figure 3-17**. It is also possible to estimate the mobile oil pore-volume map by estimate of the irreducible water saturation and residual oil saturation from oil-water relative permeability data or estimates. Mobile hydrocarbon pore volume is displayed in map view from such a calculation in **Figure 3-18.** Consistency of the reservoir-production transforms is demonstrated by comparison of oil rate maps in **Figures 3-14** and 3-**15** with mobile hydrocarbon pore volume in **Figure 3-18**.

Summary for Red River D Zone Characterizations

Some oil from the Red River D Zone has been produced at ASRRU from two wells, API 33-011-00259 and API 33-011-00305. However, it is not possible to make a quantitative assessment because the D Zone oil was commingled in the wellbore with B Zone oil. Well API 33-011-00305, located in the northeast of section 31, T130N-R103W, produced oil from a drill-stem test at an extrapolated rate of 34 bopd with an oilcut of 62%. Well API 33-011-00259, located in the northwest of section 5, T129N-R103W, was perforated in a small interval of the D Zone where log calculations indicate a water saturation of about 50%. Five other

drill-stem tests of the Red River D Zone in the ASRRU recovered fluid with oilcut of 7% or less.

After the acquisition of 3D seismic but before development and application of ICS tools, Luff Exploration Company drilled to test the new structural interpretation and thick porosity development of the Red River D Zone at well API 33-011-00915 in the southeast of section 6, T129N-R103W. Although the new interpretations for structure and D Zone porosity development were correct, the D Zone was tested to be wet. Well API 33-011-00915 encountered the D Zone porosity at a subsea depth that is 28 ft higher than the D Zone porosity in well API 33-011-00305 where the D Zone drill-stem test recovered oil at an extrapolated rate of 34 bopd and oilcut of 62%. The absence of D Zone oil at the updip well indicates a stratigraphic or hydrodynamic influence on the oil-water contact.

The reservoir characterizations of the Red River D Zone at the Amor South Red River Unit indicate a small and shallow accumulation. Close examination of structural attributes that were compiled for training of Red River D Zone production indicates that structure residual from regional trend of greater than 50 ft is necessary for commercial production where there is no updip stratigraphic trap. The maximum height above regional trend at ASRRU is 10 ft. From a blind test by external training of wells from other seismic surveys, application of ICS Tools for seismic-reservoir and reservoir-production transforms indicates a maximum initial oil rate of about 50 bopd and an oilcut of 50%. This prediction is for a vertical well placed in the most optimal position in the D Zone reservoir. Well logs and drill-stems tests at the Amor South Red River Unit confirm these predictions for the Red River D Zone. From Red River D Zone reservoir characterizations, it was concluded that there were no further exploitation opportunities for Red River D Zone oil reserves at Amor South Red River Unit.

Red River B Zone Characterizations

Development of the Red River B Zone reservoir is affected by the depositional setting as characterized by the B Cycle thickness. The B Cycle thickness is measured from the top of the overlying B Anhydrite to the top of the C Anhydrite. Red River B Zone rock-typing and depositional setting are discussed in detail in sections entitled “Geologic Rock-Typing, Red River B Zone” and “Analytical Rock-Typing, Red River B Zone.” Thickness of the B Cycle allows inference of whether the B Zone rock texture and porosity was dominated by lagoonal, intertidal or supratidal conditions (thickest to thinnest). It is desirable to place wells in an intertidal setting.

Prediction of the B Cycle thickness can be accomplished with the ICS Neural Solver. Shown in **Figure 3-20** is a map of B Cycle thickness that was produced by the ICS Neural Solver using 3D seismic attributes and training from wells located in six other 3D seismic surveys. Compare this map to the regional B

Cycle thickness map shown in **Figure 3-4**. The range of B Cycle thickness is approximately the same, from 42 to 54 ft.

A map is shown in **Figure 3-21** for a prediction of Red River B zone initial oilcut at ASRRU. A training file comprised of production, structure and reservoir attributes from 57 wells was used to make this prediction at ASRRU. As a blind test, the results from external training for initial B Zone oilcut are compared in **Figure 3-22** to the actual producing oilcut at ASRRU. The correlation coefficient R^2 of predicted and actual values for oilcut is 0.92.

A reservoir-production transform of initial oil rate is shown in **Figure 3-23** where the same database and training file was used as for the prediction of initial oilcut. From transforms or predictions made for initial oilcut and transmissibility for the Red River B Zone, a calculation can be made for oil rate for a given assumption for drawdown pressure at a vertical well. At original pressure conditions and full-drawdown, a calculated initial oil rate map is shown in **Figure 3-24** for the Red River B Zone. The productive area and range are very similar to that from the direct oil-rate transform shown in **Figure 3-23**. A graph comparing results from those shown in **Figure 3-23** and **Figure 3-24** is displayed in **Figure 3-25**. The average predicted values for initial oil rate are in good agreement for the two methods.

A map of original-oil-in-place for the Red River B Zone can be constructed from the reservoir-production transform of initial oilcut and average porosity-feet. A map is shown in **Figure 3-26** for calculated hydrocarbon pore volume for the Red River B Zone from oilcut and storage (phi-h) transforms. An oil-water relative permeability curve is used with the oilcut prediction to make a calculation of oil saturation. The resulting oil saturation is applied to the phi-h transform to produce a calculation of oil-saturated-pore-volume. The original-oil-in-place that is shown on this map is calculated to be about 7,700,000 stock-tank barrels. The technical committee for unitization of the Amor South Red River Unit made a calculation of 8,400,000 stock-tank barrels for original-oil-in-place for the Red River B Zone.

It is also possible to estimate the mobile-oil-pore-volume map by estimate of the irreducible water saturation and residual oil saturation from oil-water relative permeability data or estimates. Mobile hydrocarbon pore volume for the Red River B Zone is displayed in map view from such a calculation in **Figure 3-27.** Consistency of the reservoir-production transforms is demonstrated by comparison of oil rate maps in **Figures 3-23** and **3-24** with the mobile-hydrocarbon-pore-volume map in **Figure 3-27**.

The preceding discussions of reservoir characterization and productions transforms for the Red River B and D Zones represent a culmination of many man-hours of work gathering data at hundreds of wells and testing various training files with seismic attributes at seven 3D seismic surveys. The results are

impressive as a result of all this work, but there are simpler approaches with ICS that can produce significant results from a much lower level of effort.

ICS Clustering Tools are simple to use, yet powerful. An example of a map for oilcut is shown in **Figure 3-28** that was produced by the ICS Cluster Tool for non-interval data. Oilcut from production and drill-stem-tests from the wells located in the Amor South 3D seismic survey was used with raw seismic time at 9 horizons from the Cretaceous Eagle to the Ordovician Winnipeg. These 9 seismic horizons are clustered with the oilcut data at well locations and the top four "correlation" horizons are used to produce four clusters groups. The cluster routine determines a mean value and rank. A rank of one corresponds to the largest mean cluster value and a rank of four corresponds to the smallest mean cluster value. The map has been highlighted with red, dashed lines that delineate the area occupied by cluster rank 1 and 2 (greatest oilcut).

The ICS Cluster Tool for interval data produced the oilcut cluster map that is shown in **Figure 3-29**. This cluster tool operates similarly to the previously described cluster tool except that it makes a calculation for every combination of intervals from the 9 seismic horizons (36 intervals). The top four "correlation" intervals are used as the basis for forming four cluster groups. As with the other cluster routine, a mean value and rank is determined for each cluster group. The map has been highlighted with red, dashed lines that delineate the area occupied by cluster rank 1 and 2 (greatest oilcut).

Output from the cluster tools can be passed to the Cluster Rank Combine Tool where the ranks can be summed equally or subjectively by application of a weighting factor from 0 to 1 for each output. Shown in **Figure 3-30** is a map of the summation of cluster ranking from the two maps shown in **Figure 3-28** and **Figure 3-29**. The area of greatest oilcut is highlighted with red, dashed lines. There is very good correlation of this map with ICS Neural Solver predictions of initial oil rate and oilcut.

Summary for Red River B Zone Characterizations

Most of the oil produced at ASRRU has come from the Red River B Zone. Reservoir characterizations of the Red River B Zone using ICS Tools have been successful at predicting oil rate and oilcut at vertical wells that are consistent with actual production data from the wells in the unit. The production transforms were used in the development plan for horizontal well drilling and waterflood operations. Production transforms successfully predict the poor performance of the first horizontal well drill in the field, API 33-011-00915, located in the southeast of section 6, T129N-R103W. A new 6000-ft horizontal well for water injection was drilled on the western flank of the reservoir (API 33-011-01002) based on hydrocarbon-pore-volume constructions that were made from ICS seismic-reservoir and reservoir-production transforms. The horizontal injection well was produced for eight months prior to conversion to waterflood service.

During the production period, the oilcut averaged very close to the predicted oilcut transform along the horizontal trajectory at 48%. Four re-entry lateral completions were successfully made in the Red River B Zone with producing oilcuts that are very close to predictions made by external training for reservoir-production transforms with the ICS Neural Solver.

Graphs of production with time and cumulative oil over the entire life through October 2003 of the wells included In ASRRU are shown in **Figure 3-31** and **Figure 3-32**, respectively. Also shown with actual monthly production data are the projections, made before the ASRRU was formed, for depletion with existing wells (black dashed line) and response to waterflooding with re-entry horizontal drilling (blue dashed line). As shown in the production curves, the oil rate at ASRRU is exceeding predictions. It appears that the predicted incremental oil recovery of 1,000,000 bbl can be achieved.

References Cited

Kohm, J.A. and R.O. Louden. 1989. “Red River Reservoirs of Western North Dakota and Eastern Montana.” In *Occurrence and Petrophysical Properties of the Carbonate Reservoirs, Rocky Mountain Region: Rocky Mountain Association of Geologists 1989 Guidebook*. eds. S. Goolsby and M. Longman. 275-290.

Kumar, V.K., M.R. Fassihi and D.V. Yannimaras. 1995. “Case History and Appraisal of Medicine Pole Hills Unit Air-Injection Project.” *SPE Reservoir Engineering* 10 (3): 198-(August 1995).

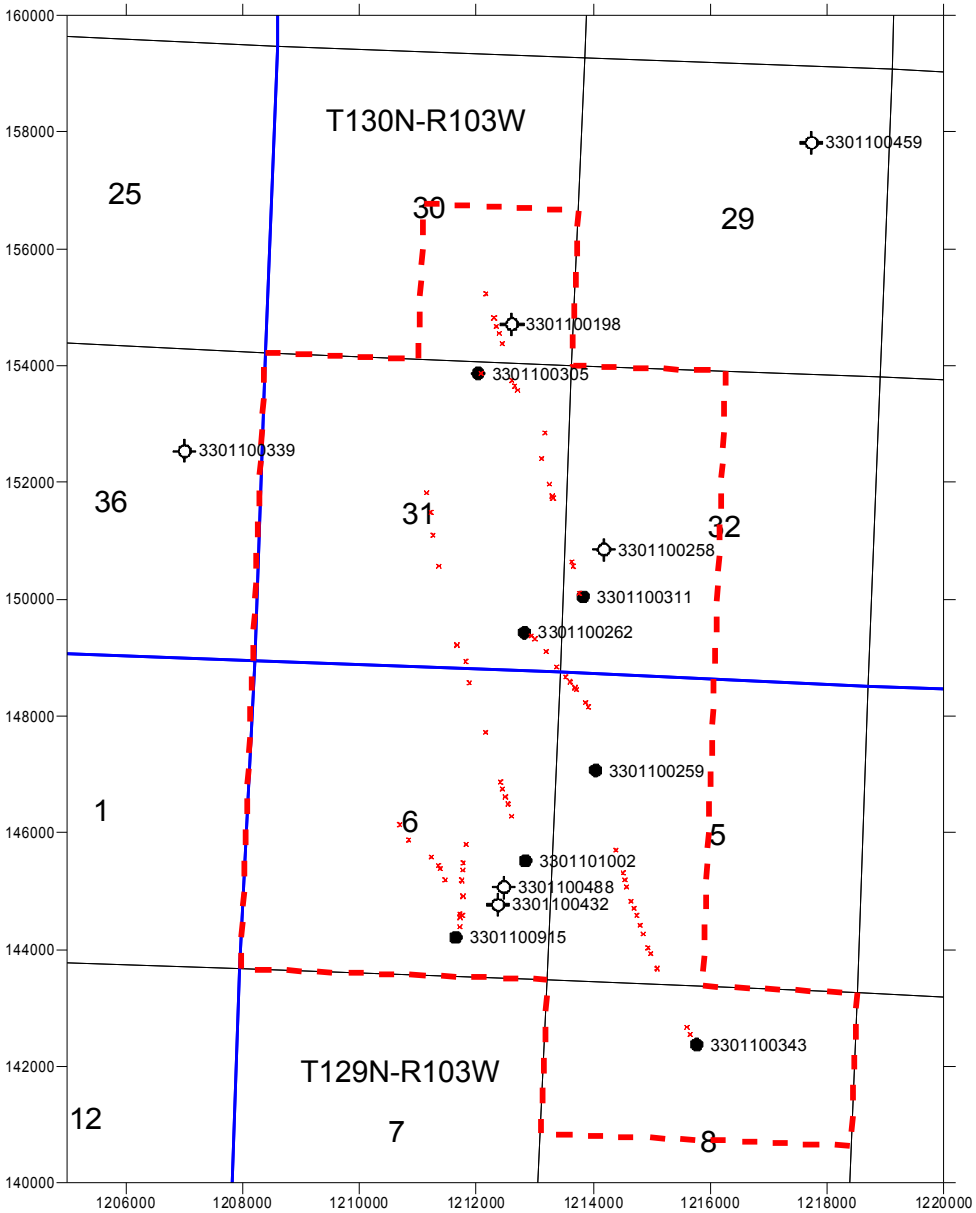

Figure 3-1. Map of the Amor South Red River Unit outline and wells. Red crosses indicate strike picks along horizontal laterals. The land grid is regular government sections. The coordinate system is state plane NAD27.

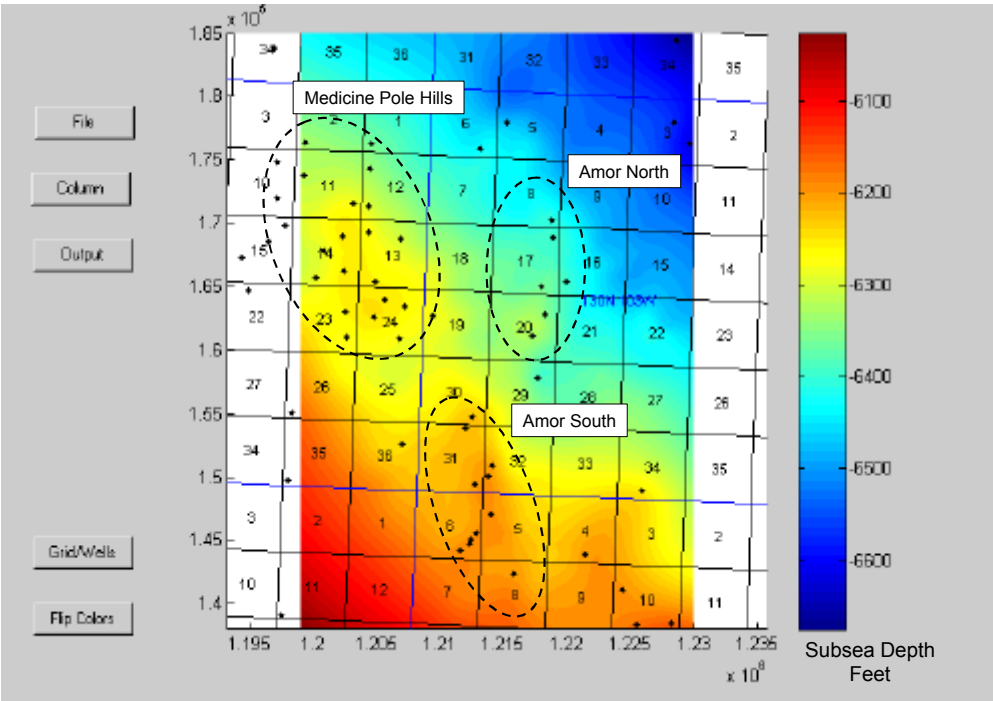

Figure 3-2. Map of regional structural setting at Red River depth for Amor South Red River Unit.

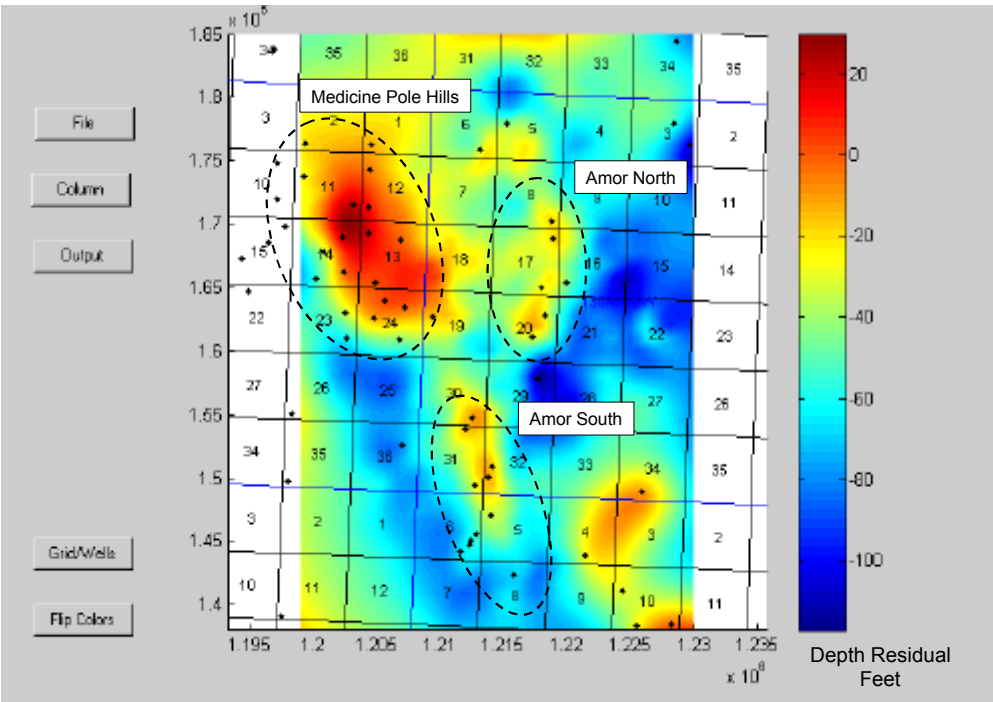

Figure 3-3. Map of structural residual from the regional trend for the Red River Formation at the Amor South Red River Unit.

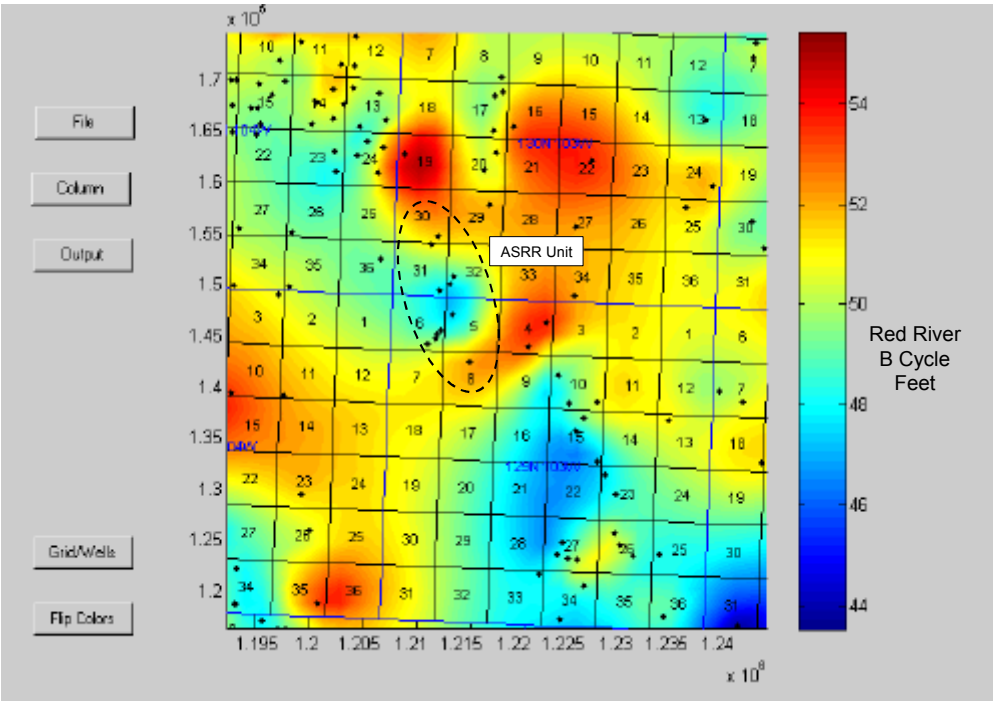

Figure 3-4. Map of regional Red River B Cycle thickness contoured from well control.

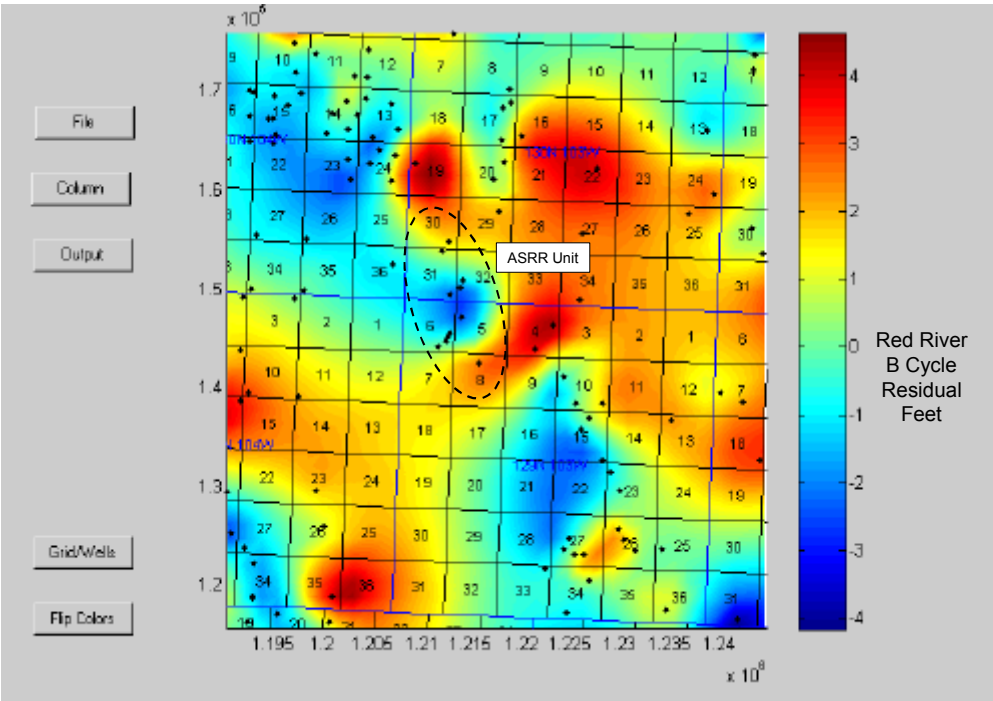

Figure 3-5. Map of residual from regional trend of the Red River B Cycle thickness contoured from well control.

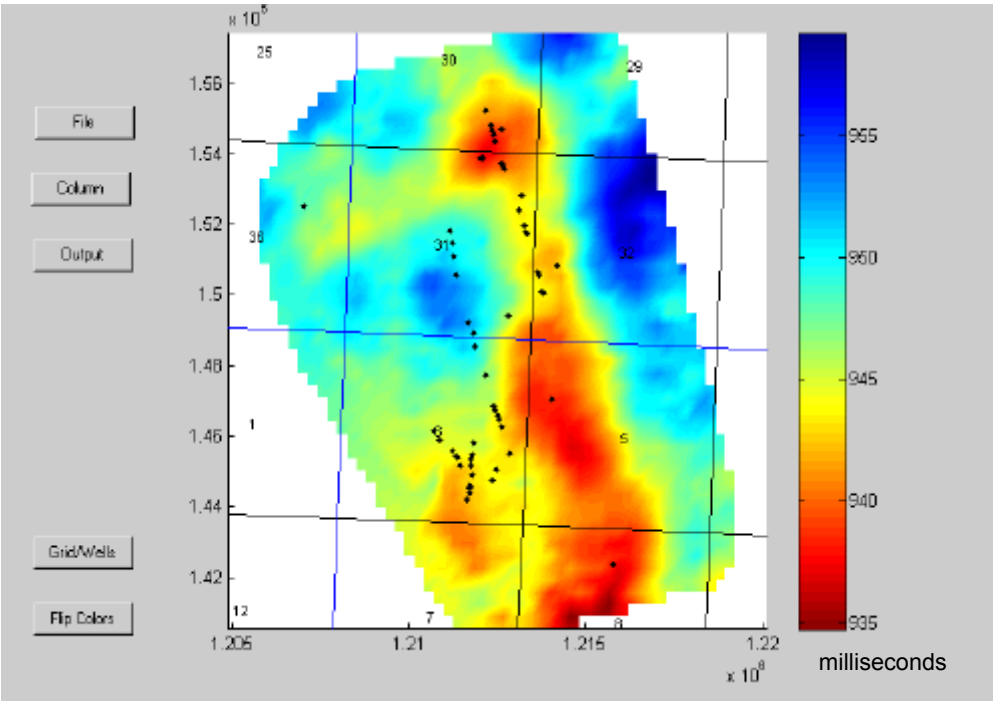

Figure 3-6. Map of seismic interval time from the Niobrara to Red River at Amor South Red River Unit.

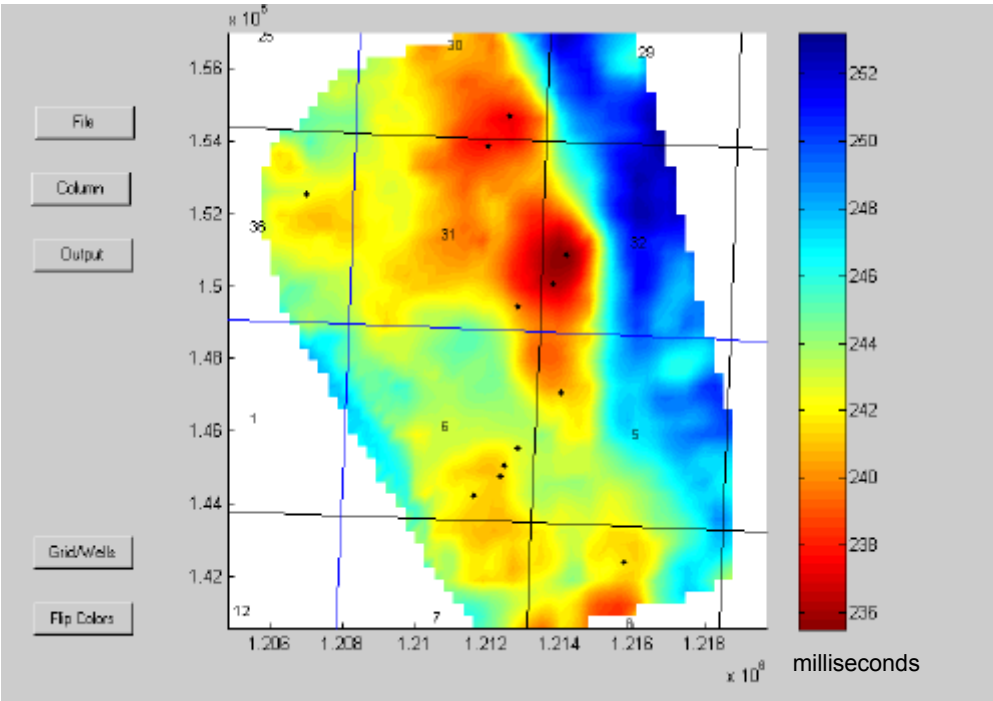

Figure 3-7. Map of seismic interval time from the Mission Canyon to Winnipeg at Amor South Red River Unit.

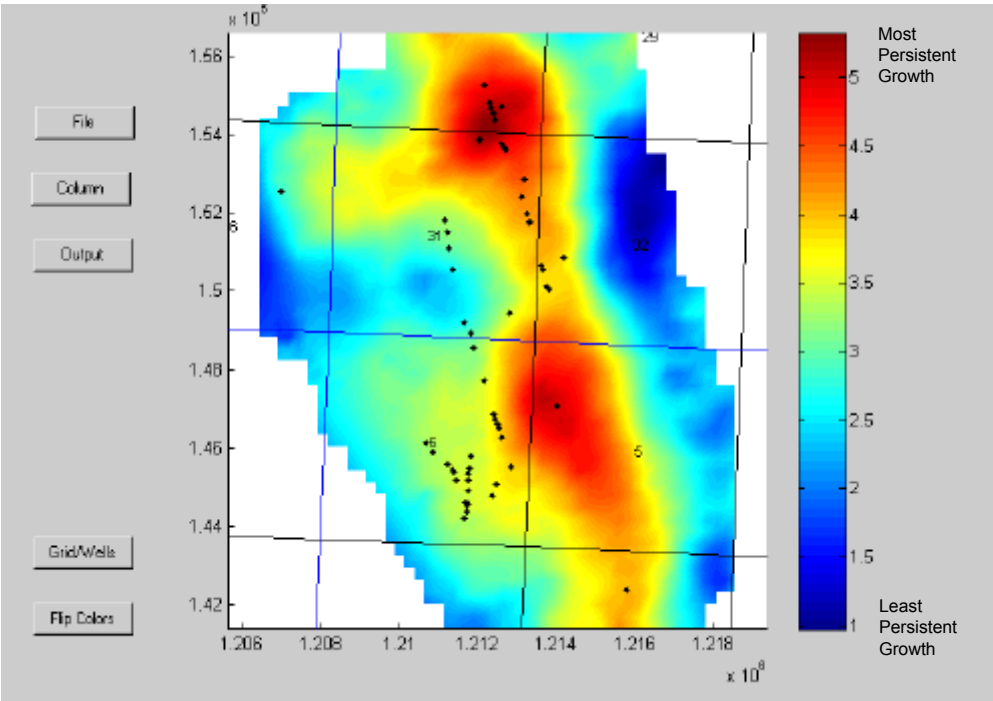

Figure 3-8. Map of structural growth index at Amor South Red River Unit.

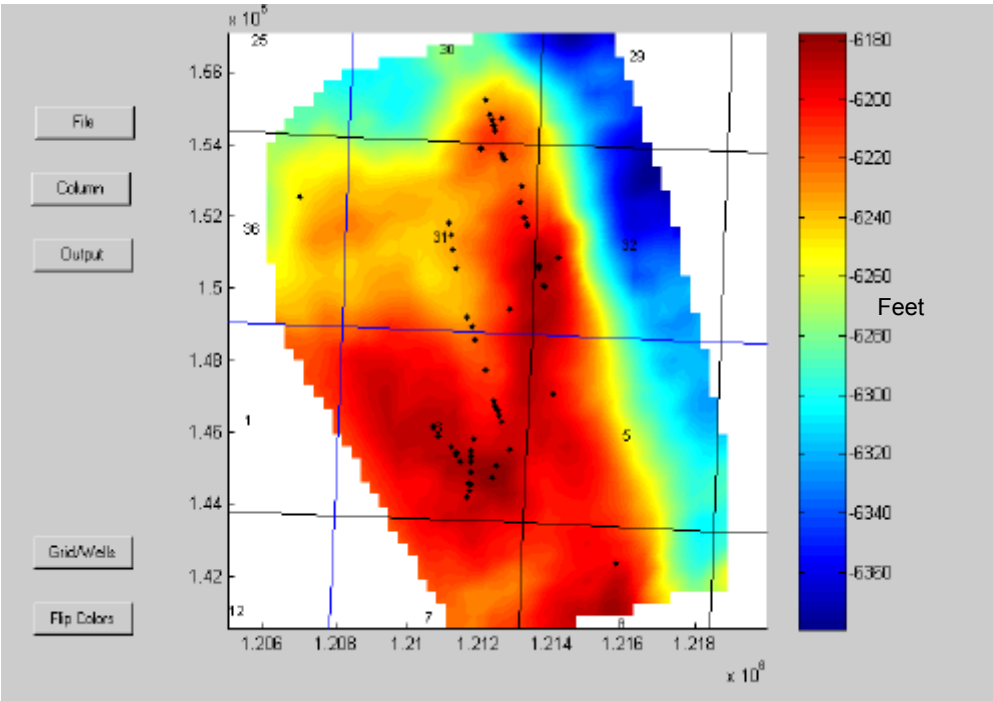

Figure 3-9. Map of computed Red River subsea depth from seismic time transforms and local well control at Amor South Red River Unit.

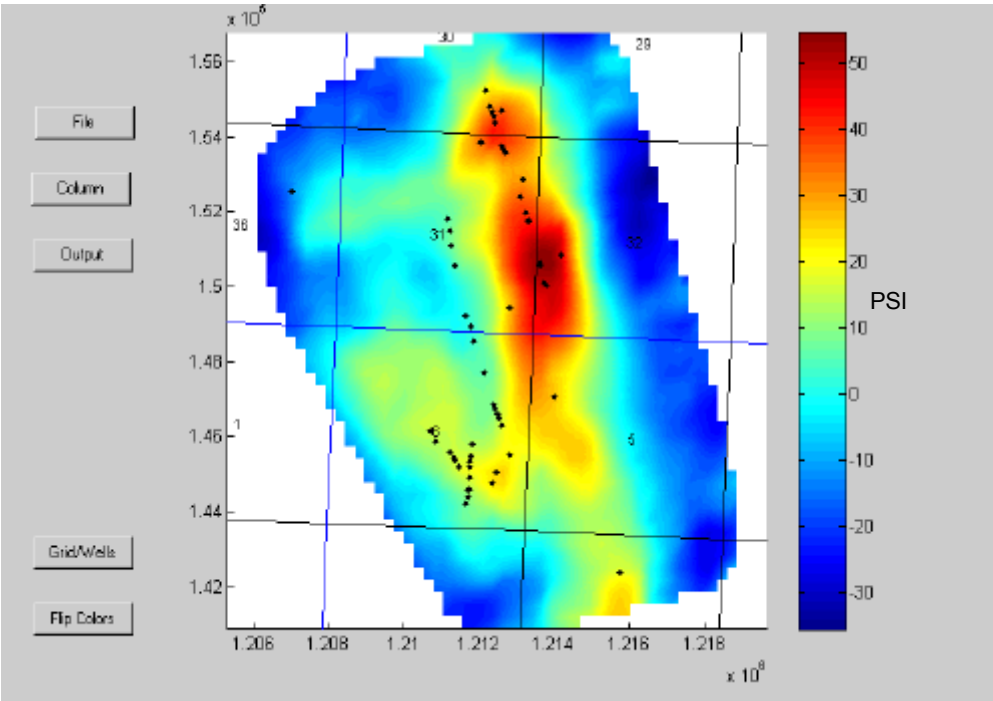

Figure 3-10. Map of composite entrapment pressure index that was created by the ICS Entrapment Tool.

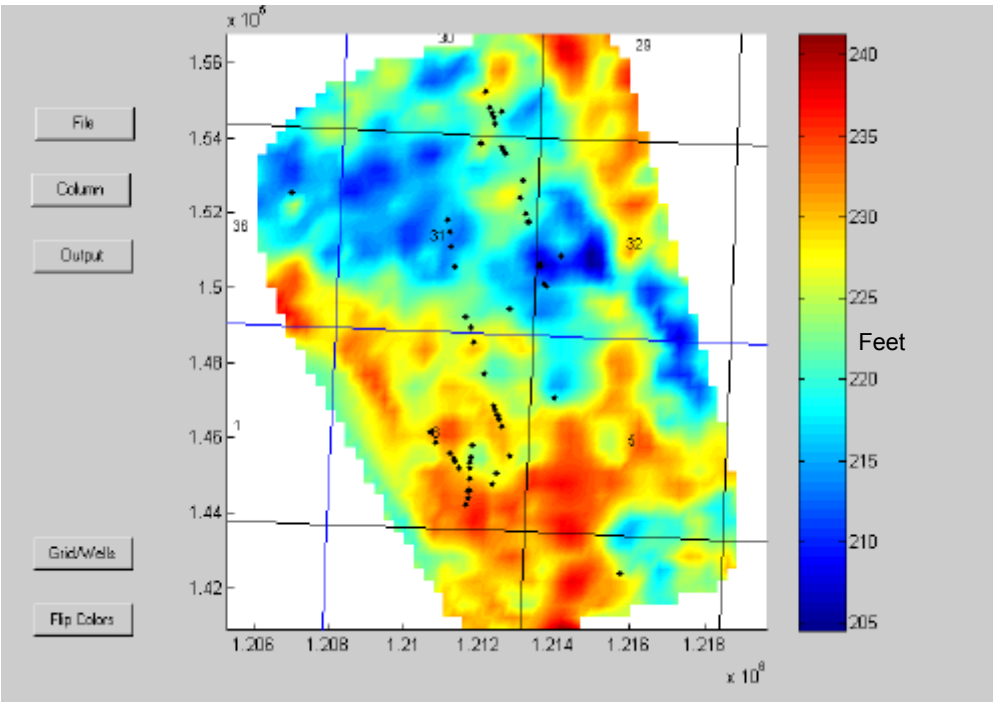

Figure 3-11. Map of thickness for upper Red River that was created by the ICS Neural Solver from seismic attributes and external training.

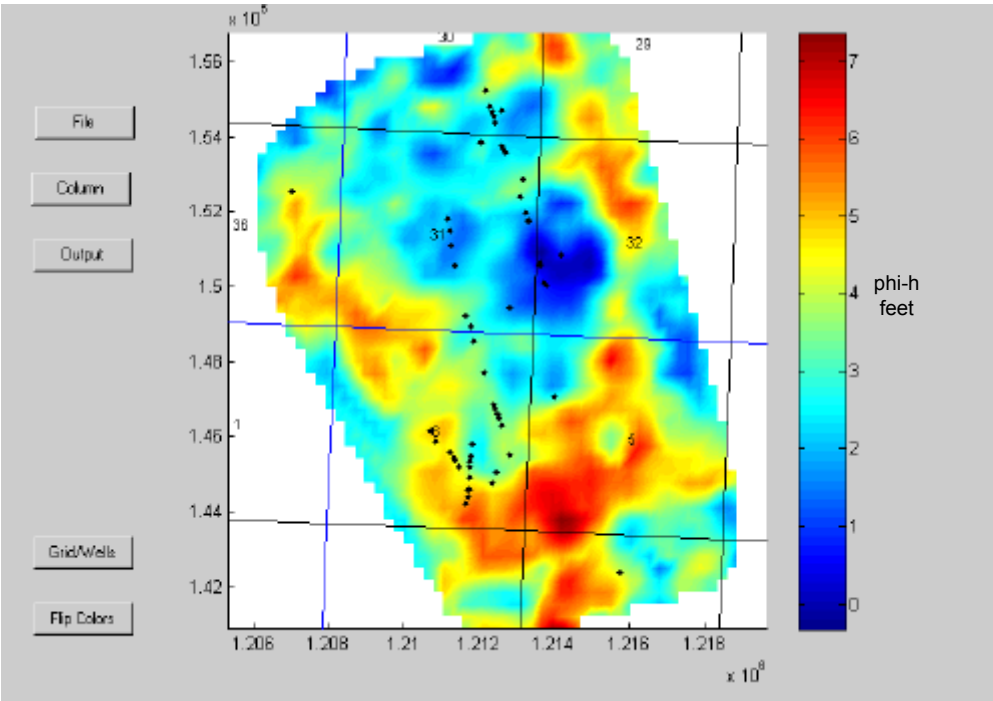

Figure 3-12. Map of porosity-feet (storage) for the Red River D Zone that was created by the ICS Neural Solver from seismic attributes and external training.

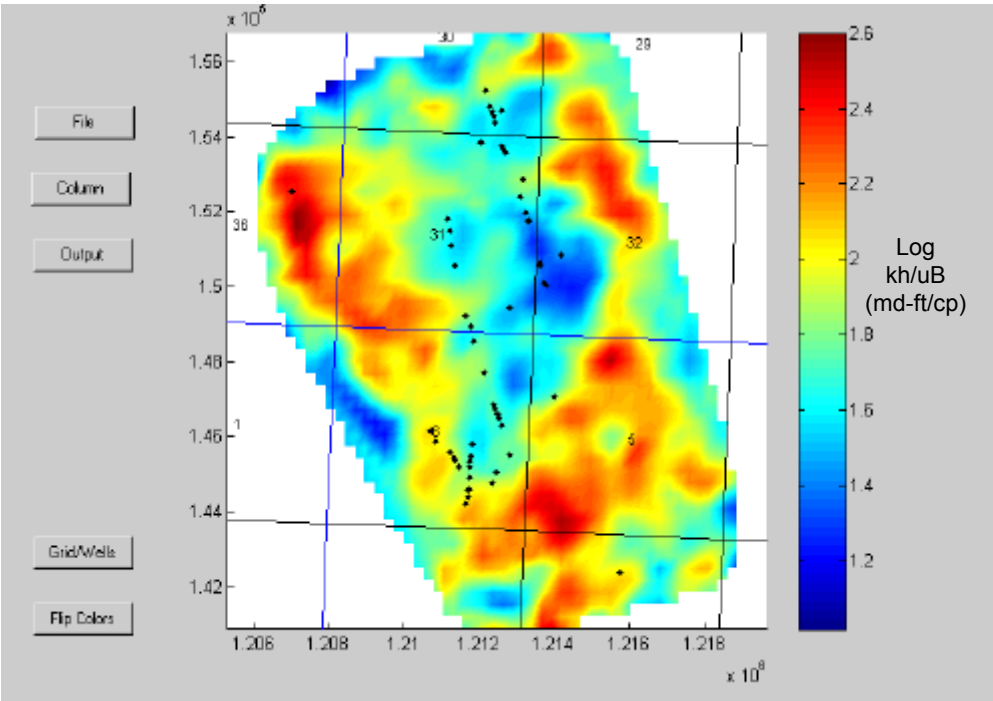

Figure 3-13. Map for logarithm of transmissibility (kh/uB) from drill-stem tests for the Red River D Zone.

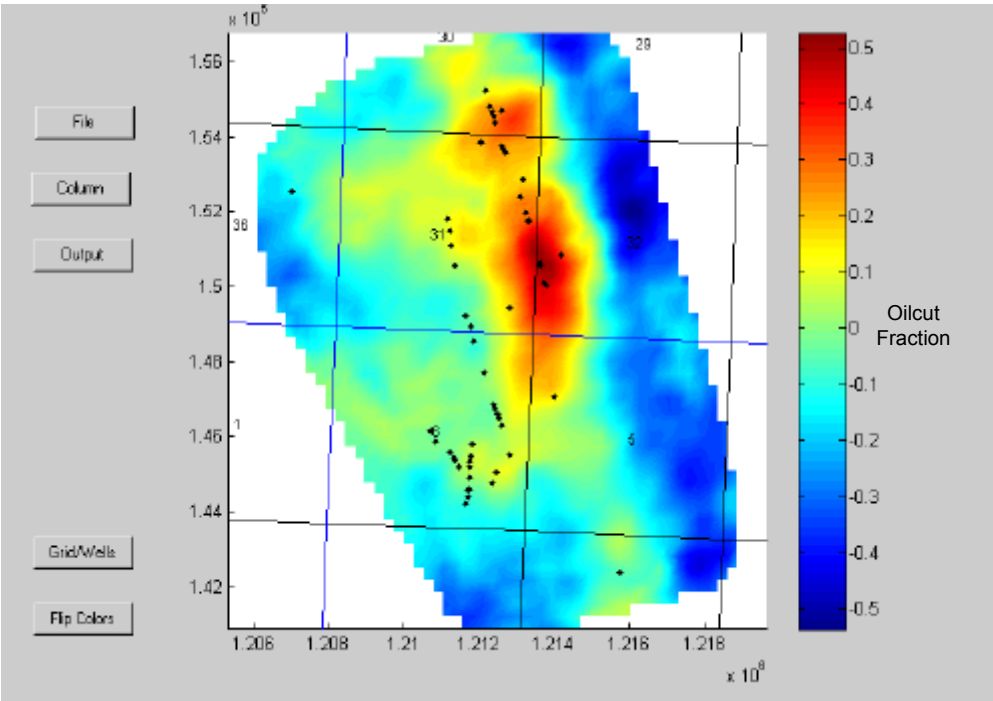

Figure 3-14. Map of initial oilcut for the Red River D Zone created by the ICS Neural Solver.

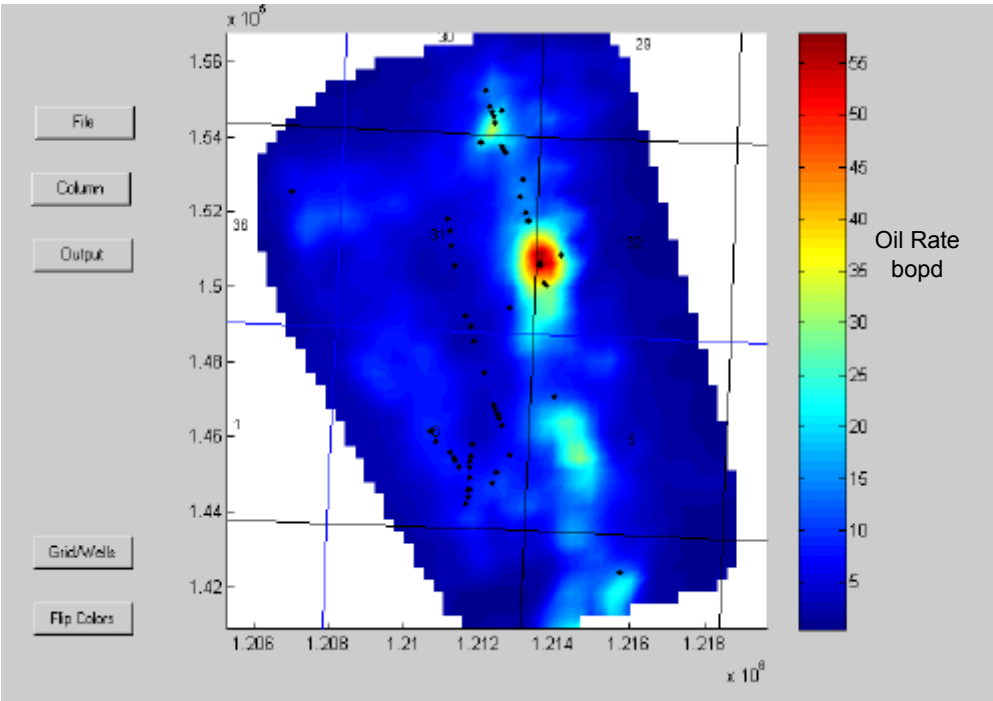

Figure 3-15. Map of initial oil rate for the Red River D Zone predicted by the ICS Neural Solver.

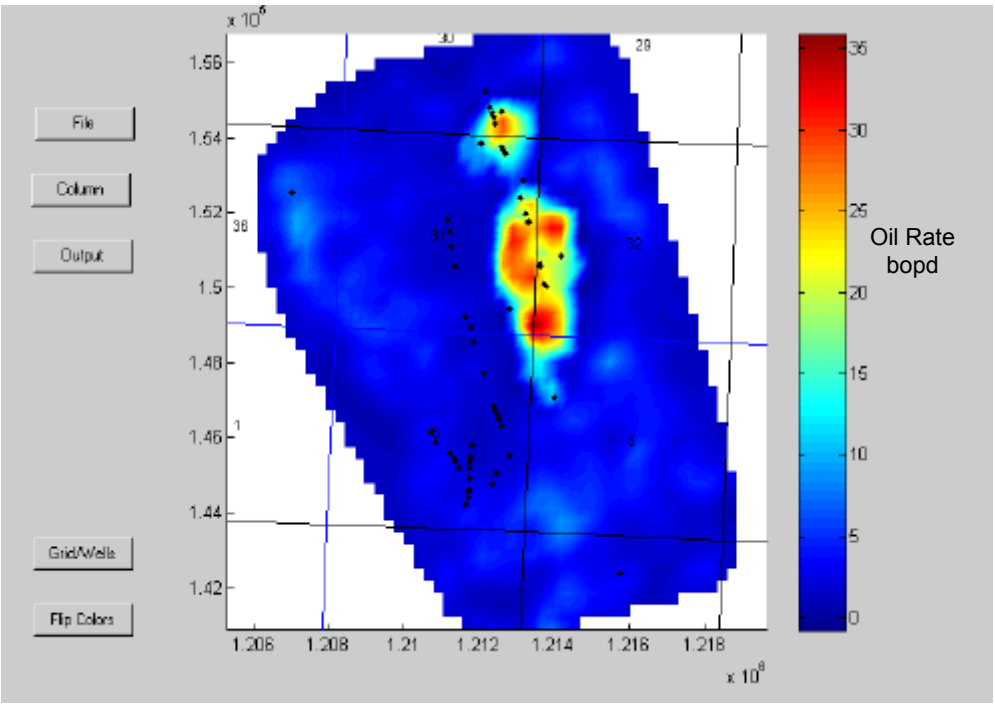

Figure 3-16. Map of initial oil rate for the Red River D Zone created by calculation from the initial oilcut and transmissibility transforms that were produced by the ICS Neural Solver.

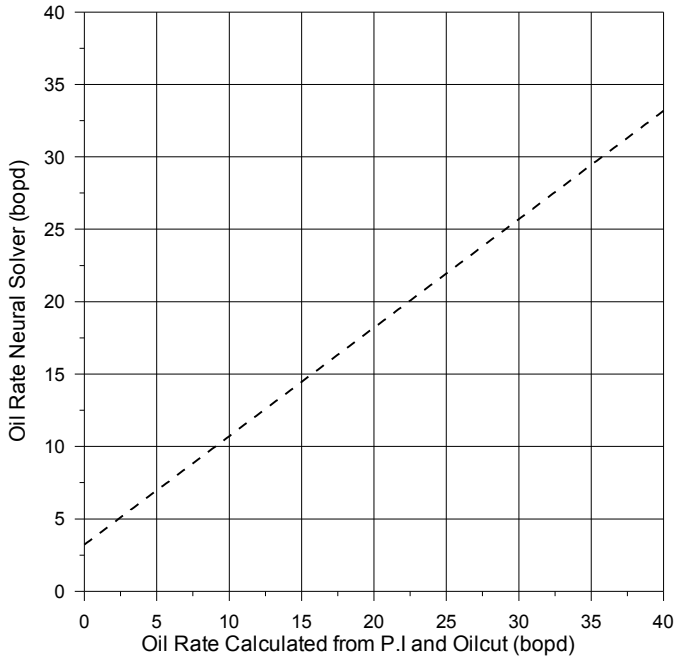

Figure 3-17. Graph comparing the calculated oil rate of Figure 3-16 with the direct transform of oil rate from the ICS Neural Solver in Figure 3-15.

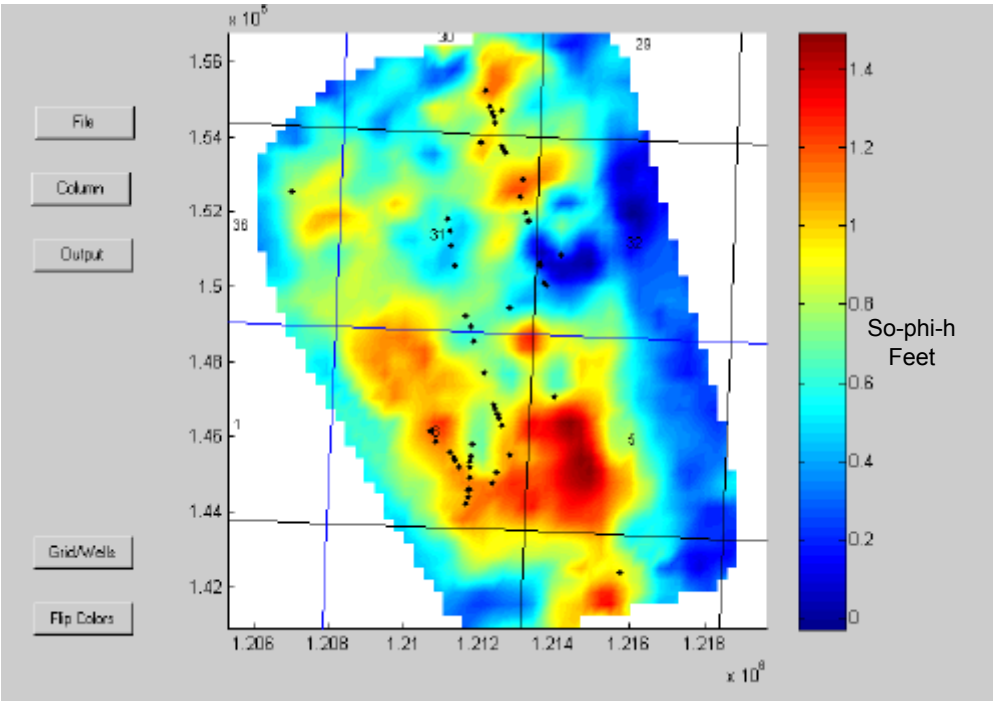

Figure 3-18. Map of calculated hydrocarbon pore volume for the Red River D Zone from oilcut and storage (phi-h) transforms.

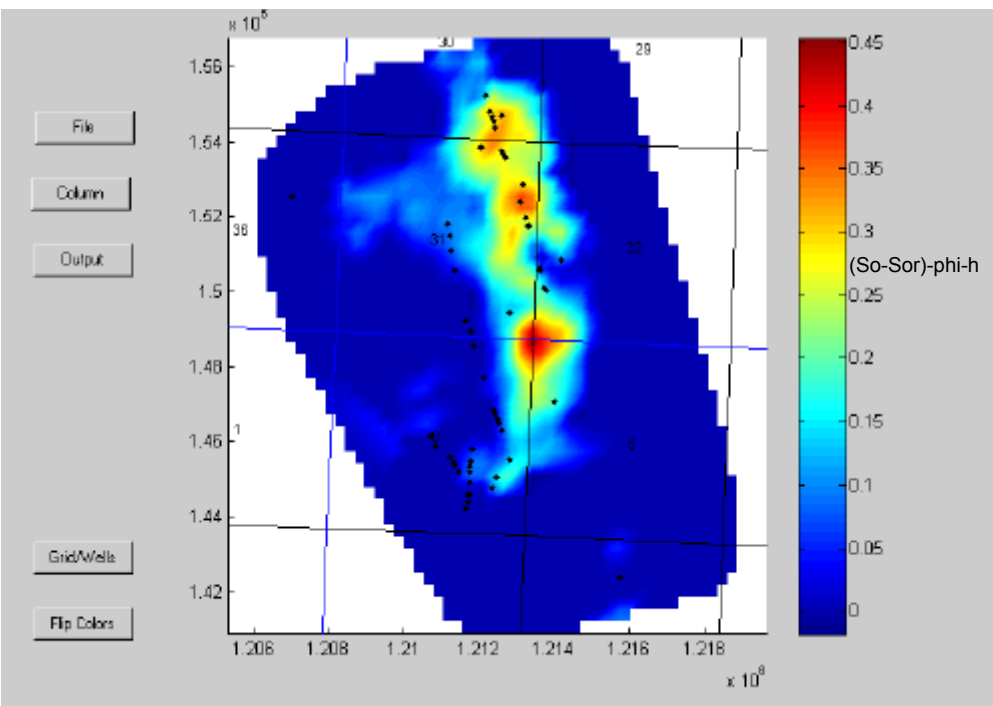

Figure 3-19. Map of calculated mobile hydrocarbon pore volume for the Red River D Zone from oilcut and storage (phi-h) transforms.

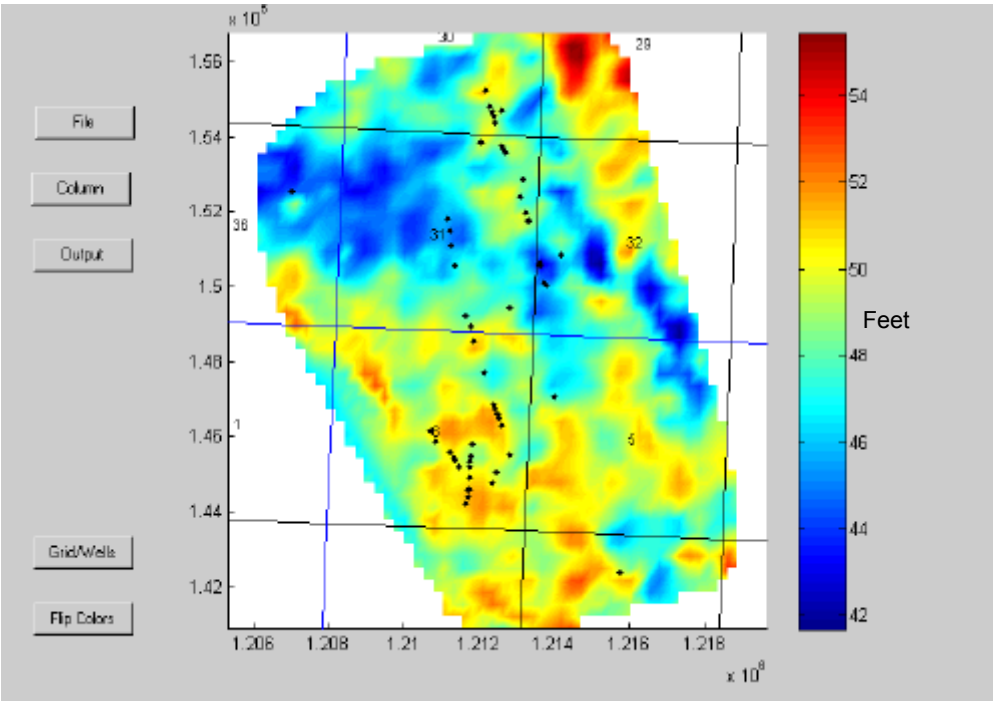

Figure 3-20. Map of Red River B Cycle thickness at Amor South Red River Unit, predicted by the ICS Neural Solver.

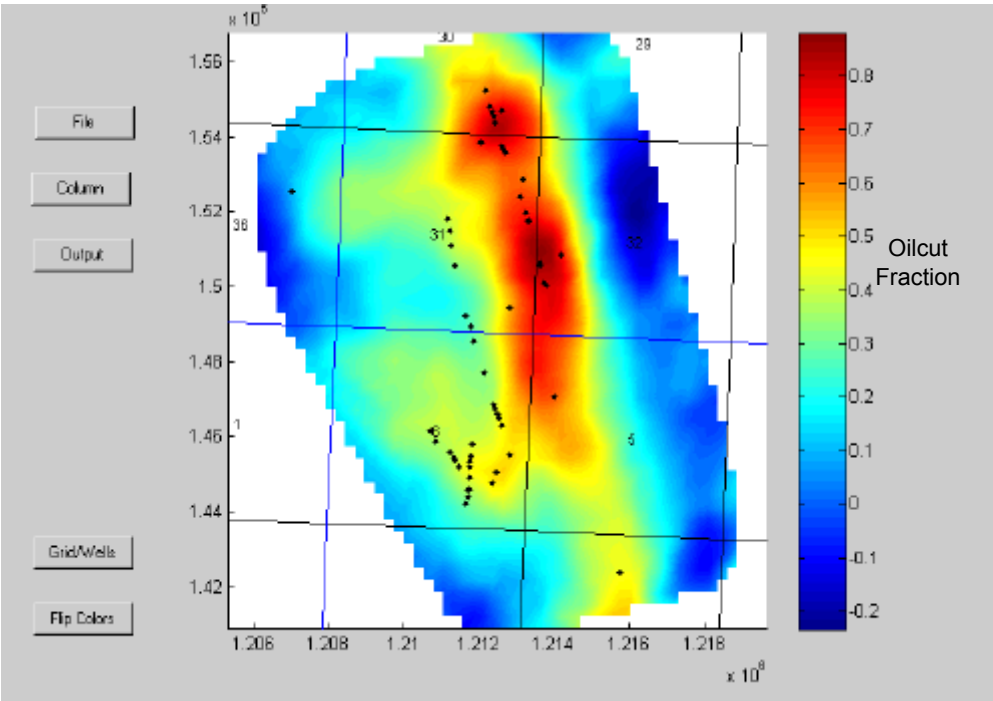

Figure 3-21. Map of initial oilcut for the Red River B zone at Amor South Red River Unit, predicted by the ICS Neural Solver.

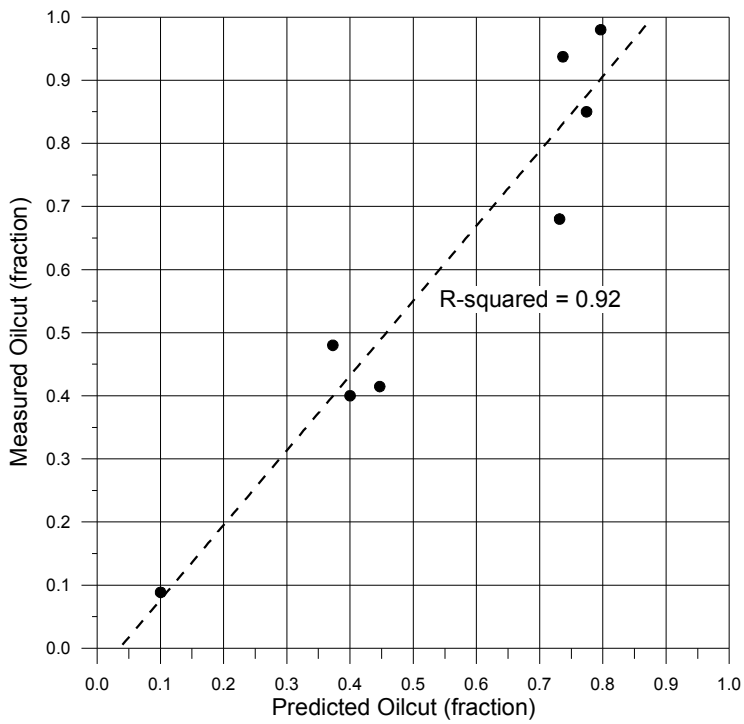

Figure 3-22. Graph comparing predicted B Zone initial oilcut with actual producing oilcut at Amor South Red River Unit.

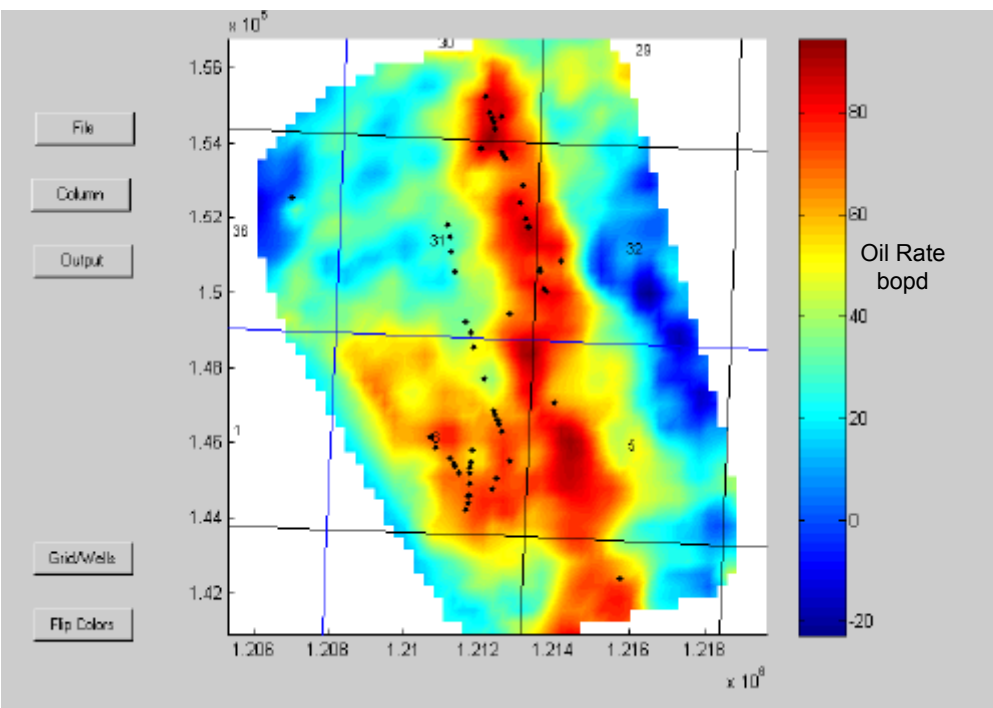

Figure 3-23. Map of predicted initial oil rate for vertical wells completed in the Red River B Zone at Amor South Red River Unit.

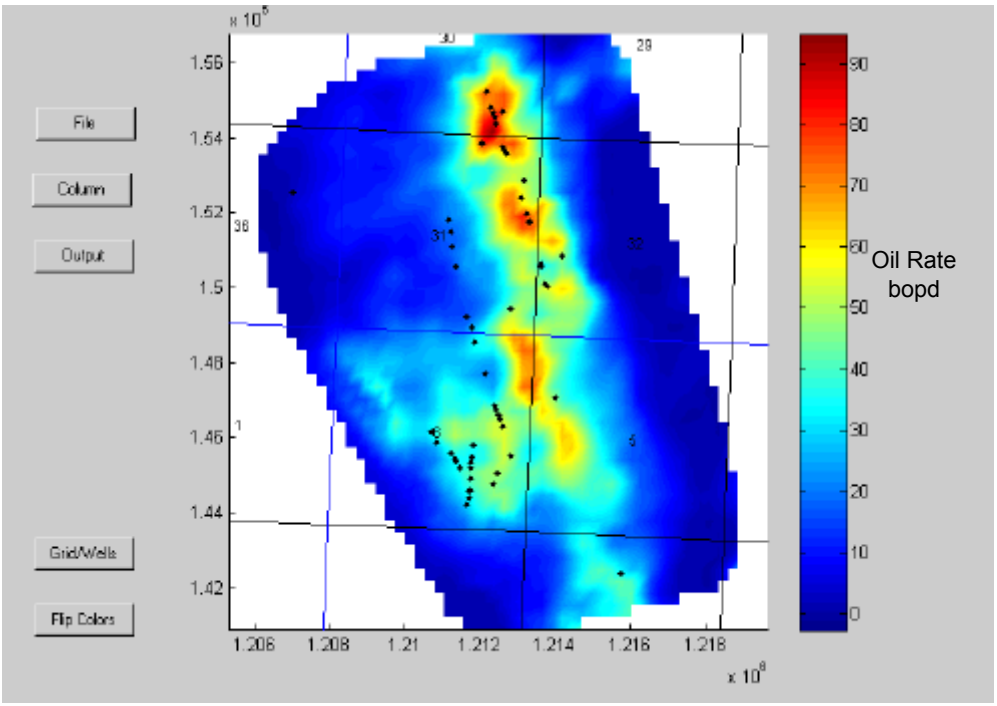

Figure 3-24. Map of initial oil rate for the Red River B Zone with vertical wells created by calculation from initial oilcut and transmissibility transforms produced by the ICS Neural Solver

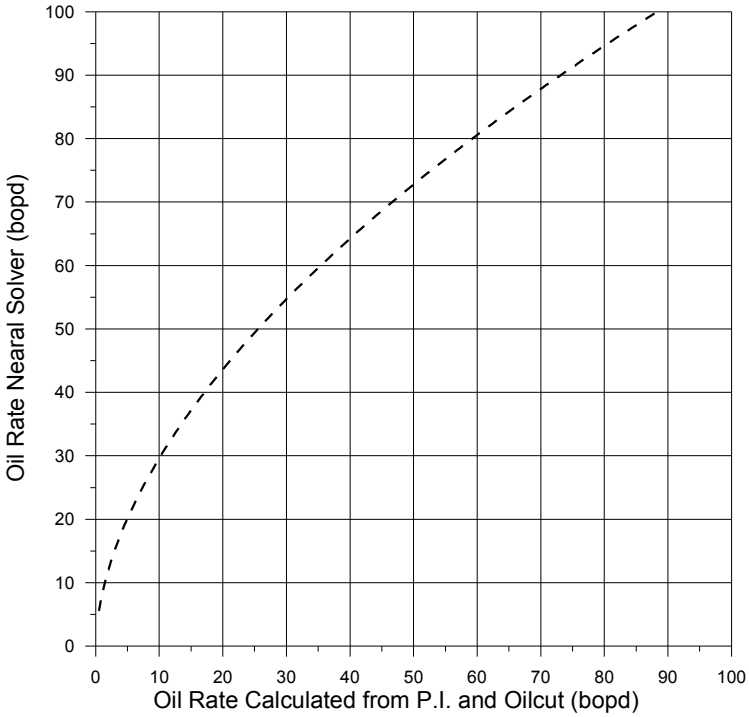

Figure 3-25. Graph comparing calculated oil rate of Figure 3-24 with the direct transform of oil rate from the ICS Neural Solver in Figure 3-23.

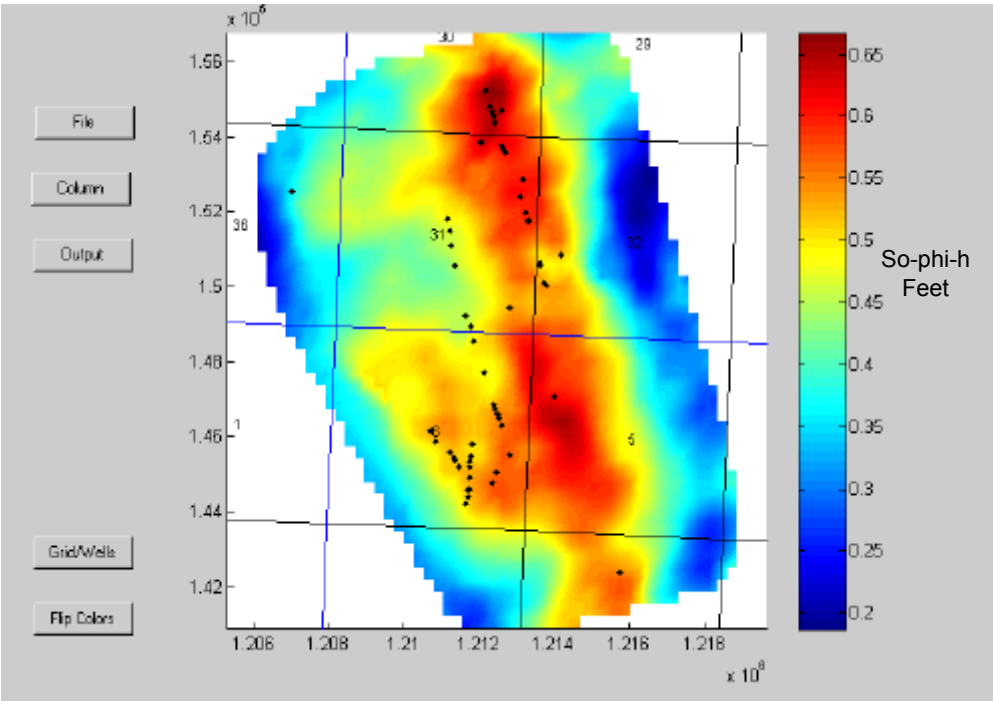

Figure 3-26. Map of calculated hydrocarbon pore volume for the Red River B Zone from oilcut and storage (phi-h) transforms.

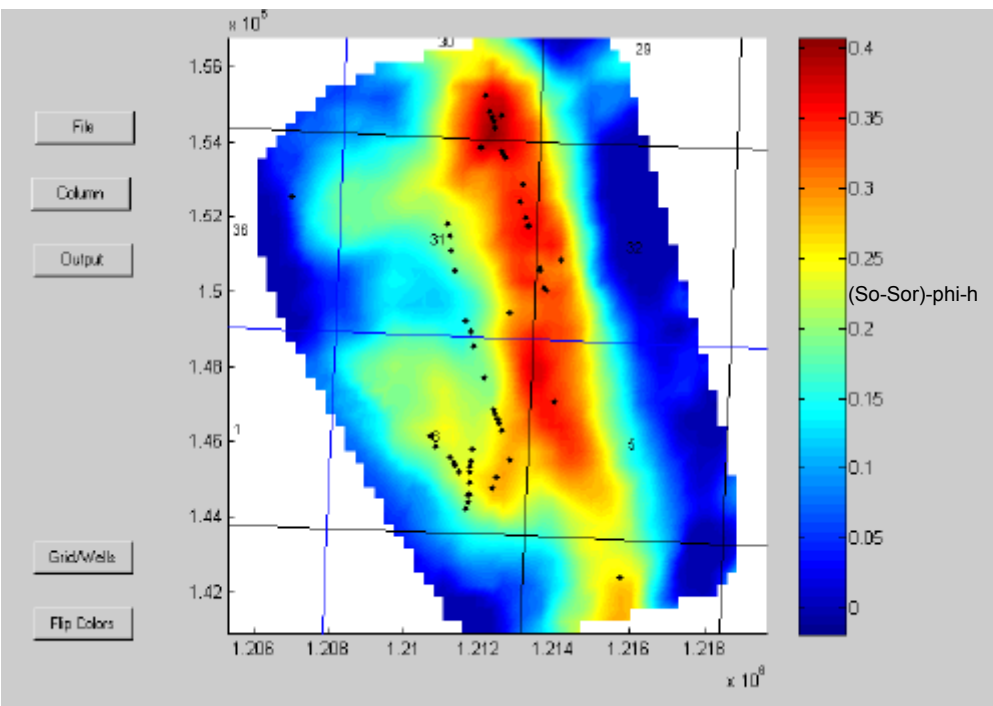

Figure 3-27. Map of calculated mobile hydrocarbon pore volume for the Red River B Zone from oilcut and storage (phi-h) transforms.

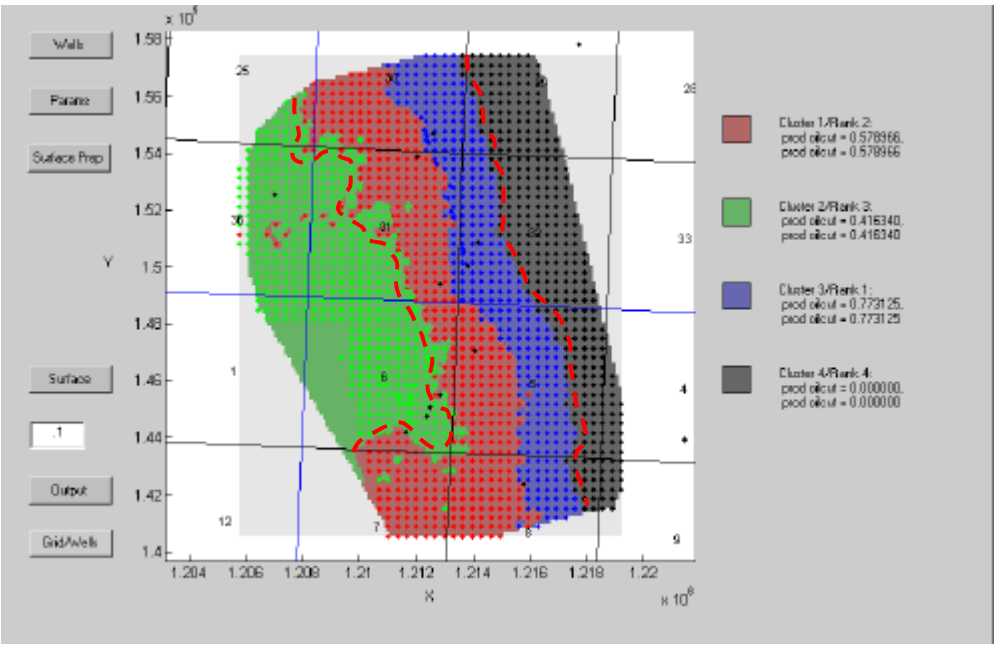

Figure 3-28. Map of four clusters for oilcut made with nine seismic-time horizons at the Amor South Red River Unit. The area of greatest oilcut is outlined by red dashed lines.

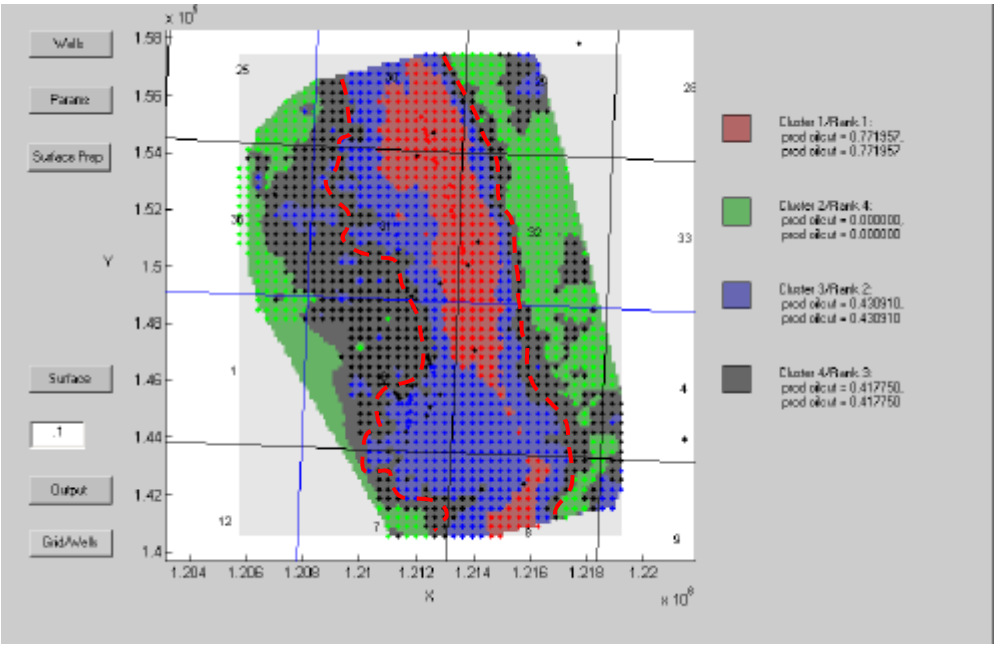

Figure 3-29. Map of four clusters for oilcut made with all combinations of interval time from nine seismic-time horizons at the Amor South Red River Unit. The area of greatest oilcut is outlined by red dashed lines.

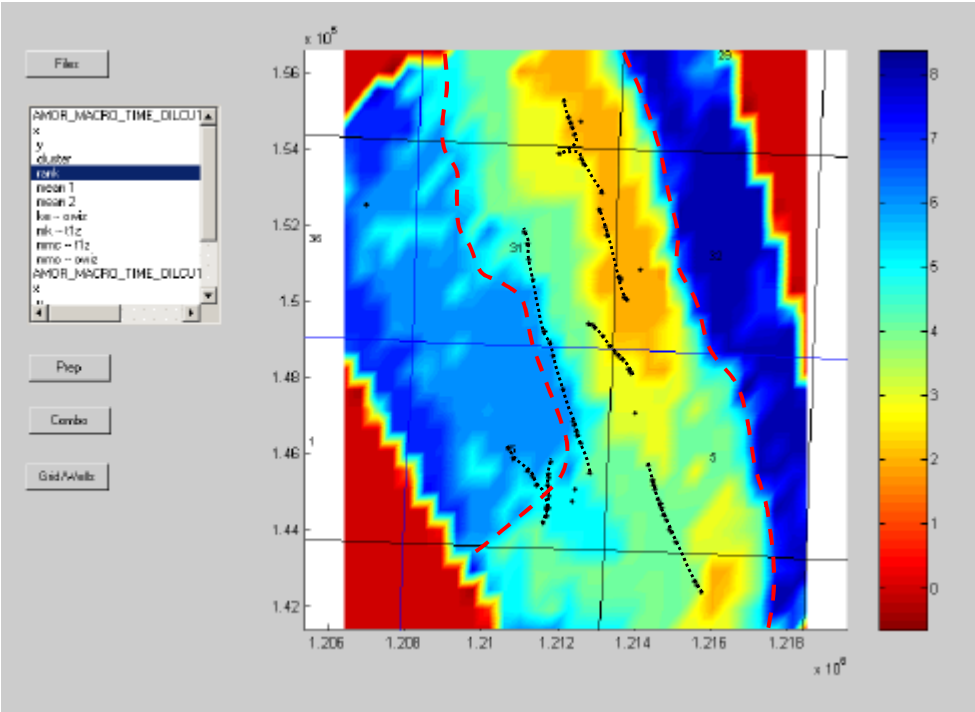

Figure 3-30. Map of cluster-rank summation for the two maps of oilcut clusters shown in Figures 3-28 and 3-29. A combined rank of 2 is the best score and a combined rank of 8 represents the lowest score. The locations are shown of current development with horizontal laterals in the Red River B Zone.

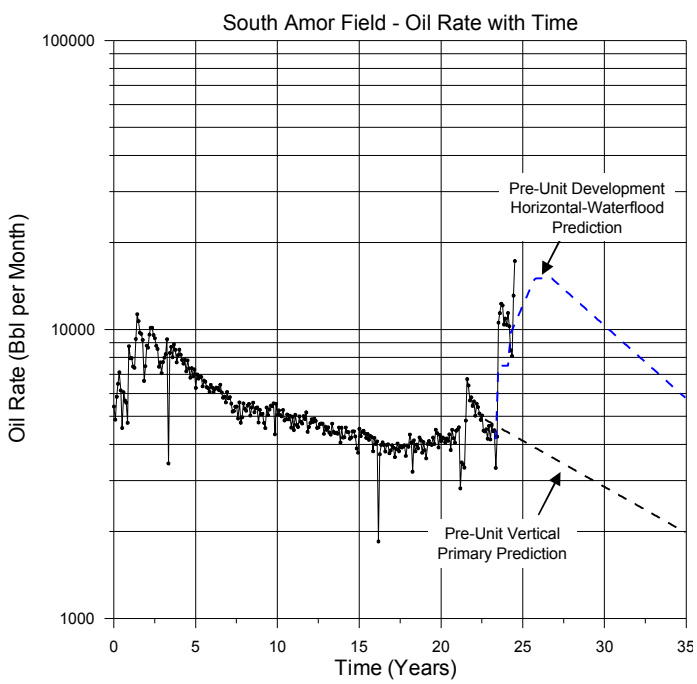

Figure 3-31. Graph of monthly oil rate with time for all wells in the Amor South Red River Unit. Projections are also shown for depletion with vertical wells and waterflooding with horizontal wells.

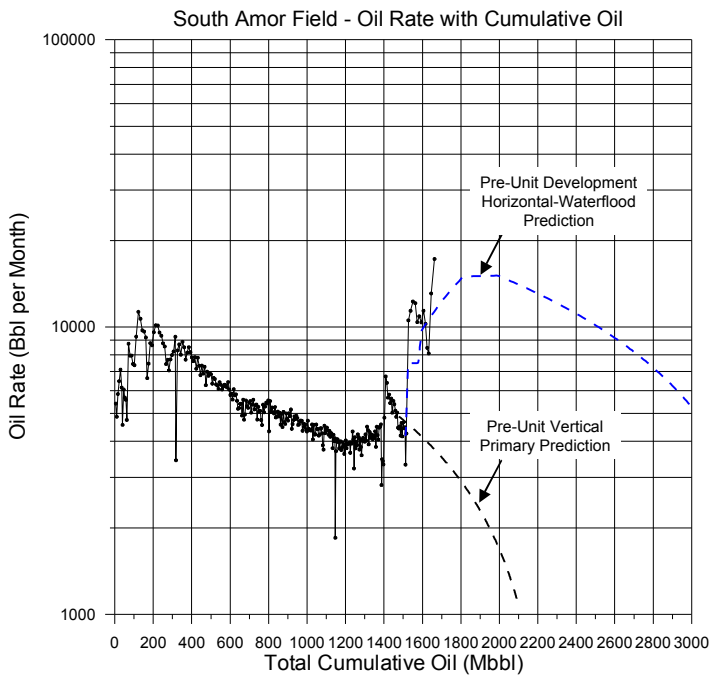

Figure 3-32. Graph of monthly oil rate with cumulative oil for all wells in the Amor South Red River Unit. Projections are also shown for depletion with vertical wells and waterflooding with horizontal wells.

Reservoir Characterization with 2D Seismic at Amor North Field

The Amor North Field was selected as a demonstration site for testing and development of ICS Tools and strategy with 2D seismic data. It is concluded that there are useful seismic attributes (amplitude and interval time) that can be extracted from 2D seismic for use in reservoir characterization beyond conventional structural interpretation. Predictions were made for oil rate and oilcut for the Red River B and D Zone reservoirs. Seismic-reservoir transforms allow calculations for oil-in-place.

Historical Background

The field area is located in township T130N-R103W in Bowman County, North Dakota. Exploration drilling began in 1972 (API 33-011-00170) and this well was successfully completed in the Red River B, C and D Zones. A total of seven wells were drilled, of which four were completed with commercial production from the Red River. Initial exploration and development efforts were based on data from 2D seismic lines that were used for identification of structure at Red River depth. Seismic interpretations of interval time and time structure were used for well placement. The four productive wells in Amor North Field had combined cumulative oil production of 1,264,640 bbl as of December 2002.

Regional Setting

The field area is located two miles east and downdip from the Medicine Pole Hills Field. The field is also located about two miles north from the northern edge of the Amor South Red River Unit, which is also described in this report. The geological setting for the Amor North Field is similar to that found at the Amor South Red River Unit. Regional structural setting for Amor North is shown in **Figures 4-1** and **4-2**. **Figure 4-1** is a structure map at the top of the Red River Formation. **Figure 4-2** shows residual structure above and below a regional trend surface of Red River depth.

2D Seismic Data

A 2D seismic grid evolved as development occurred across the Amor North Field. Various companies acquired the seismic lines in the 1970's and 1980's. Luff Exploration Company purchased rights to the seismic lines during the course of this project with the intent to determine the usefulness of 2D seismic data for use in reservoir characterization with ICS tools. Locations of the 2D seismic traces are shown in **Figure 4-3**. The seismic lines are located in an orthogonal grid with the lines separated by approximately one-quarter to one-half mile. The acquired seismic data were re-processed from the original tapes so that the line parameters would be the same. The same seismic time and amplitude attributes at Red River depth were picked as with the 3D seismic survey data that was acquired over the Amor South Red River Unit and at other surveys in the area. A

normalizing scheme was applied to amplitude data. The seismic picks at the 2D traces were exported in ASCII format to spreadsheets. Time and amplitude data at 2D seismic traces were then gridded with mapping software to create a pseudo 3D seismic grid.

Basic seismic interpretation for Red River structure in the area begins with an interval time map such as from a shallow Cretaceous marker to the Red River. **Figure 4-4** shows a map of interval time from Niobrara to Red River across the Amor North Field. Using the conventional method for computing Red River depth from seismic, a depth structure map is produced as shown in **Figure 4-5**. This map was constructed from a contoured map of Niobrara depth from wells, Niobrara-Red River interval time and contoured Niobrara-Red River seismic velocity. The regional-trend residual of the computed depth map for Red River is shown in **Figure 4-6**.

Using five isochrons from Niobrara to Winnipeg, a pre-Niobrara structural growth-index map was produced with the ICS Growth Index Tool and is shown in **Figure 4-7**. Red River depth residual and growth-index maps generally provide a good overall depiction of production limits.

The first test of using 2D seismic attributes for reservoir characterization is shown in **Figure 4-8** where a prediction of overall upper Red River thickness has been made with the ICS Neural Solver by applying external well-seismic data from six 3D seismic surveys. Normalized seismic attributes have been captured at each well location in the respective 3D seismic survey and the well control at each survey is combined into a master training file. The same training file was used as had been tested on the six 3D seismic surveys in other studies but modified slightly to match the attributes extracted from the 2D seismic data. Shown in **Figure 4-9** is another prediction for upper Red River thickness, again with the ICS Neural Solver, but in this case the training file consists of only the seven local wells covered by the 2D seismic grid. The patterns produced by the isopach maps in **Figures 4-8** and **4-9** are similar but exhibit a slight shift in scaling.

Robustness of the Amor North 2D seismic training file was tested by application with data from the Amor South Red River Unit 3D seismic survey. Comparison of results from the seven-well 2D seismic training file and a 36-well 3D seismic training file is shown in **Figure 4-10**. The same scaling shift is observed in the graph as was displayed in the isopach maps for the Amor North Field in **Figures 4-8** and **4-9**. It is concluded from these two tests, that there are useful seismic attributes (amplitude and interval time) that can be extracted from 2D seismic for use in reservoir characterization beyond conventional structural interpretation.

A structural entrapment pressure index is shown in **Figure 4-11** for the Amor North Field. This entrapment pressure index was produced by the ICS Entrapment Tool using the calculated Red River structure without parameters for rock-quality. The map was created by the difference of residual pressure and

migration pressure outputs. It is inferred from the map of entrapment pressure index that the potential for structural entrapment of oil increases with a greater value of the index pressure. Areas with negative entrapment pressure index are below critical closure.

Red River D Zone Characterization

Reservoir characterization for the Red River D Zone at Amor North Field included seismic structural and reservoir transforms. Structural transforms include seismic isotime of Niobrara to Red River, Red River depth with regional trend and residual, and entrapment pressure index. Reservoir transforms include gross D Zone thickness, porosity-thickness, upper Red River thickness and C plus D cycle thickness. These transforms were then used to predict production transforms for initial oil rate and oilcut. The predictions were made with the ICS Neural Solver using external training of D Zone production data from 53 wells as if there were no wells yet drilled at the Amor North Field. The prediction from this training for initial oil cut from the Red River D Zone is shown in **Figure 4-12**. The prediction of initial oilcut indicates a maximum oilcut of about 50% at the crest of the Red River structure located in the center of section 20.

Another production transform is for initial oil rate. Using the same wells and training file as used for the prediction of oilcut, an initial oil rate transform is produced by the ICS Neural Solver as shown in **Figure 4-13**. Similar to the prediction of oilcut, the initial oil rate map indicates a maximum oil rate of about 250 bopd at the crest of the Red River structure located in the center of section 20.

Similar to prediction of oil rate by the ICS Neural Solver, it is possible to make a prediction of transmissibility (kh/uB md-ft/cp) from drill-stem tests for the Red River D Zone. The same geologic-reservoir transforms were used as for the prediction of oil rate. Combining the transmissibility and oilcut transforms, it is possible to compute an oil-flow rate for a vertical well based on conventional equations assuming some pressure drawdown. Results from such a calculation are shown in **Figure 4-14** for the Amor North Field Red River D Zone. The maximum initial oil rate at full drawdown pressure is indicated to be about 180 bopd at the crest of the Red River structure located in the center of section 20. It is noteworthy that the production limit (0 bopd) from either map is about the same. Similar results have been achieved at other Red River D Zone reservoirs with ICS production transforms.

As a blind test, the production transforms for the Red River D Zone at Amor North Field were made from external training. External training is the application of production, geological and reservoir data from wells not in the target area. Reservoir and structural attributes are predicted from the seismic transforms. The external training is applied to those reservoir-structural attributes and predictions are made for production attributes. Validation of the predictions is made by

comparison with the actual production at wells in the target area. Well API 33-011-00170 is located on the structural crest of the feature located in section 20. That well recovered oil at an extrapolated rate of 264 bopd with an oilcut of 77% by drill-stem test of the Red River D Zone in 1972. The Red River D Zone was subsequently produced commingled in the wellbore with the Red River B and C Zones. All other Red River penetrations in the Amor North Field did not yield sufficient oil shows while drilling to warrant testing.

Volumetric estimates of oil-in-place for the Red River D Zone can be made from the seismic-reservoir and production transforms. The neural solver prediction of oilcut and storage (phi-h) are used. An oil-water relative permeability curve is used with the oilcut prediction to make a calculation of oil saturation. The resulting oil saturation is applied to the phi-h transform to produce a calculation of oil saturated pore volume. As shown in **Figure 4-15**. It is also possible to estimate the mobile oil pore-volume map by estimate of the irreducible water saturation and residual oil saturation from oil-water relative permeability data or estimates. Mobile hydrocarbon pore volume is displayed in map view from such a calculation in **Figure 4-16.** Consistency of the reservoir-production transforms is demonstrated by comparison of oil rate maps in **Figures 4-13** and 4-**14** with mobile hydrocarbon pore volume in **Figure 4-16**.

Red River B Zone Characterization

Development of the Red River B Zone reservoir is affected by the depositional setting as characterized by the B Cycle thickness. The B Cycle thickness is measured from the top of the overlying B Anhydrite to the top of the C Anhydrite. Red River B Zone rock-typing and depositional setting are discussed in detail in appendices entitled “Geologic Rock-Typing, Red River B Zone” and “Analytical Rock-Typing, Red River B Zone.” Thickness of the B Cycle allows inference of whether the B Zone porosity was dominated by lagoonal, intertidal or supratidal conditions (thickest to thinnest). It is desirable to place wells in an intertidal setting.

Prediction of the B Cycle thickness can be accomplished with the ICS Neural Solver and Clustering Tools. Shown in **Figure 4-17** is a map of B Cycle thickness that was produced by the ICS Cluster Tool using 2D seismic attributes. Four cluster groups were generated using local control from seven wells. Each cluster group is ranked from 1 to 4 (thickest to thinnest). Results from the ICS Neural Solver for prediction of B Cycle thickness at Amor North Field are shown in **Figure 4-18** where predictions at the well locations are compared to the measured thickness from well logs. The graph comparison also incorporates four additional pseudo well locations at cardinal points from each well at a distance of 150 ft. The graph shows a fairly good linear trend of predicted and measured values. The range of values for B Cycle thickness indicates that the wells are located in a lower intertidal to lagoonal depositional setting.

Reservoir characterization for the Red River B Zone at Amor North Field included seismic structural and reservoir transforms. Structural transforms include seismic isotime of Niobrara to Red River, Red River depth with regional trend and residual, and entrapment pressure index. Reservoir transforms include B Cycle thickness, and upper Red River thickness. These transforms were then used to predict production transforms for initial oil rate and oilcut. The predictions were made with the ICS Neural Solver using external training of B Zone production data from 65 wells as if there were no wells yet drilled at the Amor North Field.

The prediction from this training for initial oil cut from the Red River B Zone is shown in **Figure 4-19**. The prediction of initial oilcut indicates a maximum oilcut of about 75% at the crest of the Red River structure located in the center of section 20. Another production transform is for initial oil rate. Using the same wells and training file as used for the prediction of oilcut, an initial oil rate transform is produced by the ICS Neural Solver as shown in **Figure 4-20**.

Calculations for original-oil-in-place in the Red River B Zone were made from the predicted oilcut transform and assumption of a constant porosity-thickness from average log values. Also, the oilcut transform was used with an oil-water relative permeability relationship to compute oil saturation. **Figure 4-21** shows the map of hydrocarbon pore volume based on this calculation. A mobile hydrocarbon pore volume map for the Red River B Zone is shown in **Figure 4-22** where estimates of the irreducible water saturation and residual oil saturation were used to define the mobile oil saturation window.

Demonstration Wells

There are two demonstration wells at the Amor North Field. Both wells were re-drilled with horizontal laterals in the Red River B Zone. Each well was producing about 10 bopd and 30 bwpd from vertical completions prior to the horizontal drilling. The horizontal drilling targeted delineation of reservoir limits and predicted oilcut from ICS reservoir characterizations.

Re-entry horizontal laterals were drilled from well API 33-011-00256, located in the southeast of section 8, T130N-R103W. These laterals are in the Red River B Zone. The laterals were to test the northern end of the structural nose at Amor North Field. The vertical well was completed in the Red River B Zone during 1978 with an initial rate of about 61 bopd and 10 bwpd. A drill-stem test of the B Zone produced at an extrapolated rate of 160 bopd with no water. The ICS Neural Solver production transform (from external training) predicted an initial oil rate at this well's location of about 65 bopd. Because the well is lowest on the Amor North structural nose and had produced a low volume of water, it was thought to be a good candidate to test reservoir limits. Two bifurcating laterals were drilled northwesterly from the vertical wellbore. The westerly lateral went downdip 48 ft from the original vertical completion. While the predictions made for the Red River B Zone indicated that the lateral would encounter increasingly

water-wet rocks, drill cuttings and gas units indicated productive reservoir to the end of the lateral. The oilcut map shown in **Figure 4-19** indicates that the westerly lateral would encounter reservoir that would produce with a 25 to 30% oilcut at initial conditions (all production transforms are made for initial, undepleted conditions). After the horizontal laterals were drilled, the well was placed on pump and produced at a peak rate of 45 bopd and 290 bwpd (13% oilcut).

Another demonstration well at Amor North Field is API 33-011-00376, located in the southeast of section 17, T130N-R103W. This vertical well was completed in the Red River B Zone in 1982 with a peak oil rate of about 53 bopd. The ICS Neural Solver production transform (from external training) predicted an initial oil rate at this well's location of about 70 bopd. A re-entry lateral was drilled from the vertical wellbore in a northeasterly direction and was terminated about 300 ft from a dryhole in section 16. The horizontal lateral from this demonstration well was placed such that it would pass through an area indicated to be higher in the depositional setting (more upper intertidal) than the vertical well, refer to a map of B Cycle thickness in **Figure 4-17**. From the ICS characterizations, the predicted oilcut along the lateral is 50 to 55% (refer to the B Zone oilcut map in **Figure 4-19**). Peak production from the horizontal re-completion was 110 bopd with a 69% oilcut.

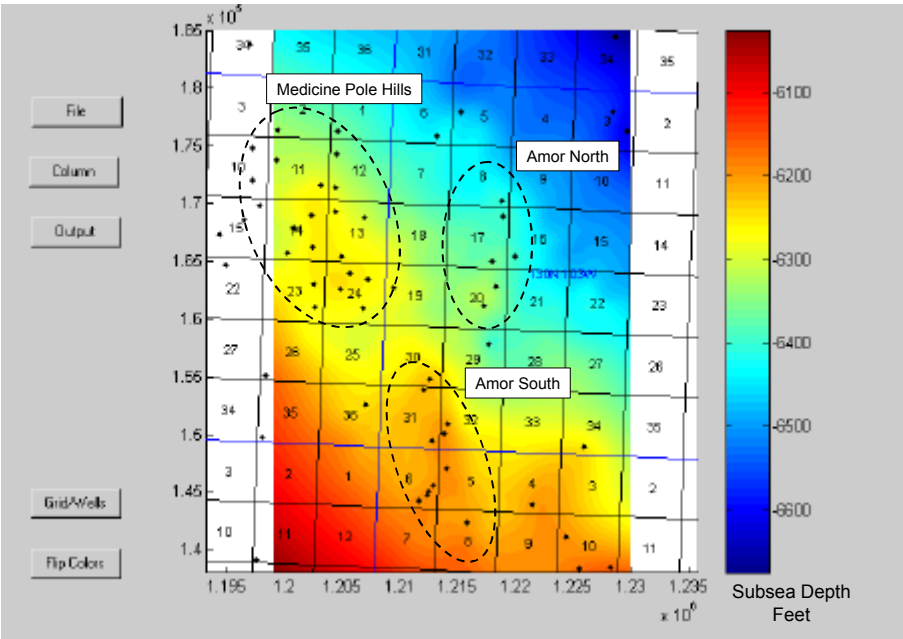

Figure 4-1. Map of regional structural setting at Red River depth for Amor North Field.

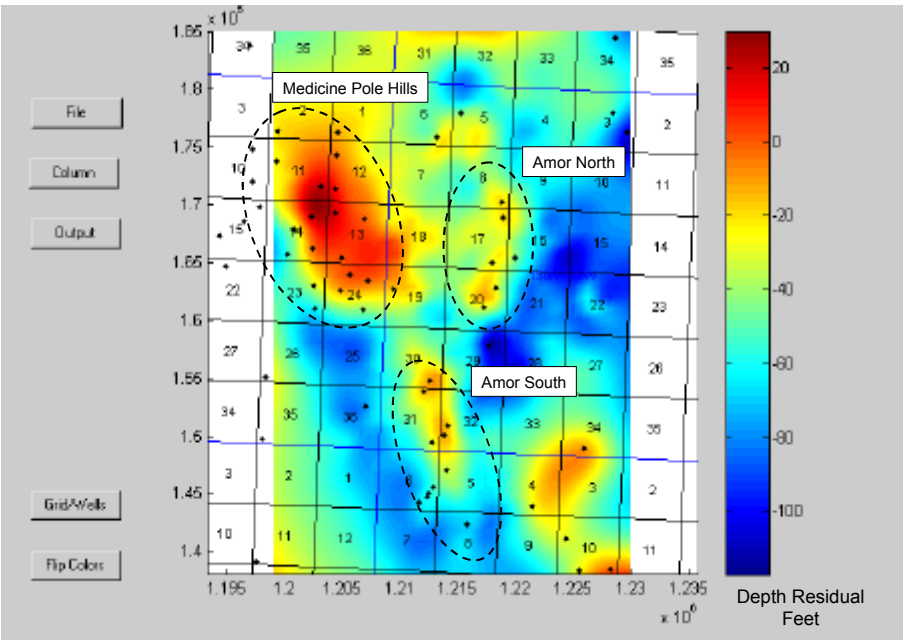

Figure 4-2. Map of residual from the regional structural trend for the Red River Formation at Amor North Field.

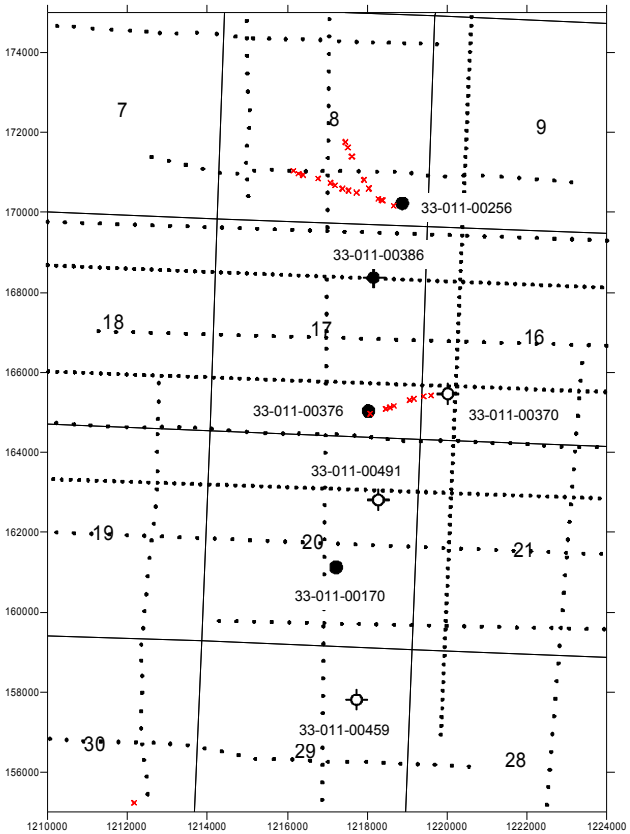

Figure 4-3. Map of well locations and 2D seismic grid at Amor North.

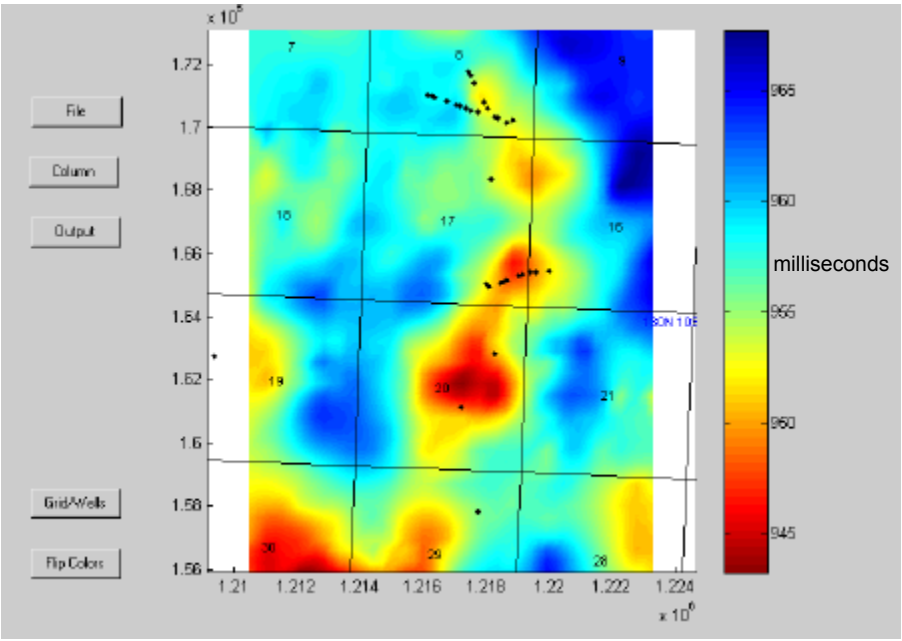

Figure 4-4. Map of seismic interval time for Niobrara – Red River.

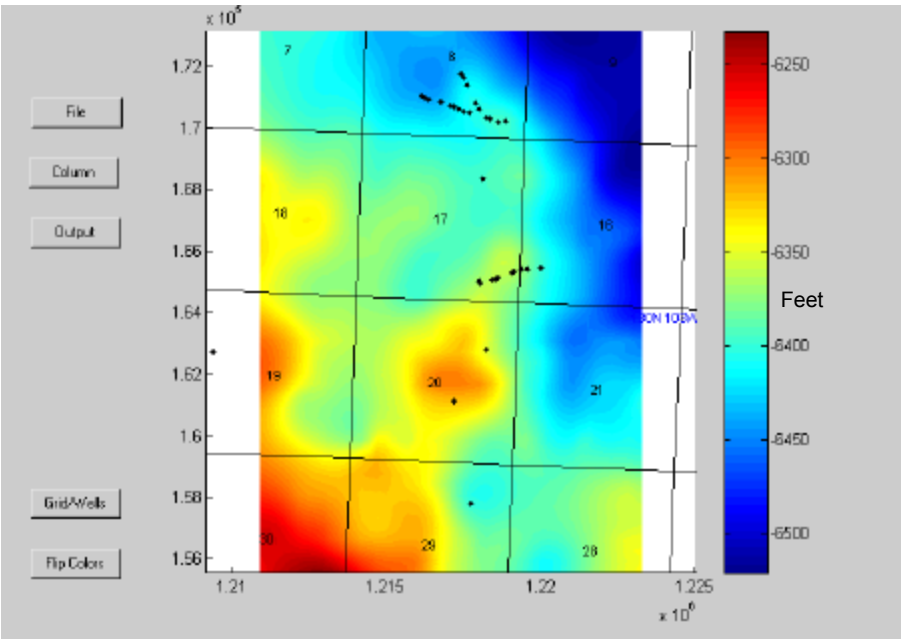

Figure 4-5. Map of computed Red River depth from seismic time and well data.

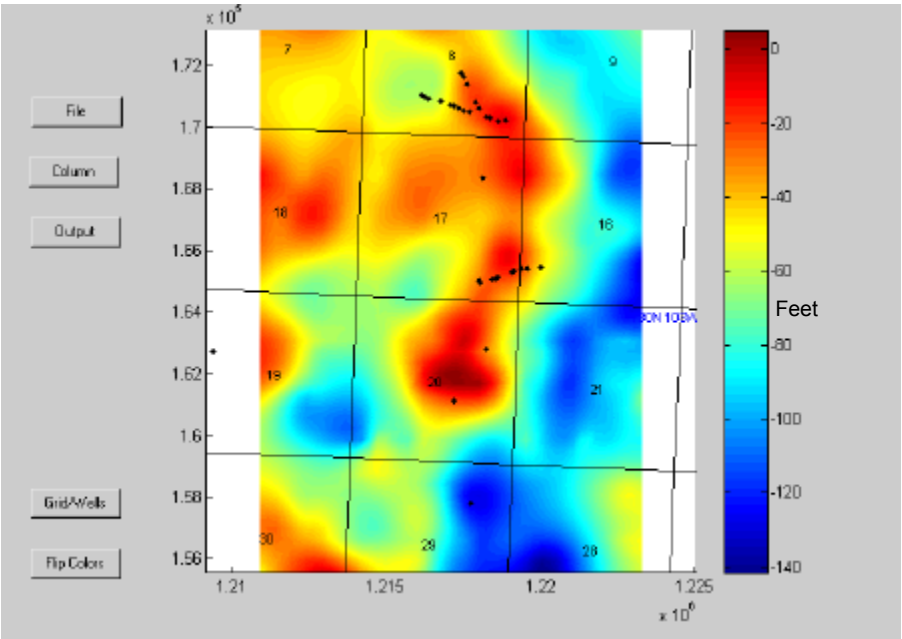

Figure 4-6. Map of regional-trend residual of Red River depth structure.

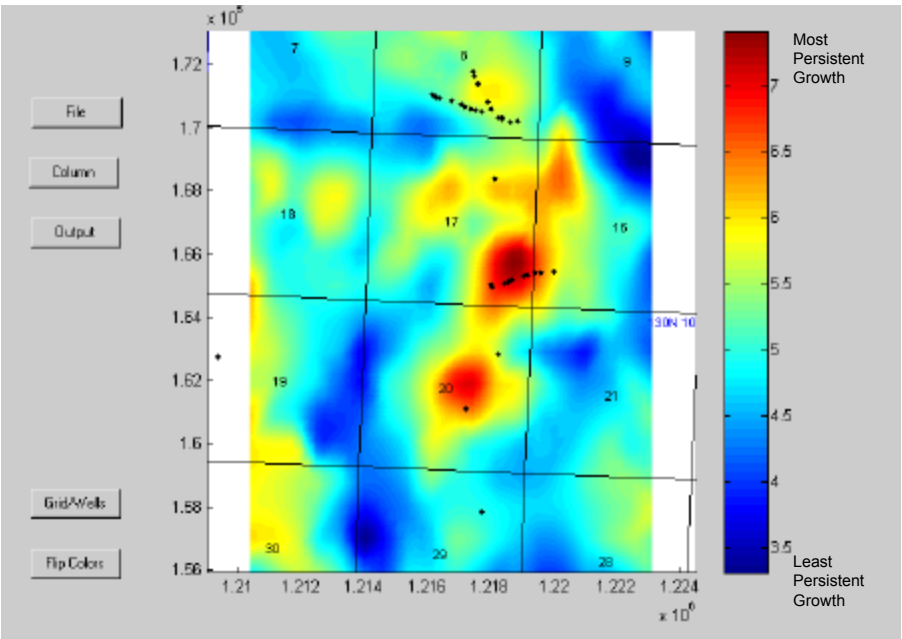

Figure 4-7. Map of structural growth index from seismic interval times.

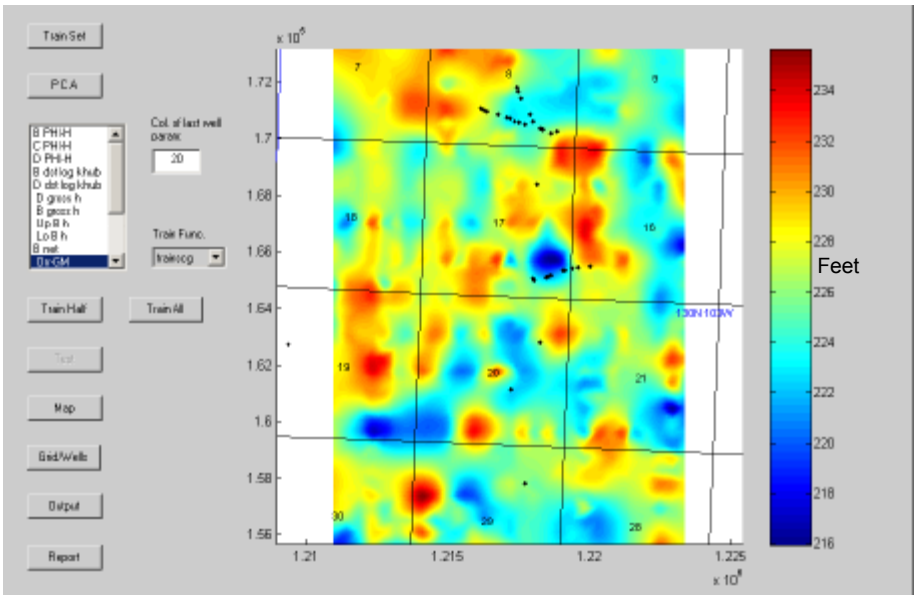

Figure 4-8. Map of the upper Red River thickness produced by the ICS Neural Solver from gridded 2D Red River seismic attributes and trained by external well-log and seismic data from six 3D seismic surveys.

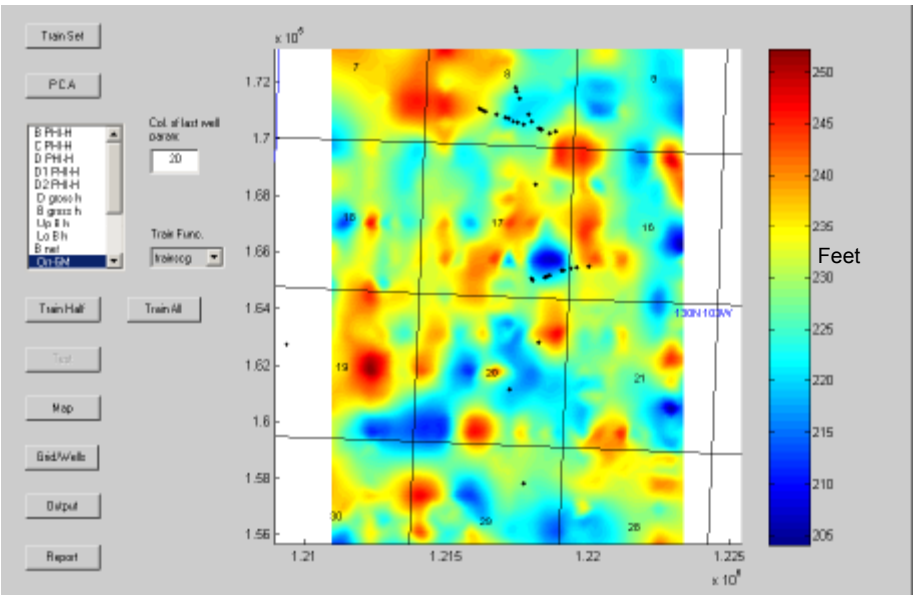

Figure 4-9. Map of upper Red River thickness produced by the ICS Neural Solver from gridded 2D Red River seismic attributes and trained by well-log data from seven local wells

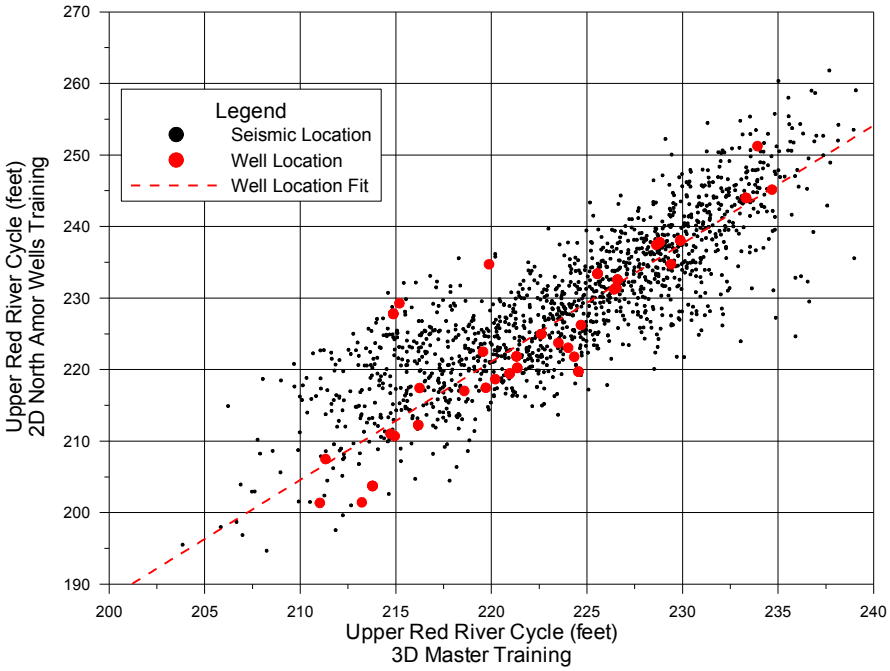

Figure 4-10. Graph compares predicted thickness of the upper Red River at Amor South Red River Unit based on ICS Neural Solver results using the master 3D seismic training file and the Amor North 2D seismic training file.

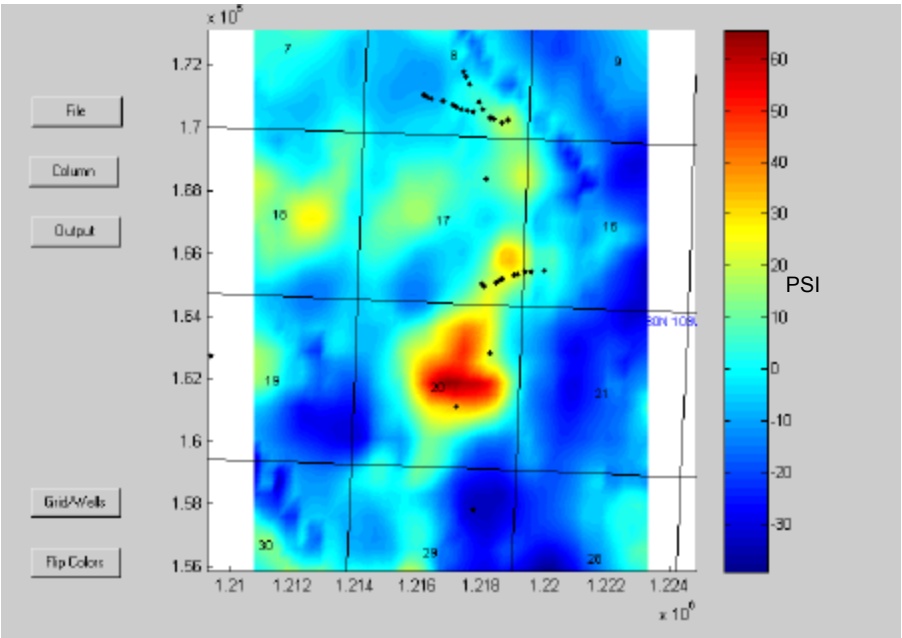

Figure 4-11. Map of Entrapment Index produced by the ICS Entrapment Tool for Amor North Field.

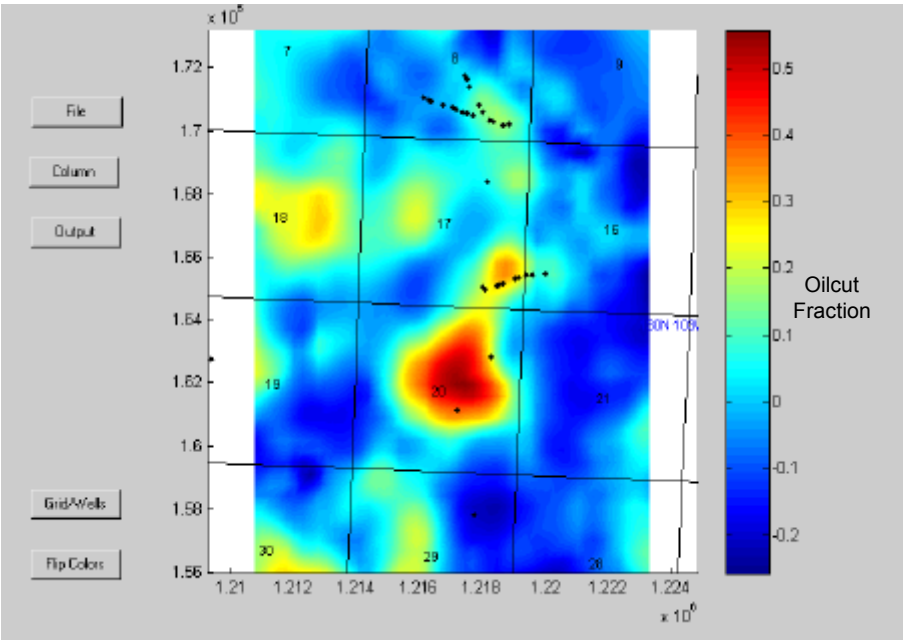

Figure 4-12. Map of initial oilcut for the Red River D Zone predicted directly by the ICS Neural Solver.

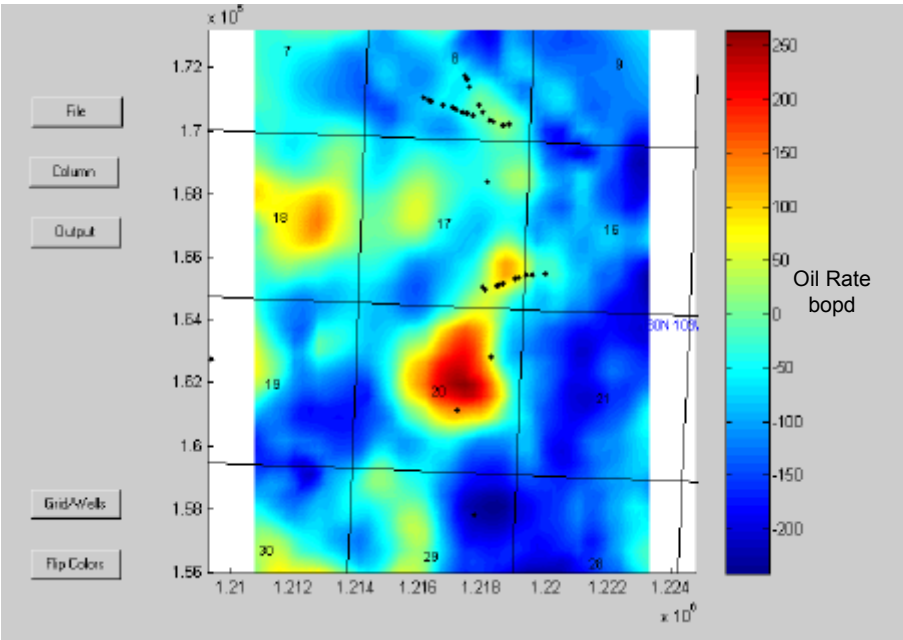

Figure 4-13. Map of initial oil rate for the Red River D Zone predicted directly by the ICS Neural Solver.

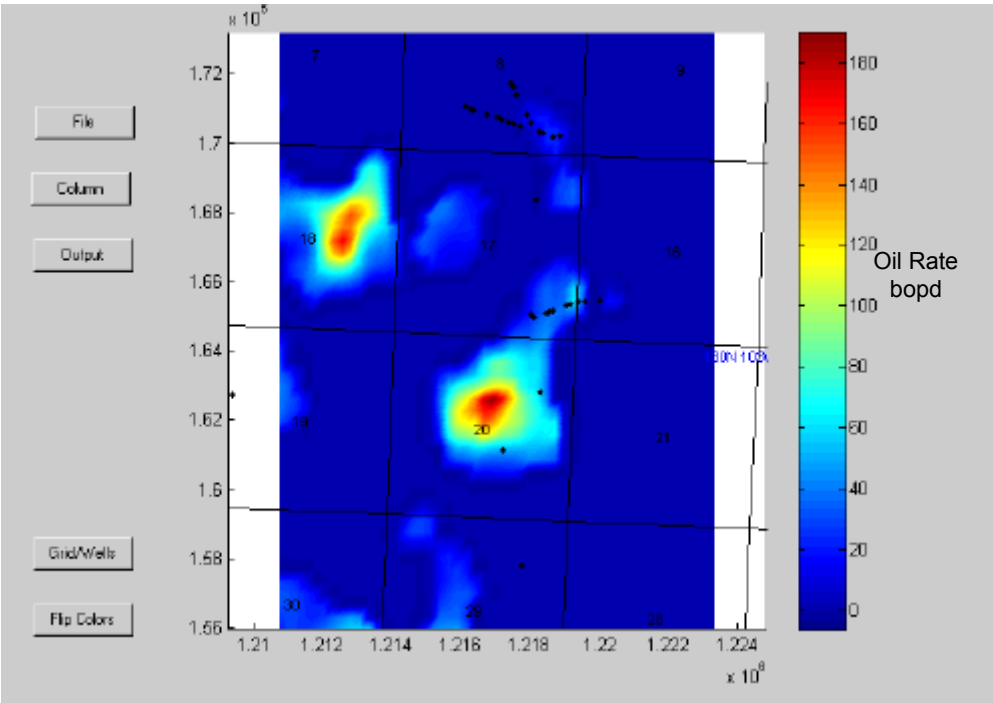

Figure 4-14. Map of initial oil rate for the Red River D Zone calculated from transforms of oilcut and drill-stem test productivity predicted directly by the ICS Neural Solver.

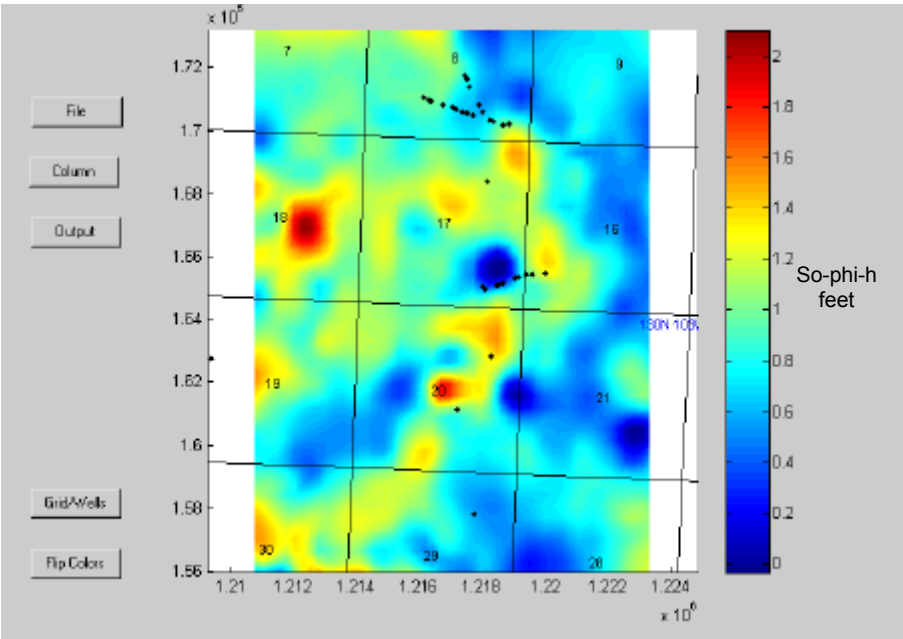

Figure 4-15. Map of hydrocarbon pore volume for the Red River D Zone calculated from transforms of oilcut and phi-h predicted directly by the ICS Neural Solver.

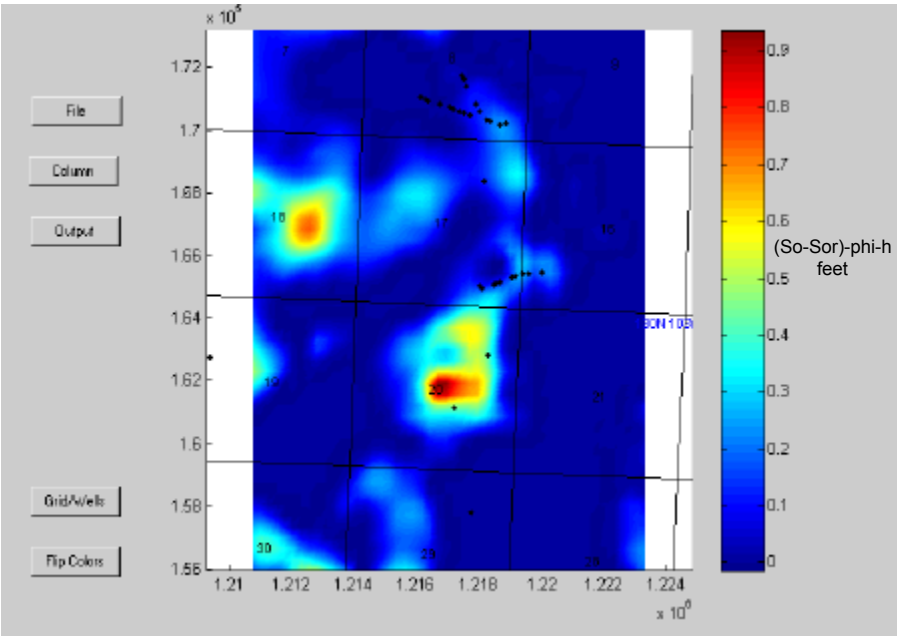

Figure 4-16. Map of mobile hydrocarbon pore volume for the Red River D Zone calculated from transforms of oilcut and phi-h predicted directly by the ICS Neural Solver.

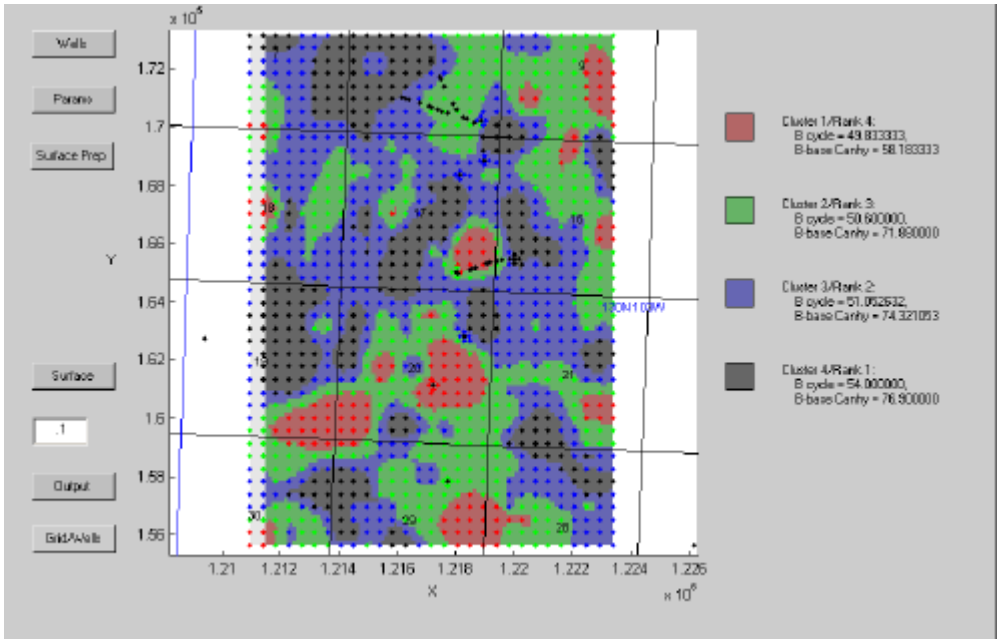

Figure 4-17. Map of the Red River B Cycle thickness produced from the ICS Cluster Tool.

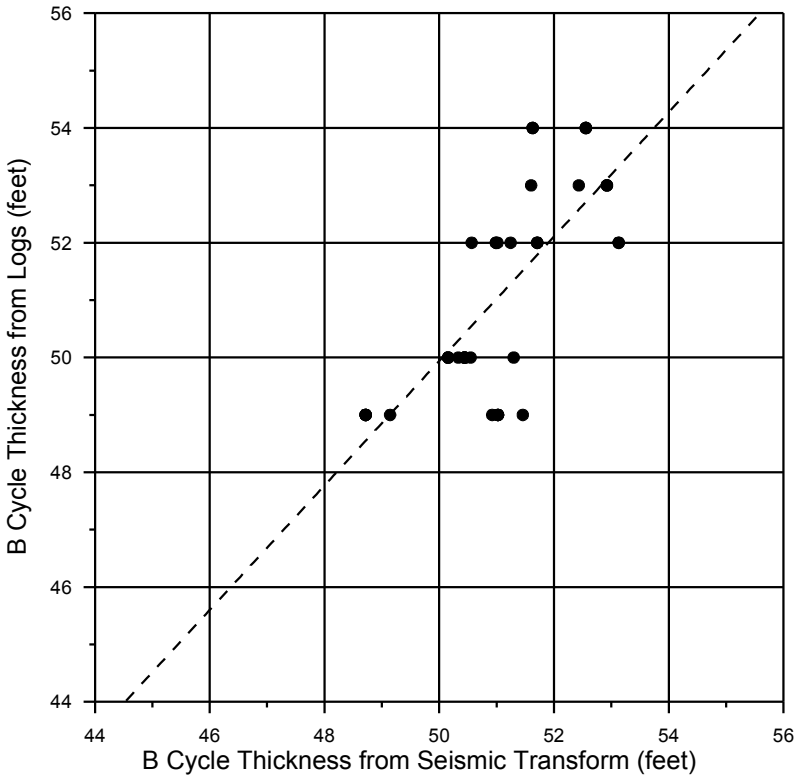

Figure 4-18. Graph of predicted B Cycle thickness from seismic attributes and measured B Cycle thickness from well logs.

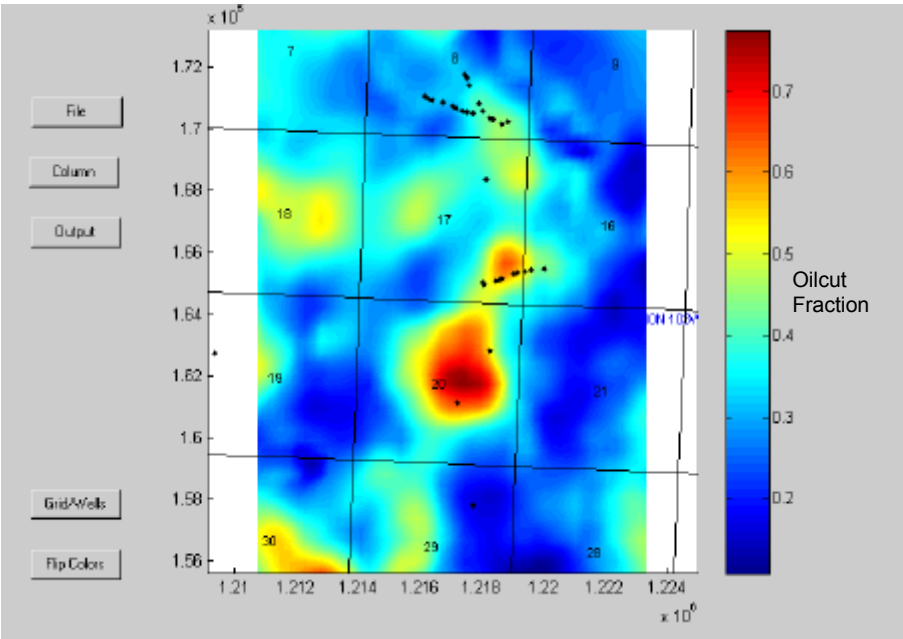

Figure 4-19. Map of predicted initial oilcut for the Red River B Zone.

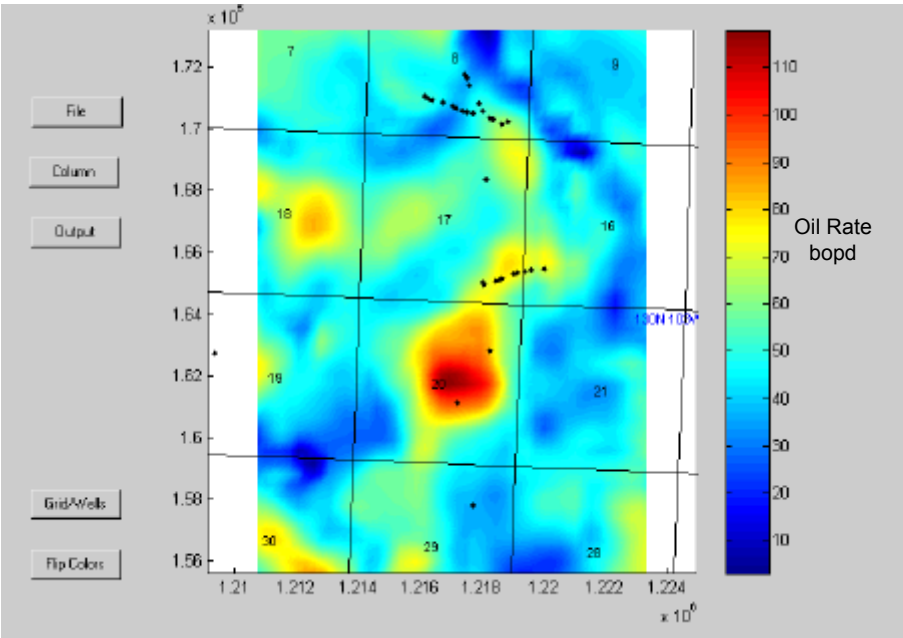

Figure 4-20. Map of predicted initial oil rate for the Red River B Zone.

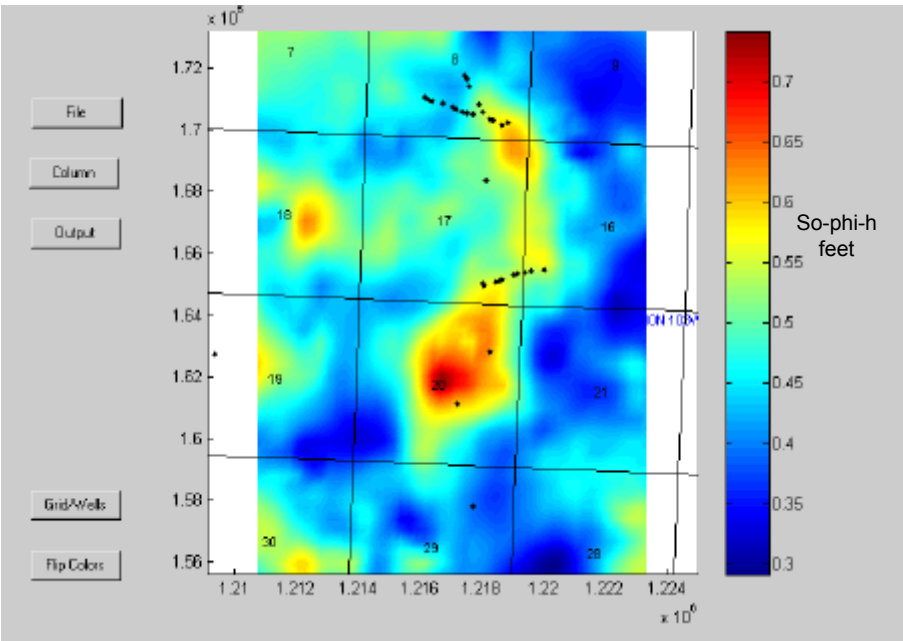

Figure 4-21. Map of hydrocarbon pore volume for the Red River B Zone calculated from transforms of oilcut and phi-h predicted directly by the ICS Neural Solver.

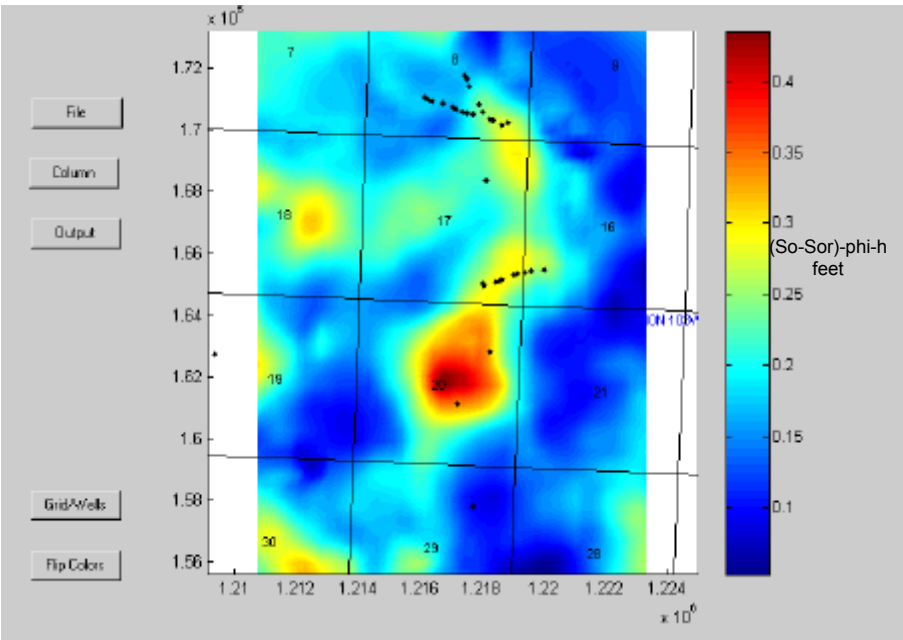

Figure 4-22. Map of mobile hydrocarbon pore volume for the Red River B Zone calculated from transforms of oilcut and phi-h predicted directly by the ICS Neural Solver.

Reservoir Characterization at East Harding Springs Area

The East Harding Springs area in Harding County, South Dakota was characterized with ICS tools and strategy using a mix of 2D and 3D seismic data. A large shelf, covering more than 6 square miles, was identified as probably containing a continuous oil reservoir in the Red River B Zone. Horizontal re-entry laterals were drilled from marginal producers and plugged wells that established peak oil rates that averaged 147 bopd per well. Reservoir characterizations from ICS used in part for establishing parameters and development plan for a waterflood project. From the initial phase of development at East Harding Springs Red River Unit, the expected additional primary and secondary oil reserves are 1,280,000 bbl.

Historical Background

East Harding Springs area is located in townships T22N-R6E and T23N-R6E, Harding County, South Dakota. The area includes regulatory field names of East Harding Springs, Pete's Creek and Corey Butte. Exploration began in 1975 with the drilling of well API 40-063-20084 that was completed in the Red River B, C and D Zones. Exploration was based on interpretation of Red River structure from 2D seismic lines. Initially, the Red River B Zone was not considered a primary reservoir target as exploration was focussed on the Red River D Zone at high-relief structures. Drill-stem tests of the Red River B Zone recovered oil at low flow rates, but with a high oilcut. At the East Harding Springs area, average oil recovery from wells completed vertically in the Red River D Zone is about 130,000 bbl per well. At the East Harding Springs Unit, the expected incremental primary and secondary oil from the Red River B Zone averages 256,000 bbl per well over 5 horizontal wells (3 producers and 2 injectors). At the time that the unit was formed, cumulative oil produced was 447,000 bbl. Pre-activity ultimate recovery is extrapolated to be 655,000 bbl.

Red River B Zone Characterization

A mix of 2D seismic lines and a 3D seismic survey were used at the East Harding Springs area for characterization of the Red River B Zone. The methodology used is the same as described for Amor South and Amor North fields. A map of predicted initial oilcut for the Red River B Zone is shown in **Figure 5-1**. The map predicts a broad area of B Zone reservoir development on a north-plunging structural platform that exhibits a relatively steep-dipping east flank. Reservoir limits for the waterflood unit were primarily defined from this map. Constructions of total and mobile hydrocarbon pore volume were used in reservoir simulation models and equity-allocation parameters for the project.

Production Results

A total of five wells were re-drilled horizontally in the Red River B Zone at the East Harding Springs-Corey Butte area. One well (API 40-063-20526) was re-drilled horizontally in 2000 before the acquisition of 3D seismic and integration with a 2D seismic grid for characterization studies with ICS. Subsequent to reservoir delineation from studies with ICS and new seismic data, four wells were re-drilled (three were not producing as uneconomic). A composite graph of total oil production with time from five wells in the East Harding Springs-Corey Butte area these wells is shown in **Figure 5-2**. A complementary graph for the same wells of oil rate with cumulative oil is shown in **Figure 5-3**. A dashed lined on both graphs indicate the timing for results of re-entry horizontal laterals from three wells after characterization studies with ICS tools and methodology (API 40-063-20084, 40-063-20141 and 40-063-20145). Well API 40-063-20084 is located one mile east from the map shown in **Figure 5-1**. From these graphs it can be seen that there was a five-fold increase in production from about 2000 bbl per month to over 10,000 bbl per month. A better representation of potential reserves from better reservoir characterization and horizontal drilling in the Red River B Zone is shown in **Figure 5-4**. The graph in **Figure 5-4** shows normalized production from five vertical completions at original reservoir pressure. Normalizing consists of starting production from all wells at the same time and calculating the average. The normalized peak rate from the vertical completions is slightly less than 2000 bbl per month per well. Combined ultimate recovery for the vertical completions is near 500,000 bbl at an economic limit of about 300 bbl per month. Also shown on the graph are normalized production rates from the first four re-entry laterals in the Red River B Zone. These four re-entry wells are from the original five vertical wells. The average peak rate from the re-entry lateral completions is slightly greater than 4000 bbl per month per well. This is a two-fold increase over the initial average rate from the vertical completions. Comparing average results with rates just prior to the re-entry lateral drilling indicates that a ten-fold increase was achieved (400 to 4000 bbl per month per well). In July 2003, the fifth well (API 40-063-20474) was re-drilled with laterals in the Red River B Zone and has averaged 3300 bbl per month for two months.

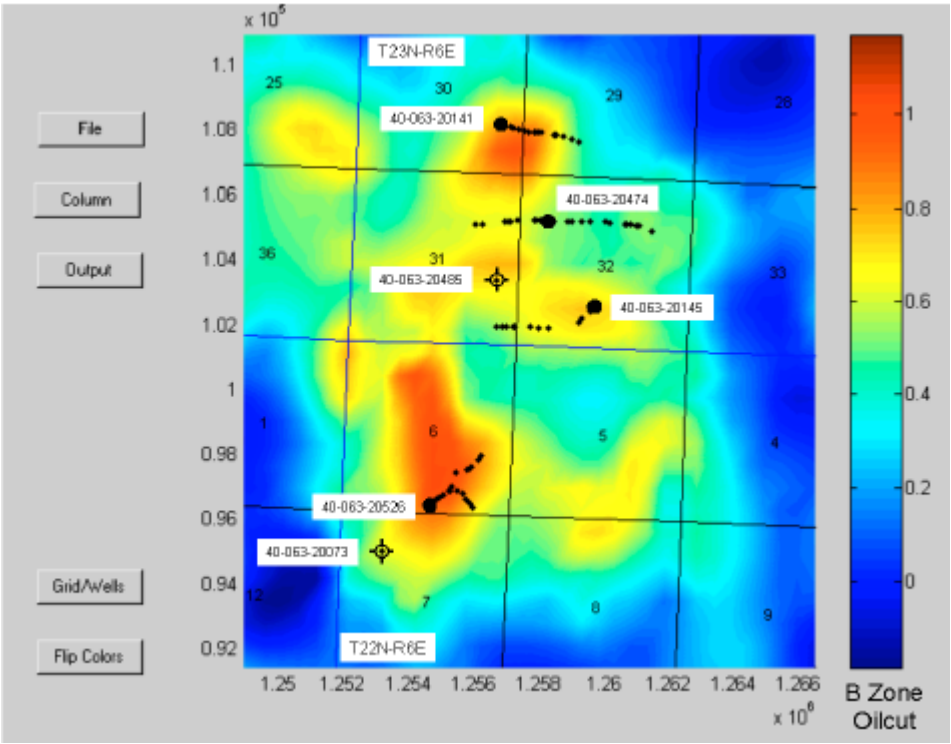

Figure 5-1. Map of predicted initial oilcut for the Red River B Zone at East Harding Springs Red River Unit.

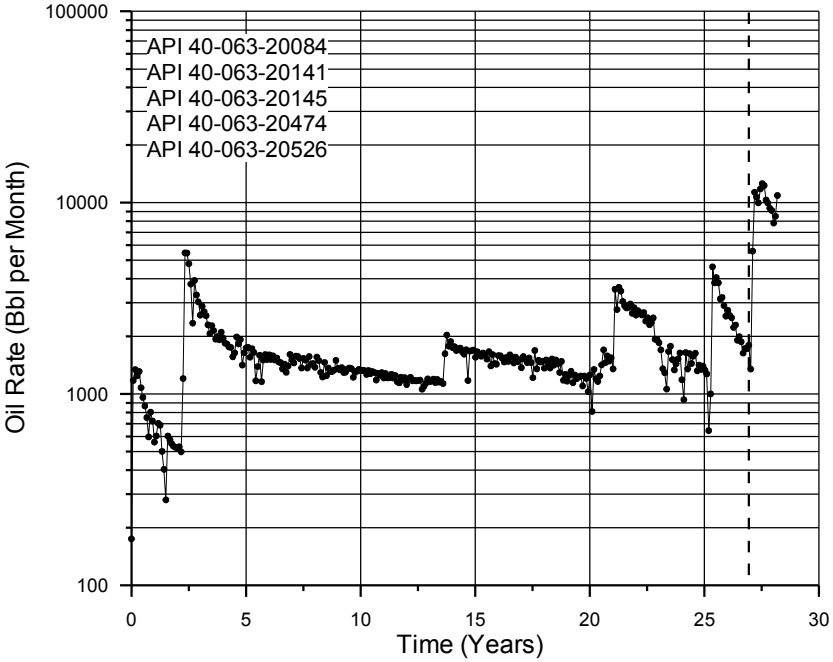

Figure 5-2. Graph of monthly oil rate with time for 5 wells at the East Harding Springs area, Harding County, South Dakota. The dashed time line references results after ICS characterizations.

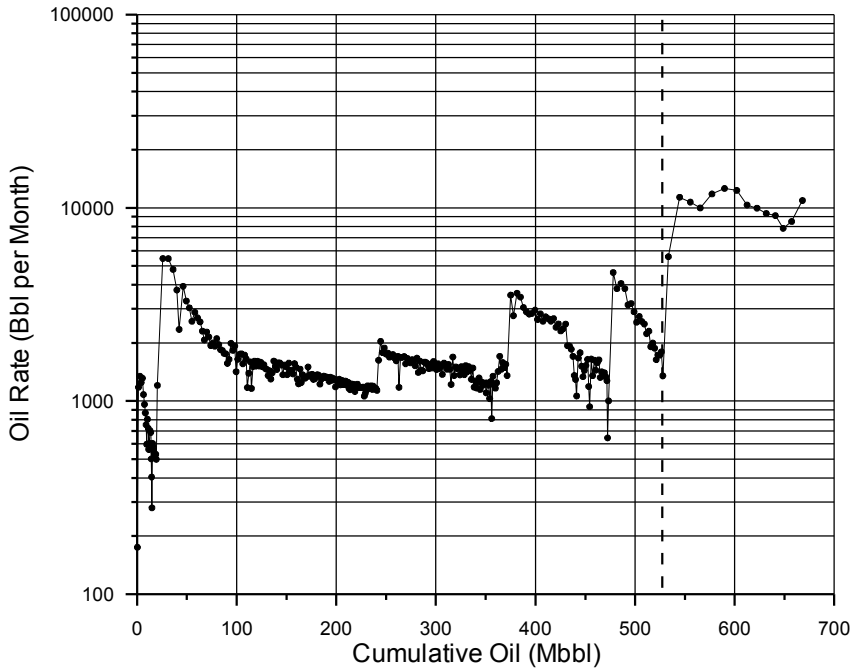

Figure 5-3. Graph of monthly oil rate with cumulative oil for 5 wells at the East Harding Springs area, Harding County, South Dakota. The dashed time line references results after ICS characterizations.

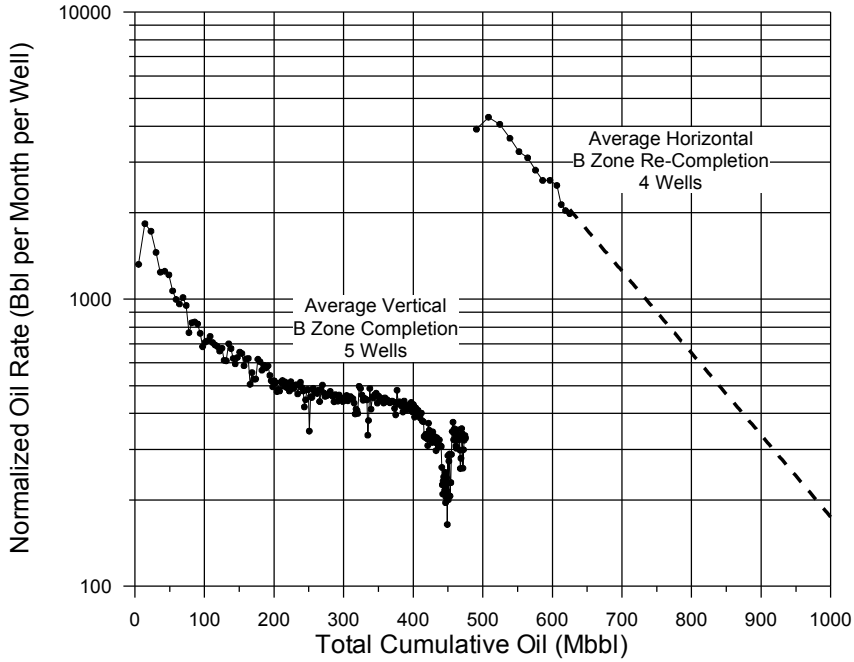

Figure 5-4. Graph of normalized average monthly oil rate at the East Harding Springs area for vertical and horizontal completions in the Red River B Zone.

Geologic Rock-Typing, Red River B Zone

Luff Exploration Company (LEC) has completed a study of core collected from the Red River B zone in of Bowman County, North Dakota and Harding County, South Dakota. The study area is located on the southwestern flank of the Williston Basin in southwestern North Dakota and northwestern South Dakota (**Figure 6-1**). The Red River formation in the area is located at a depth below ground surface of approximately 8500 to 9500 feet, and it conformably overlays the lower Ordovician Winnipeg shale. The Ordovician Red River formation in Bowman and Harding counties is a thick sequence of marine carbonate rock that range from 525 to 600 feet in thickness. The upper 260-foot section of the Red River formation often exhibits four distinct zones of porosity that are known to trap commercial quantities of oil through a combination of structural and stratigraphic means at various locations in the basin. The zones of porosity are generally dolomitic mudstones, wackestones, packstones, and grainstones that are facies members of at least three sequential cycles of a shallowing upward, restricted-marine depositional sequence. The three cycles of deposition are labeled C through A in ascending order (**Figure 6-2**). The D porosity zone, which is the lower most zone of porosity in the upper Red River formation, is often referred to as the burrowed porosity member of the Red River C depositional cycle. The B and C cycles are capped with a deposit of evaporite (anhydrite). An anhydrite cap is not present at the top of the A cycle in Bowman and Harding counties. A dark gray, calcareous shale of the upper Ordovician Stony Mountain formation overlies the Red River formation.

Recent exploitation and development success of oil reserves in the Red River B dolomite with the use of horizontal drilling techniques has helped stimulate enthusiasm by LEC for a study of B zone depositional environments from core in Bowman and Harding counties. The objective of the study was to provide a technical framework for development of a depositional model for the Red River B zone that can be used by LEC's technical team to identify and better understand reservoir geometry, and areas favorable for reservoir development. The core was acquired at six well locations and totals approximately 200 feet in length. The core intervals used in the study were limited to portions of the Red River B and lower A cycles. The six well locations in which core were available for use by LEC are identified below, and on **Figure 6-1**.

E. Fossum 1-24, NWNE Section 24, T130N, R104W; Medicine Pole Hills Field;
Schaaf 1-6, SESE Section 6, T129N, R103W, Amor Field;
Muslow B-27 State, NWNE Section 27, T130N, R102W, Cold Turkey Creek Field;
Hansen J-31, NWSE Section 31, T130N, R101W, Grand River Field;
Abrahamson D-8, NWNW Section 8, T129N, R101W, Grand River Field;
Abrahamson J-12, NWSE Section 12, T129N, R102W, Grand River Field.

K. Lyn Canter, a senior research geologist at Applied Geoscience, Inc. provided a detailed stratigraphic analysis of the core and an interpretation of facies boundaries (Appendix A). Standard core analysis was conducted by Core Lab. K. Lyn Canter compiled lithologic and facies data from each core onto lithologic strip-logs. The lithologic and facies data have been used by Luff Exploration Company to develop a depositional model for the Red River B zone in Bowman and Harding counties. The model is used by Luff Exploration Company to identify favorable areas for Red River B zone reservoir development for exploitation and development drilling. It is thought by LEC and others that primary rock fabric may be an important control on the distribution of primary and secondary porosity in reservoirs of the Red River B dolomite in Bowman and Harding counties (Canter 2002).

Red River B Zone Lithology and Facies Identification

The primary depositional facies identified in ascending order from core of the Red River B zone in the Bowman and Harding county area include the following:

B burrowed (non-reservoir) member– a nodular to burrowed, skeletal-rich lime, wackestone and packstone that may have been deposited in a low-energy, open-marine environment;

B burrowed to laminated transitional (marginal reservoir) member – a dolomitic microporous mudstone, packstone, and wackestone with Planolites that are indicative of a restricted lagoonal depositional setting (lower B dolomite member);

B laminated (reservoir) member – consists of a lower layer that is primarily a porous and permeable peloidal dolomite packstone and grainstone. Rippled to planar, laminated beds are indicative of deposition in a moderately low-energy, grain flat environment. A dolomitic grainstone and boundstone dominate the upper layer. The layer is indicative of an algal flat depositional setting in an intertidal to supratidal depositional environment (both layers constitute the upper B dolomite member);

Anhydritic laminated (marginal reservoir) member – consists of a laminated dolomitic mudstone that is indicative of a hypersaline lagoon/shelf depositional facies (upper B dolomite member);

Bedded anhydrite (non-reservoir) – nodular white-gray, anhydrite grading to bedded anhydrite. The anhydrite member of the B zone may have been deposited in an evaporative shelf/lagoonal, supratidal setting in a chemically restricted depositional condition.

Three of the five rock facies identified for the Red River B zone pertain to variations in rock fabric and reservoir development of the B dolomite. The B dolomite in the study area is a significant reservoir due to its capacity to trap and

store large quantities of oil over relatively broad areas. The B dolomite ranges in thickness in the study area from approximately 3 feet to 17 feet. In most areas, a layer of anhydrite is found overlying the B dolomite. The B dolomite is divided into a minimum of two units. A third, middle unit of siliceous dolomite or chert is recognized from field observations of drill cuttings at horizontal wells in Bowman and Harding counties (Quinn 2002, 2003). The upper layer is dominantly a grain-supported dolomitic grainstone with good reservoir properties. The lower layer is a muddy, argillaceous dolomite of lagoonal origin. The difference in reservoir properties in the two layers is directly related to primary depositional facies and early diagenesis. Differences in secondary rock fabric may be a function of variations in rates of deposition and depositional energy of the two zones. It is thought by LEC that subtle variations in water depth has influenced significant differences in the depositional and chemical environment that has directly influenced differences in the primary rock fabric of the two layers. The middle member of siliceous dolomite (chert) appears to be discontinuous, but at the same time, forms a contact or boundary between the upper and lower members of the B dolomite. The chert layer of the B dolomite may represent a geologic time-boundary that records a significant change in the physical and chemical depositional environment for the B dolomite. The source of silica for the middle member can only be speculated or hypothesized. Silica may have derived from deposition of siliceous remains of biological organisms (i.e., radiolaria), that have the ability to remove silica from water, to form a siliceous ooze. This scenario is thought to be unlikely since the cherty layer is sandwiched between shallow subtidal and intertidal deposits, requiring drastic and extremely brief fluctuation in sea level to deposit deep-water sediments in this stratigraphic position). Alternatively, it may have been derived from an inorganic sources such as a deposit of volcanic ash resulting from volcanic activity upwind of the basin, or other windblown detrital siliciclastic sediment. Overlying the Red River B zone is a open-water marine, skeletal-rich, lime wackestone and packstone that represents the maximum flooding surface (mfs) for the burrowed facies member of the A cycle (**Figure 6-3**).

Red River B Zone Depositional Model

The Red River B zone is a shallowing upward sequence of restricted, marine sedimentation. In the study area, the Red River B cycle (top B anhydrite to top C anhydrite) ranges from a minimum thickness of 39 feet at the Dworshak 1-19, section 19, T23N, R6E, to maximum thickness of 58 feet at the Fossum 1-19, section 19, T130N, R103W. On a regional scale, the B cycle thickens in a northwest direction and gradually thins in a southeast direction in the study area (**Figure 6-4**). Isopach data for the Red River B zone suggests the paleo-shoreline direction during B zone deposition was located southeast of the study area and slightly deeper water conditions may have prevailed to the northwest. A trend surface map of regional B zone isopach data shows more clearly the hypothetical basinward and shoreline directions (**Figure 6-5**). Trend surface maps of regional isopach data for the B dolomite and B anhydrite suggest

thinning of the B dolomite and slight thickening of the overlying B anhydrite occurs at the east margin of the study area (**Figures 6-6** and **6-7**). A comparison of isopach values at wells for the B cycle with thickness of the B dolomite suggest paleotopography has influenced the depositional rate of carbonate mud forming the B dolomite. Areas demonstrating relatively thin B cycle thickness exhibit a relatively thin layer of B dolomite. In contrast, areas represented by thickening of the B cycle exhibit a relatively thick layer of B dolomite.

A conceptual model of Red River B zone deposition in a shallowing upward, restricted marine setting is shown on **Figures 6-8** and **6-9**. The start of B zone deposition occurred when a land barrier, which caused restricted marine conditions to prevail during the latter stages of deposition of the Red River C zone, was removed or breached, and an open-water, normal marine depositional environment prevailed (Canter et al., 1998). Water depth in the study area reached a maximum level (40 to 60 feet), and a gray, skeletal-rich, lime wackestone and mudstone was deposited. Eventually, the basin was cut off from its marine source by rejuvenation of a barrier, and restrictive marine conditions developed. As sedimentation continued under restrictive conditions, water depth decreased and water salinity increased to form a shallowing upward, restricted marine, carbonate rock sequence. By the time deposition of carbonate sediment representing the lower B dolomite occurred, water depth might have decreased to less than 10 feet. As water depth continued to decrease in a restricted marine setting, sea-floor topography may have increasingly imposed its influence on the distribution of grain-size in carbonate mud being deposited for the B dolomite. Topographically high regions of the seafloor may have favored deposition of more dominantly grain supported carbonate particles due to a winnowing of fines by a slightly higher depositional energy base in an intertidal setting (Canter, 1998 and Canter et al., 2001). Fines may have deposited in the low-lying regions forming a more dominant area of argillaceous carbonate mud in a low-energy, lagoonal or subtidal depositional setting. Thus, deposition of grain-supported carbonate bed may have occurred in topographically high areas, and clay-dominated carbonate mud may have dominated deposition in topographically low-lying areas, where low-energy hypersaline ponds existed (**Figure 6-9**). Therefore, good reservoir properties in the B dolomite with relatively large grain and pore throat size are predicted by the model to occur on the flanks and near the crestal portions of paleo-topographically high areas. In contrast, poor reservoir conditions are thought to be favored in low-lying areas, where argillaceous carbonate mud dominated B dolomite deposition.

As proposed by Carroll (1977), and others, areas of extremely high topographic elevation during Red River B zone deposition may have experienced more sustained evaporative, and evaporative-reflux conditions during deposition of carbonate mud of the B dolomite. These areas are thought to have experienced relatively low depositional rates for carbonate mud that form the B dolomite. Thus, in extremely high topographic areas, the conceptual model predicts that

thin and relatively poor reservoir conditions may prevail in the B dolomite due to plugging of pore-space with anhydrite nodules and cement.

Near the end of the Red River B cycle, hypersaline water conditions prevailed and periodic recharge of marine water to the restricted basin may have occurred, indicating the onset of the next marine transgression. The rate of recharge of marine water may have closely equaled the rate of evaporation, allowing a continuous source of hypersaline water for continued precipitation of anhydrite (Canter, 1998 and Canter et al., 1998). As anhydrite precipitated from the brine, the Mg/Ca ratio of the brine may have increased slightly such that the brine solution became chemically favorable for dolomitization. Thus, the hypersaline brine may have served as a dolomitizing solution for carbonate deposits of the B dolomite during at least early-stage deposition of the B anhydrite. Alteration of carbonate matrix and allochems to dolomite has enhanced porosity and permeability in the middle and lower segment of the upper layer of the B dolomite. However, precipitation of anhydrite cement in uppermost, bedded layers of the B dolomite have significantly occluded pores and diminished reservoir permeability. At this juncture in the depositional cycle of the B zone, a change from a dominantly regressive marine depositional system to a slightly transgressive system likely occurred. Non-deposition and possibly erosion of the anhydrite due to local subaerial exposure may have occurred in areas of extremely high elevation. The B cycle ended when the continental barrier restricting the basin from its marine source was compromised and the area was again flooded with normal marine seawater. Open-marine conditions once more prevailed in the basin, marking a new maximum flooding surface for the Red River A cycle (Canter et al., 1998).

Using the model above, areas exhibiting significant thinning in the C anhydrite, which is directly overlain by deposition of the B cycle, may represent locations of subaerial exposure on paleo-topographic highs present at the end of Red River C and beginning of Red River B depositional time. In most instances, the paleo-topographic highs present at the end of Red River C time may have persisted during deposition of the Red River B zone cycle. In these areas, a predictive sequence of reservoir development in the B dolomite would be expected, grading from a poorly developed and relatively thin anhydritic dolomite near the crest of the paleo-structure, to a well developed, dolomitic grainstone in the higher flank area of the feature, and a poorly developed argillaceous dolomite in the low-lying lagoonal pond area.

Application of Depositional Model

An isopach of the Red River B cycle thickness has been developed from well control on both a regional and a field-scale basis for three field areas in the study. The field areas include the South Amor, Cold Turkey Creek and Grand River fields (**Figures 6-10, 6-11** and **6-12**). These fields were selected because each one contains a Red River B zone core that has been included in the LEC

study, and 3D seismic data. Isopach maps of Red River B cycle thickness that are based on transformation of seismic attributes are presented on **Figures 6-13**, **6-14** and **6-15**.

Isopach data and maps are used by LEC to re-construct a postulated topographic expression of the sea floor during Red River B zone deposition. Areas of a relatively thick B zone interval (greater than 50 feet) are thought to represent topographically low-lying areas, and relatively thin areas (<50 feet) are thought to define relatively high areas of sea-floor elevation during Red river B zone deposition. It is postulated by LEC that variation in sea-floor elevation during Red River B zone deposition may have influenced rates of deposition, the overall distribution of grain-size in carbonate sediment, and the resulting primary facies deposited.

In addition, paleo-topography may have influenced important reservoir parameters such as storage (porosity-feet) and transmissivity (permeability-feet) for the Red River B dolomite. Results of a statistical evaluation of regional isopach data for the B zone cycle and measured reservoir parameters for the B dolomite suggest reservoir storage and transmissivity increase with increasing cycle thickness (**Figure 6-16**). The data suggest that an optimum topographic setting may have existed in Bowman and Harding counties for deposition of the B dolomite that is marked by an intermediate cycle thickness range (i.e., 46 to 50 feet). It is thought that this intermediate cycle thickness may qualitatively define areas of optimum conditions of water depth, water chemistry, depositional rate, and depositional energy for deposit of a relatively thick (i.e., 3 to 4 feet), grain-supported carbonate facies in the upper B dolomite (grain flat to algal flat facies). Conditions in the defined area may also have been optimal for percolation and efficient interaction of dolomitizing solution with the carbonate sediment of the B dolomite. There is a difference in the original permeability of the sediment types as well. Grainstones and grain-dominated packstones (grain-flat deposits) contain an abundance of well-connected interparticle pores that readily function as a preferred pathway for dolomitizing fluids. Algal boundstones typically contain fenestral pores (after gas bubbles that form as the organism decays) and layers of grainstone deposited during storm surges (containing interparticle pores). This facies is also characterized by good original porosity and permeability. Both can be thought of as aquifers for dolomitizing fluids. Underlying these permeable facies are the denser/more impermeable and more heterogeneous deposits of the muddy lagoon/shelf facies (the aquitard, Canter et al., 1998).

Finally, modeling of 3D seismic data at high amplitude (~70 hertz) has shown that as porosity-feet in the B dolomite is developed and continues to increase, a “doublet” (P1a and P1b) is formed at the Red River P1 seismic reflector. In a given area, as Red River B zone phi-h increases, the difference in amplitude of the two horizons (P1b minus P1a) also increases (**Figure 6-17**). From results of seismic modeling, LEC has re-processed existing 3D seismic data at high

frequency in three field areas located in Bowman County, North Dakota. The areas of interest include the Amor, Grand River and Cold Turkey Creek Fields. A map of seismic amplitude, P1b minus P1a, has been derived from the seismic data in each area (**Figures 6-18**, **6-19** and **6-20**). The results are used to help delineate or refine model predicted facies boundaries for the B dolomite in areas where well control is sparse or non-existent. For instance, areas of moderate to high seismic amplitude are inferred as areas of relatively high phi-h that is representative of a laminated grain flat/algal flat depositional setting, and in some instances, a transitional laminated lagoonal facies (depending on the correlation with B cycle thickness map). Areas of relatively low seismic amplitude are thought to be indicative of an anhydritic laminated facies in a high, supratidal depositional setting. Thus, high frequency seismic amplitude at the Red River P1 horizon from 3D seismic data have also been used by LEC to help delineate facies boundaries for the B dolomite in three field areas in Bowman County, North Dakota.

Facies boundaries identified for the Red River B zone from a study of core have been extrapolated to open-hole logs at core wells, and nearby control wells. Using facies boundaries extrapolated to nearby well control, isopach data for the Red River B zone cycle measured at wells, and variations in high frequency seismic amplitude recorded for 3D seismic data at horizons representing the top of the Red River formation, a facies map for the Red River B dolomite has been interpreted for each field area. Facies maps on **Figures 6-21** through **6-23** were derived from transformation of seismic attributes from 3D data using intelligent computing software (ICS). Facies maps for the B dolomite on **Figures 6-24** through **6-26** were derived from geologic data from regional well control.

Amor South Field

Two facies maps for the Red River B dolomite at the Amor South Field are presented on **Figures 6-21** and **6-24**. Red River B zone core at South Amor was acquired by Tenneco at the Schaaf 1-6, NESE Section 6, T129N, R103W. Core and log measurements suggest the B dolomite at the Schaaf is approximately 7 feet thick. It consists of approximately 5 feet of argillaceous dolomite (packstone and wackestone rock fabric) of lower B dolomite, lagoonal facies, and 2 feet of a dolomitic grainstone and boundstone deposited in a grain flat and algal flat facies. A one-foot thick supratidal to hypersaline lagoonal deposit (laminated dolomitic boundstone that is anhydritic) lies at the top of the B dolomite at the Schaaf well. The B dolomite is capped with approximately one-foot of bedded anhydrite.

A facies map for the B dolomite at Amor South developed from facies boundaries correlated from the Schaaf 1-6 to surrounding well control, isopach data for the B zone cycle measured at wells, and results of seismic amplitude at the top of the Red River formation from high frequency 3D data, suggests good reservoir development is located near the crest and updip flank areas of the structural

feature (**Figure 6-24**). Reservoir facies for the B dolomite in elevated segments of the complex is generally a mixture of peloidal grain flat (grainstone) and algal flat (boundstone) rock fabric. Both facies are considered to be good to excellent reservoir. Standard core analysis from one sample in the grainstone suggest porosity and permeability in the grainstone facies is 8 percent and 13 millidarcies (Appendix B). In local segments of the crestal area of the Amor South structural trend, a relatively poor reservoir facies exists. This facies member is described as a laminated and anhydritic dolomitic boundstone. The laminated boundstone facies member is thought to occupy the highest portion of the paleo-structure at the time of Red River B zone deposition. The first well drilled on the Amor structure by LEC was the Nygaard 1-32, NWSW section 32, T130N, R103W. The Nygaard 1-32 penetrated approximately 5 feet of B dolomite that demonstrates relatively poor reservoir properties. A drill stem test of the B dolomite recovered 93 feet of oil and 443 feet of mud. Final flowing pressure measured less than 200 psi. An offset to the Nygaard 1-32 was drilled by LEC in 1980 at the Nygaard 2-32, W2SW section 32, T130N, R103W. The Nygaard 2-32 exhibits approximately 7 feet of B dolomite that is considered excellent reservoir. A drill stem test of the B dolomite recovered 2,227 feet of oil and 120 gas cut mud. Final flow pressure measured almost 700 psi. The facies member of the B dolomite at the Nygaard 2-32 is postulated to be that of a grain flat. Thickness of the B cycle at both well locations is approximately 46 feet. A capping anhydrite is absent at both locations based on open-hole log response. This information would imply that both well locations are located relatively high on a paleo-topographic feature that persisted during Red River B zone depositional time. The thickness of the C anhydrite at the Nygaard 1-32 is 15 feet, compared to 22 feet of anhydrite at the Nygaard 2-32. The isopach data for the C anhydrite imply that the location of the Nygaard 1-32 was slightly elevated to the Nygaard 2-32 during late C and early B depositional time. If the relationship persisted throughout deposition of the B cycle, then a subtle variation in elevation during the time carbonate sediment of the B dolomite was being deposited, may lend explanation for the noticeable differences in rock fabric and reservoir properties in the B dolomite at the two locations.

Lagoonal facies dominate the downdip reaches of the Amor South trend. The lagoonal facies is described as an argillaceous dolomite (packstone to wackestone rock fabric) that is dominated by fines and is characterized by relatively good porosity, small pore-throat size and poor permeability. Standard core analysis at the Schaaf 1-6 suggest reservoir properties in the lower B, lagoonal facies at Amor South range from 12 to 23 percent porosity, and <1 to 7 millidarcies of permeability.

Cold Turkey Creek Field

Two facies maps for the Red River B dolomite at the Cold Turkey Creek Field are presented on **Figures 6-22** and **6-25**. A Red River B zone core at Cold Turkey Creek was acquired by LEC at the State Muslow B-27, NWNE Section 27, T130N, R102W. Core and log measurements suggest the B dolomite at the State Muslow B-27 is approximately 7 feet thick. From bottom to top the zone consists of approximately one-half foot of argillaceous dolomite of lagoonal origin, 4 feet of dolomite (packstone and grainstone rock fabric) of the shallow higher energy grainflat facies, and 2.5 feet of upper B algal flat (boundstone) facies. Anhydrite cement is common in the uppermost laminated beds of the algal flat facies. The B dolomite at the State Muslow B-27 is capped with approximately five feet of bedded anhydrite.

A conceptual facies map for the B dolomite at Cold Turkey Creek has been constructed from facies boundaries correlated from the State Muslow B-27 to surrounding well control, isopach data for the B zone cycle measured at wells, and interpretation of seismic amplitude at the top of the Red River formation from high frequency 3D data (**Figure 6-25**). The facies interpretation suggests good reservoir development is located near the crest and updip flank areas of the structural features in the complex. Reservoir facies for the B dolomite in the updip regions of the Cold Turkey Creek complex are generally inferred as a mixture of peloidal grain flat (grainstone) and algal flat (boundstone) facies. Both facies are considered to be good to excellent reservoir. Standard core analysis suggest reservoir properties in the upper B dolomite, grainstone facies at Cold Turkey Creek Field exhibit porosity values of 20 to 25 percent and permeability of 45 millidarcies. In some local crestal locations, a relatively poor reservoir facies exists that is plugged with anhydrite cement. This facies member is described as a laminated dolomitic boundstone. The boundstone facies member is thought to represent the highest portion of paleo-structure at Cold Turkey Creek at the time of Red River B zone deposition. Lagoonal facies are inferred to dominate the downdip reach of the Cold Turkey Creek complex. The lagoonal facies is generally described as a argillaceous dolomite (burrowed wackestone to packstone rock types) that is dominated with fine-grained mud and is characterized by relatively good porosity, small pore-throat size, and poor permeability. Standard core analysis at the State Muslow B-27 from one sample point (9388.5) in the lower B, lagoonal facies suggest reservoir properties in the facies exhibit 16 percent porosity and <1 millidarcy permeability.

Grand River Field

Two facies maps for the Red River B dolomite at the Grand River Field are presented on **Figures 6-23** and **6-26**. A Red River B zone core at Grand River was acquired by LEC at the Hansen J-31, NWSE Section 31, T130N, R101W. Core and log measurements suggest the B dolomite at the Hansen J-31 is

approximately 6 feet thick. The zone consists of approximately 2 feet of argillaceous dolomite (burrowed dolomite mudstone to wackestone) of lower B - lagoonal transition facies, 2.5 feet of grain flat (dolomite grainstone) and 1.5 feet of upper B algal flat (boundstone) facies. Anhydrite cement is common in the uppermost laminated beds of the algal flat facies. The B dolomite at the Hansen J-31 is capped with approximately seven feet of nodular to bedded anhydrite (measured by open-hole logs). An attempt to acquire core of the Red River B zone was made at the Grand River Field by LEC at the Abrahamson D-8, NWNW section 8, T129N, R101W. However, jamming of anhydrite in the core barrel allowed a recovery of only 7 ft of core, most of which is from the B anhydrite. Several large pieces of "B" dolomite were found in the lower portion of the core barrel. Two lithologies were present in the rubble. The Upper B dolomite was present and was described as a dolostone, medium to dark brown, laminated in part, exhibiting a fine microsucrosic texture with occasional clear crystalline anhydrite cement, good intercrystalline and slight pin-point vugular porosity. This lithology represents that of carbonate grains deposited in a grain flat/agal flat depositional setting. The Lower B dolomite was also present and described as a dolomite, tan to mottled dark brown, chalky to microsucrosic texture, occasional microstylolites with scattered evidence of fair to good intercrystalline porosity. The middle chert member of the B dolomite was not evident in the pieces of core from the Abrahamson D-8 (Quinn, 2002).

A conceptual facies map for the B dolomite at Grand River has been constructed from facies boundaries correlated from the Hansen J-31 to surrounding well control, isopach data for the B zone cycle, and seismic amplitude at the top of the Red River formation from high frequency 3D data (**Figure 26**). Interpretation of depositional facies suggests good reservoir development is located near the crest and updip flank areas located east of the axis of the structural complex. Reservoir facies of the B dolomite in the updip regions of the Grand River Field are generally inferred as a mixture of peloidal grain flat (grainstone) and algal flat (boundstone) rock fabrics. Both facies are considered to be good to excellent reservoir. Standard core analysis from core at the Hansen J-31 and Abrahamson D-8 suggest reservoir properties in the upper B dolomite, grainstone facies at Grand River exhibit porosity values of 18 to 23 percent porosity and permeability of 10 to 29 millidarcies. In some local crestal locations, a relatively poor reservoir facies that is plugged with anhydrite probably exist within algal boundstone that contain significant anhydrite cement in larger fenestral and vuggy pores. The boundstone facies member is thought to represent the highest portion of the paleo-structure at the time of Red River B zone deposition. Core analysis in this facies member of the B dolomite show reservoir properties of 7 to 17 percent porosity and 1 to 7 millidarcies of permeability. Lagoonal facies are thought to dominate the downdip east reach of the Grand River Field. The lagoonal facies of the B dolomite is an argillaceous dolomite with a packstone to wackestone rock fabric. The zone is dominated with fine-grained mud. Relatively good porosity, but small pore-throat size, and poor permeability characterize the facies. Standard core analysis at the Hansen

J-31 from two sample points (9385.6 to 9386.8) in the lower B, lagoonal facies suggest reservoir properties in the facies exhibit 21 to 24 percent porosity and permeability of 1 to 4 millidarcies.

Luff Exploration Company has recently acquired a third core from the Red River B zone in the Grand River field. A 14-foot core was taken from the Abrahamson J-12H, NWSE section 12, T129N, R102W. Initial assessment indicate the B zone at the Abrahamson J-12 is capped with approximately 5 feet of bedded to nodular anhydrite. The anhydrite contains numerous laminae of dark brown dolomite mudstone (Quinn, 2003). A laminated algal dolomite boundstone approximately 2.0 feet thick underlies the B anhydrite. This boundstone facies contains common but patchy anhydrite cement in larger vuggy and fenestral pores, yet retains good intercrystalline and micro-intercrystalline porosity. The underlying porous grainstone unit of the grain flat facies is 2.5 feet at the Abrahamson J-12. Porosity in the upper B interval measured from open-hole logs reaches a maximum of 21 percent. The upper B grainstone facies caps approximately 2 feet of lower B dolomite, lagoonal facies. Porosity in the lower B interval measures reaches a maximum of approximately 22 percent. A total of twelve core plugs were collected on approximately one-half foot intervals from B zone core at the Abrahamson J-12. The plugs were analyzed for standard porosity-permeability and fluid saturation. Results from the analysis are presented in Appendix B. Based on the results, porosity in the upper B grainstone facies range from 17 to 25 percent and permeability varies from 10 to 57 millidarcies. In contrast, porosity in the lower B lagoonal facies range from 17 to 23 percent and permeability varies from 1.5 to 10 millidarcies.

Conclusions

LEC has used results from analysis of six core acquired from the Red River B zone to conclude that primary depositional facies and the associated rock fabric of carbonate sediment deposited under shallow, restricted marine conditions, have played a significant role in the distribution of good reservoir conditions in the B dolomite of southwestern North Dakota and northwestern South Dakota.

The industry defined Red River B cycle is a predominantly shallowing upward, restricted marine depositional sequence. The lithologies of this cycle include from bottom to top: bioturbated lime wackestone-packstone (shallow marine), to an argillaceous laminated transitional dolomitic wackestone-packstone that is indicative of a restrictive lagoon depositional environment, to a laminated grain-flat grainstone and algal flat boundstone that represent higher energy shallow marine and intertidal/supratidal depositional environments, to an anhydritic laminated dolomite that is indicative of a slightly deeper water hypersaline shelf depositional setting, to bedded anhydrite representing predominantly subaqueous evaporitic deposition. If the bedded anhydrite at the top of the Red River B cycle is in fact a subaqueous evaporative shelf/lagoonal deposit, positioned above a dolomitic algal boundstone representing high intertidal to

supratidal deposition with local subaerial exposure, then the actual sequence boundary within this part of the Red River occurs at the base of the B anhydrite, not at the contact between the uppermost anhydrite bed and the basal limestone member of the overlying Red River A cycle.

Topography of the sea floor during B zone deposition has played a significant role in the thickness and distribution of grain-size in carbonate sediment of the B dolomite. Relatively high topographic areas may have benefited from a slightly a higher depositional energy that favored deposition of a grain-supported carbonates (grain flat/algal flat facies). In contrast, topographically low-lying areas may have been dominated by a restricted lagoonal depositional setting with low depositional energy and a dominance of argillaceous muddy carbonate. The upper part of the Red River B lithostratigraphic cycle consists of nodular and bedded anhydrite, interbedded with dolomite, indicating that hypersaline water conditions prevailed and periodic recharge of marine water to the restricted basin must have occurred. The rate of recharge of marine water to the system may have closely equaled the rate of evaporation, thus, providing a continuous source of hypersaline water for precipitation of a thick layer of anhydrite. As anhydrite precipitated from the brine, the ratio of magnesium (Mg) to calcium (Ca) in the brine may have increased to a level allowing the brine solution to chemically favorable dolomitization. Thus, during at least the early-stage deposition of the B anhydrite, the hypersaline brine may have served as a solution for dolomitization of carbonate forming the B dolomite. The discontinuous but somewhat pervasive middle chert layer of the B dolomite may have served as a semi-confining layer or barrier for vertical migration of the dolomitizing solution in carbonate sediment of the B dolomite. Thus, a greater residence time for the dolomitizing solution to interact chemically with carbonate sediment of the laminated member of the upper B dolomite may have prevailed throughout most of the area allowing a complete alteration of calcite to dolomite. Cementation of many of the larger voids in the carbonate sediment with anhydrite more frequently occurred in laminated algal-rich beds of the upper B dolomite immediately beneath and in contact with the bedded anhydrite. In contrast, a relatively low residence time and somewhat incomplete process of dolomitization may have occurred in the transitional laminated facies of the lower B dolomite due to limitations in the vertical and downward migration of the dolomitizing solution by the middle chert member and /or by the more widespread argillaceous and significantly less permeably burrowed dolomite wackestones of the lagoonal facies of the B dolomite.

The topographically highest areas during Red River B deposition may have been particularly prone to cementation by anhydrite. Thin units of dolomite packstone and grainstone deposited at this position commonly contain abundant anhydrite cement.

References Cited

Canter, K.L., 2003, Red River “B” facies, stratigraphy, and reservoir characteristics, Bowman County, N.D., Study of Red River B zone core for Luff Exploration Company.

Canter, K.L. Role of Depositional Facies on Reservoir Development and Distribution: Ordovician Red River Formation, Williston Basin, Applied Geoscience Inc., 2002, 2003.

Canter, K.L., Coringrato, V.J., Stearns, D.B., and Grubbs, K., 2001, Role of depositional facies on reservoir development and distribution, Ordovician Red River Formation, Williston Basin (abs.). American Association Petroleum Geologists, 2001.

Canter, K.L., 1998, Facies, cyclostratigraphy and secondary diagenetic controls on reservoir distribution, Ordovician Red River Formation, Midale Field, southern Saskatchewan: in Core Workshop Volume, Eighth International Williston Basin Symposium, p.41-65.

Canter, K.L., Coringrato, V.J., Stearns, D.B. and Grubbs, K., 1998, Analogs for Exploration and Exploitation, Red River Formation: Case Studies of Ordovician Red River Fields: Saskatchewan, Montana and North Dakota, Applied Geoscience Proprietary Multi-client Report.

Carroll, W.K., 1979, Depositional and Paragenic Controls on Porosity Development, Upper Red River Formation, North Dakota, North Dakota Geologic Survey, Report of Investigations 66, 51p.

Kohm, J.A. and Louden, R.O., 1978, Ordovician Red River of Eastern Montana and Western North Dakota: Relationships Between Lithofacies and Production: Williston Basin Symposium, Montana Geologic Society 24th Annual Field Conference, p.99-117.

Longman, M.W., Fertal, T.G., and Glennie, J.S., 1983, Origin and Geometry of Red River Dolomite Reservoirs, Western Williston Basin. American Association of Petroleum Geologist Bulletin, V.67, No.5, p.744-771.

Quinn, C.F., 2002, Geologic Well Report for the Abrahamson D-8, Grand River Field, Bowman County, North Dakota.

Quinn, C.F., 2003, Geologic Well Report for the Abrahamson J-12H, Grand River Field, Bowman County, North Dakota.

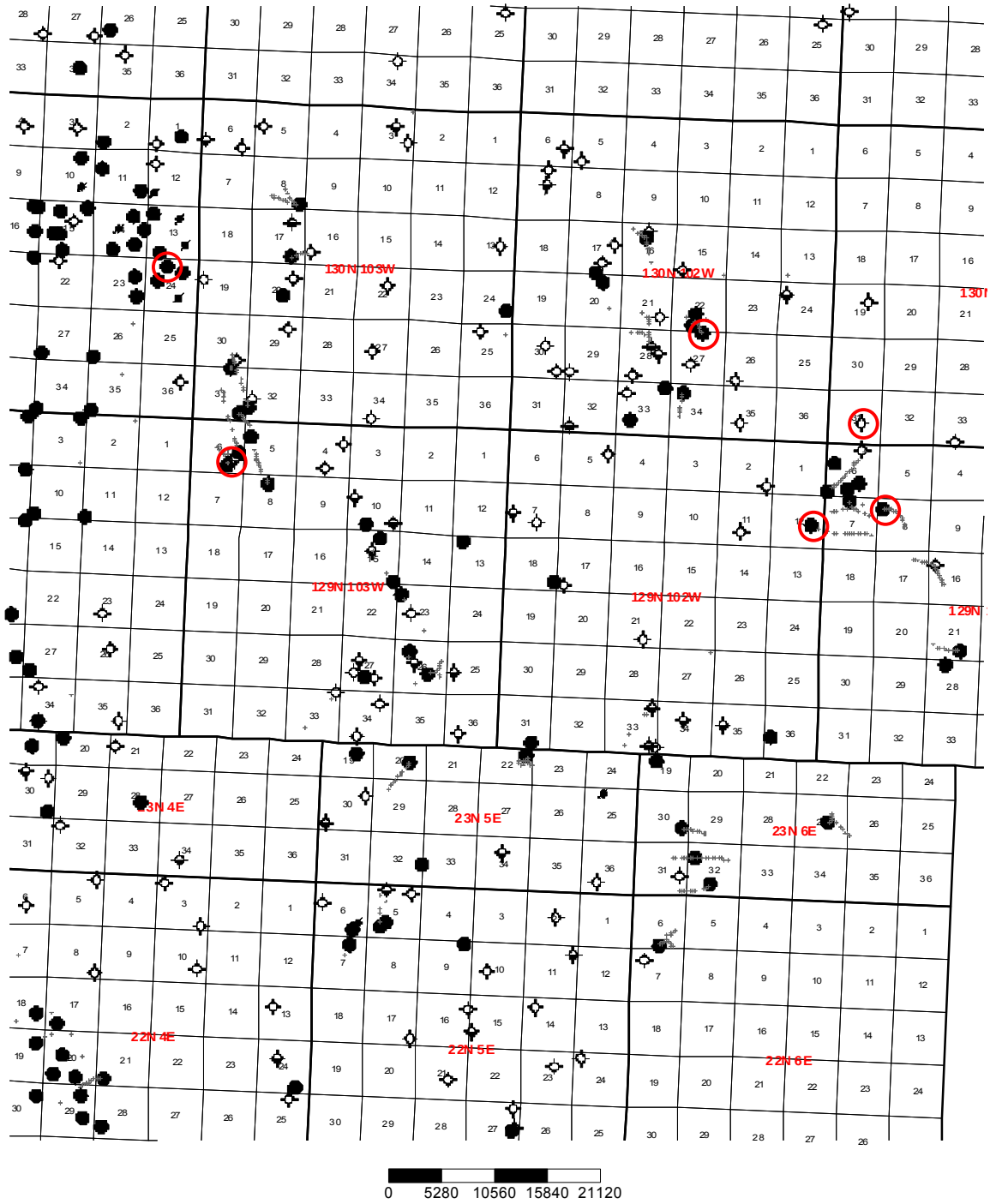

Figure 6-1. Regional map of study with location of core wells used for petrographic study

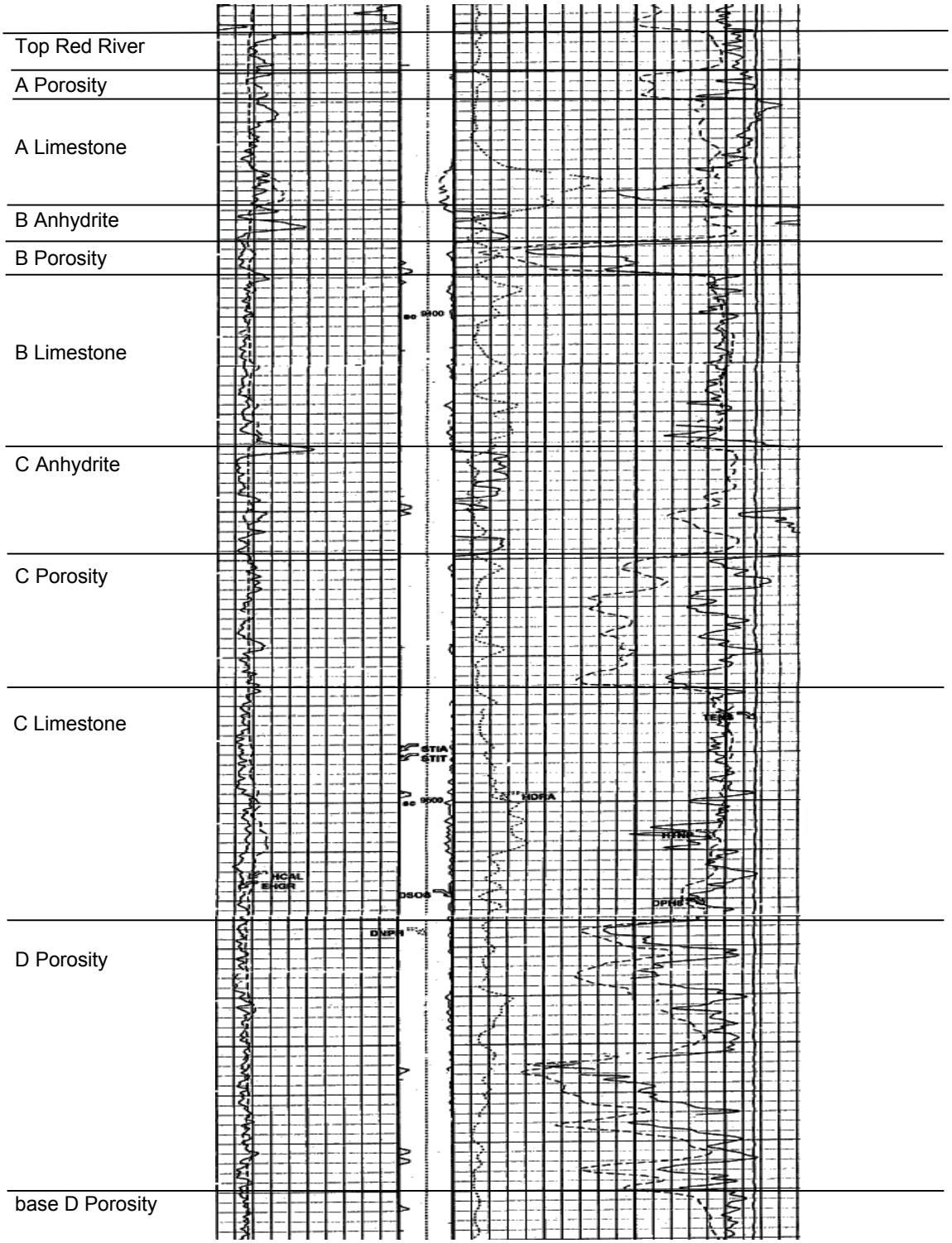

Figure 6-2. Type log of upper Red River formation from Muslow B-27 State, section 27, T130N-R102W.

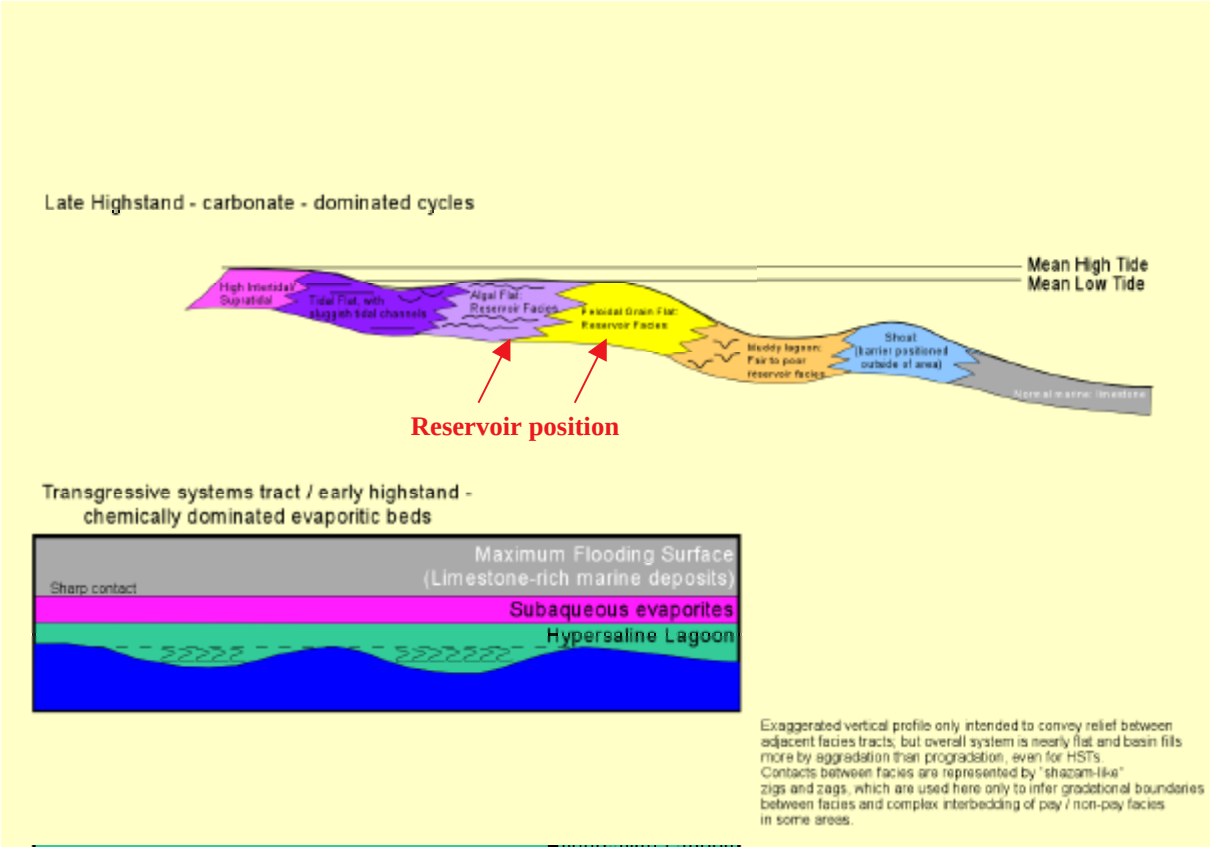

Figure 6-3. Reservoir development is mainly within the peloidal grain flat and algal flat facies, of the carbonate – dominated portions of cycles, and represent late highstand deposits on paleohighs. Peloidal grain flat facies is thicker than the algal flat facies, suggesting that this well is slightly down-dip of the local paleohigh (figure by Canter, K.L.).

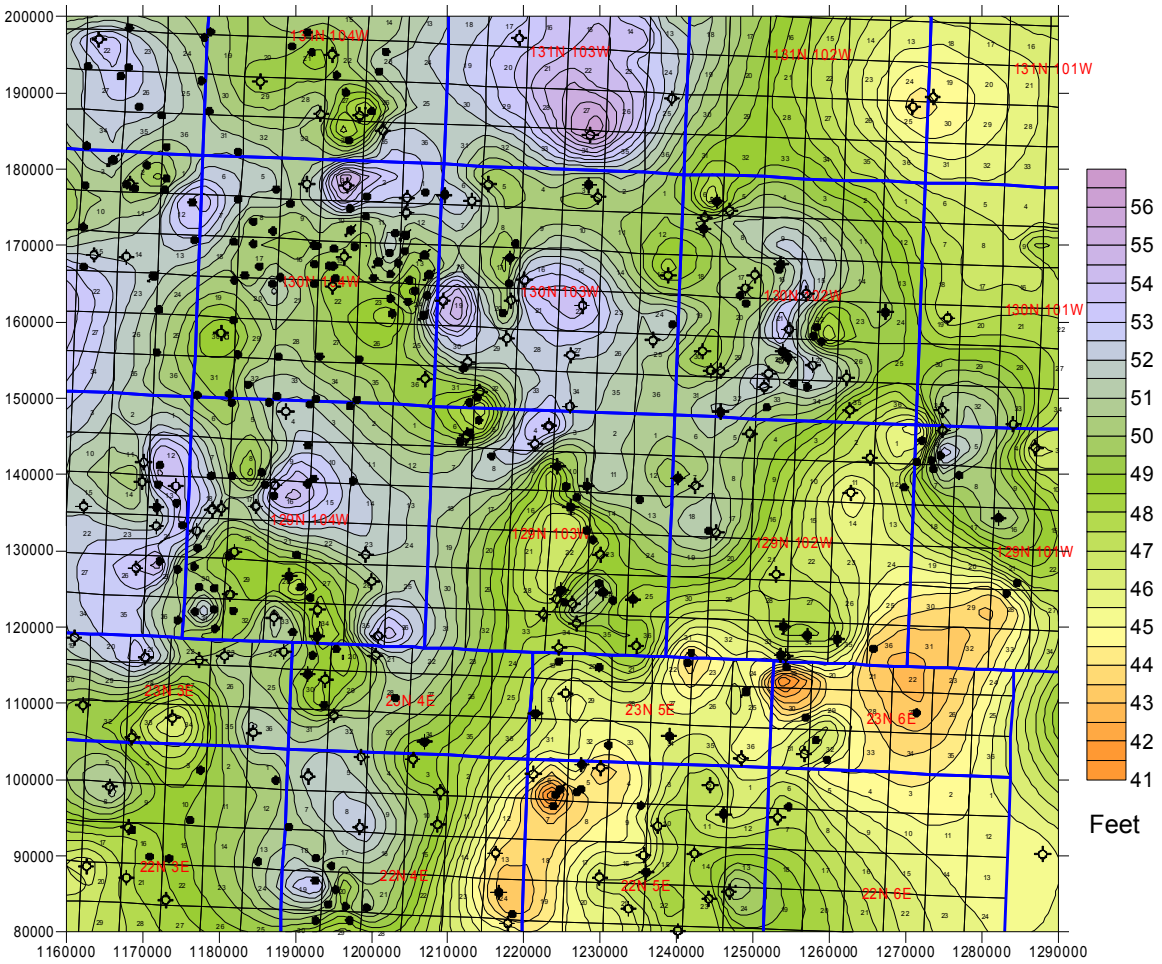

Figure 6-4. Regional isopach map of Red River B Cycle.

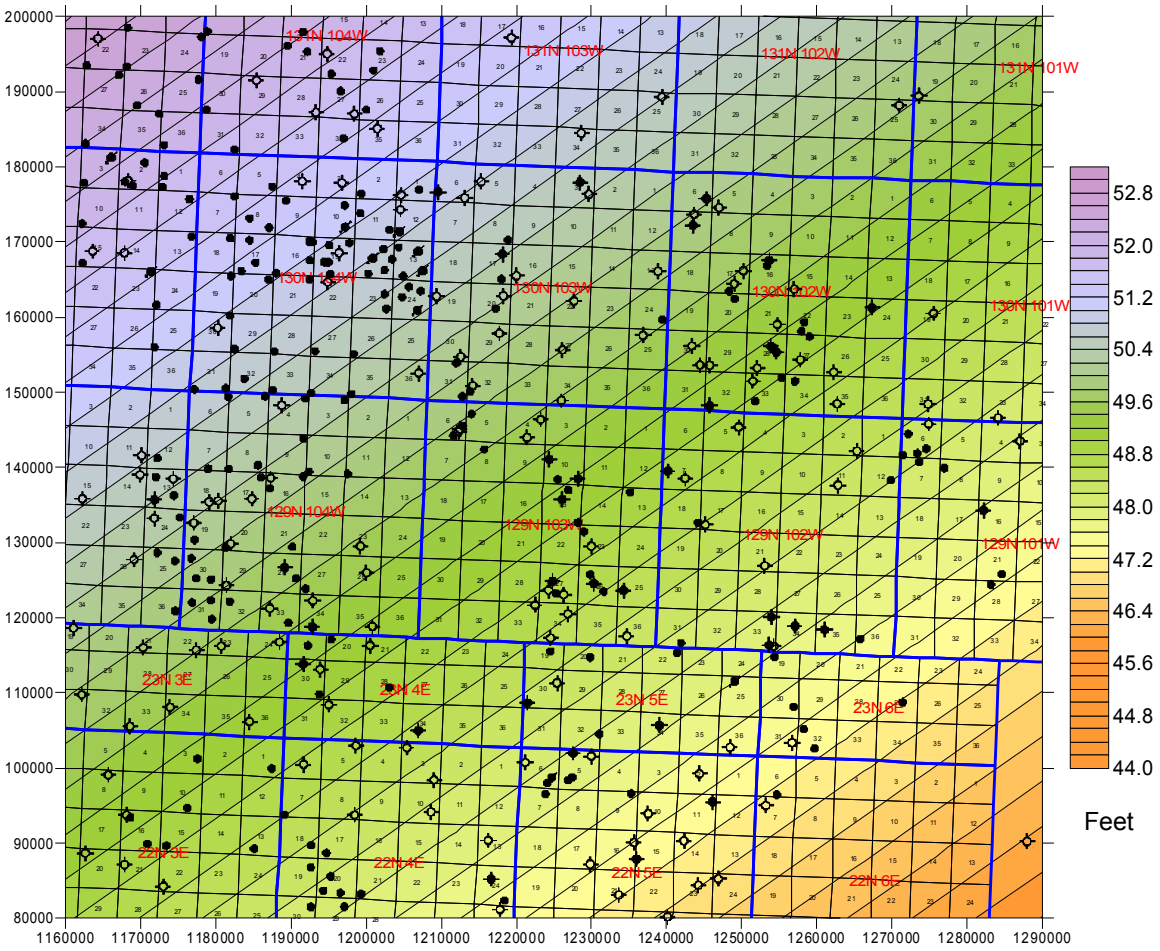

Figure 6-5. Trend surface map of Red River B Cycle isopach.

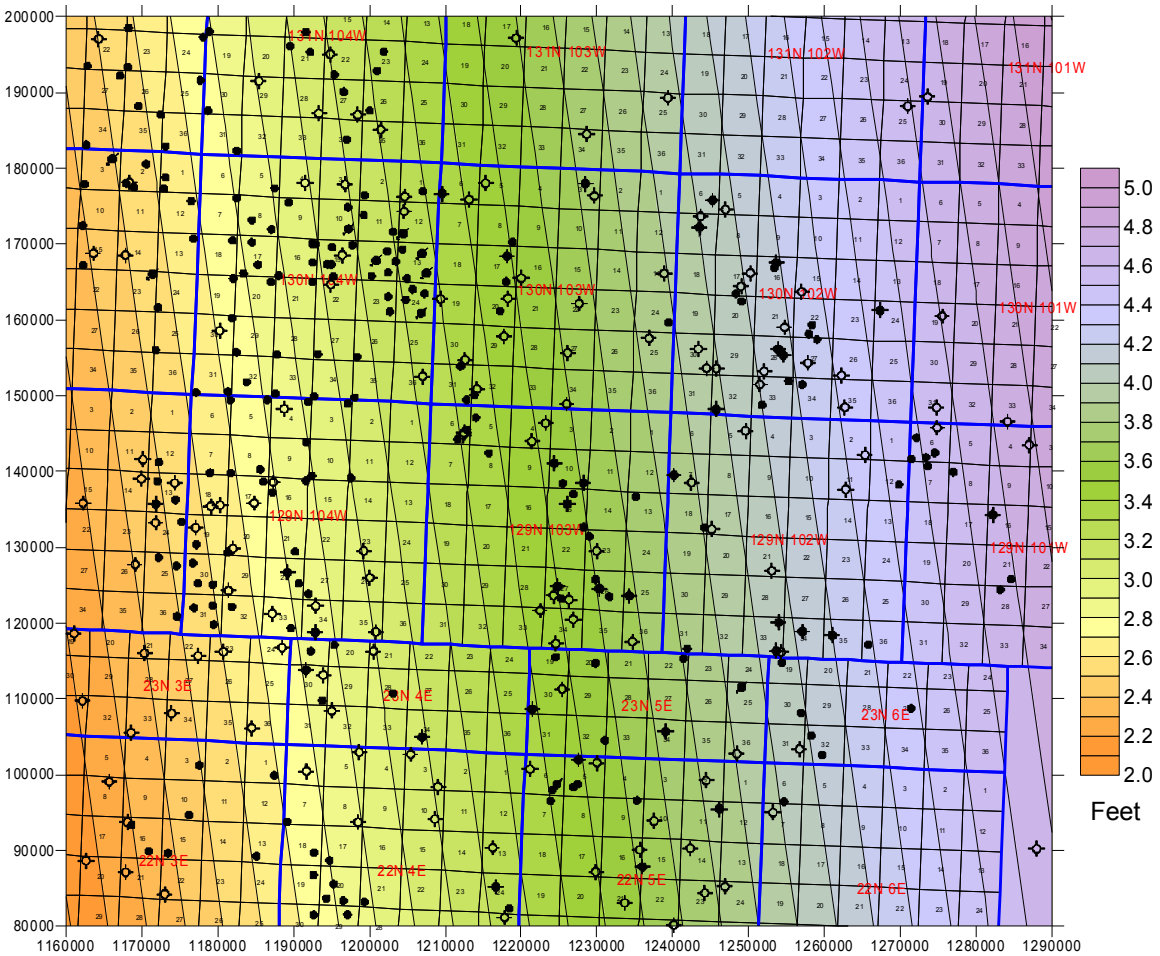

Figure 6-6. Trend surface of Red River B Anhydrite isopach.

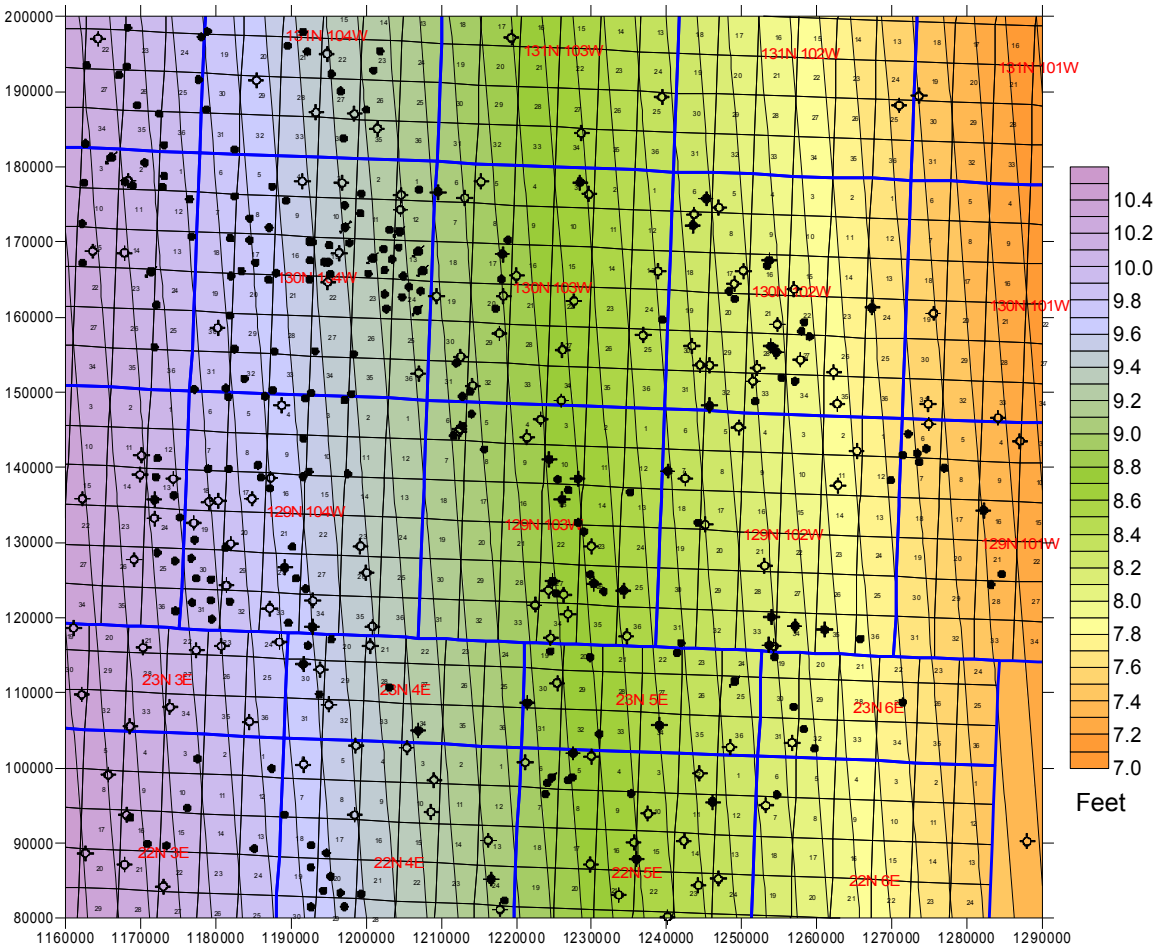

Figure 6-7. Trend surface of Red River B Dolomite isopach.

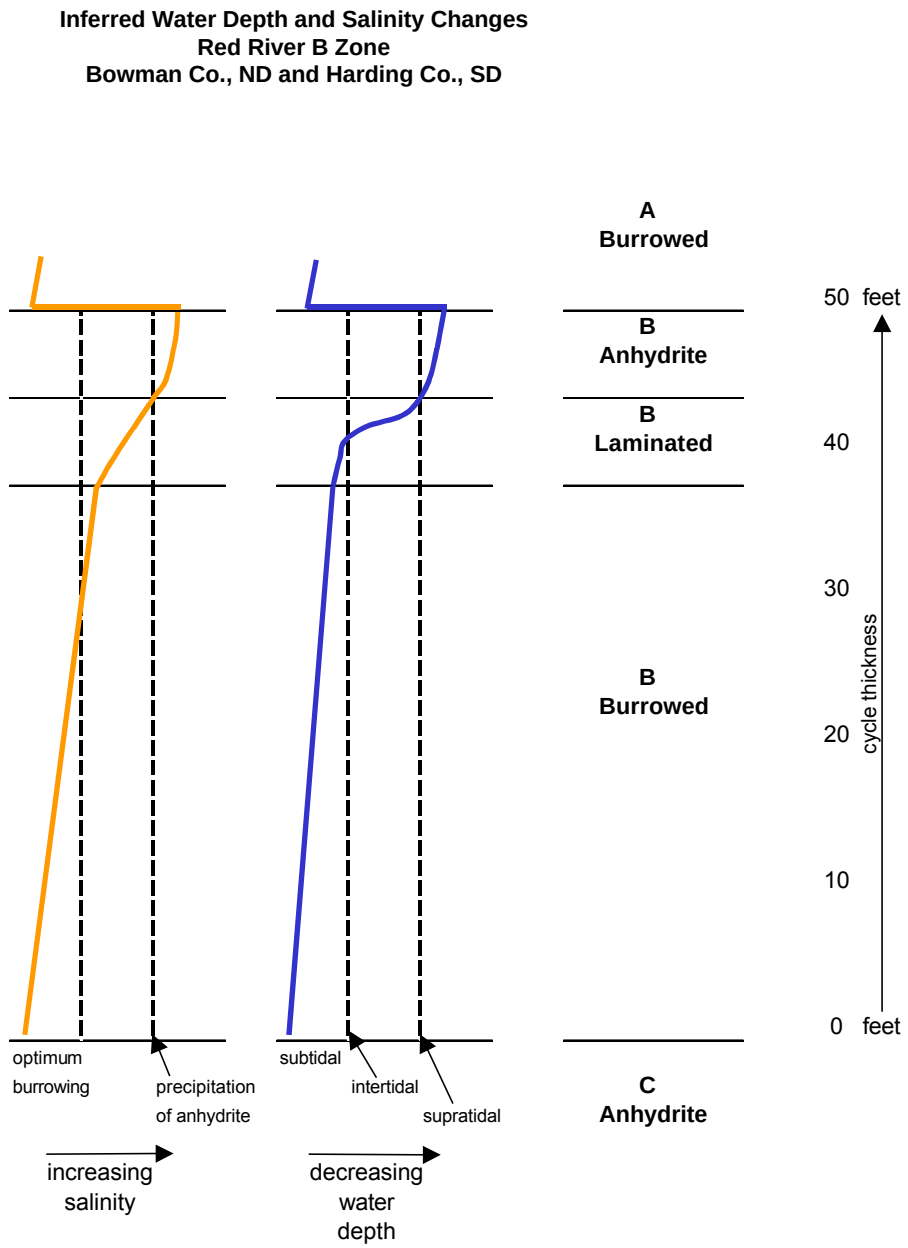

Figure 6-8. Inferred water depth and salinity changes - Red River B Zone (Longman et al., 1983).

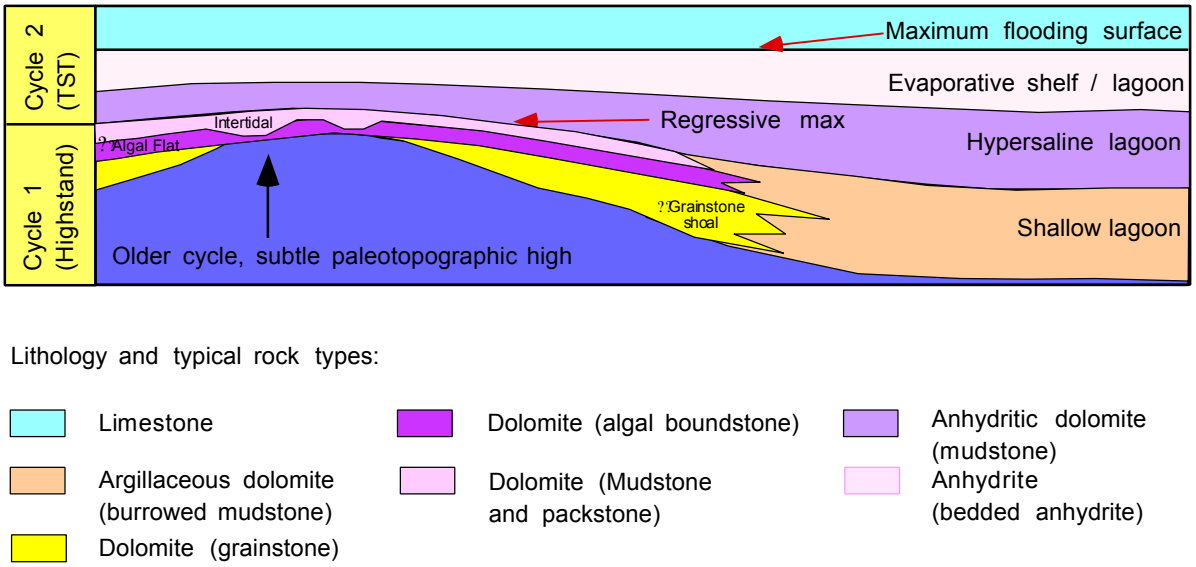

Figure 6-9. Red River B Conceptual Depositional model (Canter, K.L., 2003).

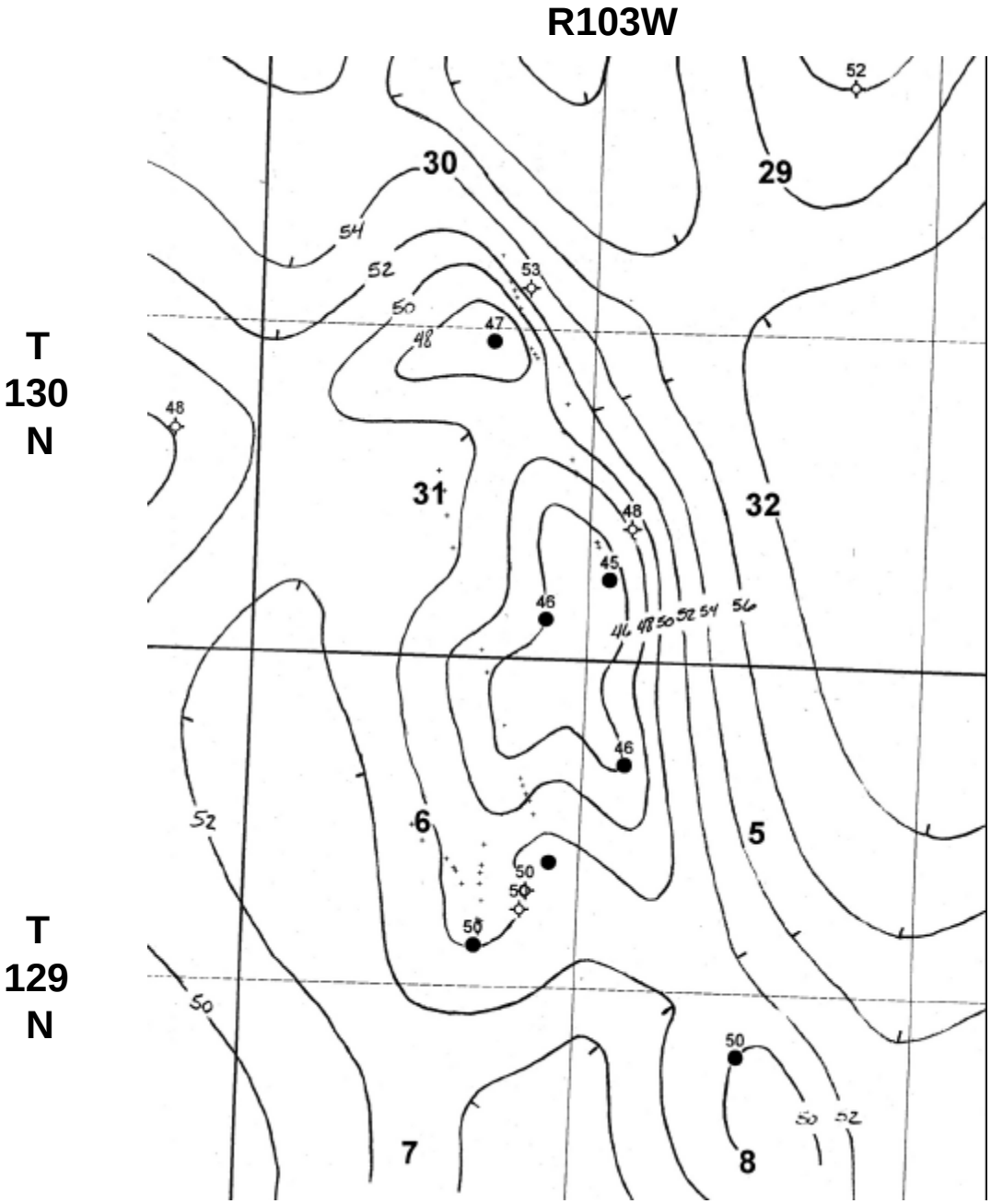

Figure 6-10. Isopach map - Red River B Cycle , Amor Field.

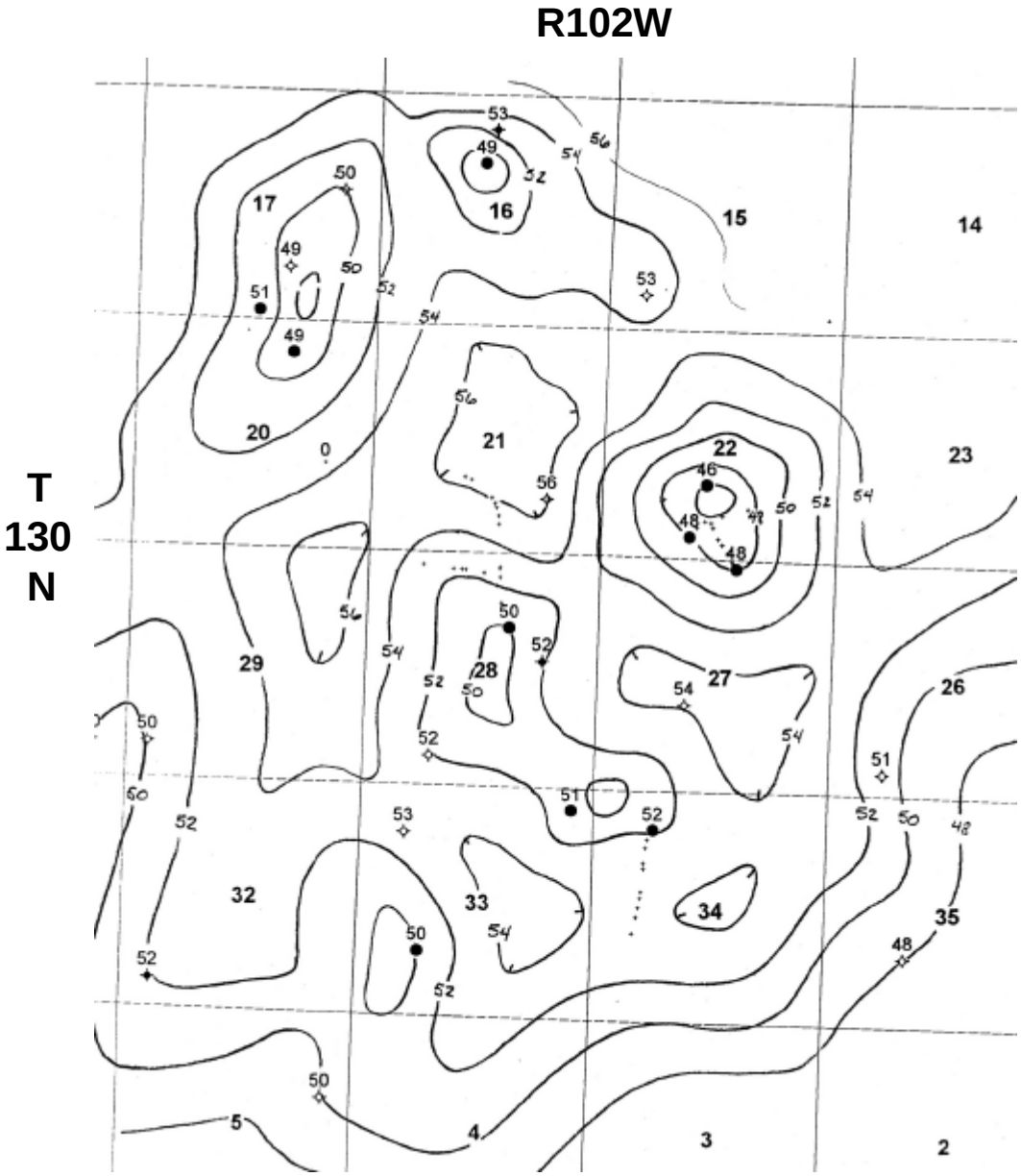

Figure 6-11. Isopach map - Red River B Cycle, Cold Turkey Creek Field.

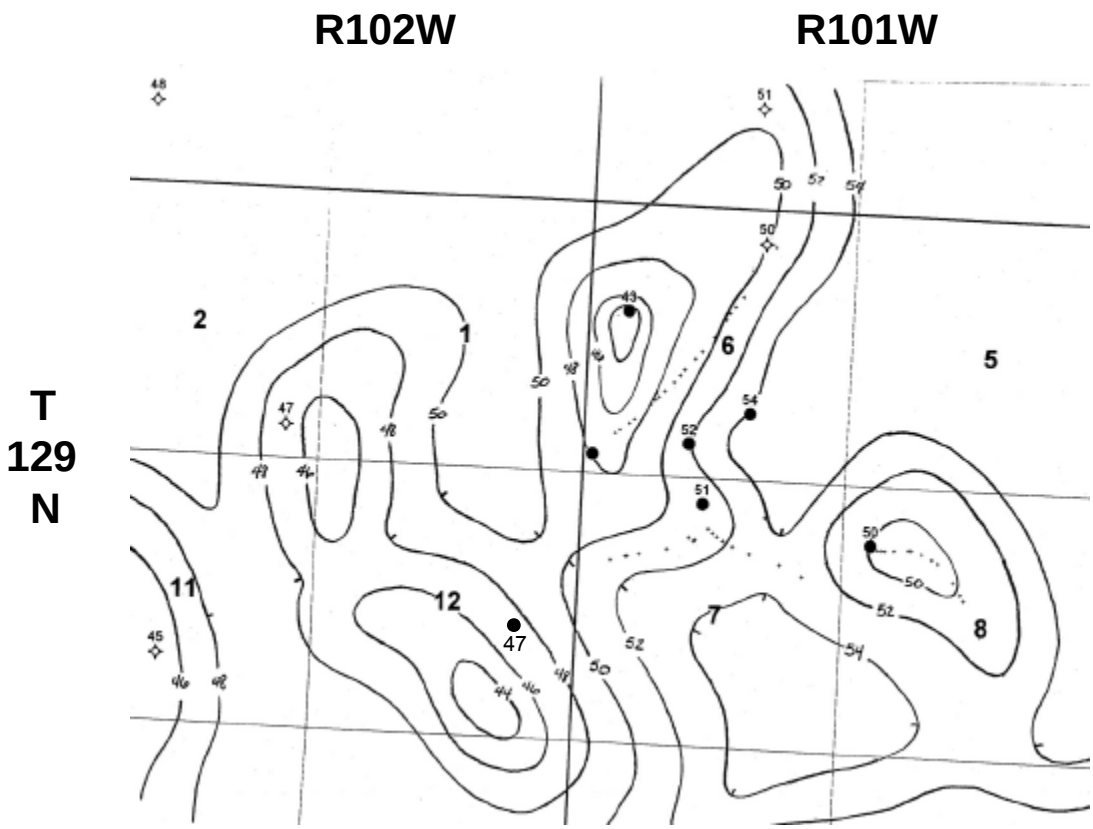

Figure 6-12. Isopach map - Red River B Cycle, Grand River Field.

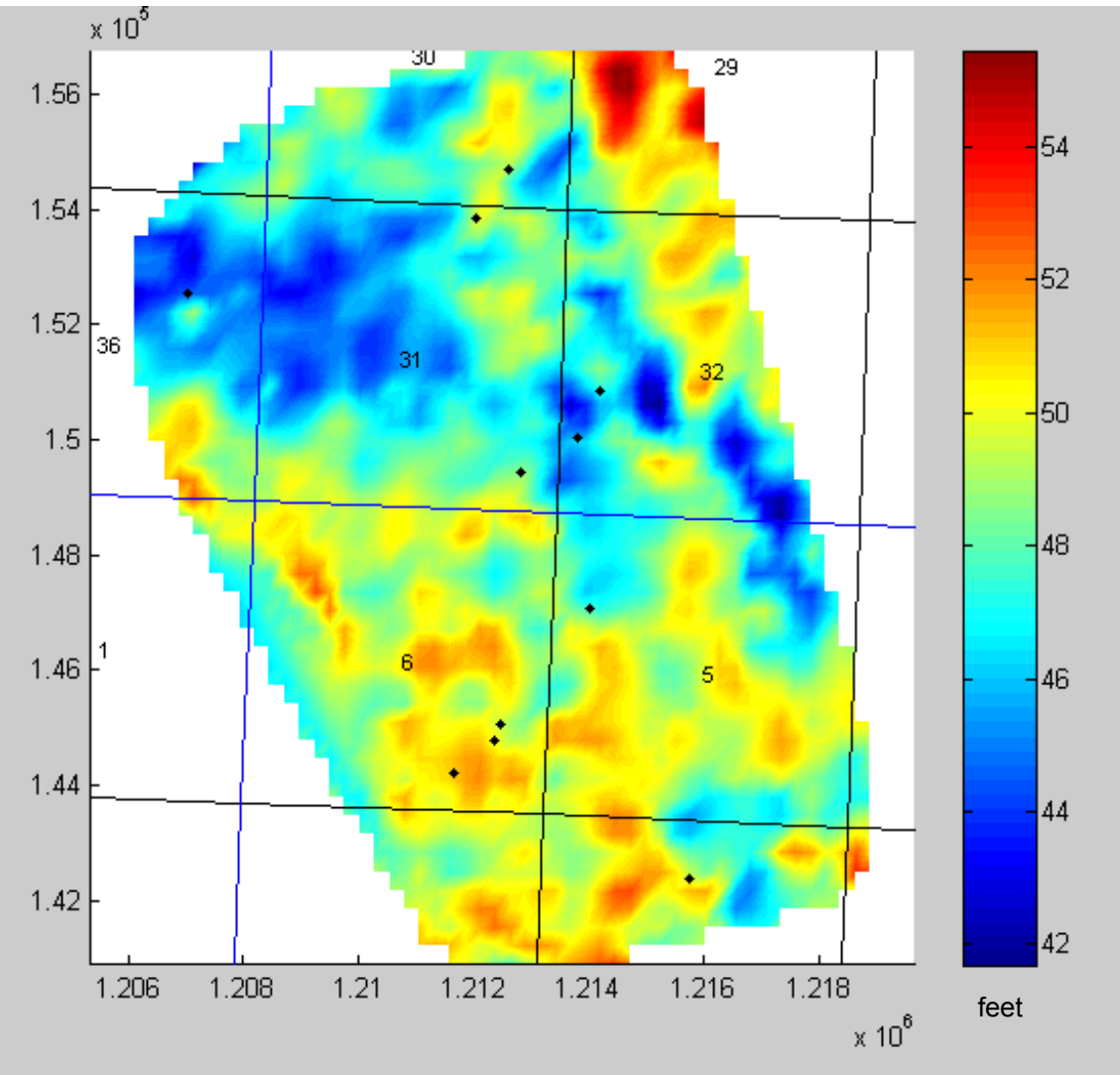

Figure 6-13. Isopach map of Red River B Cycle thickness, Amor South Field. Based on seismic attribute transforms.

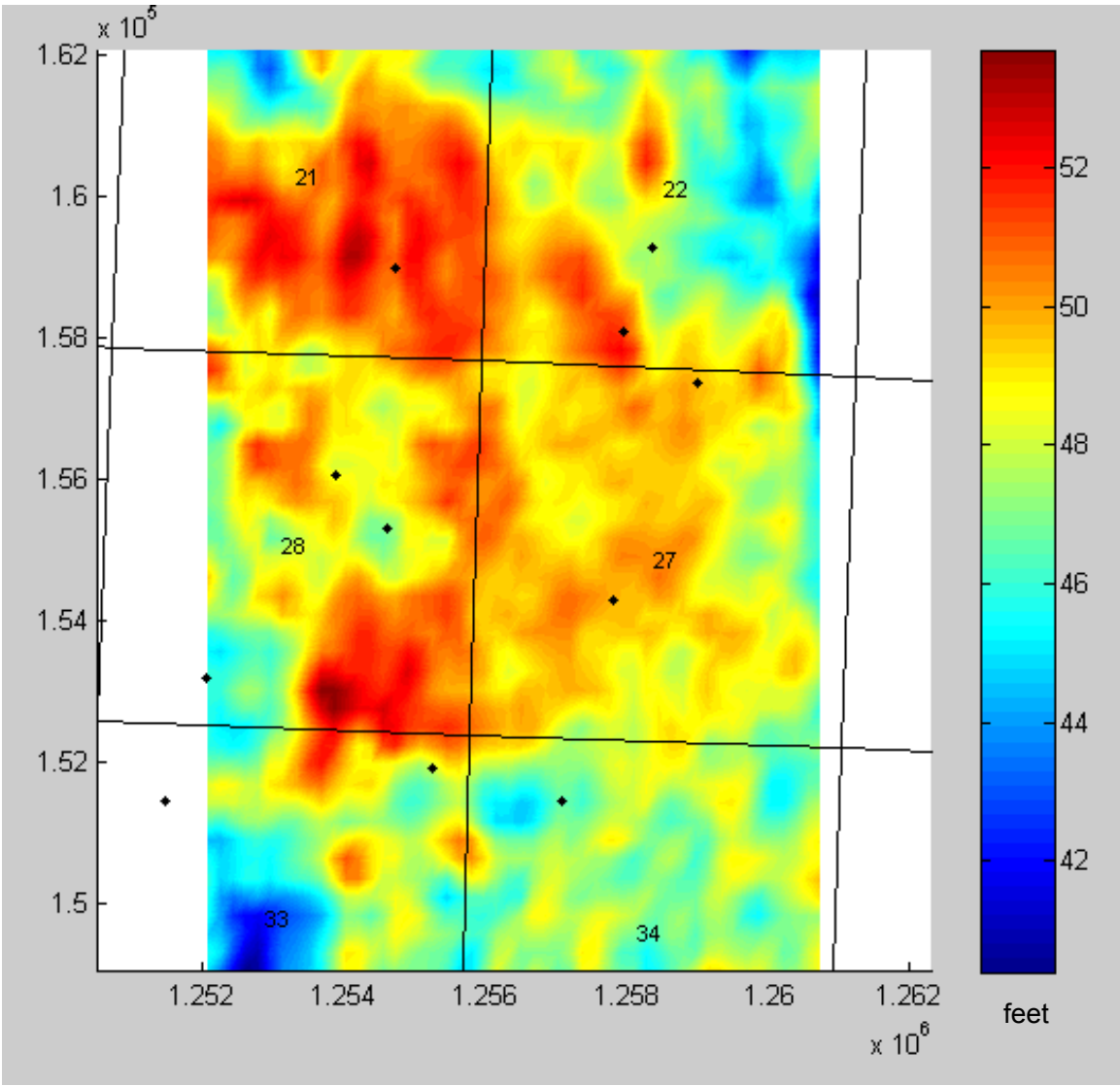

Figure 6-14. Isopach map of Red River B Cycle thickness, Cold Turkey Creek Field. Based on seismic attribute transforms.

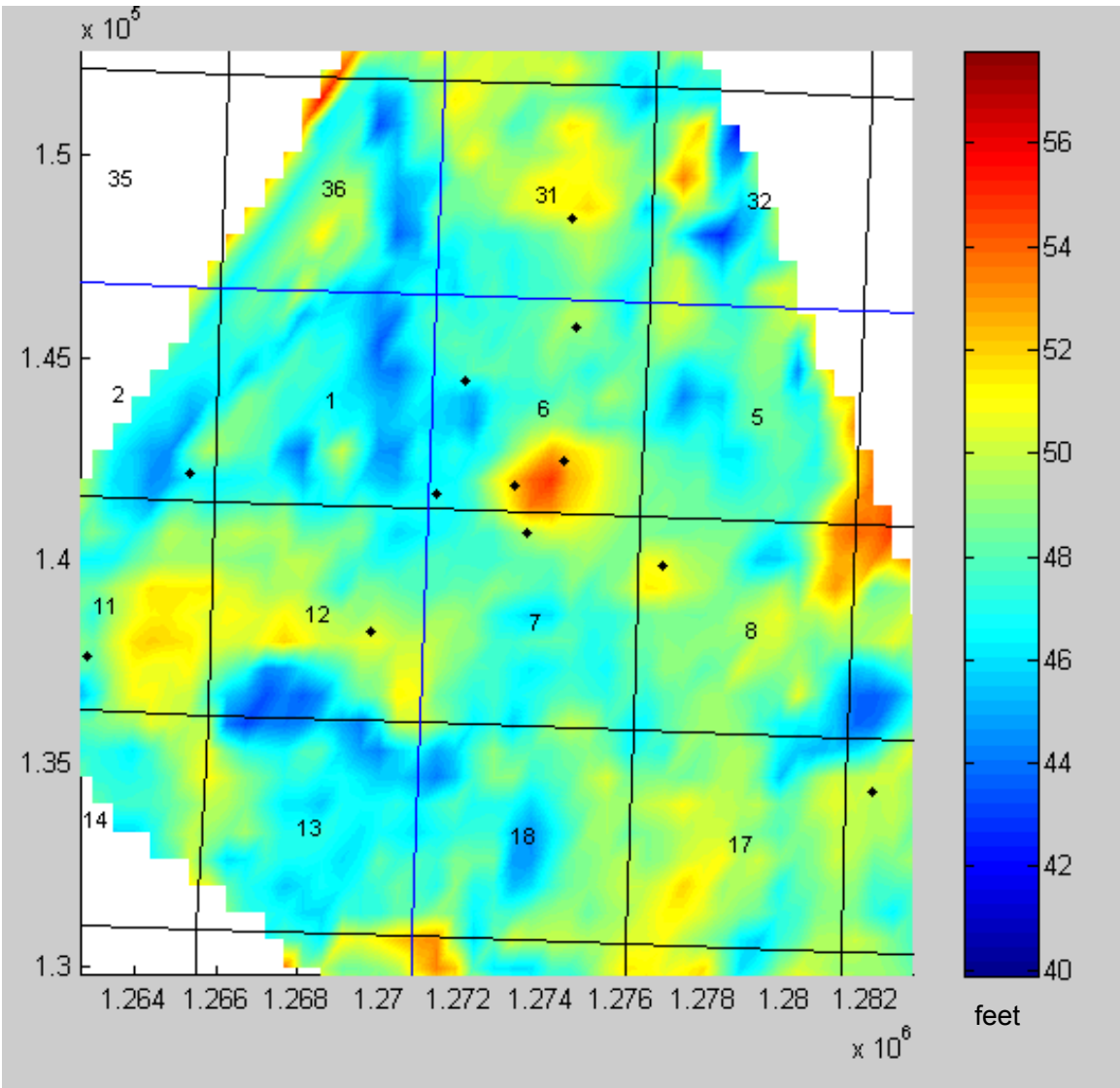

Figure 6-15. Isopach map of Red River B Cycle thickness, Grand River Field. Based on seismic attribute transforms.

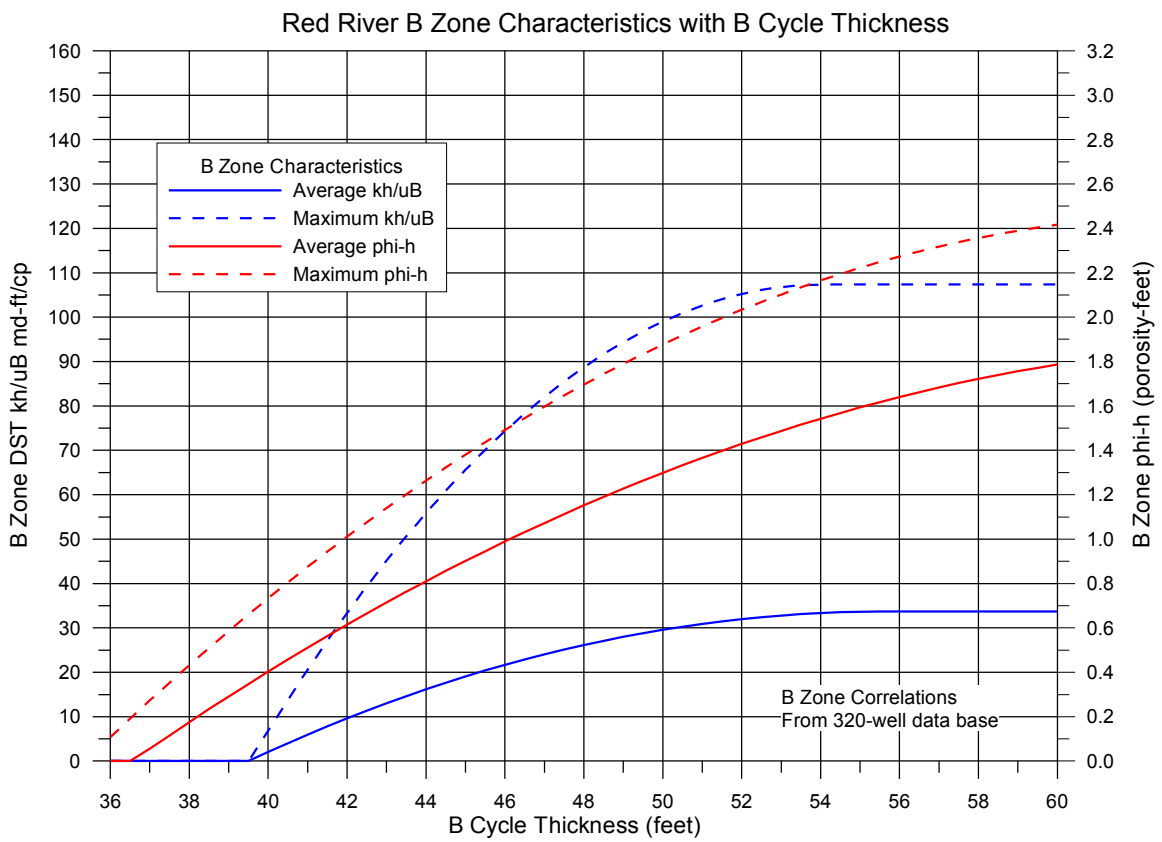

Figure 6-16. Graph showing relationship of Red River B zone reservoir properties (storage, phi-h, and transmissivity, kh/uB) and B zone cycle thickness. Data for reservoir properties collected from 320 well population located in Bowman and Harding counties.

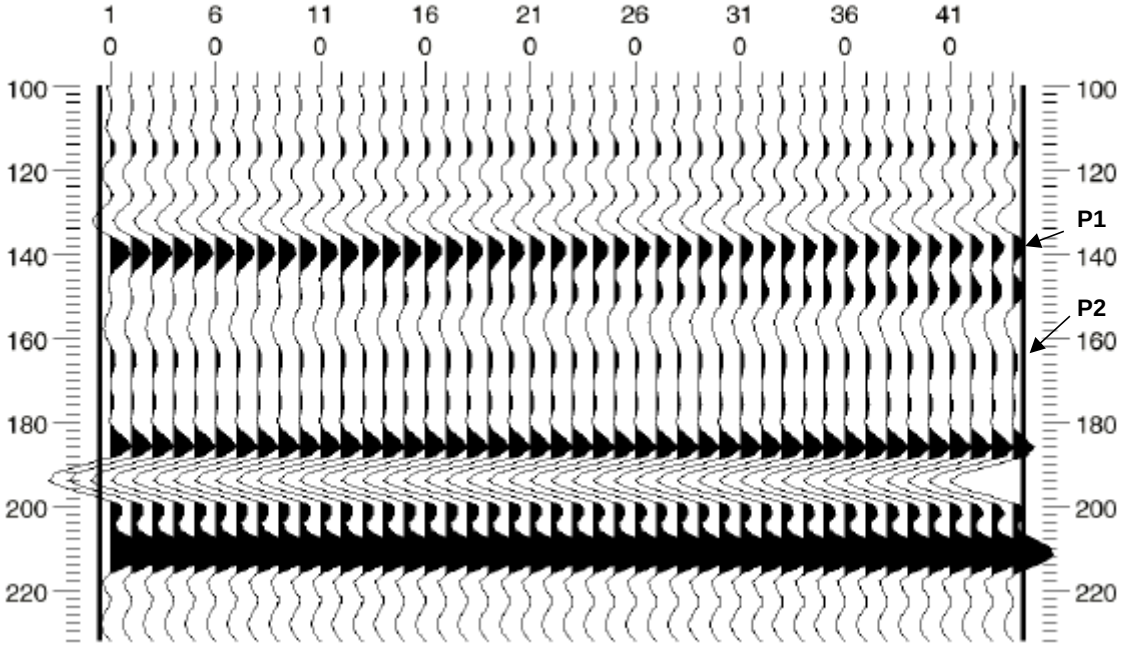

Figure 6-17. Seismic simulation of ORR B porosity development. In the model, porosity in the D zone exhibits poor development throughout the profile. In contrast, porosity thickness (phi-h) in the ORR B zone increases from very poor properties on the left to good reservoir properties on the right. A doublet forms at the P1 horizon in response to good development of phi-h in the ORR B zone.

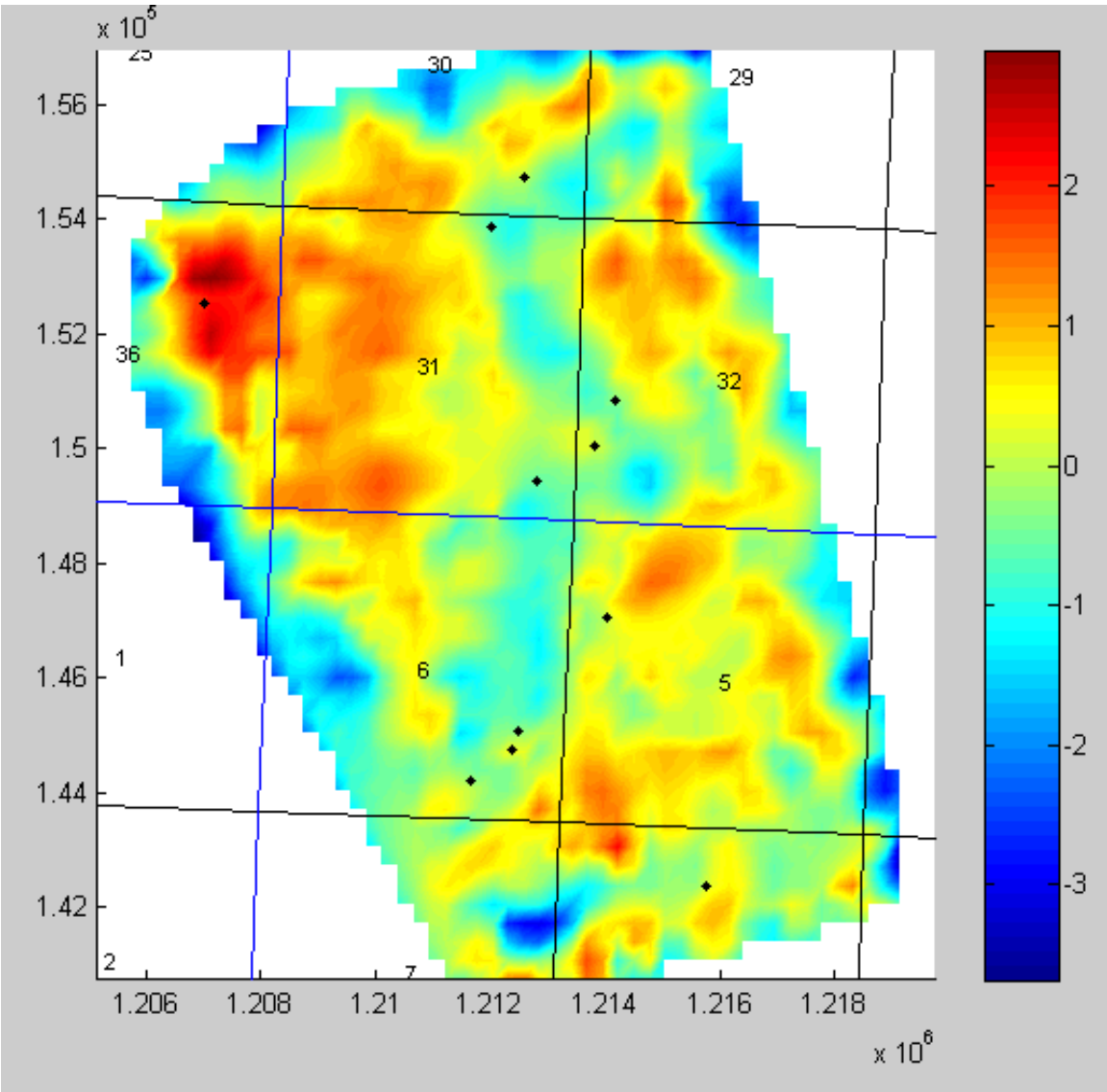

Figure 6-18. High-frequency first-peak doublet amplitude from 3D seismic, Amor Field. Scale in standard deviations from mean.

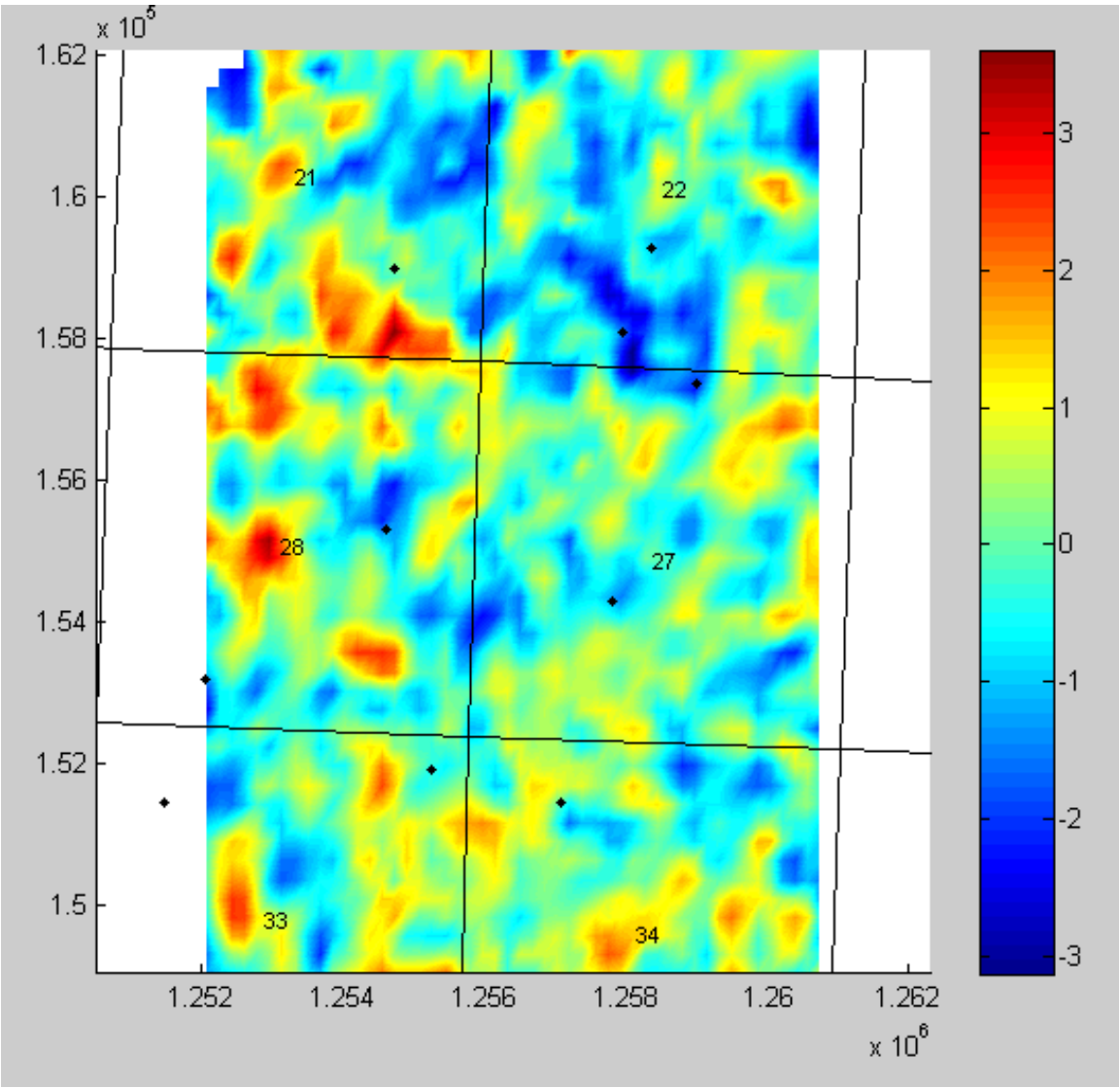

Figure 6-19. High-frequency first-peak doublet amplitude from 3D seismic, Cold Turkey Creek Field. Scale in standard deviations from mean.

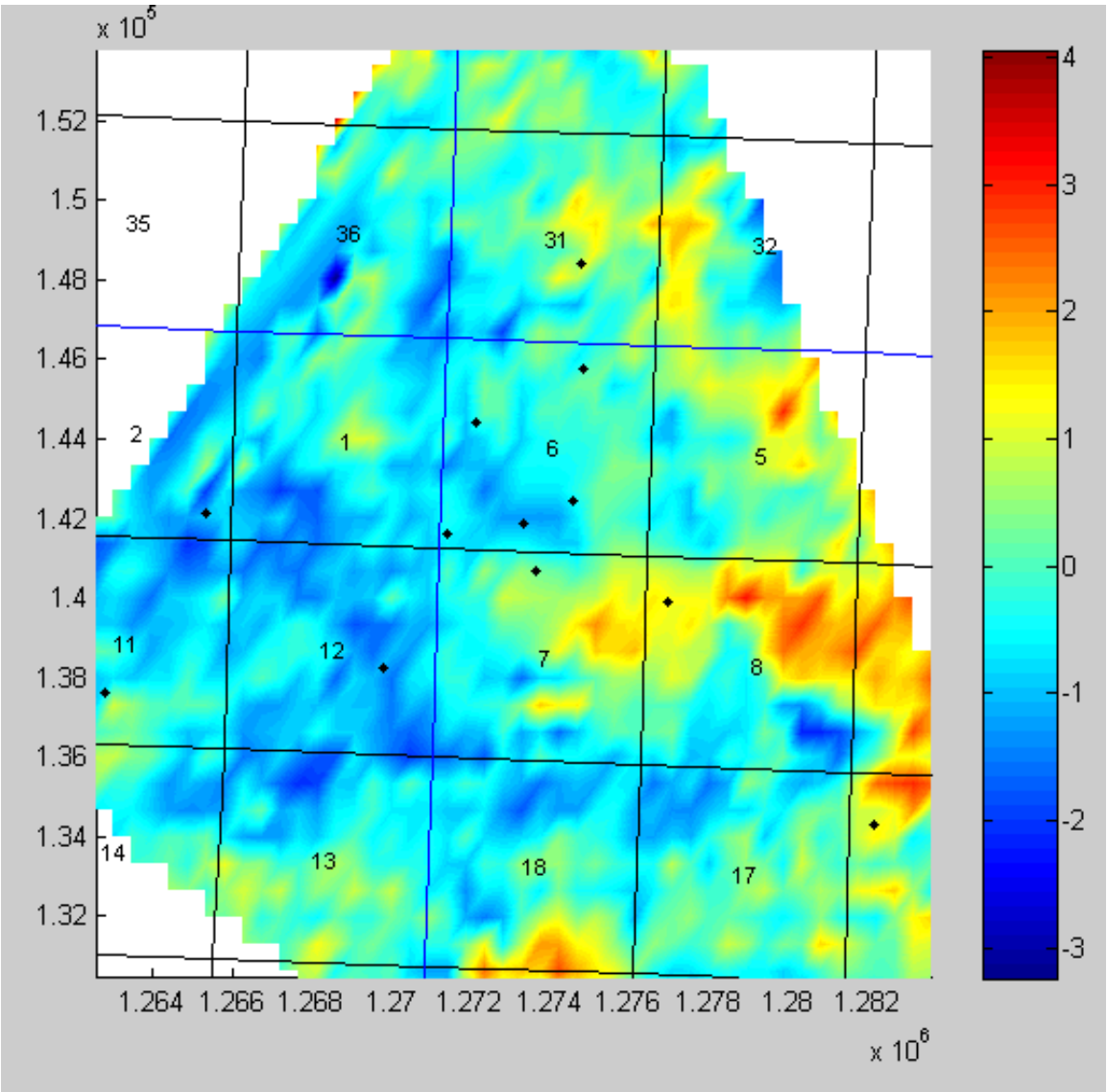

Figure 6-20. High-frequency first-peak doublet amplitude from 3D seismic, Grand River Field. Scale in standard deviations from mean.

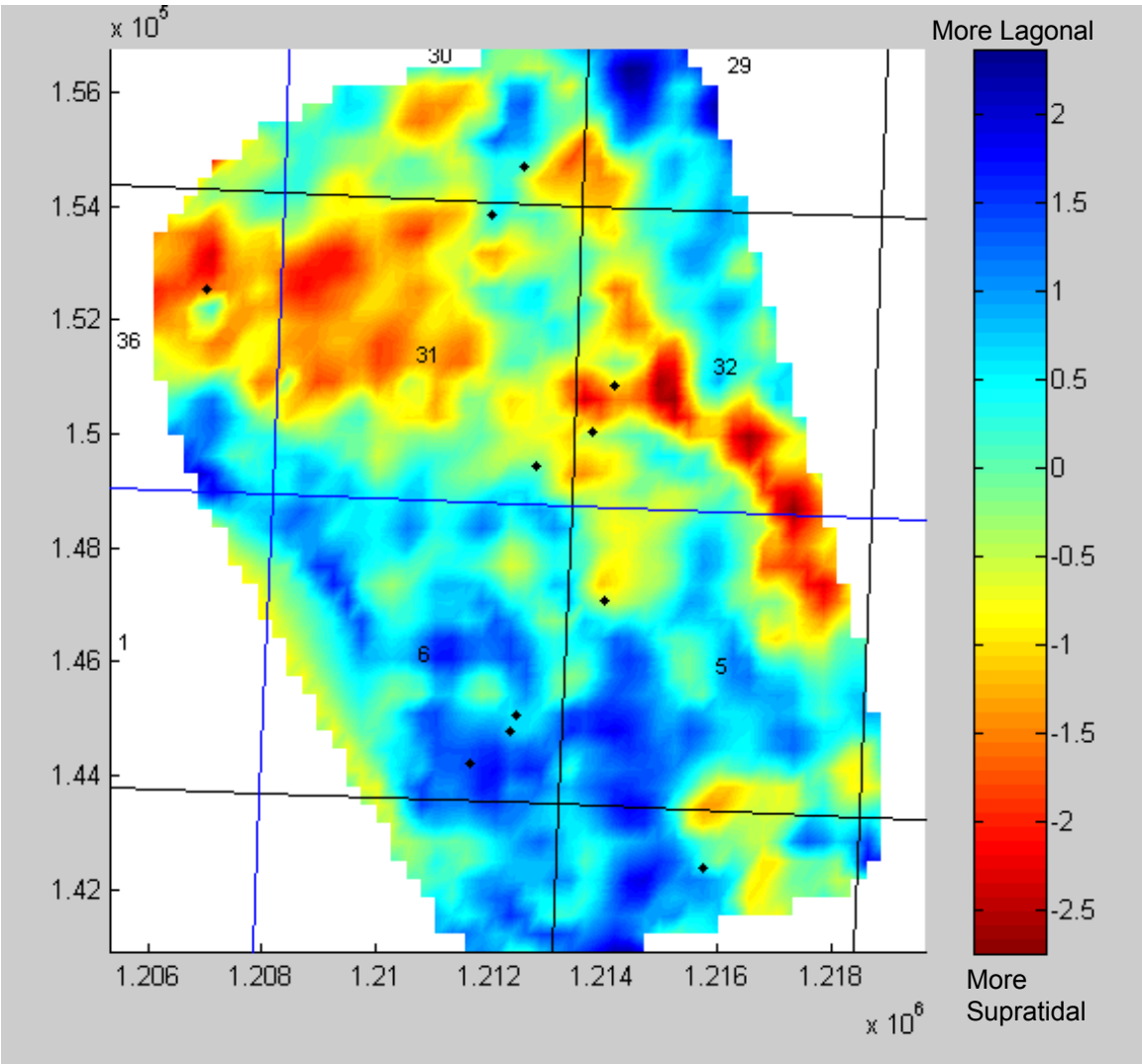

Figure 6-21. Inferred facies map - Red River B Dolomite, Amor Field, based on seismic transforms of B Cycle and C anhydrite thickness. Scale is standard deviation from mean.

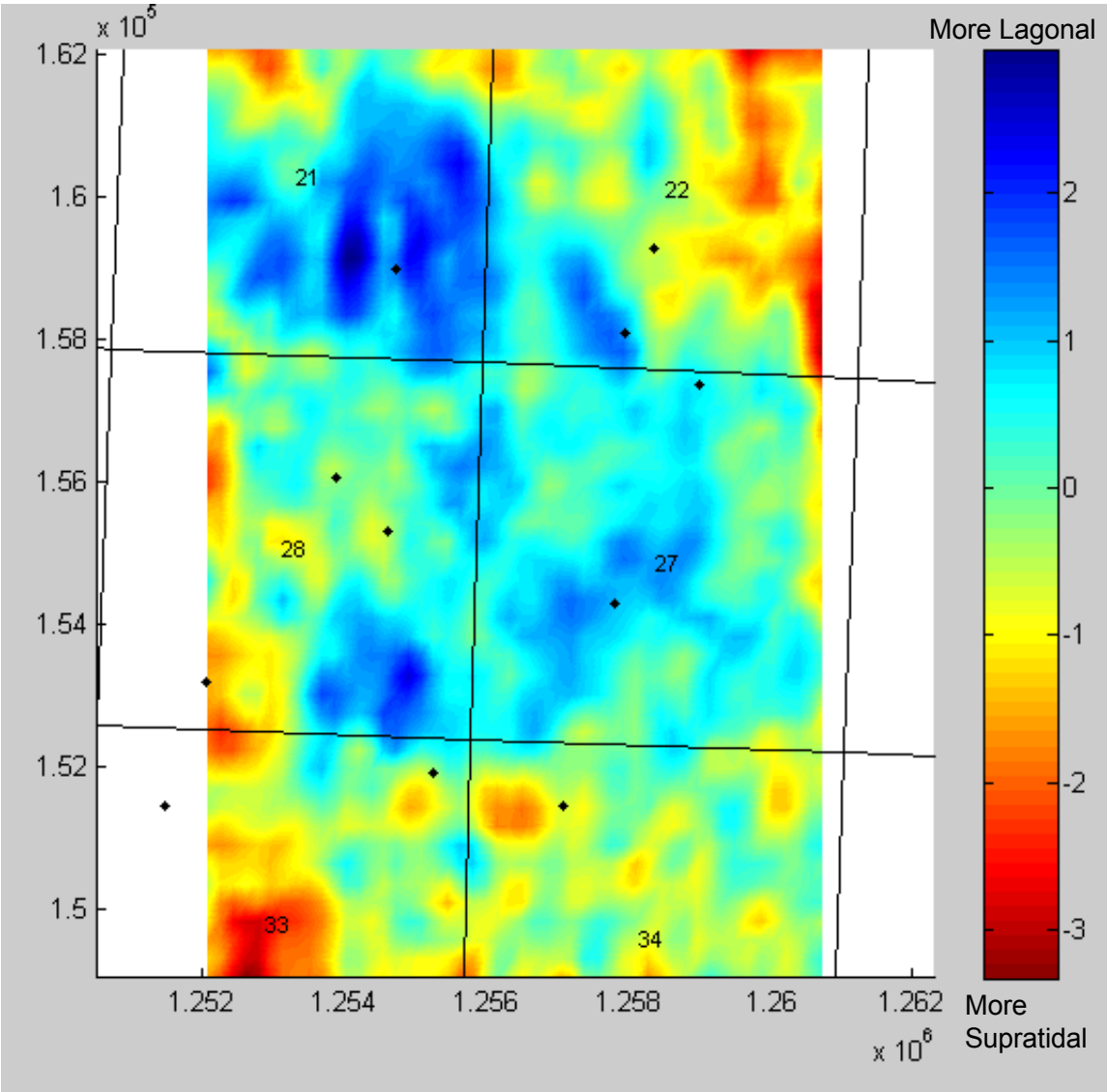

Figure 6-22. Inferred facies map - Red River B Dolomite, Cold Turkey Creek Field, based on seismic transforms of B Cycle and C anhydrite thickness. Scale is standard deviation from mean.

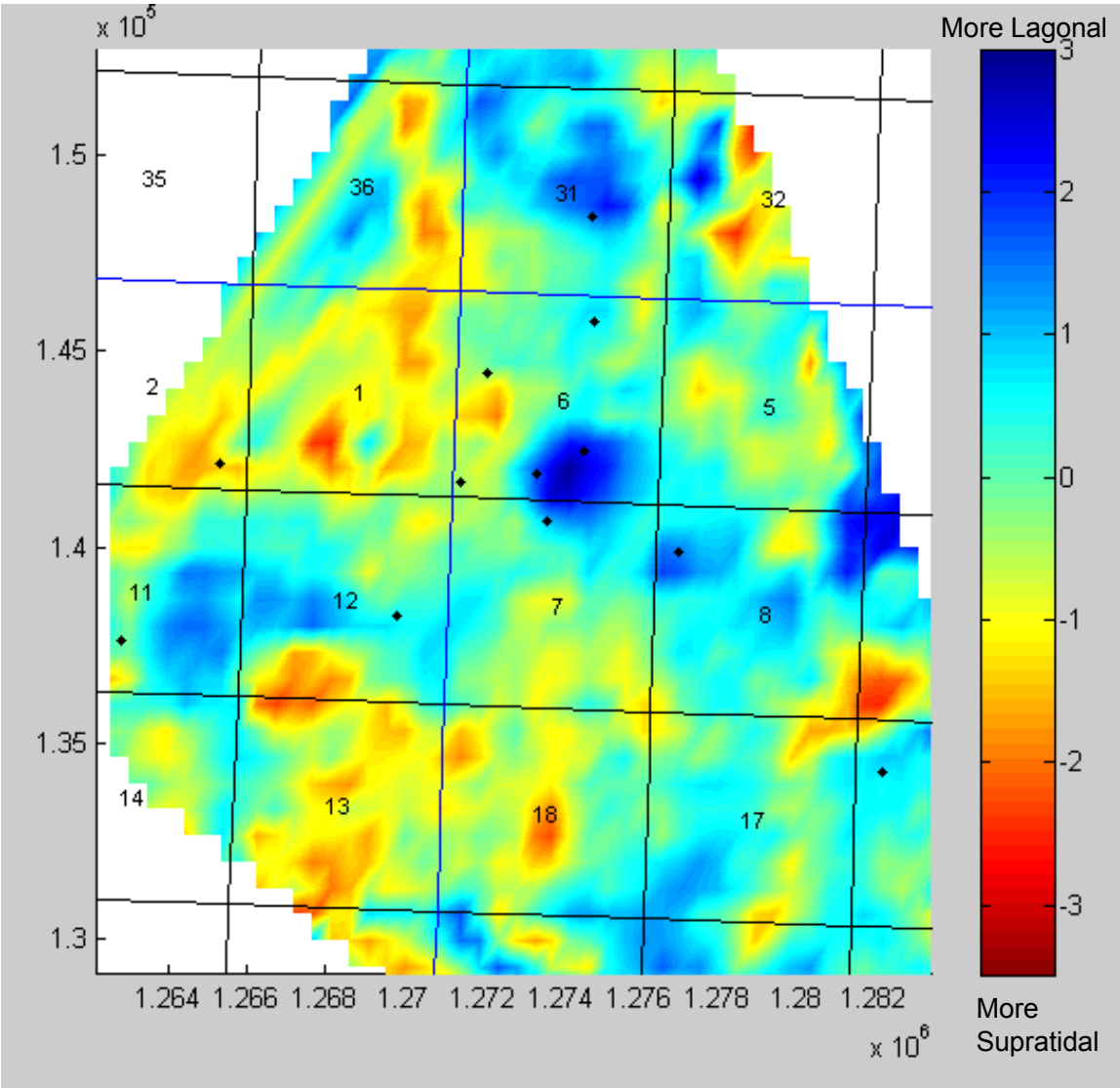

Figure 6-23. Inferred facies map - Red River B Dolomite, Grand River Field, based on seismic transforms of B Cycle and C anhydrite thickness. Scale is standard deviation from mean.

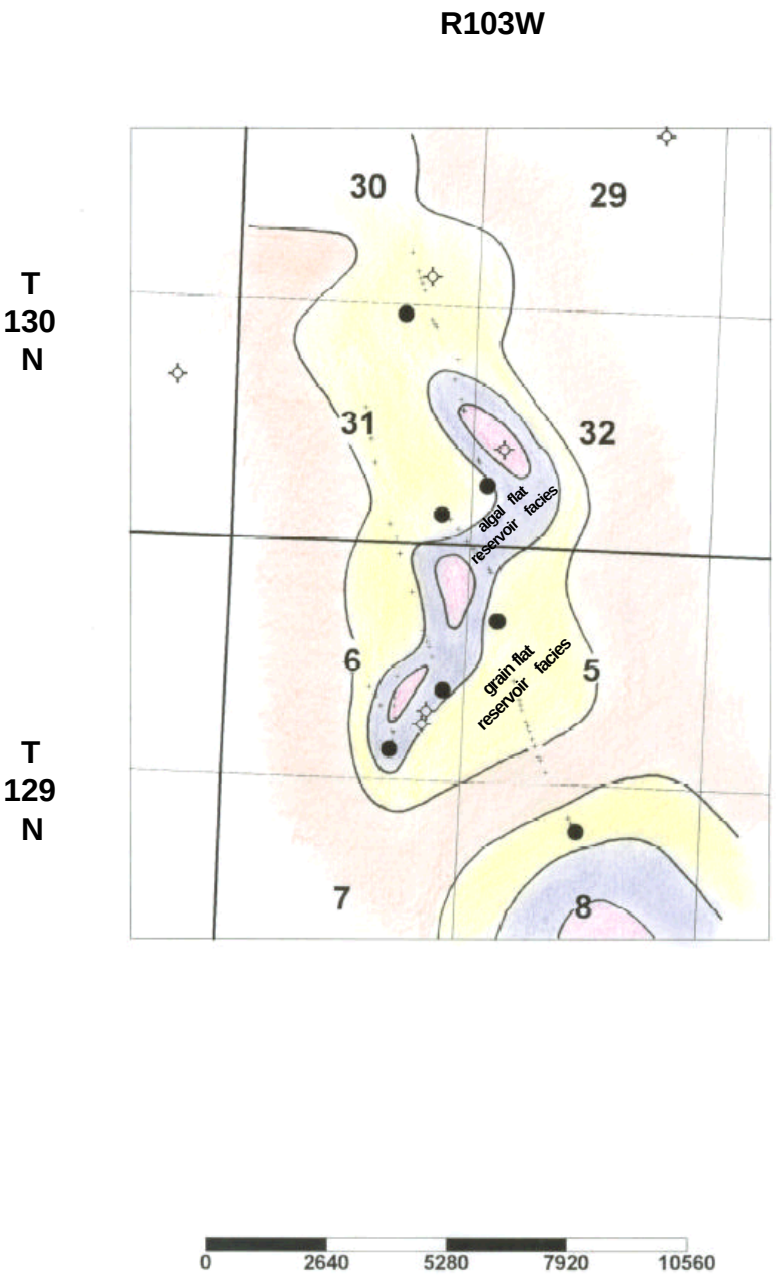

Figure 6-24. Conceptual facies map - Red River B Dolomite, Amor Field, Bowman County, North Dakota.

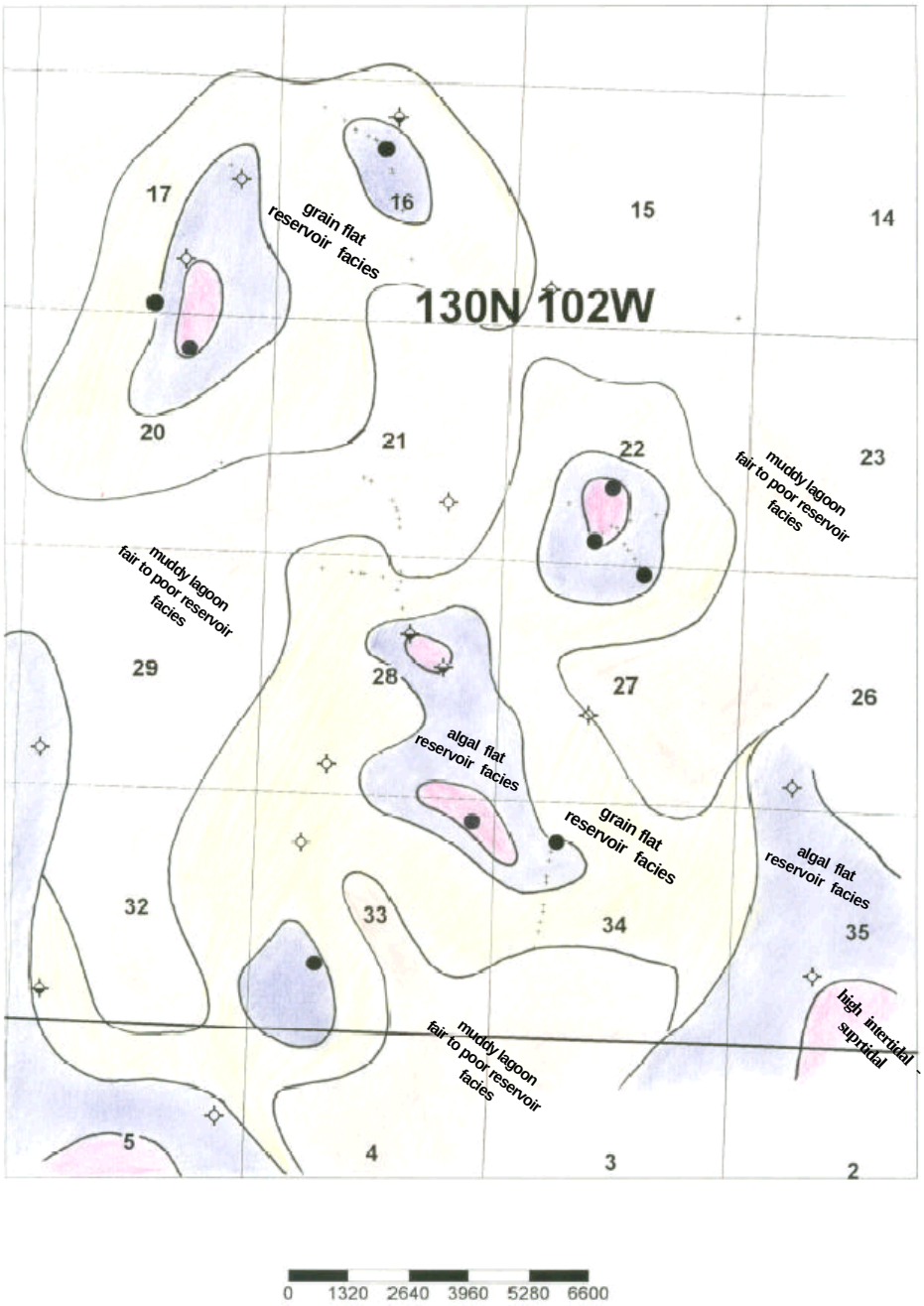

Figure 6-25. Conceptual facies map - Red River B Dolomite, Cold Turkey Creek Field, Bowman County, North Dakota.

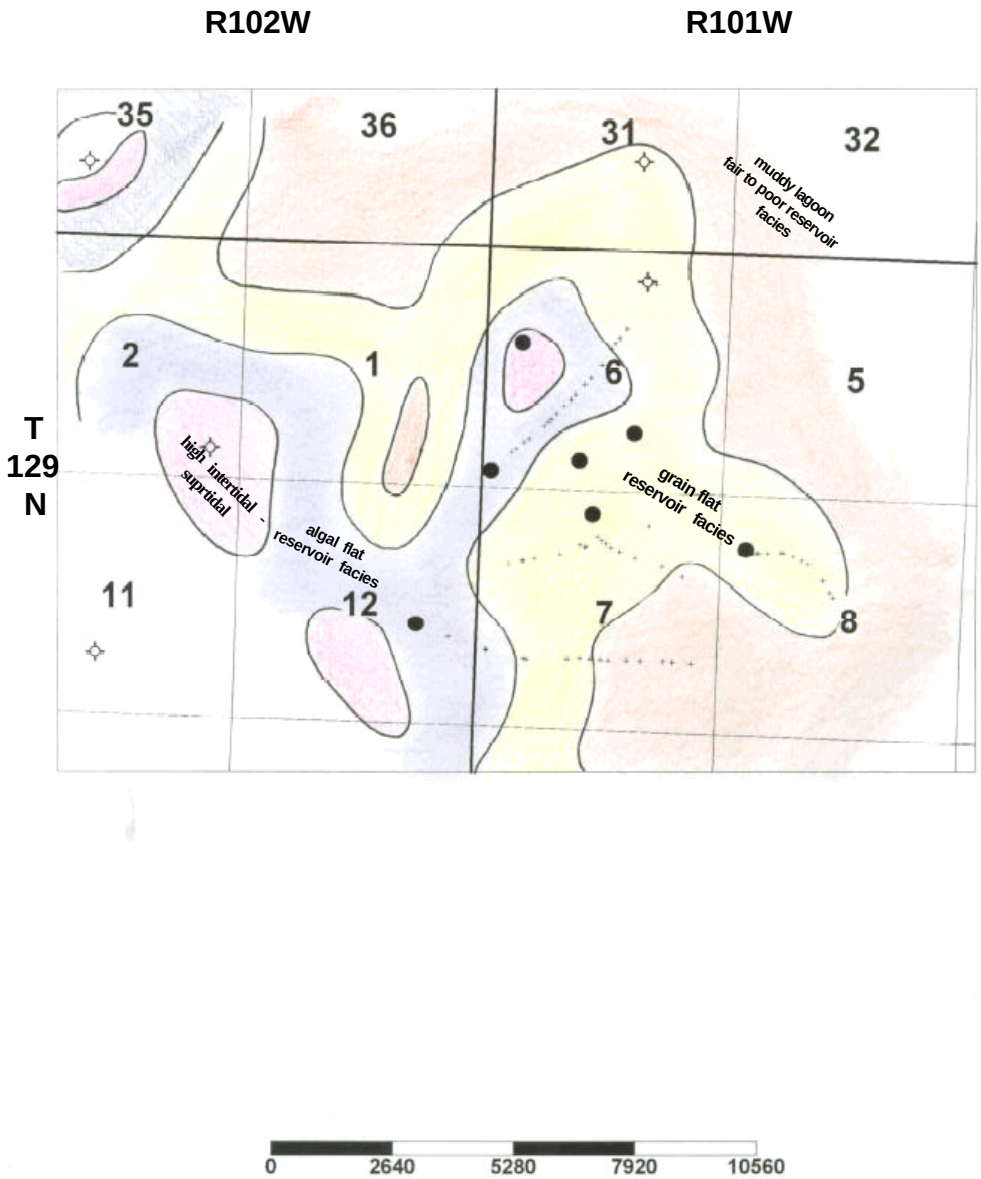

Figure 6-26. Conceptual facies map - Red River B Dolomite, Grand River School Field, Bowman County, North Dakota.

Appendix A on CD-ROM

Report: “Red River “B” Facies, Stratigraphy, and Reservoir Characteristics, Bowman County, North Dakota”, Lyn Canter
Core photographs: Ernest Fossum 1-24, T130N, R104W, Red River B
Core photographs: Schaaf 1-6, T129N, R103W, Red River B
Core photographs: Muslow State B-27, T130N, R102W, Red River B
Core photographs: Abrahamson J-31, T130N, R101W, Red River B
Core photographs: Abrahamson J-12, T129N, R102W, Red River B

Analytical Rock-Typing, Red River B Zone

Statistics obtained from well logs show that net porosity interval of the Red River B Zone has an average thickness of 8 ft +/- 2 ft. Dividing the Red River B Zone into upper and lower intervals based on well-log character indicates an average upper B thickness of 3.8 ft +/- 1 ft and an average lower B thickness of 4.3 ft +/- 2 ft. Well-log porosity-thickness (phi-h) averages 1.2 ft +/- 0.5 ft for the total B Zone. Based on an average thickness of 8.1 ft, the average porosity of the gross Red River B reservoir interval is about 15 percent. Statistics from drill-stem tests from the Red River B indicate average transmissibility (kh/uB) of 30 md-ft/cp +/- 4 md-ft/cp. An example of the Red River B Zone interval from well-log and core data is shown in **Figure 7-1**. The left side of the figure shows neutron-density porosity from wireline logs and porosity from core plugs at 0.5-ft intervals. The right side of the figure shows rock-quality index (RQI) from core porosity-permeability plotted with bulk-volume of water (BVW) from well-log porosity and water saturation. Rock-quality index (RQI) is computed from the square-root of the permeability-porosity ratio. The Red River B Zone is divided into general lithologies from visual study of the core, which are annotated on the far-right side of the figure.

Core reports of porosity and permeability from 12 wells in Bowman County, ND and Harding Co., SD indicate a difference in upper and lower Red River B Zone properties. Dividing the Red River B Zone core data into an upper and lower B rock-type by well-log character indicates that the average porosity for the upper lithology is about 22 percent while the lower lithology has an average porosity of about 16 percent. The greatest difference in the two lithologies is permeability. The average permeability for the upper B lithology is about 12 md and for the lower B lithology it is about 3 md. The average RQI is 8 and 4 for the upper B and lower B, respectively. The RQI is indicative of pore-throat size and tortuosity, which are both related to capillary pressure characteristics.

Sorting the core porosity-permeability data by RQI and plotting the data for the lower B lithology in conventional fashion yields the cross-plot shown in **Figure 7-2**. For 20 percent porosity, a permeability of 2 md is expected. A plot of porosity and permeability for the upper B lithology is shown in Figure 3 where it can be seen that permeability of 10 md corresponds to 20 percent porosity.

Special core analysis for capillary pressure further supports the contrast of functional reservoir properties within the upper and lower Red River B lithologies. Shown in **Figure 7-4** are capillary pressure with saturation relationships for representative samples from the upper and lower B. An upper-bound sample from the upper B with a RQI of 16 is contrasted with a lower-bound sample from the lower B with a RQI of 2. Based on these data, empirical relationships for other RQI rock-types of 2, 5, 10, 15 and 20 were generated and also shown graphically on **Figure 7-4**. Effective pore-throat size (radius) can be determined from the capillary pressure data and are labeled in microns with RQI for each

capillary-pressure curve. The effective pore-throat radius for typical upper B lithology is an order-of-magnitude greater than for the typical lower B lithology (3 microns for upper B and 0.3 microns for lower B).

Capillary pressure data is commonly transformed to a theoretical height above a free-water contact for the reservoir oil-water system. Converted capillary pressures to height for upper and lower B are shown in **Figure 7-5**. It can be observed on this plot that for lower B lithology, with RQI of 2 and pore-throat radius of 0.3 microns, a reservoir height of over 100 feet is required before oil can occupy the pores. For upper B lithology where RQI is 16 and at a reservoir height of 100 feet, the pores will be filled with oil to nearly irreducible water saturation. These rock-type attributes explain why water saturation in the lower B Zone is much higher than in the upper B Zone. Referring back to **Figure 7-1**, the computed bulk-volume-water (BVW) is dramatically greater in the lower B wackestone than the adjacent upper B grainstone-packstone although both well-log and core porosity are very similar.

Predicting an optimal setting for the Red River B Zone has been accomplished by working with interval thickness of the B Cycle and the underlying C Anhydrite. **Figure 7-6** shows a type-log over the Red River B Zone that is annotated for the B Cycle and C Anhydrite intervals. The thickness of these intervals was determined from over 300 wells in the Bowman-Harding area and then ranked from 0 to 1 as most lagoonal to most supratidal. **Figure 7-7** shows the ranking of depositional setting based on this sort-rank method. A depositional rank was then assigned to each well in a well database. Correlations for production attributes with this depositional rank were then performed. Production attributes from wells indicate an optimal depositional ranking of 0.60 to 0.65 where the thickness for the B Cycle ranges from 44 to 50 ft. This represents a depositional setting that is dominantly intertidal.

Average oil production over the first 24 months from 40 wells was plotted with the depositional ranking as described in the previous paragraph. The trend-fit of the data are shown in **Figure 7-8** where a peak oil rate of 65 bbl per day occurs at a ranking of 0.60. Average oil rates decrease on either side of this value.

In similar fashion, transmissibility (kh/uB) from drill-stems tests was plotted with depositional rank. The trend-fit of these data are shown in Figure **7-9** where it is observed that a peak transmissibility of 35 md-ft/cp occurs at a depositional ranking of 0.65. As with oil rate, drill-stem tests indicate a decrease in transmissibility on either side of the 0.65 ranking.

Lastly, Red River B Zone storage (phi-h) from digitized well-log data were plotted with the corresponding depositional rank and are shown in Figure **7-10**. The trend of the data show a marked decrease in storage as the depositional rank approaches a value of 1.0 (most supratidal). This is logical, as the interval becomes very thin with anhydrite plugging of the pores. Red River B Zone

storage increases with the ranking trend toward more intertidal and lagoonal settings. Values for storage reach a plateau at a depositional ranking of 0.50 to 0.60.

Plotted trends of dynamic production attributes with depositional rank indicate there is an important relationship for reservoir development in the Red River B Zone and depositional setting. The depositional setting for the Red River B Zone ranges from lagoonal to supratidal with optimal reservoir properties developing in an intertidal setting. It is concluded from these observations that predicting the B Cycle and C Anhydrite thickness can aid in successful exploitation of Red River B Zone reservoirs. This can be accomplished by mapping these intervals from well-log data and seismic-attribute transforms. **Figure 7-11** shows a plot of predicted B Cycle thickness from seismic attributes and measured thickness from well logs at one 3D seismic survey in Bowman County, North Dakota. The figure shows a good correlation of predicted and measured B Cycle thickness at a 50 percent confidence interval of +/- one-ft. Because the variation of these intervals is subtle, it is advisable to use seismic transforms as relative, not absolute, for indications of depositional setting. For areas where there is no well control, it is recommended to use seismic transforms as an aid to avoid areas that appear most supratidal (thin) or lagoonal (thick). With well control, the seismic attribute transforms can be used as a guide to drilling in the most favorable depositional setting by comparison of seismic transforms and well-log thickness. If a well is located in either a poor supratidal or lagoonal setting, the seismic can guide where to drill other wells, or a horizontal from the existing well, to areas that have a more intertidal setting.

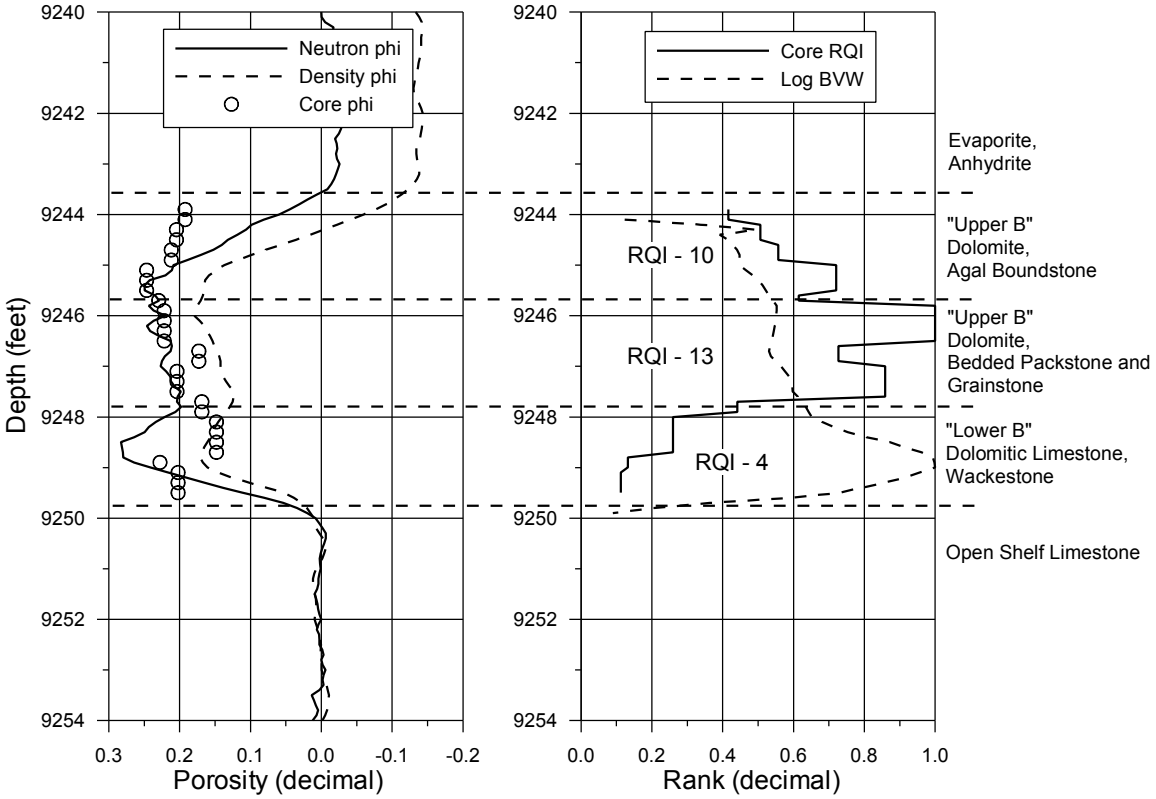

Figure 7-1. Plot of well-log and core attributes from Red River B intervals at the Abrahamson J-12, Sec. 12, T129N, R101W.

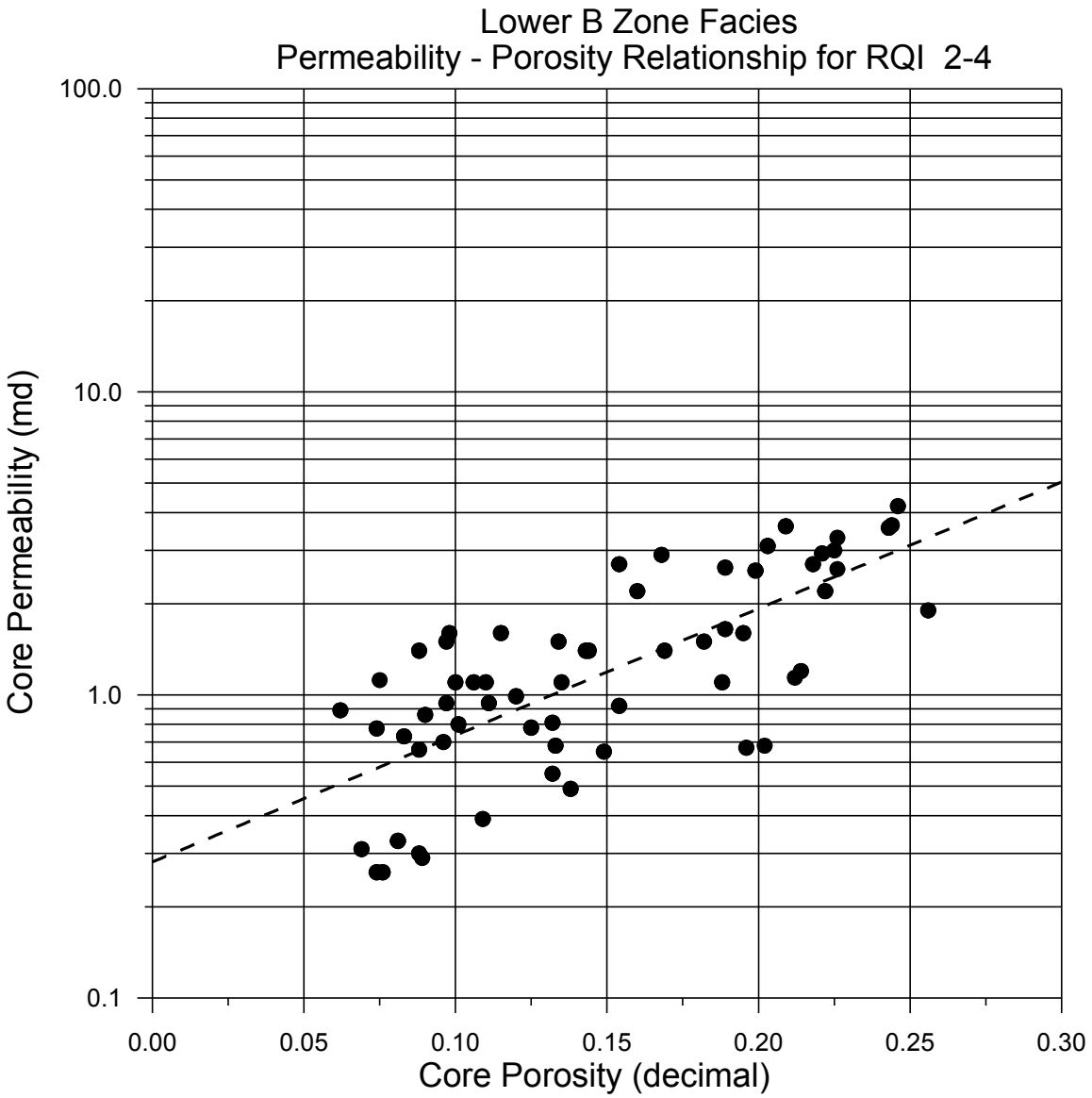

Figure 7-2. Plot of core porosity and permeability relationship for typical Red River lower B lithology.

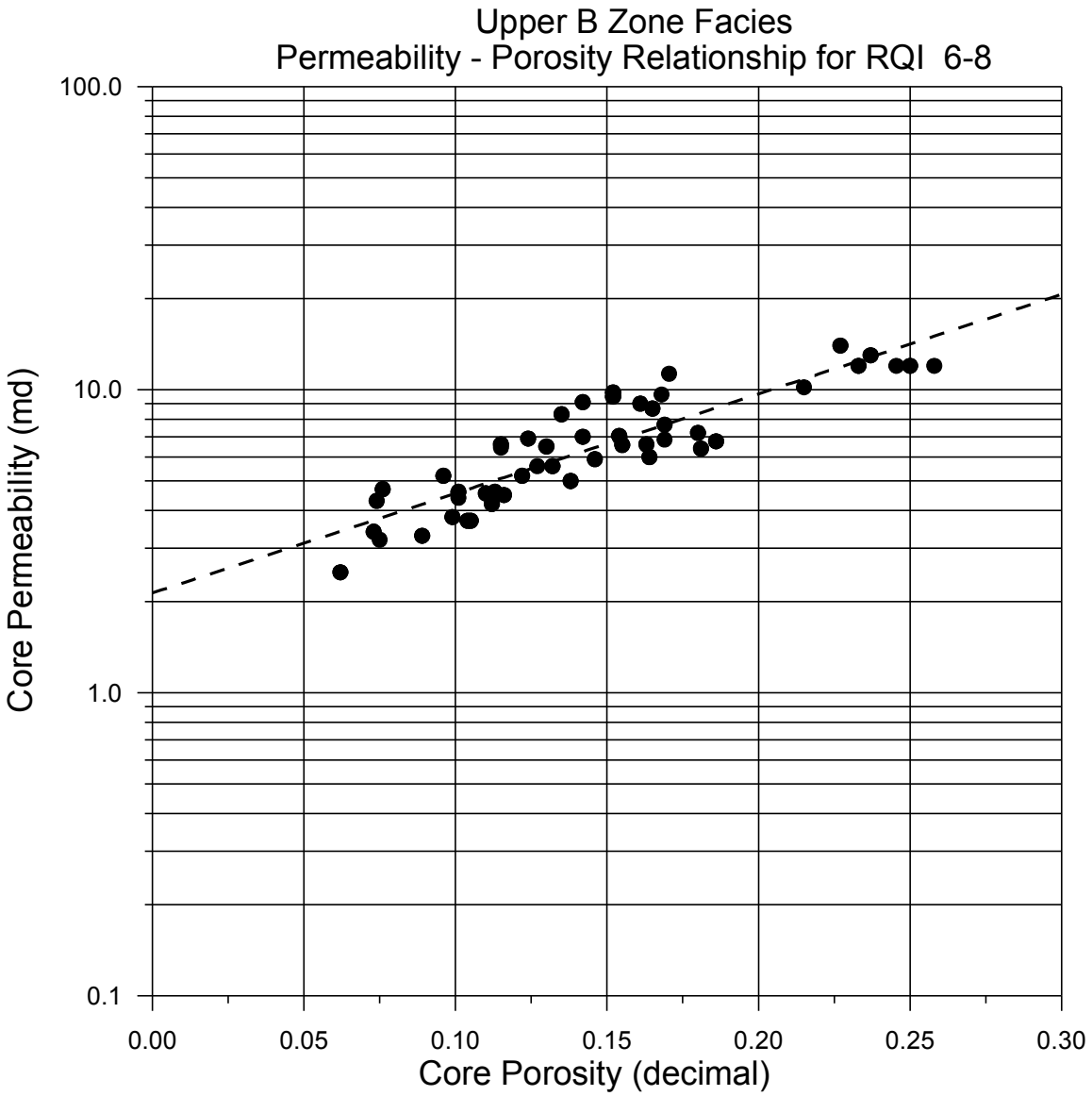

Figure 7-3. Plot of core porosity and permeability relationship for typical Red River upper B lithology.

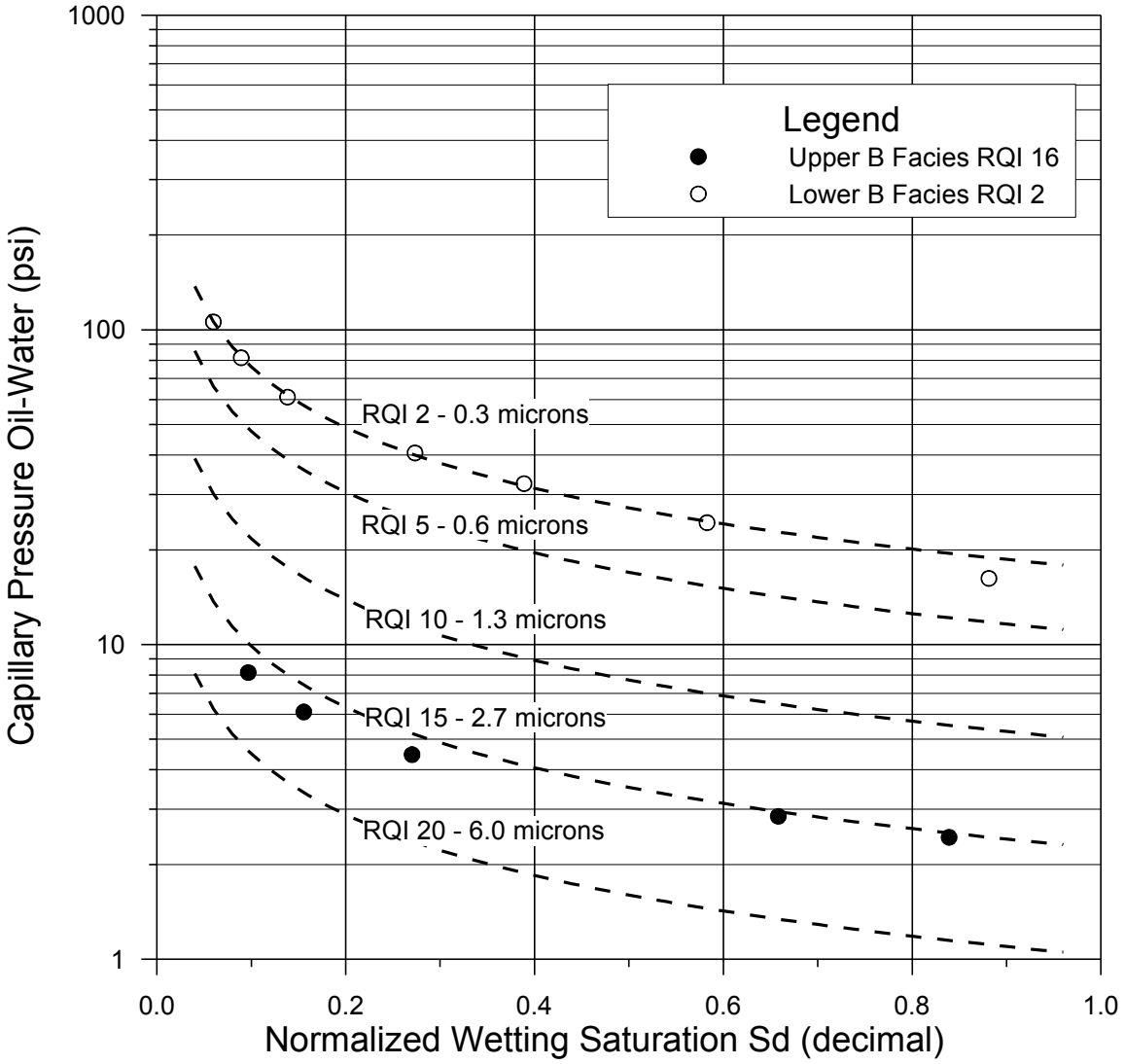

Figure 7-4. Plot of capillary pressure relationships for typical Red River B lithology.

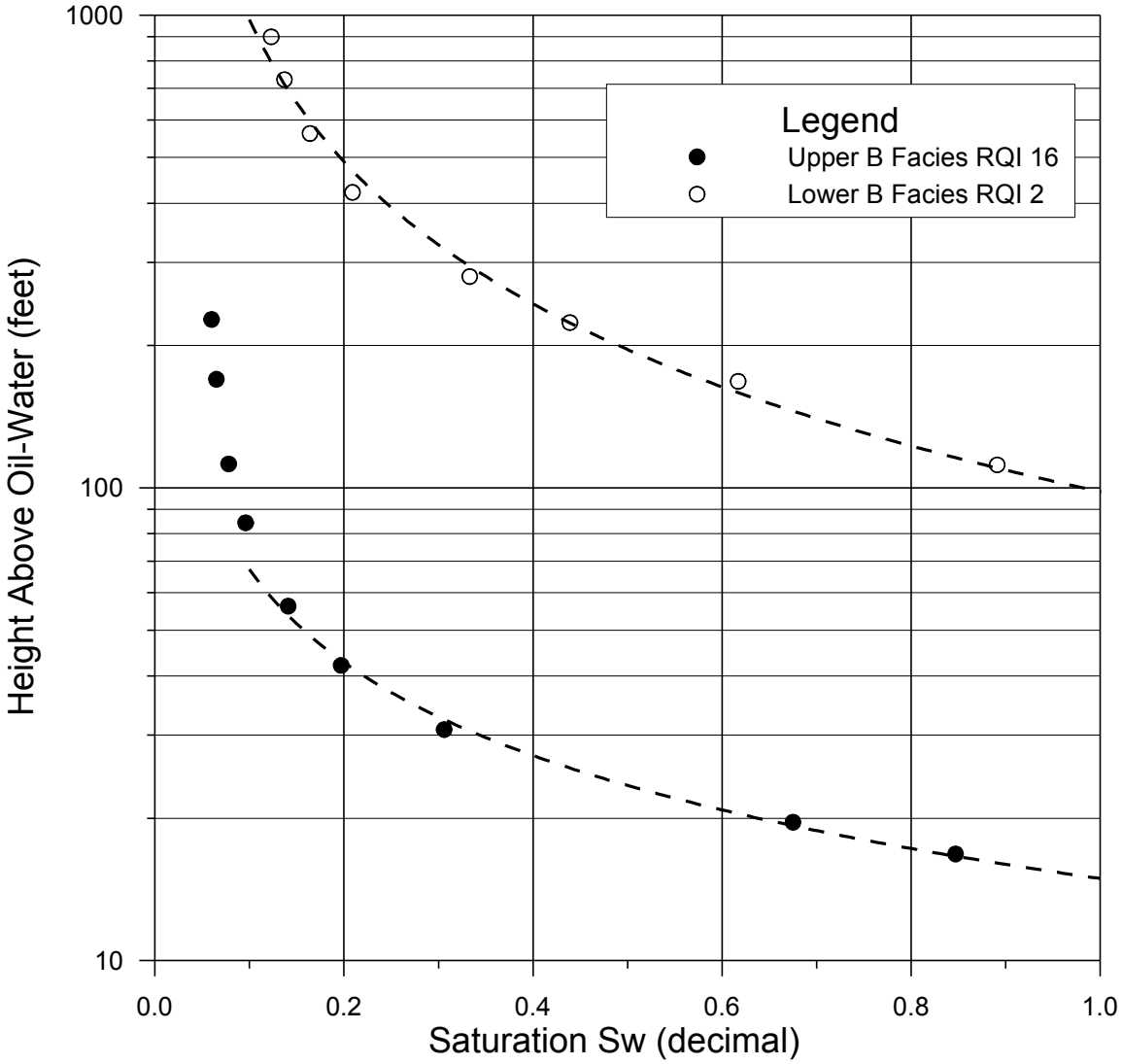

Figure 7-5. Plot of computed height above free water contact for typical Red River upper and lower B lithology.

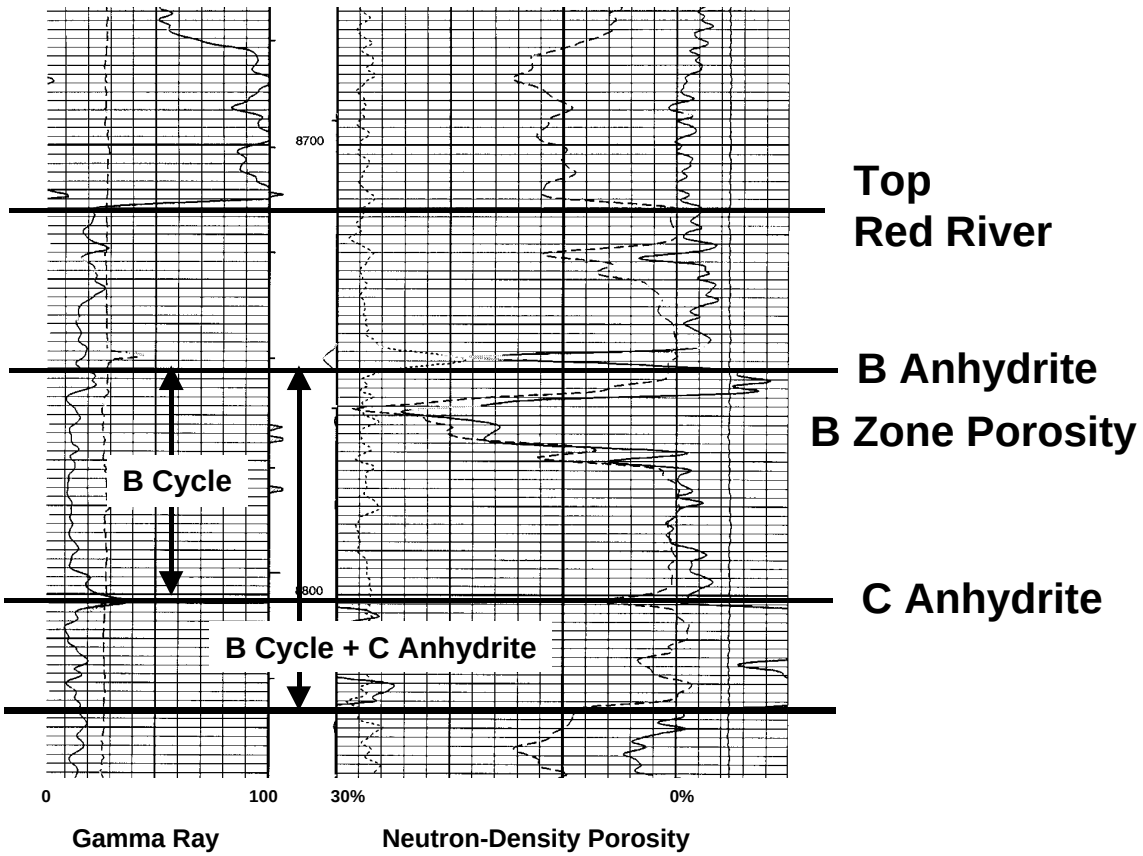

Figure 7-6. Type log for the Red River B Zone and B Cycle from Bowman County, North Dakota.

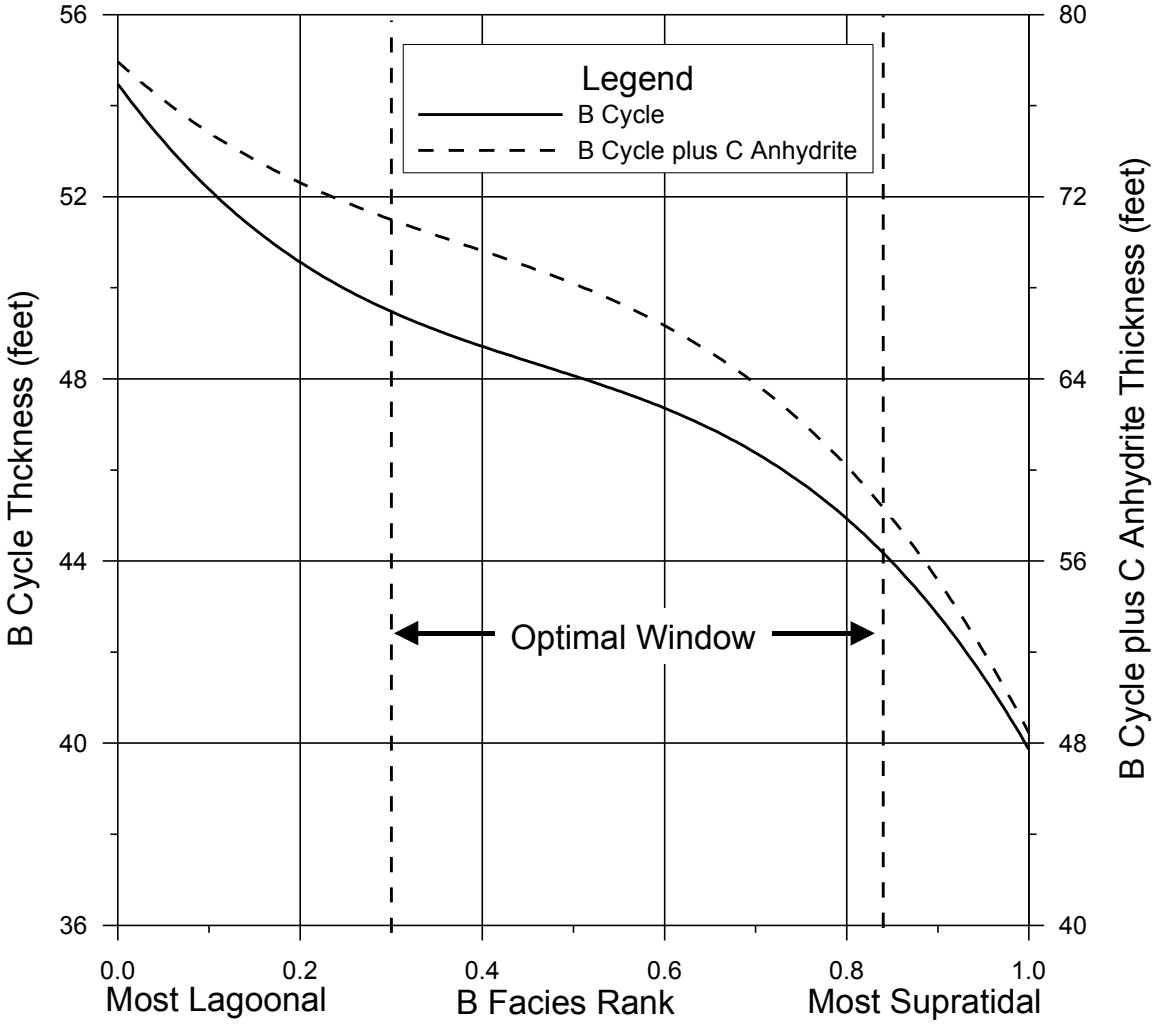

Figure 7-7. Ranking of Red River B depositional setting based on interval thickness of B Cycle and C Anhydrite.

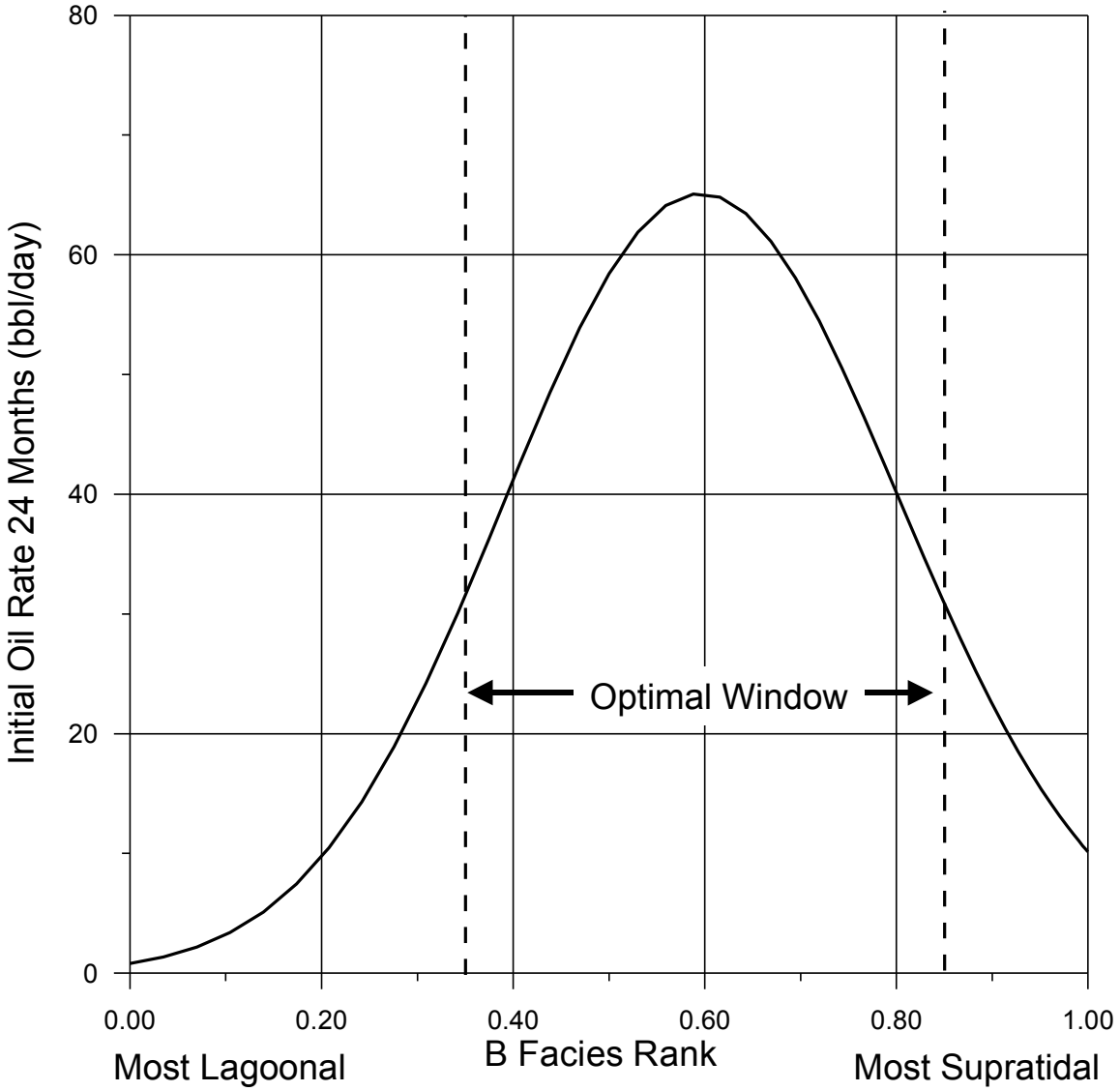

Figure 7-8. Oil production from vertical wells as a function of depositional setting based on interval thickness of B Cycle and C Anhydrite.

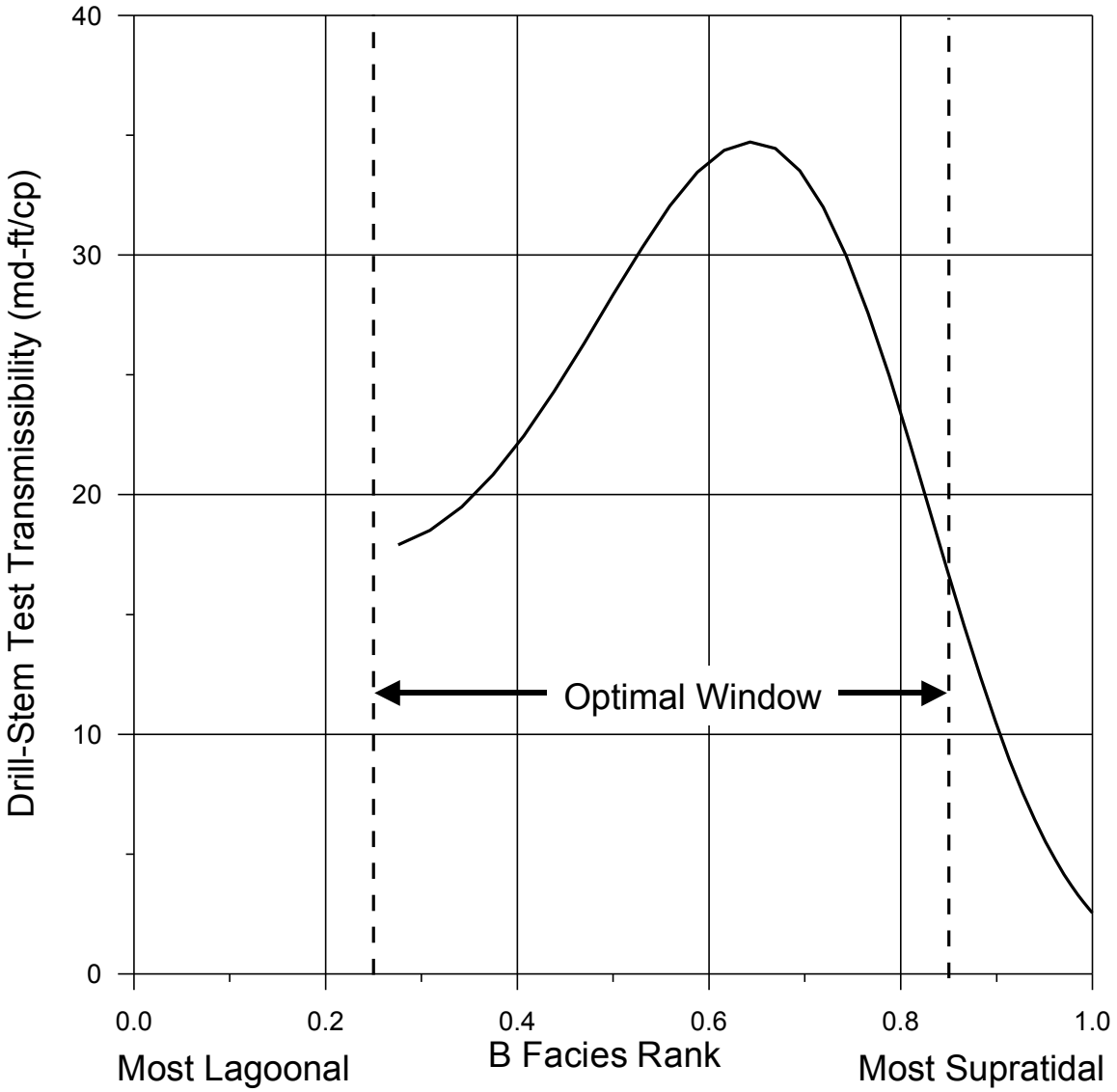

Figure 7-9. Transmissibility based on drill-stem tests as a function of depositional setting based on interval thickness of B Cycle and C Anhydrite.

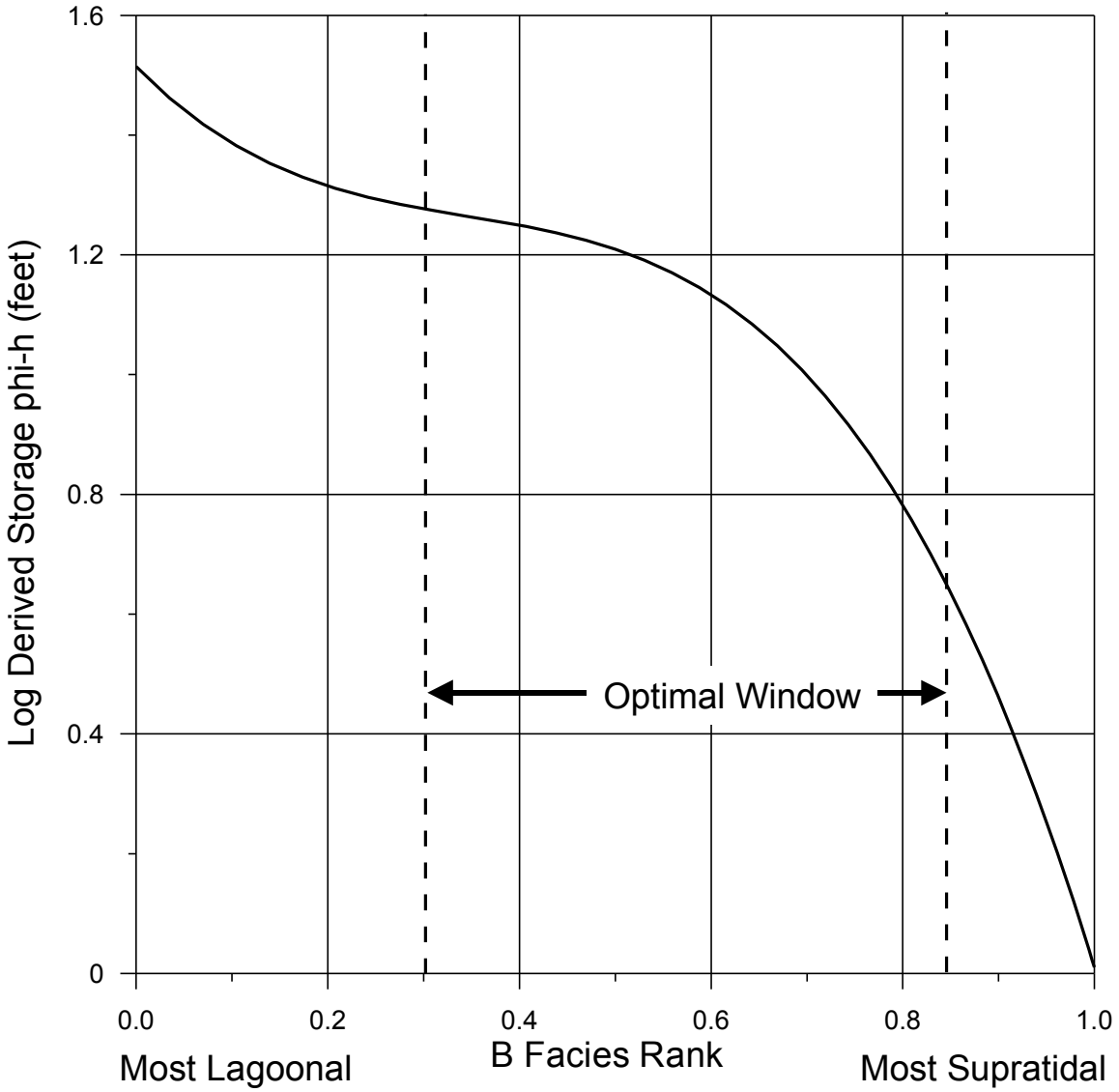

Figure 7-10. Red River B storage (phi-h) from well logs as a function of depositional setting based on interval thickness of B Cycle and C Anhydrite.

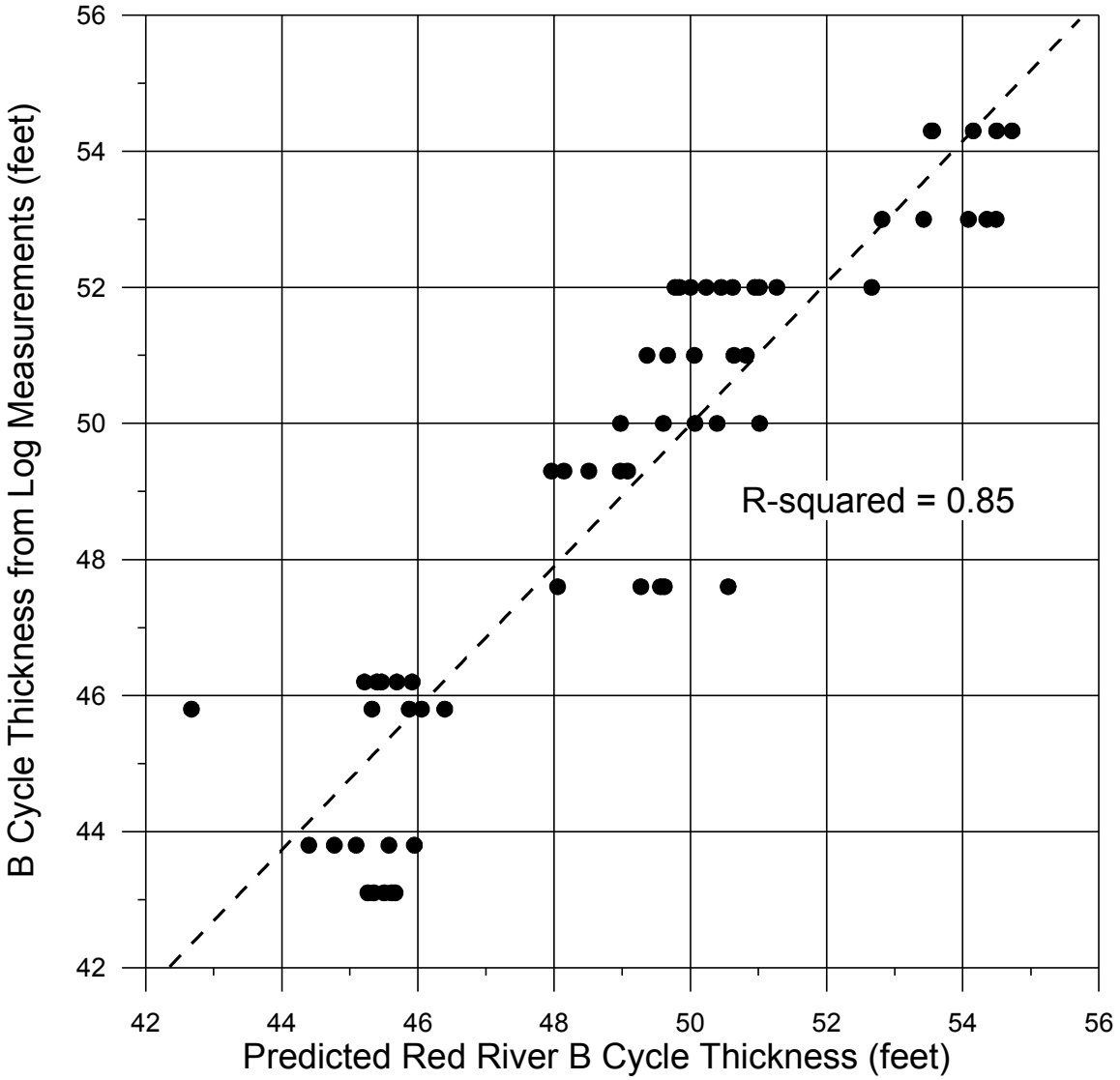

Figure 7-11. Plot of Red River B Cycle thickness predicted by seismic attribute transforms and measured thickness from well logs at one seismic survey in Bowman County, North Dakota.

Appendix B on CD-ROM

Core Laboratories, Core Analysis Report for Abrahamson J-12
Core Laboratories, Core Analysis Report for Abrahamson J-31
Core Laboratories, Advanced Rock Properties Study for Abrahamson D-8
Core Laboratories, Advanced Rock Properties Study for Abrahamson J-12
Core Laboratories, Advanced Rock Properties Study for Muslow-State B-27
BJ Testers, Drill-stem Test Report for Abrahamson J-12 B Zone

Analytical Rock-Typing, Red River D Zone

The Red River D Zone is the lower-most porosity member in the Upper Red River that is oil productive in the Bowman County, North Dakota and Harding County, South Dakota areas of the southwestern Williston Basin. The top of the D zone porosity occurs at about 175 feet below the Stony Mountain shale that overlies the Red River formation. The D Zone porosity has an average gross thickness of about 45 feet. The depositional cycle consists almost entirely of burrowed carbonate mudstones and skeletal wackestones with some interbedded organic-rich kerogenite (Longman, Fertal and Stell, 1992). From well-log analysis, the average porosity is 14.6 percent with a net thickness of 17.6 ft. Productive porosity has permeability, at the geometric mean, of 5.3 md.

Based on drill-stem test and production flow rates throughout the Bowman-Harding area, the greatest productivity from the D Zone is found where the D cycle is thickest. Several investigators have stressed the importance of mechanism and degree of dolomitization on the development of porosity and permeability in the D Zone sediments (Carroll, 1978; Gerhard et al, 1982; Kohm and Louden, 1988; Longman et al, 1992). It appears, however, that a prerequisite for reservoir development is a sediment layer that hosted a healthy environment for burrowing fauna. This environment is a more lagoonal setting off the flank of paleo structures. Predicting the occurrence of a lagoonal setting can be accomplished by mapping the combined C and D cycle thickness from the top of the C Anhydrite to the kerogenite bed at the base of the D Zone. Seismic attributes of amplitude and time isochron can be used to predict a thick D cycle thickness (Sippel et al, 1997).

The sediments that comprise the D Zone are similar throughout the vertical section. Petrographic description and photographs from ten wells in the area indicate a mottled appearance. The mottled texture is the result of large branching *Thalassinoides* burrows and small, circular *Planolites* burrows. The *Planolites* commonly demonstrate burrow within burrow morphology. In well-developed reservoir intervals, the interior of burrow structures and the surrounding mud matrix were partly to completely dolomitized. Burrow structures are preferentially dolomitized throughout. Skeletal fragments are crinoids, sparse brachiopods and occasional corals.

Typically, the D Zone cycle consists of two porosity units that can be correlated between the majority of wells in the area. The upper porosity bench is generally thinner and with less porosity-permeability that the lower bench. Reservoir storage in the D Zone is typically one-third (1.16 porosity-feet) in the upper bench and two-thirds (2.36 porosity-feet) in the lower bench. At the base of the D Zone oil-productive porosity there is a consistent thin, shaley kerogenite bed. A thin kerogenite bed is also found overlying the top of the D Zone porosity.

An analytical core study was performed for the Red River D Zone at the Hansen C-7 well, Grand River Field, Bowman County, North Dakota (API 33-011-00914). Conventional porosity-permeability measurements were supplemented with capillary-pressure tests. The Red River D Zone was initially completed as oil-productive in this well. Reservoir development of the Red River D Zone at the Hansen C-7 well is an excellent example and typical of good producers from this reservoir unit.

A total of 56 plugs were taken at one-ft intervals from the core obtained at the Hansen C-7 well. The recovered core interval is from 9410-66 ft and covered all of the D Zone. Porosity and permeability measurements were made for each plug from which a rock-quality index (RQI) was computed as the square-root of the permeability-porosity ratio (k/phi). The RQI is indicative of pore-throat size and tortuosity, which are both related to capillary pressure characteristics.

A type-log of the Red River D Zone at the Hansen C-7 well is shown in **Figure 8-1**. On the left side of the figure are porosity measurements from wire-line tools. On the right side of the figure is the computed RQI from core plugs and water saturation from wire-line measurements. The best reservoir development occurs in the middle of the lower D Zone porosity unit. This is typical for cores taken in the D Zone.

Clustering the log porosity and core porosity-permeability data produces a type-log as shown in **Figure 8-2**. The figure shows two cluster groups each for the upper and lower D Zone. The “stratigraphic layers” defined by cluster similarity would be useful for reservoir simulation studies. They also define “functional” rock-types of porosity, permeability and capillary properties.

A cross-plot of permeability with porosity is shown for upper and lower D Zone samples in **Figure 8-3**. It is observed from the plot that the upper and lower D Zone samples are overlapping and produce the same trend. A cross-plot of RQI with porosity from core measurements is shown in **Figure 8-4** that also exhibits a reasonably well-behaved trend for all the data. The RQI from the upper and lower D Zone units overlap and increases with porosity. From this analytical approach, it is concluded that the upper and lower D Zone units have similar pore systems and could be classified as being of the same rock-type.

Special core analysis for capillary pressure was performed on 10 samples. From these measurements, typical capillary pressures for a range of RQI and wetting-phase saturations were computed and are shown graphically in **Figure 8-5**. Empirical relationships for RQI of 2, 5, 10, 15 and 20 were generated and are overlain on actual core-plug measurements. There are two significant conclusions that can be made from the data and curves shown in **Figure 8-5**. Regardless of porosity, RQI or stratigraphic depth, the capillary data points from all samples indicate a bi-modal pore system. Second, all samples indicate an increasing capillary pressure trend with decreasing porosity.

From a macro perspective, the D Zone consists of one bi-modal rock-type and maybe divided into functional layers on the basis of porosity. Variations in reservoir quality are rooted in the degree of burrowing by *Thalassinoides* and *Planolites* fauna and the efficiency of subsequent dolomitization. The best reservoir development generally occurs in the middle of the lower D Zone unit where resident time of dolomitizing solution may have been greatest and the RQI often exceeds 10. Exploration and development strategies for the D Zone should focus on identification of a depositional setting that was favorable for the burrowing fauna to produce large colonies and also the infiltration and percolation of dolomitizing solution. Such a setting was in the quiet, low-lying areas below wave action and off-flank from paleo structures.

The bi-modal nature of the D Zone rock-type has important implications for oil recovery. The macro-micro pore system will result in low recovery efficiency of oil. The large pores will be preferentially depleted and flushed by natural water-drive or waterflooding. The oil in the smaller pores of the matrix surrounding the burrows will be essentially bypassed.

References Cited

Carrol, W. Kipp. 1978. “Depositional and Paragenetic Controls on Porosity Development, Upper Red River Formation, North Dakota.” In *The Economic Geology of the Williston Basin*, eds. Duane Estelle and Roger Miller, (Billings: Montana Geological Society, 1978 Williston Basin Symposium): 79-94.

Gerhard, Lee E., Sidney B. Anderson, J.A. Lefever and C.G. Carlson. 1982. “Geological Development, Origin, and Energy Mineral Resources of Williston Basin, North Dakota.” *The American Association of Petroleum Geologists Bulletin*, 76(8): 449-467 (August 1982).

Kohm, J.A., and R.O. Louden. 1988. “Red River Reservoirs in Western North Dakota and Eastern Montana.” In *Occurrence and Petrophysical Properties of Carbonate Reservoirs in the Rocky Mountain Region*, eds. S.M. Goolsby and M.W. Longman, (Denver: Rocky Mountain Association of Geologists): 275-290.

Longman, Mark W., Thomas G. Fertal, and James R. Stell. 1992. “Reservoir Performance in Ordovician Red River Formation, Horse Creek and South Horse Creek Fields, Bowman County, North Dakota.” *The American Association of Petroleum Geologists Bulletin*, 76(4): 449-467 (April 1992).

Sippel, M.A., K.D. Luff, M.L. Hendricks and D.E. Eby. 1997. “Reservoir Characterization of the Ordovician Red River Formation in Southwest Williston Basin, Bowman Co., ND and Harding Co., SD.” Topical Report to the U. S. Department of Energy, National Petroleum Technology Office, July 1997.

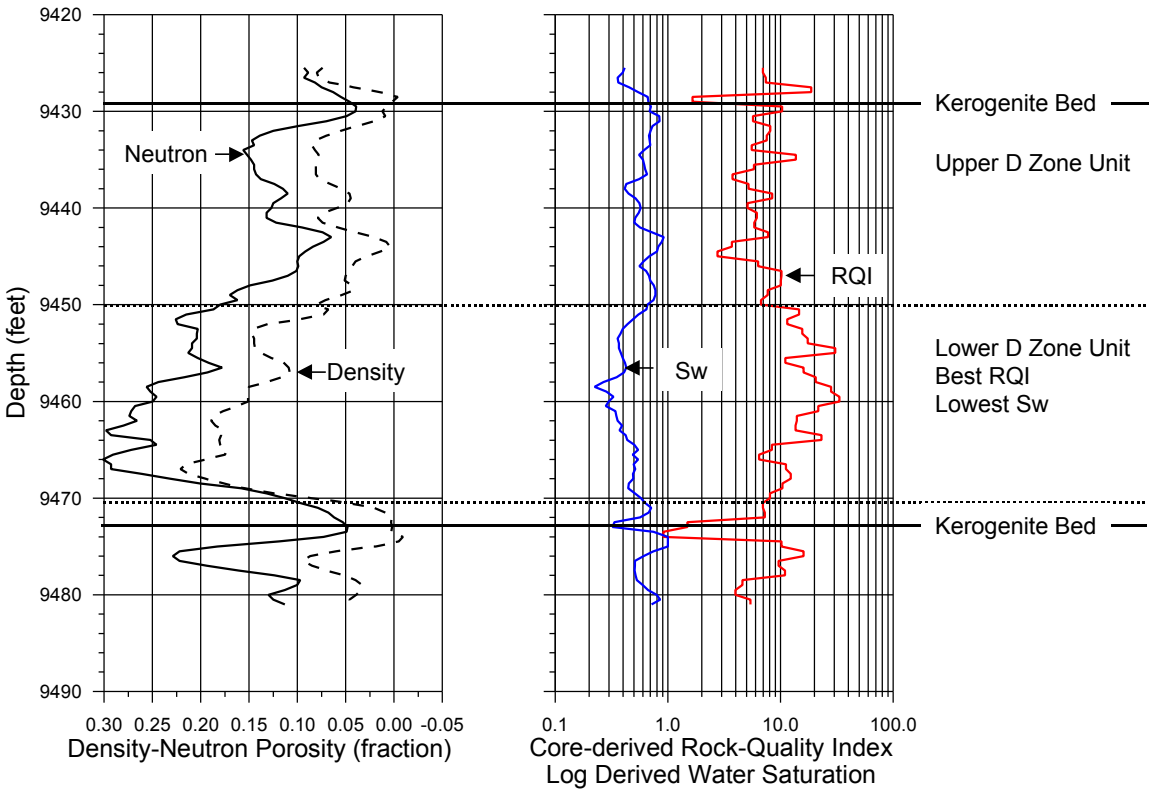

Figure 8-1. Type-log from the Hansen C-7 well in Grand River Field, Bowman County, North Dakota. The left side of the figure shows the wire-line log measurements for porosity from neutron and density tools. The right side of the figure shows the log-derived water saturation calculations and core-derived rock-quality index. The best reservoir development occurs in the middle of the lower D Zone unit.

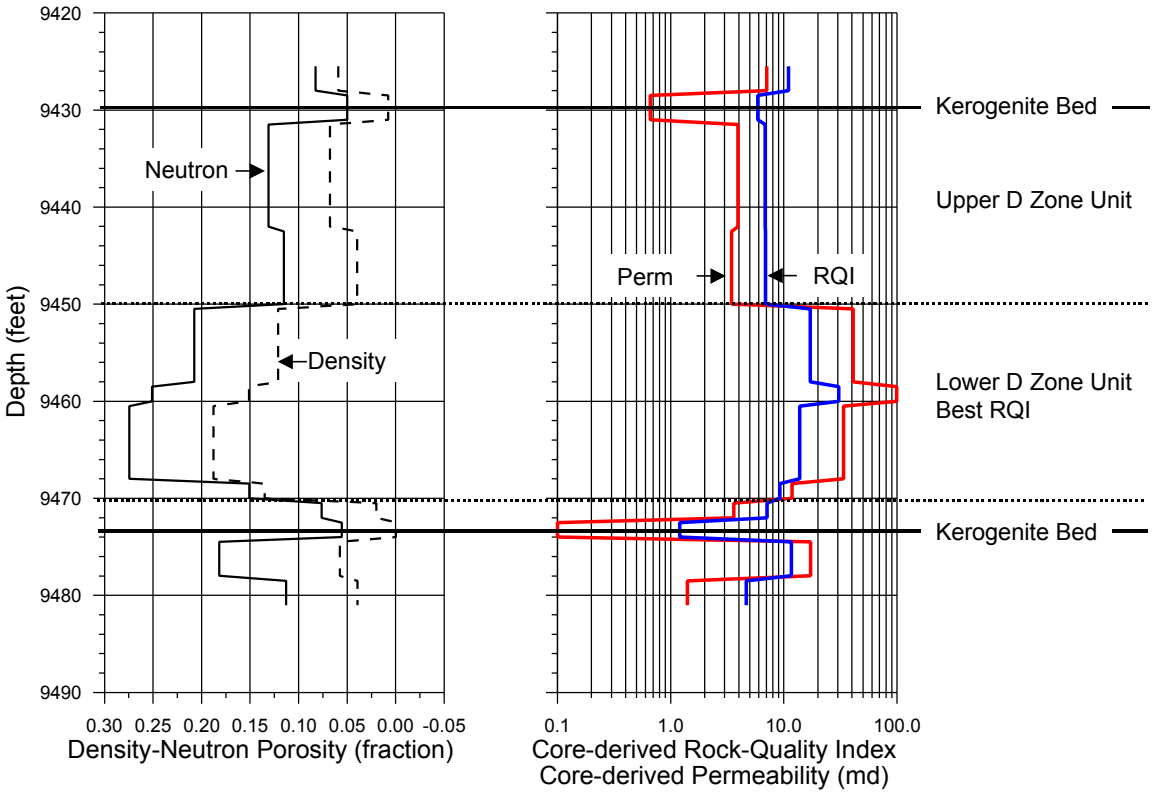

Figure 8-2. Type log for the Hansen C-7 Red River D Zone where the data have been clustered to similar groups. The upper and lower D Zone units are each divided into two stratigraphic layers by this analytical technique.

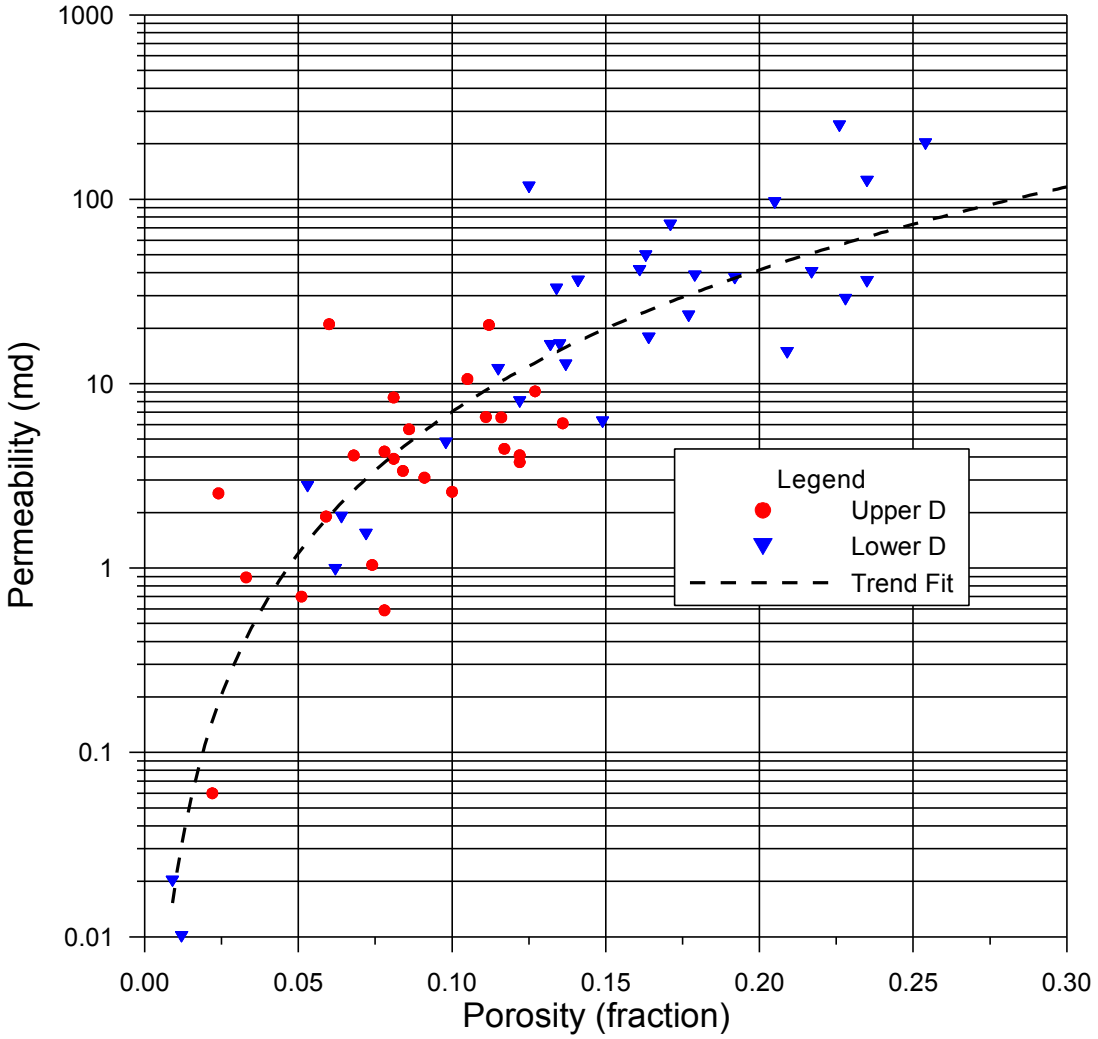

Figure 8-3. Cross-plot of porosity and permeability for the upper and lower D Zone units from the Hansen C-7 core. The data overlap and are part of the same trend. This indicates a similar pore system exists in the upper and lower D Zone units.

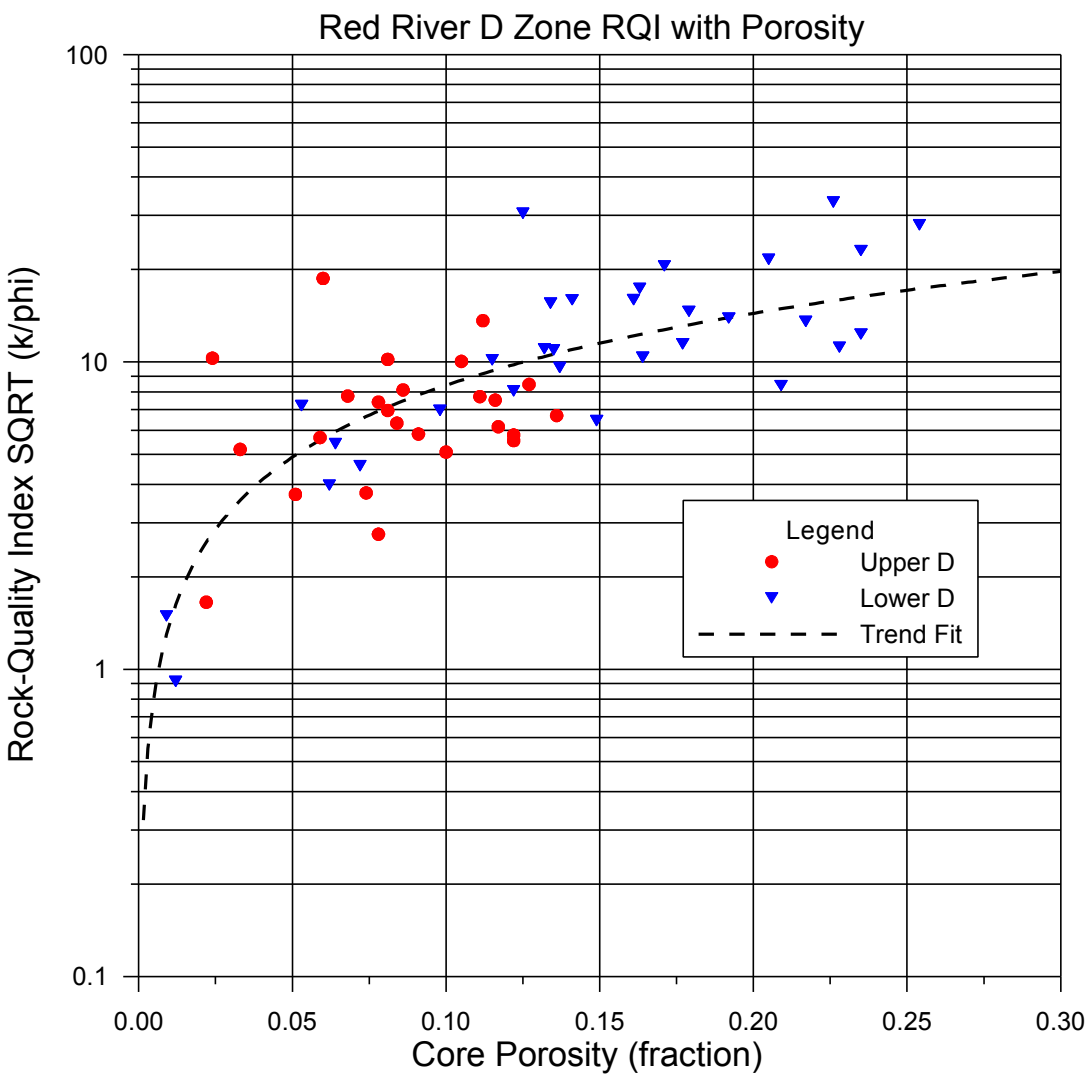

Figure 8-4. Graph of rock-quality index with porosity from measurements taken from the Hansen C-7 core. The data from the upper and lower D Zone units overlap and are part of the same trend. These common trends indicate that a similar pore system exists in the upper and lower D Zone units. RQI increases with porosity. Quality of D Zone reservoir development can be characterized by porosity.

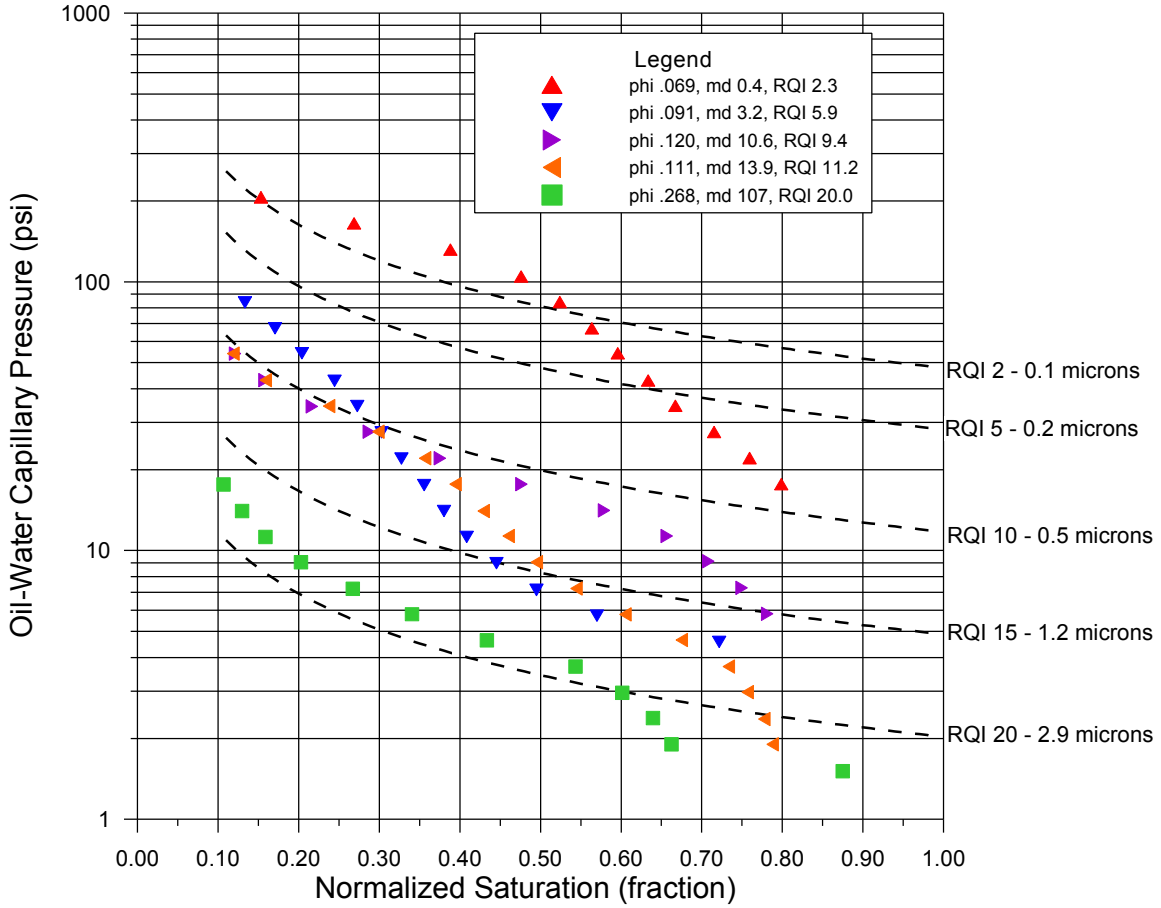

Figure 8-5. Graph of oil-water capillary pressure with normalized wetting-phase saturation. All samples indicate a bi-modal pore system that results from macro pores (burrow structures) in a micro-pore matrix. Empirical correlations are also shown for various RQI and Winland R35 effective pore radius.

Appendix C on CD-ROM

Core Laboratories, Core Analysis Report for Hansen C-7
Core Laboratories, Advanced Rock Properties Study for Hansen C-7
Core Laboratories, Core Photographs, Hansen C-7

Manual and Guide for Intelligent Computing System

The Intelligent Computing System (ICS) is a set of software tools to aid exploration and development for oil and gas. It has been designed and tested with data from the Red River Formation, Williston Basin. However, the ICS tools and approaches for addressing reservoir characterization problems should be applicable in many hydrocarbon provinces.

The software tools in ICS are for evaluating reservoir and hydrocarbon potential from various seismic, geologic and engineering data sets. The ICS tools provide a means for logical and consistent reservoir characterization. The tools can be broadly characterized as 1) clustering tools, 2) neural solvers, 3) multiple-linear regression, 4) entrapment-potential calculator and 5) combining tools. A flexible approach can be used with the ICS tools. They can be used separately or in a series to make predictions about a desired reservoir objective. The tools in ICS are primarily designed to correlate relationships between seismic information and data obtained from wells; however, it is possible to work with well data alone

The ICS tools are implemented in MATLAB™. MATLAB is an integrated programming and visualization environment that uses a proprietary interpreted language designed for easy experimental development of scientific and engineering software. MATLAB runs on UNIX or Microsoft Windows platforms, and is distributed by

The Math Works, Inc.
3 Apple Hill Drive
Natick, MA 01760-2098
http://www.mathworks.com

All ICS code development was done using version 5.3 of MATLAB running on Microsoft Windows NT. Elements of the MATLAB Neural Network Toolbox were used for those ICS components that involve artificial neural networks (ANN) algorithms. The ICS tools and utilities are both in MATLAB native code (.m files) and in compiled executable form. Using the MATLAB native code files requires that the user purchase the appropriate MATLAB products. This option provides the ability to modify the ICS source code. A full description of MATLAB products and pricing can be found by browsing the MATLAB web site. The MATLAB code has also been compiled as Microsoft Windows executables (.exe files). The Windows executable files can be run, without the purchase of additional software, on any suitable Windows platform, but cannot be modified by the user.

The ICS tool kit has been tested on seismic and well data from six 3D seismic surveys and with well data that are located outside the seismic survey boundaries. In the most general way, the user of these software tools will characterize the common physical parameters that cause a sedimentary layer to be a good or poor oil reservoir. Seismic information will be transformed to those

physical parameters. The pseudo-physical parameters will then be used to predict the reservoir potential for a sedimentary layer or unit.

Tools are not available in ICS for extraction of seismic time or waveform attributes from a seismic data file as delivered by the processing provider. It is expected that users have the ability to pick and extract relevant seismic information using seismic interpretation software. The data files imported and exported by ICS routines are in simple ASCII comma-separated-variable format.

Data Requirements

The structure of ICS is primarily designed to incorporate seismic information in a reservoir characterization process. This is not mandatory, however. The tools in ICS can work with well-log data as the sole source of geological input. The input data can be as simple or complete as is available or desired by the user. It must be stressed that characterization results will improve more significantly by adding dependent data (well information) than by adding more independent (seismic) data. Throughout the text that follows, there are references to dependent and independent data. Dependent data (or values) generally are items that are measured at wells. Dependent data are represented by a dependent variable in some function, $z = f(x,y)$ where z is the dependent variable. In this context, when we make predictions of reservoir phi-h from some seismic attributes, phi-h is represented by a dependent variable and is predicted by some function applied to the seismic attributes (independent variables).

A well data set would be comprised of items that represent reservoir storage, permeability, saturation, production and structure. The most common source of reservoir storage and saturation is from well logs. Digitized log data can be interpreted for net thickness, porosity and saturation. Drill-stem test data are a good source for permeability. Core data are also a good source for permeability, but the number of cores is often too few to provide an adequate population distribution. However, core data are invaluable for describing rock types and depositional setting. Permeability or productivity can be estimated from advanced decline-curve analysis using type-curve techniques. However, stimulation, damage or pressure depletion can significantly affect results from these methods. Production volumes and phase ratios over a normalized time period should also be included in the data set. Structure and growth history information can be obtained from depths of important geologic markers from well logs.

Once collected, the data set is then organized in an ordinary spreadsheet with data in one row representing one well or location. The location of each well must be in the same coordinate system as the seismic data. The type of information in each column will be the same. A well-master database is now constructed.

A seismic database is assembled from exported files from the user’s seismic interpretation software. Several seismic databases may be needed. One seismic

database should have time picks at major geologic events. Another seismic database may have waveform and iso-time attributes over a narrow time window that is associated with the reservoir. The selection of appropriate attributes and time window should be determined from some synthetic seismic modeling exercises.

A database from 2D seismic is possible for use with ICS. The 2D seismic grid spacing should be one-half mile or less. The lines should be processed in the same manner and the exported attributes normalized. The 2D data must be gridded with some mapping software package to create a pseudo 3D-survey database.

ICS Front Page

All tools and utilities can be executed from a simple window that is presented after starting ICS. For compiled-version users, ICS can be started in several ways. From Windows Explorer, double left-click “ICS.EXE.” From Windows START-RUN, type “ics.” Alternatively, a short can be created for the desktop. It is first necessary to edit the path environment as described under installation. If ICS is run under the MATLAB shell, the path to the directory which contains the ICS code needs to be set first. Then type “ics” at the command prompt followed by enter. The first window that is presented after starting ICS is shown in the figure below. Simply click the appropriate button to start the tool or utility.

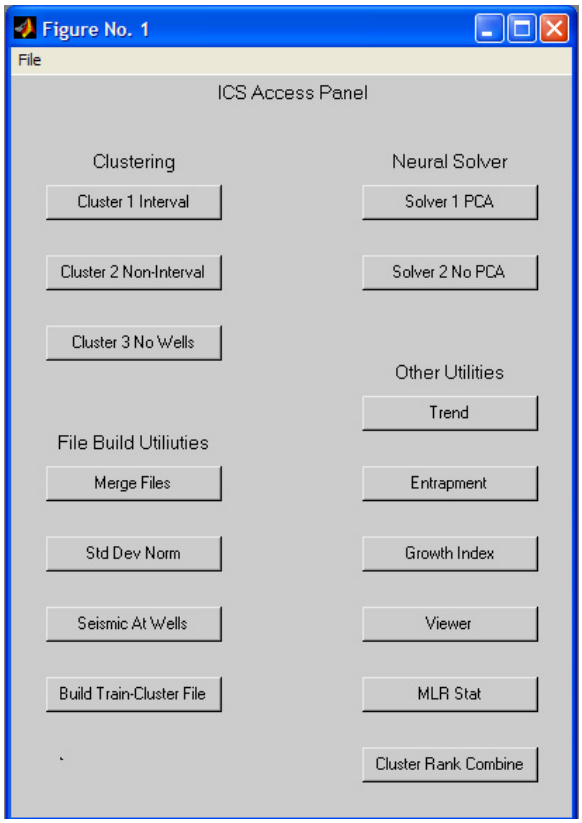

Front-page window of ICS for access to all tools and utilities is shown.

The ICS Access Panel is divided into four groups. The “File Build Utilities” are used to construct basic input files that will be used by other higher level routines. The “Other Utilities” perform some computation and file export that may be used by the Neural Solver routines. “Clustering” is an important characterization group. The “Neural Solver” group is the highest level of seismic-reservoir and reservoir-production transformation.

Land Grid and Wells

ICS tools that include map displays feature a button labeled “Grid/Wells.” This button implements a feature that allows user-supplied land grid and well spots to be overlaid on the map. This discussion provides a guide to help users build files that are needed by the “Grid/Wells” feature. If running ICS from MATLAB, the path to the directory which contains the ICS code needs to be permanently set in MATLAB. To do this, select File/Set Path from the main MATLAB window menu. A dialog will open. Select the Add Folder button in this dialog. A second dialog opens from which you select the folder that contains the code. Select OK from the second dialog and Close from the first. The path will now appear in the path list in the first dialog. When the “Grid/Wells” button is selected, the software attempts to find, in the directory set as described above, three files with the names shown below.

secs.txt
twps.txt
wells.txt

These are ASCII files that contain, one per line, the full paths to one or more data files describing, respectively, section boundaries and labels, township boundaries and labels, and well locations. The section file(s) are drawn first, in black, followed by the township files in blue and the well spots in black. The well location files are standard ICS .csv files having x and y coordinates in the first two data columns. The section and township data files are ASCII files that describe labels and polyline boundaries. These files may contain any number of label and/or polyline boundary definitions.

A label is defined by two lines of data:

L, label
x, y

where label represents the label text, and x, y the coordinates of the center of the text.

A polyline boundary is defined by *n* + 1 lines of data:

P, *n*
x1, y1
x2, y2
…
x*n*, y*n*

where n gives the number of nodes in the polyline, defined by x*n*, y*n*.

For example, the following file fragment defines the label and boundary of township 21N 3E.

```
L, 21N 3E
1171026, 57015
P, 5
1187771, 72418
1187553, 67169
1182277, 67388
1182461, 72660
1187771, 72418
```

Note that the coordinates used in these files, and the coordinates used in all ICS .csv files, are quadrant I Cartesian coordinates, not latitude/longitude.

Example files for land grid and well locations are found under the directory: ICS_MANUAL\LAND_GRID_WELLS

File Build Utilities

There are four utilities to help build training and data files for use with the Intelligent Computing System. The Merge Tool is used for file concatenation. For example, separate data exports from geophysical interpretation software can be merged together in one file with data matched to common locations. The Standard-Deviation Normal Tool will create a file where each data column will have a mean of zero and a standard deviation of one. The Seismic at Wells Tool will capture grid-type data at point locations, such as wells. The Build Train-Cluster File Tool will prepare a properly formatted file for use as training for Neural Solver 1 and MLR-STAT tools. There is also an option to create a properly formatted file for use with Cluster 1 or Cluster 2 tools.

Merge Tool, File Build Utilities

The Merge Files utility is accessed from the main ICS panel.

Example files for practice with the Merge Tool Utility are found under the directory:
ICS_MANUAL\FILE_BUILD_UTILITIES\MERGE

The ICS Merge Tool facilitates file concatenation to create a merged composite of different data files. For example, seismic amplitude picks in one file can be combined with seismic time picks from another file. Individual data may be viewed prior to merging with the draw command button. Data columns for merging are selected individually with a control left-mouse click. The common

overlapping area of each file is used for gridding operation and a rectangular grid is produced. If the survey is not rectangular, it may be desirable to capture the grid output to the original traces with the seismic-at-wells utility.

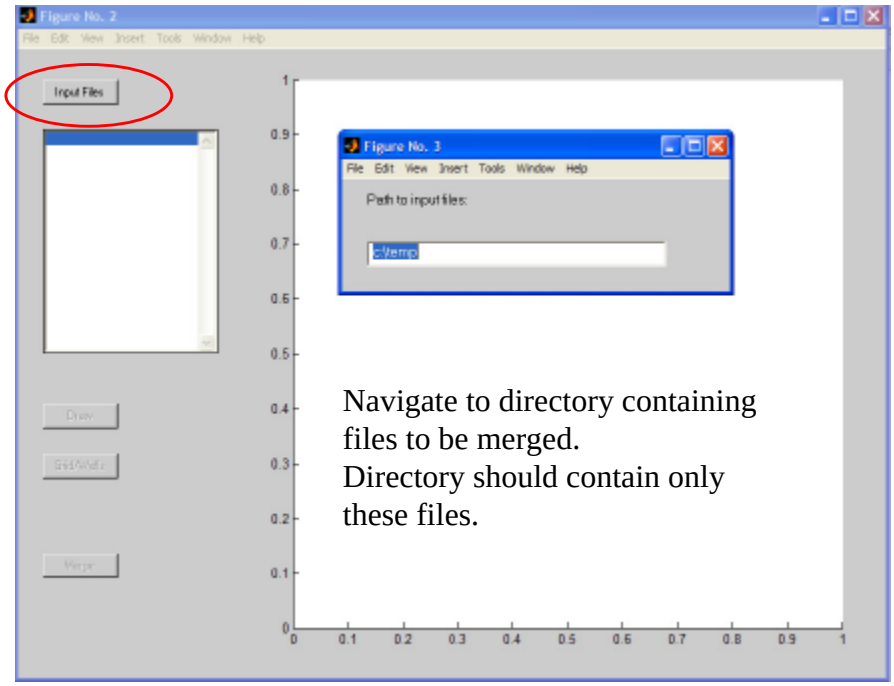

The data files to be merged must be formatted x,y,z1…zn (where n is the number of data columns) in comma-separated variable (csv) format. The first row must contain header descriptions for each column of data. The working directory for these files should be empty except for the files to be merged. The user must manually enter the complete path in the dialog window.

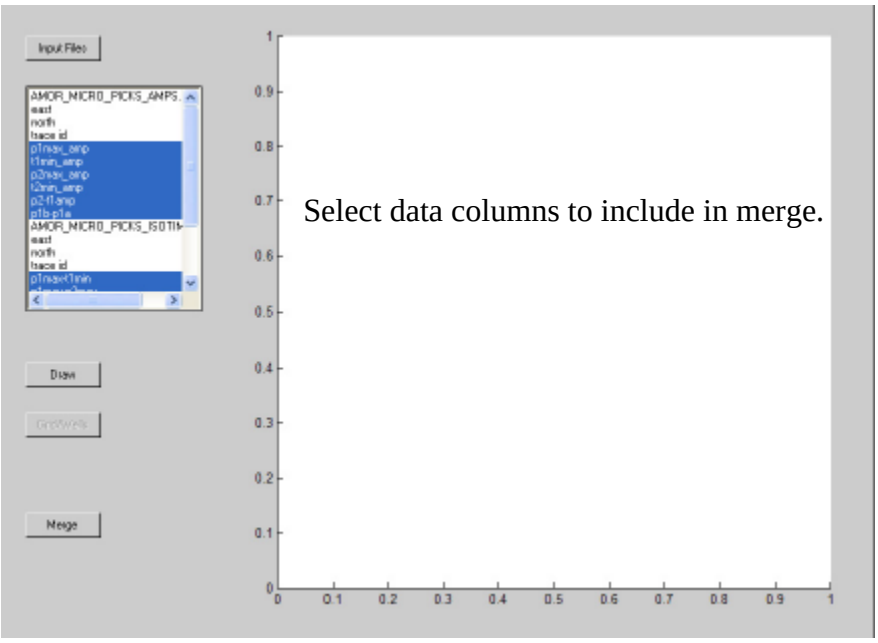

Data to be merged are selected by control-left click.

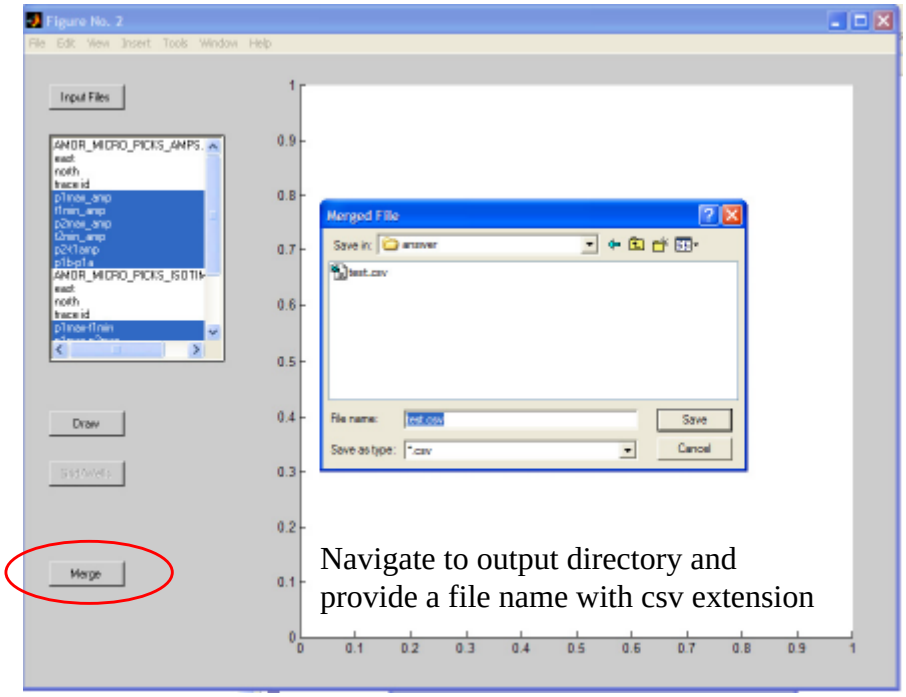

After data are selected, click on the merge button and an output file dialog window will open. Navigate to the desired directory and enter a file name with extension (csv).

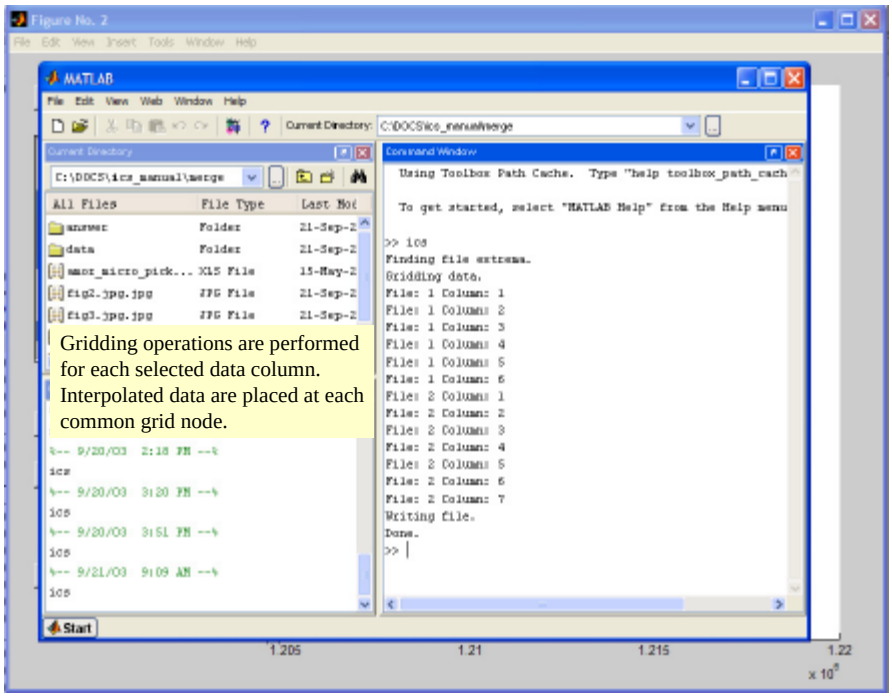

Gridding operations are performed for each selected data column. Interpolated data are placed at each common grid node.

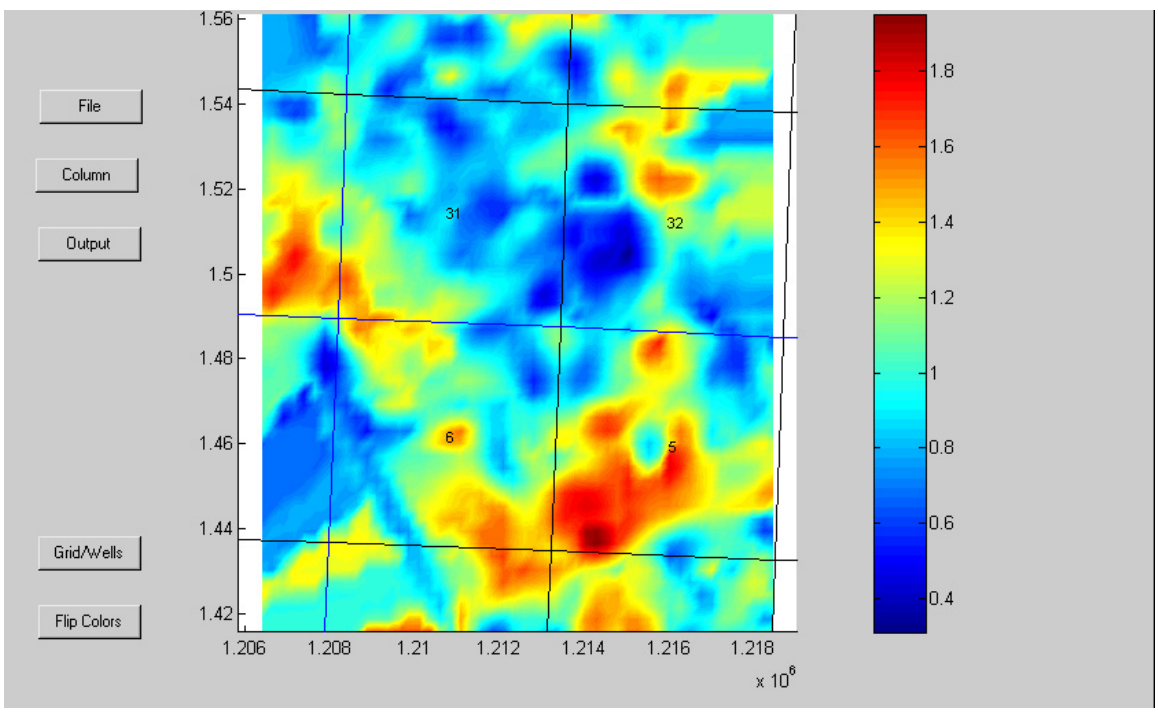

A view of data from output file with Viewer Utility that shows a rectangular grid is created. If the original survey is not rectangular, the data must be captured at original locations with the Seismic at Wells Utility.

Standard-Deviation Normal, File Build Utilities

When working with seismic attributes, it is advisable to normalize each attribute to a mean of “0” and a standard deviation of “1”. This is because some data have large numbers (such as amplitudes) and some are very small. When using data from more than one seismic survey, it is critical that the data are normalized. The Standard Deviation Norm Tool finds the mean and standard deviation of each data column. The normalized data are computed as n = (z-mean)/stddev. A new transformed data file is created that preserves trace locations and data order. Use of the tool is straightforward with only two buttons, one to read the original file and the other to write a new file.

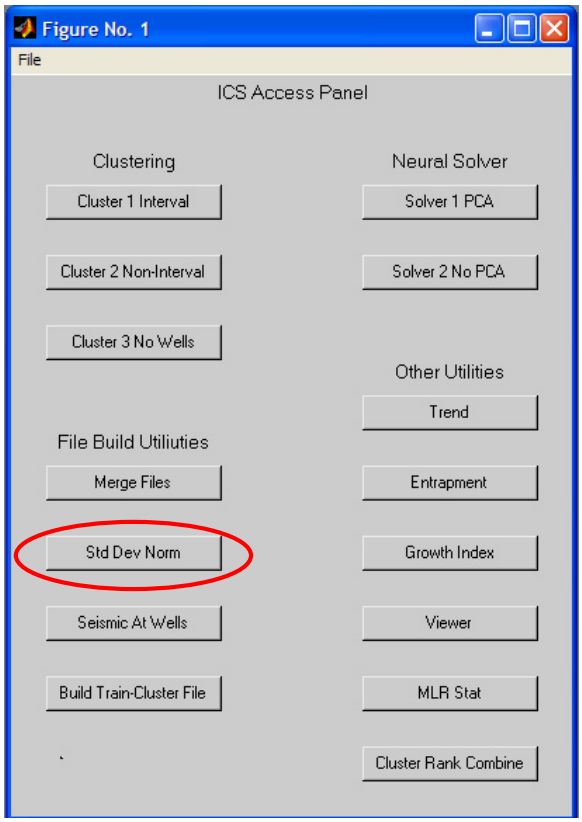

Access the standard-deviation normal utility from the main ICS control panel.

Example-practice files for the Standard-Deviation utility are found under the directory:
ICS_MANUAL\FILE_BUILD_UTILITIES\STDDEV_NORM

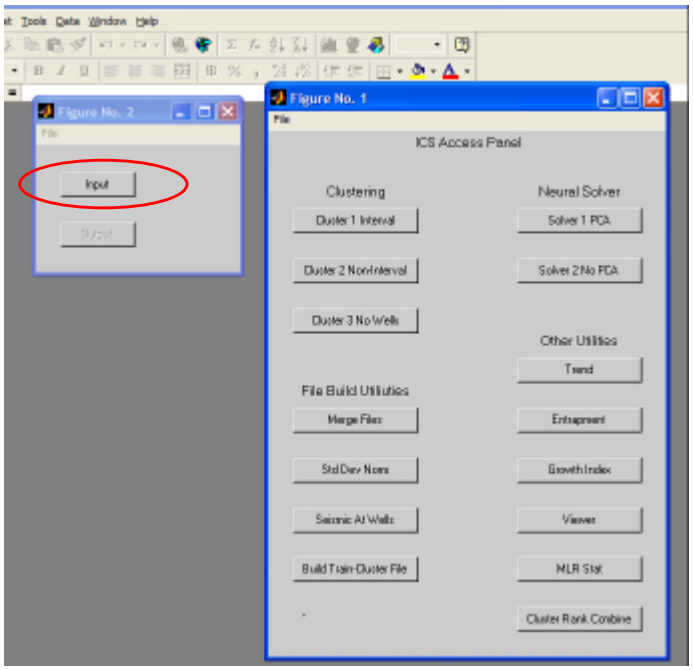

Simply click “input” to access file navigation window.

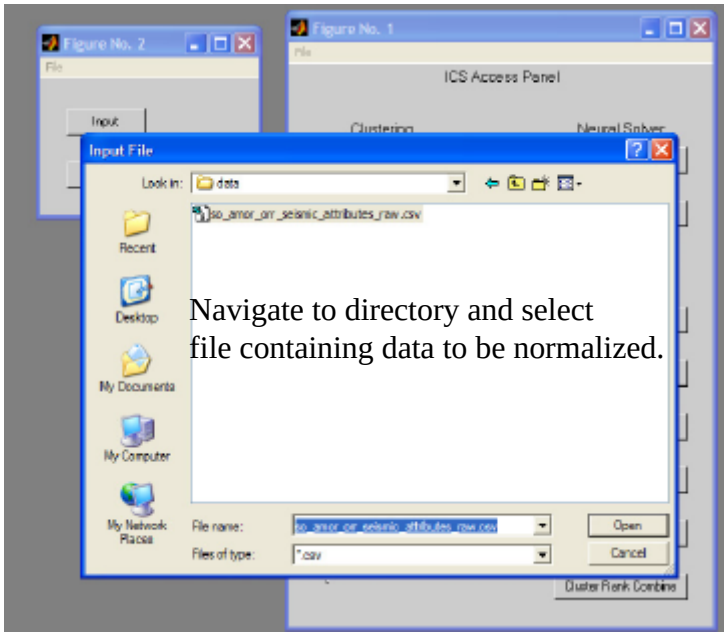

Navigate to directory and file to be processed.

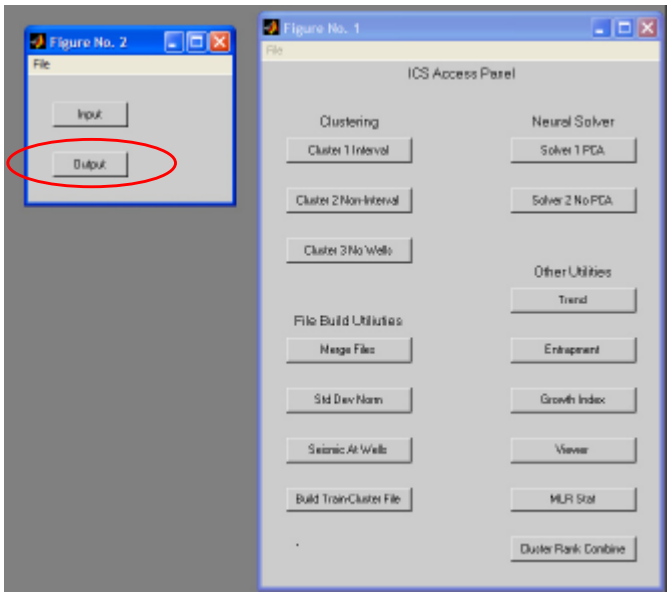

The "output" button becomes active after file normalization is complete. Click to activate file navigation window.

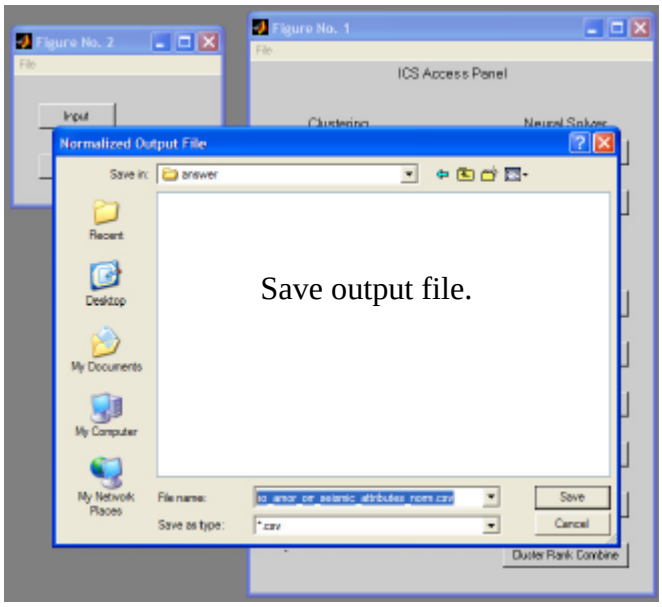

Navigate to desired directory and supply a file name for the normalized data. The locations and order of data are preserved, including the column headings.

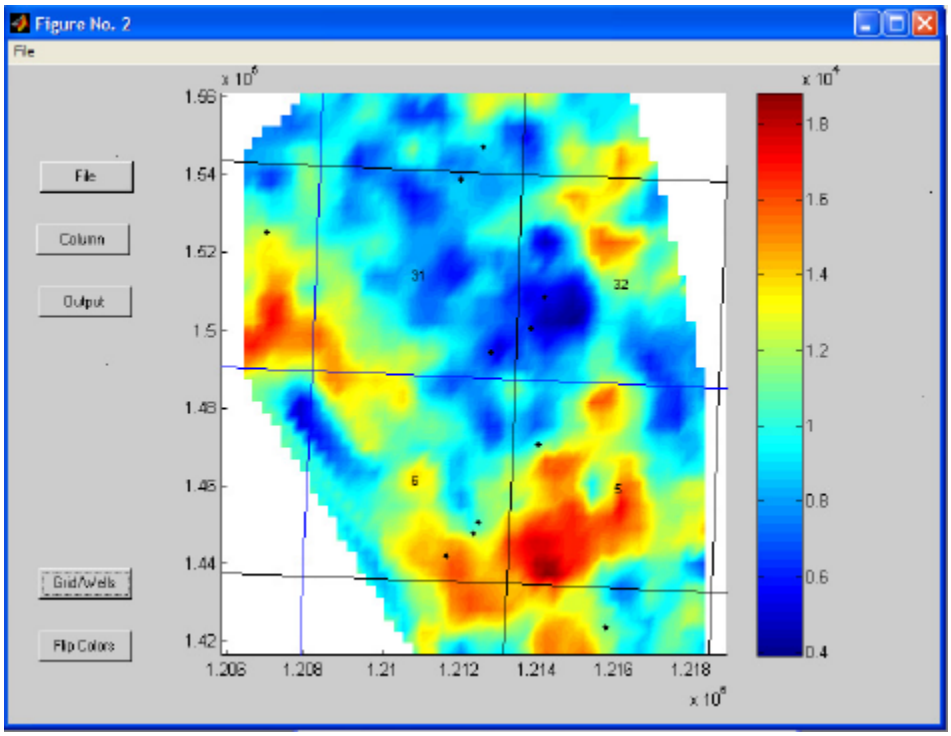

Map view of seismic amplitude attribute before normalization. Note large value of amplitude units.

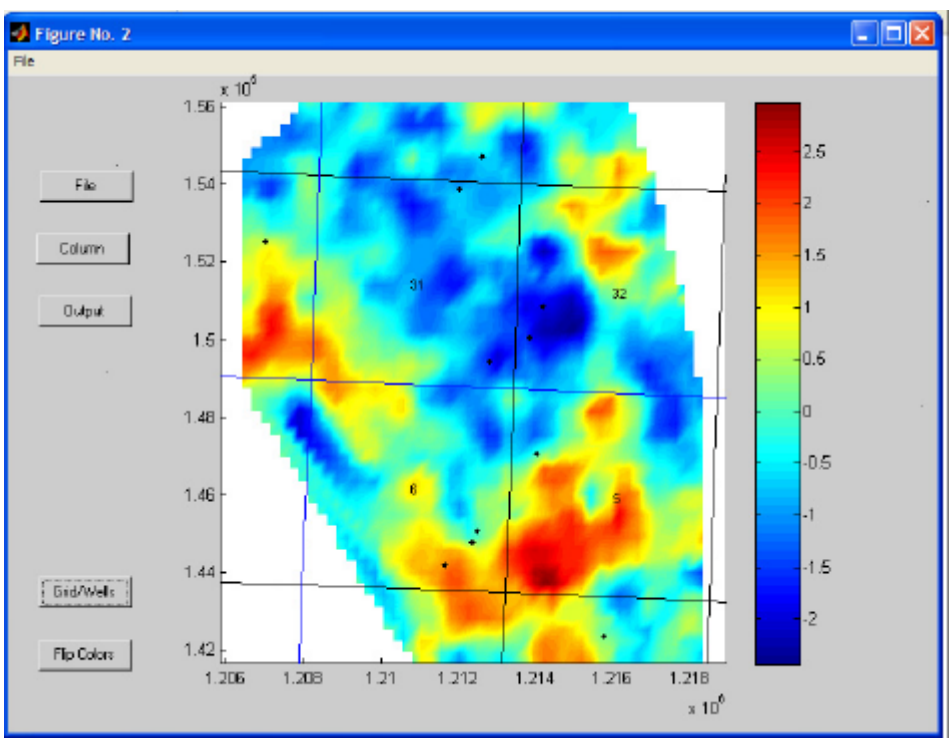

Map view of seismic amplitude attribute after normalization. Units are standard deviations.

Seismic at Wells, File Build Utilities

The Seismic-at-Wells utility helps create work files for ICS analysis. The utility captures 3D seismic or gridded data at user-supplied well or other arbitrary locations. Captured data are matched at the target x-y location using 3-point triangulation. The output file preserves the well order, x-y location and identifier to allow an easy match up for further copy-paste operations. If a target location is outside the extrema of the seismic data, that location will not be included in the output file.

It is often advantageous to work in ICS with smaller seismic data files (wider spacing) than the original seismic spacing. It is recommended to use seismic-trace spacing of 330-ft as appropriate for a first-time analysis. Unless a very fast computer is used, processing data from a 4 mile by 4-mile seismic survey with 37,000 traces will be frustratingly slow. A 4-mile by 4-mile survey reduced to 330-ft spacing will have about 4,100 traces and will be more manageable for first-pass analysis with ICS tools.

Two comma-separated-variable (csv) files are required as input for the “seismic at wells” utility. One defines target locations with three data columns: x, y, and a numeric identifier (such as API). The second input file contains the 3D seismic or other gridded data. It may have any number of columns, but the first two are assumed to be x and y. The output file columns are x, y, and identifier, followed by columns 2…n from the input seismic or gridded data file.

The output file will contain one row of data for each target location that falls within the convex hull of the seismic data points. An error message will be displayed if none of the target locations qualifies. The values for the parameters at each target location are obtained by averaging data from the three closest input data points.

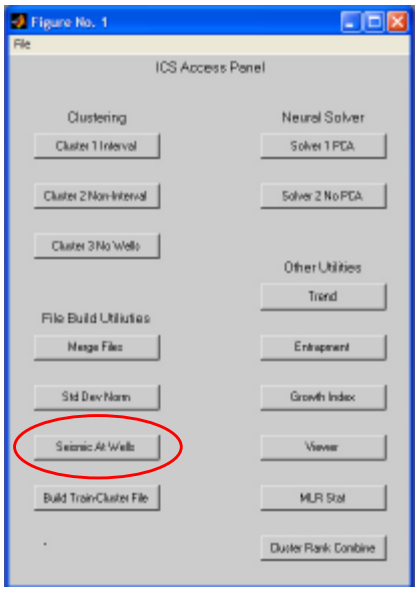

The seismic-at wells, file build utility, is accessed from the ICS main control panel.

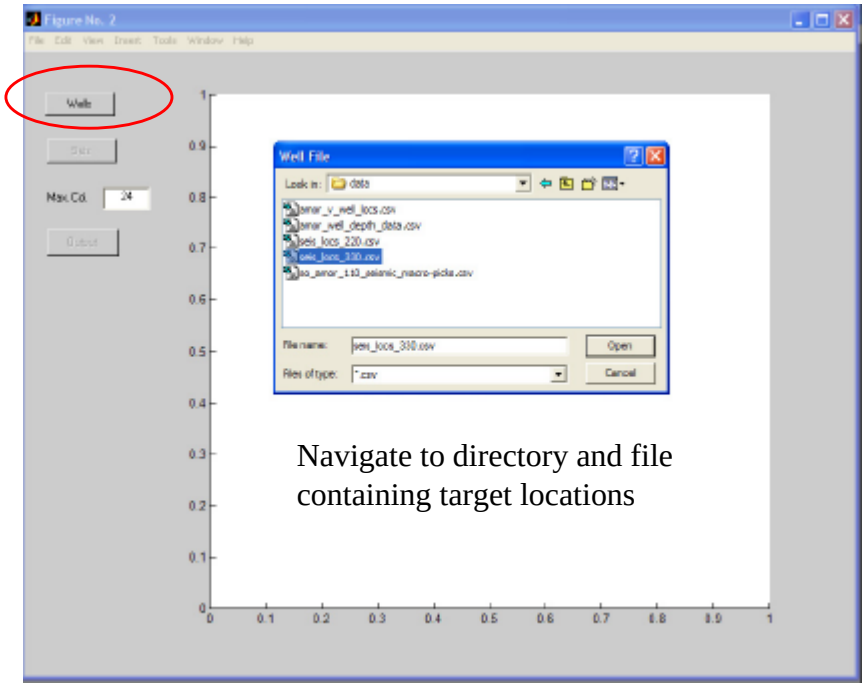

Clicking the “wells” button will open a file navigation window. Navigate to the directory containing the file with target locations.

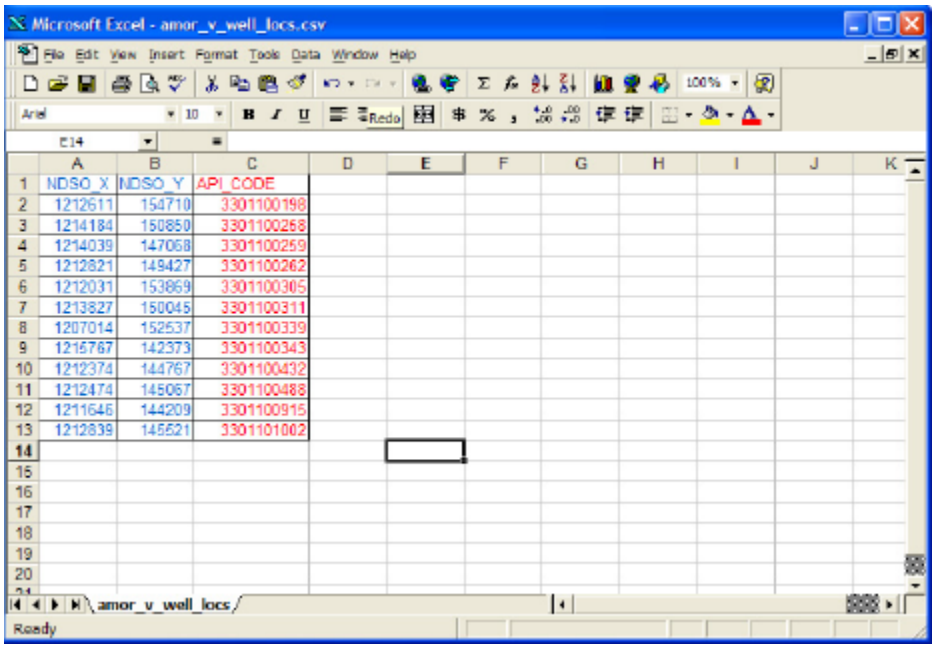

NDSO_X	NDSO_Y	API_CODE
1212611	154710	3301100198
1214184	150850	3301100268
1214039	147068	3301100259
1212821	149427	3301100262
1212031	153869	3301100305
1213827	150045	3301100311
1207014	152537	3301100339
1215767	142373	3301100343
1212374	144767	3301100432
1212474	145067	3301100488
1211646	144209	3301100915
1212839	145521	3301101002

An example of a file with well locations is shown. The file contains only three columns. The first two are x-y coordinates. The third column is a well or trace identifier. The first row contains header labels.

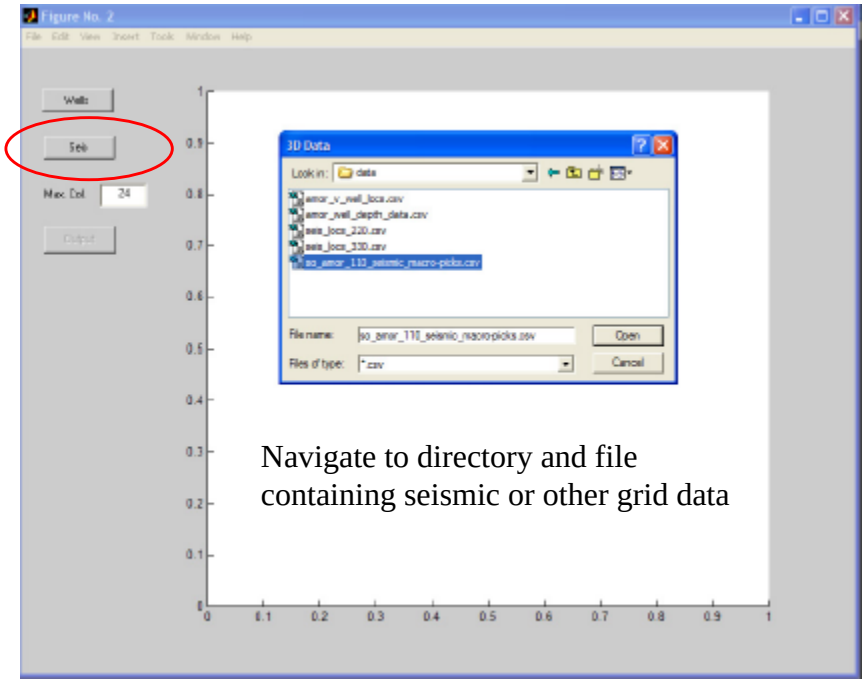

Clicking on the “Seis” button will open a file navigation window. Navigate to the directory containing the seismic or grid data.

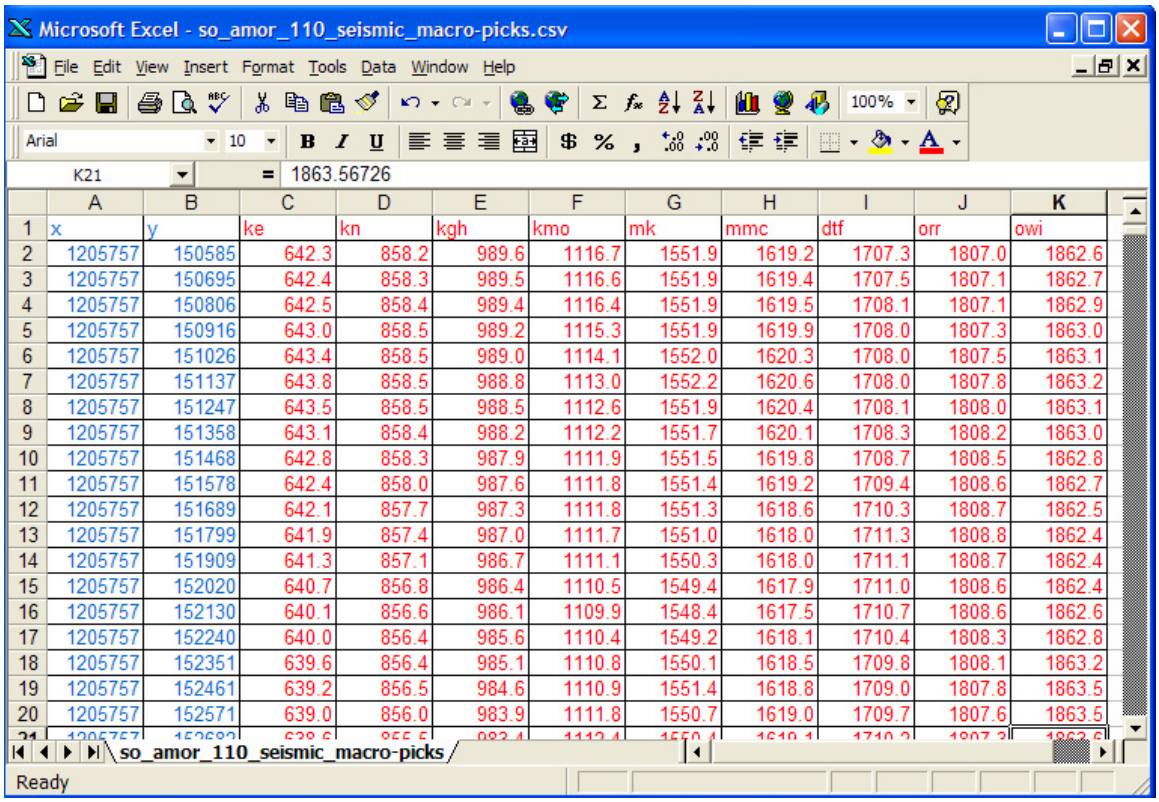

Microsoft Excel - so_amor_110_seismic_macro-picks.csv

K21 = 1863.56726

	A	B	C	D	E	F	G	H	I	J	K
1	x	y	ke	kn	kgh	kmo	mk	mmc	dtf	orr	owi
2	1205757	150585	642.3	858.2	989.6	1116.7	1551.9	1619.2	1707.3	1807.0	1862.6
3	1205757	150695	642.4	858.3	989.5	1116.6	1551.9	1619.4	1707.5	1807.1	1862.7
4	1205757	150806	642.5	858.4	989.4	1116.4	1551.9	1619.5	1708.1	1807.1	1862.9
5	1205757	150916	643.0	858.5	989.2	1115.3	1551.9	1619.9	1708.0	1807.3	1863.0
6	1205757	151026	643.4	858.5	989.0	1114.1	1552.0	1620.3	1708.0	1807.5	1863.1
7	1205757	151137	643.8	858.5	988.8	1113.0	1552.2	1620.6	1708.0	1807.8	1863.2
8	1205757	151247	643.5	858.5	988.5	1112.6	1551.9	1620.4	1708.1	1808.0	1863.1
9	1205757	151358	643.1	858.4	988.2	1112.2	1551.7	1620.1	1708.3	1808.2	1863.0
10	1205757	151468	642.8	858.3	987.9	1111.9	1551.5	1619.8	1708.7	1808.5	1862.8
11	1205757	151578	642.4	858.0	987.6	1111.8	1551.4	1619.2	1709.4	1808.6	1862.7
12	1205757	151689	642.1	857.7	987.3	1111.8	1551.3	1618.6	1710.3	1808.7	1862.5
13	1205757	151799	641.9	857.4	987.0	1111.7	1551.0	1618.0	1711.3	1808.8	1862.4
14	1205757	151909	641.3	857.1	986.7	1111.1	1550.3	1618.0	1711.1	1808.7	1862.4
15	1205757	152020	640.7	856.8	986.4	1110.5	1549.4	1617.9	1711.0	1808.6	1862.4
16	1205757	152130	640.1	856.6	986.1	1109.9	1548.4	1617.5	1710.7	1808.6	1862.6
17	1205757	152240	640.0	856.4	985.6	1110.4	1549.2	1618.1	1710.4	1808.3	1862.8
18	1205757	152351	639.6	856.4	985.1	1110.8	1550.1	1618.5	1709.8	1808.1	1863.2
19	1205757	152461	639.2	856.5	984.6	1110.9	1551.4	1618.8	1709.0	1807.8	1863.5
20	1205757	152571	639.0	856.0	983.9	1111.8	1550.7	1619.0	1709.7	1807.6	1863.5

so_amor_110_seismic_macro-picks

Ready

An example of a file is shown containing seismic data as viewed with spreadsheet software.

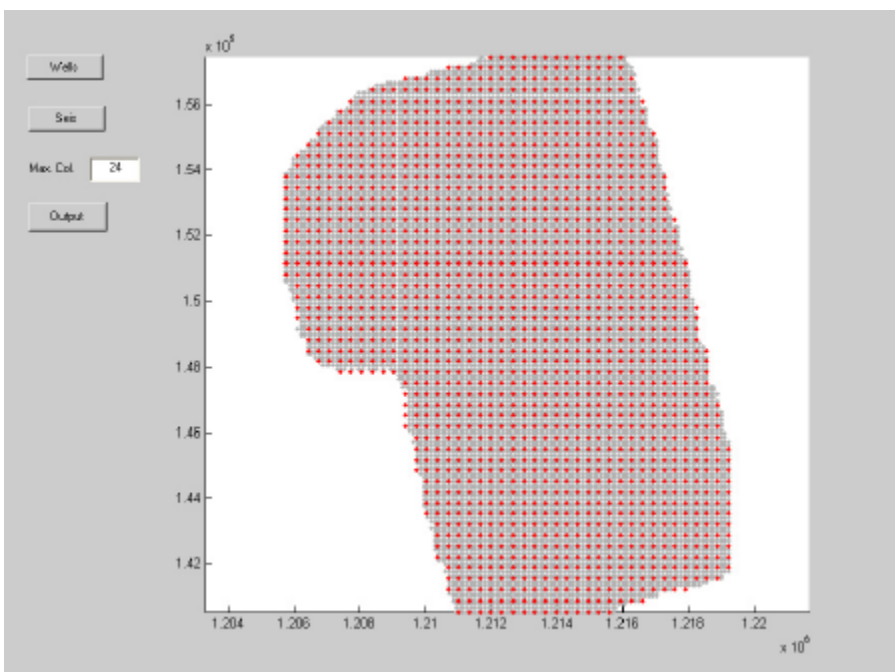

An example is shown of 110-ft seismic data captured at 220-ft locations.

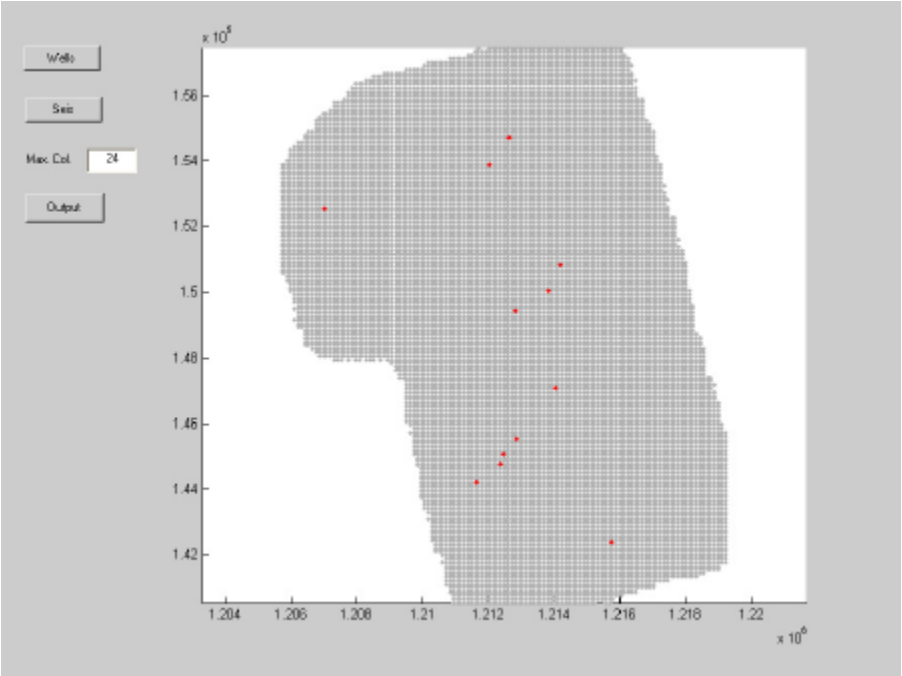

An example is shown of seismic data captured at well locations.

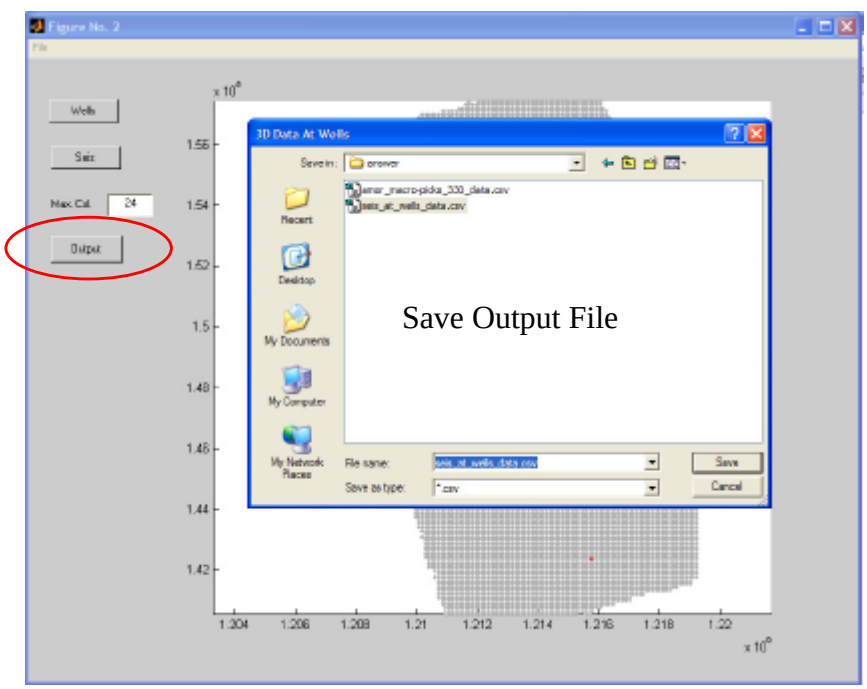

Select the “output” button that will open a file navigation window. Navigate to the appropriate directory and supply a file name with the csv extension.

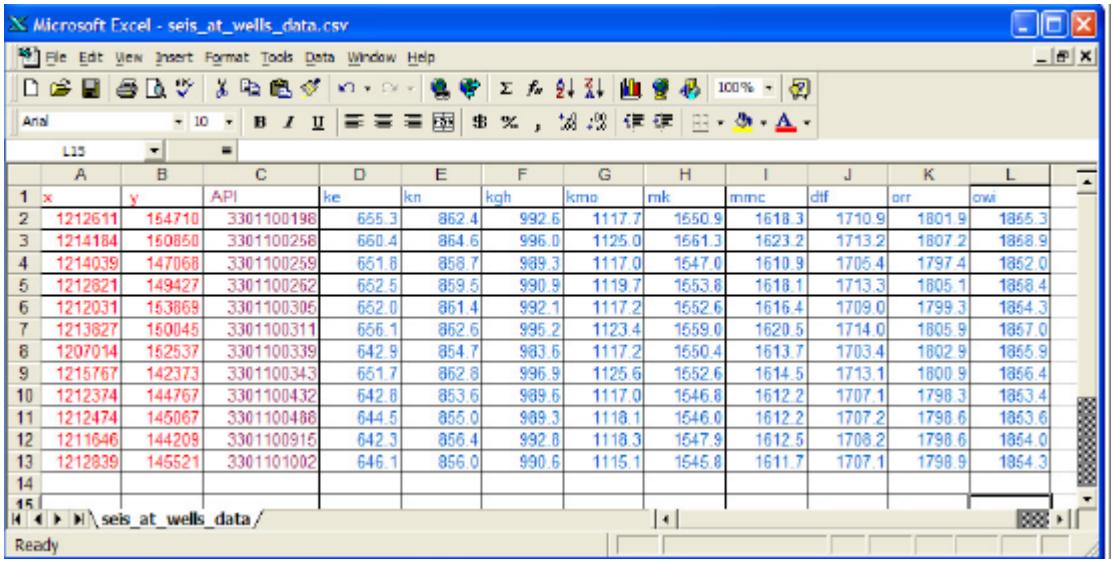

	A	B	C	D	E	F	G	H	I	J	K	L
1	x	y	API	ke	kn	kgh	kmo	mk	mmc	dtf	orr	owi
2	1212611	154710	3301100198	655.3	862.4	992.6	1117.7	1550.9	1618.3	1710.9	1801.9	1865.3
3	1214184	150850	3301100258	660.4	864.6	996.0	1125.0	1561.3	1623.2	1713.2	1807.2	1868.9
4	1214039	147068	3301100259	651.8	858.7	989.3	1117.0	1547.0	1610.9	1705.4	1797.4	1862.0
5	1212821	149427	3301100262	652.5	859.5	990.9	1119.7	1553.8	1618.1	1713.3	1805.1	1868.4
6	1212031	153869	3301100305	652.0	861.4	992.1	1117.2	1552.6	1616.4	1709.0	1799.3	1864.3
7	1213827	150045	3301100311	656.1	862.6	995.2	1123.4	1559.0	1620.5	1714.0	1805.9	1867.0
8	1207014	152537	3301100339	642.9	854.7	983.6	1117.2	1550.4	1613.7	1703.4	1802.9	1865.9
9	1215767	142373	3301100343	651.7	862.8	996.9	1125.6	1552.6	1614.5	1713.1	1800.9	1866.4
10	1212374	144767	3301100432	642.8	853.6	989.6	1117.0	1546.8	1612.2	1707.1	1798.3	1863.4
11	1212474	145067	3301100486	644.5	855.0	989.3	1118.1	1546.0	1612.2	1707.2	1798.6	1863.6
12	1211646	144209	3301100915	642.3	856.4	992.8	1118.3	1547.9	1612.5	1708.2	1798.6	1864.0
13	1212839	145521	3301101002	646.1	856.0	990.6	1115.1	1545.8	1611.7	1707.1	1798.9	1864.3

An example is shown of an output file from Seismic-at-Wells, file build utility.

Example-practice files for the Seismic-at-Wells utility are found under the directory:
ICS_MANUAL\FILE_BUILD_UTILITIES\SEIS_AT_WELLS

Build Train or Cluster Files, File Build Utilities

The “build train-cluster file” tool will create files in their proper format for neural-solver 1 training or either cluster 1 or 2. Databases (comma-separated-variable) for well information and seismic attributes are prepared before using this utility. The first step is to open the well-attribute data file. The well locations will be expanded by four additional “pseudo locations” at a user-supplied distance from the reported surface location of each well. The seismic-attribute file is read next and the routine captures the seismic (or other grid-type) data at each well and pseudo-well location. After the seismic attributes are matched to the target locations, the user selects two well attributes for cluster files or any (or all) well attributes for a neural solver training file.

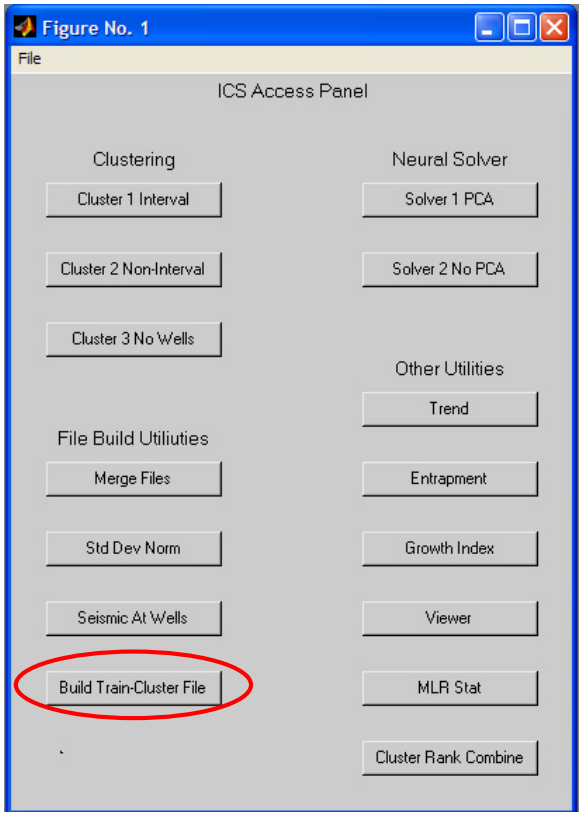

The Build Train-Cluster File utility is accessed from the main ICS control panel.

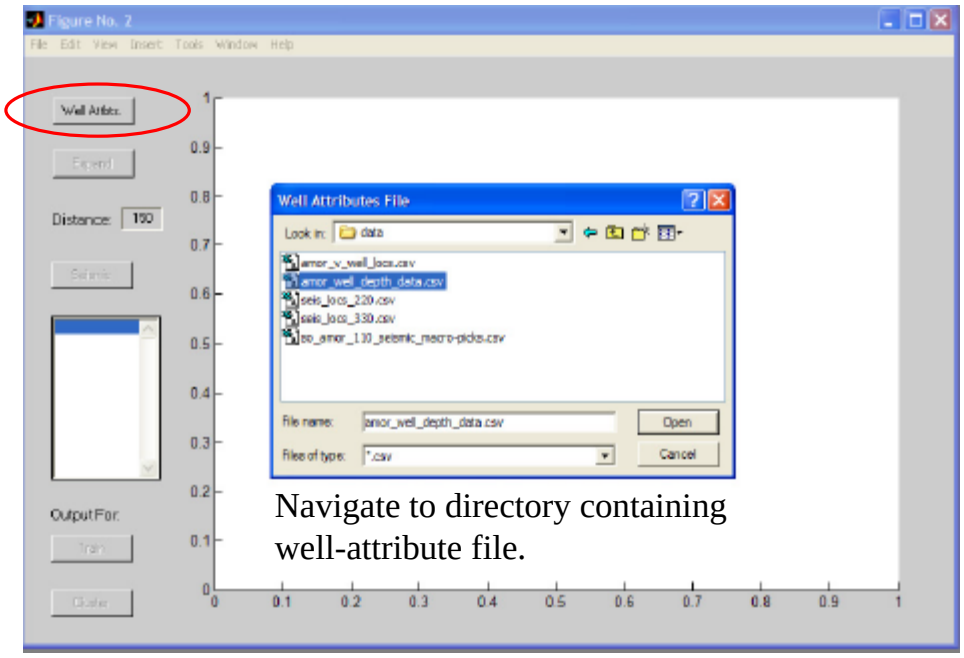

Click the “well attributes’ button will open a file navigation window. Navigate to the directory containing the well data and select the file.

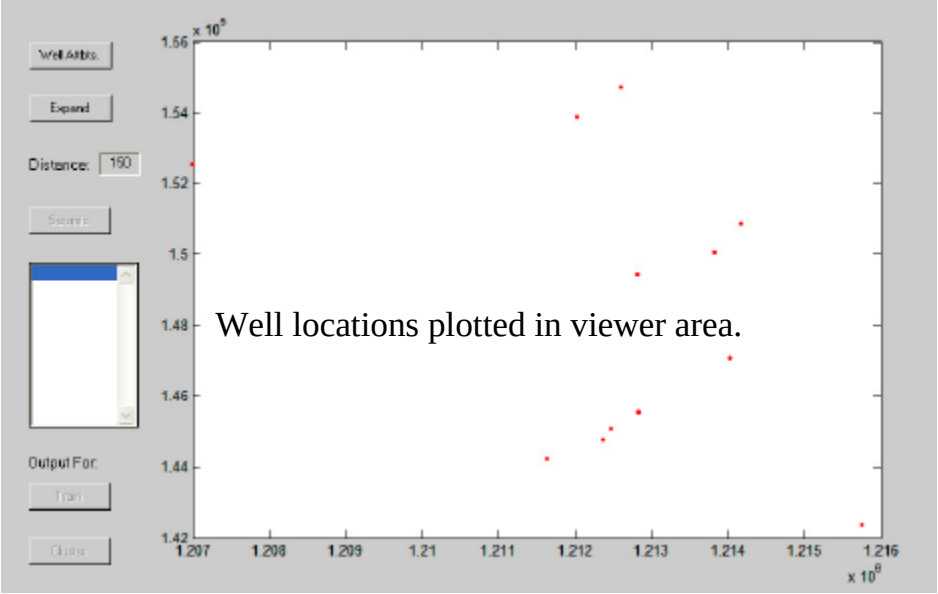

After the well file is read, the well locations are displayed in the map window.

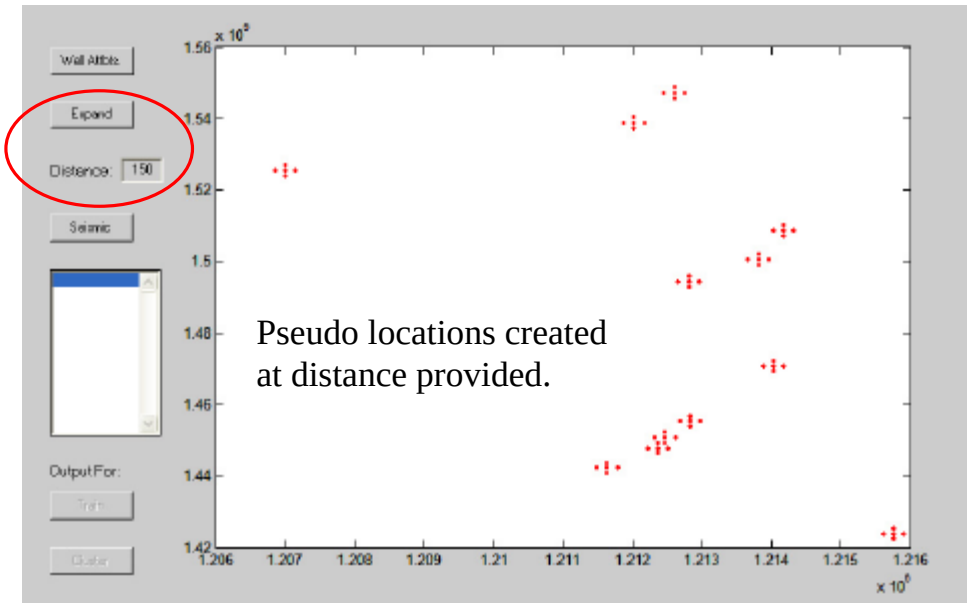

Pseudo well locations are created at each quadrant around the wells at a user specified distance.

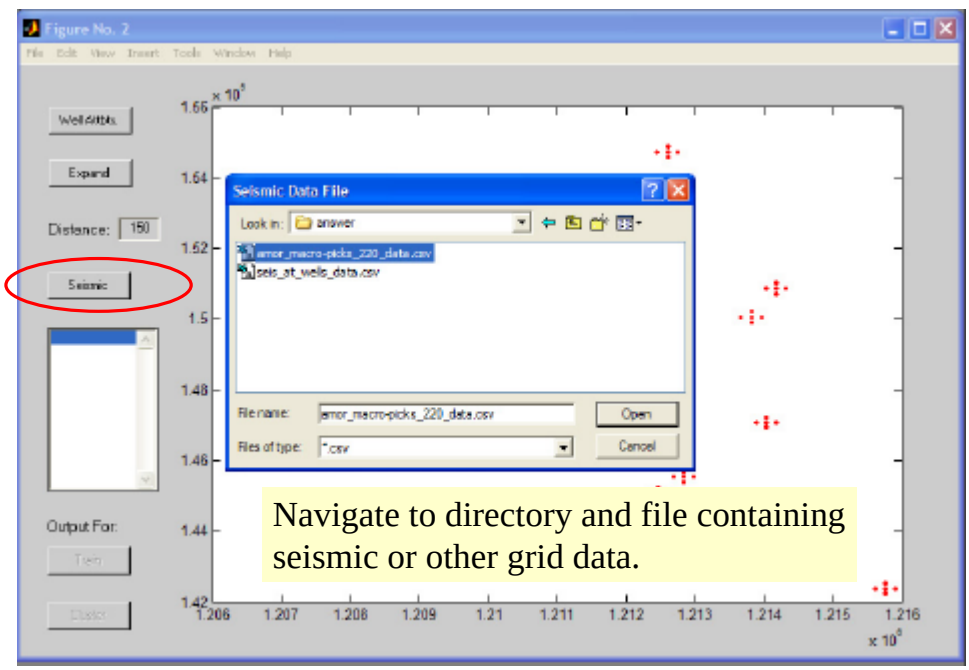

Click the ‘seismic” button and a file navigation window will open. Navigate to the directory containing the seismic or grid data and select the appropriate file.

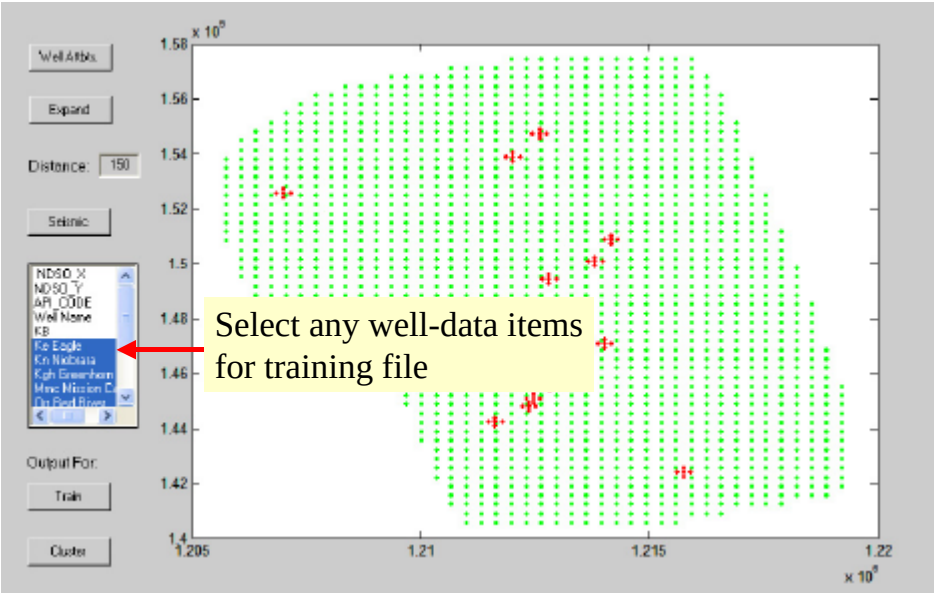

If preparing a file for training with the Neural Solver 1 tool, control-left click any well-reservoir data items.

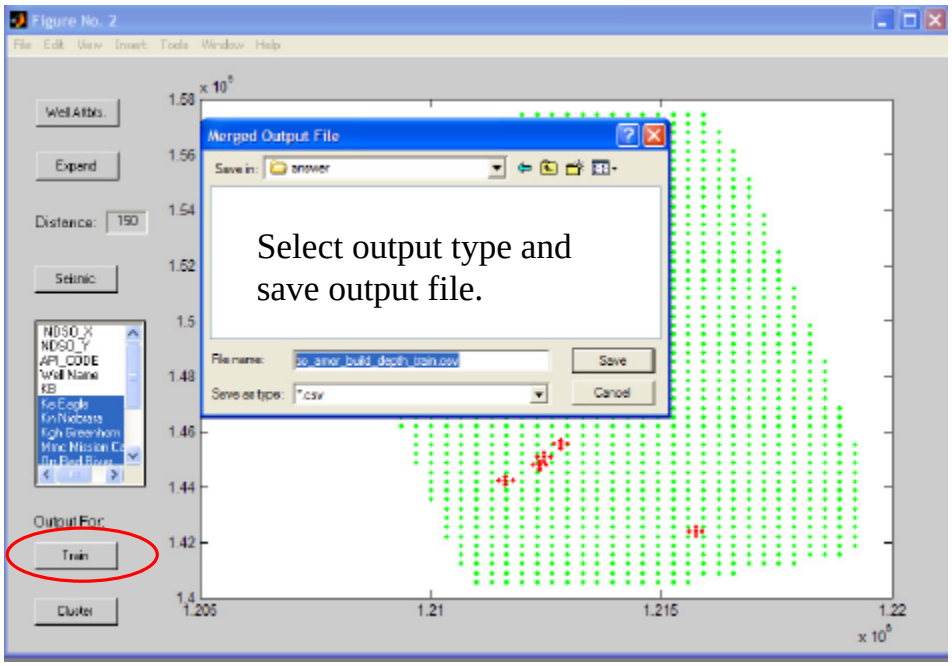

Select the output type “train” and file navigation window will open. Navigate to the appropriate directory and supply a file name with a csv extension.

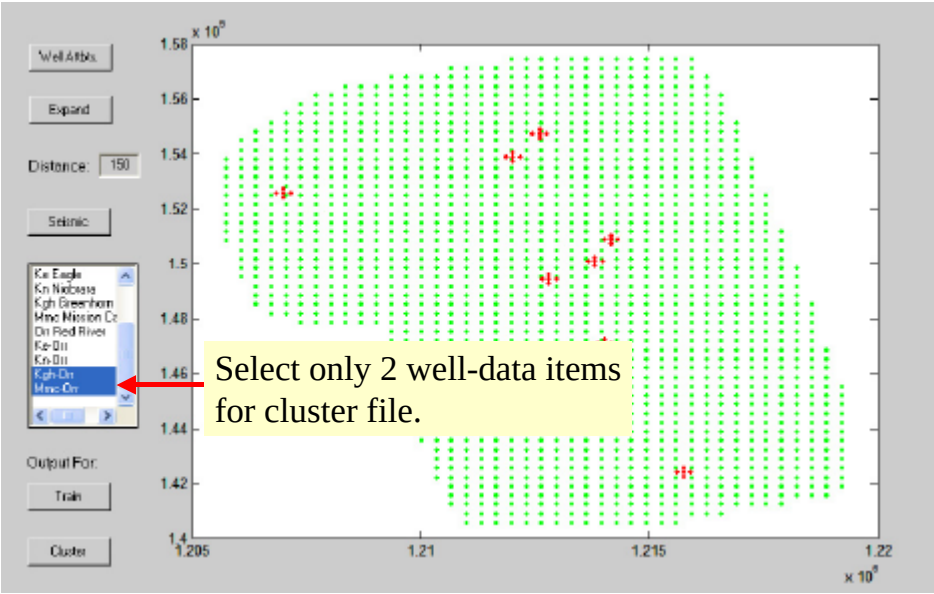

If preparing a file for clustering 1 or 2, control-left click only 2 well-reservoir data items.

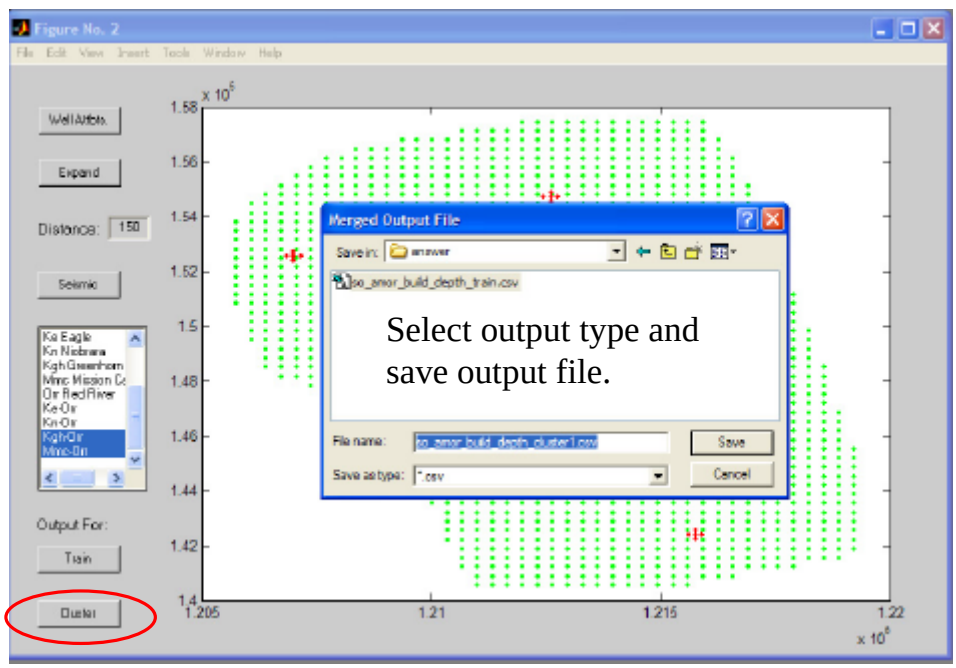

Select the output type “cluster” and file navigation window will open. Navigate to the appropriate directory and supply a file name with a csv extension.

Example-practice files for the Build Train or Cluster Files utility are found under the directory:
ICS_MANUAL\FILE_BUILD_UTILITIES\BUILD_TRAIN-CLUSTER_FILE

Other Utilities

There are six utility tools that perform various functions. The Viewer tool allows creation of map displays of data files. A trend and residual calculation of map data can be performed with the Trend tool. A Growth-Index tool can help with analyzing structural genesis. Multiple-linear regression can be performed with the MLR-STAT tool. Structural and stratigraphic entrapment can be evaluated with the Entrapment tool. Results from multiple outputs from the Cluster tool can be weighted and summed with the Combine tool. In general, these tools help create information about the reservoir that can be used alone or as an attribute for inclusion with analysis and prediction with a Neural Solver tool.

Trend Tool, Other Utilities

In many situations it is useful (and recommended) to compare local reservoir structure and depositional cycle thickness with regional data. The Trend Tool can read a file of regional well data (depths or thickness) and compute a regional surface or isopach trend. This trend is applied to the local 3D survey or field map data.

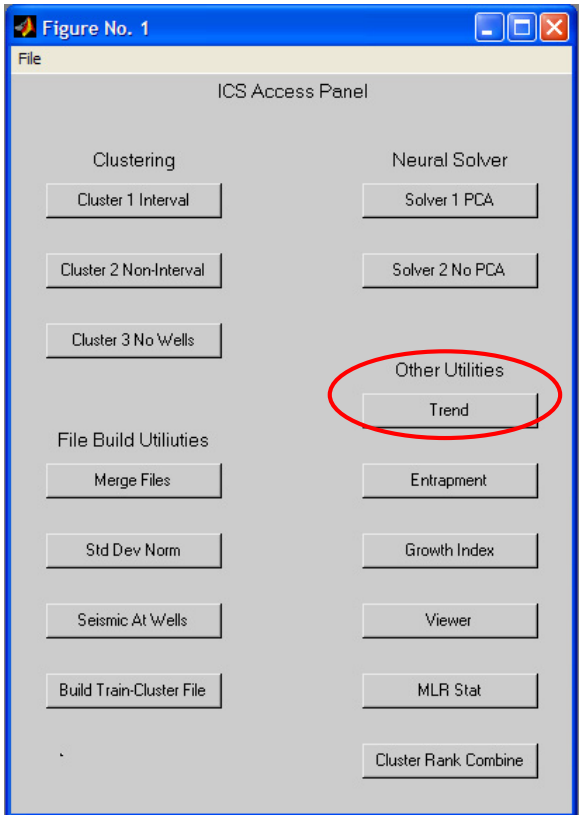

The Trend utility can be accessed from the main ICS panel.

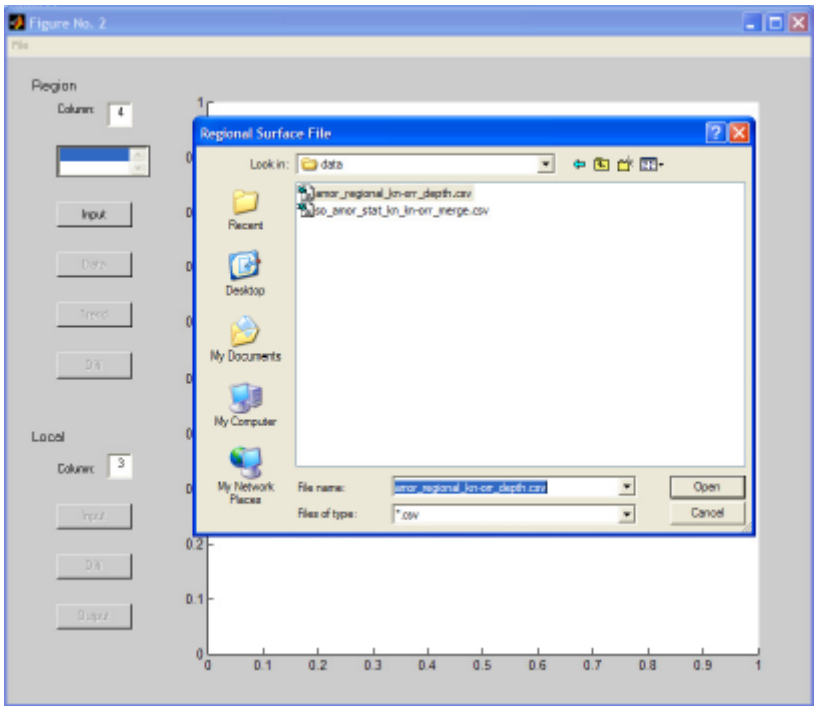

After setting the column value for the data in the regional file, click the “input” button and a file navigation window will appear. Navigate to the directory containing the regional data file.

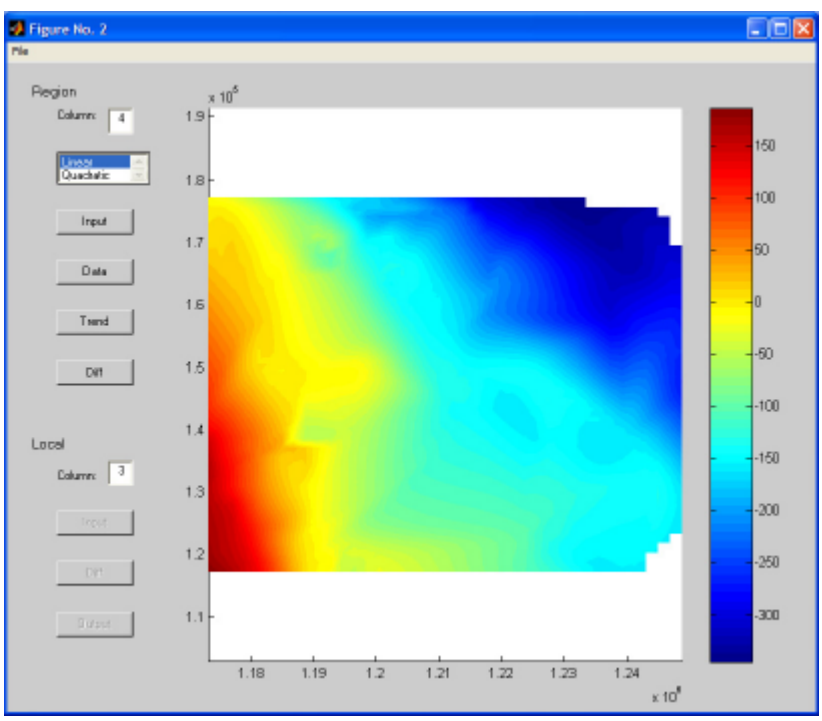

Clicking the “data” button will produce a map surface of the regional data.

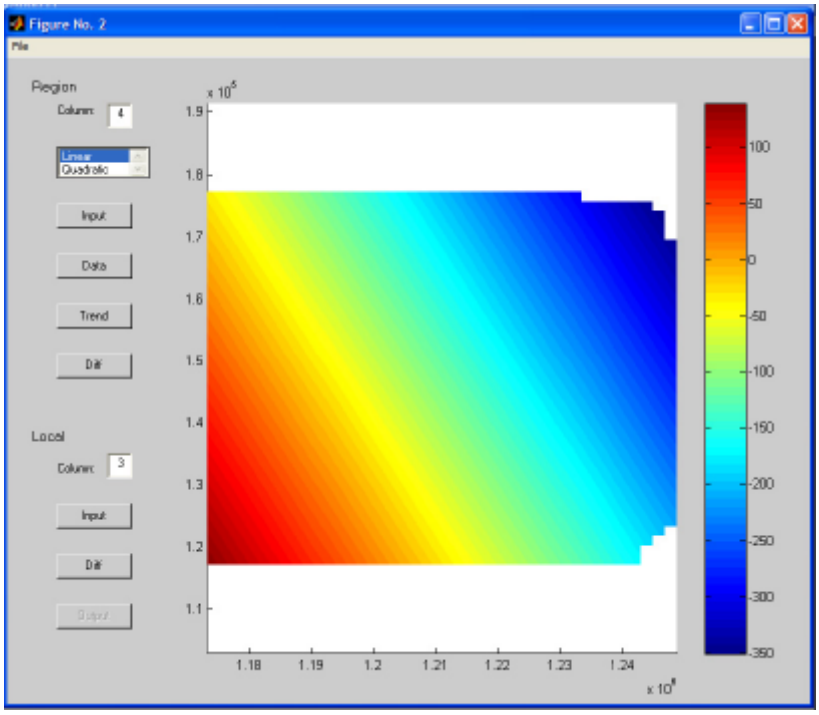

Selecting “linear” and “trend” will produce a first-order trend of the regional data.

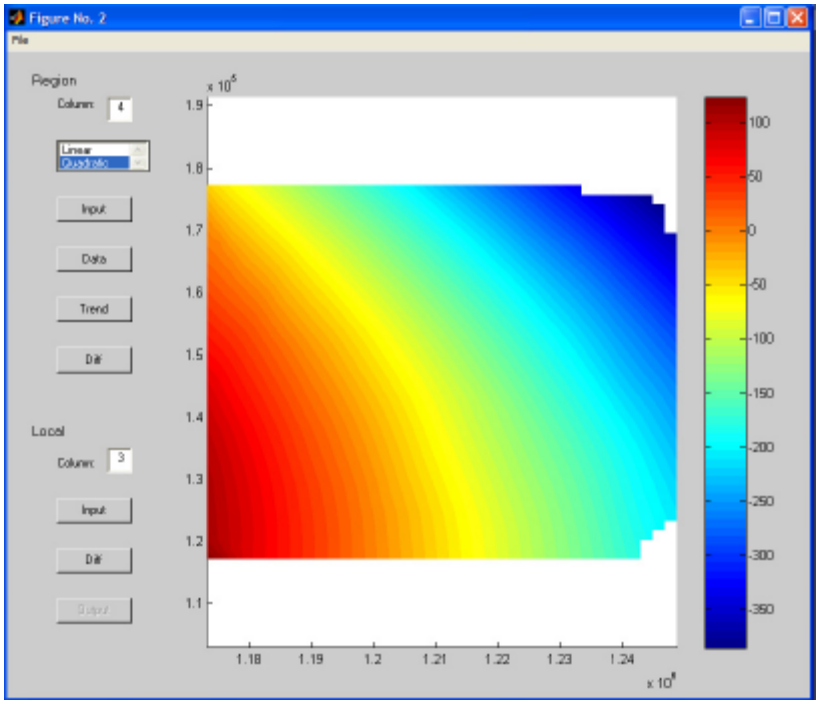

Selecting “quadratic” and “trend” will produce a second-order trend of the regional data.

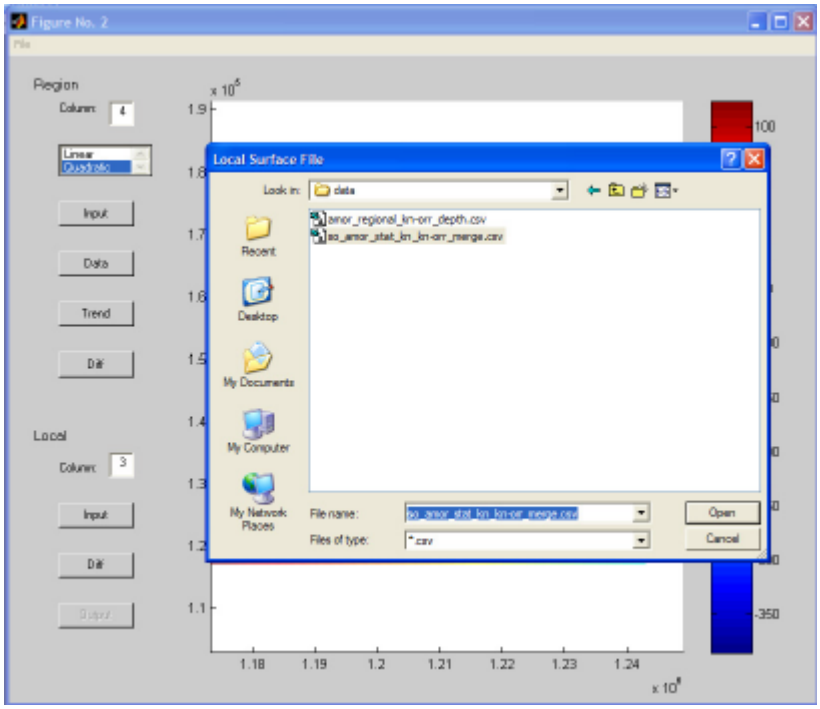

Set the data column in the local file that matches the regional map and click the local “input” button. A file navigation window will appear. Navigate to the directory containing the local data file.

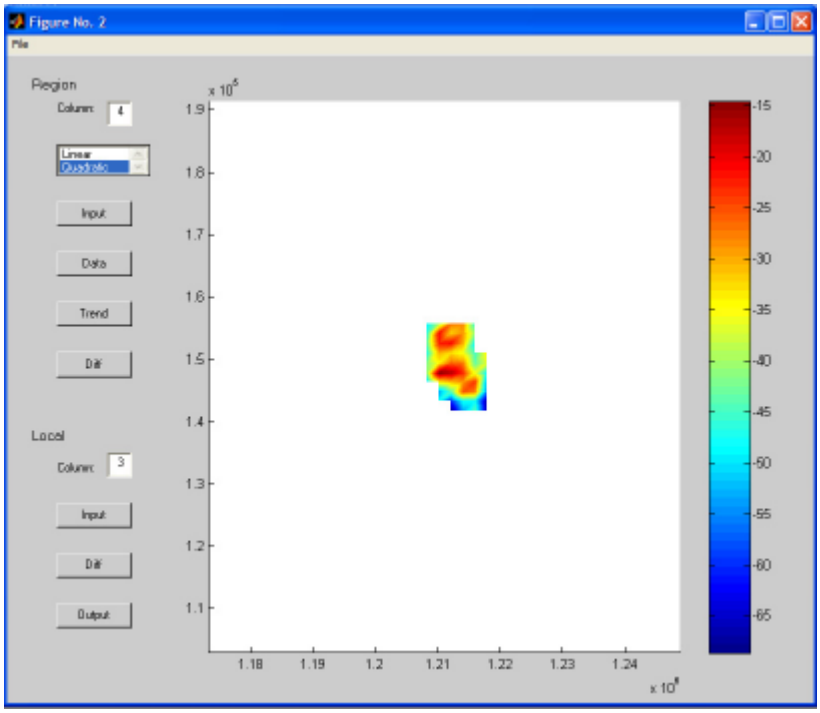

Click the “difference” button and a local residual map will be produced.

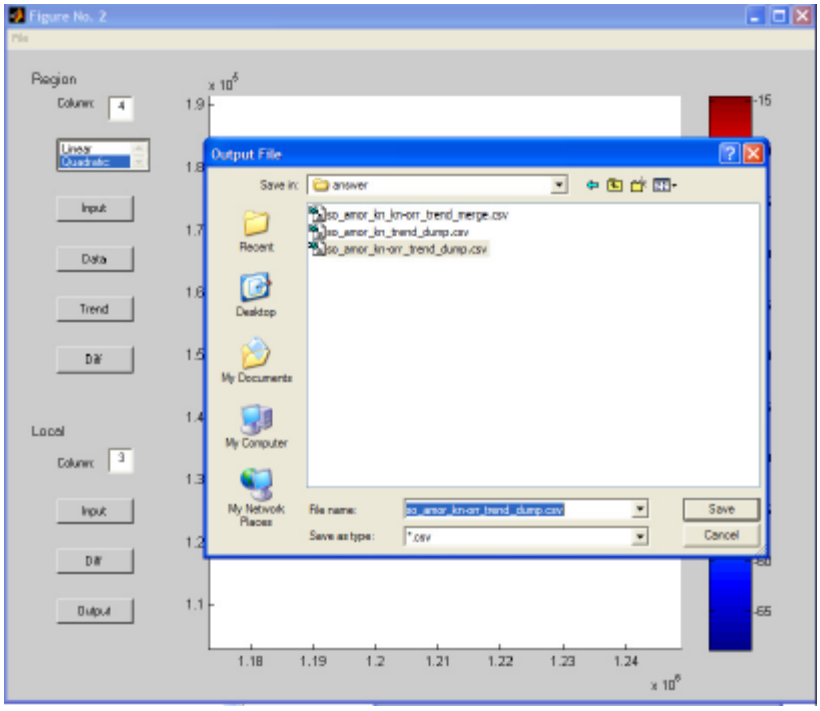

Click the “output” button and a file navigation window will appear. Save the output file.

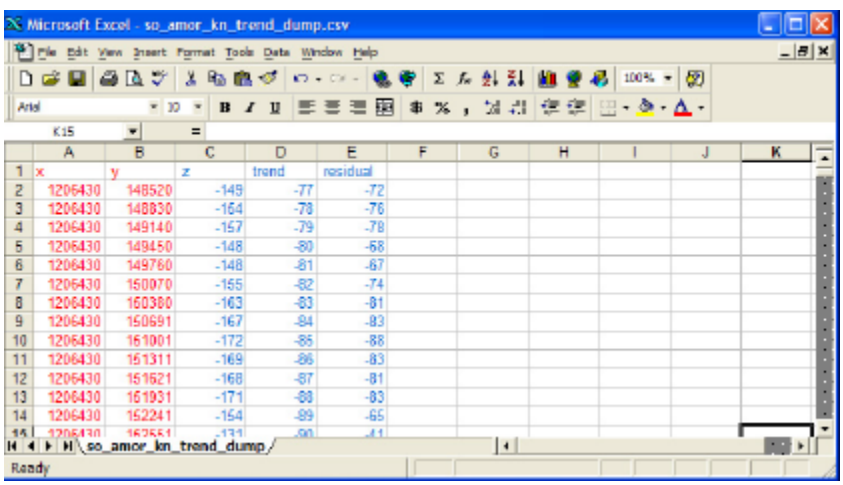

	A	B	C	D	E
1	x	y	z	trend	residual
2	1206430	148520	-149	-77	-72
3	1206430	148830	-154	-78	-76
4	1206430	149140	-157	-79	-78
5	1206430	149450	-148	-80	-68
6	1206430	149760	-148	-81	-67
7	1206430	150070	-155	-82	-74
8	1206430	150380	-163	-83	-81
9	1206430	150691	-167	-84	-83
10	1206430	151001	-172	-85	-88
11	1206430	151311	-169	-86	-83
12	1206430	151621	-168	-87	-81
13	1206430	151931	-171	-88	-83
14	1206430	152241	-154	-89	-65

The output file preserves the local traces in order with the original value. The regional trend and residual are appended to the file.

Example-practice files for the Trend utility are found under the directory: ICS_MAUAL\OTHER_UTILITIES\TREND

Entrapment Tool, Other Utilities

A reservoir-entrapment tool evaluates components of structure and rock quality for entrapment potential. The tool can produce several map views of the imported data and a map of entrapment potential in pressure units. The entrapment tool uses a depth file from seismic time conversion or grid output from a mapping package, possibly using only well control. A second source of data is imported that is related to rock quality or stratigraphic information. The source of this file is output from Cluster 1 or Cluster 2 tools. Output files can be created from the Entrapment tool for use in other ICS routines. There are several map views that can be displayed after the routine merges the depth and rank file. The “parameters” button allows modification to the reservoir pressure and capillary pressure adjustment for rock-quality rank.

There are two types of entrapment pressure calculations that can be made with the Entrapment Tool. The first, and simplest, is the residual pressure calculation. A first-order trend is computed from the pressure surface and a residual is computed. Negative values indicate a favorable situation for oil trapping. The computed dip direction and angle may be modified and the residual pressure map re-computed. The residual pressure map is indicative of hydrodynamic trapping potential.

The second entrapment pressure is iterative and CPU intensive. This is called the migration pressure. The normal spill-point of a structure or stratigraphic trap is delineated with this computation and represents non-hydrodynamic trapping. The oil migration feature is an iterative grid-based calculation, which attempts to model where oil accumulates as a result of movement along this pressure surface. Initially, one unit (or "drop") of oil is assigned to each grid cell of the calculated pressure grid. The minimum pressure is investigated in the surrounding eight cells. If this pressure is at least one psi less than the pressure in the source cell, the adjacent minimum-pressure cell becomes the destination cell, otherwise the oil drops do not move. The user specifies a pressure factor which controls how the pressure surface changes as drops move. The “psi/drop” factor determines the threshold pressure for the “oil drops” as they migrate into a structure or trap. A factor of 3 produces good results for most situations. A larger “psi/drop” factor allows greater oil charge in a trap (the spill-point moves further down the structure) and requires more iterations. A smaller “psi/drop” factor decreases the potential charge for a trap and requires less iterations. When comparing migration pressure calculations from one 3D survey to another, the “psi/drop” factors need to be the same. At the completion of the iteration process, a map is created that shows the pressure charge resulting from the oil migration.

There may be value in both calculations of entrapment pressure. Both can be attributes for prediction of oil production characteristics with the ICS Neural

Solver. The neural solver will weight each entrapment method as best fits the training data.

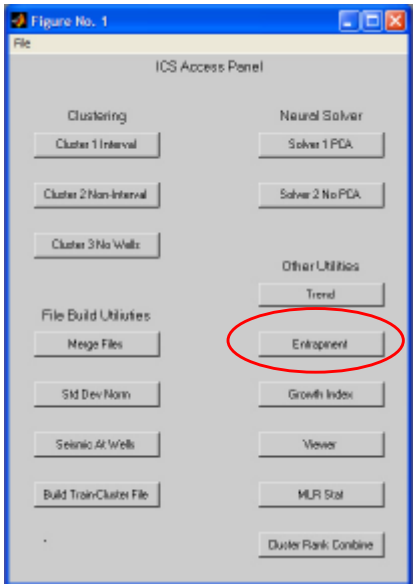

The Entrapment utility can be accessed from the main ICS control panel.

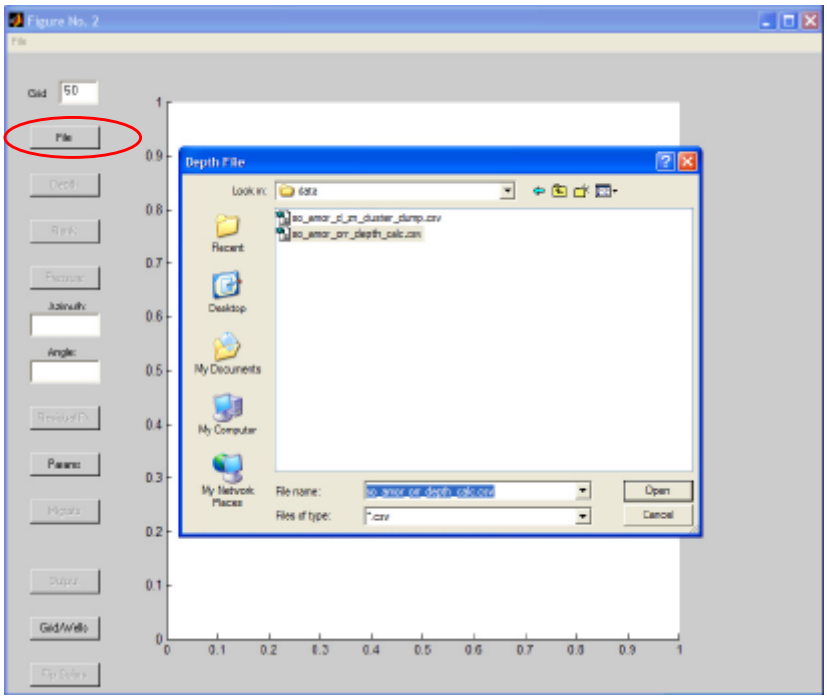

After setting the grid size (50-100), click the “file” button and a file navigation window will appear. Navigate to the directory containing the reservoir depth file. The depth file will have the depth in the fourth column. Coordinates are in the first two columns. The third column maybe blank or contain a trace number.

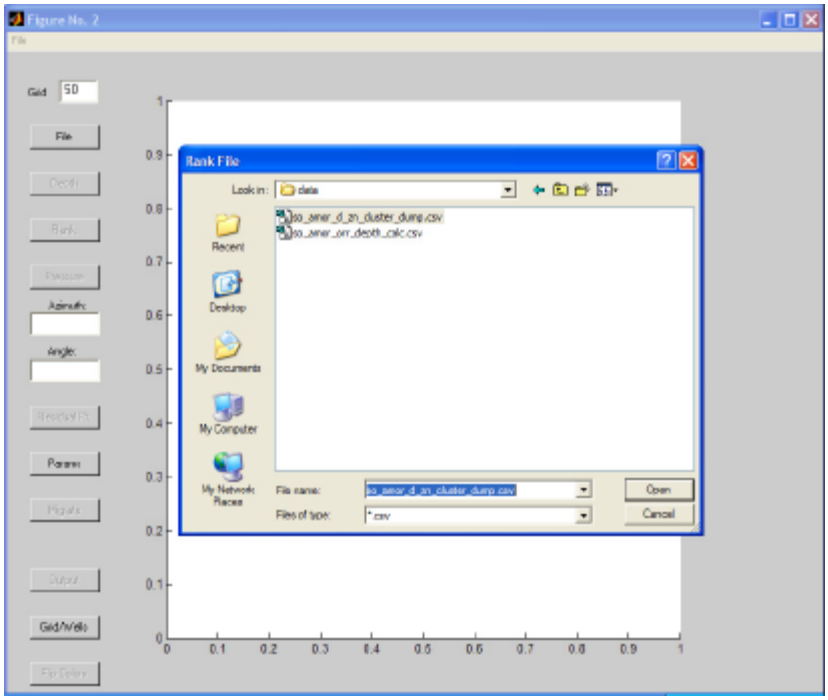

After the depth file is read, another file navigation window appears for the cluster-rank file. If none will be used, click “cancel.”

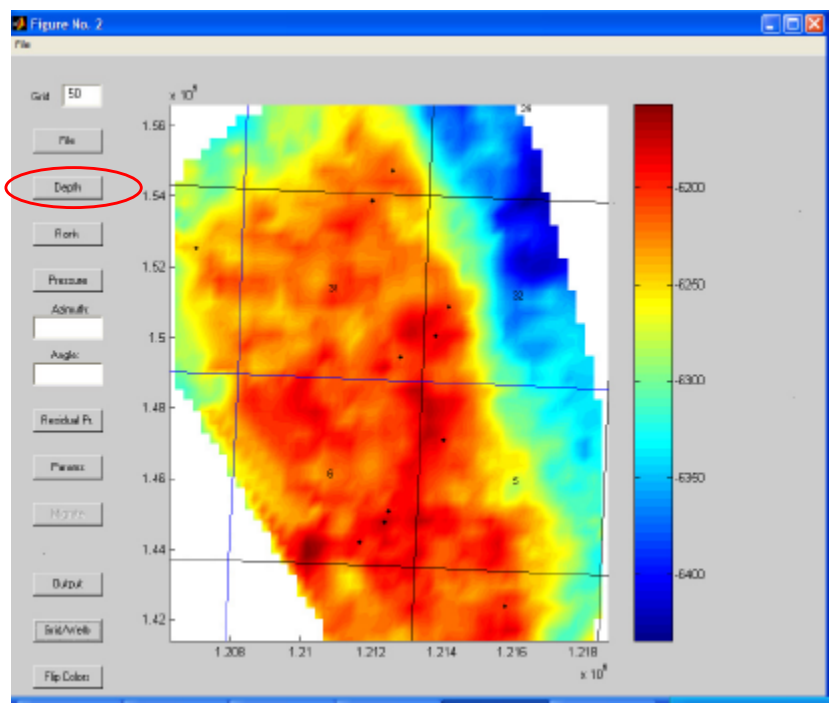

Clicking the “depth” button will display the reservoir depth map.

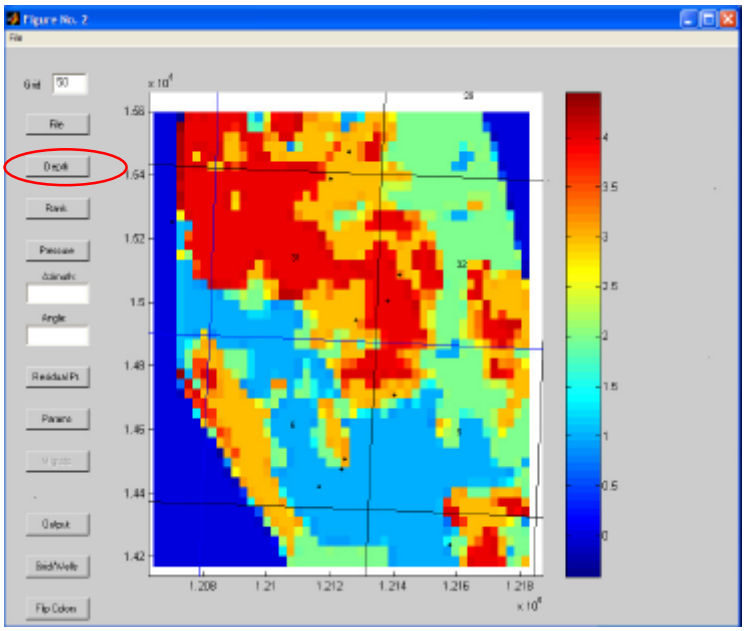

Clicking the “rank” button will display the cluster-rank map.

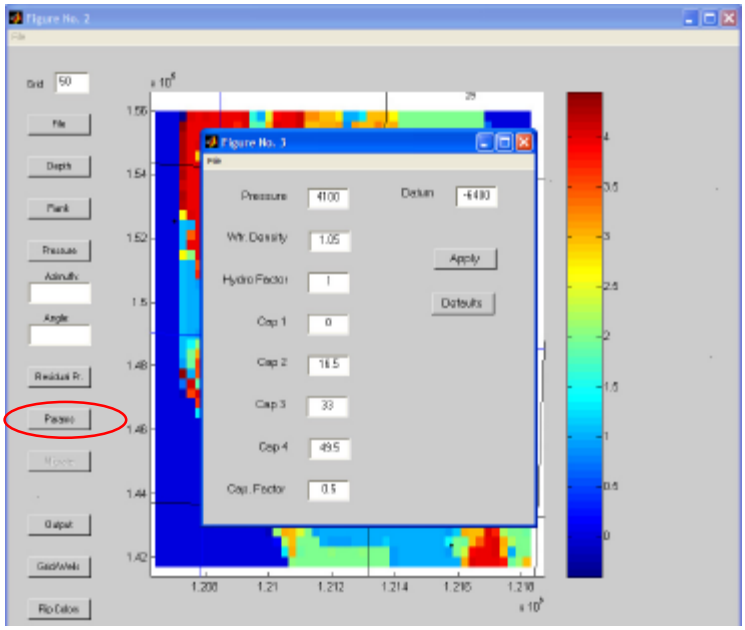

Clicking the “parameters” button will display a new window. The “parameters” button allows modification to reservoir pressure and capillary pressure adjustment for rock-quality rank. The default capillary factor of 0.5 would be appropriate for strong capillary adjustments. A factor of “zero” would cancel capillary adjustments. Capillary pressures for rock-quality rank are arbitrary and can be changed. Normal reservoir pressure at a datum is entered with a density of reservoir water. Ignore the “hydro-factor” entry. Click “apply” and close.

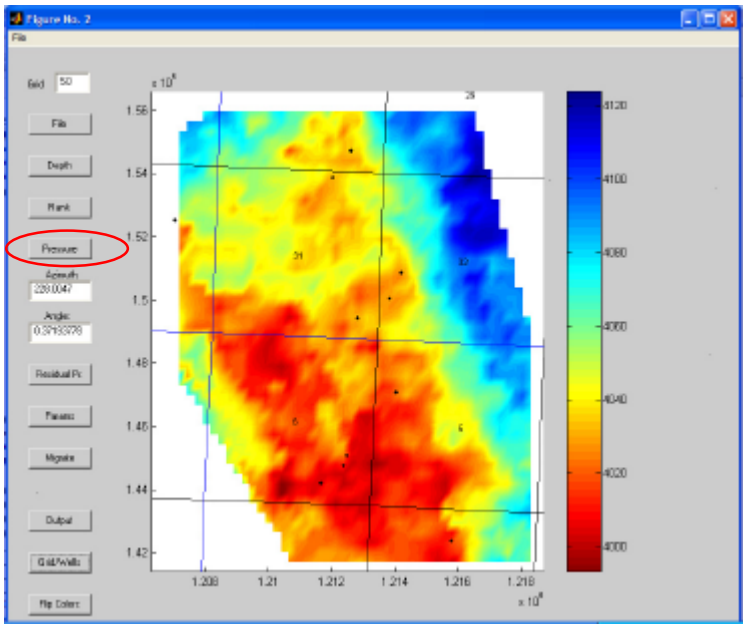

Clicking the “pressure” button will draw the reservoir pressure map that has been modified by the capillary adjustments for rock-type. The computed dip angle and azimuth are displayed.

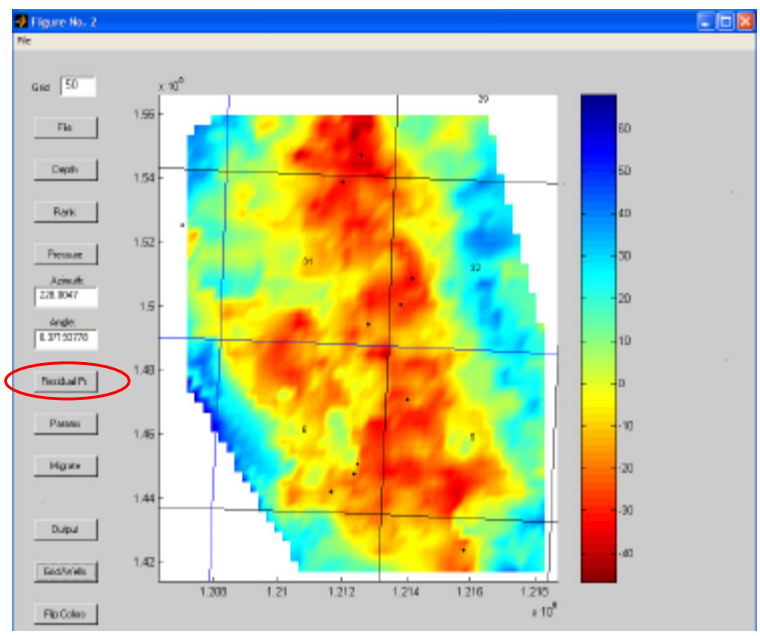

Clicking the “residual pressure” button will produce a map of the residual from the pressure trend surface. A negative pressure is to be interpreted as favorable in the context that oil will seek a minimum potential. Values for angle and azimuth may be adjusted.

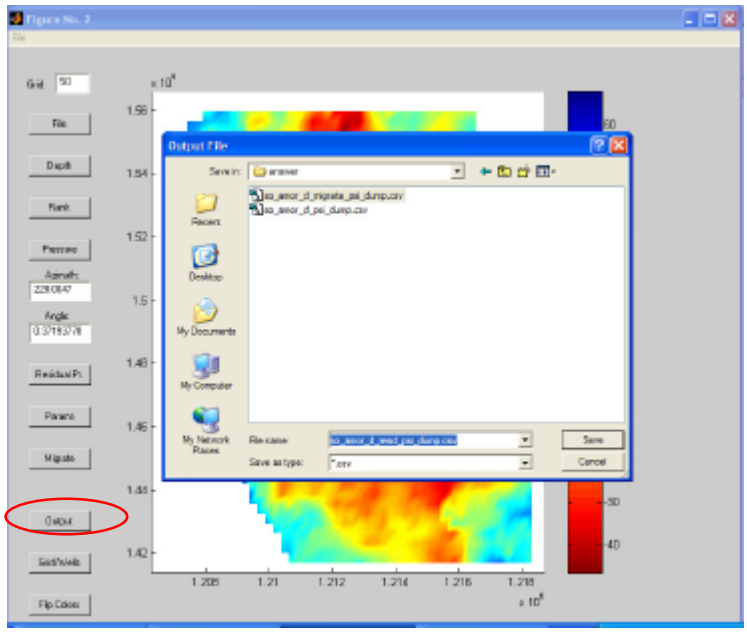

Any map that is currently in display can be saved to a file by clicking the “output” button.

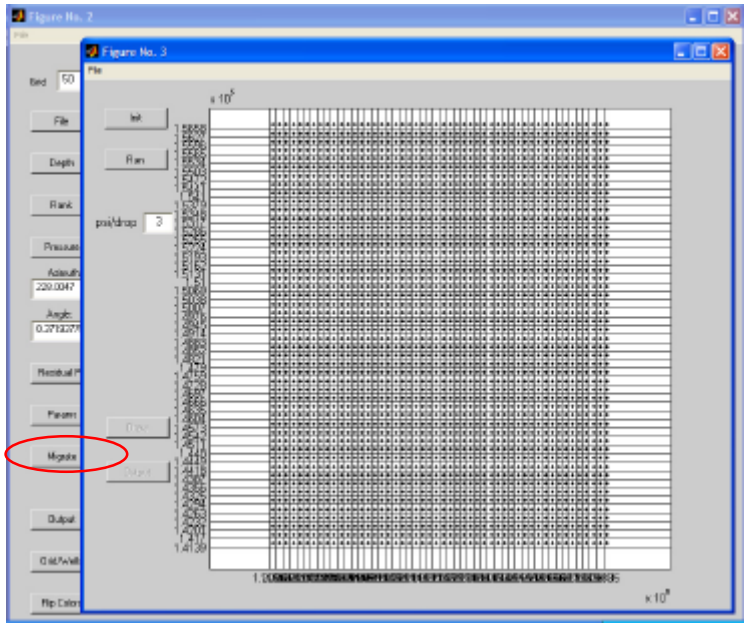

From a display of pressure, select the “migrate” button to activate a new window for calculation of another indicator of entrapment. It is informally called migration pressure. This computation is iterative and CPU intensive. First, click the “initialize” button and the grid will be drawn. Second, set the “psi/drop” factor from 1 to 5. Finally, click the “run” button to start the iterations.

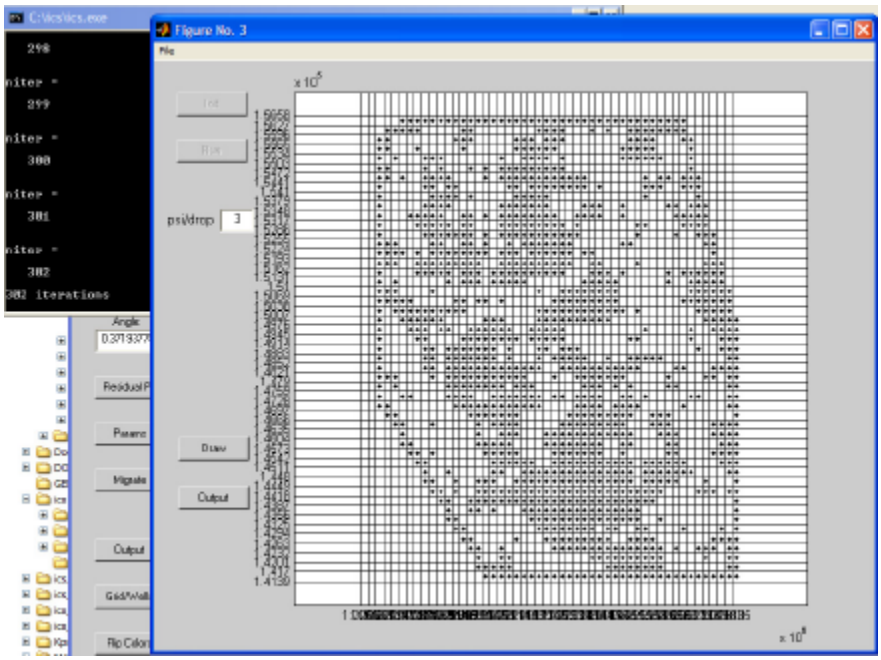

The command window will display the iteration count. At convergence, a map will be drawn that shows cells that are charged. Click the “draw” button to transfer this calculation to a color map in the main viewing area.

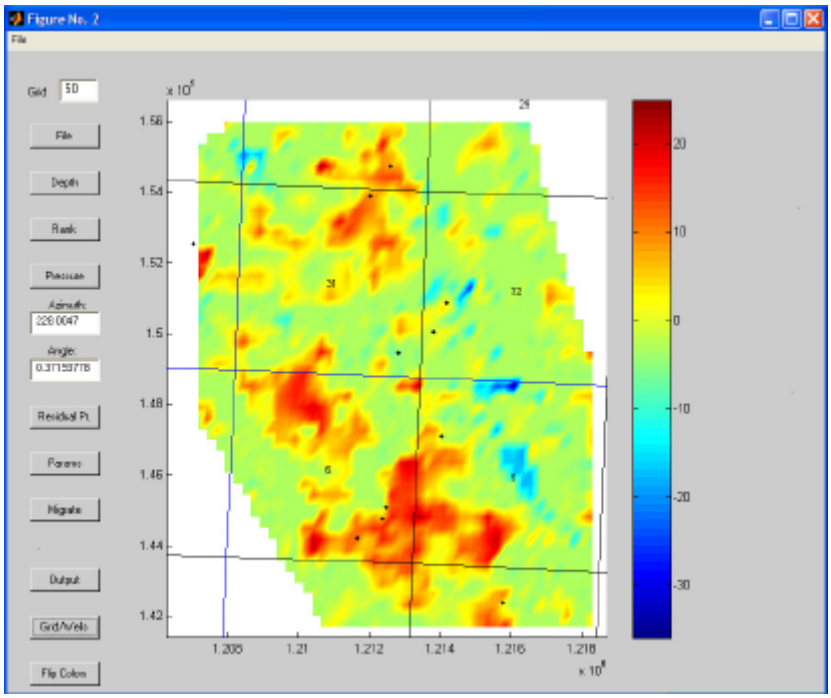

A map is shown for the results from the migration computation. Positive pressure is favorable. This map can be written to an output file.

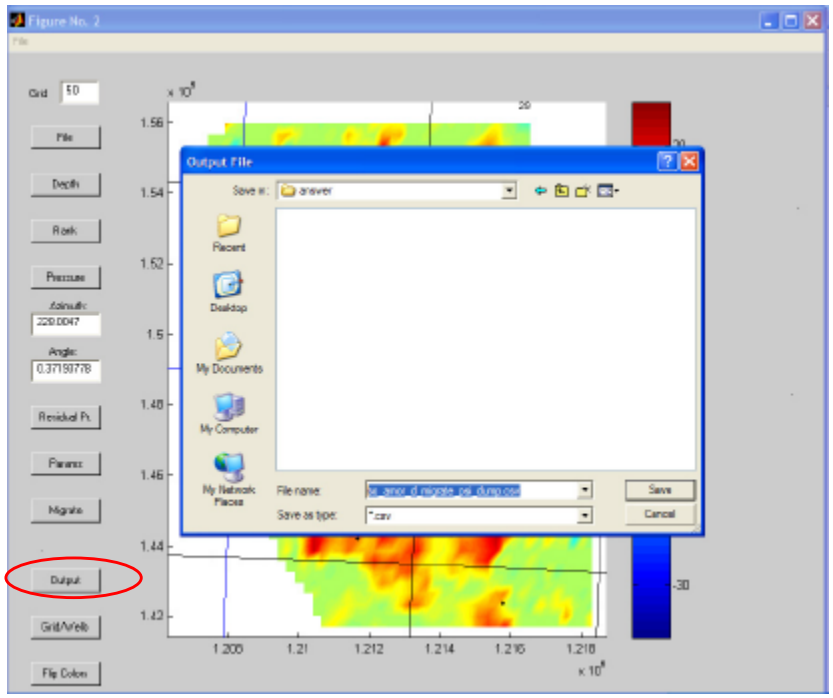

Click the “output” button and a file navigation window will be presented for saving the map results.

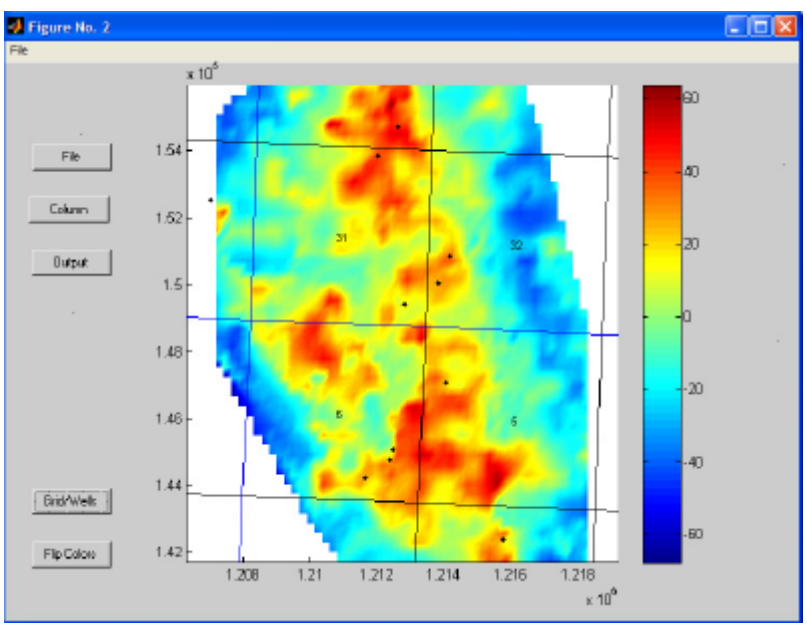

A map is shown that represents the difference of the migration and residual pressure maps.

Example-practice files for the Entrapment tool are found under the directory: ICS_MANUAL\OTHER_UTILITIES\ENTRAP

Growth Index Tool, Other Utilities

Structural drilling prospects from seismic data are frequently based on two maps. One is a map of thinning (an isochron) from a shallow marker bed to the reservoir marker. The second map is of the time structure at or near the reservoir target. Where the two maps are coincident, there is confidence that the prospect structure is valid. However, there are occasions when it is not clear which time interval is best. The ICS Growth Index Tool computes the thinning residual of all intervals and the time structure residual of all tops from the input file to produce a map showing a composite score or "growth index." Instead of looking at several isochron maps and a reservoir time map, this tool produces a value map, which previously was only subjective in the mind of the interpreter. In the example file, the are 3 seismic time horizons and "zero." The Growth Index Tool computes the residual of the 3 seismic time surfaces and the 3 interval times. Since there are 6 maps, an ideal score will be 6 for maximum thinning and structure. If the growth index from one 3D survey is to be compared (or used as training data) at another 3D survey, the same tops must be used at each survey.

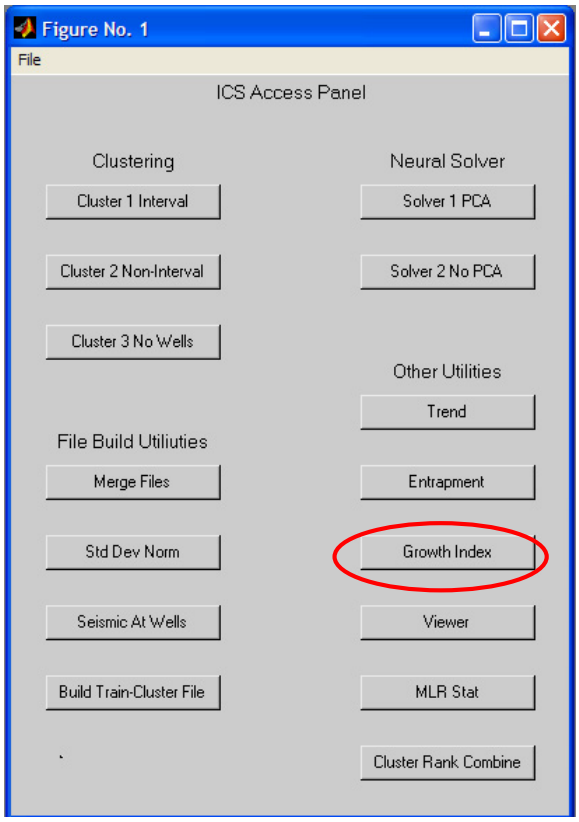

Access to the Growth Index Tool is from the ICS main panel.

Example-practice files for the Growth Index Tool are found under the directory: ICS_MANUAL\OTHER_UTILITIES\GROWTH-INDEX

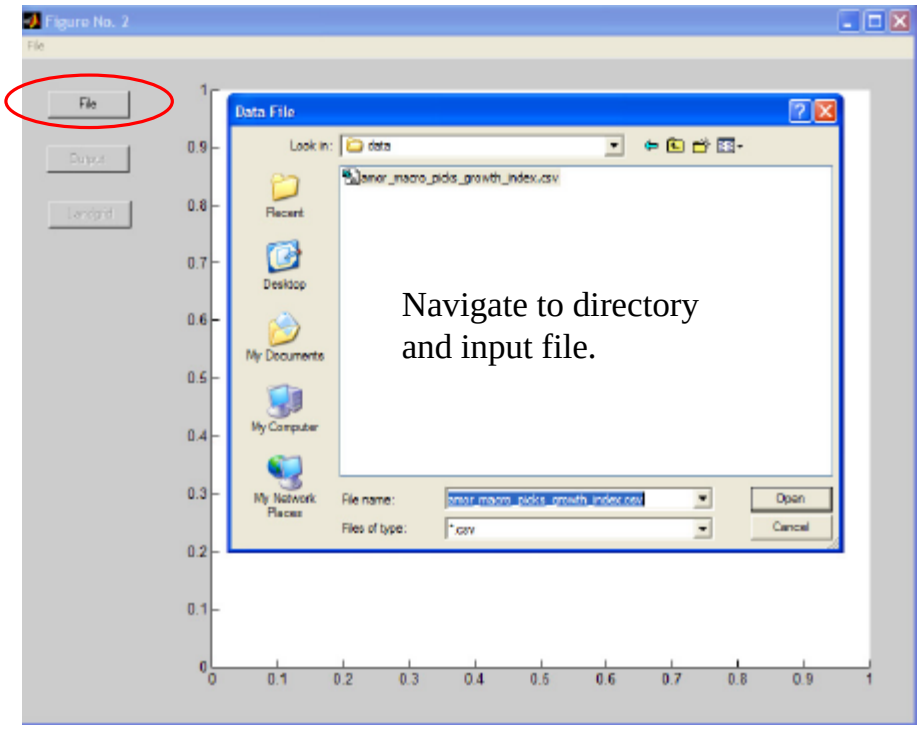

Clicking the “file” button will open a file navigation window. Navigate to the appropriate directory and select the growth-index input file.

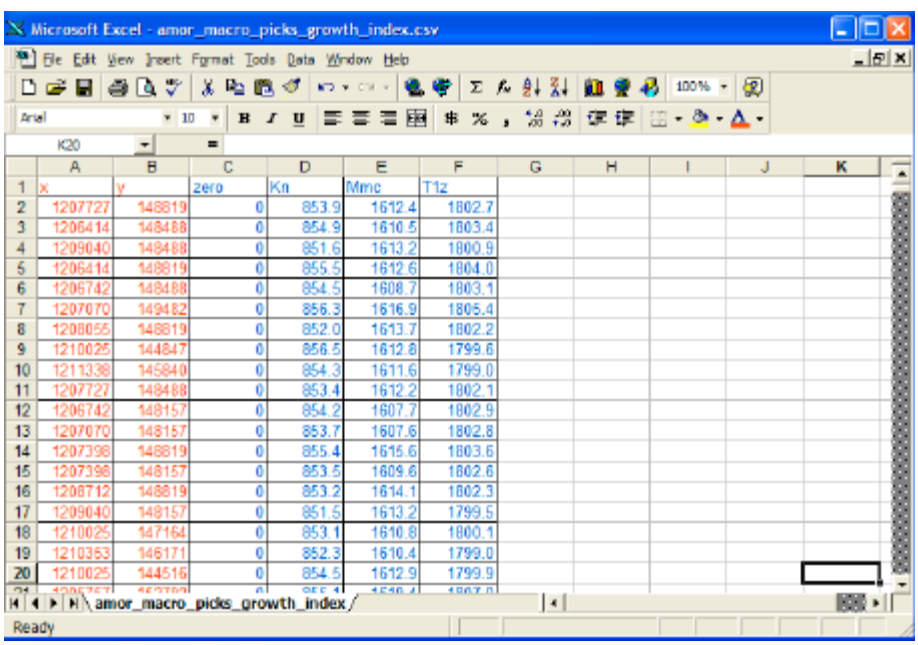

	A	B	C	D	E	F
1	x	y	zero	Kn	Mmc	T1z
2	1207727	148819	0	853.9	1612.4	1802.7
3	1206414	148488	0	854.9	1610.5	1803.4
4	1209040	148488	0	851.6	1613.2	1800.9
5	1206414	148819	0	855.5	1612.6	1804.0
6	1206742	148488	0	854.5	1608.7	1803.1
7	1207070	149482	0	856.3	1616.9	1805.4
8	1208055	148819	0	852.0	1613.7	1802.2
9	1210025	144847	0	856.5	1612.8	1799.6
10	1211338	145840	0	854.3	1611.6	1799.0
11	1207727	148488	0	853.4	1612.2	1802.1
12	1206742	148157	0	854.2	1607.7	1802.9
13	1207070	148157	0	853.7	1607.6	1802.8
14	1207398	148819	0	855.4	1615.6	1803.6
15	1207398	148157	0	853.5	1609.6	1802.6
16	1208712	148819	0	853.2	1614.1	1802.3
17	1209040	148157	0	851.5	1613.2	1799.5
18	1210025	147164	0	853.1	1610.8	1800.1
19	1210353	146171	0	852.3	1610.4	1799.0
20	1210025	144516	0	854.5	1612.9	1799.9

An example of is shown of a growth-index data file. Data are three seismic-reflection times and zero. An unlimited number of horizons or depths may be used, but three to five are recommended.

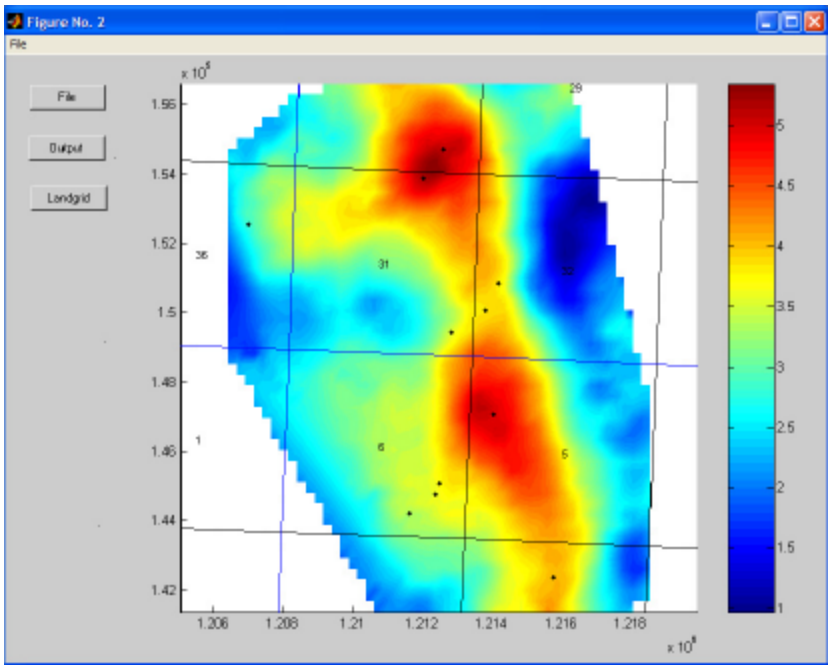

A map view is shown of a computed growth index. A value of 6 represents the maximum structure and thinning for three seismic horizons, Niobrara, Mission Canyon and Red River.

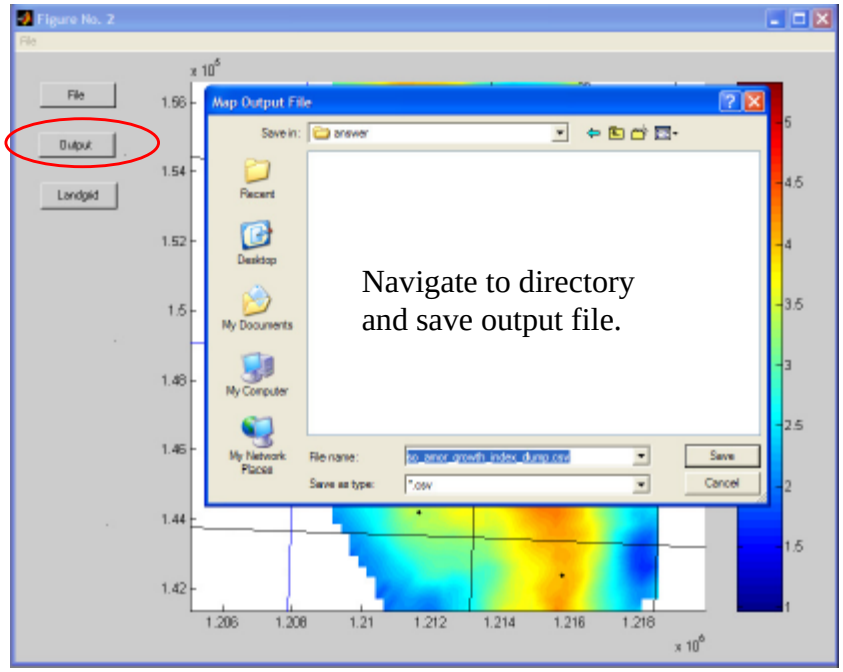

Clicking the “output” button will open a file navigation window. Navigate to the desired directory and supply a file name with csv extension.

Viewer Tool, Other Utilities

The Viewer Tool has two uses. First it can be used to display and quality check 3D seismic attribute files or any grid-type data in two-dimensional space (x,y,z). Second, linear-regression coefficients can be applied to data columns to transform attributes to another attribute.

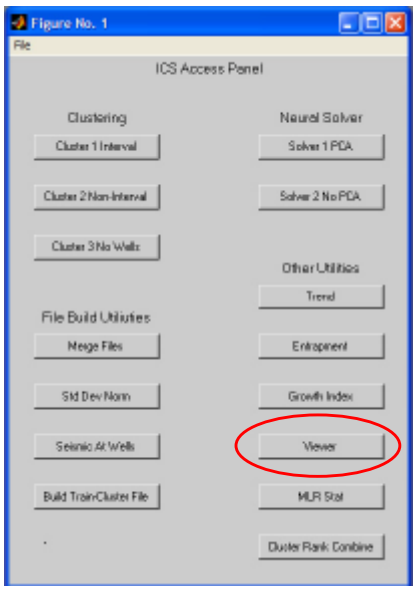

The Viewer Tool utility can be accessed from the main ICS panel.

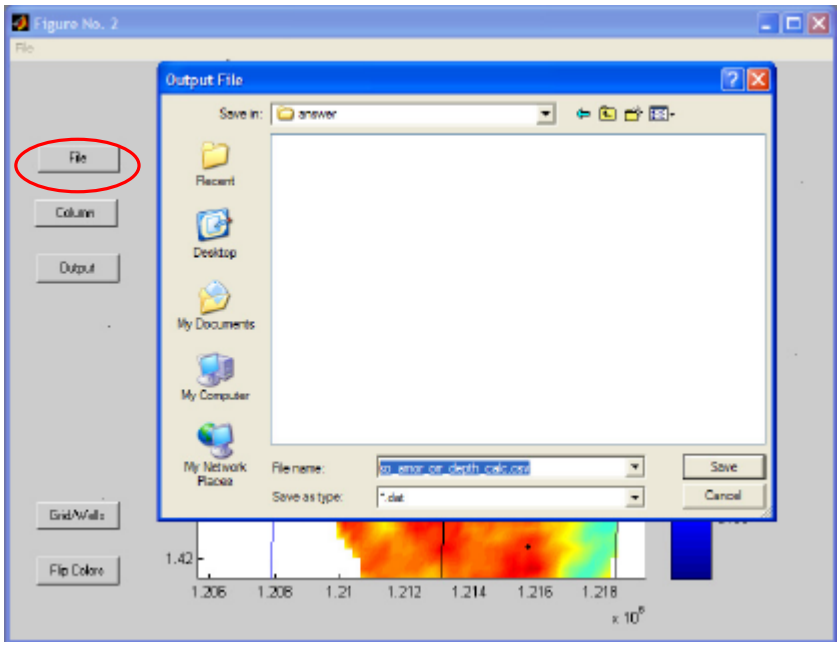

Clicking the “file” button opens a file navigation window. Navigate to the appropriate directory and select the file.

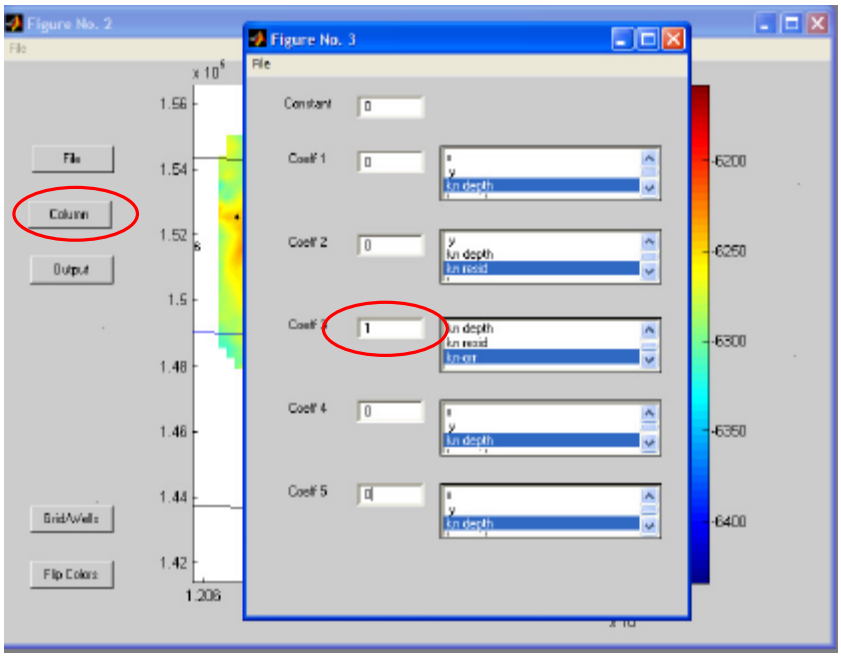

After the file is read, the “column” button becomes active. Click the “column” button and a window appears that is used to transform multiple data. Application of a coefficient of “one” and constant of “zero” will produce a map view of the data. Close window by clicking the upper-right “X.”

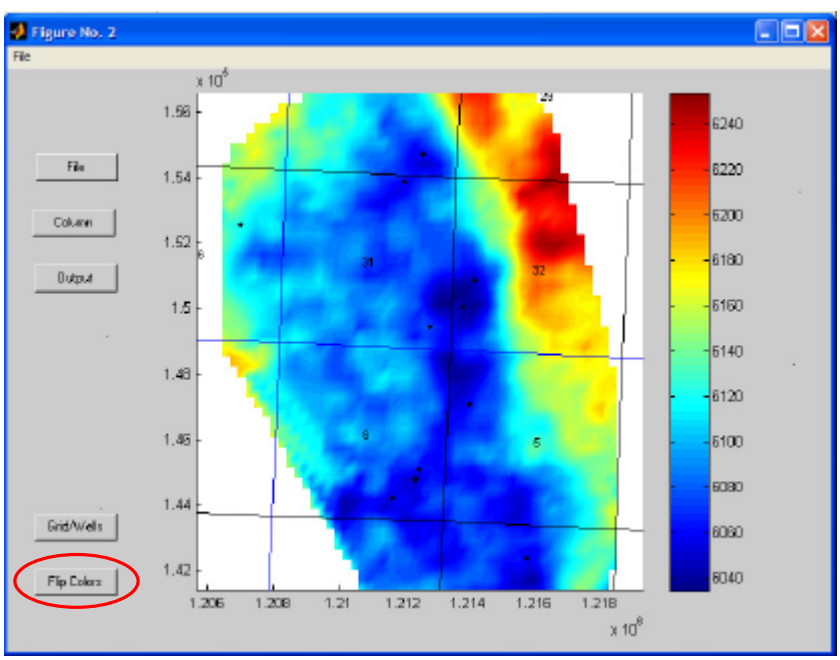

A map view of the selected data is presented in the map window. Clicking the “flip colors” button will change the color scheme. A land grid and well spots can be displayed if the appropriate files have been created.

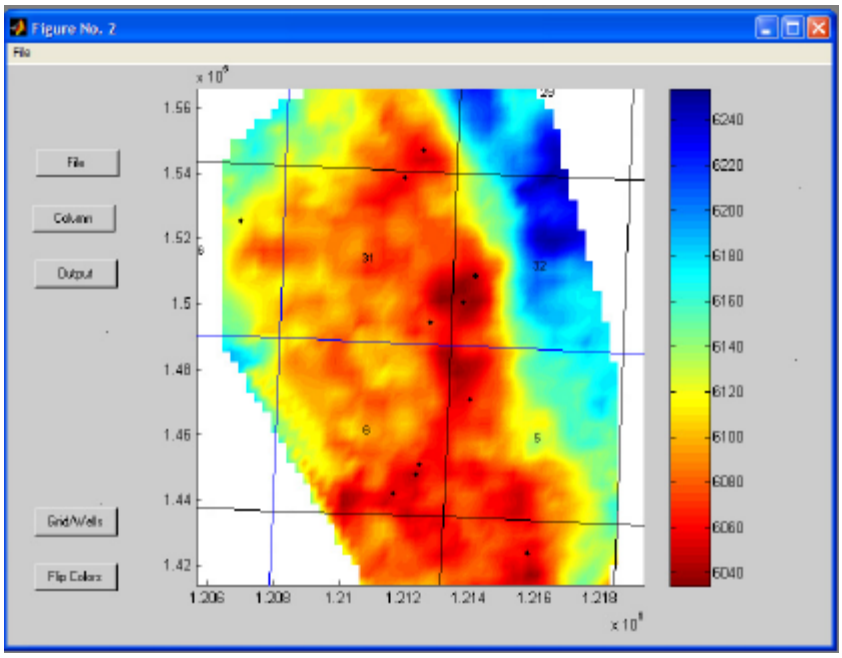

Result after clicking “flip colors” button is shown.

Practice-example files for the Viewer Tool are found under the directory:
ICS_MANUAL\OTHER_UTILITIES\VIEWER

MLR STAT, Other Utilities

The MLR-STAT utility uses standard multiple-linear-regression to correlate reservoir attribute measured at a well (such as depth) with seismic attributes (such as reflection time at various formation markers. The routine uses 2 files. The training file contains well locations, well identifier (API), measured reservoir items in any number of columns (such as formation depths) and seismic attributes at the well locations. The second file is called a map file and contains the seismic data appropriate for the problem (such as formation reflection times). The “Build-Train-Cluster-File” utility is used to construct a properly formatted training file. The MLR-STAT utility has two optional buttons for pre-processing. The filter button will remove any “NaN” found in a data column and clip the data at +/- 2 standard deviations. The PCA button will perform “principal component analysis” and reduce the seismic data columns by this mathematical method. This is optional, but is useful where there are more seismic data columns than the number of well or control data in the training file. This condition will cause multiple-linear-regression to fail. It should be noted that the tool can be used to attempt correlation of different data such as porosity-thickness with seismic amplitudes or producing oil-cut with sub-sea depth.

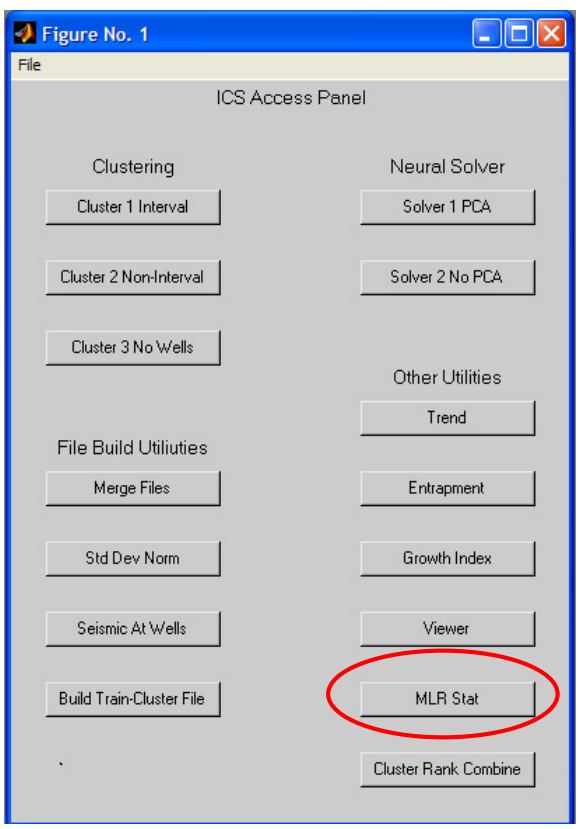

Access to the MLR-STAT utility is from the ICS main panel.

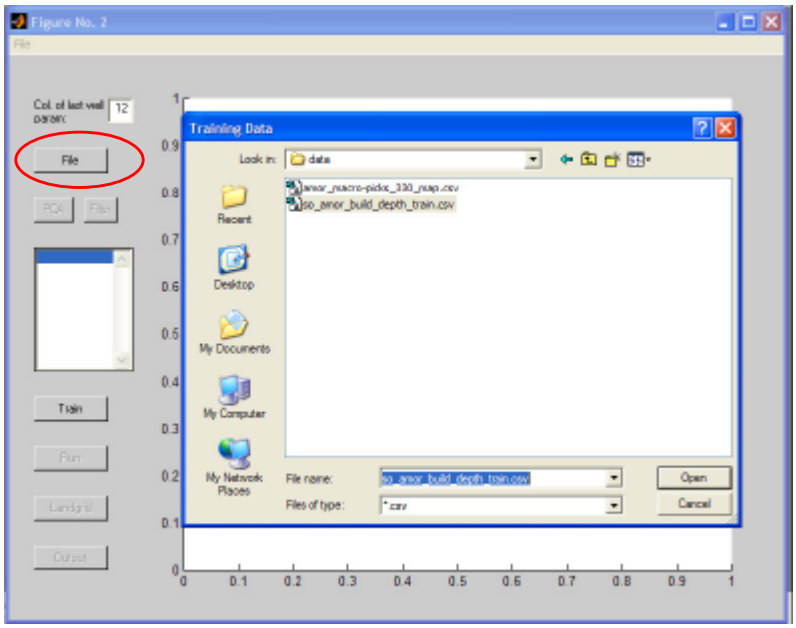

After setting the value for the last well parameter in the training file, click the “file” button and a navigation window will open. Navigate to directory containing the training file. The training file contains well locations with formation depths and intervals as the well parameters.

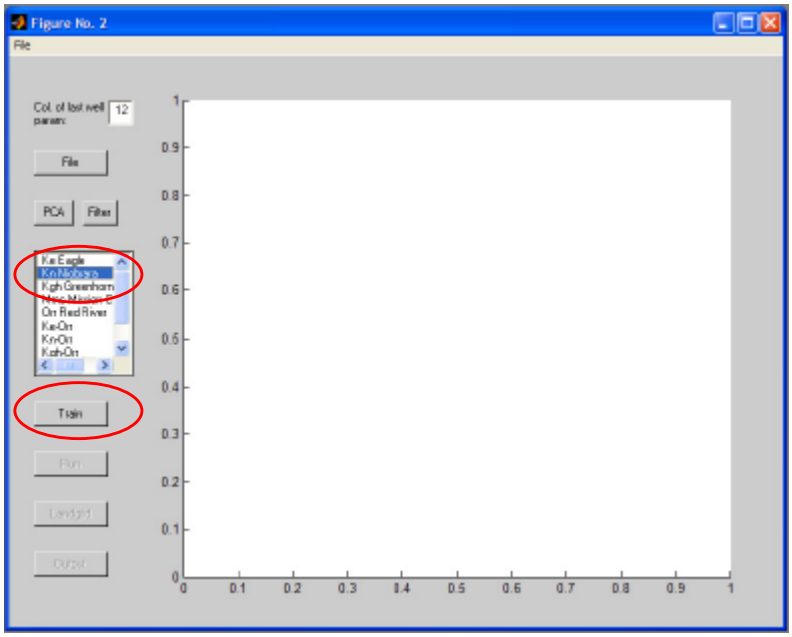

Select the well parameter for training and click the “train” button. In this example, the sub-sea depth of the Niobrara formation will be predicted from a map file containing seismic horizon times.

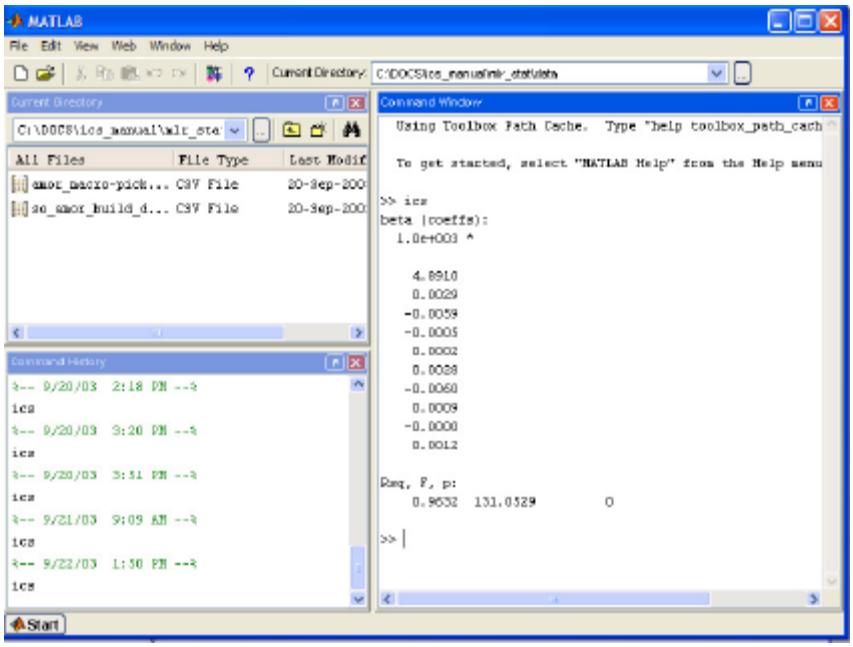

The command window will display the correlation coefficients and statistical parameters.

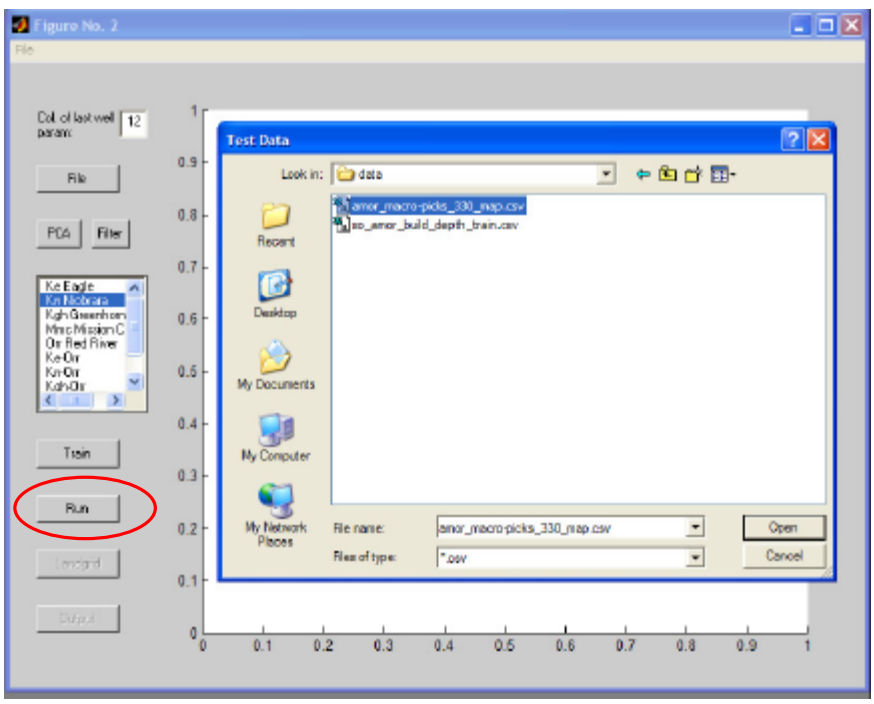

Clicking the “run” button will open a file navigation window for the map file. Navigate to the directory containing the map file. The map file contains the seismic horizon times.

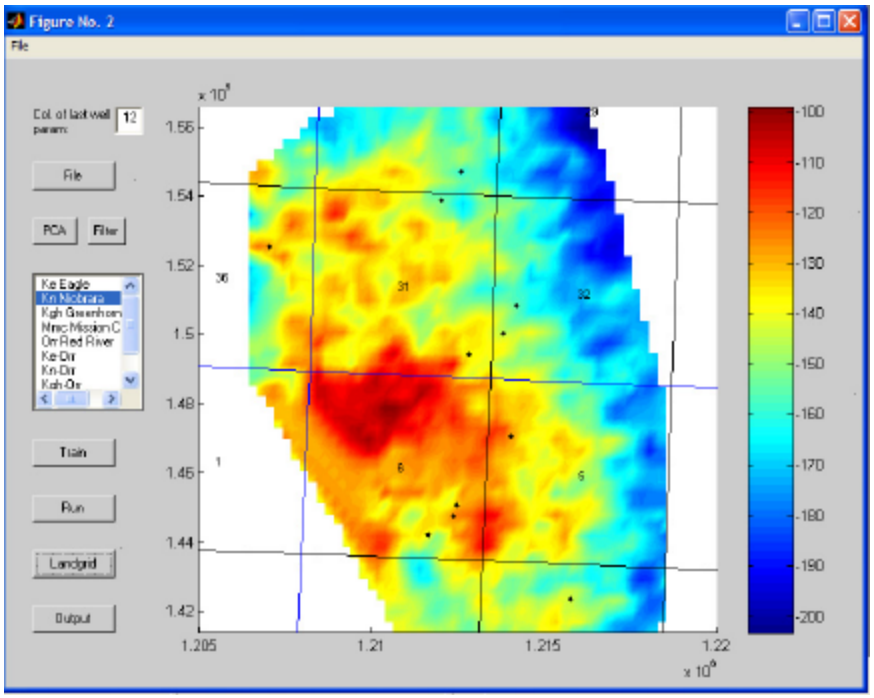

After selecting the map file, the multiple-linear-regression correlation is applied and a map of Niobrara depth will be created.

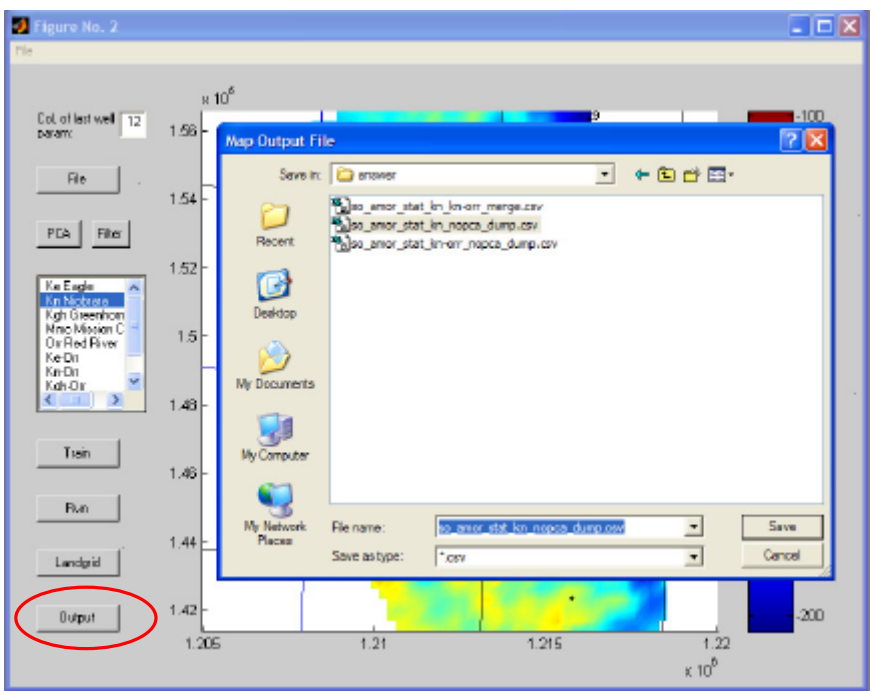

The values displayed by the map can be exported to file by clicking the “output” button.

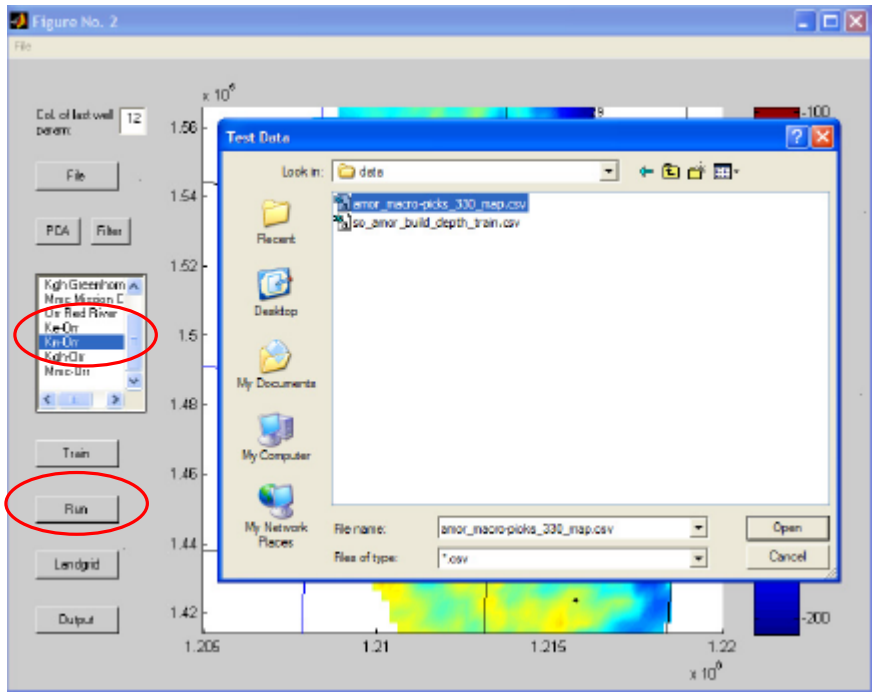

The training file is used again to predict the interval thickness from the Niobrara to Red River. After training is complete, the “run” button is selected and file navigation widow appears. Navigate to the appropriate map file.

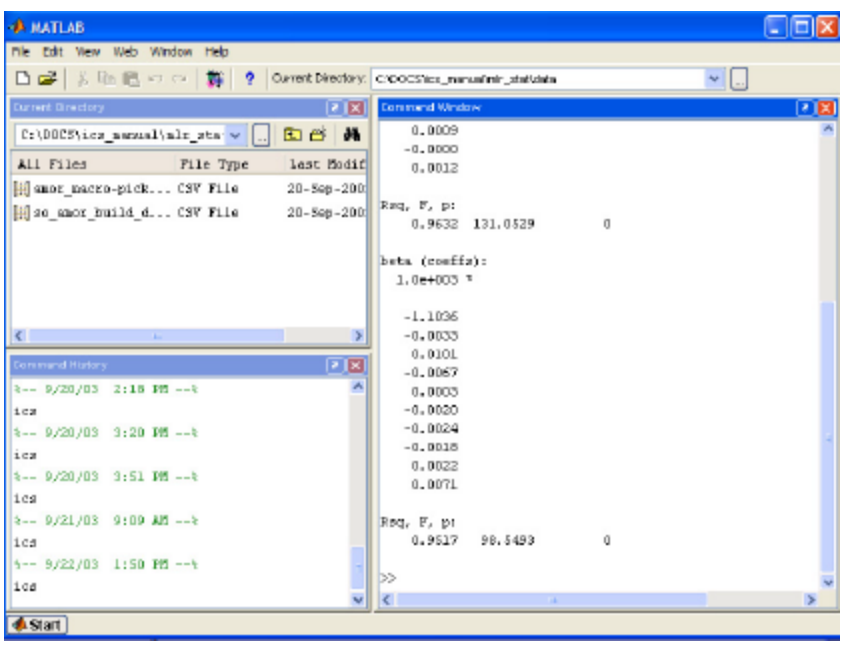

The command window will display the correlation coefficients and statistical parameters.

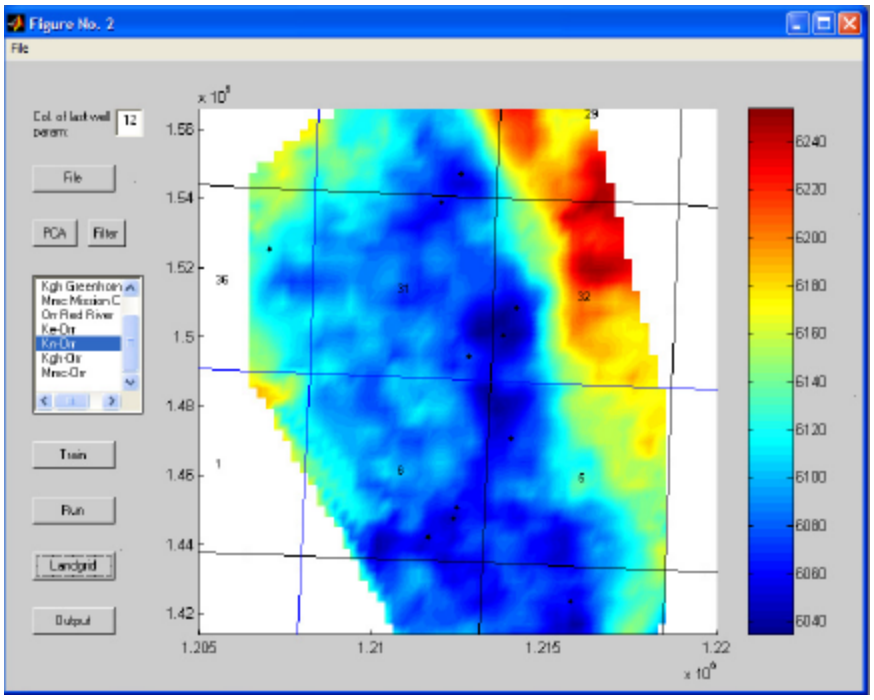

After selecting the map file, the multiple-linear-regression correlation is applied and a map of Niobrara- Red River thickness will be created.

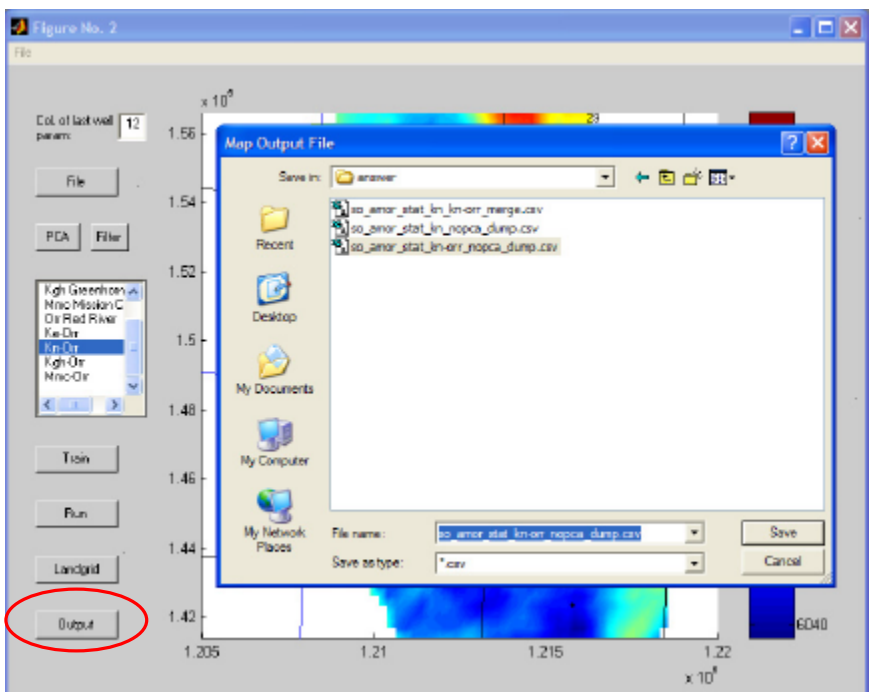

The values displayed by the map can be exported to file by clicking the “output” button.

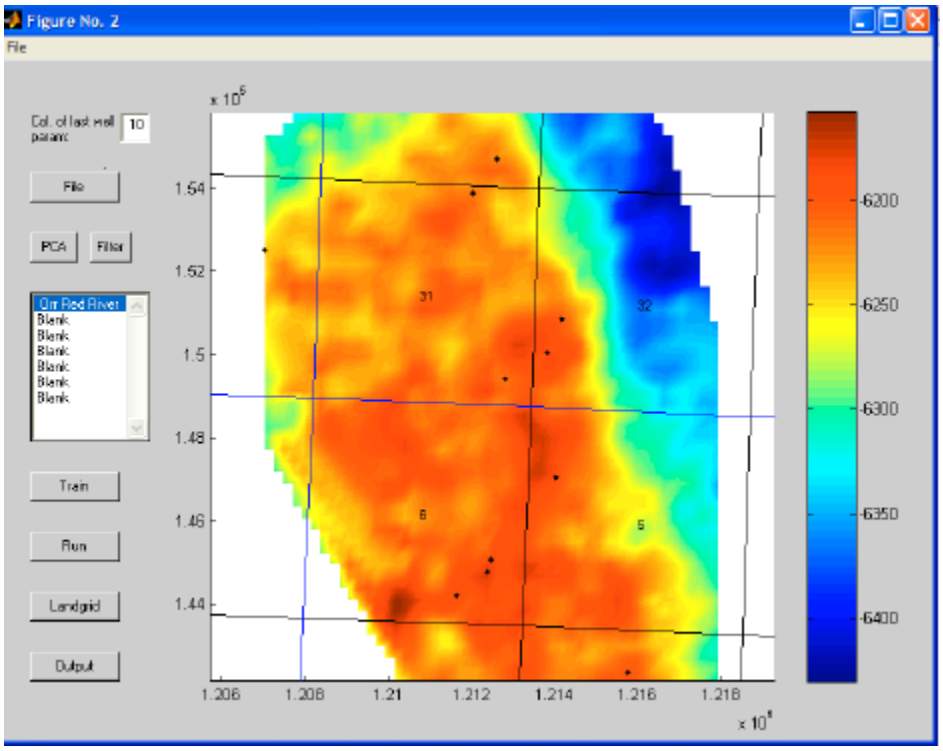

The output from the two maps can be combined with the “Merge” utility and then viewed with the “Viewer” utility. Summation of the Niobrara depth and Niobrara - Red River thickness will produce a Red River depth map as shown.

Practice-example files for MLR-STAT tool are found under the directory: ICS_MANUAL\OTHER_UTILITIES\MLR_STAT

Cluster Rank Combine, Other Utilities

The Cluster Rank Combine utility is designed to weight and sum output from either the Cluster 1 or Cluster 2 Tool. The cluster-rank output files are copied to an empty work directory. After opening the Cluster Rank Combine utility, import the cluster rank files by typing the path in the file location window (such as c:\work). Close by clicking the "X." The files will be read and data columns displayed in a window. Select the rank columns to be weighted and summed by using a control-left click with the mouse.

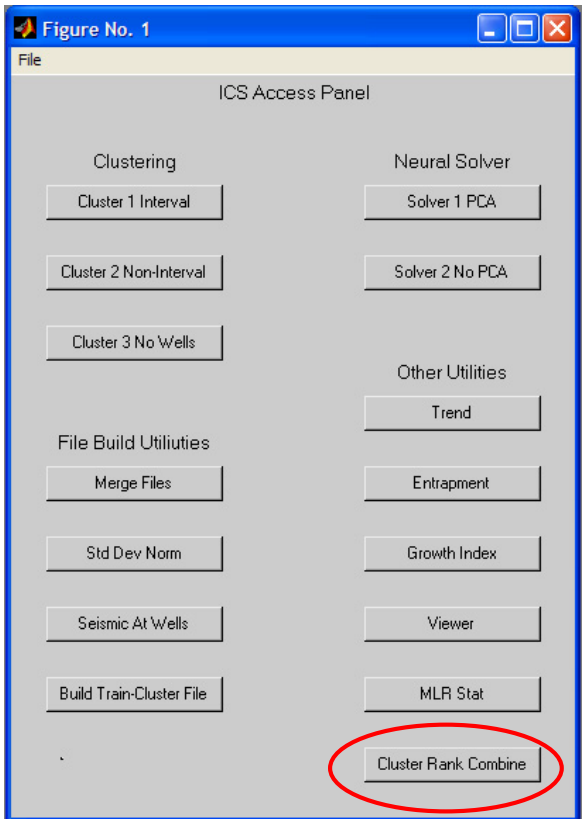

Access to the Cluster Rank Combine utility is from the ICS main panel.

Practice-example files for the Cluster Rank Combine tool are found under the directory:
ICS_MANUAL\OTHER_UTILITIES\COMBINE

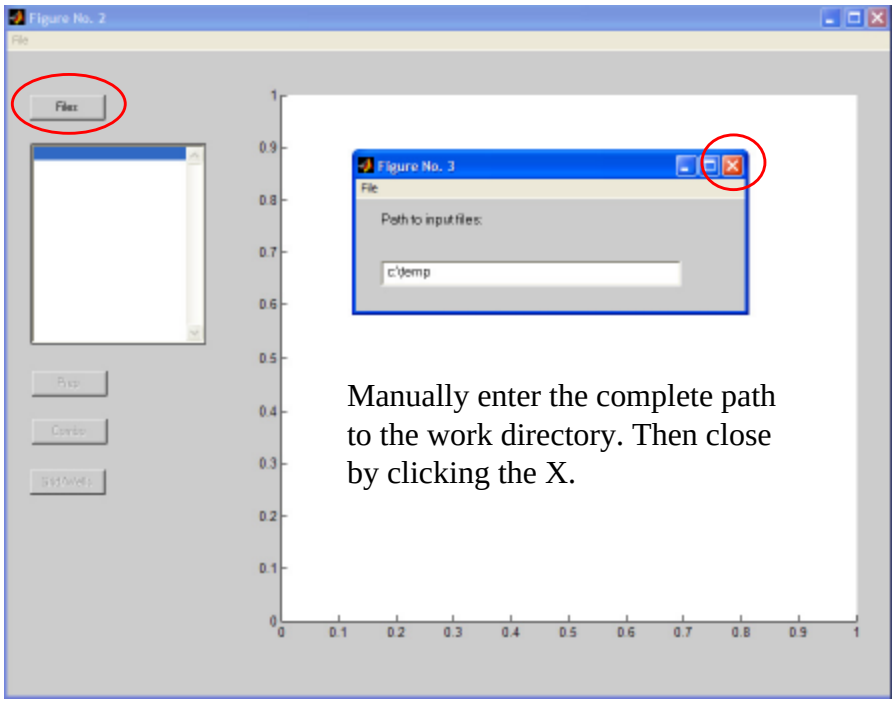

Click the “files” button and a dialog box will appear. Manually type the path and close. The working directory should contain only those cluster-output files that are to be summed.

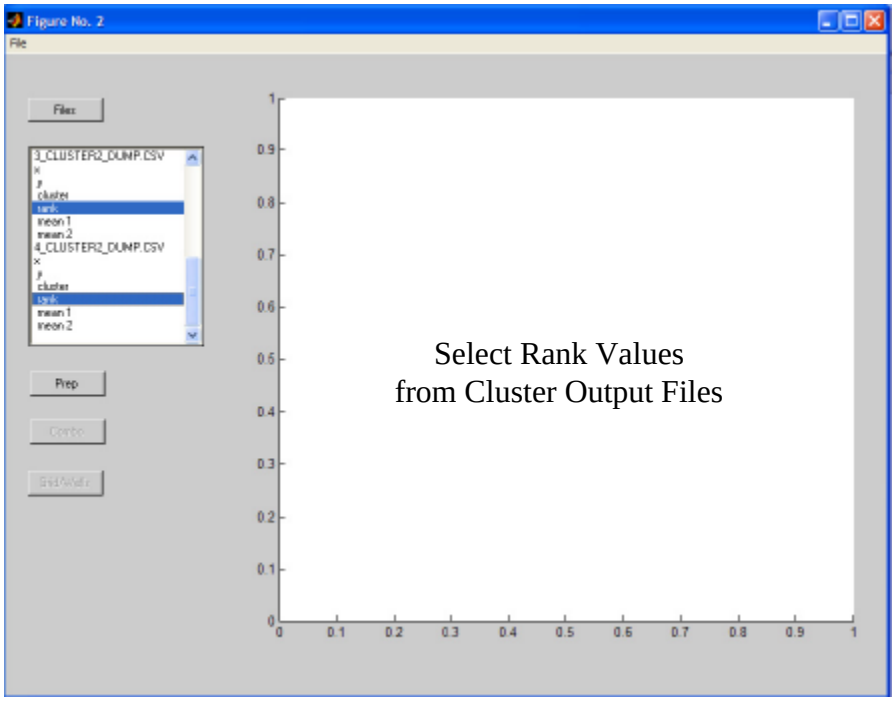

Use a control-left click to select cluster rank from all files, then click “prepare” button.

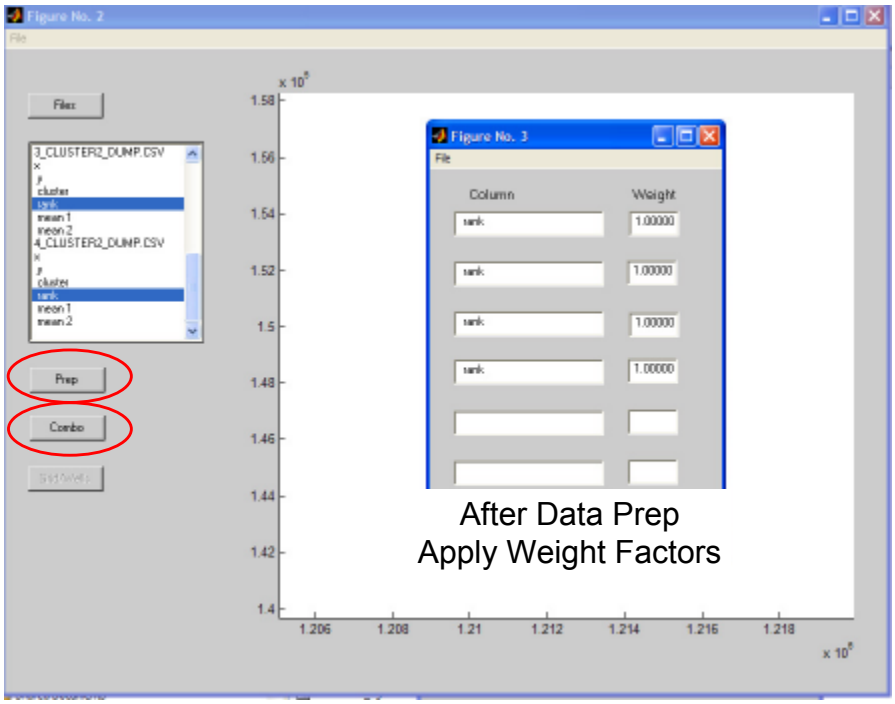

After the selected ranks are combined by gridding, click the “combine” button. Add weight factors as desired.

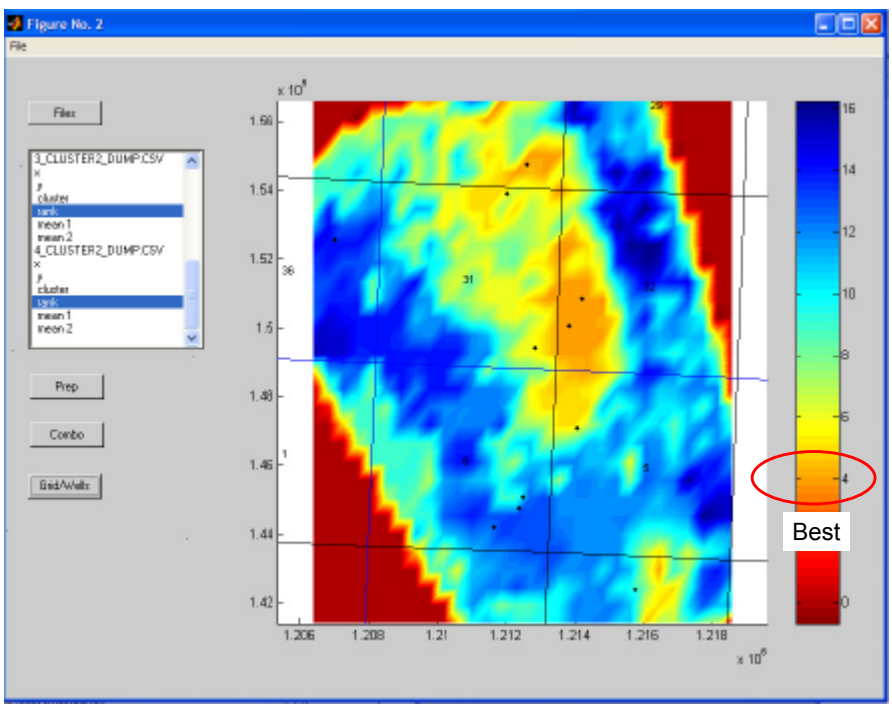

A map is produced that shows the combined equal ranking of four cluster output files.

ICS Clustering Tools

There are three versions of clustering tools in ICS. Cluster 1 Tool computes the difference of every independent data column (interval thickness or time), then calculates a trend and residual of the interval from the trend. The residual of every combination is used as a potential cluster item. Cluster 2 Tool is similar to Cluster 1 Tool except no difference or combination calculation is made. The data are used unchanged. This is useful when using seismic amplitudes with isotime data as cluster items. Cluster 3 uses no well or control data and computes only natural cluster groups. This is useful where there are few or no control wells but it is desired to see patterns in the seismic attribute data.

Cluster 1 with Intervals Tool

The Cluster 1 Tool produces clusters using differences of formation depths or seismic time (intervals). The tool is useful for clustering data that may relate to variation of thickness or interval time.

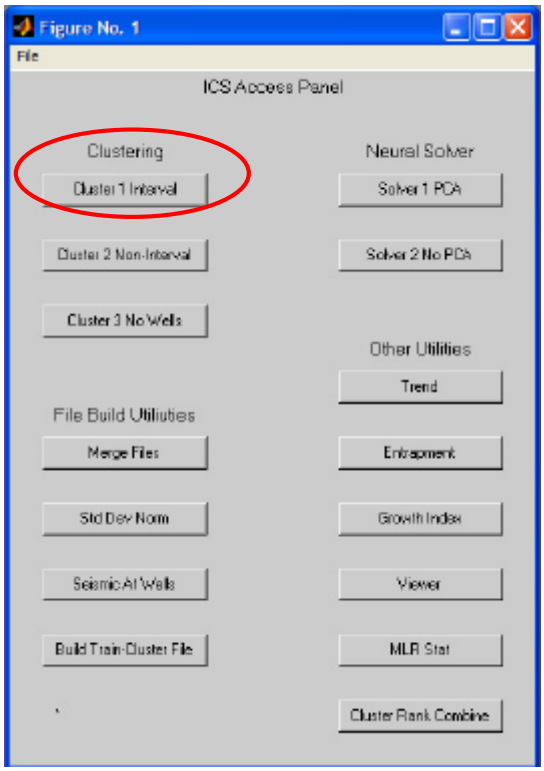

The Cluster 1 Tool is accessed from the main ICS control panel.

Practice-example files for the Cluster 1 tool are found under the directory: ICS_MANUAL\CLUSTER1

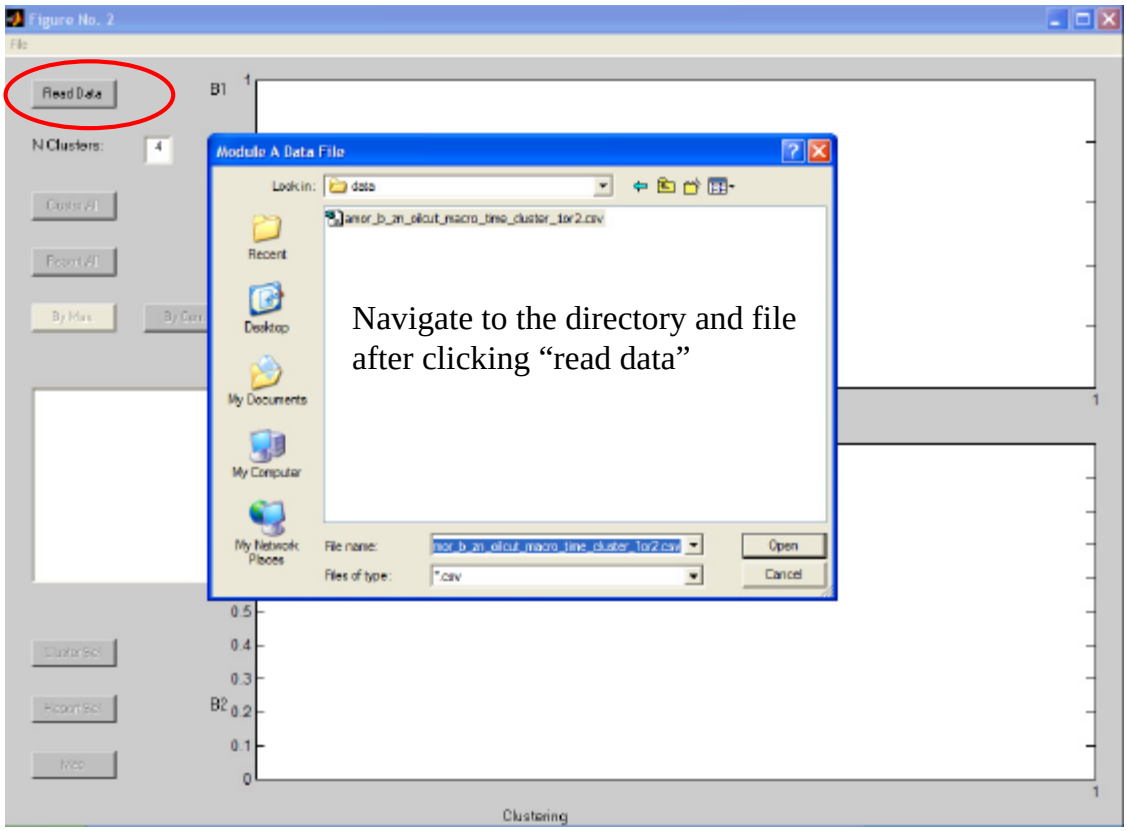

After clicking the "read data" button, a file navigation window opens. Navigate to the directory and file to use for the cluster analysis.

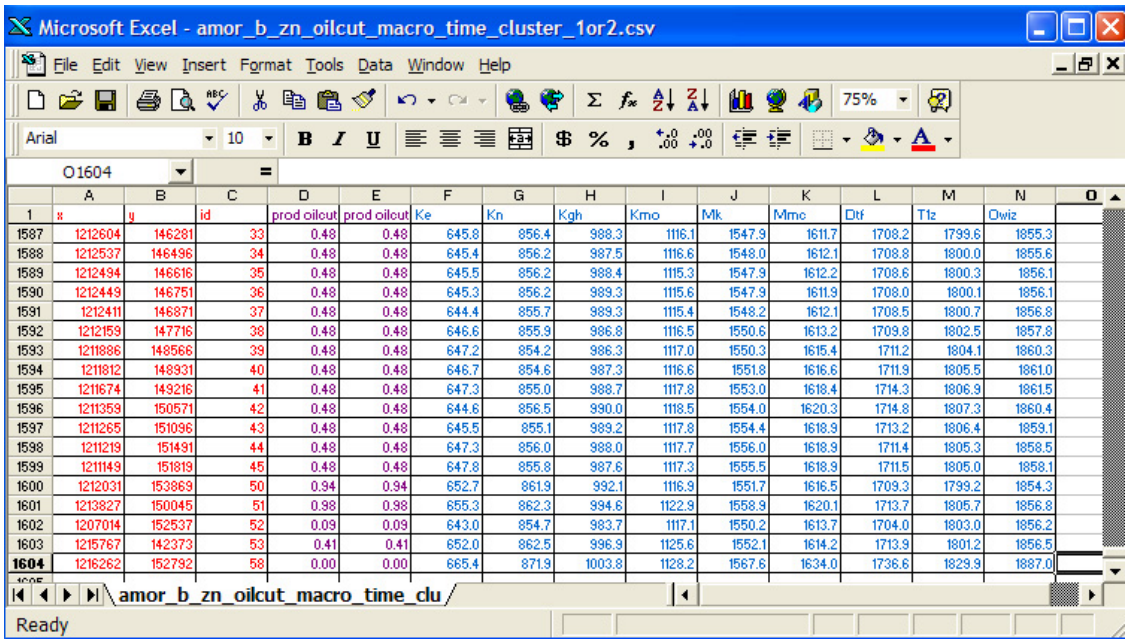

Microsoft Excel - amor_b_zn_oilcut_macro_time_cluster_1or2.csv

	A	B	C	D	E	F	G	H	I	J	K	L	M	N
1	x	y	id	prod oilcut	prod oilcut	Ke	Kn	Kgh	Kmo	Mk	Mmc	Dtf	T1z	Dwiz
1587	1212604	146281	33	0.48	0.48	645.8	856.4	988.3	1116.1	1547.9	1611.7	1708.2	1799.6	1855.3
1588	1212537	146496	34	0.48	0.48	645.4	856.2	987.5	1116.6	1548.0	1612.1	1708.8	1800.0	1855.6
1589	1212494	146616	35	0.48	0.48	645.5	856.2	988.4	1115.3	1547.9	1612.2	1708.6	1800.3	1856.1
1590	1212449	146751	36	0.48	0.48	645.3	856.2	989.3	1115.6	1547.9	1611.9	1708.0	1800.1	1856.1
1591	1212411	146871	37	0.48	0.48	644.4	855.7	989.3	1115.4	1548.2	1612.1	1708.5	1800.7	1856.8
1592	1212159	147716	38	0.48	0.48	646.6	855.9	986.8	1116.5	1550.6	1613.2	1709.8	1802.5	1857.8
1593	1211886	148566	39	0.48	0.48	647.2	854.2	986.3	1117.0	1550.3	1615.4	1711.2	1804.1	1860.3
1594	1211812	148931	40	0.48	0.48	646.7	854.6	987.3	1116.6	1551.8	1616.6	1711.9	1805.5	1861.0
1595	1211674	149216	41	0.48	0.48	647.3	855.0	988.7	1117.8	1553.0	1618.4	1714.3	1806.9	1861.5
1596	1211359	150571	42	0.48	0.48	644.6	856.5	990.0	1118.5	1554.0	1620.3	1714.8	1807.3	1860.4
1597	1211265	151096	43	0.48	0.48	645.5	855.1	989.2	1117.8	1554.4	1618.9	1713.2	1806.4	1859.1
1598	1211219	151491	44	0.48	0.48	647.3	856.0	988.0	1117.7	1556.0	1618.9	1711.4	1805.3	1858.5
1599	1211149	151819	45	0.48	0.48	647.8	855.8	987.6	1117.3	1555.5	1618.9	1711.5	1805.0	1858.1
1600	1212031	153869	50	0.94	0.94	652.7	861.9	992.1	1116.9	1551.7	1616.5	1709.3	1799.2	1854.3
1601	1213827	150045	51	0.98	0.98	655.3	862.3	994.6	1122.9	1558.9	1620.1	1713.7	1805.7	1856.8
1602	1207014	152537	52	0.09	0.09	643.0	854.7	983.7	1117.1	1550.2	1613.7	1704.0	1803.0	1856.2
1603	1215767	142373	53	0.41	0.41	652.0	862.5	996.9	1125.6	1552.1	1614.2	1713.9	1801.2	1856.5
1604	1216262	152792	58	0.00	0.00	665.4	871.9	1003.8	1128.2	1567.6	1634.0	1736.6	1829.9	1887.0

A properly formatted file for analysis with the Cluster 1 tool is shown. A properly formatted file can be created with the “Build Train-Cluster File” utility. The first two columns are reserved for coordinates. In this example we have used a state-plane system. The third column is a numeric identifier for wells or seismic traces. The cells in column 3 can be blank, but some identifier is required if the user wishes to track cluster output by well or seismic trace after creating the cluster report. Columns four and five are reserved for well information (dependent data). In this example we have chosen producing oil cut. As shown in the example, if only one dependent value is desired, duplicate the data in columns 4 and 5. Six or more dependent data (wells) should produce good results if there is a reasonable spread of values. The subsequent columns are independent data, such as seismic attributes. In this example, the independent data are seismic time at selected geologic horizons. Each cell for independent data must be filled. There is no limit to the number of independent data columns, but a practical limit for independent data columns is seven, as this will produce 21 intervals for clustering.

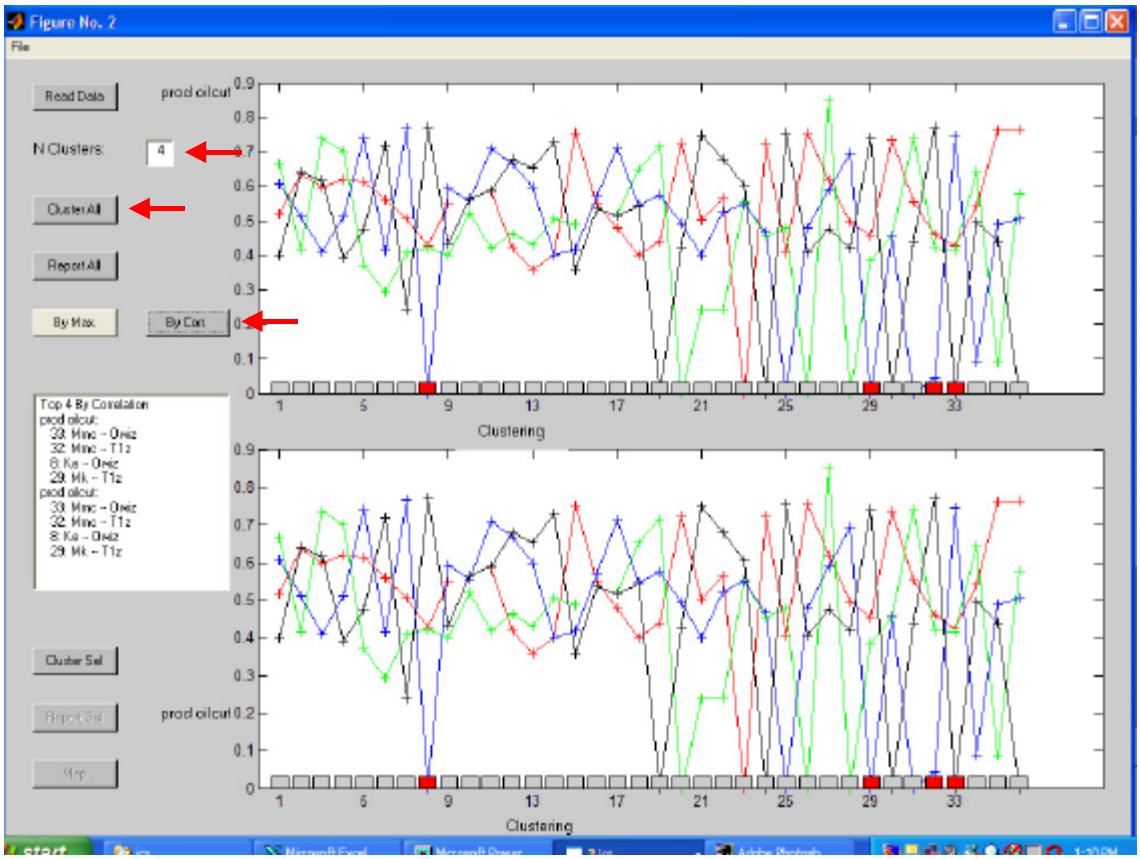

After the file is loaded, set the number of clusters from 2 to 4 and then click the “cluster all” button. When clustering is finished, select either “by max” or “by correlation.” The highest rank clusters will be displayed in the panel, both graphically and by name. The text panel will list the selected clusters in descending order of correlation. The tabs in the cluster-graph window will be red for selected clusters. Clicking the tabs in the cluster-graph window will select or deselect the cluster from the final cluster grouping.

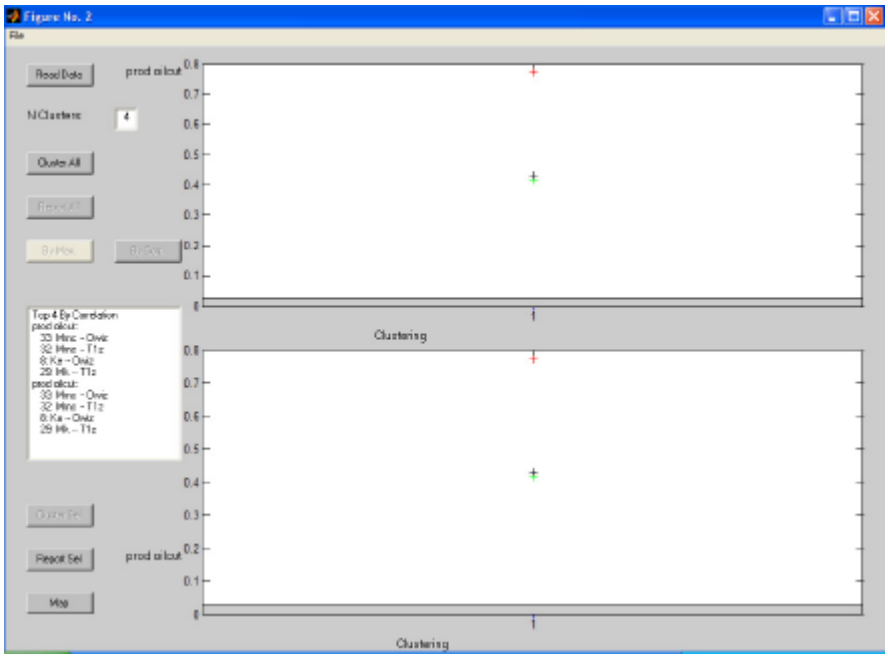

After processing the selected cluster groups, a graph displays the spread of cluster means. A wide spread of cluster means is desired. The next step is to create a report or a map view of the clusters.

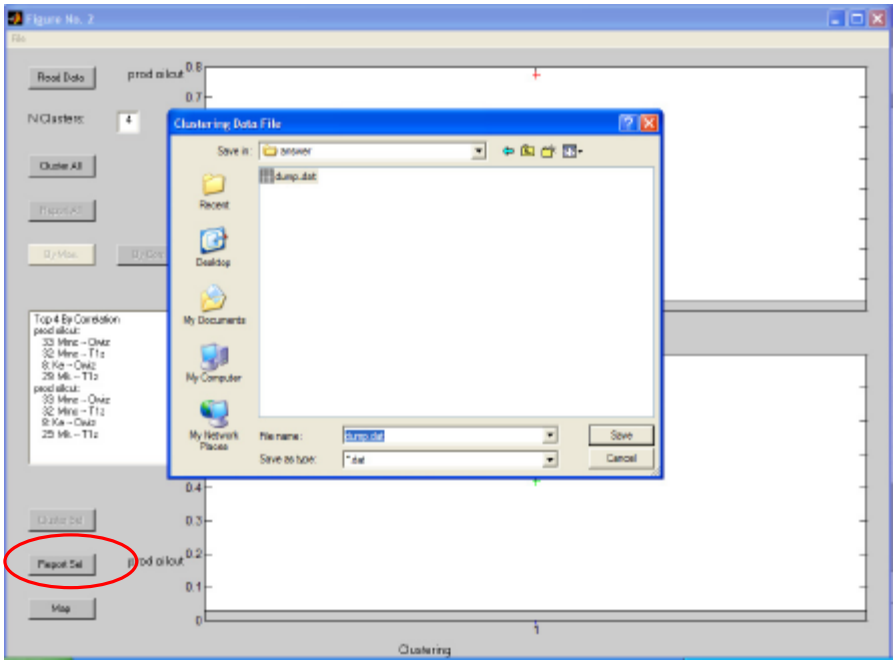

After clicking the “Report Selection” button, a navigation window is displayed. Navigate to the appropriate directory and supply a file name. A text file will be written that will summarize the cluster analysis. This file may be read with Windows Word Pad.

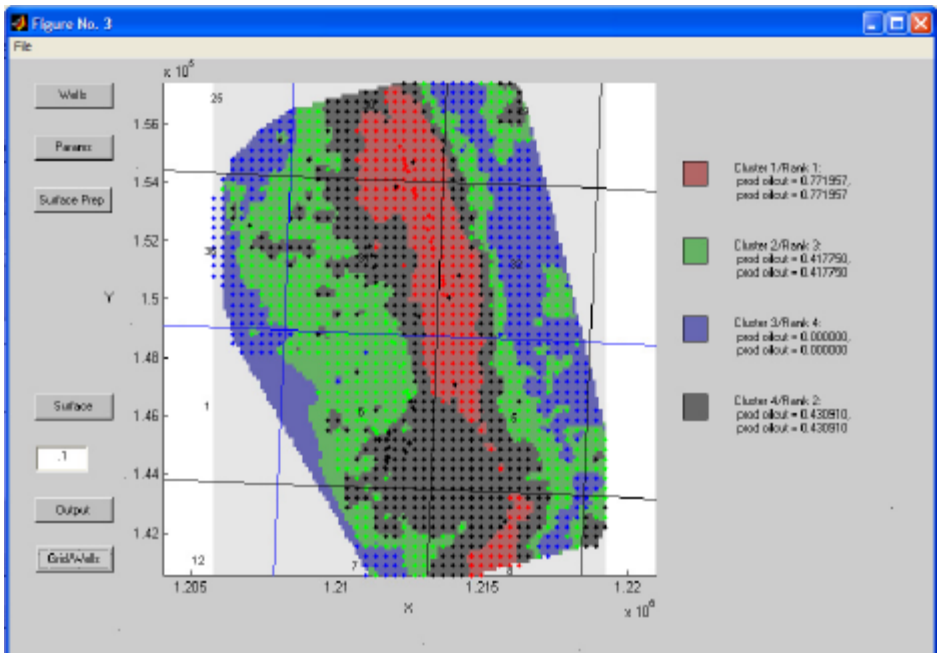

When the “map” button is selected, a new map window is displayed. Click “surface prepare” button, set the correlation coefficient from 0.1 to 0.7, and finally click the “surface” button. The cluster map will then be drawn. An optional cluster map report may be written.

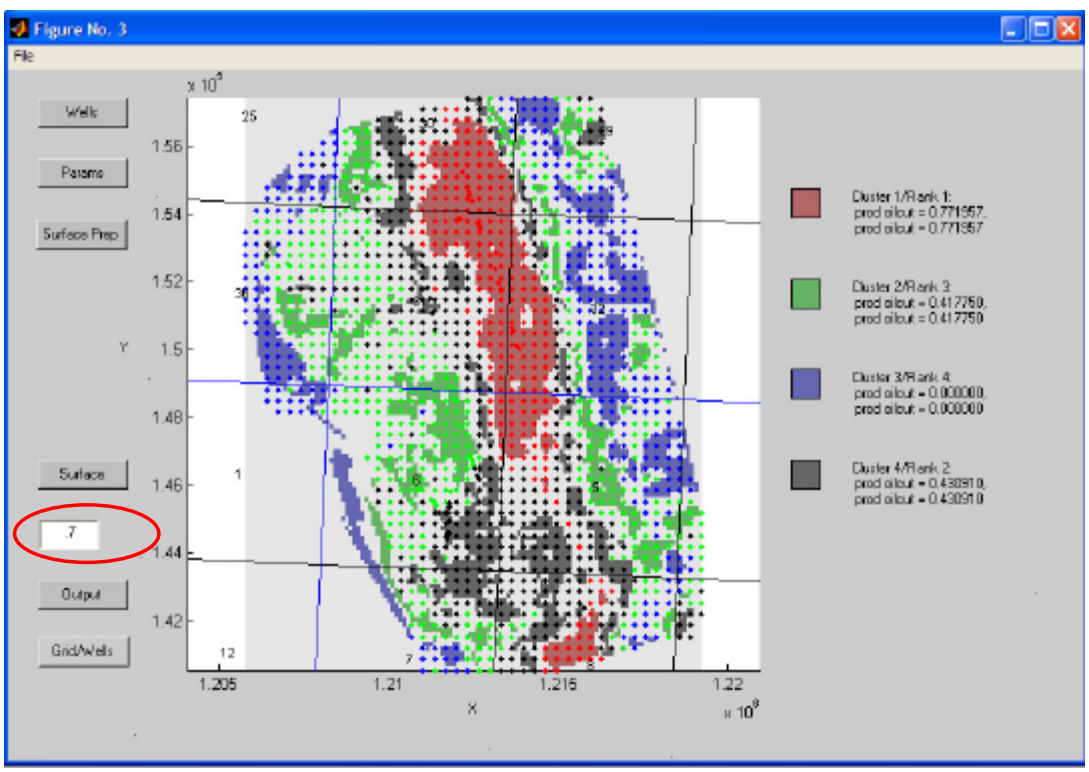

Map view shows white areas that do not meet the correlation coefficient of 0.7.

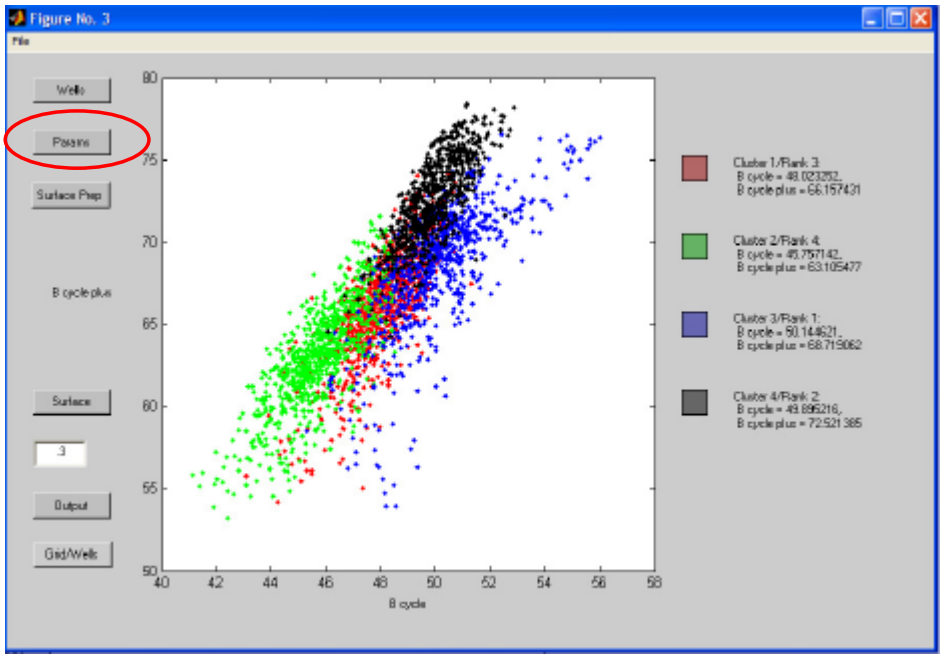

Selecting the “parameters” button will draw a graph of cluster assignments and cluster means at each location of dependent control (wells).

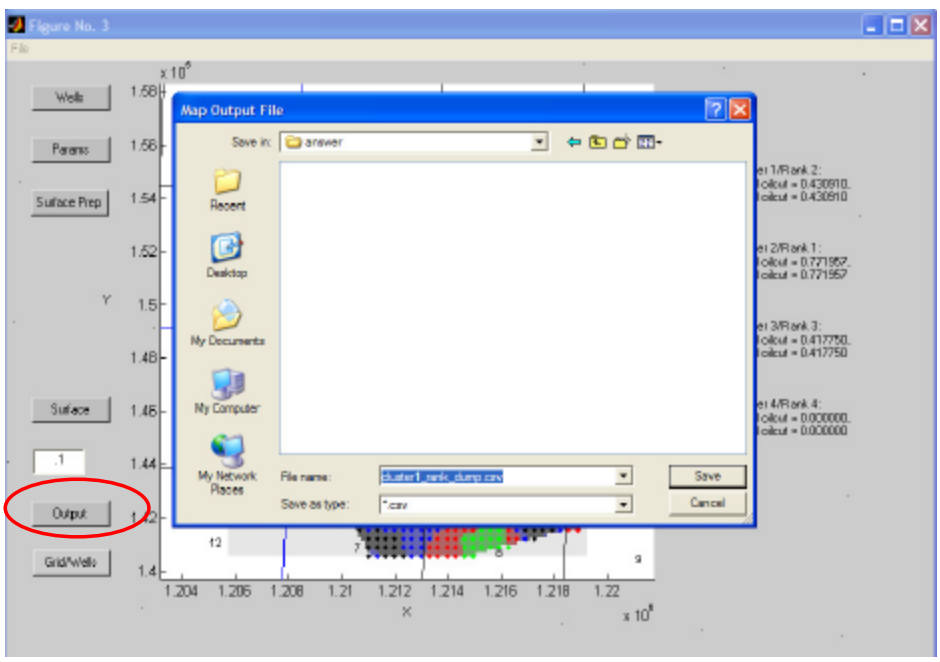

An optional cluster map report may be written. After selecting the “output” button, a file navigation window opens. The created report is in comma-separated variable format for each grid location.

Cluster 2 Non-Intervals Tool

The Cluster 2 routine works the same as Cluster 1 except that the independent data are used as imported. That is, differences or intervals are not computed. The same file can be used for both Cluster 1 and Cluster 2. When the Cluster 2 routine is called from a command line or button a work window is displayed. The windows, functions and buttons are the same as for the Cluster 1 Tool. The number of possible clusters equals the number of independent data columns after column 5.

The Cluster 2 Tool is accessed from the main ICS control panel.

Practice-example files for the Cluster 2 tool are found under the directory: ICS_MANUAL\CLUSTER2

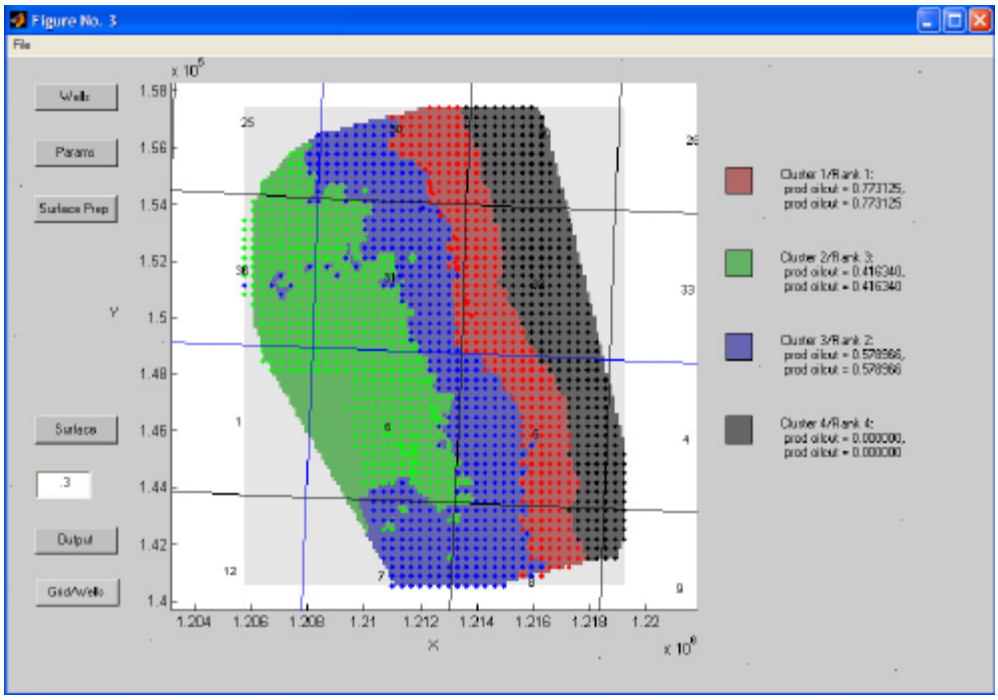

A map is displayed of results from the Cluster 2 (non-interval) Tool using the same data as shown in the previous figures that were created with the Cluster 1 (interval) Tool. Cluster 2 Tool windows and functions are the same as the Cluster 1 Tool.

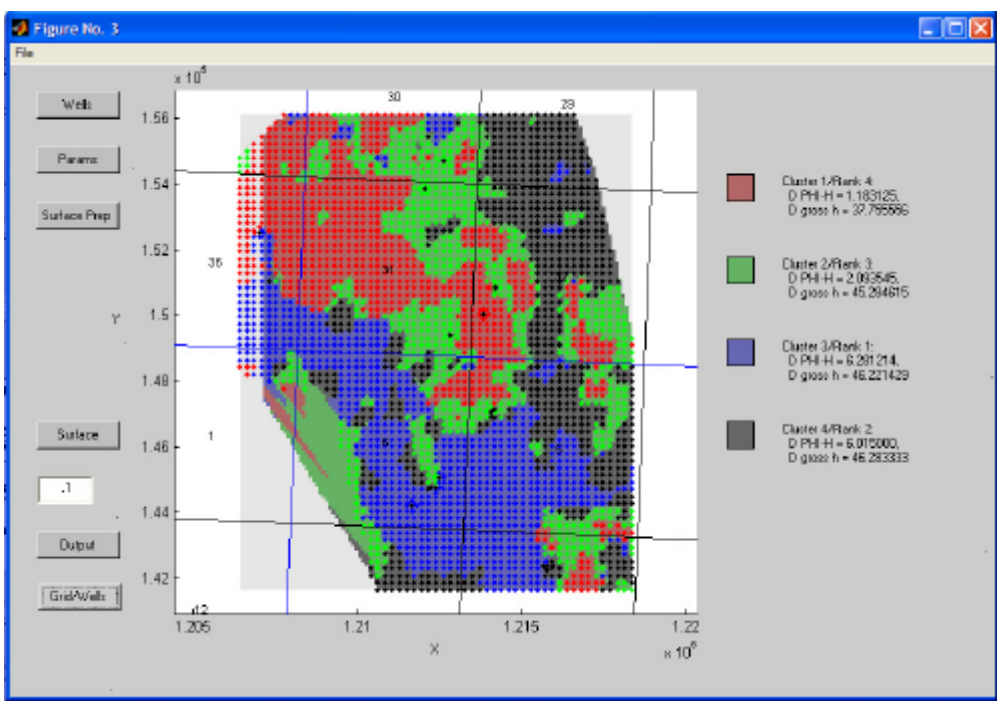

A Cluster-2 map is shown of cluster results using well-log storage (phi-h) and thickness (h) with seismic attributes at reservoir depth.

Cluster 3 Tool

The Cluster 3 routine is similar to Cluster 1 and 2. The routine uses a different file format. This format is the same as described previously for Cluster 1 and 2 except there are no columns for dependent data (wells). Cluster 3 produces intrinsic or natural clusters of the independent data. It is especially useful where there is limited control. Results from Cluster 3 should also be used for comparison with results from either Cluster 1 or 2. A map of up to 10 clusters can be created.

The Cluster 3 Tool is accessed from the main ICS control panel.

Practice-example files for the Cluster 3 tool are found under the directory: ICS_MANUAL\CLUSTER3

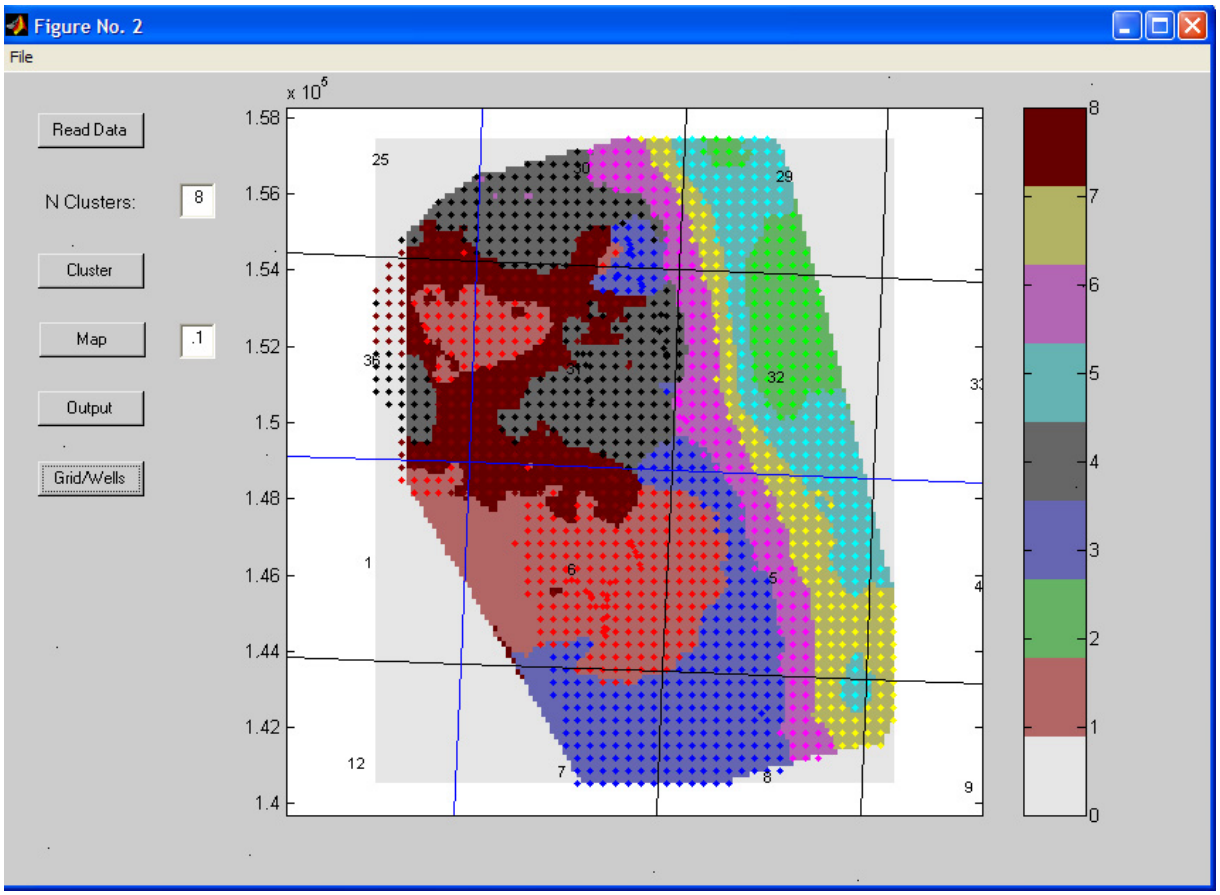

A map is displayed of results from the Cluster 3 (no wells) Tool using the same data (seismic time) as shown in the previous figures that were created with the Cluster 1 (interval) Tool. Cluster 3 Tool buttons have similar functions as the Cluster 1 or 2 Tools. The Cluster 3 Tool produces clusters of similarity without ranking.

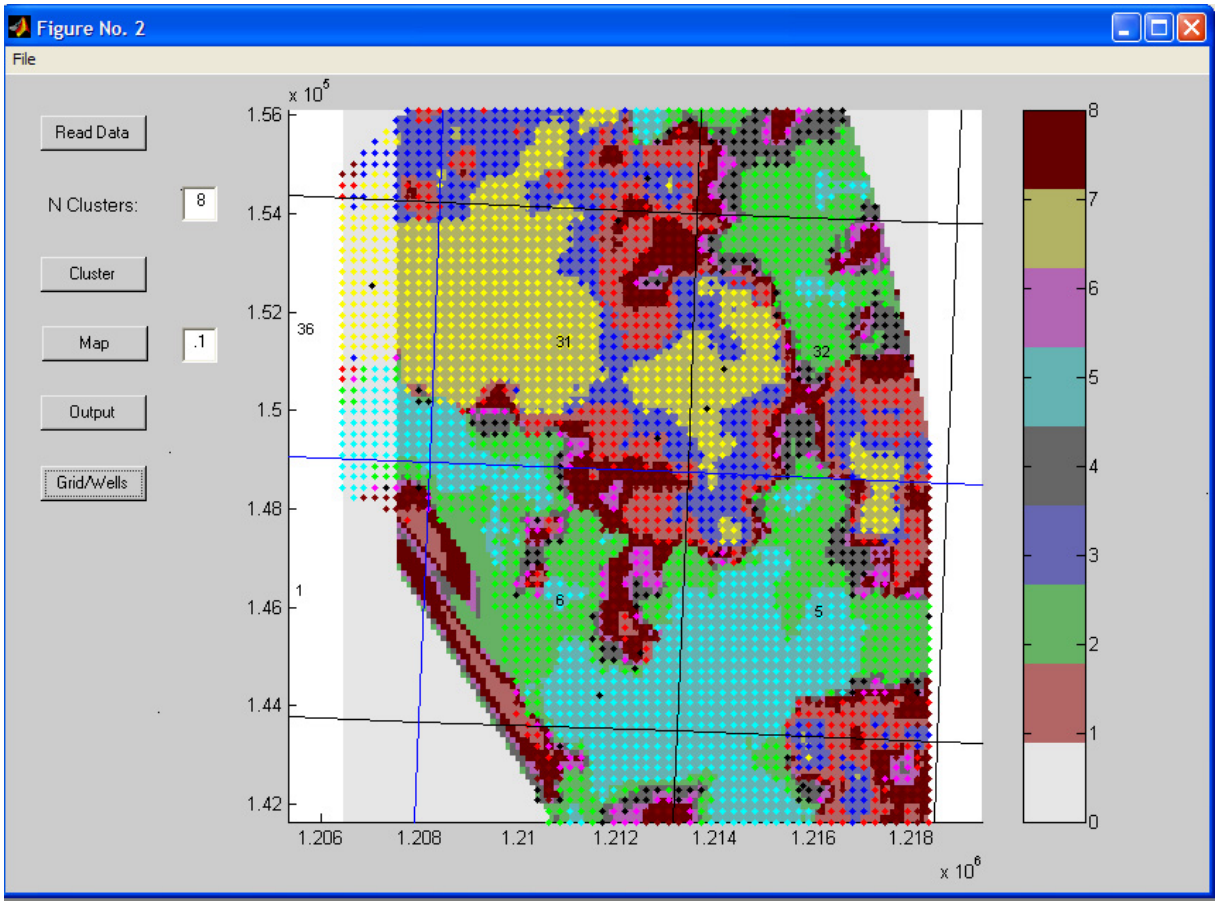

A map is displayed of results from the Cluster 3 (no wells) Tool using the same seismic attributes at reservoir depth as shown in the previous figures that were created with the Cluster (non-interval) 2 Tool.

Neural Solvers

Overview

The neural solvers are the backbone of reservoir characterization and production transforms in ICS. There are two versions of the neural solver. Neural Solver 1 (the preferred method) is useful for training from external data sources (other 3D seismic surveys). Neural Solver 1 incorporates principal-component analysis (PCA) of the independent (seismic) data. The PCA transform reduces redundant seismic or geologic data and is helpful where the number of dependent data (wells) are limited, as is often the case. Neural Solver 2 can use multiple independent data files, but trains only from dependent data (well control) within the common area of the independent data. Neural Solver 2 is more difficult to use, but provides additional crosscheck reporting. Neural Solver 2 does not incorporate PCA. With either neural solver, an output map is created for each training session that is applied to seismic or other grid-type data. Optionally, an output file may be created that can be imported into other ICS tools or external mapping software.

Neural Solver 1 Tool

The purpose of this program is to predict a parameter, that is measured at a limited number of locations, over some x-y region by using an artificial neural network (ANN) to relate it to a set of 3D seismic attributes which are known at regular grid locations over the region. The ANN used in this program is a simple linear classifier (ADALINE) having one output. The number of inputs is determined by the principal-component analysis (PCA) output matrix. A list box allows the user to choose one of three training techniques: “trainwb” and “trainlm” use variations of Levenberg-Marquardt optimization, “trainscg” is a scaled conjugate gradient method. See the MATLAB “Neural Network Toolbox User’s Guide” for details. A full description of MATLAB products and documentation can be found at the MATLAB web site, http://www.mathworks.com. If the MATLAB products are used to run ICS, the MATLAB scripts may be modified to incorporate other neural network architecture. The architecture included with ICS has been satisfactory and easy to use.

There are advantages for using Neural Solver 1. A common problem for evaluating a 3D survey with any ANN is a limited well population for control. There are no hard rules, but it is generally recommended to have at least twice the number of well control as the number of independent seismic attributes. The training file for Neural Solver 1 can be constructed from control at other 3D surveys. In this manner, a larger training population can be utilized. Caution must be exercised that the seismic data are normalized if this is attempted. For example, when using amplitudes, the gain must be the same. Acquisition and processing parameters should also be the same.

Neural solver 1 requires two files. One file is the training file that contains the dependent data (well data) and independent (seismic) data captured at well locations. A training file for Neural Solver 1 can be constructed with the “Build-Train-Cluster-File” utility. Independent (seismic) data columns must be less than dependent (well) data rows. The second file contains the seismic or other grid-type data. The independent data columns are in the same order as in the training file.

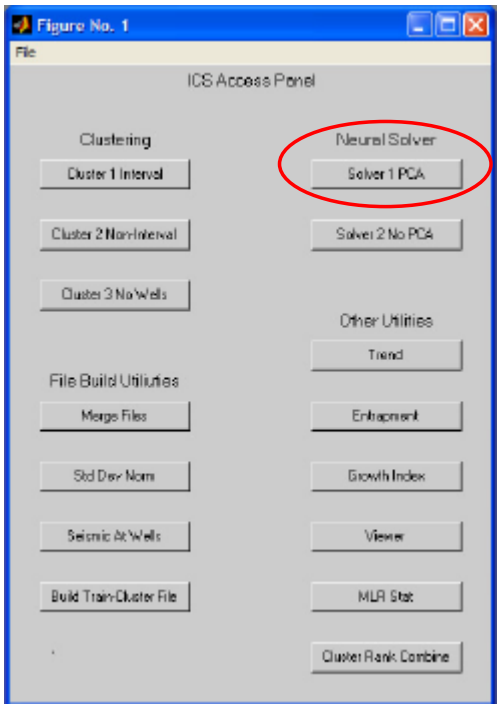

The Neural Solver 1 with PCA Tool can be accessed from the main ICS control panel.

Practice-example files for the Neural Solver 1 tool are located under the directory:
ICS_MANUAL\NEURAL_SOLVER1

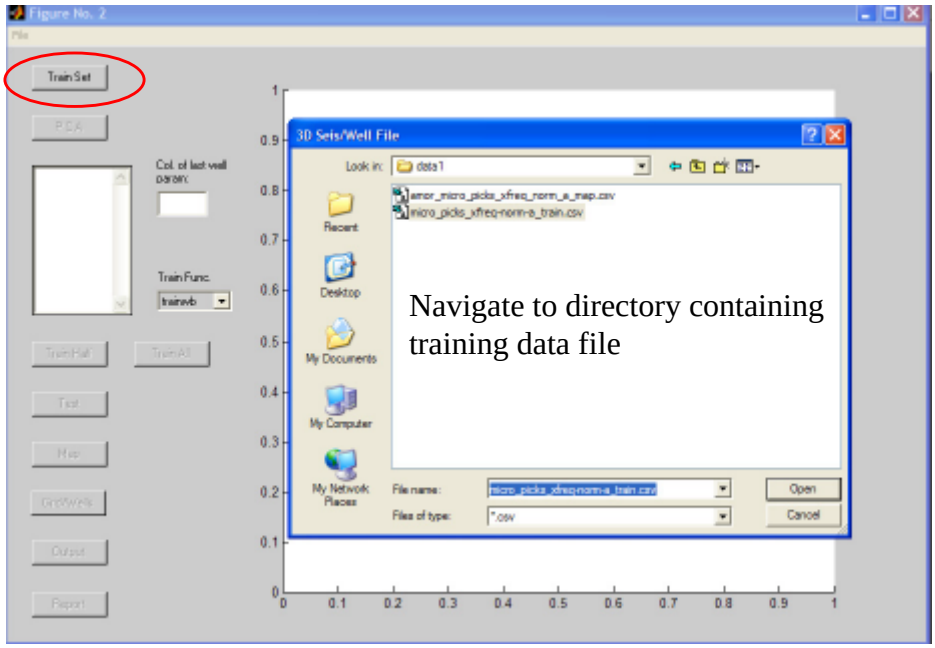

After clicking the “Train Selection” button, a file navigation window appears. Navigate to the appropriate directory and select the training file.

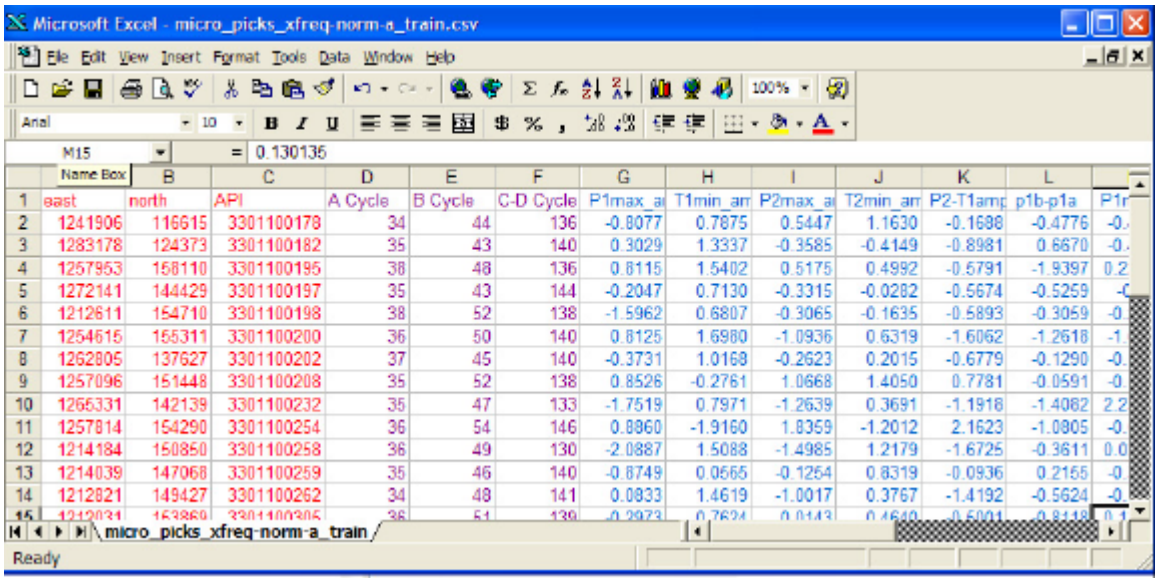

	east	north	API	A Cycle	B Cycle	C-D Cycle	P1max_a	T1min_am	P2max_a	T2min_am	P2-T1amp	p1b-p1a	P1r
2	1241906	116615	3301100178	34	44	136	-0.8077	0.7875	0.5447	1.1630	-0.1688	-0.4776	-0.
3	1283178	124373	3301100182	35	43	140	0.3029	1.3337	-0.3585	-0.4149	-0.8981	0.6670	-0.
4	1257953	158110	3301100195	38	48	136	0.8115	1.5402	0.5175	0.4992	-0.5791	-1.9397	0.2
5	1272141	144429	3301100197	35	43	144	-0.2047	0.7130	-0.3315	-0.0282	-0.5674	-0.5259	-0
6	1212611	154710	3301100198	38	52	138	-1.5962	0.6807	-0.3065	-0.1635	-0.5893	-0.3059	-0.
7	1254615	155311	3301100200	36	50	140	0.8125	1.6980	-1.0936	0.6319	-1.6062	-1.2618	-1
8	1262805	137627	3301100202	37	45	140	-0.3731	1.0168	-0.2623	0.2015	-0.6779	-0.1290	-0.
9	1257096	151448	3301100208	35	52	138	0.8526	-0.2761	1.0668	1.4050	0.7781	-0.0591	-0
10	1266331	142139	3301100232	35	47	133	-1.7519	0.7971	-1.2639	0.3691	-1.1918	-1.4082	2.2
11	1257814	154290	3301100254	36	54	146	0.8860	-1.9160	1.8359	-1.2012	2.1623	-1.0805	-0.
12	1214184	150850	3301100258	36	49	130	-2.0887	1.5088	-1.4985	1.2179	-1.6725	-0.3611	0.0
13	1214039	147068	3301100259	35	46	140	-0.8749	0.0565	-0.1254	0.8319	-0.0936	0.2155	-0
14	1212821	149427	3301100262	34	48	141	0.0833	1.4619	-1.0017	0.3767	-1.4192	-0.5624	-0

An abridged form of the training file is shown. As with all ICS input files, the training file is in comma-separated-variable (csv) format. The first three columns are always the well locations and identifier (such as API number). Columns four through six contain the dependent (such as geologic, production, well-log) data. There is no limit to the number of dependent data columns. The remainder of columns contain the independent (seismic or grid-type) data. The number of independent data columns must be less than the number of dependent (well) locations. This file can be built by the “Build-Train-Cluster-File” utility.

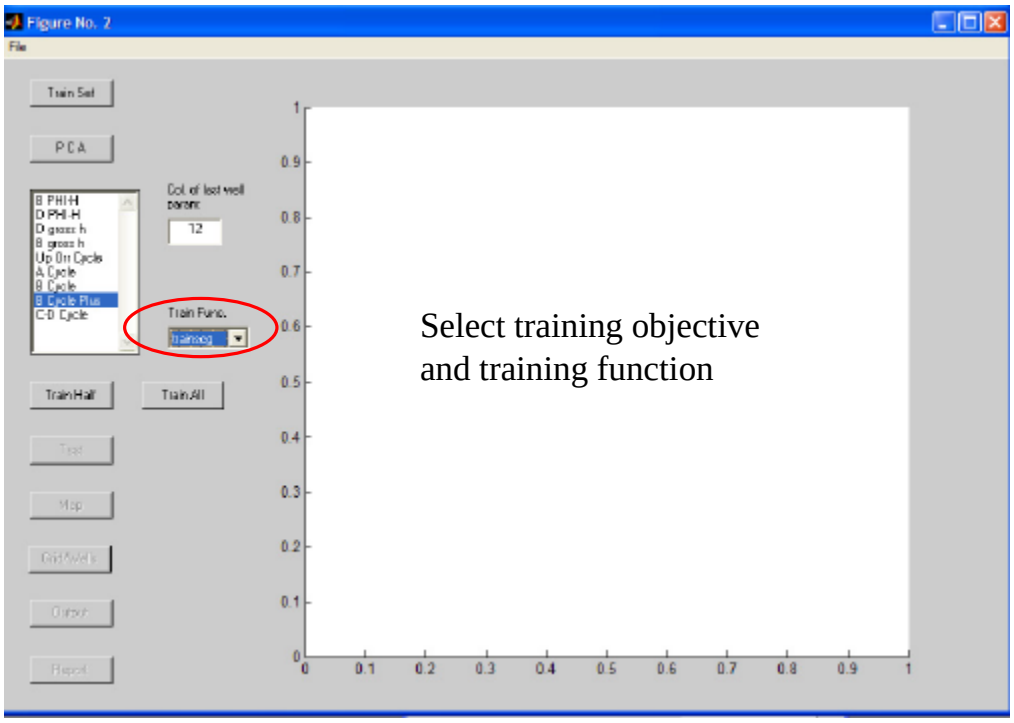

After the training file is loaded, set the column of last well parameter to match that in the file and click the “PCA” button. The dependent well parameters will be displayed in a window. Click the desired well parameter and select one of three training functions. Click either “train half” or train all.

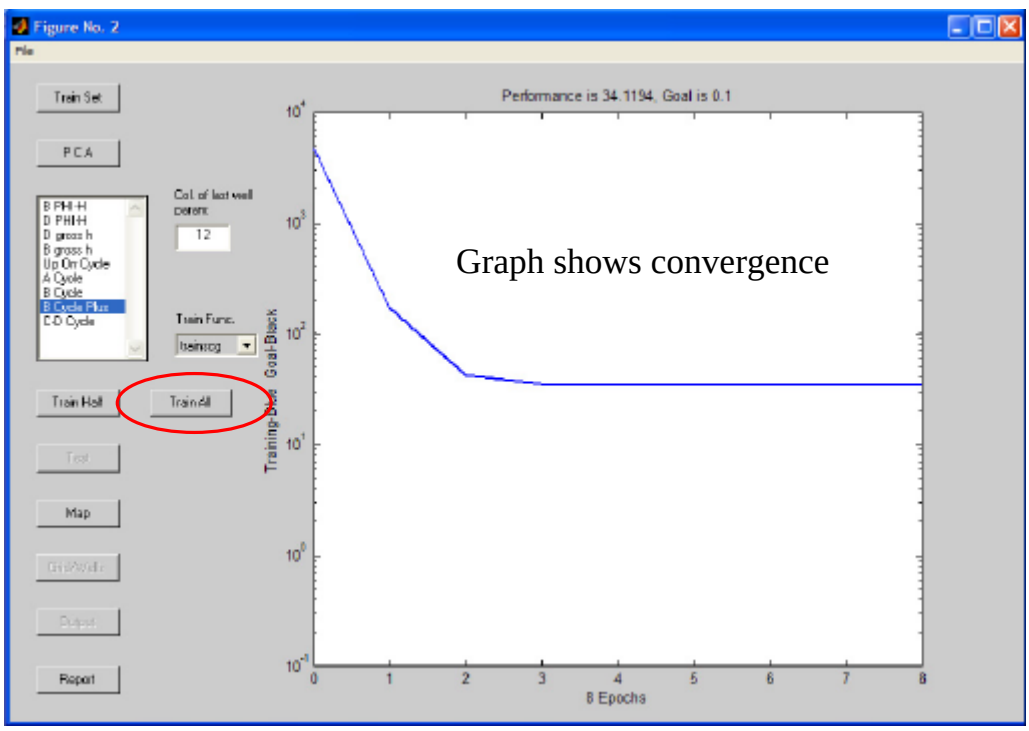

Training convergence is displayed after clicking either “train half” or “train all.”

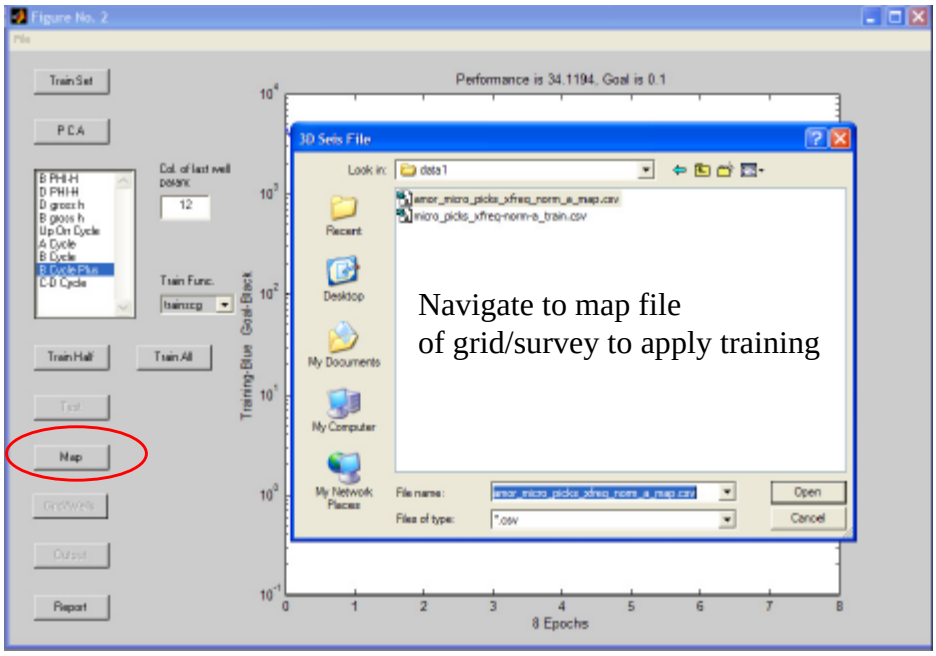

Clicking the “map” button will open a file navigation window. Navigate to the directory containing the independent seismic map file.

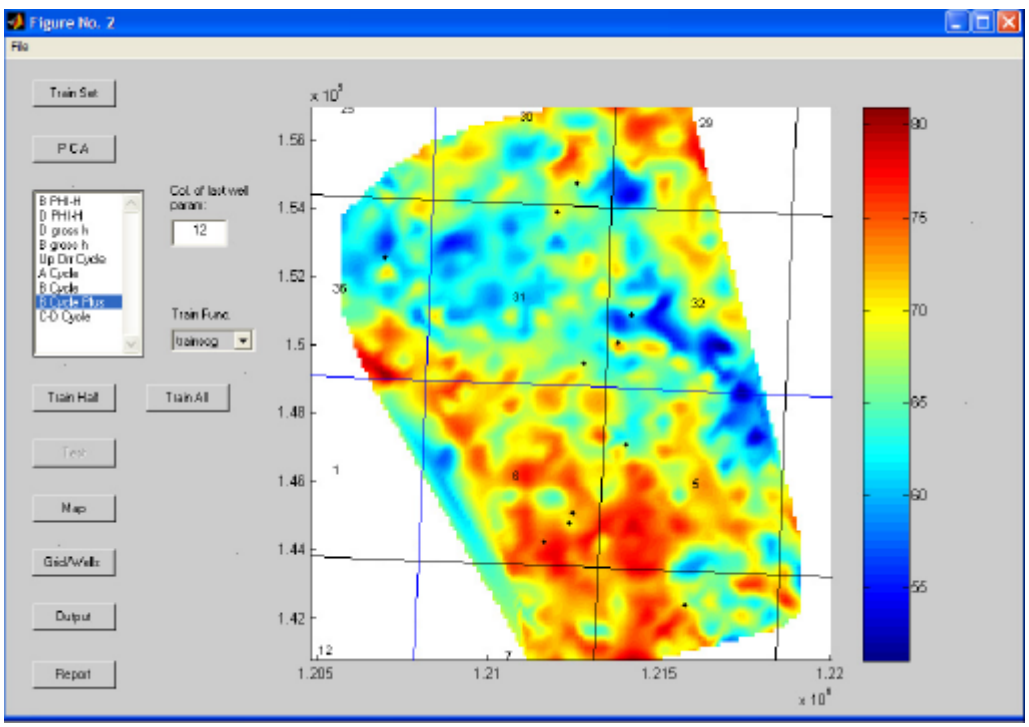

The training is applied to the independent seismic attributes and a map is drawn. The training applied in this example is for an interval thickness that is important for describing the depositional setting of a reservoir. Seismic attributes at reservoir depth are the independent data.

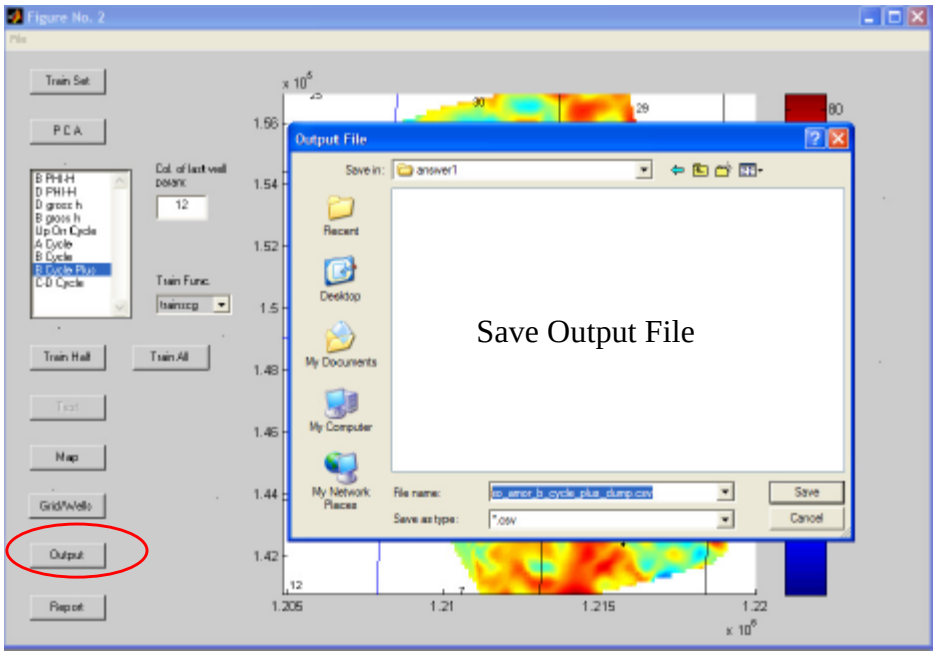

Clicking the “output” button will open a window for saving a csv text file of the map.

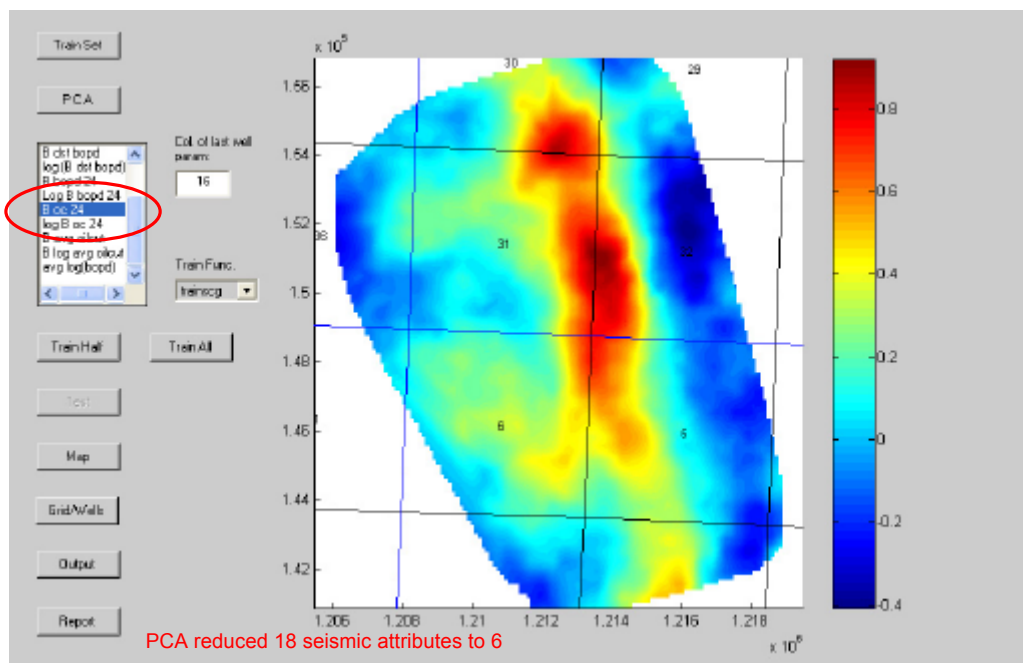

A final transform is shown using the Neural Solver 1 tool where seismic-reservoir transforms are used to predict a production transform of producing oil cut fraction.

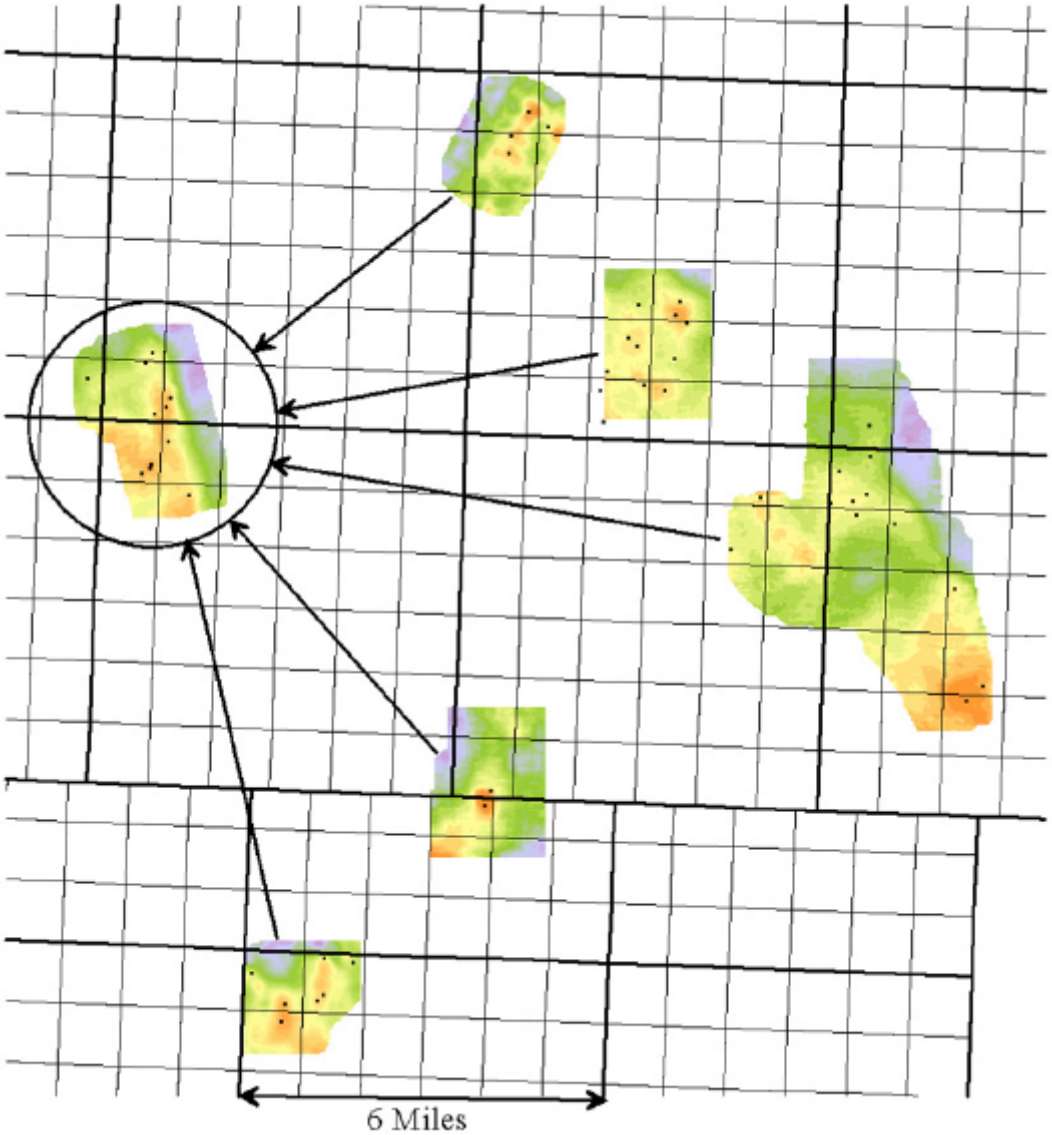

Using properly normalized data from multiple 3D seismic surveys, a larger population of wells can be used to make cross predictions and blind tests at a particular 3D seismic survey.

Neural Solver 2 Tool

The Neural Solver 2 routine is used to predict a parameter, that is measured at a limited number of locations over some x-y region, by using an ANN to relate it to a set of attributes which are known at regular grid locations. In normal use, the predicted parameter is some measure of well “goodness”, such as initial production, and the attributes are the outputs from one or more other ICS programs. All input data files are assumed to be comma-separated-variable files, with coordinates assigned in the first two columns. The first row is reserved for column labels. There are no other assumptions about the content of the files. The user specifies training data by selecting them from list boxes. An over lap of the data files is computed. Grid operations are then applied to the data within the common area. The number of inputs is by user-selection of data columns. The input data are normalized, but no PCA is done.

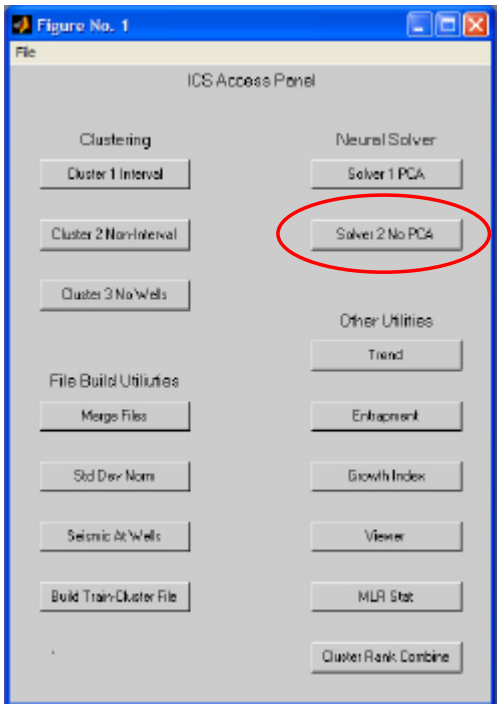

The Neural Solver 2 Tool is accessed from the main ICS control panel.

Practice-example files for the Neural Solver 2 tool are found under the directory: ICS_MANUAL\NEURAL_SOLVER2

Neural solver 2 can import multiple files containing independent data. The Neural Solver 2 routine is intended to import the output from other ICS tools that have been used to predict reservoir parameters such as porosity-thickness, growth-history and entrapment pressure. Data columns within each file can be selected as desired by the user. One file contains locations and well data. The file that

contains well data is the “objective” file. Objectives that are contained in this file will represent reservoir “goodness.” Quantities from production history such as initial 24-month production, oil-cut and estimated ultimate recovery are examples of “goodness.” When the Neural Solver 2 routine is utilized with these types of data, the output will be a “Z” map that has been objectively weighted and ranked according to the data selected from the objective file. There are some advantages for using Neural Solver 2. Separate files of independent data can be imported. These files are located in a common directory reserved for the study. The coordinates of the independent data files need not match, but there must be some common area. There is no need to capture the independent data at the location of the dependent data (wells). Interpolation of data at well locations is done by the program. There are also some disadvantages for using Neural Solver 2. If the dependent data (wells) population is small, successful training may not be possible. Although there are no hard rules, the dependent data population should be more than twice the number of independent items (3 independent items with 6 wells). Another disadvantage is that there is only one option for training.

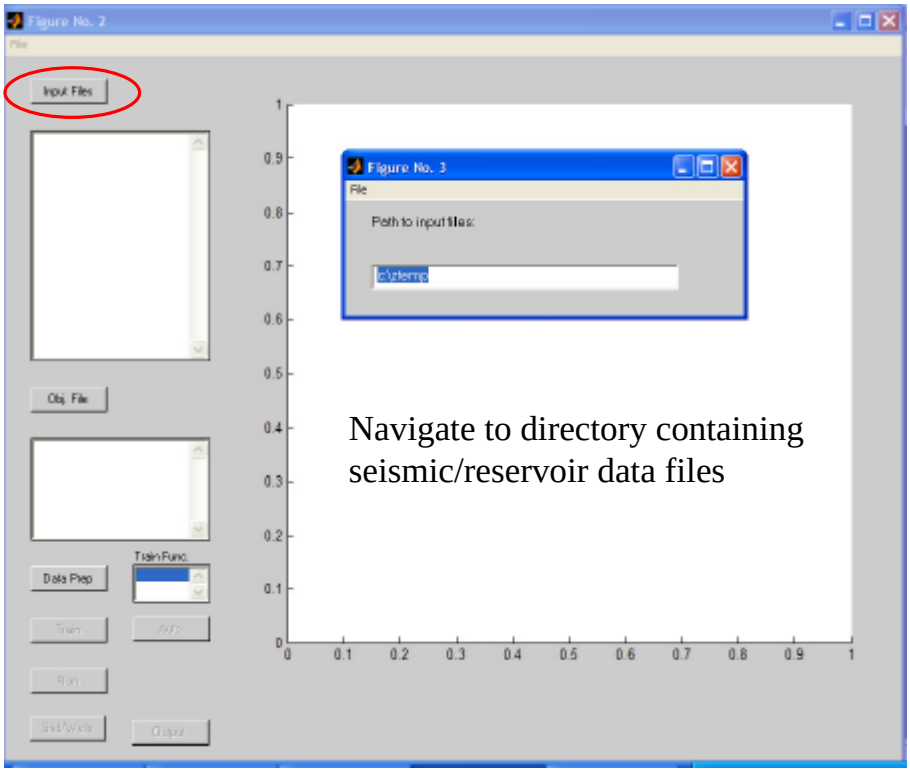

A work directory must be created to contain only files with the independent (3D seismic or grid-type) data. A sub-directory can be created to contain the objective (well) data. After clicking the “input files” button, a dialog box opens. The complete drive and path must be entered manually. Close by clicking the upper-right “X” of the dialog box.

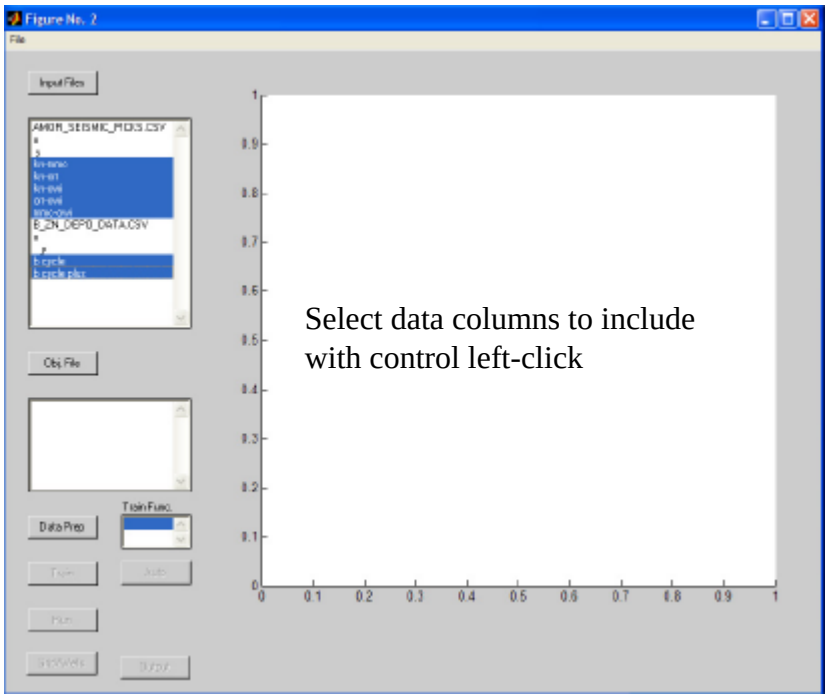

The upper-left window contains the data found in the work directory. The file name is in capitals. Select the data columns to be used with a control-left click. Then click the “objective file” button.

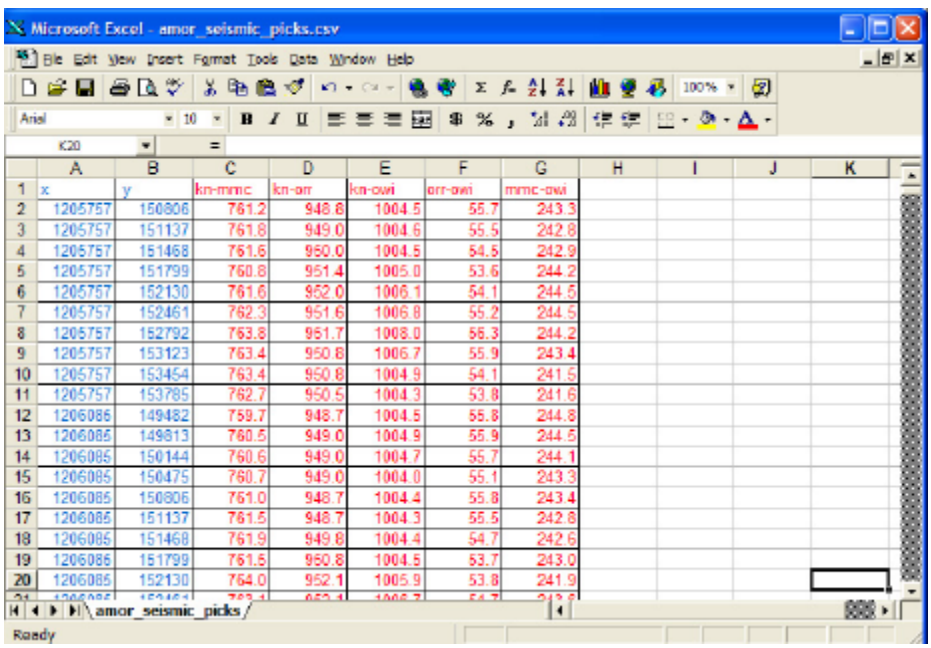

	A	B	C	D	E	F	G
1	x	y	kn-mmc	kn-orr	kn-owi	orr-owi	mmc-owi
2	1205757	150806	761.2	948.8	1004.5	55.7	243.3
3	1205757	151137	761.8	949.0	1004.6	55.5	242.8
4	1205757	151468	761.6	950.0	1004.5	54.5	242.9
5	1205757	151799	760.8	951.4	1005.0	53.6	244.2
6	1205757	152130	761.6	952.0	1006.1	54.1	244.5
7	1205757	152461	762.3	951.6	1006.8	55.2	244.5
8	1205757	152792	763.8	951.7	1008.0	56.3	244.2
9	1205757	153123	763.4	950.8	1006.7	55.9	243.4
10	1205757	153454	763.4	950.8	1004.9	54.1	241.5
11	1205757	153785	762.7	950.5	1004.3	53.8	241.6
12	1206086	149482	759.7	948.7	1004.5	55.8	244.8
13	1206086	149813	760.5	949.0	1004.9	55.9	244.5
14	1206086	150144	760.6	949.0	1004.7	55.7	244.1
15	1206086	150475	760.7	949.0	1004.0	55.1	243.3
16	1206086	150806	761.0	948.7	1004.4	55.8	243.4
17	1206086	151137	761.5	948.7	1004.3	55.5	242.8
18	1206086	151468	761.9	949.8	1004.4	54.7	242.6
19	1206086	151799	761.5	950.8	1004.5	53.7	243.0
20	1206086	152130	764.0	952.1	1005.9	53.8	241.9

A properly formatted input file is shown. The first two columns contain the coordinates of a seismic trace or grid node. Subsequent columns contain the independent (seismic or grid-type) data. The file contains seismic interval time (milliseconds).

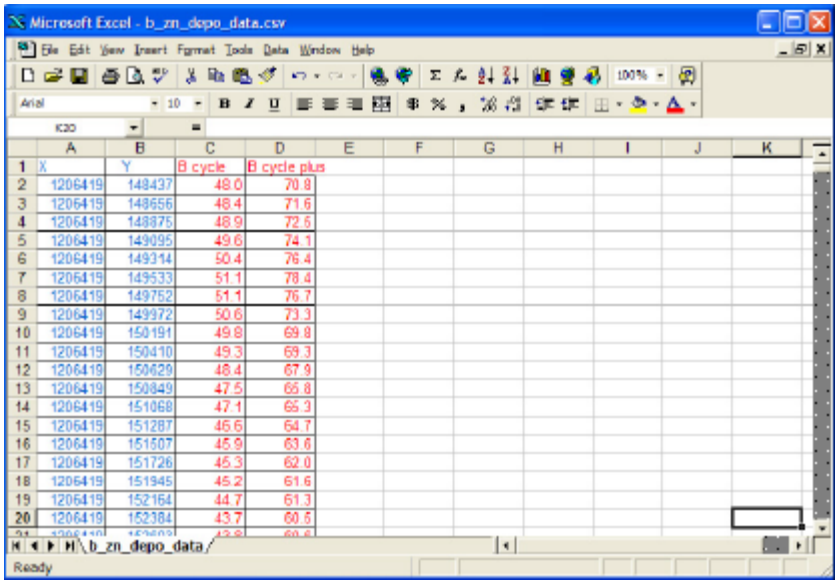

	A	B	C	D
1	X	Y	B cycle	B cycle plus
2	1206419	148437	48.0	70.8
3	1206419	148656	48.4	71.6
4	1206419	148875	48.9	72.5
5	1206419	149095	49.6	74.1
6	1206419	149314	50.4	76.4
7	1206419	149533	51.1	78.4
8	1206419	149752	51.1	76.7
9	1206419	149972	50.6	73.3
10	1206419	150191	49.8	69.8
11	1206419	150410	49.3	69.3
12	1206419	150629	48.4	67.9
13	1206419	150849	47.5	66.8
14	1206419	151068	47.1	65.3
15	1206419	151287	46.6	64.7
16	1206419	151507	45.9	63.6
17	1206419	151726	45.3	62.0
18	1206419	151945	45.2	61.6
19	1206419	152164	44.7	61.3
20	1206419	152384	43.7	60.5

A second input file is shown. It is formatted the same as the first input file. This file contains interval thickness (feet) from a previous seismic-reservoir transform.

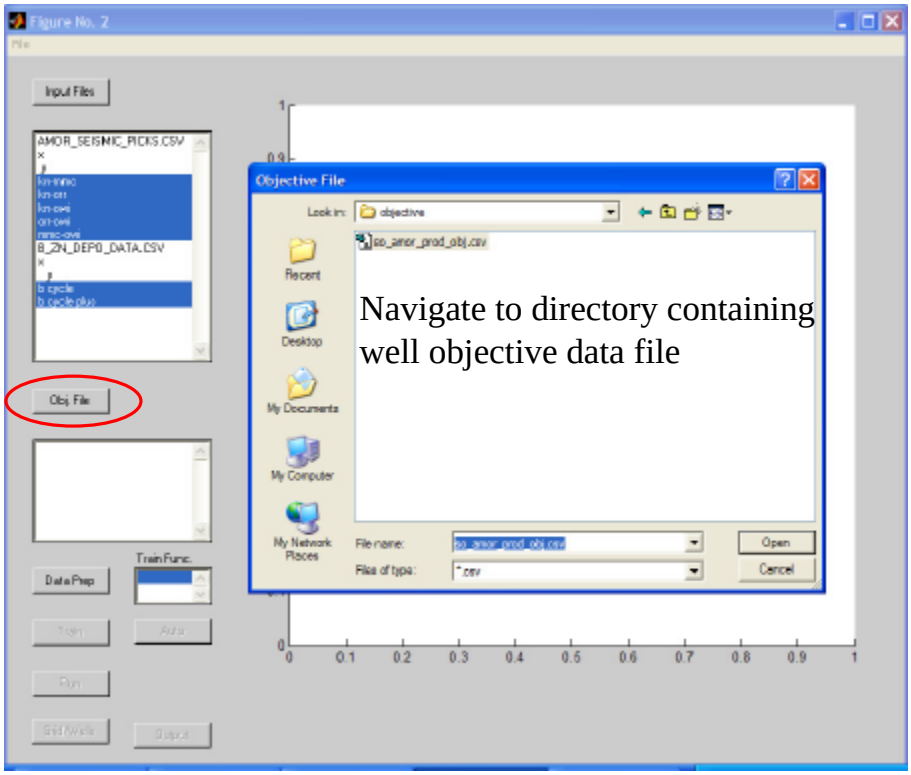

Clicking the “objective file” button opens a file navigation window. Navigate to the directory containing the objective file.

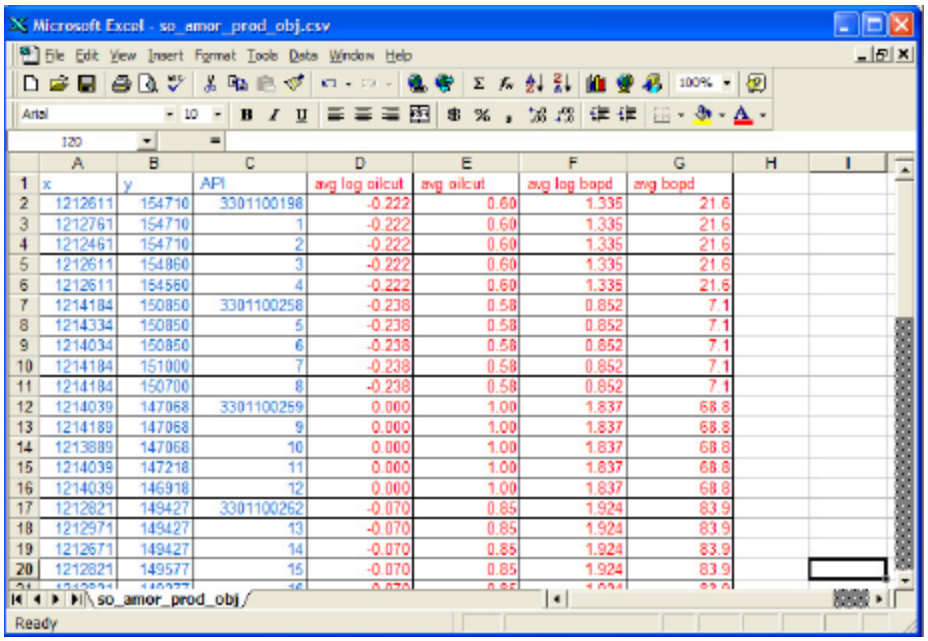

	A	B	C	D	E	F	G
1	x	y	API	avg log oilcut	avg oilcut	avg log bopd	avg bopd
2	1212611	154710	3301100198	-0.222	0.60	1.335	21.6
3	1212761	154710	1	-0.222	0.60	1.335	21.6
4	1212461	154710	2	-0.222	0.60	1.335	21.6
5	1212611	154860	3	-0.222	0.60	1.335	21.6
6	1212611	154560	4	-0.222	0.60	1.335	21.6
7	1214184	150850	3301100258	-0.238	0.58	0.852	7.1
8	1214334	150850	5	-0.238	0.58	0.852	7.1
9	1214034	150850	6	-0.238	0.58	0.852	7.1
10	1214184	151000	7	-0.238	0.58	0.852	7.1
11	1214184	150700	8	-0.238	0.58	0.852	7.1
12	1214039	147068	3301100259	0.000	1.00	1.837	68.8
13	1214189	147068	9	0.000	1.00	1.837	68.8
14	1213889	147068	10	0.000	1.00	1.837	68.8
15	1214039	147218	11	0.000	1.00	1.837	68.8
16	1214039	146918	12	0.000	1.00	1.837	68.8
17	1212821	149427	3301100262	-0.070	0.85	1.924	83.9
18	1212971	149427	13	-0.070	0.85	1.924	83.9
19	1212671	149427	14	-0.070	0.85	1.924	83.9
20	1212821	149577	15	-0.070	0.85	1.924	83.9

A properly formatted objective file is shown. The first two columns contain the coordinates of each well. The third column contains a well identifier such as API number. Subsequent columns contain the dependent data for each well location. The file must be in comma-separated-variable format.

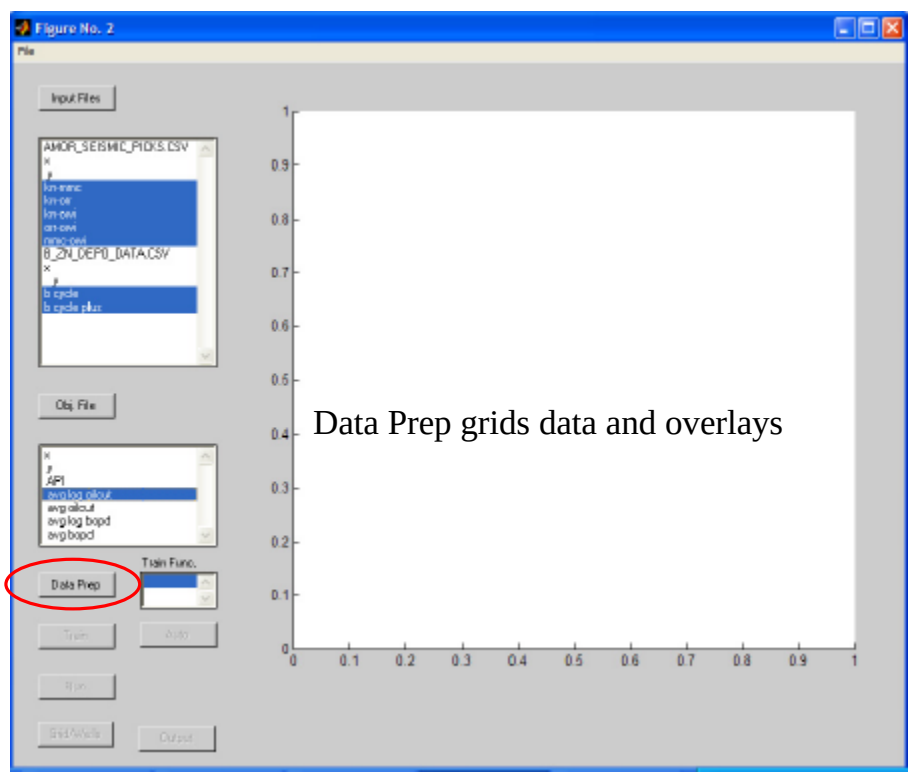

After the objective file is loaded, click the “data prepare” button. The routine will grid and overlay the data.

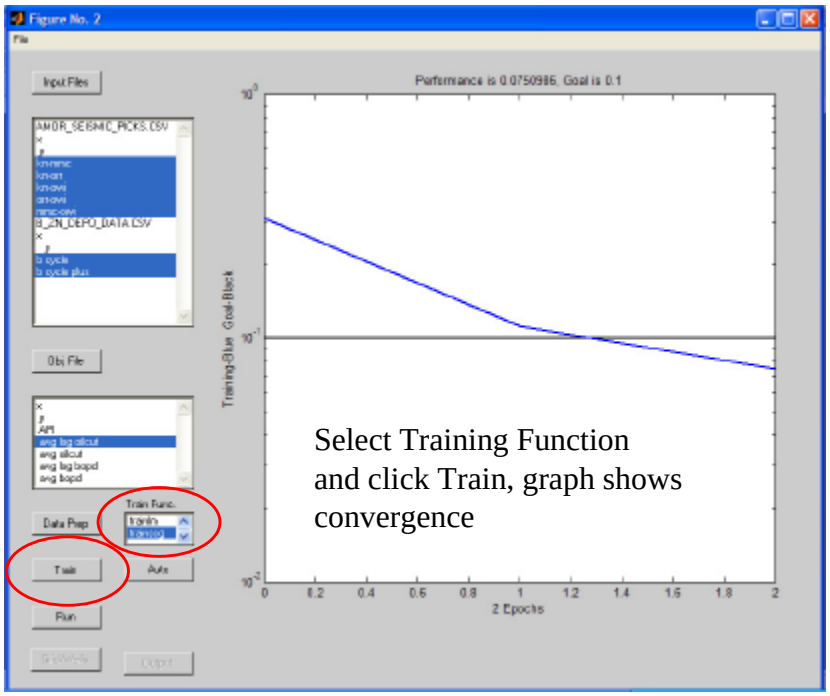

Select a dependent variable from the objective file window and one of three training functions. Finally, click the “train” button and convergence will be displayed in the graph window.

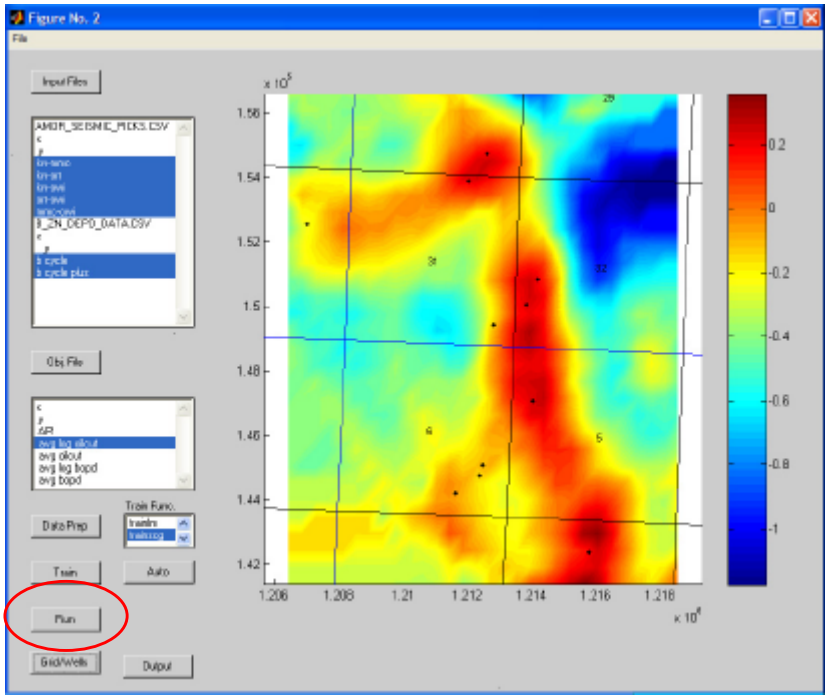

Click the “run” button and a map will be displayed of the resulting prediction. In this example, the logarithm of producing oil cut at wells has been predicted.

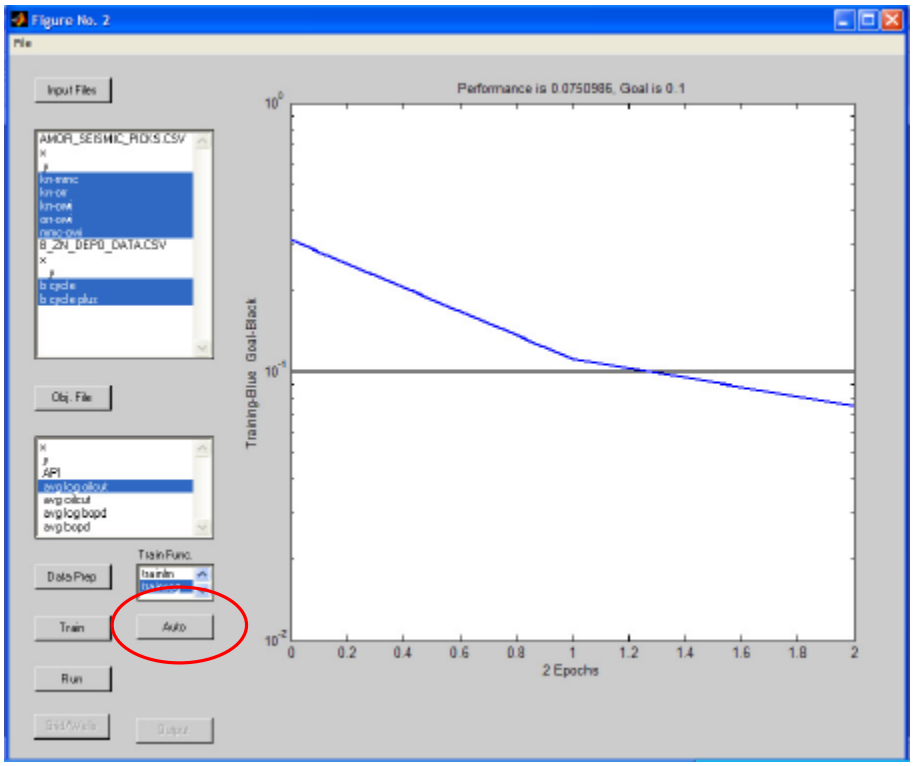

Neural Solver 2 Tool has an auto-run feature that is activated by clicking the "auto" button. This feature will do a blind test on every well with each of the dependent variables. The routine will train without data from given well and make a prediction for each dependent variable found in the "objective" file. A file is written that compares the actual and predicted dependent variable for each well.

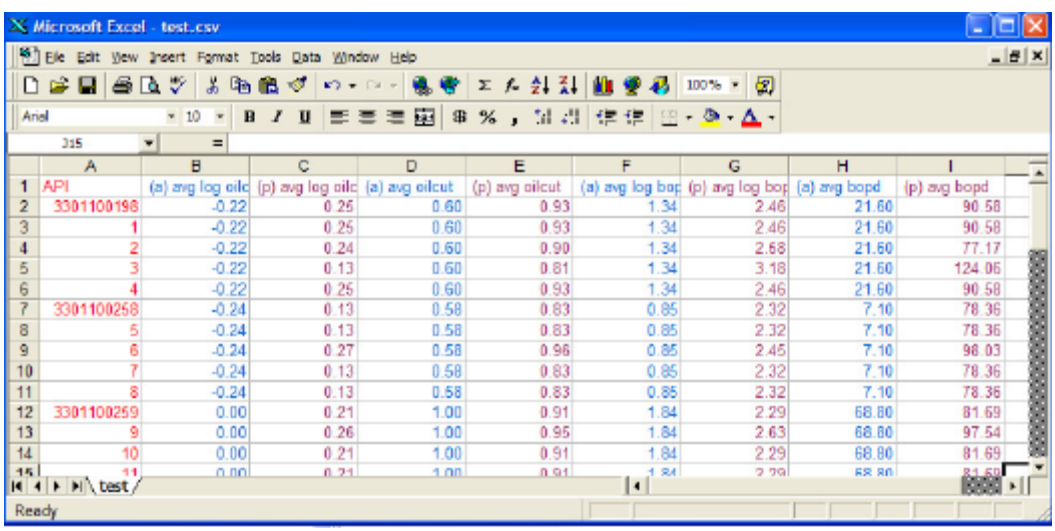

	A	B	C	D	E	F	G	H	I
1	API	(a) avg log oilc	(p) avg log oilc	(a) avg oilcut	(p) avg oilcut	(a) avg log bop	(p) avg log bop	(a) avg bopd	(p) avg bopd
2	3301100198	-0.22	0.25	0.60	0.93	1.34	2.46	21.60	90.58
3	1	-0.22	0.25	0.60	0.93	1.34	2.46	21.60	90.58
4	2	-0.22	0.24	0.60	0.90	1.34	2.68	21.60	77.17
5	3	-0.22	0.13	0.60	0.81	1.34	3.18	21.60	124.06
6	4	-0.22	0.25	0.60	0.93	1.34	2.46	21.60	90.58
7	3301100258	-0.24	0.13	0.58	0.83	0.85	2.32	7.10	78.36
8	5	-0.24	0.13	0.58	0.83	0.85	2.32	7.10	78.36
9	6	-0.24	0.27	0.58	0.96	0.85	2.45	7.10	98.03
10	7	-0.24	0.13	0.58	0.83	0.85	2.32	7.10	78.36
11	8	-0.24	0.13	0.58	0.83	0.85	2.32	7.10	78.36
12	3301100259	0.00	0.21	1.00	0.91	1.84	2.29	68.80	81.69
13	9	0.00	0.26	1.00	0.95	1.84	2.63	68.80	97.54
14	10	0.00	0.21	1.00	0.91	1.84	2.29	68.80	81.69
15	11	0.00	0.21	1.00	0.91	1.84	2.29	68.80	81.69

The output from the "auto" feature of Neural Solver 2 is shown. The first column is the well identifier. Subsequent columns are the actual (a) variable and predicted (p) result. This routine is useful for evaluation of independent (seismic) attributes for significance.

Intelligent Computing System for Reservoir Analysis and Risk Assessment of Red River Formation/Class Revisit

DE-FC26-00NT15123

Program

This project was in response to DOE's solicitation DE-PS26-99BC15144, Reservoir Class Field Demonstration Program – Class Revisit. The goal of the Class Program was to extend the economic production of domestic fields, by slowing the rate of well abandonments and preserving industry infrastructure, and to increase ultimate recovery using improved reservoir characterization and advanced technologies.

Project Goal

Develop an intelligent computing system and apply to reservoir-production models for analysis of seismic and geologic data relating to management, development and exploration problems in Class II reservoirs, shallow-shelf carbonate depostional systems.

Various software tools will be written. These tools can be broadly characterized as 1) clustering tools, 2) neural solvers, 3) multiple-linear regression, 4) entrapment-potential calculator and 5) combining tools. Evaluation of these tools will be made using at least five 3-D seismic surveys, multiple 2-D seismic surveys and a large database of geological, petrophysical and production information.

A methodology will be developed as a guide for users to effectively use the software tools. After validation and blind tests, results from the characterization tools will be used for locating drilling targets. A demonstration and capability for downloading of the software will be provided on a project web site.

Performer

Luff Exploration Company, Denver, CO

Project Results

Intelligent Computing System software has been developed and proven for predictive modeling in the Red River formaton in the Williston Basin.

Benefits

The project has developed user friendly software for neural networks solving of complex seismic and reservoir characterization problems. ICS software provides a means to correlate data from well logs, and production data, and integrate it with seismic data to make accurate stratigraphic predictions necessary for successful drilling and completions. As of July 2003, field trials conducted in the Red River formation in the Williston Basin have increased proved oil reserves by 3.25 MMbbl, and increased oil production over 2.6 M bbl/day. The horizontal wells are expected to produce over 1 MMbbl of incremental oil by 2005.

Background

Predictive tools have been used for decades by petroleum engineers and geologists to find and recover oil and gas resources. As technology advances, our understanding of subsurface geology sharpens and we often have to re-think our strategies for producing these valuable energy resources. Most of the easy to find and recover oil has been produced. The remaining oil is located in more complex environments, making it more difficult to find and more expensive to extract.

Luff Exploration has developed the Intelligent Computing System (ICS) as a tool to assist decision makers in selection of optimal drill-site locations and to reduce risks associated with drilling operations. ICS is a package of software tools and a reservoir characterization strategy to better access reservoir limits, producibility and favorable depositional setting. ICS uses clustering, artificial neural networks, and classical regression methods to combine seismic, geologic and engineering data for predictions of reservoir potential.

Project Summary

- The ICS software developed for integrated reservoir characterization and risk assessment for petroleum exploration.
- A software toolkit was designed to correlate relationships between seismic information and well data.
- ICS software tools are implemented in MATLAB™, an integration and visualization program. ICS is designed to run on Windows without purchase of MATLAB™.
- ICS toolkit tested on seismic and well data from six 3-D seismic surveys and wells within survey boundaries in the Williston Basin.
- Generic approach reservoir characterization modules that can be used: depositional setting, structure and growth history, seismic pseudo-reservoir parameters (variations in thickness and porosity), fluid saturation, structure and stratigraphic entrapment, and combining and weighting characterization parameters.
- The test site at Amor South field in the Red River formation has undergone complex depositional processes and tectonic growth since the time of deposition (450 million years ago) resulting in difficult to interpret structure and stratigraphy.
- Seismic attributes were transformed to reservoir attributes and finally to production attributes for predictive modeling of Amor South field.
- Original mobile-oil-in-place for Red River Zone B at Amor South field was calculated at 3.1 MMbbl using seismic attributes.

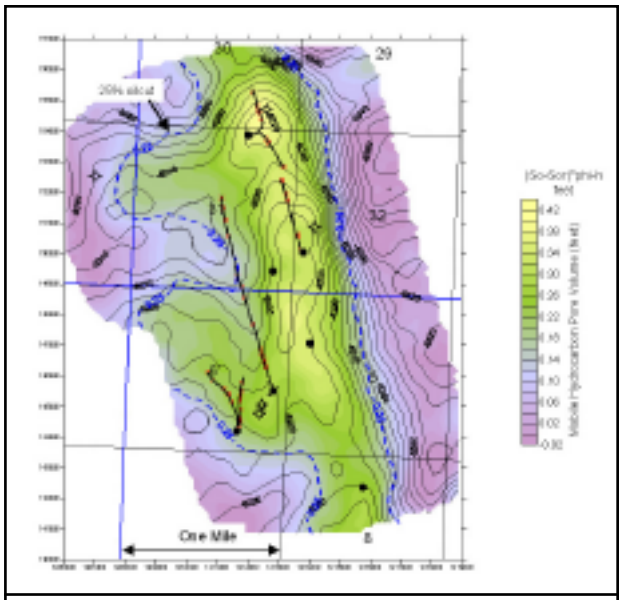

Overlay of the structure, planned and drilled horizontal wells at South Armor Field, ND.

Luff Exploration developed the ICS software to use reservoir characterization data to make predictions of where to drill and recomplete wells to optimize oil production.

Several software tools within the ICS package are used to transform seismic attributes to reservoir characteristics such as thickness, porosity, permeability, and entrapment pressure. Data from wells within seismic surveys are used as training control to transform seismic attributes to conventional reservoir attributes. Seismic-transformed reservoir characteristics can be combined with well production data from a lager database through a neural network solver to describe oil-water contacts, oil-cut and producibility.

The ICS software has been successful in exploitation field trials of the Red River B Zone in the Williston Basin at South Amor field, North Dakota. The Red River B Zone is a thin dolomite reservoir with an average thickness of 7 feet and an average depth of 9,000 ft. With a thickness ranging from only 4 to 15 feet, change in reservoir development is practically invisible to visual observation of seismic waveform character. The ICS software uses well logs, drill-stem tests and production data from several hundred wells in both the Red River B and C zones to correlate with the seismic data to overcome the resolution problems. The neural network solver was able to contour the interval revealing a tilted oil-water contact and predicting the oil-cut.

Application of ICS technology significantly reduced the risks associated in drilling horizontal wells in the Red River formation, and paid off in terms of reduced exploitation costs, increased reserves discovered and increased production. Predictions from ICS were used to re-enter and drill horizontal laterals in 16 vertical wells. These vertical wells were producing an average of 20 bbl/day each. Following completion as horizontal wells the initial production was 200-300 bbl/day/well. During the 24 months following the horizontal completions the 16 wells have produced an average of 43,300 bbl/month.

Current Status

The project ended in September, 2003. Luff continues to use the predictive modeling capabilities of ICS to develop Red River prospects in the Williston Basin. Project results, information on ICS development, and "how to use" tutorials were presented at a 2003-4 PTTC Rocky Mountain Regional symposium.

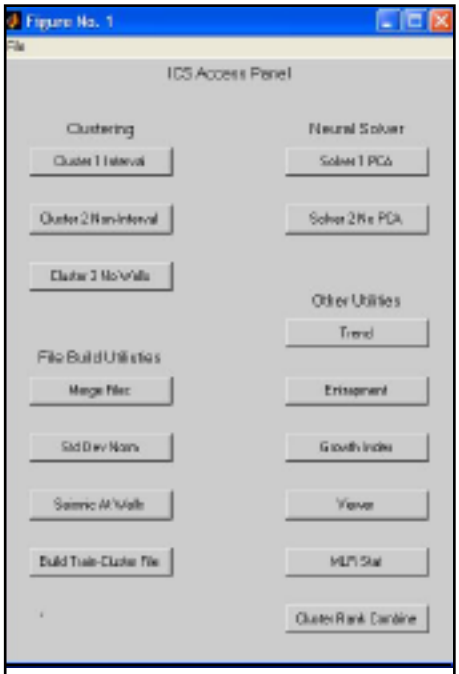

ICS control panel for access to software toolbox.

Publications/Software

An electronic copy of the final report, published in November 2003, is available from NETL at 918-699-2000.

Free ICS software is available on CD at www.netl.doe.gov/software. The ICS software is not specific to any particular region or depositional type, and users can use their own databases to populate the programs and generate predictions.

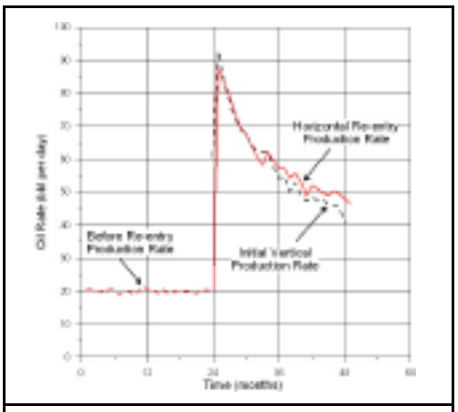

Average daily production from Red River B completions.

Project Start: February 24, 2000
Project End: August 31, 2003

Contact Information:
NETL – Paul West (paul.west@netl.doe.gov or 918-699-2035)
Luff Exploration – Kenneth Luff (303-861-2468)
1580 Lincoln St., Ste. 850, Denver, CO 80203
Petrotech Engineering – Mark Sippel (msippel@in.netcom or 303-864-9734)

CONTINUATION APPLICATION FOR BUDGET PERIOD 2

COMPANY: University of Kansas Center for Research, Inc.
2385 Irving Hill Road
Lawrence, KS 66045-7563

PROJECT TITLE: Field Demonstration of Carbon Dioxide Miscible Flooding in the Lansing-Kansas City Formation, Central Kansas

DOE CONTRACT I.D.: DE-AC26-00BC15124

PROJECT PERIOD: 03/07/00 – 03/07/10

DOCUMENT: Continuation Application for Budget Period 2

CONTACT:
NAME: Alan P. Byrnes (Project Manager – Budget Period 1)
ADDRESS: Kansas Geological Survey, 1930 Constant Ave., Lawrence, KS 66047
PHONE: 785/864-2177
E-MAIL: abyrnes@kgs.ukans.edu

DOE HEADQUARTERS PROGRAM MANAGER:
NAME: Edith C. Allison
PHONE: 202/586-1023

DOE PROJECT MANAGER:
NAME: Paul West
LOCATION: NPTO
PHONE: 918/699-2035
E-MAIL: paulwest@npto.doe.gov

CONTINUATION APPLICATION FOR BUDGET PERIOD 2

OVERVIEW OF CONTINUATION APPLICATION

It is requested that DOE approve continuation into Budget Period 2 (BP2) of the Kansas CO2 flood project, DOE Project No. DE-AC26-00BC15124 entitled "Field Demonstration of Carbon Dioxide Miscible Flooding in the Lansing-Kansas City Formation, Central Kansas" awarded to the University of Kansas Center for Research, Inc. Budget Period 1 ends on February 7, 2004, we request the continuation take place effective at the end of Budget Period 1 on February 8, 2004. We also request, as per the original proposal, that G. Paul Willhite replace Alan P. Byrnes as Project Manager. This application comprises three sections: A) Project Evaluation Report, B) Budget Period 2 Project Plan, and C) Budget Period 2 budget.

Activities performed under BP1 have principally involved: 1) Reservoir characterization and flood performance modeling; 2) Economic analysis of the pilot and miscible CO2 flooding in Kansas; 3) Wellbore remediation and facilities design and construction; 4) Initial CO2 flood testing; and 5) Technology transfer. The results of these activities will be discussed below. The original plan involved a 40-acre pattern with one injection well, five producing wells, and five water-injection containment wells. The proposed plan for BP 2, consistent with the Modified Plan approved in October 2002, involves conducting a demonstration on a 10+-acre pattern comprising one injection well, two oil producing wells, a monitoring well that may be converted to a producing well depending on flood performance, and two water-injection containment wells. The original plan involved trucking liquid CO2 from Guymon, OK. The proposed plan for BP 2 involves trucking CO2 from an ethanol plant eight miles from the demonstration site.

Assessment of the demonstration site to date, performed under Budget Period 1 activities, has defined many aspects of the reservoir. Reservoir characterization and economic analysis activities performed in Budget Period 1 have confirmed that the CO2 Pilot flood project will properly test the viability of miscible CO2 flooding in the oomolidic limestone reservoir rocks of the Lansing-Kansas City formation (L-KC), obtain the needed data to allow extrapolation and scaling of the results obtained at this site to other L-KC sites, and show small operators in Kansas that this technology can be applied to their reservoirs.

A. PROJECT EVALUATION REPORT

The following sections briefly review proposed description of work, as presented in the original approved proposal or in the modified plan approved October 2003, and the results obtained or products delivered for each of the major activities involved in the project.

ACTIVITY 1- RESERVOIR ANALYSIS AND CHARACTERIZATION

Task 1.1: Acquisition of Data and Material

Proposed Description of Work: Well, log, and production data from the proposed demonstration site and adjacent Hall-Gurney field area not in the files of the KGS and TORP will be acquired. Relevant geologic and engineering data will be entered into a digital computer database that will allow efficient storage, analysis, retrieval, editing, reporting, and output capabilities. A fully integrated digital data system accessible to internal and external users will be constructed for data handling and access.

Data to be presented will include for example: a hot-key table of contents, well drilling records, stratigraphic tops, digitized down-hole logs, well schematics, production data for the site and surrounding area, written reports, geologic sample descriptions, core and thin section photographs, cross-sections, maps, drill stem tests (DST), core analysis data, fluid analysis data, minimum miscibility pressure test(s), existing reservoir simulation models and results, and relevant regional information of similar content. Both raw and interpreted data (e.g., interpreted drill stem and production test results, stratigraphic tops, etc.) will be available through this process. Existing numerical data will be compiled and made available for downloading in spreadsheet or text form. Where data are not available numerically, such as maps or DST pressure traces, original images will be digitally scanned and made available in TIFF, JPEG, or a similar format. As the project progresses, results of the project will be added to the web site as part of technology transfer activities. Access to the data system will be modeled on the Digital Petroleum Atlas developed at the KGS (www.kgs.ukans.edu/DPA/dpaMap.html).

Project Activities/Products: Well file data were obtained from Murfin Drilling Company files, inventoried, and images scanned for presentation on the web. Wireline logs were digitized and compiled into a database for analysis and construction a reservoir model. Colliver and Carter lease production histories, pressures, and dates of when wells came online were compiled into a recurrent database for reservoir modeling and numerical simulation.

A web-based CO_2-related web site was created: http://www.kgs.ukans.edu/CO2/index.html. This site provides access to presentations, reports, well data, and important links. Well data are provided by a clickable map with links for each well to wireline logs, drillers logs, wellbore schematics, core and cuttings images is available at the CO2 website under: http://www.kgs.ukans.edu/CO2/welldata.html. Additional lease production data were collected on the adjacent Rein and Shields leases. Data were also compiled concerning plugged and unplugged wells and well ages for the entire Hall-Gurney field to aid in field-wide resource assessment and analysis of application of methodologies developed in the demonstration project. The Kansas CO2 Team utilized a proprietary website and ftp (file transfer protocol) site to share and transfer data.

Task 1.2: Reservoir Characterization

Proposed Description of Work: Reservoir characterization will consist of analysis of available core, log, fluid, well test, and production data, and integration of newly acquired data with existing data to develop descriptive and quantitative 3-D geologic, petrophysical, and fluid models of the demonstration site. Reservoir characterization will also provide data to summarize properties of the Hall-Gurney field. Models developed will be used to develop a reservoir model that describes the nature and origin of reservoir units, reservoir architecture, and 3-D storage and flow properties. The model will be used to evaluate the critical geologic and engineering parameters for optimization of development, completion and CO2 flooding strategies for the demonstration site and Lansing-Kansas City reservoirs in general. Critical to this project, the reservoir characterization models will be the basis for 3-D multi-phase reservoir numerical flow simulation to predict CO2 flood performance for decisions concerning: 1) precise location of the new CO2 injector well; 2) decisions concerning surface facilities design and CO2 flood implementation, and 3) analysis of flood results within the context of reservoir properties. Reservoir characterization is divided into three subtasks: 1) Geologic characterization, 2) Fluid Characterization, and 3) Engineering Characterization.

1.2.1 Geologic Reservoir Characterization

Logs and cuttings will be analyzed within the demonstration site and surrounding area to provide understanding of stratigraphy and depositional sequences and sequence stratigraphy. These will also provide a structure map. Typical of most leases in the Hall-Gurney, core is

unavailable from the demonstration site. Thirteen cores are available from the Lansing-Kansas City interval in the Hall-Gurney and nearby fields will be graphically logged. Representative samples will be selected for thin-section and special core analysis to assist in characterization. Cuttings for the reservoir interval will be described for all wells within the flood pattern and immediately surrounding the flood pattern. Representative larger cuttings will be utilized for thin-section and special cuttings analysis including mercury intrusion capillary pressure analysis. Photomicrographs will be taken of thin-sections to illustrate observations and interpretations.

All existing and newly acquired core and petrophysical data will be calibrated to well log response to develop a methodology for interpretation of reservoir characteristics from well logs. This will allow characterization of reservoir quality from logs in wells that were not cored, and facilitate volumetric estimation of reserves, percent recovery, and remaining oil in place. Examples of relationships to be evaluated include core porosity versus core permeability, core porosity versus log porosity, the effect of mineralogy on log response, and the feasibility of log-derived estimates of permeability. In addition, any fluid data, pressure data, and completion and production and test results (if available from cored wells) will be compared to the petrophysical data and calibrated log response.

Quantitative routine and special core and cuttings analysis will be performed on representative samples from each lithofacies present in the LKC core to characterize the complete range of petrophysical properties and identify storage and flow units.

Project Activities/Products: The Lansing-Kansas City 'C' zone reservoir was characterized geologically in the Colliver-Carter area using available cuttings and wireline logs. A summary of results were presented in two American Association of Petroleum Geologists poster presentations: 1) Byrnes, A.P., Watney, W.L., Guy, W.J., Gerlach, P., 2000, "Oomoldic reservoirs of central Kansas: controls on porosity, permeability, capillary pressure, and architecture"; and 2) Martin K. Dubois, Alan P. Byrnes, and W. Lynn Watney , 2001, "Field Development and Renewed Reservoir Characterization for CO2 Flooding of the Hall-Gurney Field, Central Kansas" (http://www.kgs.ku.edu/PRS/publication/OFR2001-38/toc1.html). This poster won the AAPG Braunstein Award for best poster at the national meeting. These are available for review and download at the CO2 website. Additional geologic and petrophysical characterization have been presented in talks and quarterly reports that are available for review and download on the website. Based on correlation with outcrop Lansing-Kansas City and log

signatures, the Lansing-Kansas City section comprises a succession of alternating marine limestones and shallow marine to nonmarine shales deposited during the Upper Pennsylvanian Series. The shoal water limestones of the Lansing-Kansas City were locally oolitic grainstones, a common lithology that serves as the main petroleum reservoir in these rocks in Kansas. The ooids are typically distributed as bars, spillover lobes, deltas, and beaches exhibiting potentially complex sets of lobes, pods, and lenses of oolite deposited during a particular cycle and sea level conditions. Geometries of beds within oolitic grainstones can include cross stratification, large foresets, and cut-and-fill structure.

Based on thin section analysis, original primary porosity was interparticle and could range up to 40 percent of the volume of the rock. This pore space was modified by early post-depositional processes including alteration by rainwater (meteoric) and shallow groundwater moving through the rock leading to both dissolution of ooids and cementation of original interparticle porosity. Most Pennsylvanian ooids were originally aragonite and tended to dissolve and recrystalize after coming into contact with percolating fresh rainwater or shallow groundwater. While Lansing-Kansas City oolitic grainstones were formed by the deposition of ooids, oomoldic grainstones in the Lansing-Kansas City of Hall-Gurney Field and the demonstration site are dominated by molds of ooids. These oomoldic pores are the dominant porosity found in oolitic grainstones of the Pennsylvanian in the Midcontinent. The geometries of the permeable (effective) reservoir rock vary considerably as a function of: 1) sedimentation of the oolites and 2) post depositional alteration including dissolution, cementation, and structural deformation.

At the demonstration site the reservoir facies were confirmed to be oomoldic limestone on the basis of cuttings description. Figure 1.2.1.1 illustrates a typical Lansing 'C' zone oomoldic limestone in core and thin section with blue-dye epoxy filling pores. Scanned images of cuttings and cores have been placed on the web site.

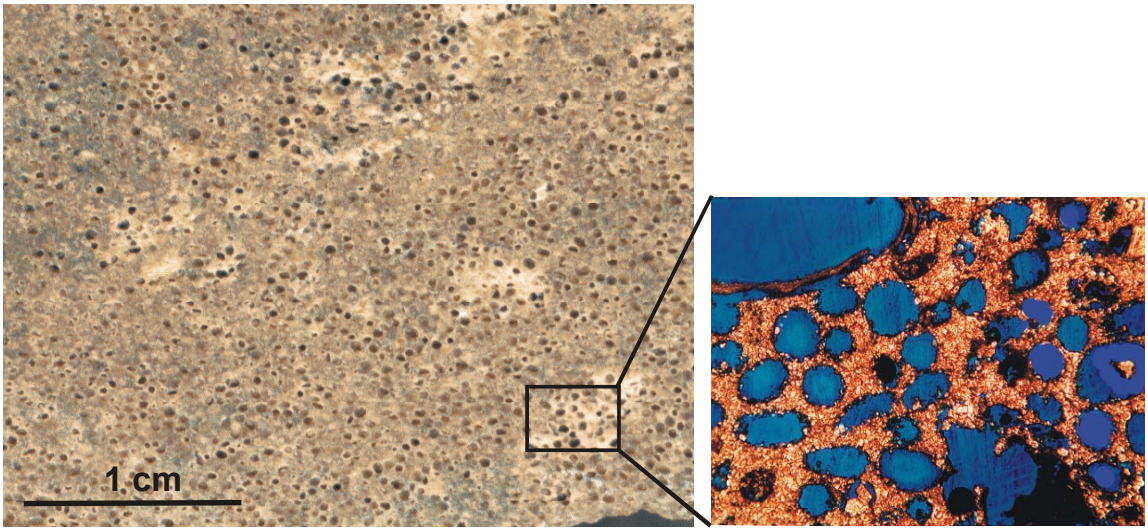

Figure 1.2.1.1. Lansing-Kansas City oomoldic limestone and plane light thin section showing blue-dye epoxy-filled pore space.

Examination of wireline log gamma ray and unscaled neutron porosity depth profiles indicates that the Lansing 'C' zone at the demonstration site consists of either three transgressive-regressive cycles or three stacked beds. For maximum numerical simulation accuracy the C zone was divided into six layers, termed C1 through C6 as described below.

Routine and special core analysis on oomoldic limestones from the Central Kansas Uplift was completed and the data analyzed. Full diameter porosity and permeability data for the Colliver #1, measured by Phillips Oil Company in 1936, were found in the well files. These full-diameter permeabilities are some of the highest values reported or measured to date though they fall below the maximum permeability versus porosity trend for Central Kansas Uplift oomoldic limestones as shown below on Figure 2. Core chips were also obtained for the Colliver #12. Porosity and grain density were measured on trimmed chips, generally measuring approximately 2-6 cm^3, after these measurements the chips were embedded in epoxy with two end faces exposed for permeability testing. Full diameter and chip permeability versus porosity trends are shown on Figure 1.2.1.2. Differences between chip and whole core permeabilities may reflect such factors as microfracturing, vuggy porosity channels, differences in oomoldic limestone properties, or other parameters.

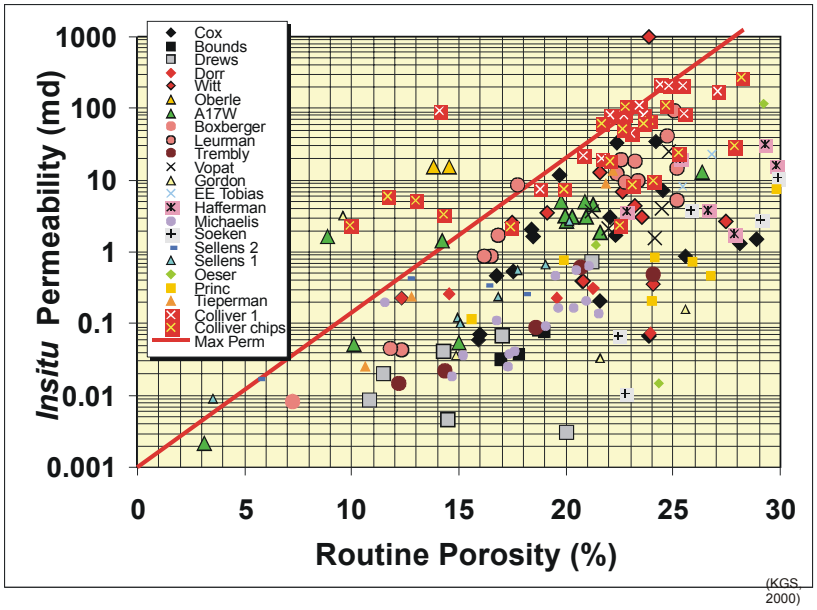

Figure 1.2.1.2. *In situ* Klinkenberg permeability versus routine porosity for Lansing-Kansas City oomoldic limestone cores obtained from wells in reservoirs lying along the Central Kansas Uplift. While scatter for total population is high, individual wells exhibit significantly less scatter.

Air-brine capillary pressure measurements were performed on a range of Lansing-Kansas City oomoldic limestone samples to obtain a trend to predict initial water saturation in the reservoir. Capillary data indicate very low irreducible water saturations for oil column heights greater than 180 feet above free water level. Analysis of the Hall-Gurney structure near the Colliver and Carter leases indicates that the reservoir lies approximately 45-55 feet above free water level which exhibit higher saturations. "Irreducible" water saturations (*Swi*) measured at an air-brine pressure equivalent to a hydrocarbon column height of 50 ft (15 m) above free water level, exhibit a trend similar to that of other L-KC oomoldic limestones (fig. 1.2.1.3) except that cores with permeability greater than 50 md exhibit Swi values as much as 25% greater than the predicted by the general L-KC trends. This represents a limited sample set in the upper-most portion of the core.

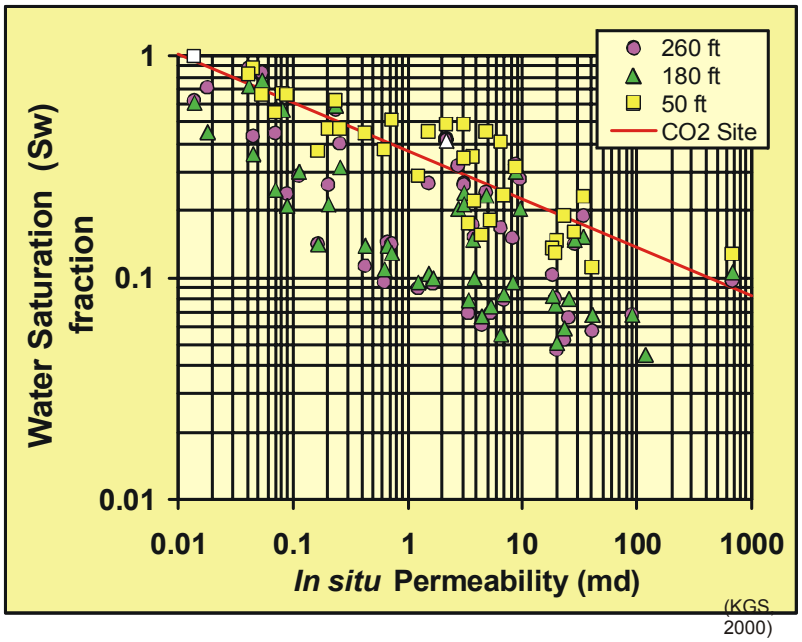

Figure 1.2.1.3. Water saturation versus permeability for L-KC oomoldic rocks and from the CO2I#1 (black squares). High permeability samples exhibit anomalously high Swi values and indicate further testing is warranted. (1md = $9.87*10^{-4}$ $u m^2$, 1 ft = 0.3048 m).

Mercury capillary pressure was measured on eight samples including oomoldic limestones distributed across the Central Kansas Uplift and a core chip from the Colliver #12. Selected samples spanned nearly the complete range in porosity (16.8%-24.9%) and permeability (0.68md – 91.9md) exhibited by the reservoir quality Lansing-Kansas City oomoldic limestones from the Central Kansas Uplift available in the study set.

Examination of the capillary pressure curves for the eight samples revealed that many samples exhibit a near log-linear trend between wetting phase saturation (assumed to be water in the reservoir) and oil-brine height above free water level. This would also translate to a log-linear relationship between wetting-phase saturation and reservoir oil-brine capillary pressure. Comparison between samples of different permeability indicates that capillary pressures decrease with increasing permeability at any given saturation. This is a typical trend for most rocks. Analyzing the relationship between the change in capillary pressure and permeability, an equation was constructed that provides approximate capillary pressure curves for any given permeability (Fig. 1.2.1.4). This equation takes the form:

$$Pc = 10^{(A\ Sw + B)} (\rho_{water} - \rho_{oil})$$

Where Pc is reservoir oil-brine capillary pressure (psia), Sw is water saturation (fraction), ρ_{water} and ρ_{oil} are water and oil density (g/cc), and A and B are constants that vary with permeability. These constants can be predicted from permeability using:

$A = -0.1663 \log_{10} Permeability\ (md) - 1.5186$

$B = 0.1088 \log_{10} Permeability\ (md) + 2.2476$

These equations provide generalized capillary pressure curves that approximate the general relationships shown by the samples studied.

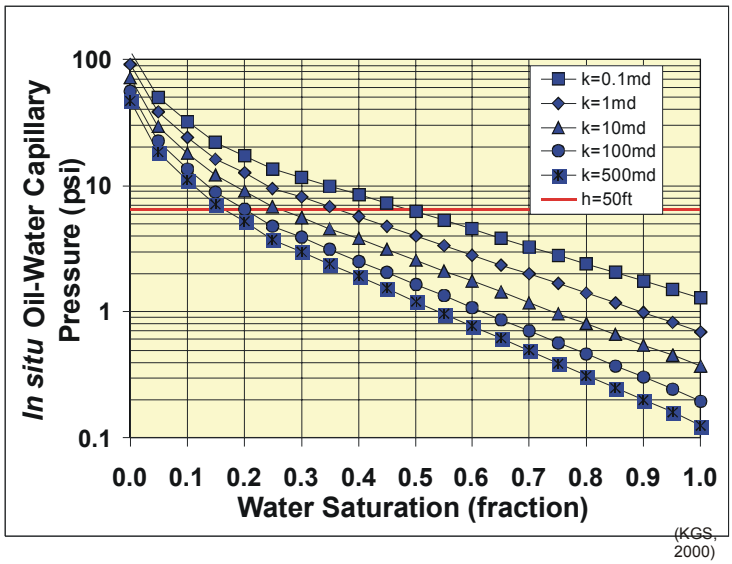

Figure 1.2.1.4. Generalized capillary pressure curves for oomoldic limestones constructed using formulas. Curvature below 15% Sw was induced by adjustment multiplier and is not predicted by the equations.

Thin sections were prepared for twenty cuttings and core chips from the Colliver lease. These are all oomoldic limestones but exhibit a range of pore types including isolated oomolds, connected oomolds, vuggy, microcrystalline, fractured, interparticle, and exhibit macroporous cement.

Log Petrophysics - Wireline logs for 41 wells in the area of the pilot were obtained, digitized and analyzed. The majority of these logs are older gamma ray – neutron logs with no resistivity logs but these appear to provide adequate porosity evaluation within ± 3 porosity percent. To convert neutron response to porosity the logs were calibrated using the standard log-linear relationship:

$$\text{Porosity (\%)} = 10^{(A*\text{Neutron} + B)}$$

Where A is the slope of the correlation between $\log_{10}$Porosity and neutron response and B is the intercept. These constants were derived using a log-linear straight-line relationship between the two points: 40% porosity-minimum Neutron response, 1% porosity-maximum neutron response. Using this correlation neutron log response was converted into porosity for the reservoir model. Porosity was used as the independent variable to predict permeability.

1.2.2 Fluid Characterization

Oil and water samples will be obtained from the demonstration site. Oil characterization tests performed included compositional analysis, minimum miscibility pressure (MMP) analysis, interfacial tension, gravity, viscosity, and Pressure-Volume-Temperature (PVT) properties. Water samples will be analyzed for total dissolved solids, composition, and resistivity.

Project Activities/Products: Oils from the Letsch #7, one mile east of the Colliver lease was analyzed for minimum miscibility pressure (MMP) prior to drilling of the CO2 injection well. MMP was measured on Letsch #10, Letsch #7, and Olson #7 oils from Hall Gurney Field. MMP is defined as the pressure at which multi-contact flooding achieves an oil recovery of 90% at one pore volume injected. Interfacial tension was measured on oil sample and found to be 28.6 dyne/cm at 25°C. Oil chemical composition and PVT properties were measured by Core Laboratories on the Letsch #7 oil sample. Water chemistries were compiled for L-KC wells in Russell County.

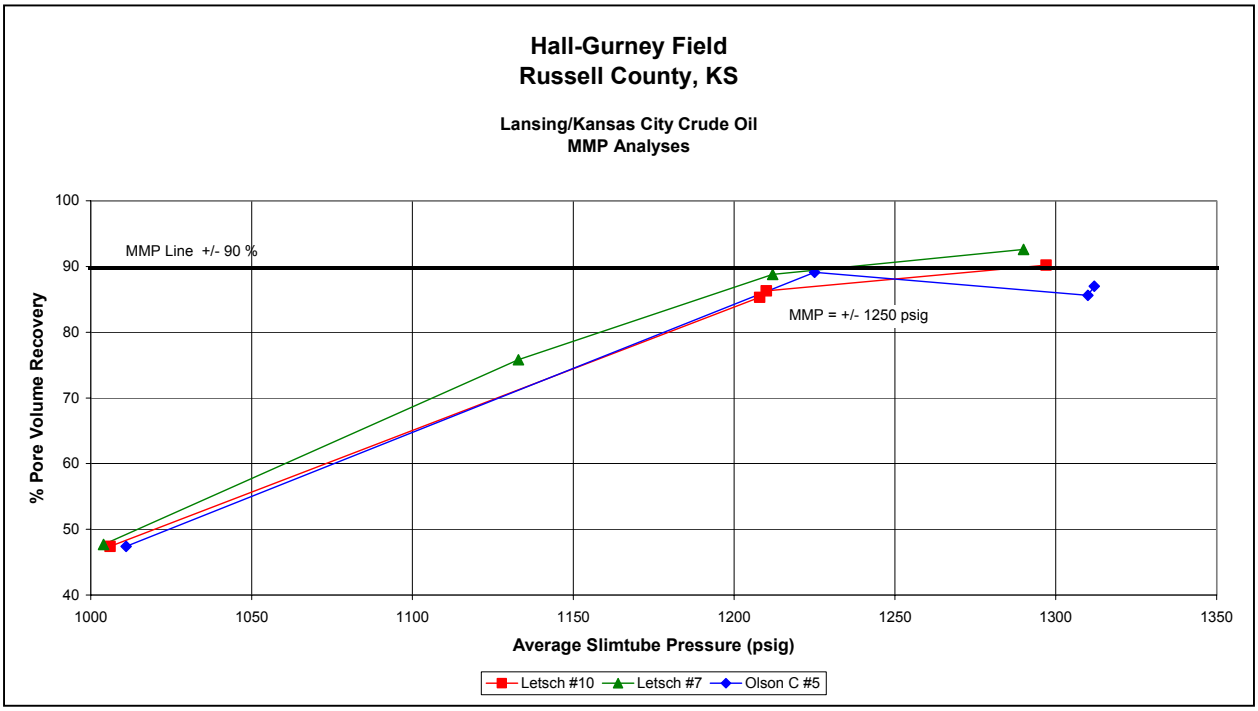

Figure 1.2.2.1 Minimum miscibility measurements on Hall-Gurney oil.

1.2.3 Engineering Characterization

Like many Hall-Gurney leases, engineering data are limited. Existing production history, including oil production on a lease basis and monthly or quarterly water production by well data will be analyzed. Additional data on well workover histories, and injection well rates and pressures will be analyzed. These data will provide input to developing a quantitative reservoir model.

Project Activities/Products: Well permeability-height, *kh*, were calculated based on known production/injection rates in 1980, wireline interpreted reservoir thickness, an assumed water relative permeability of 20% at residual oil saturation, and other basic properties assumptions (Figure 1.2.3.1). These estimates were used to modify the assigned permeabilities for each well that were based on calculated permeabilities predicted from wireline log porosities.

Gas-in-solution was estimated since records of gas production were not available.

Estimated Peremability for Colliver-Carter Wells based in Injection/Production in 1980								
Viscosity of water,cp		0.77		k_{rw} @ S_{iw}	0.2			
B_w, RB/STB		1.0079		p_e, psi	600			
r_w, ft		0.359		p_w, psi	30			
Production Wells	**h, ft**	**r_d, ft**	**q_w, B/D**	**k_w, darcy**	**k, darcy**	**kh, darcy ft**		
Colliver 1	14	664	151	0.015	0.077	1.083		
Colliver 3	11	652	91	0.012	0.059	0.651		
Colliver 5	15.5	678	137	0.013	0.064	0.986		
Colliver 6	12.5	554	115	0.013	0.064	0.805		
Colliver 7	11	1071	614	0.085	0.426	4.685		
Colliver 9	13	901	92	0.011	0.053	0.687		
Colliver 12	15	593	128	0.012	0.060	0.905		
Colliver 13	13	571	71	0.008	0.038	0.499		
Colliver 14	15	470	219	0.020	0.100	1.499		
Total-Colliver			1618					
Carter 2	12	455	14	0.002	0.008	0.095		
Carter 3	17.5	362	101	0.008	0.038	0.666		
Carter 5	17.5	441	56	0.004	0.022	0.380		
Carter 11	14	145	39	0.003	0.016	0.223		
Carter 12	11.5	212	33	0.003	0.017	0.201		
Total-Carter			243					
Total-Colliver and Carter			1861					
Injection Wells	**h, ft**	**r_e,ft**	**i_w, B/D**	**p_{wh},psi**	**p_{bh},psi @2880 ft**	**k_w darcy**	**k,darcy**	**kh, darcy ft**
Colliver 2	17	716.56	417	1100	2433.44	0.0111	0.0553	0.9396
Colliver 4	17	963.19	290	1150	2483.44	0.0078	0.0389	0.6608
Colliver 8	9.5	1196.23	274	250	1583.44	0.0259	0.1293	1.2286
Colliver 10	15	1143.23	119	415	1748.44	0.0061	0.0303	0.4544
Colliver 18	12	667.02	230	1280	2613.44	0.0078	0.0390	0.4674
Colliver 19	12	518.15	349	1275	2608.44	0.0115	0.0573	0.6872
Colliver 20	12	381.77	185	1275	2608.44	0.0058	0.0291	0.3490
Total Colliver			1864					
Carter 4	12	349.07	182	1430	2763.44	0.0052	0.0262	0.3146
Carter 10	12	530.82	288	1140	2473.44	0.0102	0.0508	0.6100

Figure 1.2.3.1. Estimates of Colliver and Carter permeabilities based on well data prior to drilling of CO2 I#1. (h=height, rd=radius, q=flow rate, k=hydraulic permeability, kh=k*h). See Table 3.1.1 for presently interpreted permeability values in the pilot area. Note that high injectivity in some injection wells may be due to injection above frac pressure.

Task 1.3: Reservoir Model

1.3.1 Develop Qualitative and Quantitative Reservoir Model

Proposed Description of Work: Both descriptive and quantitative 3-D integrated models of the reservoir interval will be developed utilizing the integrated geologic, petrophysical, engineering and production data. Elements of the descriptive reservoir model will include the nature of reservoir rock, the variability in reservoir quality, the types, scales, and causes of reservoir heterogeneity, the geometry of reservoir architecture, the definition and distribution of reservoir flow units, and the nature of reservoir traps and seals. Existing production data will be compared to the descriptive reservoir model to determine the extent to which the model corroborates fluid production history, and to identify areas of inconsistency or uncertainty. Elements of the 3-D quantitative model will include grid block parameters for dimensions (including both size of each cell and reservoir thickness), porosity, relative permeability, compressibility, capillary pressure, and fluid properties.

Project Activities/Products: A qualitative and quantitative preliminary reservoir model was constructed for the Colliver and Carter leases. The Lansing 'C' interval was characterized as being composed of three stacked units between which the vertical communication is uncertain (Figure 1.3.1.1).

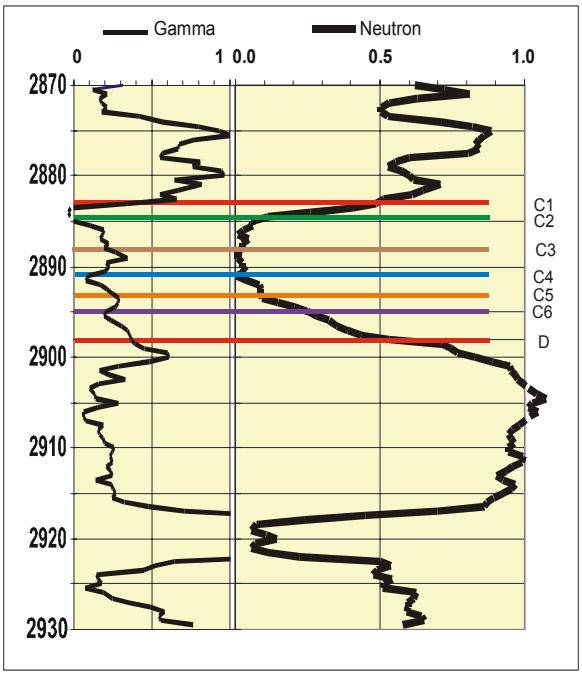

Figure 1.3.1.1. Colliver #18 normalized gamma ray-unscaled neutron log showing six C zone layers and three cycles. The Colliver #18 exhibits some of the best porosity compared to all wells in both leases.

Because permeability changes by a factor of 2 for every 1 porosity unit change, each of the three layers has been divided into an upper and lower layer to minimize permeability variance within a layer and error associated with layer averaging. Overall, the C zone deceases in porosity and permeability from top to bottom. The six layers have been termed C1 through C6. This division allows more accurate delineation of saturations and flooding behavior in each layer.

Average Layer Properties

C1: 8 md, 18.8%	set 1
C2: 150 md, 25.8%	set 1
C3: 40 md, 22.0%	set 2
C4: 6 md, 19.4%	set 2
C5: 2 md, 14.7%	set 3
C6: 0.3 md, 12.0%	set 4

Porosity and calculated permeability were mapped for each layer for the Colliver and Carter leases. An example of the porosity distribution is shown in Figure 1.3.1.2.

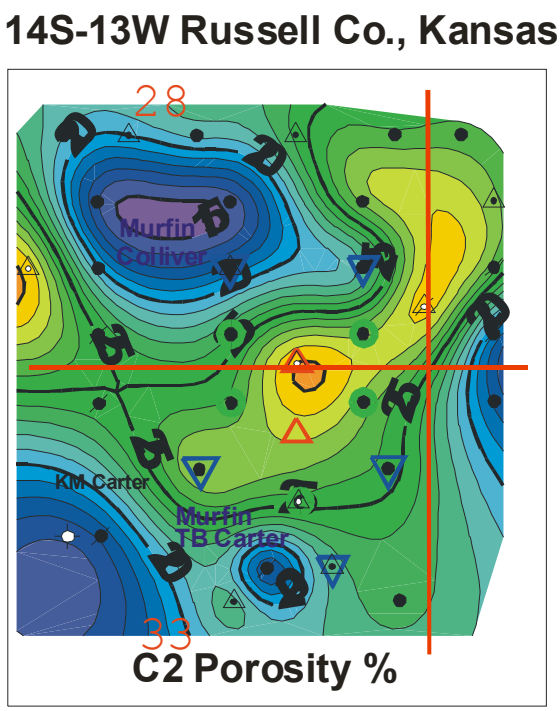

Figure 1.3.1.2. Example of porosity distribution in layer C2 for Colliver and Carter leases. Isopach created before addition of CO2I#1 and CO2#16 porosity information.

Properties of the preliminary quantitative reservoir model were modified to provide an optimum match between numerical simulator predicted production rates and cumulative production and reported values. Since permeability has been correlated with porosity, and capillary pressures and relative permeability have been correlated with permeability, changes in model reservoir porosity resulted in changes in model reservoir permeability, relative permeability, and initial water saturation. Permeabilities were predicted using two equations:

Porosity > 21%: $\quad$ *Permeability (md)* = 28.8 * *Porosity (%)* –584.4

Porosity < 21%: $\quad$ *Permeability (md)* = $10^{(0.207 * \textit{Porosity (\%)} - 3.05)}$

The high porosity equation was used because existing full-diameter core analysis data from the Colliver #1 well do not exhibit log-linear increase in permeability with increasing porosity at higher porosities.

Initial water saturations were predicted for each layer using the generalized capillary pressure curves. A single average saturation was assigned to each layer for the Colliver and Carter leases respectively. Although permeability differences between gridcells would indicate that water saturations and relative permeabilities should also vary between gridcells, the use of a single relative permeability curve for each layer (effectively a pseudo-relative permeability curve) required the use of pseudo-water saturations to avoid calculation of incorrect effective oil and water permeabilities in each gridcell.

Since relative permeability end point saturations change with permeability (e.g., "irreducible" water saturation changes with permeability), the relative permeability curves also change with absolute permeability. Starting relative permeability curves for each layer were predicted from the absolute permeability values for each layer (Figure 1.3.1.3).

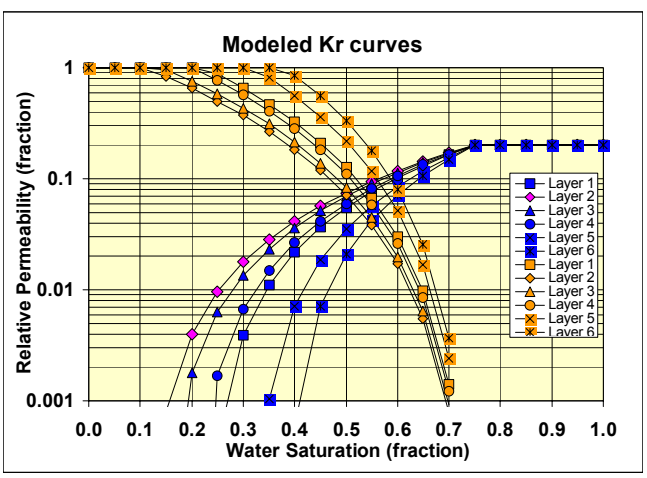

Figure 1.3.1.3. Initial oil and water relative permeability curves for Layers C1-C6.

1.3.2 Check Reservoir Model for Internal Consistency

Proposed Description of Work: Contour maps of porosity, net feet and saturation will be integrated to determine reservoir volume and initial oil in place. The primary production mechanism in Lansing-Kansas City reservoirs is solution gas drive. Material balance calculations will be made to compare estimated production from solution gas drive with primary production to assess the consistency of the reservoir description. Waterflood recovery will be estimated from simple volumetric calculations using estimated residual oil saturations and will be compared with actual field performance. Adjustments in the reservoir description will be made where necessary to correspond to field performance.

Project Activities/Products: Material is dependent on assumed/modeled starting reservoir properties and allocated production and injection. Uncertainty in these result in uncertainty in the material balance. Comparison of material balance calculations and the initial reservoir model indicated that the porosity of the reservoir model needed to be greater than values calculated from logs. Porosity was increased by ~2-3% to account for produced oil. This increase was within the error of the log-calculated porosity prediction equation. This revised model was utilized in the reservoir simulation.

Task 1.4 Reservoir Simulation(Phase I)

Proposed Description of Work: The reservoir description developed in Activity 1-Task 3 will be imported into a reservoir simulator to simulate both primary production and waterflooding of the pilot demonstration site. The reservoir simulator constructs a simulation grid of the pilot demonstration site and the surrounding area from the reservoir description. Simulation will be done using Landmark Graphics ***VIP98 Plus*** reservoir simulator installed in a Silicon Graphics Octane MXE workstation. Adjustments in reservoir and fluid properties will be made to match primary production history using the available data. Waterflood performance will be simulated and matched with production history. The capability of confinement wells to maintain the reservoir pressure near the anticipated MMP will be investigated using reservoir simulation.

Carbon dioxide injection into the pilot demonstration site will be evaluated initially using the reservoir simulator based on the saturation distribution at the end of the waterflood. The simulation will include water injection into confinement wells. Results will also be used to

evaluate recovery efficiency of the proposed demonstration project and to make preliminary economic calculations. It is anticipated that the model will be refined when core and reservoir fluids data are available from the new injection well drilled and evaluated in Activity 2-Task 1.

Project Activities/Products: Using the compiled lease production histories a recurrent database was constructed with format suitable for input to VIP. Simulation was performed on a Landmark Graphics ***VIP98 Plus*** reservoir simulator installed in a Silicon Graphics Octane MXE workstation. The pilot area was simulated using the six layer geomodel, with 48x46 gridcells in each layer, and with grid cells 110ftx110ft. History matching simulations were performed to match estimated primary and secondary production history using black oil simulation (Figure 1.4.1).

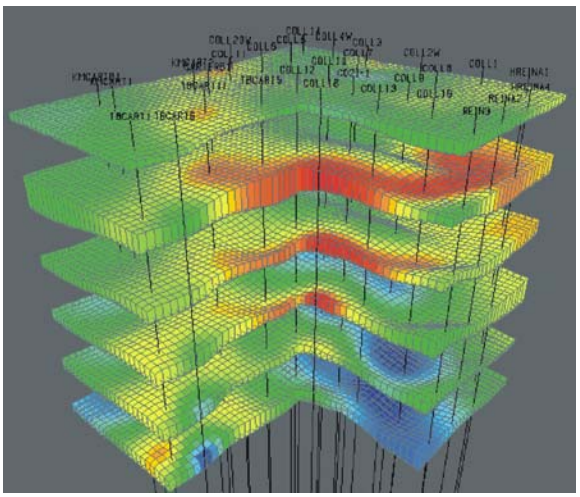

Figure 1.4.1. 3-D view of VIP model of Colliver and Carter leases showing porosity distribution for 6-layer model and well locations

For CO2 flooding a six pseudo-component fully compositional model was run. Multiple CO2 flood simulations were performed to identify the best location of the new injection well. Figure 1.4.2 illustrates an example of a simulation showing the CO2 oil bank (blue). Figure 1.4.3 illustrates the history match achieved by the reservoir simulation model developed before drilling the CO2I#1 well.

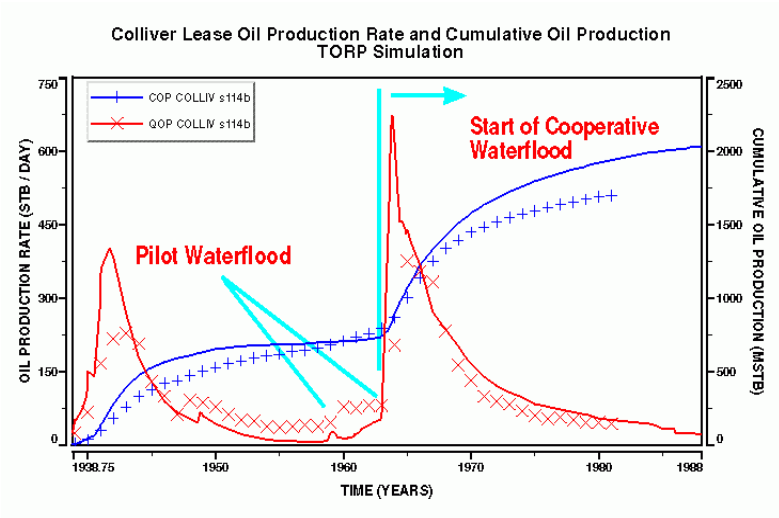

Figure 1.4.2. CO2 flood simulation showing creation of oil bank. The model results shown are based on the preliminary equation of state prior to receiving CO2 and oil pressure-volume-temperature data.

Figure 1.4.3. History match of primary and secondary production history for Colliver lease. Specific match in present pilot area exhibited high uncertainty.

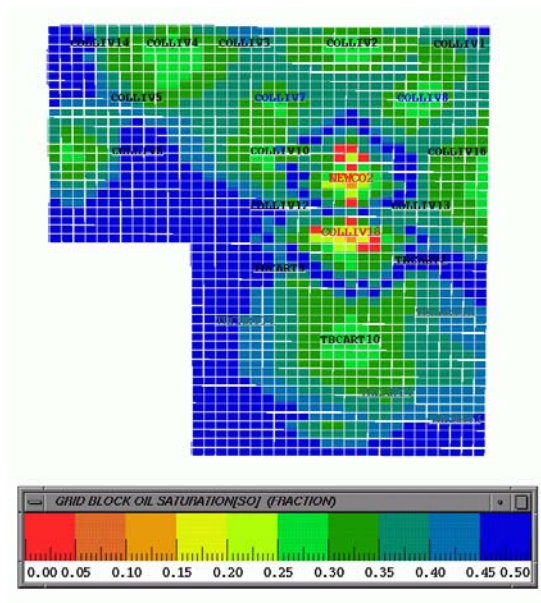

Characterization and simulations indicated that permeabilities in the Carter lease were lower than estimated before the project inception. Simulations of the original proposed injection well location indicated that this location did not provide an optimum location. A new location to the north in the Colliver lease provided good predicted oil recoveries and avoided proximity to the Colliver #7, to the northwest, which exhibits production rates that are anomalously high and may be influenced by a fracture. The new location represented an inverted 5-spot pattern with possible additional use of the Colliver #18 as a second injector creating a 2-injector, 7-producer pattern. For both patterns modeled oil recoveries indicated the pilot would be viable. Based on these models the new injection well was located in the Colliver lease. Note that flood design changed after drilling the CO2I#1 as described in Task 3.1.

ACTIVITY 2-PRODUCIBILITY PROBLEM CHARACTERIZATION AND ANALYSIS

Task 2.1: Drill, Core and Test CO_2 Injection Well

Proposed Description of Work: A new Lansing/Kansas City "C" zone CO_2 injection well be drilled, sponge cored, drill-stem tested, electric wire-line logged, and completed on the Carter lease. The location of this well will be determined using the reservoir simulation to maximize flood response. Reservoir simulation will be used to evaluate whether the nearby Colliver 18 well should be plugged and abandoned or used as a second WAG injector.

Project Activities/Products: Drilling commenced on the Murfin Drilling Company, Inc. #1CO2 I Carter-Colliver well (API# 15-167-23179), located in the S/2 SE/4 of Section 28-14S-13W, Russell County, Kansas, on September 23, 2000 and was completed on October 2, 2000 (fig. 2.1.1). Eight and five-eighths inch surface casing was set at 1435 feet with 650 sacks of cement, a 7-7/8 inch hole was drilled to a total depth of 3115 feet and five and one-half inch production casing was set at 3114 feet, one foot off bottom, with 360 sacks of cement. Drilling operations were trouble free and the maximum hole deviation was ¾ degrees from vertical. A low water loss polymer and starch mud system resulted in excellent hole conditions throughout the operation. Five cores were taken including three conventional cores at depths of 2871-2894 (L-KC 'B' and uppermost 'C' zones), 2949-54 (L-KC 'G' zone), and 2954-2981 (L-KC 'G' zone) and two pressure cores at depths of 2894-2904 (L-KC 'C' zone) and 2904-2914 (L-KC 'C' and 'D' zones). Schlumberger's Platform Express logging suite was run at total depth, including Compensated Neutron Litho Density, Array Induction Linear Correlation, and Microlog. In addition, a Borehole Compensated Sonic log was run. Schlumberger's Repeat Formation Tester tool was run following the electric logging operation on sixteen intervals to obtain pressure data. Though recovery of material cored using the high-pressure core barrel was good, a significant portion of material recovered from the good quality reservoir interval was deconsolidated and was primarily carbonate "dust." The cause for the crushing and results obtained from the core must be qualified. Given the unconsolidated nature of the retrieved core, the core is believed to have been extensively flushed.

The geologic report log for the Lansing-Kansas City interval are presented at:
http://www.kgs.ukans.edu/CO2/CO2Data/Misc/CO2I-1gr.html.

Wireline logs in the 'C' zone can be viewed at:
http://www.kgs.ukans.edu/CO2/CO2Data/1516723179.html

And complete LAS format logs can be viewed and downloaded from:
http://polaris.kgs.ukans.edu/pls/abyss/qualified.well_page.DisplayWell?f_kid=1020066130

Figure 2.1.1. NW view of Murfin Carter Colliver #1 CO2 I in background and the Colliver #13 producing well, in the SE corner of the flood pattern, in the foreground.

Formation Pressures (2.1.4)- Original plans were to perform drill stem testing of the reservoir interval. Rather than drill stem test, Schlumberger's Repeat Formation Tester tool was run following the electric logging operation on sixteen intervals to obtain pressure data. Differences in pressure between the Lansing-Kansas City 'C" zone (~800 psi, 5.9 MPa) and overlying formations (~1250 psi, 8.6 MPa) indicate that these intervals are not in communication which would indicate that wellbore integrity issues and potential loss of fluids into shallower intervals should not present a problem for the demonstration project.

Task 2.2: Producibility Characterization using New Core

Proposed Description of Work: On receipt of the new injector well core after commercial whole core analysis, whole core data will be analyzed and integrated with the core description to identify the representative lithofacies and identify samples representing the range of porosity and permeability within the reservoir interval. Core plugs will be obtained from

these selected intervals and a comprehensive suite of advanced petrophysical measurements will be performed on these samples related to fluid storage and flow and electrical properties including: 1) porosity, 2) compressibility, 3) routine permeability, 4) *insitu* water permeability, 5) air-brine and/or air-mercury capillary pressure, 6) electrical resistivity measurements for Archie cementation exponent, m, and saturation exponent, n, values; 7) *insitu* relative permeability end-point permeabilities including permeability to oil at interstitial, k_o @ ,S_{iw} and permeability to water at residual oil saturation, k_w @S_{orw}; 8) "interstitial" water saturation, S_{iw}, at reservoir capillary pressure conditions and residual oil saturation after waterflood, S_{orw}; 9) full *insitu* oil-water relative permeability curves on some and waterflood susceptibility on a larger number of samples; 11) residual oil saturation after CO2 flooding, $S_{orm}(CO2)$, for cores starting at S_{orw}; and 12) nuclear magnetic resonance T1 and T2 curve analysis. Data will be presented in both a rock catalog format and in other integrated formats.

Project Activities/Products:

Residual Oil Saturation (2.2.1) **-** Core analysis of residual oil saturation to waterflood indicates that mean residual oil saturation for "C" zone oomoldic limestones measured to date in the Carter-Colliver #1 CO2 I is 27.4% with a minimum and maximum of 14.3% and 36.9%, respectively (fig. 2.2.1.1). These core flood values are consistent with the routine core saturation and the log-measured saturations but are not consistent with the high-pressure core oil saturations.

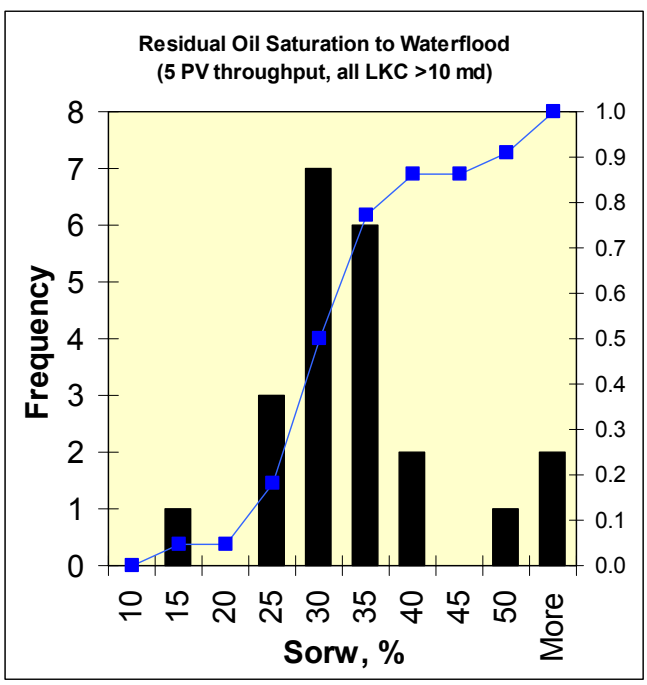

Figure 2.2.1.1. Histogram of residual oil saturation to waterflood for coreplugs from the Carter-Colliver #1 CO2 I oomoldic limestone "C" zone.

The second high-pressure core recovered from the "C" zone interval 2904-2914 ft (885.14-888.19 m) in the Carter-Colliver #1 CO2 I well is well-consolidated and exhibits decreasing porosity with increasing depth from 16% to 1% and permeabilities from 0.73 md to <0.01 md ($7.3*10^{-5}$ to $1*10^{-6}$ $u m^2$). These data indicate that model layers 5 and 6 are thicker and exhibit slightly poorer reservoir properties than predicted. The trend of decreasing permeability with increasing depth below the top of the "C" zone extends into the interval of the second core (fig. 2.2.1.2).

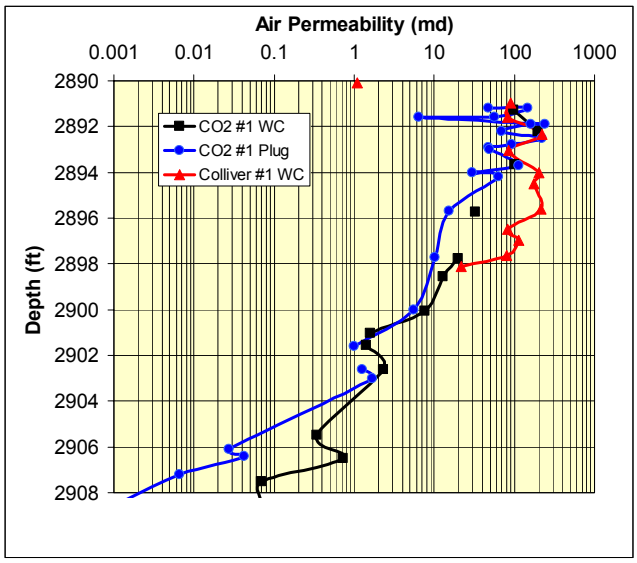

Figure 2.2.1.2. Permeability versus depth for Murfin Carter-Colliver #1 CO2 I well and the Collvier #1 well. (1md = $9.87*10^{-4}$ $u m^2$, 1 ft = 0.3048 m)

Routine and Special Core Analysis (2.2.5 & 2.2.6) **-** Permeabilities decrease with increasing depth below the top of the "C" zone and exhibit properties similar to initial reservoir simulations. Core obtained using the pressure core barrel exhibited significant damage which may have affected the representativeness of data obtained on these cores. Oil saturations measured in the routine core, taken in the top 2 feet (0.61 m) of the "C" zone exhibit an average oil saturation of 28%. The high-pressure core, taken over the remainder of the "C" zone, exhibits an average oil saturation of 10%. This low saturation is believed to be the result of extension flushing of the crushed and unconsolidated core.

Archie cementation exponents, m, for Wireline log analysis are significantly greater than the conventional value of 2.0. Cementation exponent values for "C" zone oomoldic limestones ranged from 2.2 to 3.6. Values increase with increasing porosity (fig. 2.2.5.1) and with increasing proximity to the top of the "C" zone.

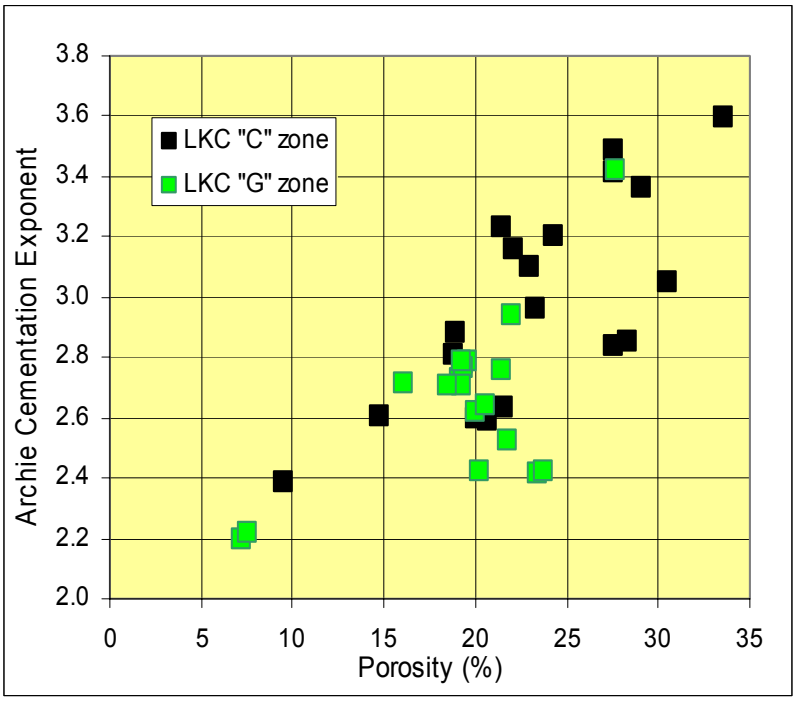

Figure 2.2.5.1. Cross-plot of Archie cementation exponents versus porosity showing increase in *m* with increasing porosity.

"Irreducible" water saturations (*Swi*) measured at an air-brine pressure equivalent to a hydrocarbon column height of 50 ft (15 m) above free water level, exhibit a trend similar to that of other L-KC oomoldic limestones (fig. 2.2.6.1) except that cores with permeability greater than 50 md exhibit Swi values as much as 25% greater than the predicted by the general L-KC trends. This represents a limited sample set in the upper-most portion of the core and must be evaluated further.

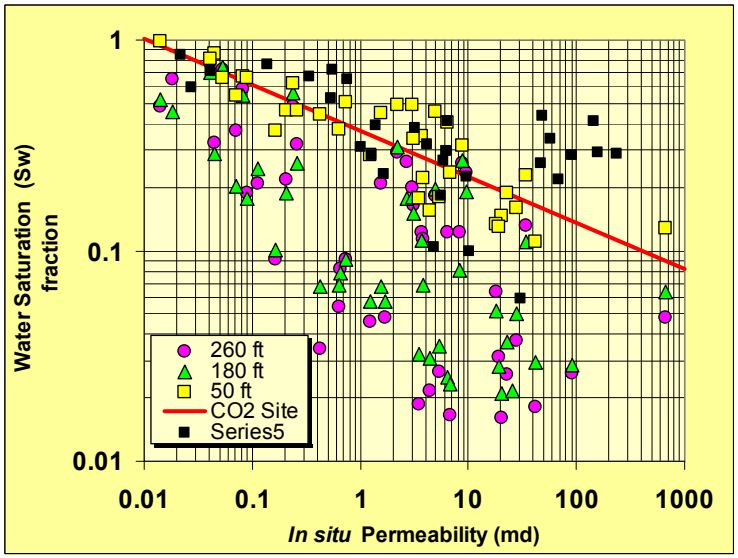

Figure 2.2.6.1. Water saturation versus permeability for L-KC oomoldic rocks and from the Carter-Colliver #1 CO2 I (black squares). High permeability samples exhibit anomalously high Swi values and indicate further testing is warranted. (1md = $9.87*10^{-4}$ $u m^2$, 1 ft = 0.3048 m).

Mercury capillary pressure intrusion measurements to 10,000 psi (1,000 kPa) provided capillary pressure curves for selected samples ranging in permeability from 0.027 md to 220 md ($2.6*10^{-6}$ to $2.2*10^{-2}$ $u m^2$). Saturation versus capillary pressure curves for these cores are consistent with capillary pressure curves measured on other Central Kansas Uplift oomoldic limestones and with the generalized model curves constructed for the reservoir simulation geomodel (fig. 2.2.6.2).

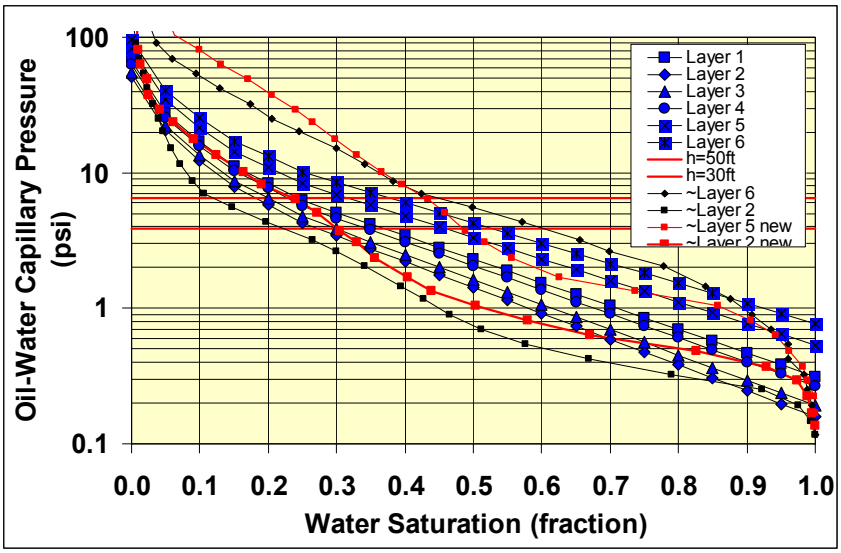

Figure 2.2.6.2. Capillary pressure curves for high and low permeability samples from the Carter-Colliver #1 CO2 I "C" zone (black and red symbols) compared with the generalized model curves developed for the reservoir simulation geomodel (blue curves).

Geologic Characterization (2.2.7) **-** The "C" zone is composed of coarse grained oomoldic grainstone exhibits a slight decrease in oomold size and deceasing packing with increasing depth below the top of the zone. Minor isopachous rim cementation and micritized ooid cortices are also present. Based on thin-section analysis, the L-KC in this region underwent similar diagenesis to that described by LeBeau (1997) and Byrnes and others (2000) (fig. 2.2.7.1).

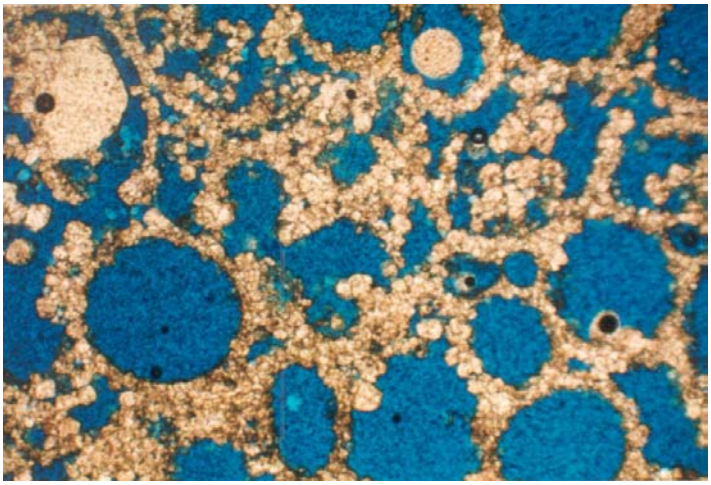

Figure 2.2.7.1. Plane light thin section of L-KC "C" zone 2903 ft (884.8 m) showing blue-dye impregnated oomoldic porosity and recrystallized limestone matrix framework. Crushing of matrix is evident.

Wireline Log Analysis (2.2.7) **-** To obtain information concerning subsurface rock types, porosity, and fluid saturations Schlumberger's Platform Express logging suite was run from casing to total depth. Logs included in this suite include Caliper, Gamma Ray, Compensated Neutron Litho-Density, Array Induction Linear Correlation, and Microlog. In addition, a Borehole Compensated Sonic log was run. Analysis of logs for this interval indicate that remaining oil saturations are near 30-40% (Fig. 2.2.7.2). Saturations of 30%-40% are sufficient for a meaningful test of CO_2 flooding.

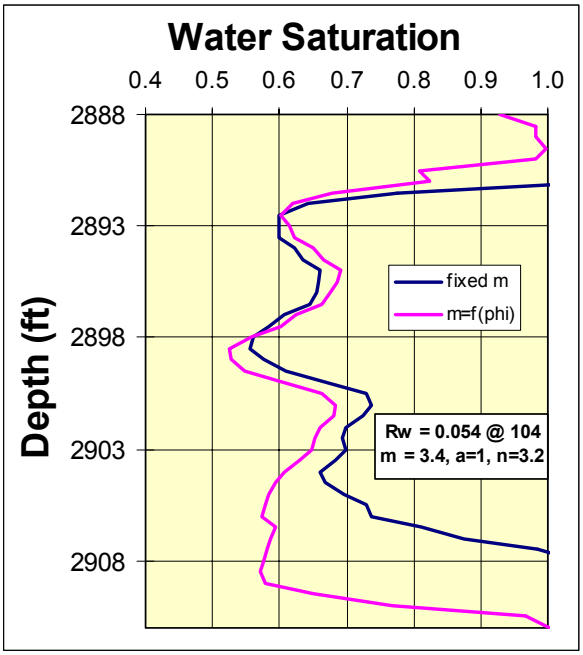

Figure 2.2.7.2. Calculated water saturations in Lansing-Kansas City "C" zone using Wireline log deep induction response and Archie parameters that are both fixed at values measured in the Laboratory or vary with porosity. Water saturations in "C" zone range from 30-40% and are sufficiently high to justify implementation of CO_2 enhanced recovery operations.

Task 2.3: Remediate and Test Wells and Pattern (WSW, Production, Containment) – (Added to original proposal in the Modified Plan approved in October 2003)

Tasks involved with injection and production well remediation and testing remain similar to those in the original SOW under Task 5.1 except that the wells involved have changed to allow a shift in the pattern location north into the Colliver lease. The number of containment is decreased from five to two. The number of producing wells is decreased from five to three and the exact remediation required has changed slightly in accordance with the remediation required for the new wells. These activities were shifted from Budget Period 2 to Budget Period 1.

2.3.1 Drill, Complete, and Equip Water Supply Well

Proposed Description of Work: A new salt water supply well will be drilled and completed to supply sufficient water for the containment water injection testing and for the CO2 Water-Alternating-Gas (WAG) water injection cycles. This well will be about 500' deep and will be completed in the Dakota, Cheyenne, or Cedar Hills. It will be equipped with pumping equipment capable of about 800-1000 BWPD. An alternative existing water supply well in an adjacent lease is also being considered. Which source of water is used will be decided based on indications of the supply rates needed and minimum costs.

Project Activities/Products: An onsite water supply well was drilled and completed in the shallow (245 ft; 74.7 m) fresh-water Dakota aquifer on 3/27/02. Supply water total dissolved solids was measured by Pace Laboratories to be 4,920 milligrams per liter. A submersible pump was run in the well. A water injection station located near the Colliver lease tank battery (near CO2 Project #10, formerly Colliver #10) comprising a 200 bbl (31.8 m^3) fiberglass tank, triplex pump, filter cartridges, metering, valves, etc. was fabricated and installed. The site was graded and the pumphouse put in place. A fiberglass injection line was laid to CO2 I#1 and CO2#10.

2.3.2 Workover and Test Producing Wells in Pilot Area

Proposed Description of Work: Activities in this task are similar to the original SOW as described under Task 5.1.2 except that the number of wells involved is decreased from five to three. Two existing wells (CO2 #12 and #13) and a shallow existing well (CO2 #16) on the Murfin CO2 Project lease will be oil-producing wells. Each of these wells will be studied in detail and reworked, completed, and equipped as necessary to isolate the producing interval to only the Lansing-Kansas City (L-KC) "C" zone.

Analysis indicates that perforated zones in all wells will probably have to be cement squeezed. These wells have 6" casing, which may make running and cementing a liner to the surface the simplest way to isolate the L-KC "C" zone. The L-KC "C" zone will be re-perforated and stimulated. The shallow-producer Colliver #16 will be used as a producer and will be drilled deeper and completed and equipped. High-pressure wellheads for CO2 service may be installed.

Project Activities/Products:

<u>CO2 Project #12</u> - A workover on the CO2 Project #12 well (formerly Colliver #12) was completed 3/6/03. For this well, the LKC G was plugged back with cement and a 4-1/2" welded liner was cemented to surface across all shallow zones leaving only the LKC C open with open-hole completion (Figure 2.3.2.1).

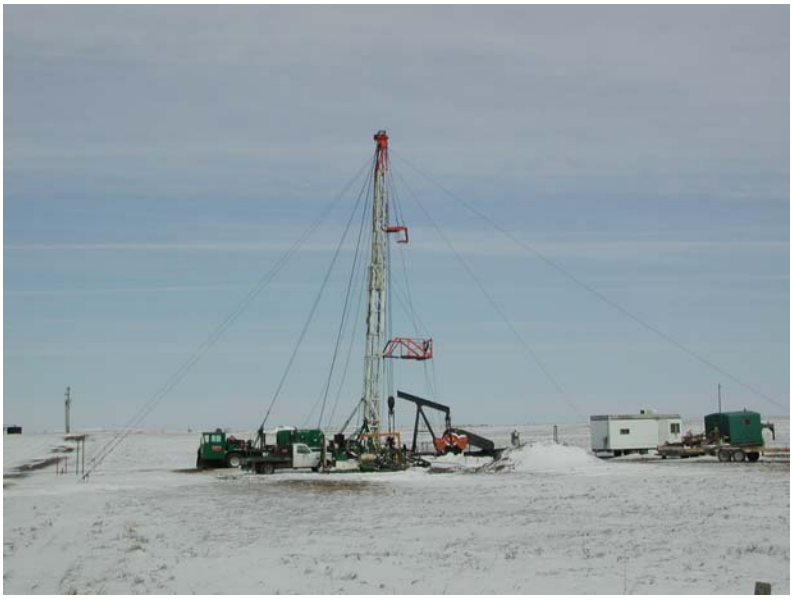

Figure 2.3.2.1. Workover of the CO2 Project #12 well in late February-early March 2003.

Wireline logs were obtained since this well was not previously logged. Porosity and distribution of depositional cycles in the CO2 Project #12 are similar to the CO2I #1 (Figure 2.3.2.2).

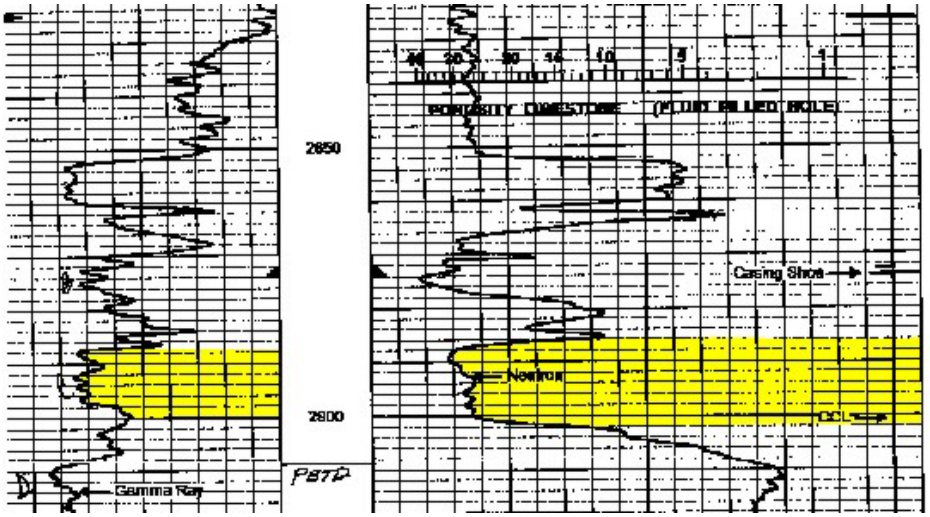

Figure 2.3.2.2. Wireline neutron log of the CO2 Project #12 logged in March 2003. High porosity in upper cycle and lower porosity in lower cycle are similar to the CO2I#1.

CO2 Project #16 – This well was a critical well because it helped define areal heterogeneties that were not interpretatble from existing wireline log interpretation but were suspected because of modeling work. The CO2 #16 was originally a shut-in Indian Cave shallow gas producer. The well's slotted liner was successfully removed in January 2003 (Figure 2.3.2.3).

Figure 2.3.2.3. Liner removed from the CO2 Project #16 well in January in preparation for drilling deeper to the LKC C interval.

The well was drilled deeper beginning 3/27/03. Cores were cut in the LKC "C" zone (2877-2905 ft; 876.9-885.4 m) and the LKC "G" zone (2936-2966 ft; 894.9-904.0 m) with 100% recovery. The cores were laid out on the catwalk, photographed, packed in dry ice and transported to Core Laboratories, Midland, TX for analysis. The well was drilled to 3253 ft (991.5 m), open-hole logged (Figure 2.3.2.4), and 4-1/2 inch (0.114 m) casing cemented to surface. The deepening of the #16 well was completed 4/15/03 with 4-1/2 inch (0.114 m) casing set at 3,252 ft (991.2 m). Core analysis, log analysis, and swab rate tests indicate that the permeability in and near #16 is lower than that of the other pilot wells. The upper portion of the #16 LKC "C" interval is interpreted to have been more heavily micritized creating poor matrix permeability and poor oomoldic pore connectivity and consequently low permeability relative to LKC oomoldic limestones. It was decided to complete the well in the LKC "C" zone and sequentially stimulate the zone with acid to attempt to contact higher quality reservoir. On 4/8/03 the well was perforated in the LKC "C" from 2883-2894 ft (878.7-882.1 m) using 4 shots/ft (13 shots/m). From 4/9/03-4/11/03, the well was treated with a total of 4,500 gallons (17,032 L) acid as follows (Table 2.3.2.1):

Table 2.3.2.1

CO2 Project #16 Acid Stimulation Program

Date	Acid Type	Acid Volume (gallons)	Maximum Rate (bpm)	Maximum Pressure (psig)	Approx. Post-treatment Swab Rate (bph)
4/9/2003	15% MCA	500	0.25	250	1.45
4/10/2003	15% MCA	1000	2.5	475	1.74
4/11/2003	XTA-15%	3000	3.2	450	3.48

(where; XTA is a retarded acid, 1 gal = 3.8 L, 1 barrel per minute bpm = 9.54 m^3/h; pounds per square inch gauge, psig = 6.90 kPa; 1 barrel per hour, bph=0.159 m^3/h). Based on the post-treatment swab rates, it was interpreted that the acid stimulation established sufficient communication with the surrounding reservoir to run tubing and monitor the well during long-term injection testing.

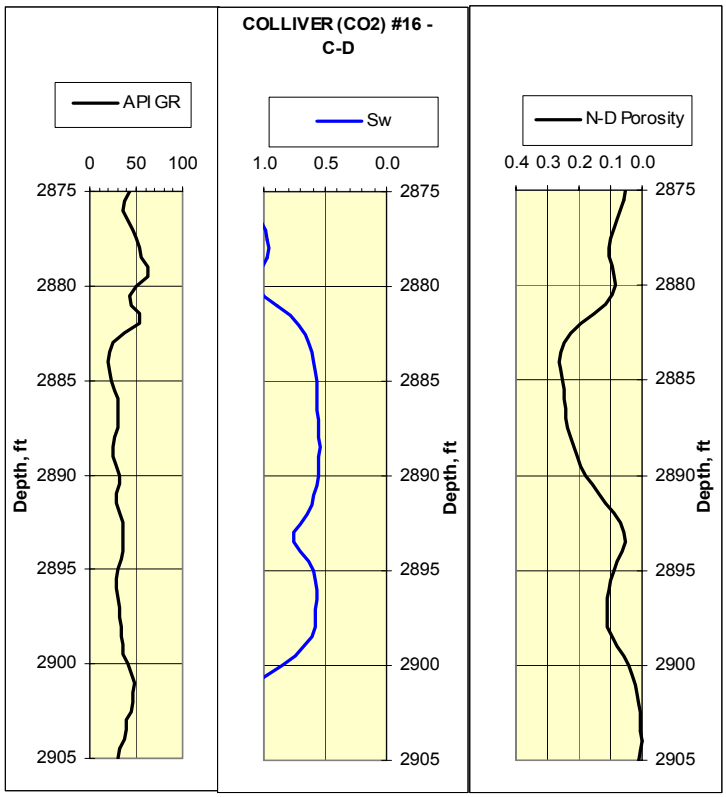

Figure 2.3.2.4 . Wireline log of CO2#16 showing API gamma ray, neutron density porosity, and interpreted water saturation using measured Archie equation exponents of A=9.59, m=1.36, n=3.4.

CO2 Project #13 – A workover to isolate the LKC "C" interval and close off other producing intervals (LKC G, Douglas, Toronto, Plattsmouth, Topeka, and Tarkio) took place from 5/15/03-5/30/03. The LKC "C" interval was isolated by cementing a 4-1/2" (0.114 m) liner from TD to surface, perforating the LKC "C" interval from 2886-2894 ft (880-882.1 m), and then acidizing the "C" interval with 2,250 gallons (8,516 L) of 15% HCL acid. New wireline logs were obtained. Production testing of the LKC-"C" interval, beginning 6/12/03, indicated that the well produced ~45 BFPD (barrels fluid per day; 7.2 m^3/d) at a bottom hole pressure (BHP) of ~417 psig (pounds per square inch gauge; 2875 kPa). Drawdown to obtain production rates for fluid levels less than 50 ft (15 m; equivalent to 23 psig, 159 kPa) above the perforations was begun on 6/27/03. Production rates at these pressures average ~93 BFPD (14.8 m^3/d) and are dropping as the well approaches long-term equilibrium. These production rates are consistent with a surrounding reservoir average absolute permeability of ~80 md. Pressure and rate tests results, partially due to the nature of the testing conducted to date, have not confirmed the nature of the CO2I#1-CO2#13 conductivity. A build-up test and conductivity test were performed to obtain reservoir properties data and establish the connectivity and conductivity between CO2 I#1 and CO2 #13 (see Section 2.3.4)

2.3.3 Workover Containment Water Injection Wells in Pilot Area

Proposed Description of Work: Activities in this task are similar to the original SOW as described under Task 5.1.3. Only the well locations and the corresponding necessary changes in required workovers for the new well conditions are changed from the original plan. Two existing wells on the Colliver lease (Colliver #10 and #18) will act as containment water injection wells for the flood pattern. Each of these wells will be worked over to allow isolation of water injection in the Lansing-Kansas City (LKC) "C" zone.

Project Activities/Products: In September 2000 the Colliver #18 well was remediated, pressure, flow, and tracer tested. Workover of the CO2 #10 (formerly Colliver #10) was performed between 3/5/03 and 3/10/03. Previously, the Colliver #10 had been stimulated in February 1960 with Dowell Duo-Frac 17,000 pound sand/15,000 gallons Dowell 3% "slick-acid" in the "C" and "G" zones and the Topeka. Well rework in 2001 cemented the "C" and "G" zones. The Colliver #10 was used as an injection well in the shallower Topeka and Plattsmouth intervals. The CO2 #10 was prepared for injection in only the LKC "C" zone by: 1) drilling out

the cement plug to +/-2925, 2) perforating the LKC "C" from 2898-2910 ft (883.3-887.0 m), 3) running a dual packer assembly across the Topeka and Plattsmouth perforations (for isolation), and 4) acidizing the LKC "C" with 500 gallons (1893 L), 15% MCA at ¼ bpm (barrels per minute; 2.38 m^3/h) with an injection surface pressure not exceeding 500 psig (pounds per square inch gauge, 3448 kPa). Flushed acid to perfs and swabbed back acid volume and two load volumes. During repressurization minimum injection rates were identified for that identified the leakoff rate and any out-of-zone injection that might exist.

2.3.4 Injection Well Testing and Analysis

Proposed Description of Work: The activities in this subtask remain the same as the original plan described under Task 5.1.4. Step rate tests and pressure falloff tests will be conducted after completion on CO2 I #1, the injection well. At an appropriate time water injection to re-pressure the pilot area will be initiated.

The major purpose of the tasks in Task 2.3 is to isolate the major Lansing-Kansas City zone of interest (the LKC "C") in the producing and injection wells in the pilot area so that the CO2 will stay in this zone and to confirm that connectivity and reservoir properties are suitable for a viable demonstration. It is necessary to isolate the LKC "C" zone in the pilot producing wells so that as the pressure increases and CO2 breaks through to the producing wellbores, the CO2 is not lost to minor zones that are not being maintained above minimum miscibility pressure (MMP) and are not major targets.

It is necessary to isolate the LKC "C" zone in the two containment water-injection wells so that water can be injected into these wells to help increase the reservoir pressure in this portion of Hall Gurney Field to above the MMP requirement before CO2 injection starts in the CO2 injection wells. Losing injection water to other zones would increase the time required to get to the required pressure. It is also important to contain the incremental CO2 oil production to the pilot-area producing wells.

The purpose of running the step rate tests is to ensure that injection is not above the breakdown pressure of the L-KC "C" zone and to determine the maximum injection rates to minimize the time to re-pressure the LKC "C" zone reservoir. Pressure falloff tests on the containment injection wells will be used to determine skin damage and estimate permeability values which can the be used to help tune the reservoir simulation.

Project Activities/Products: Initial productivity tests were conducted on the CO2I#1 after completion and continued through 2001. Beginning on 3/7/03 the CO2 Project #18 injection well was shut-in and a program of measuring fluid levels in the pattern wells was initiated (fig. 2.3.4.1). Bottom-hole pressures were calculated from the fluid levels. Long-term injection in the CO2I#1 began on 4/23/03. Based on first arrival times of 3-5 days for pressure response in the #10, #12, #18, and #16 to injection in CO2I#1, the absolute average permeability between the CO2I#1 and the #10, #12, and #18 is interpreted to range from 50-80 md. Average permeability near the CO21 #16 is ~25-35 md. These values are consistent with those in Table 3.1.1 with the exception of CO2#10. Injection rates during Repressurization in CO2#10 confirm higher values than indicated in Table 3.1.1.

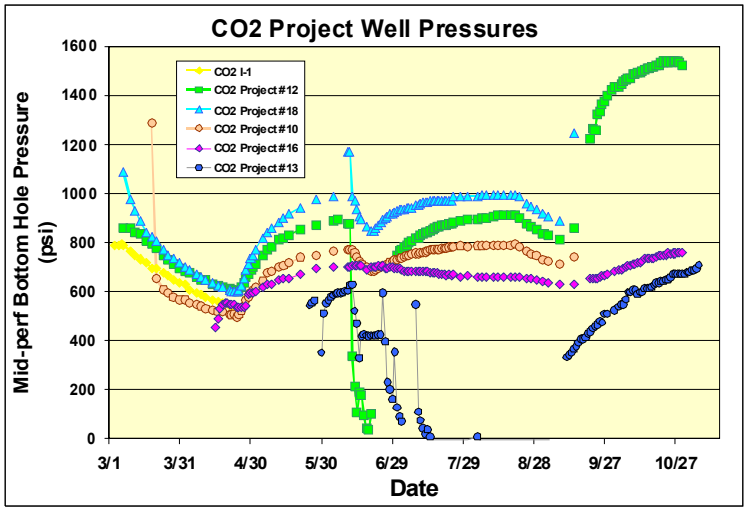

Figure 2.3.4.1. Summary of pressure response testing over the period from 03/07/03 to 09/05/03. Response after 09/05/03 is repressurization of pattern.

Pressure responses to injection in CO2I#1 give clear indication that the #10, #12, #18 and Carter #5 wells are well connected to CO2I#1. A drawdown and buildup test on the CO2#12 provided permeability values that are consistent with first arrival times from the CO2I#1. Pressure response indicates #16 communicates with flood pattern area but permeabilities in this well and the surrounding area are significantly lower than in the rest of flood pattern area. Low pressure in the #16 may result from production in the region to east. Based on these permeabilities, the rate at which the #16 would process the pore volume between the CO2I#1 and the #16 is too low to use this well effectively in its present state for the time period of the demonstration without additional stimulation.

Connectivity and conductivity between the CO2I#1 and CO2#13 were difficult to confirm because of heterogeneous reservoir properties between the two wells and probable high permeability to the east of the CO2#13. Production rate tests on the CO2#13 were consistent with an average reservoir absolute permeability of ~80 md (millidarcy; 0.079 $u m^2$) surrounding the CO2#13 but did not confirm sufficient conductivity between the CO2I#1 and the CO2#13 wells for adequate flood rates for the demonstration. To confirm adequate conductivity between the CO2 I#1 and CO2 #13 wells, a conductivity test was conducted over the period 08/20/03 through 09/05/03 in which the injection rate of CO2 I-1 was reduced from ~140 BWPD to ~70 BWPD (barrels water per day; 22.4-11.2 m^3/d) while continuing to produce and pump-off CO2 #13. The test for conductivity was based on observation of production rate falling below the pre-test hyperbolic production rate decline trend defined for CO2#13 at CO2I#1 injection rates of ~140 BWPD (22.4 m^3/d). Figure 2.3.4.2 shows that production rates from the CO2#13 decreased from ~ 72 BPD (barrels per day) to ~ 63 BPD (11.5-10.0 m^3/d) over a 2 week period. This observed production rate decline trend for the CO2#13 preceded the trend predicted by reservoir modeling, indicating slightly better conductivity. Rates are consistent with sufficient permeability between CO2I#1 and CO2#13 for a viable CO2 flood with a sufficient Process Pore Volume Rate (PPV).

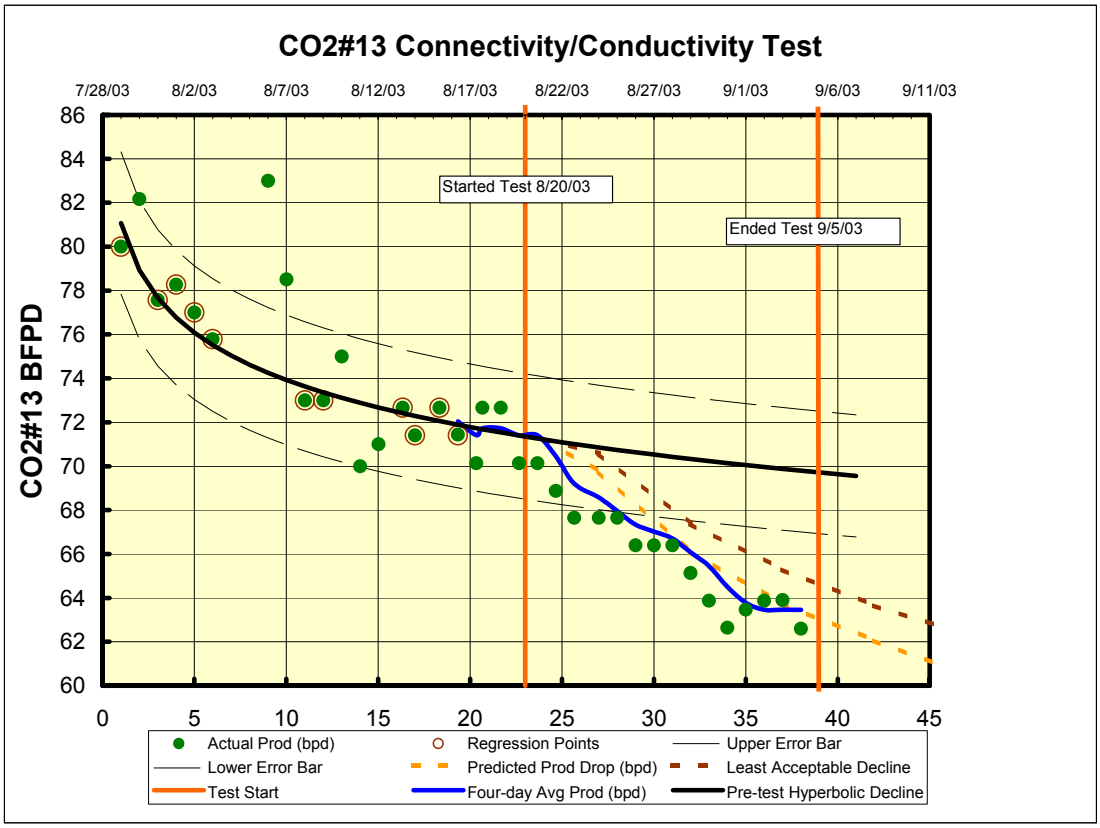

Figure 2.3.4.2. Production rates for the CO2#13 well prior to start of CO2I#1-CO2#13 conductivity test and during test. The change in CO2#13 production confirmed sufficient conductivity for adequate flood rates between the wells. (1bwpd = 0.16 m^3/d, 1 bbl = 0.16 m^3, 1 psig = 6.89 kPa)

2.3.5 Construct Surface Facilities

Proposed Description of Work: Activities in this task are similar to the original SOW as described under Task 5.3 except the exact design of the facilities is modified to conform to the needs of the newly proposed pattern.

The CO_2 pilot surface facilities can be classified in five broad categories - 1) production flowlines and injection lines, 2) produced gas/liquid separation equipment and tank batteries, 3) water injection facilities, 4) well testing and monitoring equipment, and 5) CO_2 storage and injection equipment.

Production flowlines will be run from one centrally-located tank battery to all CO_2 pilot production wells. Present design calls for flowlines that are CO_2 compatible 2" diameter fiberglass rated to 800 psig. These flowlines will transport both the produced gas and liquids.

New water and CO_2 injection lines will be run from the injection station to the new CO_2 injection well. The water injection line will be 2" diameter fiberglass rated to 1,500 psig. The CO_2 injection line will be 2" diameter externally coated carbon steel rated to 3,000 psig. A water-alternating-gas (WAG) injection skid will be installed near the injection wellhead. Existing injection lines and injection equipment will be used for the two CO_2 pilot containment wells.

The tank battery will be constructed near the pattern and will consist of a large, high-pressure two-phase (gas/liquid) separator, a gun barrel, and oil stock tanks. Historically, heater treaters and free-water-knockouts (FWKO) are not needed to treat Central-Kansas crudes; thus the use of this equipment is not anticipated for the pilot.

The two-phase separator will be large enough to handle the significant volume of CO_2 that will be present when CO_2 break-through occurs at the producing wells. The CO_2/hydrocarbon gas coming off of the separator will be vented in accordance with required environmental regulations. The separator liquids (oil and water) will be piped to the gun barrel. The water from the gun barrel will be piped to the water injection station or to disposal. The oil will be piped to stock. Both the separator and gun barrel will need to be internally coated or constructed of corrosion resistant material. The oil stock tanks will be traditional steel or fiberglass.

Existing water injection equipment will be upgraded to handle the potentially more corrosive water resulting from CO_2 flooding. Water and CO_2 injection rates will be measured using wedge or turbine meters. A test separator that is to be built near the tank battery will measure the oil, water, and gas produced from individual wells. During a test, the produced fluid from a selected well will be manually routed through the test separator and then back to the tank battery. A Barton meter will measure the gas leaving the separator and wedge or turbine meters will measure the oil and water leaving the separator. The test separator will be internally coated and rated for 250-psig service.

Project Activities/Products: The pilot water injection plant became operational 4/18/03 and began long-term injection in the CO2I#1 on 4/23/03. The injection facility consists of the shallow Dakota sandstone water supply well (WSW), a 200 barrel (31.8 m^3) fiberglass injection tank, a triplex pump, filter cartridges, metering, valves, etc (Figures 2.3.5.1-2.3.5.3). Long-term water injection began 4/23/03. Injection water is filtered to 5 microns. The incoming shallow Dakota sandstone freshwater has a dissolved oxygen concentration of approximately 2-4.4 ppm

(parts per million). After treatment with an oxygen scavenger (~2-3 quarts/d; 1.7-2.8 L/d), dissolved oxygen concentration of the injection water before the filter is 0.00-0.08 ppm. Following batch treatments using biocide WCW 5827 on 4/23/03 and 3/28/03, approximate biweekly RapidCheck™ tests have indicated no detectable levels of bacteria in the injection water before the filter.

Figure 2.3.5.1. CO2 Injection plant near CO2 Project

Figure 2.3.5.2. CO2 pilot water injection tanks battery with treatment chemicals.

Figure 2.3.5.3. CO2 Pilot injection pump and filters.

Between 09/09/03 and 09/15/03 a 350-foot (107 m) trench was dug from the water production plant to the CO2#10 wellhead and 330-foot (100 m) new Centron 2" (5 cm) 1,500 psi (pounds per square inch; 10.3 MPa) fiberglass pipe were laid. The line was pressure tested to 1,000 psi (6.9 MPa) using water and three very small seeps were repaired (Figure 2.3.5.4).

Figure 2.3.5.4. Laying fiberglass injection line from the water supply plant to the CO2#10 water injection containment well. View is looking to the northwest.

Between 09/15/03 and 09/16/03 a 240-foot trench was dug from the CO2 pump site SE to the lease road crossing and a 735-foot (224 m) trench was dug from the lease road to the CO2I#1 wellhead. Lines to the Colliver #7 and the CO2#13 were cut and modified. 980-feet (300 m) of 2" (5 cm) SCH 80 CO2 steel injection pipe were welded and pressure tested to 1,550 psi (10.7 MPa) using water and placed in the ditch and the ditch back-filled to near the CO2I#1 wellhead. On 09/16/03 the CO2#18 was treated with 500 gallons (1,890 L) of 15% NE-FE acid containing 5% solvent to improve injectivity. On 09/30/03 Murfin ordered a 3-phase separator from McDonald Tank of Great Bend, Kansas. The separator is used to individually measure the oil, water, and gas production.

2.3.6 Pattern Repressurization and Analysis

Proposed Description of Work: Activities in this task are similar to the original SOW as described under Task 5.2 except that the number of wells is decreased and initial repressurization will be conducted using only the Carter-Colliver CO2I#1 well to test for connectivity between the injection well and the oil producers and determine the nature of the pressure and its distribution resulting from injection in this well. After establishing connectivity, the two

containment wells will also be used to accelerate repressurization and insure that the reservoir exhibits properties suitable to maintain pressures above the minimum miscibility pressure.

The wells used for containment and repressurization in the approved modified plan are changed to fit the new flood pattern. The entire pilot area will be re-pressured to approximately 1,300 psi prior starting the CO2 injection. Reservoir pressure in the LKC "C" zone prior to repressurization is approximately 800 psi based on repeat formation pressure testing of the Carter-Colliver CO2 I#1. Based on present understanding of reservoir properties, simulation indicates it will require up to three months to pressure the flood pattern region up to 1,300 psi. Water injection pressures will be set at the maximum pressure below breakdown pressure or allowable by Kansas Corporation Commission permitting. This will result in the maximum safe water injection rates to increase the pressure in the LKC "C" zone as fast as possible.

The three pilot area producing wells will initially be used as pressure observation wells. Weekly/monthly fluid levels will be measured to monitor the pressure increases in the pilot area.

Project Activities/Products: Pattern Repressurization began on 09/05/03 with injection in the CO2I#1 followed by injection in the CO2#18 and CO2#10 in the subsequent weeks (fig. 2.3.4.1). Repressurization continued until 12/01/03 when a sufficient portion of the flood area was at a pressure greater than the MMP pressure allowing initial CO2 injection to begin. Repressurization approximately followed reservoir simulation predictions.

2.3.7 Test for Early CO2 Breakthrough

Proposed Description of Work: Carbon dioxide will be injected after the pattern is pressured-up using water for an initial period of time to confirm that early CO2 breakthrough is not occurring. This test will constitute the last physical test confirming viability of proper flood conditions before proceeding into Budget Period 2 Implementation of the CO2 Flood.

Project Activities/Products: Injection of CO2 was initiated on December 1, 2003 to test for the presence of a high permeability zone that would result in premature early breakthrough. Testing will continue through the end of Budget Period 1. To date no CO2 production above background has occurred at the producing wells. To prevent initiating a fracture or exceeding possible fracture parting pressure, and for optimum flood design in the pilot area fluid injection will not exceed the following conditions: 1) Water – 500 BWPD, 2) Fresh water surface pressure – 650 psi and 560 psi for produced water 3) CO2 Injection Rate – 600 mcf/d, and 4) CO2

injection surface pressure – 750 psi. Plans are to initially inject a CO_2 slug that is approximately 15% of the hydrocarbon pore volume (HCPV) of the Process Pore Volume (PPV) before initiating the Water-Alternating-Gas (WAG) process. However, WAG may be initiated earlier in response to rates of CO2 production. Initial injection rates to avoid premature CO2 breakthrough will be maintained at 2.5-3.5 (190-260 mscf/d) gallons/minute at a surface injection pressure of <750 psi. Wellhead temperature has been in the range of 32-40 ^{o}F.

ACTIVITY 3 - ADVANCED RECOVERY TECHNOLOGY IDENTIFICATION AND ANALYSIS

Task 3.1: Reservoir Simulation (Phase 2)

Proposed Description of Work: The reservoir model developed in Activity 1-Task 4 will be revised using data obtained from the new injection well drilled in Activity 2-Task 1 and the core analysis from Activity 2-Task 2. As in Activity 1-Task 4, oil production rate during primary production will be simulated from initial pressure to a pressure of about 50 psi assuming a solution gas drive mechanism. Adjustments in reservoir and fluid properties will be made to match primary production history using the available data. Waterflood performance will be simulated and matched with production history.

Carbon dioxide injection into the pilot demonstration site will be simulated based on the saturation distribution at the end of the waterflood and water injection into confinement wells to maintain reservoir pressure at desired levels for miscible displacement. Results will be used to evaluate recovery efficiency of the proposed demonstration project and to make final economic calculations of the pilot flood.

Project Activities/Products: The new reservoir properties data obtained and the well test data have indicated greater permeability architectural complexity than previously modeled, a not uncommon situation. The process pore volume rate between the CO2I#1 and the CO2#16 is sufficiently low that without additional stimulation of the CO2#16 the PPV rate is too low to properly process the region within the demonstration time period. The flood is presently planned to produce only from the CO2#12 and CO2#13 and to monitor the CO2#16 (Figure 3.1.1).

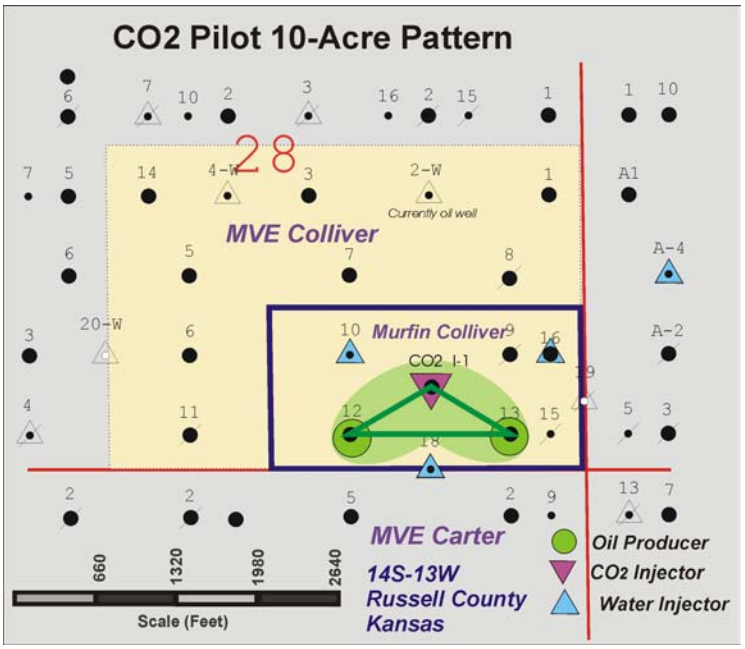

Figure 3.1.1. Present design of CO2 pilot comprising the CO2I#1 CO2 injection well, two containment wells (CO2#10, CO2#18), two producing wells (CO2#12, CO2#13) and an observation well that may be changed in status depending on response (CO2#16).

If the CO2#16 shows indications of the movement of an oil bank consideration will be given to well stimulation. Model-generated flowlines for the 2-producing well pattern indicate that this pattern should provide 80-85% containment (Figure 3.1.2) and is predicted to recover 18,000-21,000 BO (2,880-3,360 m^3). Several models have been constructed to simulate different alternate working hypotheses for reservoir permeability architecture. Table 3.1.1 illustrates predicted permeabilities at and near wellbores for leading 2-layer models and/or reservoir properties calculated from various tests interpreted by the Tertiary Oil Recovery Project (TORP) and at Transpetco Engineering (TPE; consulting for Kinder-Morgan CO2 Company). The table also shows predicted permeabilities based on porosity-permeability transforms. Due to the aerial complexity of the reservoir heterogeneity simplified two-layer models were developed for the primary CO2 flood area upper ~8-feet of the section, or layers 1-3, described in Section 1.3.1. After developing a better model(s) of the potential architecture of the pilot area, six-layer models of the primary CO2 displace areas were developed to more accurately define the CO2 displacement.

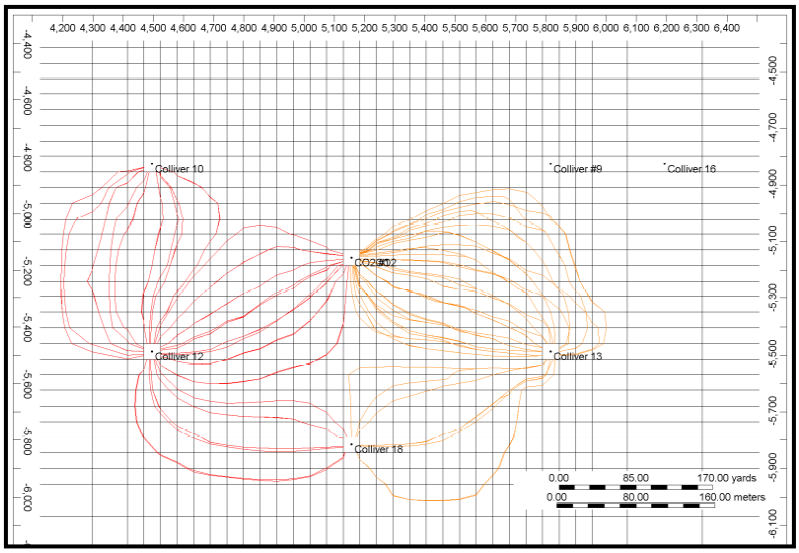

Figure 3.1.2. Flowlines generated by computer model of pilot area using permeability distributions shown in Table 1.

Well	Core Perm Avg (md)	Log ϕ only Perm Avg (md)	TPEC Perm Avg (md)	core Layer 1 Perm (md)	log ϕ only Layer 1 Perm (md)	TORP Layer 1 Perm (md)	TPEC Layer 1 Perm (md)	core Layer 2 Perm (md)	log ϕ only Layer 2 Perm (md)	TORP Layer 2 Perm (md)	TPEC Layer 2 Perm (md)
CO2 I#1	88	72	85	115	94	117	134	20	47	117	35
Colliver 10		33	48		55	117	80		14	17	15
Colliver 12		66	60		95	117f	100		37	50	19
Colliver 13		62	79		44	10	38		81	117	120
Colliver 16	25	36	26	10	58	10	17	37	26	20	34
Colliver 18		133	30		172	53f	50		108	117	10
Main Reservoir			112			117	188			117	36
W of #13			72				64				80
E of #13			110				80				140

f-indicates fracture or enhanced permeability channel may influence CO2#12-CO2#18 connection

Table 3.1.1. Summary of Lansing-Kansas City 'C' zone permeability in and near wells in pilot pattern measured from core and interpreted from well tests and used in computer models of the pilot. Permeabilities are shown for leading 2-layer models created by the Tertiary Oil Recovery Project (TORP) and Transpetco Engineering (TPE; consulting for Kinder-Morgan).

Conductivity test results between CO2I#1 and CO2#13 are interpreted to indicate the presence of a lower permeability region or barrier between the two wells that restricts but does stop flow. Based on the differences in permeability between the upper and middle intervals in the two wells, it is interpreted that the uppermost interval decreases in permeability from the CO2I#1 towards the CO2#13 and the middle interval increases in permeability. A lower permeability barrier between the upper and middle intervals, possibly reflecting a low-

permeability bedset contact, could decrease composite permeability and explain the lower conductivity between CO2I#1 and CO2#13 compared to between the CO2I#1 and CO2#12. Further analysis is being performed as the system is monitored during the early CO2 injection test phase.

Task 3.2: Economic and Recovery Analysis of Pilot

3.2.1 Determine CO_2 Source for the Pilot

Proposed Description of Work: The most economic source for CO_2 will be determined. The nearest commercial source for pipeline CO_2 is the Transpetco line whose terminus is near Guymon, Oklahoma, approximately 200 miles southwest of the proposed pilot site.

Preliminary research indicates that the most economic plan for CO_2 procurement will be to purchase CO_2 at Guymon, truck it to the site, and compress the CO_2 to injection pressure at the site. This will require special equipment at both ends for handling and compression. One arrangement that is being considered is to turnkey the CO_2 handling and delivery of the CO_2 for a fixed price per MCF. Decisions to subcontract any aspect of the handling and delivery will be weighed against the option to manage it "in-house". Selection of a subcontractor would be done on a competitive bid basis. Alternatives to trucking, such as delivery by rail or pipeline, co-generation, and sequestration of the required CO_2 from local power plants will be considered.

Project Activities/Products: When the original project plan was written the most economic source of CO_2 for the pilot was the Bravo Dome Unit in New Mexico. Shell CO_2 Company, Ltd. (Now Kinder-Morgan CO2 Company, LP) owns CO2 at Bravo Dome and it was proposed that supercritical CO_2 at the Guymon, OK, CO2 pipeline terminus would be liquefied and trucked to the lease in insulated/pressurized (300 psig) tank trailers that hold up to 20 tons ($\pm$325 Mscf) of CO_2.

The construction of the US Energy Partners, LLC (USEP) ethanol plant in Russell, Kansas, eight miles from the demonstration site, will provide a source for liquid CO2 (Figure 5.1.2.1). In preparation for CO2 injection used for testing for early breakthrough and Budget Period 2 on-going CO2 injection, Murfin Drilling Company, Inc. (Murfin) signed a contract with U.S. Energy Partners, LLC (USEP) and EPCO Carbon Dioxide Products, Inc (EPCO) for USEP and EPCO to supply CO2 to the project. USEP will supply raw carbon dioxide (CO2) in quantities

sufficient for the Murfin Carbon Dioxide Enhanced Oil Recovery demonstration project (CO2 Project) in Russell County, not to exceed 20,000 tons over a five-year period.

3.2.2 Assess Existing Facilities and Determine Necessary Modifications

Proposed Description of Work: Due to the significantly higher operating pressures and the corrosive nature of CO_2 flood produced fluids, most of the existing surface facilities, flow and injection lines are likely to be replaced. However, some of the water injection and oil separation equipment may be serviceable for the project. Plans are to utilize ten existing boreholes, after appropriate equipment upgrades are made.

A comprehensive review of well records, equipment inventories, and a field check will be made in order to determine whether boreholes can be used and what modifications will be required prior to their being utilized in the project. A preliminary survey of existing surface and well bore facilities has been made and it appears that all ten wells will require substantial workovers and significant equipment upgrades.

A thorough inventory of surface facilities and field check will be made in order to determine what existing water injection, oil separation and storage facilities may be utilized and what modifications will be required. The pilot site has no specialized equipment that is satisfactory for handling CO_2 . All of this equipment will be purchased or leased.

Project Activities/Products: Existing facilities and wellbores were evaluated. Consideration was always given to minimizing cost and existing equipment were utilized where they were suitable and would not compromise operations. For some equipment, including some existing production pipe, it was recognized that it should last through the demonstration but its' long-term integrity could only be determined by use. To keep project costs down and to determine if existing facilities that would be present in other LKC leases would be suitable, where appropriate these existing facilities were utilized.

3.2.3 Design Facilities for Pilot and Monitoring

Proposed Description of Work: The design phase for surface and wellbore facilities of the project is based on estimates of CO_2 volume, pressure and rate requirements, the likely production characteristics, and the assessment of existing facilities.

A detailed well workover and equipment plan will be made for each of the existing wells included in the pilot project. Surface facilities including the production flowlines and injection

lines, produced gas/liquid separation equipment and tank batteries, water injection facilities, CO2 injection, recovery and re-injection facilities, and well testing and electronic monitoring equipment will be designed with appropriate specifications to handle the conditions anticipated.

Some of the design aspects of the pilot may be simplified if the handling of the purchased CO2 is subcontracted, as is anticipated. The recovery, dehydration, recompression, and re-injection of produced CO2 may also be sub-contracted, further simplifying the design process.

Project Activities/Products: Facilities specifications were designated for the 10+-acre pattern and resulted in the facilities described under Task 2.3. The 3-phase separator was sized to meet or exceed 250 BFPD (40 m^3) and gas rate of 200 mcf/D (thousand cubic feet per day; 5,660 m^3/d). Gas rates are expected to average 66 mcf/d and peak around 100 mcf/D (2,830 m^3/d). Actual production rates would not exceed the injection rates. Controlling injection rates to the 14% PPV rate would result in a maximum CO2 production rate of 125-140 mcf/D (3,540-3,960 m^3/d). An approximate factor of 2.5 times the CO2 rate was used to design for the HC gas design rate due to the high density of CO2 and higher affinity it has for oil.

3.2.4 Final Cost Estimates

Proposed Description of Work: Final cost estimates for the pilot will be made for the balance of the project. based on the reservoir model, simulation of the CO2 miscible flood, and the revised design of the surface and subsurface facilities. These costs can be broken down into eight broad categories: 1) well workovers and equipment upgrades, 2) surface facilities, 3) re-pressuring, 4) lease operating expense, 5) purchase of CO2, 6) recovery and re-injection of produced CO2, 7) management, and 8) analysis of results and technology transfer.

Project Activities/Products: Costs have been continually updated for all aspects of the project and incorporated into estimates of the project cost. These have changed with different pilot designs. Costs are presented in the budget.

3.2.5 Economic Forecasts

Proposed Description of Work: Extensive economic forecasts for the pilot project as well as that of a commercial scale project will be run. We will determine whether there is sufficient funding available for completing a meaningful pilot project in a cost-effective manner based on the estimated costs outlined in Activity 3-Task 2.4 and the projected oil recovery in Budget Periods 2 and 3.

Project Activities/Products: Economic forecasts for the pilot project have been run but will be modified with improved reservoir characterization and modeling. Based on current predicted oil recovery estimates for the 2-producer pattern (CO2#12 and CO2#13 producing) economics are primarily influenced by remaining surface facilities costs, operating costs, and oil price. Table 3.2.5.1 shows estimated costs from this point forward for assumed remaining surface facilities and lease operating expenses and at an oil price of $23/barrel. These estimates indicate that the project could show profit from this point forward if lease costs can be kept low. At projected surface facilities and lease costs but with only 18,000 BO (2,880 m^3) recovery the project will show a slight loss from this time forward.

Wells in Operation	Oil Recovery BO (BO)	Surface Facilities Costs ($)	Lease Operating Expense Factor (%)	Profit (BFIT) ($)
12,13	21,000	$82,613	90	$93,152
12,13	21,000	$82,613	100	$65,767
12,13	21,000	$118,019	90	$51,162
12,13	18,000	$118,019	100	($2,224)

blue indicates modified lower cost conditions

Table 3.2.5.1. Estimated economics from this point forward for various oil recovery, surface facilities, and lease operating expense scenarios and for an oil price of $23/BO. (1bwpd = 0.16 m^3/d, 1 bbl = 0.16 m^3, 1 psig = 6.89 kPa)

Economics of CO2 flooding for Central Kansas reservoirs were summarized in a paper published in the Oil & Gas Journal, June 5, 2001, pages 37-41, entitled " Economics show CO2 EOR potential in central Kansas" by Martin K. Dubois, Alan P. Byrnes, Richard E. Pancake, G. Paul Willhite, and Lanny G. Schoeling.

Economics for leases in the Hall-Gurney field were developed and presented to operators in the field. Flood patterns for Hall-Gurney field are shown in Figure 3.2.5.1 and the economics for the different patterns are summarized in Figure 3.2.5.2.

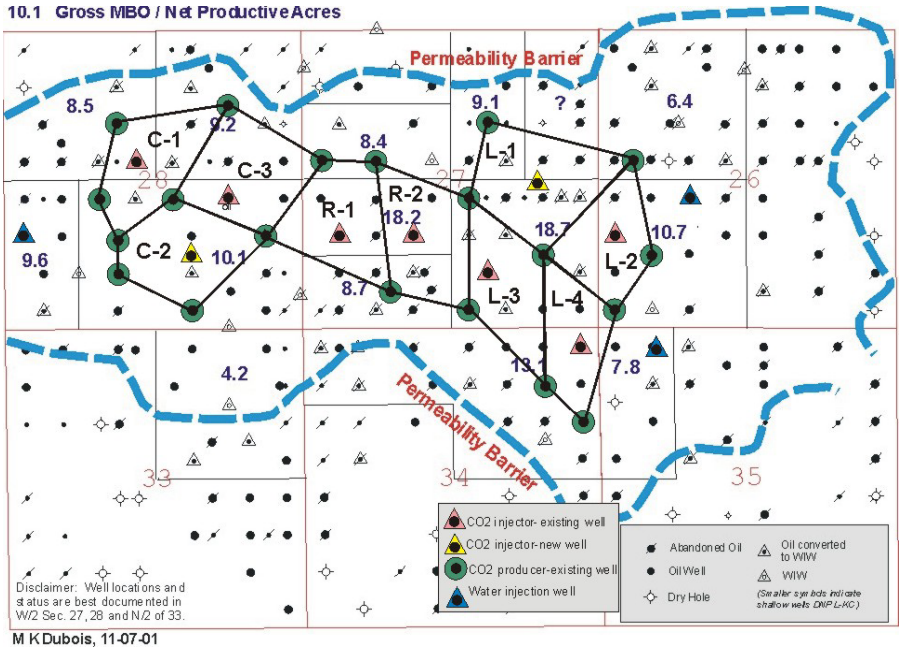

Figure 3.2.5.1. Generlized possible commercial patterns in the Hall-Gurney field (actual patterns would require greater reservoir characterization) The pilot area lies to the southeast of Pattern C-2 and is not included since flooding in it would be completed.

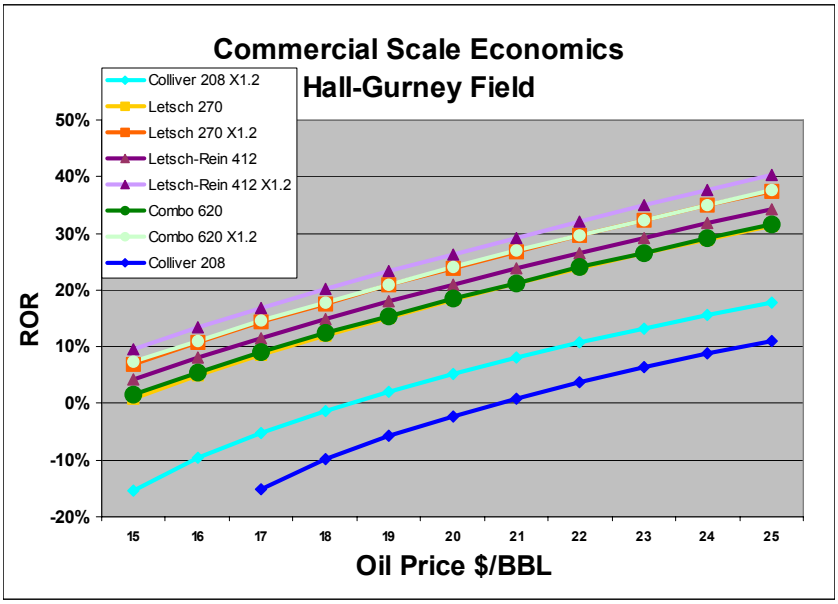

Figure 3.2.5.2. Predicted economics for patterns shown in Figure 3.2.5.1. Economics are based on several factors including lease operating expenses, surface facilities costs, CO2 costs, oil recovery and oil price.

As part of economic forecasting, a regional resource assessment was performed and integrated with the economics of a pipeline from Guymon, Oklahoma and the economics of CO2 flooding Central Kansas Uplift leases, as outlined in the Dubois and others (2000) paper discussed in the September Quarterly Report. Kinder-Morgan indicated that an economic pipeline would require a resource base of approximately ~200 million barrels of primary and secondary recovery. Lease economics indicate that at $1.00/mcf CO2 cost, $20/bbl oil price, and estimated capital costs of $1MM/lease (Dubois and others, 2000), a viable CO2 flood candidate site must have produced greater than 8MBO/acre. Regional assessment of L-KC and Arbuckle potential was performed on a section and lease-basis assuming values for the average lease size. Analysis of the Lansing-Kansas City indicates that for these economics the L-KC does not have sufficient resource base to support a pipeline alone but the Arbuckle does have sufficient resource (Table 3.2.5.2).

Table 3.2.5.2

Cumulative Oil Production for L-KC, Arbuckle, and Mississippian Based on DOR Database

Calculated MBO/acre	MBO/sec	L-KC Cumulative Production 10 County Region Lease	Arbuckle Cumulative Production 10 County Region Lease	Mississippian Cumulative Production 10 County Region Lease
>10	>6400	118,729,970	335,957,840	27,107,353
9	5760	135,266,247	393,422,559	28,659,833
8	5120	152,823,438	454,630,672	30,037,051
7	4480	177,008,452	521,019,943	33,611,084
6	3840	203,041,866	610,869,878	37,816,051
5	3200	230,641,508	712,170,200	48,535,274

note: Lease basis calculated assuming Lease cum/160acres (APB 11/21/00)

Arbuckle resource assessment is a critical task to justify Kinder-Morgan participation in the project. Aspects of Arbuckle resource assessment addressed included: preliminary mapping of Arbuckle reservoir pressure and oil production distribution, generic reservoir geomodel construction, reservoir simulation to determine the feasibility of CO2 flooding the Arbuckle, calculation of the influence of dissolved natural gas in oil on Arbuckle minimum miscibility pressure values, and initial research into identifying Arbuckle fracture pressure gradients.

Preliminary analysis of drillstem tests (DST) in the Arbuckle indicates that the Arbuckle may be divided into three classes of reservoir based on bottom hole pressures (BHP) measured after significant lease production. Low BHPs are interpreted to result from poor connection of the producing Arbuckle interval with the underlying aquifer. Intermediate and high BHPs are interpreted to indicate moderate and good connection with the underlying aquifer. Mapping of reservoir pressures shows that different portions of major Arbuckle fields exhibit different connection to the underlying aquifer, as shown for example in the Bemis South field in Figure 3.2.5.3.

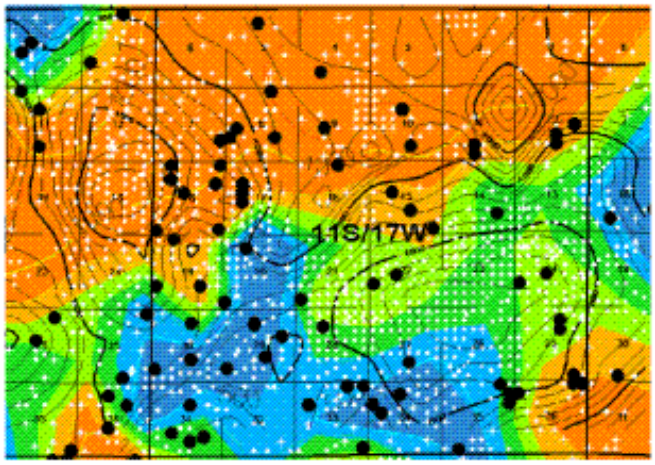

Figure 3.2.5.3. Drillstem test pressure regions in Bemis South showing low (<500 psi, blue), intermediate (green), and high (>1100 psi, orange) pressure regions.

Logs for the Bemis-Shutts were analyzed and integrated with core petrophysics (Byrnes and others, 1999) to construct generized layered reservoir models for the three classes of Arbuckle reservoir in the Beamis South field. Reservoir flow simulations on these generalized models indicate that it is possible to pressurize the Arbuckle productive intervals to pressures greater than minimum miscibility pressure for Arbuckle oil (fig. 3.2.5.4)

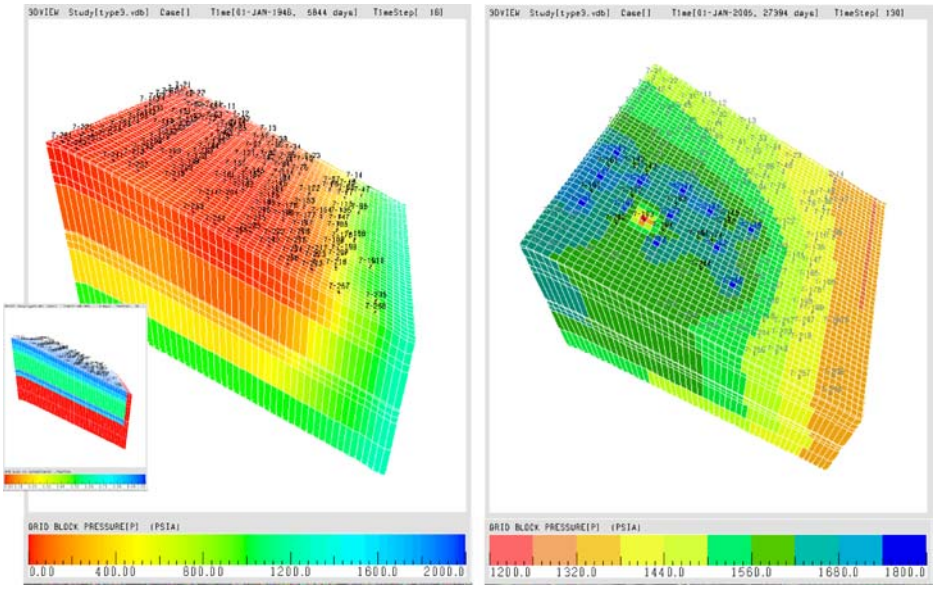

Figure 3.2.5.4. Reservoir simulation of present pressure and post-injection pressure in generalized isolated Arbuckle reservoir showing ability to reach MMP pressures in Arbuckle.

Present data indicate that in the 10-county central Kansas area oil production from known high producing Arbuckle reservoirs, which exhibit pressures indicating isolation from the underlying aquifer and which are capable of being pressured up to MMP, is approximately 150-186 million barrels (MMBO; 23.8-29.6 $*10^6 m^3$). To recover 25% of this oil using CO2, and assuming it required 4mcf/bbl for recovery, then this would require approximately 150-186 billion cubic feet (BCF, 4.2-5.3$*10^9 m^3$) of CO2. Total regional Arbuckle production for leases estimated to produce over 8,000-10,000 bbls/acre is 337-454 MMBO (53.6-72.2 $*10^6 m^3$), respectively. Approximately 75-112 MMBO (11.9-17.8$*10^6 m^3$) are in areas for which connection to the aquifer has not been determined but based on regional distribution is likely to be floodable. A remaining 112-140 MMBO (17.8-22.3$*10^6$ m^3) were produced from high-pressure reservoirs that are well connected to the aquifer and may or may not be suitable for CO2 flooding. Though more investigation is needed, the present data and results indicate that a significant fraction of the Arbuckle may be a viable resource for CO2 enhanced oil recovery. Lansing-Kansas City (LKC) leases which have produced >8,0000-10,000 bbl/acre are estimated to have produced from 70-120 MMBO (11.1-19.1$*10^6$ m^3), where the range expresses differences due to the method for assessing production. The combined production of potential areas is approximately 295-320 MMBO, which exceeds the required 200 MMBO. CO2 demand for the Arbuckle (225-298 BCF; 6.4-8.4$*10^9$ m^3) and the L-KC (70-120 BCF; 2.0-3.4 $*10^9$ m^3) indicate there is sufficient resource to require at least 295-320 BCF (8.3-9.1 $*10^9$ m^3) of CO2 which would support an 8- to 10-inch pipeline.

ACTIVITY 4 - REVIEW OF BUDGET PERIOD 1 ACTIVITIES AND DEMONSTRATION

Proposed Description of Work: We will evaluate the technical and economic potential of the proposed field demonstration project in Budget Period 1. Reservoir data, reservoir characterization, estimated oil recovery and projected economics will be integrated into this decision making task. Effects of uncertainties in data will be included. A decision will be made whether to implement carbon dioxide miscible flooding in the proposed pilot pattern or to terminate the project. The Project Evaluation Report will be prepared. A Continuation Application will be submitted if a decision is made to continue the project.

Project Activities/Products: Full technical and economic analysis have been performed to decide whether to proceed into Budget Period 2 both to insure that the demonstration meets its objective of providing results that can be scaled and applied to other oomoldic reservoirs as well as knowing what cost/benefit/risk is involved with Budget Period 2. Table 3.2.4.1 illustrates a range in predicted economics for different recoveries and lease operating expenses. Additional analyses were performed that have not been summarized here. The technical decision to proceed was based on the results of the many activities involved in reservoir characterization, well test and interference testing, modeling, and initial CO2 injection testing. Technical analysis of all available data that were interpreted to indicate that the project would be technically scalable to typical LKC field size. Scalability is dependent on knowing: 1) Representativeness of LKC in flood pattern area to LKC (e.g., k, ϕ, Pc, kr, thickness, geology, history), 2) Pore volume processed, 3) Total PPV throughput and distribution of PPV throughput, 4) initial Sorw, 5) oil recovery, 6) reservoir properties-especially permeability distribution, 7) CO2 utilization – gross and net. While it is recognized that unknown reservoir properties may result in a pilot that does not have the results predicted, data collected to date indicate that this site should provide an appropriate test that will meet the objectives of the project.

The objective of this Class II Revisited project is to demonstrate the viability of carbon dioxide miscible flooding in the Lansing-Kansas City formation on the Central Kansas Uplift and to obtain data concerning reservoir properties, flood performance, and operating costs and methods to aid operators in future floods. The project addresses the producibility problem that these Class II shallow-shelf carbonate reservoirs have been depleted by effective waterflooding leaving significant trapped oil reserves. The objective is to be addressed by performing a CO_2 miscible flood in a 10-acre (4.05 ha) pilot in a representative oomoldic limestone reservoir in the

Hall-Gurney Field, Russell County, Kansas. At the demonstration site, the Kansas team will characterize the reservoir geologic and engineering properties, model the flood using reservoir simulation, design and construct facilities and remediate existing wells, implement the planned flood, and monitor the flood process. The results of this project will be disseminated through various technology transfer activities.

ACTIVITY 7-PROJECT MANAGEMENT

Proposed Description of Work: This project requires management of activities involving geologists, engineers and field operators. Project management is continuous through all Budget Periods. A significant amount of time and effort is required and is shown in this task in the budget in Volume III. The project management plan is discussed in Section II.C.3. We included a task to recognize the amount of time required in four categories: 1)Overall Project Management, 2)Management of Reservoir Characterization, 3)Management of Reservoir Engineering and 4) Management of the Field Operations.

Project Activities/Products: The project has undergone several major changes in partnership roles including replacement of two original partners due to buy-out and merger. MV Energy LLC and Shell CO2 Company, were replaced by Murfin Drilling Company and Kinder-Morgan CO2 Company LLC, respectively. New partners were added to the lease ownership; John O. Farmer Oil Company and White Eagle Resources, and new partners were added to CO2 supply; US Energy Partners LLC and EPCO Carbon Dioxide Products, Inc.. These many changes have resulted in time delays and project restructuring, but the project management has kept the project on-track and brought the project to the stage that it is ready to move into Budget Period 2.

Management has involved continual contact between the various partners. Various members of the Kansas CO2 Team communicated on a nearly daily basis by telephone and email over specific technical or business issues. Group conference calls and meetings were held as needed. The following personnel have participated in one or more calls, emails, and meetings: Murfin Drilling) James Daniels; Stan Froetschner, Kevin Axelson, Tom Nichols, Larry Jack; Tertiary Oil Recovery Project) Paul Willhite, Don Green, Richard Pancake, Rodney Reynolds, Jun Syung; Kansas Geological Survey) Alan Byrnes, Martin Dubois; Tim Carr, W. Lynn Watney, W.J. Guy, John Doveton, Dana Adkins Heljesen, Ken Stalder, Michael Magnuson, Paul

Gerlach; Kinder-Morgan) Russell Martin, Paul Nunley, Lanny Schoeling, William Flanders (Transpetco Engineering working for K-M), Don Schnacke (Representing K-M in Topeka); John O. Farmer) John Farmer III., John Farmer IV; US Energy Partners LLC) Dave Vander Griend, Eric Mork, Paul Cantrell, John Neufeld; EPCO Carbon Dioxide Products, Inc.) Richard Wiesemann.

ACTIVITY 8- TECHNOLOGY TRANSFER AND REPORTING REQUIREMENTS

Proposed Description of Work: Technology transfer will be an on-going process throughout the course of this project. The different activities are designed to complement project time schedules and to target alternate audiences. The technology transfer program will be the responsibility of the KU Energy Research Center and will involve university staff with cooperation from the participating companies. These activities will focus on transferring the knowledge gained, methodologies used, data required and necessary for evaluation, and the techniques used for solving the specific producibility problems. Instruction in accessing the results and understanding and utilizing the results of this project will be disseminated by web-based information, publications, workshops and seminars to the public, government, academia, and industry, newsletters, site visits and direct one-on-one discussion that involves true two-way communication between operators and KUERC staff. All reporting requirements of the Department of Energy, other federal agencies, and state and local governments will be fulfilled in timely manner

Project Activities/Products: Technology transfer has been a major activity of this project. Since inception the project has created the following transfer products: 1) six newspaper article published; 2) one Oil & Gas Journal article; 3) two American Association of Petroleum Geologist poster papers presented at annual meetings, one of which won the AAPG Braunstein Award for best poster at the annual convention. A third poster utilizing some of the data from the project won a second AAPG Braunstein Award and the AAPG AI Leverson Award; 4) Over 42 technical presentations; 5) a web-site providing access to presentations and data which has a high "hit" rate; 6) a PTTC workshop on CO2 flooding the Morrow formation in southwest Kansas.

Nearly every oil operator in the state, state representative, and federal representative is aware of the project. Another large independent operator in the state is in the final stages of

evaluating a CO2 flood similar in design to the commercial patterns shown in Figure 3.2.5.1. These efforts are recognized as important and will continue through the next Budget Period.

The goals of the technology transfer have been to disseminate information obtained from this project, which should encourage operators of similar reservoirs in this reservoir class to apply these technologies to enhance their oil production and economics. Most of the operators of these reservoir types in Kansas have no or minimal technical staff. Thus, the operators are often not fully aware of current technology or how to proceed with implementation of a technology that is new to them. They also have no program for research and development. The technology transfer program in place works to show operators how results apply to their fields. Finally, most of the reservoirs are mature and are being operated under marginal economics with low production and relatively high operating costs per barrel of oil produced. Operators are hesitant to implement technologies because of the initial cost and lack of confidence in the technologies. The fact that the project is being successfully run by a Kansas independent operator has already lent confidence to many that if the project is successful they could also perform a flood.

B. BUDGET PERIOD 2 PROJECT PLAN

ACTIVITY #5-FIELD DEMONSTRATION AND ANALYSIS

In the proposed modified plan Activity #5 is modified from the original SOW. Activities in Tasks 5.1, 5.2, and 5.3 have been moved from Activity #5 to Activity #2.3 in Budget Period 1. To keep task numbers similar to the original proposal for easier reference the task numbers for the modified plan in Budget Period 2 have remained the same as in the original proposal. Other modifications to tasks in this activity are primarily related to: 1) Changes needed for the 10+-acre pattern from the originally proposed 40-acre pattern, 2) Changes needed to obtain CO2 from the USEP ethanol plant, and 3) Extension of time for Activity #5 tasks to compensate for time taken by Task 2.3 (Well Remediation and Testing). The following sections review changes to the original activity #5 tasks.

Task 5.4: Implement CO_2 Flood - Operations

<u>5.4.1 Perform Flood – Operations</u>

Description of Work: Injection of CO_2 will continue following initial test injection of CO_2 to test for early CO2 breakthrough (Task 2.3.7) performed in Budget Period 1. In Task 5.4.1 CO2 and fresh water from the Dakota formation water supply well will be injected in the CO2 I#1 and both fresh and produced water will be injected in the CO2 #10 and CO2#18 containment wells. Wells CO2 #12 and CO2#13 will act as producers (Figure 5.4.1.1). CO2 #16 will be monitored and depending on response to the flood may be converted to a producer.

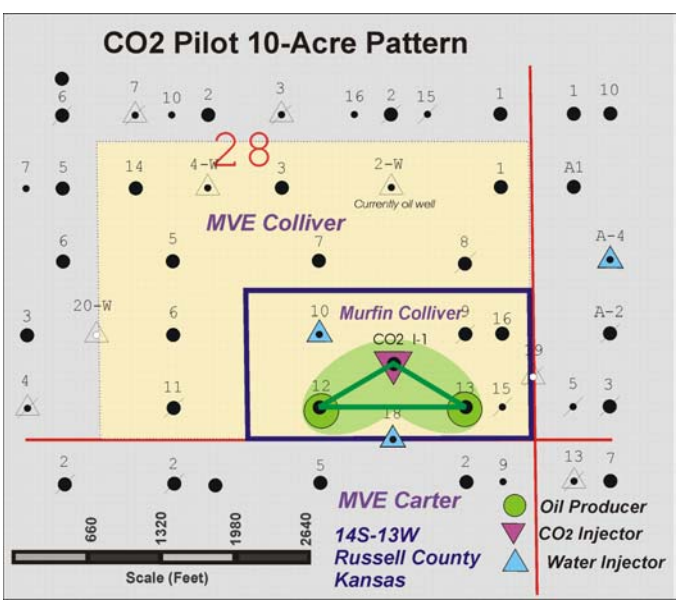

Figure 5.4.1.1. Flood pattern for Budget Period 2 utilizing two producers and the single CO2 injector. CO2#16 will be monitored and if it shows appropriate response will be stimulated and put on production.

Both CO2 and water injection rates and pressures will be adjusted to maximize flood response and maintain flood control. To prevent initiating a fracture or exceeding possible fracture parting pressure, and for optimum flood design in the pilot area fluid injection will not exceed the following conditions: 1) Water – 500 BWPD, 2) Fresh water surface pressure – 650 psi and 560 psi for produced water 3) CO2 Injection Rate – 600 mcf/d, and 4) CO2 injection surface pressure – 750 psi. Plans are to initially inject a CO_2 slug that is approximately 15% of the hydrocarbon pore volume (HCPV) of the Process Pore Volume (PPV) before initiating the Water-Alternating-Gas (WAG) process. However, WAG may be initiated earlier in response to rates of CO2 production. Initial injection rates to avoid premature CO2 breakthrough will be maintained at 2.5-3.5 (190-260 mscf/d) gallons/minute at a surface injection pressure of <750 psi. Wellhead temperature has been in the range of 32-40 ^{o}F.

Containment water injection will continue at rates that will maintain the reservoir pressure at the set-point location between the CO2 I#1 and the producing wells at a pressure greater than 1,200 psi. Produced water from the pilot producing wells will be re-injected into the containment injection wells.

When large volumes of CO_2 breakthrough occur a water-alternating-gas (WAG) process will be implemented. We estimate that the WAG will begin at a ratio of 1:1 or less and may employ cycles of approximately 1-3 months. The selection of cycle period will be dependent on the flood response and modeling of performance. Through Budget Period 2 the WAG ratio will be adjusted and the water ratio increased to improve conformance. The purpose of the WAG cycle is to minimize gas production.. WAG will continue for approximately four to five years or until flood conditions warrant initiation of final water injection. Water will be injected to complete the project in Budget Period 3. Model simulations, analysis of pressure and production, and 4-D seismic imaging will help fine tune project operational procedures.

CO2#16 is connected to CO2I#1 but does not have adequate conductivity to be used as a pattern production well for a successful sweep during the time period of the demonstration. It will not be produced to prevent reducing CO2 efficiency in the pattern. CO2#16 will be monitored to guide management of the pilot flood – if monitoring indicates its status should be changed this will be done at that time. If CO2#16 provides evidence of an oil bank and indicates that permeability between the CO2I#1 and CO2#16 is sufficiently high that a cost-effective

stimulation of the CO2#16 would make this a viable producing well, then CO2#16 will be stimulated and put on production

5.4.2 Contract for Delivery and Injection of CO_2

When the original project plan was written the most economic source of CO_2 for the pilot was the Bravo Dome Unit in New Mexico. Shell CO_2 Company, Ltd. (Now Kinder-Morgan CO2 Company, LP) owns CO2 at Bravo Dome and it was proposed that supercritical CO_2 at the Guymon, OK, CO2 pipeline terminus would be liquefied and trucked to the lease in insulated/pressurized (300 psig) tank trailers that hold up to 20 tons ($\pm$325 Mscf) of CO_2.

The construction of the US Energy Partners, LLC (USEP) ethanol plant in Russell, Kansas, eight miles from the demonstration site, will provide a source for liquid CO2 (Figure 5.1.2.1). In preparation for CO2 injection used for testing for early breakthrough and Budget Period 2 on-going CO2 injection, Murfin Drilling Company, Inc. (Murfin) signed a contract with U.S. Energy Partners, LLC (USEP) and EPCO Carbon Dioxide Products, Inc (EPCO) for USEP and EPCO to supply CO2 to the project. USEP will supply raw carbon dioxide (CO2) in quantities sufficient for the Murfin Carbon Dioxide Enhanced Oil Recovery demonstration project (CO2 Project) in Russell County, not to exceed 20,000 tons over a five-year period. It is anticipated that the amount of CO2 required will be approximately 14,500 to 17,500 tons over a four to five year period more specifically outlined in Table 1.

EPCO will process the USEP raw CO2 earmarked for Murfin to a minimum ninety-nine percent pure CO2 (99%) and deliver it as liquid CO2 to the CO2 Project site. The CO2 delivered will be under usual pressure and temperature conditions for commercial use unless agreed upon by Murfin and EPCO. Delivery will be made on a regular basis to the CO2 Project site so that Murfin has an adequate supply for continuous injection.

To make supply, transportation, on-site storage, and injection of CO2 economically viable for USEP, EPCO and Kinder-Morgan, the value of CO2 delivered to the demonstration site during the pilot project will be similar to that charged by EPCO to regular customers. This price will be approximately $3.00/mcf but will vary with market conditions. In addition, the City of Russell charges EPCO an energy surcharge to offset increases in gas prices and consequent increases in the costs they incur supplying EPCO with electrical power for CO2 operations. EPCO will pass these additional surcharges on to Murfin. Liquid CO2 will be trucked to the demonstration site where a supply for several days will be stored in an insulated 50-ton tank.

At the pilot site liquid CO2 will be pressurized and injected into the CO2I#1 well using an injection pump skid. On-site equipment will be leased from FLOCO2. Lease CO2 injection equipment costs will be provided as an in-kind contribution by Kinder-Morgan CO2 Company, LLC through an arrangement with FLOCO2. On-site equipment being provided include: 1) An insulated, skid mounted 50-ton liquid CO_2 storage tank; 2) An injection skid capable of pumping 300 to 600 MCFD of liquid CO_2 at between 1100 and 1400 psig; 3) A CO_2 transfer pump between the CO_2 storage and the injection skid; 5) A CO_2 flow meter at the injection skid; 6) A programmable logic controller (PLC) to monitor and control the injection rate and pressure; 7) An inline CO_2 vaporizer to heat the CO_2 if required but is not currently being used and is only planned to be used if the injection wellhead temperature is too low. Current operations during cold winter months indicate it should not be required but is available if needed.

5.4.3 Monitor Flood and Collect Samples and Data

Monitoring of the CO2 flood is necessary both for flood management and assessment of flood results and for scaling of results to other locations. The CO_2 pilot flood will be monitored by collecting injection and production data on all wells in the pilot area including the containment injection wells. The following data will be obtained and reported:

- A field report of oil, water, and gas production will be generated approximately daily. This is important to define displacement and flag production problems early.
- Confinement wells CO_2 #10 and #18 will have injection pressure, cumulative injection, time of meter reading, and injection rate recorded approximately daily.
- CO_2 I#1 will have injection pressure, cumulative injection, time of meter reading, injection rate, and temperature recorded approximately daily.
- Production wells will have tubing and casing pressure, pump run time, and on/off cycle recorded approximately daily.
- Fluid level on production wells will be taken and reported generally twice a week.
- Fluid level will be obtained and reported generally once a week on wells CO_2 #16, and an attempt will be made to obtain data on the adjoining lease wells Carter #2 and #5.

- Well test will be performed 1-3 times a month or when there is a significant change in the field production.
- Iron counts will be measured on produced water from production wells prior to chemical treatments.
- Test for bacteria will be performed on injected and produced water monthly.
- Weekly pressure will be measured up- and down-stream of the injection filter.
- Gas composition of the total production stream will be measured weekly, monthly or when there is a major change in rates and will decrease in frequency through the demonstration as the gas composition becomes more consistent. Individual wells will be tested as needed. Composition will be measured using either Draeger tube or gas chromatography methods.
- Monthly production and injection information will be allocated and summarized by well and the total field. This will include monthly and daily average oil, water, gas, average injection pressure, maximum injection pressure, average injection temperature, minimum and maximum injection temperature.
- Data will be maintained in an easily accessible database to facilitate easy analysis.
- Oil samples will also be collected at the CO_2 battery approximately once a month. These will be analyzed as necessary to monitor possible changes in the composition of the oil as the CO_2 project proceeds.

Task 5.5: Analyze CO_2 Flooding Progress

Murfin Drilling personnel with assistance, as needed from TORP/KUERC personnel will monitor the performance of the carbon dioxide miscible flood throughout Budget Periods 2 and 3 on a regular basis. Production data will be entered into a database that will be on line and accessible to all members of the **Kansas CO2 Team**. In some cases, additional data may be required to analyze flood performance. The data will be analyzed at regular intervals and summary reports distributed electronically to the **Kansas CO2 Team**.

Simulation of carbon dioxide miscible flooding in the demonstration area will resume as soon as there are sufficient data to analyze flood performance. Actual production will be

compared with simulated production. Injection rates or pressures will be compared with simulated values to check the accuracy of the simulator. Adjustments in reservoir properties will be made as appropriate. Simulations will be used to guide operation of the pilot test and to estimate total oil recovery. In addition, information provided by the 4-D seismic project will be utilized to manage the flood. Members of the **Kansas CO2 Team** will meet regularly to discuss field performance and develop plans to improve performance of the field test.

Lease- and field-wide projections of potential oil recovery will be developed to support plans for expansion of the Colliver lease CO2 flood and to bring a carbon dioxide pipeline into Central Kansas from the Oklahoma panhandle.

ACTIVITY #6 - ANALYZE POST-CO2 INJECTION RESULTS

Carbon dioxide injection will be terminated at the end of Budget Period 2 and the project will be converted to continuous water injection. Simulation indicates that more oil may be recovered if the WAG cycle is continued into Budget Period 3. Whether this is economic is dependent on the WAG cycle used in the flooding operations. The decision as to whether to continue CO2 injection into Budget Period 3 or convert to continuous water injection will be made before the beginning of Budget Period 3 and will be based on the predicted flood response. Additional oil recovery following termination of the project will be estimated from decline curve analysis and reservoir simulation. Results of the simulation will be used to guide operation of the waterflood. Following analysis of the flood response the partners in the demonstration project will evaluate whether a larger-scale demonstration is appropriate and each will evaluate whether they will be involved in a larger demonstration and what their role may be.

ACTIVITY #7-PROJECT MANAGEMENT

This project requires management of activities involving geologists, engineers and field operators. Project management is continuous through all Budget Periods. A significant amount of time and effort is required and is shown in this task in the budget.

The ***Kansas CO2 Team*** will work collaboratively throughout the field demonstration project. Regular meetings will be held to coordinate activities, review progress, identify problems and develop solutions to unexpected problems. During the past years, members of the ***Kansas CO2 Team*** at five different geographical locations communicated extensively by email

and by telephone. Team members shared problems, asked for help and distributed proposed solutions through email to the entire project team. Day to day and sometimes hour by hour communication between team members is well developed. Collaboration will continue in this project.

Project Review Meetings will be held in Lawrence and Wichita. The frequency of Project Review Meetings will be based on project needs. Time and travel has been budgeted for monthly or bi-monthly meetings throughout the project. Subtask project meetings will be held where appropriate and will probably occur more frequently as a large part of the project team is located in Lawrence. Every major project encounters unanticipated problems that affect the time of the project and possibly the performance of the project. We will identify these problems as soon as possible and reallocate the personnel and resources necessary to resolve the problem. We will keep all members of the ***Kansas CO2 Team*** informed as to major problems, schedule changes, etc.

The project management plan is based on three distinct groups with clearly identified responsibilities: These are: 1) Murfin Drilling Company (Murfin); 2) Operations Committee (OC) - Bill Flanders (K-M)-Chair, Tom Nichols (Murfin), Rich Pancake (TORP/KU); 2) Technical Committee (TC) - Paul Willhite (TORP/KU)-Chair, Don Green (TORP/KU), Alan Byrnes (KGS/KU).

Each group has specific responsibilities as outlined in this section. Joint meetings and or conference calls will be scheduled at the request of either Murfin Drilling Company or the two chairs.

Murfin Drilling Company - Field activities of the project will be managed and performed by Murfin Drilling Co. and its' personnel. This includes field operations, purchase and maintenance of all equipment and wells, and the purchase of carbon dioxide.

Plans/activities for the flood will be proposed by the Technical Committee to the Operations Committee which will review, clarify, justify and recommend plans/activities to Murfin management. Murfin may accept or reject proposed plans/activities. Implementation of all plans/activities, including any instructions to the field and any changes in field operations, will originate from Murfin (Tom Nichols or James Daniels).

Murfin is responsible for obtaining the field data necessary for analysis of process performance, management of the project and providing the data to the Operations and Technical Committees on a timely basis.

Operations Committee - The Operations Committee will review, clarify, justify and recommend to Murfin management field activities as required for maintenance of the project. Approved recommendations for field implementation will be documented (by email or word documents) and distributed to members of both the Operations and Technical Committees. Communication between the Operations and Technical Committees will be done through the chairs (Flanders and Willhite). In the event that members of the Operations Committee cannot reach consensus on a course of action, a simple majority vote will prevail.

The Operations Committee is responsible for reviewing field status, plan implementation and analysis of the flood as required to verify that the flood is proceeding properly and to identify as quickly as possible any changes that may be needed in the proposed plan or field operations. Concerns identified by the Operations Committee involving process performance will be communicated to Murfin and the Technical Committee by email or word document.

The Operations Committee may request specific technical analysis and clarification of analysis from the Technical Committee as needed. Members of the Technical Committee will also review field data in the context of interpreting performance and can raise any issue regarding field implementation to the Operations Committee.

The Operations Committee is responsible for checking the quality and accuracy of data and other information coming from the field and making corrections in data that are not accurate. The Operations Committee is responsible for insuring that all critical data are distributed to Murfin, members of the Operations Committee and Technical Committee in a timely manner.

Technical Committee - The Technical Committee is responsible for technical analysis, reporting, and support related to the CO2 flood (and not significantly involving routine oil field operations) including: reservoir model modification to model flood response, flood and well analysis to manage the flood and document development of the flood, analysis to address specific technical questions that arise, technical analysis for technology transfer, and reporting of analysis results

There will be a continuous dialogue between the Technical and Operations Committees, primarily through the Chairs (Willhite and Flanders) to make sure that critical issues are addressed and that recommended actions can be carried out. Either Murfin or the Operations Committee may request technical analysis from the Technical Committee.

Recommendations (in email or Word document format) from the Technical Committee will be forwarded by the Chair of the TC to the Chair of the Operations Committee for review, clarification, justification and recommendation to Murfin management. In the event that members of the Technical Committee cannot reach consensus on a course of action, a simple majority vote will prevail.

Planning

Planning calendars will be maintained by the TC and OC or Murfin. As needed, the OC will supply the TC with necessary plan changes including activities and scheduling.

Planning will be initiated by the Technical Committee with four time horizons that will be continually updated. These are:

1. One month
    a. Overall plan for the coming month will be developed
    b. A monthly calendar of field activities will be developed
    c. A schedule for analysis of the data will be completed as appropriate and results of the analysis of data will be distributed to the technical group
2. Three month
3. Six month
4. Total Project (General Plan)

Calendar(s) will be distributed monthly to Murfin and OC or more frequently when significant changes are made.

To the extent possible, project planning will anticipate changes that are likely to occur but will probably not be able to predict the timing. The project plan will be revised periodically as results become available.

Action items will be developed for each time horizon with tentative deadline dates for completion as well as absolute deadlines for completion of the each action item. Priority will be assigned to each item to insure that efforts are directed toward the most critical items in a timely sequence.

Progress will be reviewed weekly for monthly planning activities, monthly for the three-month horizon and at three-month intervals for the six-month time horizon. The level of detail decreases with increasing time horizons.

Analysis of Data

Data required for analysis of the flood performance will be identified by the Technical Committee and recommended to the Operations Committee. Recommendations for collection of data will be accompanied by an explanation of specifically how the data are to be used in project analysis, how data may improved performance, a recommended and minimum collection frequency and specifications on the necessary accuracy of the data.

Data will be analyzed and results reported to the Operations Committee on the time schedule developed in the project plan. Results will be reported to Murfin management as requested.

Information Storage and Retrieval

A common data repository for common input and access to data, reports, and other information will be established that can be accessed by all partners through a password-protected ftp (file transfer protocol) system. Data to be stored on this site and the format for the data and site will determined by Technical and Operations Committees.

Emergency Contact Chain

There may be situations that require decisions on a short time frame and key personnel are out of the office or out of town. A contact chain will be established that will enable Murfin to contact the technical group for advice. Project personnel will share schedules of when they will be out of the office for extended periods of time. Murfin is responsible for field implementation and safety of their personnel. Bill Flanders will be the principal contact for the Operations Committee. Paul Willhite will be the principal contact for the Technical Committee.

Preparation of Reports

Several types of reports are required to keep all parties informed of the progress of the project. Quarterly and annual reports will be submitted to the USDOE. These will be prepared by KU along with required accounting reports. Drafts of reports will be circulated to all parties for comment prior to submission to DOE. Reports that summarize progress are needed to develop a common understanding of field performance and will be created on a monthly basis early in Budget Period 2 and quarterly later in the period. The Technical Committee will prepare individual analyses of specific tests and share results with the Operations Committee for discussion. Reports will be provided to Murfin field personnel by Murfin management if they determine that reports will help field personnel understand how the flood is progressing, how present or future activities relate to the flood, and what is expected to happen.

ACTIVITY #8- TECHNOLOGY TRANSFER AND REPORTING REQUIREMENTS

Technology transfer has been a major focus in Budget Period 1 and will continue to be in Budget Periods 2 and 3 and subsequent to the demonstration project. The website for the project is growing and will contain more information as the results obtained in Budget Period 1 are compiled and summarized. The different activities are designed to complement project time schedules and to target alternate audiences. The technology transfer program will be the responsibility of the KU Energy Research Center and will involve university staff with cooperation from the participating companies. These activities will focus on transferring the knowledge gained, methodologies used, data required and necessary for evaluation, and the techniques used for solving the specific producibility problems. Instruction in accessing the results and understanding and utilizing the results of this project will be disseminated by web-

based information, publications, workshops and seminars to the public, government, academia, and industry, newsletters, site visits and direct one-on-one discussion that involves true two-way communication between operators and KUERC staff.

All reporting requirements of the Department of Energy, other federal agencies, and state and local governments will be fulfilled in timely manner.

C. BUDGET PERIOD 2 – BUDGET

The attached budget details costs for Budget Period 2. This budget is identical to the previously submitted Modified Plan Budget that was approved in October, 2003 with three minor modifications: 1) the dates from 2003-2008 were increased by one year to account for no-cost time extensions and get the budget properly synchronized with the real calendar, 2) 50,000 mcf of CO2 were added to Task 5.4.2 to provide for possible greater use of CO2 due to cooler reservoir temperatures (cost $63,000), and 3) the number of months for lease operating expense in 2004 in task 5.4 was increased from 9 to 11 months to account for the present calendar of events (cost $13,927). These additional costs do not increase requested DOE costs share greater than the cost share approved by DOE in the original proposal.

In addition to these costs certain monies not spent on surface facilities under Task 2.3 in Budget Period 1 are requested to be carried over into Budget Period 2. Most of these planned expenditures did not take place in Budget Period 1 for several reasons: 1) the existing equipment might be able to last for the duration of the project so that not buying replacement equipment would save all parties money, 2) by keeping the existing equipment in place we are able to evaluate how long it is usable under operating conditions which is important information for future application of the technology at other leases; and 3) some testing expenditures for CO2#16 were deferred awaiting further reservoir properties data.

At present remaining DOE dollars in BP1 are $80,373. It is estimated that funds left at the end of BP1 will be $40,870. We request that $40,762 be carried over from Budget Period 1 to Budget Period 2.

Budget Period 1 monies we request to be carried over into Budget Period 2 include:

	Total	DOE BP1 cost-share
1. Flow lines -	$39,262	$17,668
2. Pump & injection pump CO2#12 -	$18,500	$8,325
3. CO2 injection testing CO2#16	$15,000	$6,750
4. Meters	$7,500	$3,375
5. Site structure & improvements	$4,800	$2,160
6. Data line & communications	$5,520	$2,484
TOTAL	$90,582	$40,762

Field Demonstration of Carbon Dioxide Miscible Flooding in the Lansing-Kansas City Formation, Central Kansas/Class Revisit

DE-FC26-00BC15124

Program

This project was in response to DOE's solicitation DE-PS26-99BC15144, Reservoir Class Field Demonstration Program – Class Revisit. The goal of the Class Program was to extend the economic production of domestic fields, by slowing the rate of well abandonments and preserving industry infrastructure, and to increase ultimate recovery using improved reservoir characterization and advanced technologies.

Project Goal

The goal of the project is to determine the economic and technical feasibility of using CO_2 miscible flooding to recover residual and bypassed oil in the Lansing-Kansas City Field in central Kansas.

Performer

University of Kansas, Kansas Geological Survey, Lawrence, KS

Projects Results

The 1st CO_2 flood in central Kansas is being conducted using alternative CO_2 sources from local industries.

Benefits

Carbon dioxide flooding demonstrated in this project may prevent up to 6,000 mature oil fields in Kansas from being abandoned. The economic potential of CO_2 flooding in Kansas may recover over 250-500 million barrels of oil, equivalent to 5-10 years of additional Kansas production. The project's original objective, to demonstrate to Kansas Independents the feasibility of CO_2 flooding, and find a viable supply of CO_2 is being met by joint industry ventures; which will benefit agriculture, ethanol production and electrical generation in addition to independent oil producers.

The electrical co-generation, ethanol production and EOR project is unique in that it brings together three distinctly separate industries in a way that improves the economics of each while also providing a mechanism for value-added geologic sequestration of CO_2. At the same time the public will gain the environmental benefit of less carbon dioxide in the atmosphere. If the full CO_2 stream from the ethanol plant is utilized for EOR for a ten-year period the benefits from the links would realize $88 million.

Background

The CO_2 miscible flood demonstration project represents the first use of CO_2 for enhanced oil recovery (EOR) in Kansas. The goal is to demonstrate the technical feasibility of the process in a major Kansas reservoir. The Hall-Gurney field, the largest Lansing-Kansas City oil field in Kansas, is one of several CO_2 flood candidate fields in central Kansas. There are no miscible CO_2 floods in Kansas primarily due to the distance from CO_2 sources.

The electrical co-generation, ethanol fuel production and CO_2 EOR project is a unique scalable model for linked energy systems. Waste heat from a municipal 15-megawatt gas-fired turbine electric generator provides heat inputs for a 25 MM gallon per year ethanol plant. CO_2, a fermentation byproduct of ethanol production, will be utilized by the CO_2 miscible flood project in Hall-Gurney field. The full CO_2 stream from the ethanol plant could supply a small oil field capable of producing 5 MMbbl of oil and sequestering 1.5 MM tons of CO_2 over twenty years.

Project Summary

- Reservoir characterization and flood performance modeling completed.
- Economic analysis of the pilot and miscible CO_2 flooding in Kansas completed.
- Confirmed that the CO_2 pilot will be viable for miscible CO_2 flooding in the Lansing-Kansas City formation.
- Evaluation of the pilot demonstrates that this technology can be applied to other reservoirs in Kansas.
- Wellbore remediation and facilities design and construction completed.
- Technology transfer at state, regional and national meetings; presentations and posters.
- Project received the AAPG National, Best Poster, Jules Brunstein Memorial Award for 2001 and again in 2003.
- Original plans called for trucking liquid CO_2 from western Oklahoma. However, a local ethanol plant became the CO_2 source. The pilot area is a 10-acre+ pattern with one injection, two producing wells, a monitoring well that may later be converted to production and two water injection containment wells.

Hall-Gurney field and nearby ethanol plant, Russell, KS.

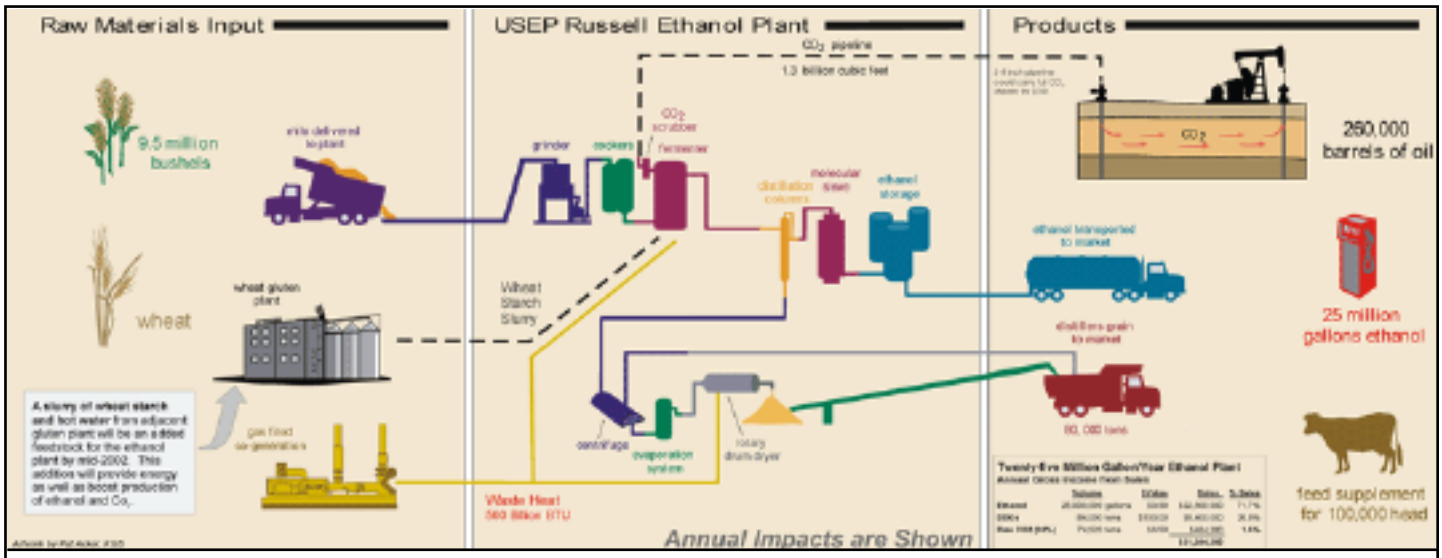

Linked systems will benefit six industries: agriculture, electrical generation, gluten, and ethanol production, cattle feeding and CO_2 EOR.

• Initiated the first CO_2 flood in Kansas in December, 2003.

Initial studies of the Lansing-Kansas City carbonate reservoir have determined the technical and economic feasibility of using CO_2 miscible flooding to recover residual and bypassed oil in central Kansas. The demonstration will mark the first time that CO_2 from an ethanol plant has been used for EOR. If proven to be technically and economically feasible the project offers potential to add significant value to waste CO_2 through EOR. Modeling indicates that the 25 MM gallon /year ethanol plant running at full capacity may increase production to 40 million gallons /year by the end of year. Current legislation in Congress will potentially double the demand for ethanol. 10-20% of the CO_2 stream will be used for the nearby demonstration at Hall-Gurney field. Inputs from the agricultural community will be the grains used to produce ethanol. An additional byproduct of ethanol production will be cattle feed.

The official beginning of carbon dioxide flooding in Kansas began in December, 2003. The CO_2 is trucked 7 miles from the ethanol plant in Russell, Kansas and injected into the depleted Lansing-Kansas City reservoir. If the technology is determinded to work the estimated incremental oil production in the State of Kansas is 600 million barrels ($$15 billion @$25/bbl) over 20 years.

Current Status

The project is in Budget Period II, and has completed 6 months of CO_2 injection. Modification of the original plan allowing provision for an alternate CO_2 source and revisions in the CO_2 flood and monitoring period extended the time necessary to fulfill the project obligations. No-cost extensions have increased the length of the project from 2003 to 2008.

Publications

The Budget Period 1 report (Jan. 2004) is available at NETL, 918-699-2000.

Project Start: March 8, 2000
Project End: March 7, 2010

Contact Information:
NETL – Paul West (paul.west@netl.doe.gov or 918-699-2035)
Kansas Geological Survey – Paul Willhite (willhite@ukans.edu or 785-864-2906) University of Kansas, Lawrence, KS
Partners – *Murfin Drilling Company,* Wichita, KS
MV Energy, Princeton, NJ
Kinder-Morgan CO_2, Houston, TX
ICM, Inc., Colwich, KS
Kansas Dept. of Commerce, Topeka, KS

Exploitation and Optimization of Reservoir Performance in Hunton Formation, Oklahoma

ANNUAL TECHNICAL PROGRESS REPORT

Reporting Period
October 1, 2002 – September 30, 2003

Principal Investigator
Mohan Kelkar, The University of Tulsa

Report Issued
October 2003

DOE Award No.
DE-FC26-00NT15125

Submitted By
Mohan Kelkar
Department of Petroleum Engineering
The University of Tulsa
600 S. College Ave., KEH #L-117
Tulsa, Oklahoma 74104-3189

http://www.tucrs.utulsa.edu/Hunton

Disclaimer

This report was prepared as an account of work sponsored by an agency of the United States Government. Neither the United States Government nor any agency thereof, nor any of their employees, makes any warranty, express or implied, or assumes any legal responsibility for the accuracy, completeness, or usefulness of any information, apparatus, product, or process disclosed, or represents that its use would not infringe privately owned rights. Reference herein to any specific commercial product, process, or service by trade name, trademark, manufacturer, or otherwise does not necessarily constitute or imply its endorsement, recommendation, or favoring by the United States Government or any agency thereof. The views and opinions of authors expressed herein do not necessarily state or reflect those of the United States Government or any agency thereof.

Acknowledgements

The research effort described in this report was supported by the U.S. Department of Energy under Contract No. DE-FC26-00NT15125. Additional support is provided by Marjo Operating Company, Inc., the University of Houston, Joe Podpechan and James R. Derby and Associates, Inc. The computer facilities were provided by The University of Tulsa.

We would like to thank Brian Keefer from Marjo Operating Company, Inc. for his valuable contribution and insight to our work. Our special thanks also go to Paul West from the Department of Energy for their enthusiasm and valuable suggestions.

October 2003
Mohan Kelkar

Abstract

This report presents the work done so far on Hunton Formation in West Carney Field in Lincoln County, Oklahoma. West Carney Field produces oil and gas from the Hunton Formation. The field was developed starting in 1995. Some of the unique characteristics of the field include decreasing water oil ratio over time, decreasing gas-oil ratio at the beginning of production, inability to calculate oil reserves in the field based on log data, and sustained oil rates over long periods of time.

To understand the unique characteristics of the field, an integrated evaluation was undertaken. Production data from the field were meticulously collected, and over forty wells were cored and logged to better understand the petrophysical and engineering characteristics. Based on the work done in this budget period so far, some of the preliminary conclusions can be listed as follows:

- Based on PVT analysis, the field most likely contains volatile oil with bubble point close to initial reservoir pressure of 1,900 psia
- The initial oil in place, which is contact with existing wells, can be determined by newly developed material balance technique. The oil in place, which is in communication, is significantly less than determined by volumetric analysis, indicating heterogeneous nature of the reservoir. The oil in place, determined by material balance, is greater than determined by decline curve analysis. This difference may lead to additional locations for in fill wells.
- The core and log evaluation indicates that the intermediate pores (porosity between 2 and 6 %) are very important in determining production potential of the reservoir. These intermediate size pores contain high oil saturation.
- The limestone part of the reservoir, although low in porosity (mostly less than 6 %) is much more prolific in terms of oil production than the dolomite portion of the reservoir. The reason for this difference is the higher oil saturation in low porosity region. As the average porosity increases, the remaining oil saturation decreases. This is evident from log and core analysis.
- Using a compositional simulator, we are able to reproduce the important reservoir characteristics by assuming a two layer model. One layer is high permeability region containing water and the other layer is low permeability region containing mostly oil. The results are further verified by using a dual porosity model. Assuming that most of the volatile oil is contained in the matrix and the water is contained in the fractures, we are able to reproduce important reservoir performance characteristics.
- Evaluation of secondary mechanisms indicates that CO_2 flooding is potentially a viable option if CO_2 is available at reasonable price. We have conducted detailed simulation studies to verify the effectiveness of CO_2 huff-n-puff process. We are in the process of conducting additional lab tests to verify the efficacy of the same displacement.
- Another possibility of improving the oil recovery is to inject surfactants to change the near well bore wettability of the rock from oil wet to water wet. By changing the wettability, we

may be able to retard the water flow and hence improve the oil recovery as a percentage of total fluid produced. If surfactant is reasonably priced, other possibility is also to use huff-n-puff process using surfactants. Laboratory experiments are promising, and additional investigation continues.

- Preliminary economic evaluation indicates that vertical wells outperform horizontal wells.

Future work in the project would include:

- Build multi-well numerical model to reproduce overall reservoir performance rather than individual well performance. Special emphasis will be placed on hydrodynamic connectivity between wells.
- Collect data from adjacent Hunton reservoirs to validate our understanding of what makes it a productive reservoir.
- Develop statistical methods to rank various reservoirs in Hunton formation. This will allow us to evaluate other Hunton formations based on old well logs, and determine, apriori, if additional potential exists from these reservoirs.
- To develop more complex well test model so that we can obtain reservoir parameters based on the well test data
- To conduct additional laboratory experiments to validate the feasibility of CO_2 huff-n-puff process as well as evaluate surfactant injection as another process of recovering more oil.
- To collect additional economic data from many vertical and horizontal wells to determine if horizontal wells add value in exploiting Hunton reservoir.

On the technology transfer front, we will continue to update our web site (http://www.tucrs.utulsa.edu/Hunton), and publish more papers to disseminate technology. To this end, we will be presenting two papers in the upcoming IOR meeting to be held in Tulsa in April 2004.

Table of Contents

Disclaimer……ii

Acknowledgements……...…iii

Abstract……...…iv

Table of Contents……...…vi

Executive Summary ……1

Experimental……2

Results and Discussion……..……...…10

Geological Analysis……..……...…10

Engineering Analysis…….…...…45

Fluid Properties Analysis…….……..45

Material Balance Analysis……..…49

Petrophysical Analysis…….…..62

Simulation Evaluation……....79

Economic Analysis……...……...…90

Technology Transfer…….....……..……...…103

Web Development……...……..……...…105

Conclusions…….....……..….....…….……106

References……...……...…….……107

Appendix A……..……..……....……108

Appendix B……..……118

Appendix C……..……146

Executive Summary

Hunton Formation in West Carney Field can be considered as an enigma in terms of its production characteristics. The formation produces significant quantities of water up front; has unique gas-oil ratio characteristics; is geologically extremely complex, but is hydrodynamically connected; and the log characteristics at the well locations do not provide representative information about the reserves in place.

This investigation was undertaken to explain some of the production characteristics present in Hunton Formation. Further, the investigation also concentrated on the field characteristics, which can be extrapolated to other fields so that the success in West Carney Field can be reproduced in other places where Hunton Formation is present.

This report covers the progress we have made so far during the first year of Budget Period II. We have identified the fluid present in the reservoir as volatile oil. This characterization helps us in explaining some of the gas and oil production characteristics observed in the field. We have also developed a new material balance equation, which can be used to calculate oil in place using traditional p/z plot, typically used for gas reservoirs. We were able to calculate the oil in place values using available field information, and compare that to volumetric as well as decline curve analyses. This comparison helped us to understand the difference between geological differences observed in different parts of the field. We have also conducted extensive petrophysical evaluation to understand the relationship between log characteristics and production performance. We have identified statistical log characteristics, which can explain the difference in the performance of the reservoir in various parts. We observed that a clear relationship exists between trapped oil saturation and porosity of a particular region in the reservoir. Typically, higher the oil saturation, better has been the recovery. Our lab evaluations confirm the oil wetting characteristic of the reservoir. This helps us explain the unique trapping mechanism we have postulated to explain the water oil ratio production characteristics. Our simulation results are able to explain most of the production behavior observed in the field, validating our model assumptions. In addition to validating single well characteristics, we also examined the use of huff-n-puff CO_2 injection to recover additional oil. We observed that if the CO_2 is available at reasonable cost, such huff-n-puff procedure can add significant reserves.

We will continue to refine our reservoir model and extend it other fields operating in similar environment. Our laboratory studies will explore the use of surfactants and CO2 injection to improve the oil recovery from the rock. Laboratory studies for CO2 injection are important to validate our simulation results. We will also examine the importance of horizontal wells in exploiting these types of reservoirs, as compared to vertical wells. We hope that by the end of the Budget Period II, we should have identified important statistical characteristics, which can allow us to high and low grade reservoirs for additional recoveries from Hunton formation in other areas.

Experimental

Experimental Analysis

Kishore Mohanty, University of Houston

Objective

The objective of the second phase of this project is to study the effect of near well bore surfactant treatment on productivity enhancement. In water-wet gas reservoirs, water saturation is high in the near well bore region (or at fracture faces). This leads to low gas relative permeability and low productivity. Treatment of the near-well bore region by a surfactant solution can make the surface hydrophobic and thus increase the gas-water contact angle. This can lead to a decrease in water saturation and an increase in gas flow. In gas condensate reservoirs, condensates (or oil) accumulate in the near well bore regions (and fracture faces). Removal of the oil from this region can improve gas productivity.

Methodology

Two different studies are made. The first study investigates the wettability of gas and water in the absence of oil. The second study investigates the effect of surfactants on oil mobilization.

Gas-Water Wettability

We equilibrated calcite and silica plates with synthetic brine for a day. The water/air contact angle was measured and then the plate was treated with a surfactant solution for a day. We again measured water/air contact angles on the plate. The change in contact angle quantifies the effect of surfactant on wettability. This experiment was repeated with different surfactant solutions to study structure property relationships. We are treating cores with the same surfactant solutions and will measure the effect on gas/water relative permeability.

Oil Mobilization

Mary Marie dead oil was used for these experiments. The surfactants evaluated for solubilization and wettability alteration are: Alfoterra –38 (Sasol), SS-6656 (Oil Chem Technology) and DTAB (Dodecyl trimethyl ammonium bromide). The first two are anionic, where as the last one is cationic. The following sets of experiments were conducted:

Phase Behavior: Dilute surfactant solutions (0.05 active wt% for anionics and 1wt% for cationic) were prepared with varying concentrations of Na_2CO_3 (0M–0.5M). These solutions were equilibrated with equal volume of oil on a tube shaker for a period of two days. Thereafter the tubes were removed and left to settle for a day. The shift from Winsor type II- to type II+ was observed with the increase in salinity of the solution and thus over-optimum and under-optimum regions were identified.

IFT Determination

The equilibrated oil and brine from the phase behavior test were injected into a spinning drop tensiometer to measure interfacial tension (IFT).

Wettability Alteration: The calcite mineral plate was polished on a 600 mesh diamond lap and equilibrated with the synthetic brine for a day. The initial (before aging in oil) wettability state of the plate was determined by measuring the advancing and recently receded contact angle of oil with the calcite surface immersed in brine. The plate was removed from brine and aged with oil at elevated temperature (~80^0C) in the oven for about 72 hours. This step mimics the exposure of reservoir rock to oil for geologic periods of high temperature. After removing from the oven, the plate was contacted with synthetic (sodium carbonate) brine for an hour and the advancing contact angle was measured. Thereafter, the synthetic brine was replaced by the surfactant-brine solution and the evolution of contact angle was studied for a period of two days. In cases where the drops were too small, it was difficult to measure the contact angle accurately and a post-wettability test was performed wherein the calcite plate was washed with brine to remove oil. This plate was then placed in the brine solution and an oil drop was deposited on the bottom of the surface with the help of an inverted needle. The contact angle was then measured. This gave the final wettability state of the plate. For the cationic surfactant, the field brine was used instead of the synthetic brine.

Results

Gas-Water Wettability

The drop shapes during contact angle measurement are shown in Figure 1. We have identified some surfactants (OSA and WSA supplied by Oil Chem Technology) that can increase the contact angle on calcite and silica plates. The change in contact angles is quantified in Table 1. Before the surfactant treatment, the plates were water wet with contact angles of 33 and zero. After the treatment, the contact angles changed to 107 and 93 respectively. At these contact angles, capillary pressures are very small.

Table 1: Air-water contact angle on mineral plates before and after treatment with surfactant solutions

Plate	Surfactant	Contact Angle Before Treatment	Contact Angle After Treatment
Calcite	OSA	33^0	107^0
Silica	WSA	0^0	93^0
Silica	Furofac 1157	0^0	63^0

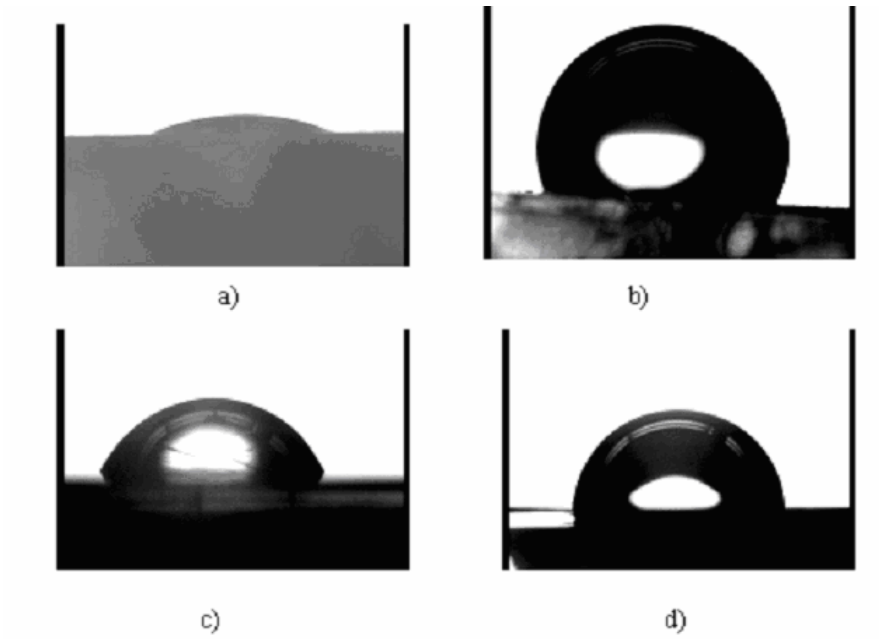

Figure 1: Contact Measurements (a) Calcite Plate before treatment with OSA, 0=33°, (b) Calcite Plate after treatment, 0=107°, (c) Silica Plate after treatment with DTAB, Furofac, 0=63°, (d) Silica Plate after treatment with WSA, 0=93°

Another observation that was made in contact angle measurements was the spreading of the drop after treatment with surfactants. After washing the plate and measuring the drop contact angle again, the time of spreading increased (the time drop took to spread from an initial state to final equilibrium state). This is shown in Figure 2. To observe this phenomenon a random spot was chosen after treatment and that spot was repeatedly washed. It was observed that the drop was spreading initially and the time of spreading decreased as number of washes was increased. And a final equilibrium angle was established after 20-25 washes. This phenomenon is illustrated in Figure 3. Probable reason for this phenomenon is the change in nature of the surface from a bilayer hydrophilic surface to a monolayer hydrophobic surface.

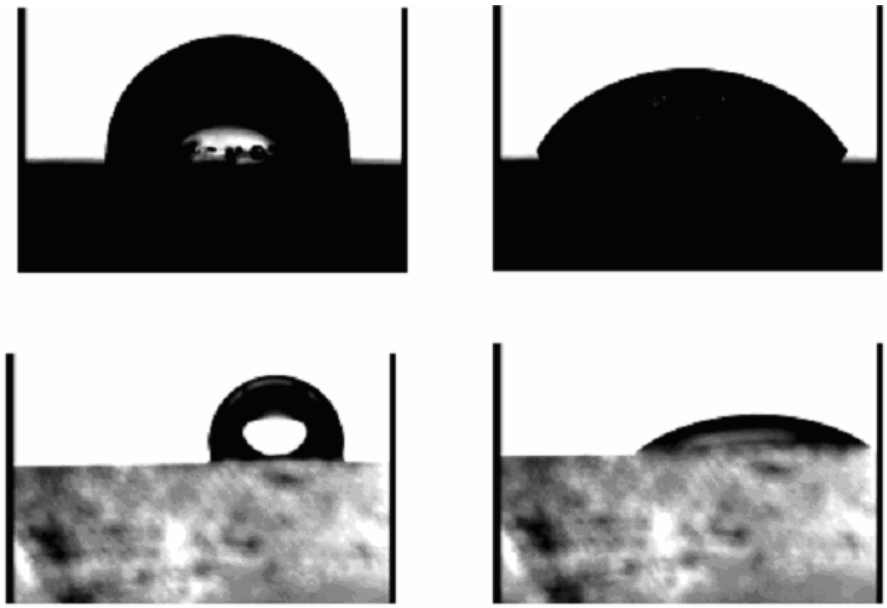

Figure 2: Spreading of Drop after treatment with surfactant. The time for spreading varied from few seconds to 4-5 minutes as the plate was repeatedly washed.

Figure 3: Hydrophilic Nature for an unwashed spot and hydrophobic nature for a washed spot suggesting change in nature of surface with washing from a bilayer to a monolayer adsorption.

Oil Mobilization

The phase behavior of oil-brine-surfactant solutions is shown in Figure 4. The surfactant concentration is 0.05 wt%. The tube at the left most position has no Na_2CO_3. Na_2CO_3 concentration increases by 0.1M for each tube to the right. For Alfoterra38, the second tube from the left (0.1 M Na_2CO_3) has the most colored brine phase. Na_2CO_3 forms in situ surfactant by reacting with some of the acid groups of the oil. The surfactant micelles solubilize some oil,

giving some color to the brine phase. As the Na_2CO_3 concentration increases, electrolyte concentration increases in the brine phase, which drives the surfactants into the oil phase, thus brine phase becomes more clear. The colored phase salinity is the optimum. For Alfoterra38, it is 0.1 M. For SS6656 surfactant, the optimum salinity occurs at 0.4 M Na_2CO_3. Three phases occur for the second surfactant.

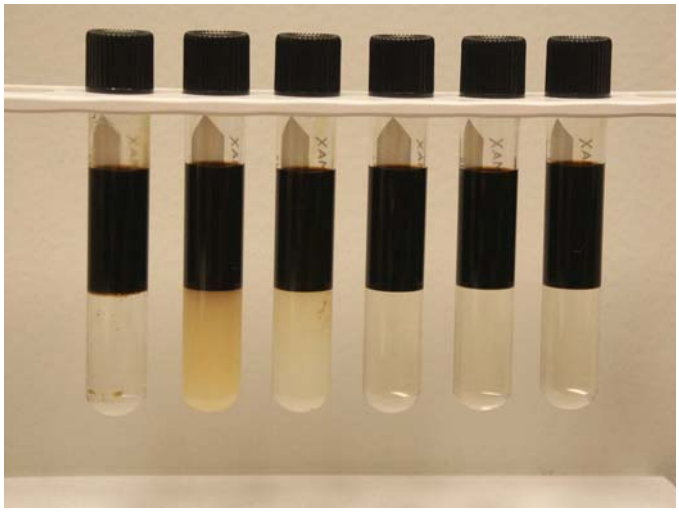

a) Alfoterra-38 (0.05wt% active) with Na_2CO_3

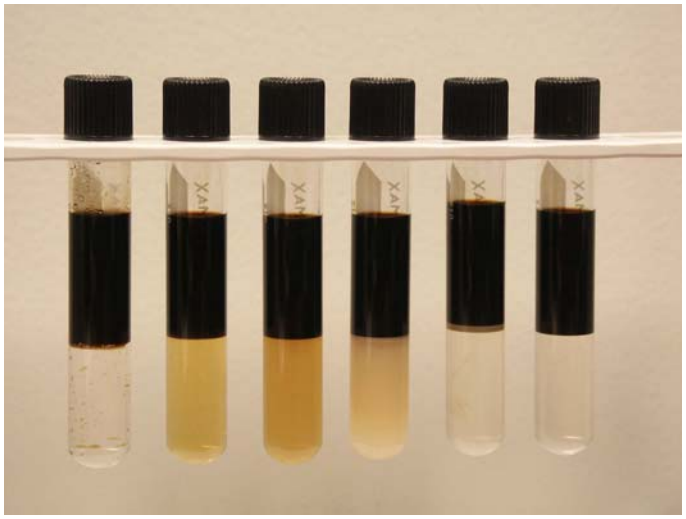

b) SS-6656 (0.05wt% active) with Na_2CO_3

Figure 4: Phase behavior of brine, oil, and surfactant

The interfacial tension for these solutions is plotted in Figure 5. The tensions remain higher than 0.1 dyne/cm for Alfoterra38 solutions. For SS 6656, the tensions decrease to about 0.001 dyne/cm. Note that the lowest IFT corresponds to the optimal salinity for both the solutions. The

oil can be displaced easily at such low tension in the near well bore region. The IFT for DTAB (1 wt%) solution with oil was 0.053 dynes/cm.

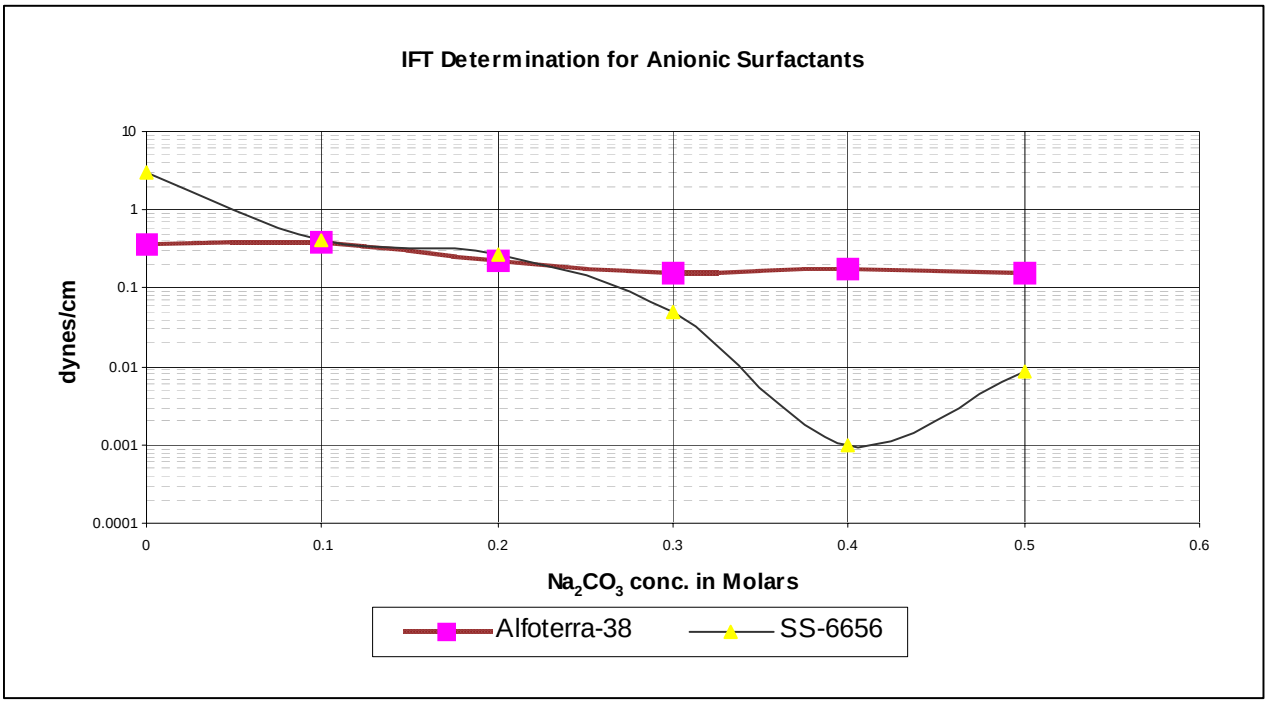

Figure 5: Interfacial tension between equilibrated oil and water phases.

The oil-water wettability results are listed in Table 2. Before aging with oil, the calcite plate had a receding contact angle of ~30^0 and advancing contact angle of ~90^0. After aging with Mary Marie well, the contact angle was 180, completely oil-wet. After treating with Alfoterra-38, the oil-wet calcite plate was altered to an intermediate-water-wet state (contact angle ~66^0). After treating with SS-6656, the oil-wet calcite plate was altered to a water-wet state (contact angle ~34^0). After treating with DTAB, the oil-wet calcite plate was altered to an intermediate-water-wet state (contact angle ~83^0). The change of oil wettability can help mobilize oil and reduce the condensate saturation in the near-well bore region.

Table 2: Oil-water contact angle on calcite

Contact angle	**Alfoterra-38 (0.05wt%, 0.4M Na2CO3)**	**SS-6656 (0.05wt%, 0.4M Na2CO3**	**DTAB (1wt%, in Hunton brine)**
Before aging with oil:			
Equilibrium Angle	34^0	34^0	24^0
Advancing Angle	102^0	102^0	88^0
After aging with oil at 80^0 C:			
In Synthetic Brine			***In Hunton Brine***
- 5-10 mins	180^0	180^0	180^0
- 60 mins	180^0	180^0	180^0
In 0.05 wt % surfactant			***In 1.0 wt % surfactant***
- 30 mins	161^0-166^0	Drops departing from the surface	145^0
-1 hour	154^0-167^0	Solution turbid, Drops too small	135^0
-24 hours	Hardly any oil left, drops too small to measure	Drops very small; Angle less than 70^0	80^0-85^0
-48 hours	Status-quo	Drops very small ;	73^0-85^0
Post-wettability test	66^0	34^0	83^0

Summary

A surfactant has been identified which can change the air-water wettability of calcite to intermediate wettability. Some surfactants have also been identified which can change the oil-water wettability to intermediate wettability and reduce oil-water interfacial tension to about 0.001 dyne/cm.

Future Work

- Corefloods will be conducted to see the impact of surfactant treatment on gas permeability.
- Corefloods will be conducted to evaluate the impact of CO_2 injection on residual oil recovery.

Results and Discussion

Geological Analysis

Jim Derby, James R. Derby & Associates

Geological Goals for Budget Period II include:

1. Describe and elucidate the stratigraphy and depositional model of the field
2. Define and describe the lithologic nature of the reservoir, including:
   a. Depositional facies
   b. Diagenetic facies
   c. Karst and structural overprint
3. Reconcile petrophysical log data with core analysis data by petrographic microscopy and detailed core study.

Review:

In Budget Period 1 we described 14 cores and outlined an "Island model" of a field created by a high standing "island" of the Cochrane Limestone, surrounded by a younger dolomite reservoir unit, the Clarita Formation (see Figure 6). Distal to the field we postulated a carbonate mudstone facies based on well-log and preliminary core data. This simple picture was complicated by recognition of two phases to the Cochrane. The older unit, the Lower Cochrane is present throughout the field and appears to be present in the western, thicker part of the limestone facies at positions stratigraphically (and paleotopographically) higher than the younger Upper Cochrane and Clarita formations. The Upper Cochrane, overlain by Clarita dolomite, was identified in only two wells in the eastern part of the field. Clarita was also positively identified in dolomite facies in one well west of the western thick Lower Cochrane wells. These stratigraphic units were positively identified by paleontologic age determination, specifically by conodonts.

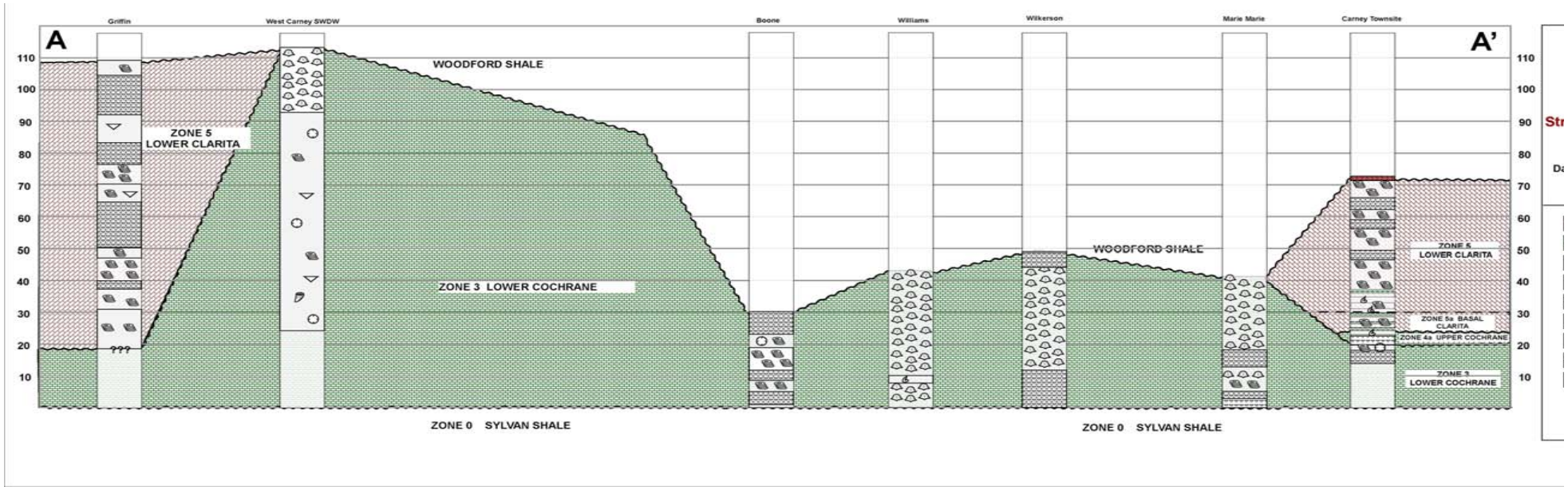

Figure 6: Stratigraphic Cross-section of WCHF, by Jason Andrews from data by J. Derby.

Logistical Progress

We now have 28 cores, 26 in the field and 2 from outside the field, that provide critical regional stratigraphic information. A major part of our effort to date, since the beginning of work in Budget Period II, is compiling the data on all 28 wells, transporting the cores to Derby's office site for description, taking of samples for paleontological analysis and thin sections, and preparing the slabbed core for description (cleaning and polishing). The data management is summarized on the attached well summary tables (Table 3 and Table 4). Twenty-one wells have been sampled for paleontology, 24 sampled for thin sections, and 26 sets of core slabs have been cleaned and prepared for description. Core-log plots have been prepared on 27 wells.

Table 3: Table of Wells Cored

DOE/TU West Carney Hunton Project

TABLE OF WELLS CORED: Thickness, Core/Log adjustment, Data

X = top or base of Hunton not cored;; (footage) = top or base of core; *italicized depth* is "core depth" of fm top or base picked on logs

	Well #	Well Name	Twp-Rng	Hunton Top		Core/log	Hunton Base		Thickness	Status & Data, * = Completed							
				Core	Log	adjustment.	Core	Log	ft.	Wk	TS	PC	SEM	Cono	UH	Wett	Lithology
1	5705	Mary Marie 1-11	11-15N-2E	4961	4944	17	5003.5		42.5 cored	C	33	C	4	14*	10	4	Ls/ 2'dol
2	5712	Wilkerson 1-3	3-15N-2E	4953.4	4937.5	15.8	4999.8	4984	46.4 cored	C	17*	C	1	11	8	1	Ls/ 2'dol
3	5733	Toles 1	10-15N-2E	4964	X	na	5003.7	X	39.7 cored	C	8*	C					Ls/ 2'dol
4	5818	Henry 1-3	3-15N-2E	X (4966)	4958	7.5	X (4996.6)		30.6+ cored	C		C					Ls/5' dol/ls
5	5838	Danny 2-34	34-16N-2E	X (4930)	4918	10.8	4984.3		54.3+ cored	C		C		11	4	1	Ls
6	5874	Joe Givens 1-15	15-15N-2E	5017.8	5010	9	5044		26.2 cored	C		C		4			Ls/ 0.1' dol
7	5887	Williams 1-3	3-15N-2E	4943.5	4934	9.5	4983.7	4974	40.2 cored	C		C		5	8		Ls/ 5' dol
8	5899	McBride South 1-10	10-15N-2E	X (4962)	4947	13.3	4996.2	4983	34.3 cored *36 log*	C	1*	C		1*	4		Ls/dol/ls
9	5913	Boone 1-4	4-15N-2E	X (5037)	5028	6.5	5066.5	5060	29.5+ cored *32 log*	C	6*	C		6*	4	1	Ls/ dol Ls/ 4' dol
10	5934	Carter 1-14	14-15N-2E	X (4940)	4927	13.3	4995.8	4983	56.1 cored *56 log*	C	16	C		18*	4	2	1'dol/ Ls/ 2'dol
11	5943	Anna 1 - 15	15-15N-2E	4967.1	4947	20.1	5004.7	4985	37.6 cored	C	10	C					Dol
12	5992	Carney Twnste 2-5	5--15N-3E	X (4906)	4907	0	X (4966); *4978L.*	4978	60 cored; *71 log*	C	8*	C		12*	4		Dol/Ls
13	6011	Bailey 2-6	6-15N-3E	X(4876)	4875	-2.8	X(4934)	4964	58 cored; *89 log*	C	20	C		25* 30			14' Dol/Ls
14	6029	Kathyrn 2-14 P	14-15N-2E	X(4994)	4990	2.5	5030.5	5028	36.5 core *38 log*								Ls/Dol/Ls/Dol
15		Geneva 2-32 (not analyzed)	32-16N-3E						9 ft cored		1						Dol? Ls(Cri pkstn)
16	6051	Carter Ranch 2	15-15N-2E	5006	5000	6	5035.1	5030	29.1 cored	C	5	C					
17	6061	W Carney Ext SWDW # 1	14-15N-1E	5042.7	5038.0	4.7	X(5131); *=5156 L*	5151	88.7 cored *113 log*		15			10			Ls
18	6088	Cal 1-11 NE-SE	11-15N-1E	X(5034)	5025	1.8	5135.8	5134	101.8 cored *108.5 log*					21			no pent br facies? Wkstn Karst/ 12' mdstn/ 6' burr mdstn
19	6100	Mark Houser 1-11	11-15N-!E	X(4961)	4940		X(5077.6)	5066	116.6core *126 log*								need log
20	6112	JB 1-13	13-15N-1E	4971.9	4966	5.9	X(5058.8)	5120	86.9 cored *154 log*					24			
21	6131	Saunders 1-13 SE-NE (xerox only	13-15N-1E	4917.3	4911	6.3	X(4940.5) 5059.3L	5053	23.2 cored *142 log*					4			
22	6143	Points 1-13 NE-SE	13-15N-1E	4989.5	4978	11.5	X(5107)	5096	117.5 cored *118 log*								2.5' Wfd, 60' big br, vuggy, 57'wkstn,
23	6150	Mercer 1-28	28-17N-2E	X(4527)	4526	0 ?	X(4583)	4606	56 cored *80 log*					17*			
24	6209	Griffen 1-14 NW-NW-SW	14-15N-1E	X (5082)	5077	5	X(5142); *5191.5*	5186.5	60 cored *109.5 log*					14*			Ls/dol/limy dol
25	6247	Morrow 1-27	27-16n-2E	X(4905)	4886	0.5	4956.5	4956	53 cored *69 log*					15*			
26	6281	Chandler SWDW # 1 33	5-14N-3E	X(4810)	4797.5	5+ ?	X(4869.8)	4865	59.8 cored *68 log*					14*			
27	6302	Stevenson 1-14 NW	14-15N-1E	X(5143)	5103	2	X(5167.6) 5188L	5186	24.6 cored *85 log*					7			
28	6563	W Carney Ext SWDW # 2 NW	10-15N-1E	X(5140)	5135	6	X(5232) 5275L	5271	92 cored *135.5 log*								

Wk = Work status (Core description), C = Completed IP = In Process; PC = Porosity Codes.
TS = Thin Sections,# made, * described ; SEM = Scanning Electron Microscopy, Cono = Conodont micropaleontology, # of samples, * completed
UH = Core Plug samples at Univ. Houston; Wett = Wettability Analysis,
Hg Inj = Mercury injection porosimetry
Numbers in front of Well Name is StimLab well Identification Number

Table 4: Table of Work Progress

				Hunton Top				Hunton Base			Status & Data, * = Completed									Core Analysis		Core Photos			Logs C = CBL Only		Core Log Plots				Pore & Facies			Typed Form		# of Samples	Core Description					Core Slab	
	Well #	Well Name	Twp-Rng	Core	Log	Core log Adj	Top LAS Log	Core	Log	Thickness Feet	Wk	TS	PC	SEM	Cono	UH	Wett	Hg Inj	Lithology	Print	File	Book	CD	Paper	Paper	LAS	Core	Log	Samples	Pore & Facies	Form Prepped	Data Entered	Corrected	Conodonts	Thin Sections	Mega Fossils	Prelim	Core - Final	Karst	Fractures	Stylolites	Slab at JRD	Slab at Carney
1	5705	Mary Marie 1-11	11-15N-2E	4961	4944	17	4924	5003.5		42.5 cored	C	33	C	4	14*	10	4		Ls/ 2'dol	x	x	x	x		x	x	x	x	x	x	x	x		x	x			X				X	
2	5712	Wilkerson 1-3	3-15N-2E	4953.4	4937.5	15.8	4917	4999.8	4984	46.4 cored	C	17*	C	1	11	8	1		Ls/ 2'dol	x	x	x	x		x	x	x	x	x	x	x	x						X				X	
3	5733	Toles 1	10-15N-2E	4964	X	na	na	5003.7	X	39.7 cored	C	8*	C						Ls/ 2'dol	x	x	x	x				x	x	x	x	x	x			x			X	x	x	x	X	
4	5818	Henry 1-3	3-15N-2E	X (4966)	4958	7.5	4938	X (4996.6)		30.6+ cored	C		C						Ls/5' dol/ls	x	x	x	x			x	x	x	x	x	x	x						X	x	x	x	X	
5	5838	Danny 2-34	34-16N-2E	X (4930)	4918	10.8	4898	4984.3		54.3+ cored	C		C		11	4	1		Ls	x	x	x	x			x	x	x	x	x	x	x						X	x	x	x	X	
6	5874	Joe Givens 1-15	15-15N-2E	5017.8	5010	9	4990	5044		26.2 cored	C		C		4				Ls/ 0.1' dol	x	x	x	x			x	x	x		x	x	x						X	x	x	x	X	
7	5887	Williams 1-3	3-15N-2E	4943.5	4934	9.5	4914	4983.7	4974	40.2 cored	C		C		5	8			Ls/ 5' dol	x	x	x	x		x	x	x	x	x	x	x	x						X				X	
8	5899	McBride South 1-10	10-15N-2E	X (4962)	4947	13.3	4927	4996.2	4983	34.3 cored *36 log*	C	1*	C		1*	4			Ls/dol/ls	x	x	x			x	x	x	x	x	x	x	x						X	x	x	x	X	
9	5913	Boone 1-4	4-15N-2E	X (5037)	5028	6.5	5008	5066.5	5060	29.5+ cored *32 log*	C	6*	C		6*	4	1		Ls/ dol Ls/ 4' dol	x	x	x	x		x	x	x	x	x	x	x	x		x	x			X	x	x	x	X	
10	5934	Carter 1-14	14-15N-2E	X (4940)	4927	13.3	4917	4995.8	4983	56.1 cored *56 log*	C	16	C		18*	4	2		1'dol/ Ls/ 2'dol	x	x	x			x	x	x	x	x	x	x	x		x	x			X				X	
11	5943	Anna 1 - 15	15-15N-2E	4967.1	4947	20.1	4928	5004.7	4985	37.6 cored	C	10	C						Dol	x	x	x		x	x	x	x	x	x	x	x	x						X				X	
12	5992	Carney Twnste 2-5	5--15N-3E	X (4906)	4907	0		X (4966); *4978L;*	4978	60 cored; *71 log*	C	8*	C		10* / 16	4			Dol/Ls	x	x	x	x		x	x	x	x	x	x	x	x		x	x			X	x	x	x	X	
13	6011	Bailey 2-6 P	6-15N-3E	X(4876)	4875	-2.8		X(4934)	4964	58 cored; *89 log*	C	20	C		25* / 35				14' Dol/Ls	x	x	x			x	x	x	x	x	x	x	x		x	x			X	x	x	x	X	
14	6029	Kathyrn 2-14 P	14-15N-2E	X(4994)	4990	2.5		5030.5	5028	36.5 core *38 log*									Ls/Dol/Ls/Dol	x	x	x	x		x	cd					x	x										X	
15		Geneva 2-32 (not analyzed)	32-16N-3E							9 ft cored		1			8				Dol? Ls(Cri pkstn)												x											X	
16	6051	Carter Ranch 2	15-15N-2E	5006	5000	6		5035.1	5030	29.1 cored	C	5	C		6					x	x	x				x	x	x	x	x	x	x			x	1	X				X	
17	6061	W Carney Ext SWDW # 1	14-15N-1E	5042.7	5038.0	4.7		X(5131); *=5156 L*	5151	88.7 cored *113 log*		15			10				Ls	x	x	x	x		x	x	x	x		x	x				x							X	
18	6088	Cal 1-11 P NE-SE	11-15N-1E	X(5034)	5025	1.8		5135.8	5134	101.8 cored *108.5 log*					21				no pent br facies? Wkstn Karst/ 12' mdstn/ 6' burr mdstn	x	x	x	x		x	x	x	x		x	x		X			X						X	
19	6100	Mark Houser 1-11 P	11-15N-!E	X(4961)	4940			X(5077.6)	5066	116.6 cored *126 log*									need log	x	x	x	x								x	x										X	
20	6112	JB 1-13 P	13-15N-1E	4971.9	4966	5.9		X(5058.8)	5120	86.9 cored *154 log*					24					x	x	x	x	x	c						x	x										X	
21	6131	Saunders 1-13 SE-NE (xerox only	13-15N-1E	4917.3	4911	6.3		X(4940.5) 5059.3L	5053	23.2 cored *142 log*					4					x	x	x	x		c						x	x		X			X					X	
22	6143	Points 1-13 P NE-SE	13-15N-1E	4989.5	4978	11.5		X(5107)	5096	117.5 core *118 log*								L	2.5' Wfd, 60' big br, vuggy, 57'wkstn,	x	x	x	x		c						x	x										X	
23	6150	Mercer 1-28 *	28-17N-2E	X(4527)	4526	0 ?		X(4583)	4606	56 cored *80 log*					17*					x	x		x	x	c	x	x	x	x		x	x		X	x		X					X	
24	6209	Griffen 1-14 NW-NW-SW	14-15N-1E	X (5082)	5077	5		X(5142); *5191.5*	5186.5	60 cored *109.5 log*					14				Ls/dol/limy dol	x	x	x	x	x	x	x	x	x			x	x		X								X	
25	6247	Morrow 1-27	27-16n-2E	X(4905)	4886	0.5		4956.5	4956	53 cored *69 log*					15*					x	x		x	x	x	x	x	x			x	x		X			X					X	
26	6281	Chandler SWDW #1 33	5-14N-3E	X(4810)	4797.5	3.3		X(4869.8)	4865	59.8 cored *68 log*					14*					x	x		x	x	x	x	x	x	x		x	x		X	x		X					X	
27	6302	Stevenson 1-14 NW	14-15N-1E	X(5143)	5103	2		X(5167.6) 5188L	5186	24.6 cored *85 log*					7					x	x		x		x	x	x	x			x	x										X	
28	6563	W Carney Ext SWDW # 2 NW	10-15N-1E	X(5140)	5135	6		X(5232) 5275L	5271	92 cored *135.5 log*										x	x		x		x	x	x	x			x	x										X	

Wk = Work status (Core description), C = Completed; IP = In Process; PC = Porosity Codes.
TS = Thin Sections,# made, * described ; SEM = Scanning Electron Microscopy, Cono = Conodont micropaleontology, # of samples, * completed
UH = Core Plug samples at Univ. Houston; Wett = Wettability Analysis,
Hg Inj = Mercury injection porosimetry
Numbers in front of Well Name is StimLab well Identification Number

* Mercer not logged, but 75' offset (WFC Petroleum # 1-28 Cruse) was logged (N-D, Sonu;lateral og - same thickness - 80') -Sandeep to digitize, Import digitized log data for Cruse 1-28 into Mercer 1-28

Conodont studies have now been completed on 14 wells, the 13 shown in the figure “Wells with Conodont Studies”, (Figure 7) and the Saunders, which only yielded indeterminate material to date. The data from the two wells outside the field, the Mercer to the north and Chandler SWDW to the southeast and additional data within the field shows that the original simple stratigraphic model was generally correct, but far more complex than initially envisioned.

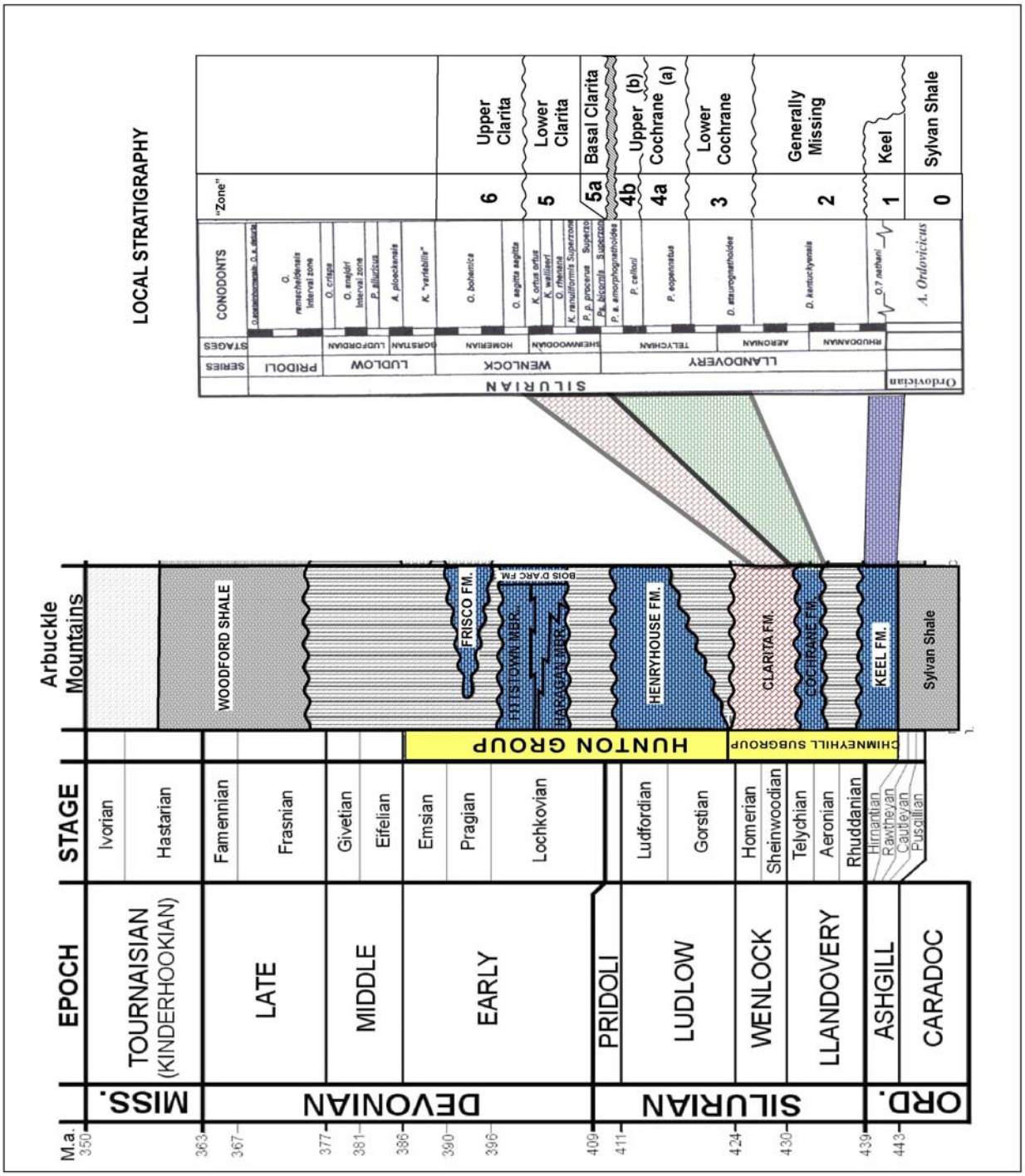

Figure 7: Stratigraphic Chart For Hunton Group, comparing Arbuckle Mtn. Sequence (modified from Stanley, 2001, fig 2)[4], with WCHF sequence, by Barrick and Derby.

Stratigraphic Interpretation

Figure 7 shows the new stratigraphic classification developed for the field, with comparison to the Hunton outcrop in the Arbuckle Mountains. These new subdivisions are displayed in the field cross-section (Figure 6). Figure 8 summarizes the conodont data upon which the interpretation is based, and also shows which zones are present on the outcrop. New information includes: recognition of the Keel Formation in the Morrow well, subdivision of the Upper Cochrane into two units, informally designated A and B, that correlate with two separate sea level highstands, and recognition of both shallow and deep water facies and faunas in most units. It should be noted that the Hunton units in WCHF are quite different lithologically from the units that crop out in the Arbuckle Mountains. In addition, the two upper Cochrane units are not present on the outcrop, whereas the upper Clarita is present on the outcrop but not present in WCHF (Figure 7).

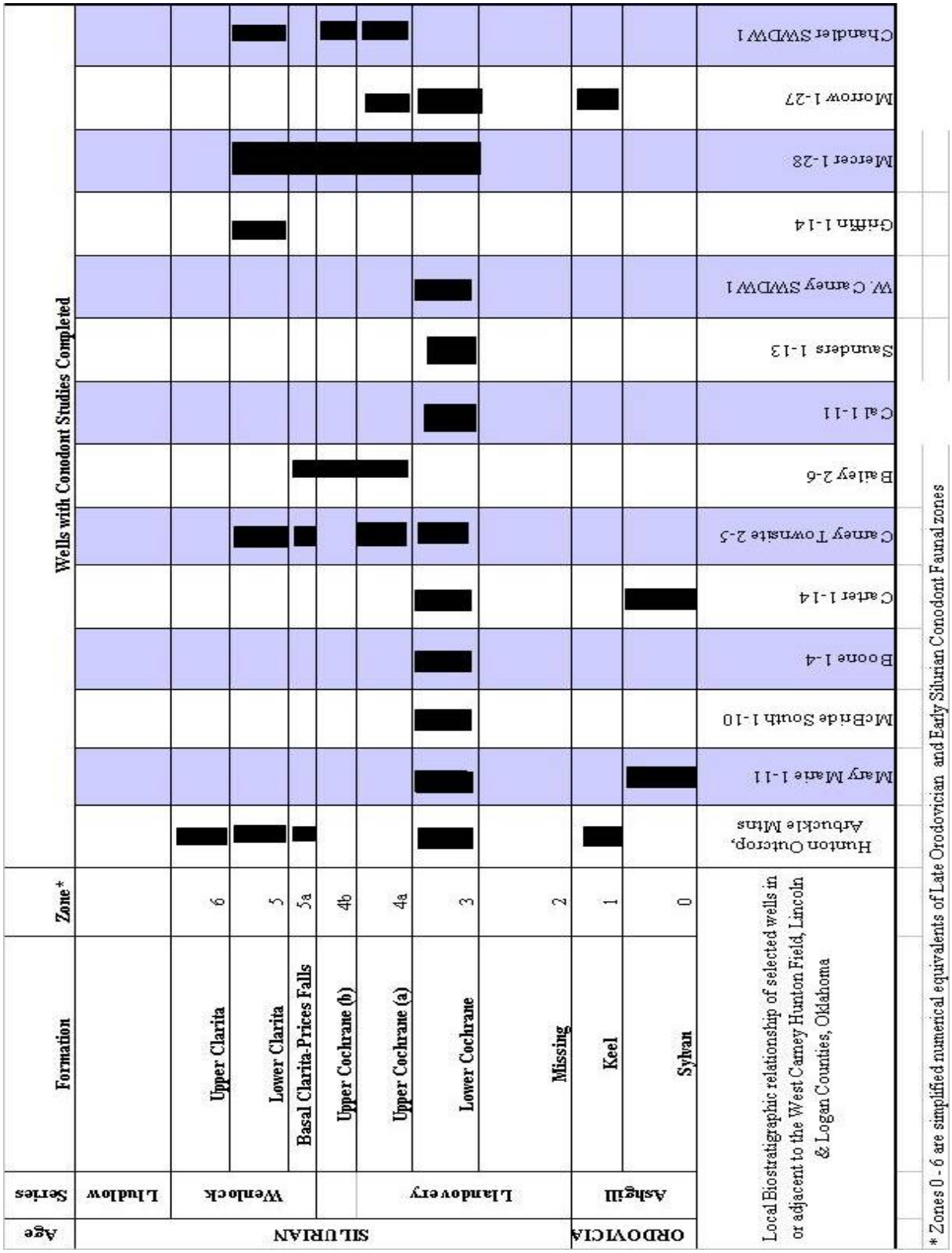

Figure 8: Wells With Conodont Studies

Critical to understanding the stratigraphy of WCHF is recognition that the lithostratigraphic units are sequences formed during 5 cycles of sea level change from lowstand to highstand during the late Ordovician and earliest Silurian. (See Figure 9; from Johnson, 1996)[2]. The bathymetric changes produced a complex of depositional and diagenetic facies that directly affects the development of reservoir facies in the Hunton Group. Each depositional sequence is unconformably separated from the super- and subjacent sequences; consequently subaerial exposure of each sequence caused extensive diagenesis and karsting immediately following deposition. Additionally, most sequences have both a shallow-water and a deep-water facies, we are in the process of defining these sets of facies and their faunas.

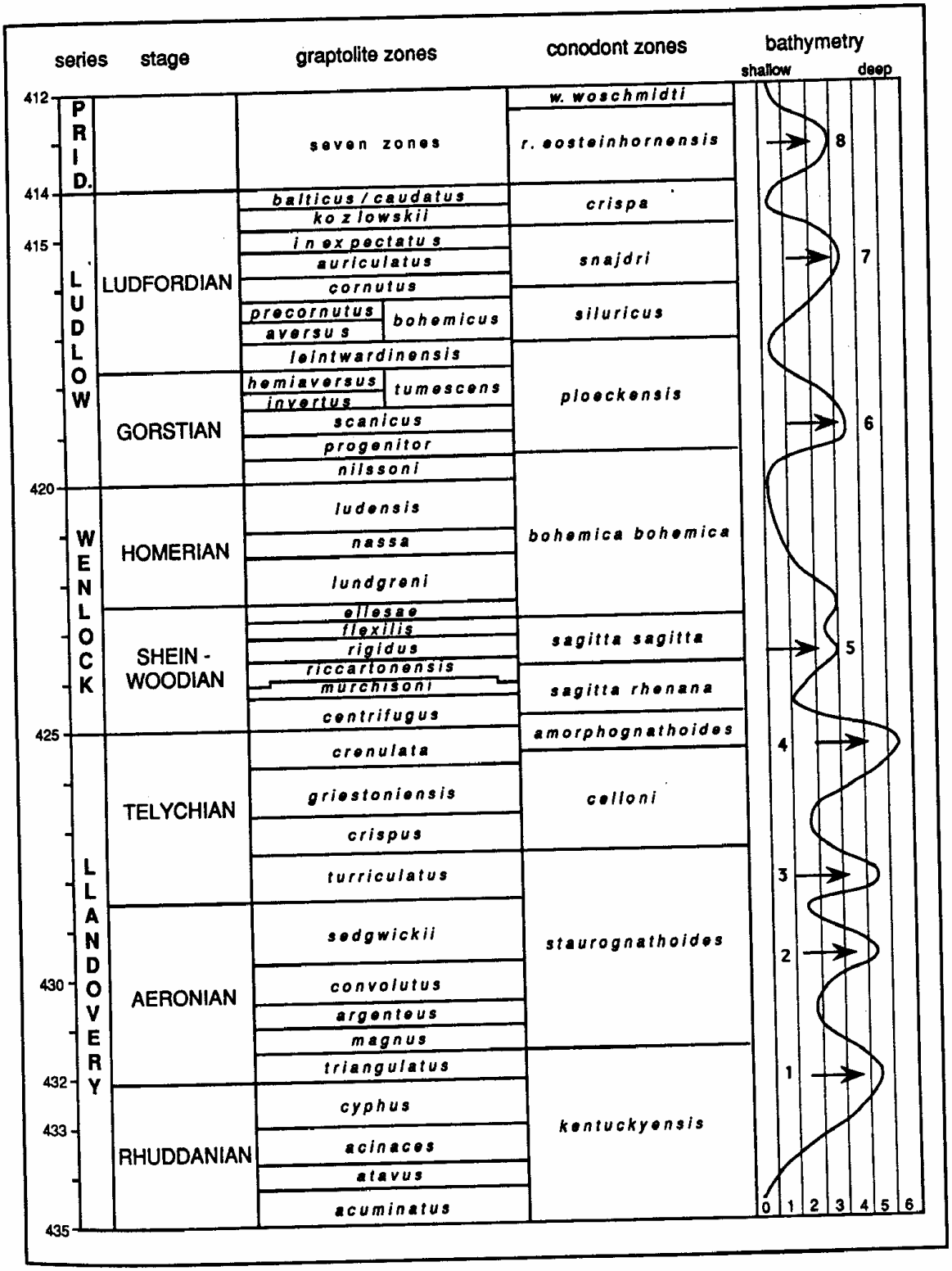

Figure 9: Silurian Sea Level Curve (from Johnson 1996, fig 1)[2]

Description of 14 cores and conodont analyses of 8 wells was included in the Final Report for Budget Period I. Revised descriptions of two of those 14, the Bailey and the Carney Townsite, and updated conodont sample results are repeated the Appendix following, to show the new stratigraphic classification resulting from more complete paleontological studies. These data demonstrate a more complex stratigraphy and structure than previously envisioned.

Structural Control?: Marjo Bailey and Thick Altex Wells

The Bailey is the only Marjo well that lies in a trend of thick Hunton (81 to 100 feet in thickness) in an area largely drilled by Altex.in the eastern part of the field. The Bailey appears anomalous compared to other Marjo wells (Figure 10), but should be compared rigorously to the logs of these thick Altex wells, and that set then compared to the thinner sequences of Hunton both west (*e.g.* Marjo Mary Marie) and east (*e.g.* Marjo Carney Townsite). Perhaps much of this thick section is the Upper Cochrane B unit only found in shallow water facies in the Bailey of the Marjo wells. The stratigraphic relationships shown in Figure 10 are impossible without structural movements to provide accommodation space for deposition of thicker sections relative to adjacent areas. The shape of the thick isopach suggests a northwest trending basement graben creating a localized thick trend in the Hunton.

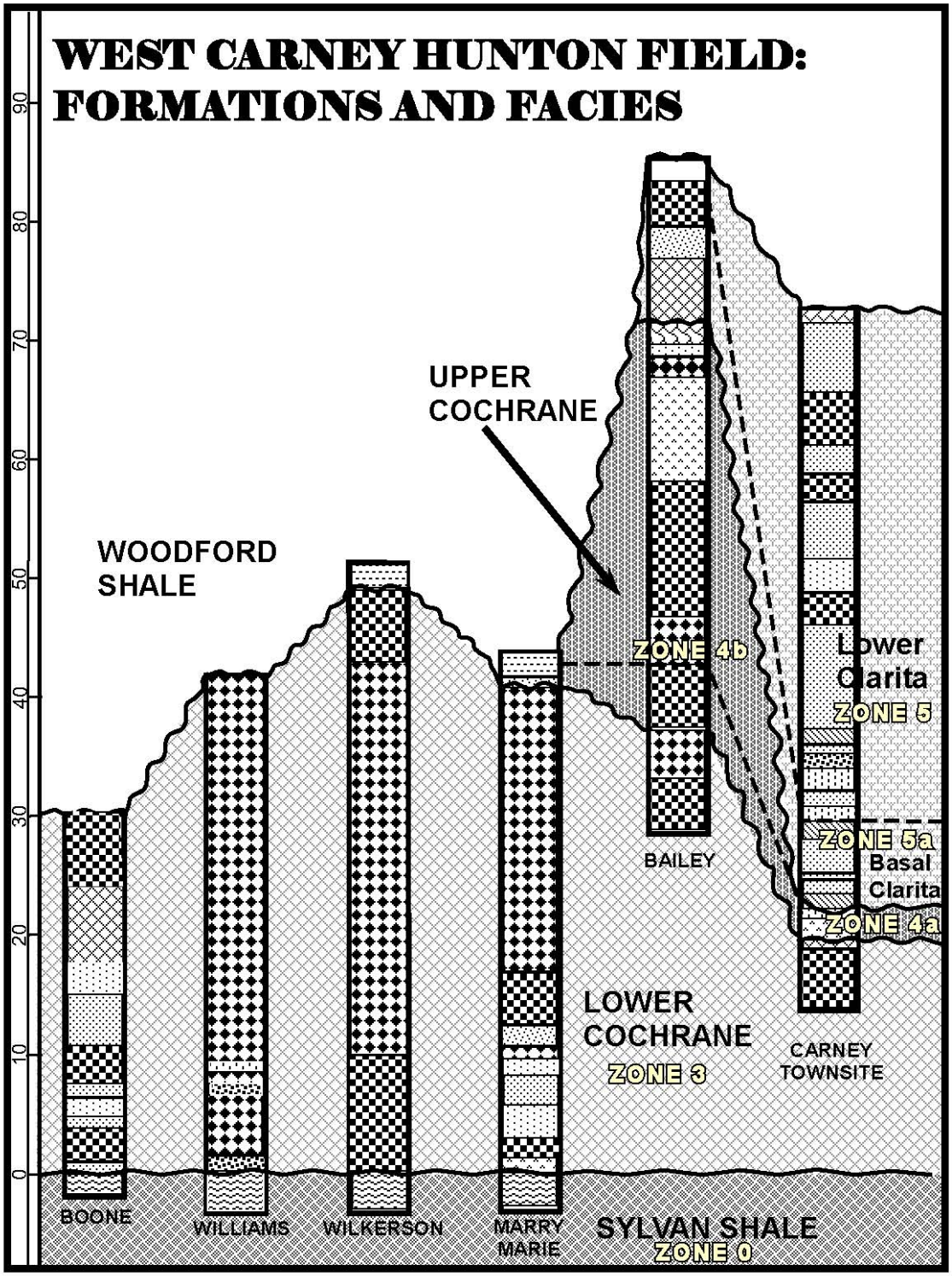

Figure 10: 6-well Cross-section comparing Carney Townsite and Bailey wells to central field wells.

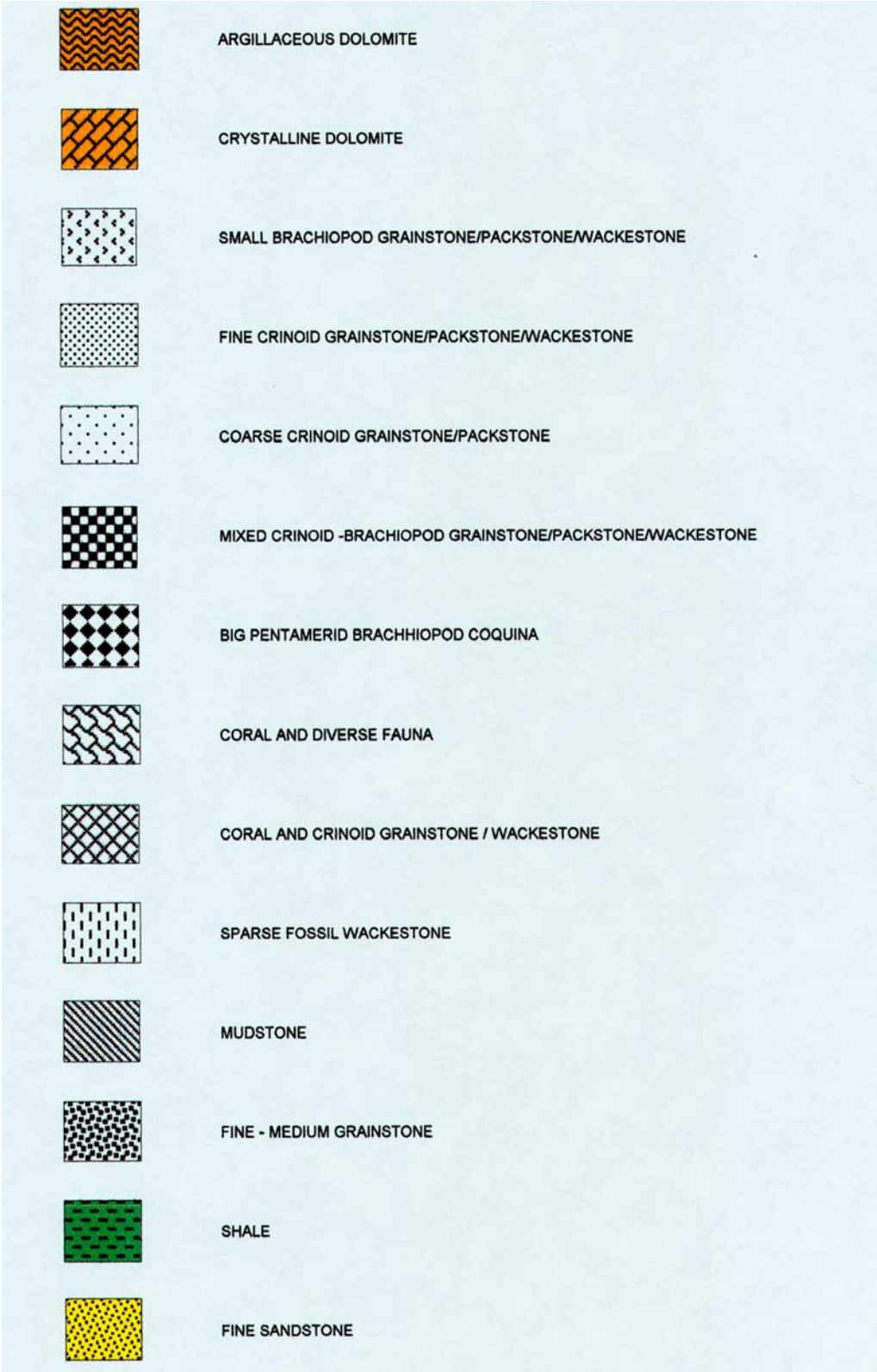

Figure 11: Explanation for Facies Type Symbols in Figure 10

Stratigraphic Revisions

Preliminary core descriptions of the Mercer and the Chandler SWDW cores, as well as for the Cal, Morrow, and Saunders wells are included in Appendix A. Also included are the revised descriptions of the Bailey and Carney Townsite wells, which include the revised formation boundaries. Details of the conodont analyses for 3 additional wells, the Mercer, Chandler SWDW, and Morrow, and updated tables for the Bailey and Carney Townsite are given in the individual Conodont Sample tables (Appendix A).

The Mercer, Chandler, and basal Cal contain shaly lime mudstone and siliciclastic shale sequences that are not present in the WCHF central portion. Our preliminary interpretation during Budget Period I was that the shaly intervals recognized on well logs from outside WCHF represented the Prices Falls Member of the Clarita Formation (see Figure 6). This is simply not true in the Chandler and Cal, and only partly true in the Mercer.

In the Chandler, the Clarita is entirely in a dolomite grainstone facies with much dissolution (moldic) porosity. The dolomite extends downward into the Upper Cochrane for at least 5 feet, in what I interpret to be "Diagenetic Terrain" facies (as defined by Roehl, 1967)[3]. No Prices Falls has been identified in this well, sample spacing is so close that only 1.4 ft is the possible thickness of a Prices Falls unit. Limy shale and nodular shaly limestones extend downward into units identified as Upper Cochrane B and Upper Cochrane A.

In the Mercer, six feet of Lower Clarita dolomite is underlain by 12 feet of porous, gilsonitic and oil stained, dolomite grainstone containing a Prices Falls conodont fauna. Beneath is the Upper Cochrane B, 20.1 ft thick, consisting of pale brown burrow-mottled shaly limestone with sparse crinoids and small brachiopods. At the base is 4.7 feet of limy shale and shaly lime mudstone containing 2 intervals of abundant small fossils, dominantly crinoids. The underlying Upper Cochrane A (9.4 feet) and Lower Cochrane (6.7 feet cored) contain interbedded light-colored nodular shaly lime mudstones, light green limy shales, and dark-gray, apparently organic rich shales.

The Cal has not yet been described in detail nor its conodont fauna fully picked and analyzed, however its position relative to the West Carney SWDW #1 and conodont results to date suggests that the core is in the Lower Cochrane interval. The shaly nodular limestone facies is probably a deeper-water facies, analogous to facies zone 4 or 5 of Stanley, 2001, (see Figure 12) deposited during the initial flooding event and prior to establishment of the Lower Cochrane grain–supported carbonate bank that grew to over 100 feet in thickness less than one mile away.

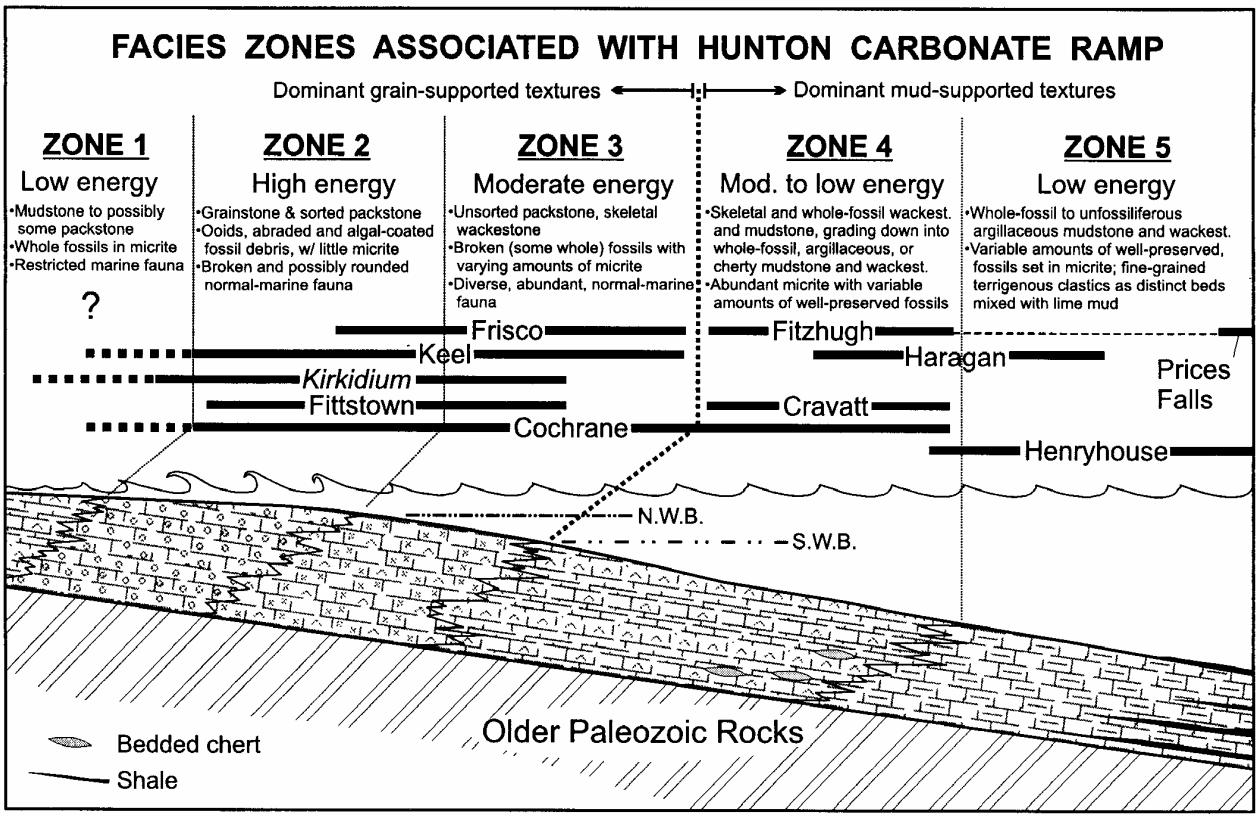

Figure 12: Idealized Standard Facies Model For Hunton Group (from Stanley 2001, fig. 6)[4]

My preliminary hypothesis is that these interbedded sequences are off-bank condensed sequences representing both highstand (dark, laminated, organic-rich shales) and lowstand (light-colored, burrowed, local "birdseye" calcite) depositional environments. Conodont faunas (see below) confirm the presence of a deeper water facies. In terms of the facies zones described by Stanley (2001), these would be Zones 1 and 5. (Figure 12) However, the spatial distribution of the facies in the WCHF area suggests that a modified platform model, as opposed to a ramp model, may be more applicable to WCHF (see Figure 13). In this model, the light-colored muddy carbonates are deposited in the quiet peritidal waters during extreme lowstand., while the thick shell banks of the central part of WCHF (Final Report, Budget Period I) are deposited in somewhat deeper water on the platform during highstand. The dark-colored shales and shaly limestones are deposited in deep water, during sea level rise, either off bank, or prior to bank/platform development.

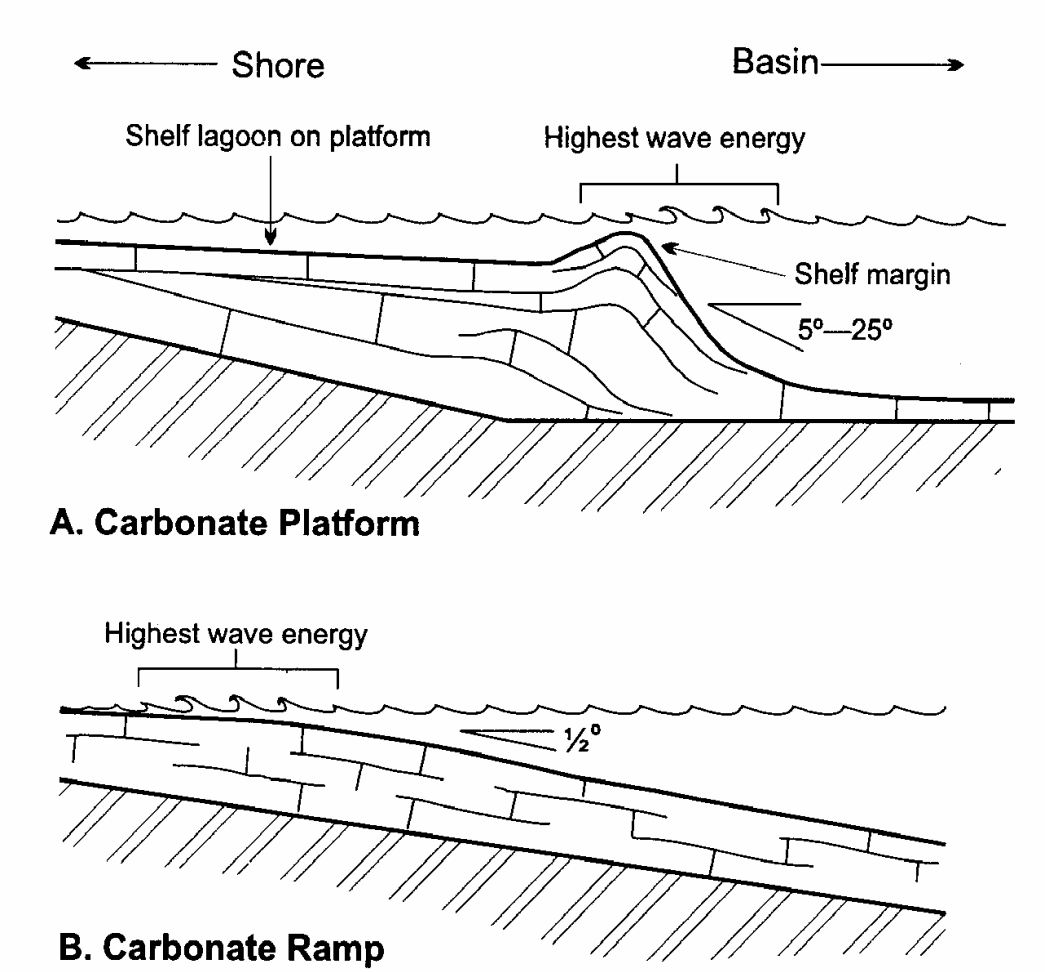

Figure 13: Comparisons Of Carbonate Platform Vs Carbonate Ramp Models (from Stanley 2001, fig 4)

Clearly the depositional model and, therefore, the diagenetic model for WCHF is being continuously modified as new data is obtained.

Petrography

One hundred forty (140) thin sections and 5 Scanning Electron Microscope (SEM) from 12 wells have been studied for this project. Representative thin section samples are being taken from each well as it is processed. Ideally the thin sections are available for study at the time of describing the well, so that different rock types and porosity systems can be accurately characterized at the first pass. In many cases, however, the process is iterative. It is not clear where thin sections are needed until the core is examined in detail under low power magnification, and then the high magnification examination of the thin sections reveals features that must be re-examined in the core at low magnification.

We are in the process of redescribing the existing 140 thin sections, and having additional thin sections made, primarily on undescribed wells, or in intervals lacking microscopic work. This work, which demands good visual acuity, has been delayed while the principal investigator in this field has had his lenses replaced.

Thin section and SEM work has revealed that the major porosity systems in the WCHF are secondary, that is they are the result of dissolution of original rock fabric. Even in cases where the pore systems appear to be primarily intergranular or intercrystalline suggesting that the porosity might be primary, examination shows that it is dissolution of fine matrix between grains, or dissolution of pre-existing cement that creates the existing porosity.

The following illustrations are selected to demonstrate the variety of pore systems present in WCHF, in a variety of rock types. These photos make it clear that pore geometry in WCHF is extremely complex. In general pore systems are extremely variable in the wackestones through grainstones of the Cochrane, and much more uniform and predictable in the dolomitized grainstones and packstones of the Clarita. In one well, the Carter, thin section analysis demonstrates that an interval that calculates a high Sw and has no fluorescence has more than adequate porosity and permeability and, therefore, must be "wet" in the conventional sense.
Most other "wet" appearing intervals in the field are holding bound water due to fine pore throats, or have such fine pore throats as to preclude entry of hydrocarbons during generation and migration.

Figures of thin sections and SEM photos follow:

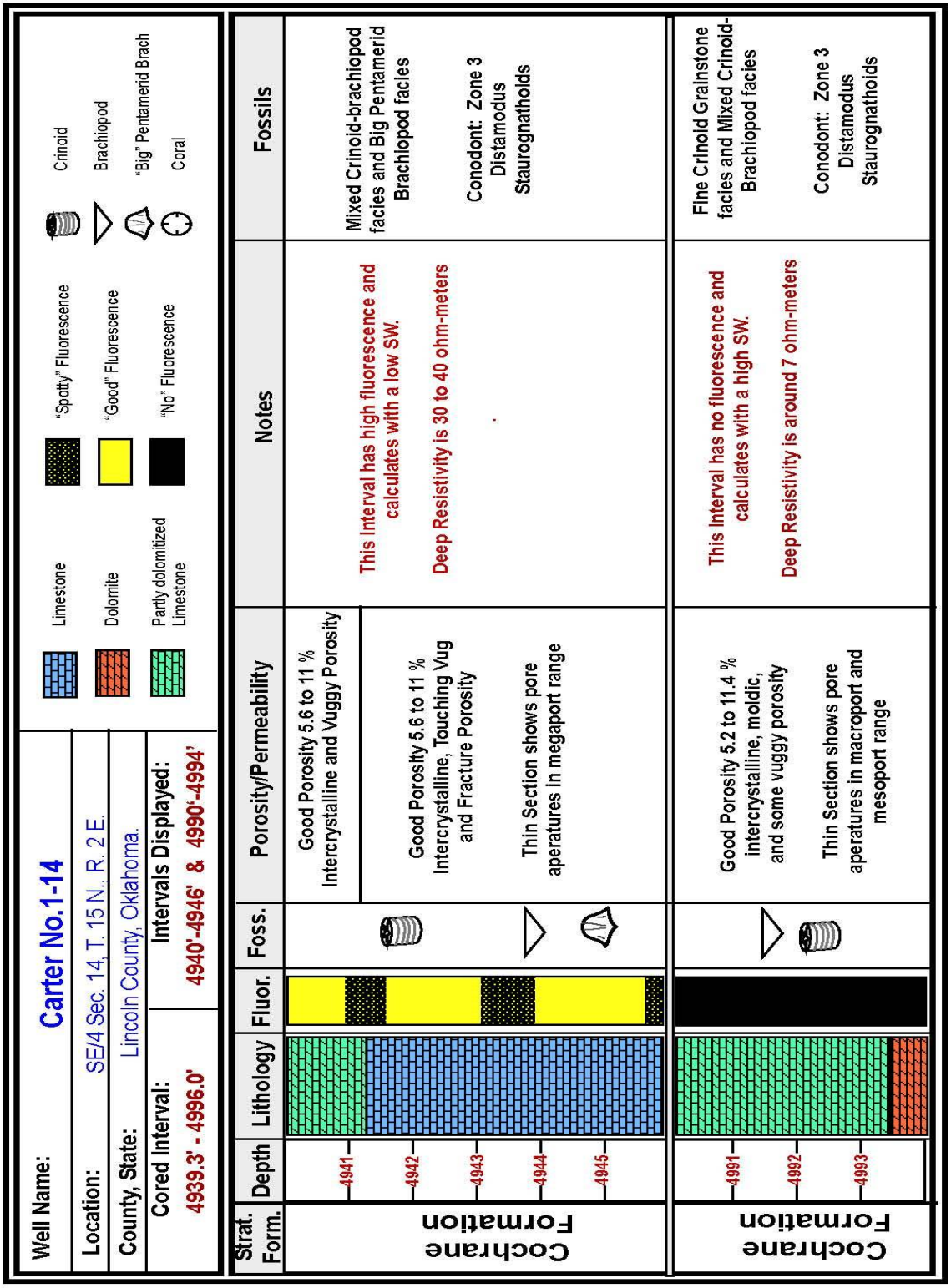

Figure 14: Core graphic of selected intervals of the Carter 1-14

Marjo Carter 1-14, SE-14-15N-2E, Lincoln Co., OK. Cochrane Fm.

The Carter is one of the few wells that displays a high Sw and no fluorescence in pore systems that higher in the well have low Sw and good fluorescence. It appears there is a true oil/water contact in this well, unlike most wells in the field. The Carter also lies SE of a fault cutting the east side of the field, and exhibited very low initial pressure.

4940 - 4946' Good porosity, 5.6 to 11.0 %, in dolomite with intercrystalline and vuggy porosity, and limestone with intergranular, touching vug, and fracture porosity. This interval has high fluorescence and calculates low Sw. Deep resistivity is 30-40 ohms. Facies are the Mixed Crinoid-Brachiopod facies and the Big Pentamerid Brachiopod facies.

4990 – 4994' Good porosity, 5.2 to 11.4%, in limestone and partially dolomitized limestone with intergranular and some vuggy and moldic porosity. This interval has no fluorescence and calculates high Sw. Deep resistivity is about 7 ohms. Facies are Fine Crinoid Grainstone and Mixed Crinoid-Brachiopod Grainstone.

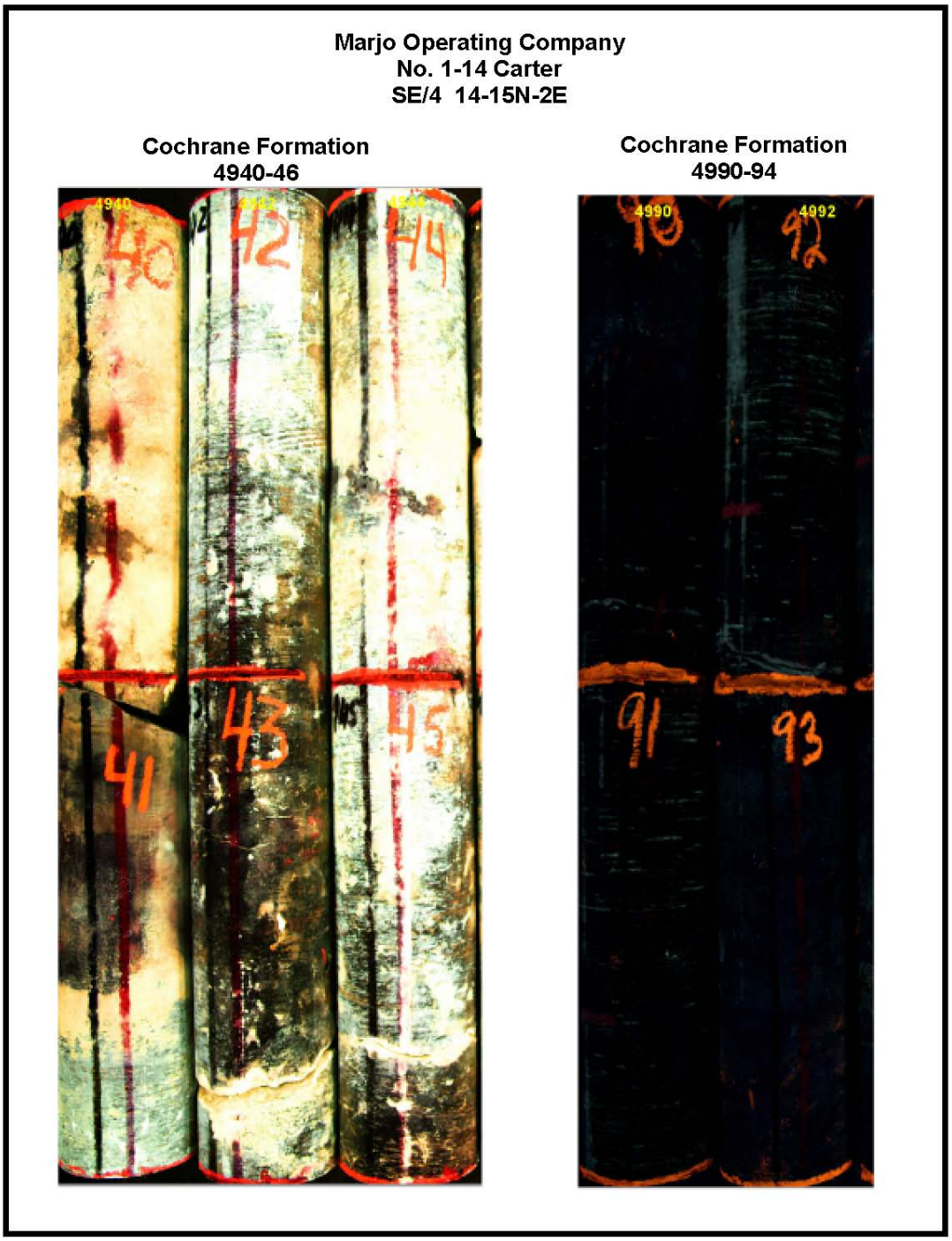

Figure 15: Whole core fluorescence photograph of the above captioned intervals in the Marjo Carter 1-14

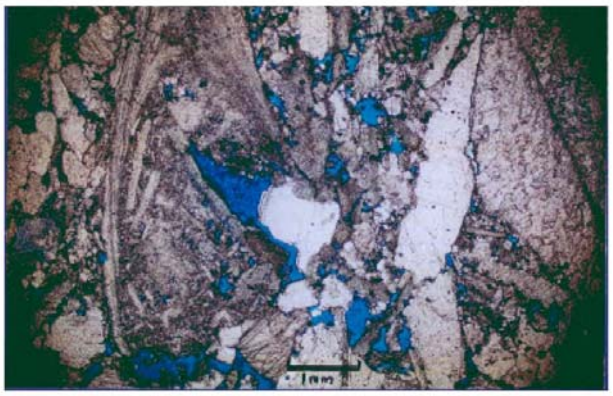

Marjo Operating Company No. 1-14 Carter
Depth : 4945.1 Porosity: 9 %
Facies: Coarse Brachiopod grainstone
Scale bar = 1 mm, X18

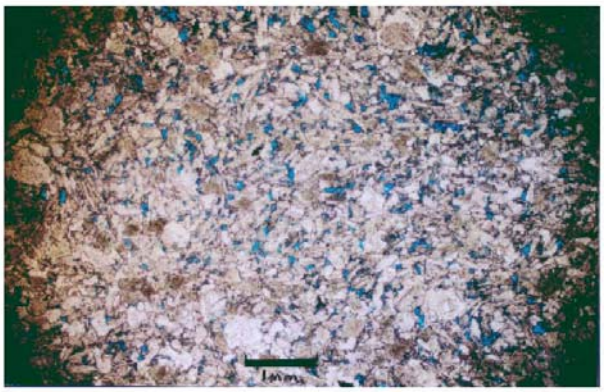

Marjo Operating Company No. 1-14 Carter
Depth : 4991.3 Porosity: 10 %
Facies: Medium crinoid brachiopod grainstone
Scale bar = 1 mm, X18

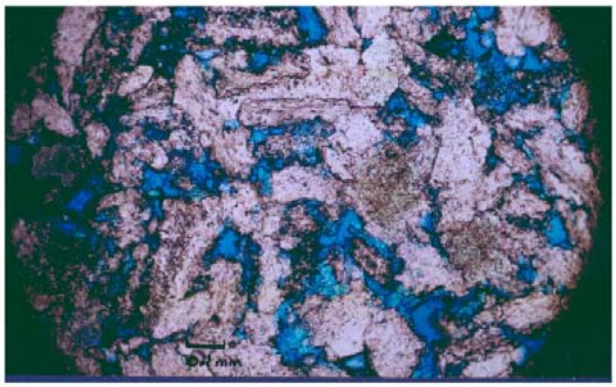

Marjo Operating Company No. 1-14 Carter
Depth : 4991.3 Porosity: 10 %
Facies: Medium crinoid brachiopod grainstone
Scale bar = 1 mm, X89

Figure 16: Thin section photos from Carter 1-14

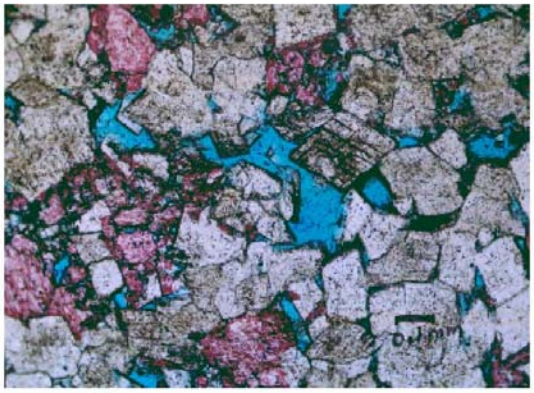

Marjo Operating Company No. 2-4 Carney Townsite
Depth : 4924.3 Porosity: 15%
Facies: medium crystalline calcitic dolomite
Scale: bar = 0.1 mm, X89

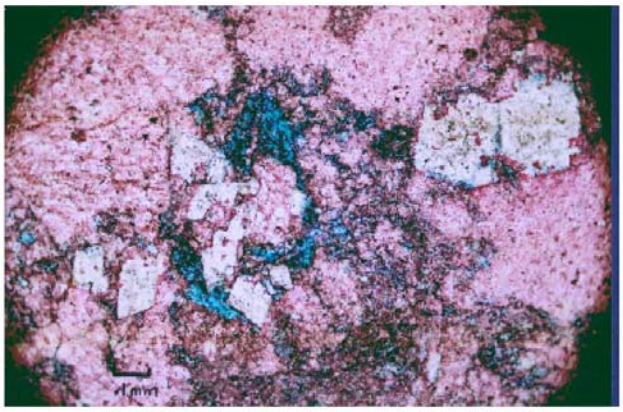

Marjo Operating Company No. 2-4 Carney Townsite
Depth : 4931.3 Porosity: 5%
Facies: Partly dolomitized crinoid packstone
Porosity by dissolution of matrix
Scale: bar = 0.1 mm, X89

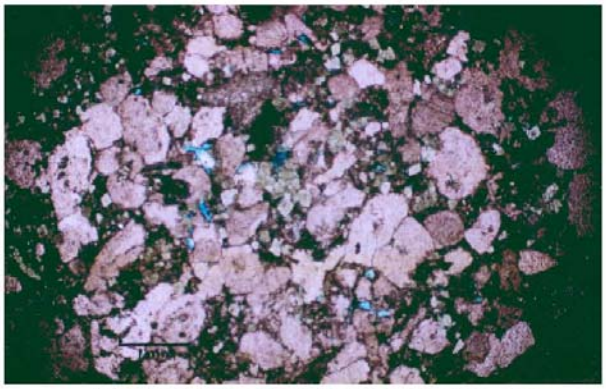

Marjo Operating Company No. 2-4 Carney Townsite
Depth : 4931.3 Porosity: 5%
Facies: Partly dolomitized crinoid packstone
Porosity by dissolution of matrix
Scale: bar = 0.1 mm, X18

Figure 17: Thin section photos from the Carney Townsite 2-4

Marjo Carney Townsite 2-5, NW-5-15N-3E, Lincoln Co., OK. Clarita Formation

This figure is the only one of two examples, in this report, of the good dolomite porosity in the Clarita Fm. The upper 34 feet of this well has good porosity, good oil saturation and strong fluorescence throughout. Vuggy porosity is developed in coarsely crystalline dolomites and dolomitic limestones, originally fine to coarse crinoid grainstones and packstones, locally with minor brachiopods. The Clarita overlies the Upper Cochrane Fm at 4957 feet, and the Lower Cochrane at 4962 feet.

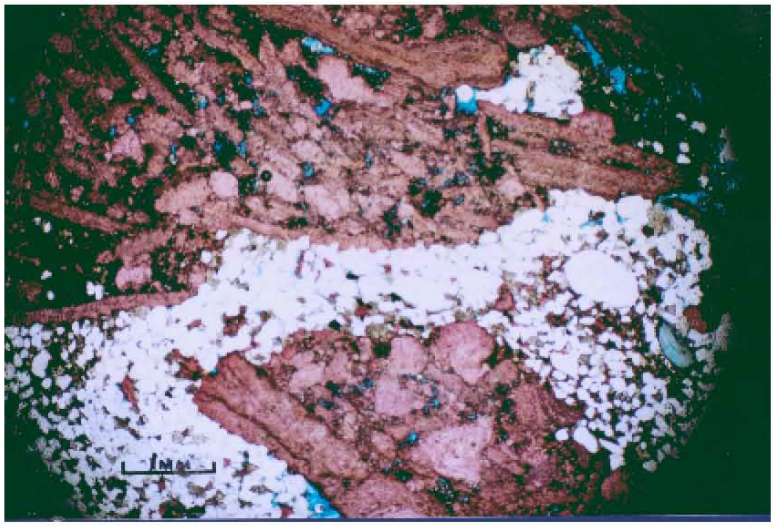

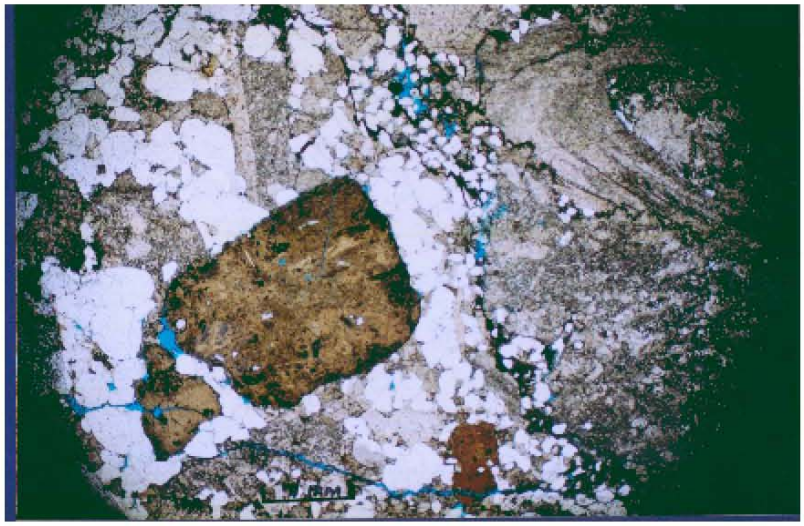

Marjo Operating Company No. 1-3 Wilkerson
Depth : 4953 Porosity: 7 %
Qrtz Sand and Phosphate, from Misener, filling karst
cavity in brachiopod packstone
Scale: bar = 1 mm, X18

Figure 18: Thin section photos from the Wilkerson 1-3

Marjo Wilkerson 1-3, NE-3-15N-2E, Lincoln Co., OK. Woodford, Misener and Cochrane Fm.

This core displays good porosity, oil saturation and fluorescence in porous zones developed in limestones of the Big Pentamerid Brachiopod Facies. Major vuggy porosity and good permeability is interspersed with tightly cemented zones. The Woodford/Misener contact at 4952.4 and the Misener/Hunton (Cochrane Fm) contact at 4953.4 feet are displayed. Note the karst dissolution in the upper part of the Hunton; fissures and cavities are filled with Misener sand as shown by these thin sections.

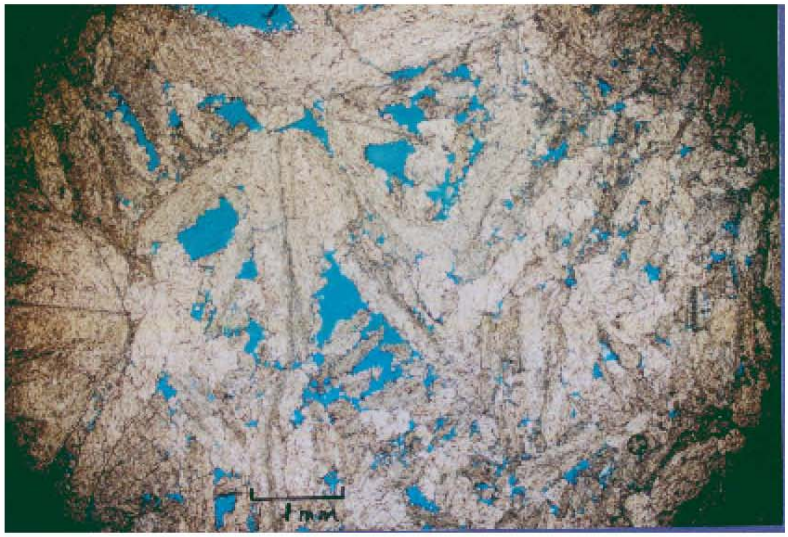

Marjo Operating Company No. 1-11 Mary Marie
Depth : 4478.3,
Medium crystalline dolomite with vuggy and fossil moldic porosity
Scale: bar = 1 mm, X18

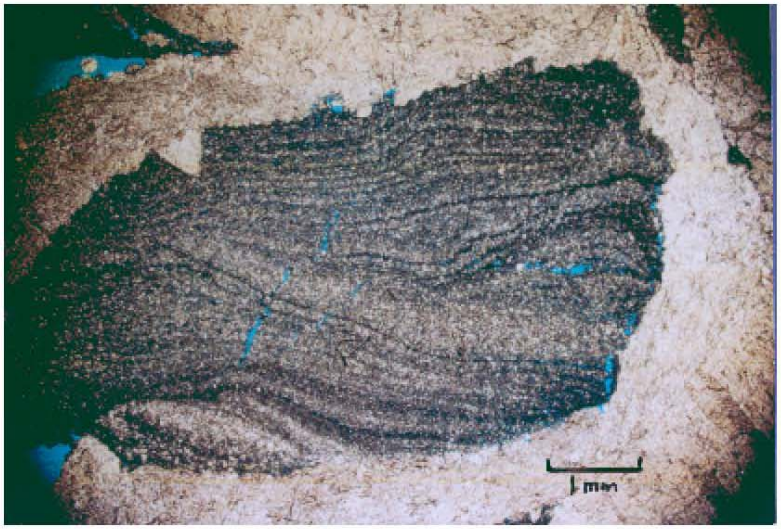

Marjo Operating Company No. 1-11 Mary Marie
Depth : 4981.8
Laminated karst silt, very fine quartz fills a microcavern in the Lower Cochrane
Scale: bar = 1 mm, X18

Figure 19: Thin section photos from the Mary Marie 1-11

Marjo Mary Marie 1-11, SE-11-15N-2E, Lincoln Co., OK. Cochrane Fm.

Like many of the wells in the center of WCHF, the Mary Marie is dominated by the Big Pentamerid Brachiopod facies, and displays both tightly cemented zones and extremely good porosity developed by dissolution of matrix and cement as shown here. Also shown is a common karst feature in the field, a large vug or micro-cavern, completely filled with siliclastic karst silt, derived from the overlying Misener Formation.

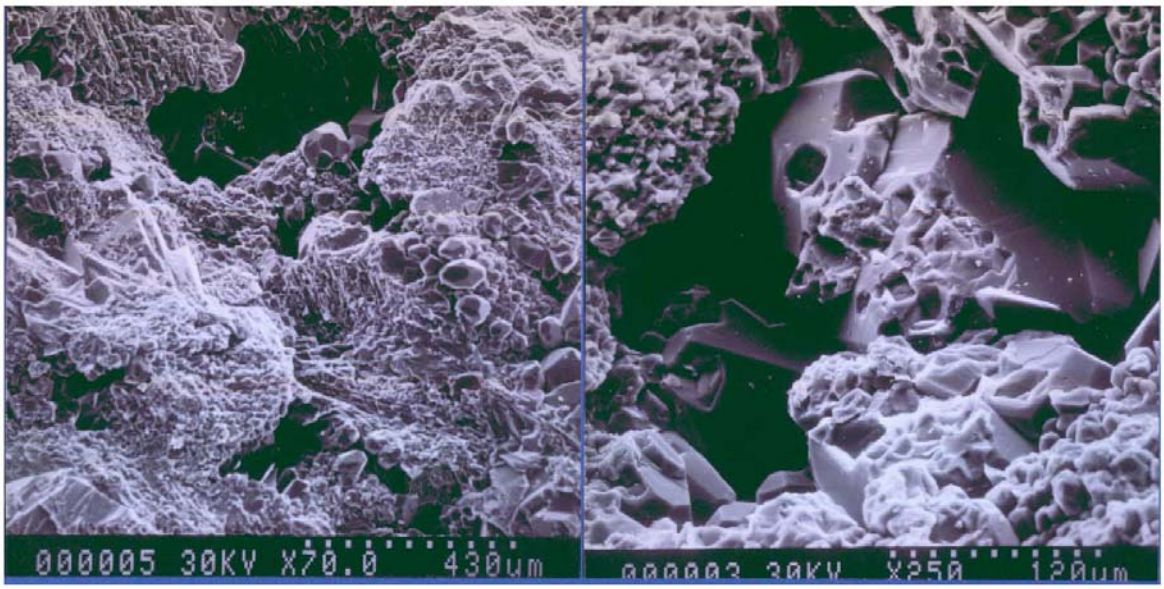

Marjo Operating Company No. 1-11 Mary Marie
Depth : 4966.5, Cochrane Formation
Large secondary dissolution pore surrounded by calcite cement
Scale: X70

Marjo Operating Company No. 1-11 Mary Marie
Depth : 4966.5, Cochrane Formation
Large secondary dissolution pore partly filled by blocky calcite. Pitted surfaces are evidence of subsequent dissolution
Scale: X250

Figure 20: Scanning Electron Microscope photos from the Mary Marie 1-11

SEM studies in the Mary Marie illustrate the dissolution of both grains and cement seen in thin sections.

Marjo Operating Company No. 1-4 Boone
Depth : 5051.1 Porosity: 7 %
Facies: Coarse crinoid packstone
Scale: bar = 1 mm, X18

Figure 21: Thin section photos from the Boone 1-4

Marjo Boone 1-4, SE-4-15N-2E, Lincoln Co., OK. Cochrane Fm.

This core displays good porosity, strong fluorescence, and logs calculate a low Sw. This well is dominated by Crinoid Facies, and totally lacks the pentamerid brachiopod coquina. This exemplifies the rapid lateral facies changes common in WCHF. Intergranular and intercrystalline porosity systems in partially dolomitized limestone were enhanced by dissolution of mud matrix and sparry cement, as shown in this thin section. Also visible are the clear calcite spar overgrowths on the crinoid grains.

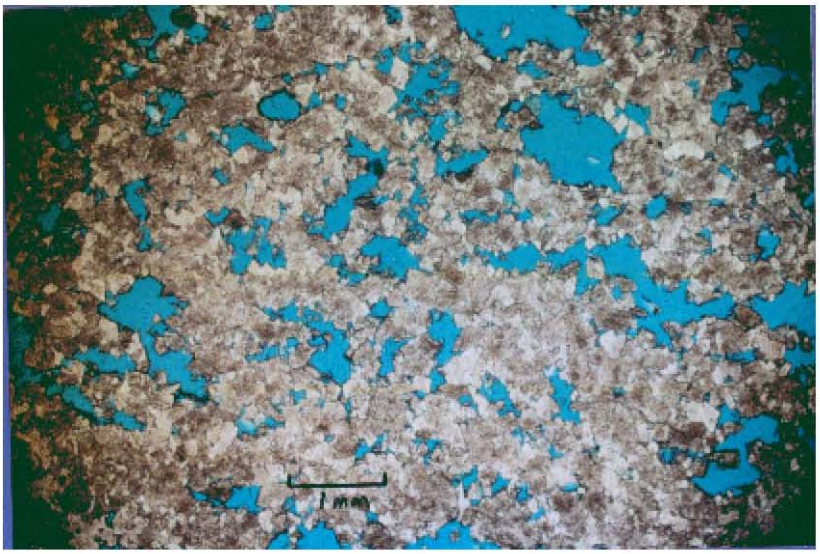

Marjo Operating Company No. 2-6 Bailey
Depth : 4478.3
Facies: Medium crystalline dolomite, with
vuggy and fossil moldic porosity
Scale: bar = 1 mm, X18

Marjo Operating Company No. 2-6 Bailey
Depth : 4916.3, No Porosity
Facies: Brachiopod Packstone
Fine Matrix completely fills brachiopod shell. Collapsed and compacted brach grains below
Scale: bar = 1 mm, X18

Figure 22: Thin section photos from the Bailey 2-6

Marjo Bailey 2-6, SW-6-15N-1E, Lincoln Co., OK, Clarita and Upper Cochrane Fm.

The upper photo illustrates excellent porosity and permeability developed by both dolomitization and dissolution in a crinoid-brachiopod grainstone. Core analysis of the (mislabeled sample) interval 4878-4879 shows 16.9 % porosity and 1002 md K90 permeability. Both fossil moldic and intercrystalline porosity are present. Basal Clarita (Prices Falls equivalent), Zone 5a at 4878.3 core depth.

The lower photo is a coarse brachiopod wackestone in which the original porosity is completely filled with fine matrix, and solution collapse and compaction has destroyed porosity in the grainstone underlying the big brachiopod shell. By core analysis, porosity is 1.1 %, permeability is 0.06 md. Upper Cochrane B, Zone 4b at 4916.3.

Paleontology

This section provides a summary of work to date in Budget Period II on conodont faunas of WCHF, adapted and modified from a memo by Dr. James Barrick of Texas Tech University, August 25, 2003. After a discussion of each faunal unit, the samples containing that fauna in each studied well are listed.

Keel Faunas

"Zone 1" : The Keel is characteristically a thin oolitic unit at the base of the Hunton, containing an Ordovician to earliest Silurian fauna (Amsden and Barrick, 1986)[1]. It has been recognized only in one 0.9 ft interval of oolitic grainstone and packstone at the bottom of the Morrow core. Its conodont fauna contains definite Ordovician elements, but lacks the characteristic Hirnatian fauna.

Cochrane Faunas

"Zone 3": The majority of core samples assigned to this unit contain conodont elements that can be assigned to a mid-Llandovery conodont fauna that comprises shallow to deeper water biofacies. It is correlated with the Cochrane that crops out in southern Oklahoma. The most typical biofacies is dominated by an *Oulodus* species with robust elements, *O. sigmoideus*, and robust elements of *Panderodus unicostatus*, as used in the broadest sense. This assemblage is characteristic of brachiopod-rich beds and associated carbonates. The *O. sigmoideus* biofacies grades into a mixed biofacies that includes *Aulacognathus* sp. A, *Distomodus staurognathoides, Panderodus recurvatus* (in the broadest sense), *Walliserodus* sp., *Asplelundia fluegeli,* and rare *Rexroadus kentuckyensis and Pseudooneotodus tricornis.* In argillaceous carbonates deposited in the deeper, more quiet water settings, the biofacies becomes dominated by *Asplelundia fluegeli,* and a diverse coniform fauna including common *Decoriconus fragilis* and *Dapsilodus praecipuus,* in addition to *Panderodus* and *Wallisderodus* species. *Ozarkodina clavula* is rare, and *Oulodus sigmoideus* is uncommon.

The presence of *Distomodus staurognathoides* in many samples places a firm lower age on the fauna; it is no older than Aeronian C_2. The presence of *Ozarkodina clavula* at the base of the Silurian section in the CAL well restricts the age of the base of the section to no younger than C_2. The ranges of other taxa, *Oulodus sigmoideus, Asplelundia fluegeli, Rexroadus kentuckyensis*, and *Aulacognathus* sp. A, all suggest a late Aeronian age C_2, perhaps extending up into C_3 for the biofacies assemblages. Amsden had earlier assigned a C_2 age to the outcrop Cochrane based on brachiopods, as well as to the "Brassfield limestone" of the Cason Shale in Arkansas, the conodont fauna of which includes *Ozarkodina clavula.*

[Mercer 13, 12, 17; CAL 5135-5034 (*not all analyzed); Morrow 4956 up through 4919 (*not all analyzed); Mary Marie all?; Boone all?; Carter all?; Carney SW ext all?; Carney Townsite 4965-4964]

"Zone 4a": A slightly younger fauna occurs in some cores of the Cochrane interval. The most characteristic feature of the fauna of "Zone 4a" is the replacement of *Oulodus sigmoideus* by *Ozarkodina polinclinata*. Elements of P*anderodus unicostatu*s comprise a greater proportion of the fauna and robust elements of this species may be the only conodonts present in samples from high-energy settings. Elements transition to and including *Aulacognathus kuehni* occur with *Oz. polinclinata*. The appearance of *Ozakodina polinclinata* and *Aulacognathus kuehni* places this fauna in the *eopennatus* Zone, even in the absence of the nominate species. The *eopennatus* Zone fauna occurs with graptolites of the early to middle Telychian *turriculatus* to *griestoniensis* zones, which should correspond to Telychian C_4 toC_5.

[Chandler 14, 13, 12, 11, 10; Mercer 16, 11, 10, 9; Bailey 2-6 4921-4919; Morrow 4906 (*not all analyzed); Carney Townsite 4962-4958]

"Zone 4b": Fauna 4b lies at the top of the "Cochrane" interval and includes a shallow water biofacies and a deeper water facies. The shallow water facies in the Bailey 2-6 well is characterized by the occurrence of *Pterospathodus amorphognathoides angulatus*, which appears at the base of the *Pt. celloni* Zone. Some specimens may be transitional to *Pt. am. lennarti*, which would indicate a middle *celloni* Zone assignment and a few *Pt. celloni* are present. The fauna is dominated by an abundant, but undiagnostic coniform association: *Panderodus unicostatus, P. recurvatus, Walliserodus* sp., *Dapsilodus praecipuus*, and *Pseudoonetodus tricornis.* Elements of *Ozarkodina polinclinata* and *Oulodus petila* occur infrequently. The deeper water biofacies was recovered from argillaceous limestones in the Mercer and Chandler wells. This biofacies contains abundant *Pt. celloni,* as well as less common *Pt. am. angulatus* and *Pt. am. lennarti. Distomodus staurognathoides, Ozarkodina polinclinata, Oulodus petila, Apsidognathus* sp. and a diverse coniform association are present. "Zone 4b" is approximately C_5 in age; *spiralis* graptolite Zone.

[Chandler 9, 8, 7, 6; Mercer 8, 7, 6; Bailey 2-6 4918.7-4891]

Outside of the study area, faunas of "Zone 4a and 4b" have been recovered from strata assigned to the Cochrane only in one well, the Phillips 1-D Franklin, Gray County, Texas, in the western Anadarko Basin. Here Zone 4a and 4b faunas occur successively through a thickness of 25 feet, and overlie at least 170 feet of Cochrane carbonates that have yielded only few undiagnostic Silurian conodonts and the C_2 brachiopod *Stricklandia protriplesiana*, which is characteristic of the outcrop Cochrane.

The Cochrane faunas are difficult to correlate with Johnson's sea level curves, partly because the conodonts zones are miscorrelated with the graptolite zones as revealed by newer data. Sea level high 2 appears to correspond to "Zone 3". Sea level 3 may correspond with "Zone 4a" and sea level high 4 with "Zone 4b". This assumes that the sea level highs are correctly correlated with the graptolite zones in his charts.

Clarita Faunas

"Zone 5a", Amorphognathoides Fauna. Samples that include the species *Pterospathodus amorphognathoides amorphognathoides,* diagnostic of the *Pt. am. amorphognathoides Zone* occur in a few cores. This *amorphognathoides* fauna is a diverse association that includes *Distomodus staurognathoides*, *Ozarkodina polinclinata, Oulodus petila*, and many coniform species. Sometimes only a thin interval bearing this species (1-3 feet) lies just below the typical lower Wenlock conodont fauna of the Clarita, as is the case in outcrop sections in southern Oklahoma [Carney Townsite 4952-4953]. However, in two cores the *amorphognathoides* fauna ranges through a thicker interval of strata [13 feet in Bailey 2-6, 4889-4876; 8.7 feet in Mercer, 4546-4537.3]. Whether these beds are Clarita or not depends on lithological criteria. For now we are labeling these beds as "Clarita", as they correlate with the Clarita.

The *Pt. am. amorphognathoides* Zone ranges from the latest Telychian C_6 (*lapworthi* graptolite Zone) well into the lower Sheinwoodian (*murchinsoni* graptolite Zone).

Lower Clarita Fauna, "Zone 5"

The lower Clarita fauna is readily identified by the lack of Llandovery taxa and the presence of either, usually both, of two coniform species: *Dapsilodus obliquicostatus* (in a restricted sense) and *Pseudooneotodus bicornis. Panderodus unicostatus, Decoriconus fragilis* and *Walliserodus* sp. may be common. Few elements of non-coniform species occur, usually just elements of *Ozarkodina excavata* or rarely *Kockelella* sp. The common occurrence of *Walliserodus* elements indicates that the fauna is mostly likely Sheinwoodian, early Wenlock, in age, for Homerian samples from the southern United States usually lack *Walliserodus* elements.

[Griffen – all; Mercer 3, 2, 1; Chandler 5, 4, 3, 2, 1; Carney Townsite 4949-50, ?4946, 4932-4906].

The Lower Clarita faunas match Johnson's sea level high 5.

Upper Clarita "Zone 6"

Faunas characteristic of the Homerian Stage are present in the upper Cochrane in the Arbuckle Mountain outcrops of south-central Oklahoma. None have been found in the Carney area.

Summary

Geologic studies provide documentation of stratigraphic interpretations previously based only on limited evidence and documented a much greater complexity to the stratigraphic history and facies relations of the reservoir units. New data shows that the field contains five distinct stratigraphic units in the "Hunton reservoir", each is tentatively correlated with a eustatic a widely recognized sea level rise. The field appears to be divided into numerous major "compartments" by a combination of faults, unconformities between major stratigraphic units, and facies changes within stratigraphic units. Previous work postulated that tight lime mudstones surround the porous limestone facies (Cochrane Formation) of the central portion of WCHF. Stratigraphic and paleontologic work demonstrate that three distinct stratigraphic units are present within the Cochrane Formation. Each unit passes laterally from a shoal water facies in the central part of the field, to a deep-water, shaly, facies to the north, southeast, and (in the lower portion) to the west. Detailed stratigraphic analysis in the Marjo Bailey 2-6, suggests that the trend of thick Hunton in wells in sections 1 & 12, 15N-2E, sections 7 & 6, 15N-1E, and sections 25, 26, 35, 36, 15N-2E may be controlled by a northwest trending fault graben that was active during deposition of the uppermost Cochrane and basal Clarita. This creates another subdivision of the field that should be investigated.

Regional geologic evidence for the Carney area being a regional high and possibly a major "paleo-oil field" by the end of the Paleozoic was presented in the Budget Period I report. This scenario was developed by Joe Podpechan in two presentations [Podpechan, *et al*, *Workshop;* Podpechan, *et al*, *AAPG MidContinent presentation*], demonstrating the critical paleostructural data and tilting of the field to its present SW dip. A critical element in the proposed trapping mechanism is the explanation of the change from porous facies in central WCHF, to non-porous facies on the updip flanks. Facies change of the midshelf bioclastic and biohermal facies of the Cochrane units in the central WCHF to non-porous, non-permeable shaly deep water facies on the flanks provides, in part, the required trapping mechanism.

The more shoal environment of deposition of the central WCHF facies, relative to deeper water facies on the flanks, explains the extensive karst development and predominance of secondary porosity in the field. During periods of sea level lowstand, the central portion of WCHF would stand high, as an island in the Silurian sea, and the previously deposited limestones would be

subjected to subaerial weathering and freshwater diagenesis. Evidence in the cores suggests at least 3 different periods of karst development throughout the thickness of the Hunton in WCHF.

Engineering Analysis

Fluid Properties Analysis

Rahul Joshi, The University of Tulsa

Introduction

Because of the unique behavior of reservoir performance, it was critical that we understand what type of fluid is present in the reservoir. PVT analysis of reservoir fluid samples was carried out to study the nature of reservoir fluid and to generate a representative reservoir fluid model. Fluid samples were collected from two wells, Schwake 1-10 and Morrow 1-27 and were analyzed by PENCOR Reservoir Fluid Specialists. Schwake 1-10 lies in the depleted region of the reservoir, whereas Morrow 1-27 lies in a relatively virgin part of the reservoir.

Fluid samples were analyzed by flashing the sample at standard conditions and recombining vapor and liquid at surface GOR to determine the well-stream fluid composition. The report also gave the detailed well stream composition along with a characterized component and the properties (Molecular Weight/Specific Gravity) of each component and flash summary results. Standard laboratory tests such as Constant Composition Expansion (CCE) were carried out to determine the bubble/dew point of the fluid system and to calculate the two-phase properties below saturation pressures. The data from these tests was used in developing the fluid model that would generate fluid properties that are consistent with those observed in the field.

Schwake Well Sample

Fluid samples were collected from Schwake Well No.1-10 and were analyzed for PVT properties. The fluid was flashed at surface conditions and recombined at a GOR of 4130 SCF/STB to generate the well stream composition. The well stream consisted of 15 components with C7+ as the characterized component. Appendix Table B- 1 shows the well stream fluid composition. PENCOR also performed a CCE test (Appendix Table B-1) and calculated the dew point of the fluid. The dew point was reported as 7,000 psia. The fluid is probably a gas condensate but it has an unusually high dew point, which does not agree well with the initial reservoir pressure of 1,900 psia. Also log data has indicated the presence of oil in the reservoir. Since this fluid sample was collected from a depleted reservoir region, it is also possible that the fluid may not be a representative sample. The fluid sample was not considered for any further processing and a new fluid sample from a virgin zone was analyzed.

Morrow Well Sample

The fluid sample obtained from Morrow Well 1-27 was flashed at surface conditions and recombined at a GOR of 3,017 SCF/STB to generate the well stream composition. The well stream consisted of 35 components with C30+ as the characterized component. Well

stream compositions and CCE test results are shown in Table B- 1. The bubble point of the fluid sample was reported as 1,869 psia. The result was encouraging as the initial reservoir pressure was 1900 psia and the bubble point was found to be very close to initial pressure. Also since the fluid sample was collected from a virgin reservoir region, the fluid may be considered as a representative sample. Further processing of the fluid sample is done to generate the fluid model to be used in modified material balance procedure and compositional simulation.

Generation of Reservoir Fluid Model

The fluid model was generated using a 3 parameter Soave-Redlich-Kwong (SRK) Equation of State (EOS). The EOS determines fluid properties at different fluid pressure, temperature and composition, which helps in performing compositional simulation. GEOQUEST PVTI module is used for fluid modeling. The components of Morrow well fluid were grouped into pseudo-components (grouping consecutive components with small mole fractions) such that the monotonocity is preserved. Using the composition of the Morrow well fluid and the EOS, a phase plot for the reservoir fluid was generated. Figure 23 shows the phase plot. A CCE test was simulated using the PVTI module and the results of simulated test were plotted with the laboratory observed test. Figure 24 shows comparison between experimental CCE and simulated pressure-volume relation. As can be seen from the plot, there is a significant difference between the simulated and observed curves. The aim here is to match the simulated values with the laboratory observed values. This involves tuning the EOS, which is achieved by performing regression.

The tuned EOS was used to simulate a CCE and pressure-volume plot was generated. Figure 25 shows the regressed pressure-volume plot from CCE test. It can be seen from the figure that there is a good match between simulated and laboratory observed data. This tuned EOS was then used to generate the phase plot for the initial reservoir fluid. Figure 26 shows the phase plot obtained from using the regressed 3-parameter SRK EOS. It can be seen from this plot that the initial reservoir fluid (marked in the figure) lies close to the critical point and can be categorized as volatile oil. This fluid model was used for performing compositional simulation as well as generating necessary fluid properties for material balance calculations.

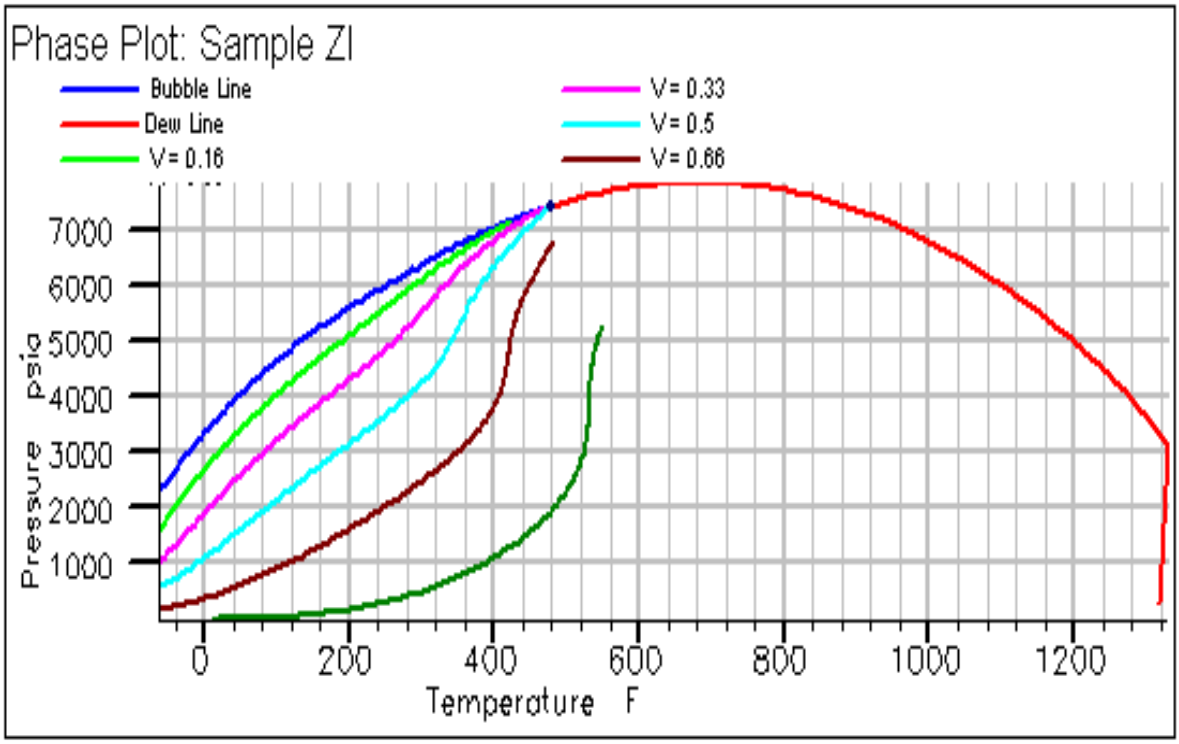

Figure 23: Non Regressed Phase Plot

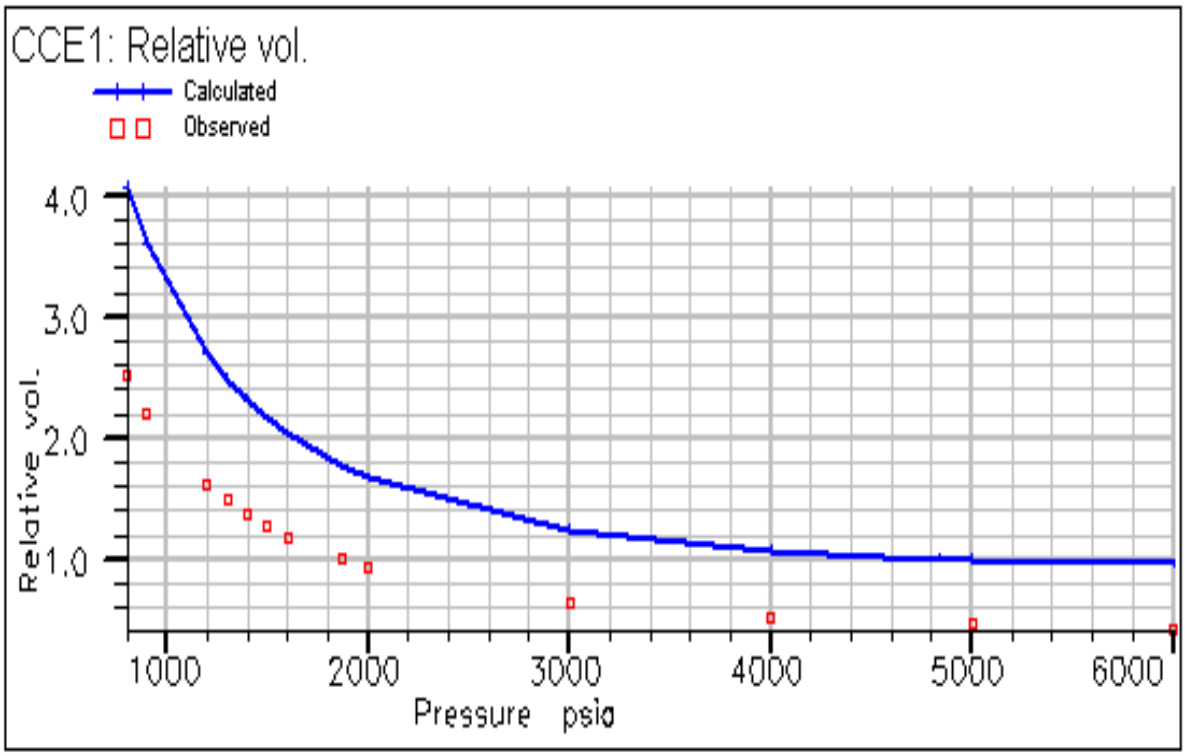

Figure 24: Non Regressed CCE Plot

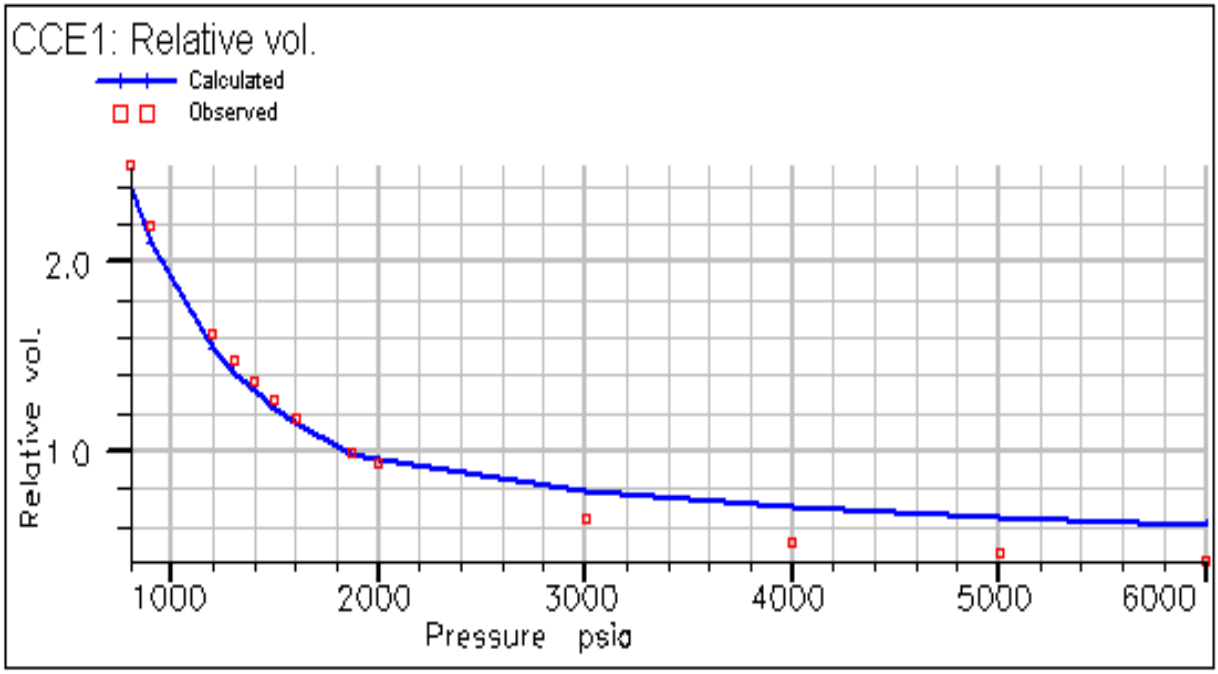

Figure 25: Regressed CCE Plot

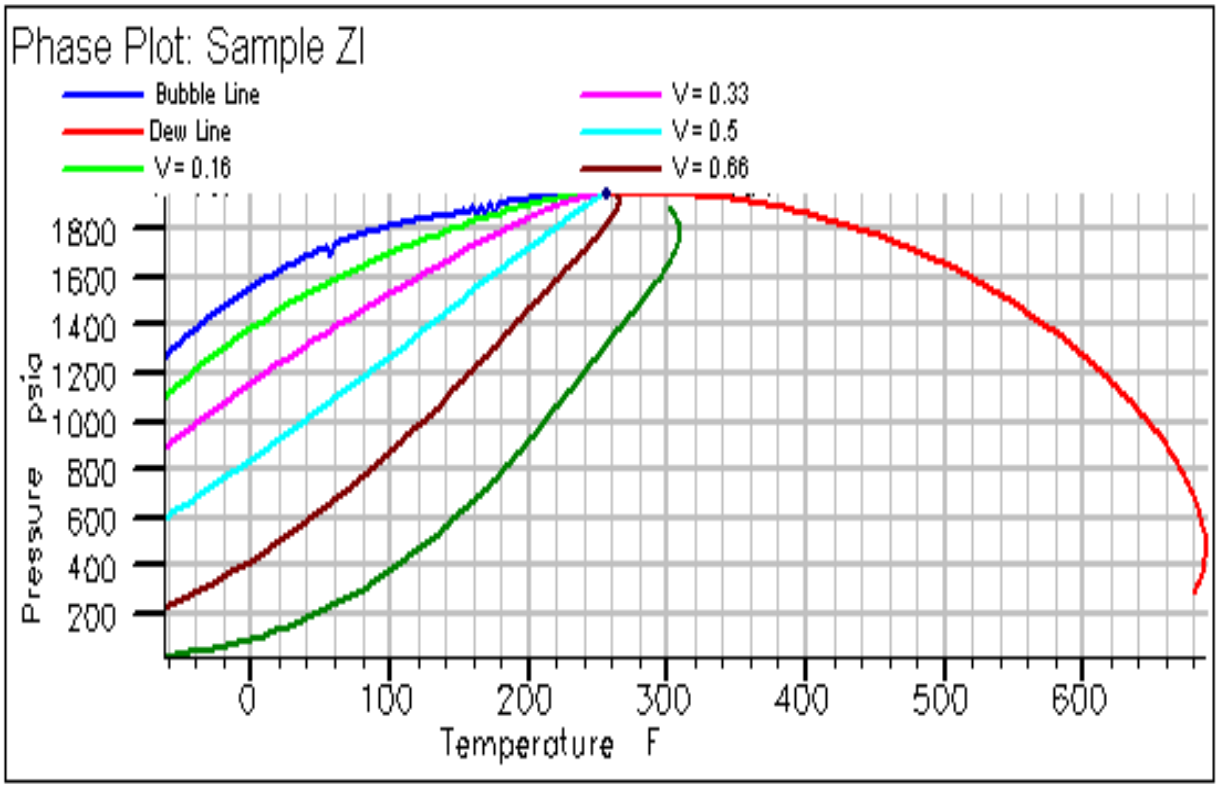

Figure 26: Regressed Phase Plot

Material Balance Analysis

Rahul Joshi, The University of Tulsa

Introduction

In Fluid Properties section, we already have established the hydrocarbons present can be represented by volatile oil. In this section, we present the material balance technique used for such system. The Material Balance procedure is used to estimate the amount of hydrocarbon in place using the field cumulative production data. This is important since it helps in calculating the field recoveries and also helps in identification of potential locations for infill wells. In this section, we present a modified method of $\frac{p}{Z}$ plots for volatile oil systems. A synthetic case was used for validating the applicability of this method to volatile oils and then the procedure was applied to field data. It can be seen that the material balance predicts the in place reserves that are mostly consistent with the results from decline curve analysis. We also compare material balance method with volumetric analysis to understand the difference between total oil volume vs. connected oil volume.

Material Balance Equation for Volatile Oil

The equation used in this case is the standard gas material balance given by the following equation:

$$\frac{\overline{p}}{\overline{Z}} = \frac{p_i}{Z_i}\left(1 - \frac{G_p}{G_i}\right)$$

Equation 1

The same equation can also be used to evaluate volatile oil reservoirs with some modifications. In the above equation p_i, Z_i are the initial field pressure and single-phase Z factor respectively. G_i is the initial fluid in place that is to be estimated. $\overline{p}$ is the average field pressure at given time and G_p is the equivalent cumulative gas production at pressure $\overline{p}$. $\overline{Z}$ is the two phase Z factor at pressure $\overline{p}$. $\overline{Z}$ is calculated using the following expression:

$$\overline{Z} = LZ_L + VZ_V$$

Equation 2

where L, V are the mole fractions of liquid and vapor respectively and Z_L, Z_V are the Z factors of liquid and vapor respectively. We need to use two phase Z factor to account for the presence of both gas and liquid in the reservoir. This method has been successfully used for condensate reservoirs in the past, but has not yet been applied for volatile oil reservoirs.

Development of Representative Two-Phase Z factors

In calculating two phase Z factor, we can consider two possibilities: Constant Volume Depletion (CVD) experiment and Constant Composition Expansion (CCE). In CVD experiment, we assume that liquid dropping out of the two phases is immobile and only the free gas is produced. The overall composition in the cell will change over time, getting richer as more and more liquid is dropped. For CCE experiment, we assume that the composition is constant through out the depletion phase. Therefore, the proportion of liquid and gas would be different in CCE experiments compared to CVD experiments. Traditionally, in simulating gas condensate reservoirs, we assume that CVD experiment mimics gas condensate reservoir. We assume that gas is always mobile and liquid has to reach high critical saturation before it becomes mobile. The question is, can we use CVD experiment to mimic the volatile oil reservoir? The reason that the answer to this question is important is because the reservoir originally contains volatile oil. Therefore, we have to assume that originally oil is a mobile phase. However, as the pressure depletes, large amount of gas is released from volatile oil making gas as the dominant mobile phase. It is possible that the behavior of volatile oil could fall somewhere between CVD and CCE experiments.

We can mimic both CVD as well as CCE experiments using PVTI module in ECLIPSE OFFICE Suite. By knowing L, V, Z_L and Z_V at different pressures, we can calculate two-phase Z factor as a function of pressure using either CVD or CCE experiments.

A way to determine the best method to calculate two phase Z factor is to simulate a synthetic case in a flow simulator. By knowing the fluid produced and the initial fluid in place (molar amounts), we can back-calculate the two phase Z factor. The density of the initial reservoir fluid can be obtained as an output from the simulator. A slight rearrangement of Equation 1 gives the two-phase Z factor as:

$$Z_{2p} = \frac{\overline{p}}{\beta_i RT\left(1 - \frac{G_p}{G_i}\right)}$$

Equation 3

The initial gas in place G_i and the initial reservoir fluid density β_i are obtained from the simulator. Knowing these and the other constants, two-phase Z factors can be calculated for each average reservoir pressure value. This back-calculated Z factor value will accurately represent the material balance equation. By comparing the back-calculated Z factor with two-phase Z factors calculated from CVD and CCE experiments, we can determine which method reasonably represents the depletion of volatile oil in our reservoir.

We ran several cases mimicking the reservoir performance and obtained back-calculated two- phase Z factors using Equation 3. The synthetic cases consisted of running ECLIPSE 300 simulator, simulating a standard reservoir filled with volatile oil. Figure 27 shows the

back-calculated two-phase Z factors plot for the different cases. Each case involves using different values of critical oil and gas saturations and different relative permeability curves that would represent different reservoir depletion processes (from being mainly oil depletion to mainly gas depletion). As can be seen from the figure, all the depletion processes are bounded by the CVD and CCE tests.

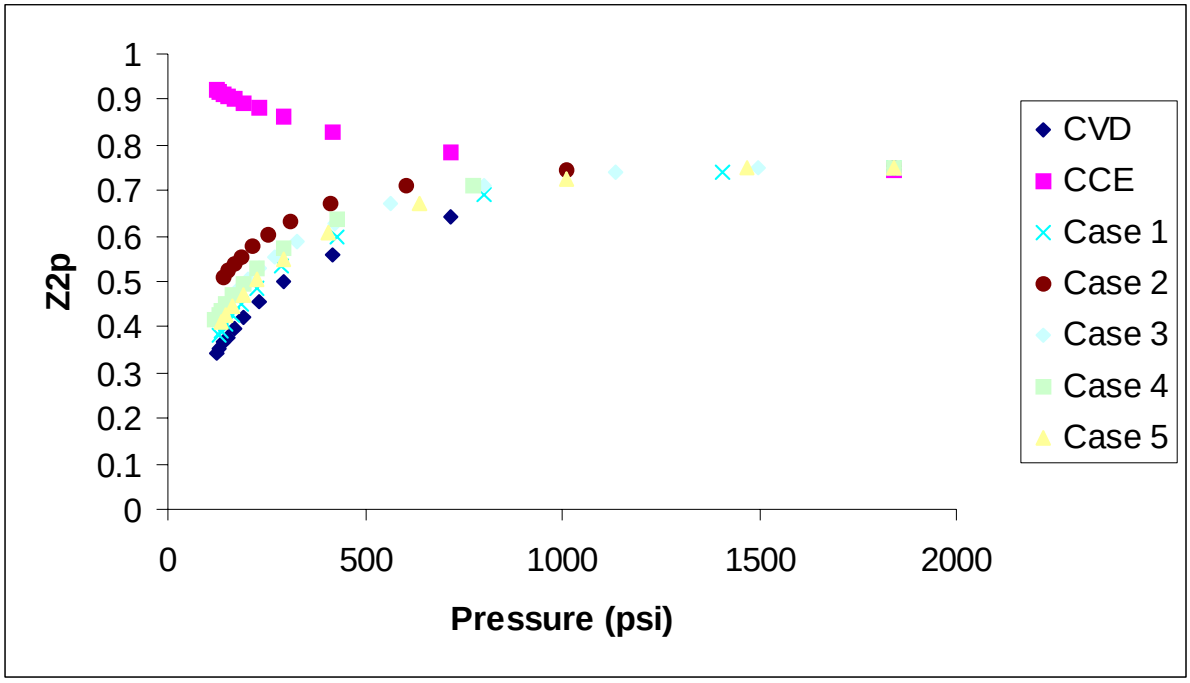

Figure 27: Two-Phase Z Factors bound by CCE and CVD

An important aspect of generating the representative two-phase Z factors is the determination of averaging method for the CCE and CVD obtained values. The averaging method depends on the reservoir depletion process especially the relative permeability curves and the critical saturation of oil and gas phases. For the cases with high critical oil saturation, more amount of gas is depleted from the reservoir and the two-phase Z factors match closely with those obtained from the CVD data. Two different averaging methods were tried. In one case, a simple arithmetic average of Z factors from CCE and CVD was used. In other case, a weighting method based on average reservoir pressures is used and the results are compared with the back-calculated two-phase Z factors. The equation used for pressure averaged method is:

$$Z_{2p} = \left(1 - \frac{p}{p_i}\right)\left(Z_{2p}\right)_{CVD} + \frac{p}{p_i}\left(Z_{2p}\right)_{CCE}$$

Equation 4

In the equation above, the CVD experiment is weighed more as the pressure is reduced. Figure 28 and Figure 29 show two different reservoir depletion processes with different

relative permeabilities. Figure 28 is high critical oil saturation (0.3), so that mainly gas is removed from the reservoir. The calculated two-phase Z factors match well with pressure averaged Z factors, because for the pressure-averaged values, the CVD is weighed more at lower pressures. Figure 29 shows a case where gas has a critical saturation and the calculated two-phase Z factors deviate away from pressure-averaged values. In general, it can be concluded that the CCE and CVD data form the upper and lower bounds for the two-phase Z factors values. In most cases, pressure averaging is more appropriate than arithmetic averaging.

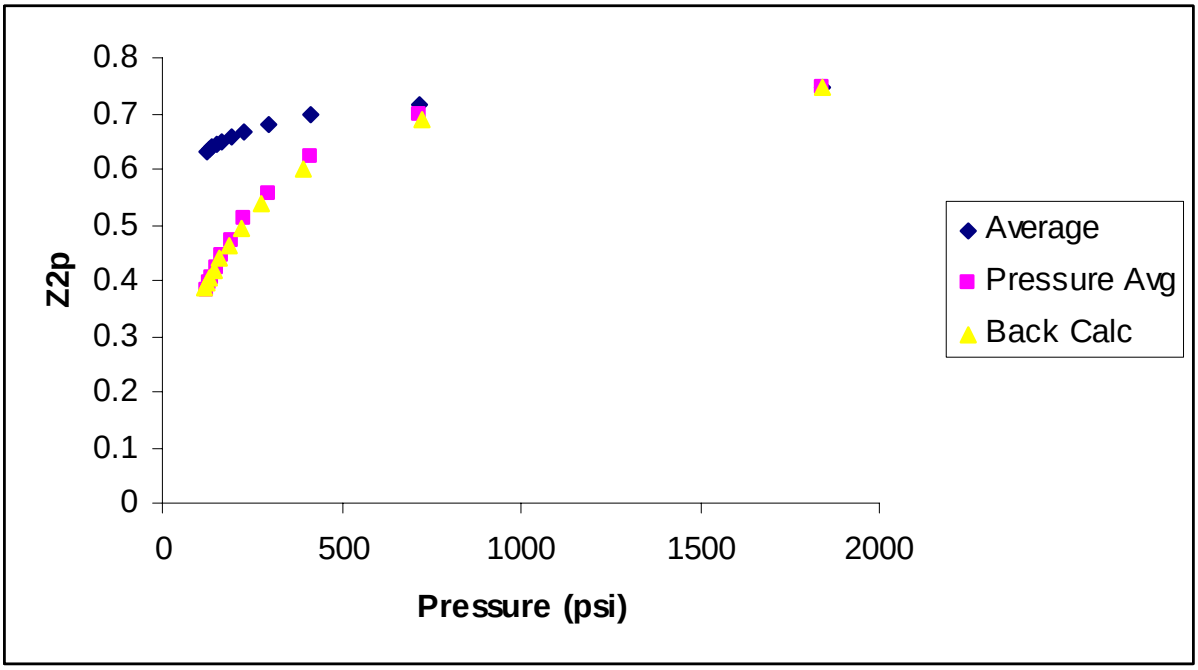

Figure 28: Two-Phase Z factors for High Critical Oil Saturation

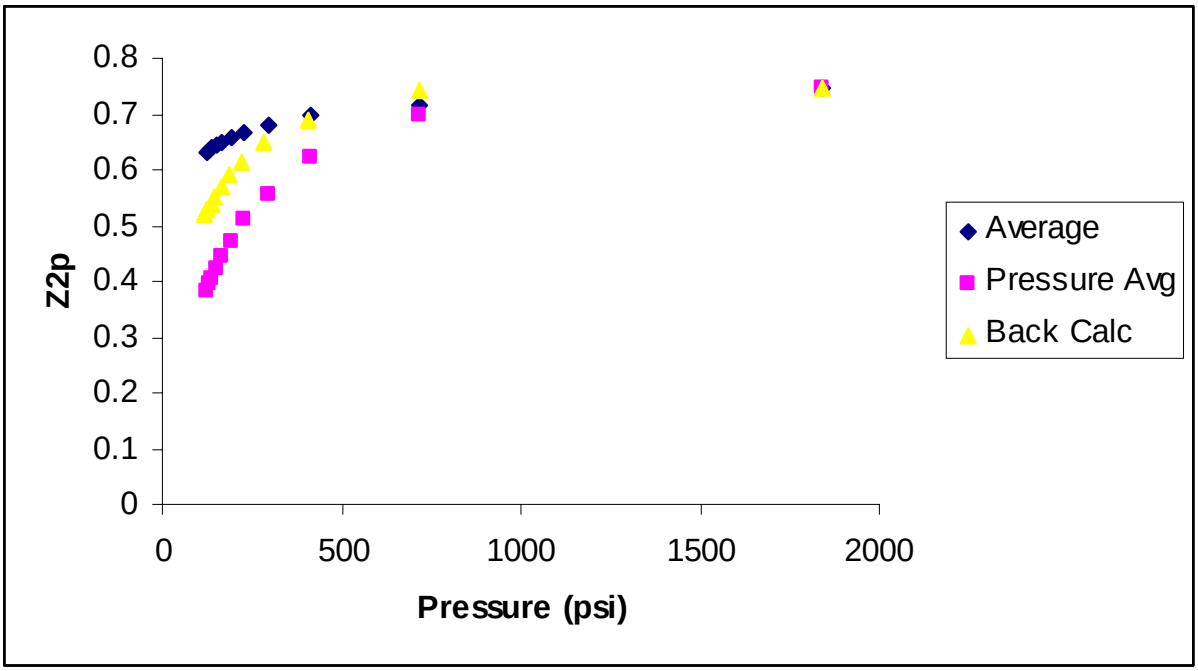

Figure 29: Two-Phase *Z* factors for Critical Gas Saturation

After having established the above mentioned averaging methodology, we try to apply it to our reservoir model.

Figure 30 shows a comparison of material balance plot using two-phase Z factors calculated by three different processes i.e. CVD, CCE and back-calculated using Equation 3 for our reservoir model. It is known that all reservoir depletion processes lie somewhere between those simulated CVD and CCE tests. Hence the back-calculated two-phase Z factors should be limited by CVD and CCE as in Figure 27. However, this is not the case. The back-calculated Z factors are even lower than those calculated by CVD test. The reason for this behavior is that in our case the reservoir is slightly different than conventional oil and gas reservoir where the oil and gas are produced because of expansion. In our case, the efflux of water results in lowering of pressure, which, in turn, results in expansion of oil and gas from matrix into high permeability regions. The removal of gas from matrix and its movement into regions of high permeability causes liquid drop out in the reservoir. Liquid is first dropped in the matrix, followed by additional drop in the fracture. As a result of this the two-phase Z factor is even lower than that calculated by a CVD test (which simulates gas depletion from a reservoir). Therefore in our case, the only option is to use back-calculated two-phase Z factors. A pressure-Z factor correlation is developed and is used in calculating field reserves. This procedure is explained in the next section.

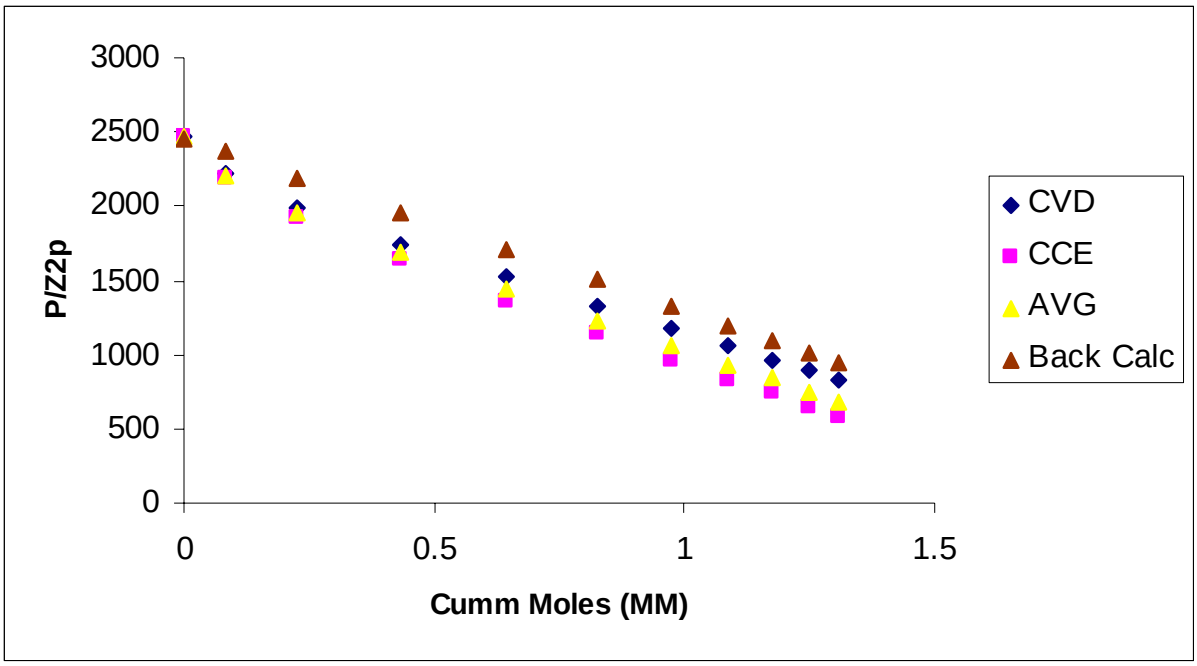

Figure 30: Material Balance Plot for Synthetic Case

Validation with Synthetic Data

The material balance procedure was first verified with synthetic data. The reservoir model used is the history-matched model described in the previous chapter. The in place oil at initial conditions was 950,300 rbbl. This oil is flashed at surface conditions to yield 97,700 STB of oil and 773.94 Million SCF of gas. The oil at surface conditions was converted to equivalent gas G_{eq} by using the following equation:

$$G_{eq} = G_{sc} + V_0 N_{sc}$$

Equation 5

where G_{sc}, N_{sc} are the gas and oil produced at surface from flashing the reservoir oil and V_0 is given by:

$$V_0 = 133316 \frac{\gamma_o}{M_o}$$

Equation 6

where γ_o and M_o are the specific gravity and molecular weight of the oil. The value of V_o is obtained as 300 SCF/STB and the equivalent gas at surface is calculated as 803.26 Million SCF. This data is obtained from initial reservoir conditions and from the generated fluid model. The simulation was run for two years and field pressure, cumulative oil and gas produced is recorded. CVD and CCE tests are simulated using PVTI module at recorded field

pressures and the two-phase Z factors are calculated at the corresponding pressures using Equation 2.

In this case, the back calculated two-phase Z factors are used to develop a correlation between average field pressure and two-phase Z factors. Table 5 shows the back-calculated values obtained by running a synthetic case. Figure 31 shows the plot of correlation between pressure and back calculated two-phase Z factor values.

Table 5: Back-Calculated Two-Phase Z Factors

Pressure (psi)	Cumm Moles Produced(MM)	P/z2p back calculated
1839	0	2458.99645
1627.5	0.081715	2364.187169
1438.7	0.228342	2194.064174
1231.4	0.435062	1954.218679
1038.4	0.646009	1709.468835
879.46	0.82639	1500.182988
754.21	0.971373	1331.967433
656.58	1.086019	1198.950179
580.16	1.176826109	1093.591839
519.73	1.249415769	1009.370172
471.35	1.30814111	941.2344889

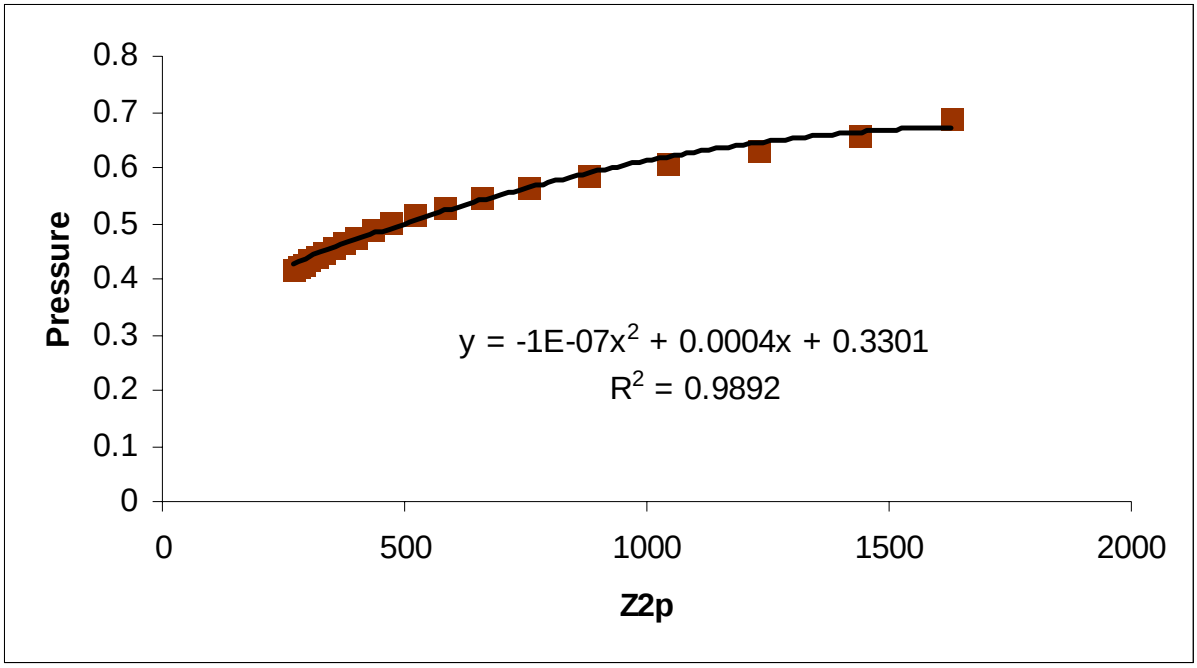

Figure 31: Plot of 2-phase Z factor

Application to Field Data

The material balance procedure was applied to field data after validating with the synthetic case. The field data is divided in four regions due to different local geologies and different initial pressures. Material balance was performed separately for each region and recovery for each region is calculated based on the quantity of initial oil in place as calculated by log data and the total recoverable amount based on estimates from material balance. Figure 32 shows the map of the area divided in four distinct regions. The orange color indicates the West Carney region, green indicates Central West, purple indicates Central East, and violet shows East Carney. West and East Carney regions consist of dolomite lithology, whereas the central region is made up of limestone lithology. The central region is divided in two regions by a fault that passes through it. The initial pressure in the Central East region is less than initial pressure in the Central West. The pressure data are collected from initial pressures observed in newly drilled wells in individual region. The production data were collected from public domain database (NRIS). A table of all pressures in drilled wells and cumulative oil and gas production in each region of the field in provided in Appendix B, in the Material Balance Analysis section. Figure 33 through Figure 36 show the material balance plots for each region with estimated gas in place. Table 6 shows the summary of results obtained from three different methods. The two decline curve methods are slightly different from each other. One is based on regional decline curve while other is based on individual well declines. The regional decline uses all the production data from each region and declines it till the point of abandonment. The individual well decline method declines each well rate till the point of abandonment. The reserves from all the wells within region are added to calculate the total

reserves. It can be seen that material balance results are slightly greater than what is predicted by decline curve analysis. The difference could be due to two reasons. One reason is that material balance represents all the oil or gas which is connected in the reservoir. It may not be mobile but isolated. Another reason is that the existing wells are not capable of producing the hydrocarbons which are connected. The second reason may indicate the need to drill more in fill wells, whereas, the first reason simply implies the need of minimum critical saturation before gas and/or oil can become mobile within high permeability system. The difference between material balance and decline curve analysis is significant in the East region. This is appropriate since the region is currently being developed and several new wells are being drilled in the region. Table 7 shows the recovery factors obtained from material balance.

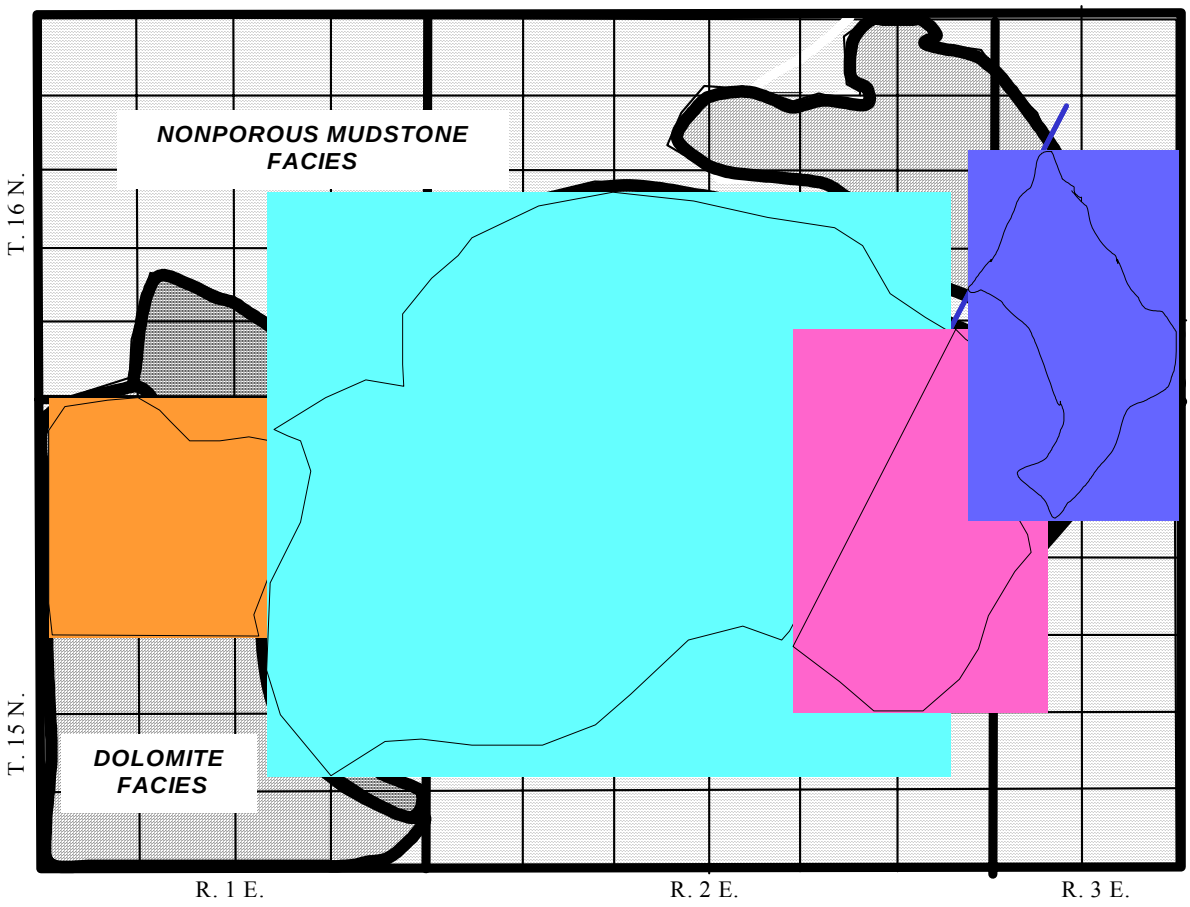

Figure 32: Map of West Carney Field Regions

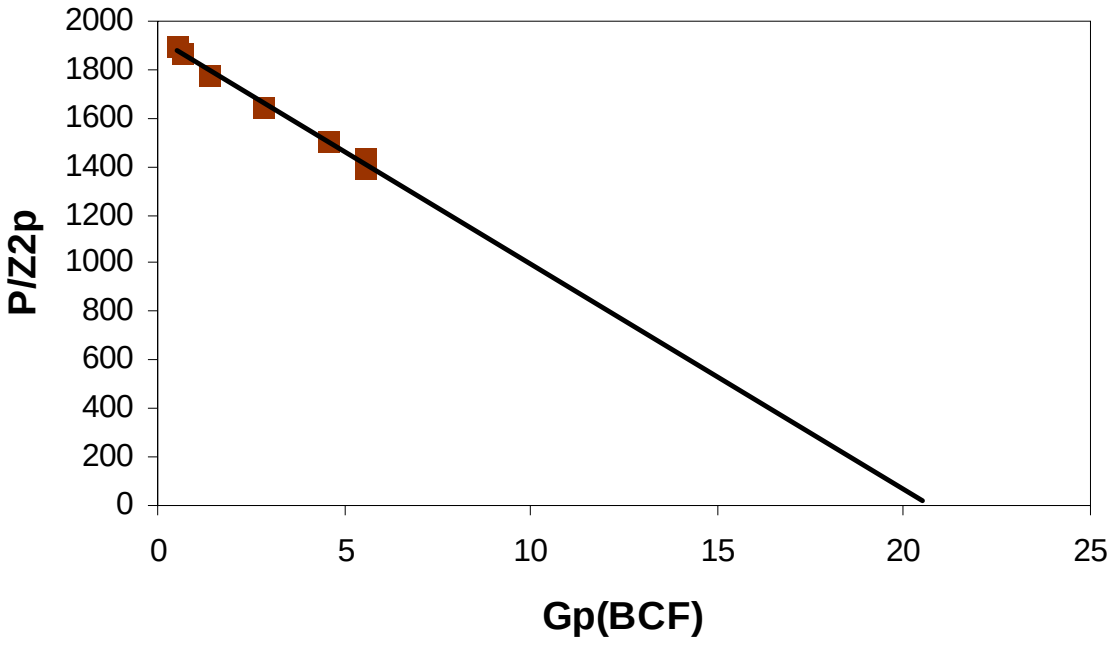

Figure 33: Material Balance West Carney Region

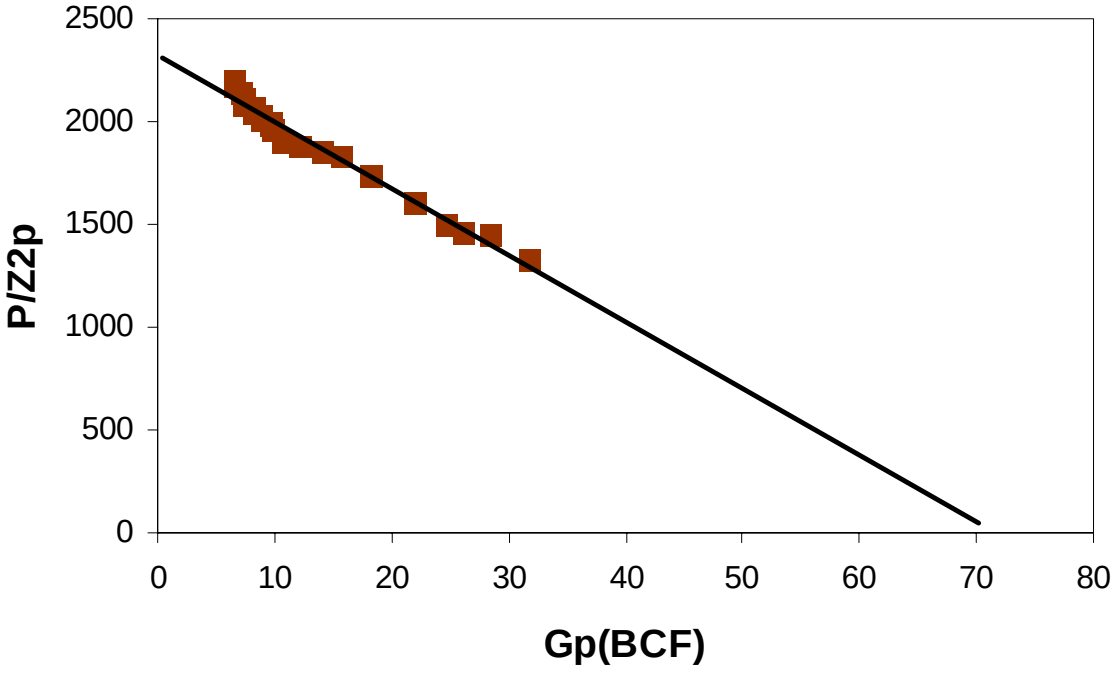

Figure 34: Material Balance Central West Carney Region

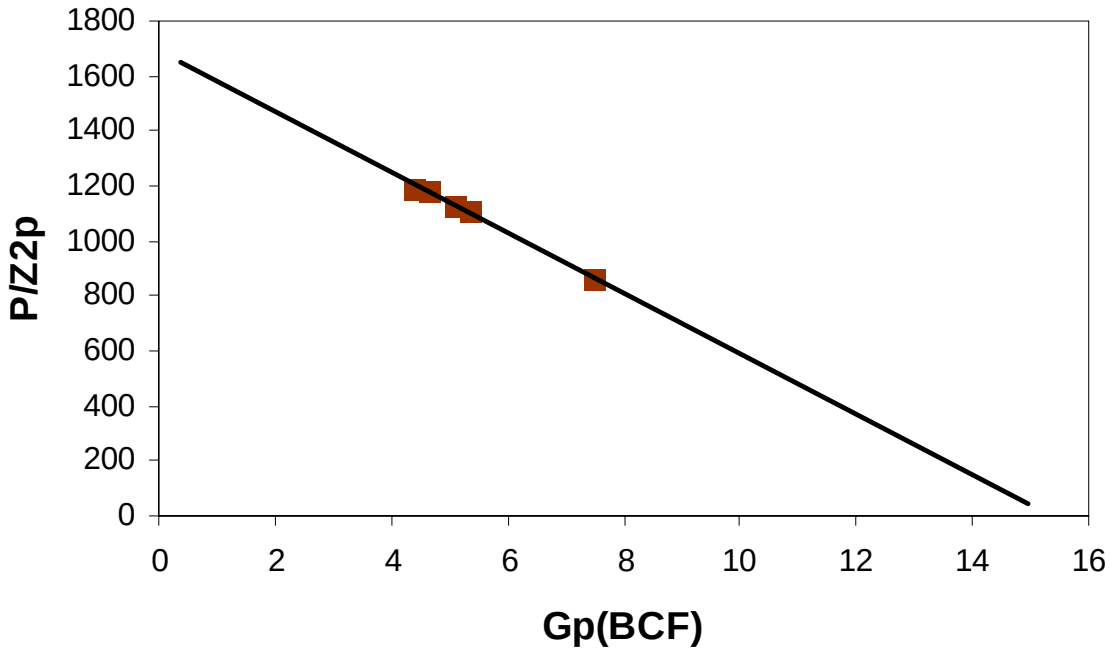

Figure 35: Material Balance Central East Carney Region

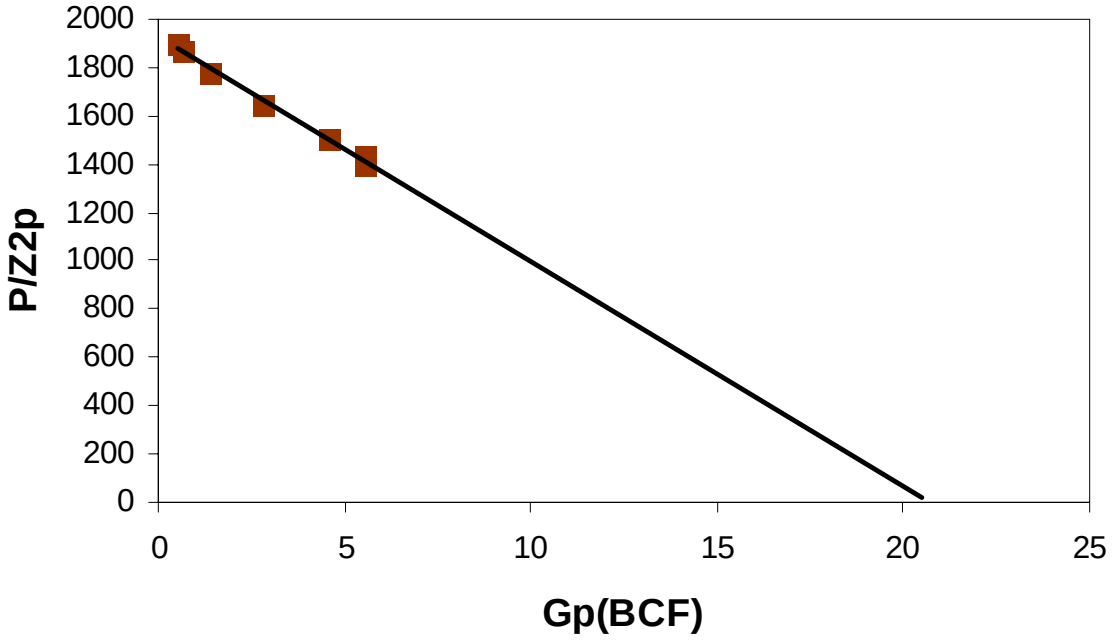

Figure 36: Material Balance East Carney Region

Table 6: Comparison of In place Hydrocarbon Values

Area	Log Data(BCF)	Material Balance (BCF)	Well Decline Curve (BCF)	Regional Decline Curve(BCF)
West Carney	57	20	15	11
Central West	192	71	61	57
Central East	45	15	11	10
East Carney	51	31	19	20

Table 7: Comparison of Recovery Factors

Area	Log Data (BCF)	Material Balance (BCF)	RF% (Material Balance)
West Carney	57	20	35
Central West	192	71	37
Central East	45	15	33
East Carney	51	31	61

Summary

As discussed in this section, there is a consistency in estimating the oil in place values obtained from material balance and decline curve analysis. Material balance gas-in -place always predicts higher values than those predicted by decline curve analysis. This is consistent since the difference indicates access to the regional oil-in-place. The larger the discrepancy, the larger is the potential for infill wells. The potential for infill wells is greater in the east region as can be seen by the difference in the values calculated by material balance and decline curves. The plots also indicate high recovery values for the east and west regions, due to the presence of more homogeneous dolomite. The study also shows that material balance is a simple and effective tool in estimating the oil in place when only the field pressure and cumulative hydrocarbon production are available.

Petrophysical Analysis

Sandeep Ramakrishna, Orca Exploration
Manas Gupta, The University of Tulsa

Introduction

One of the important goals of this project is to use log data to understand the behavior of the reservoir. This type of analysis is important because we would like to extend what we learn to other fields in the Hunton formation. Unfortunately, with the exception of log data, rarely are any other type of data available.

Pore Throat Size Evaluation

Our evaluation for correlating the core and log data to production performance continued during this period. In previous reports, we reported that the wettability of samples was observed to be correlated to the permeability of the rock samples. The higher the permeability, the more oil wet was the core. Since permeability is related to the pore opening, i.e. the pore throat size, we assumed that the bigger the pore throat, the more oil wet will be the rock. Pore throat sizes have been recognized based on the Winland R_{35} [1] technique. This technique is used to identify and characterize petrophysical flow units in carbonate rocks. It represents carbonate rocks as combinations of different groups of flow units, each group having a uniform pore throat size distribution. The concept behind the use of R_{35} is that, once different flow unit types have been identified and quantitatively characterized; then the wells are subdivided into smaller units having predictable flow characteristics.

The ranges of R_{35} have distinguished five petrophysical flow units.

1. Megaport: Flow unit with R_{35} ranging above a threshold of 10 microns. Production of medium gravity crude's could be around tens of thousands of barrels per day from these pore throats, given that zonal thickness and other factors are constant.
2. Macroport: Flow unit with R_{35} ranging between 2 to 10 microns. With all other constraints held constant, these are capable of moving thousands of barrels of oil per day.
3. Mesoport: Flow unites with R_{35} ranging between 0.5 and 2 microns, allows hundreds of barrels of oil per day, with all the constraints being constant. For maximal production, the well needs to have good thickness of the zone and continuity of this pore type.
4. Microport: Flow units with R_{35} values in the range of 0.5 to 0.2 microns. These make about a few barrels of oil per day on pump, when all other constraints are considered constant.
5. Nanoport: Flow units with R_{35} values less than 0.2 microns. There is not production from these pore throats, when all other constraints are said to be constant.

R_{35} values can be calculated using the Winland R_{35} [5] equation when porosity and permeability for a rock type are known. Figure 37 shows a porosity permeability plot with R_{35} values superimposed on the plot. The data has been quantified into groups of limestone, partly dolomitized limestone and dolomite based on their grain density values. From the figure, we have tried to distinguish three flow units, the fracture flow, fracture flow imposed on matrix flow and the matrix flow.

The Winland[1] equation to calculate R_{35} for samples with inter-granular or inter-crystalline porosity is

$$\text{Log } R_{35} = 0.732 + 0.588 \log K_a - 0.864 \log \phi$$

Equation 7

Where:

K_a = air permeability, md
ϕ = porosity, % (not decimal)

Solving for R_{35}, we get

$$R_{35} = 10^{0.732 + 0.588 \log Ka - 0.864 \log \phi}$$

Equation 8

We used the porosity and permeability values from the core analysis data and solved for R_{35}.

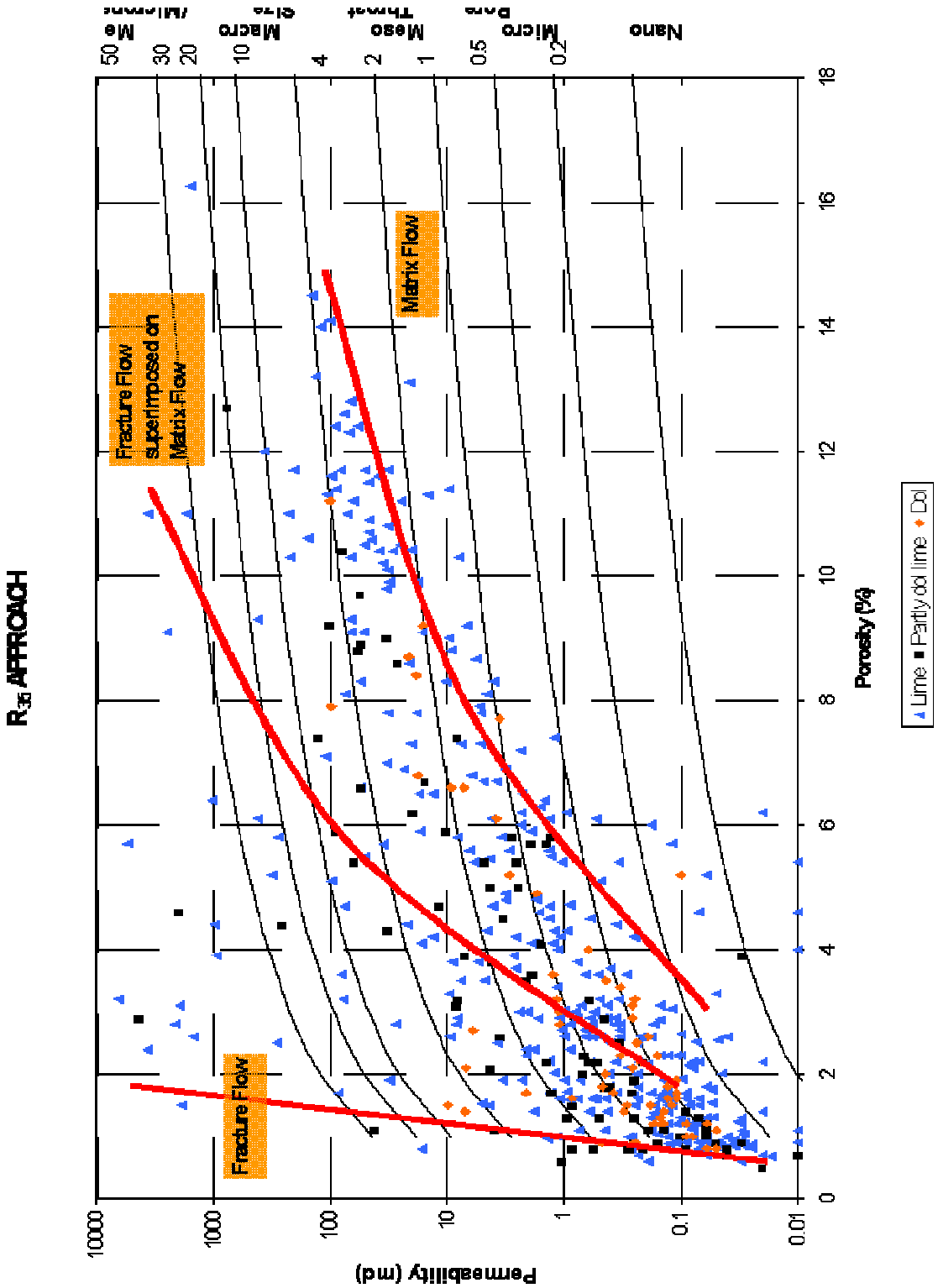

Figure 37: Porosity permeability plot with R_{35} values and lithology

We were not able to correlate the pore throat sizes to any particular lithology. We also tried to use the four different pore types; vugs, coarse matrix, fine matrix and fractures. Figure 38 shows a Porosity permeability plot with superimposed R_{35} values using the different pore types. Observations from the figure did not show any correlation between the pore type and the pore throat size. We also tried to correlate the observed fluorescence with the pore throat sizes. Porosity and Permeability data from each well was sorted based on the percentage fluorescence observed in the cores and plotted along with the R_{35} values. Low fluorescence indicates high water saturation. Although it is difficult to generalize any particular relationship, typically, for low fluorescence, <10%, we observed permeability porosity correlation approaching that of fracture flow. See, for example, Figure 39 and Figure 40 for two Marjo wells. This indicates the presence of water in fractured zones. This also confirms that the bulk of the water is flowing in fractures.

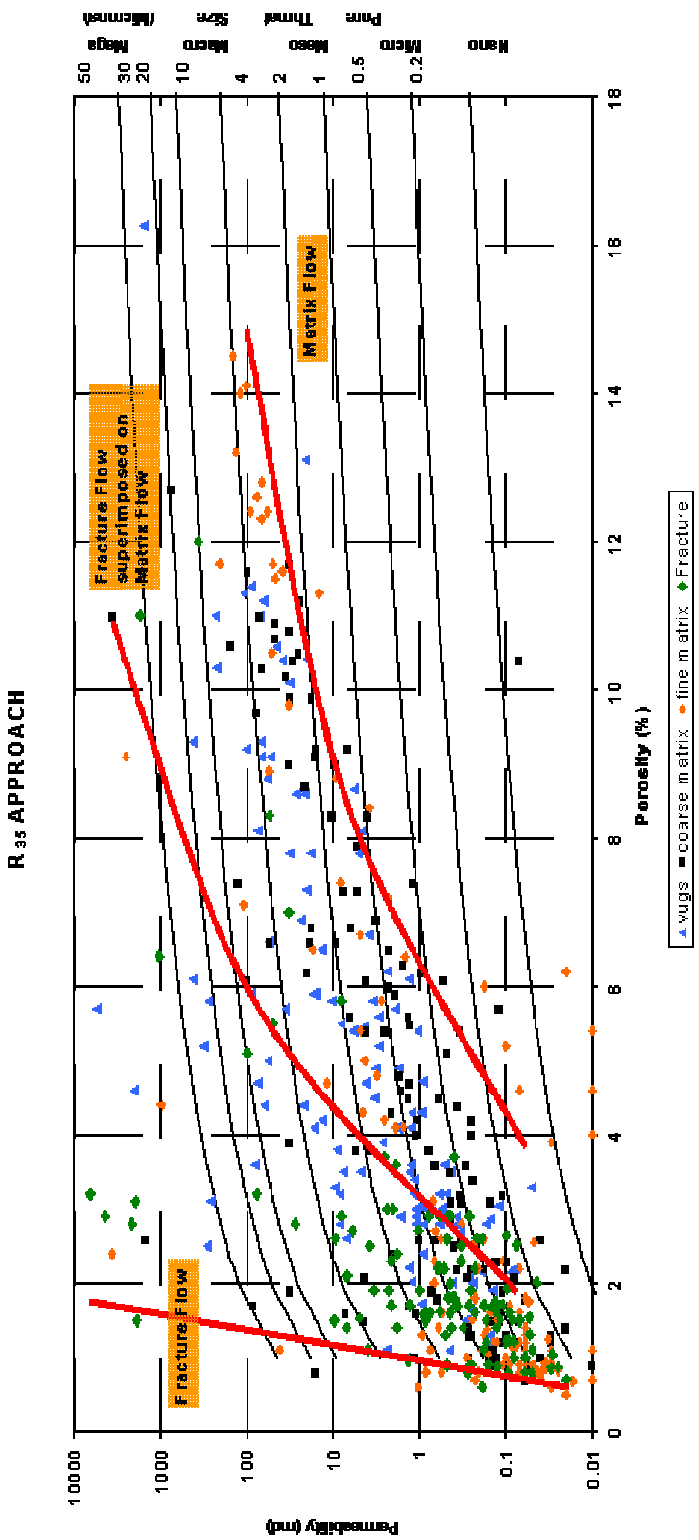

Figure 38: Porosity permeability plot with R35 values and Pore types

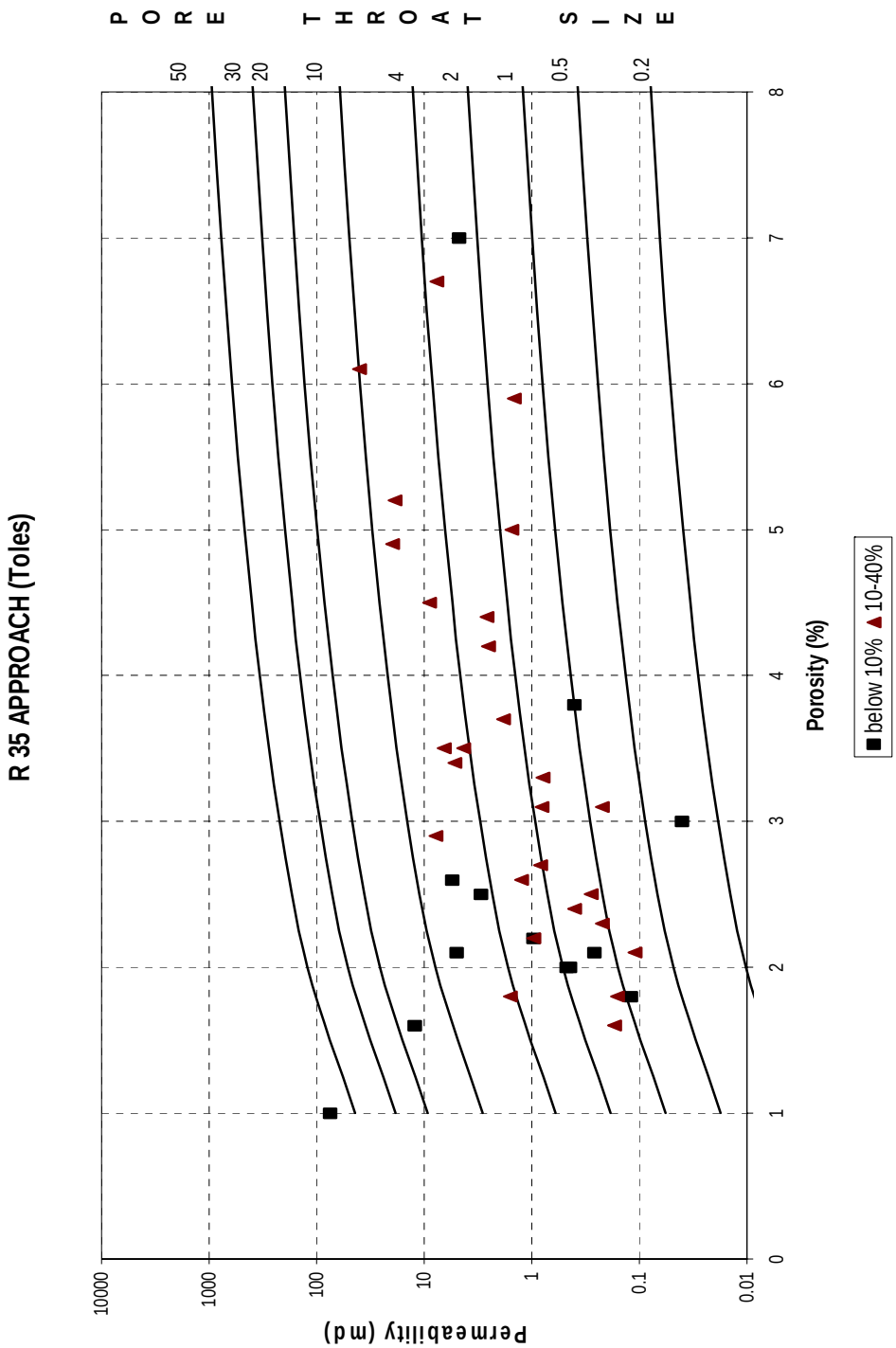

Figure 39: Porosity & Permeability data for Marjo Toles sorted based on the percentage fluorescence on a R_{35} plot.

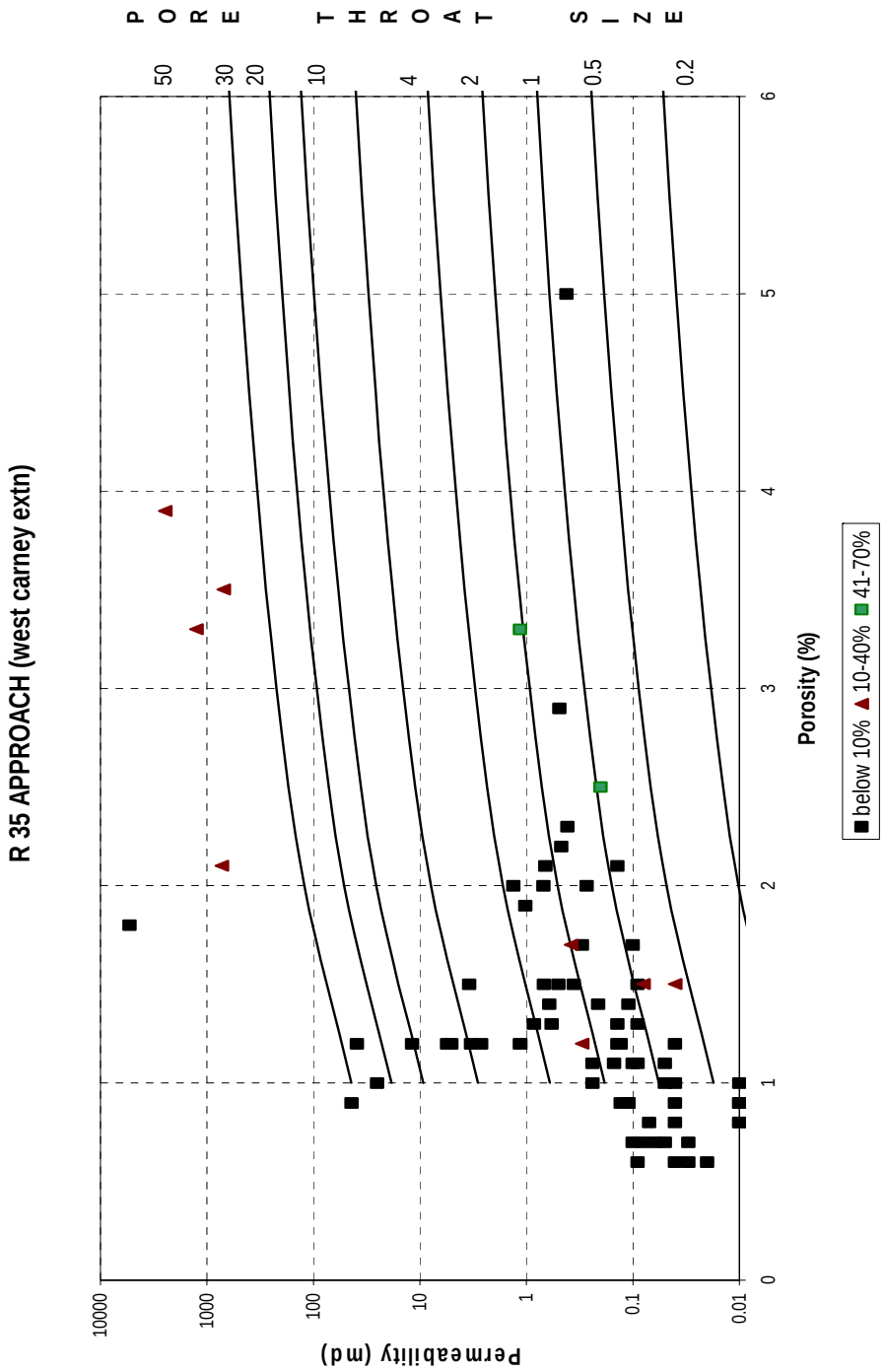

Figure 40: Porosity & Permeability data for Marjo West Carney Extension SWDW sorted based on the percentage fluorescence on a R_{35} plot.

Encouraged by the preponderance of water in the fractured zones, we envisioned the following scenario:

Under initial conditions, the reservoir only contained water. During the primary drainage, oil migrated into the rock. In very tight rock (porosity less than 2% and also very small pore throats), oil never migrated. Those pores always remained filled with water. Figure 41 shows how the pores are filled with oil during primary drainage. The rocks with the smallest pore throat is filled with water, whereas, the rock with the largest pore will be filled with oil. During the geological times, as oil remained in the rock, the wettability of the rock was altered. Over time, the rock became oil wet, with increasing oil wettability with increasing pore throat size. At some time, the reservoir seal was breached, and oil started migrating upwards, which resulted in encroachment of water one more time. Because of the change of the wettability, water preferentially entered the largest pore throats first and selectively swept through the pores. The intermediate pores throats are least affected by the invading water. Therefore, we expect that those pores contain the most oil. Schematically, Figure 42 shows the current distribution of oil.

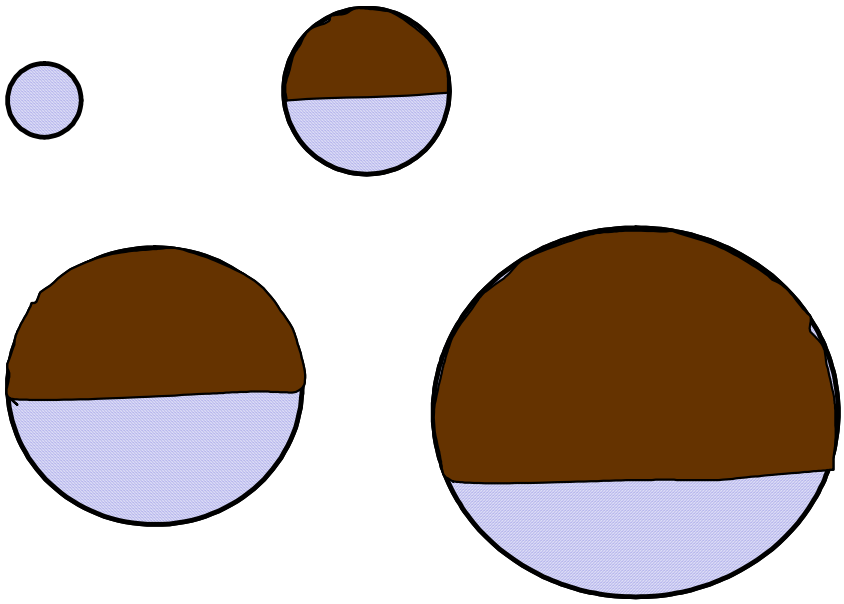

Figure 41: Distribution of Oil after Primary Drainage

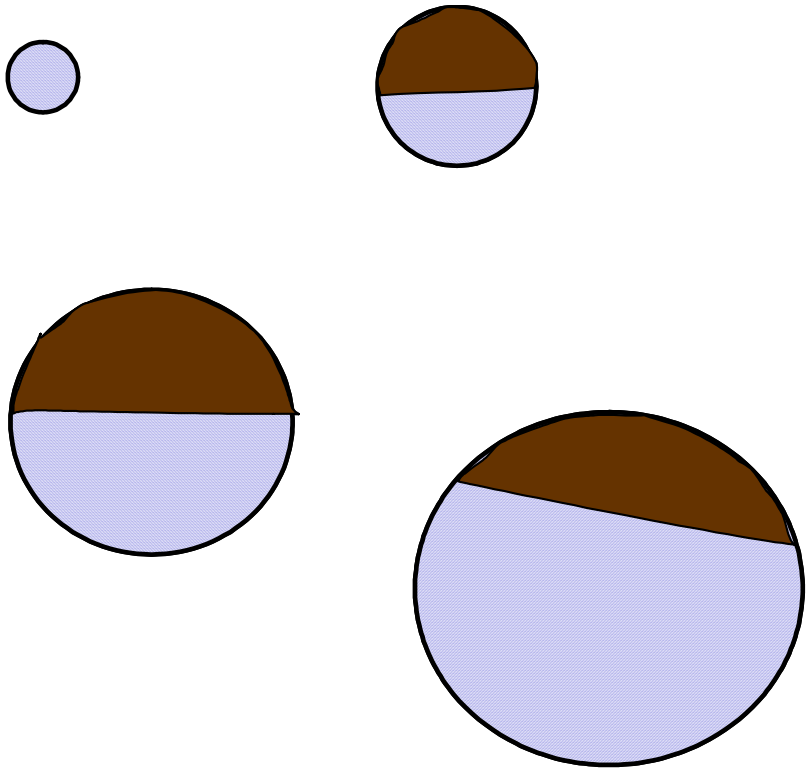

Figure 42: Oil Distribution after Water Displacement

This hypothesis can also verified by examining the fluorescence data observed in the existing core samples. If we examine the fluorescence as a function of porosity, we observe that the least fluorescence is observed in extremely low porosity cores and the large porosity cores. As shown in Figure 43, for fluorescence is less than 10% (very low oil saturation), bulk of less than 2% porosity cores fall in this category. Notice that a large number of core samples with porosity between 6 to 12% also fall into this category.

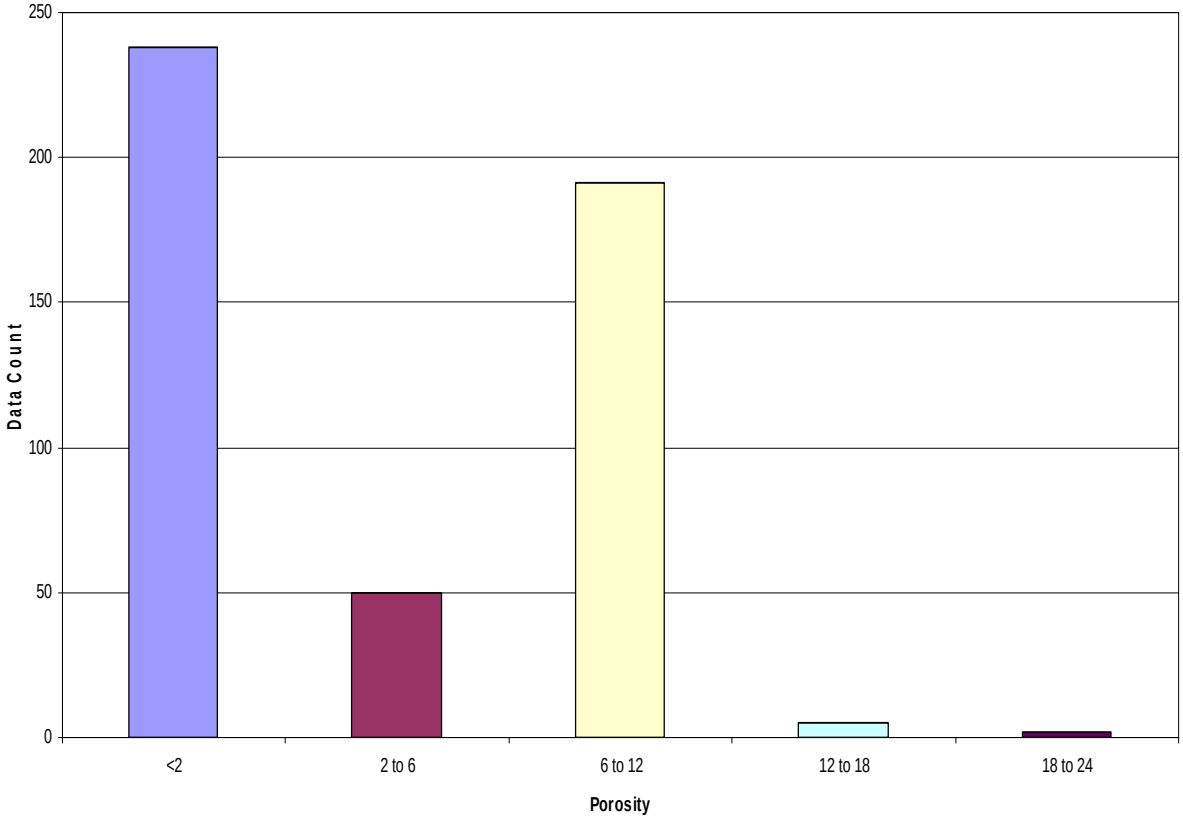

Figure 43: Histogram of Porosity Data for Fluorescence Less than 10%

For fluorescence between 10% and 40% (still low oil saturation), we have a large number of samples falling in the 6 to 12% category as shown in Figure 44. That is, the majority of core samples between 6 and 12% porosity have very low fluorescence indicating that the oil from these cores has been swept out. If we examine the core samples with fluorescence between 40% and 70% and between 70% and 90% (see Figure 45 and Figure 46), we observe that a large number of intermediate core samples fall into this category indicating that oil saturation in these intermediate core samples remains quite high.

The implication of this finding on recovery mechanism can be potentially significant. If we understand the conduit of water and where the oil is located, as we extrapolate our findings to potentially new plays, we can look for both ingredients based on porosity cut-offs.

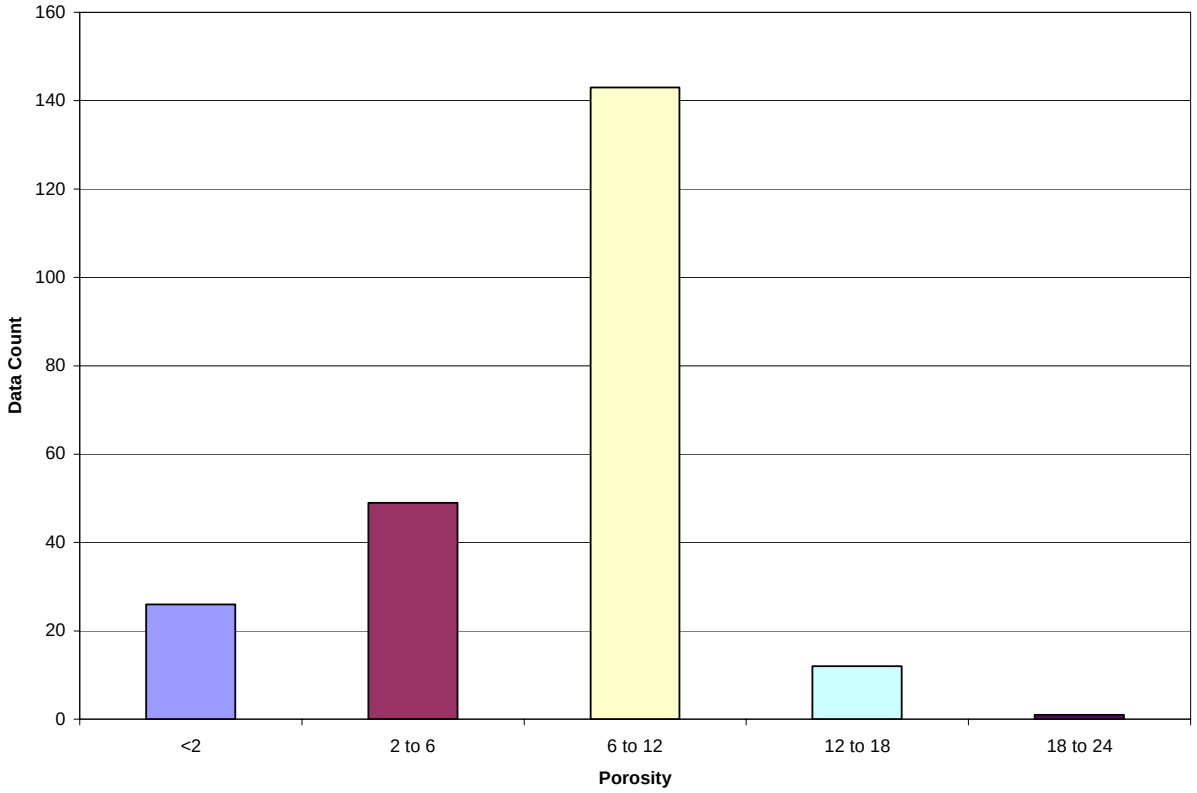

Figure 44: Porosity Distribution for Fluorescence between 10 and 40%

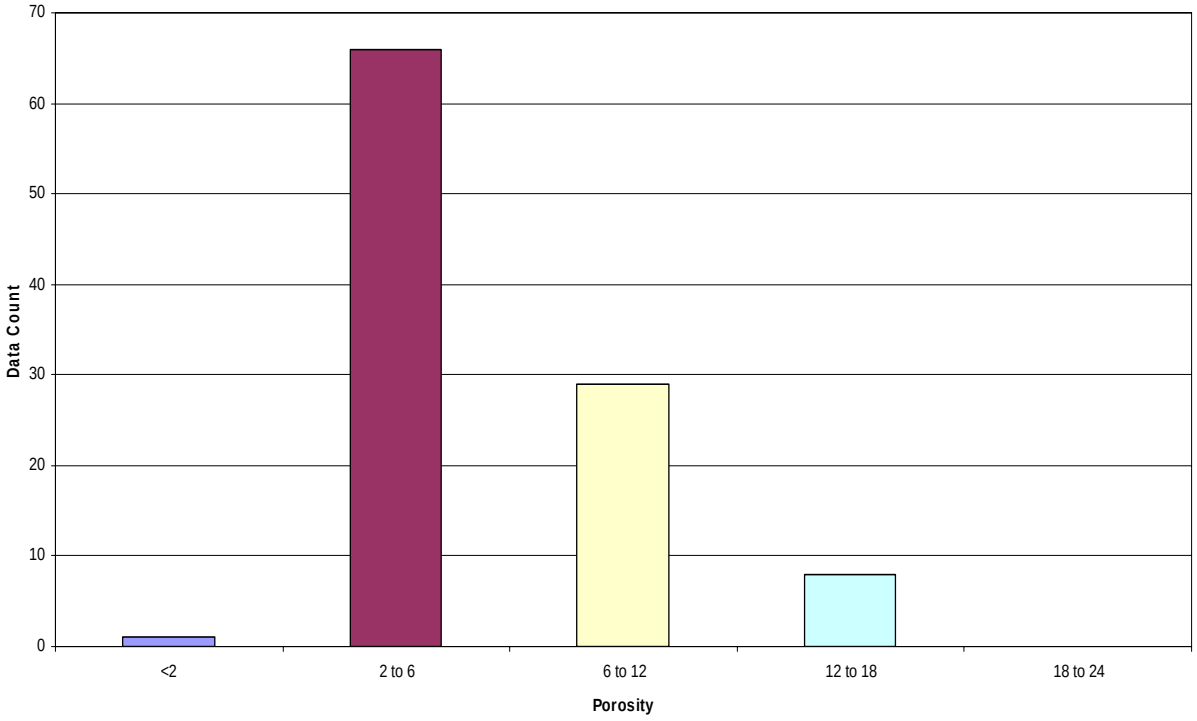

Figure 45: Porosity Distribution for Fluorescence between 40% and 70%

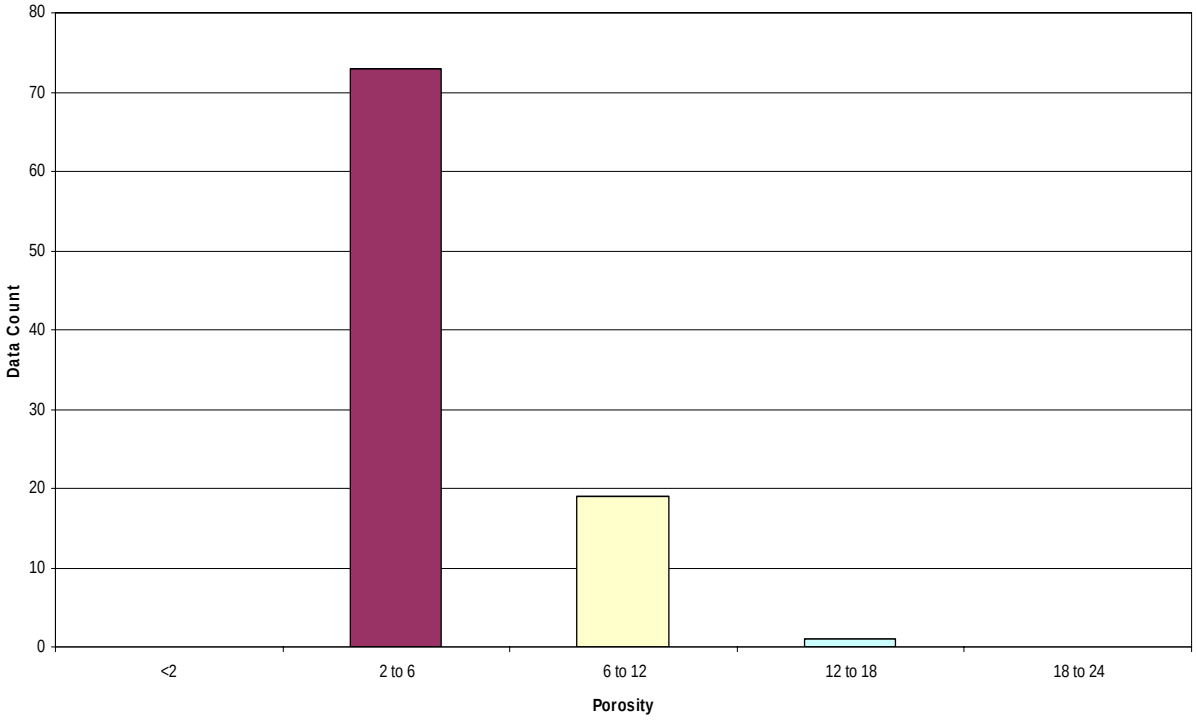

Figure 46: Porosity Distribution for Fluorescence between 70% and 90%

Statistical Evaluation

In the previous section we presented hypothesis about how the field exists under current conditions. Most of the work was based on core data and fluorescence analysis. Although extremely useful, the evaluation is difficult to extrapolate to other regions unless we can develop better understanding based on Log Data only.

In this section we discuss an evaluation of Log Data to understand the possible relationship between log data and the production performance. For this evaluation we divided the data into Four Regions: Central East, Central West, West and East Carneys. (See Figure 32.) As explained in Material Balance section, Central East and Central West regions represent limestone lithology, whereas East and West regions represent dolomite lithology. The field observations also indicate that the Central East and Central West regions are prolific in terms of oil and gas production compared to both East and West regions. The East region is a good gas producer; whereas West region is the poorest producer.

The Log Data we used were resistivity, Neutron and Density Logs. We calculated Porosity and Saturation based on these three logs. Porosity was the average of the Neutron and Density porosities. We had Log data available for all the regions. We had 129 Well data for Central West region, 33 Well Data for Central East region, 36 Well Data for West region and

39 Well Data for East region. We digitized data for all the Logs and calculated porosity and saturation for each well. We then examined the average and standard deviation for both porosity and saturation at each well. We observed that no relationship is evident to the production performance on an individual well basis. Therefore we concentrated on the average properties for the entire region. We observed the following properties for each region shown in Table 8.

Table 8: Statistical Distribution of Log Data

	Central East	Central West	West	East
Avg. Porosity for 0.02<Φ<0.06	**0.0368**	**0.0373**	**0.0394**	**0.0379**
Avg. Porosity for Φ>0.06	**0.0569**	**0.0588**	**0.0953**	**0.075**
Average Porosity	**0.0452**	**0.0454**	**0.0796**	**0.0675**
Avg. Saturation for 0.02<Φ<0.06	**0.4211**	**0.4013**	**0.2755**	**0.3115**
Avg. Saturation for Φ>0.06	**0.5523**	**0.5587**	**0.2829**	**0.4532**
Standard Deviation for 0.02<Φ<0.06	**0.0107**	**0.0099**	**0.0107**	**0.0106**
Standard Deviation for Φ>0.06	**0.0252**	**0.0235**	**0.0349**	**0.0227**
Standard Deviation of Saturation	**0.2201**	**0.2033**	**0.1949**	**0.1701**
Standard Deviation of porosity	**0.0275**	**0.0245**	**0.0454**	**0.0338**

From this table, certain distinguishing characteristics emerge. The average porosity for Central East and Central West region are very similar and this in consistent with limestone lithology. The average porosity in East region is slightly lower than average porosity in West region. Both these regions exhibit dolomite lithology; however West Region has slightly higher value indicating more dolomatization. Instead of calculating average oil saturation, we divided the saturation into two regions: for Φ <0.06 and for Φ >0.06. Recall the discussion in the previous section. The average saturation for porosity values within 2% to 6% shows the trend which indicates higher values in the Central West and the Central East regions; whereas in the West region the value is the smallest. See Figure 47 where a plot is made of average porosity as a function of average saturation. For porosities less than 6%, average saturation is not dependent on average porosity; whereas, for porosity greater than 6%, the average saturation decreases dramatically as the porosity increases. The reduction in saturation below 6% may also be influenced by how well connected low porosity regions are to high porosity regions.

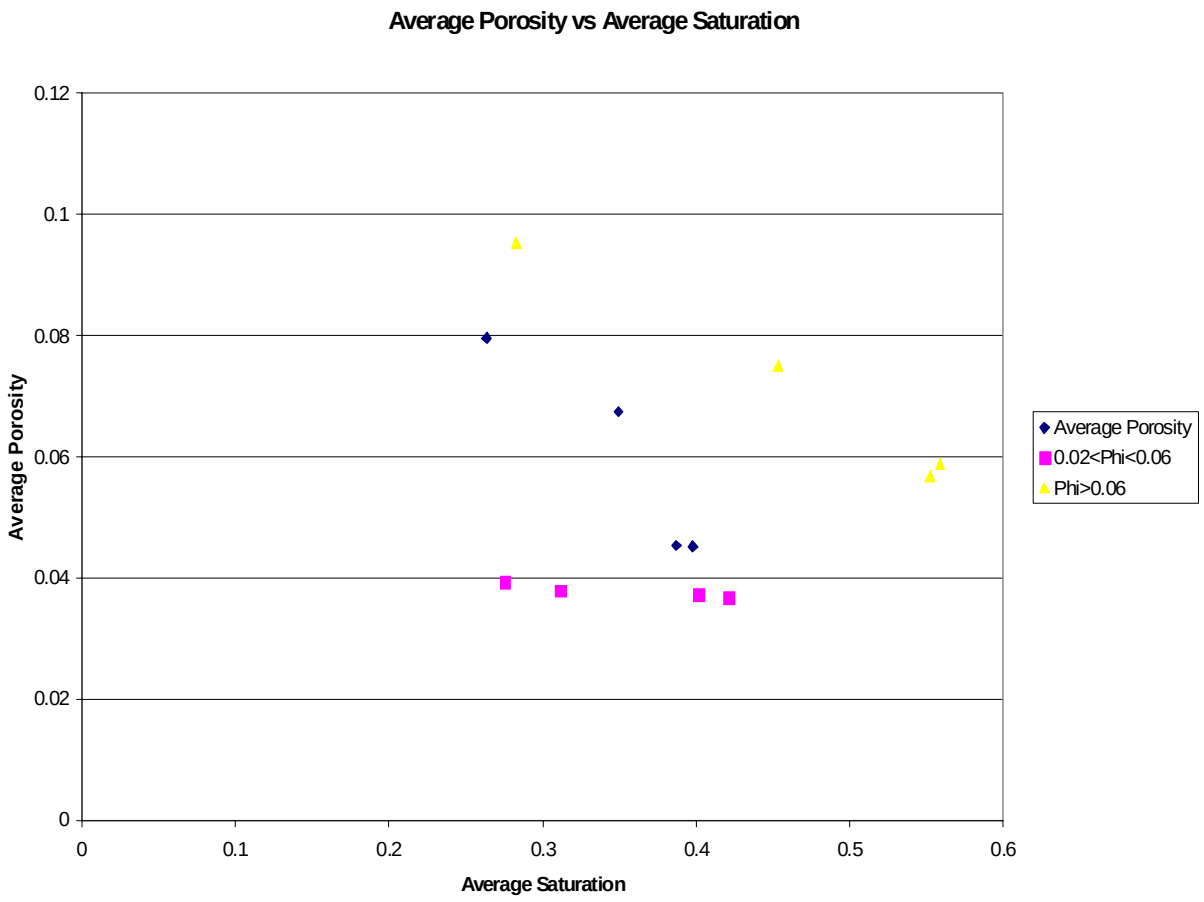

Figure 47: Effect of Average Porosity on Average Saturation

The West region has significantly lower saturation compared to the other three regions. When one examines standard deviation of porosity values within 2% to 6%, one will notice the values to be almost identical. However, the standard deviation for porosity for values exceeding 6% is significantly greater for West region than other three regions.

The production performance behavior of Central East and Central West regions is similar and so are the log properties. The East region is less productive and the West region is the least productive. Based on the Log analysis, we can make the following observations:

- High Porosity values indicate low productivity because of low oil saturation.
- The low oil saturation values for high porosity regions ($\Phi>0.06$) indicate low productivity. This is because low saturations in high porosity region are indicative of low amount of remaining oil in place.

- Higher the porosity variation, lower is the remaining oil saturation. That means, if the rock has overall high Porosity and high Standard Deviation, the remaining oil is smaller. This also causes low productivity.

To confirm this further, we calculated equivalent gas produced by each well in different regions and compared that to Gas in-Place at each well by the following equation:

Gas in Place/Area= 7758* Φ*So*300*h

This calculation provides equivalent Gas in-Place by converting Oil into Gas by assuming one barrel of oil is equivalent to 300SCF of Gas. We have explained this equivalence in Material Balance section. When we plotted equivalent gas produced from each well as a function of Gas in Place (see Figure 48), we observed a general increasing trend in recovery as the gas in place increases. However the data still exhibit a clear differentiating between Central regions compared to either East or West regions. The recovery in the Central East and Central West is better than especially West region. The West region clearly shows very low recovery compared to the other regions. This means that the low oil saturation does not alone explain the low recovery in the West region. Although the oil saturation in the West region is low, because of high porosity, oil in place (or equivalent Gas in Place) is high. The possible explanation for this discrepancy may lie in mobile oil saturation. That is, although West region contains significant quantities of Oil in Place (or equivalent Gas in Place) only portion of it is mobile making it difficult to produce.

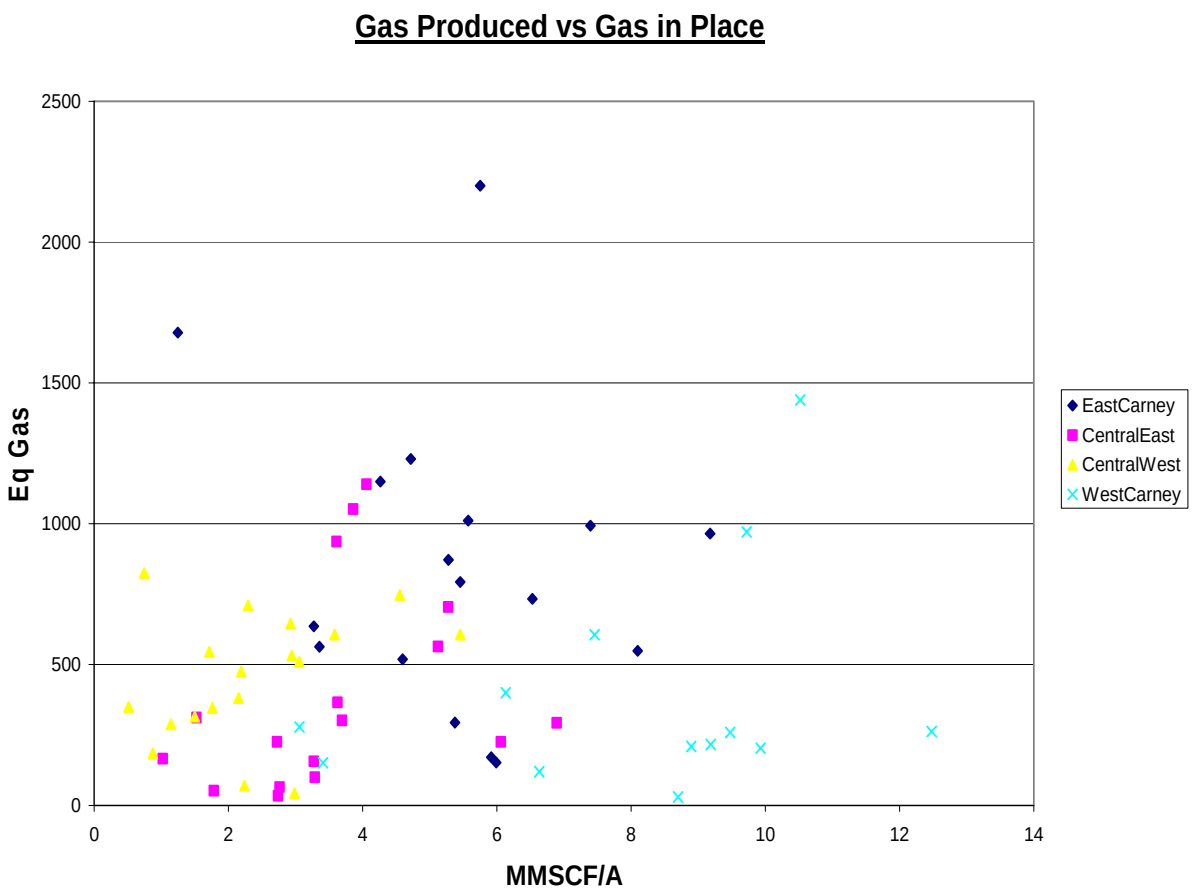

Figure 48: Gas Produced vs. Gas in Place

We need to investigate this further. We intend to evaluate the Well Performance by using different values of mobile saturation and evaluate its impact on the recovery. We will also expand our work in other regions to understand if our hypothesis will hold in these regions as well.

Simulation Evaluation

Primary Recovery Mechanism

Rahul Joshi, The University of Tulsa

Introduction

One of the objectives of this study is to reproduce some of the important characteristics observed in the field. Eclipse 300 simulator was used to simulate the reservoir. We considered Schwake # 1 well to be representative of reservoir behavior. Many unique characteristics typical of this reservoir are observed in the well performance of Schwake well. These include large water production at initial conditions followed by delayed breakthrough of gas followed by breakthrough of oil, jump in GOR after shut-in, and decrease in WOR over time.

A single well radial model was considered to explain the primary production mechanism. The drainage area for one well is about 160 acres. The radius of the model is about 1500 ft., divided into 12 grids increasing geometrically in size. There is only one grid in the angular direction. This was done because increasing the number of grids in the angular (6-12) causes extremely small size of the grids near the wellbore and results in stability problems while running the simulation. The model consists of two layers in the vertical direction, consistent with the geology. The top layer is matrix with a low permeability, which stores all the oil. The bottom layer is the fracture layer with high permeability, which is responsible for production. The fracture layer is connected to the wellbore whereas the matrix layer is isolated. One reason for isolating the matrix layer is that oil cut is observed only after 5-6 days after the well is put on production. This indicates that oil does not exist in the immediate vicinity of the wellbore and has to travel some distance before it reaches the wellbore. Figure 49 shows the schematic of the conceptual reservoir model. The initial reservoir pressure is 1869 psia at a temperature of 117 F. As discussed in Fluid Properties section, this is approximately the bubble point of the reservoir fluid. As the well is put on production, water is produced from the fracture layer and there is a reduction in the reservoir pressure. This causes oil from the matrix layer to flow down into the fracture. This pressure reduction causes the reservoir pressure to drop below the bubble point causing gas to be released from oil. Water, oil and gas flow through the fracture and are produced at the wellbore.

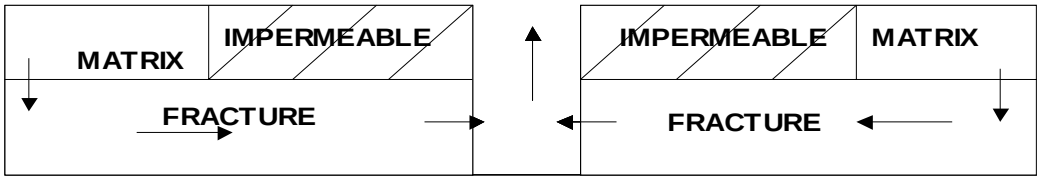

Figure 49: Conceptual Reservoir Model

The fracture relative permeabilities are linear with no residual saturations. It is assumed that oil, water and gas flow independent of each other. Once the model is defined, the input parameters are adjusted so that results from simulation can match the field production values and field production behavior.

History Matching

History matching for the data was done by manually changing the input parameters until the desired field output was observed. The objective of the exercise as defined in the previous section was to match the normalized (rates divided by pressure drop) oil, gas and water production rates and also the gas oil ratio (GOR). The field data was obtained from Schwake Well 1-10 as it showed all the unique field characteristics. The rates were normalized because the field bottom-hole pressure (BHP) is not constant and decreases gradually with time. For simulation purposes, the BHP is kept constant at 100 psi. To account for this difference, normalized rates are used to match production history. A satisfactory oil rate and GOR match was obtained using the following parameters. Figure 50 and Figure **51** show the oil rates and GOR plots obtained by history matching. It can be seen from the plots that the normalized oil rate matches well with the field rate through 100 days after which it starts to decline faster than the field value. The GOR in actual field data indicate flattening trend, whereas, in the field data, the GOR starts increasing rapidly. Part of the reason for this difference is the rapid drop in oil rate in the model, whereas, the gas rate is matched reasonably well. Due to excellent dynamic continuity in the reservoir, it is possible that aquifer is connected over larger distance than indicated by 160 acre spacing. This will allow oil to be brought to the well from distances farther than 160 acre spacing. Our single well model did not account for such possibility. This is under investigation. We will build the next generation model by allowing for larger size of aquifer and investigate potential improvements in the result.

Table 9 shows parameter values of the reservoir model obtained by history matching.

Table 9: Parameter Values from History Match

Parameter	Value
Matrix Thickness (d1)	30 ft
Fracture Thickness (d2)	20 ft
Matrix Horizontal Permeability (kh1)	0
Vertical Permeability (kv)	20 md
Fracture Horizontal Permeability (kh2)	20 md
Matrix Residual Oil Saturation (Sor1)	0.3
Fracture Residual Oil Saturation (Sor2)	0
Matrix Residual Gas Saturation (Sgr1)	0
Fracture Residual Gas Saturation (Sgr2)	0
Distance from Wellbore (D)	636 ft
Connate Water Saturation (Swc)	0.2
Water Relative Permeability	Linear
Oil Relative Permeability	Linear
Gas Relative Permeability	Linear

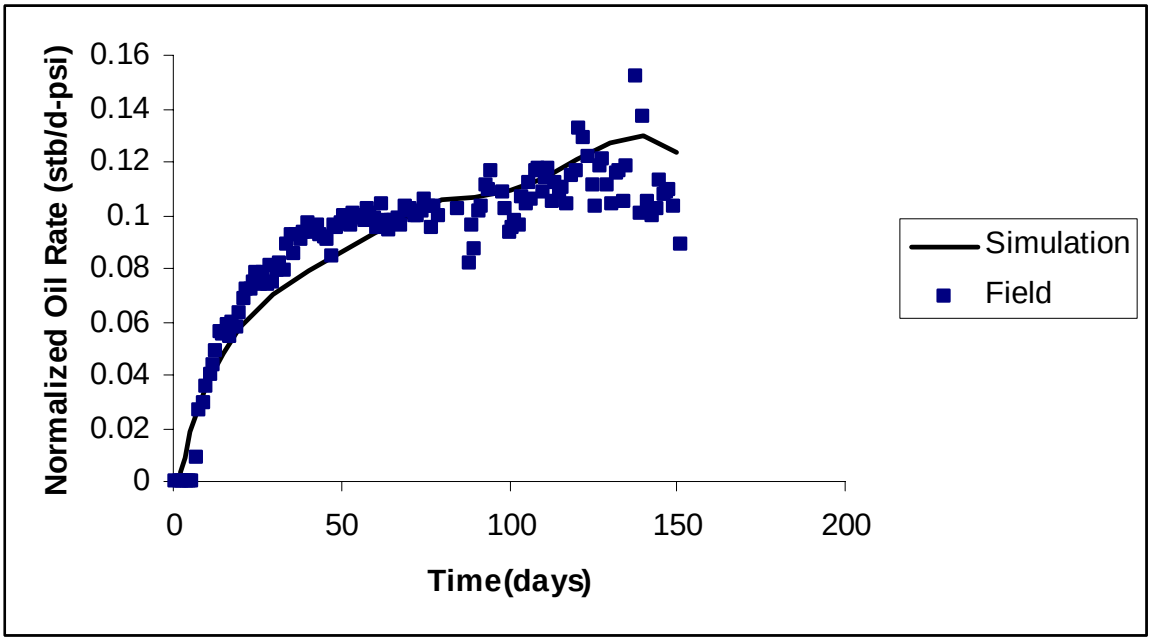

Figure 50: Oil Rate match for Schwake 1-10

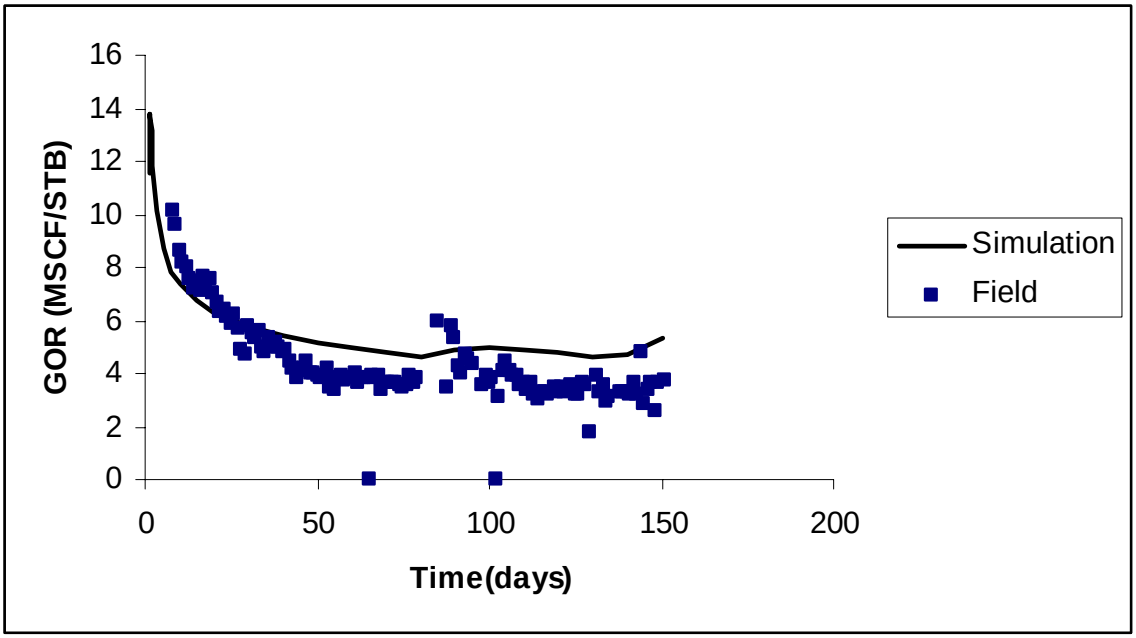

Figure 51: GOR match for Schwake 1-10

Wells Producing Only Gas

Certain wells in the region of study exhibit an interesting behavior. These wells produce large quantities of water in early stages, followed by slow breakthrough of rich gas. Even after producing for several months, these wells never produce any oil, except rich gas. Since our hypothesis requires that the trapped hydrocarbons are represented by volatile oil, we wanted to examine the possibility of wells producing only gas. The model can reproduce the behavior of these wells by making small changes to its input parameters. The changes include reducing the proportionate depth of matrix layer to about 20% of the total formation depth (consistent with log data), increasing porosity in both layers to 10% (consistent with dolomite region in the reservoir) and introducing residual oil saturation in the fracture layer. Figure 52 shows the production profile of such a well. It can be seen that the well produces only water and gas and no oil. In general the model is able reproduce the behavior of only gas production, although the reservoir initially contains volatile oil.

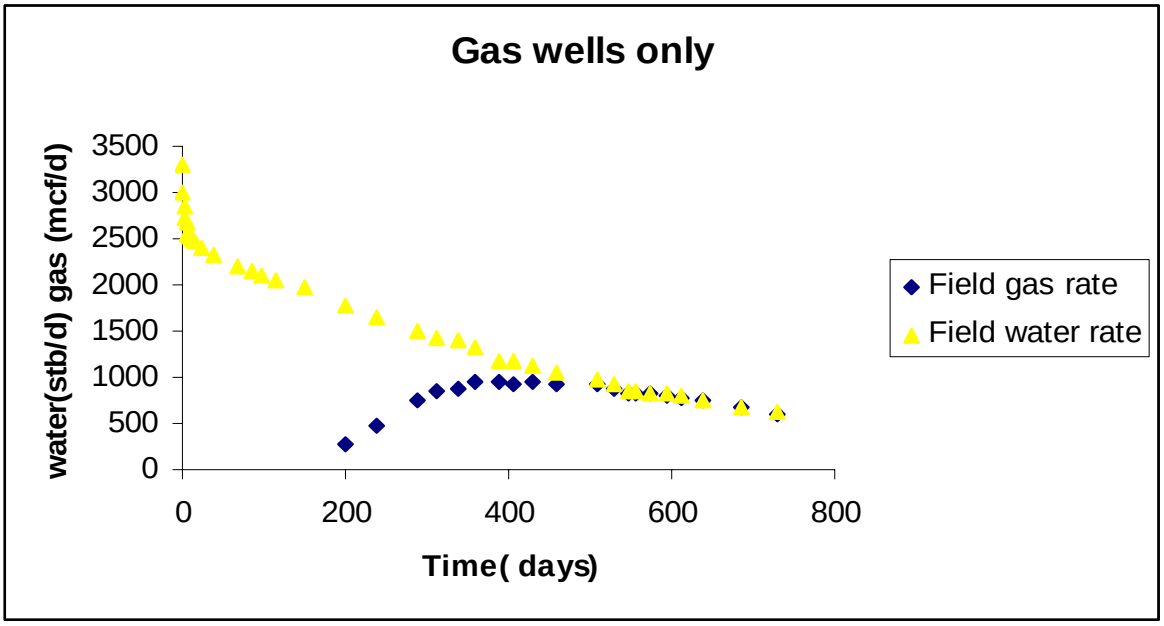

Figure 52: Production Profile of Gas Wells

Summary

The Hunton reservoir exhibits several unique characteristics. Using compositional simulator and geologically consistent, reservoir model, we were able to re-produce most of the characteristics of the well production. These characteristics include: increasing Oil/Water Ratio, decreasing GOR followed by increase, delayed production of oil and gas, spike in GOR after shut-in, and only gas production in some wells from reservoir containing volatile oil. Some late time characteristics could not be matched well. Additional investigation is under way to resolve these discrepancies.

Secondary Recovery Mechanism

Rahul Joshi, The University of Tulsa

Introduction

The West Carney field is declining very rapidly. Part of the reason for such a rapid decline is relatively low compressibility of water, and limited aquifer. As water is produced, the reservoir pressure declines. Since the primary mechanism of oil and gas production is water efflux, as the reservoir pressure declines, the ability of water to carry oil and gas also decreases rapidly. The average decline in many wells is close to 50% indicating that the wells will become uneconomical to produce within three to five years.

We cannot use water flooding to increase the production since water will only increase the pressure in the reservoir resulting in further reduction in oil and gas production. Conventional CO_2 flooding is also not feasible since injected CO_2 will move through the high permeability system resulting in quick breakthrough. In this section, we evaluate the feasibility of huff-n-puff methods. These include injection of gases including Carbon-dioxide (CO_2), Flue Gas (88% Nitrogen, 12% CO_2) and methane. The aim of an enhanced recovery process is to revitalize the depleted wells and produce maximum recoverable oil. The important factor in determining the feasibility of the process is the economics of the recovery project. Although this study does not deal with the economics of secondary recovery process, it provides a vital insight into the engineering aspects of the recovery process.

Field Application

Enhanced recovery methods are used to produce the residual oil in the reservoir. Methane, flue gas and CO_2 injection is studied and the results are discussed. The procedure for enhanced recovery is simulated (using ECLIPSE 300) in following steps:

1. Primary Depletion: Primary depletion is carried out for a period of two years during which the reservoir pressure is depleted to a low value (500 psi). The composition of reservoir fluid changes with depletion and heavier components remain in the reservoir during the end of the primary depletion process.
2. Calculation of Minimum Miscibility Pressure (MMP): Once primary depletion is carried out, the composition of the remaining reservoir fluid is used to determine the MMP for the injection gas. The MMP test is carried out using the GEOQUEST PVTI module.
3. Gas Injection: Gas is injected in the reservoir at the constrained bottom hole pressure until the reservoir attains the MMP. The injection period depends on injection pressure, MMP and the nature of injection gas.
4. Shut in Period: After the gas has been injected, the reservoir is shut in for a 30-day period, which allows the reservoir to re-pressurize and achieve MMP throughout the reservoir. This is also the period during which the vaporizing-gas drive is achieved.

5. Production Period: The well is reopened and produced for a period that is economical or until a certain reservoir pressure is reached. For continuing cycles of enhanced recovery the production period and depleted reservoir pressure may need to be optimized.

CO_2 Injection Study

A CO_2 injection study was performed to estimate the oil and gas production from the secondary process. Figure 53 shows the production cycle. It can be seen from the plot that the maximum oil production rate decreases with each cycle. The reservoir was depleted for a period of 2 years. Depleted reservoir pressure was about 520 psi. The MMP test was conducted using PVTI and the MMP was calculated to be 1490 psi. CO_2 was injected at an injection pressure of 2500 psi for 70 days until the reservoir pressure was equal to the MMP. The well was put back on production after a 30-day shut in period. The well was produced for 400 days during which a maximum oil rate of 70 STB/D was recorded. A second CO_2 injection cycle was carried out. The MMP was calculated to be 1295 psi. CO_2 was injected at a pressure of 2500 psi for 60 days until the reservoir reached the MMP. The well was produced for 400 days after a 30-day shut in period. Maximum oil production during this cycle was 15STB/D. A third injection cycle was performed but it showed very low oil production rates (less than 5 STB/D) and is not discussed here.

The gas produced consisted of 73% CO_2 indicating that it was not saleable without separation. Although an economic analysis of CO_2 injection was not performed in this study, it can still be concluded based on these results that CO_2 injection in its current state may not a viable unless it can be secured at low price (about $ 0.5/MSCF).

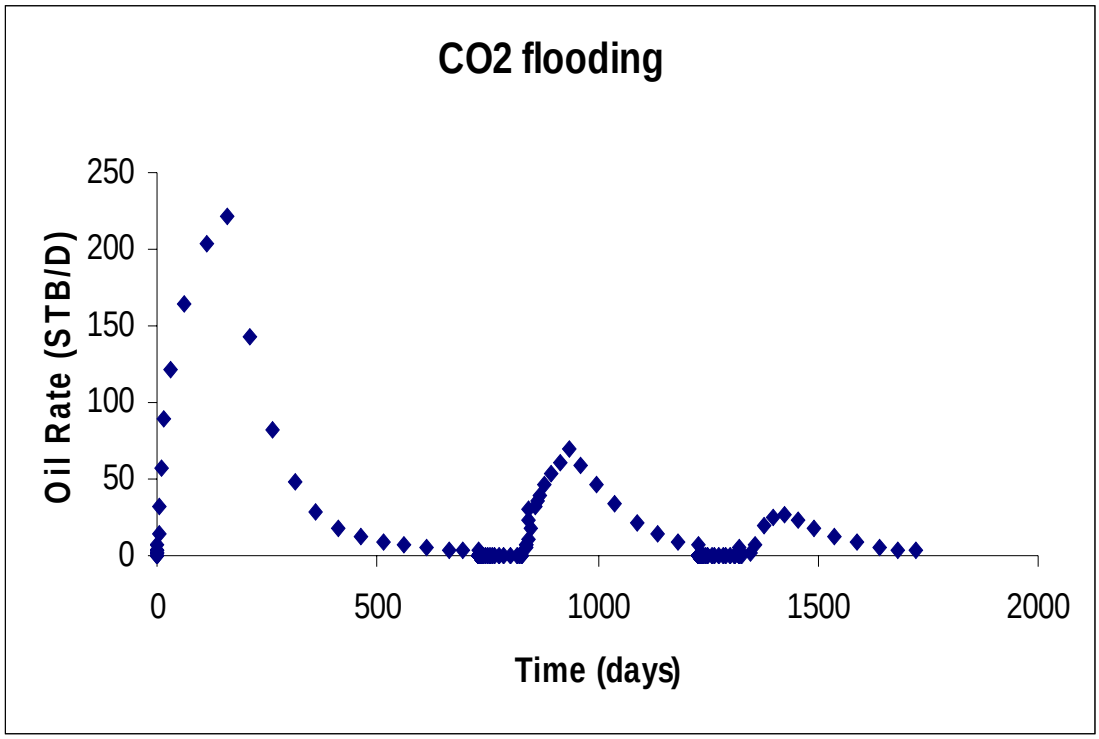

Figure 53: CO_2 Injection Study

Flue Gas Injection Study

Apart from CO_2, flue gas and methane injection studies were also carried out. Flue Gas (88% N2, 12% CO_2) has a higher MMP than CO_2. This was confirmed by simulating a MMP test for the depleted reservoir fluid composition. The MMP was obtained as 2152 psi, which is considerably higher than the MMP for CO_2. Flue gas was injected at a pressure of 2500 psi for 115 days. Production was resumed from the well after a 30-day shut in period. Oil production was very low when compared to CO_2 injection. The produced gas consisted of 63% Nitrogen and 16 % CO_2. Figure 54 shows the plot of flue gas injection study. As can be seen from the plot, only one injection cycle is performed and the oil rates are very low (5 STB/D). Further injection cycles were not performed, as the oil rate in the first cycle itself was very low.

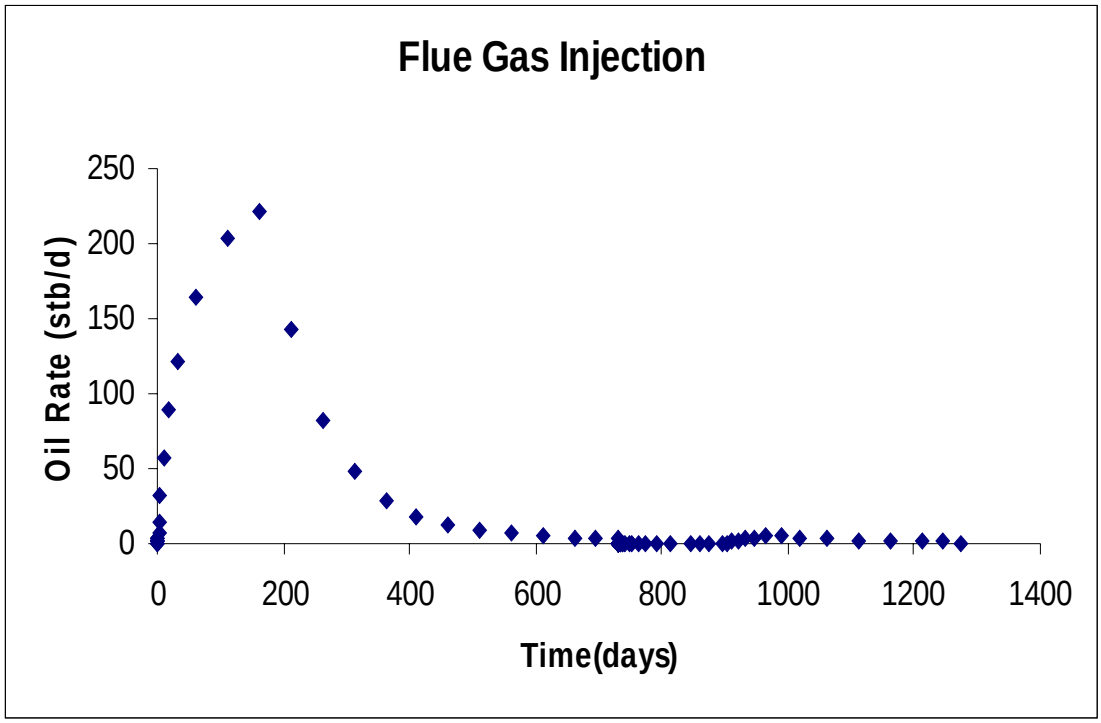

Figure 54: Flue Gas Injection Study

Methane Injection Study

A methane injection study was carried to see if higher oil production could be obtained as compared to flue gas. The MMP for methane was obtained at 2126 psi, same as that for flue gas. Methane was injected at a pressure of 2500 psi for 80 days until the reservoir attained the MMP. The well was shut in for 30 days and put on production for 400 days. Production data indicated very low oil rates. Due to low oil recoveries in the first injection cycle, subsequent recovery cycles were not performed. Figure 55 shows methane injection study results.

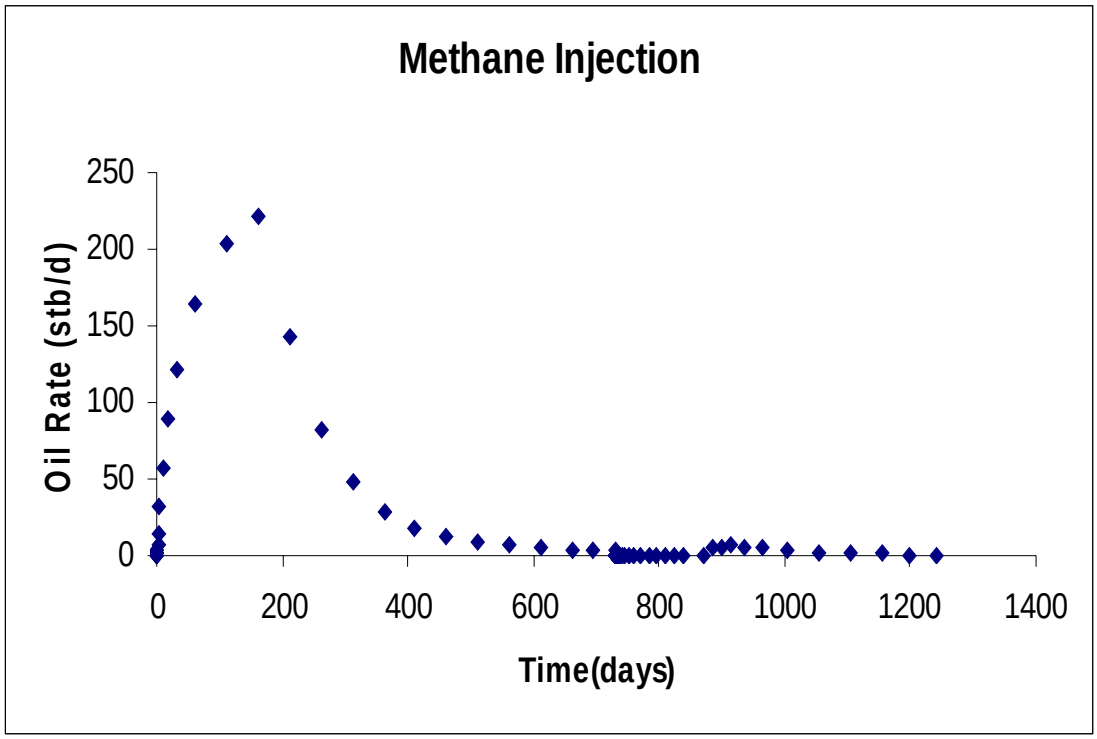

Figure 55: Methane Injection Study

Summary

The enhanced recovery study by huff-puff method was carried out using three injection gases. It was observed that only CO_2 injection can increase oil recovery, although the produced gas contained 73% CO_2 which makes the recovery process economically difficult to justify. Enhanced recovery using CO_2 is only possible if the price of CO_2 is reasonable. Methane and flue do not show good oil recovery and, hence, are not suitable as enhanced recovery agents for this reservoir.

Economic Analysis

Samarth Patwardhan, The University of Tulsa

The early development of West Carney field was mostly accomplished through vertical wells. However, in the last two years, the new wells drilled are mostly horizontal wells. This section evaluates the performance of representative vertical wells with representative horizontal wells. It should be emphasized that the work presented in this section is preliminary in nature because of limited amount of data used and the analysis presented. Specifically, the questions we need to address are:

- What is Net Present Value obtained by drilling vertical well vs. horizontal well?
- What is the probability of success in drilling vertical vs. horizontal well?
- How does the horizontal well benefit by holding bigger section of the lease compared to vertical well?
- How does the length of horizontal well affect the performance of horizontal well?

A preliminary analysis between the horizontal and vertical wells is undertaken in this report. A total of 16 wells were considered – eight horizontal and eight vertical. Some of these wells have been drilled recently, i.e. around January 2003, and have not developed long historical record. The lease operating cost, before completion costs (BCP) and after completion costs (ACP) were taken into account for each well. The analysis is before taxes, so we did not take depreciation or income taxes into account in conducting our analysis.

Table 10 provides the names of the wells, which were studied in this project

Table 10: Names of Horizontal and Vertical Wells

Vertical wells	Horizontal wells
Wilkerson 1	Wilkerson 2
Griffen 1	Gilmore 1
Suzie Q	Gilmore 2
Shons 1	Mr. B
Danny 2	Jennifer
Anna Givens 1	Julie Ann
Stevenson 1	44-Horizontal
Schwake 1	Blackstuff

The data provided for all the wells was only till the month of June 2003. In order to perform a preliminary economic analysis, a planning horizon of 72 months (6 years) was taken into account, with month 0 being the one in which the BCP and the ACP occur. We assumed that the well has a maximum life of six years.

Table 11 gives the values of the BCP, ACP and Equipment costs for the vertical wells considered.

Table 11: Costs of Vertical Wells

Vertical Wells			
Well Name	**BCP ($)**	**ACP ($)**	**Equipment ($)**
Wilkerson 1	139,461.78	57,500.76	177,624.34
Griffen 1	226326.01	85938.7	193,896.52
Suzie Q	189,958.12	127,594.83	238,204.31
Shons 1	10,126.45	67,674.50	100,918.71
Anna Givens 1	158,639.61	63,508.17	139,476.03
Stevenson 1	213,489.31	65,838.97	150,648.60
Danny 2	124,471.62	60,271.20	151,599.11
Schwake 1	132,883.19	39,145.06	254369.06

Table 12 gives the values of the BCP, ACP and Equipment costs for the horizontal wells considered.

Table 12: Costs for Horizontal Wells

Horizontal Wells			
Well Name	**BCP ($)**	**ACP ($)**	**Equipment ($)**
Wilkerson 2	490,648.63	48,456.47	245,776.72
Gilmore 1	344,084.39	78,266.10	108,828.84
Gilmore 2	320,003.09	127,973.69	180,337.19
Blackstuff	389,177.10	148,137.09	185,567.76
Jennifer	491,910.69	120,999.91	174,580.16
Mr. B	569,666.32	103,341.31	220,245.42
Juli Ann	496,904.22	81,434.77	95,922.13
44-Horizontal	431,472.27	151,346.17	251,968.17

To extrapolate the revenue up to six years, we plotted ln (gross revenue) vs. time. By fitting the best line through it, we could extrapolate the revenue up to six years. This assumes that revenue is proportional to oil and gas production and the price of oil and gas remain reasonably constant. In addition, the following assumptions were made in conducting this economic analysis.

1) In case the average lease operating expense up till June' 03 was too high, a value between $1000 and $5000 was assumed. This is a reasonable value for the expense, based on the data from other wells. The lease operating expense is dependent on amount of fluid produced. Larger the amount of water, more is the operating cost.
2) If sufficient production data were not available to estimate decline, we assumed about 4 % per month or 50 % per year decline in revenues. This is consistent with other wells in the field.

3) If gross revenue was not available for some wells, we calculated gross revenue by assuming oil price of $ 25 per barrel and gas price of $ 4 per MSCF.

Using the information for all the wells, we evaluated all the vertical and horizontal wells and calculated the Net Present Value at 20 % annual interest rate. The details about the gross revenue as a function of time can be found in Appendix C.

Table 13 shows the NPV values of the vertical wells at 20%.

Table 13: NPV at 20% for Vertical wells

Vertical Wells	
Well Name	**NPV at 20%**
Wilkerson 1	2,272,218.89
Griffen 1	272,573.39
Suzie Q	169,137.47
Shons 1	(277,671.73)
Anna Givens 1	(164,621.75)
Stevenson 1	1,074,768.63
Danny 2	2,187,104.19
Schwake 1	2,716,735.16

Figure 56 shows the NPV at 20 % for the above given vertical wells.

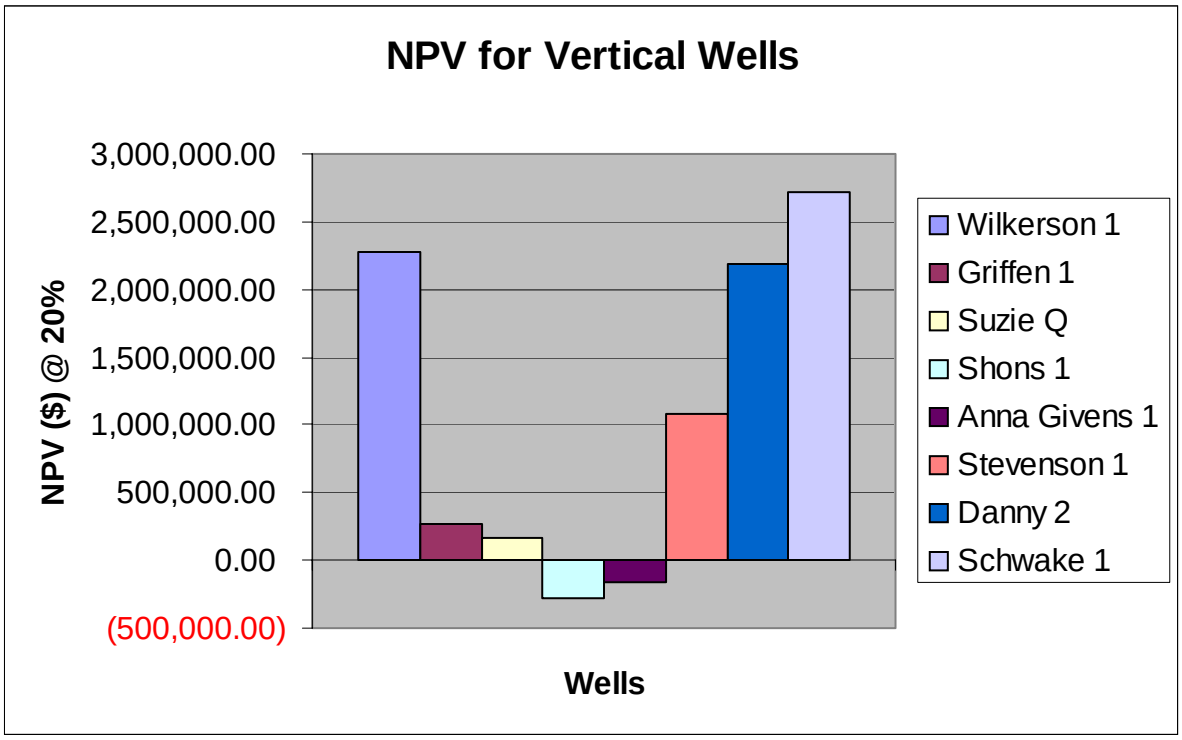

Figure 56: NPV @ 20% for Vertical Wells

It can be seen from the figure that 6 out of 8 wells considered have a positive NPV at an annual interest rate of 20%.

Table 14 shows the NPV values for the vertical wells at 10%.

Table 14: NPV @ 10% for Vertical Wells

Vertical Wells	
Well Name	**NPV @ 10%**
Wilkerson 1	2,691,488.24
Griffen 1	451,610.33
Suzie Q	297,213.42
Shons 1	(311,342.33)
Anna Givens 1	(150,889.65)
Stevenson 1	1,299,454.95
Danny 2	2,466,229.56
Schwake 1	3,566,024.67

Figure 57 shows the NPV values of the vertical wells, at an annual interest rate of 10 %

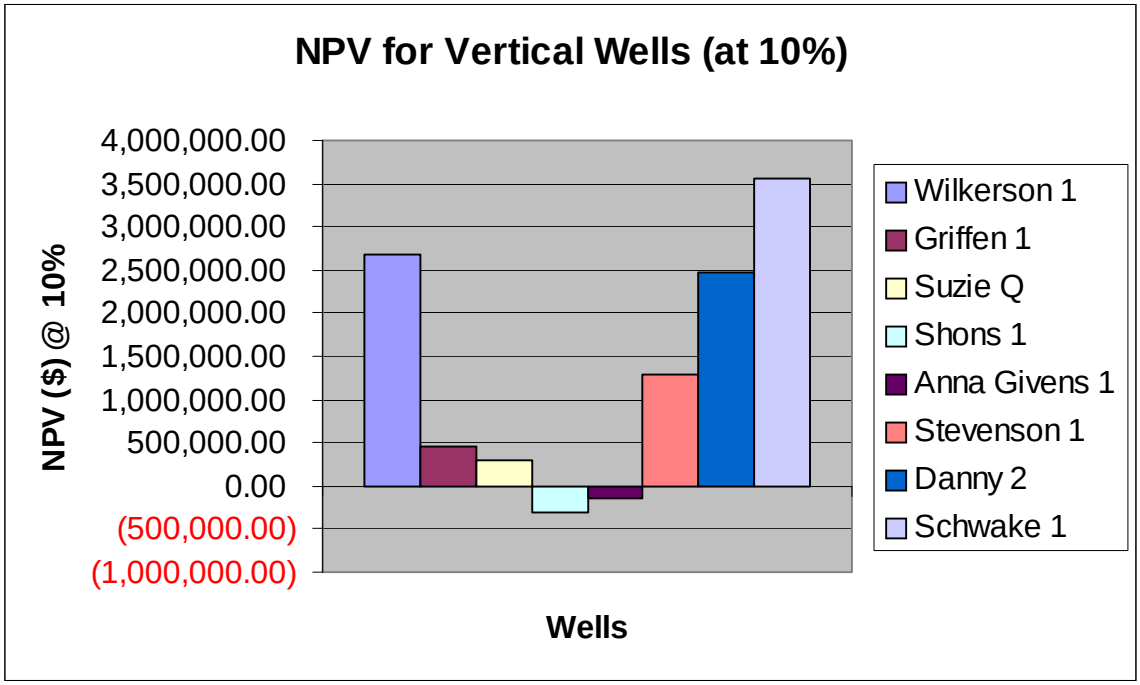

Figure 57: NPV @ 10% for Vertical Wells

The wells show a similar behavior as when evaluated at 20%. It can be seen that Shons 1 and Anna Givens 1 still have a negative NPV value, even when the annual interest rate is considered as 10%. The other wells have a higher value of NPV though, which is normal. There is a substantial increase in the NPV values of the wells at 10%.

Table 15 gives the NPV values for horizontal wells at an annual interest rate of 20%.

Table 15: NPV @ 20% for Horizontal wells

Horizontal Wells		
Well Name	**NPV at 20%**	**Length of Well**
Wilkerson 2	1,374,244.33	1116
Gilmore 1	631,059.08	166
Gilmore 2	(121,355.90)	1235
Blackstuff	1,081,457.83	1126
Jennifer	(186,148.27)	2654
Mr. B	742,721.08	1,354.00
Julie Ann	(398,887.11)	2,732.00
44-Horizontal	120,441.19	2,060.00

Figure 58 shows the NPV values for the horizontal wells.

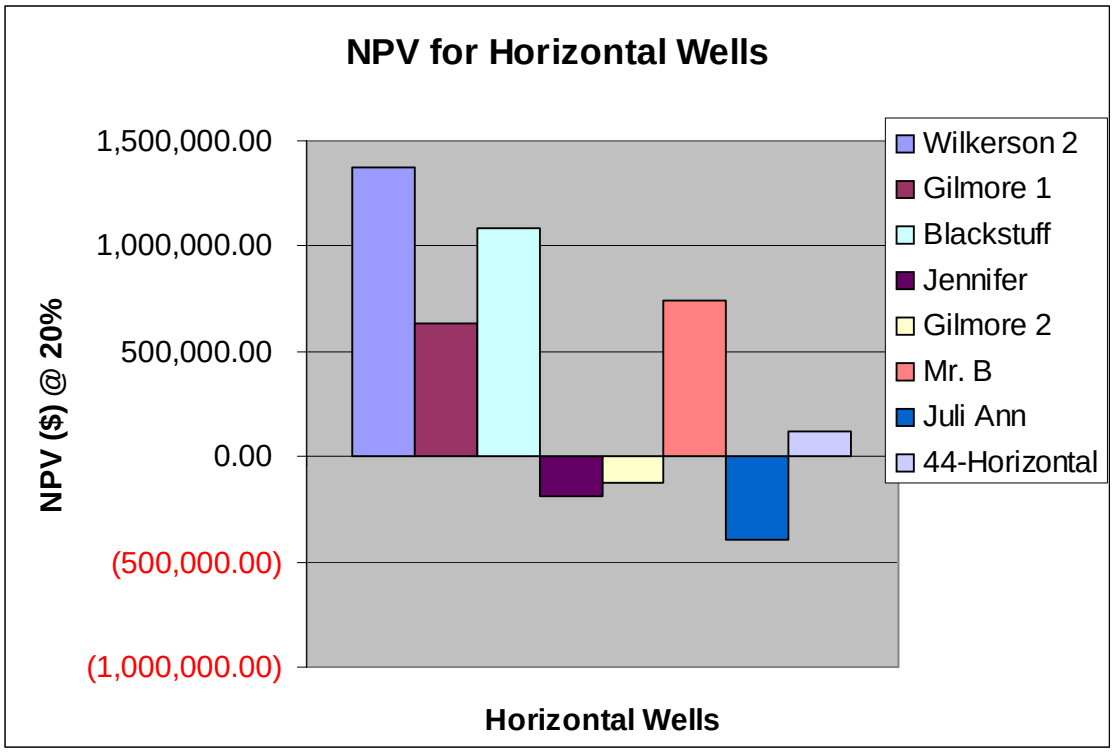

Figure 58: NPV @ 20% for Horizontal Wells

Figure 58 shows that out of 8 wells, 5 have a positive NPV at 20%.

Table 16 gives the NPV values for the horizontal wells, when evaluated at an annual interest rate of 10%.

Table 16: NPV @ 10% for Horizontal Wells

Horizontal Wells	
Well Name	**NPV @ 10%**
Wilkerson 2	1,807,676.91
Gilmore 1	1,001,838.60
Gilmore 2	(45,276.16)
Blackstuff	1,465,940.72
Jennifer	(72,166.96)
Mr. B	982,973.37
Juli Ann	(355,353.63)
44-Horizontal	300,149.62

Figure 59 shows the NPV values for the horizontal wells, when evaluated at an annual interest rate of 10%.

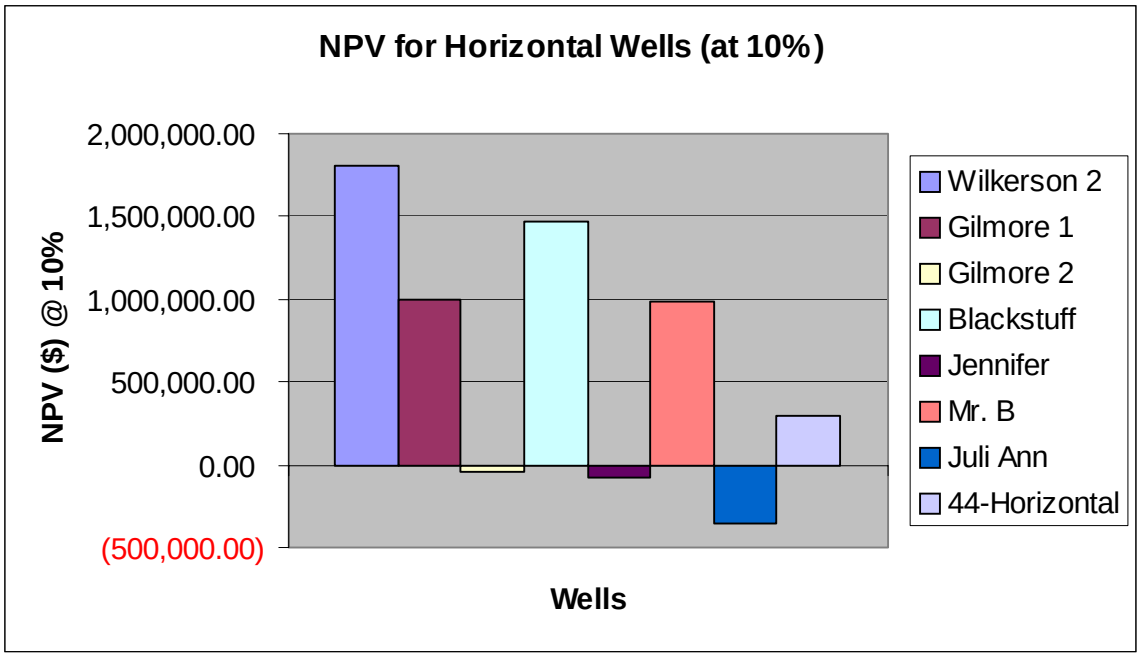

Figure 59: NPV @ 10% for Horizontal Wells

It can be seen from the above figure that there is a substantial increase in the NPV of the wells, when compared to the NPV obtained at an annual interest rate of 20%.

Figure 60 shows the relation between NPV @ 20% with the length of the horizontal well. It can be seen that there is no correlation between the NPV and the length of well. If any, it can be seen that as the length increases, the NPV decreases.

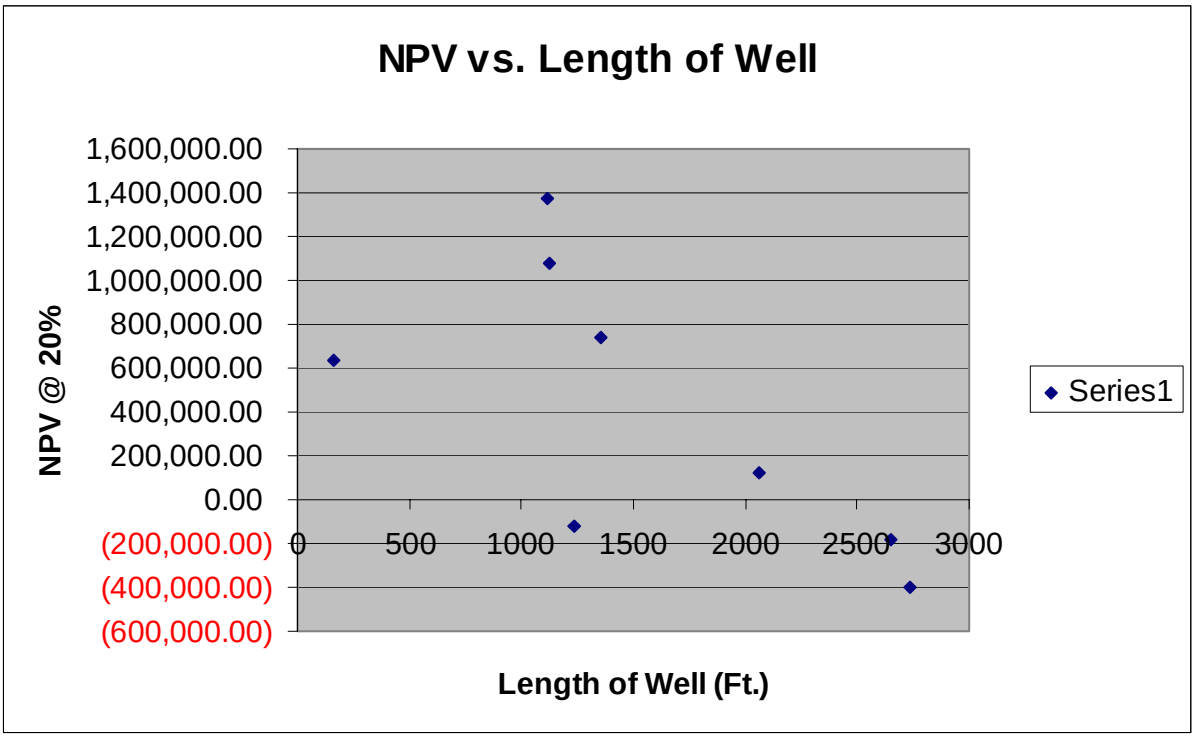

Figure 60: NPV @ 20% vs. Length of well

Figure 61 shows the values of NPV for various interest rates for horizontal wells. It can be seen that only Julie Ann, Jennifer and Gilmore 2 have their NPV less than 0 for all interest rates.

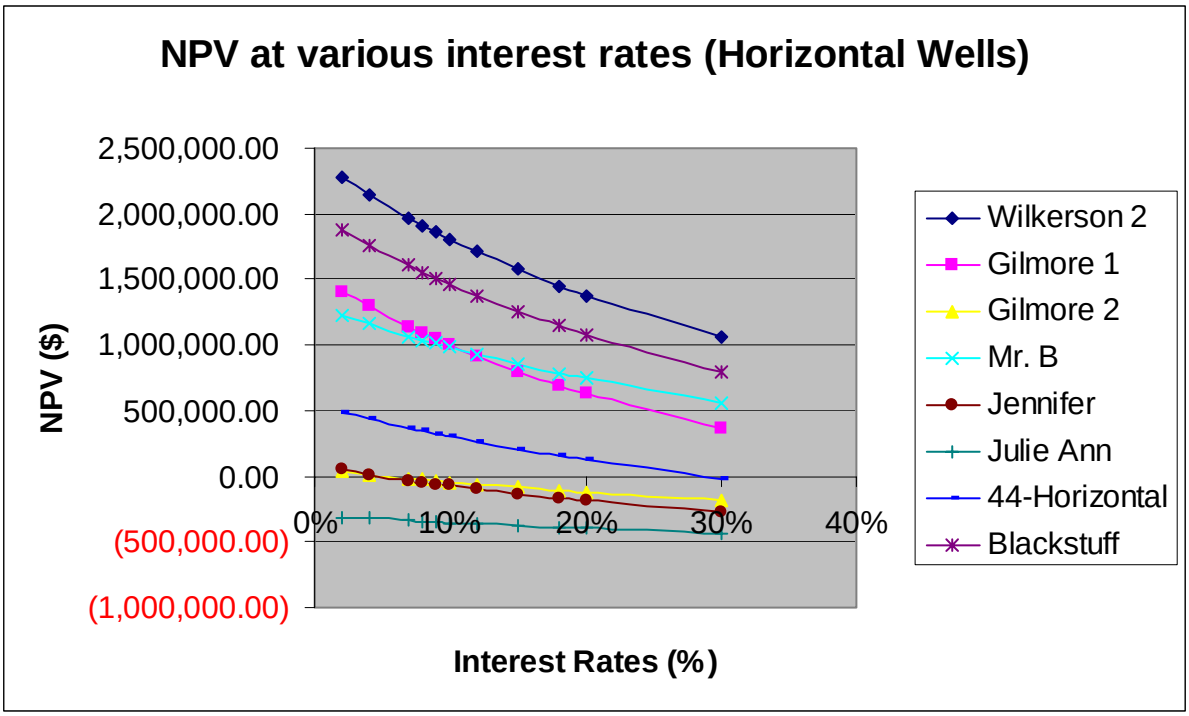

Figure 61: Figure 6: NPV at various interest rates for horizontal wells

Figure 62 shows how the NPV varies for the vertical wells, when the interest rate changes. Only Anna Givens and Shons 1 have their NPV values below 0 at all interest rates.

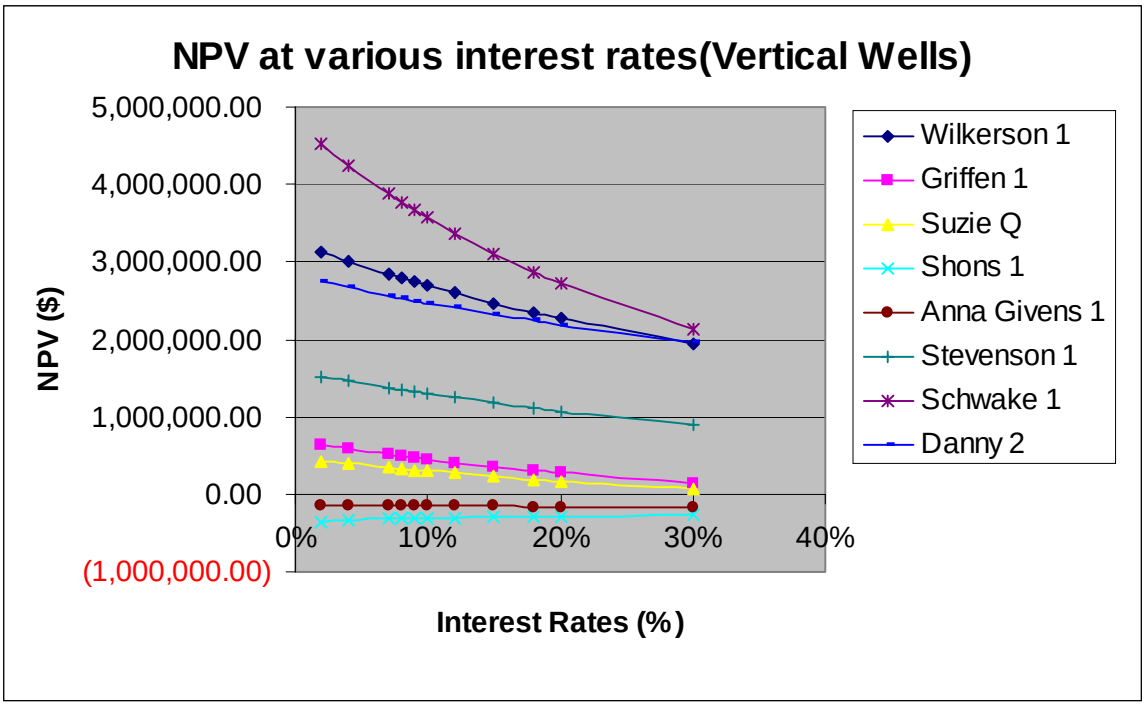

Figure 62: NPV at various interest rates for vertical wells

The Net present values of all the wells were added up and an average was taken across all wells, for a particular annual percentage rate. In this manner, the average NPV for the vertical as well as horizontal wells was calculated.

Table 17 gives the average values of the net present values obtained across the wells.

Table 17: Average values of NPV for various annual percentage rates

Annual Rate	Average NPV (V)	Average NPV (H)
2%	1560710	879112
4%	1485943	812250
7%	1383709	719766
8%	1350311	690862
9%	1319033	662859
10%	1288724	635723
12%	1230861	583919
15%	1150429	511937
18%	1076874	446166
20%	1031281	405442
30%	837669	233195

Figure 63 shows how the average values of these above calculated NPV's vary with the annual percentage rate. Clearly, based on the analysis, the vertical wells provide superior value to horizontal wells.

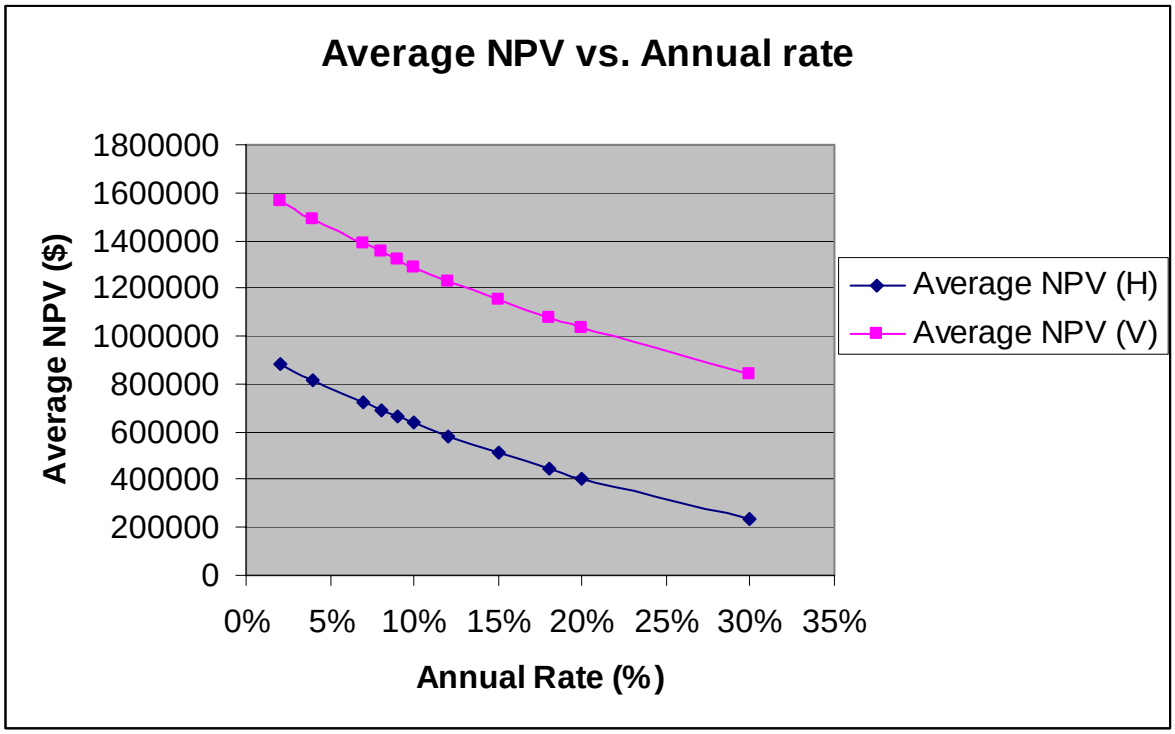

Figure 63: Figure 8: Average NPV values across wells

Summary

Based on the analysis of the limited number of wells, we can reach preliminary conclusions:

- The probability of success for horizontal wells is about the same as that of vertical wells.
- The vertical wells provide better NPV than horizontal wells.
- The length of the horizontal wells does not correlate with the NPV of that well.

Technology Transfer

The following presentations and publications were made:

1. U.S. DOE-Sponsored Study of West Carney Hunton Field, Lincoln & Logan Co., OK: A Preliminary Report
   By James R. Derby, F. Joe Podpechan and Jason Andrews, and Sandeep Ramakrishna.
   Shale Shaker (Journal of the Oklahoma City Geological Society, vol 53, no. 1, pages 9-19, and vol. 53, no. 2, pages 39-48, 2002.

2. Development Case Study of a Karsted Carbonate "Island" Hydrocarbon Reservoir: West Carney Hunton Field, Oklahoma
   By James R. Derby, F. Joe Podpechan, Jason Andrews, and Sandeep Ramakrishna.
   American Association of Petroleum Geologists, Electronic Publication: Search and Discovery, Article #20008 (2002)

3. U.S. DOE- Sponsored Study of West Carney Hunton Field, Lincoln & Logan Co., OK: A Preliminary Report
   By James R. Derby*, F. Joe Podpechan*, Jason Andrews, and Sandeep Ramakrishna. *Speakers
   Presented at noon luncheon meetings of the Tulsa Geological Society, Nov. 13, 2001, and the Oklahoma City Geological Society, Jan. 23, 2002.

4. Development Case Study of a Karsted Carbonate "Island" Hydrocarbon Reservoir: West Carney Hunton Field, Oklahoma
   By James R. Derby, F. Joe Podpechan, Jason Andrews, and Sandeep Ramakrishna.
   Presented by James R. Derby on May 16, 2002 at the International Symposium on the 21st Century Petroleum Exploration and the 2nd Forum on Marine Carbonate Reservoirs in China, Hangzhou, China, May 14-17, 2002. [This paper was presented at the request of the American Association of Petroleum Geologists who provided travel arrangements and expenses for the presenter].

5. Development Case Study of a Karsted Carbonate "Island" Hydrocarbon Reservoir: West Carney Hunton Field, Oklahoma
   By James R. Derby, F. Joe Podpechan, Jason Andrews, and Sandeep Ramakrishna.
   Presented by James R. Derby, May 21, 2002, at the invitation of the Tulsa Geological Study Group, at their evening meeting. (A repeat of the Hangzhou presentation).

6. Development Case Study of a Karsted Carbonate "Island" Hydrocarbon Reservoir: West Carney Hunton Field, Oklahoma
   By James R. Derby, F. Joe Podpechan, Jason Andrews, and Sandeep Ramakrishna.
   Presented by James R. Derby, Oct. 30, 2002, at the invitation of the University of Tulsa Department of Geoscience, Noon Seminar Series.

7. Development Case Study of a Karsted Carbonate "Island" Hydrocarbon Reservoir: West Carney Hunton Field, Oklahoma
   By James R. Derby, F. Joe Podpechan, Jason Andrews, and Sandeep Ramakrishna.
   Presented by James R. Derby at the invitation of the Tulsa Geological Society, for their evening meeting Nov. 5, 2002, in conjunction with a talk by David Chernicky and Scott Schad of New Dominion on the discovery and development of West Carney Hunton Field

8. Exploitation and Optimization of Reservoir Performance in Hunton Formation, Oklahoma
   By Mohan Kelkar, Ph.D., J.D.
   Presented by Mohan Kelkar at the U.S. DOE Class II Shallow Shelf Carbonate Review, December 12, 2002, at The University of Texas, Permian Basin, Odessa, TX.

9. Hunton Dewatering Project: Mystery Solved?
   By Brian Keefer, presented at 15th Oil Recovery Conference, TORP, University of Kansas, Wichita, KS (March 17, 2003)

10. Dewatering of the Hunton Reservoir in West Carney Field: Mystery Solved?
    Technical Workshop, presented at the DoubleTree Hotel, Tulsa, OK (April 16, 2003)

11. Dewatering of the Hunton Reservoir in West Carney Field: Mystery Solved?
    Technical Workshop, presented at Metro Technology Center, Oklahoma City, OK (April 21, 2003)

12. Exploitation and Optimization of Reservoir Performance in Hunton Formation, Oklahoma
    By Rahul Joshi, first place paper, Masters division, SPE Student Paper Contest, Mid-Continent Division, presented at the University of Missouri – Rolla (April 5, 2003)

13. Correlating Static Data to Dynamic Characteristics: Hunton Reservoir
    By Sandeep Ramakrishna, Brian Keefer, and Mohan Kelkar, submitted for publication by the University of Kansas (May, 2003)

14. Limestone and Dolomite Cores from the Hunton Formation, West Carney Field, Oklahoma
    By Joe Podpechan, Jim Derby, and Jason Andrews, presented at the Poster/Core Sessions, 2003 Mid-Continent Section Meeting, American Association of Petroleum Geologists (October 13-14, 2003)

15. Dewatering as a Production Technique in a Dual Permeability Reservoir: West Carney Hunton Field, Lincoln and Logan Counties, Oklahoma
    By Joe Podpechan, Jim Derby, Jason Andrews, and Sandeep Ramakrishna, presented at the 2003 Mid-Continent Section Meeting, American Association of Petroleum Geologists (October 13-14, 2003)

Web Development

The project web software was converted to Dreamweaver MX due to technology issues between The University of Tulsa's servers and Microsoft Frontpage. With this conversion, cascading style sheet (CSS) technology was applied to provide a uniform appearance and allow for quick formatting changes in the future. The new site, located at http://www.tucrs.utulsa.edu/Hunton will be the point of contact for all future technology transfer. (July, 2003)

Conclusions

Based on the work presented in the report, following conclusions can be drawn:

- The Hunton reservoir exhibits predominantly oil wet characteristics. Most of the oil is located within intermediate sized pores.
- The reservoir contains volatile oil at bubble point pressure of approximately 1,900 psia.
- The remaining oil saturation has big influence on the productivity of the reservoir. A relationship exists between porosity of the reservoir and the remaining oil saturation. Higher the porosity, lower is the remaining oil saturation. Among the four compartments investigated, we observed that the dolomitized regions, having high porosity, typically have low oil saturations and hence low productivity. The other two compartments, which are primarily limestone reservoirs, have low porosity and high oil saturation, and hence better recovery.
- The core analysis indicates that the reservoir contains high permeability conduits mostly filled with water.
- A new material balance method is developed to calculate original oil in place. By using an appropriate two phase Z factor, we can apply traditional p/Z method to calculate the initial oil in place. The applicability of the method is demonstrated by applying it to synthetic case as well as the four compartments investigated thus far.
- The difference between oil in place calculated using decline curve analysis and material balance may either indicate potential for new in fill wells or isolated oil globules. Additional investigation about the relationship between isolated oil and the lithology needs to be conducted.
- By using a compositional simulator, the important characteristics of the West Carney field are captured – thus validating the reservoir model consisting of matrix and fractures. Matrix contains oil, whereas, fractures/high permeability zones contain water.

Two potential secondary mechanisms can help us recover additional amount of oil. CO_2 flooding in a simulator indicates that additional oil can be recovered through huff-n-puff mechanism so long as the price of CO_2 is reasonable. Other possibility is to inject surfactant so that the wettability of the rock can be altered, thus improving the imbibition recovery. Both these processes need to be investigated further.

References

1. Amsden, T.W., and J.E. Barrick, 1986, Late Ordovician-Early Silurian Strata in the Central United States and the Hirnatian Stage: Oklahoma Geological Survey Bull. 139, 95 p.

2. Johnson, M.E., 1996, Stable Cratonic Sequences and a Standard for Silurian Eustasy: Geological Society of America, Special Paper 306, p. 203-211.

3. Roehl, P.O., 1967, Stony Mountain (Ordovician) and Interlake (Silurian) facies analogs of Recent low-energy marine and subaerial carbonates, Bahamas: American Association of Petroleum Geologists Bulletin, v. 51, no. 10, p. 1979-2032.

4. Stanley, T.M., 2001, Stratigraphy and Facies Relationships of the Hunton Group, Northern Arbuckle Mountains and Lawrence Uplift, Oklahoma: Oklahoma Geological Survey Guidebook 33, 73 p.

5. Martin, A.J., Solomon, S.T., Hartman, D.J.: Characterization of Petrophysical Flow Units in Carbonate Reservoirs, AAPG Bulletin (1997) 81 (5) 734-759.

Appendix A - Geological Analysis

Preliminary or Revised Core Descriptions

Table A- 1: Mercer 1-28 Preliminary Stratigraphic Description, Quick Review of Slabbed Core

UNIT	FROM	TO	THK	DESCRIPTION
Top of Core = 4527				
Woodford Shale (not cored)				
Misener Sandstone (not cored)				
Hunton Group (55 ft. cored)				
Lower Clarita Fm (6.7 ft.)				
	4527	4533.7	6.7	Dol, pale brown, med fossilif. grnstn-pkstn, much moldic porosity.
Clarita-Prices Falls Member (12.1 ft)				
	4533.7	4545.8	12.1	Dol, dark gry to black, abund. gilsonite & oil stain, fossilif., moldic porosity, burrowed. disturbed bedding, possibly diagenetic terrane. abund. small crinoids
Upper Cochrane B (20.1 ft)				
	4545.8	4555.3	9.5	Ls, shaly, pale brown burrow-mottled shaly lime mdstn, sparse fossilif., rare crinoids & brachioids. Pyrite nodules at base. Up Cochrane top to be better defined by cono sampls
	4555.3	4561.2	5.9	Ls, shaly, pale brown-gray burrow-mottled shaly lime mdstn. Sharp upper contact, abund small crinoids at top.
	4561.2	4565.9	4.7	Shale, limy & Ls, shaly. Abrupt top & bottom contacts. Two intervals of abund. fossil fragments, dom. crinoids.
Upper Cochrane A (9.4 ft.)				
	4565.9	4569.3	3.4	Ls, buff to light gray, burrowed mdstn, "birdseye" crystals common. Grades to shale below.
	4569.3	4570.6	1.3	Sh, dk grn-gry, limy, thinly laminated, part nodular.
	4570.6	4575.3	4.7	Ls, shaly, lt gry-greenish gray, nodular mdstn with thin shaly partings. Basal contact obscure, place at a parting, based on conodont faunal change.
Lower Cochrane (6.7 ft cored)				
	4575.3	4576.6		Ls, shaly, lt gry-greenish gray, nodular mdstn with thin shaly partings and 0.5' of shale at base.
	4576.6	4582	5.4	Ls, pale brown, burrow mottled mdstn & v.f. fossilif. wkstn; sparse shaly partings.
Base of Core = 4582				

Table A- 2: Chandler SWDW Preliminary Stratigraphic Description, Quick Review of Slabbed Core

UNIT	FROM	TO	THK	DESCRIPTION
Hunton (entire core, 59.75 ft. cored)				
Lower Clarita FM. (24.9 ft.)				
H	4810	4834.9	24.9	Dol, md dk gy, abund vuggy moldic porosity, some Karst fractures with fill, 2ndry tight zones NOTE: is this sabkha crusts? Small cavities with lam fill; TS at 4822.5 dol- TS 4834.8 - 4835 poss TS at 4833 - sel Cono s.l. poss TS at 4825 photo karst fill at 4817
Upper Cochrane B (15.3 ft.)				
G	4834.9	4839.9	5	Dol, burrowed, prob "diagenetic terrane", sparse isolated vugs; altered burrowed wkstn + mdstn, laminated at top
F	4839.9	4842.4	2.5	Ls, dolomitic, fine foss wkstn to foss mdstn, burrowed, partly dolomitized, sparse large crinoid
E	4842.4	4844.3	1.9	LS, grnst + sh, limy;loc lg grains in shale. Spare brach, crinoid; Shale, limy to Shaly Ls med grn-gy, vuggy, with lime mdstn lenses, burrow fill. Large white chert nodule TS 4843 - 43.3 grnstn TS 4843.6 - .7 with blk center Grades at top-top 2' has thin lime grnstn bed
Upper Cochrane A. (25.45 ft cored)				
D	4844.3	4850.2	5.9	Shale, med grn gy, with lime mdstn nodules, grades up in top ft to burrowed cherty mdstn
C	4850.2	4853.5	3.3	Ls, lt gy burrowed mdstn with shaly laminae, black chert nodule, sparse large crinoid; TS 4862.0 burrowed mdstn
B	4853.5	4859.5	6.5	Shale, med grn gy, with lime mdstn nodules, grades up in top ft to burrowed cherty mdstn
A	4859.4	4869.75	10.35	Limestone, nodular burrowed mudstone, with shaly laminae and beds up to 1 cm thick. With 7 large black chert nodules; shaly at top 0.5' and basal 2 ft. TS 4867.4 chert nodule
Note: Formation assignments based on conodont analysis as of10/6/03.				
Note: no Lower Cochrane, nor no Prices Falls has been found in this well.				

Table A- 3: Marjo Cal 1-11 Preliminary Stratigraphic Description, Quick Review of Slabbed Core

UNIT	FROM	TO	THK	DESCRIPTION
Hunton Group (101.8 ft. cored)				
Lower Cochrane				
J	5034	5051	17	Ls; sparse pentamerid brach pkstn;
I	5051	5111	60	Ls, fine crinoid-brach wkstn with intrbdd mdstn, loc. Intensly fractured.
H	5111	5115.5	4.5	Ls, mdstn, with fractures and soln cavity fill, with cave flowstone
G	5115.1	5115.6	0.5	Ls, cavern fill Parabreccia? With vertical open fracture filled with Karst mud. (get TS of this)
F	5115.6	5129.7	14.1	Ls, pale-br mdstn, sparsely fossilif. rare crinoids; fractured, Karst fill in dissol.cavites, Crackle breccia, both V & H
E	5129.7	5133.9	4.2	Ls, Shaly, nodular, pale yellow-brn mdstn, with abund dark gry shale layers; prob burrowed mottled strongly pyritic 32 - 33.7;, glauconite pellets at 5130.3 to 5131 large white chert 33.7 - 33.9;
D	5133.9	5135.4	1.5	Ls, mdstn, pale yellow brn, burrowed mottled, sparse shaly laminae
C	5135.4	5135.8	0.4	Ls, pale yellow brn - (buff); mdstn, burrowed corrasion contacts top and bottom
Sylvan Shale (9.8 ft. cored)				
B	5135.8	5138	2.2	Dol, mdstn argill; pale grn - gry at top, grades down to med grn gry with incr argill pyrite in top 0.2; blk chert nodule in top 0.2 with thin shale layers
A	5138	5145.6 TD	7.6	Shale, med grn gry, Dolomitic, burrowed grades in part, mod - strongly fissile, up to Dolomite

Note: The entire Hunton is very tightly cemented with no significant matrix porosity. Permeability is entirely due to solution-enlarged fractures. The lower 20 ft. of the Hunton appears to be a deeper water facies than seen in most field wells. This facies appears to be BA 4 & 5 (below storm wave base), as opposed to BA 3 & 2 for most Carney limestone wells.

Table A- 4: Marjo Morrow 1-27 Preliminary Stratigraphic Description, Quick Review of Slabbed Core

Morrow 1-27 Preliminary Core Description; with Conodont age assignments

UNIT	FROM	TO	THK	DESCRIPTION
				Note 1: Unit D looks like dolomitized upper part of Chandler SWDW - with tight streaks alternating with grnstn Note 2: Core log correction very close to Core depth = Log depth, by visual inspection
Hunton (51.5 ft cored)				
Upper Cochrane A (6.2)				
E	4905	4911.2	6.2	Ls, fine foss grnstn & pkstn, sharp basal contact at corrosion surface.
Lower Cochrane (45.2 ft).				
D	4911.2	4951.2	40	Ls, fine foss grnstn + pkstn; loc mdstn; thin intervals of Pent. Brachs, small brachs at 4947 - 46, 4922 - 24, 4908 Porosity is moldic (?) or micro vug., appears uniformly oil stained
C	4951.2	4956.4	5.2	Dol, variegated, shaly in part, loc. Fossilif. with small brachs, burrowed - Diagenetic Terrane? No obv. Karst, mostly tight. Pyrile nodules, Dol nodules - photos
Keel FM	4955.6			
B	4955.6	4956.5	0.9	Oolite, chert and dolomite, lt gy to pale grn-gy, with ovate white & black chert nodule, 0.1 ft thick, with white ooids. TS
Sylvan Shale				
A	4956.5	4959	2.5	Dolomite, argillaceous; & dolomitic siltstone, greenish-gray

Table A- 5: Saunders 1-13 Preliminary Stratigraphic Description, Quick Review of Slabbed Core

UNIT	FROM	TO	THK	DESCRIPTION
Woodford/Misener				
	4915	4915.3	2.3	Shale blk, with 3" basal ss, f. gr, dgy, pebbly at 4915.1 - .3 irreg corroded surface at contact
Hunton (25.2 ft. cored)				
	4915.3	4940.5	25.2	Ls, v.c. pentamerid brachiopod coquina; brachs up to 3" long, vuggy, drusy calcite fills in brach cavities, Woodford shale in cavity fill, @ 4920 - 20.5. mostly tightly cemented with scattered large vugs. Vugs are open, with drusy calcite linings.

Table A- 6: Bailey 2-6 Preliminary Stratigraphic Description, Quick Review of Slabbed Core

Final Core Description (Formations Revised 10-6-03)
Marjo Bailey 2-6, Sec.6 , T15N, R3E, Lincoln Co. OK

Depth From	Depth To	Lith	Fabric	Pore Types	Av Pore %	% TV	Chalky	Facies	Description
4876	**Top of Core**								
	Woodford Shale		(not cored)						
		Shale		nil	nil				
	Misener Sandstone (not cored)								
		SS		nil	nil				
4876	**Hunton Limestone (58.15)**								
4876	**Basal Clarita (Zone 5a) (13.8 feet)**								
4876	4880.45	Dol	xln	TV,SF,MO,IX	11	7	N	6	Dol, fine to med xln, lt gy N7 to yellowish gy 5Y 7/2, strongly rexln, originally cri brac pkstn and grnstn. Crudely interbedded, tightly cemented zones and zones of abundant moldic and vuggy porosity, vertically solution enhanced frac connect karst solution cavities .05 by .01 ft, filled with coarse to med quartz sand and phosphate grains, certainly misener.
4880.45	4881.95	Ls	pkstn	IG, Vug	4	0	N	4	Ls, partly dolomitized, med cri pkstn, finely xln dol in part, pinkish gy 5 YR 8/1, porosity is dissolved intergrannular matrix
4881.95	4889.8	Dol	pkstn	SF, Vug, Mo	5	4	N	9	Dol, fine to med xln, color a/a, fine to med cri coral pkstn, sparse brac and bryzoans. Mostly tight with thin zones of abundant moldic porosity, abscured dolomitization but probably coral layers
4889.8	**Upper Cochrane B (Zone 4b) (29.5 feet)**								
4889.8	4891.4	Ls	pkstn	SF, SV	2.5	2	N	8	Ls, partly dolomitized, v lt gy to med gy N6 - N8, med to coarse coral-cri-brac-bryzoan-trilobite pkstn, strongly rexln, much coarse pore filling spar
4891.4	4899.75	Ls	grnstn	SF, Vug	1.5	1.5	N	3	Ls, pinkish gy with mottles and crude banding of moderately reddish orange 10 R 6/5 wich are Terra Rossa, brac grnstn and pkstn mostly small brac facies with the big pent brac facies present 4892.5 to 4893.5, porosity is dominantly SF
4899.8	4901.7	Ls	grnstn	SF, Vug	1.5	1,5	N	3	Ls, partly dolomitized, med lt gy to lt brnsh gy 5YR7/1, med to carse small brachiopod grainstone. Mottled stained med gy by karst silt. Contains small pentamerid and other brachs.
4901.7	4914.2	Ls	pkstn	FR	1	-	N	6	Ls, lt pinkish gy, fine to med small brac cri pkstn, tightly cemented, sparse frac, @ 4912.5 to 4913.2 are dissolution cavities with small amount of karst silt and cavity largely filled with white coarse calcite spar, fractured unit partially dolomitized for 0.1 ft @ 4913
4914.2	4919.3	Ls	pkstn	Vug	1.5	-	N	7	Ls, lt pinkish gy to lt gy, coarse brac pkstn, big pent brac facies with sparse cri and thin layers of small brac facies, partially dolomitized at base with solution fracturing, dissolution and coarse xln calcite infill
4919.3	**Upper Cochrane A (Zone 4a) (7.0 feet)**								
4919.3	4926.3	Ls	pkstn	Vug, fine matrix	2	1	N	6	Ls, color a/a, mixed brac cri facies, locally v large thin shelle brac, abundant karst mosaic frac and dissolution with karst infill of v fine laminated carbonate silt. At the top of the interval and locally throughout are large cavities filled with coarse calcite. From 4924 to base is Terra Rossa and possible palaeosol horizons
4926.3	**?Lower Cochrane (7.85 feet cored; 34.9 feet by log)**								
4926.3	4928.7	Ls	pkstn	Vug	3	3	N	7	Ls, color a/a to lt gy, coarse brac pkstn, large vugs and solution frac in upeer 1.5 ft
4928.7	4934.15	Ls	pkstn	SF, IG	2	1	N	6	Ls, lt to med gy, med grn brac cri pkstn, locally dense dark gy matrix, possibly carbonate silt
4934.15	**Bottom of core**								

Table A- 7: Carney Townsite 2-5 Core Description

Depth From	Depth To	Lith	Fabric	Pore Types	Av Pore %	% TV	Chalky	Facies	Description
4906	Top of Core								
	Woodford Shale		(not cored)						
		Shale		nil	nil				
	Misener Sandstone (not cored)								
		SS		nil	nil				
4906	**Hunton Group (60 feet Cored, 73.3 ft total thickness))**								
4905	Lower Clarita Formation, Zone 5 (46 feet cored)								
4906	4907	Dol	XLN	IX,SF	9	2	N	2	Dol, limy, f xln , v pale orange 10 YR 8/2, equant subhedral crystalls, faint foss allochems, vertical frac
4907	4910	Ls	XLN pkstn	IX, SF	11	3	N	4	Ls, strongly dolomitic gysh orange 10YR 7/3, fine to med foss pkstn with minor wkstn, vague thin bedding, allochems largely fine cri grains, sparse large cri & small brac, sli MO & SV porosity, prominent vertical SF 4907 to 4908.3 with associated large vugs
4910	4912	Dol	XLN	IX,SF	12	1	N	4	Dol, limy, gysh orange, dolomitized f cri pkstn & wkstn, SF 4910 to 4910.6 & associated minor vuggy porosity. Thin horizontal zones of dense rexln matrix possibly are rexln stylolite zones
4912	4916	Ls	grnstn	IX, SV	10.5	-	N	5	Ls, strongly dolomitized, gyish orange, med cri brac grnstn? With numerous coarse cri grains & sparse small brac
4916	4927	Dol	XLN pkstn	IX,SF	13	2	N	4	Dol limy gysh orange, dolomitized f cri pkstn with thin intervals of moderately abundant small brac fragments, irregularly thin bedded, apparently grainsize sorted, numerous sub horizontal tightly cemented layers or possibly rexln stylolites. Scattered foss moulds & SV. @ 4921.9 is karst cavity .04 ft X 0.2 ft wide filled with laminated carbonate silt. Vertical SF 4919.4 to 4919.7 & 4925.5 to 4927. Thin collapse breccia @ 4926.7 to 4926.9
4927	4940.3	Ls	pkstn/grnstn	IG,SF,MO	10	3	N	4	Ls, strongly doltzd, gysh orange, f to c cri pkstn, grnstn with 3 ft of mixed cri brac pkstn 4931 to 4934. Large vugs associated with SF & minor mosaic breccia scattered through the interval. Also contains thin intervals of karst solution cavities filled with carbonate silt. v c cri debri @ 4930 to 4930.4. Numerous subhorizontal tight cemented zones, possibly recrystallised stylolites or possibly mdstn layers
4940.3	4941	Dol	pkstn	SF,Vug,IX	6.9	5	N	4	Dol, limy, gysg orange to lt gy, f cri pkstn with tight cemented zones a/a, SF with large xln vuggy porosity and 3 karst cavities filled with carbonate silt
4941	4943.7	Ls	pkstn/wkstn	IG, Mo	4	1	N	4	Ls, lt gy to pinkish gy 5 YR 8/1, f to med cri pkstn/wkstn thin inetrvals of MO and sli SF porosity in wkstn layers, numerous calcite filled frac & silt filled karst fissures
4943.7	4944.6	Dol	mdstn	IX, Sf	6	2	N	11	Dol, limy pinkish gy mottled med gy, f mdstn , probably sabkha mdstn
4944.6	4946.4	Ls	pkstn/wkstn	MO, SF	2.75	-	N	4	Ls, lt gy to pinkinsh gy interbedded, f cri pkstn with localised MO porosity & SF porosity where tightly cemented. Irregular karst micro caverns with carbonate silt fill
4946.4	4948.6	Dol	XLN/pkstn/wkstn	MO, SF, IX	9	3	N	10	Dol, limy, lt gy to pinkish gy interbedded, f sparsely foss pkstn/wkstn, strongly dolomitized, f matrix largely dolomitic, vertical SF
4948.6	4950.1	Ls	pkstn	IG, MO	3.5	-	N	4	Ls, ltgy to pinkish gy mottled, possibly burrow mottled f cri pkstn with Mo & sparse Sv porosity
4950.1	4952	Dol	mdstn, wkstn	SF, MO	2	2	N	11	Dol, limy, interbedded lt pinkish gy to lt gy, burrow mottled mdstn to sparsely foss wkstn with thin (0.1ft intervals of fine foss pkstn), dolomite with good IX & SF porosity @ 4950.1 - 4950.2
Basal Clarita, "zone" 5a (5.1 ft)									
4952	4957.1	Ls	pkstn/wkstn	Sf,MO	4	4	N	4,11	Ls, dolomitic, pinkish gy mottled to lt gy, f cri pkstn with interbedded mdstn & sparse wkstn, MO porosity connected by vertical SF
4957.1	Upper Cochrane A Fm. "Zone 4a (5.4 feet)								
4957.1	4962.5	Ls	pkstn	SF,MO	2	2	N	6	Ls, pinkish gy, med to f cri brac pkstn, tightly cemented with corals @ 4916.6 .
4962.5	Lower Cochrane, Zone 3 (5.4 ft cored, 16.8 total thickness)								
4962.5	4966	Ls	pkstn	SF,MO	1	1	N	6	Ls, mottled lt brn to pinkish gy, large brachs @ 4962.6 to 4963.5, contains intevals of collapsed grnstn with 0 preserved porosity, well developed vertical solution fractures and widely spaced small vugs, small karst micro cavities with silt infill
Base of core: 4966 feet; Base of Hunton Not Cored.									

Conodont Samples and Results

Table A- 8: Conodont Samples - Marjo Mercer 1-28, 28-17N-2E

[On log-plots, enter the top or "to" depth]

Depth FROM	Depth TO	Spl #	Gp/Fm	LITHOLOGY	Grams	# Cono	Age	Series	"Zone"	Strat Position	TS
			Hunton				Silurian				
4527.4	4528	1	Lower Clarita	Dol, Vuggy , foss grnstn				Wenlock	5	78	x
4528.4	4529	2	Lower Clarita	aa, . v oily					5	77	x
4531.2	4532	3	Lower Clarita	aa				Wenlock	5	74	x
4537.3	4538	4	Prices Falls	aa,v. vuggy, moldic; gilsonite pore fill				Up Lland	5a	68	x
4543.1	4543.8	14		Shaly crinoidal wkstn						62.2	
4545.2	4546	5	Prices Falls	Ls, foss burr wkstn				Llandov	5a	60	x
4550.1	4550.8	6	Up Cochrane B	AA-tite, burr mdstn				Llandov	4b	55.2	
4553.2	4553.9	15	Up Cochrane B	AA-tite				Llandov		52.1	x
4558.3	4559	7	Up Cochrane B	AA				Llandov	4b	47	x
4564.1	4564.7	8	Up Cochrane B	Burr muddy ls, sl. foss wkstn				Llandov	4b	41.3	x
4566.4	4567	9	Up Cochrane A	LS, wkstn 0.5' below base of dK shale				Llandov	4a	39	x
4570	4570.5	10	Up Cochrane A	bottom of shale, muddy foss mdstn/wkstn				Llandov	4a	35.5	x
4570.5	4571	11	Up Cochrane A	Foss mdstn/wkstn clean				Llandov	4a	35	x
4574.6	4575	16	Up Cochrane A	Foss mdstn/wkstn				Llandov	4a	31	
4575.4	4576	17	Lower Cochrane	Ls, w burrowed mudrock streaks, shaly at base				Llandov	3	30	
4577.2	4577.9	12	Lower Cochrane	Dense ls, mdstn clean				Llandov	3	28.1	x
4582	4582.7	13	Lower Cochrane	aa				Llandov	3	23.3	x

Strat Position is footage above or below (-) the Hunton/Sylvan contact at 4606 ft, by gamma-ray & CBL log..

Note : Lithology is limestone, unless mentioned otherwise

TS = Thin Section of this sample

"Zone" = "Zones" 1-6 of of simplified conodont zoanation adopted for this study

Table A- 9: Conodont Samples - Chandler SWDW1-5, 5-14N-3E

[On log-plots, enter the top or "To" depth]

Depth FROM	TO	Spl #	Gp/Fm	LITHOLOGY	Grams	# Cono	Age	Series	"Zone"	Strat Position	TS
			Hunton				Silurian				
4810	4810.6	Ch-1	Lower Clarita	Dol					5	67.7	
4816.4	4817	Ch-2	Lower Clarita	Dol					5	61.3	
4822.5	4823	Ch-3	Lower Clarita	Dol				Wenlock	5	55.3	x
4824.9	4825.7	Ch-4	Lower Clarita	Dol, Vuggy, Diag Terrane					5	52.6	
4833	4833.6	Ch-5	LowerClarita, Misener leak	Dol, Vuggy, Diag Terr				Wenlock	5	44.7	
4835	4835.6	Ch-6	Up Cochrane B	Dol, Diag Terr				high Llandov	4b	42.7	x
4838.7	4839.4	Ch-7	Up Cochrane B	Dol, Burrowed, Diag Terr				Llandov	4b	38.9	x
4840	4840.7	Ch-8	Up Cochrane B	Foss Wkstn				Llandov	4b	37.6	
4843	4843.7	Ch-9	Up Cochrane B	Shaly, f grnstn				Llandov	4b	34.6	x
4847.2	4847.8	Ch-10	Up Cochrane A	Shaly ls				Llandov	4a	30.5	
4853.5	4854.4	Ch-11	Up Cochrane A	Burr, Mdstn				Llandov	4a	23.9	
4862	4862.7	Ch-12	Up Cochrane A	Burr, Mdstn				Llandov	4a	15.6	x
4866.4	4867	Ch-13	Up Cochrane A	Burr, Mdstn				Llandov	4a	11.3	x
4868.9	4869.7	Ch-14	Up Cochrane A	Burr, Mdstn, Shaly lam				Llandov	4a	8.6	x

Note: All samples, #1-14, were shipped to Barrick on 6/4/03; Barrick provided prelim results 6/22
Note: No Prices Falls, no Lower Cochrane in this well
Strat Position is footage above or below (-) the Hunton/Sylvan contact at ft. 4878.3, core depth; log base is 4865, 13.3 ' correction.

Note : Lithology is limestone, unless mentioned otherwise
TS = Thin Section of this sample
"Zone" = "Zones" 1-5 of of simplified conodont zoanation adopted for this study

Table A- 10: Conodont Samples - Morrow 1-27, 27-16N-2E

[On log-plots, enter the top or "from" depth]

Depth FROM	TO	Spl #	Gp/Fm	LITHOLOGY	Grams	# Cono	Age	Series	"Zone"	Strat Position	TS	Comment
			Hunton				Silurian	Llandov.				
4905	4906		U Cochrane A	LS			Silurian	Llandov.	4a	51.5		
4911	4912		Low Cochrane	Ls, burrowed mdstn			Silurian	Llandov.	3	45.5		*Aulognathus sp A*
4915	4915.7		Low Cochrane	LS Burrd, mdst			Silurian	Llandov.	3	41.5		*Aulognathus sp A*
4919	4919.7		Low Cochrane	LS			Silurian	Llandov.	3	37.5		*Aulognathus sp A*
4926	4926.7		Low Cochrane	LS			Silurian	Llandov.	3	30.5		
4933	4933.6		Low Cochrane	LS, moldic, microvugs			Silurian	Llandov.	3	23.5		
4941	4941.7		Low Cochrane	LS, f grnst			Silurian	Llandov.	3	15.5		
4946	4946.7		Low Cochrane	LS, sli above Brachs			Silurian	Llandov.	3	10.5		
4950	4951		Low Cochrane	LS, loc vuggy			Silurian	Llandov.	3?	6.5		
4951.2	4951.6		Low Cochrane	Dol			Silurian	Llandov.	3?	5.3		
4951.6	4951.8		Low Cochrane	Dol, dk gy, mottled (?sabkha); pyritic			Silurian	Llandov.	3?	4.9		
4952.3	4953		Low Cochrane	Dol, Diag Terr				Llandov.		4.2		
4955.4	4955.7		Keel	Oolitic Chert & Dol,\ Algal fragment grnst						1.1	X	
4955.7	4956		Keel	Dol, oolitic, grn-tan			Ordov.	Ashgill	1	0.8		
4956.4	4956.5		Keel	Oolitic Chert-TS			Ordov.	Ashgill	1	0.1	X	
4956.6	4957		Sylvan	Shaly dol			Ordov.	Ashgill	1	-0.1		
4957.6	4958.4		Sylvan	Shaly dol						-1.1		

Strat Position is footage above or below (-) the Hunton/Sylvan contact at 4956.5 ft.

Note : Lithology is limestone, unless mentioned otherwise
TS = Thin Section of this sample
"Zone" = "Zones" 1-6 of of simplified conodont zoanation adopted for this study

Table A- 11: Conodont Samples - Marjo 2-6 Bailey, 6-15N-3E

Depth FROM	TO	Spl #	Fm	LITHOLOGY	Grams	# Cono	Age	Series	ZONE	Position	TS	Barrick	Cono Zone
Top of Core=4876													
Basal Clarita (= Prices Falls)(,Zn 5a, 13.8 ft)													
4876.0	4876.3	1	Clarita	Dol, moldic, foss			Silurian	Llandov	5a	85.20	x	8/31/2001	*Ps.bicornis zn ? (Prices Falls)*
4876.3	4877.4	24	Clarita	Dol, moldic, foss						84.90			
4878.3		2	Clarita	Dol, dk, oil stn			Silurian	Llandov	5a	82.90	x		
4878.4	4879.0	25	Clarita	Dol, mottled, moldic fossil pores					5a	82.80			
4879.2	4879.8	20	Clarita	Dol, vuggy						82.00		5/2/2003	*indet fauna.*
4881.2	4881.9	3	Clarita	Doltc ls, crin. pkstn			Silurian	Llandov	5a	80.00	x	8/31/2001	
4883.0	4883.6	26	Clarita	Doltc Ls, mdstn & pkstn, moldic & burrowed					5a	78.20			
4884.3	4885.0	27	Clarita							76.90			
4885.6	4886.4	28	Clarita						5a	75.60			good 5a
4887.0	4887.4	4	Clarita	Ls, cri grnstn			Silurian	Llandov	5a	74.20	x	9/19/2001	*P. a. amorphognathoides zn; def 5a*
4888.5	4889.3	29	Clarita	Ls, f foss pkstn					5a	72.70			def 5a
4889.8 Upper Cochrane B (Zn 4b; 29.5 ft.)					Lithologic boundary, top of coral-bearing pkstn								
4890.7	4891.0	5	?	Ls, br-cri pkstn			Silurian	Llandov	4b	70.50	x	8/31/2003	
4891.4	4892.0	6	Up Cochrane	Dolc br-cri pkstn			Silurian	Llandov	4b	69.80	x		Celloni zn def 4b
4892.4	4893.0	30								68.80			
4895.4	4896.0	31		LS, Sparse pent br,-Terra rosa						65.80			
4897.2	4897.8	32								64.00			
4899.4	4900.0	7	Up Cochrane	Ls, cri, small brachs			Silurian	Llandov	4b	61.80	x	9/19/2001	*lower Pt. celloni zn*
4903.4	4904.0	33								57.80			
4905.0	4905.2	8	Up Cochrane	Big brach coquina, ?Ts only			Silurian	Llandov	4b	56.20	x		
4905.3	4906.0	21	Up Cochrane	Dolc ls, burrow mottled						55.90		5/2/2003	
4907.4	4908.0	34	?							53.80			
4910.1	4911.0	35	?							51.10			
4910.8	4911.0	9	Up Cochrane	? Ts only			Silurian	Llandov	4b	50.40	x		
4912.0	4913.0	34								49.20			
4913.0	4913.1	10	Up Cochrane	O.I.ft, ? Ts only			Silurian	Llandov	4b	48.20	x		
4915.0	4915.6	11	Up Cochrane	Big Br, micrite infill			Silurian	Llandov	4b	46.20	x	9/19/2001	*Pt. eopennatus zn*
4916.0	4916.7	12	Up Cochrane	brachs			Silurian	Llandov	4b	45.20	x	8/31/2001	*Pt. eopennatus zn*
4918.0	4918.7	22	Up Cochrane	Ls, dns, small brach wkstn, microfoss?					4b	43.20		5/2/2003	index cono -Pterospathodus
4919.3 Upper Cochrane A (Zone 4a, 7.0ft)													
4919.4		13	Up Cochrane	Poss seq bndry, paleosol?			Silurian	Llandov	4a	41.80	x	9/19/2001	prob Pterosp. Zn
4920.3	4921.0	14	Up Cochrane				Silurian	Llandov	4a	40.90	x	9/19/2001	*Pterospathodus interval*
4921.7	4922.5	23	? Up Cochrane						indet Sil	39.50		5/2/2003	
4923.0	4923.4	15	? Up Cochrane	Karst mud infill, lam			Silurian	Llandov	indet Sil	38.20	x	9/19/2001	*Non-diagnostic, early Silurian*
4925.0	4925.2	16	? Up Cochrane	? TS, only			Silurian	Llandov	indet Sil	36.20	x	9/19/2001	
4926.3 Lower Cochrane ?				Indet Silurian fauna,									
4927.4	4928.0	17	indet.	Brachs; vuggy & tite			Silurian	Llandov	indet Sil	33.80	x	9/19/2001	
4930.0	4930.5	18	indet.	Foss wk/pkstn, small brachs			Silurian	Llandov	indet Sil	31.20	x	9/19/2001	
4932.0	4932.6	19	indet.	F. br/cri ls; soln fract & fill			Silurian	Llandov	indet Sil	29.20	x		

Indet Silurian, v. low recovery 1-4 conos/spl.; big br facies et
Simply cannot say if have lower Cochrane or Upper Cochrane below 4921.0.
Strat Position is footage above or below (-) the Hunton/Sylvan contact at 4961.2 ft., equivalent to core footage.
Contact is at 4964 log depth. All footages are core depth.

Note : Lithology is limestone, unless mentioned otherwise

Table A- 12: Conodont Samples - Carney Townsite 2-5, Sec. 5, T15N-R3E

Depth From	Depth To	Spl #	FM	LITHOLOGY	Detailed Lithology	Grams	# Cono	Age	Series	"Zone"	Position	TS	Barrick
4906.2	4906.9	CT-1	Lower Clarita	Dol, lt gy f xln	open vert fract, with xln lining 4906-4908.4	900	7	Silurian	Wenl.	5	71.1	x	8/31/2001
4916.3	4917	CT-2	Lower Clarita	Dol, limy f xln	micro vug + 1 lining 1"x11/2" vug	680	26	Silurian	Wenl.	5	61	x	8/31/2001
4924.3	4925	CT-3	Lower Clarita	Dol, limy, v lt gy	many microvugs	620	30	Silurian	Wenl.	5	53	x	8/31/2001
4931.3	4932	CT-4	Lower Clarita	Ls, sli dol v lt gy	chalky, pp, foss, f foss wkstn-pkstn with spares lg cri	550	22	Silurian	Wenl.	5	46	x	9/19/2001
4946	4946.7	CT-5	Lower Clarita	Ls, lt gy, dense hard	mdstn/wkstn, sli pp, with tan silt cavity fill	600	71	Silurian	Wenl.	5	31.3	x	9/19/2001
4947.3	4948	CT-6	Lower Clarita	Dol, f xln, lt gy	intersecting vertical fractures, sli xtls in fractures	not picked					30		?
4949	4950	CT-13	Clarita	Doltc Ls & Dol,	f cri wkstn,pkstn					5	28		6/4/2003
4951.3	4952										26		
4952.2	4953	CT-14	Basal Clarita	Doltc Ls & Dol,	f cri wkstn/pkstn					5a	25		6/4/2003
4955	4956										22		
4956.9	4957.9	CT-7*	Clarita/Up Coch	Ls, lt tan gy	open vert fract in tight Ls, healed frac below 4959, Ls very dense, foss, wkstn/pkstn	not processed?					20.1		?
4958.6	4959.3	CT-15	Upper Cochrane A	Ls, f foss, wkstn/pkstn						4a	18.7		5/4/2003
4959.3	4959.8	CT-8	Upper Cochrane A	Ls, f foss, wkstn/pkstn	v dense and tight 1% porosity	650	>100	Silurian	Llandov	4a	18.2	x	9/19/2001
4960	4960.6	CT-16	Upper Cochrane A	Ls, f foss, wkstn/pkstn						4a	17.4		6/4/2003
4961	4962	CT-11	Upper Cochrane A	.s, f-m grnstn, crinoids & coral	dense, tite					4a	16		5/2/2003
4962	4963	CT-9	Lower Cochrane	Ls, c brac pkstn	huge soln enhanced frac 0.5" long x 0.2"wide, a pipeline !						15		?
4964	4964.7	CT-12	Lower Cochrane	Ls, dense mdstn						3	13.3		5/2/2003
4964.7	4965	CT-10	Lower Cochrane							3	13	x	?

Strat Position is footage of base of sample above base of Hunton at 4978 ft, by log. Core depth appears to = log depth.
* Sample originally labeled 4956.8-4959, an error. Clarita/Cochrane contact at 4957.1, believed to fall within this sample

The data above show that all units are present in this well except Upper Cochrane B (4b)

Appendix B - Engineering Analysis

Fluid Properties Analysis

Table B- 1: Schwake Wellstream Composition

Wellstream Fluid Composition

Recombination Summary

Basis of Recombination	4130	scf separator gas at 15.025 psia and 60 °F/bbl separator liquid
Separator Gas Gravity	0.8417	(Air = 1.00)
Separator Liquid Density	0.7876	g/cc at 43 psig and 95 °F

Component (Symbol / Name)		Separator Gas (mole%)	Separator Liquid (mole%)	Molecular Weight	Specific Gravity (Water = 1.0)	Wellstream Fluid (mole %)
N_2	Nitrogen	7.179	0.048	28.01	0.809	6.179
CO_2	Carbon Dioxide	0.103	0.004	44.01	0.818	0.089
H_2S	Hydrogen Sulfide	0.000	0.000	34.08	0.801	0.000
C1	Methane	67.363	1.244	16.04	0.232	58.093
C2	Ethane	10.305	0.917	30.07	0.405	8.989
C3	Propane	7.917	2.187	44.10	0.507	7.114
iC4	i-Butane	0.842	0.584	58.12	0.563	0.806
nC4	n-Butane	3.307	3.550	58.12	0.584	3.341
iC5	i-Pentane	0.681	1.902	72.15	0.624	0.852
nC5	n-Pentane	1.031	3.758	72.15	0.631	1.413
C6	Hexanes	0.783	9.276	85.78	0.673	1.974
C7	Heptanes	0.303	12.911	98.42	0.704	2.071
C8	Octanes	0.136	10.485	113.44	0.710	1.587
C9	Nonanes	0.017	8.831	126.32	0.731	1.253
C10	Decanes	0.033	44.302	241.88	0.876	6.239
Total		100.000	100.000			100.000
Molecular Weight		24.38	159.04			43.18

Table B- 2: Schwake CCE Test

Constant Composition Expansion at 110 °F
Pressure-Volume Relations

Pressure (psia)	Fluid Condition	Relative Volume (V / V^{sat})	Gas Density (g/cm^3)	Absolute Liquid Volume (%)	Deviation Factor (z)	Gas Viscosity (cP)
962		3.769		11.82	0.718	
1210	Curr. Res.	2.951		13.26	0.708	
1510	Orig. Res.	2.351		16.41	0.704	
2000		1.793		23.71	0.711	
3000	↑	1.320		40.52	0.785	
4000		1.150		45.66	0.912	
5000		1.072		42.33	1.063	
6000	Two-Phase	1.028		23.16	1.222	
6200		1.021		13.11	1.255	
6400		1.016		7.12	1.288	
6600		1.010		3.59	1.321	
7000	**Dew Point**	**1.000**	**0.571**	**0.00**	**1.387**	**0.168**
7500		0.989	0.577		1.471	0.175
8000		0.979	0.583		1.553	0.183
8500		0.970	0.588		1.635	0.190
9000		0.963	0.593		1.717	0.196
9500		0.955	0.598		1.799	0.203
10000		0.948	0.602		1.879	0.209

Table B- 3: Well stream Composition for Morrow 1-27

Original Wellstream Fluid Composition (two-phase at Reservoir conditions)

Recombination Summary

Basis of Recombination	3017	scf separator gas at 14.65 psia and 60 °F/bbl separator liquid
Separator Gas Gravity	0.815	(Air = 1.00)
Separator Liquid Density	0.818	g/cc at 30 psig and 74 °F

Component (Symbol / Name)		Separator Gas (mole%)	Separator Liquid (mole%)	Molecular Weight	Specific Gravity (Water = 1.0)	Wellstream Fluid (mole %)
N_2	Nitrogen	9.681	0.019	28.01	0.809	8.087
CO_2	Carbon Dioxide	0.463	0.005	44.01	0.818	0.387
H_2S	Hydrogen Sulfide	0.000	0.000	34.08	0.801	0.000
C1	Methane	69.229	0.273	16.04	0.258	57.850
C2	Ethane	8.411	0.227	30.07	0.423	7.061
C3	Propane	5.973	0.854	44.10	0.507	5.128
iC4	i-Butane	0.643	0.282	58.12	0.563	0.583
nC4	n-Butane	2.523	1.758	58.12	0.584	2.397
iC5	i-Pentane	0.613	0.984	72.15	0.624	0.674
nC5	n-Pentane	1.003	1.744	72.15	0.631	1.125
C6	Hexanes	0.658	4.153	85.75	0.672	1.235
C7	Heptanes	0.585	10.176	96.35	0.692	2.168
C8	Octanes	0.181	11.873	110.40	0.722	2.110
C9	Nonanes	0.035	10.165	123.62	0.746	1.707
C10	Decanes	0.002	8.904	137.33	0.750	1.471
C11	Undecanes		6.584	151.07	0.763	1.086
C12	Dodecanes		5.562	164.81	0.775	0.918
C13	Tridecanse		5.238	178.55	0.785	0.864
C14	Tetradecanes		4.259	192.29	0.794	0.703
C15	Pentadecanes		3.542	206.04	0.802	0.585
C16	Hexadecanes		2.612	219.78	0.809	0.431
C17	Heptadecanes		2.507	233.52	0.816	0.414
C18	Octadecanes		2.234	247.26	0.821	0.369
C19	Nonadecanes		1.980	261.01	0.826	0.327
C20+	Eicosanes Plus		1.556	274.75	0.831	0.257
C21	Heneicosanes		1.418	288.49	0.835	0.234
C22	Docosanes		1.147	302.23	0.839	0.189
C23	Tricosanes		1.033	315.98	0.843	0.170
C24	Tetracosanes		0.880	329.72	0.846	0.145
C25	Pentacosanes		0.928	343.46	0.850	0.153
C26	Hexacosanes		0.619	357.20	0.852	0.102
C27	Heptacosanes		0.676	370.95	0.855	0.112
C28	Octacosanes		0.626	384.69	0.858	0.103
C29	Nonacosanes		0.544	398.43	0.860	0.090
C30+	Tricontanes Plus		4.637	711.24	1.208	0.765
Total		100.00	100.00			100.00
Molecular Weight		23.6	184.57			50.14

Table B- 4: CCE Test for Morrow Fluid

Pressure (psia)	Fluid Condition	Relative Volume (V / V_{sat})	Gas Density (g/cm^3)	Absolute Liquid Volume (%)	Deviation Factor (z)	Gas Viscosity (cP)
6000		0.422	0.270		1.173	0.032
5000		0.459	0.248		1.063	0.029
4000		0.522	0.218		0.968	0.025
3000		0.642	0.177		0.892	0.020
2000		0.932	0.122		0.864	0.016
1869	**Reservoir**	**1.000**	**0.114**	**0.000**	**0.866**	**0.016**
1600	Two-Phase	1.181		0.028	0.876	
1500	↓	1.268		0.037	0.881	
1400		1.368		0.044	0.887	
1300		1.486		0.049	0.895	
1200		1.625		0.053	0.903	
900		2.190		0.059	0.921	
800		2.513		0.060	0.927	

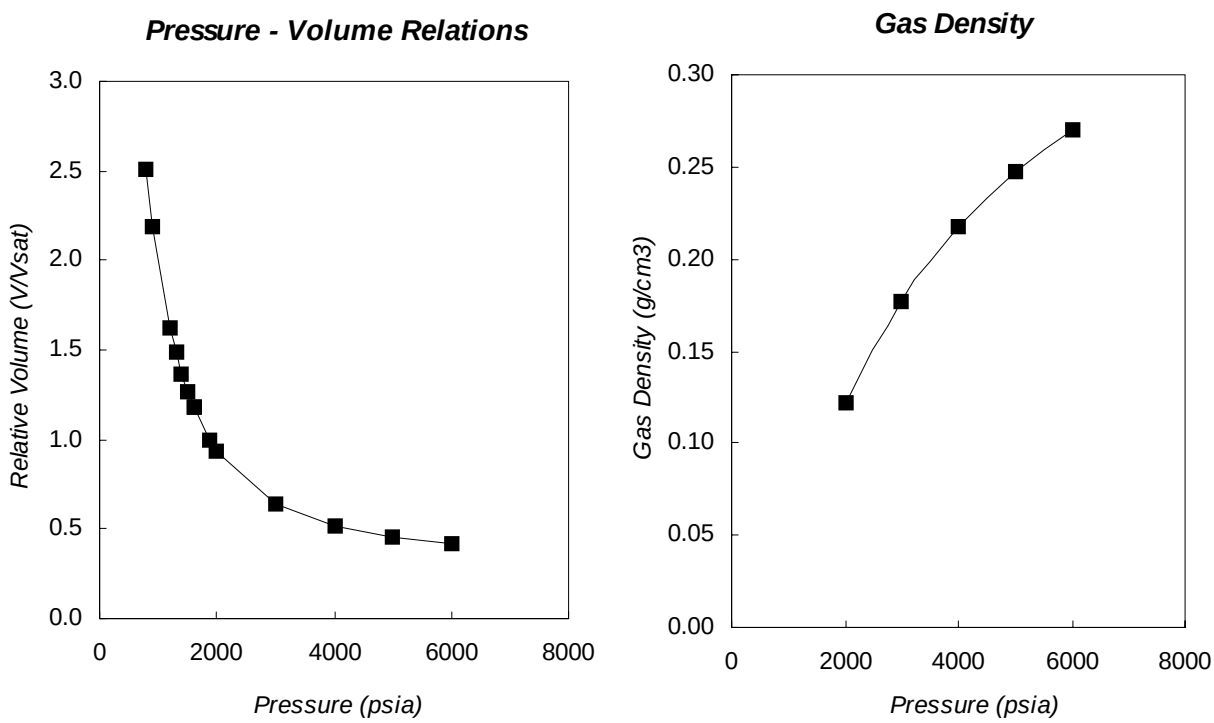

Figure B- 1: CCE Test Plots

Table B- 5: CVD Data for Synthetic Case

Pressure	v	l	zv	zl	z2p
1836	0	1	0.8486	0.746	0.746
1627.5	0.3016	0.6984	0.8514	0.7007	0.74615112
1438.7	0.3872	0.6128	0.8604	0.6566	0.73551136
1231.4	0.4575	0.5425	0.8708	0.6024	0.725193
1038.4	0.4929	0.5071	0.881	0.5449	0.71056369
879.46	0.5034	0.4966	0.8897	0.4911	0.69175524
754.21	0.5012	0.4988	0.8966	0.4439	0.67079324
656.58	0.4931	0.5069	0.902	0.4036	0.64936104
580.16	0.4823	0.5177	0.9062	0.3696	0.62840218
519.73	0.4706	0.5294	0.9096	0.3412	0.60868904
471.35	0.459	0.541	0.9122	0.3172	0.590305

Table B- 6: Field Data for East Carney Region

Well	BHP	Corrected BHP	Cumm Oil (STB)	Cumm Gas (MSCF)
Wilson # 1-6	1442.65	1528	433931	2080409
Geneva #1-32	1562.26	1509.115	464794	2233471
Carney Townsite 1-5	1416.21	1482.0465	529877	2520854
Denney #1-31	1527	1374.402	745808	3897744
Carney Townsite #2-5	1435	1314.5995	869027	4591368
Geneva #2-32	1115	1273.682	953516	5064184
Denney #2-31	1091	1106.8645	1314553	8007914

Table B- 7: Field Data for Central East Carney Region

Well	BHP	Corrected BHP	Cumm Oil (STB)	Cumm Gas (MSCF)
Alan Ross 1-11	769.4	655.27	1690477	3889578
Franny 1-11	697.01	649.407	1736672	4096707
Pearl #1-12	553.03	643.544	1736672	4096707
Lewis #1-14	619.7	605.4345	1842686	4563392
Townsend #1-13	516.34	587.8455	1892022	4783902
Carter #1-14	298	412.5418	2233787	6795666
Kathryn #2-14	433.49	332.2187	2322586	7196697

Table B- 8: Field Data for West Carney Region

Well	BHP	Corrected BHP	Cumm Oil (STB)	Cumm Gas (MSCF)
Cal #1-11	1193	1444.8	8491	109793
Griffin #1-14	1598	1292.5908	15098	515849
Houser #1-11 A	1187	1265.2712	20768	658182
Stevenson #1-14	1346.4	1176.4825	51938	1360511
Susie Q #1-15	1008.76	1060.3742	118568	2780711
Steffanie #1-15	1008	924.7519	197748	4542470
Jennifer #1-10	656	865.2342	238724	5450843
Mr. B #1-3	861	829.1333	238724	5450843

Table B- 9: Field Data for Central West Region

Well	BHP	Corrected BHP	Cumm Oil (STB)	Cumm Gas (MSCF)
Schwake #1-10	1509.62	1561.8	906417	6169676
Garrett 1-11	1385.02	1547.962	906417	6169676
Mary Marie #1-11	1399.78	1511.48	988686	6748538
Wilkerson #1-3	1535.75	1493.868	171141	7254694
Toles #1-10	1307.1	1466.192	171141	7254694
Parkview #1-3	1685.64	1462.418	171141	7254694
Christy 1-15	1475.75	1451.096	1189727	7812124
McBride North #1-10	1607.09	1430.968	1189727	7812124
Danny 1-34	1344.04	1412.098	1306570	8481249
Ables 1-34	1532.51	1395.744	1306570	8481249
Henry #1-3	1610.57	1389.454	1452336	9236998
Mary Marie #2-11	1384	1368.068	1452336	9236998
Danny 2-34	1164	1356.746	1616943	9236998
Joe Givens #1-15	1078	1301.394	1780124	10054662
Williams #1-3	1510	1278.75	1780124	11628664
McBride South #1-10	1277	1251.074	1959159	13310743
Boone #1-4	1332	1228.43	2137428	15040818
Wilkerson #2-3	1195	1139.112	2626538	17410895
Carter Ranch #2-15	1007	1014.57	3230124	20891802
JB #1-13	733	922.736	3789028	23568449
Saunders #1-13	925	891.286	3947709	24864835
Points #1-13	544	872.416	3947709	27149522
Gilmore Price Horizontal #1-33	892	775.55	4211862	30521472
Rollins #1-13	281	191.838	5142326	42114356

Table B- 10: Phase Z Factors CVD Data

Pressure	v	l	Zl	Zv	Z2p
1838	0	1	0.746	0.8486	0.746
1800	0.0825	0.9175	0.7378	0.8433	0.74650375
1750	0.1444	0.8556	0.7272	0.8457	0.7443114
1700	0.1909	0.8091	0.7165	0.848	0.74160335
1650	0.2295	0.7705	0.7056	0.8503	0.73880865
1600	0.2621	0.7379	0.6945	0.8526	0.73593801
1550	0.29	0.71	0.6831	0.855	0.732951
1500	0.3143	0.6857	0.6714	0.8573	0.72982837
1450	0.3355	0.6645	0.6593	0.8597	0.7265342
1400	0.3541	0.6459	0.6469	0.8622	0.72313773
1350	0.3706	0.6294	0.6342	0.8646	0.71958624
1300	0.3852	0.6148	0.621	0.8671	0.71579772
1250	0.3982	0.6018	0.6075	0.8697	0.71190804
1200	0.4098	0.5902	0.5934	0.8722	0.70765224
1150	0.4201	0.5799	0.5789	0.8748	0.70320759
1100	0.4292	0.5708	0.5639	0.8775	0.69849712
1050	0.4372	0.5628	0.5483	0.8801	0.69336296
1000	0.4441	0.5559	0.5322	0.8828	0.68790146
950	0.4501	0.5499	0.5154	0.8854	0.681937
900	0.4552	0.5448	0.4981	0.8881	0.675628
850	0.4594	0.5406	0.48	0.8909	0.66876746
800	0.4627	0.5373	0.4613	0.8936	0.66132521
750	0.465	0.535	0.4417	0.8963	0.653089
700	0.4665	0.5335	0.4214	0.8991	0.64424705
650	0.467	0.533	0.4003	0.9018	0.6345005
600	0.4665	0.5335	0.3782	0.9046	0.6237656
550	0.465	0.535	0.3552	0.9074	0.611973
500	0.4624	0.5376	0.3311	0.9101	0.5988296
450	0.4586	0.5414	0.3059	0.9128	0.58422434
400	0.4535	0.5465	0.2795	0.9155	0.567926
350	0.447	0.553	0.2519	0.9182	0.5497361
300	0.4391	0.5609	0.2228	0.9207	0.52924789
250	0.4298	0.5702	0.1922	0.9232	0.5063838
200	0.4197	0.5803	0.1599	0.9255	0.48122232
150	0.411	0.589	0.1256	0.9278	0.4553042
100	0.4115	0.5885	0.089	0.9307	0.43535955

Petrophysical Analysis

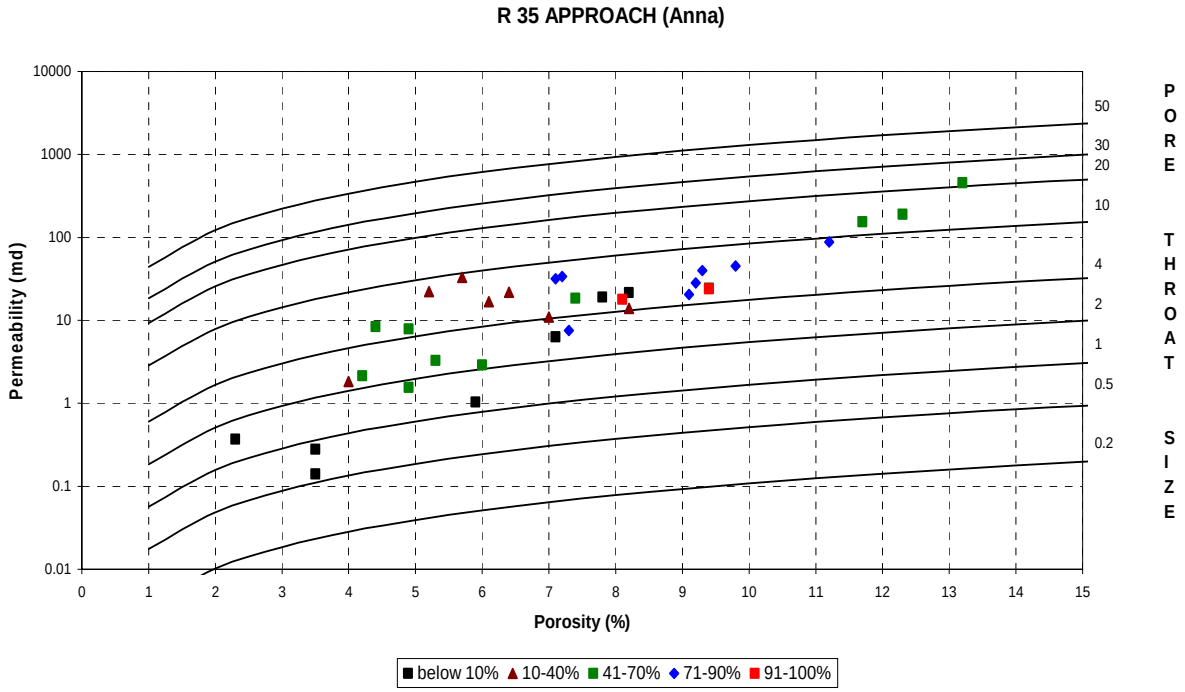

Figure B- 2: Porosity & Permeability data for Marjo Anna sorted based on the percentage fluorescence on a R_{35} plot.

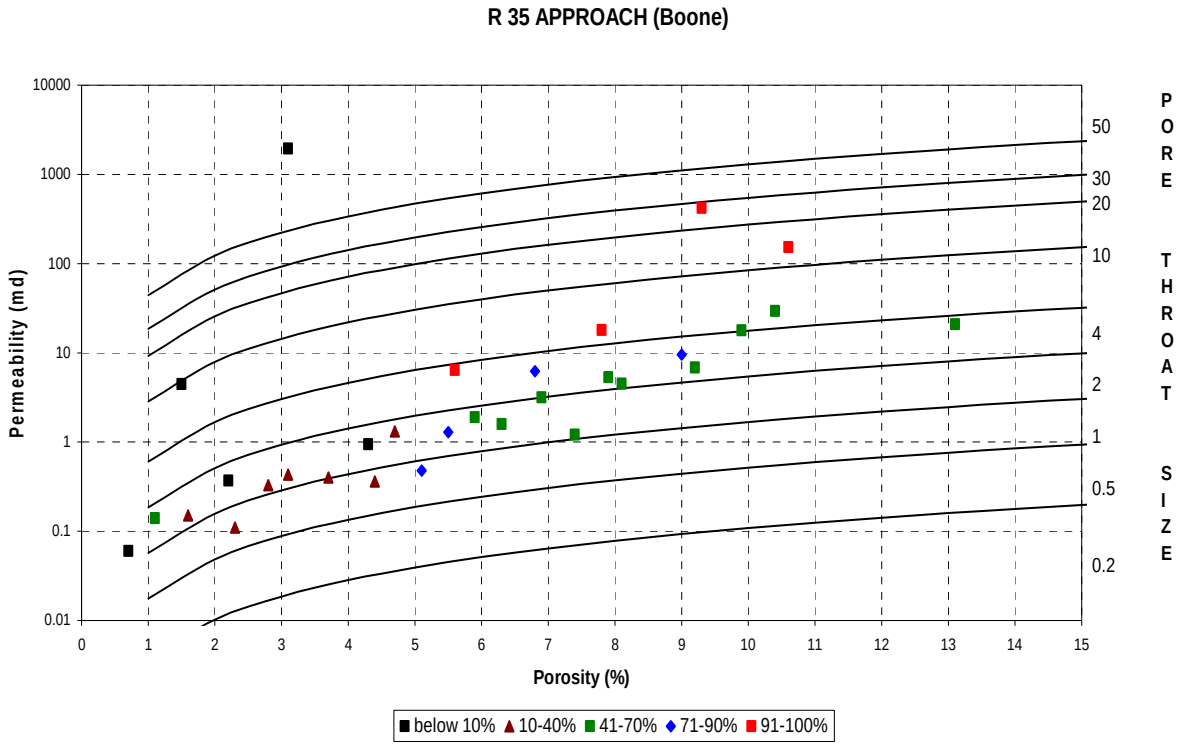

Figure B- 3: Porosity & Permeability data for Marjo Boone sorted based on the percentage fluorescence on a R_{35} plot.

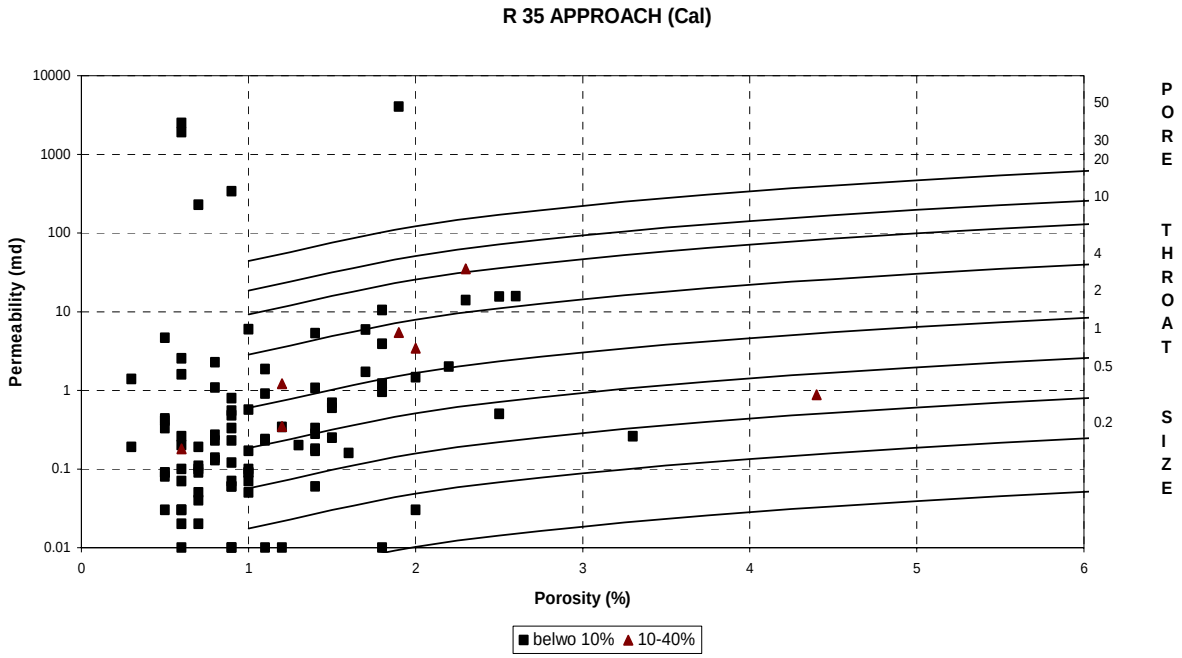

Figure B- 4: Porosity & Permeability data for Marjo Cal sorted based on the percentage fluorescence on a R_{35} plot.

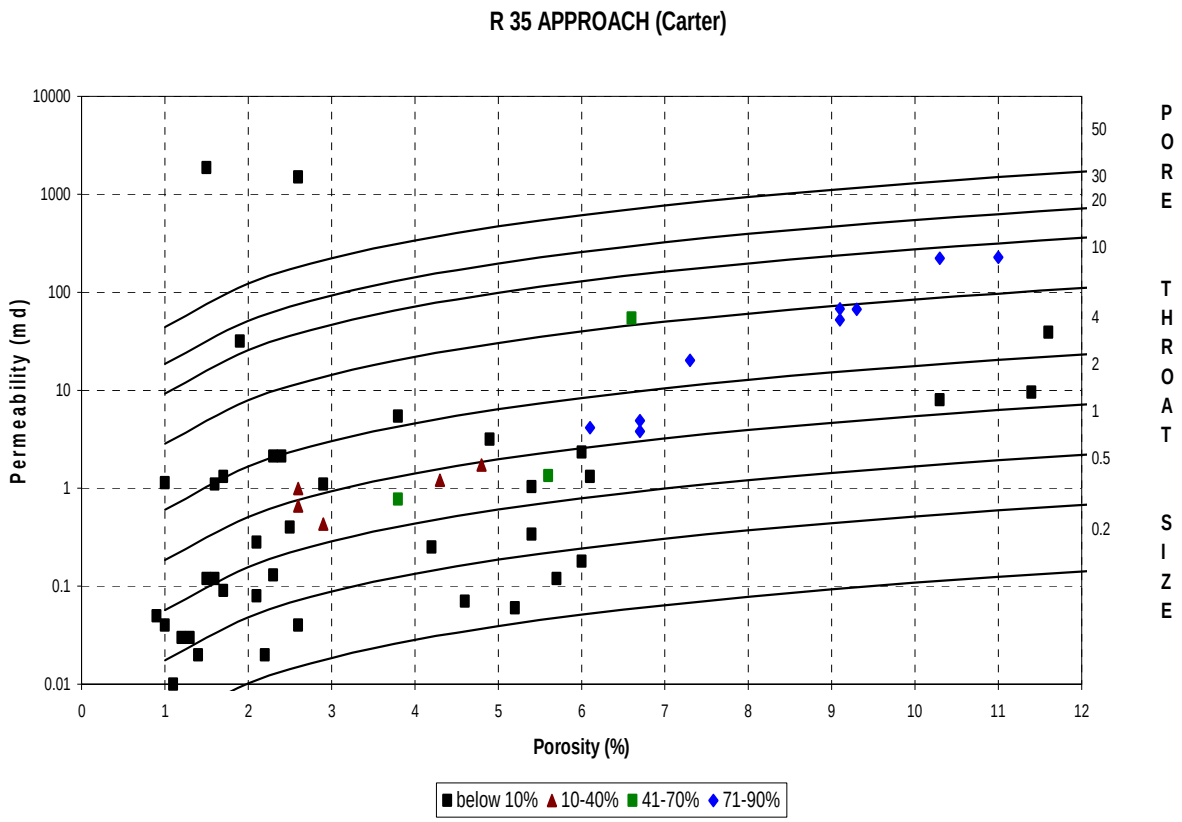

Figure B- 5: Porosity & Permeability data for Marjo Carter sorted based on the percentage fluorescence on a R_{35} plot.

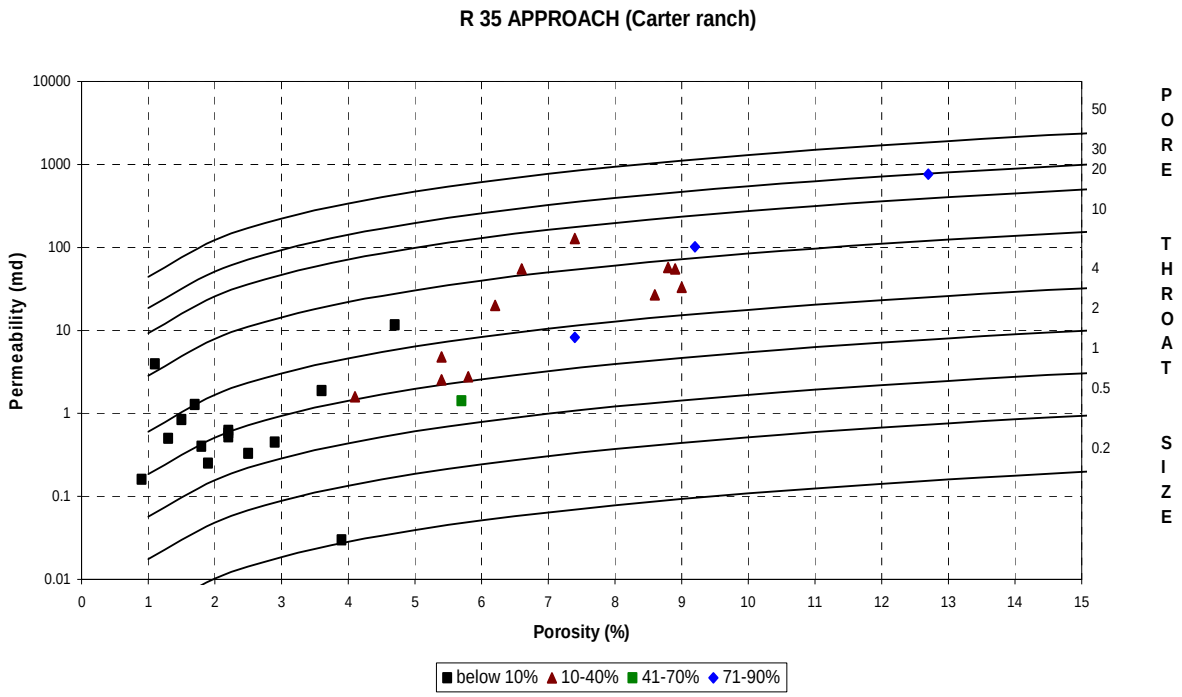

Figure B- 6: Porosity & Permeability data for Marjo Carter Ranch sorted based on the percentage fluorescence on a R_{35} plot.

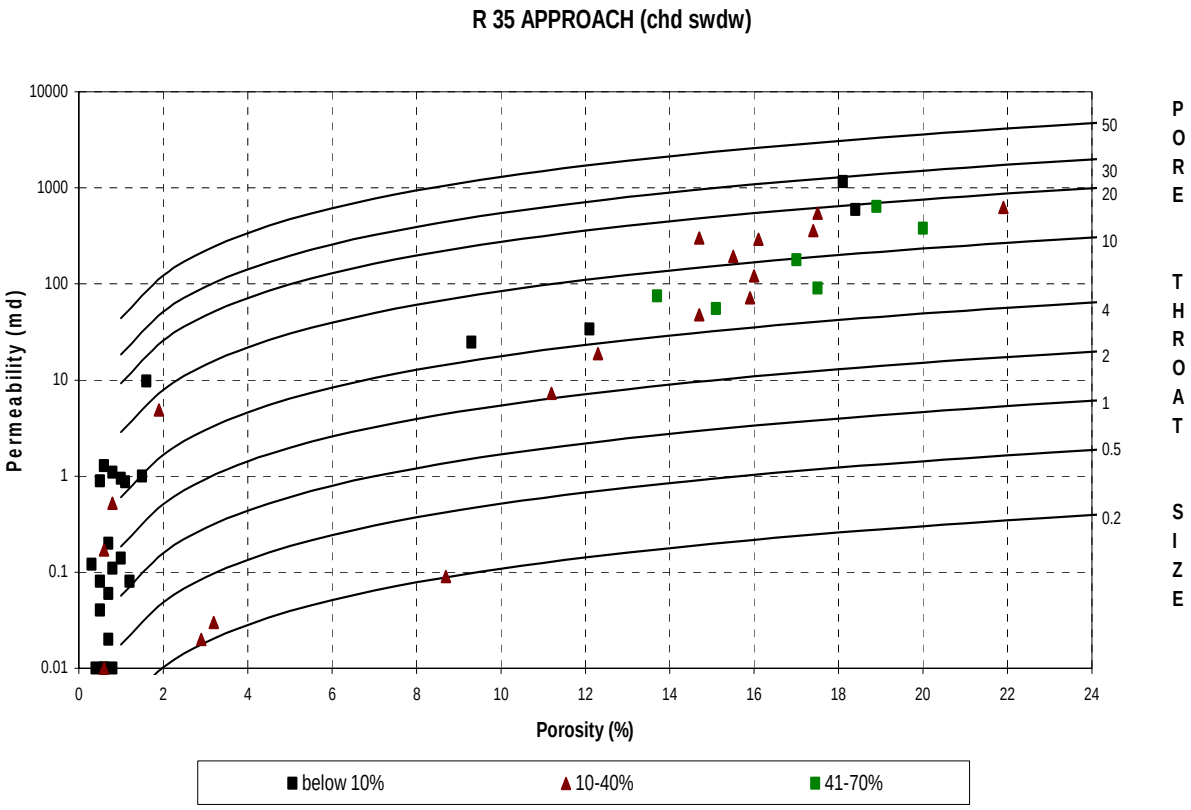

Figure B- 7: Porosity & Permeability data for Marjo Chandler SWDW sorted based on the percentage fluorescence on a R_{35} plot.

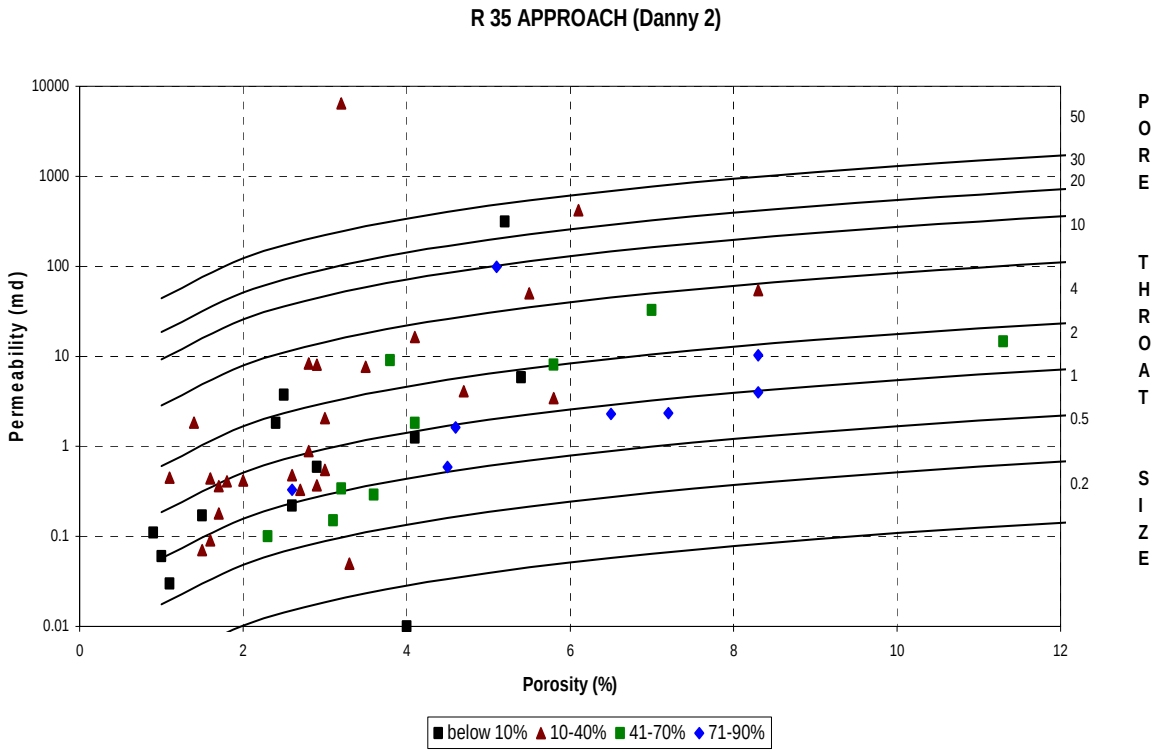

Figure B- 8: Porosity & Permeability data for Marjo Danny sorted based on the percentage fluorescence on a R_{35} plot.

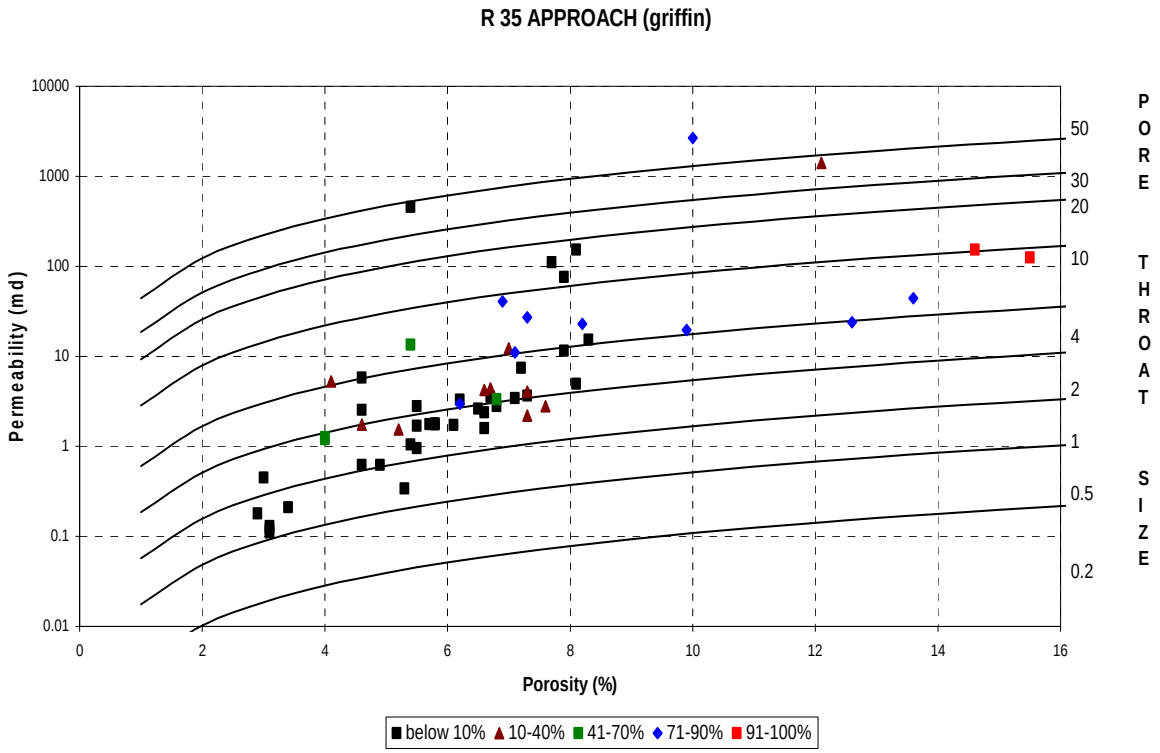

Figure B- 9: Porosity & Permeability data for Marjo Griffin sorted based on the percentage fluorescence on a R_{35} plot.

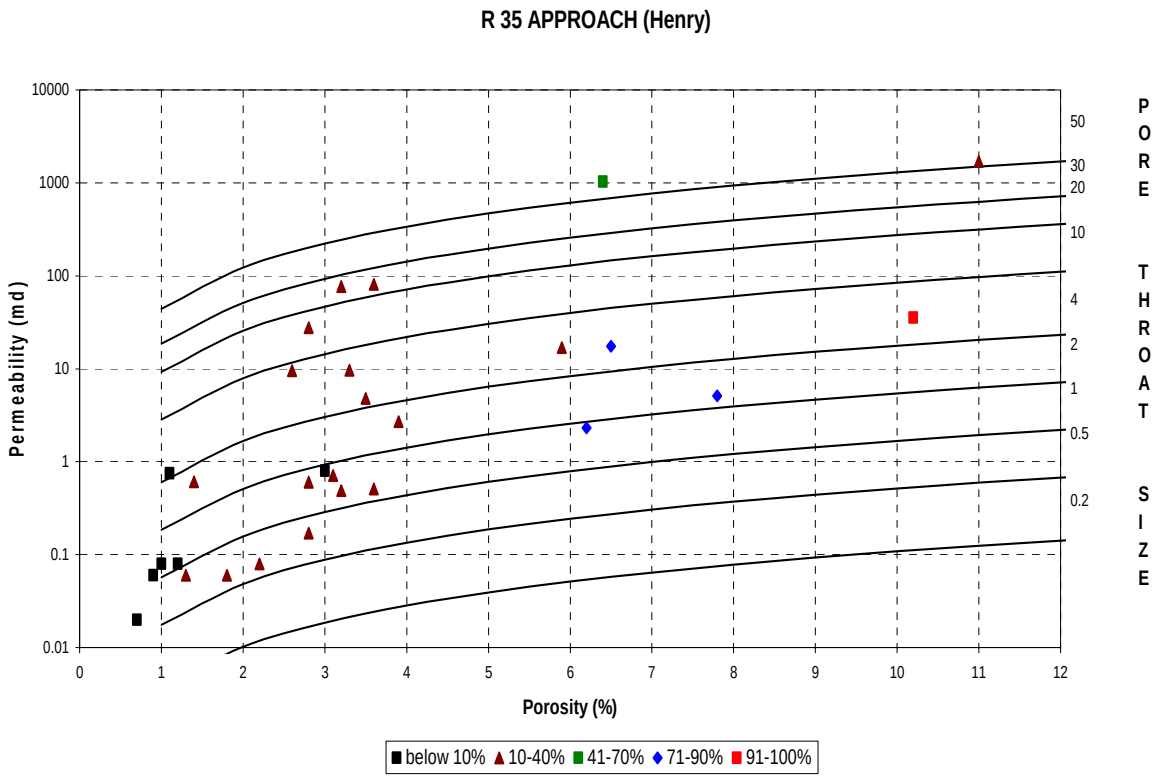

Figure B- 10: Porosity & Permeability data for Marjo Henry sorted based on the percentage fluorescence on a R_{35} plot.

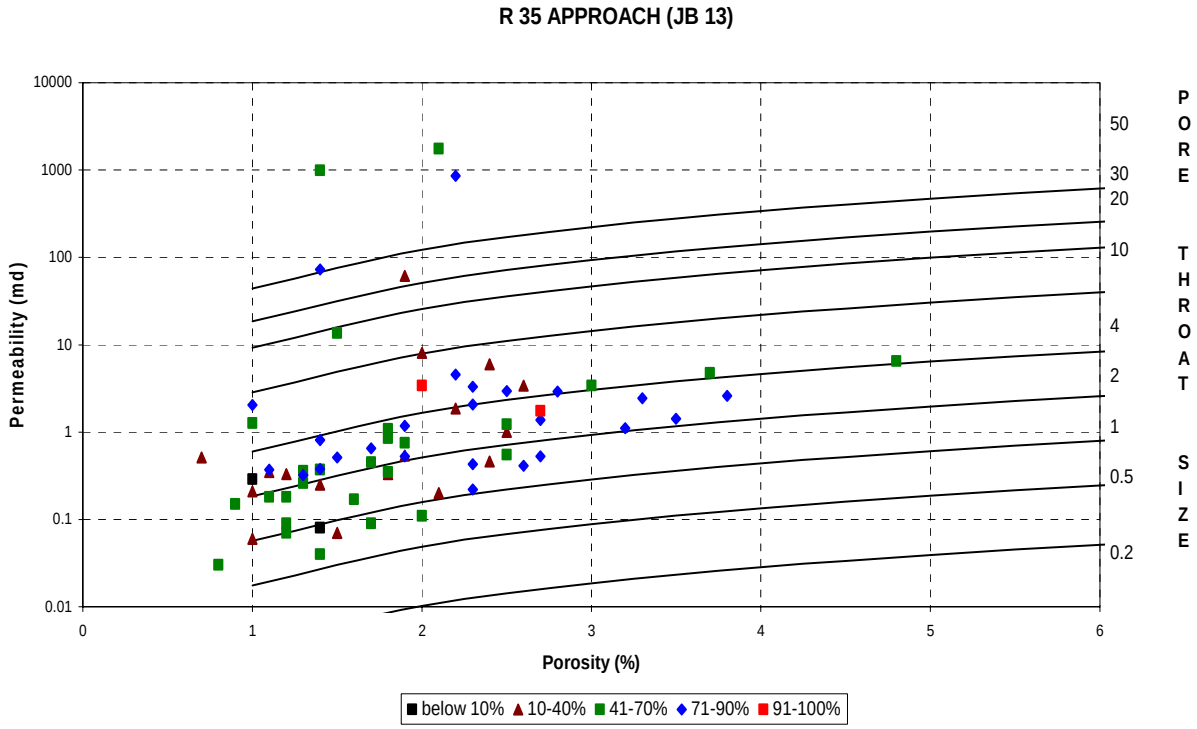

Figure B- 11: Porosity & Permeability data for Marjo JB-13 sorted based on the percentage fluorescence on a R_{35} plot.

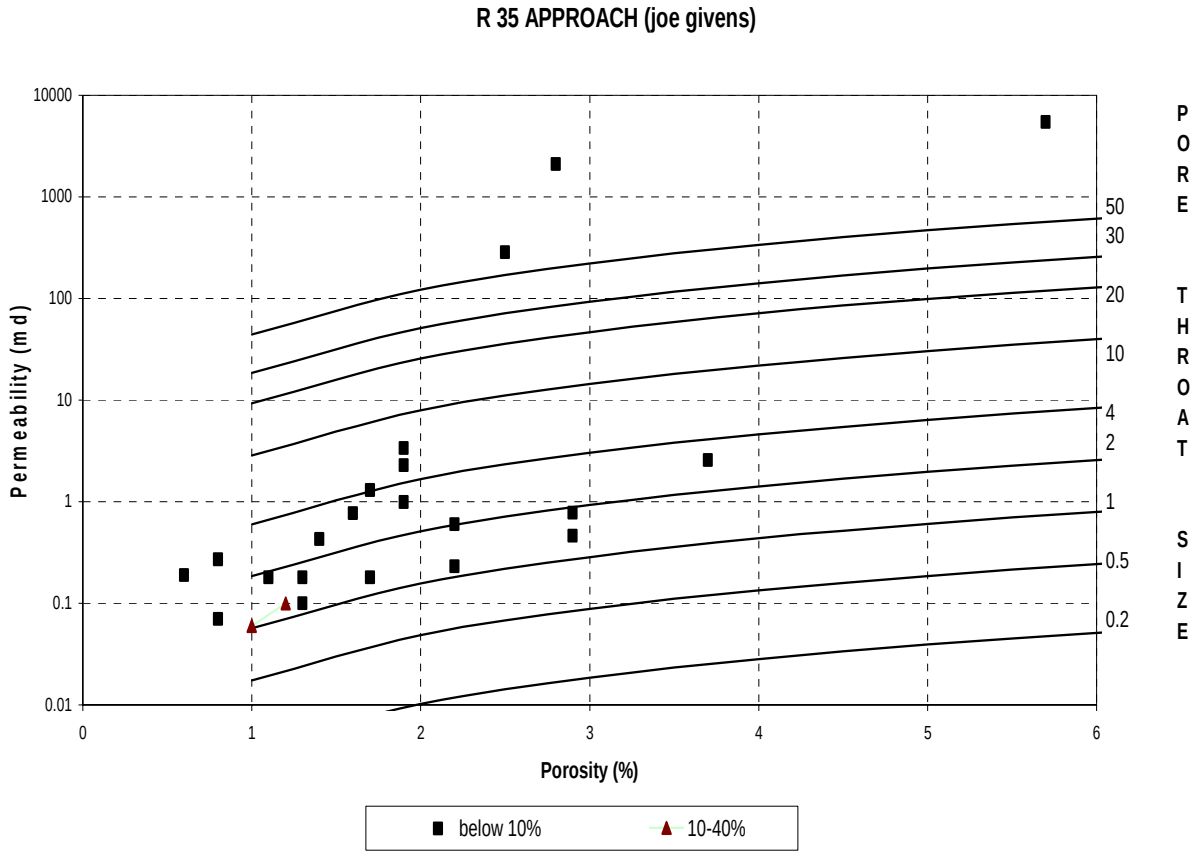

Figure B- 12: Porosity & Permeability data for Marjo Joe Givens sorted based on the percentage fluorescence on a R_{35} plot.

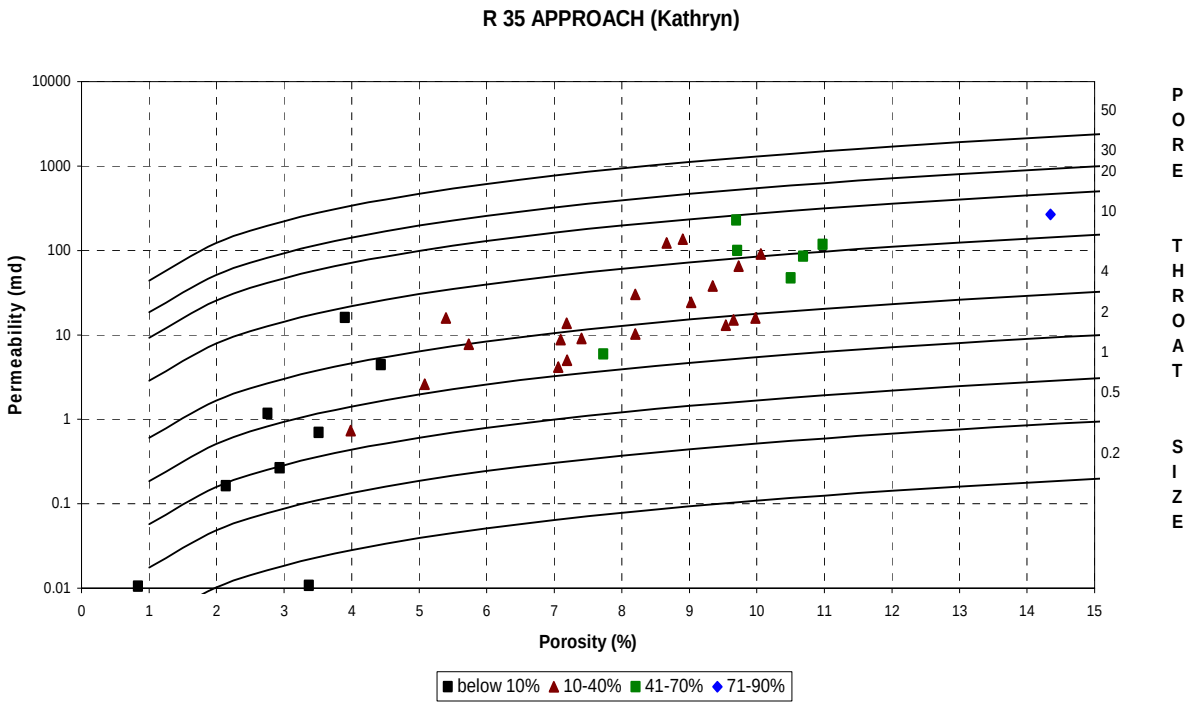

Figure B- 13: Porosity & Permeability data for Marjo Kathryn sorted based on the percentage fluorescence on a R_{35} plot.

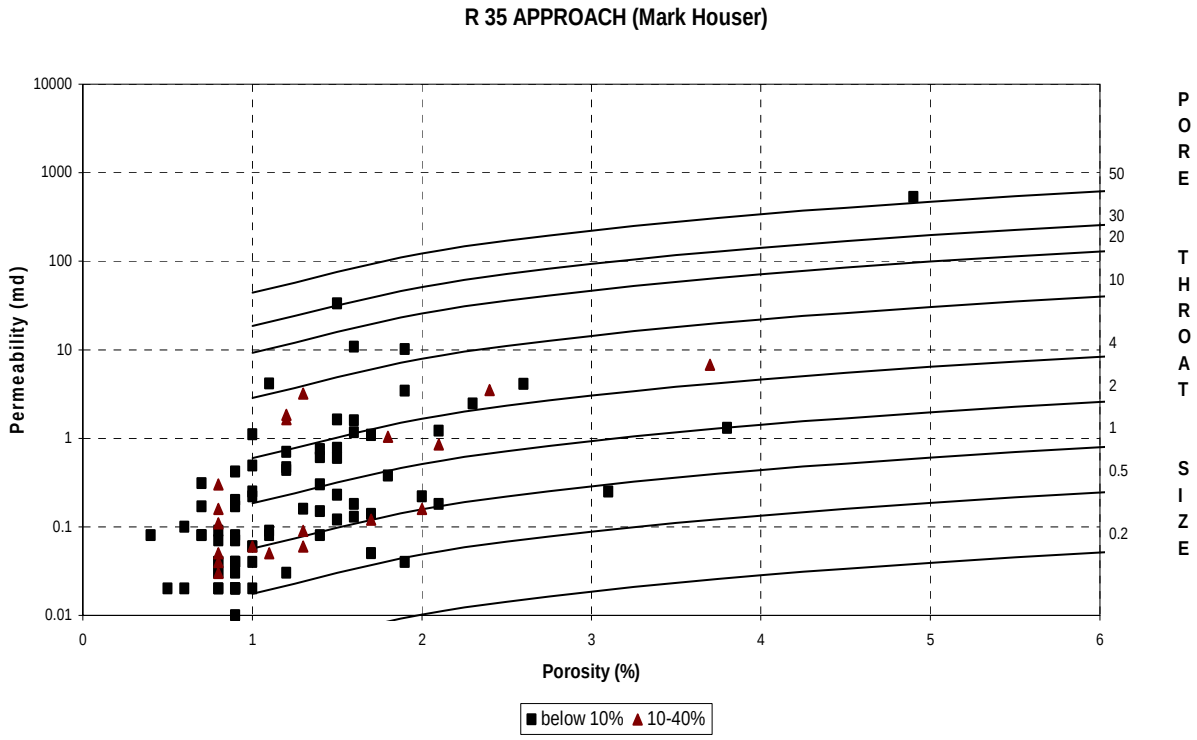

Figure B- 14: Porosity & Permeability data for Marjo Mark Houser sorted based on the percentage fluorescence on a R_{35} plot.

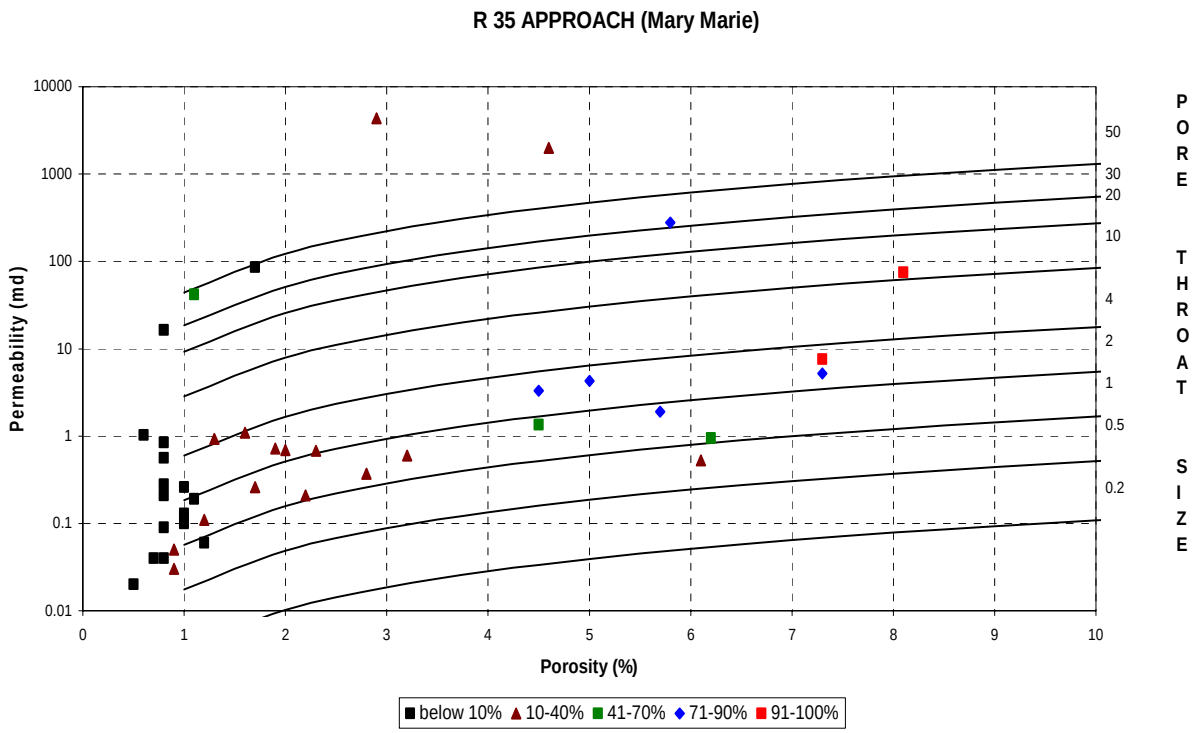

Figure B- 15: Porosity & Permeability data for Marjo Mary Marie sorted based on the percentage fluorescence on a R_{35} plot.

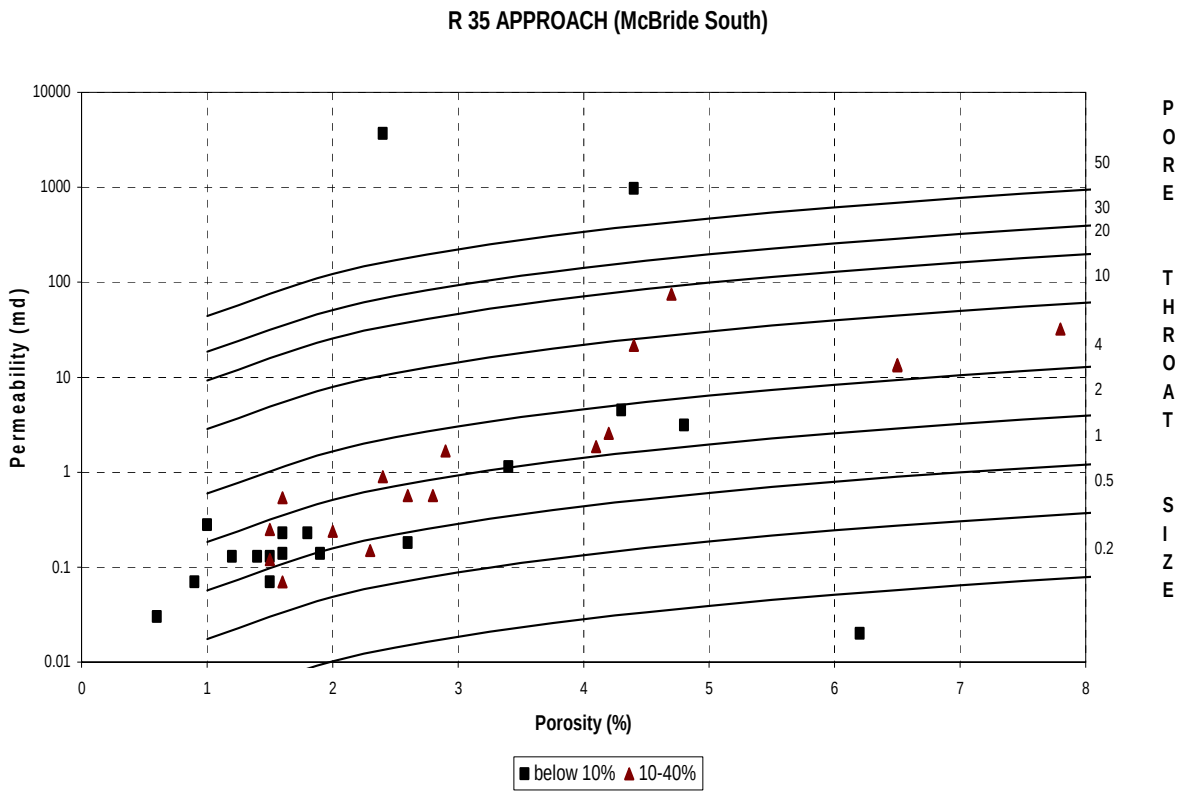

Figure B- 16: Porosity & Permeability data for Marjo Mc Bride South sorted based on the percentage fluorescence on a R_{35} plot.

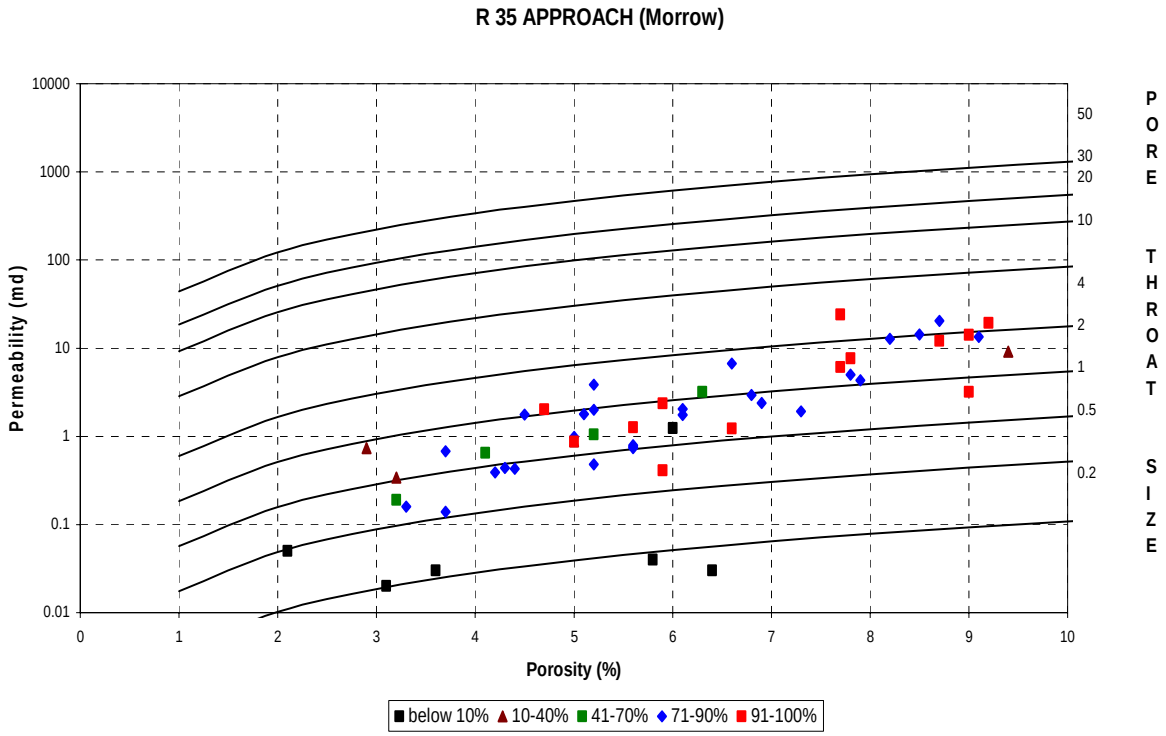

Figure B- 17: Porosity & Permeability data for Marjo Morrow sorted based on the percentage fluorescence on a R_{35} plot.

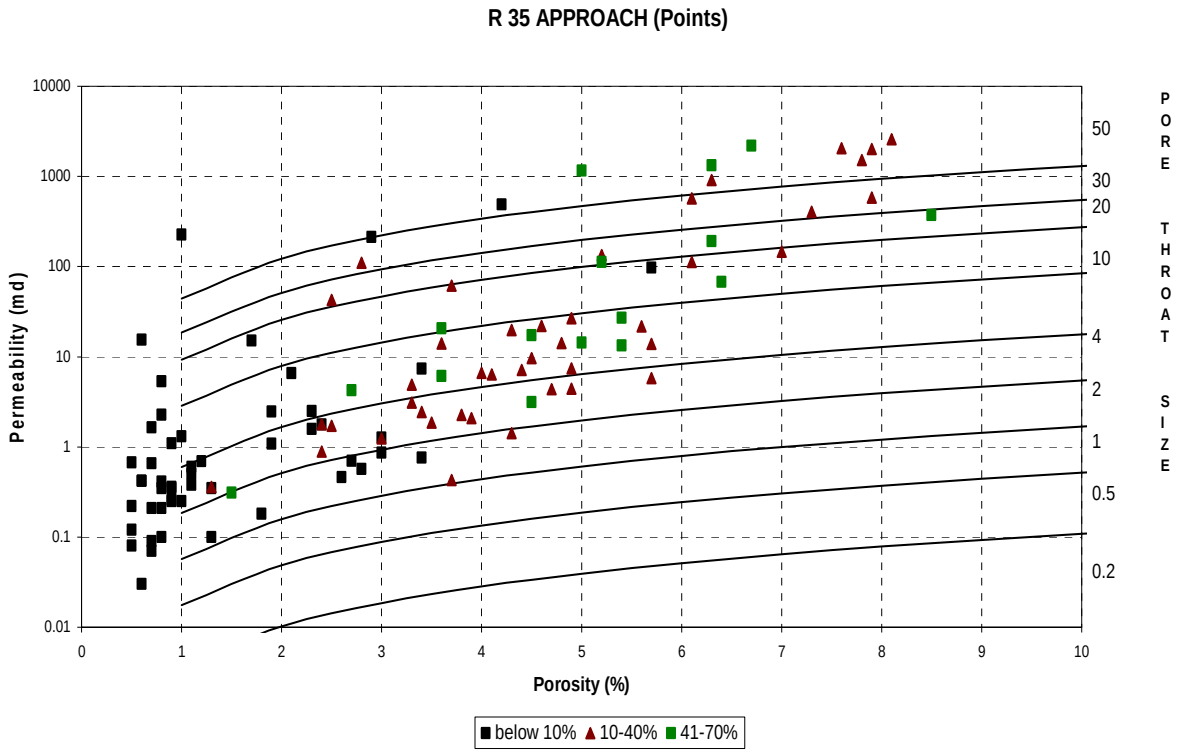

Figure B- 18: Porosity & Permeability data for Marjo Points sorted based on the percentage fluorescence on a R_{35} plot.

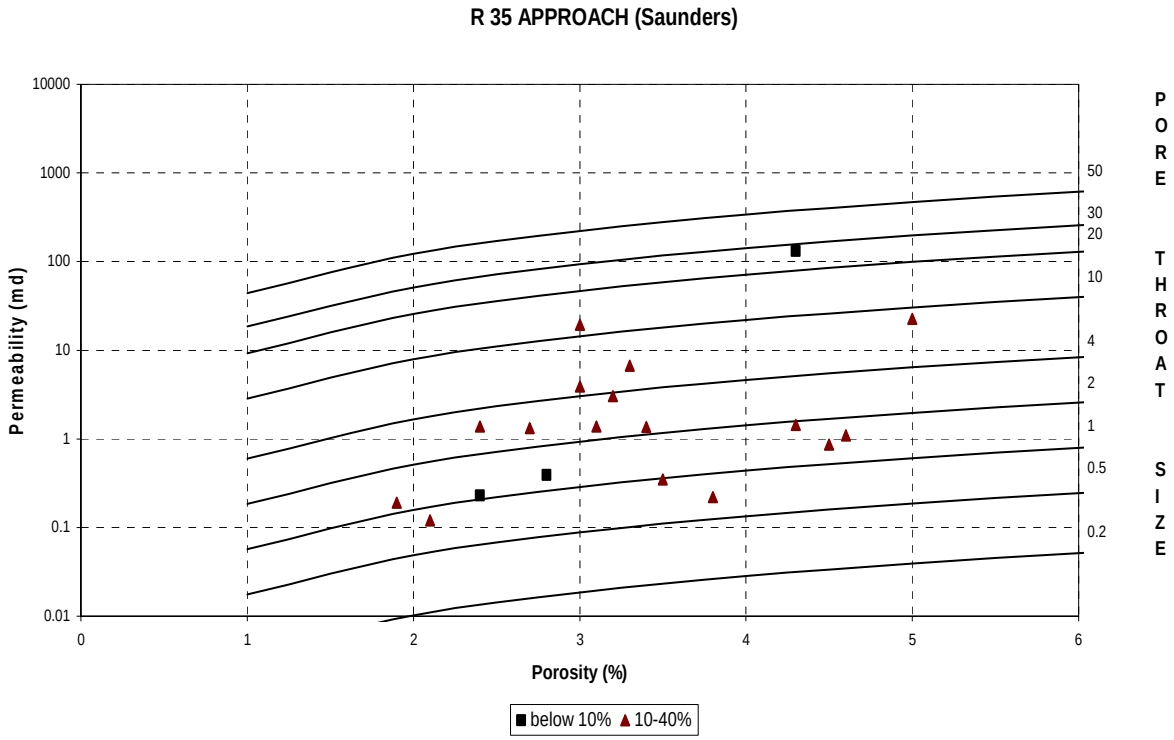

Figure B- 19: Porosity & Permeability data for Marjo Saunders sorted based on the percentage fluorescence on a R_{35} plot.

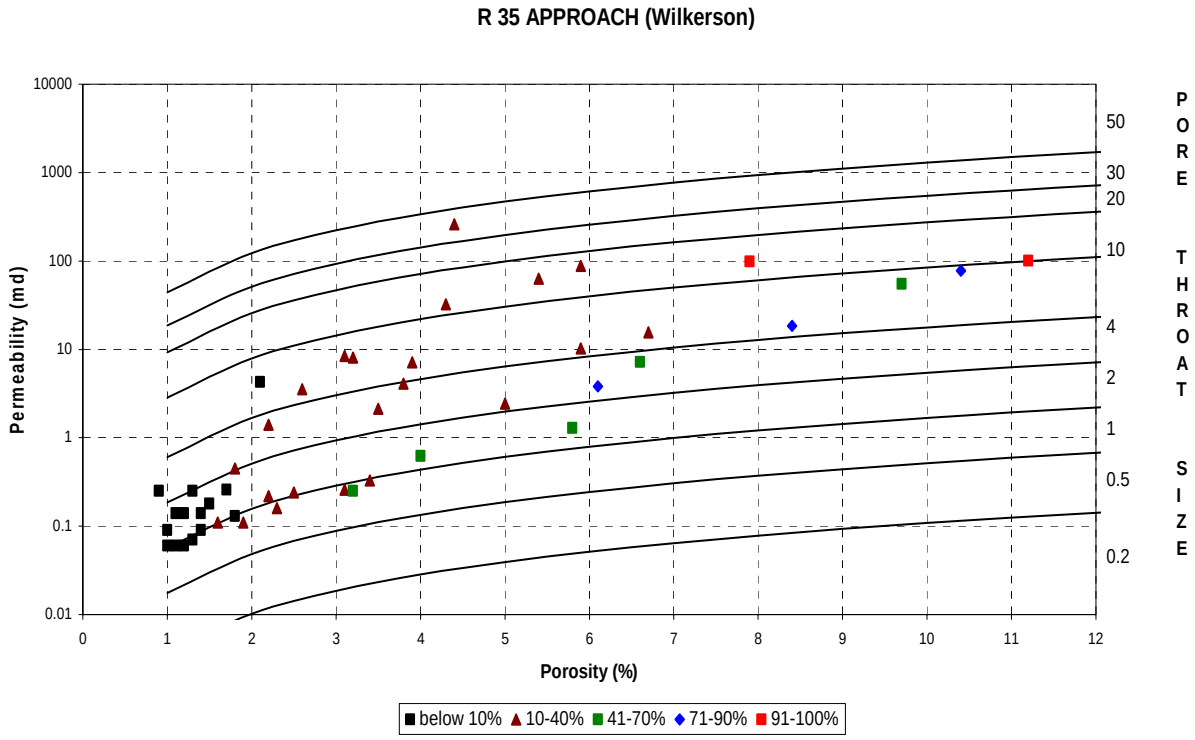

Figure B- 20: Porosity & Permeability data for Marjo Wilkerson sorted based on the percentage fluorescence on a R_{35} plot.

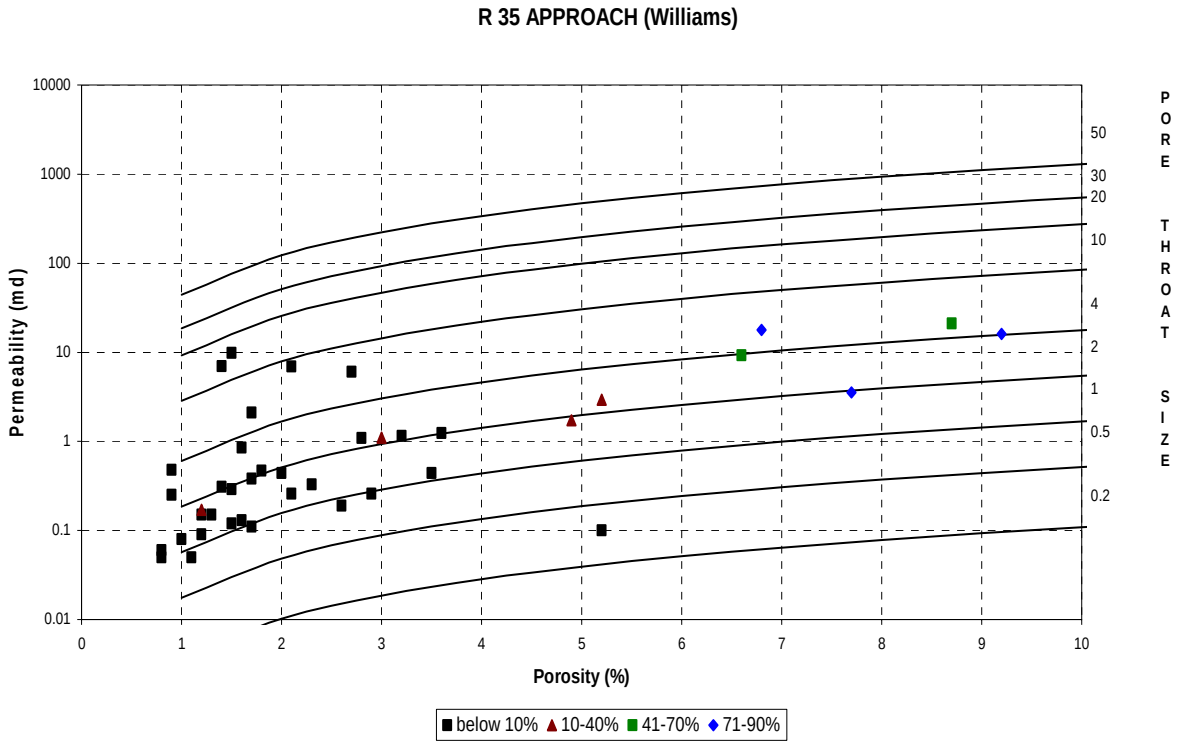

Figure B- 21: Porosity & Permeability data for Marjo Williams sorted based on the percentage fluorescence on a R_{35} plot.

Appendix C - Economic Analysis

This appendix presents the analysis of revenue as a function of time for all the vertical and horizontal wells.

Vertical Wells:

1) **Wilkerson 1 –**

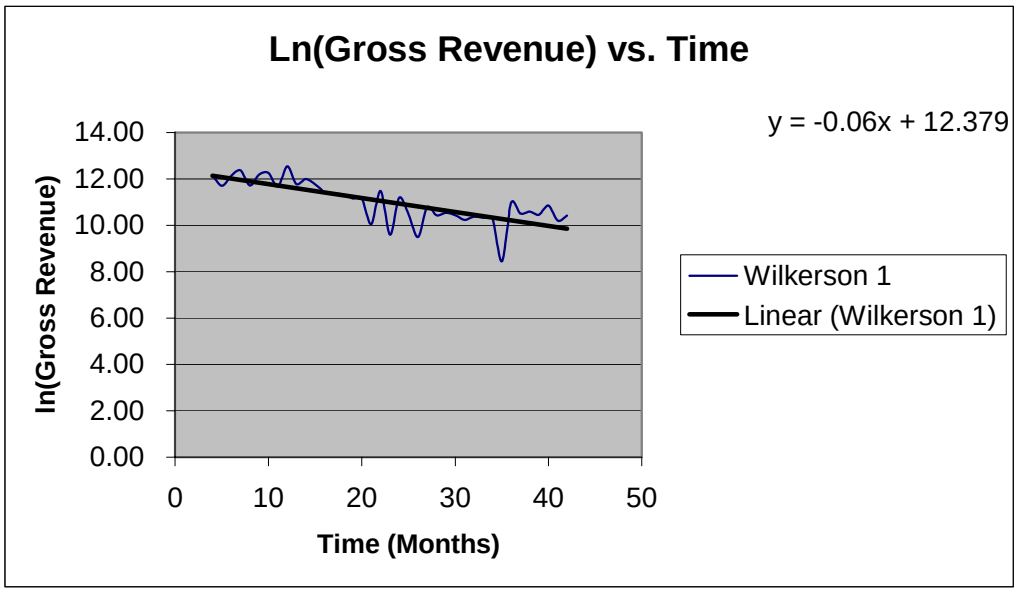

Figure C- 1: Wilkerson 1

The equation of the above graph for the data provided gave a slope of (-0.06). This slope was used in extrapolating the values of gross revenue till the end of the planning horizon. A plot of the extrapolated values vs. time was made, which gave the extrapolated value of the Gross revenue at the end of 6 years as $10,137.81.

The figure below shows the graph for the extrapolated values of gross revenues.

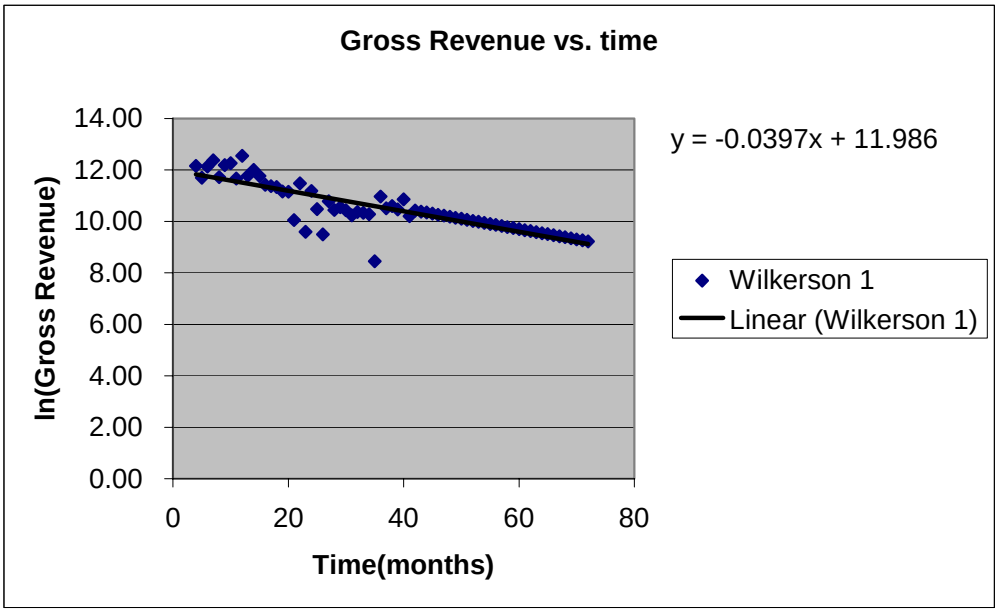

Figure C- 2: Wilkerson 1

2) Griffen 1

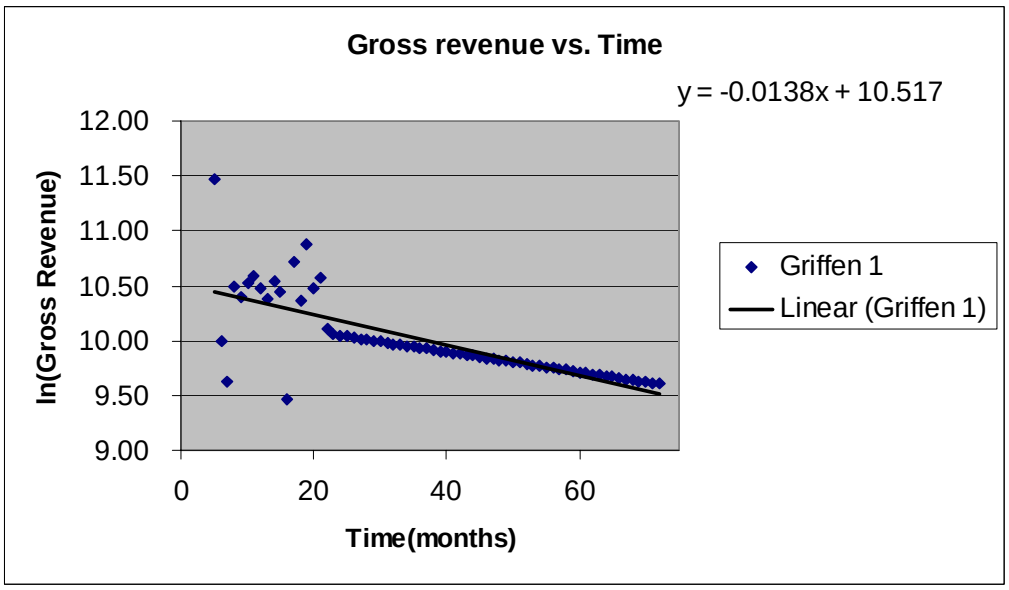

Figure C- 3: Griffen 1

The extrapolated value for the gross revenue at the end of 6 years for Griffen 1 was calculated as $14,802.38.

3) Suzie – Q

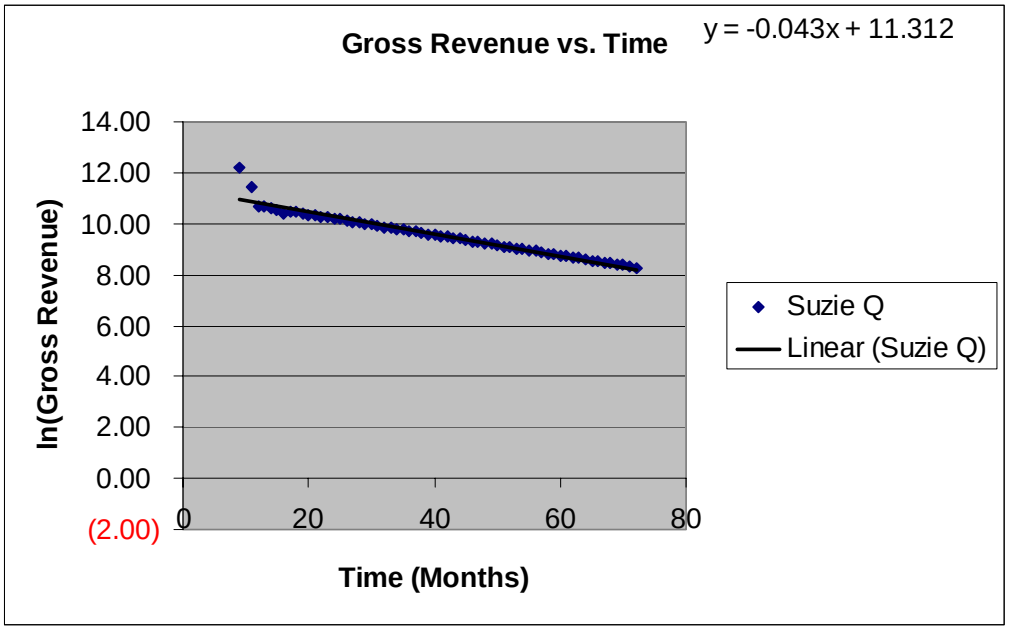

Figure C- 4: Suzie - Q

The Gross Revenue at the end of 6 years, i.e. at the 72nd month is calculated as $ 3931.68

4) Shons 1

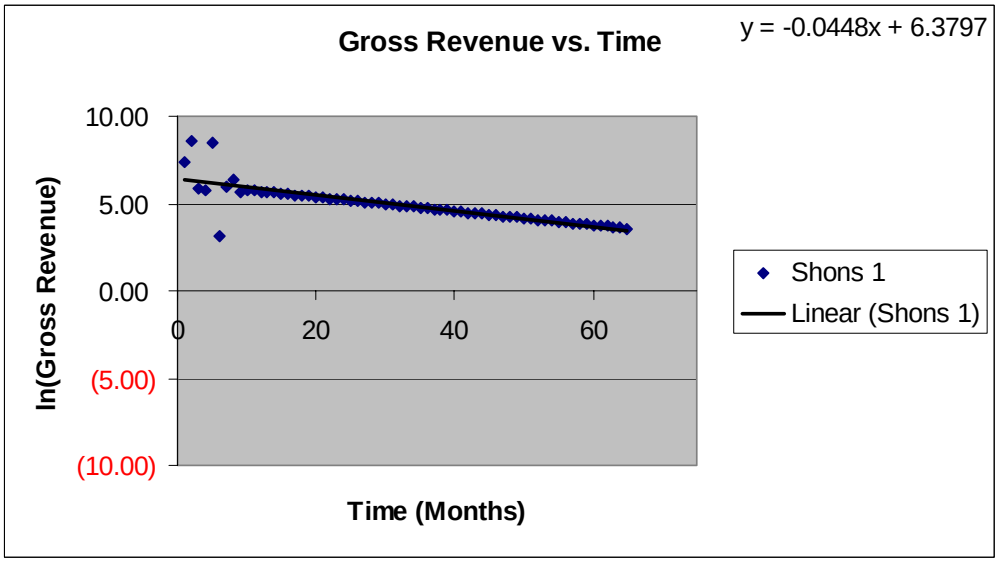

Figure C- 5: Shons 1

Shons 1 has been operating since almost 1 year, and the net revenues it has generated is always a negative value. Data is available up till the month of June' 03, at the time when a negative net revenue value is observed. So, it might be advisable to terminate the well, after it continually gives a negative revenue value. The extrapolated value of the gross revenue at the 72nd month for Shons 1 is $35.44.

5) Danny 2

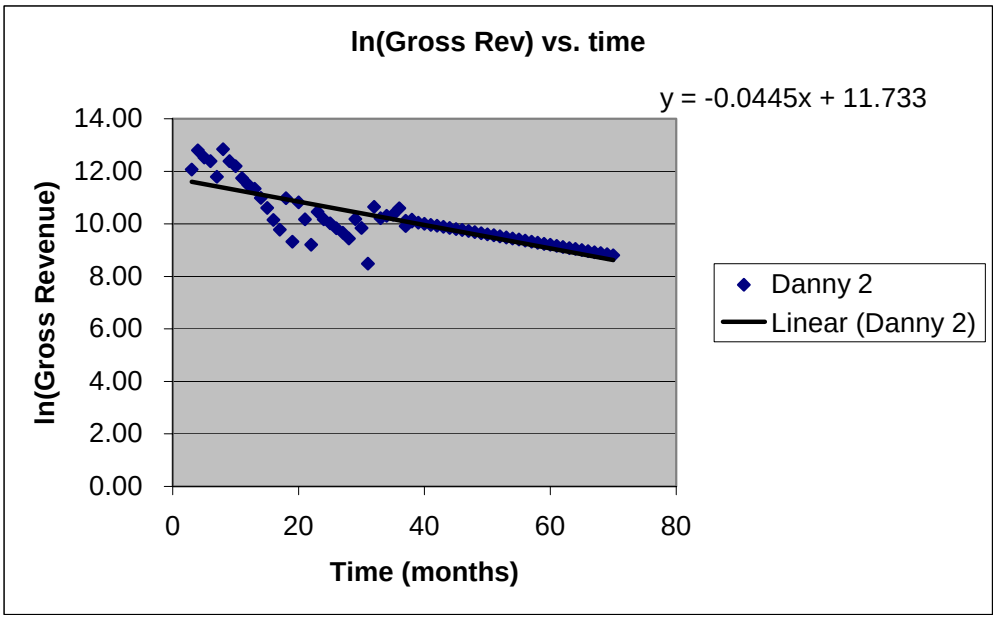

Figure C- 6: Danny 2

The gross revenue at the end of the 6th year is calculated as $6654.29.

6) Schwake 1

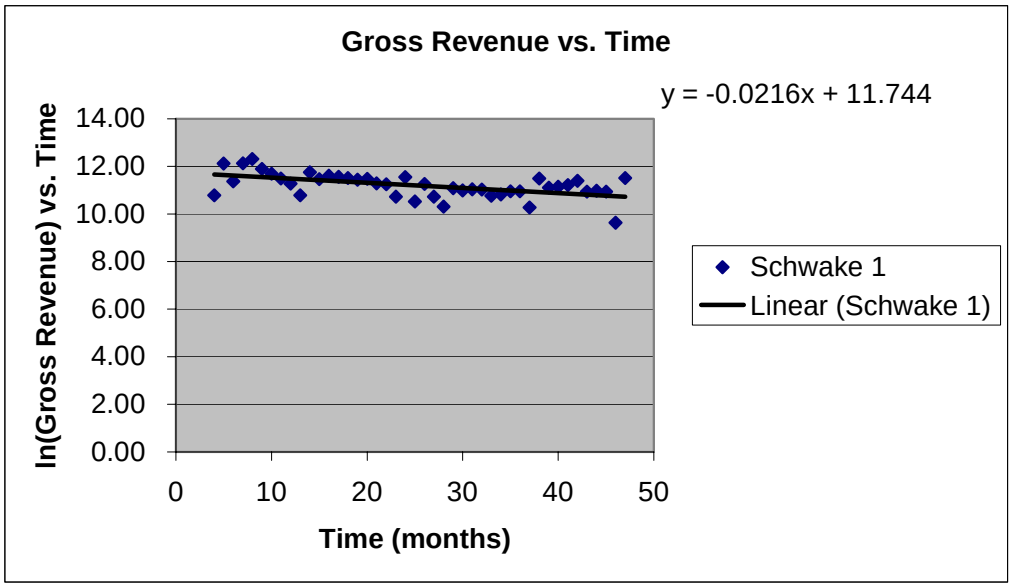

Figure C- 7: Schwake 1

The Gross Revenue at the 72nd month for the above figure is calculated as $57,962.15.

7) Anna Givens 1

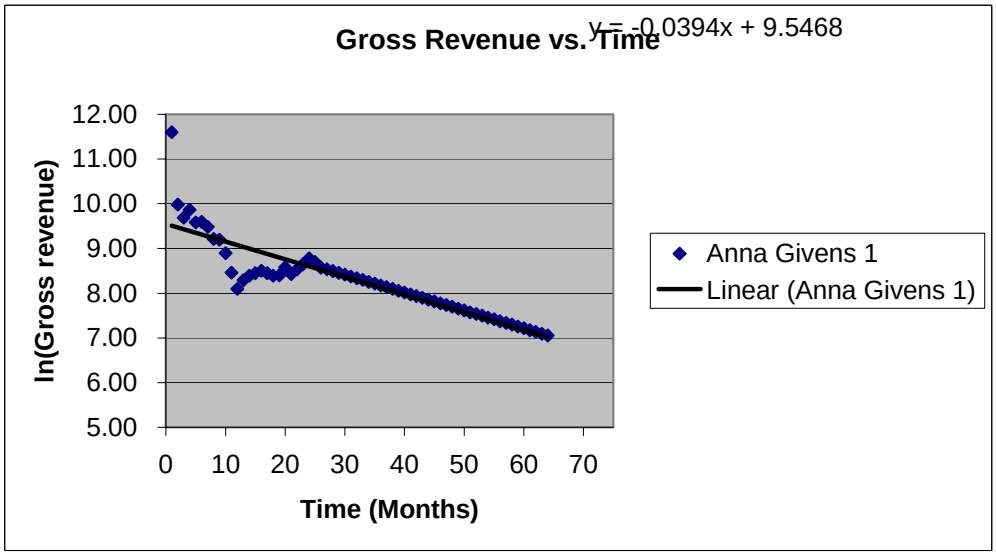

Figure C- 8: Anna Givens 1

Anna givens gives a consistent value of positive net revenue up till the January of 2005, from where onwards, it starts giving negative net revenue. After observing the revenues, if the well continues to give negative revenues, it would be advisable to terminate the well at this point in time. The gross revenue at the end of 6 years is $1158.45.

8) Stevenson 1

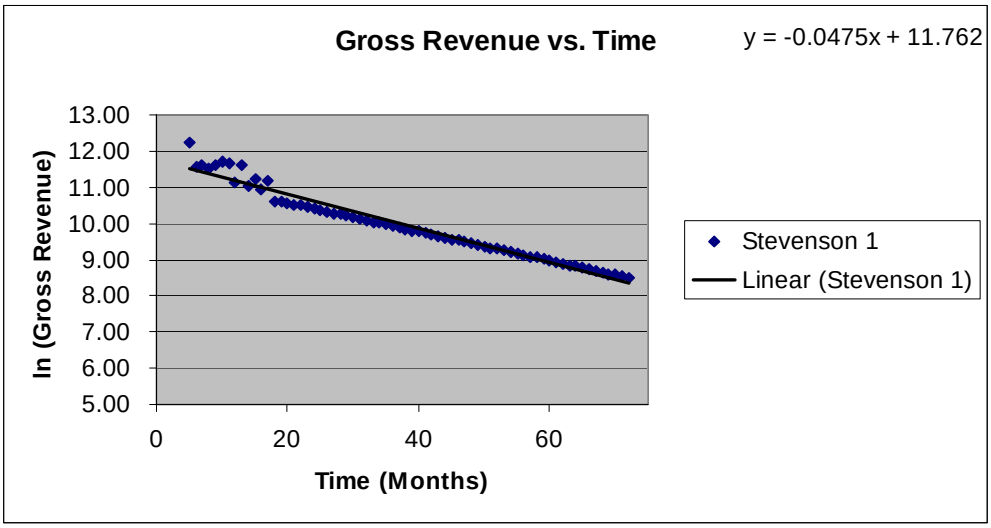

Figure C- 9: Stevenson 1

The gross revenue for Stevenson 1 at the end of 6 years is calculated as $4875.23.

Horizontal Wells:

1) Wilkerson 2

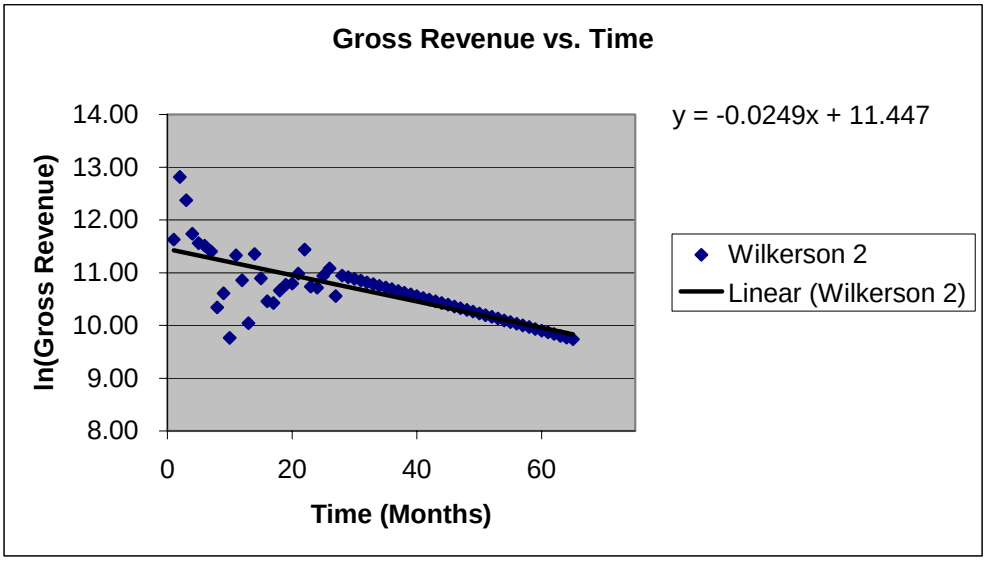

Figure C- 10: Wilkerson 2

The extrapolated gross revenue for Wilkerson 2 is calculated as $16,934.78.

2) Gilmore 1

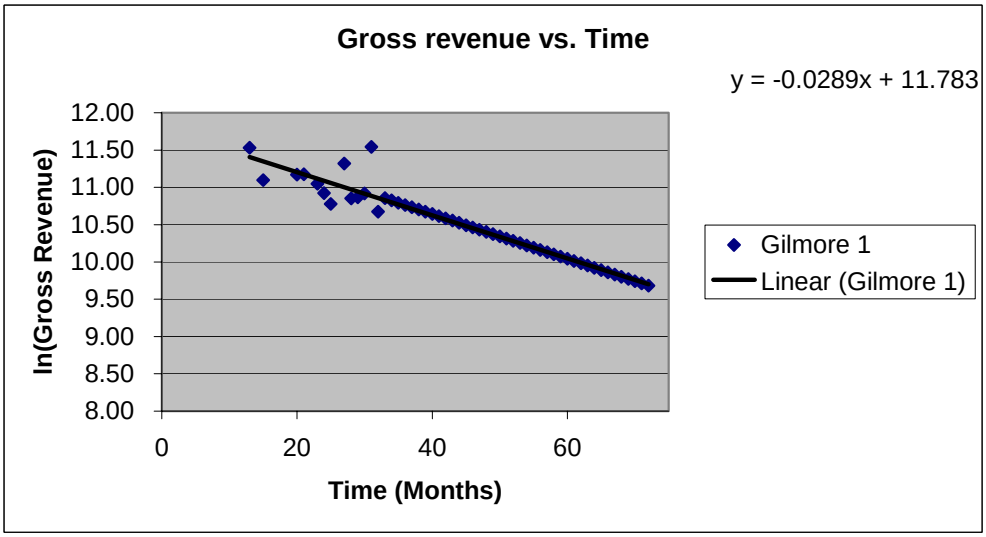

Figure C- 11: Gilmore 1

The gross revenue at the 72nd month is calculated as $16,009.05

3) Gilmore 2

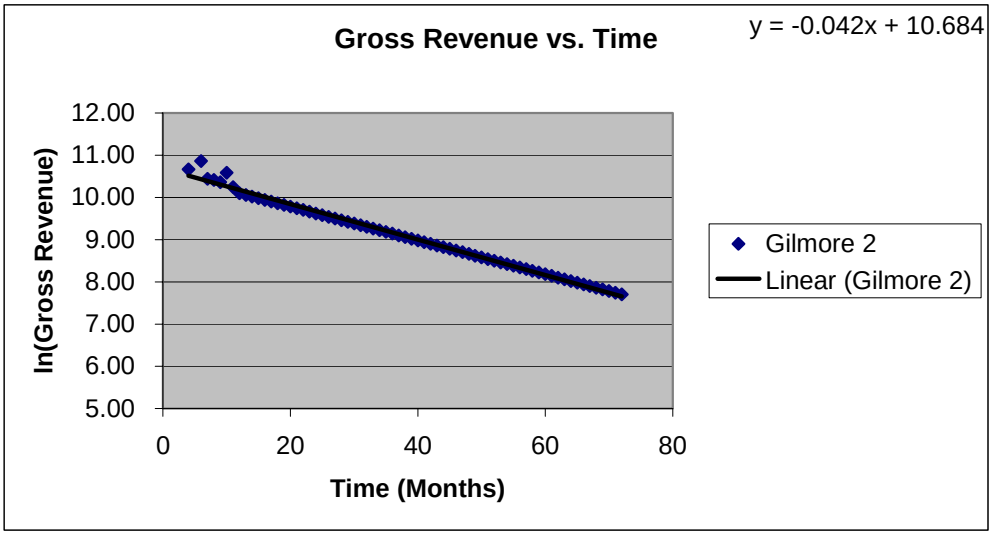

Figure C- 12: Gilmore 2

The gross revenue of Gilmore 2 at the end of 6 years is calculated as $2211.96.

4) Blackstuff

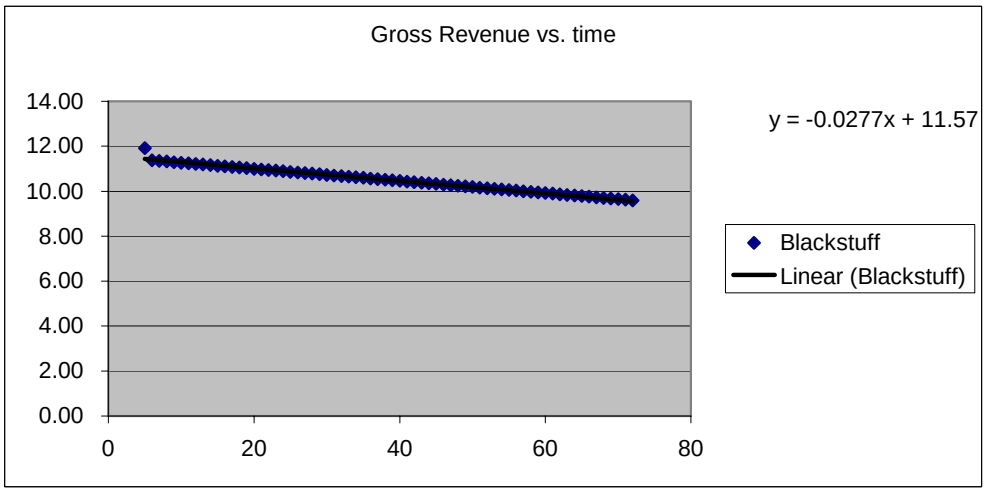

Figure C- 13: Blackstuff

The gross revenue at the end of 6 years is calculated as $14,670.75.

5) Jennifer

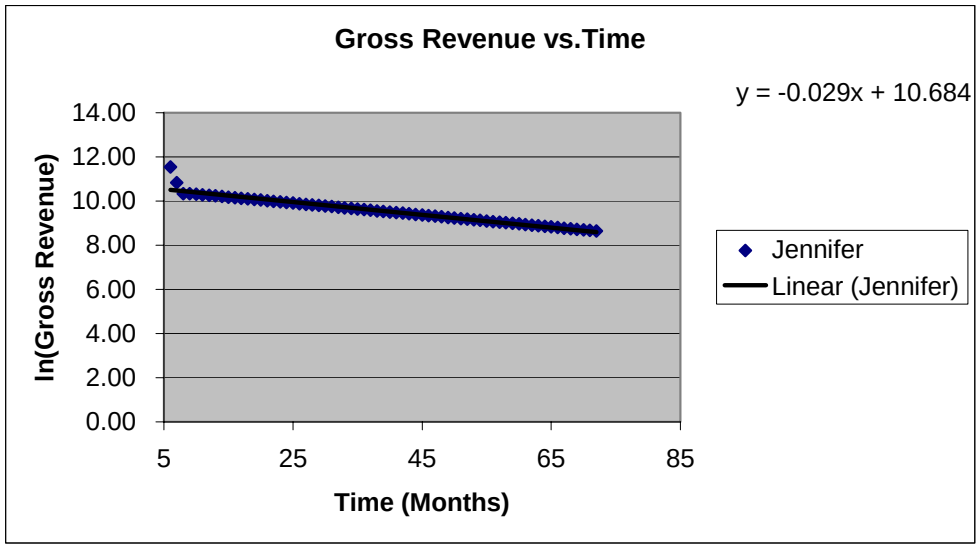

Figure C- 14: Jennifer

The gross revenue calculated at the end of 6 years is $5652.00.

6) Mr. B

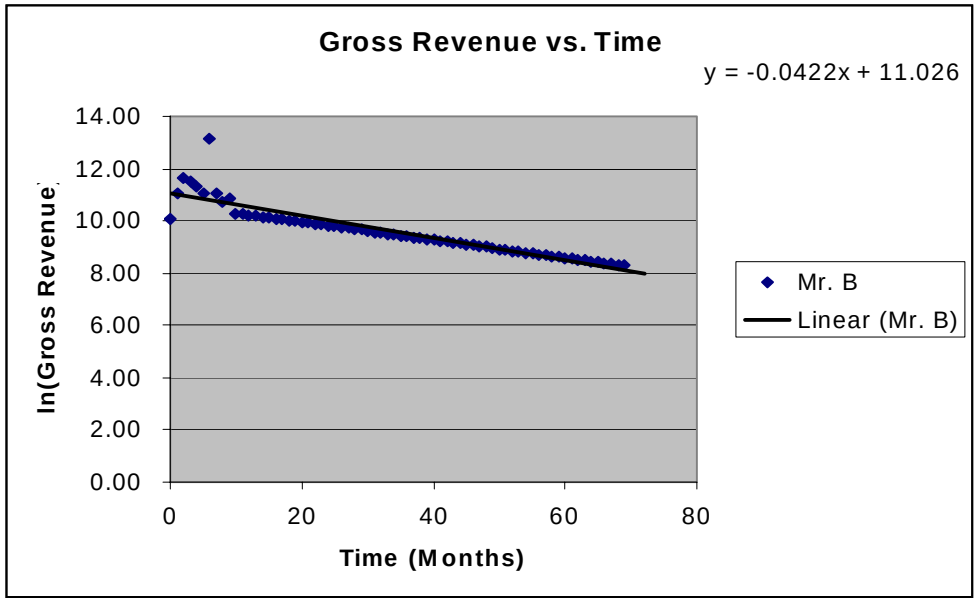

Figure C- 15: Mr. B

The production data available for Mr. B is till the October of 2003. But, as the complete data is not available, September is considered as the last month for availability of production data. From there on, the slope of the trend line is used in calculating the further values of gross revenues. The gross revenue at the end of 6 years is calculated as $6770.12.

7) Julie Ann

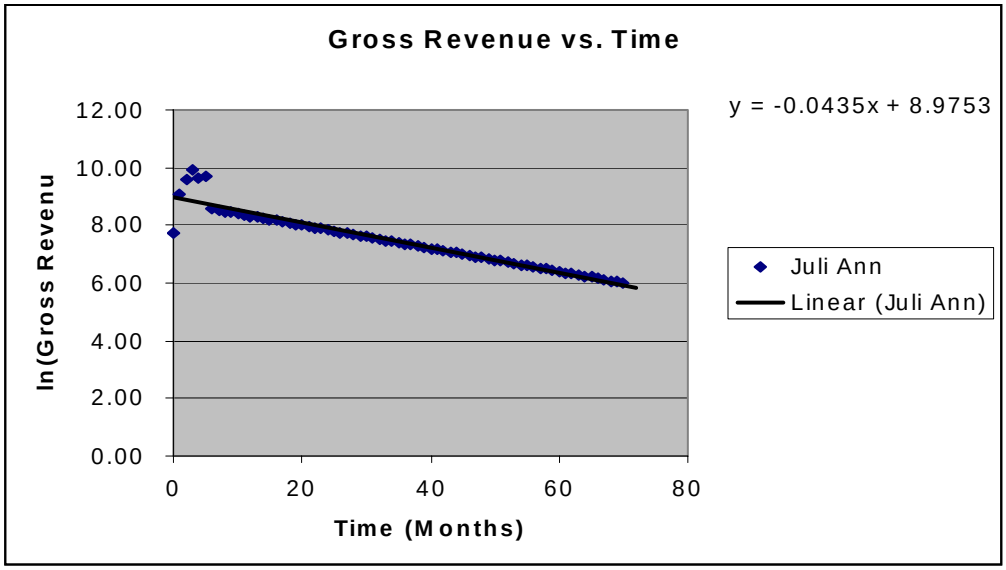

Figure C- 16: Julie Ann

Similar to the case of Mr. B, Julie Ann and 44-horizontal also have data which is available till the mid of October. But, September is taken as the final month for all these cases. The gross revenue of the above shown well is $4372.67.

8) 44-Horizontal

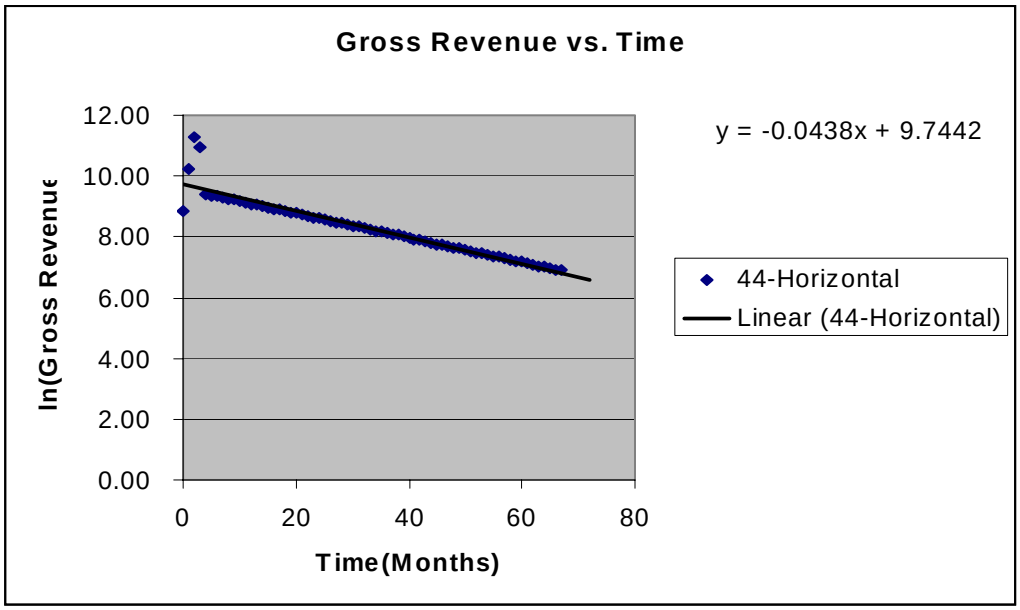

Figure C- 17: Horizontal

The gross revenue at the end of the 6 year period for the well 44-Horizontal is calculated as $4372.67.

An Advanced Fracture Characterization and Well Path Navigation System for Effective Re-Development and Enhancement of Ultimate Recovery from the Complex Monterey Reservoir of the South Ellwood Field, Offshore California

DE-AC26-00BC15127

Program

This project was in response to DOE's solicitation DE-PS26-99BC15144, Reservoir Class Field Demonstration Program – Class Revisit. The goal of the Class Program was to extend the economic production of domestic fields, by slowing the rate of well abandonments and preserving industry infrastructure, and to increase ultimate recovery using improved reservoir characterization and advanced technologies.

Project Goal

Redevelop the Monterey Formation, a slope and basin turbidite reservoir at South Ellwood Field, Offshore Santa Barbara, CA. The target is to locate oil reserves in large fracture blocks, where 3-D seismic surveys can not be used.

Performer

Venoco, Inc.
Carpenteria, CA
University of Southern California
Santa Barbara, CA

Results

The project has used advanced technologies to reprocess 20 year old 2-D seismic data, resulting in the identification of three previously unknown fault block targets containing over 80 MMbbl of oil reserves. New technologies have been applied to reduce the water cut-off to economically position horizontal wellbores, resulting in 6 MMbbl incremental recovery by August 2003. South Ellwood field production has risen to 3,500 bbl/day by July 2004. Siginificant environmental benefits have been achieved.

Benefits

The first horizontal kickoff using reprocessed seismic and lithologic data has come in at 800 BOPD and paid for itself in only a few months.

Use of the Thru-tubing bubble and plug back technology reduced water production from 10 times the amount of oil to nearly equal volumes of water and oil. The cost of the Thru-tubing bubble for each well pays for itself in 20 days of production at South Ellwood Field, and has significant potential for other high water cut oil fields. The initial $30 K investment added 6 million barrels production ($150 million at $25/bbl).

Reprocessed 1982 seismic data was used to locate wellpaths for drilling the South Ellwood lease, and identified three previously unknown fault block targets with over 80 million barrels of reserves. The Pipeline Network Fracture Simulation Model and algorithm released to the public provides a valuable tool for analysis of fractured reservoir characteristics.

The impact of removing the natural gas using the seep tents has reduced pollution of the Santa Barbara Channel, increased the marine mammal population of the area, and resulted in a favorable impression on offshore production in California.

Background

Due to the tectonic history of the Santa Barbara channel, the geology of the Monterey shale is very complex. As of December 1998, the Monterey sands at South Ellwood Field had produced 48.5 MBO, 29.2 BCF of gas, and 38 MB of water. This represents only about 5% of OOIP. Reserves have been targeted at over one billion barrels of oil. High water cuts across the field had rapidly deteriorated the economics. Substantial additional recovery of ROIP (up to 50 million barrels of oil) can be realized if fracture patterns can be characterized and aquifer movement within the fracture conduits can be managed.

Cleaner water in Santa Barbara Channel attracts seals to Holly Platform.

Offshore Platform Holly, South Ellwood Field, CA.

Well productivity in South Ellwood field varies significantly, and is primarily affected by the position of the wellbore path with respect to macro and micro faulting and fracturing in the Monterey reservoir, the resulting heterogeneity, and the degree of aquifer support. To redevelop the field and optimize reservoir management the project is mapping and characterizing the field wide fracture patterns and the reservoir conduit system. The preliminary research has improved production 3-fold and identified over 80 million barrels of reserves in the Offshore Monterey.

California law has prohibited seismic surveys in the Santa Barbara Channel due to the abundant marine mammal population. This has been a challenge to exploration technology to identify reserves in the complex faulted Monterey formation. South Ellwood field is currently operating from a single offshore platform, Holly with 30 well slots used for multi-directional horizontal wells into the 1,000 ft thick Monterey fractured chert.

The former operator, ARCO Western, build two cement pyramid shaped collecting tents over natural gas seeps in the Santa Barbara channel. Venoco maintains the seep tents and produces ½ million cubic feet of gas per day from them.

Project Summary

- Successful re-development has resulted in effective new geologic mapping and characterized new geologic structures, field fracture patterns and identified the reservoir's petroleum conduit system.
- State of the art borehole imaging technologies including FMI, interference tests and production logs have been employed to characterize fractures and micro faults.
- These data along with the existing database were used for construction of a novel geologic model of the fracture network and revised reservoir structural interpretations.
- A Pipeline Network Fracture reservoir simulator was developed by the University of Southern California to monitor and manage the aquifer's role in pressure maintenance and water production.
- The new fracture simulation model, along with reformulated 2-D seismic data, originally collected by ARCO Western in 1982, was used for both planning optimal paths for new wells and improving potential ultimate recovery from recently identified new geologic structural reservoir traps.
- An off-the-shelf seismic reprocessing software (costing only $20,000) was applied to the 2-D data and used to map the Monterey fault block pattern in the Ellwood field area.
- A better understanding of the fractured Monterey chert was obtained using Schlumberger's Thru-tubing bubble and plug back technology.
- Thru-bubble and plug technology led to positioning well paths and setting bridge plugs to significantly decrease the water cut and reduce operating costs.

Environmental issues at South Ellwood field are of intense concern, because of the marine mammal population and the naturally occurring gas seeps. The gas seep collection tents have proved to be an important component of improved water quality. Collection of the gas is credited with lowering the gas pressure from the seeps and decreasing the surface oil accumulation, resulting in cleaner beaches and surface waters and healthy marine mammal population in the Santa Barbara Channel. Advances in production and drilling multiple horizontal wells from a single offshore operating platform have reduced the surface disturbance at South Ellwood field. The Thru-tubing bubble and plug back technology has achieved a 10-fold reduction of produced water brought to the surface. This means significantly lower volumes of water to be transported onshore for processing and disposal.

Current Status

The probable reserves at the newly identified North Flank area are estimated at 30 MMB. On the basis of the drill stem test (DST) results, well productivity potential appears to be very high. An appraisal well will be drilled to test the structure at an updip location from a previous well drilled and abandoned in 1977. The new well will be spudded in September 2004 and it should be on production by October 2004. The well is anticipated to produce 800 BOPD after acid treatment. If successful, five follow-up drilling locations have been defined in the North Flank area of South Ellwood field.

To further reduce operating costs and increase environmental compliance, Venoco is preparing to use compact oil/water separators installed on Holly platform. The separators, developed by the University of Tulsa under a separate DOE grant, will allow immediate reinjection of produced water to deep reservoirs, and avoid the costly and environmentally challenging necessity of bringing produced water onshore for separation and disposal.

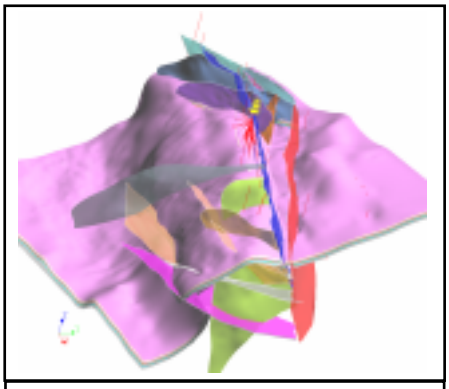

Cross-section of Monterey strata showing major faults and multi-layered wells from Platform Holly.

Project Start: July 31, 2000
Project End: July 30, 2005

Contact Information:
NETL – Gary Walker (gary.walker@netl.doe.gov or 918-699-2083)
Veneco – Steve Horner (shorner@venocoinc.com or 805-745-2285)
5464 Carpenteria Ave., Ste. J, Carpenteria, CA 93013

HETEROGENEOUS SHALLOW-SHELF CARBONATE BUILDUPS IN THE PARADOX BASIN, UTAH AND COLORADO: TARGETS FOR INCREASED OIL PRODUCTION AND RESERVES USING HORIZONTAL DRILLING TECHNIQUES

SEMI-ANNUAL TECHNICAL PROGRESS REPORT April 6, 2003 - October 5, 2003

by

Thomas C. Chidsey, Jr., Principal Investigator/Program Manager,
Kevin McClure and Craig D. Morgan
Utah Geological Survey
David E. Eby, Eby Petrography & Consulting, Inc.
and
Stephen T. Nelson, Brigham Young University

UTAH GEOLOGICAL SURVEY

November 2003

Contract No. DE-FC26-00BC15128

Gary D. Walker, Contract Manager
U.S. Department of Energy
National Petroleum Technology Office
1 West 3rd Street
Tulsa, OK 74103-3532

DISCLAIMER

This report was prepared as an account of work sponsored by an agency of the United States Government. Neither the United States Government nor any agency thereof, nor any of their employees, makes any warranty, express or implied, or assumes any legal liability or responsibility for the accuracy, completeness, or usefulness of any information, apparatus, product, or process disclosed, or represents that its use would not infringe privately owned rights. Reference herein to any specific commercial product, process, or service by trade name, trademark, manufacturer, or otherwise does not necessarily constitute or imply its endorsement, recommendation, or favoring by the United States Government or any agency thereof. The views and opinions of authors expressed herein do not necessarily state or reflect those of the United States Government or any agency thereof.

Although this product represents the work of professional scientists, the Utah Department of Natural Resources, Utah Geological Survey, makes no warranty, expressed or implied, regarding its suitability for a particular use. The Utah Department of Natural Resources, Utah Geological Survey, shall not be liable under any circumstances for any direct, indirect, special, incidental, or consequential damages with respect to claims by users of this product.

HETEROGENEOUS SHALLOW-SHELF CARBONATE BUILDUPS IN THE PARADOX BASIN, UTAH AND COLORADO: TARGETS FOR INCREASED OIL PRODUCTION AND RESERVES USING HORIZONTAL DRILLING TECHNIQUES

SEMI-ANNUAL TECHNICAL PROGRESS REPORT April 6, 2003 - October 5, 2003

by

Thomas C. Chidsey, Jr., Principal Investigator/Program Manager,
Kevin McClure and Craig D. Morgan
Utah Geological Survey
David E. Eby, Eby Petrography & Consulting, Inc.
and
Steve Nelson, Brigham Young University

Date of Report: November 2003

Contract No. DE-FC26-00BC15128

Gary D. Walker, Contract Manager
U.S. Department of Energy
National Petroleum Technology Office
1 West 3rd Street
Tulsa, OK 74103-3532

Submitting Organization: Utah Geological Survey
1594 West North Temple, Suite 3110
P.O. Box 146100
Salt Lake City, Utah 84114-6100
(801) 537-3300

US/DOE Patent Clearance is not required prior to the publication of this document.

CONTENTS

ABSTRACT iv

EXECUTIVE SUMMARY vi

INTRODUCTION 1
Project Overview 1
Project Benefits and Potential Application 4

CASE-STUDY FIELDS 4
Cherokee Field 5
Bug Field 5

PRODUCTION ANALYSIS – RESULTS AND DISCUSSION 6
Well-Test Data Evaluation 6
Cumulative Production 14

ISOTOPIC GEOCHEMISTRY – RESULTS AND DISCUSSION 14
Previous Work 16
Methodology 23
Carbon and Oxygen Isotopes from Lower Desert Creek Dolomites 23
Carbon and Oxygen Isotopes from the Upper Ismay of Cherokee Field 28
Carbon and Oxygen Isotopes from an Upper Ismay Buildup, Patterson Canyon Field 31

TECHNOLOGY TRANSFER 34
Utah Geological Survey *Survey Notes* and Internet Web Site 35
Technical Presentations 35
Project Publications 36

CONCLUSIONS 36

ACKNOWLEDGMENTS 38

REFERENCES 39

FIGURES

Figure 1. Map showing the project study area and fields within the Ismay and Desert Creek producing trends, Utah and Colorado 1
Figure 2. Pennsylvanian stratigraphy of the southern Paradox Basin 2
Figure 3. Block diagrams displaying major depositional facies for the Ismay (A) and Desert Creek (B) zones, Pennsylvanian Paradox Formation 3
Figure 4. Initial potential flow of oil and gas, from upper Ismay producing wells, in Cherokee field 6

Figure 5. Bubble map of initial potential flow of oil from upper Ismay producing wells in Cherokee field 7
Figure 6. Initial potential flow of oil and gas, from lower Desert Creek producing wells, in Bug field 8
Figure 7. Bubble map of initial potential flow of oil from lower Desert Creek producing wells in Bug field 9
Figure 8. Map of combined top of "clean carbonate" structure and isochore of porosity units 1 through 5, upper Ismay zone, Cherokee field 10
Figure 9. Upper Ismay zone facies map, Cherokee field 11
Figure 10. Map of combined top of structure and isochore of lower Desert Creek zone mound, Bug field 12
Figure 11. Lower Desert Creek zone facies map, Bug field 13
Figure 12. Historical oil (A), gas (B), and water (C) production for Cherokee field. 15
Figure 13. Cumulative production of oil and gas, from upper Ismay producing wells, in Cherokee field 16
Figure 14. Bubble map of cumulative production of oil from upper Ismay producing wells in Cherokee field. 17
Figure 15. Photomicrograph of a peloidal packstone/grainstone dominated by microporosity, Cherokee No. 22-14 well 17
Figure 16. Historical oil (A), gas (B), and water (C) production for Bug field. 18
Figure 17. Cumulative production of oil and gas, from lower Desert Creek producing wells, in Bug field 19
Figure 18. Bubble map of cumulative production of oil from lower Desert Creek producing wells in Bug field 19
Figure 19. Photomicrograph showing dolomite dissolution including micro-box-work pores, Bug No. 10 20
Figure 20. Diagenetic sequence diagram for Bug and Cherokee fields 20
Figure 21. Graph of carbon versus oxygen isotope compositions 21
Figure 22. Graph of carbon versus oxygen compositions for Bug and Tin Cup Mesa fields 21
Figure 23. Core photos of typical Bug field components sampled for stable carbon and oxygen isotope analysis 25
Figure 24. Graph of carbon versus oxygen compositions for Bug field dolomites 26
Figure 25. Graph comparing carbon versus oxygen compositions for Bug field dolomites by Roylance (1984) versus those completed for this study. 26
Figure 26. Summary graph of carbon versus oxygen compositions for all components sampled for this study and previously published by Roylance, 1984 28
Figure 27. Core Photos of typical Cherokee field components sampled for stable carbon and oxygen isotope analysis 29
Figure 28. Graph of carbon versus oxygen compositions for Cherokee field components 30
Figure 29. Core photos of whole rock and cement components sampled for stable carbon and oxygen isotope analysis in the upper Ismay buildup of the Samedan Bonito 41-6-85 well 32
Figure 30. Graph of carbon versus oxygen compositions for whole rock and cement components in an upper Ismay buildup, Samedan Bonito No. 41-6-85 well 33

TABLES

Table 1. Location of cores used in the isotope geochemistry study 22
Table 2. Previous stable carbon and oxygen isotope data from lower Desert Creek zone, Bug and Tin Cup Mesa fields 22
Table 3. New stable carbon and oxygen isotope data from lower Desert Creek zone Bug field dolomites 23
Table 4. New stable carbon and oxygen isotope data from upper Ismay zone Cherokee field 24
Table 5. New stable carbon and oxygen isotope data from upper Ismay buildup zone Samedan Bonito No. 41-6-85 core 24

ABSTRACT

The Paradox Basin of Utah, Colorado, Arizona, and New Mexico contains nearly 100 small oil fields producing from carbonate buildups within the Pennsylvanian (Desmoinesian) Paradox Formation. These fields typically have one to 10 wells with primary production ranging from 700,000 to 2,000,000 barrels (111,300-318,000 m^3) of oil per field and a 15 to 20 percent recovery rate. At least 200 million barrels (31.8 million m^3) of oil will not be recovered from these small fields because of inefficient recovery practices and undrained heterogeneous reservoirs.

Several fields in southeastern Utah and southwestern Colorado are being evaluated as candidates for horizontal drilling and enhanced oil recovery from existing vertical wells based upon geological characterization and reservoir modeling case studies. Geological characterization on a local scale is focused on reservoir heterogeneity, quality, and lateral continuity, as well as possible reservoir compartmentalization, within these fields. This study utilizes representative cores, geophysical logs, and thin sections to characterize and grade each field's potential for drilling horizontal laterals from existing development wells. The results of these studies can be applied to similar fields elsewhere in the Paradox Basin and the Rocky Mountain region, the Michigan and Illinois Basins, and the Midcontinent region.

This report covers research activities for the first half of the fourth project year (April 6 through October 5, 2003). The work included (1) analysis of well-test data and oil production from Cherokee and Bug fields, San Juan County, Utah, and (2) diagenetic evaluation of stable isotopes from the upper Ismay and lower Desert Creek zones of the Paradox Formation in the Blanding sub-basin, Utah.

Production "sweet spots" and potential horizontal drilling candidates were identified for Cherokee and Bug fields. In Cherokee field, the most productive wells are located in the thickest part of the mound facies of the upper Ismay zone, where microporosity is well developed. In Bug field, the most productive wells are located structurally downdip from the updip porosity pinch out in the dolomitized lower Desert Creek zone, where micro-box-work porosity is well developed. Microporosity and micro-box-work porosity have the greatest hydrocarbon storage and flow capacity, and potential horizontal drilling target in these fields.

Diagenesis is the main control on the quality of Ismay and Desert Creek reservoirs. Most of the carbonates present within the lower Desert Creek and Ismay have retained a marine-influenced carbon isotope geochemistry throughout marine cementation as well as through post-burial recycling of marine carbonate components during dolomitization, stylolitization, dissolution, and late cementation. Meteoric waters do not appear to have had any effect on the composition of the dolomites in these zones. Light oxygen values obtained from reservoir samples for wells located along the margins or flanks of Bug field may be indicative of exposure to higher temperatures, to fluids depleted in ^{18}O relative to sea water, or to hypersaline waters during burial diagenesis. The samples from Bug field with the lightest oxygen isotope compositions are from wells that have produced significantly greater amounts of hydrocarbons. There is no significant difference between the oxygen isotope compositions from lower Desert Creek dolomite samples in Bug field and the upper Ismay limestones and dolomites from Cherokee field. Carbon isotopic compositions for samples from Patterson Canyon field can be divided into two populations: isotopically heavier mound cement and isotopically lighter oolite and banded cement.

Technology transfer activities consisted of exhibiting a booth display of project materials at the annual national convention of the American Association of Petroleum Geologists, a technical presentation, a core workshop, and publications. The project home page was updated on the Utah Geological Survey Internet web site.

EXECUTIVE SUMMARY

The project's primary objective is to enhance domestic petroleum production by demonstration and transfer of horizontal drilling technology in the Paradox Basin of Utah and Colorado. If this project can demonstrate technical and economic feasibility, then the technique can be applied to approximately 100 additional small fields in the Paradox Basin alone, and result in increased recovery of 25 to 50 million barrels (4-8 million m^3) of oil. This project is designed to characterize several shallow-shelf, carbonate reservoirs in the Pennsylvanian (Desmoinesian) Paradox Formation, choose the best candidate field(s) for a pilot demonstration project to drill horizontally from existing vertical wells, monitor well performance(s), and report associated validation activities.

The Utah Geological Survey heads a multidisciplinary team to determine the geological and reservoir characteristics of typical, small, shallow-shelf, carbonate reservoirs in the Paradox Basin. The Paradox Basin technical team consists of the Utah Geological Survey (prime contractor), Colorado Geological Survey (subcontractor), Eby Petrography & Consulting Inc. (subcontractor), and Seeley Oil Company (subcontractor and industry partner). This research is funded by the Class II Oil Revisit Program of the U.S. Department of Energy, National Petroleum Technology Office (NPTO) in Tulsa, Oklahoma. This report covers research activities for the first half of the fourth project year (April 6, 2003, through October 5, 2003). This work included (1) analysis of well-test data and oil production from Cherokee and Bug fields, San Juan County, Utah, and (2) diagenetic evaluation of stable isotopes from the upper Ismay and lower Desert Creek zones of the Paradox Formation in the Blanding sub-basin, Utah. From these, and other, project evaluations, untested or under-produced reservoir compartments and trends can be identified as targets for horizontal drilling. The results of this study can be applied to similar reservoirs in many U.S. basins.

Production "sweet spots" and potential horizontal drilling candidates were identified for Cherokee and Bug fields. In Cherokee field, the most productive wells are located on the crest of the structural nose where the upper Ismay zone buildup developed and in the thickest part of the mound facies. These wells likely penetrated a thick section of microporosity - pore type with the greatest hydrocarbon storage capacity and potential horizontal drilling target in the field. In Bug field, the most productive wells are located structurally downdip from the updip porosity pinch out that forms the trap, and in the main part of the lower Desert Creek zone carbonate buildup. These wells likely penetrated significant micro-box-work porosity - the diagenetic pore type with the greatest hydrocarbon storage and flow capacity in this dolomitized reservoir.

Diagenesis is the main control on the quality of Ismay and Desert Creek reservoirs. Most of the carbonates present within the lower Desert Creek and Ismay have retained a marine-influenced carbon isotope geochemistry throughout marine cementation as well as through post-burial recycling of marine carbonate components during dolomitization, stylolitization, dissolution, and late cementation. Meteoric waters do not appear to have had any effect on the composition of these lower Desert Creek dolomites. Based on Bug field dolomite samples, the lower Desert Creek zone shows carbon isotope compositions that are very close in value to modern marine carbonates and Holocene botryoidal, marine, aragonite cements. As with the Bug field dolomite samples, the Cherokee field carbonates fall within the same range of carbon isotope compositions as modern marine sediments, skeletons, and marine cements.

Light oxygen values obtained from reservoir samples for wells located along the margins or flanks of Bug field may be indicative of exposure to higher temperatures, to fluids depleted in ^{18}O relative to sea water, or to hypersaline waters during burial diagenesis. The samples from Bug field with the lightest oxygen isotope compositions are from wells that have produced significantly higher amounts of hydrocarbons. There is no significant difference between the oxygen isotope compositions from lower Desert Creek dolomite samples in Bug field and the upper Ismay limestones and dolomites from Cherokee field.

Carbon isotopic compositions for samples of an upper Ismay cemented limestone buildup in Patterson Canyon field can be divided into two populations with regard to carbon isotopic composition: isotopically heavier mound cement and isotopically lighter oolite and banded cement. Mound cements were confined to a "closed hydrologic system" that allowed a fluid with heavier carbon to evolve. The oolite and banded cement therein may have formed in a more open system allowing exchange with isotopically lighter waters which were involved in the lithification and diagenesis of the capping oolite.

Technology transfer activities consisted of exhibiting a booth display of project objects and results at the 2003 annual national convention of the American Association of Petroleum Geologists in Salt Lake City, Utah. The technical team also presented a project short course/ core workshop and a poster technical presentation at the convention. Cores, regional facies maps, diagenetic analysis, and horizontal drilling recommendations were part of these presentations. The project home page was updated on the Utah Geological Survey Internet web site. Project team members also published an abstract and semi-annual report detailing project progress and results.

INTRODUCTION

Project Overview

Over 400 million barrels (64 million m^3) of oil have been produced from the shallow-shelf carbonate reservoirs in the Pennsylvanian Paradox Formation in the Paradox Basin of southeastern Utah and southwestern Colorado (figure 1). The two main producing zones of the

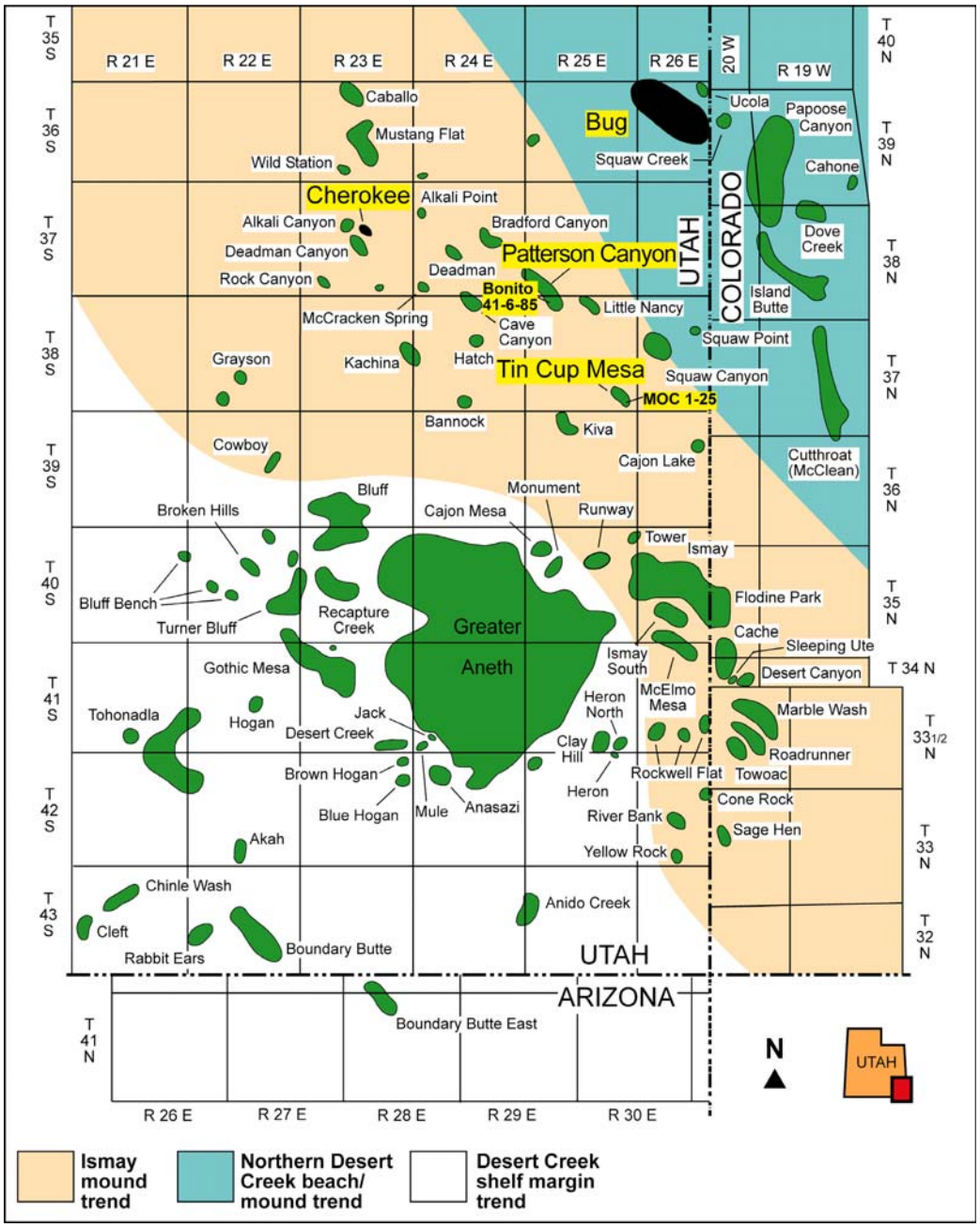

Figure 1. Map showing project study area and fields (case-study fields in black) within the Ismay and Desert Creek producing trends, Utah and Colorado. Fields sampled for isotope analyses are highlighted in yellow.

Paradox Formation are informally named the Ismay and the Desert Creek (figure 2). Reservoirs within the Utah portion of the upper Ismay zone of the Paradox Formation are dominantly limestones composed of small, phylloid-algal buildups; locally variable, inner-shelf, skeletal calcarenites; and rare, open-marine, bryozoan mounds (figure 3A). The Ismay produces oil from fields in the southern Blanding sub-basin (figure 1). The Desert Creek zone is dominantly dolomite comprising regional, nearshore, shoreline trends with highly aligned, linear facies tracts (figure 3B). The Desert Creek produces oil in fields in the central Blanding sub-basin (figure 1). Both the Ismay and Desert Creek buildups generally trend northwest-southeast. Various facies changes and extensive diagenesis have created complex reservoir heterogeneity within these two diverse zones.

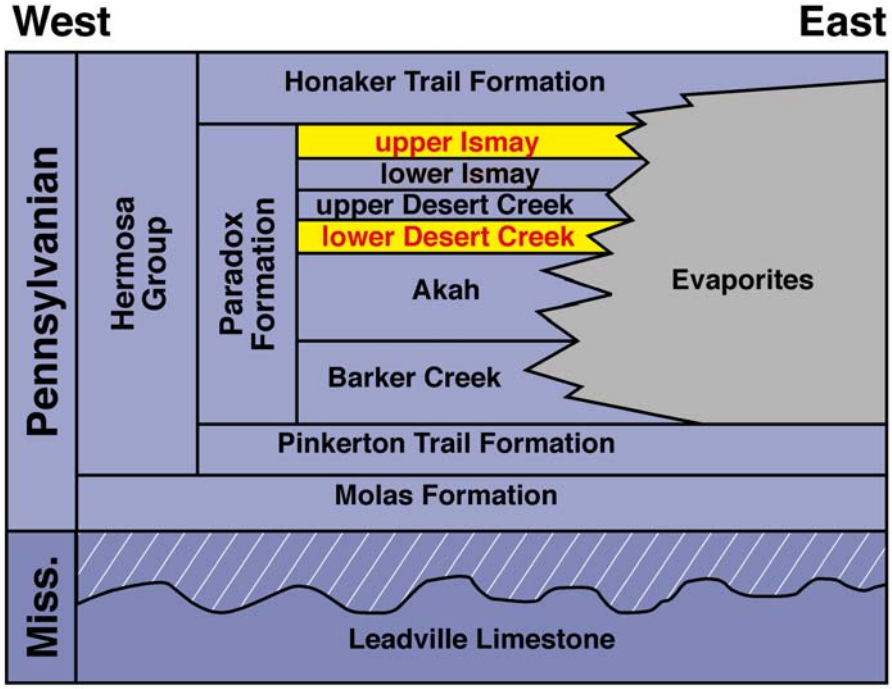

Figure 2. Pennsylvanian stratigraphy of the southern Paradox Basin including informal zones of the Paradox Formation; the upper Ismay and lower Desert Creek zones productive in case-study fields are highlighted.

With the exception of the giant Greater Aneth field, the other 100-plus oil fields in the basin typically contain 2 to 10 million barrels (0.3-1.6 million m^3) of original oil in place. Most of these fields are characterized by high initial production rates followed by a very short productive life (primary), and hence premature abandonment. Only 15 to 25 percent of the original oil in place is recoverable during primary production from conventional vertical wells.

An extensive and successful horizontal drilling program has been conducted in the giant Greater Aneth field. However, to date, only two horizontal wells have been drilled in small Ismay and Desert Creek fields. The results from these wells were disappointing due to poor understanding of the carbonate facies and diagenetic fabrics that create reservoir heterogeneity. These small fields, and similar fields in the basin, are at high risk of premature abandonment. At least 200 million barrels (31.8 million m^3) of oil will be left behind in these small fields because current development practices leave compartments of the heterogeneous reservoirs undrained. Through proper geological evaluation of the reservoirs, production may be increased by 20 to 50 percent through the drilling of low-cost, single, or multilateral, horizontal legs from existing vertical development wells. In addition, horizontal drilling from existing wells minimizes surface disturbances and costs for field development, particularly in the environmentally sensitive areas of southeastern Utah and southwestern Colorado.

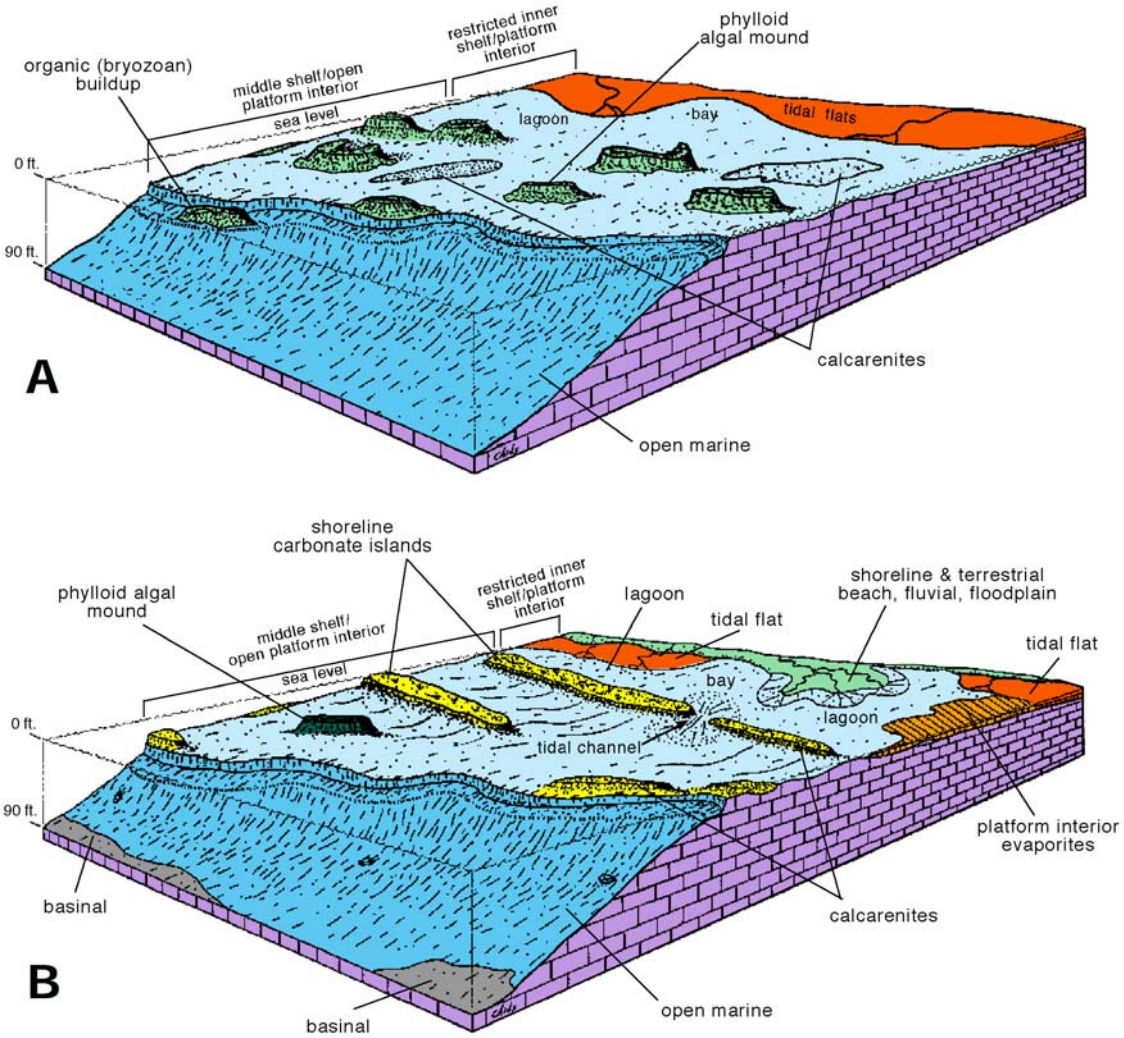

Figure 3. Block diagrams displaying major depositional facies, as determined from core, for the Ismay (A) and Desert Creek (B) zones, Pennsylvanian Paradox Formation, Utah and Colorado (tan and blue areas shown in figure 1).

The Utah Geological Survey (UGS), Colorado Geological Survey (CGS), Eby Petrography & Consulting, Inc., and Seeley Oil Company have entered into a cooperative agreement with the U.S. Department of Energy (DOE) as part of its Class II Oil Revisit Program. A three-phase, multidisciplinary approach will be used to increase production and reserves from the shallow-shelf carbonate reservoirs in the Ismay and Desert Creek zones of the Paradox Basin.

Phase 1 is the geological and reservoir characterization of selected, diversified, small fields, including Cherokee and Bug fields in San Juan County, Utah (figure 1), to identify those field(s) having the greatest potential as targets for increased well productivity and ultimate recovery in a pilot demonstration project. This phase includes: (a) determination of regional geological setting; (b) analysis of the reservoir heterogeneity, quality, lateral continuity, and compartmentalization within the fields; (c) construction of lithologic, microfacies, porosity, permeability, and net pay maps of the fields; (d) determination of field reserves and recovery; and (e) integration of geological data in the design of single or multiple horizontal laterals from existing vertical wells.

Phase 2 is a field demonstration project of the horizontal drilling techniques identified as having the greatest potential for increased field productivity and ultimate recovery. The demonstration project will involve drilling one or more horizontal laterals from the existing vertical field well(s) to maximize production from the zones of greatest potential.

Phase 3 includes: (a) reservoir management and production monitoring, (b) economic evaluation of the results, and (c) determination of the ability to transfer project technologies to other similar fields in the Paradox Basin and throughout the U.S.

Phases 1, 2, and 3 will have continuous, but separate, technical transfer activities including: (a) an industry outreach program; (b) a core workshop/seminar in Salt Lake City; (c) publications and technical presentations; (d) a project home page on the Utah Geological Survey and Colorado Geological Survey Internet web sites; (e) digital databases, maps, and reports; (f) a summary of regulatory, economic, and financial needs; and (g) annual meetings with a Technical Advisory Board and Stake Holders Board.

Project Benefits and Potential Application

The overall benefit of this multi-year project would be enhanced domestic petroleum production by demonstrating and transferring an advanced-oil-recovery technology throughout the small oil fields of the Paradox Basin. Specifically, the benefits expected from the project are: (1) increasing recovery and reserve base by identifying untapped compartments created by reservoir heterogeneity; (2) preventing premature abandonment of numerous small fields; (3) increasing deliverability by horizontally drilling along the reservoir's optimal fluid-flow paths; (4) identifying reservoir trends for field extension drilling and stimulating exploration in Paradox Basin fairways; (5) reducing development costs by more closely delineating minimum field size and other parameters necessary for horizontal drilling; (6) allowing for minimal surface disturbance by drilling from existing, vertical, field well pads; (7) allowing limited energy investment dollars to be used more productively; and (8) increasing royalty income to the federal, state, and local governments, the Ute Mountain Ute Indian Tribe, and fee owners. These benefits may also apply to other areas including: algal-mound and carbonate buildup reservoirs on the eastern and northwestern shelves of the Permian Basin in Texas, Silurian pinnacle and patch reefs of the Michigan and Illinois Basins, and shoaling carbonate island trends of the Williston Basin.

The results of this project are transferred to industry and other researchers through establishment of Technical Advisory and Stake Holders Boards, an industry outreach program, digital project databases, and project web pages. Project results will be disseminated via technical workshops and seminars, field trips, technical presentations at national and regional professional meetings, and papers in various technical or trade journals.

CASE-STUDY FIELDS

Two Utah fields were selected for local-scale evaluation and geological characterization: Cherokee in the Ismay trend and Bug in the Desert Creek trend (figure 1). This evaluation included (1) analysis of well-test data and oil production, and (2) diagenetic evaluation of stable isotopes from the upper Ismay and lower Desert Creek zones of the Paradox Formation. This geological characterization focused on reservoir heterogeneity,

quality, and lateral continuity, as well as possible compartmentalization within the fields. From these evaluations, untested or under-produced compartments can be identified as targets for horizontal drilling. The models resulting from the geological and reservoir characterization of these fields can be applied to similar fields in the basin (and other basins as well) where data might be limited.

Cherokee Field

Cherokee field (figure 1) is a phylloid-algal buildup capped by anhydrite that produces from porous algal limestone and dolomite in the upper Ismay zone. The net reservoir thickness is 27 feet (8.2 m), which extends over a 320-acre (130 ha) area. Porosity averages 12 percent with 8 millidarcies (md) of permeability in vuggy and intercrystalline pore systems. Water saturation is 38.1 percent (Crawley-Stewart and Riley, 1993).

Cherokee field was discovered in 1987 with the completion of the Meridian Oil Company Cherokee Federal 11-14, NE1/4NW1/4 section 14, T. 37 S., R. 23 E., Salt Lake Base Line and Meridian (SLBL&M); initial potential flow (IPF) was 53 barrels of oil per day (BOPD) (8.4 m^3), 990 thousand cubic feet of gas per day (MCFGPD) (28 MCMPD), and 26 barrels of water (4.1 m^3). There are currently three producing (or shut-in) wells, one abandoned producer, and two dry holes in the field. The well spacing is 80 acres (32 ha). The present field reservoir pressure is estimated at 150 pounds per square inch (psi) (1,034 Kpa). Cumulative production as of June 1, 2003, was 182,071 barrels of oil (28,949 m^3), 3.65 billion cubic feet of gas (BCFG) (0.1 BCMG), and 3,358 barrels of water (534 m^3) (Utah Division of Oil, Gas and Mining, 2003). The original estimated primary recovery is 172,000 barrels of oil (27,348 m^3) and 3.28 BCFG (0.09 BCMG) (Crawley-Stewart and Riley, 1993). The fact that both these estimates have been surpassed suggests significant additional reserves could remain.

Bug Field

Bug field (figure 1) is an elongate, northwest-trending carbonate buildup in the lower Desert Creek zone. The producing units vary from porous dolomitized bafflestone to packstone and wackestone. The trapping mechanism is an updip porosity pinchout. The net reservoir thickness is 15 feet (4.6 m) over a 2,600-acre (1,052 ha) area. Porosity averages 11 percent in moldic, vuggy, and intercrystalline networks. Permeability averages 25 to 30 md, but ranges from less than 1 to 500 md. Water saturation is 32 percent (Martin, 1983; Oline, 1996).

Bug field was discovered in 1980 with the completion of the Wexpro Bug No. 1, NE1/SE1/4 section 12, T. 36 S., R. 25 E., SLBL&M, for an IPF of 608 BOPD (96.7 m^3), 1,128 MCFGPD (32 MCMPD), and 180 barrels of water (28.6 m^3). There are currently seven producing (or shut-in) wells, six abandoned producers, and two dry holes in the field. The well spacing is 160 acres (65 ha). The present reservoir field pressure is 3,550 psi (24,477 Kpa). Cumulative production as of June 1, 2003, was 1,622,020 barrels of oil (257,901 m^3), 4.47 BCFG (0.13 BCMG), and 3,181,448 barrels of water (505,850 m^3) (Utah Division of Oil, Gas and Mining, 2003). Estimated primary recovery is 1,600,000 bbls (254,400 m^3) of oil and 4 BCFG (0.1 BCMG) (Oline, 1996). Again, since the original reserve estimates have been surpassed and the field is still producing, significant additional reserves likely remain.

PRODUCTION ANALYSIS – RESULTS AND DISCUSSION

Before reservoir-modeling studies could be conducted for the Cherokee and Bug fields, analyses of production data were required. These data were compiled through two principal tasks: (1) review of existing well-completion data, and (2) determination of production history from monthly production reports available through the Utah Division of Oil, Gas and Mining. This information was merged with geological characterization data and incorporated into the interpretation of reservoir models. Production "sweet spots" and potential horizontal drilling candidates, both wells and fields, were identified. Using the results, various horizontal drilling methods and the ultimate recovery can be estimated for Cherokee and Bug fields.

Well-Test Data Evaluation

Well-test data can provide key insight into the nature of reservoir heterogeneities, and also provide "large-scale" quantitative data on actual reservoir properties and facies from case-study reservoirs. Although a number of well tests have been conducted in all of the target reservoirs, only the IPF well tests were determined to provide quantitative reservoir property information. IPF well tests were graphed and plotted for each well (figures 4 through 7). The graphs include both oil (in BOPD) and gas (in MCFPD) production.

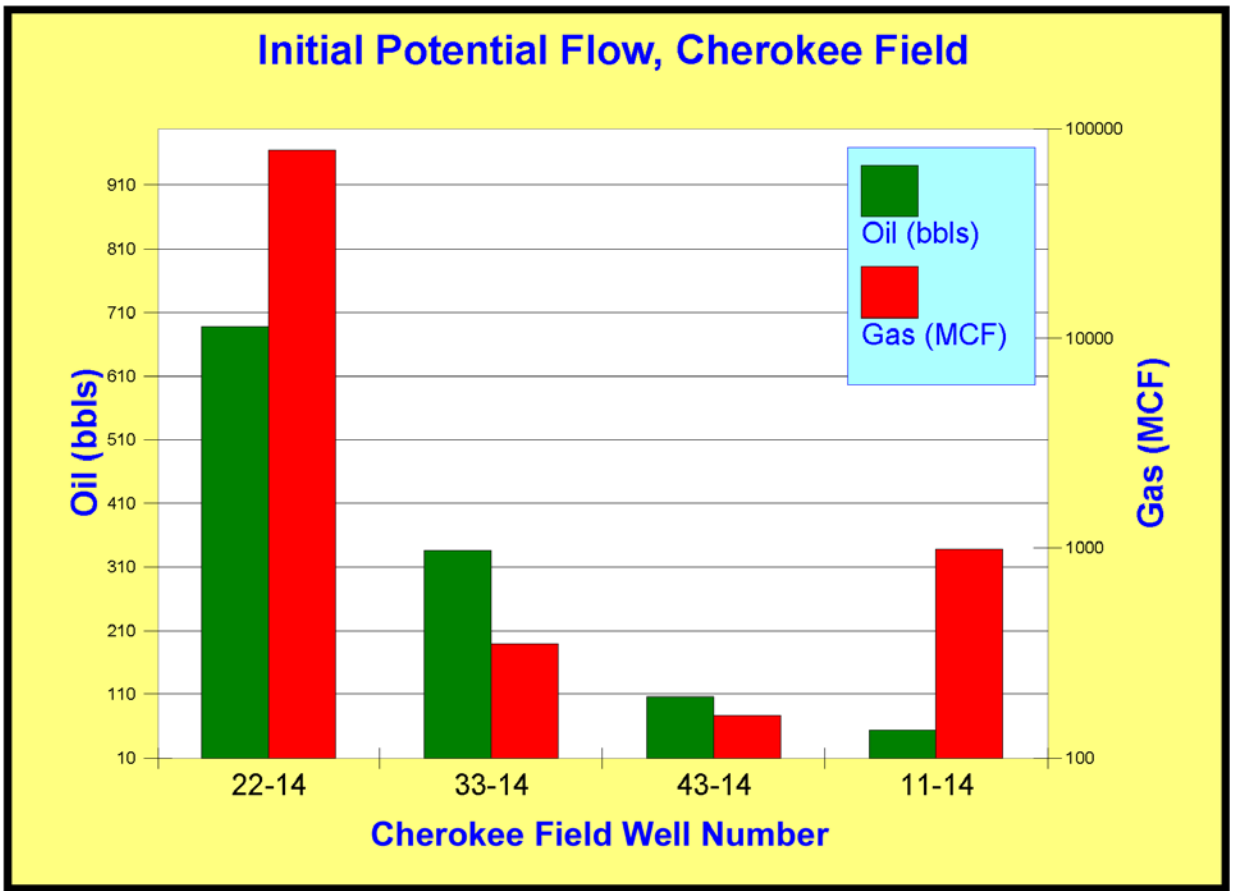

Figure 4. Initial potential flow of oil and gas, from upper Ismay producing wells, in Cherokee field, San Juan County, Utah (data source Utah Division of Oil, Gas and Mining).

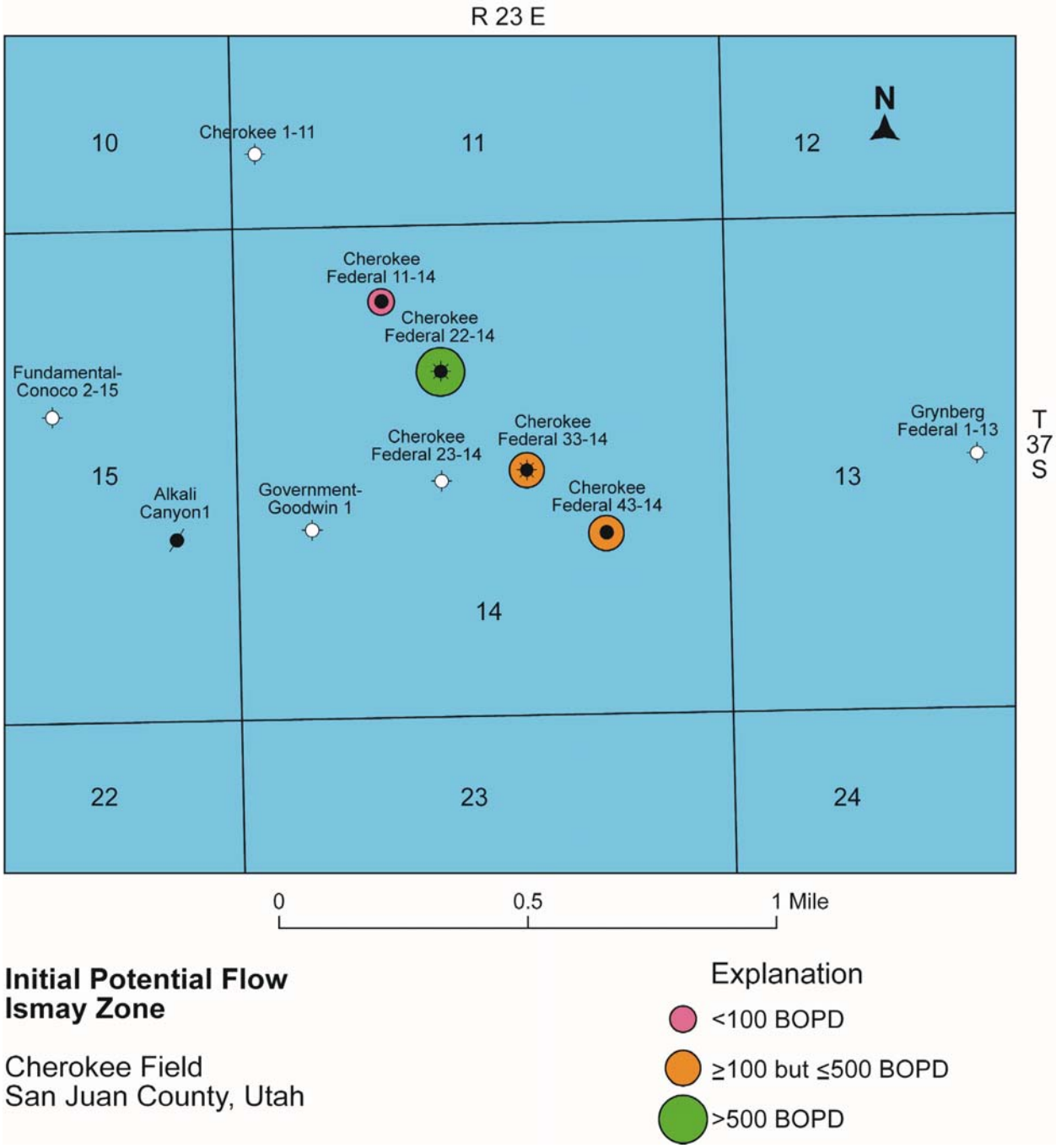

Figure 5. Bubble map of initial potential flow, of oil in BOPD, from upper Ismay producing wells in Cherokee field, San Juan County, Utah (data source Utah Division of Oil, Gas and Mining).

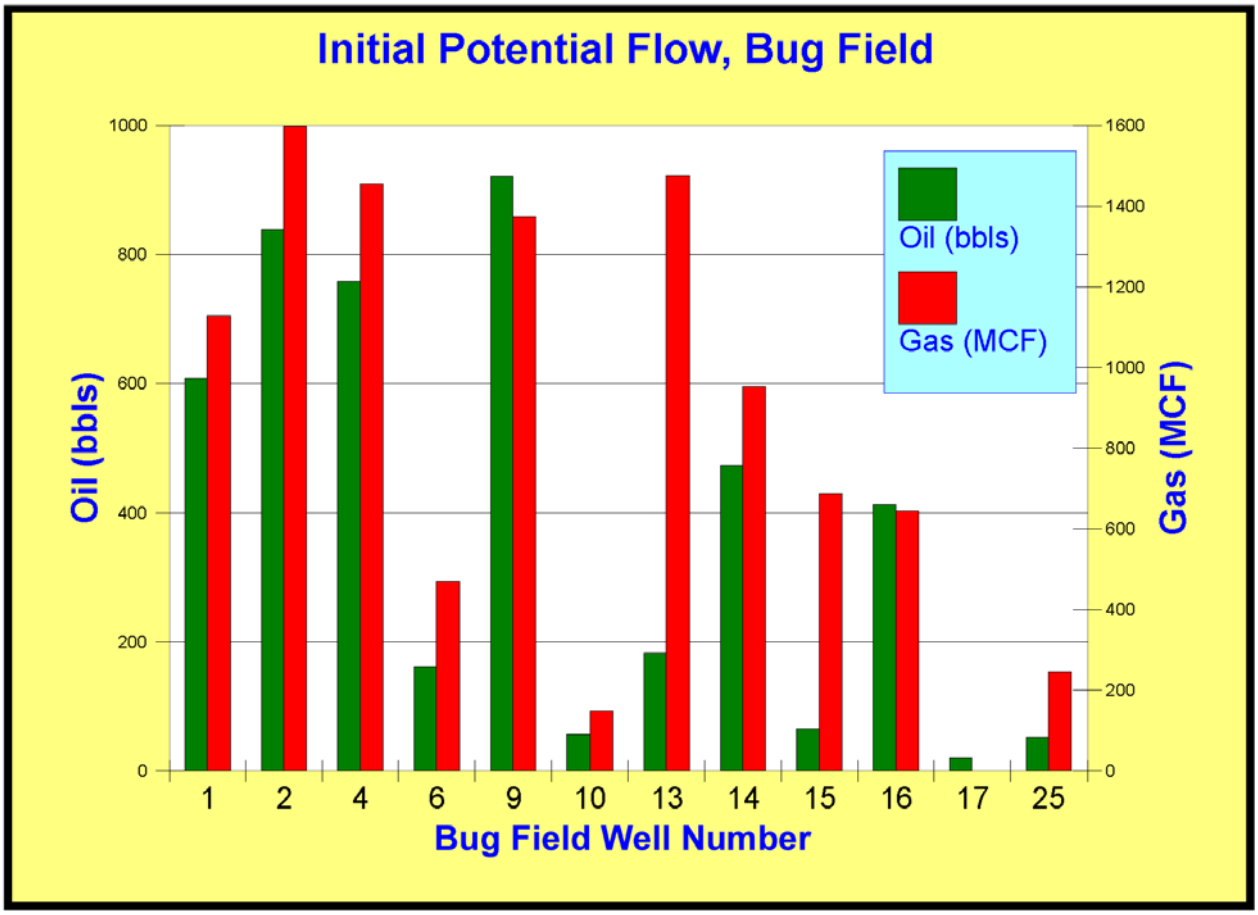

Figure 6. Initial potential flow of oil and gas, from lower Desert Creek producing wells, in Bug field, San Juan County, Utah (data source Utah Division of Oil, Gas and Mining).

In Cherokee field, the highest IPF was recorded from the Cherokee Federal No. 22-14 well (figures 4 and 5), located on the crest of the structural nose where the upper Ismay zone buildup developed and in the thickest part of the mound facies (figures 8 and 9). The lowest recorded IPF was recorded from the Cherokee Federal No. 11-14 well (figures 5 and 6), located on the structural low and on the thin flank of the mound buildup (figures 8 and 9). Both wells had relatively high gas-to-oil ratios (GOR) in comparison to the other two producing field wells (figure 4) in the southeastern part of the field (figure 5).

In Bug field, the highest IPFs were recorded from the Bug No. 1, May Bug No. 2, Bug No. 9, and Bug No. 4 wells (figures 6 and 7), located structurally downdip from the updip porosity pinch out that forms the trap, and in the main part of the lower Desert Creek zone carbonate buildup (figures 10 and 11); Bug No. 9 was tested from the thickest section of the mound. These wells penetrated both the phylloid-algal mound and the shoreline carbonate island facies of the carbonate buildup. The lowest recorded IPFs were from wells closest to the updip porosity pinch out, or downdip near the oil/water contact (figures 6, 7, and 10). These wells penetrated only the phylloid-algal mound facies (figure 11).

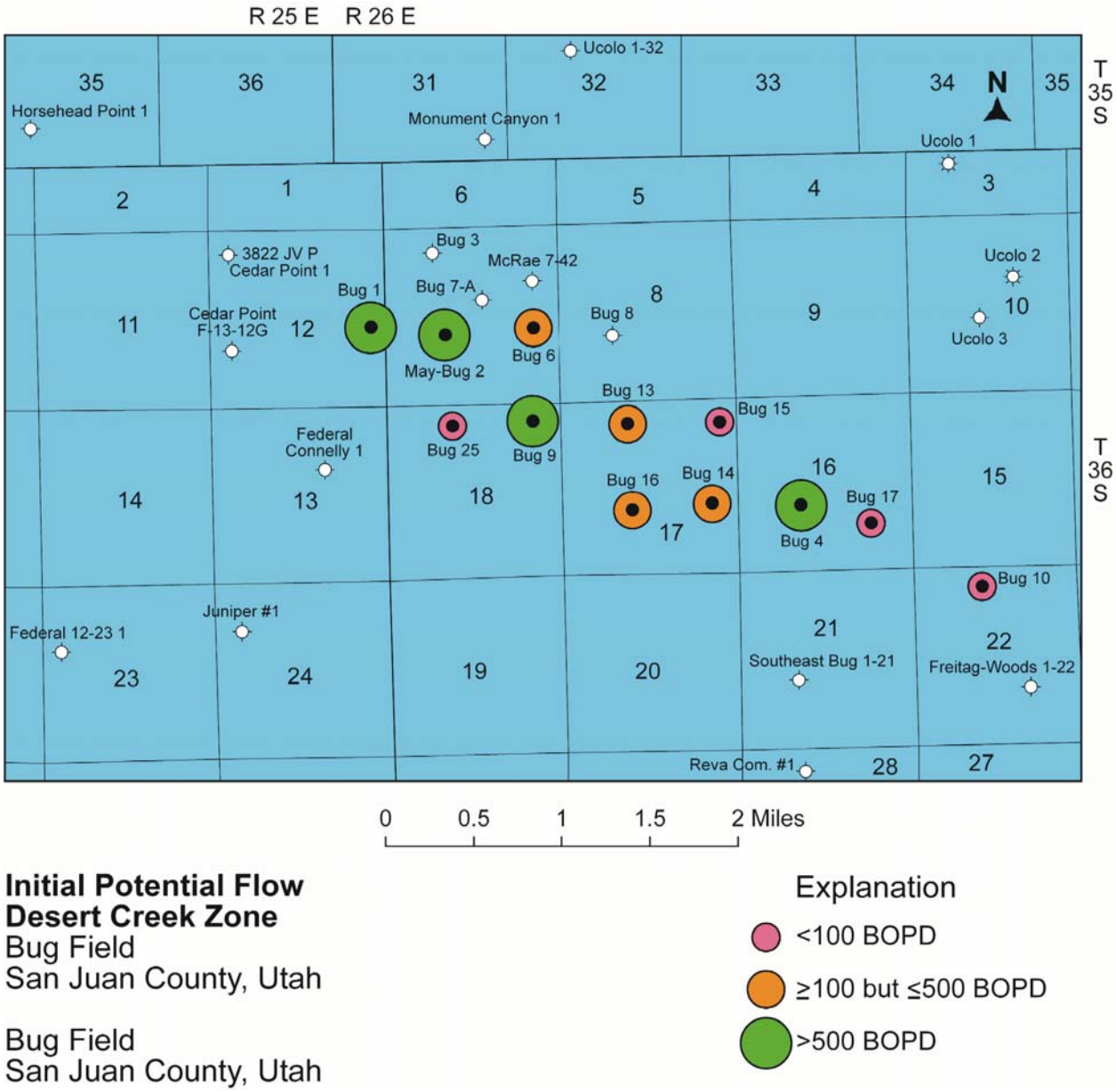

Figure 7. Bubble map of initial potential flow, of oil in BOPD, from lower Desert Creek producing wells in Bug field, San Juan County, Utah (data source Utah Division of Oil, Gas and Mining).

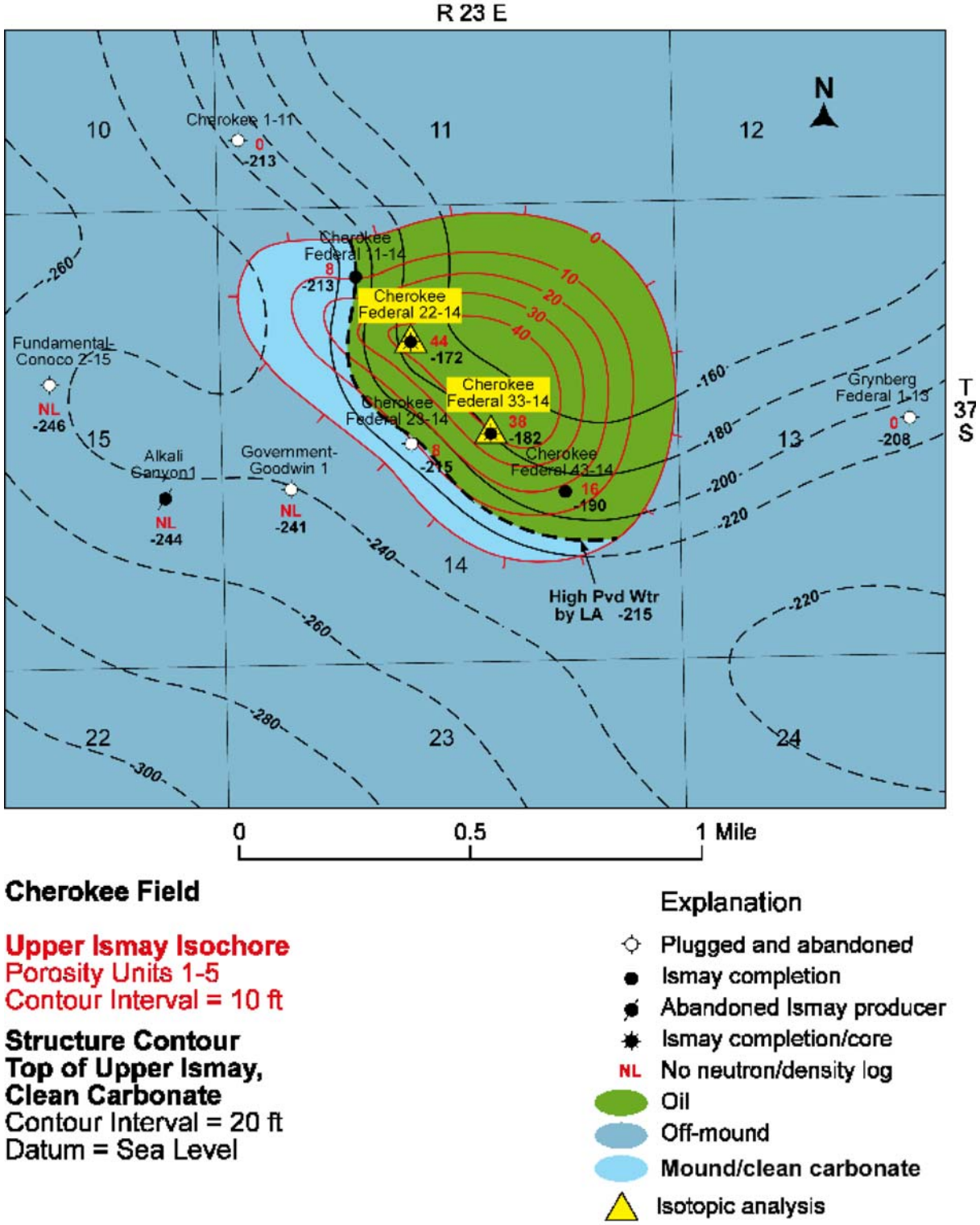

Figure 8. Map of combined top of "clean carbonate" structure and isochore of porosity units 1 through 5, upper Ismay zone, Cherokee field, San Juan County, Utah. Well cores used for isotope sampling for this study are highlighted with a yellow triangle.

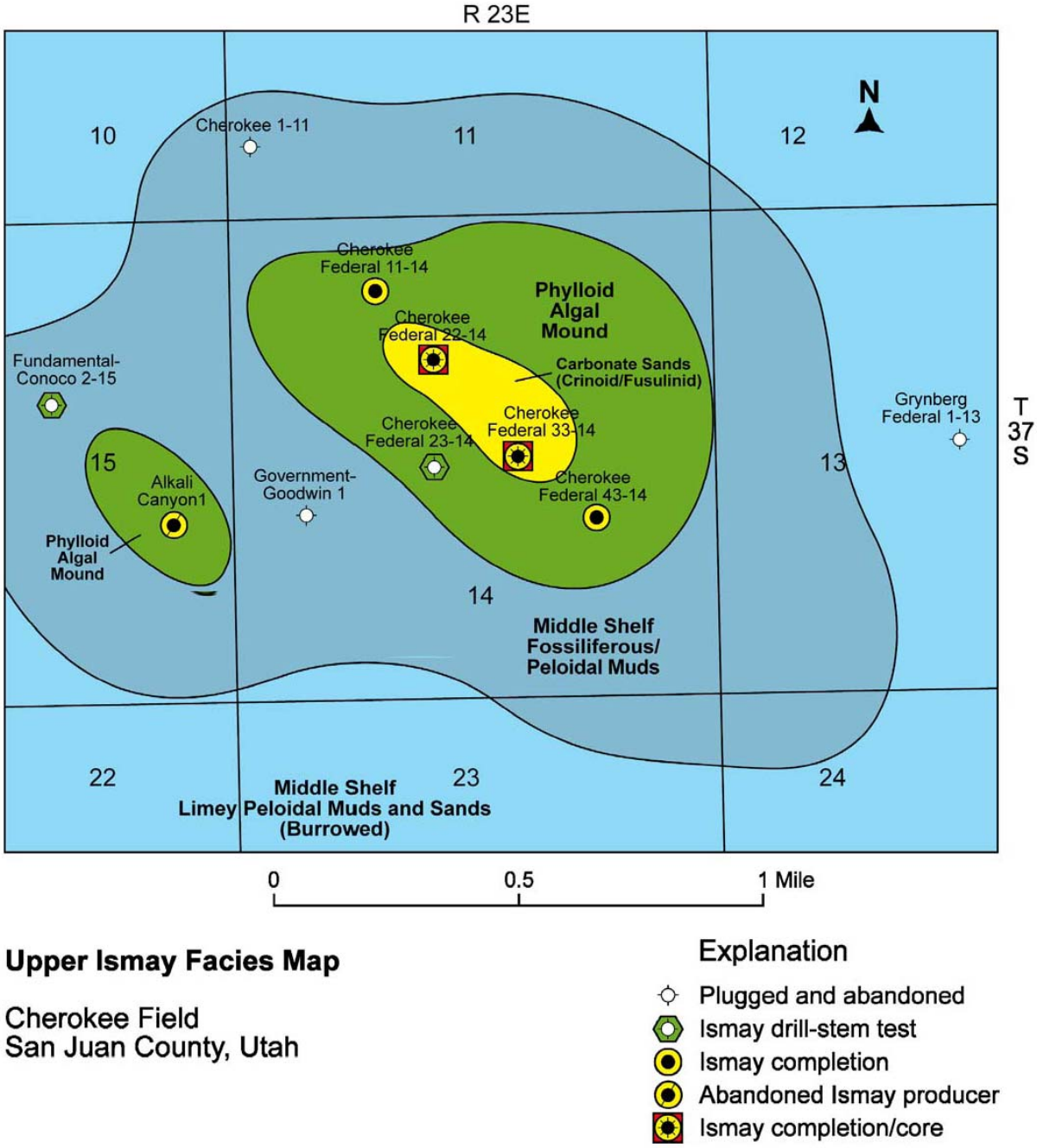

Figure 9. Upper Ismay zone facies map, Cherokee field, San Juan County, Utah.

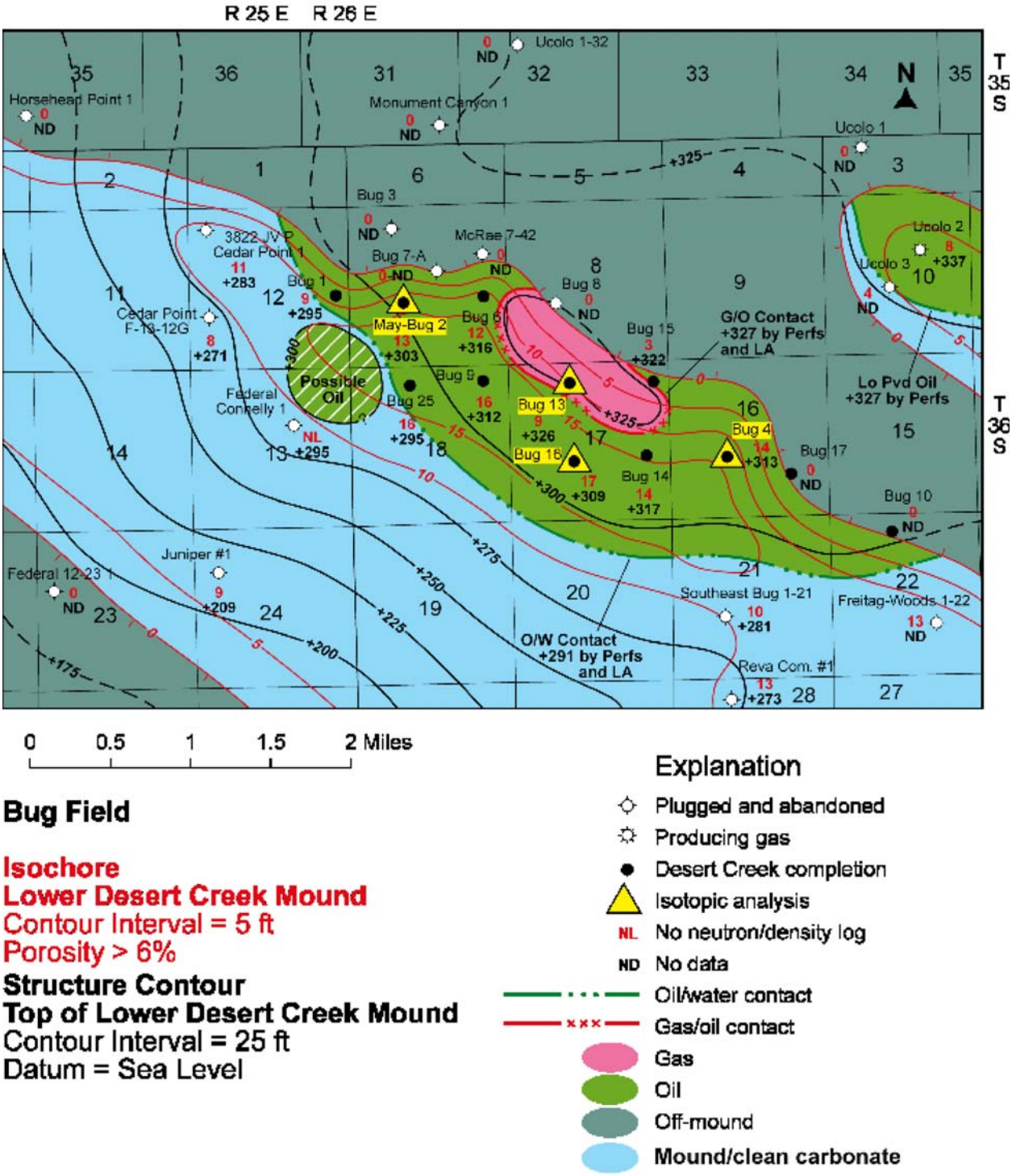

Figure 10. Map of combined top of structure and isochore of lower Desert Creek zone mound, Bug field, San Juan County, Utah. Well cores used for isotope sampling for this study are highlighted with a yellow triangle.

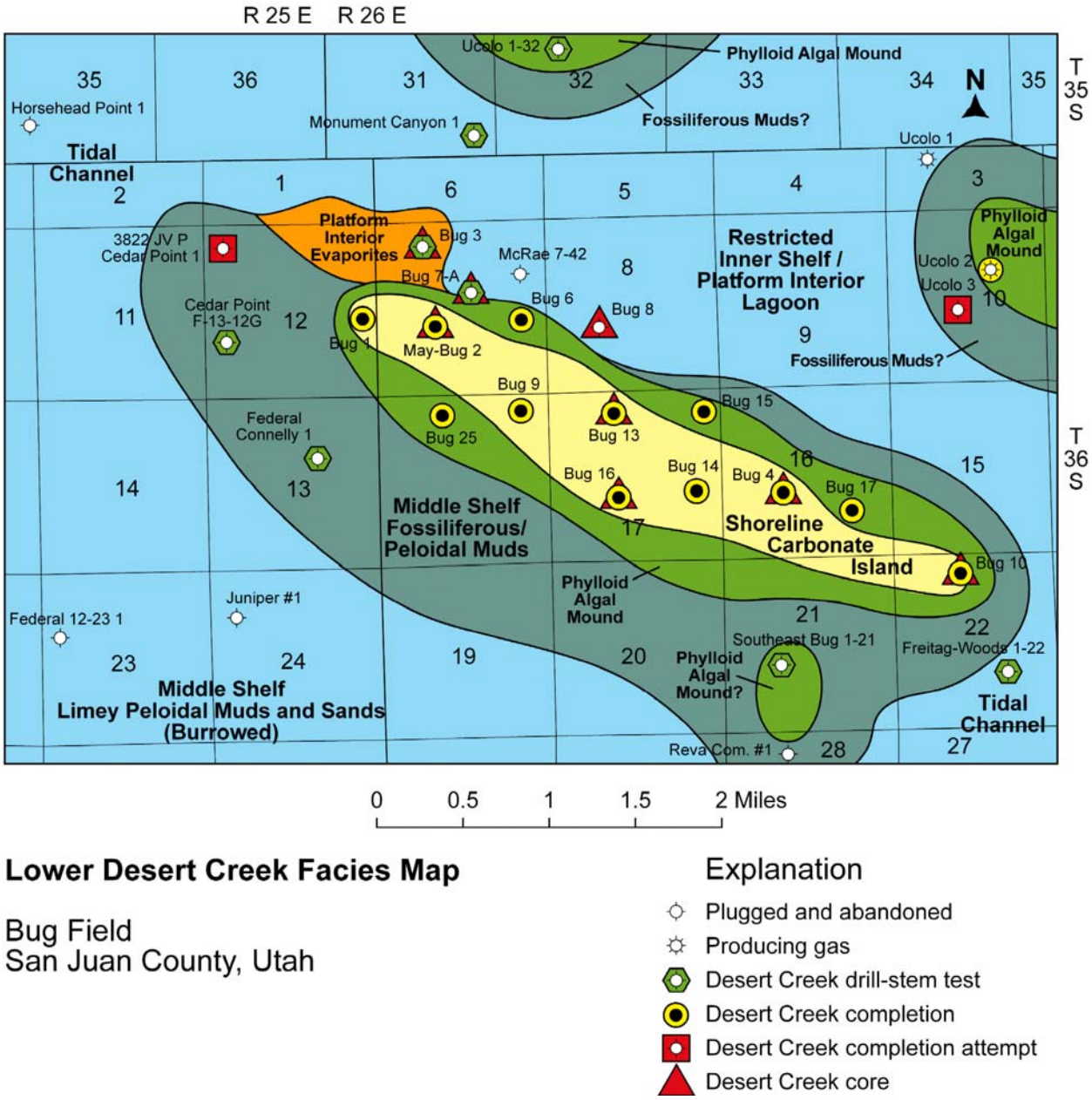

Figure 11. Lower Desert Creek zone facies map, Bug field, San Juan County, Utah.

Cumulative Production

Oil and gas production from Cherokee field has shown a steady decline since peaking in the late 1980s (figure 12). Cumulative production was graphed and plotted for each well (figures 13 through 16). The graphs include both oil and gas production. In Cherokee field, the largest volume of oil has been produced from the Cherokee Federal No. 33-14 well, while the highest volume of gas has been produced from the Cherokee Federal No. 22-14 well (figures 13 and 14). Both wells are located on the crest of the structural nose and in the thickest part of the mound facies (figures 8 and 9). The Cherokee Federal No. 22-14 well is slightly higher structurally than the Cherokee Federal No. 33-14 well, possibly accounting for the significantly greater volume of gas production. These wells penetrated both the phylloid-algal mound and the crinoid/fusulinid-bearing carbonate sand facies of the carbonate buildup (figure 9). The Cherokee Federal No. 33-14 well may have encountered a significantly thicker section of microporosity and microfractures than other wells resulting in greater oil production. Microporosity is present in cores from both the Cherokee Federal No. 33-14 and Cherokee Federal No. 22-14 wells (figure 15). This unique pore type represents the greatest hydrocarbon storage capacity and potential horizontal drilling target in the field. The lowest volumes of hydrocarbon production are from wells on both the structural and mound flanks. These wells are likely close to the oil/water contact (its exact elevation is unknown) and have penetrated only the phylloid-algal mound buildup.

In Bug field, oil and gas production peaked in 1982, and has shown a steady decline in oil and gas since 1985 and 1989 respectively (figure 16). The largest volumes of oil have been produced from the May Bug No. 2 and Bug No. 14 wells (figures 17 and 18). These wells, plus the Bug No. 4 and Bug No. 9 wells, have each produced over 200,000 barrels of oil. They are all located structurally downdip from the updip porosity pinch out, and in the main part of the lower Desert Creek zone carbonate buildup (figures 10 and 11). These wells penetrated both the phylloid-algal mound and the shoreline carbonate island facies. However, there are other wells that penetrated this same facies combination, such as Bug No.16 well, yet have produced lower volumes of oil. These wells may have encountered fewer microfractures and less micro-box-work porosity (figure 19), a prime diagenetic pore type in this dolomitized reservoir, which is thought to account for the greatest hydrocarbon storage and flow capacity in the field. The lowest volumes of hydrocarbon production are from wells closest to the updip porosity pinch out (Bug No. 15 and No. Bug 17) or downdip near the oil/water contact (Bug No. 25) (figures 10, 17, and 18). These wells penetrated only the phylloid-algal mound facies (figure 11). The Bug No. 13 and Bug No. 15 wells are the structurally highest wells in the field and are located near a presumed gas cap, thus their production history shows high GORs.

ISOTOPIC GEOCHEMISTRY – RESULTS AND DISCUSSION

Modification of rock fabrics and porosity within the lower Desert Creek and upper Ismay zones of the Blanding sub-basin study area is quite complex. Diagenesis played a major role in the development of reservoir heterogeneity in Bug, Cherokee, and Patterson Canyon fields as well as throughout the Paradox Formation fields. Diagenetic processes started during deposition and continued throughout burial history (figure 20).

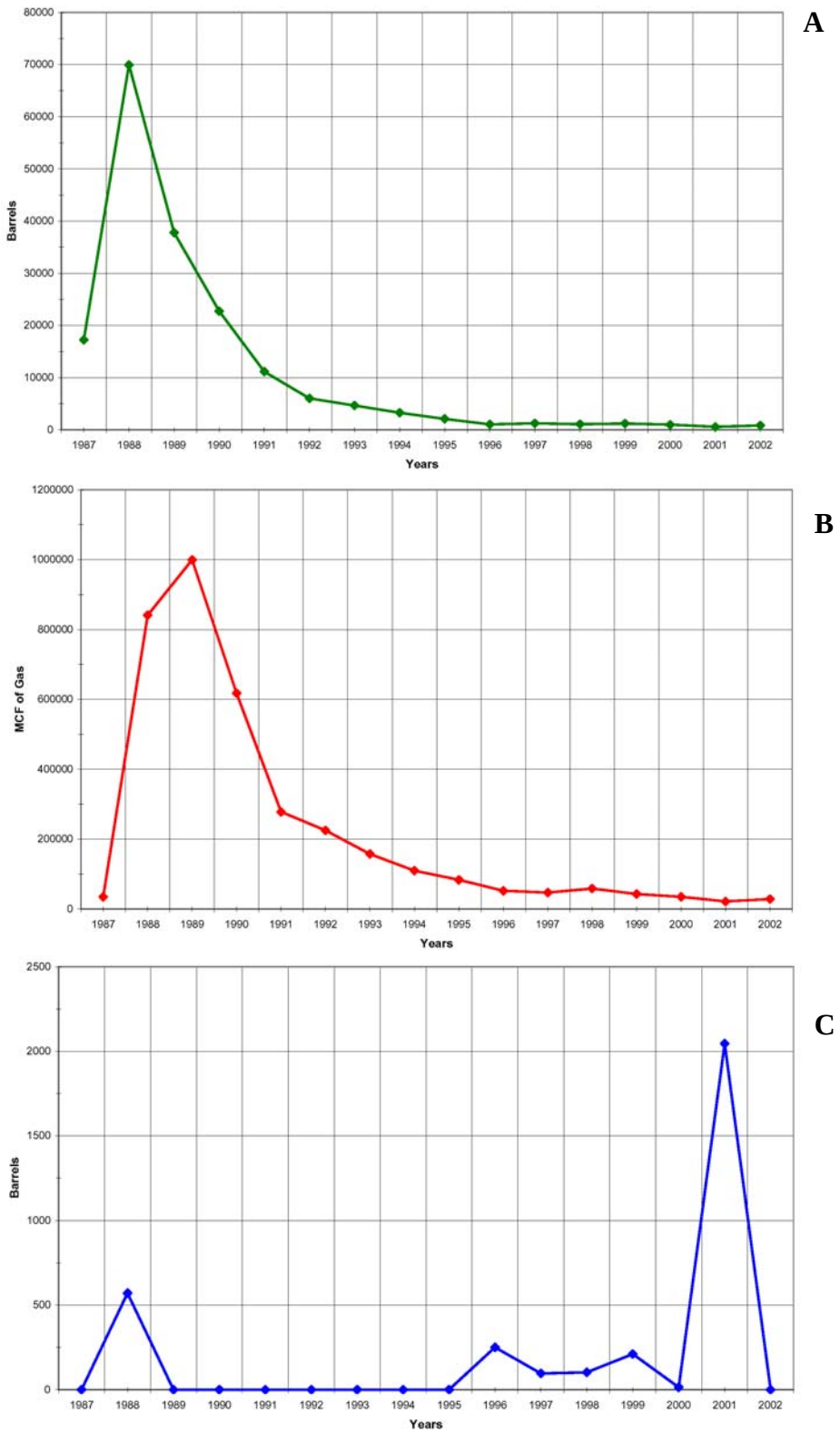

Figure 12. Historical oil (A), gas (B), and water (C) production for Cherokee field (data source Utah Division of Oil, Gas and Mining).

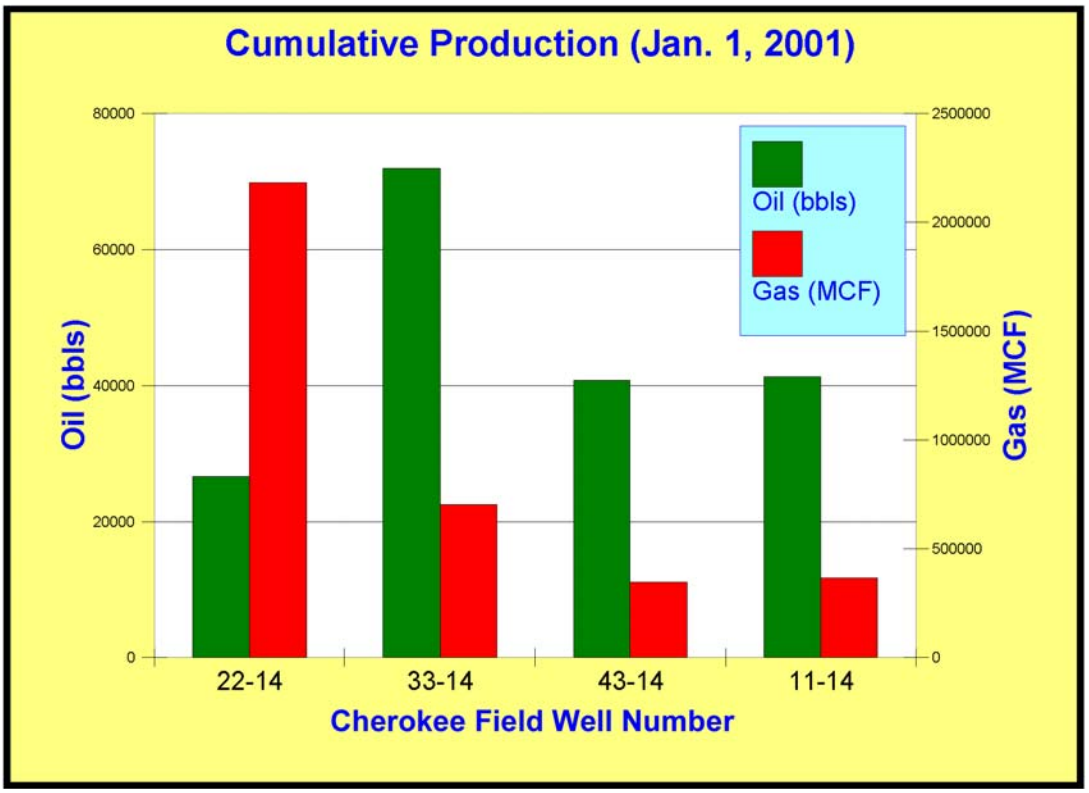

Figure 13. Cumulative production of oil and gas, from upper Ismay producing wells, in Cherokee field, San Juan County, Utah (data source Utah Division of Oil, Gas and Mining).

Stable isotope geochemistry has been used in recent years to provide insights into the chemical differences between preserved remnants of depositional components from various diagenetic events in carbonate rocks as recognized from core examination and thin section petrography. Figure 21 shows a graph of carbon versus oxygen isotope compositions for a range of carbonate rock types from various published sources as compiled by Roylance (1990). Broad fields of carbon and oxygen isotope compositions for various carbonate rock settings are indicated, including modern marine ("subsea") cements, various marine skeletons and sediments, deep-water ("pelagic") limestones, Pleistocene carbonates, and meteoric carbonates ("speleothems and veins").

Previous Work

The only previously published isotope composition data for lower Desert Creek rocks for the project area was completed at the Marathon Petroleum Technology Lab in Littleton, Colorado for the M.S. thesis work of Roylance (1984). That data and the location of the wells sampled can be seen in tables 1 and 2, and figures 10 and 22. Brinton (1986) collected and interpreted a robust data set of carbon and oxygen isotopes (84 samples) from four cores in Ismay field, Utah and Colorado, which is outside the project area. Comments about the general isotopic ranges of various diagenetic rock components within the Ismay zone in cores from Ismay and Greater Aneth fields (outside of the Blanding sub-basin project area) have been published by Dawson (1988).

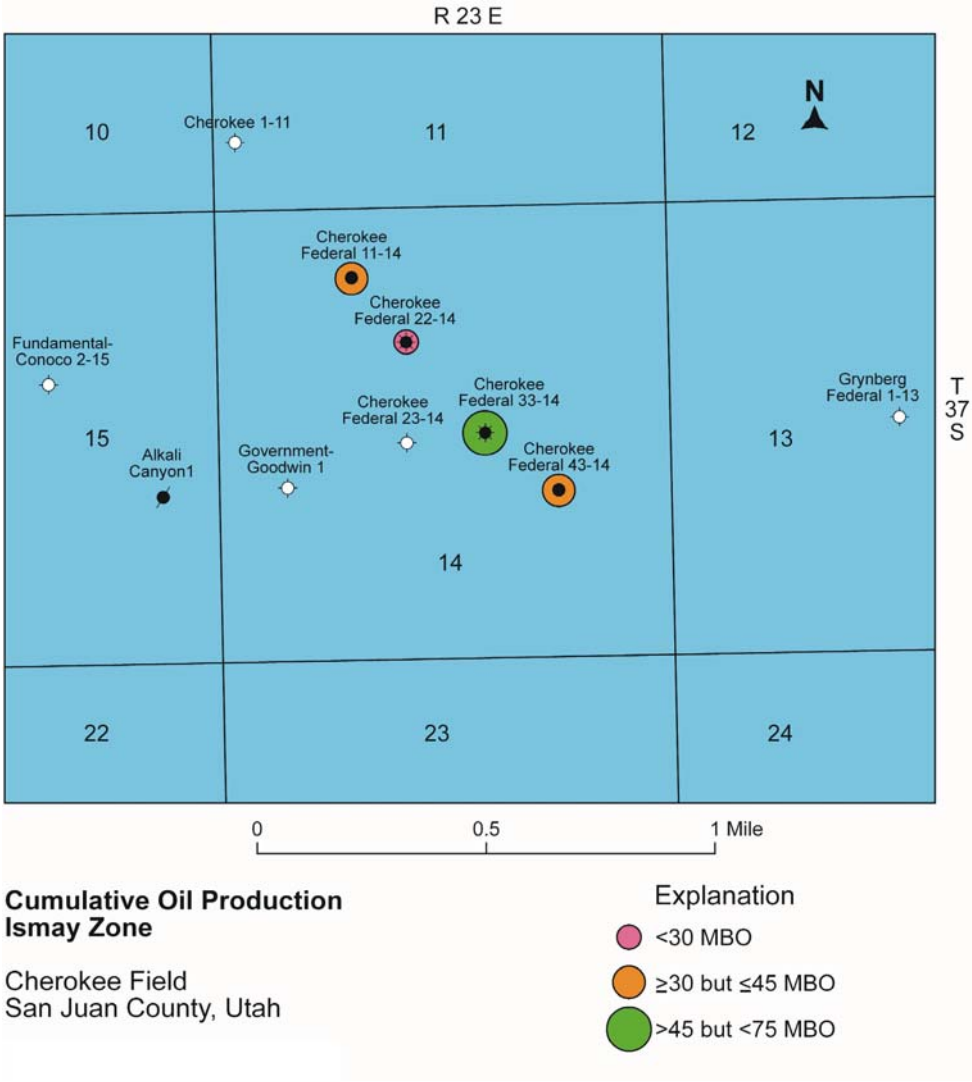

Figure 14. Bubble map of cumulative production, of oil in thousands of barrels of (MBO), from upper Ismay producing wells in Cherokee field, San Juan County, Utah (data source Utah Division of Oil, Gas and Mining).

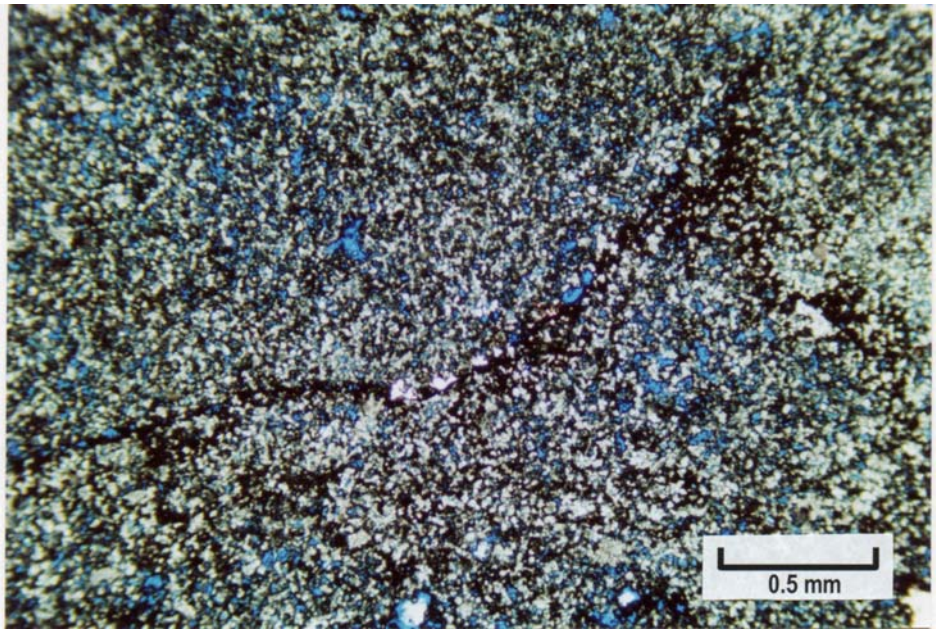

Figure 15. Photomicrograph (plane light) of a peloidal packstone/ grainstone dominated by microporosity (in blue). Cherokee No. 22-14, 5,768.7 feet (1,758.2 m), porosity = 22.9 percent, permeability = 215 millidarcies.

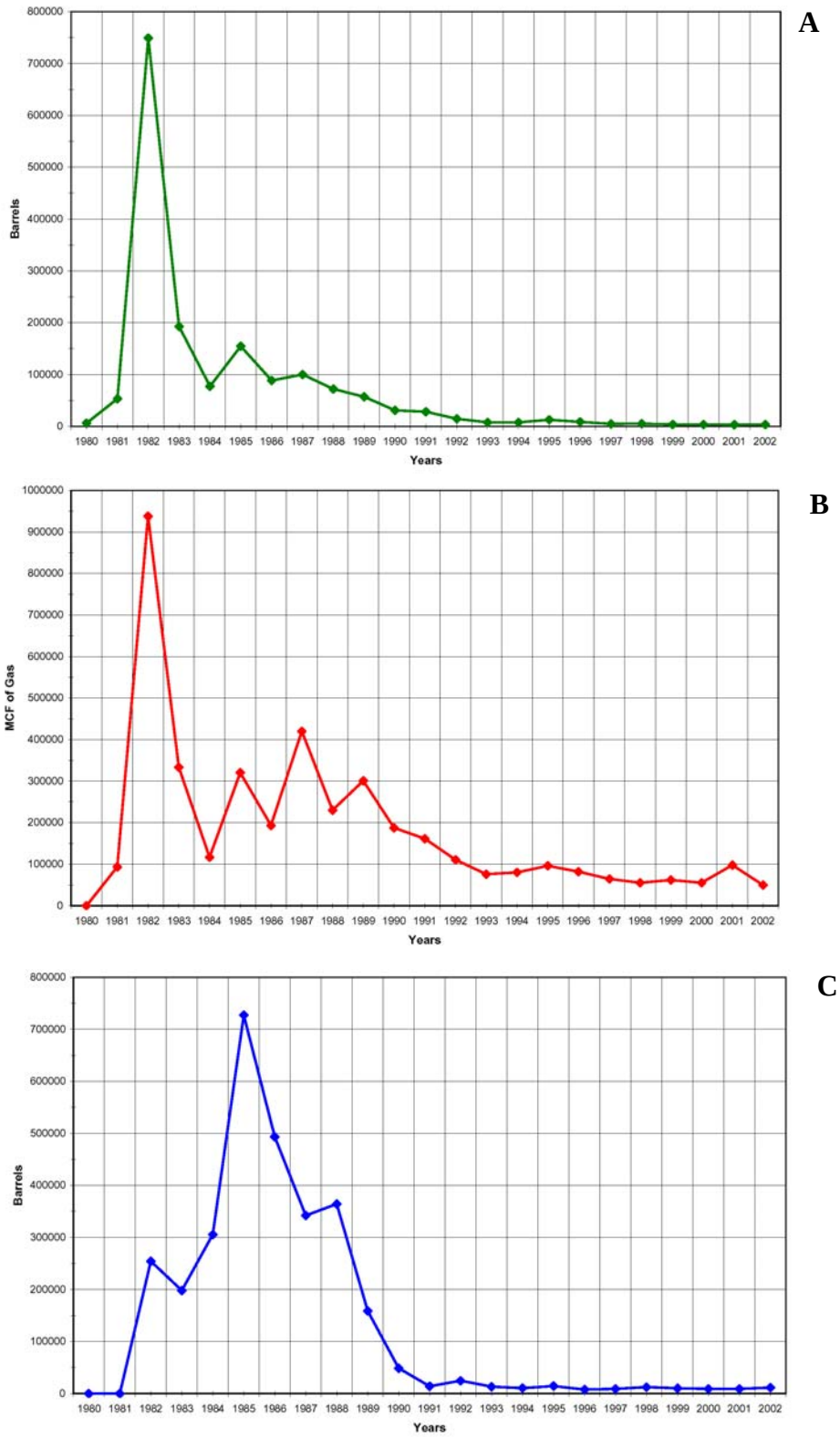

Figure 16. Historical oil (A), gas (B), and water (C) production for Bug field (data source Utah Division of Oil, Gas and Mining).

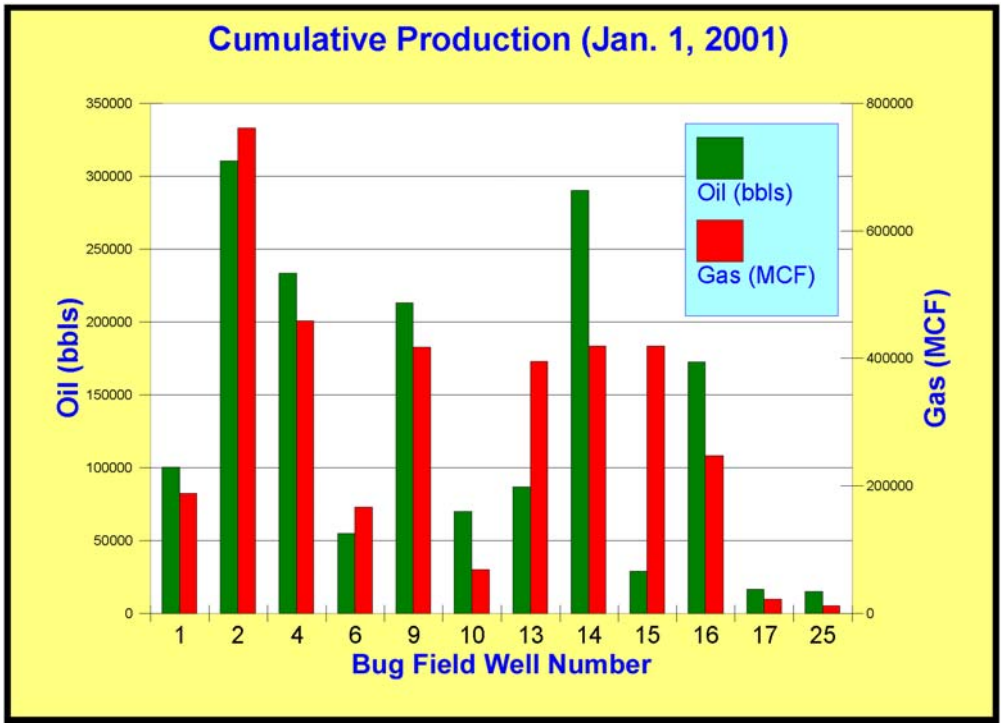

Figure 17. Cumulative production of oil and gas, from lower Desert Creek producing wells, in Bug field, San Juan County, Utah (data source Utah Division of Oil, Gas and Mining).

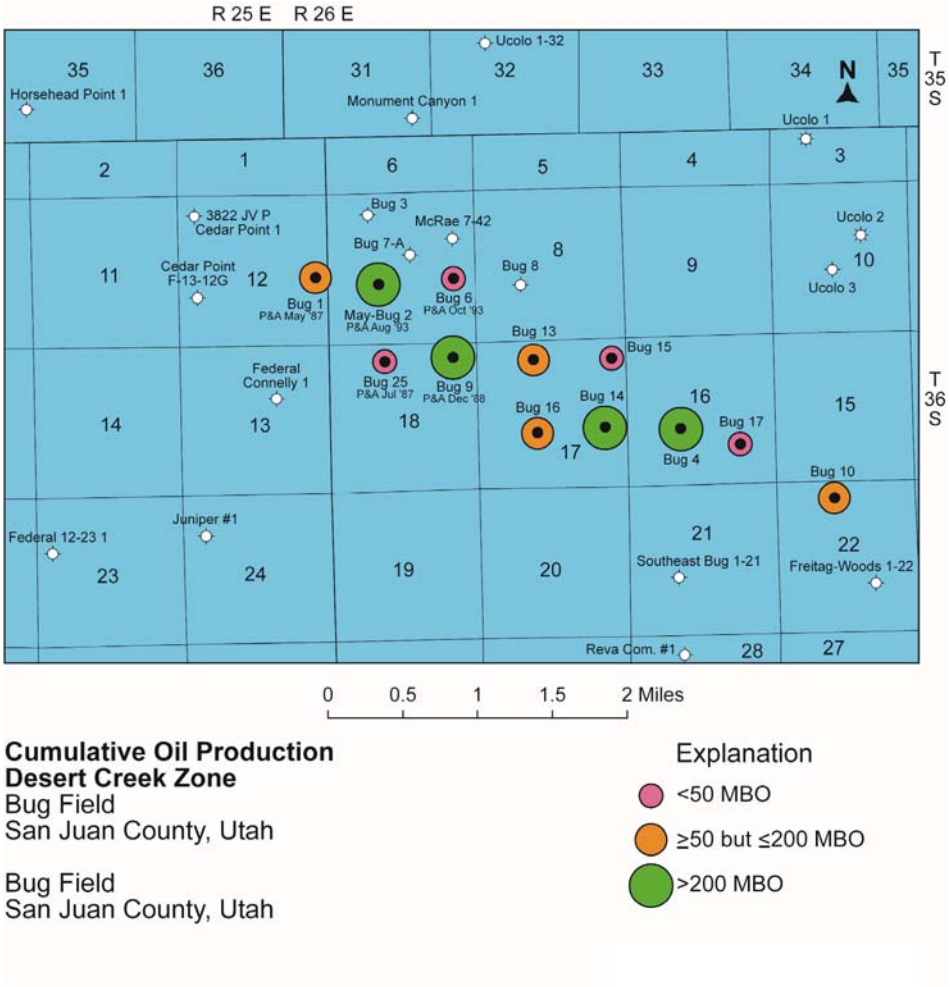

Figure 18. Bubble map of cumulative production, of oil in thousands of barrels of (MBO), from lower Desert Creek producing wells in Bug field, San Juan County, Utah (data source Utah Division of Oil, Gas and Mining).

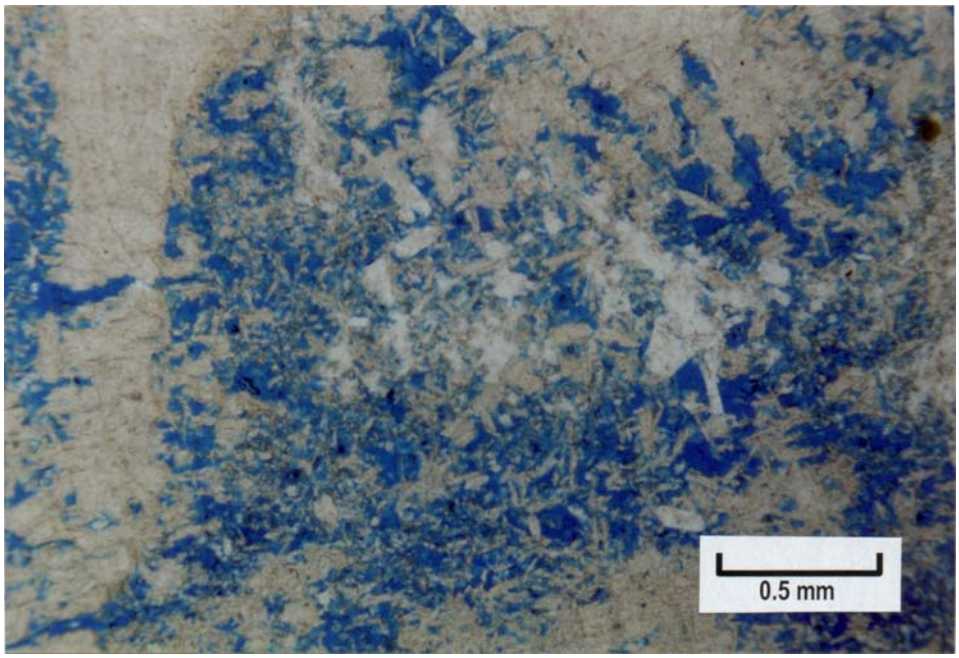

Figure 19. Photomicrograph (plane light with white card technique [diffused light using a piece of paper on the stage of the microscope]) showing a pattern of patchy dolomite dissolution which includes a "micro-box-work" pattern of pores (in blue). Bug No. 10, 6,327.5 feet (1,928.5 m), porosity = 10.5 percent, permeability = 7.5 millidarcies.

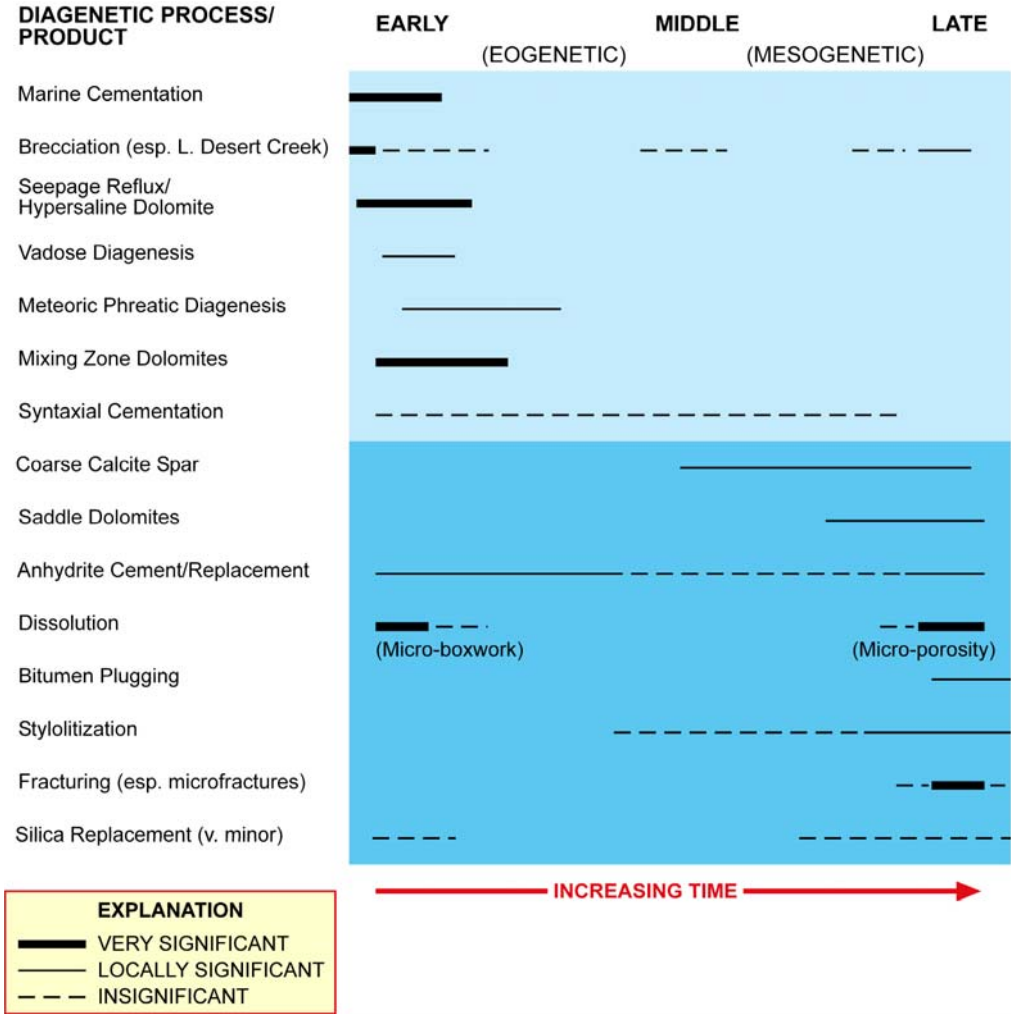

Figure 20. Diagenetic sequence diagram for Bug and Cherokee fields.

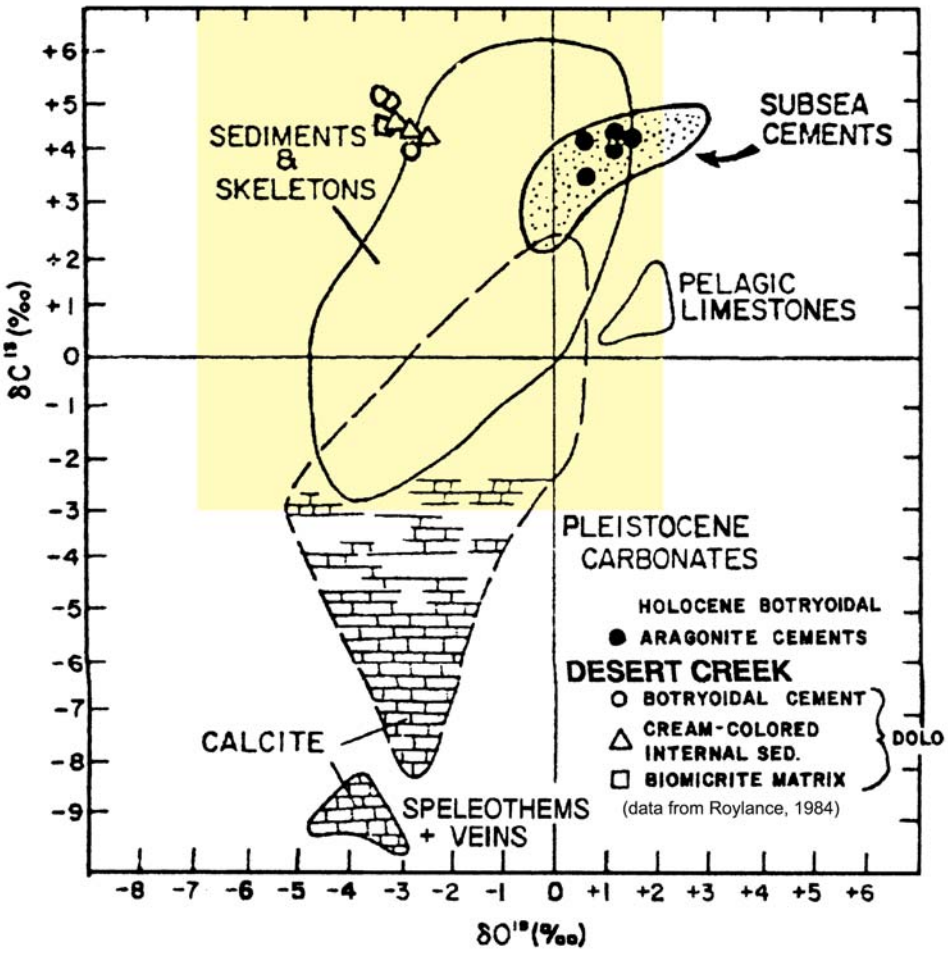

Figure 21. Graph of carbon versus oxygen isotope compositions. Other compositional facies compiled from various published work (modified from James and Ginsburg, 1979 by Roylance, 1990). The yellow area in this cross plot is the same part of the graph shown in figures 22, 24, 25, 26, 28, and 30 of this study.

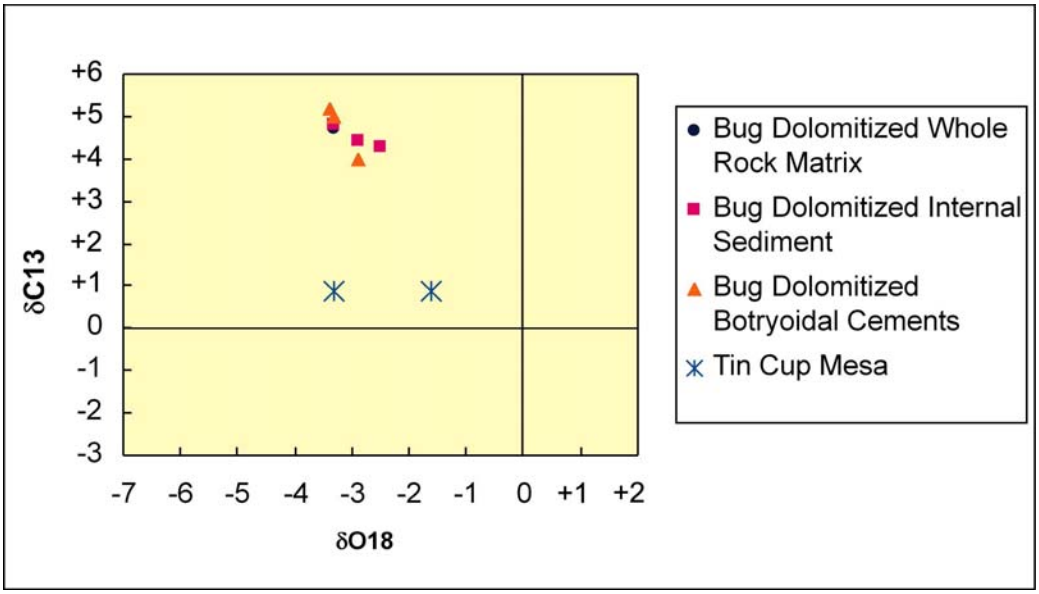

Figure 22. Graph of carbon versus oxygen compositions for Bug and Tin Cup Mesa fields determined by Roylance, 1984.

Table 1. Location of cores used in the isotope geochemistry study.

Zones	Well Name	Location
Lower Desert Creek	*Wexpro May-Bug 2 (this study)	NE1/4 SW1/4 Sec. 7, T36S, R26E UT
	*Wexpro Bug 4 (this study)	NE1/4 SW1/4 Sec. 16, T36S, R26E UT
	*Wexpro Bug 13 (Roylance, 1984)	NE1/4 NW1/4 Sec. 17, T36S, R26E UT
	*Wexpro Bug 16 (Roylance, 1984)	NE1/4 SW1/4 Sec. 17, T36S, R26E UT
	MOC Tin Cup Mesa 1-25	SW1/4 NW1/4 Sec. 25, T38S, R25E UT
Upper Ismay	†Cherokee 22-14 (this study)	SE1/4 NW1/4 Sec. 14, T38S, R23E UT
	†Cherokee 33-14 (this study)	NE1/4 NW1/4 Sec. 14, T38S, R23E UT
	Samedan Bonito 41-6-85 (this study)	NE 1/4 NE1/4 Sec. 6, T38S, R25E UT

*Well locations are shown in figure 8
†Well locations are shown in figure 10

Table 2. Previous stable carbon and oxygen isotope data from lower Desert Creek zone, Bug and Tin Cup Mesa fields (analyses from Roylance, 1984).

Sample Groups:	del 13C	del 18O
BUG FIELD - Lower Desert Creek Cores Dolomitized Whole Rock Matrix (biomicrite in algal bafflestone)		
Bug 13: 5940.7'C	+4.7	-3.3
Dolomitized Internal Sediment (within phylloid-algal bafflestone)		
Bug 13: 5939.3'A	+4.4	-2.9
Bug 13: 5940.7'A	+4.3	-2.5
Bug 16: 6313.4'A	+4.8	-3.3
Dolomitized Botryoidal Cements		
Bug 13: 5939.3'B	+5.0	-3.3
Bug 13: 5940.7'B	+4.0	-2.9
Bug 16: 6313.4'B	+5.2	-3.4
TIN CUP MESA FIELD - Lower Desert Creek Cores Limestone Whole Rock Matrix (calcite fraction [micrite and crinoid, bryozoan and brachiopod fragments] of dolomitized bioclastic wackestone)		
Tin Cup Mesa #1-25: 5667' calcite	+0.9	-3.3
Dolomite Fraction of Whole Rock Matrix (dolomitized micrite matrix of bioclastic wackestone)		
Tin Cup Mesa #1-25: 5667' dolomite	+0.9	-1.6

Methodology

Isotopic composition analyses for carbon and oxygen were completed for a variety of whole rock and diagenetic phases for core samples from the lower Desert Creek zone from Bug field and the upper Ismay zone from Cherokee field (tables 1, 3, and 4). In addition, a series of samples from whole rock, dolomite, and various cement generations were selected from an upper Ismay buildup in a recently drilled well at Patterson Canyon field (the Samedan Bonito No. 41-6-85, completed in July 2002) containing well-cemented oolitic beds and phylloid-algal mound fabrics (table 5). Figure 1 shows the location of the fields or well names sampled for isotope geochemistry. Individual samples were collected as powdered rock using a Dremel drill equipped with precision bits. All analyses were completed at the Brigham Young University (BYU) Department of Geology Stable Isotope Laboratory, Provo, Utah. The internal standard used in the BYU lab is the UCLA Carrara marble. The accepted values for this internal standard were matched consistently during the analysis of the Paradox core samples selected for this study. All isotopic compositions are reported relative to PeeDee Belemnite (PDB) (see Land, 1980, figure 6 for definition relative to SMOW).

Table 3. New stable carbon and oxygen isotope data from lower Desert Creek zone Bug field dolomites.

Sample Groups:	del 13C	del 18O
BUG FIELD - Lower Desert Creek Cores		
Whole Rock Dolomite		
May Bug 2: 6304'A (phylloid-algal mound & marine sediment)	+4.49	-4.72
May Bug 2: 6315' B (phylloid-algal mound fabric)	+4.03	-4.42
Dolomitized Internal Sediment (cream-colored)		
May Bug 2: 6304'B	+4.30	-4.50
May Bug 2: 6315'A	+4.16	-4.15
May Bug 4: 6297.4'B	+4.52	-4.67
Dolomitized Micro-Boxwork Fabric (probably botryoidal cements)		
May Bug 2: 6304'C	+4.40	-4.56
May Bug 4: 6289.7'	+4.77	-4.58
May Bug 4: 6297.4'A	+4.76	-4.46

Carbon and Oxygen Isotopes from Lower Desert Creek Dolomites

Isotopic composition analyses for carbon and oxygen were completed for a variety of whole rock and diagenetic phases for core samples from the lower Desert Creek dolomite interval from Bug field (table 1, figure 10). Values obtained in this project were compared to stable carbon and oxygen isotopic measurements reported by Roylance (1984, 1990), and included in this report in figure 22 and table 2. A total of eight powdered samples were drilled from core samples from two Bug field wells and analyzed (table 3). The samples were selected

Table 4. New stable carbon and oxygen isotope data from upper Ismay zone Cherokee field.

Sample Groups:	del 13C	del 18O
CHEROKEE FIELD - Upper Ismay Cores		
Whole Rock		
Cherokee 22-14: 5827.7' (mostly dolomite, w/ moldic porosity)	+5.41	-2.90
Cherokee 22-14: 5836.8' (limestone; phylloid-algal mound fabric)	+5.02	-4.55
Cherokee 33-14: 5781.2'A (mostly dolomite)	+4.67	-6.08
Micro-Porous Dolomite Zones (often w/ pyrobitumen)		
Cherokee 22-14: 5768.7'	+3.57	-2.92
Cherokee 33-14: 5781.2'B	+4.85	-4.54

Table 5. New stable carbon and oxygen isotope data from upper Ismay buildup zone Samedan Bonito No. 41-6-85 core.

Sample Groups:	del 13C	del 18O
Whole Rock (dolomitized oolite)		
Bonito 41-6-85: 5544'A	+4.53	-5.10
Dolomitized Cements (in oolite)		
Bonito 41-6-85: 5544'B	+4.51	-5.15
Calcite Cements (within phylloid-algal buildup)		
Bonito 41-6-85: 5592'A (black cement)	+6.30	-5.10
Bonito 41-6-85: 5592'B (gray cement)	+5.67	-5.68
Bonito 41-6-85: 5592'C (brown cement ? w/sediment?)	+5.56	-5.87
Bonito 41-6-85: 5592'D (white cap cement; no sediment)	+5.73	-5.05
Bonito 41-6-85: 5592'E (coarse blocky cement)	+5.69	-6.41

to analyze dolomitized phylloid-algal mound fabrics and breccias, cream-colored dolomitized internal sediments, and dolomitized void-filling cements (mostly botryoids and blunt-ended fibrous fans). Annotated close-up core photos (figure 23) show the approximate locations of the drilled and powdered samples from the May Bug No. 2 and Bug No. 4 wells. A plot of carbon versus oxygen compositions for all Bug field samples obtained in this study is shown on figure 24 (see also table 3). Comparison of the new data with previously reported Bug field isotope compositions (Roylance, 1984, 1990) is shown in figure 25.

Carbon isotopic compositions for the eight Bug field dolomite samples (figure 24) all cluster very close around a mean value of +4.43‰ PDB (range of +4.03 to +4.77‰). Interestingly, the range for del ^{13}C values is slightly higher for the Bug 4 well (+4.03 to +4.77‰) for the May Bug No. 2 well (+4.52 to +4.77‰), although their means (+4.28 versus 4.68‰) may not be significantly different. The carbon isotope values for Bug field dolomites are remarkably similar for all the rock components analyzed, including "whole rock" samples from the phylloid-algal mound fabrics and associated marine sediments, internal sediments

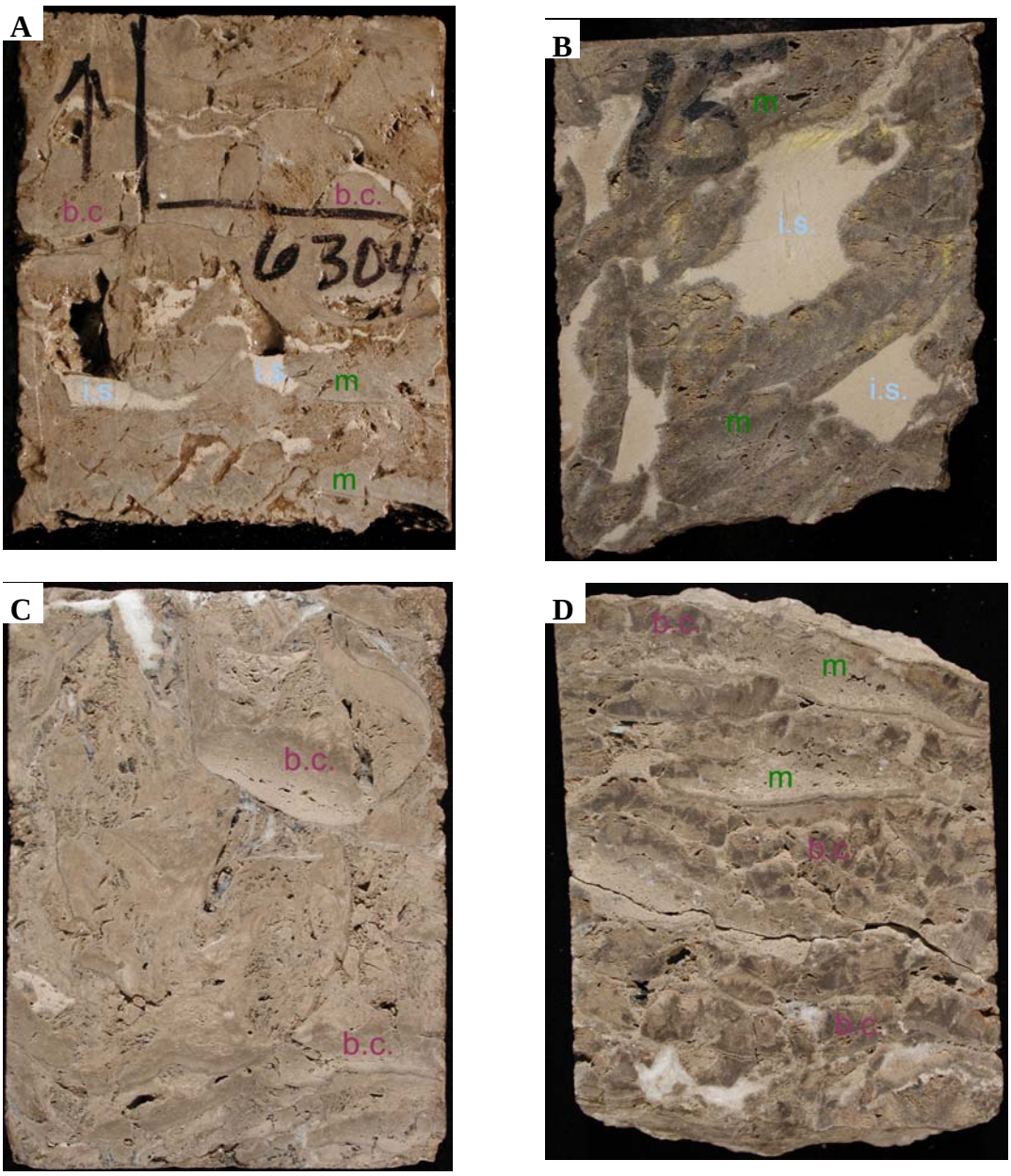

Figure 23. Core photos of typical Bug field components sampled for stable carbon and oxygen isotope analysis. (A) May Bug No. 2: 6,304 feet - the "whole rock" dolomitized phylloid-algal mound fabric (m; sample 6,304' A) in medium gray, the dolomitized cream-colored internal sediment (i.s.; sample 6,304' B), and dark gray dolomitized botryoidal cements (b.c.; sample 6,304' C) as well as associated micro-box-work fabric were sampled for isotopic analysis. (B) May Bug No. 2: 6,315 feet - both the "whole rock" dolomitized phylloid-algal mound fabric (m; sample 6,315' B) in dark gray and the dolomitized cream-colored internal sediment (i.s.; sample 6,315' A) were sampled for isotopic analysis. (C) Bug No. 4: 6,289.7 feet - dolomitized, dark gray botryoidal cements (b.c.; sample 6,289.7') displaying micro-box-work fabric were sampled for isotopic analysis. (D) Bug No. 4: 6,297.5 feet - "whole rock" dolomitized phylloid-algal mound fabric (m; sample 6,297.5' B) and dark gray dolomitized botryoidal cements (b.c.; sample 6,297.5' A) as well as associated micro-box-work fabric were sampled for isotopic analysis.

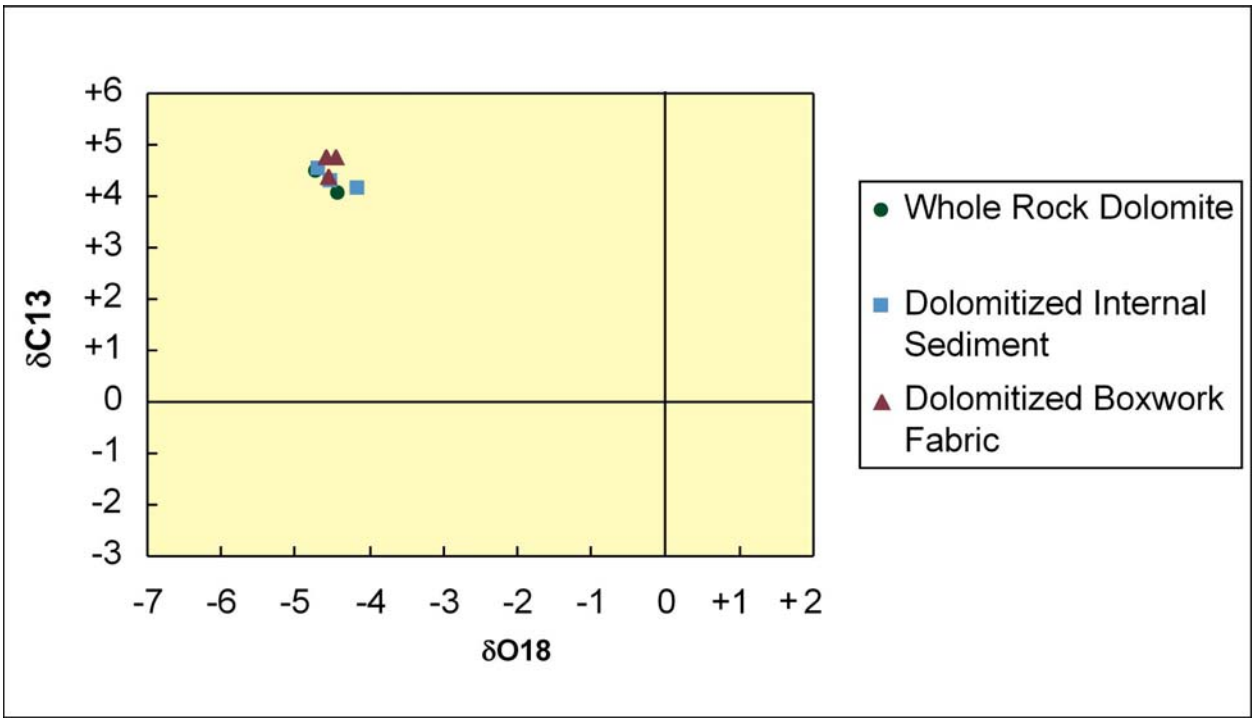

Figure 24. Graph of carbon versus oxygen compositions for Bug field dolomites completed for this study.

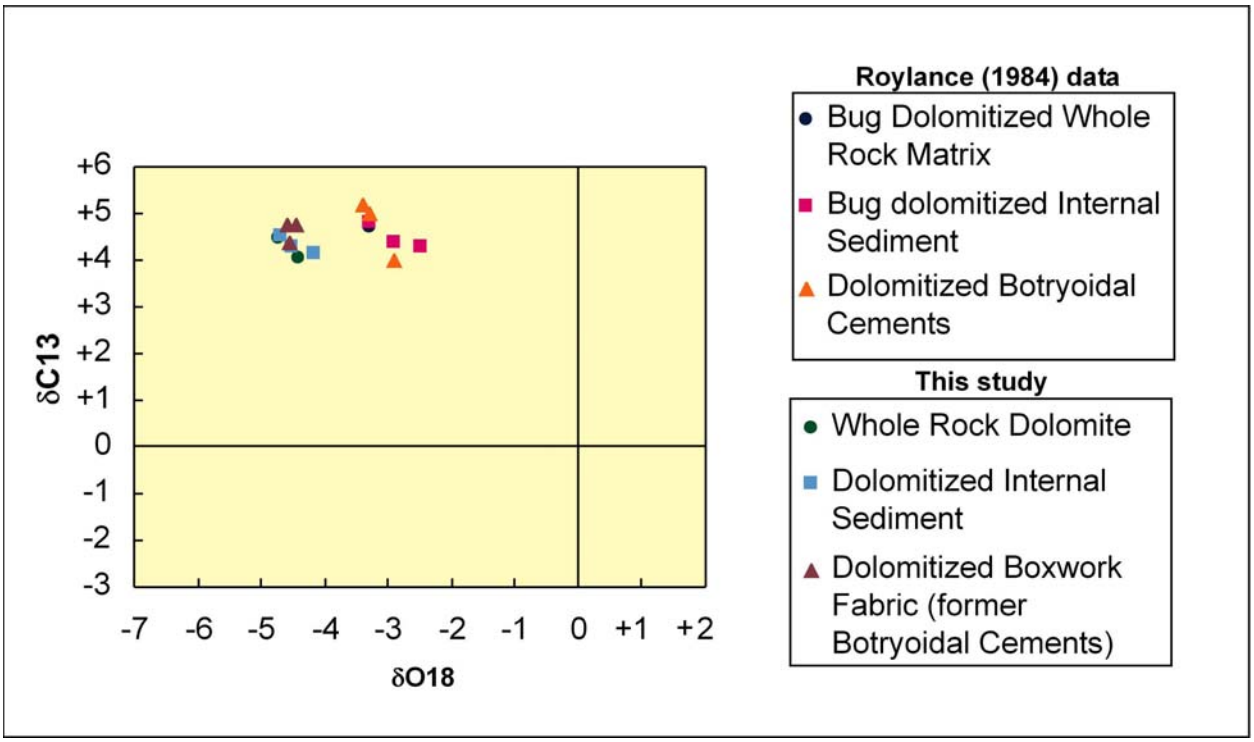

Figure 25. Graph comparing carbon versus oxygen compositions for Bug field dolomites by Roylance (1984) versus those completed for this study.

within shelter pores, and early cements lining original pores. The mean value of del ^{13}C for all Bug field samples in this study is also very close to the mean of +4.6‰ (range of +4.0 to +5.2‰) for seven samples from two other Bug field cores (Bug No. 13 and Bug No. 16) analyzed by Marathon's lab (see table 3, p. 125 in Roylance, 1984; see figure 22). Despite dolomitization, all of the lower Desert Creek samples from Bug field analyzed in this project and by Marathon show carbon isotope compositions that are very close in value to modern marine carbonates ("sediments and skeletons" on figure 21) and Holocene botryoidal marine aragonite cements (James and Ginsburg, 1979; "subsea cements" on figure 21). Furthermore, carbon isotopic compositions for former aragonite marine cements from the Late Permian Capitan Reef complex in southeastern New Mexico are calculated to be about +5.3‰ by Given and Lohmann (1985). Hence, it appears that the carbon isotope geochemistry of all of the lower Desert Creek dolomites at Bug field have retained a strong influence from Pennsylvanian marine water composition. Meteoric waters, which typically would tend to lower the carbon isotope values significantly (Hudson, 1975), do not appear to have had any effect on the composition of these lower Desert Creek dolomites.

Oxygen isotopic compositions for the eight Bug field dolomite samples (figure 24 and table 3) also cluster in a very narrow range around a mean value of -4.51‰ PDB (range of -4.15 to -4.72‰). There is no significant difference in oxygen values between the two Bug wells studied. However, the oxygen compositions in the dolomites sampled here for May Bug No. 2 and Bug No. 4 are significantly different from the values reported by Roylance (1984, 1990) for seven samples processed from the same stratigraphic interval in the Bug No. 13 and Bug No. 16 wells (figures 24 and 25, table 2). The mean oxygen isotope composition for the latter wells is -3.1‰ PDB (range of -2.5 to -3.4‰). Thus, the oxygen values in the May Bug No. 2 and Bug No. 4 cores are more negative by nearly 1.5‰. The oxygen isotope composition data from Bug No. 13 and Bug No. 16 cores, which are situated near the center of the Bug field buildup (figure 10), are rather close to the values for modern marine carbonates ("sediments and skeletons" on figure 21) and to values inferred for unaltered Pennsylvanian marine cements (Lohmann, 1983).

Oxygen isotopic compositions for former aragonite and magnesium calcite marine cements from the Late Permian Reef complex in southeastern New Mexico are calculated to be between -2.8 and -2.5‰ by Given and Lohmann (1985, 1986). The lighter oxygen values obtained from samples in the May Bug No. 2 and Bug No. 4 cores, which are located along the margins or flanks of Bug field (figure 10), may be indicative of exposure to higher temperatures, to fluids depleted in ^{18}O relative to sea water, or to hypersaline waters (Land, 1980, 1982) during burial diagenesis. It is also interesting to note that the two wells with the lightest oxygen isotope compositions in the lower Desert Creek dolomites (May Bug No. 2 and Bug No. 4) have produced significantly greater amounts of hydrocarbons. Production through May 2003 is 340,562 BO (54,149 m^3) and 0.76 BCFG (0.02 BCMG) for May Bug No. 2, and 236,248 BO (37,563 m^3) and 0.48 BCFG (0.01 BCMG) for Bug 4, while Bug No. 13 and Bug No. 16 have produced only 86,786 BO (13,799 m^3) and 0.4 BCFG (0.01 BCMG), and 24,385 BO (3,877 m^3) and 0.84 BCFG (0.02 BCMG), respectively (Utah Division of Oil, Gas and Mining, 2003). The gross productive lower Desert Creek reservoir zone within each of these wells is less than 20 feet (6 m) thick. Clearly, there are economically significant changes in the reservoir quality and the diagenetic history between these well pairs.

Two samples of regional, non-reservoir, open-marine lower Desert Creek zone from Tin Cup Mesa field were analyzed by Marathon's lab for carbon and oxygen isotope composition (MOC No. 1-25 well; figure 1, table 2). The isotopic values for these samples (a limestone and

a dolomite) are significantly different from the Bug field reservoir dolomites (figure 22 and 26). The biggest difference is the much lighter (by greater than 3‰) carbon isotope compositions in the Tin Cup Mesa lower Desert Creek samples than at Bug field. For oxygen isotope composition, the limestone (calcite fraction) is significantly heavier (at -1.6‰ PDB) than either the dolomite sample in the Tin Cup Mesa sample (at –3.3‰ PDB) or the mean values in the two different Bug field dolomite data sets (-3.1‰ for the two poor wells and –4.51‰ for the two excellent wells).

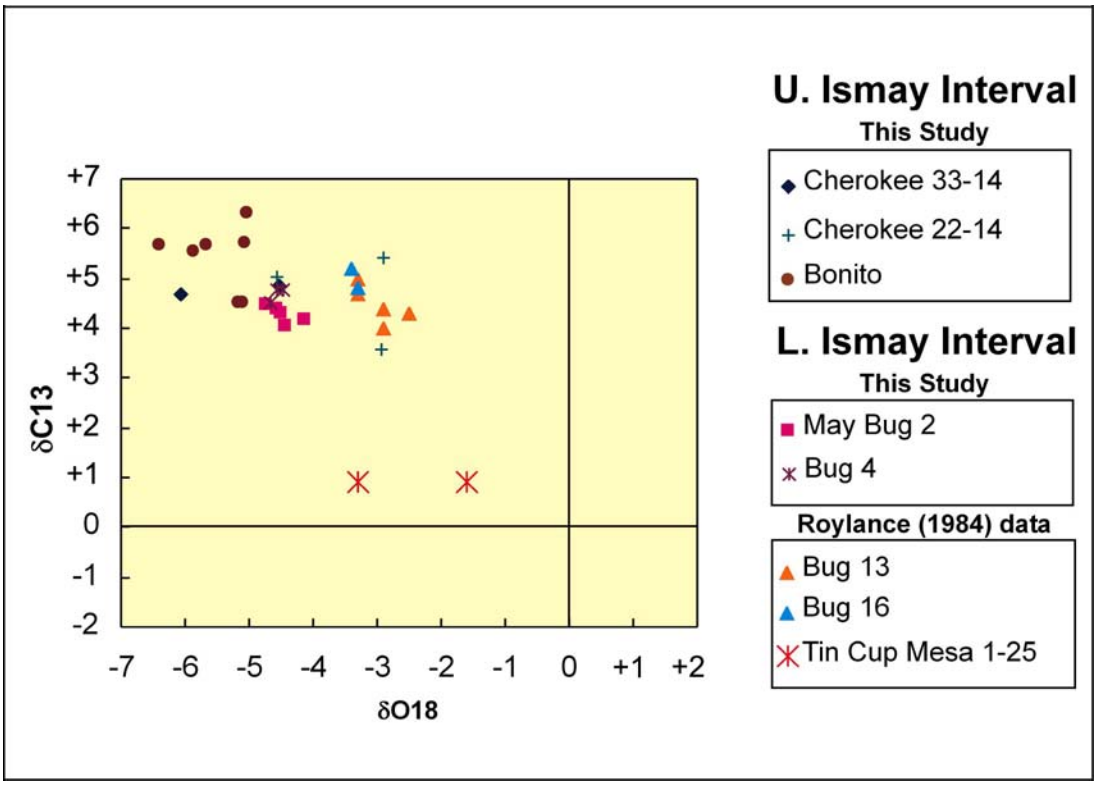

Figure 26. Summary graph of carbon versus oxygen compositions for all components sampled for this study and previously published data by Roylance (1984).

Carbon and Oxygen Isotopes from the Upper Ismay of Cherokee Field

Isotopic composition analyses for carbon and oxygen were completed for a variety of whole rock and diagenetic phases for core samples from the upper Ismay zone in Cherokee field (figures 1 and 8; table 1). A total of five powdered samples were drilled from core samples of the two cored, upper Ismay wells at Cherokee field and were analyzed (table 3). The samples were selected to analyze typical dolomitized calcarenite (bioclastic grainstone), limestone phylloid-algal fabric, dolomitized cryptalgal (stromatolitic) laminites, and microcrystalline, microporous dolomite. Annotated close-up core photos (figure 27) show the approximate locations of the drilled and powered samples from the Cherokee No. 22-14 and Cherokee No. 33-14 wells. A plot of carbon versus oxygen compositions for all Cherokee field samples obtained in this study is shown on figure 28 (see also table 4).

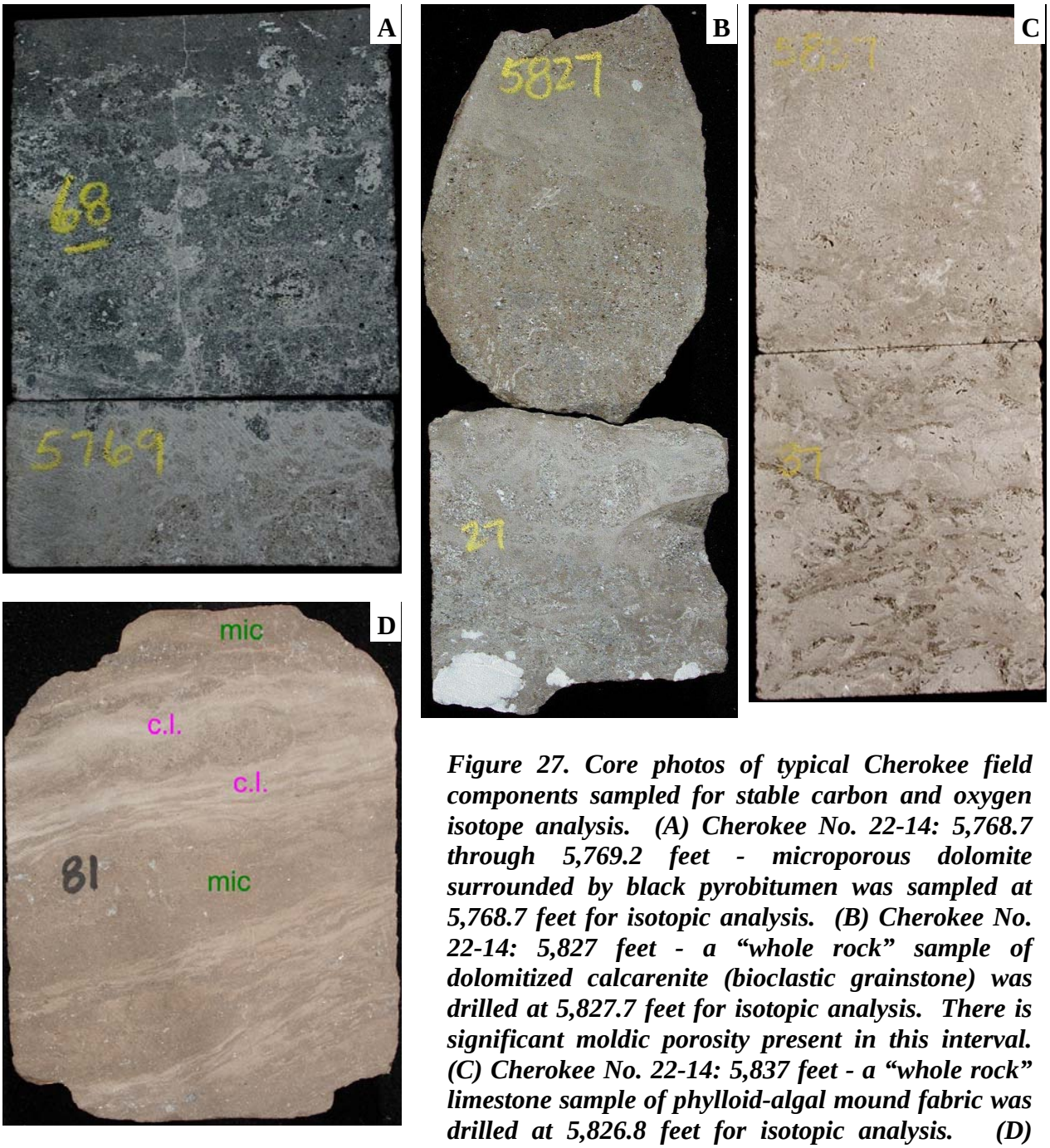

Figure 27. Core photos of typical Cherokee field components sampled for stable carbon and oxygen isotope analysis. (A) Cherokee No. 22-14: 5,768.7 through 5,769.2 feet - microporous dolomite surrounded by black pyrobitumen was sampled at 5,768.7 feet for isotopic analysis. (B) Cherokee No. 22-14: 5,827 feet - a "whole rock" sample of dolomitized calcarenite (bioclastic grainstone) was drilled at 5,827.7 feet for isotopic analysis. There is significant moldic porosity present in this interval. (C) Cherokee No. 22-14: 5,837 feet - a "whole rock" limestone sample of phylloid-algal mound fabric was drilled at 5,826.8 feet for isotopic analysis. (D) Cherokee No. 33-14: 5,781 feet - both the "whole rock" dolomitized cryptalgal laminite (c.l.; sample 5,781.2' A) and microporous dolomite (mic; sample 5,781.2' B) were sampled for isotopic analysis.

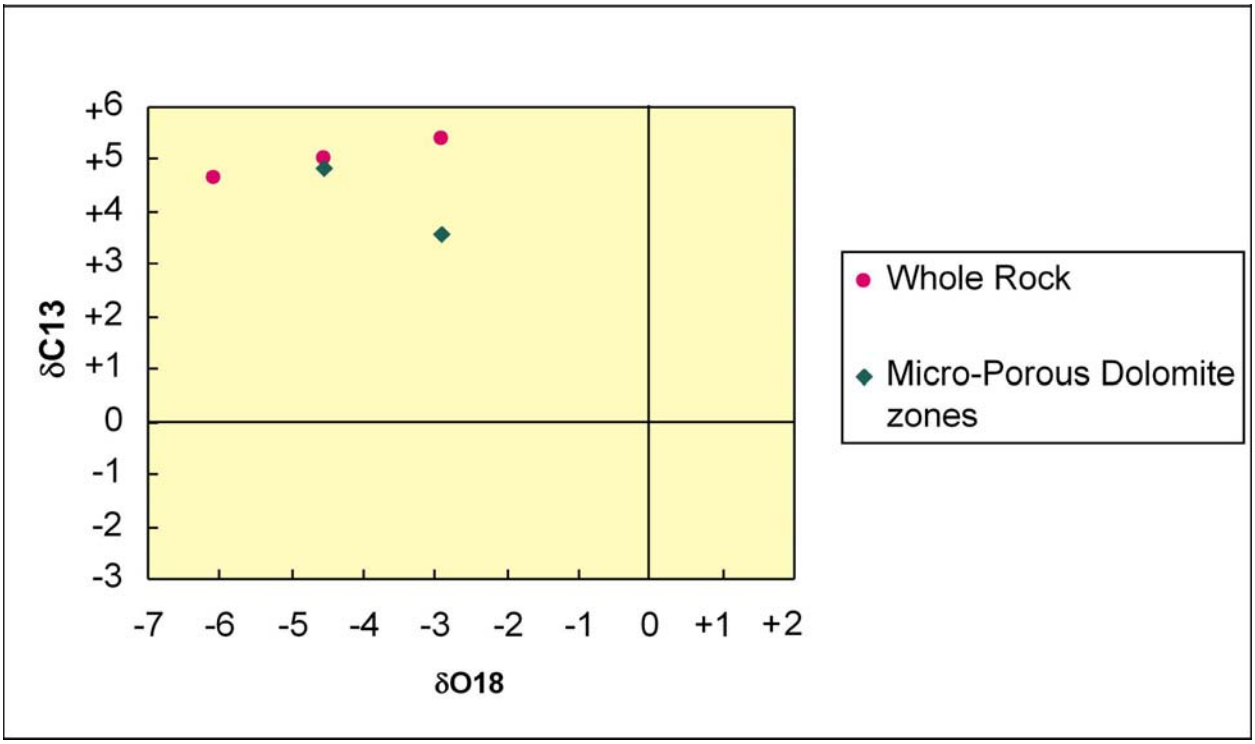

Figure 28. Graph of carbon versus oxygen compositions for Cherokee field components completed for this study.

Carbon isotopic compositions for the five upper Ismay dolomite samples from Cherokee field (figure 28) have a mean value of +4.70‰ PDB (range of +3.57 to +5.11‰). Although the mean carbon isotopic composition appears to be higher in the upper Ismay carbonate samples from Cherokee field than in the lower Desert Creek dolomites at Bug field, the values are not distinguishable at the 95 percent confidence level (t-test). In addition, the limestone (calcite) sample from representative phylloid-algal mound fabrics displays a del ^{13}C value within the same range as the dolomite samples (table 4). Brinton (l986, p. 217-218) reported a possible mean marine del ^{13}C value of +3.9‰ PDB during the time of Ismay deposition from analysis of unaltered brachiopods from Ismay field core. Carbon isotopic compositions for former aragonite marine cements from the Late Permian Capitan Reef complex in southeastern New Mexico are about +5.3‰ (Given and Lohmann, 1985). This may suggest that the fluids responsible for upper Ismay carbonates within Cherokee field have slightly heavier carbon isotope compositions than marine brachiopods at Ismay field, or slightly lighter than late Paleozoic seawater. But as with the Bug field dolomite samples, the Cherokee field carbonates fall within the same range of carbon isotope compositions as modern marine sediments, skeletons, and marine cements (see figure 21).

The del ^{13}C values of the Cherokee field upper Ismay components overlap or are slightly heavier than any of the diagenetic components reported by Dawson (1988) in Ismay field for meteoric-phreatic cements (del ^{13}C = +2.5 to +4.8‰), and are uniformly heavier than either deep burial ferroan calcite cements (del ^{13}C = +1.8 to +3.2‰) or saddle dolomites (mean del ^{13}C = +3.4‰). The range of del ^{13}C values at Cherokee field has a better overlap with values reported from marine botyroidal-fibrous (marine) cements and "neomorphosed matrix sediments" in Ismay field cores (Brinton, 1986) that range between +4.2 to +5.0‰. In addition, Brinton (1986, figure 62) shows that various forms of microcrystalline dolomite in Ismay field have isotopic values that cluster between +3.0 and +6.0‰ for del ^{13}C. As with the lower Desert

Creek dolomites in Bug field, it does not appear that meteoric waters, which typically would precipitate carbonates with more depleted carbon isotope values, have had major effects on the composition of the Ismay carbonate components in Cherokee field. Rather, it is likely that most of the carbonates present within Ismay carbonates (as well as throughout the lower Desert Creek) have retained a marine-influenced isotope geochemistry throughout marine cementation as well as through post-burial recycling of marine carbonate components during dolomitization, stylolitization, dissolution, and late cementation. Such an explanation is in agreement with the model for the positive carbon isotope values of many ancient carbonates proposed by Hudson (1975).

Oxygen isotopic compositions for the Cherokee field limestone and dolomite samples (figure 28 and table 4) form a wide range of values around a mean value of -4.20‰ PDB (range of –2.90 to –6.08‰). As with the carbon isotope data, there is no significant difference between the oxygen isotope compositions from lower Desert Creek dolomite samples in Bug field and the upper Ismay limestones and dolomites from Cherokee field. There is no apparent pattern in the Cherokee field del ^{18}O values other than the deeper samples contain the more depleted (more negative) values. However, the range of values is probably too wide to suggest a depth-related temperature increase for the lowered del ^{18}O values. A similar range of del ^{18}O values was reported by Dawson (1988) from a variety of cement generations from Ismay field cores. Only very late ferroan calcites and baroque dolomites in Dawson's (1988) data displayed more negative oxygen isotope compositions than the Cherokee field limestones and dolomites.

Brinton (l986, p. 217-218) reported a possible mean marine del ^{18}O value of –4.7‰, during the time of Ismay deposition, from analysis of unaltered brachiopods from Ismay field core. This proposed Ismay marine value is very close to two of the Cherokee field values (see table 4), and to the mean value of all the samples. However, two of the samples (at –2.90 and –2.92‰) are significantly heavier than Brinton's marine del ^{18}O value calculated from unaltered marine fossils. They are closer to Given and Lohmann's (1985, 1986) marine diagenesis as determined from former aragonite and magnesium calcite marine cements in the Captian Reef. These heavier del ^{18}O samples (both dolomites) contain oxygen values similar to two cement-filled crinoids and many of the microcrystalline dolomites analyzed by Brinton (1986). One of the dolomitized samples in Cherokee field, from cryptalgal laminites, has a much lighter oxygen composition (-6.08‰). Only certain saddle dolomite cements, late equant calcite spars, and neomorphosed calcites commonly had such light compositions in Brinton's (1986) work on Ismay field cores. The depleted del ^{18}O value of this one dolomite sample (Cherokee No. 33-14: 5,781.2' A [1,762 m]) suggests neomorphism, cementation, and/or dolomitization from warm or isotopically light subsurface waters.

Carbon and Oxygen Isotopes from an Upper Ismay Buildup, Patterson Canyon Field

Carbon and oxygen isotopic analysis was completed on various whole rock and diagenetic cement generations from the upper Ismay oolite/phylloid-algal buildup along the southwest margin of Patterson Canyon field (figure 1, table 1). The Samedan Bonito No. 41-6-85 well cored approximately 25 feet (8 m) of very well-cemented, phylloid-algal mound limestone (a "reef wall" at the margin of the Patterson Canyon phylloid-algal reservoir) and 31 feet (10 m) of overlying tight oolitic and pelloidal calcarenites. Two samples were drilled from

core near the top of the oolitic grainstone section, and five samples were drilled from the cements near the base of the well-cemented mound section. Annotated close-up core photos (figure 29) show the approximate locations of the drilled and powdered samples from the oolite and "reef cementstone" interval selected in the Bonito No. 41-6-85 well. This particular core was analyzed, despite its location outside of either of the two project fields (Bug and Cherokee) because of the spectacular development of cements that display visual characteristics suggesting different generations of development, most of which appear to have been early, or prior to significant burial. A plot of carbon versus oxygen compositions for all Samedan Bonito No. 41-6-85 limestone samples obtained in this study is shown on figure 30 (see also table 5).

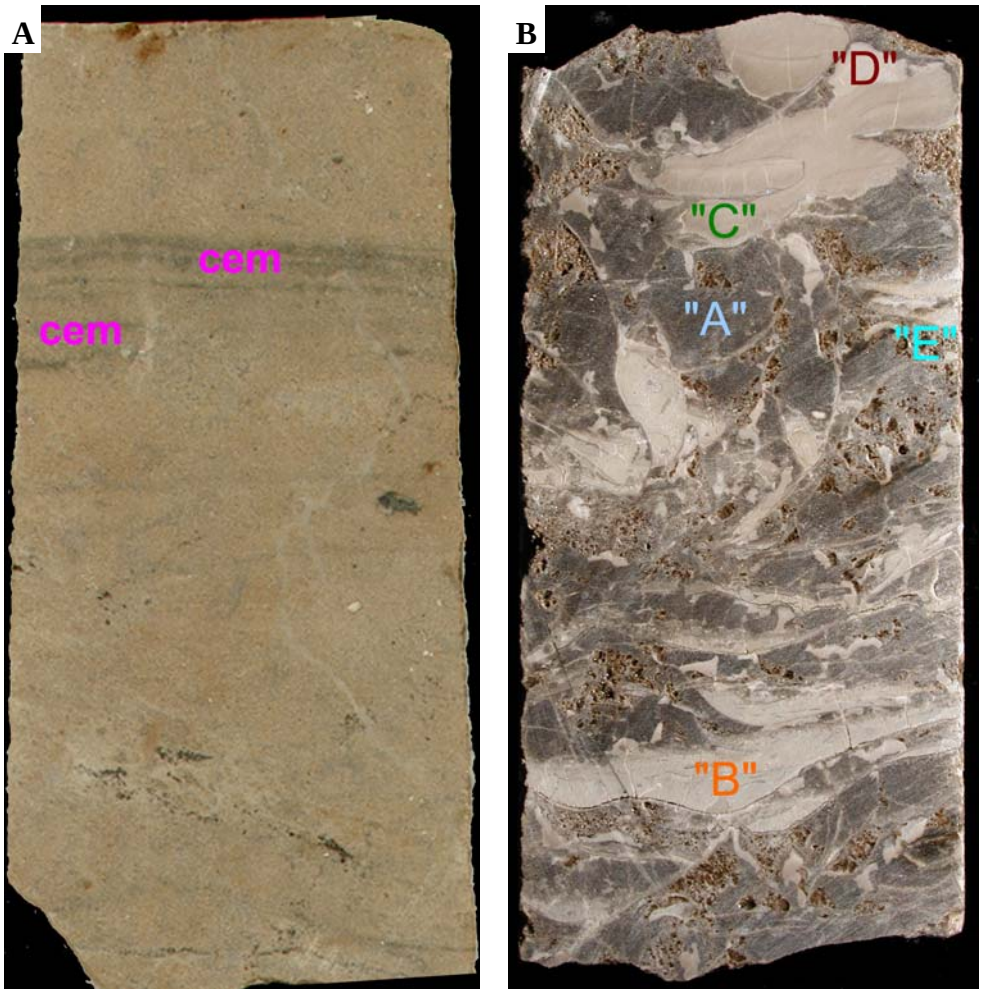

Figure 29. Core photos of whole rock and cement components sampled for stable carbon and oxygen isotope analysis in the upper Ismay buildup of the Samedan Bonito No. 41-6-85 well. (A) Bonito No. 41-6-85: 5,544 feet - both the "whole rock" limestone (an oolitic grainstone; sample 5,544' A) and calcite cement bands (cem; sample 5,544' B) along bedding were sampled for isotopic analysis. (B) Bonito No. 41-6-85: 5,592 feet – five calcite cement generations were sampled for isotopic analysis. Sample 5,492' A – black cements that appear to have originally been botryoidal cement fans. Sample 5,492' B – gray marine cements. Sample 5,492' C – brown cements containing sediments at the bottoms of pores, often display geopetal relationships. Sample 5,492' D – white cements that fill the tops of geopetal cores. Sample 5,492' E – coarse, blocky calcite spar cements.

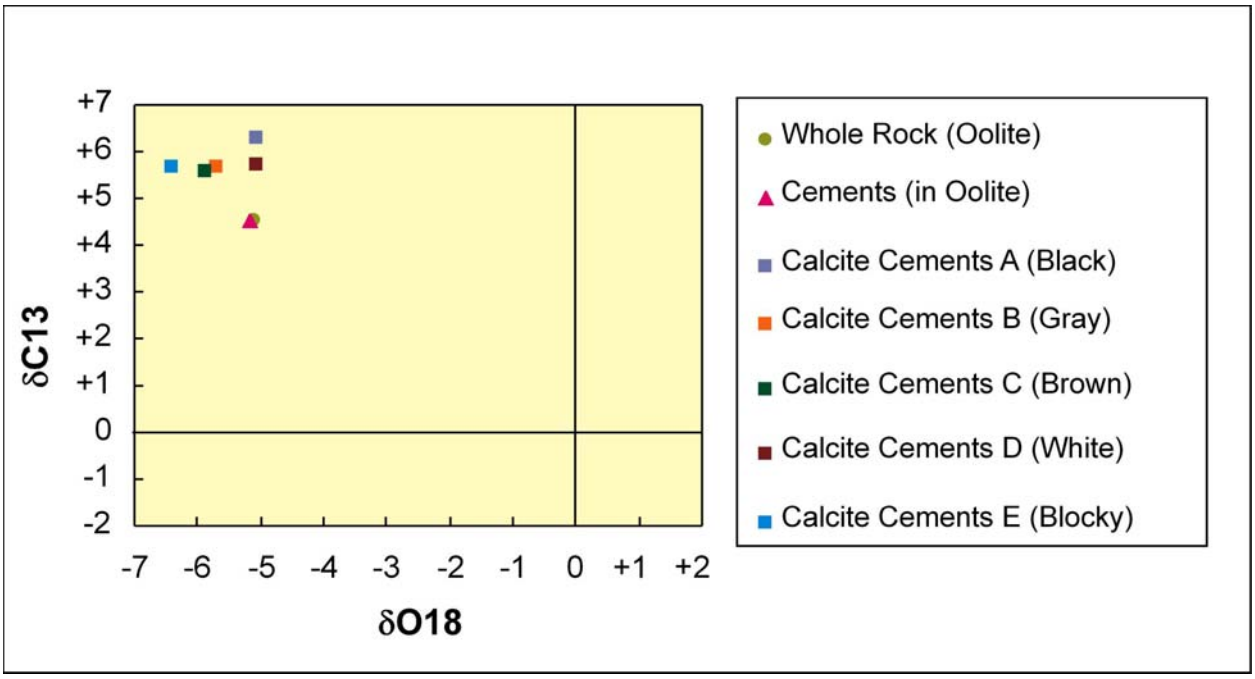

Figure 30. Graph of carbon versus oxygen compositions for whole rock and cement components in an upper Ismay buildup, Samedan Bonito No. 41-6-85 well, completed for this study.

Carbon isotopic compositions for the seven upper Ismay limestone samples in the core from the cemented buildup in Patterson Canyon field have a mean value of +5.43‰ PDB (range of +4.51 to +6.30‰). These values are distinguishable at the 95 percent confidence level (t-test) from the Cherokee field carbonate samples and at the 90 percent level from the Bug field dolomites, but like the Bug and Cherokee values of del ^{13}C, they are much heavier than the mean value of +0.56‰ (standard deviation of 1.55) for a large sampling (n = 272) of Phanerozoic marine limestones (Hudson, 1975). However, the samples can really be divided into two populations with regard to carbon isotopic composition. The five calcite samples from the deeper cemented phylloid-algal buildup have a mean value of +5.79 ‰ PDB (range of +5.56 to +6.30‰) while the oolite and cement samples from the capping grainstone have a mean value of +4.52‰ PDB (range of +4.51 to +4.53‰). Since both of these carbon isotope populations are significantly heavier than Brinton's (1986) value for unaltered brachiopods from Ismay field, it is likely that an isotopically heavier fluid, possibly from concentrated (higher salinity) or closed-system sea water, is recorded in both populations.

Interestingly, Given and Lohmann's (l985) calculated value (+5.3‰ PDB) from Late Paleozoic marine cements from the Permian Basin reef front falls between the two Bonito No. 41-6-85 well populations. It does not appear that meteoric waters, which typically would precipitate calcites with more depleted carbon isotope values, were involved in the diagenesis of the tight Patterson Canyon well buildup. But why the significant difference in del ^{13}C values between the well-cemented oolite samples and the cements present in the underlying reef? Clearly the waters were somehow different in composition between the phylloid-algal mound cements and the lithified oolites. One possible scenario is that the waters responsible for the several generations ("A" through "E") of mound cement were confined to a "closed hydrologic system" that allowed a fluid with heavier carbon to evolve. The oolite and cement bands

therein may have been in a more open system allowing water exchange such that waters with a composition slightly lighter than Brinton's proposed Ismay marine value (derived from unaltered brachiopods) were involved in the lithification and diagenesis of the capping oolite.

Oxygen isotopic compositions for the seven upper Ismay limestone samples of the cemented buildup in Patterson Canyon field form a moderate range of values around a mean value of –5.48‰ PDB (range of –5.05 to –6.41‰). As with the carbon isotope data, there is a significant difference (at the 95 percent confidence level) between the Bonito No. 41-6-85 oxygen isotope compositions and those from both the lower Desert Creek dolomites and the upper Ismay at Cherokee field. There is no significant difference in the del ^{18}O values between the deeper mound, early cement samples (mean value of -5.62‰ PDB) and the overlying lithified oolite (mean of -5.58‰ PDB). All seven of the Bonito No. 41-6-85 limestone samples, regardless of component or cement type, are lighter on average by about 1.0‰ PDB than the Bug and Cherokee field samples. These Patterson Canyon samples' del ^{18}O values from diagenetic components are also lighter than either Brinton's marine del ^{18}O value calculated from unaltered marine fossils or Given and Lohmann's (1985, 1986) values of –2.8 to -2.5‰ for former aragonite and magnesium calcite marine cements from the Late Permian Reef complex in southeastern New Mexico. The reasons for these significant differences are not immediately clear. It is possible that the oxygen isotope signatures indicate waters with depleted ^{18}O characteristics evolved in the mound cavities and ooid grainstone pores, without any influence by hypersaline waters. Alternatively, the limestones in this sample set may have all been modified via neomorphism by isotopically light subsurface waters.

TECHNOLOGY TRANSFER

The UGS is the Principal Investigator and prime contractor for three government-industry cooperative petroleum-research projects, including two in the Paradox Basin. These projects are designed to improve recovery, development, and exploration of the nation's oil and gas resources through use of better, more efficient technologies. The projects involve detailed geologic and engineering characterization of several complex heterogeneous reservoirs. The two Class II Oil (this report covers the Class II Revisit project) projects include practical oil-field demonstrations of selected technologies in the Paradox Basin. The third project involves establishing a log-based correlation scheme for the Tertiary Green River Formation in the southwestern Uinta Basin to help identify new plays and improve the understanding of producing intervals. The DOE and multidisciplinary teams from petroleum companies, petroleum service companies, universities, private consultants, and state agencies are co-funding the three projects. The UGS is also the Principal Investigator and prime contractor for the DOE Preferred Upstream Management (PUMP II) project titled *Major Oil Plays in Utah and Vicinity* which will describe and delineate oil plays in the Thrust Belt, Uinta Basin, and Paradox Basin. Finally, the UGS is just beginning a new project that will evaluate exploration methods and map regional facies trends for independents interested in the Mississippian Leadville Limestone play of the Paradox Basin.

The UGS intends to release selected products of the Paradox Basin project in a series of formal publications. These publications may include data, as well as the results and interpretations. Syntheses and highlights will be submitted to refereed journals, as appropriate, such as the *American Association of Petroleum Geologists (AAPG) Bulletin* and *Journal of*

Petroleum Technology, and to trade publications, such as the *Oil and Gas Journal*. This information will also be released through the UGS periodical *Survey Notes* and be posted on the UGS Paradox Basin project Internet web page.

The Technical Advisory Board advises the technical team on the direction of study, reviews technical progress, recommends changes and additions to the study, and provides data. The Technical Advisory Board is composed of 13 field operators from the Paradox Basin (Seeley Oil Co., Legacy Energy Corp., Pioneer Oil & Gas, Hallwood Petroleum Inc., Dolar Oil Properties, Cochrane Resources Inc., Wexpro Co., Samedan Oil Corp., Questar Exploration, Tom Brown Inc., PetroCorp Inc., Stone Energy LLC., and Sinclair Oil Corp.). This board ensures direct communication of the study methods and results to the Paradox Basin operators. The Stake Holders Board is composed of groups that have a financial interest in the study area including representatives from the Utah and Colorado state governments (Utah School and Institutional Trust Lands Administration, Utah Division of Oil, Gas and Mining, and Colorado Oil and Gas Conservation Commission), Federal Government (U.S. Bureau of Land Management and U.S. Bureau of Indian Affairs), and the Ute Mountain Ute Indian Tribe. The members of the Technical Advisory and Stake Holders Boards receive all semi-annual technical reports and copies of all publications, and other material resulting from the study.

Project plans, objectives, and results were through a PowerPoint™ display at the UGS booth during the AAPG annual national convention, May 11-14, 2003, in Salt Lake City, Utah. Four UGS scientists staffed the display booth at this event. Project displays will be included as part of the UGS booth at professional meetings throughout the duration of the project.

Utah Geological Survey *Survey Notes* and Internet Web Site

The purpose of *Survey Notes* is to provide non-technical information on contemporary geologic topics, issues, events, and ongoing UGS projects to Utah's geologic community, educators, state and local officials and other decision makers, and the public. *Survey Notes* is published three times yearly. Single copies are distributed free of charge and reproduction (with recognition of source) is encouraged. The UGS maintains a database that includes those companies or individuals (more than 300 as of April 2003) specifically interested in the Paradox Basin project or other DOE-sponsored UGS projects. They receive *Survey Notes* and notification of project publications and workshops.

The UGS maintains a web site on the Internet, http://geology.utah.gov. The UGS site includes a page under the heading *Economic Geology Program*, which describes the UGS/DOE cooperative studies (Paradox Basin, Ferron Sandstone, Bluebell field, Green River Formation, PUMP II), and has a link to the DOE web site. Each UGS/DOE cooperative study also has its own separate page on the UGS web site. The Paradox Basin project page http://geology.utah.gov/emp/Paradox2/index.htm contains: (1) a project location map, (2) a description of the project, (3) a list of project participants and their postal addresses and phone numbers, (4) a reference list of all publications that are a direct result of the project, and (5) semi-annual technical progress reports.

Technical Presentations

The following technical presentations were made during the first six months of the fourth project year as part of the technology transfer activities.

Poster Presentation: "Regional Facies Trends in the Upper Ismay Zone of the Blanding Sub-basin of the Paradox Basin, Utah – Aids for Identifying Possible Targets for Horizontal Drilling" by David E. Eby, Thomas C. Chidsey, Jr., Craig D. Morgan, and Kevin McClure, at the AAPG annual convention, Salt Lake City, Utah, May 13, 2003. Core photographs of facies types, regional facies maps, and horizontal drilling recommendations were part of the presentation.

Short Course/Core Workshop: "Pennsylvanian Heterogeneous Shallow-Shelf Buildups of the Paradox Basin: A Core Workshop," instructed by David E. Eby, Thomas C. Chidsey, Jr., and Laura L. Wray, at the UGS Core Research Center, May 10, 2003, as part of the AAPG annual convention in Salt Lake City. The short course was co-sponsored by the DOE. Core from representative Ismay and Desert Creek fields was examined. All core displayed was placed into regional paleogeographic settings. The core workshop was organized into topical modules with participants performing a series of exercises using core, geophysical well logs, and photomicrographs from thin sections. These modules included: describing reservoir versus non-reservoir facies, determining diagenesis and porosity from core, recognizing barriers and baffles to fluid flow, correlating core to geophysical well logs, and identifying potential completion zones and candidates for horizontal drilling. There were 25 participants from oil companies around the world.

Project Publications

Chidsey, T.C., Jr., 2003, An up close and personal view of Cherokee oil field, San Juan County, Utah: Utah Geological Survey, Survey Notes, v. 35, no. 2, p. 1-3.

Eby, D.E., Chidsey, T.C., Jr., McClure, Kevin, and Morgan, C.D., 2003, Heterogeneous shallow-shelf carbonate buildups in the Paradox Basin, Utah and Colorado: targets for increased oil production and reserves using horizontal drilling techniques – semi-annual technical progress report for the period October 6, 2002 to April 5, 2003: U.S. Department of Energy, DOE/BC15128-6, 29 p.

Eby, D.E., Chidsey, T.C., Jr., Morgan, C.D., and McClure, Kevin, 2003, Regional facies trends in the upper Ismay zone of the Blanding sub-basin of the Paradox Basin, Utah – aids for identifying possible targets for horizontal drilling [abs.]: American Association of Petroleum Geologists Annual Convention, Official Program with Abstracts, v. 12, p. A48.

CONCLUSIONS

The Blanding sub-basin within the Pennsylvanian Paradox Basin developed on a shallow-marine shelf that locally contained algal-mound and other carbonate buildups. The two main producing zones of the Paradox Formation are the Ismay and the Desert Creek. The Ismay zone is dominantly limestone comprising equant buildups of phylloid-algal material.

The Desert Creek zone is dominantly dolomite comprising regional nearshore-shoreline trends with highly aligned, linear facies tracts. This study was undertaken to provide a useful database and methodology for identifying potential horizontal drilling targets within heterogeneous carbonate rocks containing porous phylloid-algal buildups and associated facies.

Production "sweet spots" and potential horizontal drilling candidates were identified for Cherokee and Bug fields. In Cherokee field, the highest IPFs as well as the largest volumes of oil and gas produced are from wells located on the crest of the structural nose where the upper Ismay zone buildup developed and in the thickest part of the mound facies. These wells penetrated both the phylloid-algal mound and the crinoid/fusulinid-bearing, carbonate sand facies of the carbonate buildup where there may be a thick section of microporosity. This unique pore type represents the greatest hydrocarbon storage capacity and potential horizontal drilling target in the field. In Bug field, the highest IPFs and largest volumes of oil were recorded from wells located structurally downdip from the updip porosity pinch out that forms the trap, and in the main part of the lower Desert Creek zone carbonate buildup. These wells penetrated both the phylloid-algal mound and the shoreline carbonate island facies where significant micro-box-work porosity has likely developed - the diagenetic pore type with the greatest hydrocarbon storage and flow capacity in this dolomitized reservoir.

Diagenesis is the main control on the quality of Ismay and Desert Creek reservoirs. Much of the porosity development occurred in a mesogenetic (burial) setting, mostly post-dating stylolitization. Maximum porosity is developed as dissolution adjacent to stylolites, especially in phylloid-algal mounds. It is likely that most of the carbonates present within the Ismay zone (as well as throughout the lower Desert Creek) have retained a marine-influenced isotope geochemistry through marine cementation as well as post-burial recycling of marine carbonate components during dolomitization, stylolitization, dissolution, and late cements. Such an explanation is in agreement with the model for the positive carbon isotope values of many ancient carbonates proposed by Hudson (1975).

Specific conclusions of the isotopic analyses conducted for the project are as follows:

1. Carbon isotopic compositions for Bug field dolomite samples have a mean value of +4.43‰ PDB. Despite dolomitization, all of the lower Desert Creek samples from Bug field show carbon isotope compositions that are very close in value to modern marine carbonates and Holocene botryoidal marine aragonite cements.

2. The carbon isotope geochemistry of all of the lower Desert Creek dolomites at Bug field has retained a strong influence from Pennsylvanian marine water composition. Meteoric waters do not appear to have had any effect on the composition of these lower Desert Creek dolomites.

3. Oxygen isotopic compositions for the Bug field dolomite samples have a mean value of -4.51‰ PDB. The lighter oxygen values obtained from wells located along the margins or flanks of Bug field may be indicative of exposure to higher temperatures, to fluids depleted in ^{18}O relative to sea water, or to hypersaline waters during burial diagenesis.

4. The wells in Bug field with the lightest oxygen isotope compositions in the lower Desert Creek dolomites have produced significantly greater amounts of hydrocarbons.

5. Carbon isotopic compositions for the upper Ismay dolomite samples at Cherokee field have a mean value of +4.70‰ PDB. As with the Bug field dolomite samples, the Cherokee field carbonates fall within the same range of carbon isotope compositions as modern marine sediments, skeletons, and marine cements. It does not appear that meteoric waters, which typically would precipitate carbonates with more depleted carbon isotope values, have had major effects on the composition of the Ismay carbonate components.

6. Most of the Ismay carbonates (as well as those throughout the lower Desert Creek) have retained a marine-influenced carbon isotope geochemistry throughout marine cementation as well as post-burial recycling of marine carbonate components during dolomitization, stylolitization, dissolution, and late cementation.

7. Oxygen isotopic compositions for the Cherokee field limestone and dolomite samples form a wide range of values around a mean value of -4.20‰ PDB. There is no significant difference between the oxygen isotope compositions from lower Desert Creek dolomite samples in Bug field and the upper Ismay limestones and dolomites from Cherokee field.

8. One of the dolomitized samples in Cherokee field, from cryptalgal laminites, has a much lighter oxygen composition. The depleted del ^{18}O value of this one dolomite sample suggests neomorphism, cementation, and/or dolomitization from warm or isotopically light subsurface waters.

9. Carbon isotopic compositions for upper Ismay limestone samples in the cemented buildup of Patterson Canyon field have a mean value of +5.43‰ PDB. However, the samples can be divided into two populations with regard to carbon isotopic composition: isotopically heavier mound cemented and isotopically lighter oolite and cement bands.

10. Mound cements were confined to a "closed hydrologic system" that allowed a fluid with heavier carbon to evolve. The oolite and cement bands therein may have been in a more open system allowing water exchange such that waters with a composition slightly lighter were involved in the lithification and diagenesis of the capping oolite.

11. Oxygen isotopic compositions for upper Ismay limestone samples of the cemented buildup in Patterson Canyon field have a mean value of –5.48‰ PDB, lighter than Bug and Cherokee samples.

12. The oxygen isotope signatures indicate waters with depleted ^{18}O characteristics evolved in the mound cavities and ooid grainstone pores, without any influence by hypersaline waters. Alternatively, the limestones in this sample set may have all been modified via neomorphism by isotopically light subsurface waters.

ACKNOWLEDGMENTS

Funding for this ongoing research was provided as part of the Class II Oil Revisit Program of the U.S. Department of Energy, National Petroleum Technology Office, Tulsa,

Oklahoma, contract number DE-FC26-00BC15128. The Contracting Officer's Representative is Gary D. Walker. Support was also provided by the Colorado Geological Survey and David E. Eby, Eby Petrography & Consulting, Inc.

Core and petrophysical data were provided by Burlington Resources, Anadarko Petroleum Company, Wexpro Company, Seeley Oil Company, Marathon Oil Company, and Samedan Oil Corporation. Isotopic analysis was conducted by Melissa Schlegel, Brigham Young University Department of Geology Stable Isotope Laboratory, Provo, Utah. Carolyn Olsen, Cheryl Gustin, and Jim Parker, of the Utah Geological Survey, prepared samples, photographed core, generated graphs, and drafted figures. The report was reviewed by Bryce Tripp, David Tabet, and Michael Hylland of the Utah Geological Survey. Cheryl Gustin, Utah Geological Survey, formatted the manuscript.

REFERENCES

Brinton, Lisë, 1986, Deposition and diagenesis of Middle Pennsylvanian (Desmoinesian) phylloid algal banks, Paradox Formation, Ismay zone, Ismay field and San Juan Canyon, Paradox Basin, Utah and Colorado: Golden, Colorado School of Mines, M.S. thesis, 315 p.

Crawley-Stewart, C.L., and Riley, K.F., 1993, Cherokee, *in* Hill, B.G., and Bereskin, S.R., editors, Oil and gas fields of Utah: Utah Geological Association Publication 22, non-paginated.

Dawson, W.C., 1988, Ismay reservoirs, Paradox Basin - diagenesis and porosity development, *in* Goolsby, S.M., and Longman, M.W., editors, Occurrence and petrophysical properties of carbonate reservoirs in the Rocky Mountain region: Rocky Mountain Association of Geologists, p. 163-174; 442-443.

Given, R.K., and Lohmann, K.C., 1985, Derivation of the original isotopic composition of Permian marine cements: Journal of Sedimentary Petrology, v. 55, p. 430-439.

---1986, Isotopic evidence for the early meteoric diagenesis of the reef facies, Permian reef complex of West Texas and New Mexico: Journal of Sedimentary Petrology, v. 56, p. 183-193.

Hudson, J.D., 1975, Carbon isotopes and limestone cements: Geology, v. 3, p. 19-22.

James, N.P., and Ginsburg, R.N., 1979, The seaward margin of Belize barrier and atoll reefs: International Association of Sedimentologists Special Publication 3, 191 p.

Land, L.S., 1980, The isotopic and trace elements geochemistry of dolomite - the state of the art, *in* Zenger, D.H., Dunham, J.B., and Ethington, R.L., editors, Concepts and models of dolomitization: Society for Sedimentary Geology (SEPM) Special Publication 28, p. 87-110.

---1982, Dolomitization: American Association of Petroleum Geologists Short Course Note Series No. 24, 20 p.

Lohmann, K.C., 1983, Diagenetic history of carbonate reservoirs – integration of petrographic and geochemical techniques, *in* Wilson, J.L., Wilkinson, B.H., Lohmann, K.C., and Hurley, N.F., editors, New ideas and methods of exploration for carbonate reservoirs: Dallas Geological Society, unpaginated.

Martin, G.W., 1983, Bug, *in* Fassett, J.E., editor, Oil and gas fields of the Four Corners area, volume III: Four Corners Geological Society, p. 1073-1077.

Oline, W.F., 1996, Bug, *in* Hill, B.G., and Bereskin, S.R., editors, Oil and gas fields of Utah: Utah Geological Association Publication 22 Addendum, non-paginated.

Roylance, M.H., 1984, Depositional and diagenetic control of petroleum entrapment in the Desert Creek interval, Paradox Formation, southeastern Utah and southwestern Colorado: Lawrence, University of Kansas, M.S. thesis, 178 p.

---1990, Depositional and diagenetic history of a Pennsylvanian algal-mound complex - Bug and Papoose Canyon fields, Utah and Colorado: American Association of Petroleum Geologists Bulletin, v. 74, p. 1087-1099.

Utah Division of Oil, Gas and Mining, 2003, Oil and gas production report, May: non-paginated.

Report Title

"Improved Oil Recovery from Upper Jurassic Smackover Carbonates through the Application of Advanced Technologies at Womack Hill Oil Field, Choctaw and Clarke Counties, Eastern Gulf Coastal Plain"

Type of Report

Topical Annual Progress Report for Year 2 and Continuation Application for Year 3

Reporting Period Start Date

May 1, 2001

Reporting Period End Date

April 30, 2002

Principal Author

Ernest A. Mancini (205/348-4319)
Department of Geological Sciences
Box 870338
202 Bevill Building
University of Alabama
Tuscaloosa, AL 35487-0338

Date Report was Issued

May 6, 2002

DOE Award Number

DE-FC26-00BC15129

Name and Address of Contacts for Participants

Ernest A. Mancini Dept. of Geological Sciences Box 870338 Tuscaloosa, AL 35487-0338	David Cate Pruet Production Co. 217 West Capitol St., Suite 201 Jackson, MS 39201	Thomas Blasingame Dept. of Petroleum Engineering Texas A&M University College Station, TX 77843-3116
R. P. Major Dept. of Geology & Geological Engr. University of Mississippi University, MS 38677	Lewis Brown Dept. of Biology Mississippi State University Mississippi State, MS 39762	Wayne Stafford 558 Highway 468 Brandon, MS 39042

Disclaimer

This report was prepared as an account of work sponsored by an agency of the United States Government. Neither the United States Government nor any agency thereof, nor any of their employees, makes any warranty, express or implied, or assumes any legal liability or responsibility for the accuracy, completeness, or usefulness of any information, apparat us, product, or process disclosed, or represents that its use would not infringe privately owned rights. Reference herein to any specific commercial product, process, or service by trade name, trademark, manufacturer, or otherwise does not necessarily constitute or imply its endorsement, recommendation, or favoring by the United States Government or any agency thereof. The views and opinions of authors expressed herein do not necessarily state or reflect those of the United States Government or any agency thereof.

Heterogeneous Shallow-Shelf Carbonate Buildups in the Blanding Sub-Basin of the Paradox Basin, Utah and Colorado: Targets for Increased Oil Production and Reserves Using Horizontal Drilling Techniques

DE-AC26-00BC15128

Program

This project was in response to DOE's solicitation DE-PS26-99BC15144, Reservoir Class Field Demonstration Program – Class Revisit. The goal of the Class Program was to extend economic production of domestic fields, by slowing the rate of well abandonments, preserving industry infrastructure, and to increase ultimate recovery using improved reservoir characterization and advanced technologies.

Project Goal

Increase production and reserves from the shallow shelf carbonate reservoirs in the Ismay and Desert Creek zones of the Pennsylvania age Paradox Formation, in the Paradox Basin of Utah and Colorado. The project proposed using horizontal laterals from existing vertical field development wells to optimize production.

Performers

Utah Geological Survey,
Salt Lake City, UT
Eby Petrography & Consulting,
Salt Lake City, UT
Colorado Geological Survey, Denver, CO
Seeley Oil Company

Project Results

Production "sweet spots" have been identified at Bug and Cherokee fields as potential horizontal well targets. Vertical wells have penetrated the Ismay phylloid-algal mound and crinoid/fusulinid facies at Cherokee field, and the areas of highest microporosity have been confirmed. At Bug field the best potential drilling facies are the updip porosity pinch-out in the Desert Creek phylloid-anglo mound and shoreline carbonate facies.

Benefits

Detailed reservoir characterization and analysis of horizontal wells by the Utah and Colorado Geological Surveys will provide information and assessment of horizontal drilling of prospects in the Blanding Subbasin of the Paradox Basin which small independent operators could not afford on their own. Work by the Geological Surveys will not be restricted to individual leases or time constraints and can thus provide a more comprehensive and objective analysis available to all companies working in the area. Methodologies to identify drilling prospects in the over 100 small carbonate mound fields in the Paradox Basin holds the key to recovery of an estimated 200 MM barrels of oil.

Background

Most of the Pennsylvania Paradox Formation fields are characterized by high initial production rates followed by a very short production life (primary). Only 15 to 25% of the original oil-in-place (OOIP) is recoverable during primary production with conventional vertical wells. The previous DOE Class II study of the Paradox Basin demosntrated that secondary recovery by waterflood is not feasible.

The small Ismay and Desert Creek fields are at risk of premature abandonment. At least 200 MM barrels of oil is at risk of being left behind in them because of inefficient development practices that leave undrained these very heterogeneous reservoirs. Because of the wide spread nature of the carbonate mound fields, the Desert Creek and Ismay zones have not been adequately characterized. Small independent operators of single fields do not have the time, money or expertise to perform this analysis. The Utah Geological Survey serves the public by conducting regional studies which small companies can not under take by themselves.

The proposal sugguested a three-phase, multi-disciplinary approach to increase production and reserves from the shallow-shelf carbonate reservoirs in the Ismay and Desert Creek zones of the Paradox Formation using horizontal laterals from existing vertical field development wells.1) Conduct detailed geologic analysis of fields, 2) Drill horizontal wells from existing vertical wells to test hypothesis developed in Phase 1, and 3) extended monitoring to determine impact of Phase 1 & 2.

Project Summary

- Data from representative field and wildcat wells was used to correlate logs and construct regional maps and cross sections of facies for the Desert Creek and Ismay Zones.
- A three-dimensional model was constructed of environmental facies and potential undrained zones that may be suitable for horizontal drilling.
- Diagenesis has been determined to be the main control of reservoir quality of Desert Creek and Ismay reservoirs.
- Reservoir characterization of the Ismay and Desert Creek zones has identified Bug and Cherokee fields as the best candidates for horizontal wells.
- Potential horizontal drilling targets are based on analysis of the porosity distribu-

Phylloid algal mound outcrops along the San Juan River, Paradox Basin.

tion, which is highly dependent on the diagenetic history of each facies.

- At Cherokee field the best production zones are related to microporosity in the phylloid-algal mound and crinoid/fusulinid facies of the Ismay zone.

- At Bug field the best production zones are related to micro-box-work porosity of the Desert Creek phylloid-algal mound and shoreline carbonared island facies.

The shallow-shelf carbonate reservoirs in the Pennsylvanian Paradox Formation (primarily the Ismay and Desert Creek zones) in the Paradox Basin of Utah, Colorado and Arizona contain over 100 small fields with heterogeneous carbonate reservoirs, which had not previously been adequately characterized. The Ismay zone is dominantly limestone comprising equant buildups of phylloid-algal with local, rapidly changing small-scale subfacies. The Desert Creek zone is dominantly dolomite, comprising regional shoreline trends with highly aligned, linear facies tracts.

Most of the carbonates present within the lower Desert Creek and Ismay have retained a marine-influenced carbon isotope geochemistry throughout marine cementation as well as through post-burial recycling of marine carbonate components during dolomitization, stylolitization, dissolution, and late cementation. Porosity development necessary for oil production is dependent on the geochemical history and diagenesis of the carbonate mounds. Meteoric waters do no appear to have had any effect on the composition of the Desert Creek dolomites. Samples from Cherokee and Bug fields dolomites indicate that the lower Desert Creek zone shows carbon isotope compositions that are very close in value to modern marine carbonates.

Wells in Bug field have lower oxygen(O^{18}) isotope composition in the lower Desert Creek dolomites have produced significantly greater amounts of hydrocarbons. Oxygen isotope analysis from the upper Ismay limestone at Cherokee field have lower oxygen(O^{18}) than samples from the dolomites at either field. The oxygen isotope signatures indicate waters depleted of the heavy oxygen isotope (O^{18}), characteristic of mound cavities and ooid grainstone pores where the influence of hypersaline waters were limited during diagenesis.

With the exception of the giant Greater Aneth field in Utah, the small oil fields in the basin contain 2 to 10 MMbbl of OOIP per field. Proper geological evaluation of the reservoirs may increase production by 20 to 50% by the application of horizontal, possibly multilateral horizontal drilling projects at lower costs than vertical wells.

Current Status

The second phase of the project, drilling horizontal wells at Bug and/or Cherokee fields to test the predictive theories based on the mapping and carbon and oxygen isotope analysis is scheduled to begin in mid-late 2004. Presentations at the AAPG Rocky Mountain annual meeting in August 2004 will be used to reach independent operators, and invite them to participate in Phase 2, the horizontal drilling project.

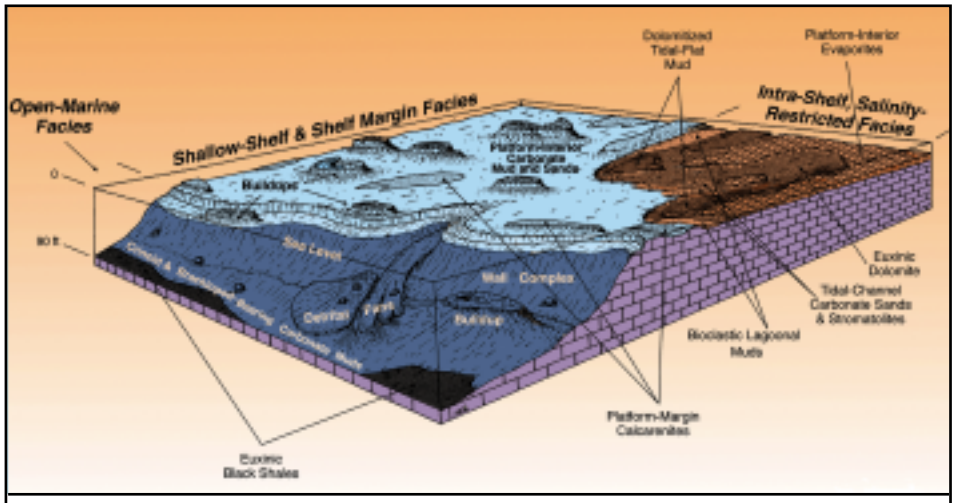

Block diagram of the Desert Creek facies showing the shoreline carbonate deposits in the Paradox Formation of AZ,CO, and UT.

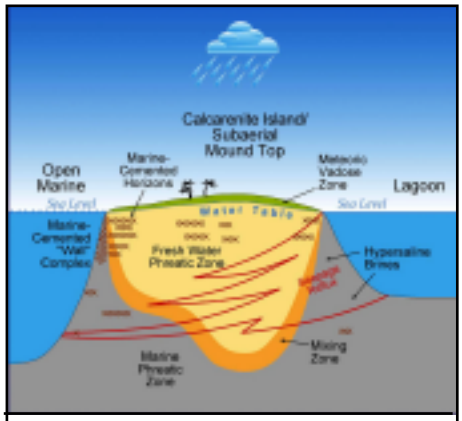

Schematic showing the diagenetic processes affecting porosity in carbonate mounds..

Project Start: April 6, 2000
Project End: April 5, 2005

Contact Information:
NETL – Gary Walker (gary.walker@netl.doe.gov or 918-699-2083)
Utah Geological Survey – Thomas Chidsey (tomchidsey@utah.gov or 801-537-3364) Salt Lake City, UT

IMPROVED OIL RECOVERY FROM UPPER JURASSIC SMACKOVER CARBONATES THROUGH THE APPLICATION OF ADVANCED TECHNOLOGIES AT WOMACK HILL OIL FIELD, CHOCTAW AND CLARKE COUNTIES, EASTERN GULF COASTAL PLAIN

Annual Report
May 1, 2001-April 30, 2002

By:
Ernest A. Mancini
Charles Haynes
Joe Benson
David Hilton
David Cate
Thomas Blasingame
Wayne Ahr
Rosalind Archer
R. P. Major
Lewis Brown
Alex Vadie
Wayne Stafford
Brian Panetta
William Tedesco
Tiffany Hopkins
Juan Avila
Ekene Chijuka
Ammi Tan
Leo Lynch
Todd French
Karen Thompson
Magan Green
John Sorrell

Work Performed Under Contract No. DE-FC26-00BC15129

University of Alabama
Tuscaloosa, Alabama

National Energy Technology Laboratory
National Petroleum Technology Office
U.S. DEPARTMENT OF ENERGY
Tulsa, Oklahoma

ABSTRACT

Pruet Production Co. and the Center for Sedimentary Basin Studies at the University of Alabama, in cooperation with Texas A&M University, Mississippi State University, University of Mississippi, and Wayne Stafford and Associates are undertaking a focused, comprehensive, integrated and multidisciplinary study of Upper Jurassic Smackover carbonates (Class II Reservoir), involving reservoir characterization and 3-D modeling and an integrated field demonstration project at Womack Hill Oil Field Unit, Choctaw and Clarke Counties, Alabama, Eastern Gulf Coastal Plain.

The principal objectives of the project are: increasing the productivity and profitability of the Womack Hill Field Unit, thereby extending the economic life of this Class II Reservoir and transferring effectively and in a timely manner the knowledge gained and technology developed from this project to producers who are operating other domestic fields with Class II Reservoirs.

The principal research efforts for Year 2 of the project have been reservoir characterization, which has included three (3) primary tasks: geoscientific reservoir characterization, petrophysical and engineering property characterization, and microbial characterization and recovery technology analysis, which has included 3-D geologic modeling. In the second year, the research focus has primarily been on completion of the geoscientific reservoir characterization and 3-D geologic modeling tasks. This work was scheduled for completion in Year 2.

Overall, the project work is on schedule. Geoscientific Reservoir Characterization has been completed. Petrophysical and Engineering Characterization and Microbial Characterization are essentially on schedule with minor problems with well downhole pressure testing and the acquisition of whole core material. 3-D Geologic Modeling has been completed.

TABLE OF CONTENTS

	Page
Report Page	i
Disclaimer	i
Title Page	ii
Abstract	iii
Table of Contents	iv
Introduction	1
Executive Summary	8
Experimental	13
Work Accomplished in Year 2	13
Work Planned in Year 3	142
Results and Discussion	150
Conclusions	157
References	161

INTRODUCTION

Pruet Production Co. and the Center for Sedimentary Basin Studies at the University of Alabama, in cooperation with Texas A&M University, Mississippi State University, University of Mississippi, and Wayne Stafford and Associates are undertaking a focused, comprehensive, integrated and multidisciplinary study of Upper Jurassic Smackover carbonates (Class II Reservoir), involving reservoir characterization and 3-D modeling and an integrated field demonstration project at Womack Hill Oil Field Unit, Choctaw and Clarke Counties, Alabama, Eastern Gulf Coastal Plain (Fig. 1).

Estimated reserves for Womack Hill Field are 119 million barrels of oil. During the production history of the field, which began in 1970, 30 million barrels of oil have been produced. Conservatively (additional 10-20 percent), another 12 to 24 million barrels of oil remains to be recovered through the application of advanced technologies in optimizing field management and production. Womack Hill Field is one of 57 Smackover fields in the regional peripheral fault trend play of the eastern Gulf Coastal Plain. To date, 674 million barrels of oil have been produced from these fields. The fields in this play have a common petroleum trapping mechanism (faulted salt anticlines), petroleum reservoir (ooid grainstone and dolograinstone shoal deposits), petroleum seal (anhydrite), petroleum source (microbial carbonate mudstones), overburden section, and timing of trap formation and oil migration. Therefore, the proposed work at Womack Hill Field is directly applicable to these 57 fields and can be transferred to Smackover fields located along this fault trend from Florida to Texas.

Phase I (3.0 years) of the proposed research involves characterization of the shoal reservoir at Womack Hill Field to determine reservoir architecture, heterogeneity and producibility in order to increase field productivity and profitability. This work includes core and well log analysis; sequence stratigraphic, depositional history and structure study; petrographic and diagenetic study; and pore system analysis. This information will be integrated with 2-D seismic data and probably 3-D seismic data to produce an integrated 3-D stratigraphic and structural model of the reservoir at Womack Hill Field. The results of the reservoir characterization and modeling will be integrated

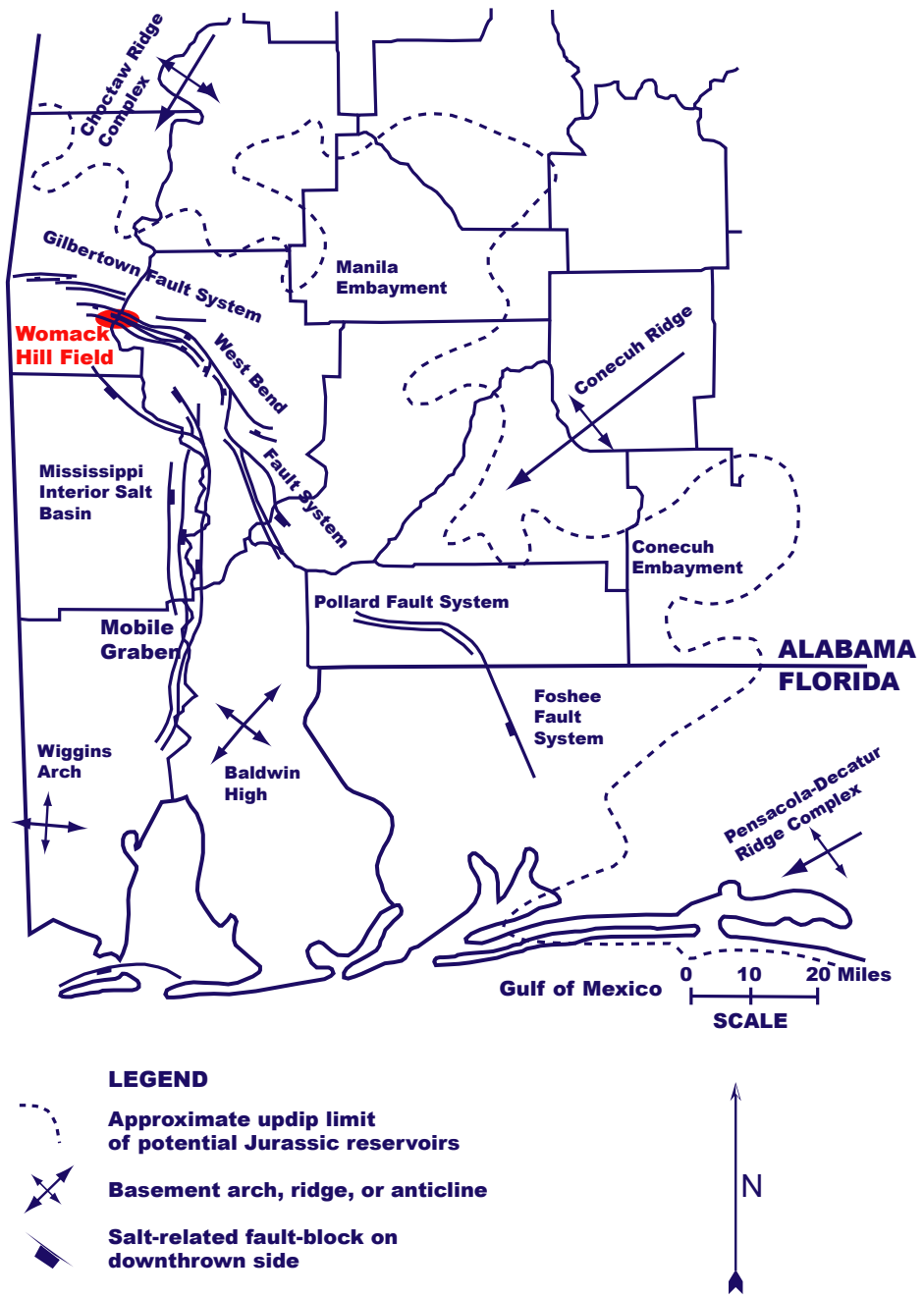

Figure 1. Regional setting and location of Womack Hill Oil Field

with petrophysical and engineering data and pressure communication analysis to perform a 3-D reservoir simulation of the field reservoir. The results from the reservoir characterization and modeling will also be used in determining whether undrained oil remains at the crest of the Womack Hill structure (attic oil), in assessing whether it would be economical to conduct strategic infill drilling in the field, and in determining whether the acquisition of 3-D seismic data for the field area would improve recovery from the field and is justified by the financial investment. Parallel to this work, engineers are characterizing the petrophysical and engineering properties of the reservoir, analyzing the drive mechanism and pressure communication (through well performance data), and developing a 3-D reservoir simulation model. Further, the engineering team members will determine what, if any, modifications should be made to the current pressure maintenance program, as well as assess what, if any, other potential advanced oil recovery technologies are applicable to this reservoir to extend the life of the field by increasing and maintaining productivity and profitability. Also, in this phase, researchers are studying the ability of *in-situ* micro-organisms to produce a single by-product (acid) in the laboratory to determine the feasibility of initiating an immobilized enzyme technology project at Womack Hill Field Unit.

Phase II (2.5 years) of the proposed research will proceed along three lines if the results from Phase I justify the continuance of this work. Line 1 involves the integration of the 3-D seismic imaging of the structure and reservoir into the 3-D geologic model to assess the merits of conducting a strategic infill drilling program in the field, including drilling in the interwell area and a crestal well, and if new well(s) are drilled assess by using fracture identification log technology whether a lateral-multilateral completion for these wells would be successful. Line 2 involves integrating the data obtained from the 3-D seismic imaging, petrophysical and engineering data acquired from drilling new wells using lateral-multilateral well completions, and the results of the analysis of the well performance data (field/well pressure and rate histories). These integrated data will be used to refine the 3-D reservoir simulation model, implement modifications to the pressure maintenance program, and initiate any additional activities, such as further infill drilling and/or advanced oil technology applications to improve recovery. Line 3 involves confirming the ability of

in-situ micro-organisms to produce a single by-product (acid) and injecting nutrients into the field reservoir to sustain the cells rather than to support cell proliferation for initiation of the immobilized enzyme technology project .

Phase III (0.5 year) of the proposed project involves monitoring the enhanced pressure maintenance program and advanced technology application project, and evaluating the viability of entering existing field wells for lateral-multilateral well completions to improve field productivity and profitability. Also, the immobilized enzyme technology project will be monitored to evaluate the impact of this technique on overall oil recovery from the field.

The objectives of this project are as follows:

1. Increase the productivity and profitability of the Womack Hill Field Unit, thereby extending the economic life of this Class II Reservoir and enhancing National economic and energy security.
2. Demonstrate the feasibility of transferring the knowledge gained and technology developed from previous studies of Class II Reservoirs to the analysis of the Womack Hill shallow shelf (ramp) carbonate reservoir.
3. Demonstrate to producers in the Eastern Gulf Region the significance and procedures for developing an integrated reservoir approach based on geological, geophysical, petrophysical, and well performance data, highlighting reservoir characterization activities and utilizing 3-D reservoir simulation as mechanisms for making decisions regarding field operations, such as selecting well locations for strategic infill drilling, identifying wells for recompletion (and/or simulation), as well as for constructing and implementing programs of reservoir surveillance.
4. Demonstrate to producers in the Eastern Gulf Region the value of 3-D reservoir simulation in the design, implementation, and maximizing of a pressure maintenance program, including optimization of injection wells, well locations, and injection-production balancing, and the value of chemistry and chemical agents that can be used to improve injection conformance and increase oil recovery.

5. Demonstrate the usefulness of 3-D seismic imaging in defining the productive limits of the reservoir.
6. Demonstrate the value and utility of strategically targeted infill drilling to improve the productivity and profitability of heterogeneous carbonate reservoirs, including drilling wells that are optimal in the sense of location, well completion components, and well stimulation.
7. Demonstrate the usefulness of lateral-multilateral well completions in naturally fractured carbonate reservoirs to increase reservoir producibility.
8. Demonstrate the utility of an immobilized enzyme technology project to increase oil recovery effectiveness and efficiency.
9. Transfer the knowledge gained, technology developed and successes and failures of this project to producers who are operating other fields with Class II Reservoirs through technology workshops, presentations at professional meetings, and publications in scientific and trade journals.
10. Contribute to the knowledge base on carbonate sequence stratigraphy, depositional systems, lithofacies analysis, diagenesis, and pore systems and to the understanding of carbonate reservoir architecture, heterogeneity and producibility, carbonate petroleum systems, fluid-rock interactions, petrophysical properties of carbonates, reservoir drive mechanisms and pressure communication in carbonates, immobilized enzyme recovery process, 3-D seismic imaging in carbonates, lateral-multilateral well completions in fractured carbonate reservoirs, and the dynamics of effective and balanced pressure maintenance in heterogeneous grainstone and dolograinstone reservoirs.

The principal problem at Womack Hill Field is productivity and profitability. With time, there has been a decrease in oil production from the field, while operating costs in the field continue to increase. In order to maintain pressure in the reservoir, increasing amounts of water must be injected annually. These problems are related to cost-effective, field-scale reservoir management, to reservoir connectivity due to carbonate rock architecture and heterogeneity, to pressure

communication due to carbonate petrophysical and engineering properties, and to cost-effective operations associated with the oil recovery process.

Improved reservoir producibility will lead to an increase in productivity and profitability. To increase reservoir producibility, a field-scale reservoir management strategy based on a better understanding of reservoir architecture and heterogeneity, of reservoir drive and communication and of the geological, geophysical, petrophysical and engineering properties of the reservoir is required. Also, an increased understanding of these reservoir properties should provide insight into operational problems, such as why the reservoir is requiring increasing amounts of freshwater to maintain the desired reservoir pressure, why the reservoir drive and oil-water contact vary across the field, how the multiple pay zones in the field are vertically and laterally connected and the nature of the communication within a pay zone.

Several potential opportunities have been identified which could lead to increased reservoir productivity. First, the drilling of the Dungan Estate Unit 14-5 well in Sec. 14, T.10N., R.2W. suggests that undrained oil (attic) may be present on the crest of the Womack Hill Field structure. The 14-5 well encountered oil in the Norphlet and Smackover at a horizon that previously was not productive in the field. These productive zones were structurally higher in this well then encountered in any of the field wells prior to the drilling of the 14-5 well.

Second, field scale heterogeneity affects the producibility of the reservoir. A major barrier to flow separates the field reservoir into a western portion and an eastern portion and results in structural compartmentalization in Womack Hill Field. This flow barrier dramatically impacts production strategy in the field. Only the western portion of the field has been unitized and only this part of the reservoir is experiencing pressure maintenance. The reservoir drive mechanism in the eastern portion of the field is a strong bottom-up water drive, while the drive mechanism in the western portion of the field is primarily solution gas. This flow barrier has been interpreted to be a major fault (megascopic heterogeneity) or change in permeability. If the barrier to flow is a result of lower permeability, the reduction in permeability could be due to a change in mesoscopic heterogeneity (depositional facies change), a change in microscopic heterogeneity (diagenetic

change), or a combination of the two processes. Also, there are multiple shoal lithofacies in the field. The nature of the communication among and within these multiple pay zones is unclear at this time. Carbonate depositional systems involve the complex interaction of biological, chemical and physical processes. Further, the susceptibility of carbonates to alteration by early to late diagenetic processes dramatically impacts reservoir heterogeneity. Diagenesis is the fundamental influence in determining which carbonate deposits will become seals, which will become reservoirs, and what the nature of the reservoir quality and producibility will be. Reservoir characterization and the study of heterogeneity, therefore, becomes a major task because of the physiochemical and biological origins of carbonates and because of the masking of the depositional rock fabric and reservoir architecture principally due to dolomitization. Thus, greater lithofacies and/or diagenetic variability (greater reservoir heterogeneity) translates into more difficulty in predicting between wells (interwell areas) at any spacing but particularly at Womack Hill Field were the well spacing is as great as 120 acres.

Third, prior investigations have suggested that Smackover carbonate reservoirs should be naturally fractured at depths of 11,000 ft. Therefore, well completions, such as lateral-multilateral completions, that utilize the fractured nature of these carbonates should lead to increased producibility of the field.

Fourth, understanding and accurately predicting the flow units and barriers to flow in this heterogeneous reservoir is vital to improving producibility. An enhanced pressure maintenance program, advanced oil recovery application, and/or immobilized enzyme technology project that accounts for inherent properties of this heterogeneous reservoir, multiple pay zones, and the nature of the variable drive mechanisms and oil-water contacts in the field should result in increased producibility of Womack Hill Field. The improved connectivity in this compartmentalized reservoir should result in the production of more incremental oil.

The project will build on the experiences and lessons learned from the previous Class II Reservoir studies. Techniques, methods and technologies utilized in previous studies will be applied and modified accordingly for application to the Womack Hill reservoir. These technologies and techniques include reservoir characterization and modeling, reservoir simulation, 3-D seismic

imaging, infill drilling, horizontal/lateral drilling, and waterflood design for Class II reservoirs. The particular advanced technologies applied will include developing an integrated geoscientific and engineering digital database for Womack Hill Field, characterizing the Smackover reservoir and modeling (in 3-dimensions) these heterogeneous carbonates for cost-effective management of the reservoir on a fieldwide scale and for making decisions regarding field operations. These data and this modeling will be integrated with petrophysical properties of the reservoir, field pressure and production data, and other engineering information and used in 3-D reservoir simulation to evaluate the effectiveness of the existing pressure maintenance program and to assess the viability of initiating other advanced oil recovery applications in the field. These data and 3-D geologic modeling will also be utilized in developing an infill drilling strategy for this heterogeneous reservoir.

The project results will be vigorously transferred to producers through five technology workshops in project Years 4, 5 and 6. The first workshop (Year 4) will focus on the results of Phase I of the project and will include carbonate reservoir characterization, data integration, carbonate reservoir modeling, and 3-D reservoir simulation. The second workshop (Year 5) will focus on aspects of the integrated field demonstration project and will include the results of the 3-D seismic imaging and the new wells drilled in the field. Workshops 3, 4 and 5 (Year 6) will focus on the results of using lateral-multilateral well completions in the field, results of the enhanced pressure maintenance program and advanced oil recovery application project, and the results of the immobilized enzyme technology project. These workshops will be conducted in cooperation with the Eastern Gulf Region (EGR) of the Petroleum Technology Transfer Council (PTTC).

EXECUTIVE SUMMARY

Pruet Production Co. and the Center for Sedimentary Basin Studies at the University of Alabama, in cooperation with Texas A&M University, Mississippi State University, University of Mississippi, and Wayne Stafford and Associates are undertaking a focused, comprehensive, integrated and multidisciplinary study of Upper Jurassic Smackover carbonates (Class II Reservoir), involving reservoir characterization and 3-D modeling and an integrated field

demonstration project at Womack Hill Oil Field Unit, Choctaw and Clarke Counties, Alabama, Eastern Gulf Coastal Plain.

Phase I (3.0 years) of the proposed research involves characterization of the shoal reservoir at Womack Hill Field to determine reservoir architecture, heterogeneity and producibility in order to increase field productivity and profitability. This work includes core and well log analysis; sequence stratigraphic, depositional history and structure study; petrographic and diagenetic study; and pore system analysis. This information will be integrated with 2-D seismic data and probably 3-D seismic data to produce an integrated 3-D stratigraphic and structural model of the reservoir at Womack Hill Field. The results of the reservoir characterization and modeling will be integrated with petrophysical and engineering data and pressure communication analysis to perform a 3-D reservoir simulation of the field reservoir. The results from the reservoir characterization and modeling will also be used in determining whether undrained oil remains at the crest of the Womack Hill structure (attic oil), in assessing whether it would be economical to conduct strategic infill drilling in the field, and in determining whether the acquisition of 3-D seismic data for the field area would improve recovery from the field and is justified by the financial investment. Parallel to this work, engineers are characterizing the petrophysical and engineering properties of the reservoir, analyzing the drive mechanism and pressure communication (through well performance data), and developing a 3-D reservoir simulation model. Further, the engineering team members will determine what, if any, modifications should be made to the current pressure maintenance program, as well as assess what, if any, other potential advanced oil recovery technologies are applicable to this reservoir to extend the life of the field by increasing and maintaining productivity and profitability. Also, in this phase, researchers are studying the ability of *in-situ* micro-organisms to produce a single by-product (acid) in the laboratory to determine the feasibility of initiating an immobilized enzyme technology project at Womack Hill Field Unit.

The principal problem at Womack Hill Field is productivity and profitability. With time, there has been a decrease in oil production from the field, while operating costs in the field continue to increase. In order to maintain pressure in the reservoir, increasing amounts of water must be

injected annually. These problems are related to cost-effective, field-scale reservoir management, to reservoir connectivity due to carbonate rock architecture and heterogeneity, to pressure communication due to carbonate petrophysical and engineering properties, and to cost-effective operations associated with the oil recovery process.

Improved reservoir producibility will lead to an increase in productivity and profitability. To increase reservoir producibility, a field-scale reservoir management strategy based on a better understanding of reservoir architecture and heterogeneity, of reservoir drive and communication and of the geological, geophysical, petrophysical and engineering properties of the reservoir is required. Also, an increased understanding of these reservoir properties should provide insight into operational problems, such as why the reservoir is requiring increasing amounts of freshwater to maintain the desired reservoir pressure, why the reservoir drive and oil-water contact vary across the field, how the multiple pay zones in the field are vertically and laterally connected and the nature of the communication within a pay zone.

The principal research efforts for Year 2 of the project have been reservoir characterization, which has included three (3) primary tasks: geoscientific reservoir characterization, petrophysical and engineering property characterization, and microbial characterization and recovery technology analysis, which has included 3-D geologic modeling. In the second year, the research focus has primarily been on completion of the geoscientific reservoir characterization and 3-D geologic modeling tasks. This work was scheduled for completion in Year 2.

Geoscientific Reservoir Characterization has been completed. The upper part of the Smackover Formation is productive from carbonate shoal complex reservoirs that occur in vertically stacked heterogeneous porosity cycles (A, B, and C). The cycles typically consist of carbonate mudstone/wackestone at the base and ooid and oncoidal grainstone at the top. The carbonate mudstone/wackestone lithofacies has been interpreted as restricted bay and lagoon sediments, and the grainstone lithofacies has been described as beach shoreface and shoal deposits. Porosity has been enhanced through dissolution and dolomitization. The grainstone associated with Cycle A is dolomitized (upper dolomitized zone) in much of the field area. Although Cycle A is present across

the field, its reservoir quality varies laterally. Dolomitization (lower dolomitized zone) can be pervasive in Cycle B, Cycle C and the interval immediately below Cycle C. Cycle B and Cycle C occur across the field, but they are heterogeneous in depositional texture and diagenetic fabric laterally. Porosity is chiefly solution-enlarged interparticle, grain moldic and dolomite intercrystalline pores with some intraparticle and vuggy pores. Pore systems dominated by intercrystalline pores have the highest porosities. Median pore throat aperture tends to increase with increasing porosity. Probe permeability strongly correlates with median pore throat aperture, and tortuosity increases with increasing median pore throat aperture. Larger tortuosity and median pore throat aperture values are associated with pore systems dominated by intercrystalline pores.

Petrophysical and Engineering Characterization is on schedule except for a delay in well downhole pressure testing. Extensive efforts have been made to integrate and correlate the core and well log data for the field. Reservoir permeability has been correlated with core porosity, gamma ray well log response, and resistivity well log response. The petrophysical data have been segregated into flow units prescribed by the geological data, and for the data in these flow units a histogram of core porosity and the logarithm of core permeability were prepared. These histograms yield statistical measures, such as the mean and median values, which will be used to develop spatial distributions and to provide data for the numerical simulation model. Evaluation of production, injection and shut-in bottomhole pressure data for the field have been interpreted and analyzed using appropriate mechanisms, such as decline type curve analysis and estimated ultimate recovery analysis. The volumetric results are relevant as virtually every well yielded an appropriate signature for decline type curve analysis. However, a discrepancy in the estimate of total compressibility for this system has arisen, and the absolute volumetric results will need to be revised. The estimation of flow properties, such as permeability and skin factor has emerged as a problematic issue because little early time data, which are required for this analysis, are available. Therefore, the results of these analyses should be considered qualitative. The correlation of estimated ultimate recovery and the Nc_{+}- product is consistent suggesting that a strong relationship exists between contacted oil-in-place and recovery.

Microbial Characterization is on schedule with the recent acquisition of Smackover core material from south Alabama. Initially water samples and core samples taken from wells in the Womack Hill Field yielded no micro-organisms capable of growing at 90˚C. This result was due to a combination of factors, including the fact that the core samples were exposed to air for decades and the equipment necessary to maintain an anaerobic environment was inadequate. Well cuttings from the Smackover Formation acquired from a field near Womack Hill Field were analyzed for micro-organisms. Growth of micro-organisms was evident in the samples prepared from these well cuttings in association with oil from the Womack Hill Field. These organisms consumed ethanol and are presumed to produce carbon dioxide or the gas was derived from organic acids produced from the oil reacting with carbonate. These findings suggest that micro-organisms capable of producing acetic acid from ethanol have a high probability of being present in Womack Hill Field and of being induced to grow and be metabolically active at the subsurface temperature in the reservoir.

A 3-D Geologic Model has been constructed for the Womack Hill Field structure and reservoir(s). The 3-D geologic modeling shows that the petroleum trap is more complex than originally interpreted. The geologic modeling indicates that the trap in the western part of the field is a fault trap with closure to the south against the fault, and that the trap in the central and eastern parts of the field is a faulted anticline trap with four-way dip closure. The pressure difference between wells in the western and central parts of the field and wells in the eastern part of the field may be attributed to a flow barrier due to the presence of a north-south trending fault in the field area. The modeling shows that the Smackover reservoirs are heterogeneous. Four reservoir intervals are identified in the field area: Cycle A, Cycle B, Cycle C, and the interval immediately below Cycle C. A permeability barrier to flow is present potentially between the western and eastern parts of the field.

EXPERIMENTAL

Overview

The principal research efforts for Year 2 of the project have been reservoir characterization, which has included three (3) primary tasks: geoscientific reservoir characterization, petrophysical and engineering property characterization, and microbial characterization and recovery technology analysis, which has included 3-D geologic modeling. In the second year, the research focus has primarily been on completion of the geoscientific reservoir characterization and 3-D geologic modeling tasks (Table 1). This work was scheduled for completion in Year 2.

Work Accomplished in Year 2

Task RC-1. Geoscientific Reservoir Characterization

Description of Work.--This task is designed to characterize reservoir architecture, pore systems and heterogeneity based on geological and geophysical properties (Tables 1 and 2).

Rationale. Reservoir characterization is fundamental to determining reservoir architecture, pore systems, and heterogeneity. It is critical in the design of a cost-effective fieldwide reservoir management strategy and for making sound operational decisions. Deformational (structural), depositional, and diagenetic processes exert the major influences on reservoir quality and evolution and produce heterogeneities at various scales. To predict accurately changes in reservoir quality, heterogeneity, and producibility in interwell areas, it is crucial to characterize and understand the processes that produce carbonate rock textures and the diagenetic fluid-rock interactions that have altered the primary rock fabric and pore system.

This task has been completed and the data and results from this work have been presented in the Year 1 Report for this project and are presented herein.

Core Description.--Reservoir characterization begins with core description and analysis. Six slabbed cores from Womack Hill field were described following the methodology of Bebout and Loucks (1984). Graphic logs were constructed for each of the cores (Figs. 2 through 7). One hundred eighteen thin sections were cut from the cores, with care taken to sample all diagenetic and stratigraphic changes. In addition, 66 thin sections were available from the Alabama State Oil and

Table 1

Milestone Chart—Project

Task	Year/Quarter																							
	2000			2001				2002				2003				2004				2005				
Phase I	2	3	4	1	2	3	4	1	2	3	4	1	2	3	4	1	2	3	4	1	2	3	4	1
1. Reservoir Characterization																								
Task RC-1—Geoscientific	xxxxxxxxxxx																							
Task RC-2—Petrophysical and engineering			xxxxxxxxxxx																					
Task RC-3—Microbial			xxxxxxxxxxx																					
Task RC-4—Data integration					xxxxxxxx																			
2. Recovery Technology Analysis																								
Task RTA-1—3-D Geologic model							xxxxxxxx																	
Task RTA-2—3-D Simulation									xxxxxxxx															
Task RTA-3—Core experiments									xxxxxxxx															
3. Recovery Technology Evaluation																								
Task RTE-1—3-D Seismic										xxxxxxxx														
Task RTE-2—Pressure maintenance												xx												
Task RTE-3—IET concept												xx												
4. Decision to Implement Demonstration Projects												x												

Table 2
Milestone Chart—Year 2

Tasks (Phase I)	M	J	J	A	S	O	N	D	J	F	M	A
Reservoir Characterization												
Geoscientific	xxxxxxxxxx											
Petrophysical and Engineering	xxxxxxxxxxxxxxxxxxxxx											
Microbial	xxxxxxxxxxxxxxxxxxxxx											
Data Integration	xxxxxxxxxxxxxxxxxxxxxxxxxxxxxxxx											
Recovery Technology Analysis												
3-D Geologic Model									xxxxxxxxxxxxxxx			

Work Planned
Work Accomplished xx

Well: Counselman 18-12

Logged By: W. A. Tedesco

Stratigraphic Interval: Smackover Formation 11460 - 11540

Date: January 10, 2001

Depth (ft.)	Pore Type	Mineral Composition (Incl. Porosity) 0% 50% 100%	Structures	Texture	Fabric	Grain Size (mm)	Color	Cement	Comments
11460	BC			Peloidal	WS	.004 - .25	B	D	
	WP BP M V WP BP M V			Oolitic	GS	.004 - 4.0	G	C	Anhydrite laths Very fossiliferous: algae, pelecypods,gastropods, echinoids, crinoids
				Oolitic Peloidal	GS	.004 - 4.0	B	C	Anhydrite healed pores Echinoids and pelecypods
11470		No Recovery							
	WP BP M V M BP			Oolitic Peloidal	PS WS	.004 - 1.0	B	C	Interbedded Packstone and Wackestone Wackestone lamina seem more dolomitized
11480	M BP M BP BP BP		Shale Partings	Oolitic Peloidal	WS	.004 - .5	DG	C	Pelecypod shell frags.
				Peloidal	WS	.004 - .125	DG	C	Anhydrite along shale partings
		No Recovery							
11490	M BP M BP M BP BC			Peloidal	WS	.004 - .25	G	C	Anhydrite filled molds
				Oolitic Peloidal	PS	.004 - 1.0	LB	C	Algae and Pelecypods common
11500	BC BC BC		Shale Partings	Peloidal	MS	.004 .062 .004 - 1.0	B LB	C	Silty Large anhydrite healed molds of oncoids & pelecypods
11510		No Recovery							
	V M BP			Peloidal	MS	.004 .062	LB	C	Anhydrite laths common
11520	V M BP		Vague Bedding	Oncoidal Peloidal	WS	.004 - 1.0	LB	C	Algae & Pelecypods
		No Recovery							
	BC BC			Micritic	MS	.004 - .125	LG	C	Anhydritic
11530	BC M BC M BC M		Shale Partings	Oncolitic	WS	.004 - 1.0	LG	C	Numerous oncoids
		No Recovery							
	BC BC		Shale Partings	Peloidal	MS	.004 - 1.0	LG	C	Anhydrite vugs and pelecypod shell frags Selective dolomitization of rare grains
11540									

Figure 2. Graph of the core for the 18-12 well.

KEY

Mineral Composition

Porosity

Calcite

Dolomite

Anhydrite

Pore Types

BP - Interparticle
WP - Intraparticle
BC - Intercrystalline
M - Moldic
F - Fenestral
FR - Fracture
V - Vuggy

Carbonate Fabrics

MS - Micrite
WS - Wackestone
PS - Packstone
GS - Grainstone

Structures

Stylolite

Fracture

Brecciation

Bedding

Streaky Laminations

Ripple Marks

Vertical Burrow

Horizontal Burrow

Cross-Bedding

Cements

C - Calcite
D - Dolomite
A - Anhydrite

Colors

G - Gray
B - Brown
W - White

Color Modifiers

L - Light
D - Dark
M - Mottled
VD - Very Dark

Well: Scruggs, Parker, Norton 9-14

Logged By: W. A. Tedesco

Stratigraphic Interval: Smackover Formation, 11402 - 11555

Date: August 15, 2000

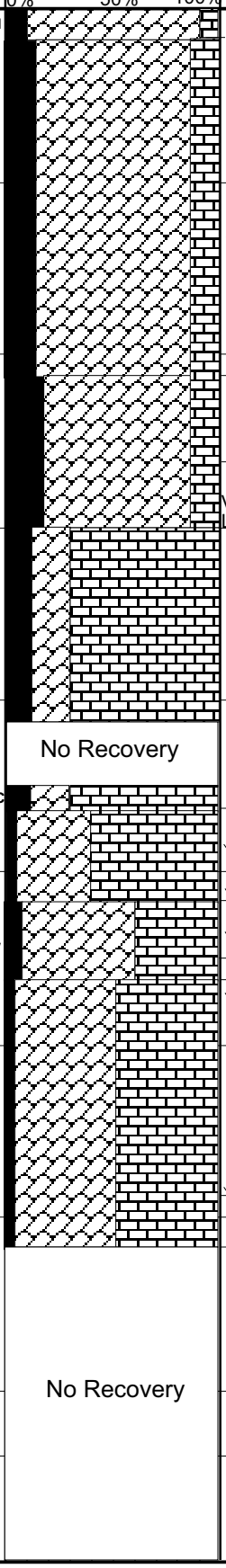

Depth (ft.)	Pore Type	Structures	Texture	Fabric	Grain Size (mm)	Color	Cement	Comments
11402	WP, M		Peloidal	WS	.004 - .25	LG	D	Anhydrite filled vugs
	WP BC	Shale Partings				B		
	WP BC							
11412	WP BC	Cloudy, Shale Partings	Peloidal Pelletal	WS	.004 - .125	MGB	D	
	WP BC							
11422	BC WP M		Ooid Pelletal Peloidal	WS	.004 - .25	B	D	
	BC	Vague Laminations	Peloidal	MS	.004 - .062	DG	D	
11432	BC							Anhydrite healed vugs
	BP	Shale Partings, Cloudy	Ooid Pelletal Peloidal	WS	.004 - .125	MG	C	
	BC							
11442	No Recovery							
	WP BC					DG		
	WP	Shale Partings	Ooid Peloidal	PS	.004 - .25	DG	C	
11452	WP							
	BC V	Cloudy	Pelletal	WS	.004 - .125	B	D	Shaley
	BC V							
	BC		Peloidal	MS	.004 - .031	VDG	D	Poor Recovery
	BC							
11462	BC	Shale Partings	Peloidal	WS	.004 - .062	LB	D	Poor recovery through bottom of core segment (11473)
11472	BC		Peloidal	MS	.004 - .031	LG	D	
11482								

Figure 3. Graph of the core for the 9-14 well.

Well: Scruggs. Parker. Norton 9-14

Logged By: W. A. Tedesco

Stratigraphic Interval: Smackover Formation 11402 - 11555

Date: August 15, 2000

Depth (ft.)	Pore Type	Mineral Composition (Incl. Porosity) 0% 50% 100%	Structures	Texture	Fabric	Grain Size (mm)	Color	Cement	Comments
11492		No Recovery							
	BC		Shale Partings	Peloidal	WS	.004 - .062	DG	C	Very Shaley Increasing Organics
	BC, F								
11502	BP			Ooid Peloidal Pelletal	WS	.004 - .062	DG	C	Crumbly till top of cored segment (11495)
	BC		Shale Partings	Pelletal	WS	.004 - .062	LB	D	
11512	BC		Vague Laminations	Pelletal	WS	.004 - .125	DB	D	Significant Oil Stain
	BC								
11522	BC		Vague Laminations	Pelletal	WS	.004 - .125	DB	D	Interbedded brown/gray laminations
	BC			Peloidal	MS	.004 - .031	LG	D	
11532	BC		Shale Partings Vague Laminations	Peloidal	WS	.004 - .125	LB	D	Shaley, vague laminations
	BC			Peloidal Pelletal	WS	.004 - .062	DG	D	Shaley, vague laminations
11542	BC		Shale Partings Vague Laminations	Peloidal Pelletal	WS	.004 - .125 .004 - .062	G G	D	Shaley, vague laminations
11552									
11555									

Figure 3 (continued). Graph of the core for the 9-14 well.

Well: Turner 13-25

Logged By: W. A. Tedesco

Stratigraphic Interval: Buckner Anhydrite / Smackover Formation 11421 - 11451

Date: August 16, 2000

Depth (ft.)	Pore Type	Mineral Composition (Incl. Porosity) 0% 50% 100%	Structures	Texture	Fabric	Grain Size (mm)	Color	Cement	Comments
11421			Shale Partings	Chickenwire Anhydrite	--	--	W	A	Buckner Anhydrite Sabkha
11431				Sucrosic	MS	.004 - .125	G	D	Pyrite Common
	M BC		Cloudy						
	M BC		Shale Partings	Peloidal Oolitic	WS	.004 - .5	B	D	Oomoldic Porosity
11441	M BC								
	M BC								
				Micrite	MS	.004 - .031	DG	D	Silty
	WP M			Oolitic Peloidal	PS	.004 - .5	G	C	
	WP M								
	WP M			Algal Oolitic	BS/GS	.004 - .5	G	C	Top Patch Reef?
11451									

Figure 4. Graph of the core for the 13-25 well.

Well: Turner 13-5

Stratigraphic Interval: Smackover Formation 11318 - 11500

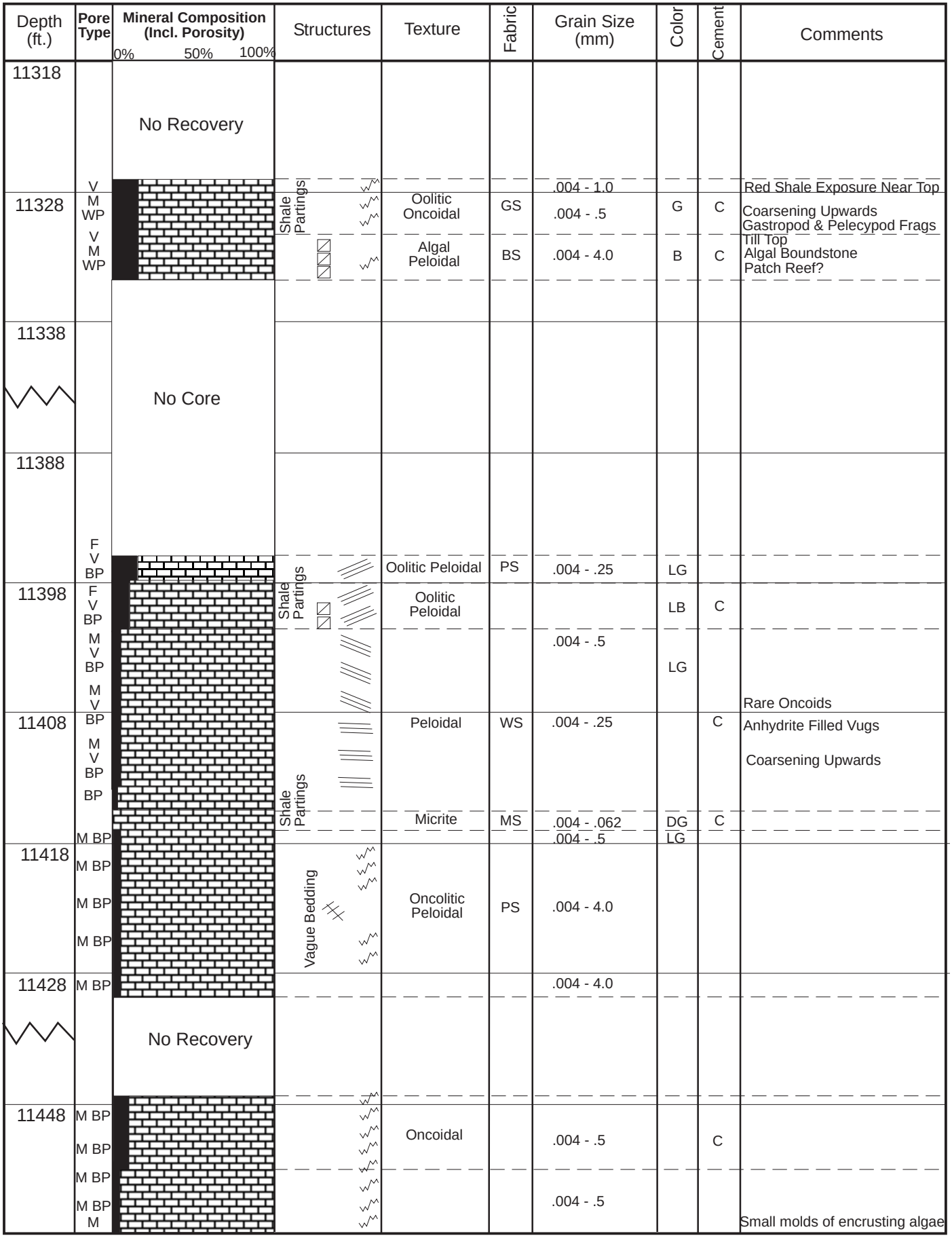

Figure 5. Graph of the core for the 13-5 well.

Well: Turner 13-5

Logged By: W. A. Tedesco

Stratigraphic Interval: Smackover 11318 - 11500

Date: August 16, 2000

Depth (ft.)	Pore Type	Mineral Composition (Incl. Porosity) 0% 50% 100%	Structures	Texture	Fabric	Grain Size (mm)	Color	Cement	Comments
11458	M M WP M WP			Peloidal	WS	.004 - .25	LG	C	Many small molds of round colonial algae
11468		No Recovery							
	M			Oncolitic					Abundant large oncoids
11478	M M			Peloidal	WS	.004 - 4.0	G	C	and rounded colonial algae
				Peloidal	MS	.004 - .062	DG	C	
	M			Anhydritic Peloidal	WS	.004 - .5	DG	C	Abundant Anhydrite Vugs
11488				Peloidal	MS	.004 - .062	DG	C	Anhydrite laths along laminations
11498									Vague laminations
11508									

Figure 5 (continued). Graph of the core for the 13-5 well.

Well: Turner 13-6

Logged By: W. A. Tedesco

Stratigraphic Interval: Smackover Formation 11400 - 11525

Date: August 15, 2000

Depth (ft.)	Pore Type	Mineral Composition (Incl. Porosity) 0% 50% 100%	Structures	Texture	Fabric	Grain Size (mm)	Color	Cement	Comments
11400	V			Oolitic	GS	.031 - 1.0	G	C	cross-bedded
	WP			Oolitic Peloidal	PS	.031 - .25	LB	C	
	M								
	V			Peloidal	WS	.004 - .062	LB	C	
	WP								
	M								
	V			Oolitic Peloidal	PS	.031 - .5	LB	C	
	WP								
11410	M			Oolitic Peloidal	WS	.031 - .25	LB	C	
	V								
	WP								
	M								
	V			Oolitic Peloidal	GS	.031 - .5	LB	C	
	WP								
	M								
11420	V								
	WP								
	BP			Oolitic Peloidal	PS	.004 - .25	LB	C	Some ooids dolomitized
		No Recovery	Shale Parting						
11430	V			Oolitic Peloidal	PS	.004 - .25	LB	C	Some ooids dolomitized
	WP								
	BP								
	BP			Oolitic Peloidal	WS	.004 - .25	LG	C	Some ooids dolomitized
	BP								
	BP								
11440		No Recovery							
11450	M			Oolitic Peloidal Skeletal	WS	.004 - .5	G	C	Pelecypod shell fragments common
	WP								
	V								
	M								
	WP								
	V								
	M								
	WP								
	V								
11460	M WP			Oolitic Peloidal	WS	.004 - .5	MG	C	Oncoids and pelecypods
	M WP								Bioturbated
	M WP								
	WP			Oolitic Peloidal	PS	.004 - .5	LB	C	Oncoids
	M								
	BP								
	WP								
11470	WP			Peloidal	WS	.004 - .5	LB	C	Oncoids
	WP								
	WP			Peloidal	GS	.004 - .5	LB	C	Oncoids
	FR								
	WP			Peloidal	WS	.004 - .5	LB	C	
	WP								
	WP F								
11480	WP			Oolitic Peloidal	WS	.004 - .25	LG	C	Oncoids and pelecypods
	WP								
		No Recovery							

Figure 6. Graph of the core for the 13-6 well.

Well: Turner 13-6

Logged By: W. A. Tedesco

Stratigraphic Interval: Smackover Formation 11400 - 11525

Date: August 15, 2000

Depth (ft.)	Pore Type	Mineral Composition (Incl. Porosity) 0% 50% 100%	Structures	Texture	Fabric	Grain Size (mm)	Color	Cement	Comments
11490		No Recovery							
	WP			Peloidal	WS	.004 - .25	LB	C	
	WP								
11500	WP								
	WP		Shale Partings	Peloidal	PS	.031 - .5	G	C	Healed fractures off of stylolite Pelecypods and oncoids
	WP								
	WP BP			Oolitic Peloidal	WS	.031 - .5	DG	C	
11510	WP BP			Peloidal	WS	.004 - .125	LG	C	
		No Recovery							
	WP BP V					.004 - .25			
11520	WP BP V		Shale Partings	Oolitic Peloidal	WS	.004 - .125	LG	C	Oncoids
11530									

Figure 6 (continued). Graph of the core for the 13-6 well.

Well: Womack Hill Field Unit 14-5 #2

Logged By: W. A. Tedesco

Stratigraphic Interval: Smackover Formation 11115 - 11206

Date: August 14 - 15, 2000

Depth (ft.)	Pore Type	Mineral Composition (Incl. Porosity) 0% 50% 100%	Structures	Texture	Fabric	Grain Size (mm)	Color	Cement	Comments
11115			Shale Partings	Ooilitic Intraclasts	WS	.004 - 4.0	LG	C	Red Shale - Exposure Surface Dense Limestone
	M WP V			Oolitic Peloidal Oncoidal	PS	.062 - .5	LB	D	Anhydrite Laths Pelecypods, Gastropods, Oncoids, and Forams Finger Stromatolite
11125	M WP V M WP V		Cloudy	Oolitic	GS	.031 - .5	MGB	C	Dissolution Surface? Large Anhydrite Nodules Bitumen healed fracture
11135	WP M WP M WP M		Shale Partings Cloudy	Oolitic Peloidal	WS	.004 - .5	LB	D	Shaley Resembles Lagoonal Depositional Environment Shaley
11145	WP M WP M			Oolitic Peloidal	PS	.004 - 1.0 .004 - .5 .031 - .25	LB G	D C	Vague cross-laminations pelecypods
11155	WP M M Wp V			Oolitic	GS	.125 - 1.0	G	C	Numerous Pelecypods
11165	WP M WP M WP M			Oolitic Peloidal Peloidal	PS WS	.004 - 1.0 .004 - 1.0	LB LB	D D	Small Nautiloid Fossil
11175	M WP V WP BC V			Peloidal	MS	.004 - .25	DB	D	Pelecypods and Gastropods Pelecypods, Gastropods, Oncoids
11185	BC BC BC		Faint Laminations	Peloidal	WS	.004 - .5	DB	D	Chert Nodules Bioturbation, Oncoids Fabric probably destroyed
11195 11206	BC BC V BP V		Faint Laminations Shale Partings	Peloidal	MS	.004 - .25 .004 - .5	LB	D	Oncoids Finely Laminated

Figure 7. Graph of the core for the 14-5 #2 well.

Gas Board. Thin section petrography was conducted using standard-sized, polished thin sections, with one half of each section stained with Alizarin Red-S and Potassium ferricyanide. Thin sections were described using a Nikon microscope and Swift Model F point counter. Stable carbon and oxygen isotopic analysis were conducted at the Stable Isotope Laboratory of the University of Miami Resensteil School of Marine and Atmospheric Science following standard procedures and are reported relative to the Peedee Belemnite standard (PDB). Reproducibility for isotope data is better than 0.05 ‰ for oxygen and better than 0.1 ‰ for carbon. Cathodoluminescence petrography was conducted on polished thin sections using a Technosyn Cold Cathode Luminescence Model 8200 MK II with a 450 – 550 nA current, 15-20 kw KV, and a 0.05 torr vacuum. Detailed component microsampling was done using a JEOL 733 Superprobe. Probing was completed with an accelerator voltage of 15 kV, 12 nA sample current and a 10 µ spot.

Well Log Study.--Electrical and geophysical well logs were obtained and analyzed for 42 wells within and immediately adjacent to Womack Hill Field (Fig. 8) and core analysis for 24 cores in the field area were studied. Log types studied include resistivity, compensated neutron, bulk density, gamma ray, SP, and acoustic. Compensated neutron, bulk density and resistivity logs were used to pick and distinguish the Smackover, Buckner, and Norphlet units. Three upward-shoaling cycles in the upper Smackover Formation (labeled A, B, and C) were also determined and picked on all logs (Fig. 9). These picks were correlated across the field and used to create cross-sections (Fig. 10). Core descriptions were also added to the logs, allowing correlation of rock types, facies, and reservoir units across the field. The core data were calibrated to the well log patterns to establish electrofacies for correlation, mapping and modeling.

The three shallowing-upward cycles (A, B, and C) (Fig. 11) are generally composed of a basal peloidal carbonate mudstone, overlain by peloidal wackestone. The tops of each cycle are comprised of peloidal to ooid packstone and are capped by ooid and oncoidal grainstone. The cycles suggest a gradual regression of sea level. There are general increases in porosity, permeability, and dolomite toward the tops of each cycle suggesting some stratigraphic control on reservoir development at Womack Hill Field.

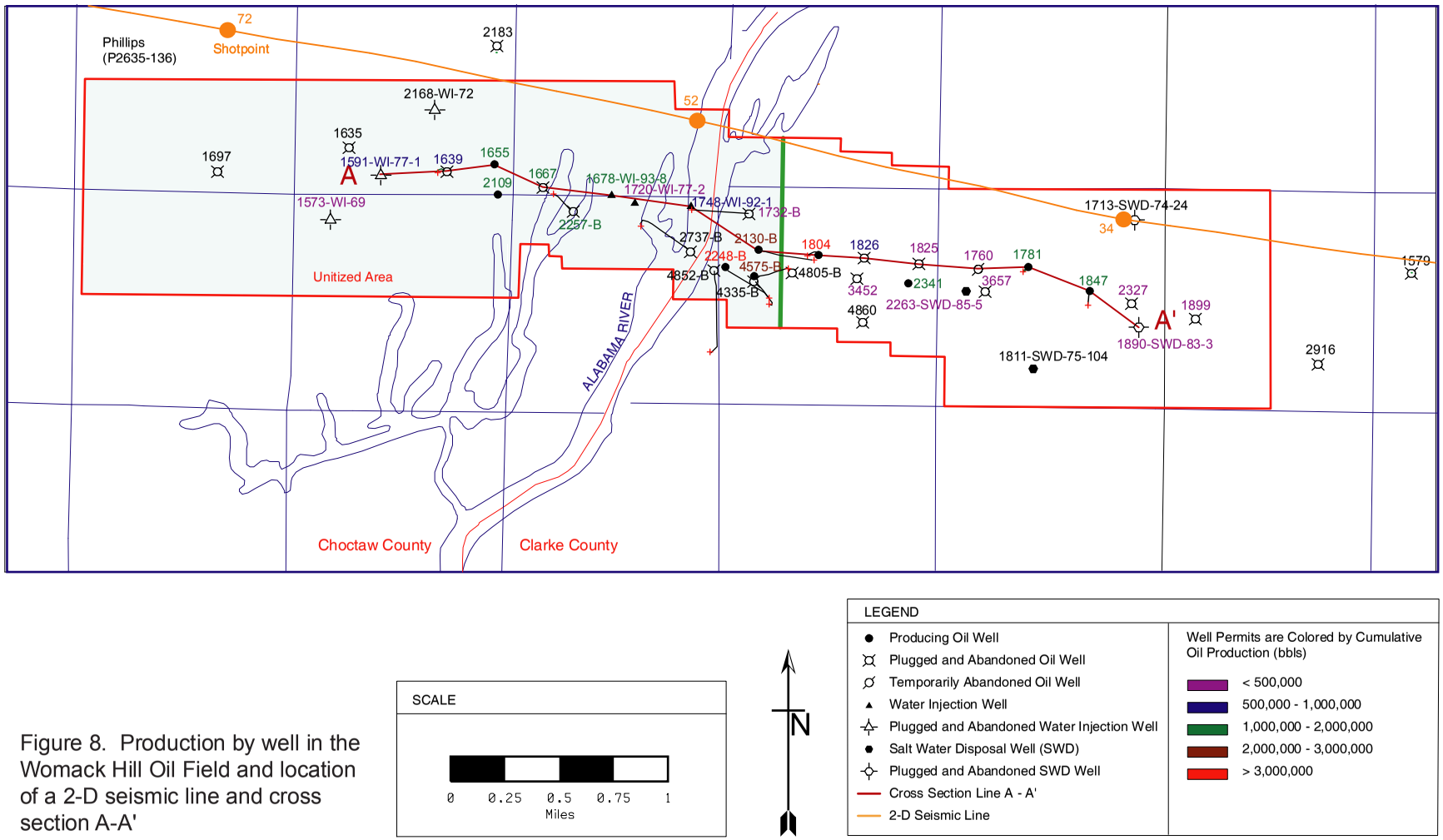

Figure 8. Production by well in the Womack Hill Oil Field and location of a 2-D seismic line and cross section A-A'

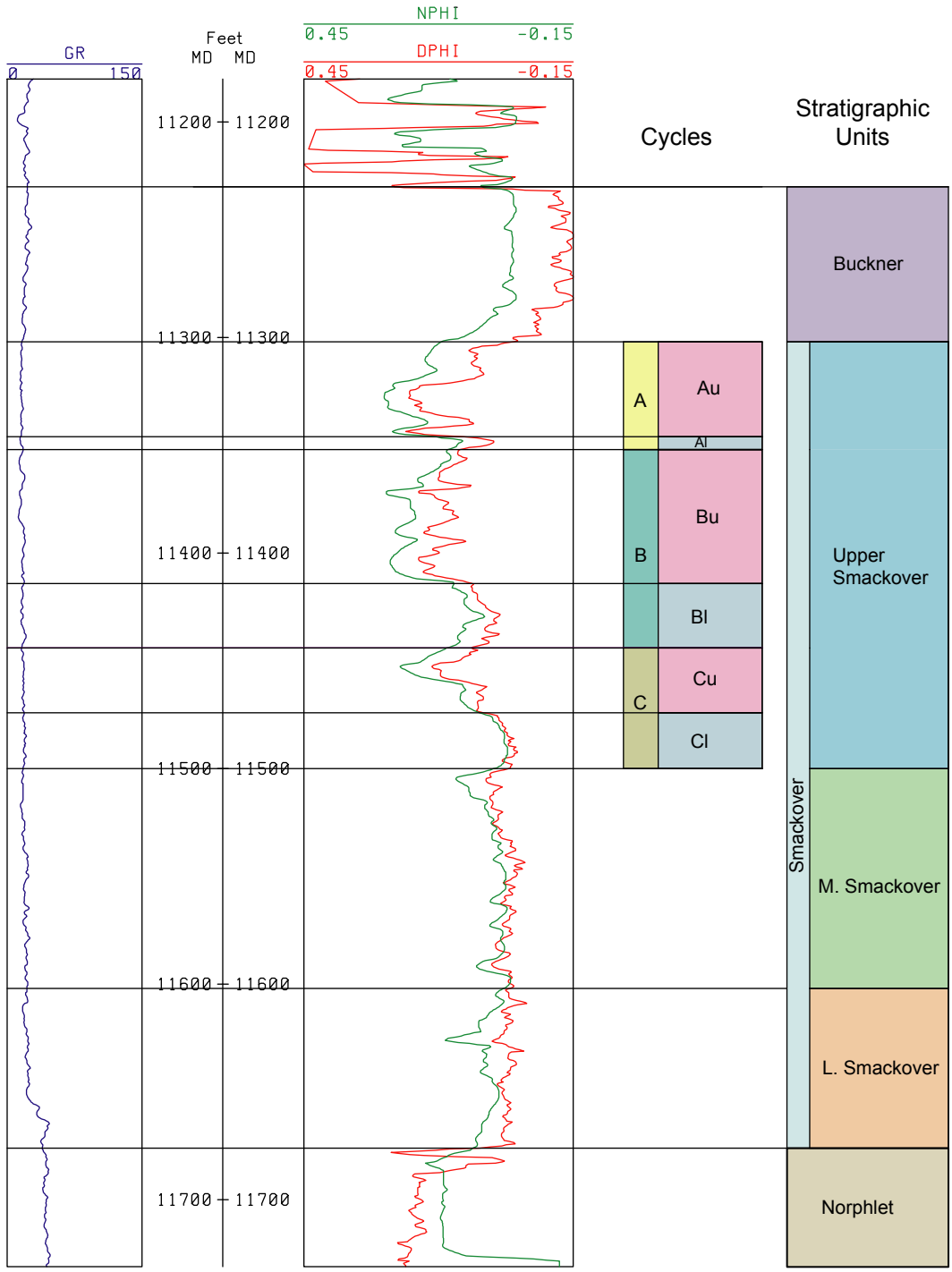

Figure 9. Well log patterns of the Louise Locke 10-14 well (Permit #1667) illustrating Smackover stratigraphic units and upper Smackover cycles at Womack Hill Oil Field. GR=gamma ray log, NPHI=neutron porosity log, DPHI=density porosity log; Au=upper Cycle A, Al=lower Cycle A, Bu=upper Cycle B, Bl=lower Cycle B, Cu=upper Cycle C, Cl=lower Cycle C. See Figure 8 for location of well.

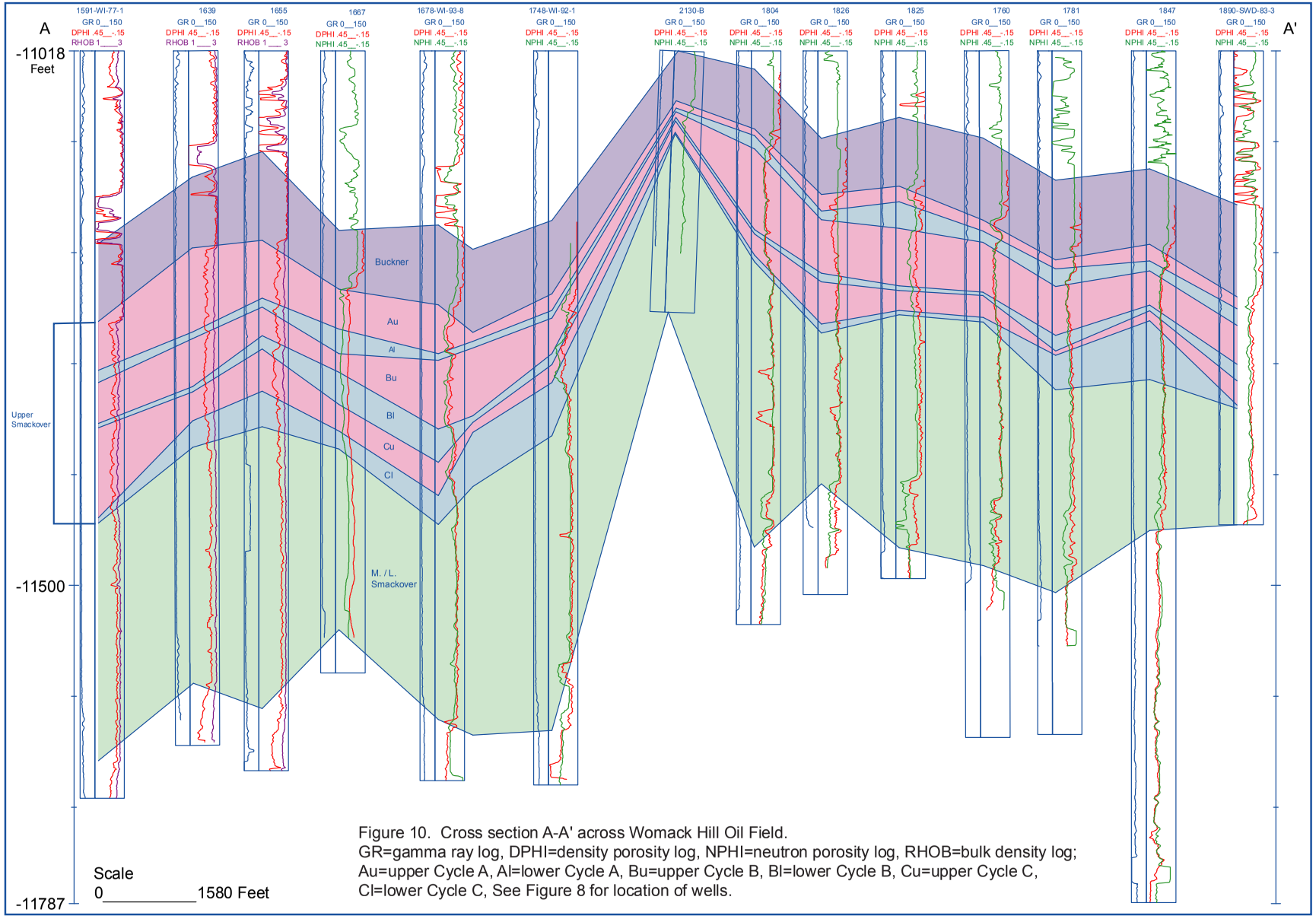

Figure 10. Cross section A-A' across Womack Hill Oil Field.
GR=gamma ray log, DPHI=density porosity log, NPHI=neutron porosity log, RHOB=bulk density log;
Au=upper Cycle A, Al=lower Cycle A, Bu=upper Cycle B, Bl=lower Cycle B, Cu=upper Cycle C,
Cl=lower Cycle C, See Figure 8 for location of wells.

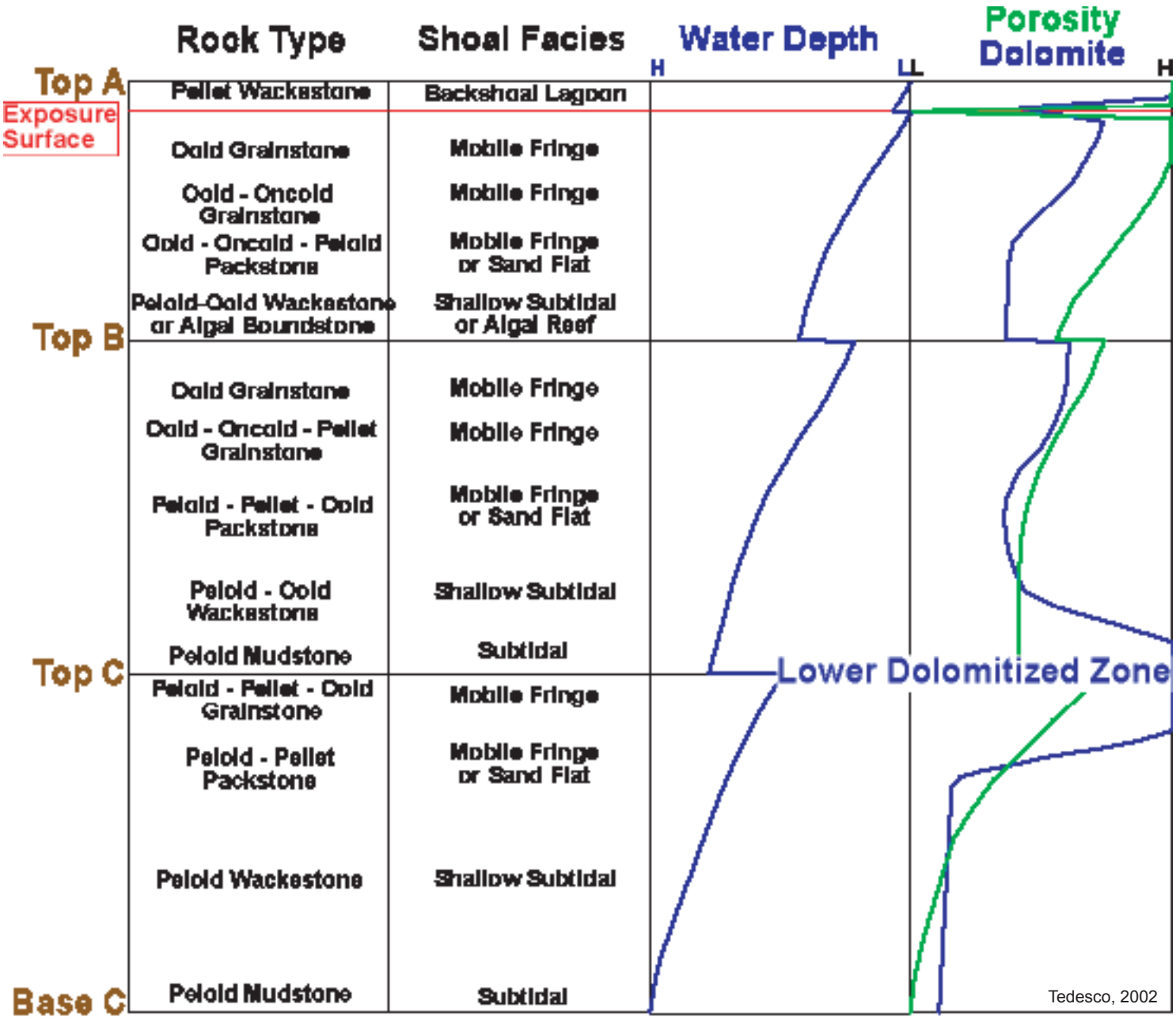

Figure 11. Idealized cycle facies in Upper Smackover at Womack Hill Field. Each cycle comprised of an upward-shallowing sequence of facies on an ooid shoal. Porosity, permeability and dolomite percents generally increase towards the top of each cycle. Location of lower dolomitized zone idealized for a well near the crest of the field structure. Upper dolomitized zone at top of Cycle A.

Two completely dolomitized zones (Fig. 12) were identified and named the upper and lower dolomitized zones. These zones consist of completely dolomitized carbonate rock and are the best reservoir zones at Womack Hill Field. The upper dolomitized zone is found in the upper 10-15 feet of the Smackover Formation, just beneath the Buckner Anhydrite Member. The lower dolomitized zone cuts across depositional lithofacies in the field. This zone is commonly 40 to 50 feet thick and is stratigraphically higher in the structurally lower parts of the field.

Subsurface Mapping.--Several different subsurface maps of the Womack Hill Field have been constructed to assist with analysis of production controls in the field. Structure maps of the top of the Smackover Formation (Fig. 13) and Buckner Anhydrite Member of the Haynesville Formation (Fig. 14) have been made using depths determined from the geophysical logs. Isopach maps of the Smackover (Fig. 15), upper Smackover (Fig. 16), Cycle A (Fig. 17), Cycle B (Fig. 18), and Cycle C (Fig. 19) have been made using log derived thicknesses.

Seismic Interpretation.--Seismic reflection data (2-D) have been acquired from Seismic Exchange, Inc. These data (Fig. 20) were reprocessed by Geo-Seis Processing and interpreted. Figure 8 shows the location of the seismic data acquired.

Petrographic Analysis.--Thin section petrographic analysis is completed. All 184 thin sections available at Womack Hill field have been described. A clasticity index was determined for all thin sections and then compared to porosity and permeability data. Clasticity index is a measure of the largest coated grain present in each sample (Carozzi, 1958; Erwin *et al.*, 1979; Humphrey *et al.*, 1986). In general, a direct relationship with permeability and porosity was found with the clasticity index. With increasing clasticity there is a corresponding increase in porosity and permeability. The only zones not following this trend are zones with complete or near complete fabric-destructive dolomitization. In these zones, clasticity index drops to zero, whereas porosity and permeability increase. At the top of Cycle A, a low clasticity index also correlates well with an exposure surface identified and mapped across the field.

One hundred twenty-two powders for isotope analysis were prepared from thin section butts and core pieces for stable carbon and oxygen isotopic analysis. Sampling ensured that all rock

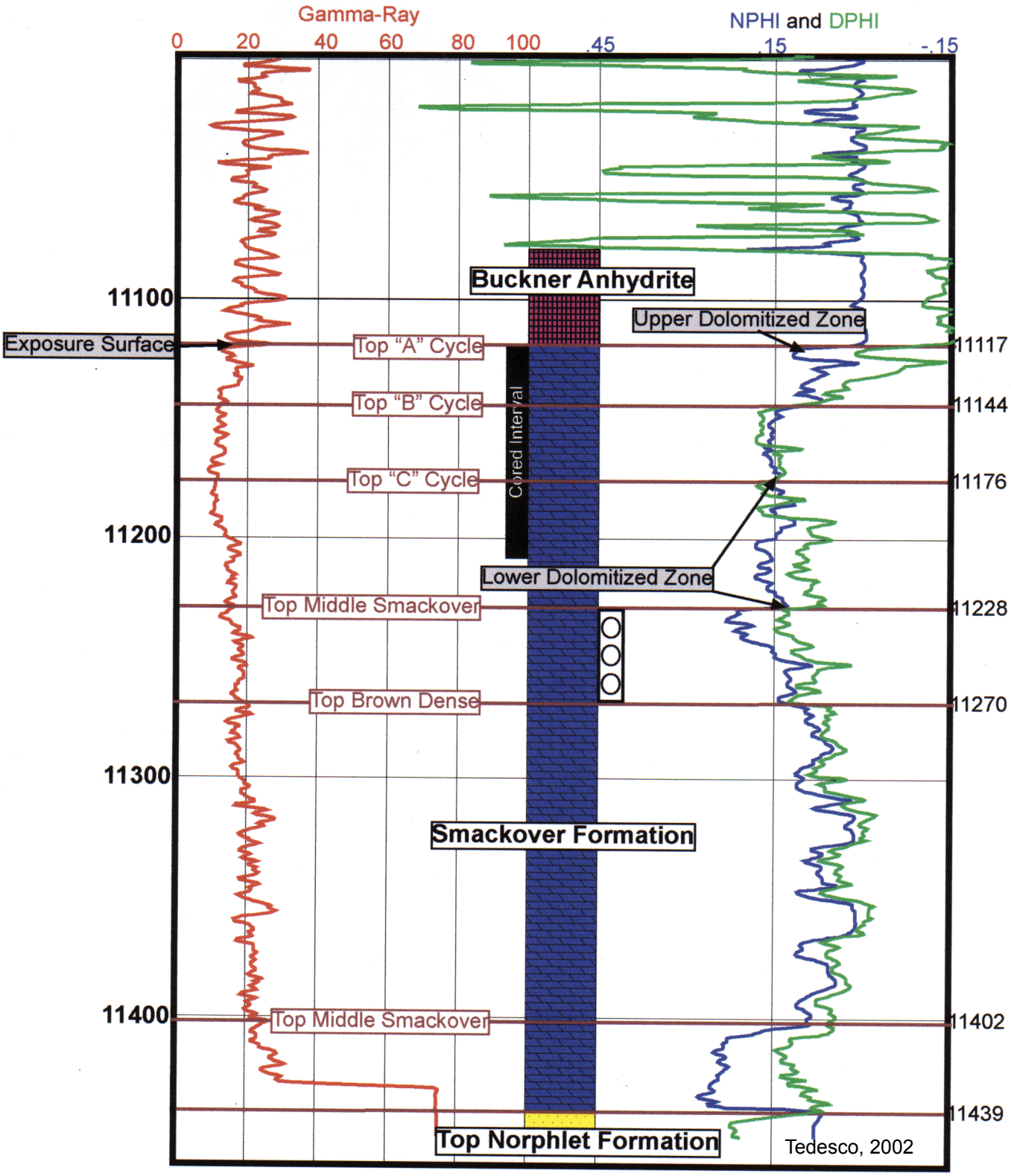

Figure 12. Porosity and gamma-ray logs for Womack Hill Field Unit 14-5 No. 2 well. Formation boundaries and cycles denoted by brown lines. Exposure surface identified at top of Smackover Formation from core data correlates with gamma-ray spike near Buckner-Smackover contact. "Type 1" dolomitizated zone just below exposure. Lower dolomitized zone comprised of "Types 2 & 3" dolomite.

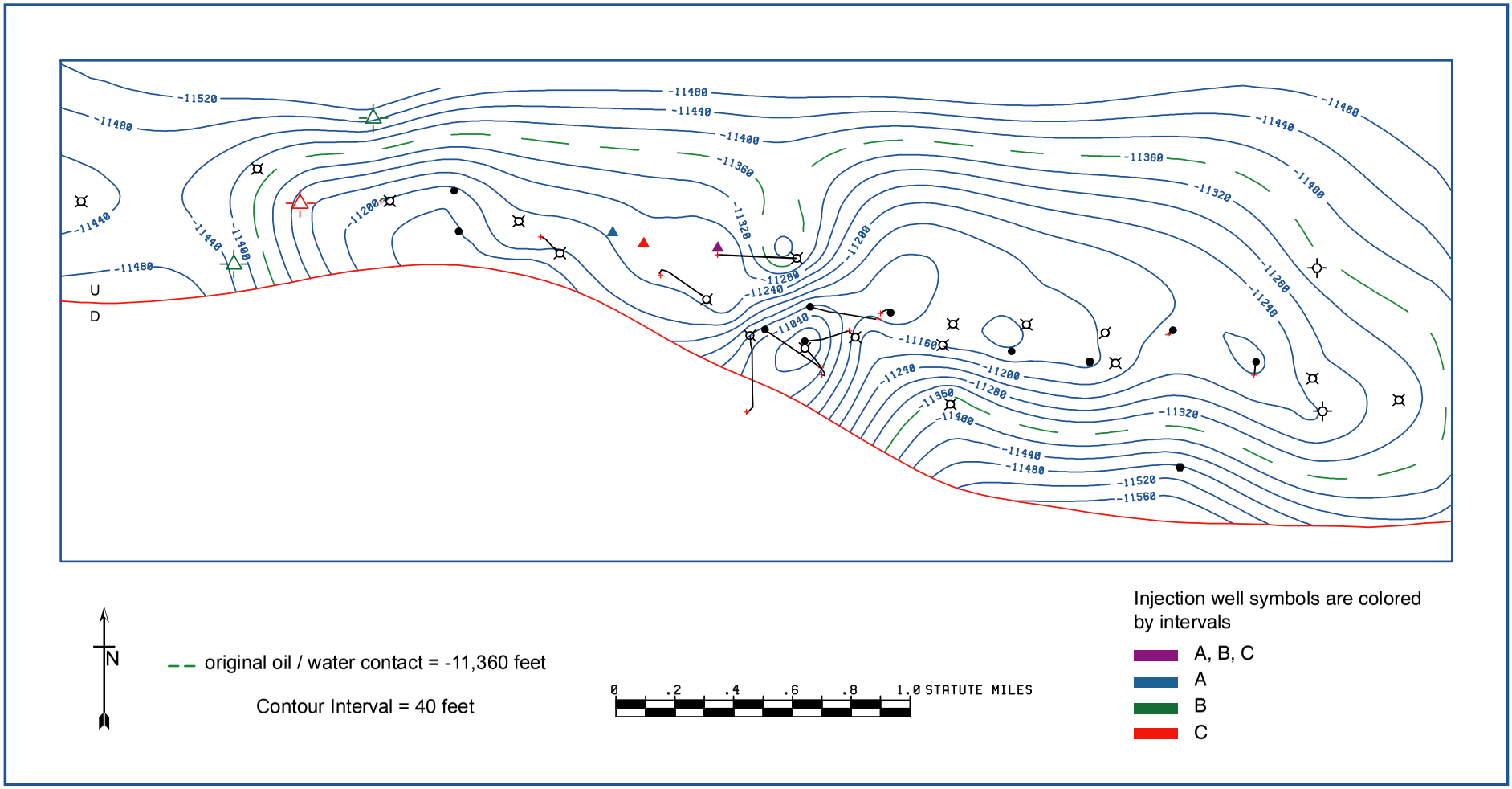

Figure 13. Structure map on top of the Smackover Formation at Womack Hill Oil Field. See Figure 8 for well symbols.

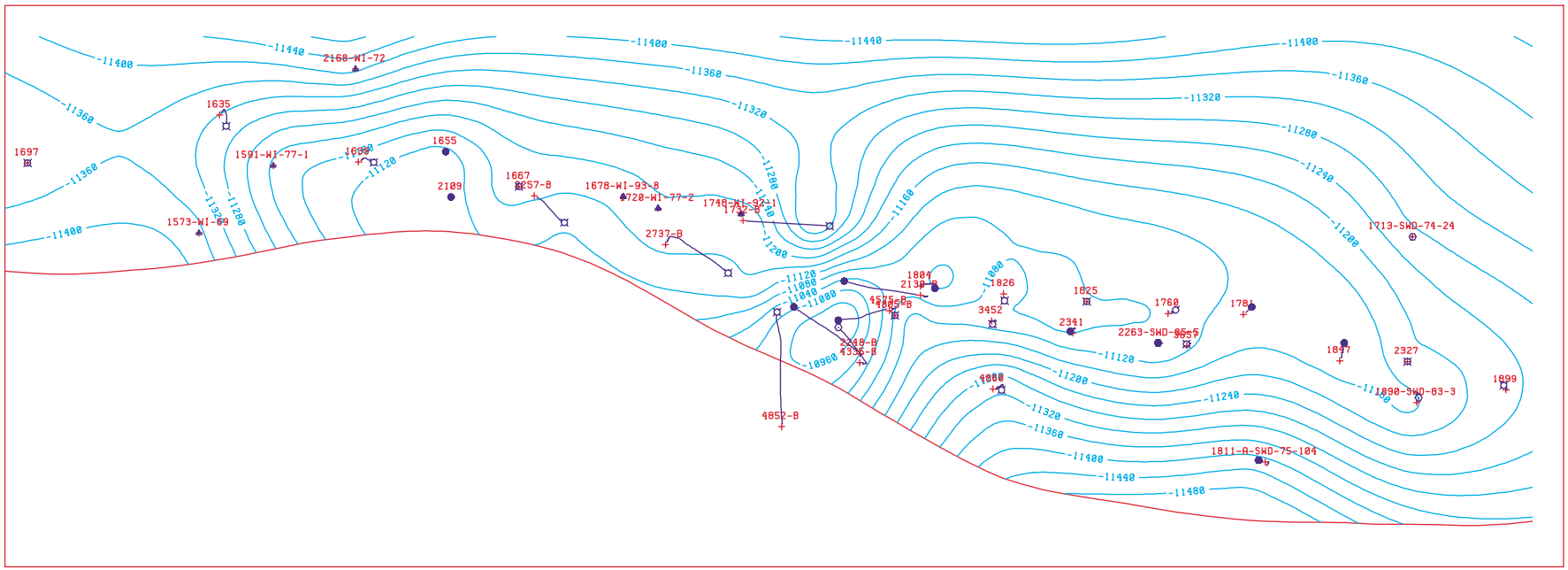

STATUTE MILES 0 .2 .4 .6 .8 1.0 STATUTE MILES

FEET 0 2000 4000 6000 8000 10000 FEET

N

Figure 14. Structure map on top of the Buckner Formation.

Contour Interval = 40 feet

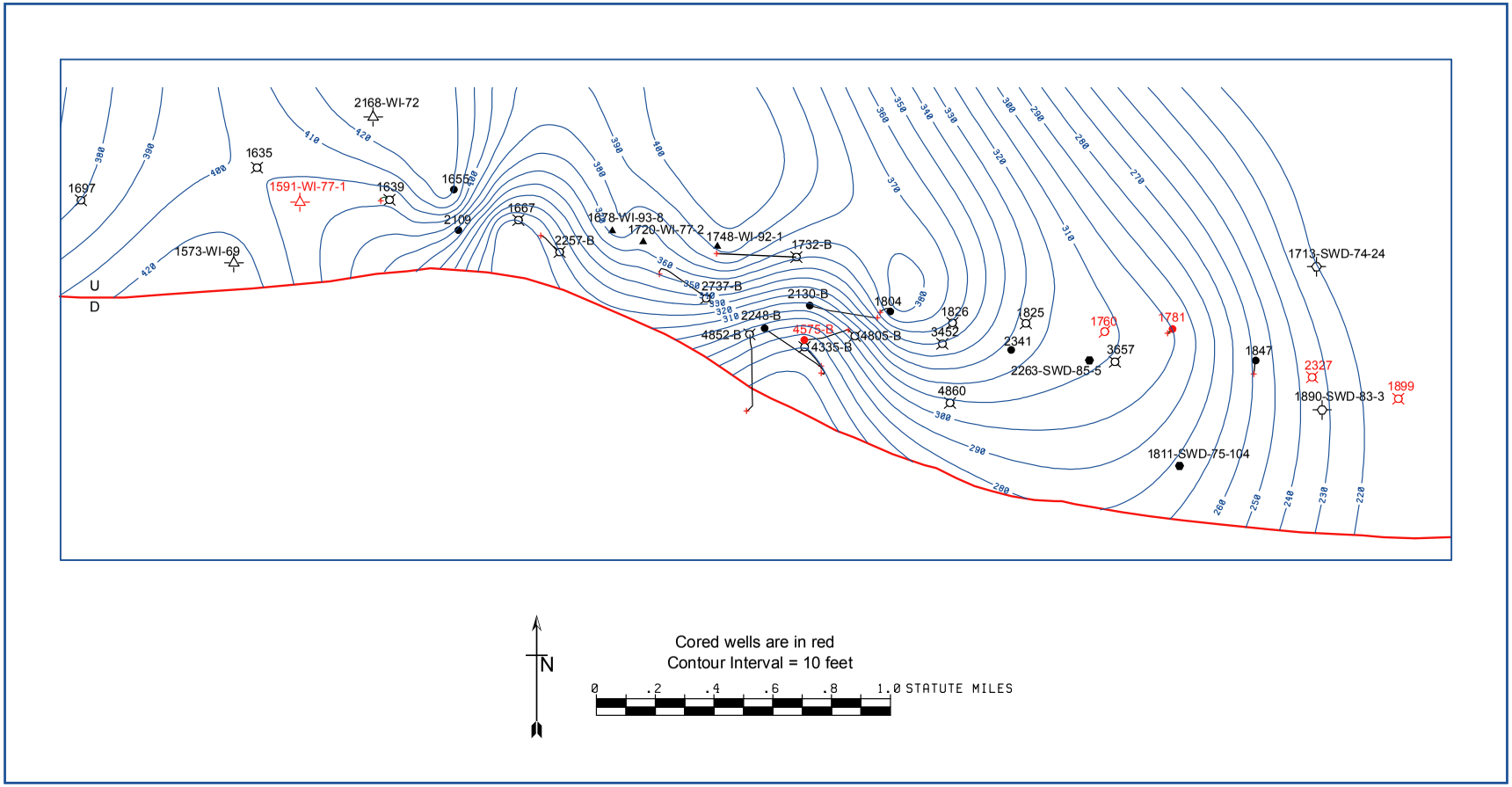

Figure 15. Isopach map of the Smackover Formation at Womack Hill Oil Field.
See Figure 8 for well symbols.

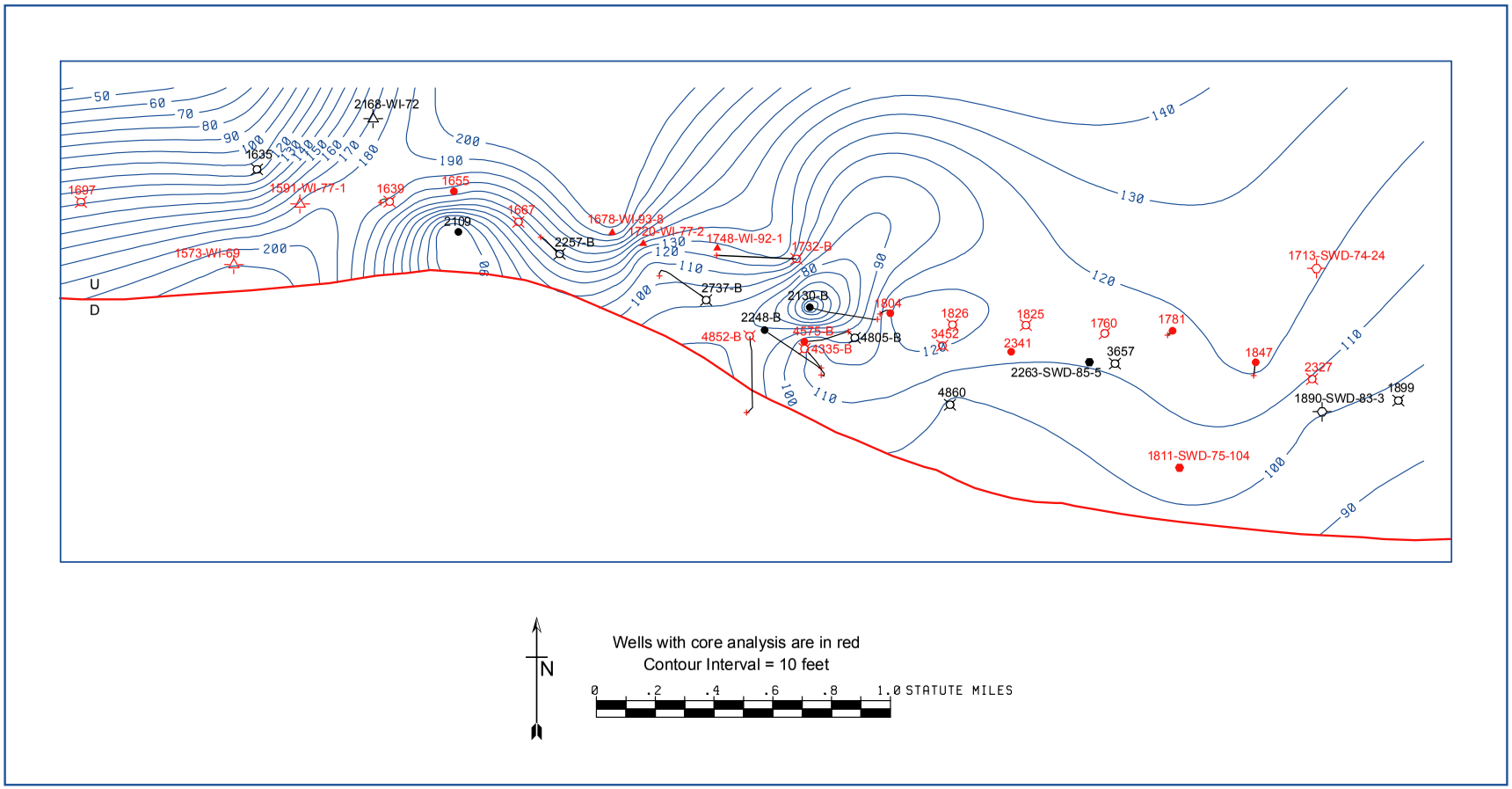

Figure 16. Isopach map of the upper part of the Smackover Formation at Womack Hill Oil Field and location of wells with core analysis data. See Figure 8 for well symbols.

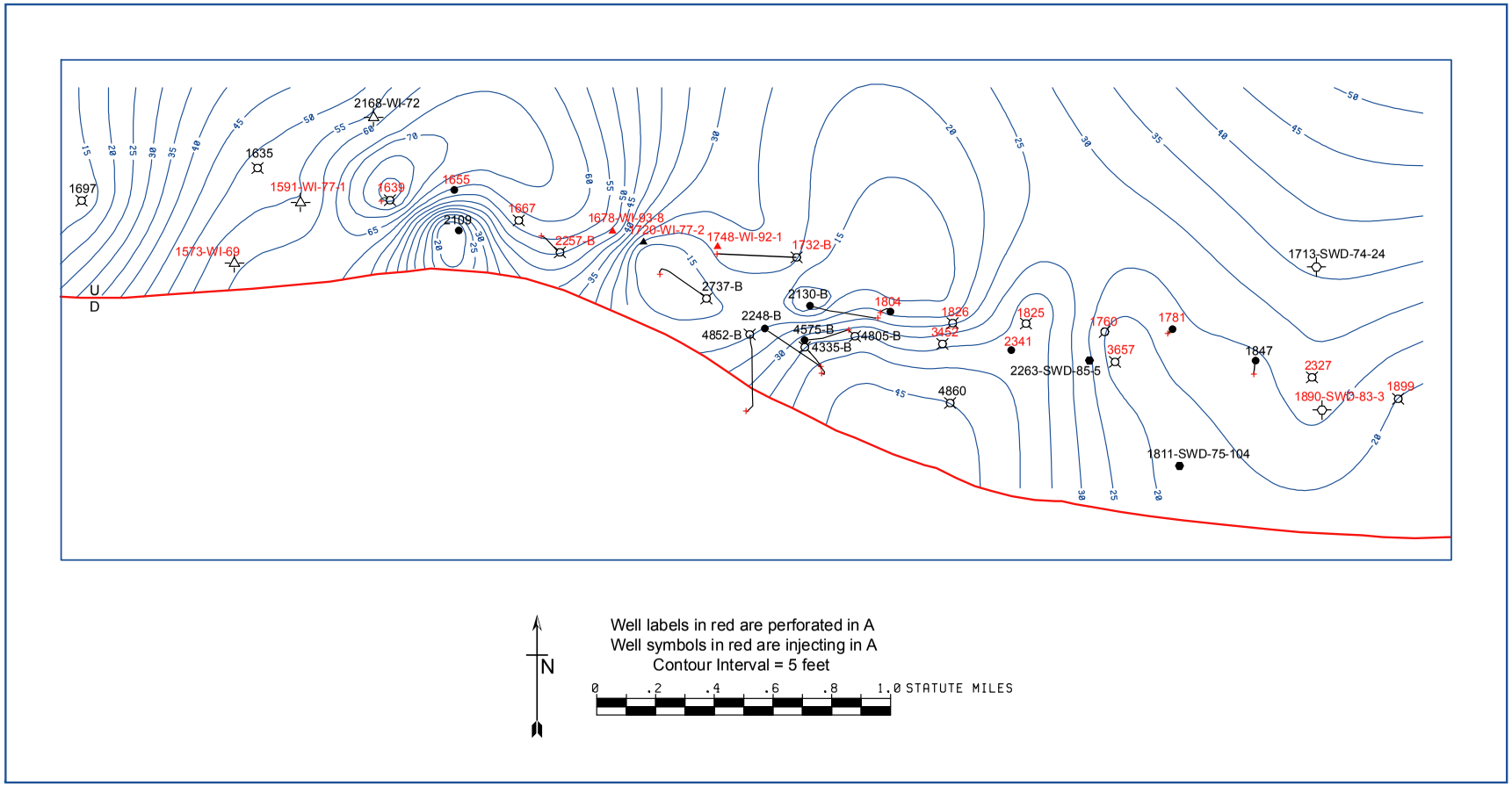

Figure 17. Isopach map of Cycle A and locations of wells perforated in Cycle A and wells injecting water into Cycle A. See Figure 8 for well symbols.

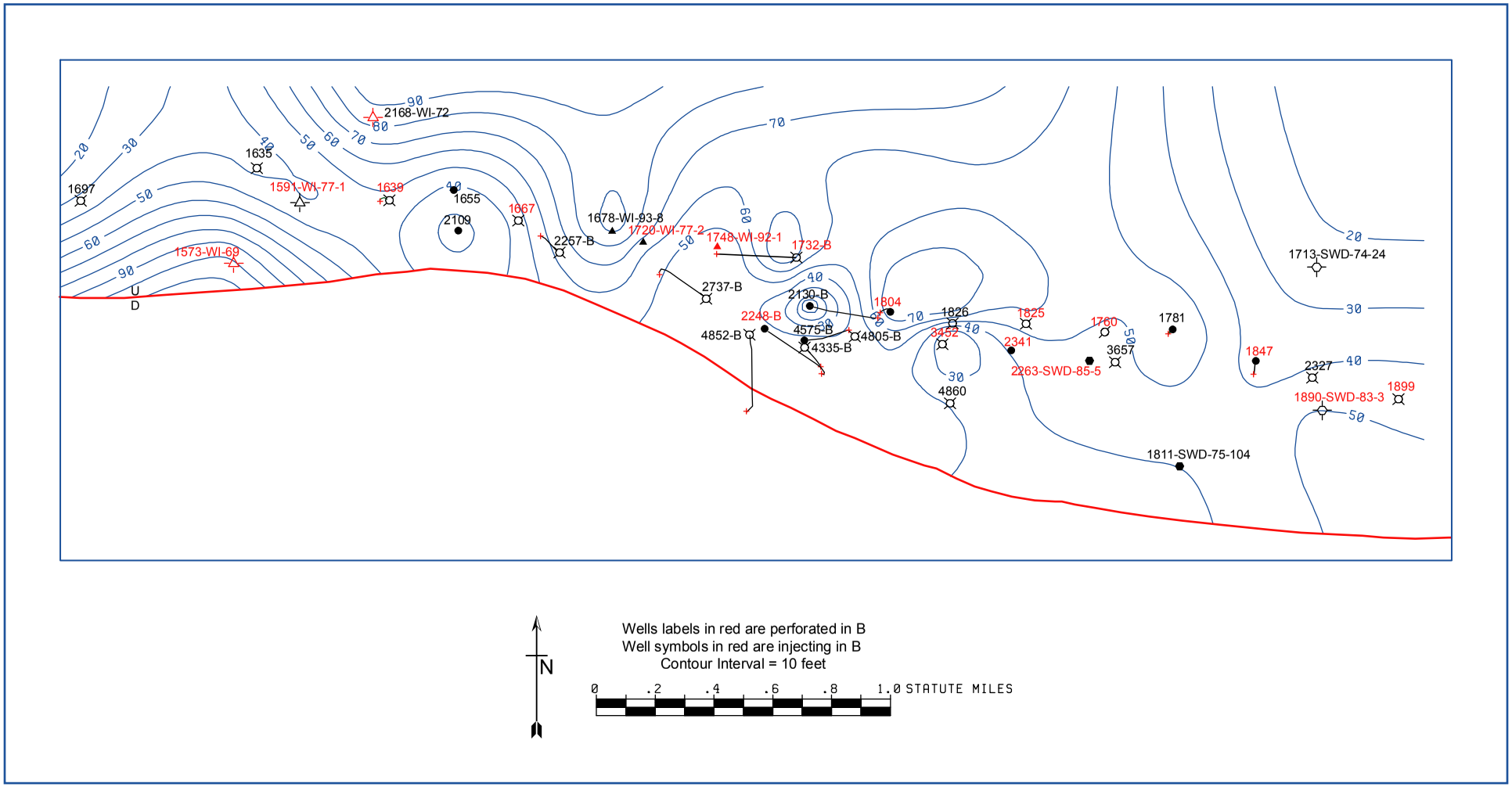

Figure 18. Isopach map of Cycle B and locations of wells perforated in Cycle B and wells injecting water into Cycle B.
See Figure 8 for well symbols.

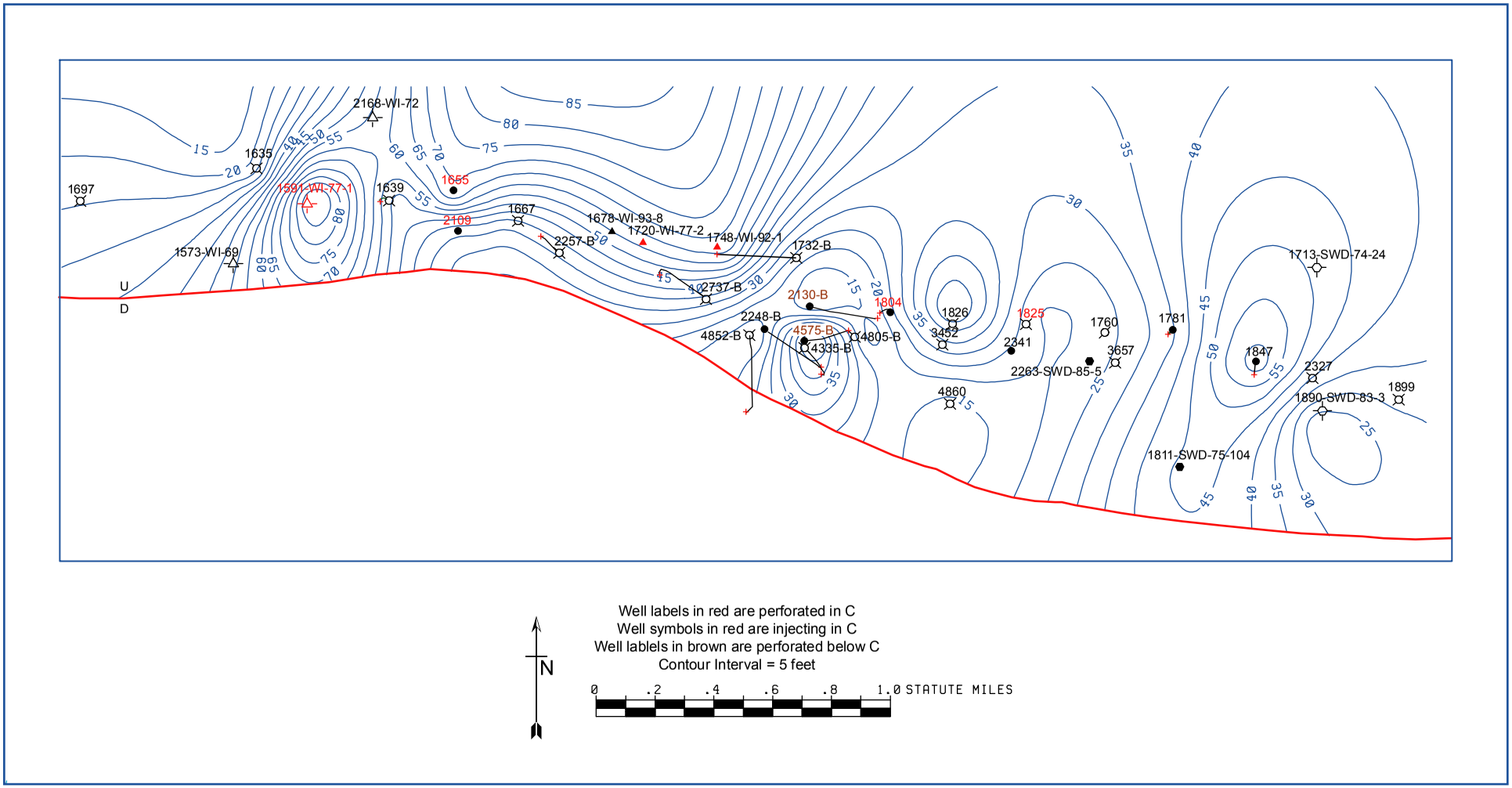

Figure 19. Isopach map of Cycle C and locations of wells perforated in Cycle C, wells perforated immediately below Cycle C, and wells injecting water into Cycle C. See Figure 8 for well symbols.

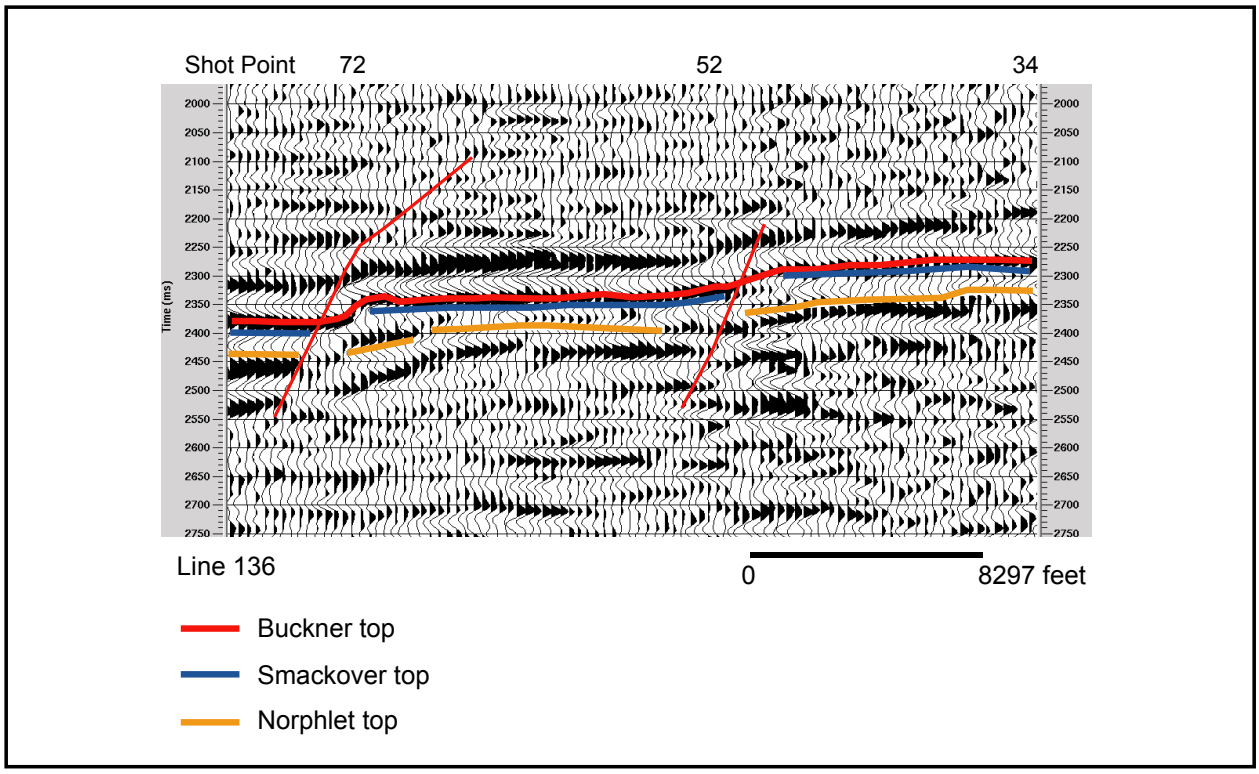

Figure 20. 2-D reflection profile, west-east line, Phillips P2635-136. See Figure 8 for location of seismic line.

types present in each of the cores were analyzed. Data from isotopic analysis (Fig. 21) show clear separation of the upper and lower dolomitized zones. Dolomite in the upper dolomitized zone has isotopically enriched δO^{18} values compared to the lower dolomitized zone. This suggests that the dolomitizing fluid for the upper zone was supersaturated brine at relatively low temperature. Analysis of the lower dolomitized zone isotopic data is ongoing. Calcite cements form a linear trend probably reflecting a transition from earlier precipitated cement at cooler temperature through later burial calcite cements.

Cathodoluminescence (CL) petrography was conducted on all petrographically identified dolomite and calcite cements and grains. Zoned cements and bimineralic ooid grains were recognized during petrography. In addition, changing CL intensities in some dolomite crystals suggests changing fluid chemistry during precipitation. Detailed CL mapping was used to determine traverse and sampling locations for microprobe study. Results of CL study will be discussed in the diagenesis section below.

Strontium, calcium, magnesium, iron, and manganese concentrations have been determined through detailed component microsampling using a JEOL 733 Superprobe. We collected 98 data points, which include data from each dolomite type identified during transmitted light and cathodoluminescence petrography. Analysis of probe data is currently be conducted at The University of Mississippi.

Diagenetic Study.--Core descriptions, openhole well log analysis, thin section petrography, and stable isotope geochemistry have been used to create a model of Smackover diagenesis at Womack Hill Field. Smackover diagenesis began with early marine cementation of grains by fibrous aragonite and development of micrite envelopes through algal borings. Partially preserved fabrics in ooids suggest these grains had three different original compositions: aragonite, Mg-calcite, and bimineralic. These unstable sediments were highly altered in the meteoric diagenetic realm, creating large amounts of moldic porosity. Isopachous rim and equigranular drusy spar cements precipitated in intergranular and moldic pores. Both cements precipitated

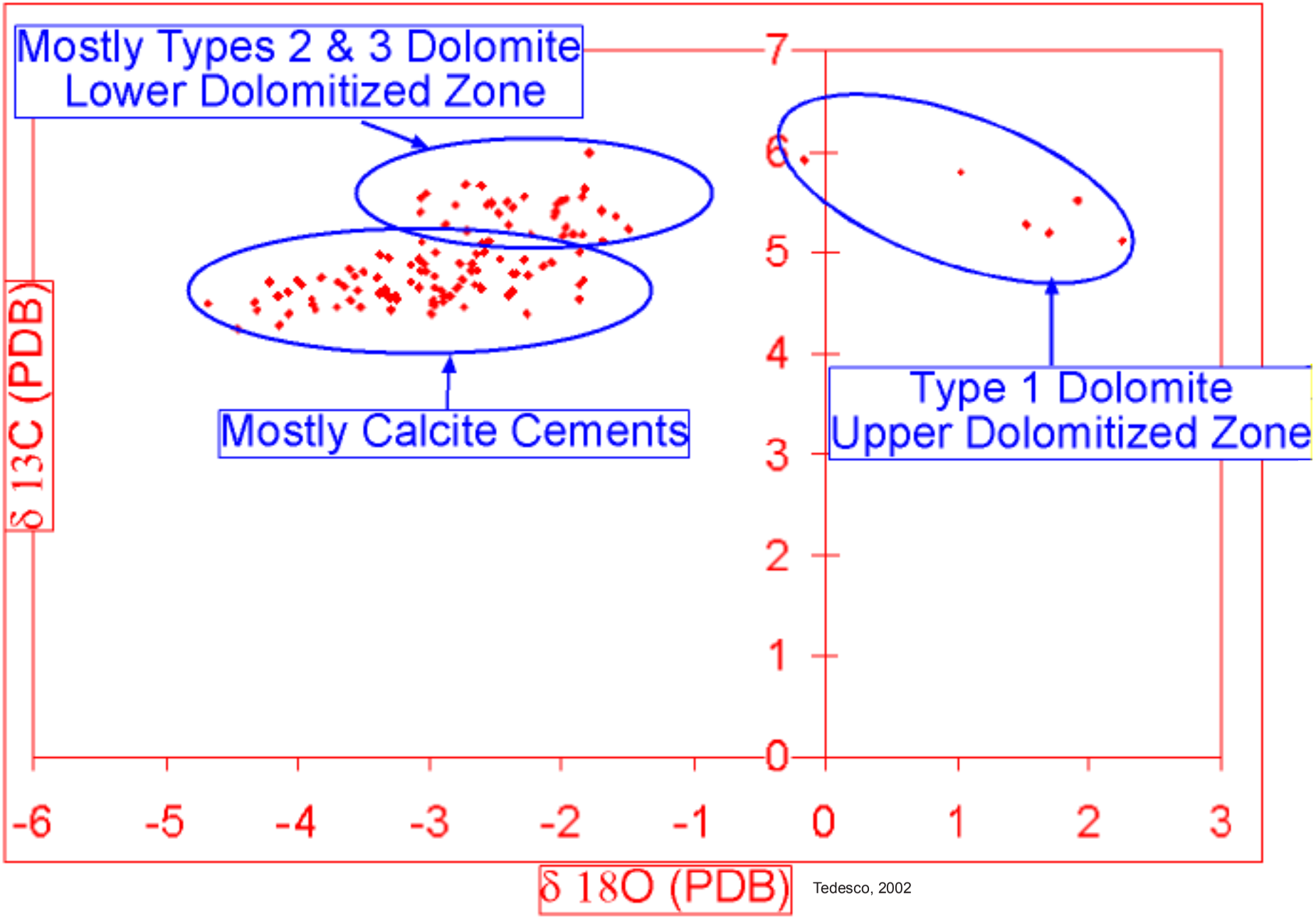

Figure 21. Stable isotope geochemistry. Upper dolomitized zone enriched relative to lower dolomitized zone suggesting two seperate dolotimizing fluids. Upper dolotimized zone isotropic signiture suggests dolotimization by hypersaline brine at near-surface tempeartures.

contemporaneously with dissolution and can be found in intergranular and moldic pores. Meteoric cementation was followed by at least four major phases of dolomitization.

The first event was a fabric-destructive dolomitization in the uppermost Smackover (Cycle A; upper dolomitized zone) (Fig. 22). This event likely occurred soon after deposition by penecontemporaneous, downward-moving, evaporitically-concentrated brine. The dolomite phase is associated with an exposure event identified from core and petrographic analysis (Fig. 23). At wells located on the structural high area of the field, the exposure is located above the phase 1 dolomitized zone near the Buckner-Smackover contact. In wells off the structural high, the exposure is located at or near the base of the dolomitized zone. A gamma-ray spike commonly occurs at the exposure surface, allowing for recognition and correlation of this surface. The dolomite is composed of inclusion-rich, euhedral to subhedral dolomite crystals, is completely fabric destructive, and exhibits a dull red luminescence (Fig. 22). The dolomitized zone is commonly 4 to 15 feet thick, has high porosity (15-30%) and high permeability (5-45 md). This first dolomitization event can be recognized on logs across the entire field.

The second phase of dolomitization likely occurred during or immediately following meteoric leaching of unstable aragonite grains, occluding much of the moldic porosity. The dolomite is characterized by inclusion-rich, xenotopic, fine-crystalline to microcrystalline (commonly less than 50 microns), anhedral crystals selectively replacing ooids and peloids (Fig. 24). The dolomite has a slightly brighter red luminescence than other dolomite phases. This event occluded moldic porosity and is a porosity destructive event.

The third dolomitizing event was fabric-destructive, creating large amounts of intercrystalline porosity and increasing permeability. This dolomite event is the most common throughout the wells, except where dolomite type 1 is present. Reservoir zones in the lower part of Cycle A, Cycle B, and Cycle C are commonly associated with dolomite phase 3. The lower dolomitized reservoir zone, which is primarily composed of type 3 dolomite, climbs stratigraphically higher in north to south transects. Two distinct dolomite crystal morphologies are recognized in this phase. The two morphologies may represent two separate phases of dolomitization from different brines or may

A.

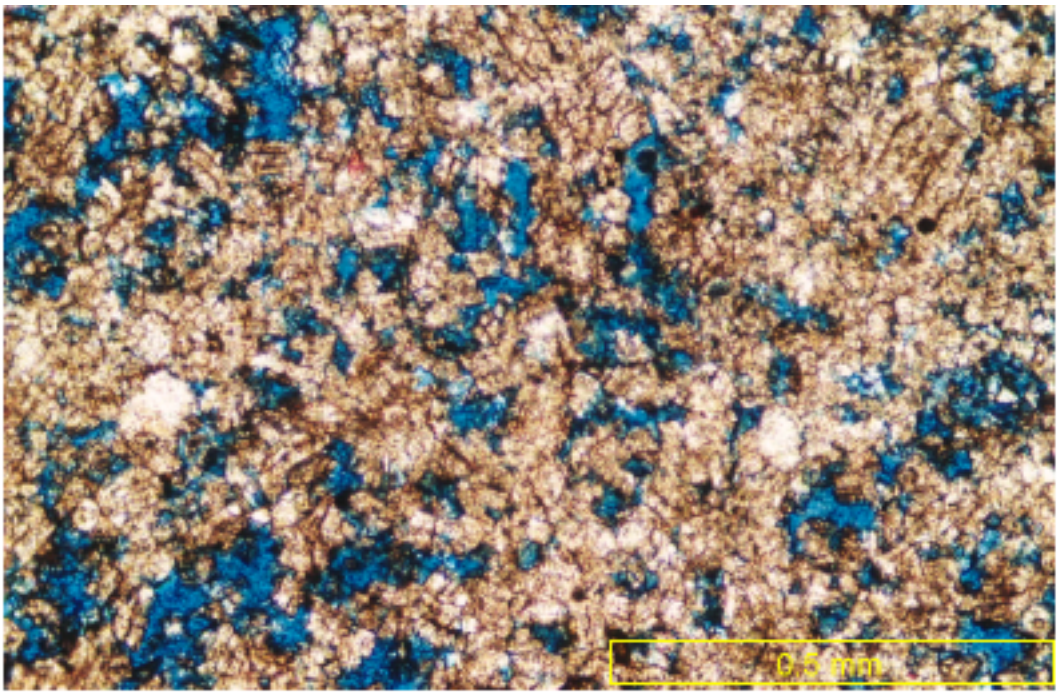

B.

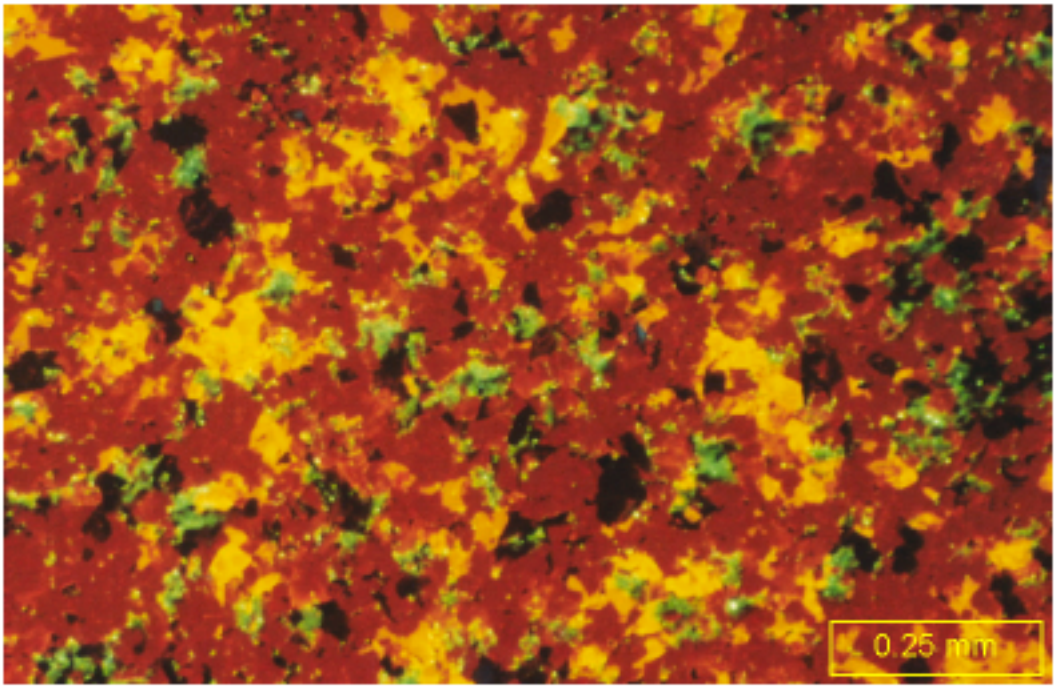

Figure 22. "Type 1" dolomite from near the top of the Smackover Formation.
A. Note inclusion-rich sucrosic dolomite crystals and large amount of intercrystalline porosity, Turner 13-25 well (11,434.4 ft).
B. Cathodoluminescence in Type 1 dolomite. Dolomite has red luminescence, burial calcite cement exhibits yellow luminescence, and bitumen exhibits green luminescence, Counselman 18-12 well (11,462 ft.).
(photographs by Tedesco).

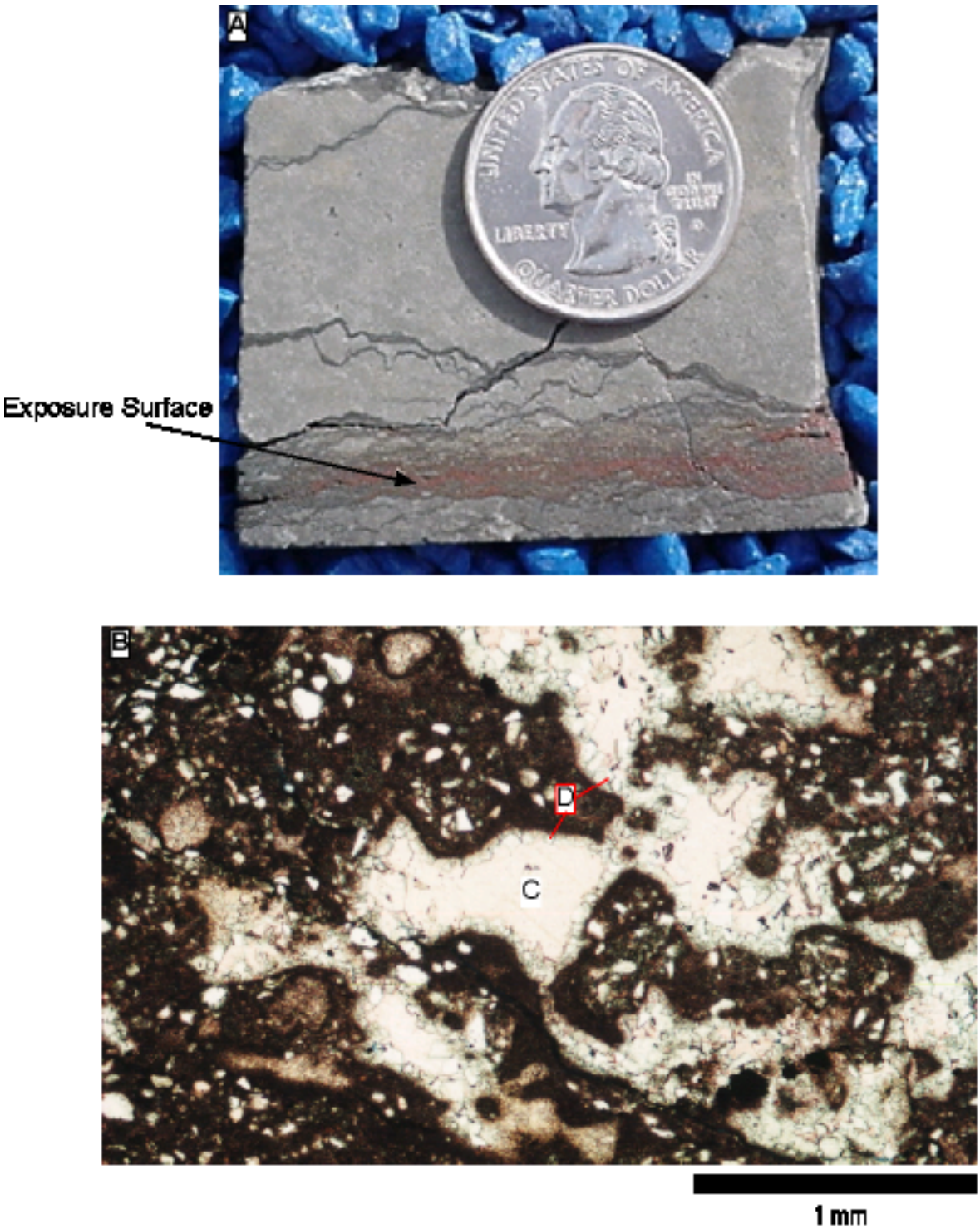

Figure 23. Upper "A" cycle exposure surface. Turner 13-5 well (11,326 ft.).
A. Red shale lamina at exposure surface.
B. Phtomicrograph at exposure surface. Dark brown groundmass composed of microcrystalline dolomite. Note alveolar texture. Pore lined idiotopic-C dolomite cement (D) followed by blocky calcite (C) cements that completely occlude porosity. Note high clastic content which is responsible for gamma ray spike characteristic of exposure surface.
(photographs by Tedesco).

A.

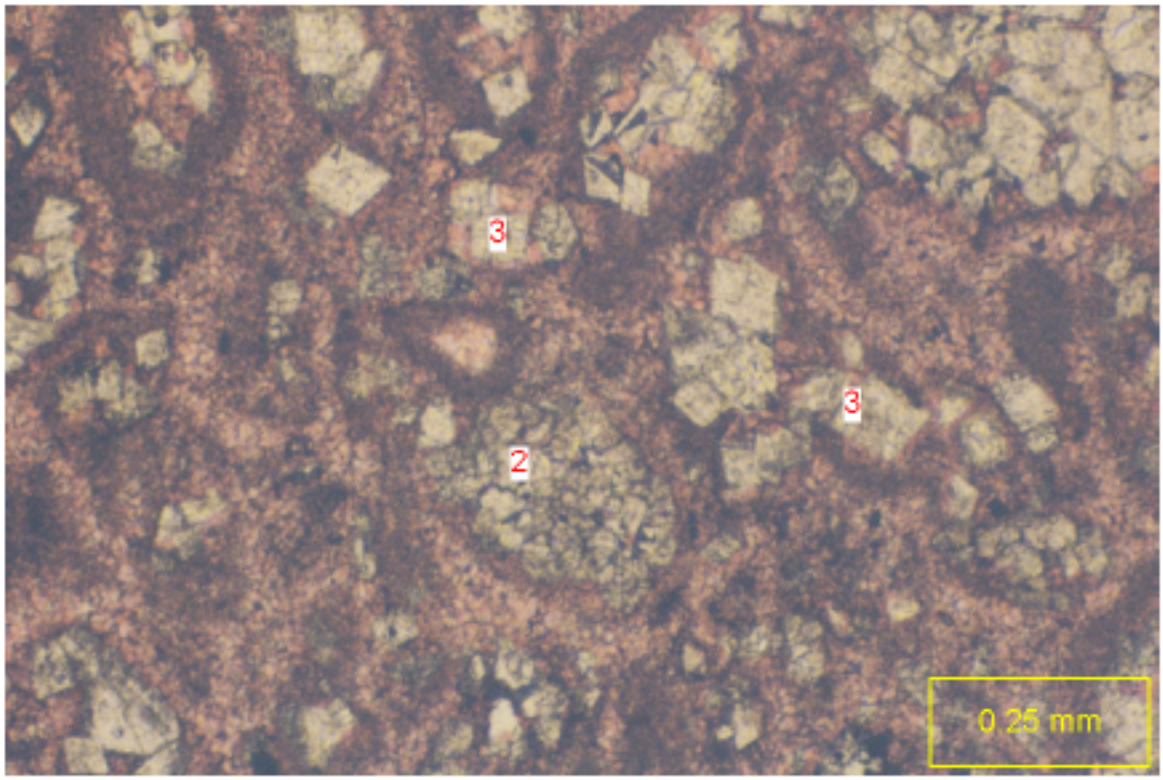

B.

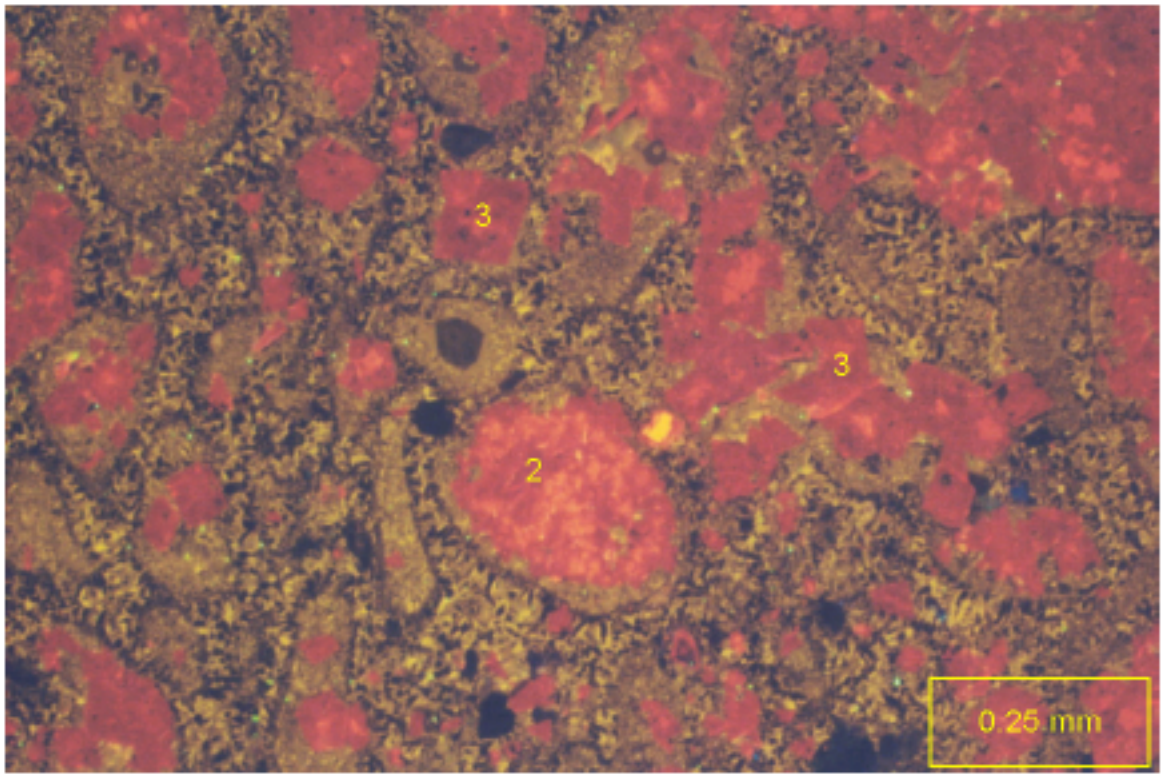

Figure 24. "Types 2 and 3" dolomite. Womack Hill Field Unit 14-5 well (11,116.5 ft.).
A. Note Type 2 (2) fabric selective replacement of grains by anhedral fine-crystalline dolomite and Type 3 (3) fabric destructive dolotimization by euhedral rhombs.
B. Cathodoluminescence view of A. Note brighter luminescence by Type 2 (2) dolomite.
(photographs by Tedesco).

represent a continuum of dolomitization with changing water chemistry. The first dolomite morphology is characterized by subhedral hypidiotopic to idiotopic, relatively inclusion-free crystals 50 to 100 microns in diameter (Figs. 24 and 25). The second morphology is comprised of euhedral, ideotopic, inclusion-free crystals 50 to 150 microns in diameter. Larger crystals commonly have an inclusion-rich core and more inclusion-free outer zone (Fig. 25). Both morphologies are commonly associated with stylolites and fractures throughout the cores, suggesting stylolites may have been fluid migration pathways.

The fourth dolomitization phase is comprised of idiotopic-c (Gregg and Sibley, 1984) dolomite cement lining vuggy pores in the Cycle A (Fig. 26). The cement commonly follows an early phreatic isopachous calcite cement and is followed by syntaxial blocky calcite spar cement. This cement is found in Cycle A near the identified exposure surface. The dolomite commonly has a bright red luminescence with quenched crystal terminations, suggesting changing fluid chemistry during precipitation. Microprobe data indicate a decrease in Mn concentration across the crystals, explaining the change in luminescence.

A minor dolomitization phase occurred in the deep burial environment and is characterized by precipitation of large saddle dolomite rhombs in fractures and vuggy pores. Other late burial cements include syntaxial and poikilotopic calcite spar cements, potassium feldspar overgrowths, blocky and poikilotopic anhydrite and celestite cement, and rare gypsum and sulfur cements.

Burial effects include both physical and chemical compaction (Fig. 27). These have led to significant reductions of porosity and permeability in sediments not already dolomitized or altered to stable calcite. Burial features include crushed and deformed or broken grains, spalled oolites, stylolites and microstylolites, stylolitic grain contacts, interpenetrating grains, and fractures.

Pore System and Petrophysical Study.--The pore systems in the Smackover reservoir at Womack Hill Field have been studied and classified using the classification of Choquette and Pray (1970). Pore types include interparticle, intraparticle, vuggy, intercrystalline and moldic (Table 3). The probe permeameter (mini-permeameter) was used to determine horizontal and vertical permeabilities from the 118 billets cut from the cores for thin sections. Average log vertical

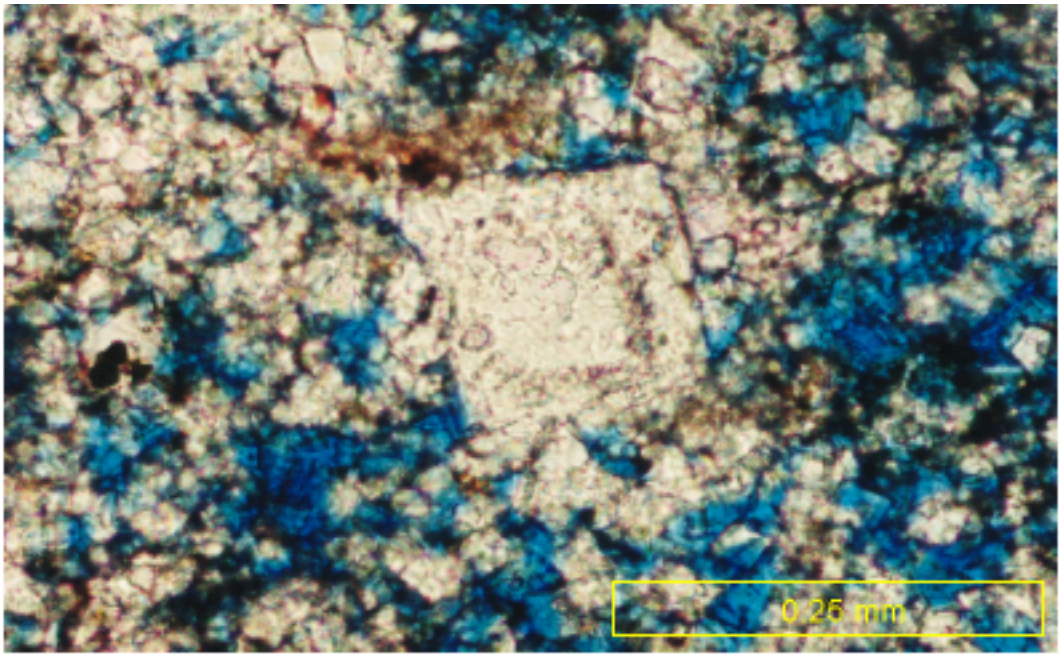

Figure 25. Close-up of "Type 3" dolomite crystal. Zones of inclusions toward center of crystal is a common observation across the field. Scruggs, Parker, Norton 9-14 well (11,413 ft.). (photograph by Tedesco).

A.

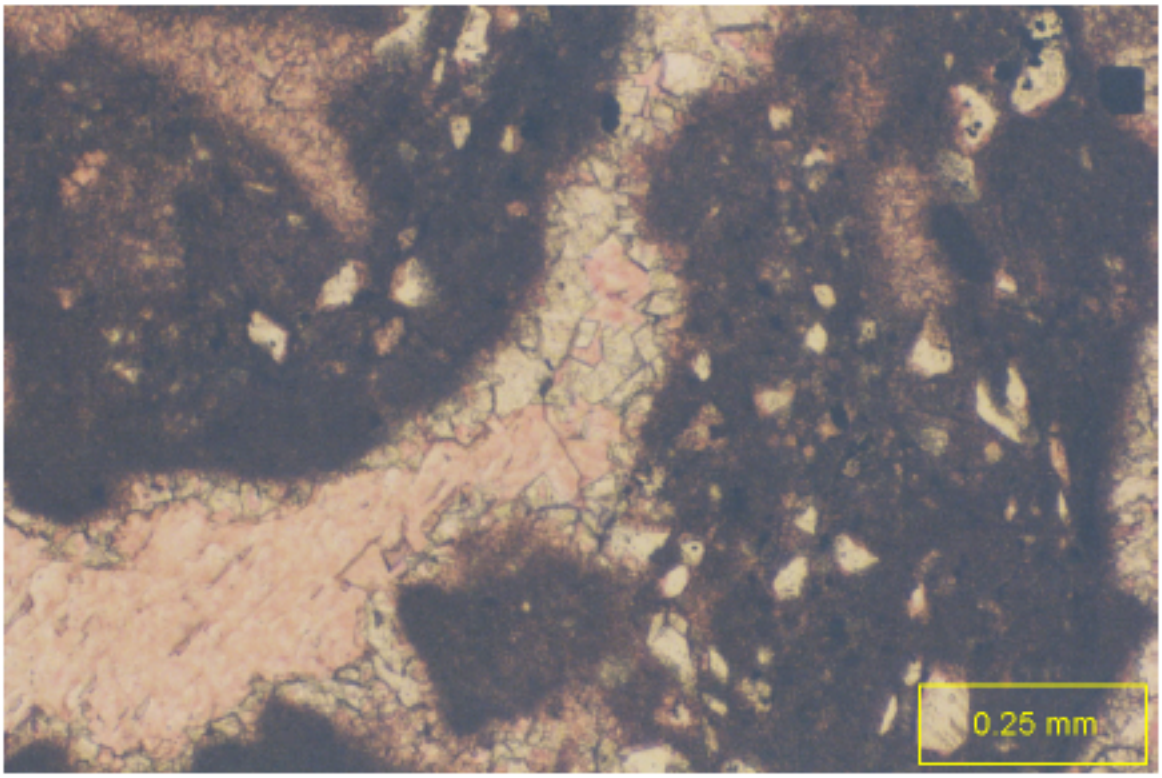

B.

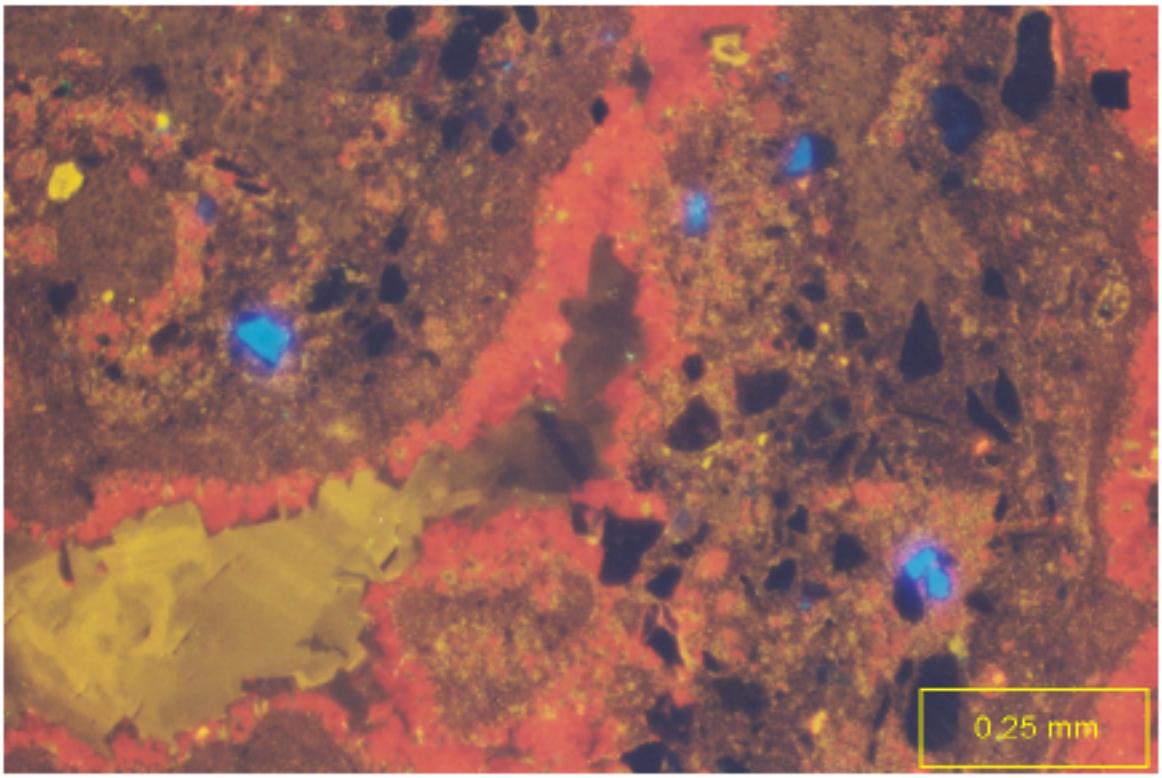

Figure 26. Idiotopic-C dolomite cement. Turner 13-5 well (11,327 ft.).

A. Note dolomite cement lining pore walls and following isopachous calcite cement. Dolomite followed by coarse syntaxial calcite cement which completely occludes porosity.

B. Cathodoluminescence of same view as in A. Note red luminescence and quenched crystal edges in dolomite cement.

(phtographs by Tedesco).

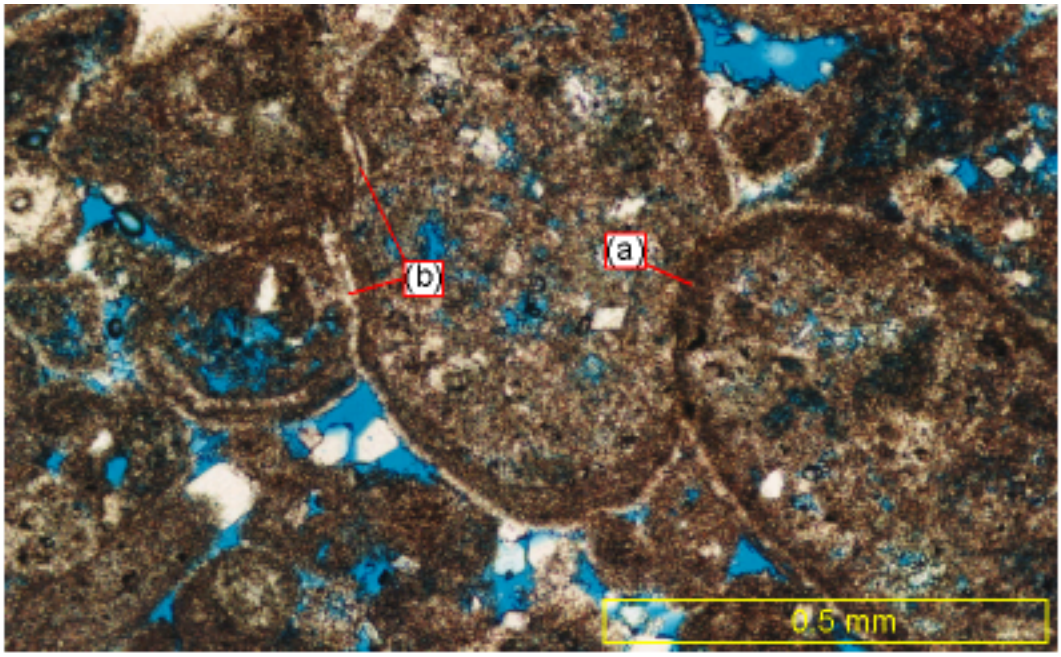

Figure 27. Deformation features in calcite-dominated zones. Note interpenetration and deformation of grains. These features can significantly reduce porosity. Deformation occurred both before (a) and following (b) early marine cementation. Rare "Type 3" dolomite rhombs scattered in interparticle pores. Turner 13-6 well (11,412 ft.). (photograph by Tedesco).

Table 3. Data on plugs chosen for capillary pressure testing (from Hopkins, 2002).

Well Permit #	Cycle	Core Depth	Lithology	*Est* % Dolomite	Pore Types	(Cleaned) He % Porosity	Cleaned Pr Permeability (md)
1591	A	11,405.0	pel, oo ws	*90*	ic 21.	52	35.07
1591	A	11,411.0	ms	*80*	ip, vg	12.10	5.60
1591	A	11,413.0	oo, pel ws	*80*	ic 17.	15	8.19
1591	C	11,515.0	pel ws	*88*	ic 18.	33	41.83
1591	C	11,528.0	pel ms	*90*	ic 16.	39	9.04
4575b	A	11,120.0	oo, pel ps	*20*	vg 8.	56	19.90
4575b	A	11,129.0	oo, pel ps	*10*	ip, ap, vg	20.73	22.40
4575b	B	11,146.0	onc, pel, oo gs	*15*	ip, ap	17.68	6.87
4575b	B	11,156.0	onc, oo gs	*15*	ip, ap, vg	18.22	7.46
4575b	B	11,174.0	onc, pel, oo gs	*20*	ip, ap, vg	15.25	2.27
4575b	C	11,192.0	pel ws	*87*	ic 17.	27	42.67

ms=mudstone
ws=wackestone
ps=packstone
gs=grainstone

ip=interparticle
ap=intraparticle
vg=vuggy
ic=intercrystalline
mo=moldic

Est - Visually Estimated
He - Helium Porosimeter
Pr - Probe Permeameter

permeabilities were plotted with average log horizontal permeabilities, and no significant difference was observed between vertical and horizontal permeabilities (Figs. 28 and 29). High pressure mercury injection capillary pressure (MICP) analysis was performed on 11 core plugs representative of the pore systems (Table 4). See Figures 30 through 42 for results of the MICP testing.

Porosity and permeability data representative of the pore systems and acquired from the plugs were combined with mercury derived data to compare porosities and permeabilities (Table 5). Helium derived porosity values were found to average 2% higher than the mercury derived values (Figs. 43 and 44). Probe permeability values closely approximate the mercury derived permeabilities, except where the permeability value is below 1 md (Figs. 45 and 46). Capillary pressure permeability correlates with measured probe permeabilities (Fig. 47). Capillary pressure porosity has a high correlation with helium derived porosity values (Fig. 48); however, porosity from core analysis correlates poorly with the mercury and helium derived porosities (Figs. 48 and 49). There is a general relation between porosity and permeability (Fig. 50). See cross plots of porosity and permeability for the range of correlation values between these two parameters (Figs. 51 through 53).

Pore types exhibit general trends to their relation to porosity and median pore throat aperture (Table 6). See Figures 54 through 64 for median pore aperture size distribution for certain depths in well Permits #1591 and 4575B. Median pore throat aperture (MPA) increases with increasing porosity (Fig. 65), and probe permeability and mercury derived permeability strongly correlate with MPA (Fig. 66). The intercrystalline pore system is characterized by the highest porosities.

Capillary pressure data were available for wetting phase (air) saturations. Wetting phase saturation at 77 psia was approximated from its relation with MPA through the equation graphed on Figure 67. No clear relation was observed for entry pressures (displacement pressures) and any parameters. Utilizing a series of equations where porosity, permeability, and capillary radius (=MPA) can be determined, the equation: $y=\tau=(\phi r^2)/8k$ was graphed to solve for π or tortuosity

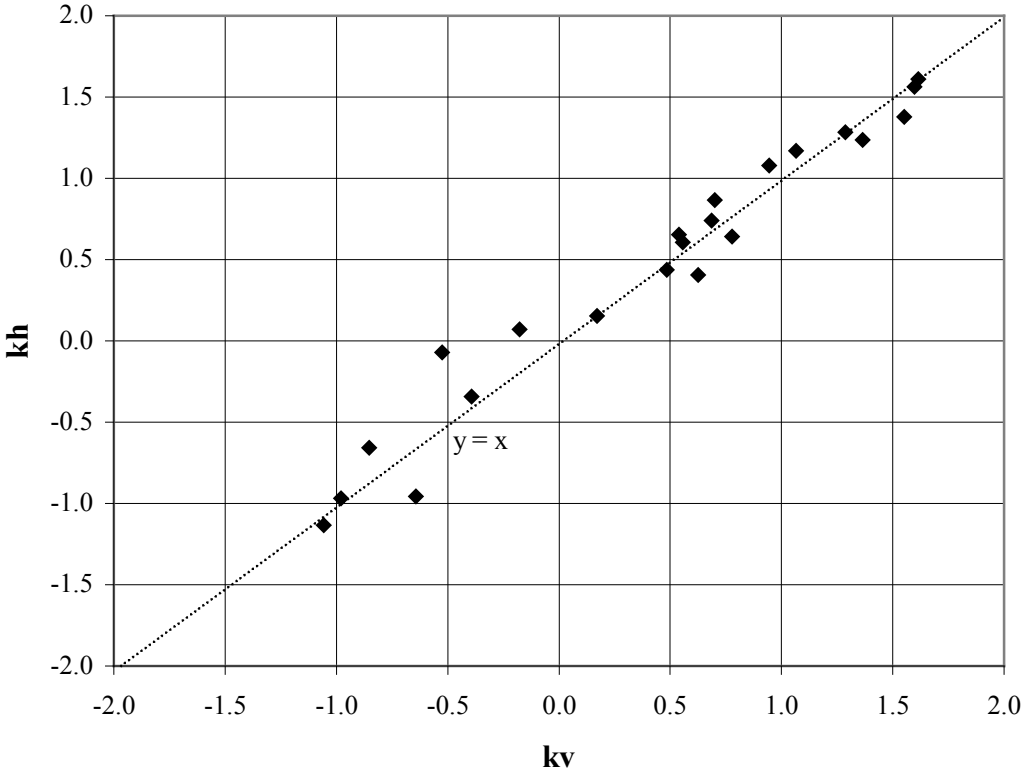

Figure 28. Average log vertical permeability (kv) vs. average log horizontal permeability (kh) measured from the probe pemeameter for Well Permit 1591 (from Hopkins, 2002).

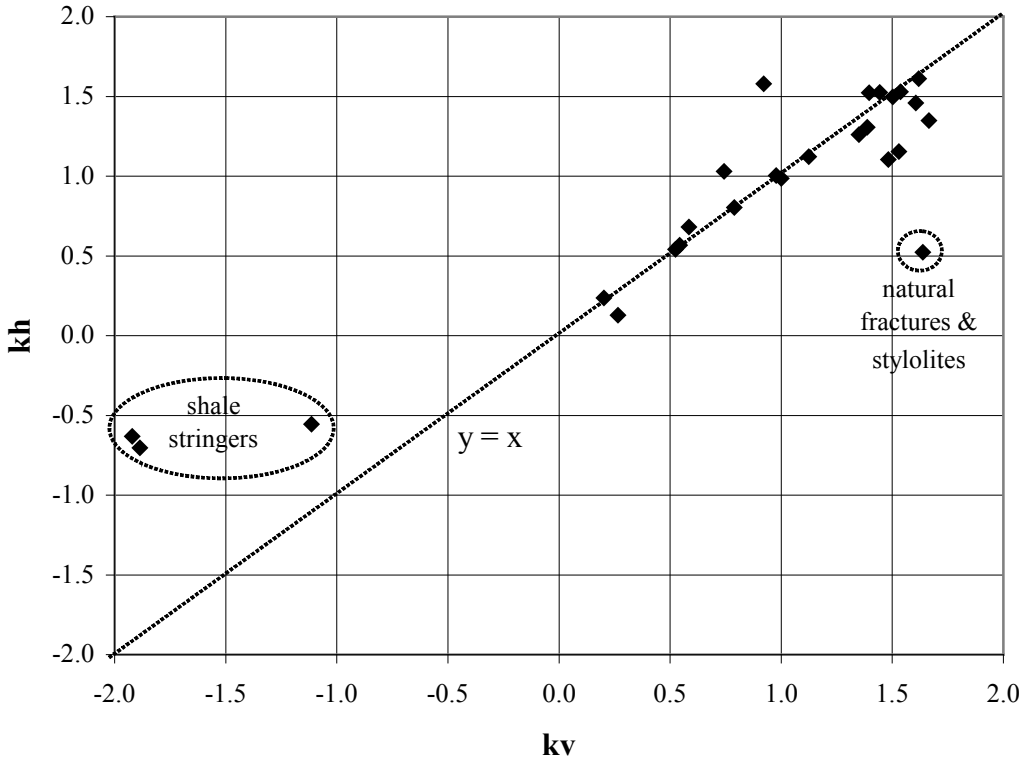

Figure 29. Average log vertical permeability (kv) vs. average log horizontal permeability (kh) measured from the probe pemeameter for Well Permit 4575-B (from Hopkins, 2002).

Table 4. List of mercury injection capillary pressure plugs and associated data (from Hopkins, 2002).

Permit #	Sample Depth (ft)	Plug #	Core Analysis		Mercury Derived		Median Pore Aperture (μm)	Saturation At End of Initial		Pore Structure
			phi (%)	k (md)	phi (%)	k (md)		Drainage Cycle	Imbibition Cycle	
1591	11,405.0	1	21.52	35.1	19.6	35.3	4.62	3	34	unimodal sharp
	11,411.0	2	12.10	5.6	9.02	0.982	1.07	12	25	unimodal broad
	11,413.0	3	17.15	8.19	15.3	8.83	2.59	7	29	unimodal sharp
	11,515.0	4	18.33	41.8	16.4	34.7	5.20	4	24	unimodal sharp
	11,528.0	5	16.39	9.04	15.0	8.95	2.33	2	52	unimodal sharp
4575b	11,120.0	11	8.56	19.9	2.27	0.021	0.262	44	46	poorly defined
	11,129.0	12	20.73	22.4	18.7	17.8	3.33	3	44	unimodal broad
	11,146.0	14	17.68	6.87	16.6	8.67	2.36	2	37	unimodal sharp
	11,156.0	15	18.22	7.46	15.9	7.19	2.22	4	44	unimodal broad
	11,174.0	16	15.25	2.27	12.9	2.07	1.28	8	40	unimodal broad
	11,192.0	18	17.27	42.3	16.0	49.5	6.75	3	23	unimodal sharp

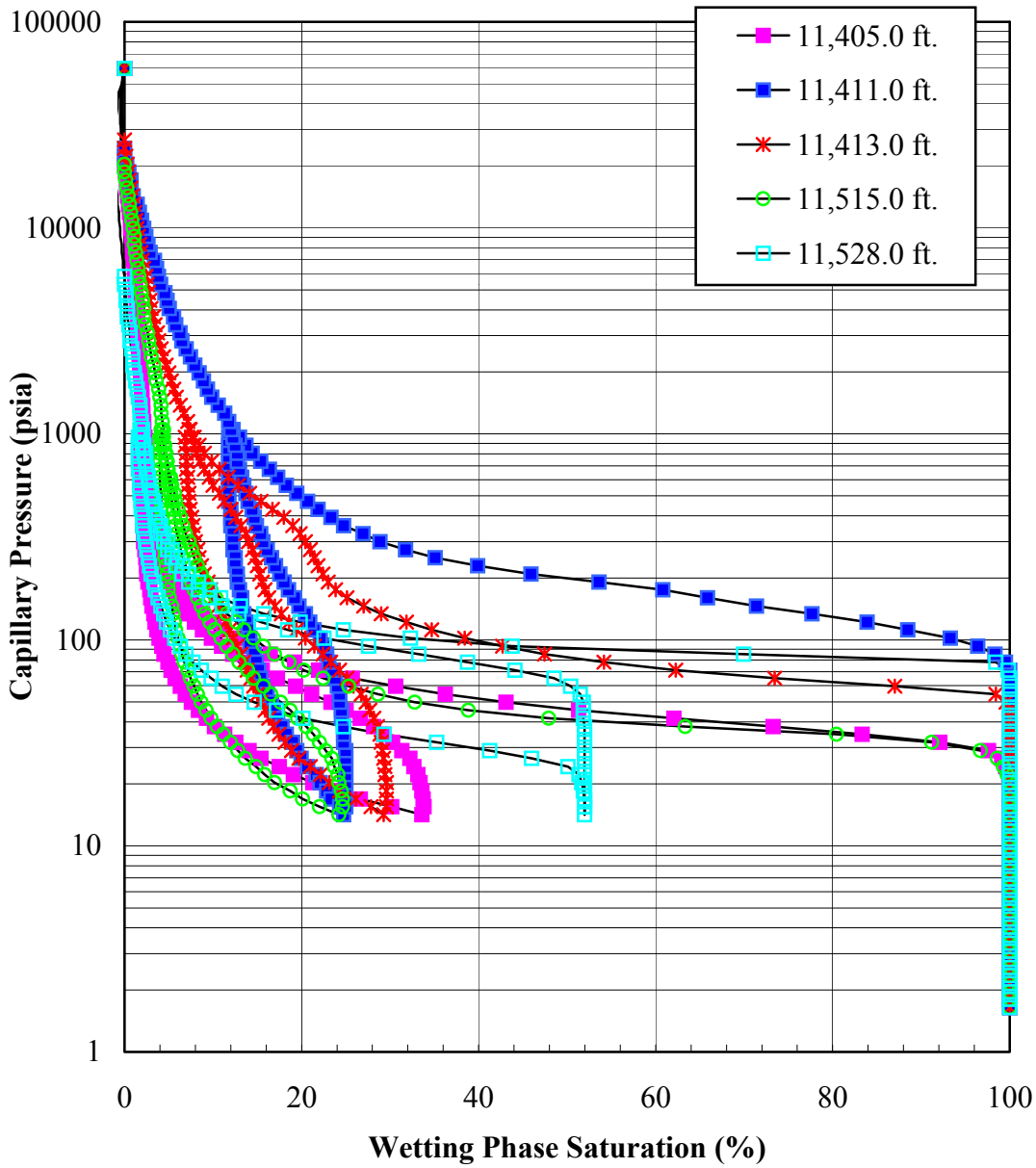

Figure 30. Mercury injection capillary pressure (pore volume) for Well Permit 1591 (from Hopkins, 2002).

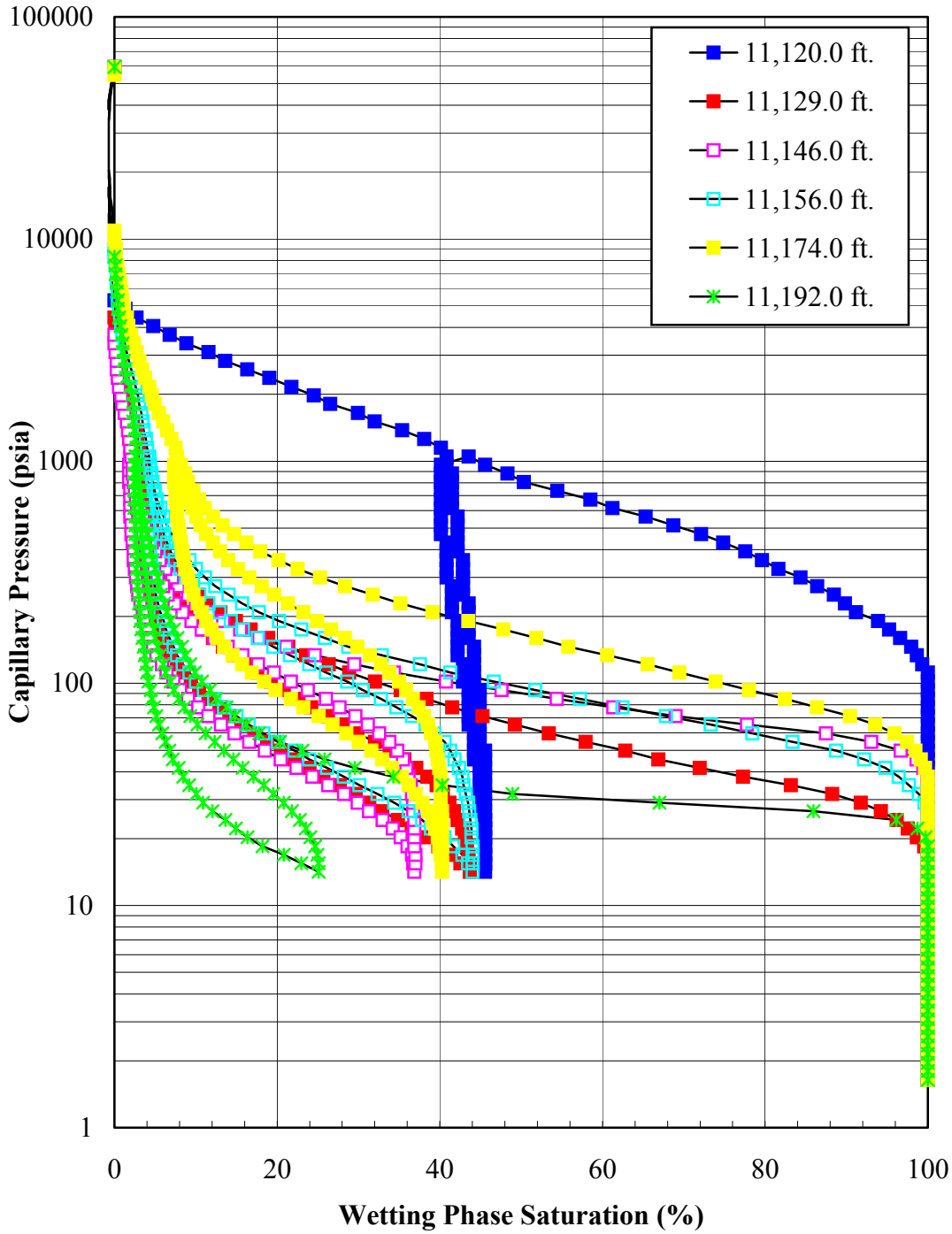

Figure 31. Mercury injection capillary pressure (pore volume) for Well Permit 4575-B (from Hopkins, 2002).

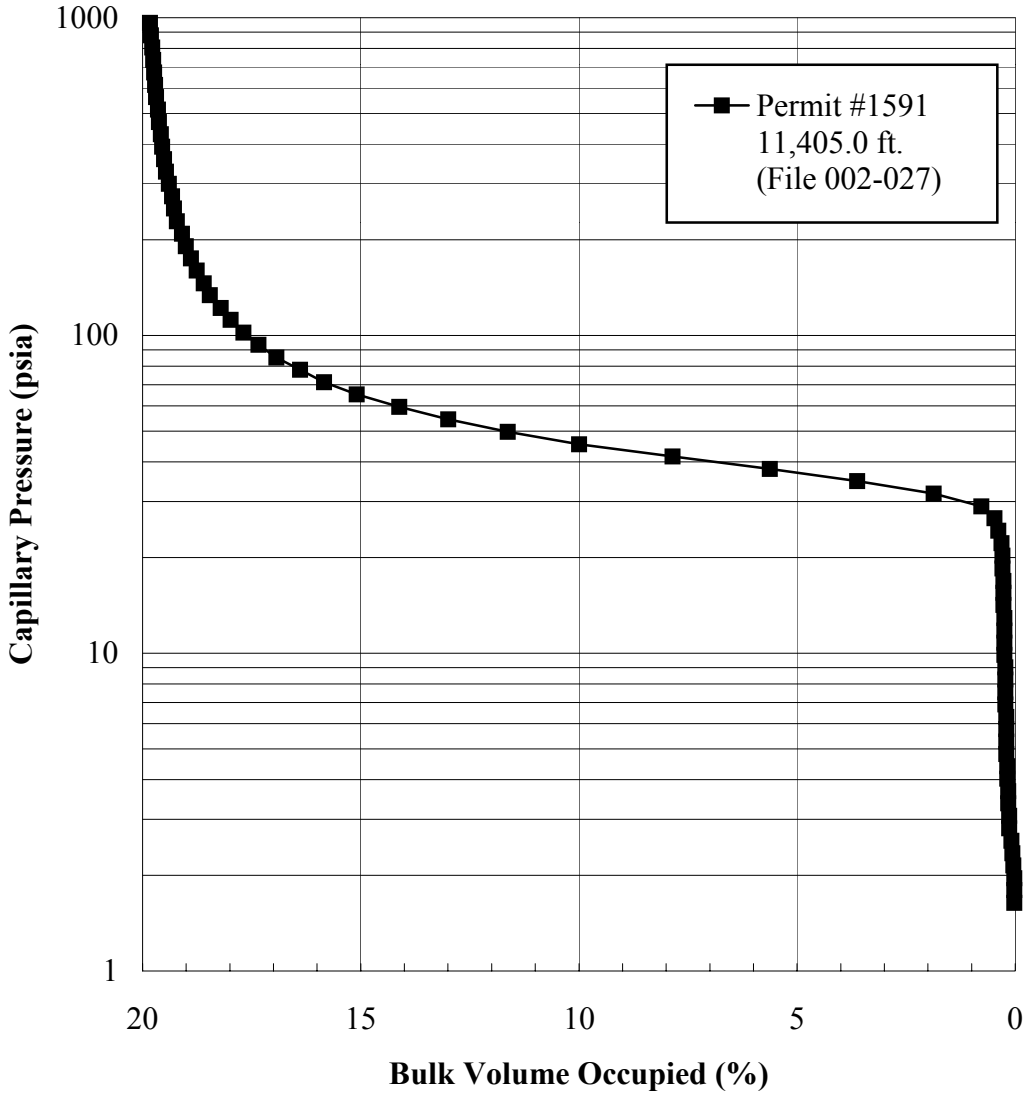

Figure 32. Mercury injection capillary pressure (pore volume) for Well Permit 1591 at 11,405 ft (from Hopkins, 2002).

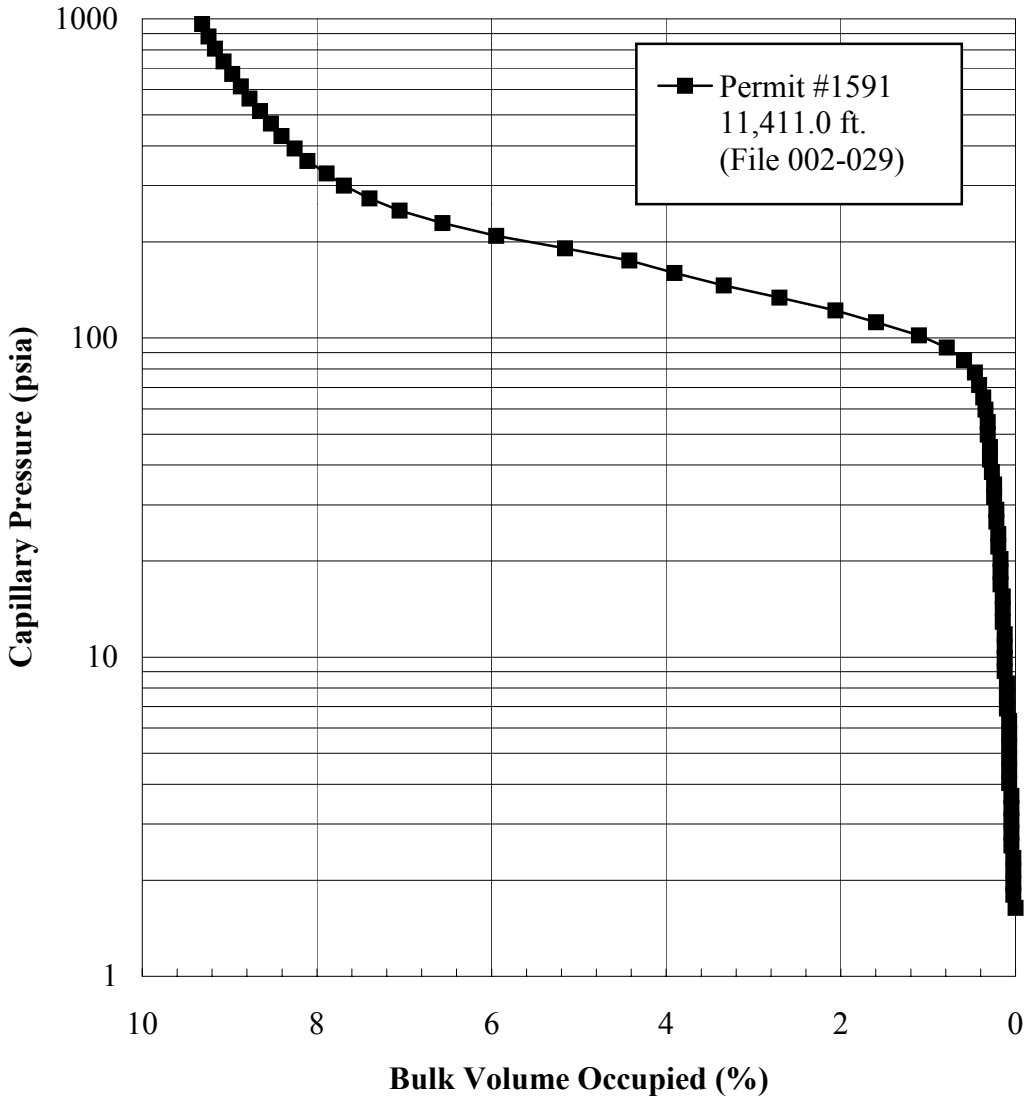

Figure 33. Mercury injection capillary pressure (pore volume) for Well Permit 1591 at 11,411 ft (from Hopkins, 2002).

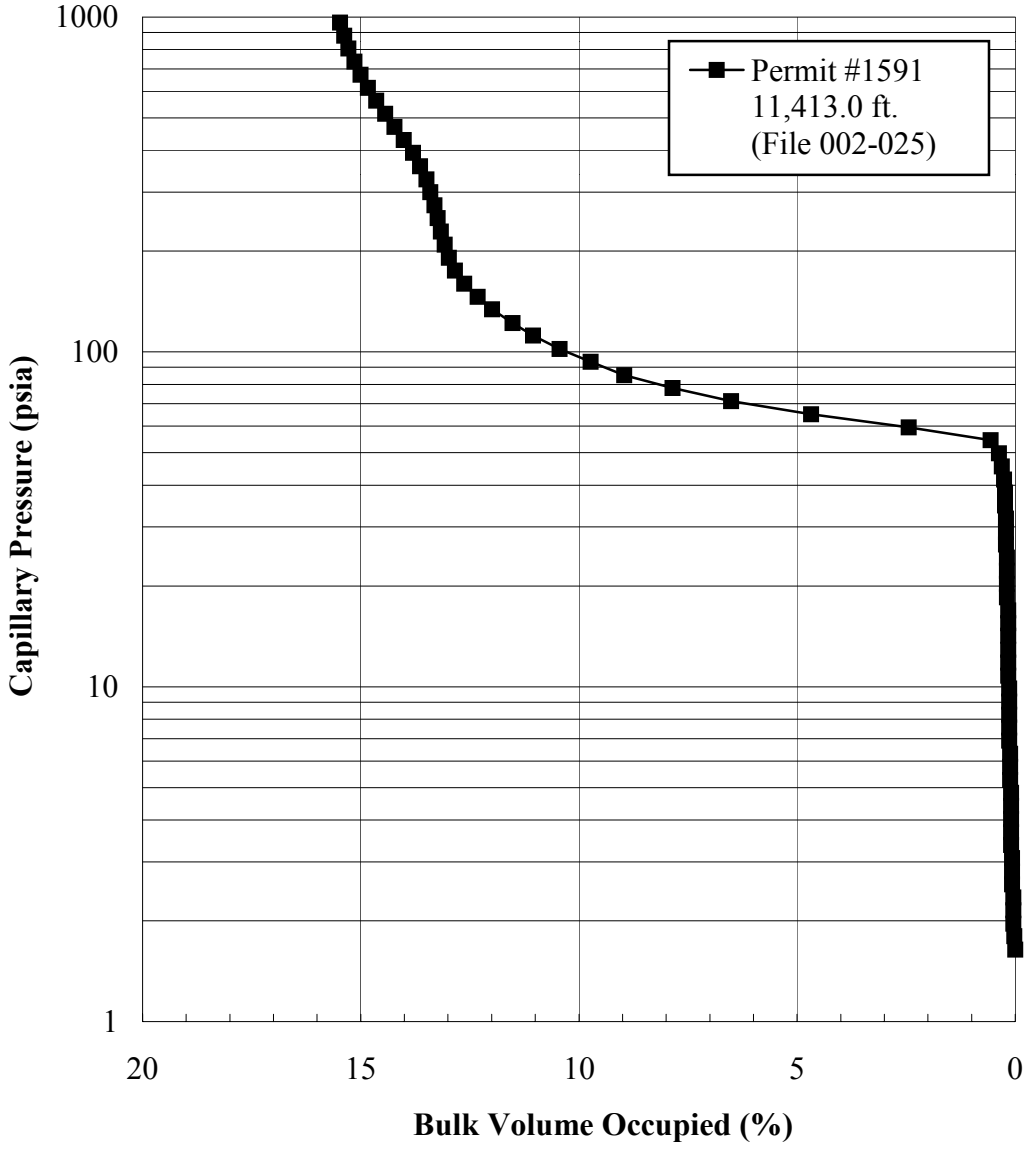

Figure 34. Mercury injection capillary pressure (pore volume) for Well Permit 1591 at 11,413 ft (from Hopkins, 2002).

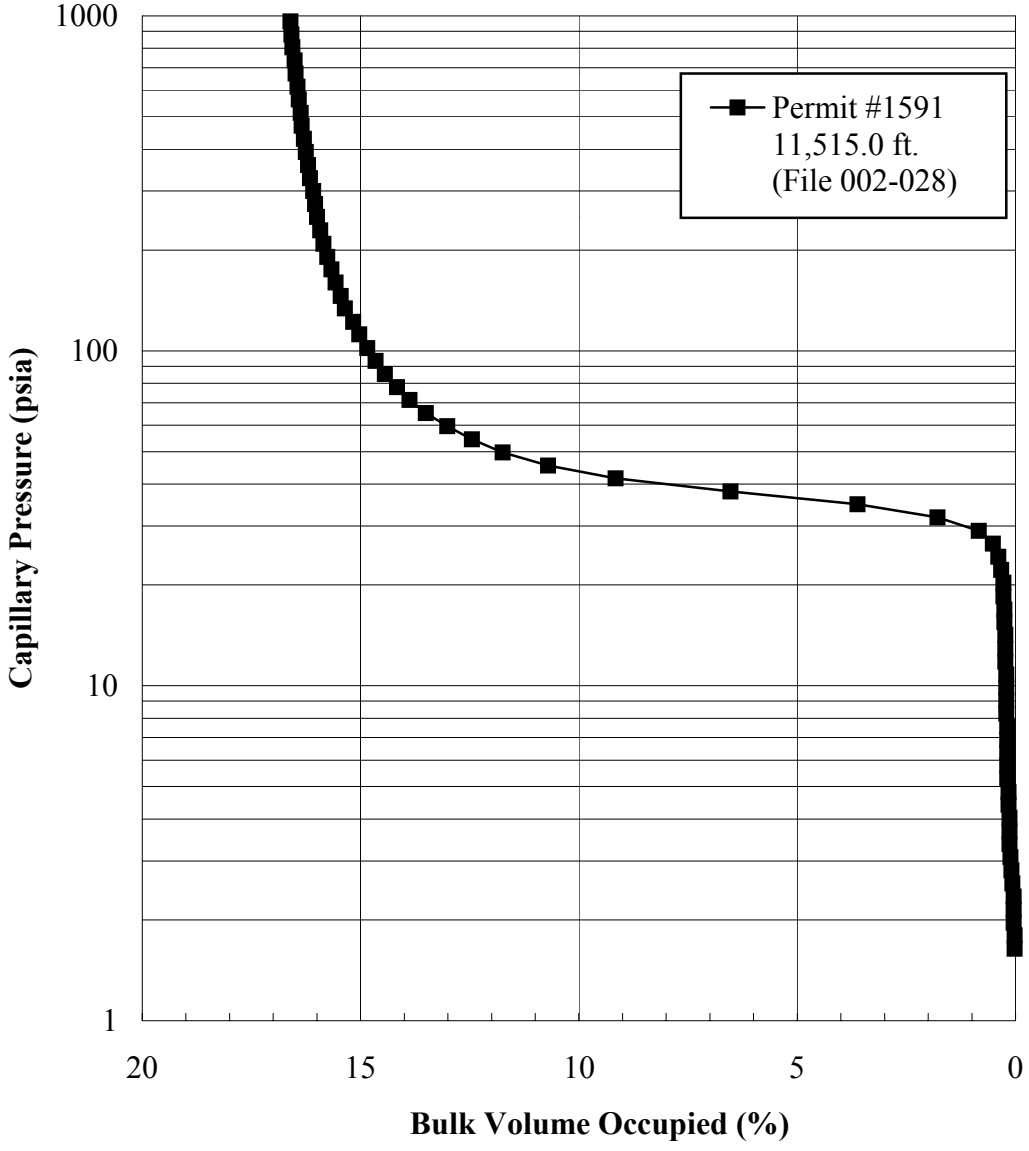

Figure 35. Mercury injection capillary pressure (pore volume) for Well Permit 1591 at 11,515 ft (from Hopkins, 2002).

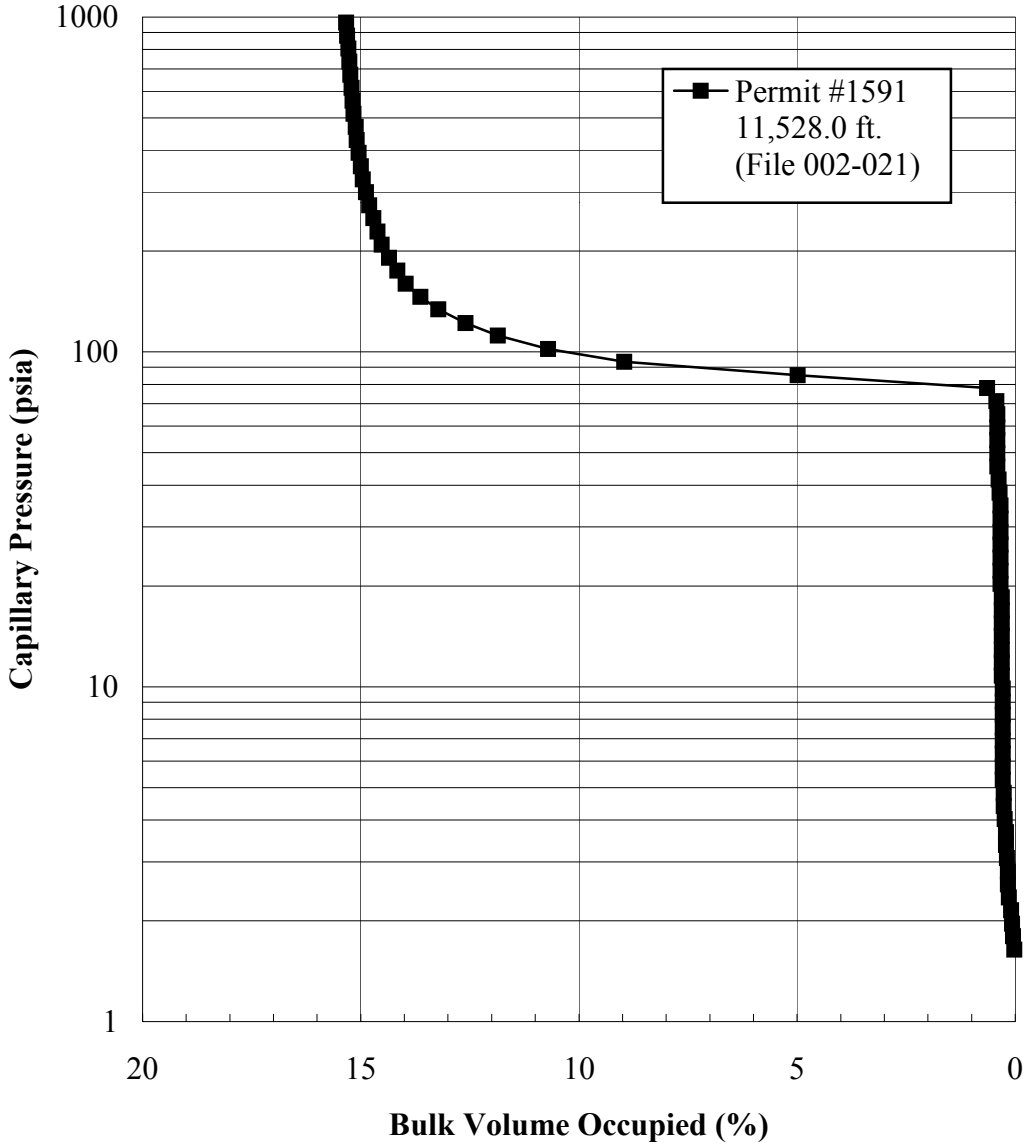

Figure 36. Mercury injection capillary pressure (pore volume) for Well Permit 1591 at 11,528 ft (from Hopkins, 2002).

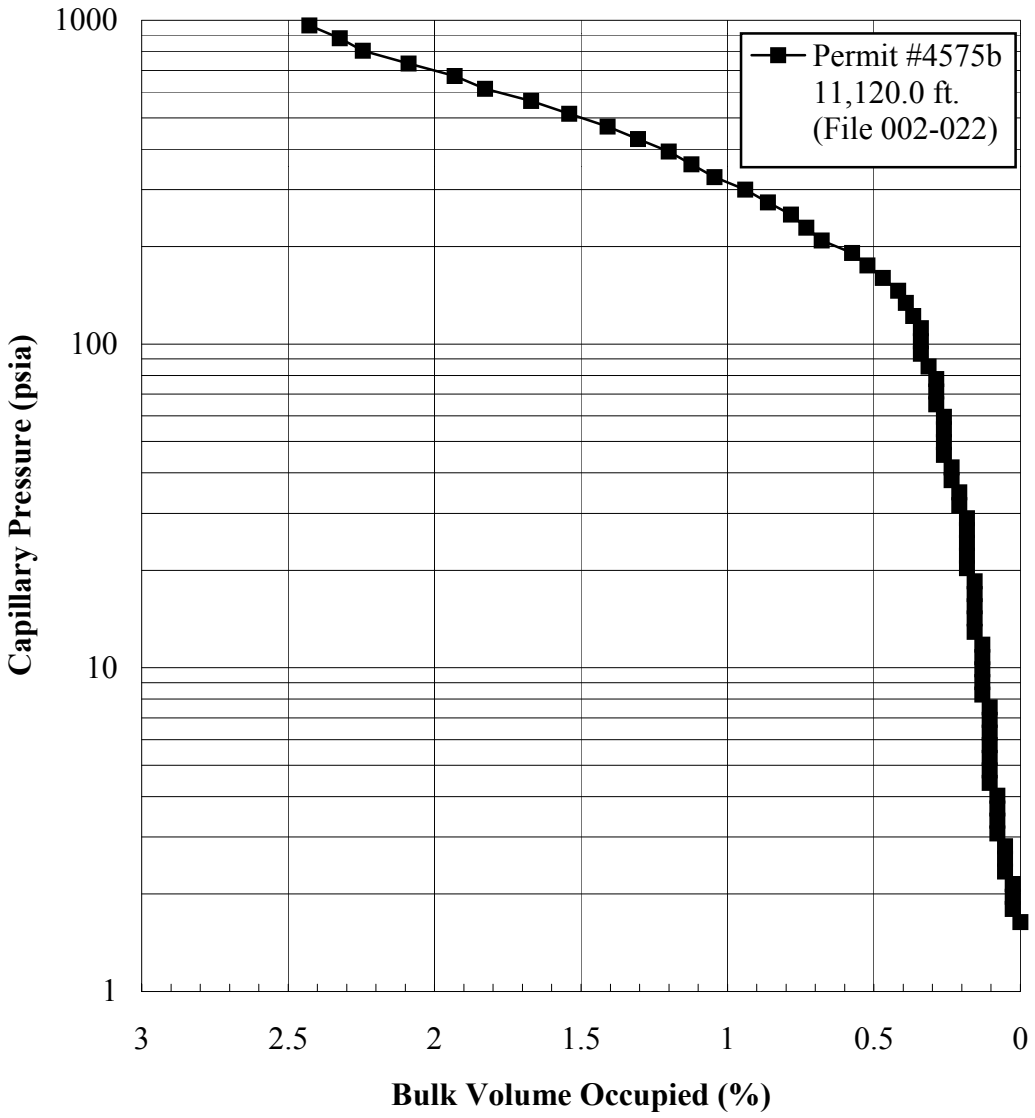

Figure 37. Mercury injection capillary pressure (pore volume) for Well Permit 4575B at 11,120 ft (from Hopkins, 2002).

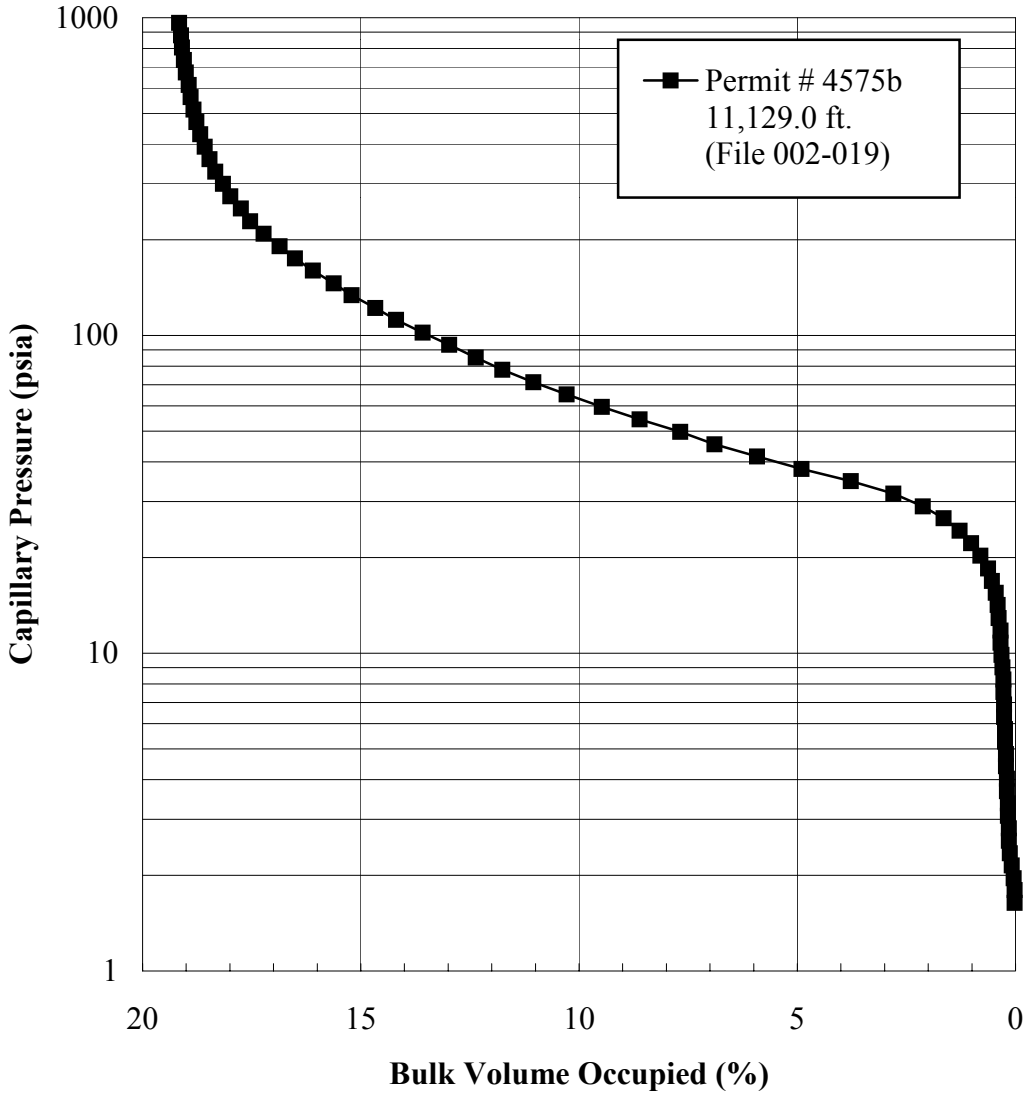

Figure 38. Mercury injection capillary pressure (pore volume) for Well Permit 4575B at 11,129 ft (from Hopkins, 2002).

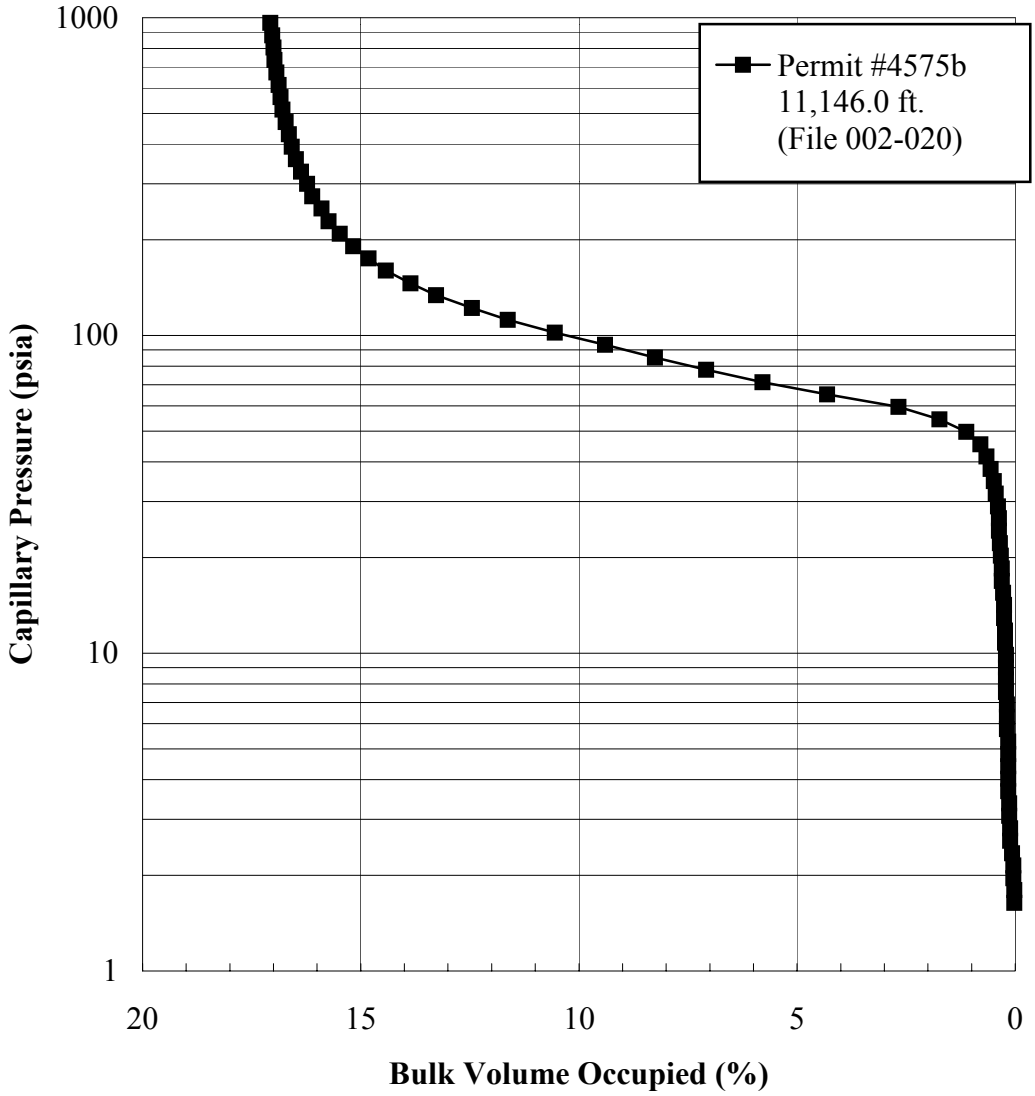

Figure 39. Mercury injection capillary pressure (pore volume) for Well Permit 4575B at 11,146 ft (from Hopkins, 2002).

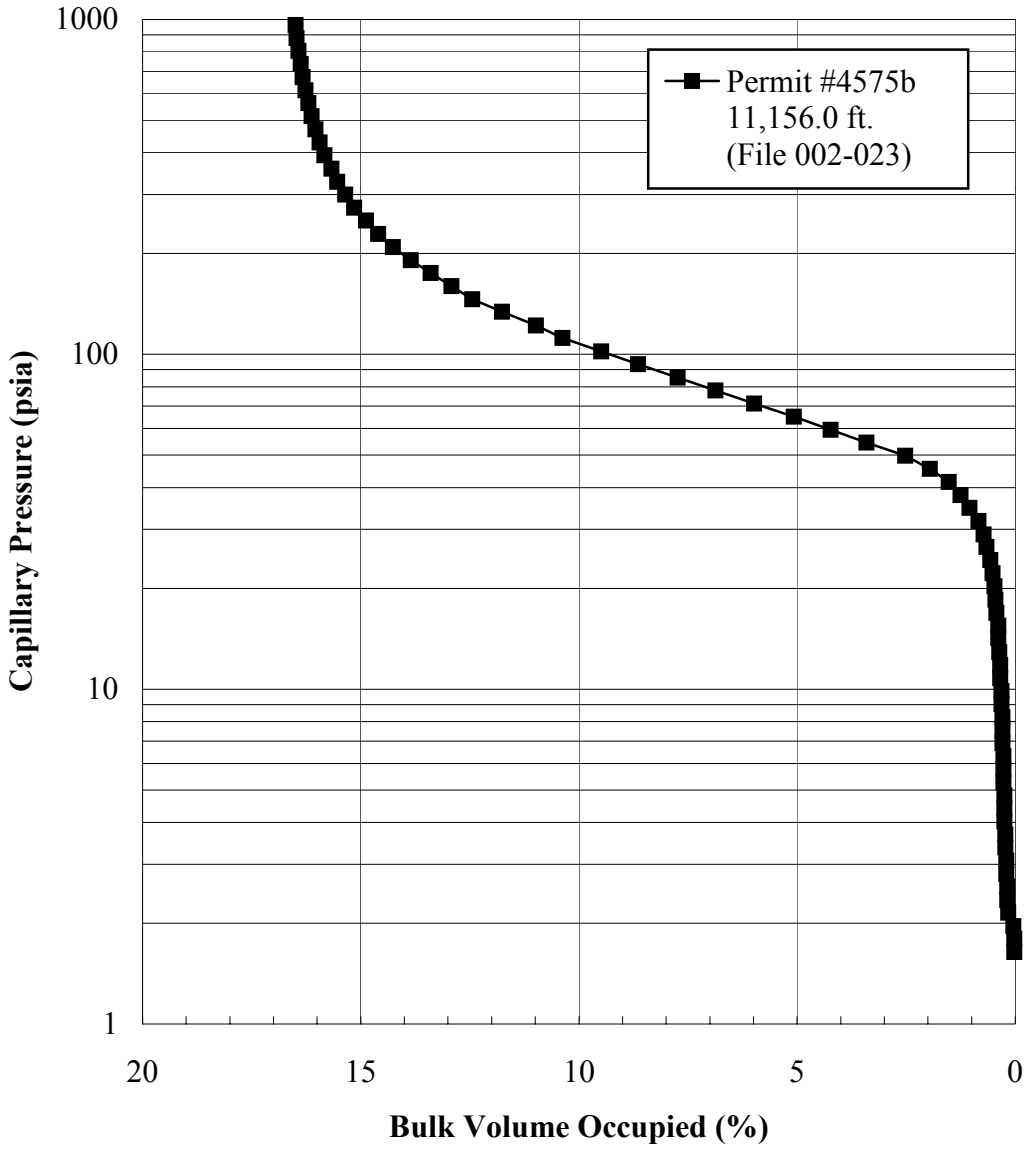

Figure 40. Mercury injection capillary pressure (pore volume) for Well Permit 4575B at 11,156 ft (from Hopkins, 2002).

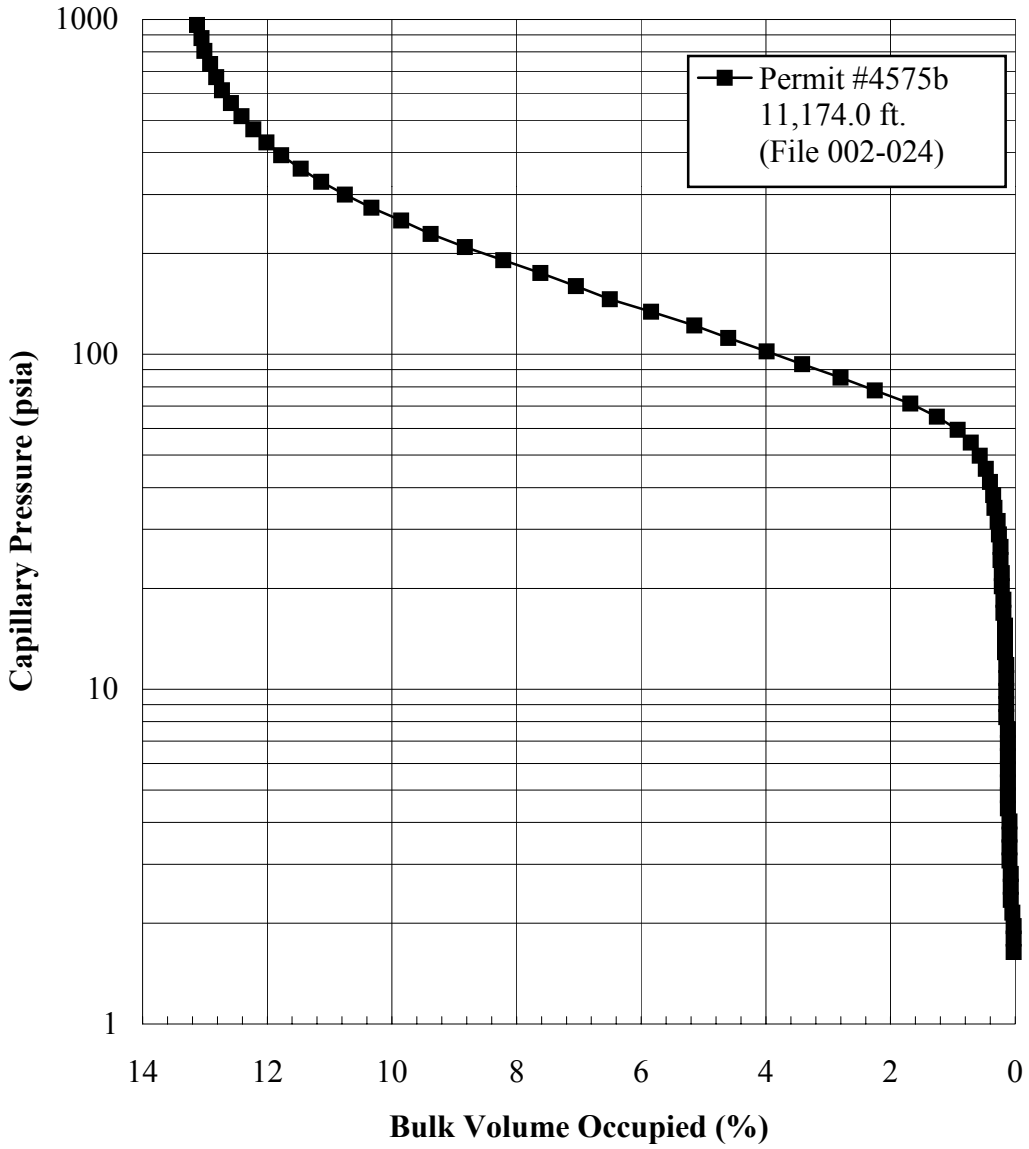

Figure 41. Mercury injection capillary pressure (pore volume) for Well Permit 4575B at 11,174 ft (from Hopkins, 2002).

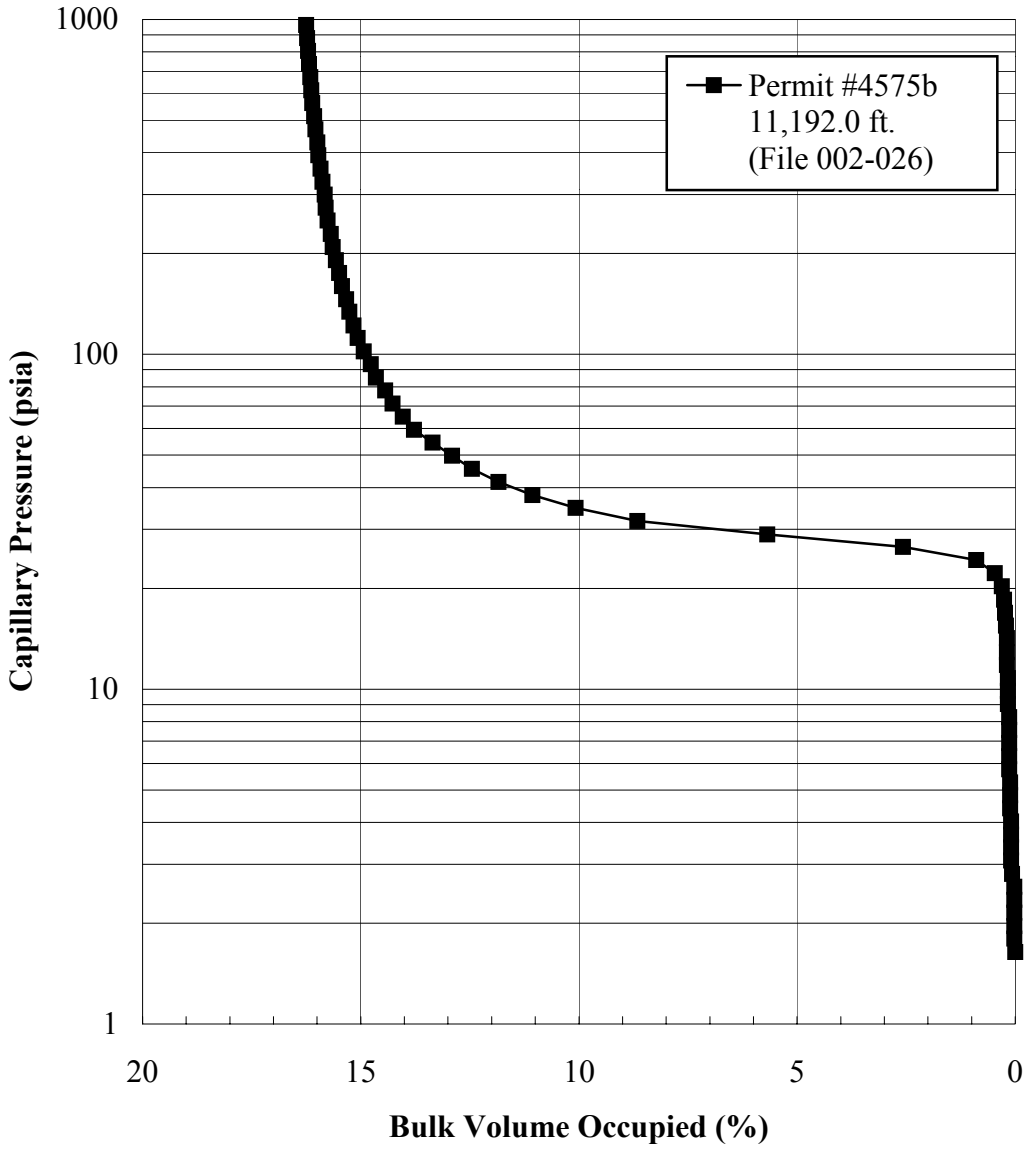

Figure 42. Mercury injection capillary pressure (pore volume) for Well Permit 4575B at 11,192 ft (from Hopkins, 2002).

Table 5. Plug data: measured values versus mercury (Hg) derived values (from Hopkins, 2002).

Plug Number	Well Permit #	Core Depth	Pore Types	Hg Median Pore Aperture (µm)	He % Porosity	Hg % Porosity	Pr Permeability (md)	Hg Permeability (md)
1	1591	11,405.0	ic	4.62	21.52	19.6	35.07	35.3
2	1591	11,411.0	ip, vg	1.07	12.10	9.02	5.60	0.98
3	1591	11,413.0	ic	2.59	17.15	15.3	8.19	8.83
4	1591	11,515.0	ic	5.20	18.33	16.4	41.83	34.7
5	1591	11,528.0	ic	2.33	16.39	15.0	9.04	8.95
11	4575b	11,120.0	vg	0.26	8.56	2.27	19.90	0.02
12	4575b	11,129.0	ip, ap, vg	3.33	20.73	18.7	22.40	17.8
14	4575b	11,146.0	ip, ap	2.36	17.68	16.6	6.87	8.67
15	4575b	11,156.0	ip, ap, vg	2.22	18.22	15.9	7.46	7.19
16	4575b	11,174.0	ip, ap, vg	1.28	15.25	12.9	2.27	2.07
18	4575b	11,192.0	ic	6.75	17.27	16.0	42.67	49.5

ic=intercrystalline
ip=interparticle
vg=vuggy
ap=intraparticle

Hg - Mercury Derived
He - Helium Porosimeter
Pr - Probe Permeameter

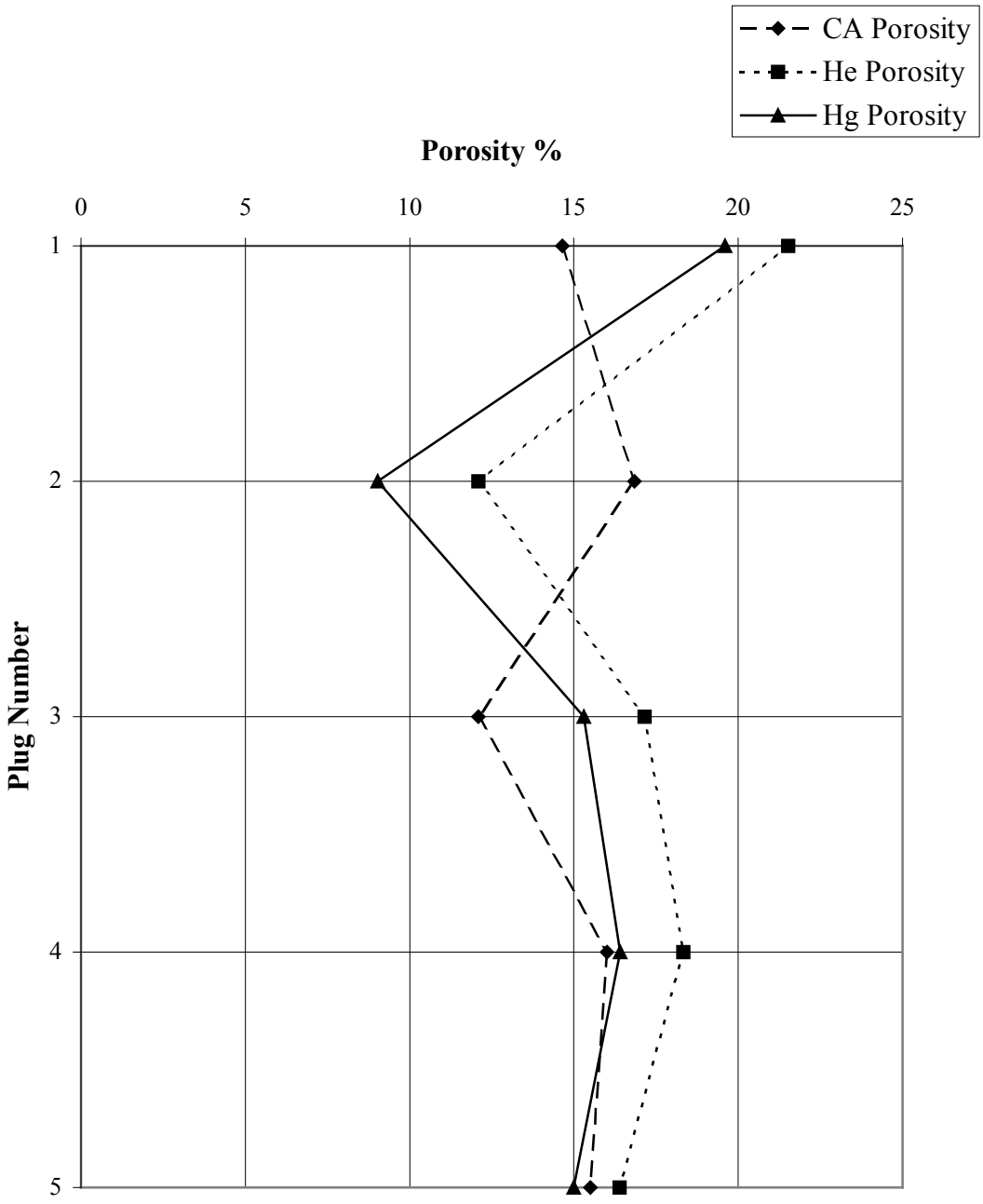

Figure 43. Comparison of porosities derived from various tests for Well Permit 1591. CA=core analysis, He=helium derived, Hg=mercury derived (from Hopkins, 2002).

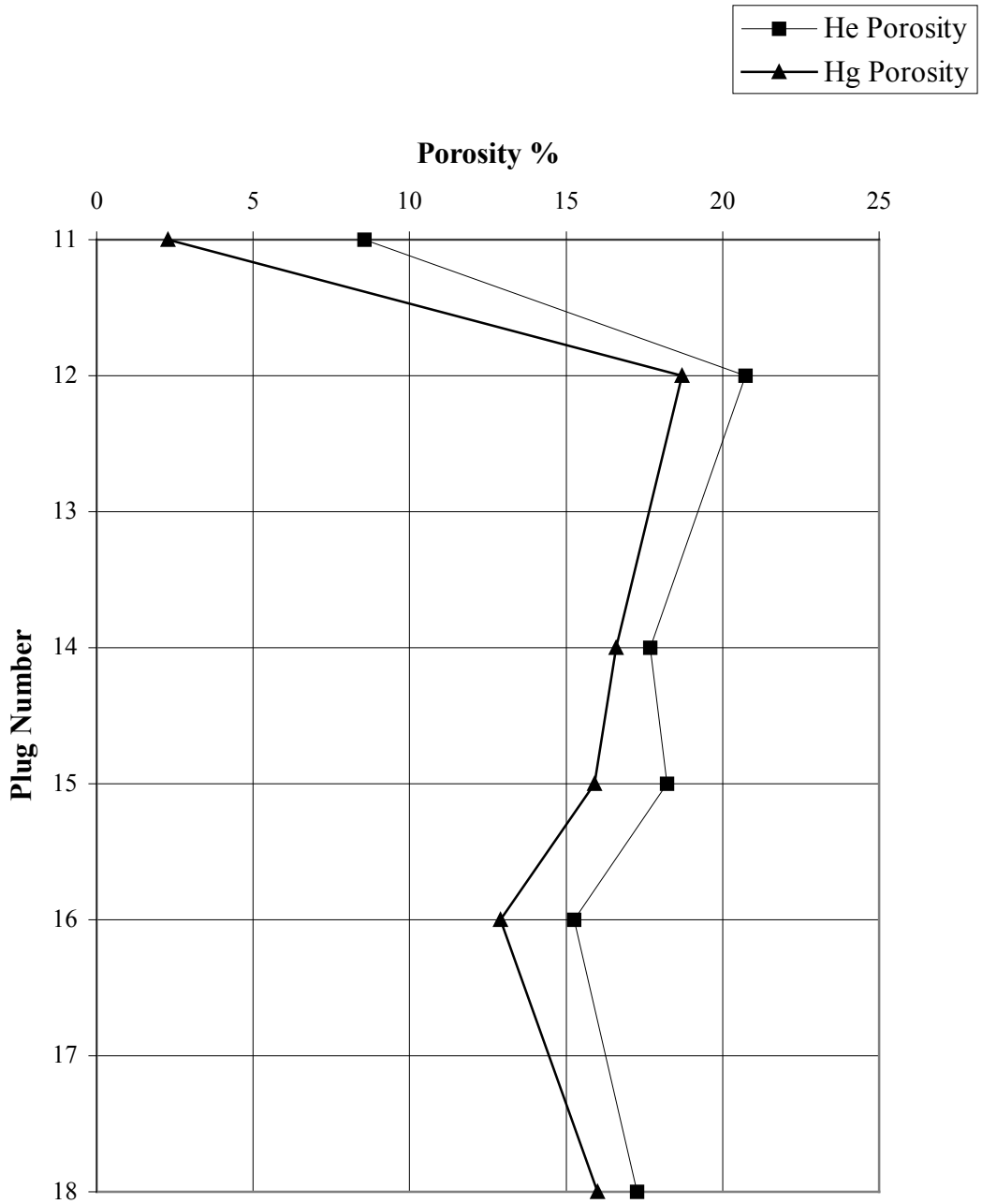

Figure 44. Comparison of porosities derived from various tests for Well Permit 4547B. CA=core analysis, He=helium derived, Hg=mercury derived (from Hopkins, 2002).

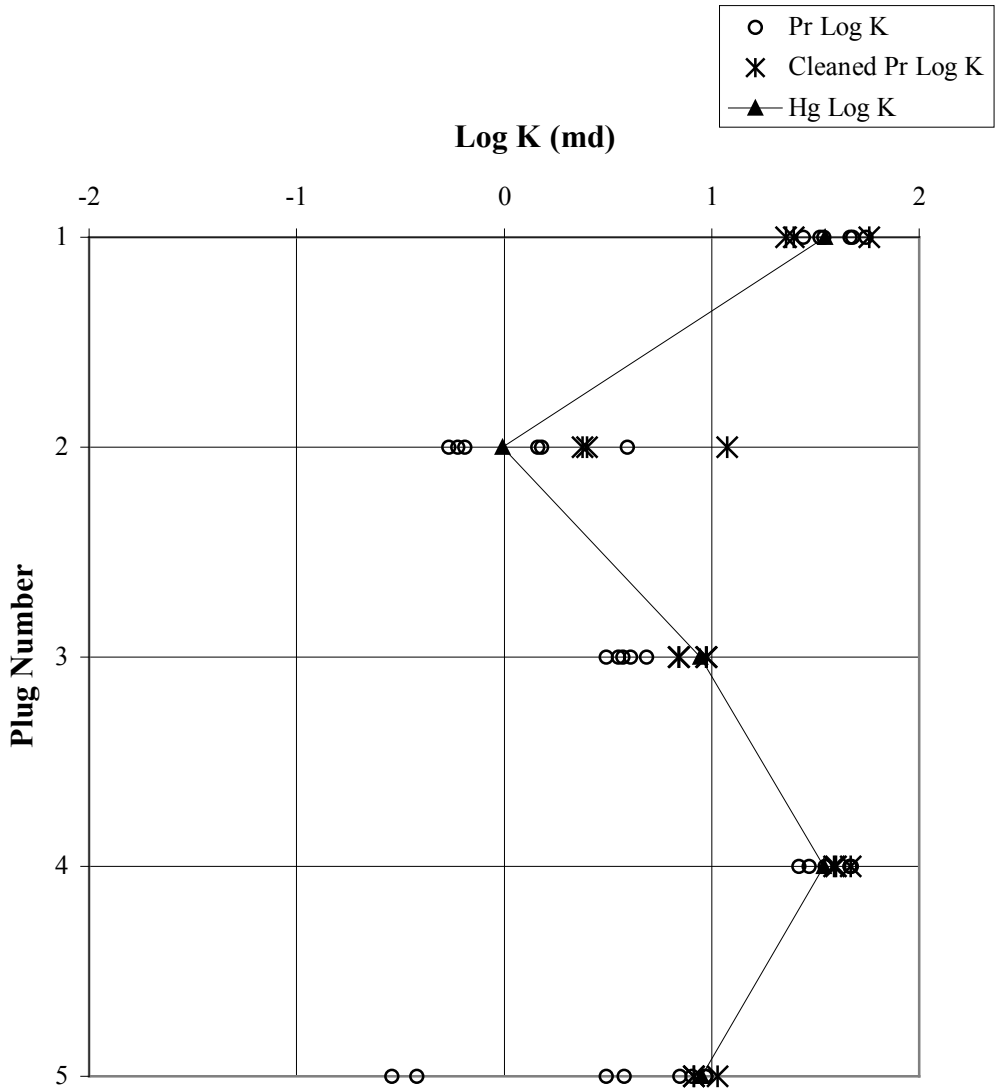

Figure 45. Comparison of log permeabilities derived from various tests for Well Permit 1591 (from Hopkins, 2002).

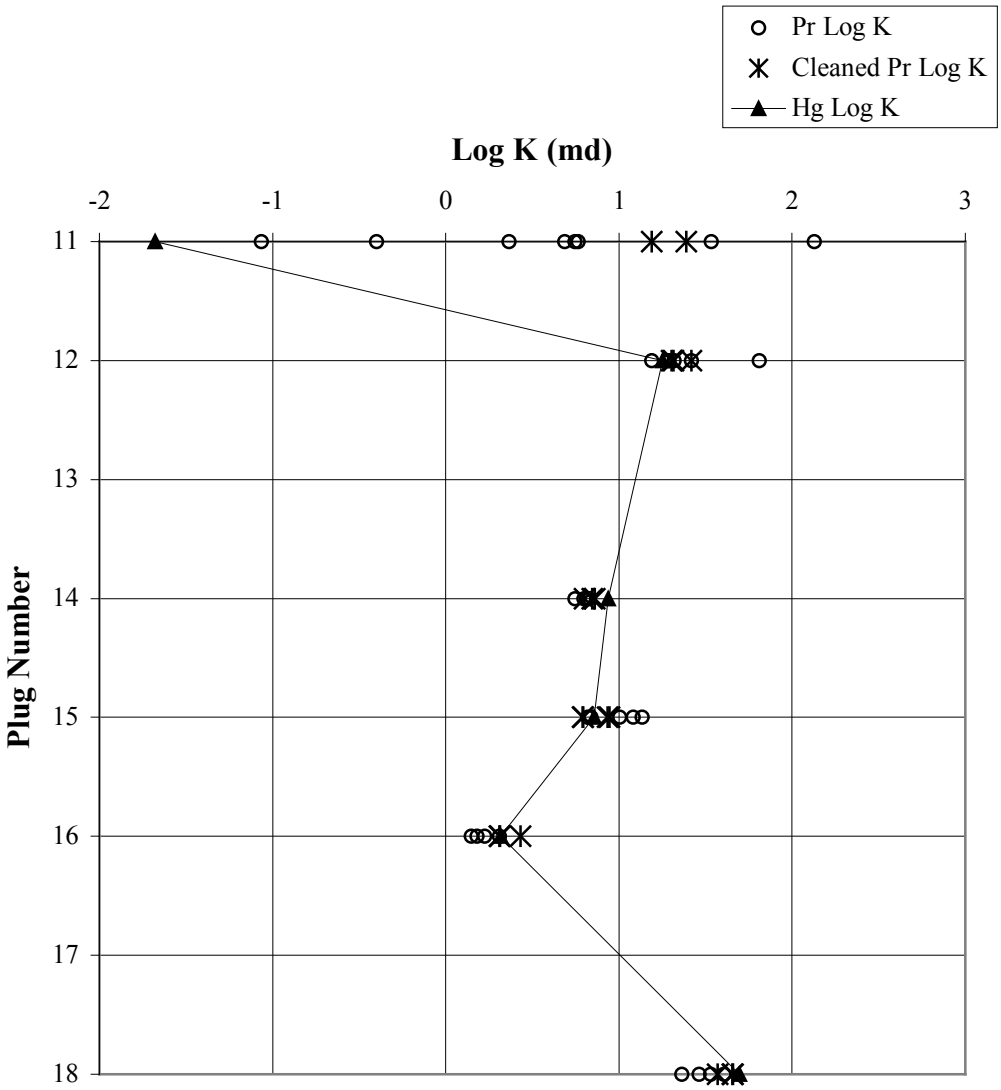

Figure 46. Comparison of log permeabilities derived from various tests for Well Permit 4575B (from Hopkins, 2002).

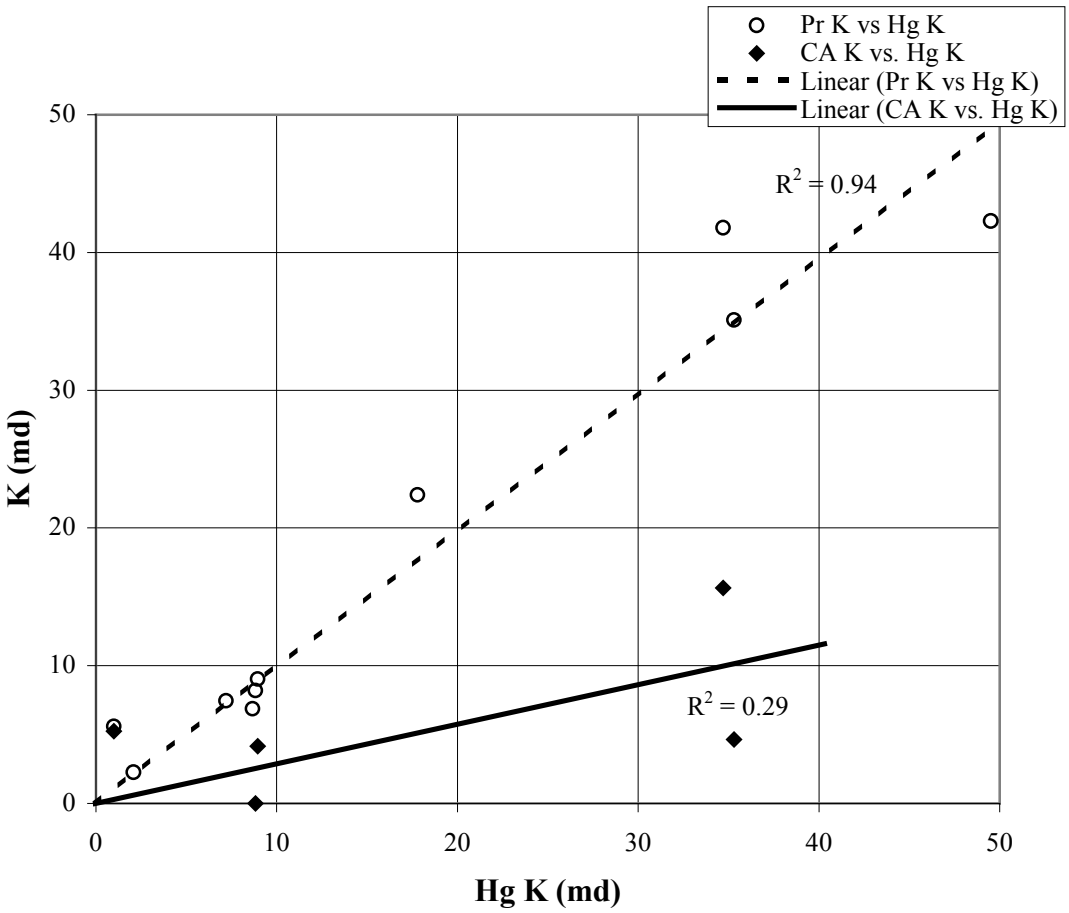

Figure 47. Comparison of mercury derived (Hg), core analysis (CA), and probe permeability (Pr) data (from Hopkins, 2002).

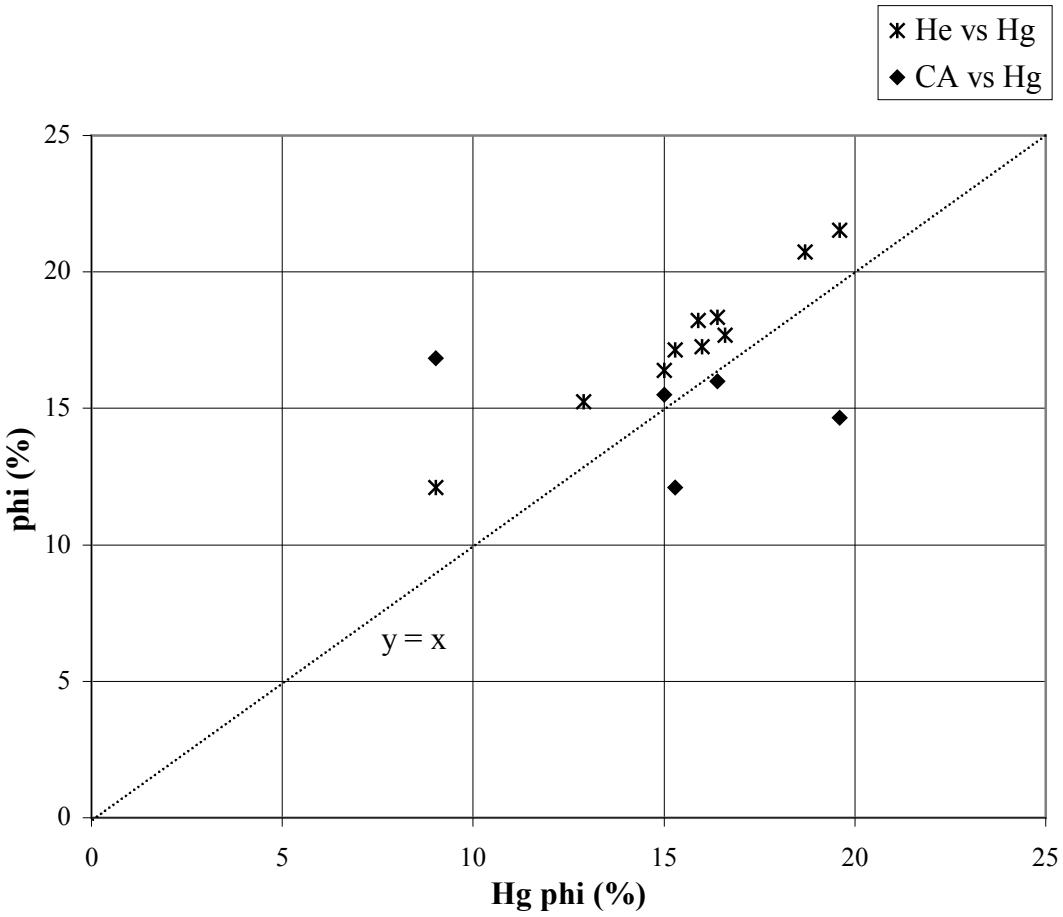

Figure 48. Comparison of helium and core analysis porosities with mercury (capillary pressure) porosity (from Hopkins, 2002).

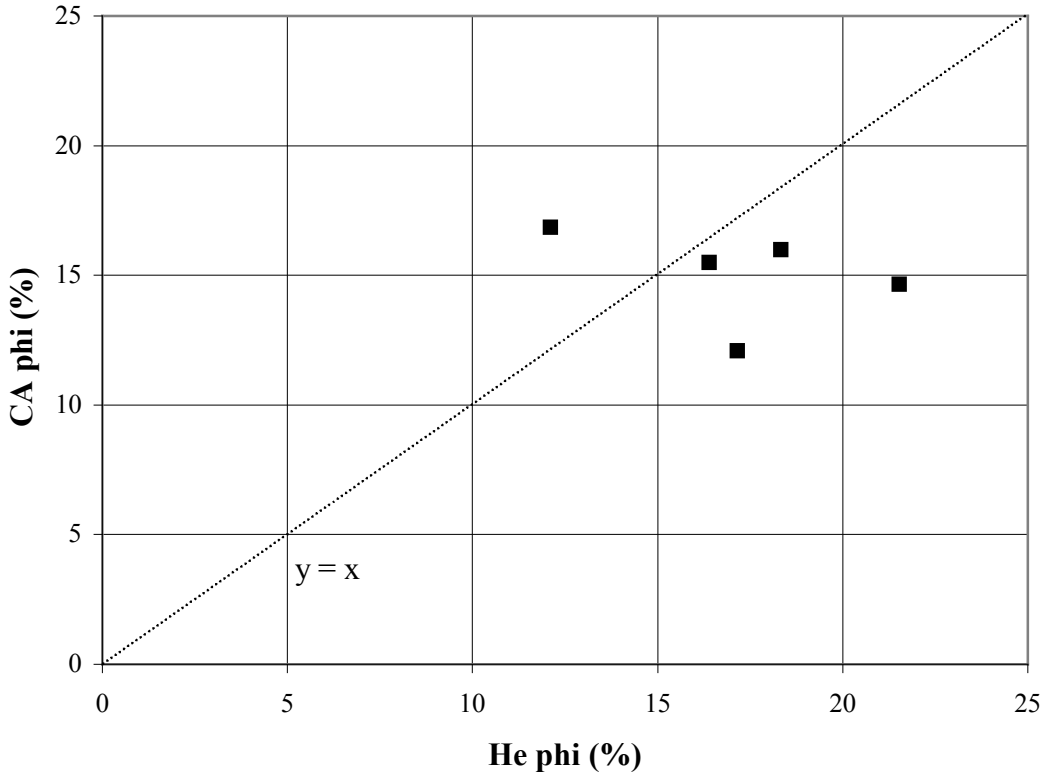

Figure 49. Comparison of core analysis porosity and helium porosity (from Hopkins, 2002).

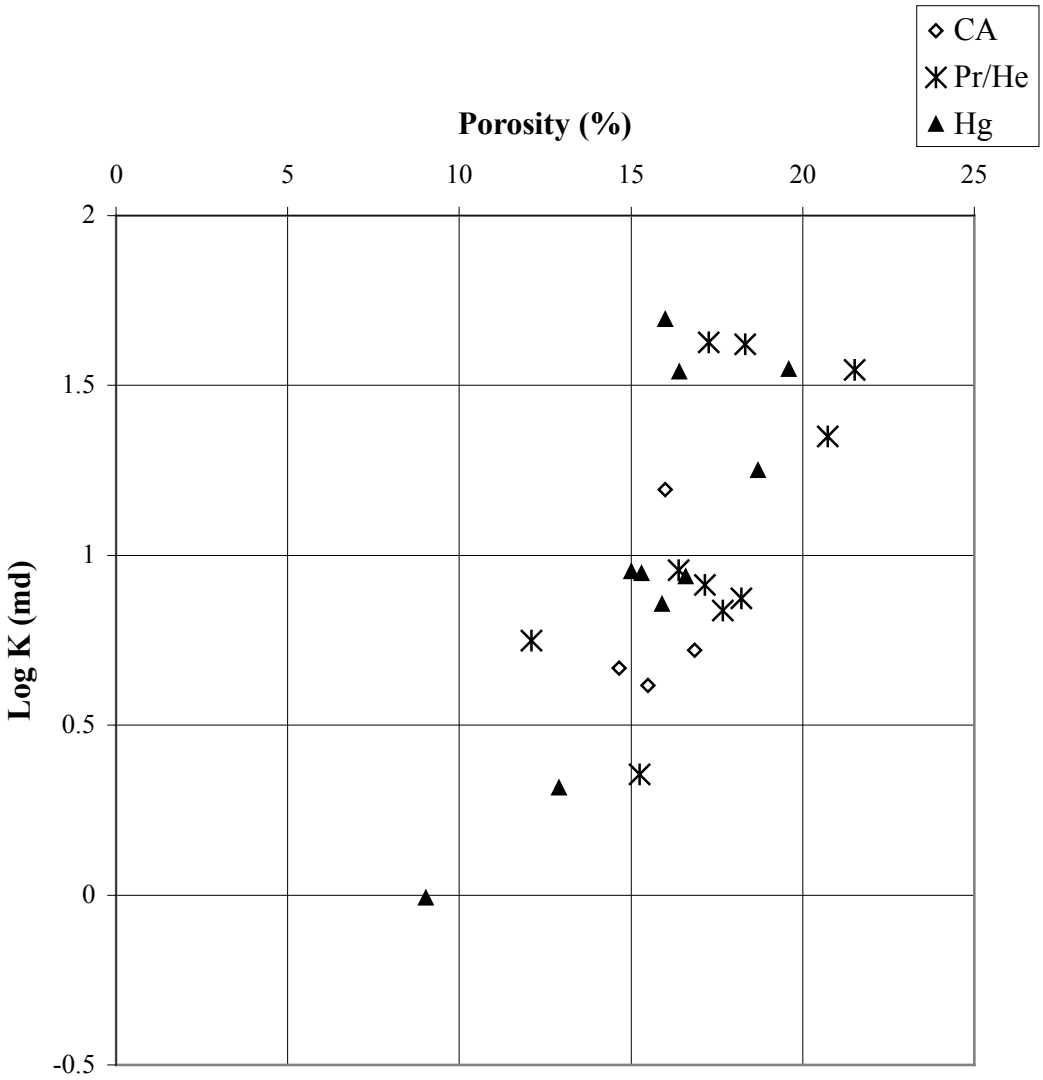

Figure 50. Comparison of porosity and permeability relationships from each method used. CA=core analysis porosity and permeability, Pr/He=plugs measured with the probe permeameter and helium porosimeter, Hg=mercury derived porosity and permeability (from Hopkins, 2002).

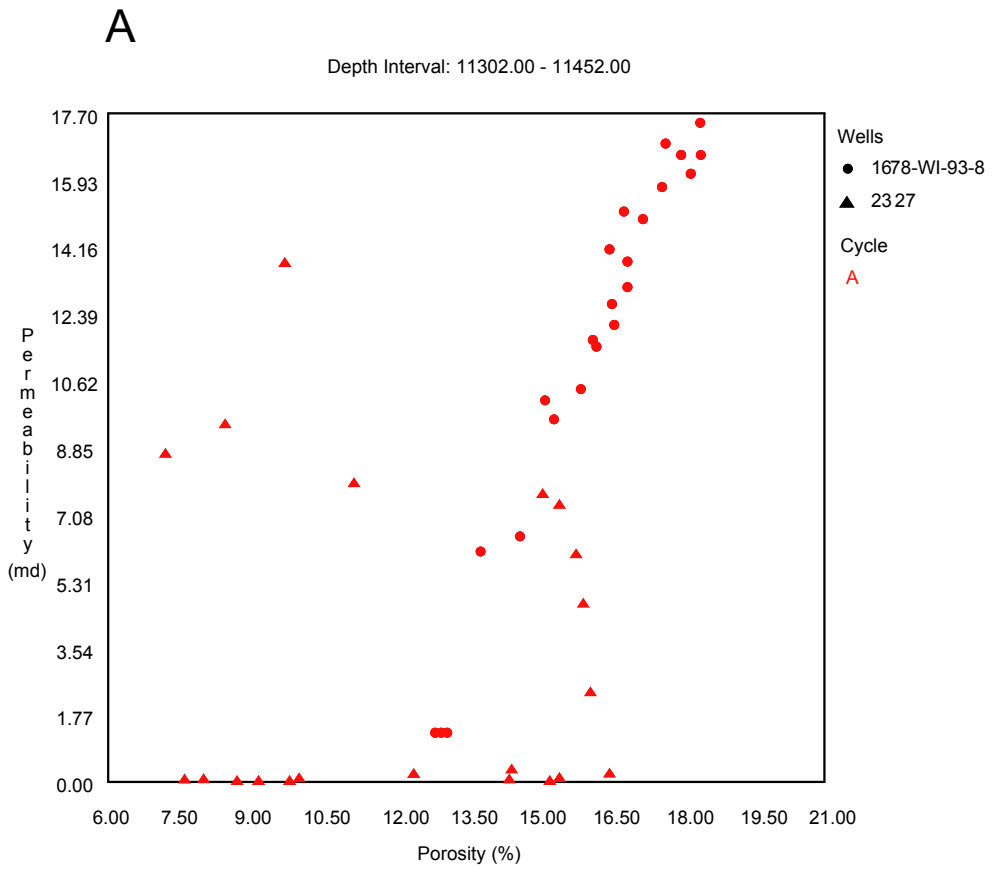

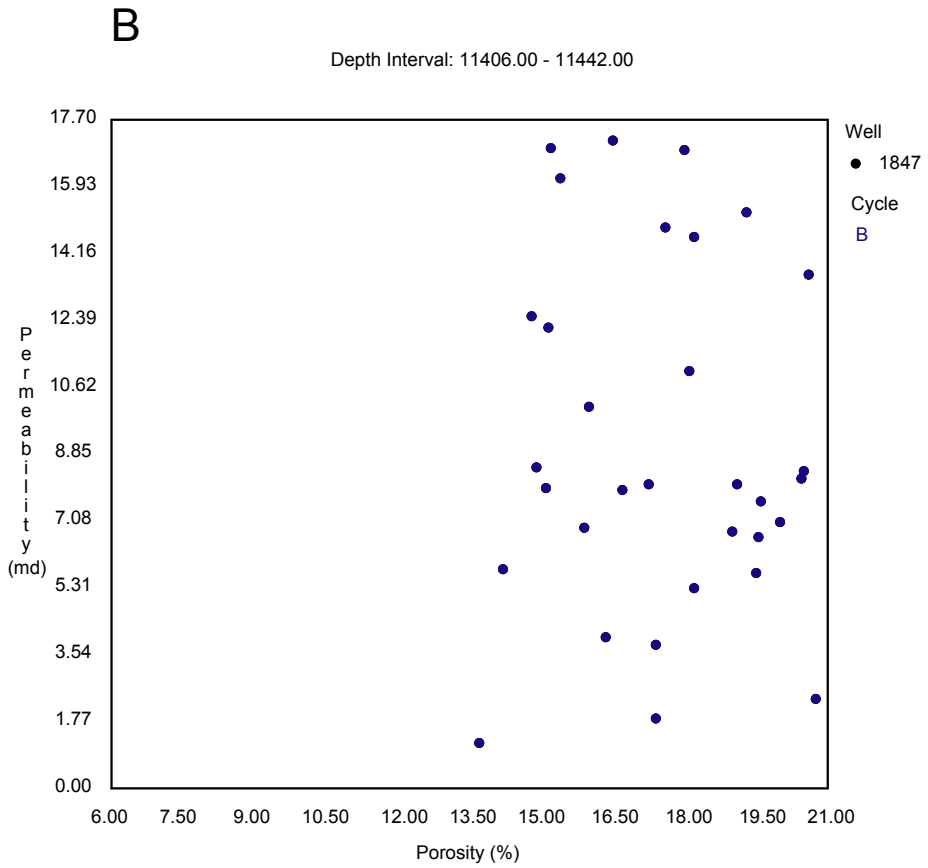

Figure 51. Porosity vs. permeability plots for: (A) Cycle A for wells, Permit # 1678, high production well and Permit #2327, low production well, (B) Cycle B for well, Permit #1847.

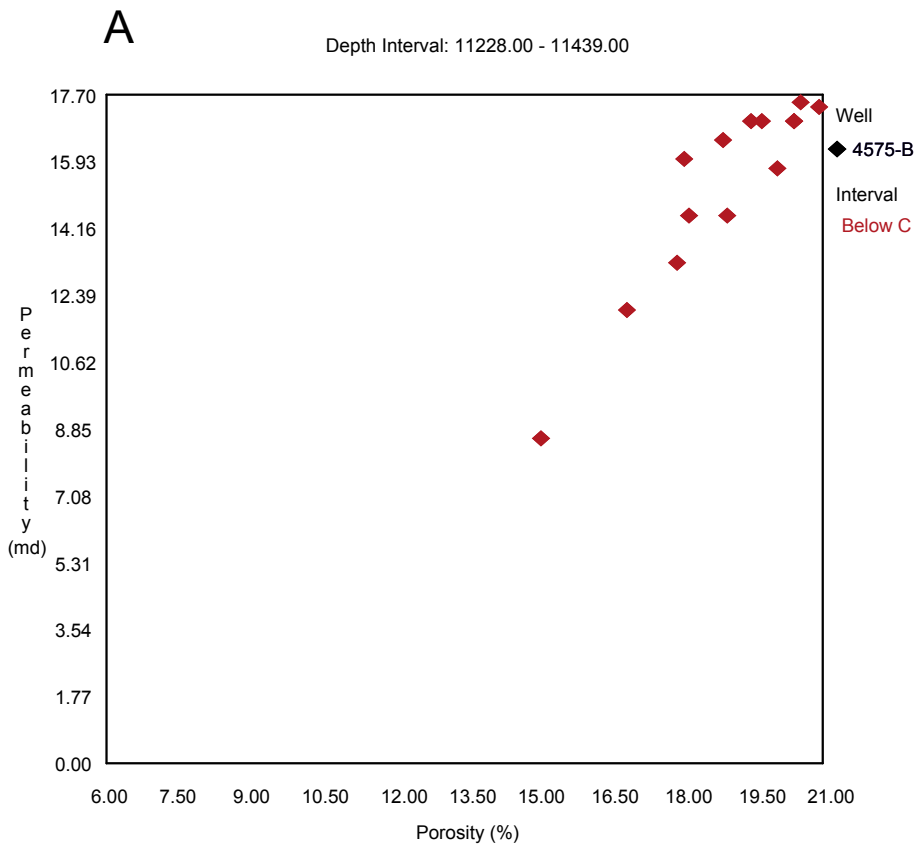

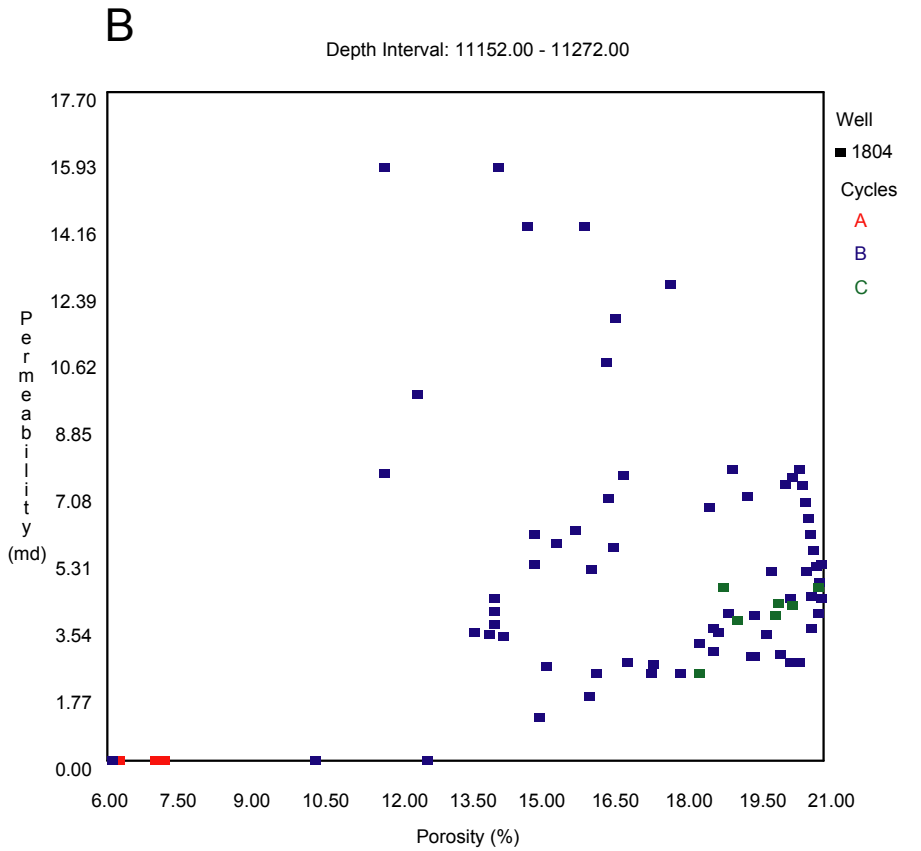

Figure 52. Porosity vs. permeability plots for: (A) Interval immediately below Cycle C for well Permit #4575B, (B) Cycles A, B, and C for well, Permit #1804.

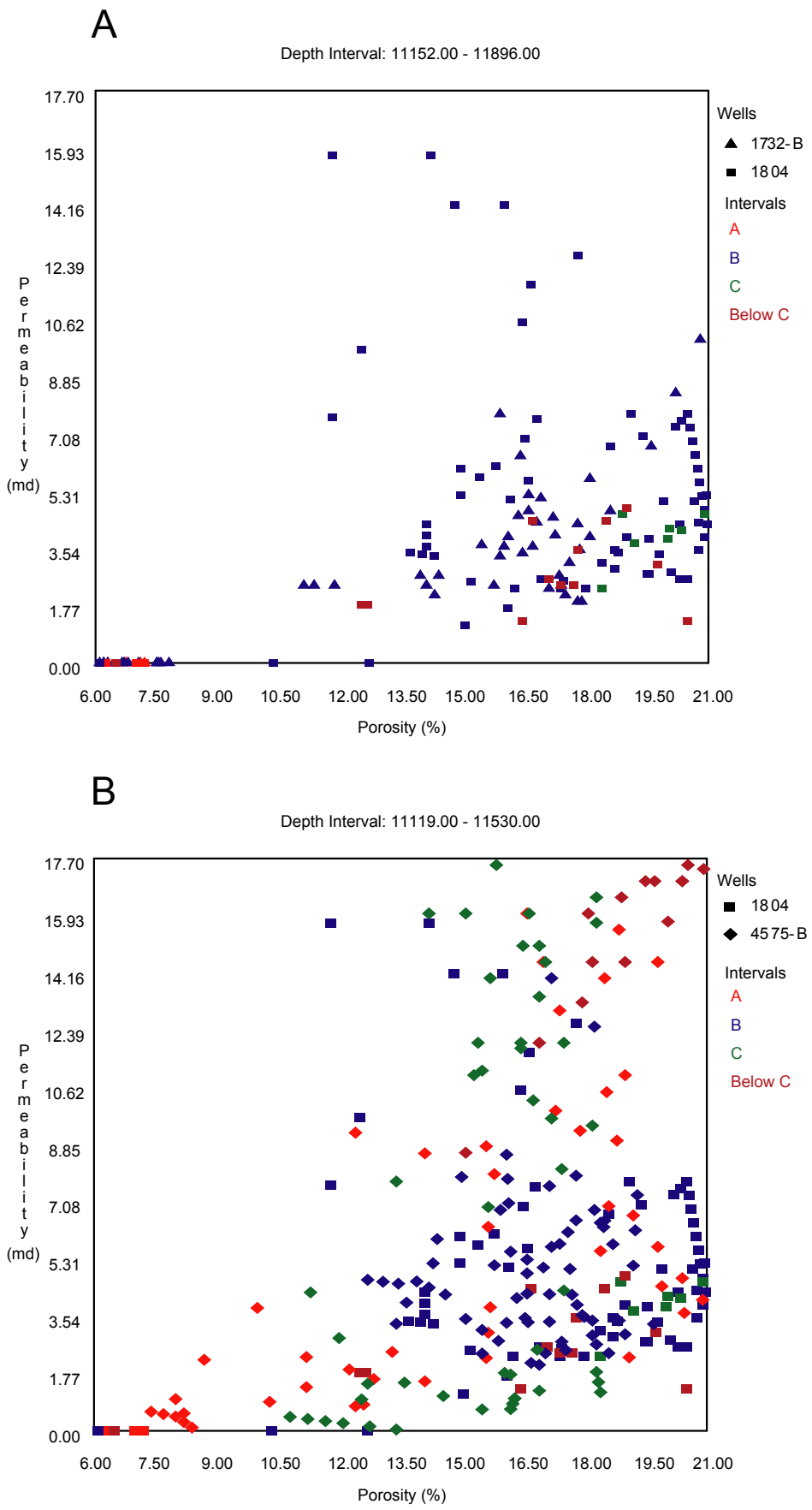

Figure 53. Porosity vs. permeability plots for: (A) Cycles A, B, C and interval immediately below Cycle C for wells, Permit #1732B and Permit #1804, and (B) Cycles A, B, C and interval immediately below Cycle C for wells, Permit #1804 and Permit #4575B. See Figure 8 for location of wells.

Table 6. Common pore type associations in the mercury injection capillary pressure sample set, with the average porosity and median pore throat aperture (from Hopkins, 2002).

Common Pore Type Associations	Average Sample Porosities (%)	Average MPA (μm)
intercrystalline 1	6.5	4.3
interparticle, intraparticle, moldic	16.3	2.3
interparticle, intraparticle	15.8	2.3
interparticle, vuggy	9.0	1.1
channel, vuggy	2.3	0.3

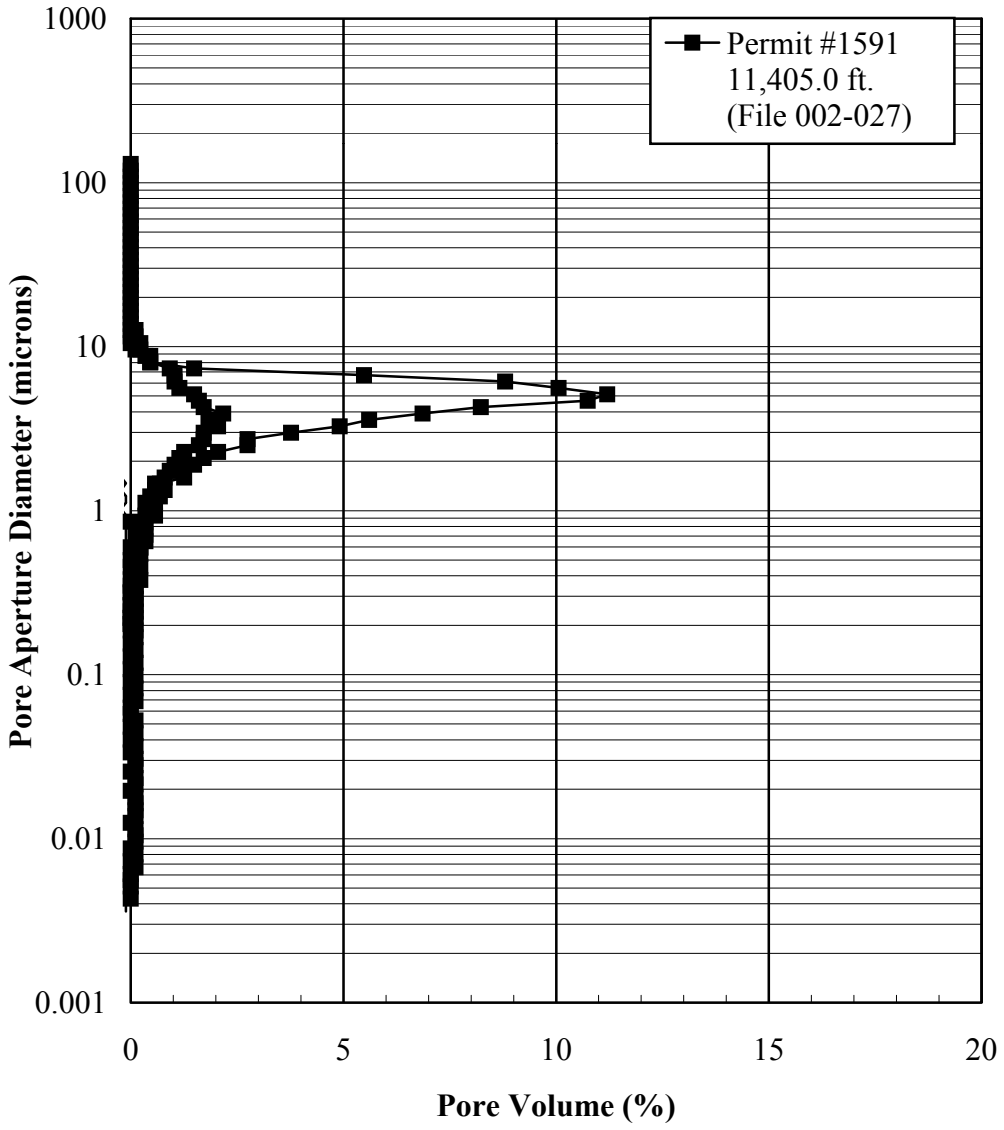

Figure 54. Pore aperture size distribution for Well Permit 1591 at 11,405 ft. (from Hopkins, 2002).

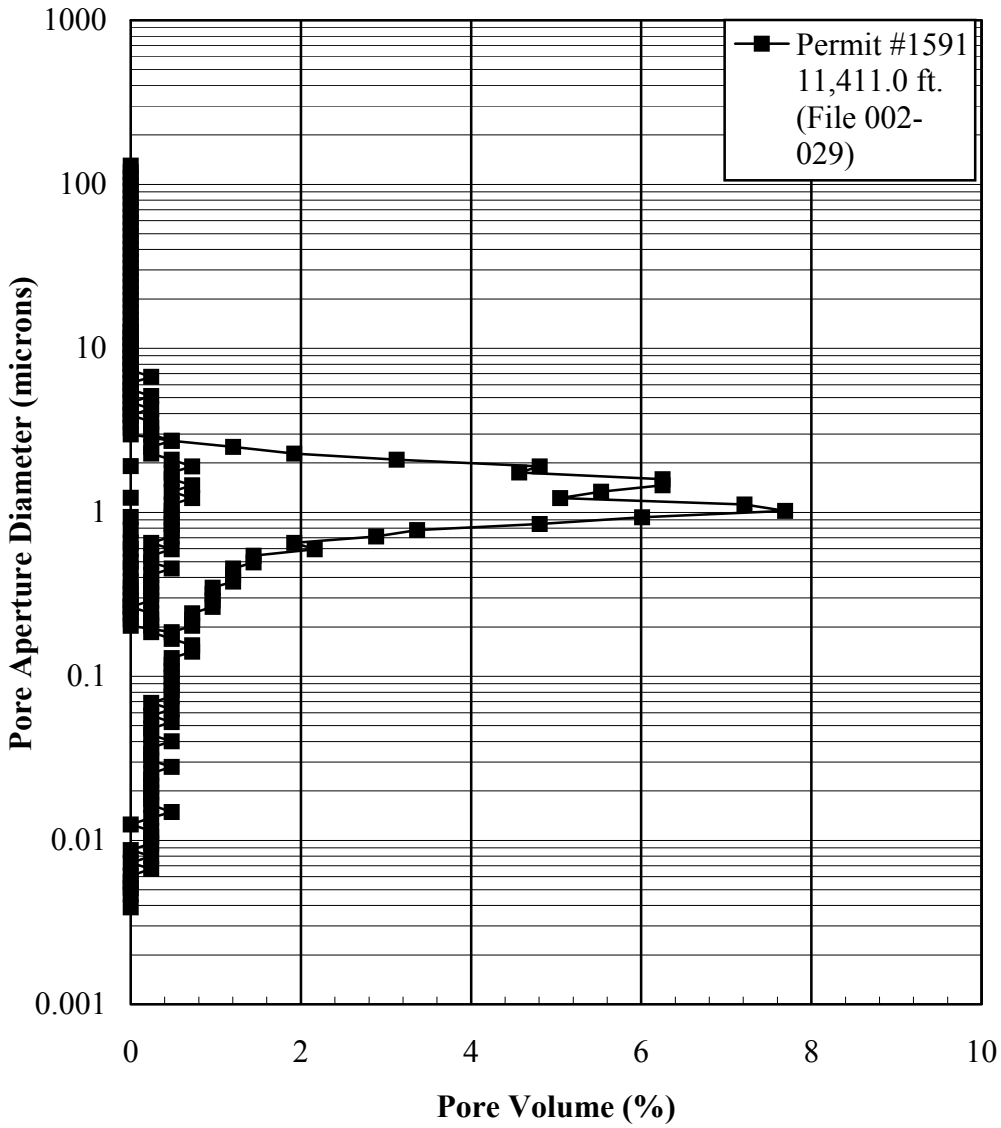

Figure 55. Pore aperture size distribution for Well Permit 1591 at 11,411 ft. (from Hopkins, 2002).

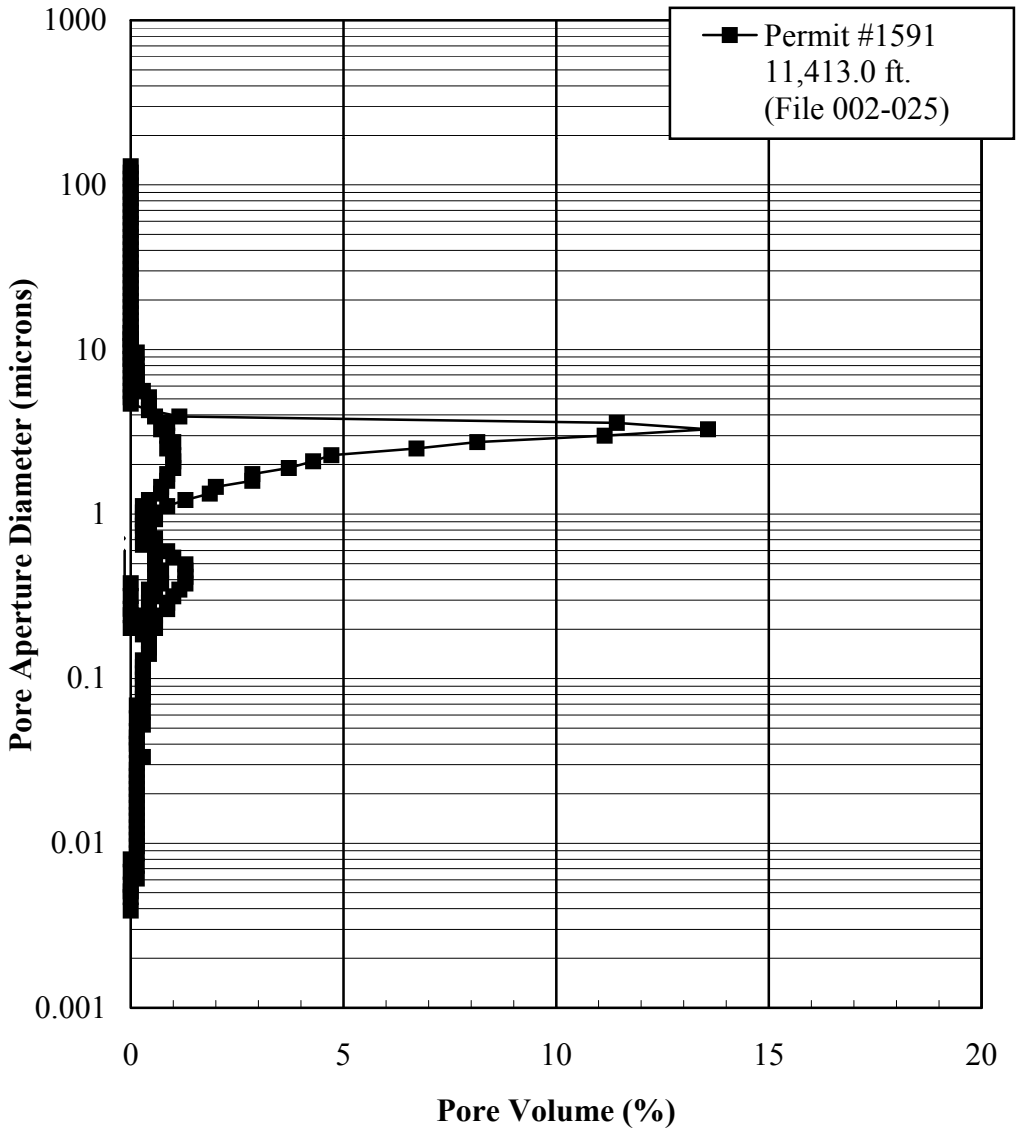

Figure 56. Pore aperture size distribution for Well Permit 1591 at 11,413 ft. (from Hopkins, 2002).

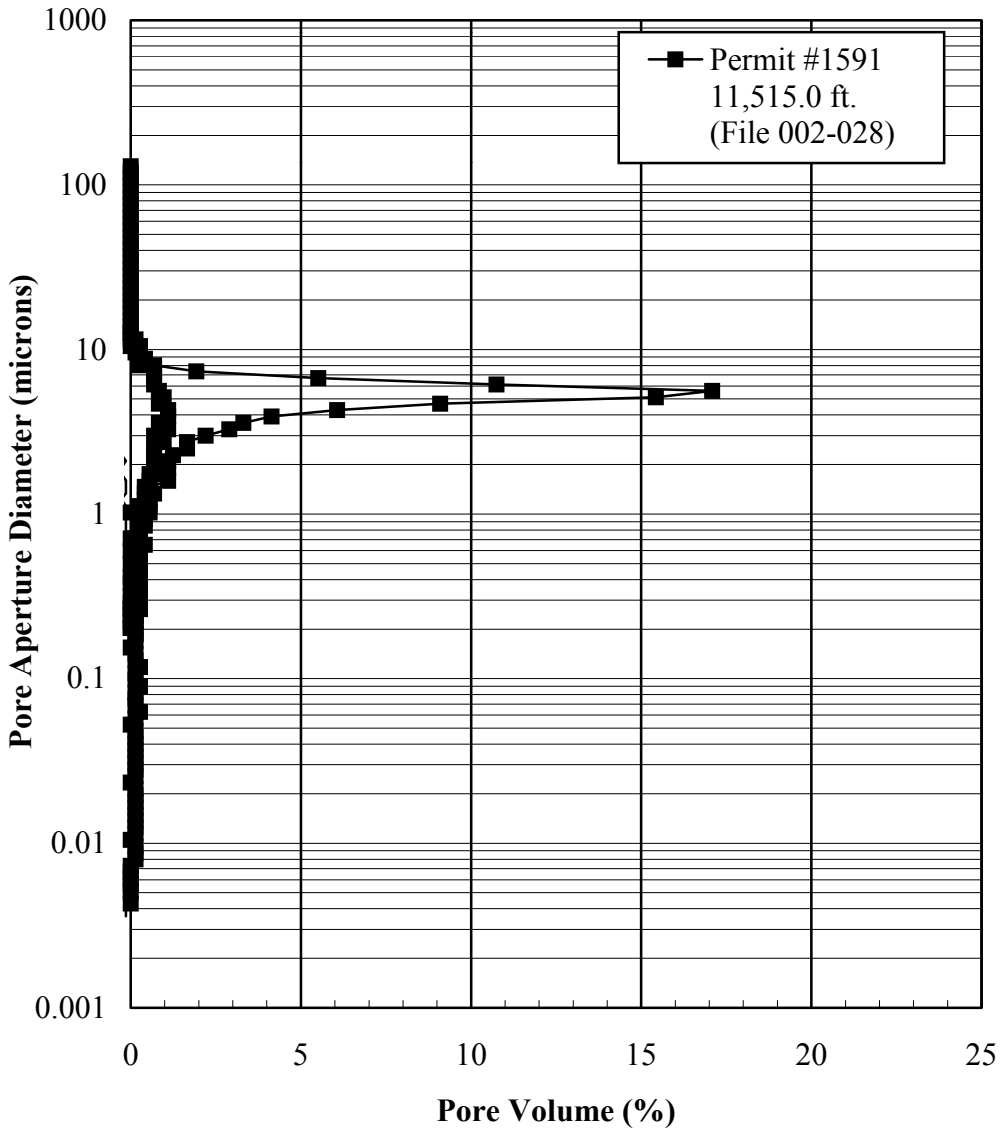

Figure 57. Pore aperture size distribution for Well Permit 1591 at 11,515 ft. (from Hopkins, 2002).

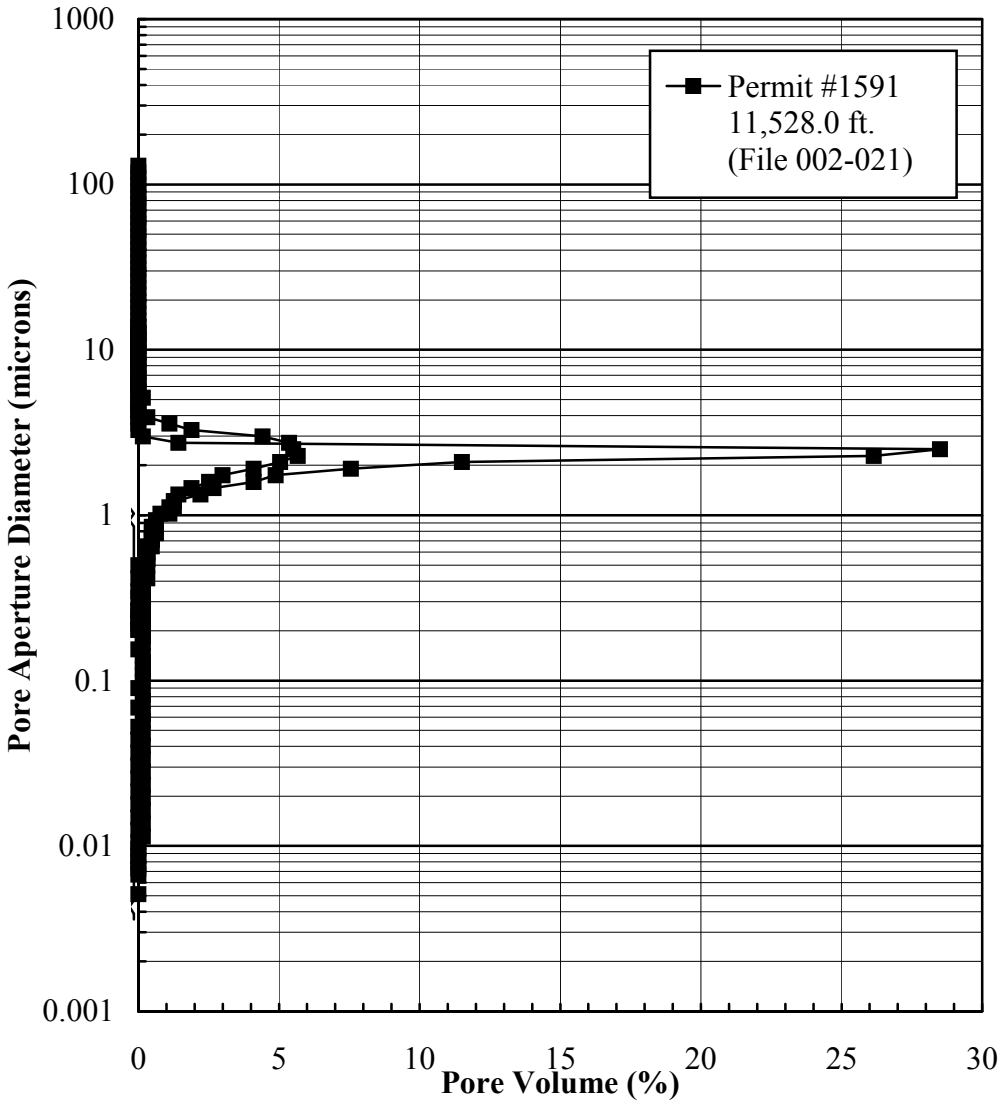

Figure 58. Pore aperture size distribution for Well Permit 1591 at 11,528 ft.

(from Hopkins, 2002).

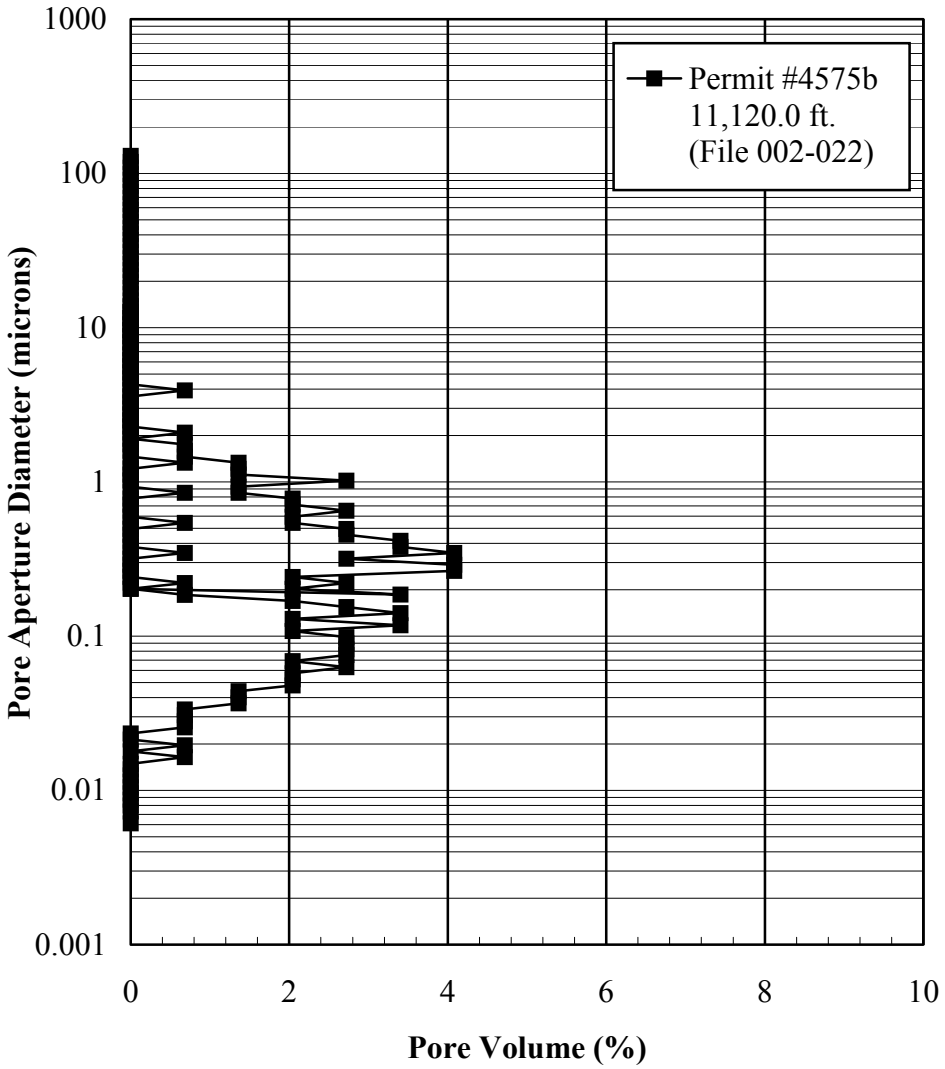

Figure 59. Pore aperture size distribution for Well Permit 4575B at 11,120 ft. (from Hopkins, 2002).

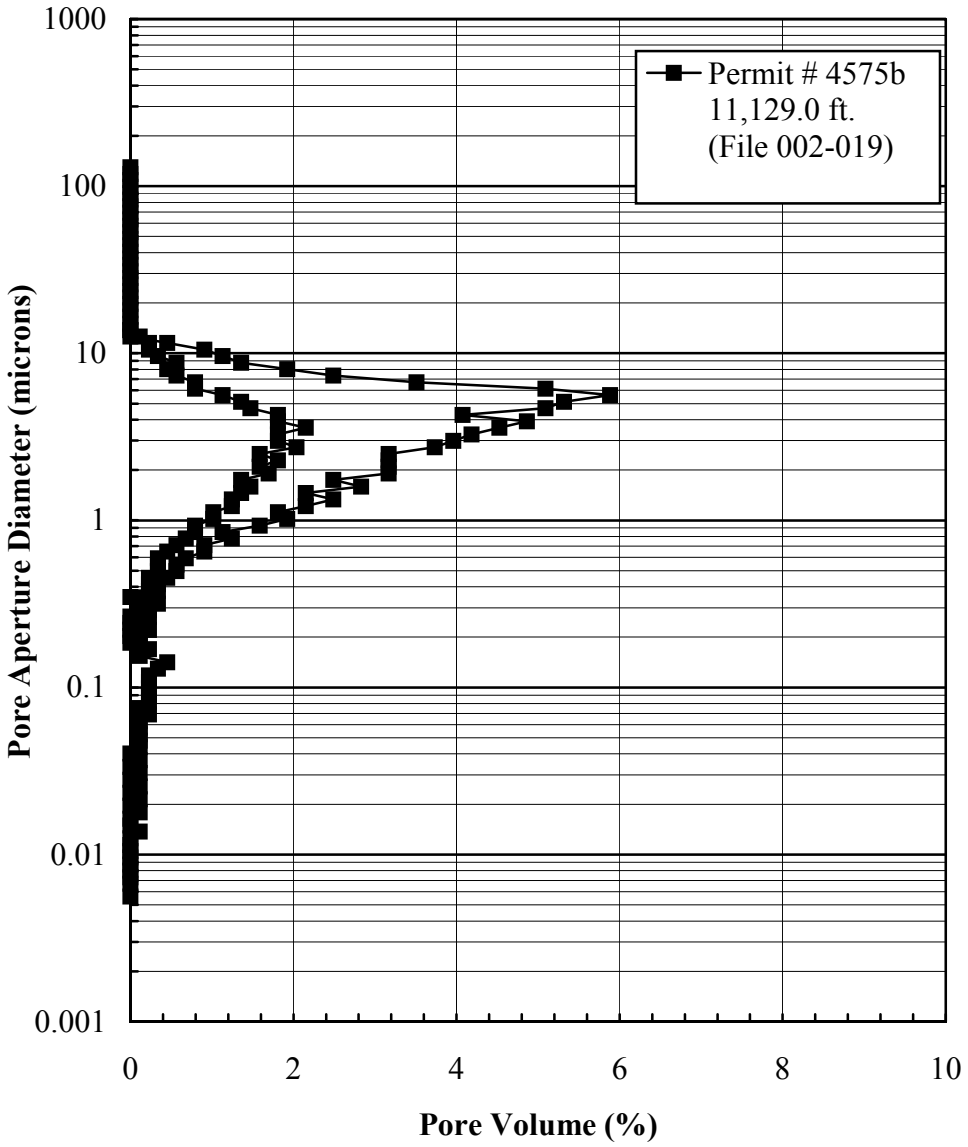

Figure 60. Pore aperture size distribution for Well Permit 4575B at 11,129 ft. (from Hopkins, 2002).

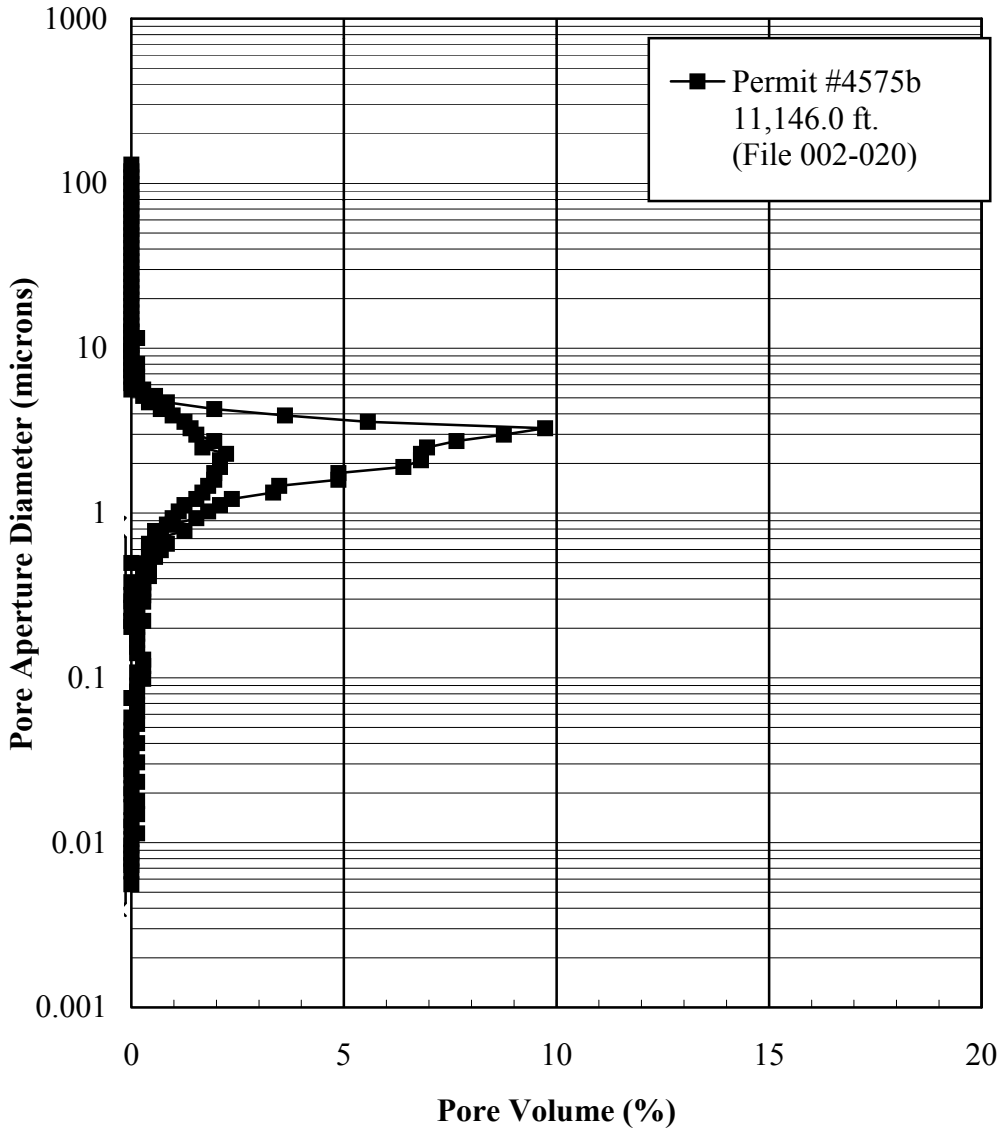

Figure 61. Pore aperture size distribution for Well Permit 4575B at 11,146 ft. (from Hopkins, 2002).

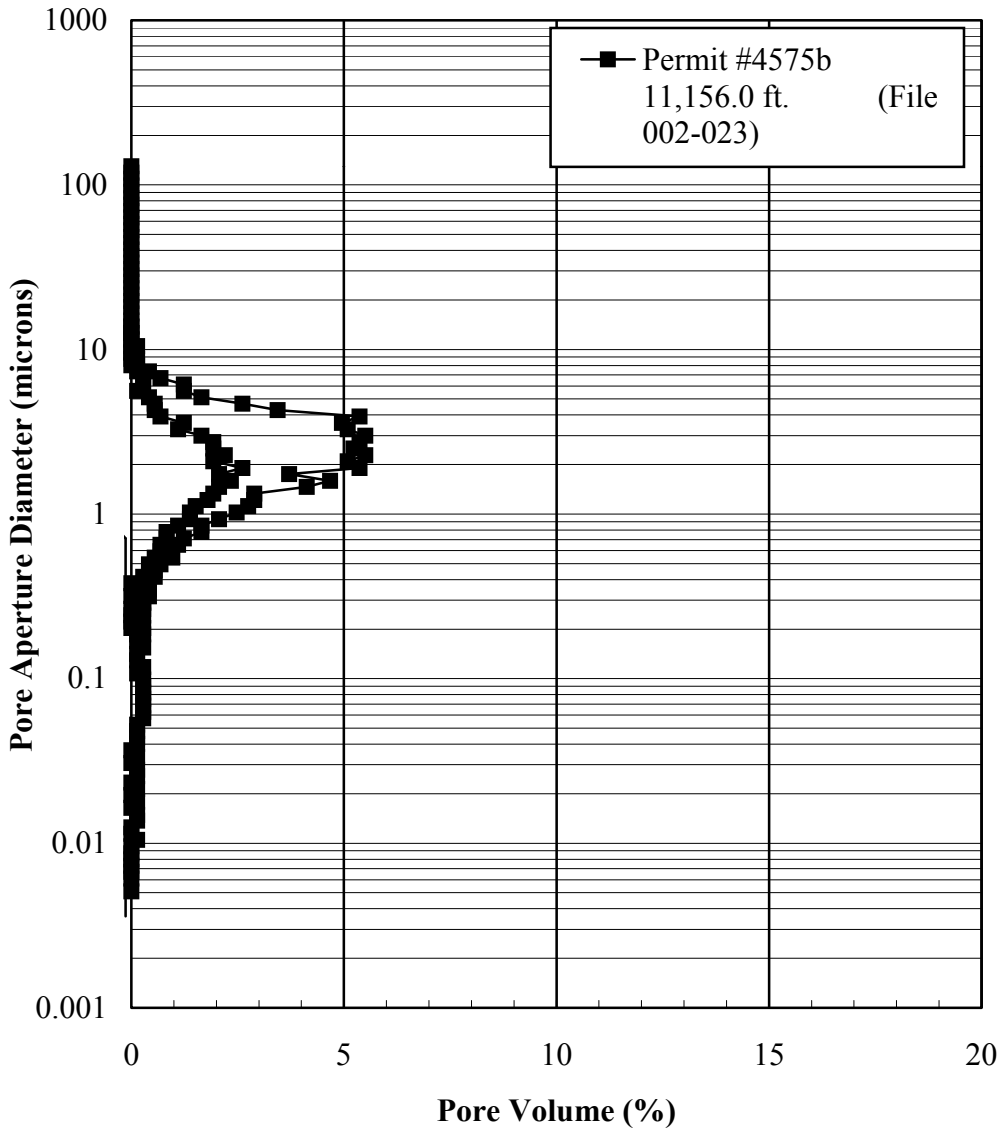

Figure 62. Pore aperture size distribution for Well Permit 4575B at 11,156 ft. (from Hopkins, 2002).

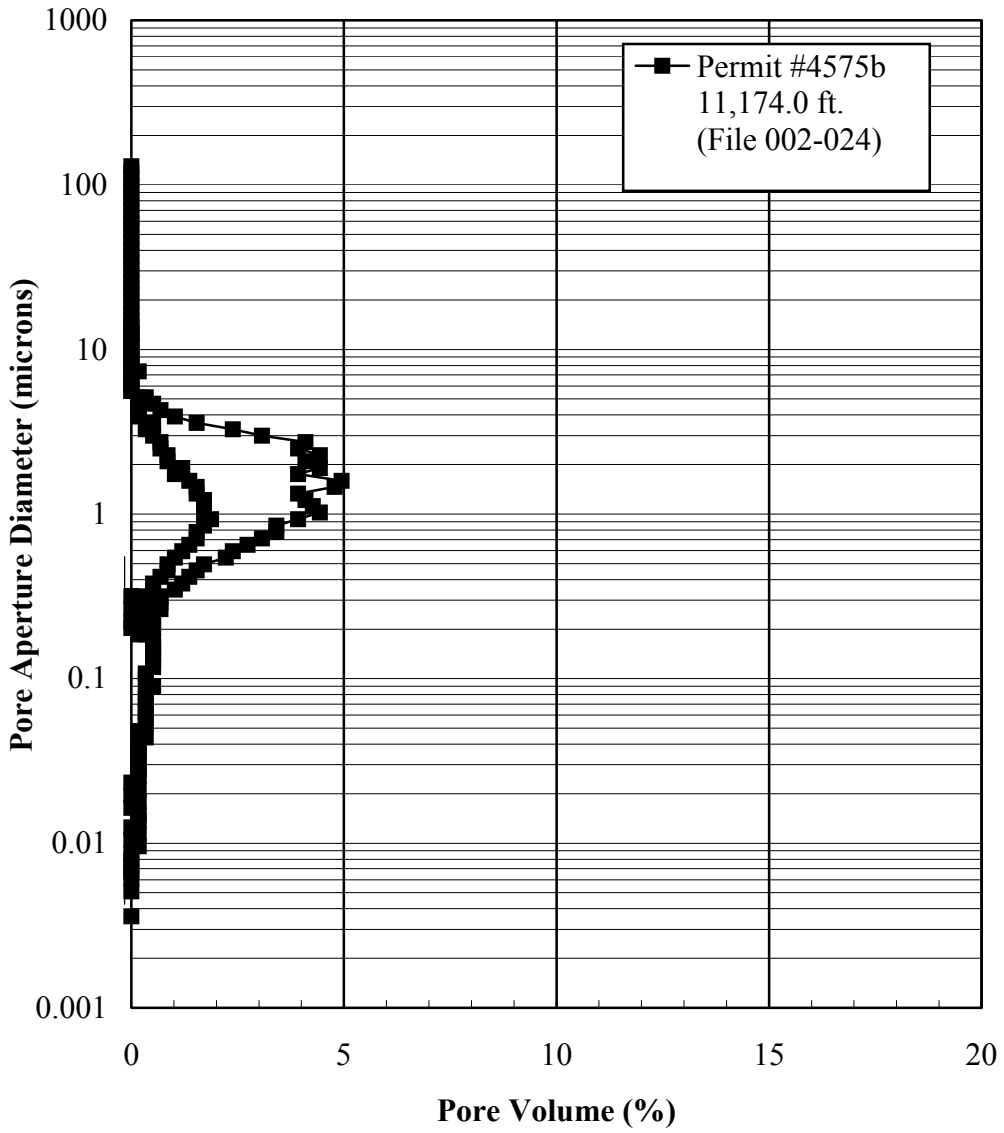

Figure 63. Pore aperture size distribution for Well Permit 4575B at 11,174 ft. (from Hopkins, 2002).

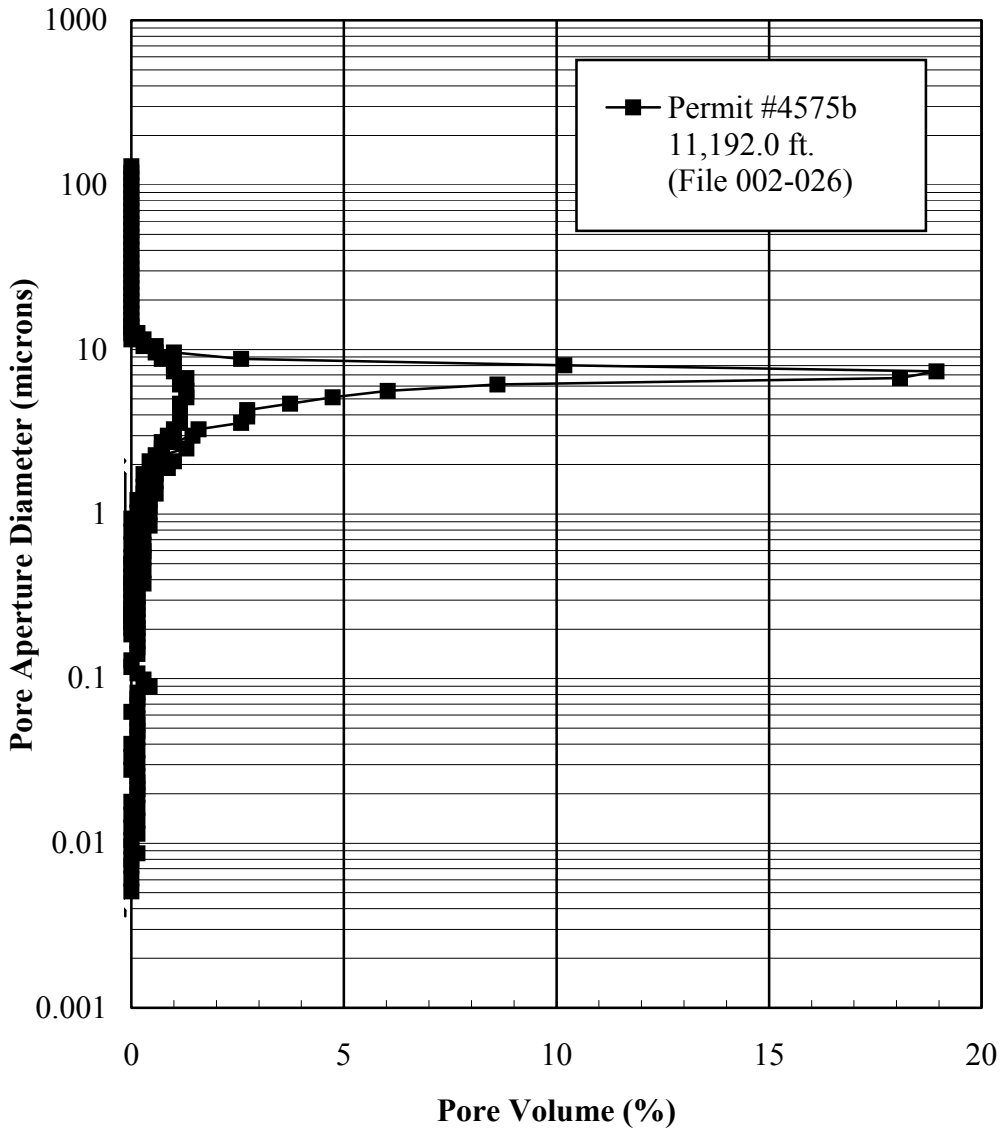

Figure 64. Pore aperture size distribution for Well Permit 4575B at 11,192 ft. (from Hopkins, 2002).

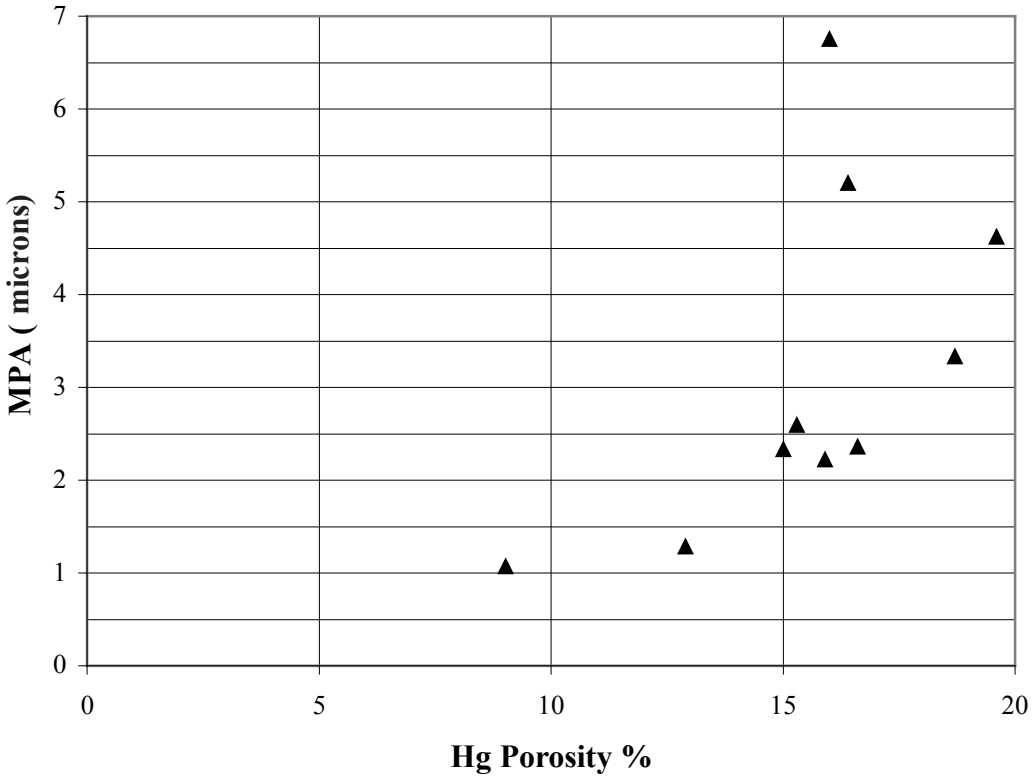

Figure 65. Graph of median pore throat aperture versus mercury derived porosity (from Hopkins, 2002).

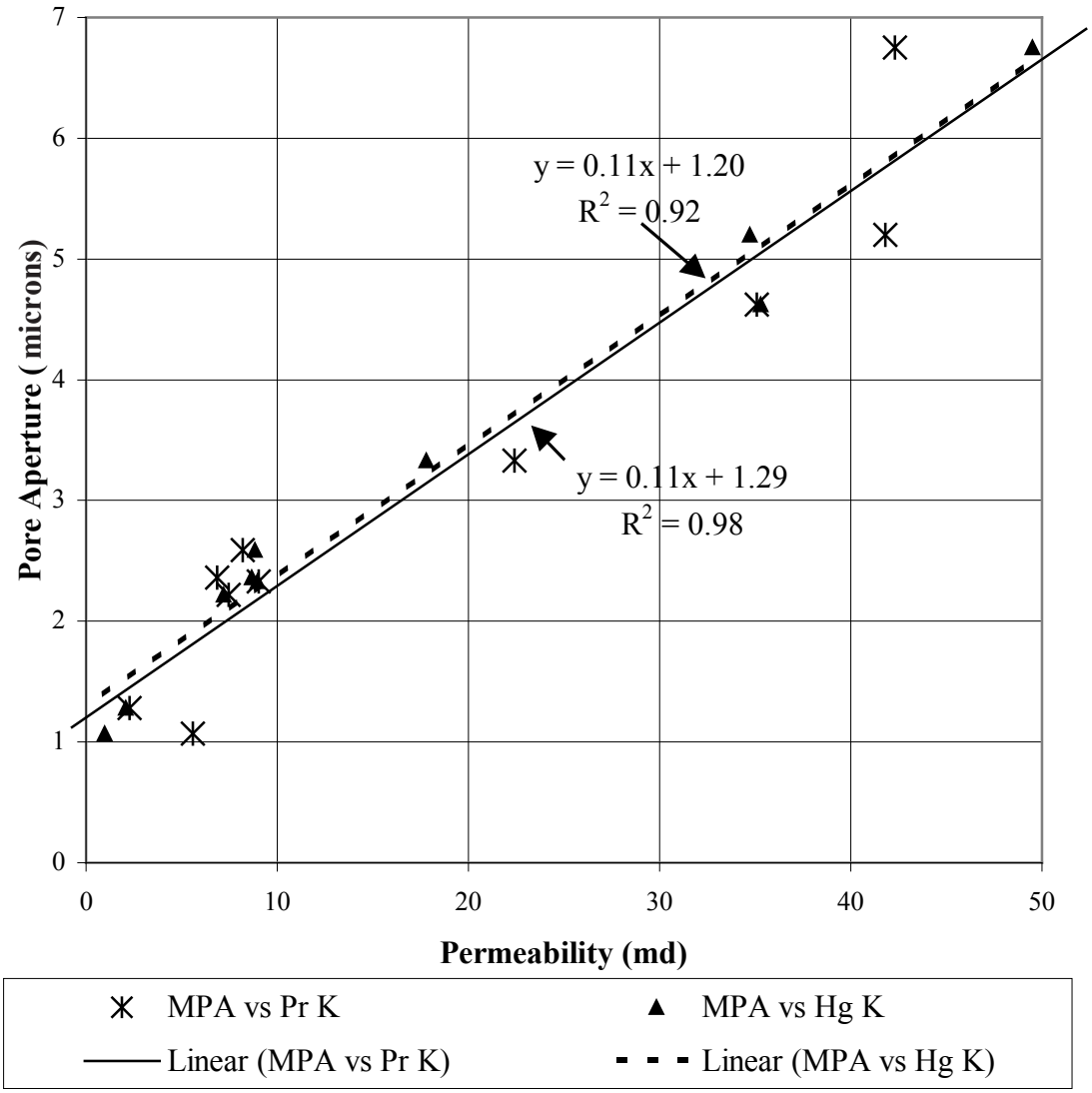

Figure 66. Graph showing the relationship between median pore throat aperture and probe permeability (from Hopkins, 2002).

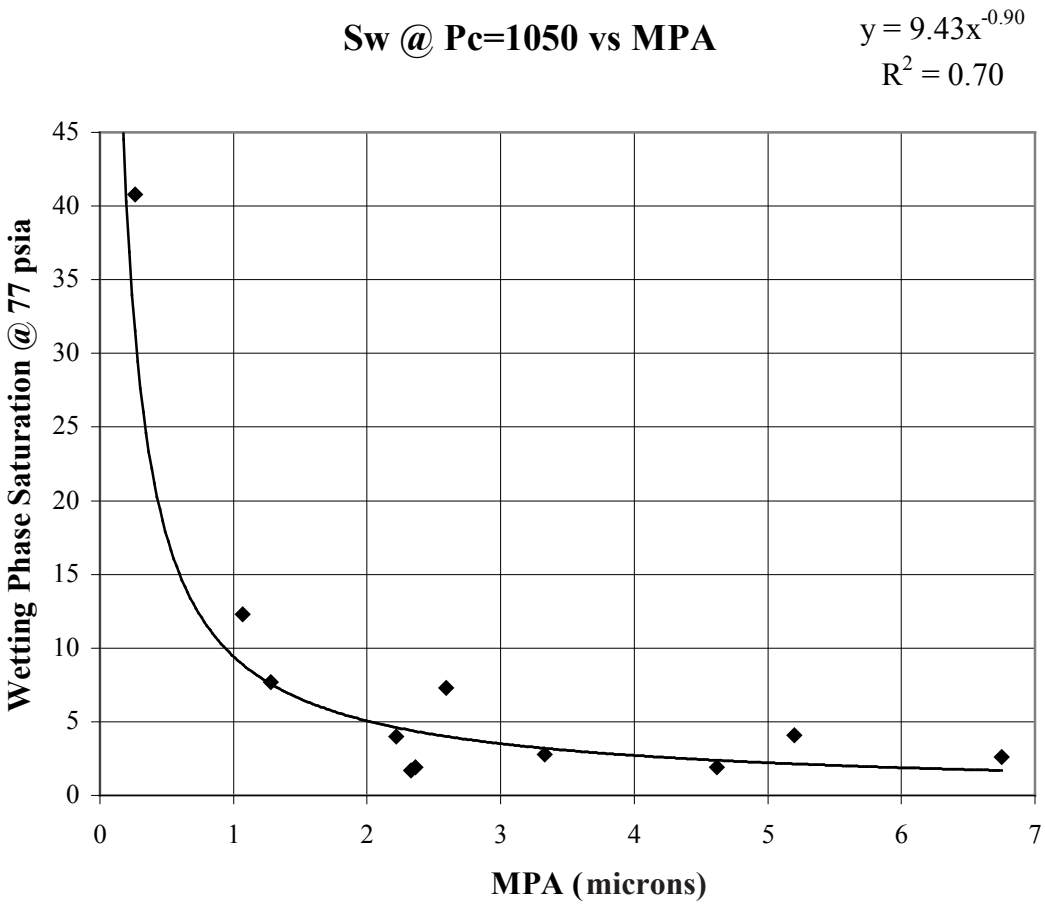

Figure 67. Wetting phase saturation at 77 psia versus median pore throat aperture (from Hopkins, 2002).

(Fig. 68). Figure 68 shows that tortuosity increases with increasing MPA. This relation is related to pore type: the larger MPA and tortuosity values are observed to be associated with intercrystalline pores. Figure 69 shows that entry pressure conditions can be predicted using the inverse of the pore throat radius.

Task RC-2. Petrophysical and Engineering Property Characterization

Description of Work.--This task is designed to focus on the characterization of the reservoir rock, fluid, and volumetric properties. These properties can be obtained from petrophysical and engineering data. This task will assess the character of the reservoir fluids (oil, water, and gas), as well as quantify the petrophysical properties (rock type, grain density, porosity, permeability, electrical properties, etc.) of the reservoir rock. In addition, considerable effort is devoted to the fluid-rock behavior (i.e., capillary pressure and relative permeability). The production rate and pressure histories are cataloged and analyzed for the purpose of estimating reservoir properties such as permeability, well completion efficiency (skin factor), average reservoir pressure, as well as in-place and movable fluid volumes. A major goal is to assess current reservoir pressure conditions and develop a simplified reservoir model (i.e., drive mechanism). New pressure and tracer survey data are scheduled to be obtained in Year 2 to assess communication within the reservoir fieldwide, including among and within the various pay zones in the Smackover. This work will both serve as a guide and provide bounds for the reservoir simulation modeling.

Rationale. Petrophysical (core, well logs, etc.) and engineering data (production rate and pressure histories, pressure tests, well completion data) are fundamental to the reservoir characterization process. Petrophysical data are often considered static (non-time dependent) measurements, while the engineering data are considered dynamic. The reservoir characterization concept is (almost by definition) the coupling or integration of these two classes of data. The data are analyzed to identify fluid flow units (reservoir-scale flow sequences), barriers to flow, as well as reservoir compartments. The petrophysical data are essential for defining the quality of the reservoir rock, and engineering data (performance data) are crucial for assessing the producibility of the

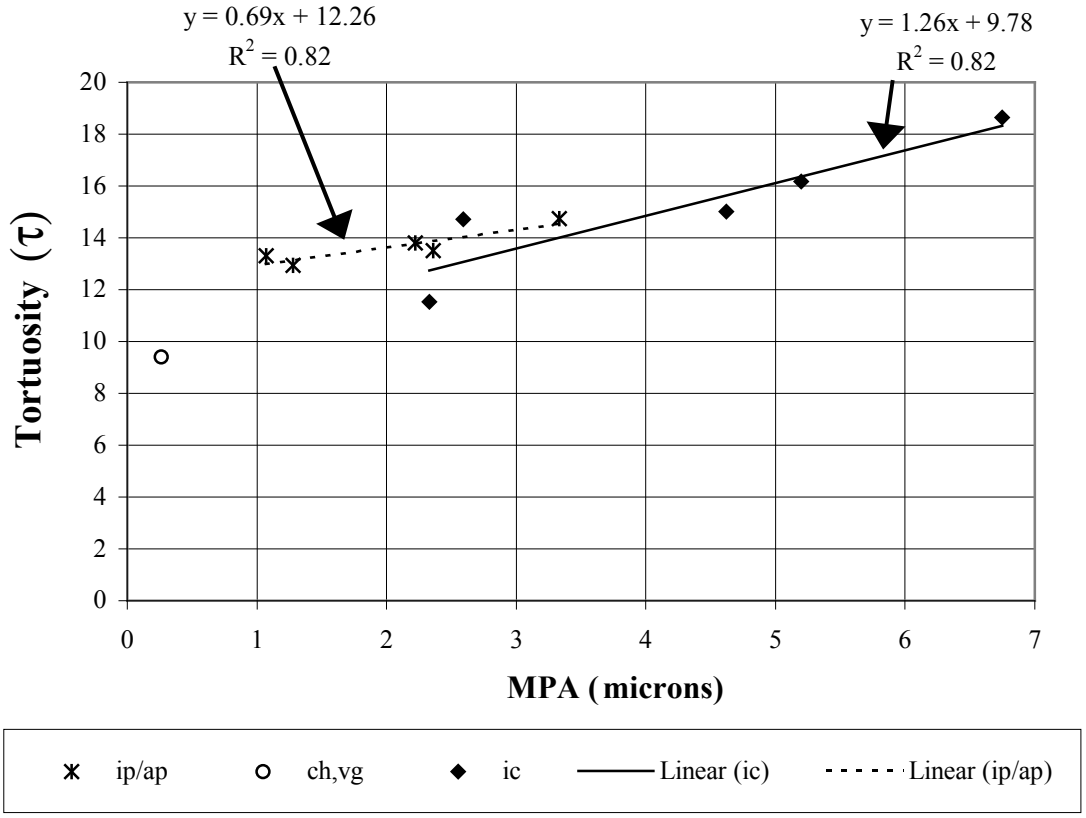

Figure 68. Graph of equation to determine tortuosity (τ) (from Hopkins, 2002).

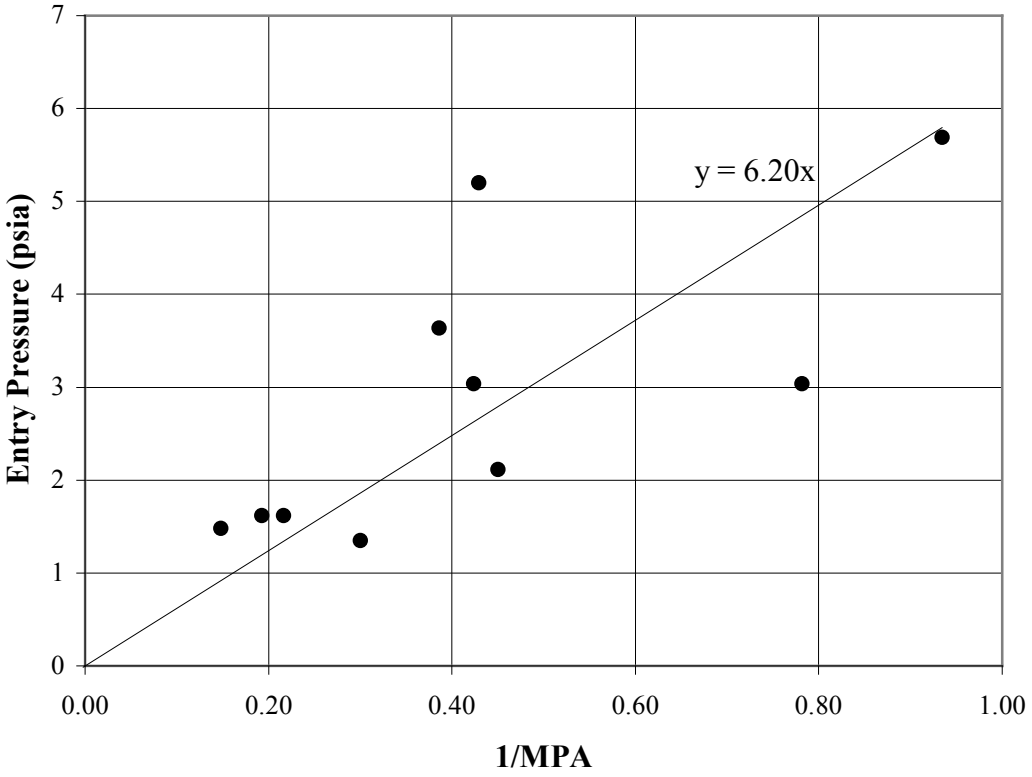

Figure 69. Predicting entry pressure from the inverse of pore throat radius (from Hopkins, 2002).

reservoir. Coupling these concepts, via reservoir simulation or via simplified analytical models, allows for the interpretation and prediction of reservoir performance under a variety of conditions.

Analysis/Interpretation/Integration Procedure.--Womack Hill Field is a mature oil field (Figs. 70 and 71). Since the discovery of the field production rates have steadily declined. The following tasks are employed as the mechanisms to analyze, interpret, and integrate the petrophysical and engineering data from Womack Hill Field.

1. Collect and catalog the well log, core, and production data.
2. Convert these data into an appropriate electronic format.
3. Develop correlations between core and well log data to predict reservoir permeability using well log responses.
4. Analyze and interpret the reservoir performance data using decline type curve analysis and estimated ultimate recovery analysis.
5. Integrate the geological data and the results of reservoir performance analysis by generating maps of distributions of reservoir properties throughout the field.
6. Establish recommendations to optimize the reservoir management strategies, such as: infill drilling, producer/injector conversions, special testing procedures to obtain more information regarding reservoir behavior, etc.

Our work to date has essentially focused on points 1-5.

Correlation of Petrophysical Data—Core-Well Log Data Correlation.--At Womack Hill Field the following well log responses are typically available:

- (SP) Spontaneous potential
- (ILM) Shallow resistivity
- (LLS) Deep resistivity
- (GR) Gamma ray
- (ROHB) Bulk density
- (DPHI) Density derived porosity
- (NPHI) Neutron derived porosity

In addition, substantial volumes of whole and sidewall core data are available. Admittedly, all of these data are 1970's vintage, and we have encountered significant difficulty in trying to correlate the core and well log data.

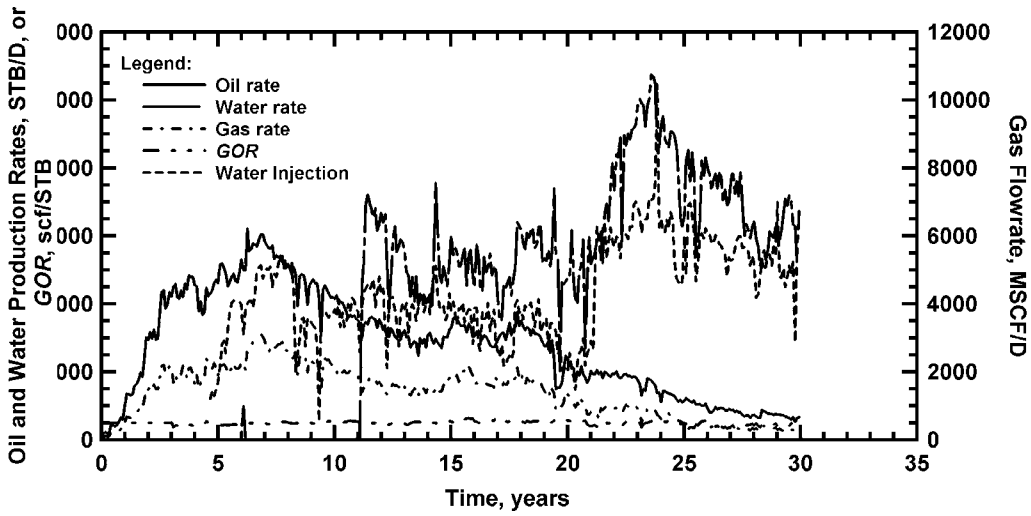

Figure 70. Production history of Womack Hill Field. Since 1997, oil and gas rates have steadily declined, while the water production rate has increased. *GOR* has remained essentially constant.

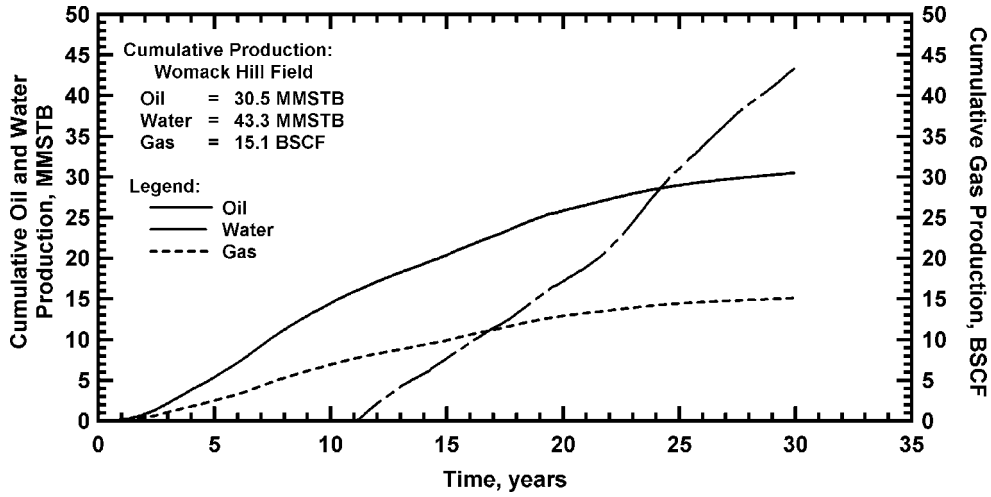

Figure 71. Cumulative production of Womack Hill Field. Oil and gas curves are on the plateau and the water continues rising.

As an example, in Figure 72 we provide a presentation of the core and well log data—showing the well log data and core permeability profiles for well Permit #1639. The reservoir has been divided into three flow units, based originally on geological data, and we note that our work with the core and well log data also confirmed these assignments. As shown, the core permeability data are quite scattered, giving us an indication of the level of heterogeneity in the reservoir. The wells at Womack Hill Field produce from the upper Smackover carbonate reservoir, which is typically characterized by a high level of heterogeneity. This makes it difficult to find correlations between the petrophysical variables on a regional scale. Therefore, our approach is to establish correlations for each of the three flow units at a local scale (i.e., for individual wells).

As part of our characterization of the petrophysical data, we distributed the core data (porosity and permeability) into the appropriate flow units and aligned the corresponding well log measurements to construct the data tables for correlation purposes. We selected the core and well log data for 9 wells. We find that there is no consistent suite of well logs for all wells; however, we do note that the GR, LLS and some sort of porosity log are generally available. As such, we selected GR, LLS, and (core) porosity as independent variables to keep the same set of input data for all correlations.

To develop our correlations of the petrophysical data we selected a nonparametric technique that is based on estimating the optimal transformation of each variable (the dependent as well as the independent variables). This method has an advantage over conventional multiple regression algorithms in that it does not require an assumed correlating function (i.e., model) between the variables—where a pre-established model could yield an inaccurate representation. The nonparametric method uses an iterative process involving a set of "alternating conditional expectations" (ACE) to generate a transform value for each data point of the dependent and independent variables. Once the transform for each of the variables has been established, a nonparametric correlation is generated between the dependent variable and the sum of the transform values, this is called the optimal transformation. Parametric correlations can be generated by fitting these curves using the appropriate functions, generally polynomial functions (GRACE (1996)) The

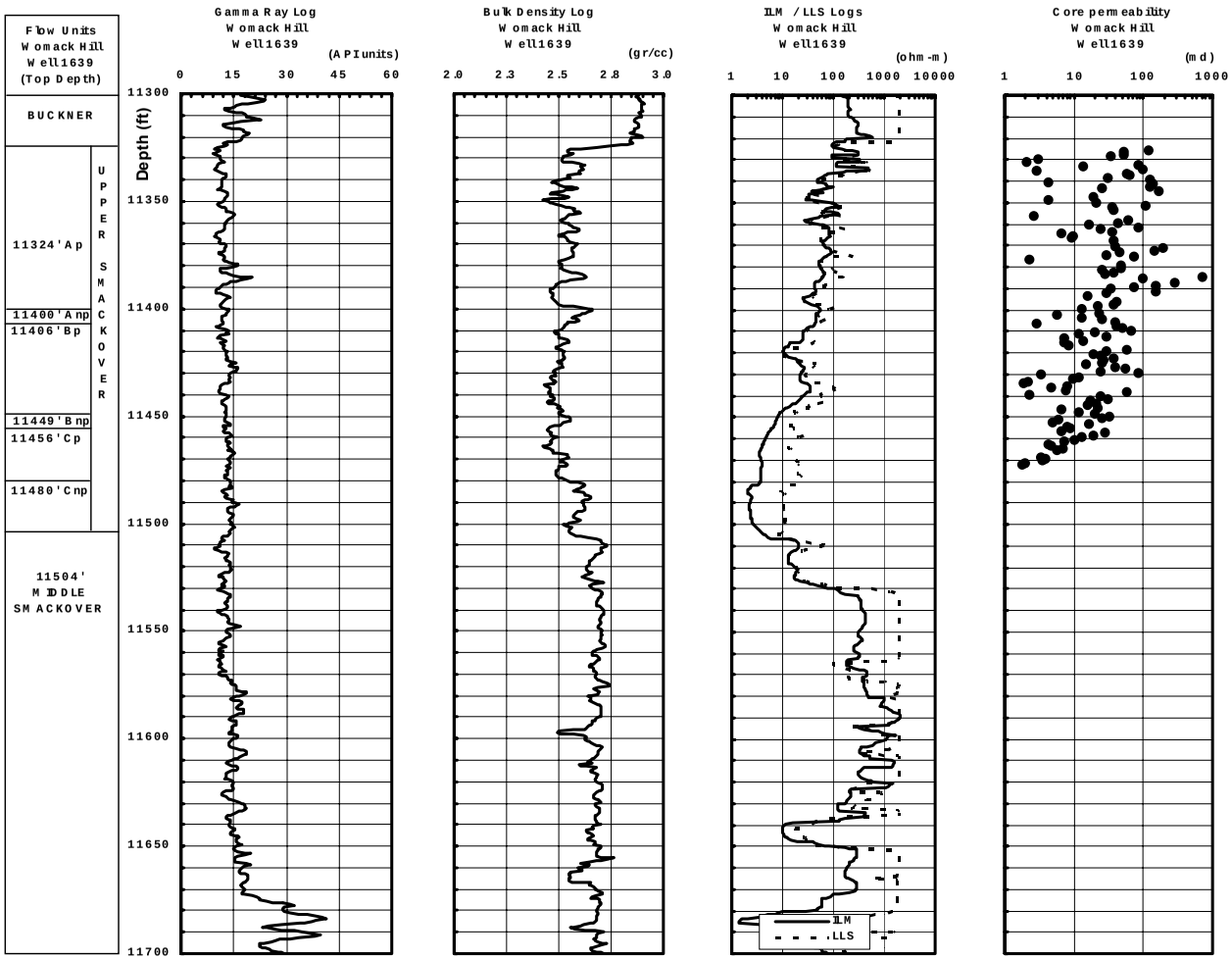

Figure 72. Example of log and core permeability profiles — Well 1639, Womack Hill Field, Alabama.

dependent variable is estimated by determining the inverse of the optimal transform. The details for this process are given by Breiman and Friedman (1985).

Our first approach in developing the core-log correlations was to analyze simple relationships between the variables, which could allow us to obtain less complex correlations if a strong relationship is found between these variables. We then studied the relationship between core permeability and each well log signal. Figure 73 presents crossplots of core permeability against GR, RHOB, LLS, and ILM for flow unit in well Permit #1639. No single plot indicates a clear tendency between the core permeability and any of the well log variables. GR and RHOB do not provide significant character to the correlation since the behavior of these variables is essentially constant through the section. Although the resistivity data do exhibit some variation, the overall relationship of resistivity with the core permeability is quite random (no clear pattern is evident).

This behavior (i.e., the lack of a univariate relationship) was found in each of the three flow units for each well. This observation leads us to pursue the application of regression on several well log variables simultaneously as a mechanism to generate correlations between the core permeability and the well log data We believe that the use of several well log variables in these correlations will improve the overall behavior of a correlation and establish a more consistent statistical model (when we move to convert the non-parametric relation into a parametric relation).

During the depth shifting effort we observed that a significant variation exists between the core and well log-derived porosity, over the entire scale of porosity values. As an effort to try to resolve these differences, we considered the relationship between these two variables (core and well log porosity) on the flow unit scale. Figure 74 shows the relation between the porosity derived from the bulk density log and the core porosity for well Permit #1639 (Flow unit A). We note that the relationship is extremely poor, and that the only positive comment is that the data appear evenly distributed (although randomly) about the 45° line (i.e., the perfect correlation line).

Generally speaking, well log derived porosity values are among the most consistent variables that can be estimated—unfortunately, this is not the case in Womack Hill Field. To use the well log

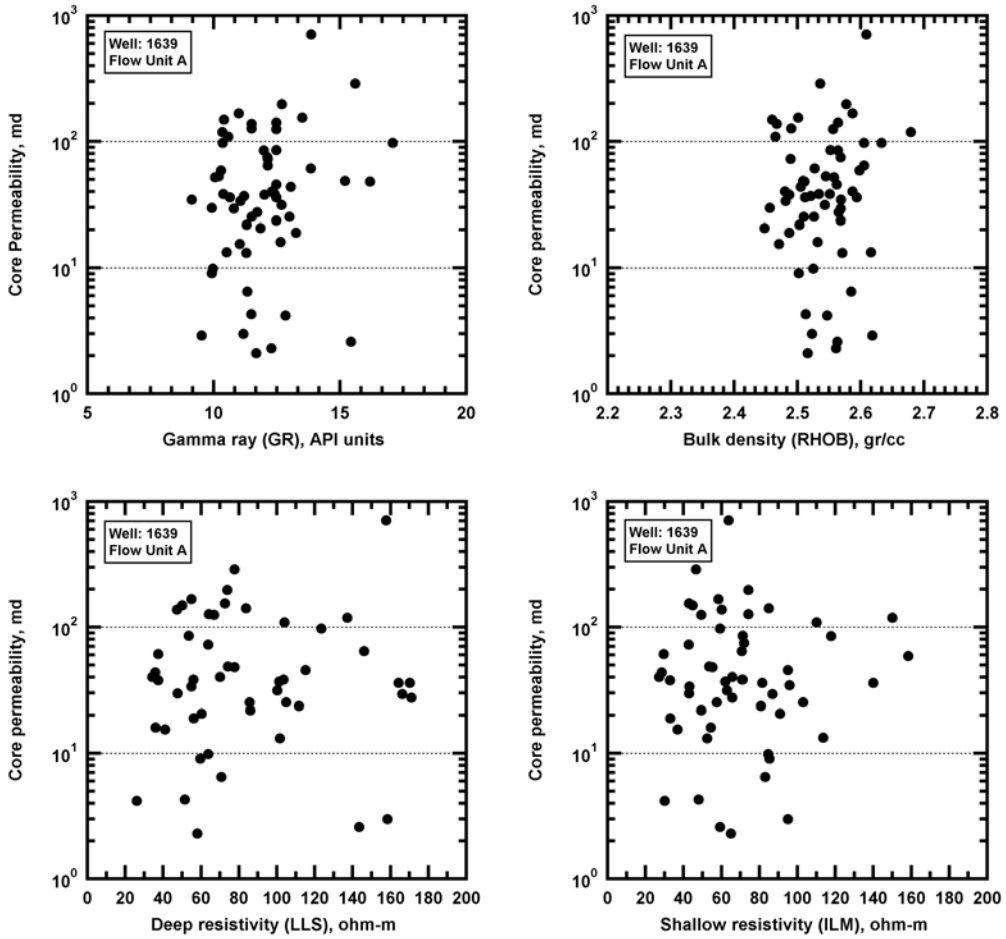

Figure 73. Core permeability univariate correlations — Womack Hill Field, Well 1639 (Flow unit A). No clear trend is present.

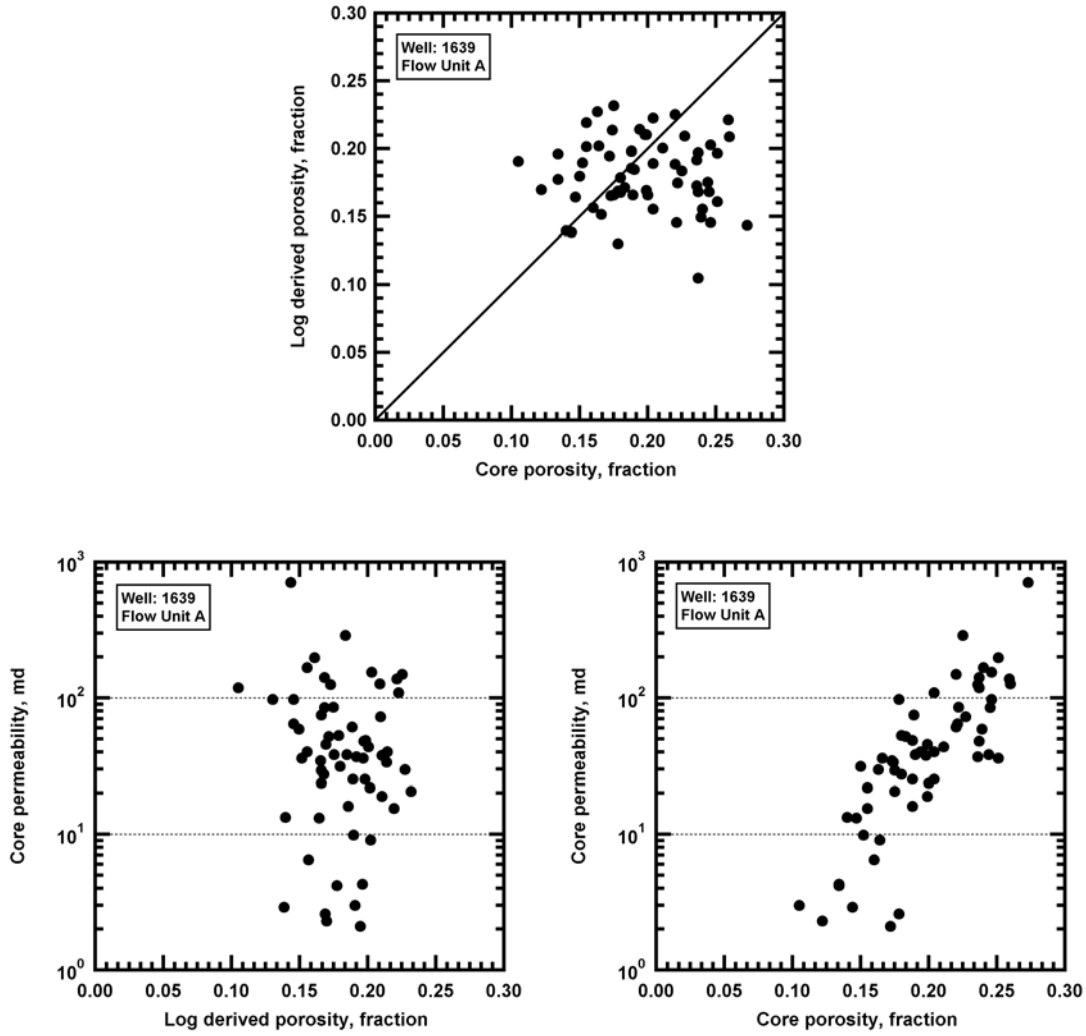

Figure 74. Core permeability and porosity plots — Womack Hill Field, Well 1639 (Flow unit A). Log derived porosity does not match either core porosity or have a clear trend with core permeability — core porosity and permeability show a clear relationship.

derived porosity as input data for the correlation would produce significant errors, as it has little or no relation to the formation permeability. However, a comparison of the logarithm of the core permeability with core porosity yields a reasonably linear trend (Fig. 74). As such, we elected to use the core porosity in lieu of the well log-derived porosity to obtain more consistent results. To generate correlations that can be used for most of the wells, we selected the GR, LLS, and core porosity as input data for the correlations. Although the GR log is thought to have relatively little character, it does provide certain petrophysical characteristics, as the accuracy of the correlation tends to improve when the GR data are included. Typically, the ILM and LLS responses follow essentially the same tracks; however, we prefer the deep resistivity (LLS) over the shallow resistivity (ILM) because the LLS resistivity utilizes information at distances further into the reservoir, and because the LLS is the more common well log acquired in Womack Hill Field.

Having prepared the data sets for correlation, we use the GRACE program (1996) to establish the nonparametric correlations for each variable—generating the corresponding optimal transformations. As we require some functional form, in order to apply the correlation, we utilize parametric correlations that are generated by fitting the data using quadratic polynomials (a feature of the GRACE program). As an example, in Figure 75 we present the transformations for each variable (well Permit #1639—Flow unit A). Finally, the correlation that is used to predict the dependent variable is obtained by calculating the inverse of the optimal transformation. We noted that the correlating function matches the tendency exhibited by the measured data, which confirms the robustness of the non-parametric method.

Correlation of Petrophysical Data—Statistical Analysis of Core-Data.--In order to generate a petrophysical model of the reservoir we need to establish a distribution of the formation properties throughout the reservoir drainage area. Our ultimate goal in this effort is to provide a reservoir description that can be used for numerical simulation. To accomplish this goal we segregate the data according to flow units and develop histograms of porosity and the logarithm of permeability. These histograms confirm that porosity and the logarithm of permeability both follow a normal distribution.

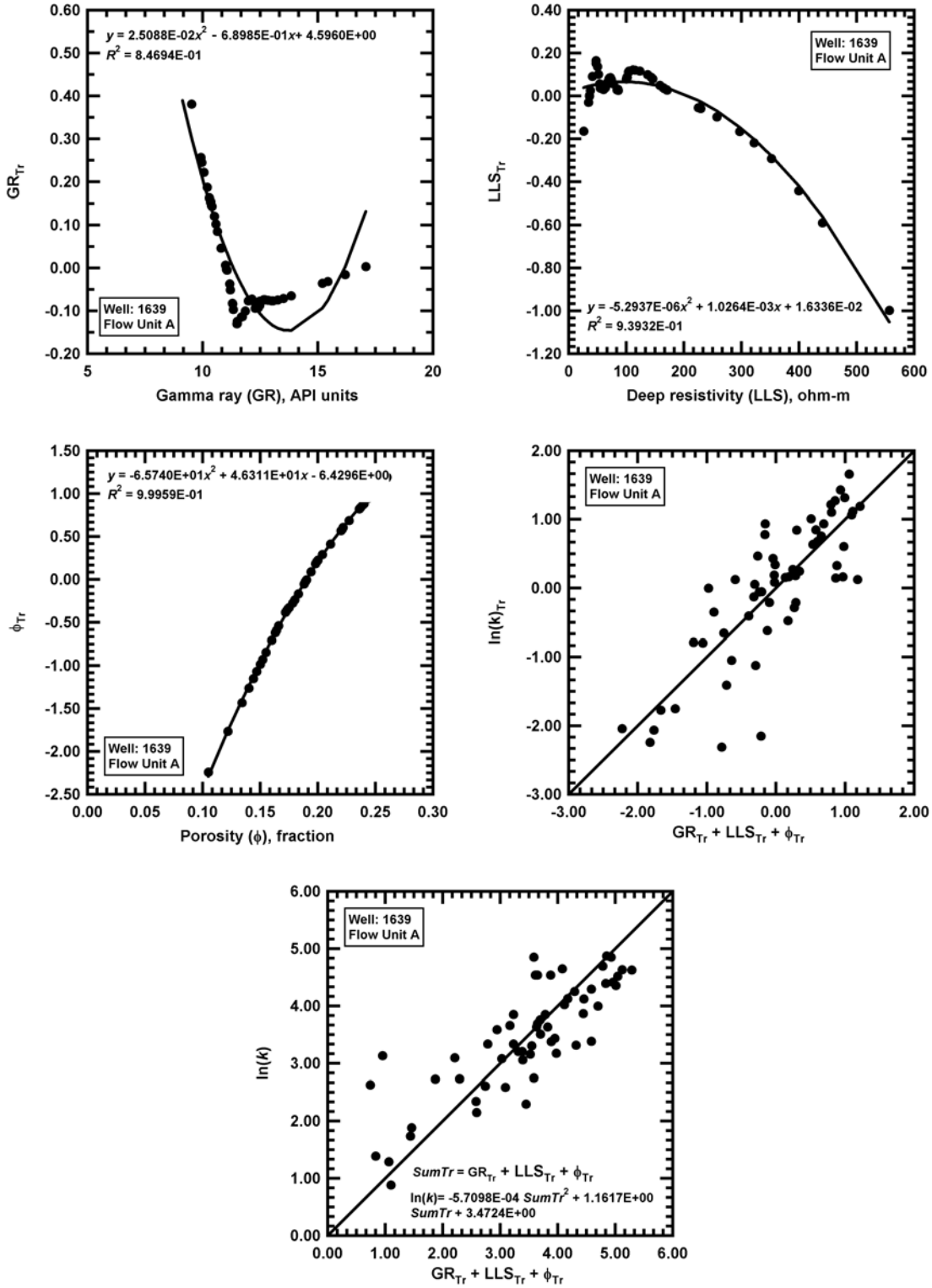

Figure 75. Optimal transformations for independent and dependent variables and core permeability correlation — Womack Hill Field, Well 1639 (Flow unit A).

Figure 76 provides an example of this behavior for well Permit #1639—Flow unit A. We note that most of the wells in Womack Hill Field yield similar histogram trends. It is our intention to use the mean value of porosity and the logarithm of permeability established from a particular histogram to represent the average for a particular flow unit. Using these results we developed maps of porosity and permeability based on the average values for each flow unit—which will be part of our proposed geological model for numerical simulation.

Analysis of Reservoir Performance—General.--Figure 70 presents the historical behavior of the oil, gas, and water production rates at Womack Hill Field since production began in December 1970. Oil and gas production peaked in 1977 at 6,200 STB/D and 3,200 MSCF/D of oil and gas, respectively. Since then, oil and gas flow rates have steadily declined, while the water rate has consistently increased. This production decline has reduced the profitability of the field—which leads to the current program of production optimization and field management strategies to improve the performance and overall recovery. Currently there are 3 injection wells (in the Smackover) which are active, although there are also some injection wells which are also used periodically. The producing gas-to-oil ratio (GOR) has remained relatively constant (approximately 500 scf/STB) indicating that the reservoir pressure remains above the bubblepoint pressure (approximately 1925 psia).

Figure 71 presents the fieldwide cumulative production for oil, gas, and water. The oil and gas curves are nearing their respective "plateaus" and should not be expected to change their behavior without substantial intervention (i.e., infill drilling, well stimulation, improved artificial lift, etc.). We also note from Figure 71 that the cumulative water production curve is still increasing at a substantial rate although it does appear to be trending towards a plateau (probably in the range of 55-60 MMSTB of water). To date, the total oil production is 30.5 MMSTB, along with 43.3 MMSTB of water and 15.1 BSCF of gas. The field is divided the field into two areas—the Eastern and Western Unit areas, based presumably on geological information. In Figure 77 we present the production profiles for the Eastern area, and in Figure 78 the hydrocarbon production for the Western Unit area is presented.

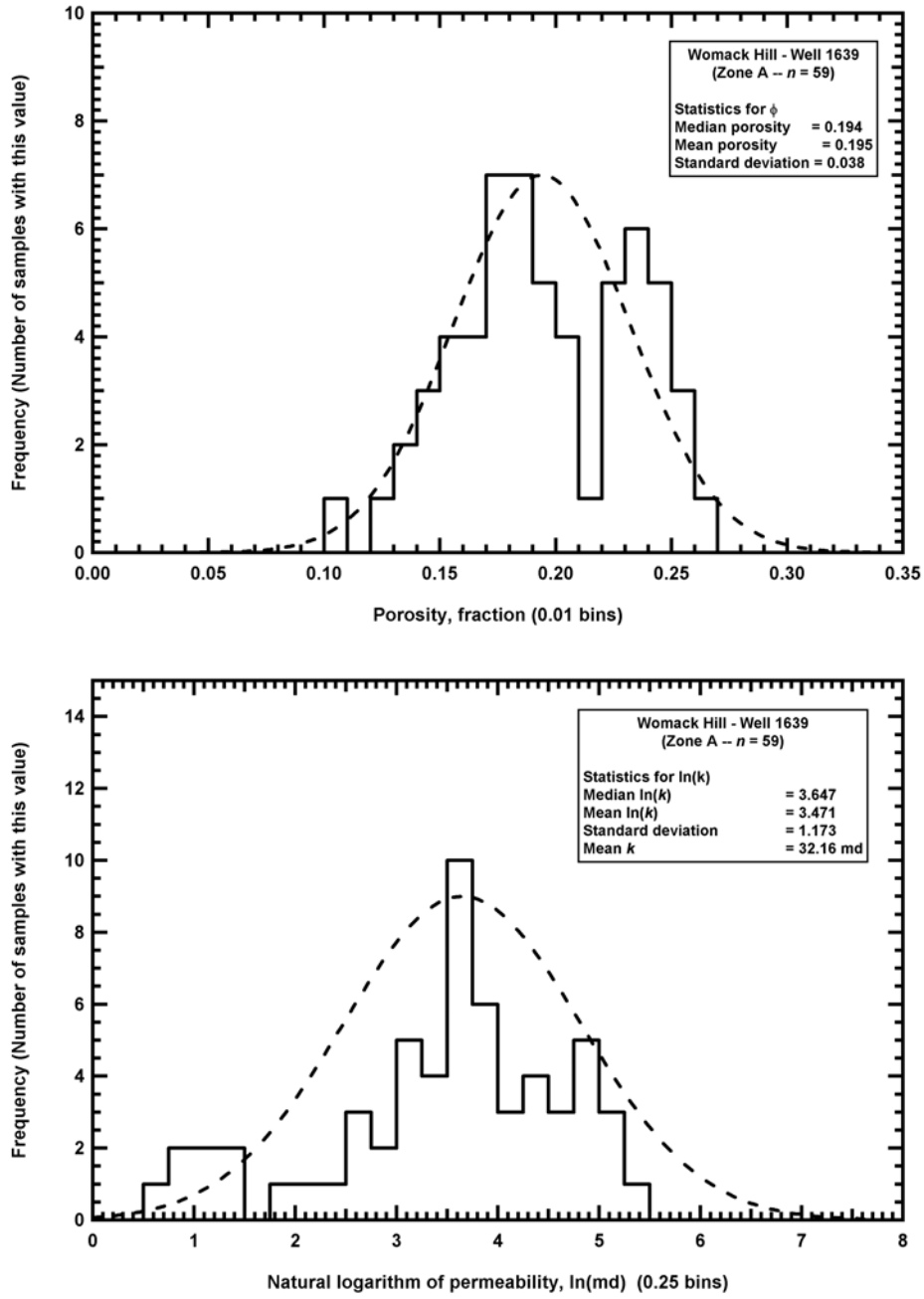

Figure 76. Core porosity and logarithm of core permeability histograms — Womack Hill Field, Well 1639 (Flow unit A). Both porosity and the logarithm of permeability have a normal distribution.

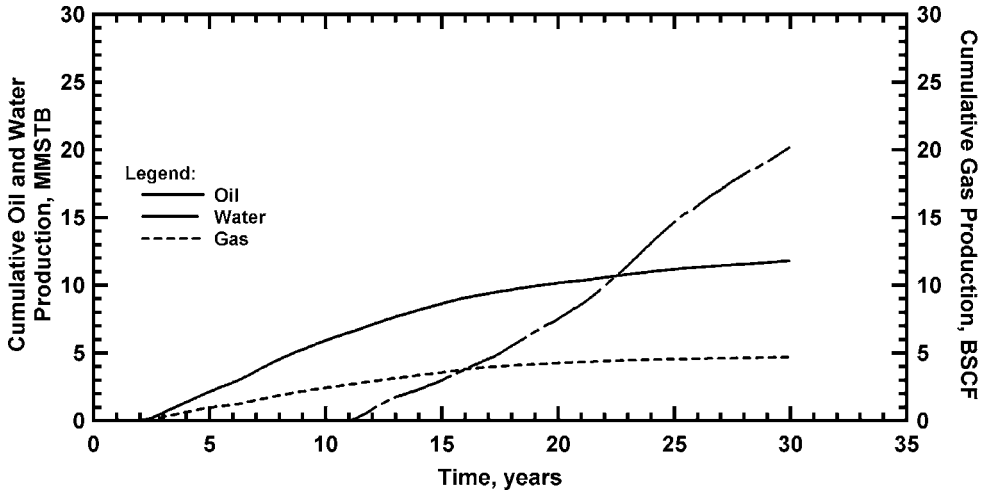

Figure 77. Cumulative Production in Eastern Area — Womack Hill. This area produces 38.7 percent of total oil production.

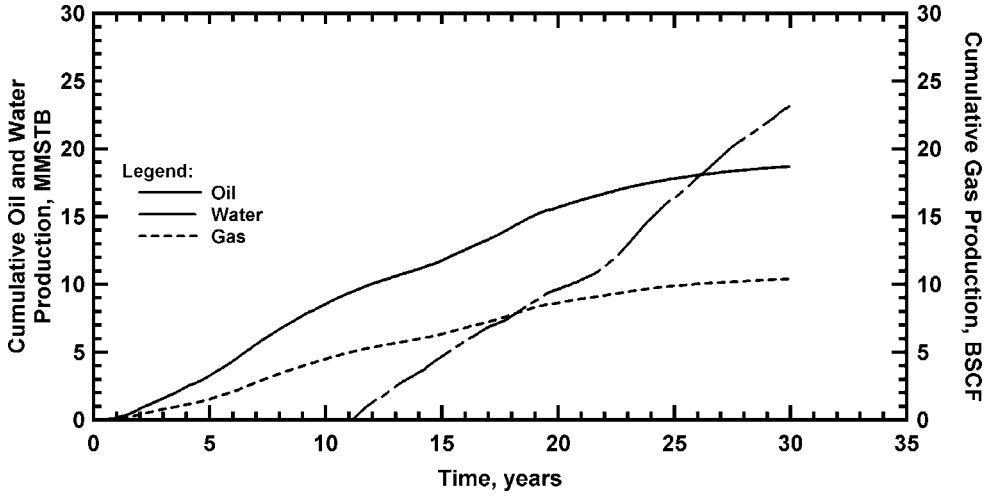

Figure 78. Cumulative Production in Western Area — Womack Hill. This area produces 61.3 percent of total oil production.

In Figure 79 we present a curve of the logarithm of the fractional flow of water (f_w) versus cumulative oil production (N_p)—these plots are widely used for evaluation and prediction of reservoir performance—in particular, to estimate total recovery at 100 percent water production. The technique only applies at later times and presumes a log-linear relationship of WOR (or fw) and oil recovery, which allows us to extrapolate the presumed straight-line trend to any desired water cut in order to determine the corresponding oil recovery. In our case, this extrapolation yields an oil recovery of approximately 34.5 MMSTB, which is consistent with the result obtained by the hyperbolic extrapolation of the cumulative oil curve (34.6 MMSTB).

Another way to estimate remaining reserves is using "estimated ultimate recovery" (or *EUR*) analysis on the production performance for each well. *EUR* analysis is a semi-empirical technique that consists of extrapolating the production rate (q_o) versus cumulative production (N_p) curve to q_o=0. The corresponding value of N_p at q_o=0 represents the "recoverable" oil ($N_{,p,max}$). In Figure 80 we illustrate this process for well Permit #1591. For the wells at Womack Hill Field the recoverable oil estimate is often close to current cumulative production because of the lateness in the productive life of an individual well (as well as the field). We performed this analysis on all of the producing wells in the field as a mechanism to estimate the remaining field-wide recoverable oil at current conditions.

In Figure 81 we summarize the *EUR* analysis results by plotting the cumulative oil production (N_p) for each well against its corresponding *EUR*. As expected, a strong correlation of N_p with *EUR* emerges because of the mature status of the field. The slope of this curve represents the percentage of oil produced with respect to the total recoverable oil. As a fieldwide average, we estimate that 94 percent of the total oil at current conditions has been recovered—which means that 6 percent of recoverable oil remains to be produced.

Analysis of Reservoir Performance—Field-Scale Flow Behavior.--Early in the productive life of Womack Hill Field a concept emerged that the field had two compartments (or areas)—one in the west and one in the east. For field management purposes, and based on the belief that a geological division exists in the field, Womack Hill Field has been developed and managed in two

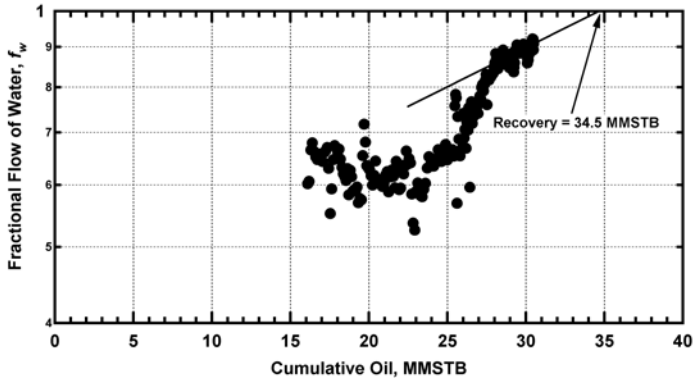

Figure 79. Logarithm of the fractional flow of water versus cumulative oil production. The straight-line extrapolation at f_w=1 yields an oil recovery of 34.5 MMSTB.

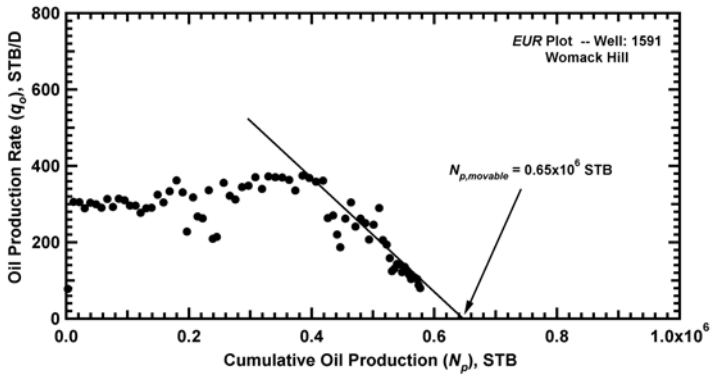

Figure 80. *EUR* plot for Well 1591 — Womack Hill Field. Cumulative production is approaching total recoverable oil.

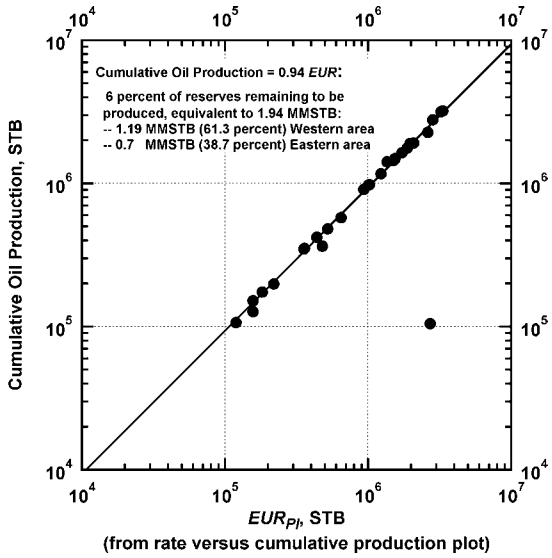

Figure 81. Summary of *EUR* Analysis — Womack Hill Field. Strong correlation — likely a consequence maturity of production.

independent areas. It appears, however, that some pressure support is benefiting wells in the Eastern area, while all of the injection wells are in the Western Unit area.

A "flow barrier" in the Womack Hill Field area was identified early in the development of the field and was used as demarcation to separate the Western Unit area from the Eastern area. It is important to note that all of the water injection wells are located in the Western Unit area, so the water injection influence should not affect the Eastern area if a "barrier" exists. Figure 71 shows that the water injection rate has always exceeded the oil production rate—the cumulative water injected has reached 42 MMSTB, which is 11.5 MMSTB higher than the oil withdrawal. So the amount of injected water appears to be more than sufficient to maintain the reservoir pressure. Figures 82 and 83 present the limited pressure data available for the Western Unit and Eastern areas, respectively. Figure 82 illustrates clearly the pressure increase (or maintenance) in the Western Unit wells due to the water injection. However, the pressure maintenance has not been as effective in the Eastern area (Fig. 83), where the pressure in most of the wells has declined (although there are exceptions). This pressure data suggests that a geological separation could exist between the two areas—but it does not serve to confirm this concept. As noted, some of the wells in the Eastern area have experienced pressure maintenance—which suggests that the "barrier" is not completely sealing and that some flow paths may communicate to both areas.

Figure 84 presents the historical field-wide oil production and water injection rates. We first note that from the beginning of the water injection program up to about year 20 (1990), the reservoir performance was approximately a 1:1 ratio (the volume of injected water per volume produced oil). Since then the injected water has increased steadily and the oil production has declined. This sharp change almost certainly cannot be attributed to a reservoir mechanism—it is far more likely to be a consequence of operational practices. In fact, in 1990 the operator first installed hydraulic "jet pumps" in the production wells in order to improve the productivity—but as revealed in Figure 84, this installation has not been as effective as desired.

We also consider the phenomenon of "overproduction" of water where the ratio of water production rate to water injection rate ratio versus time is presented in Figure 85. This profile shows

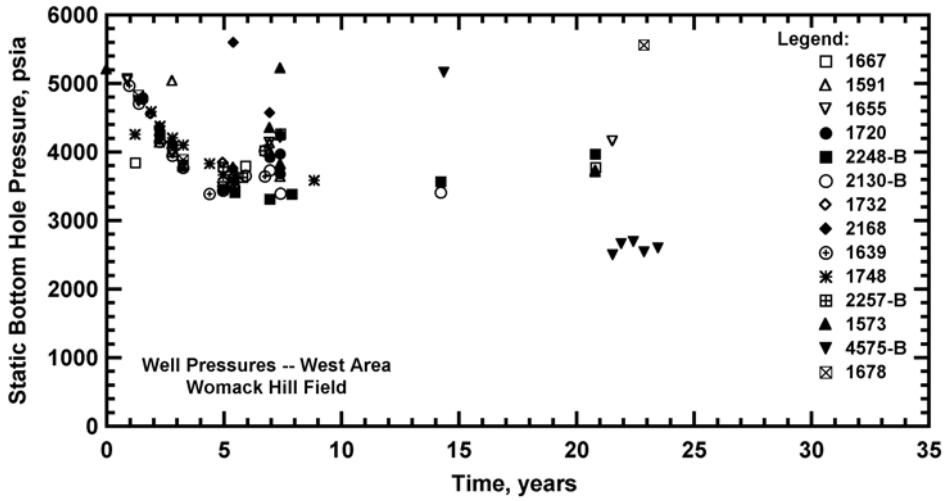

Figure 82. Well pressures in Western Area — Womack Hill Field. The effect of water injection is clearly shown from year 5.

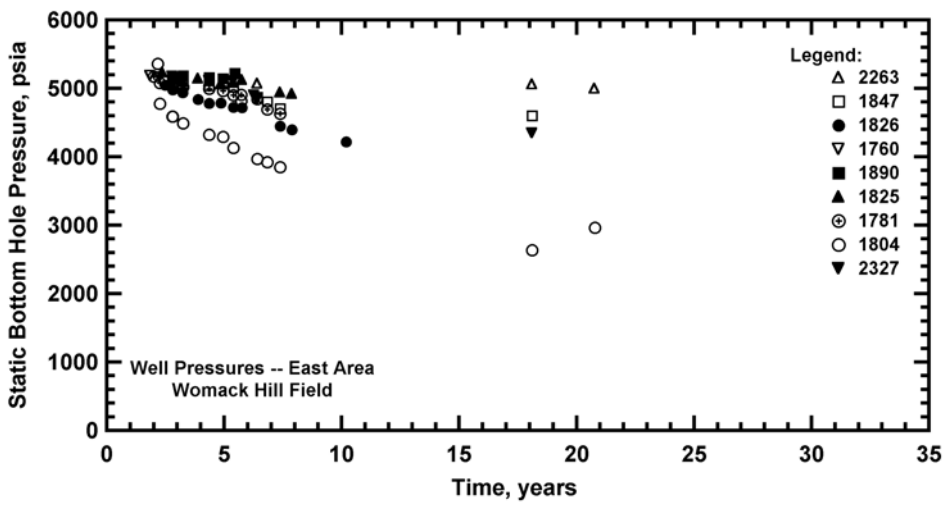

Figure 83. Well pressures in Eastern Area — Womack Hill Field. Despite water injection, well pressures for some wells are declining "normally," while other wells appear to be receiving pressure support.

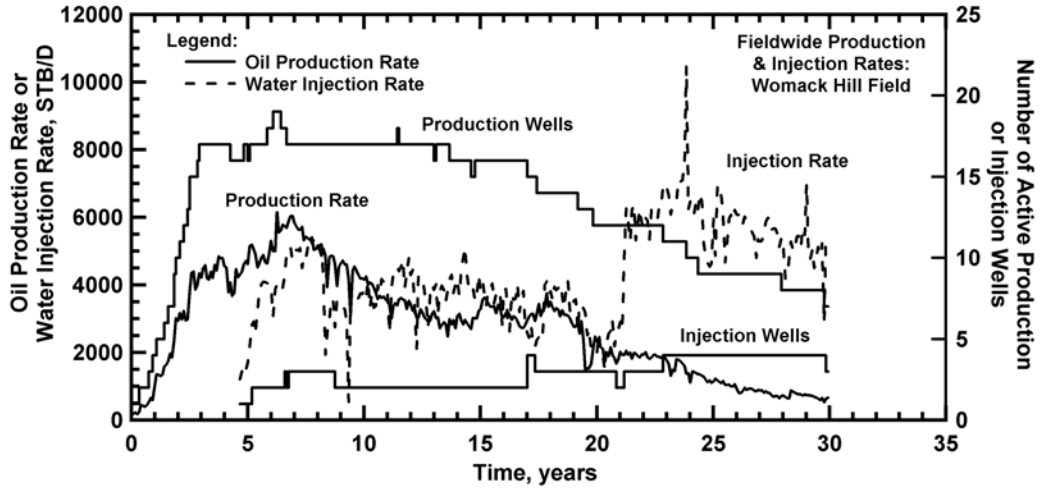

Figure 84. Water injection and oil production rate profiles — Womack Hill Field. Water injection appears to be less efficient over the last 10 years.

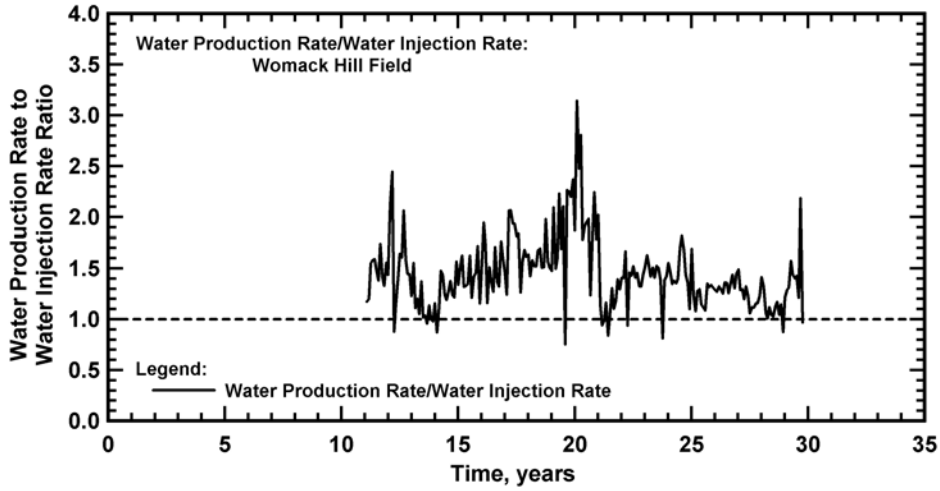

Figure 85. Water production rate to water injection rate ratio — Womack Hill Field. The higher volume of produced water is likely due to water coning or a strong water influx.

a ratio over unity—so the volume of produced water is higher than the volume of injected water. Water coning, water channeling, and/or strong water influx can cause this phenomenon. Empirical evidence from a site visit to Womack Hill Field suggests the possibility of water channeling and water influx. A numerical simulation model should consider the causes and effects of this "overproduction" of water phenomenon.

Analysis of Reservoir Performance—Decline Type Curve Analysis.--To analyze and interpret the well production profiles for each well we used the decline type curve technique (Fetkovich, 1980; Doublet *et al.*, 1994; Doublet and Blasingame, 1996). The application of this methodology is based in theory, but in practice we must often apply the technique without certain data — typically wellbore pressure data are not available. This is a limitation, and it is the case for our analysis of the production performance at Womack Hill Field.

For this work we have specifically used the Fetkovich-McCray family of decline type curves (Doublet, *et al.* (1994)) where these type curves are formulated based on pseudosteady-state (or boundary-dominated) flow behavior. We use pressure-drop normalized rate functions as well as a "material balance time" formulation to eliminate the constant p_{wf} constraint associated with the original Fetkovich method. In addition, by adding the rate integral and the rate integral-derivative functions to this analysis technique, we are able to achieve much more consistent (*i.e.*, unique) type curve matches and we generally obtain better matches of transient data for the estimation of formation flow properties.

The software *WPA* (Blasingame, *et al.*, 1998) provides us a mechanism to apply this technique. The input data required for the *WPA* program consists of a table containing the following production data functions:

Time, t (days)	Flowing bottomhole pressure, p_{wf} (psia)	Flow rate, q (STB/D)
xxx	xxx	xxx
xxx	xxx	xxx
xxx	xxx	xxx
xxx	xxx	xxx

In addition to production data, we also require reservoir and fluid properties, as well as an estimate of the initial reservoir pressure. Once the analysis process is completed in the *WPA* software, we should obtain estimates of the following parameters:

Flow terms:	Volumetric results:
•Effective permeability, k_o, md	•Reservoir radius, r_e, ft
•Skin factor for near-well damage/stimulation, s	•Drainage area, A, acres
•Fracture-half length, x_f	•Nc_t product, STB/psi

Figure 86 illustrates the type curve match we obtained for Well 1847. As shown, the $q/\Delta p$, the "integral" of $q/\Delta p$, and the "integral-derivative" of $q/\Delta p$ are matched against the corresponding type curves. We note that most of the data lie in the "boundary-dominated flow region"—which is logical since the "transient flow region" contains few (if any) representative data (due to the proration of the field). Further, a lack of wellbore pressure data amplifies the problems encountered with the transient flow region—we simply have to provide a "best guess" analysis in this region, which really implies that the "flow property" results are qualitative at best.

As noted, we can only use the transient "flow property" results qualitatively, but we can utilize the "volumetric" results in a somewhat more quantitative fashion because for each well analyzed we clearly observe the late-time "harmonic" trend—which confirms the material balance correctness of this technique. Unfortunately, the parameters estimated using the "late time" data are tied to the value of total compressibility (c_t) specified for the analysis—this is not a value for which we have substantial confidence. Having prescribed a value for c_t we can calculate the oil-in-place (N) and the reservoir drainage area (A). In this particular case we believe that it may be more valuable to report the Nc_t-product because our estimate of c_t yields estimates of N and A which are clearly unrealistic. Our intention is to obtain a "tuned" value of c_t and calibrate our analysis.

Therefore, for this case, we will use the Nc_t product as a surrogate variable to represent the distribution of oil in the reservoir. Figure 87 presents a crossplot EUR_{PI} versus Nc_t for all of wells that were analyzed. As shown, this plot shows a very strong correlation between EUR_{PI} and Nc_t, even though these results are estimated independently. EUR_{PI} is estimated from the rate versus

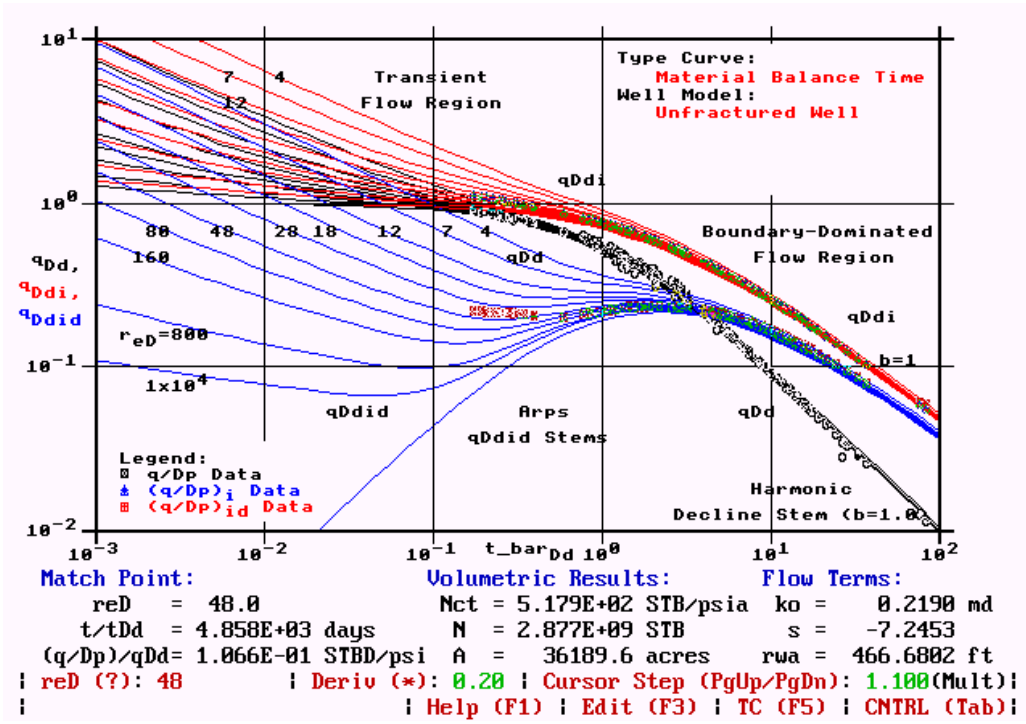

Figure 86. Decline type curve analysis — match plot, Womack Hill Field Well 1847. Most of the data lie in the boundary-dominated flow region 1848. The transient flow regime is less well-defined.

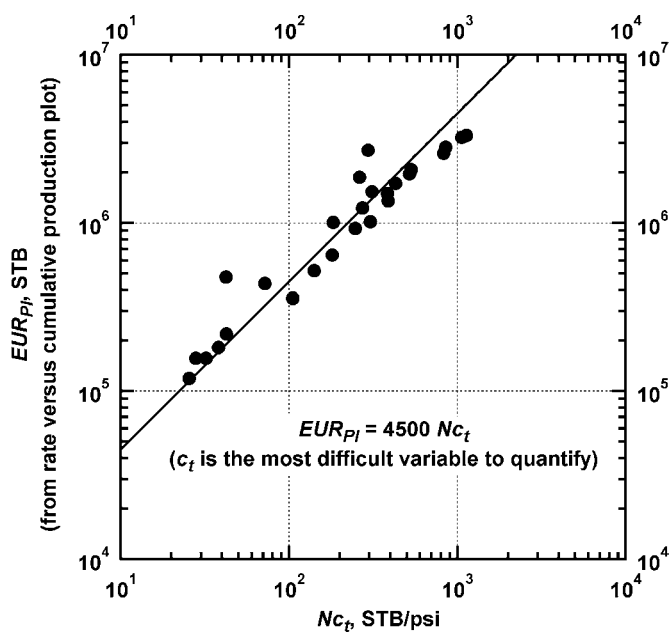

Figure 87. EUR_{PI} versus. Nc_t — Womack Hill Field. EUR_{PI} and. Nc_t are estimated using independent mechanisms — however, these variables are clearly correlated.

cumulative production plot and Nc_t from using decline type curve analysis. The observation of this strong relationship is logical, and it suggests that the recovery is proportional to the fluid-in-place (which is logical — but this evidence does confirm this behavior).

In Table 7, we present a summary of the results we obtained using decline type curve analysis for each well. The "flow properties," effective permeability (k_o) and skin factor (s) are only qualitative estimates at best due to the lack of competent data in the transient flow region. The N and A estimated depend on an accurate estimate of c_t, and these values are also suspect since a "tuned" estimate of c_t has not been defined. At this point in our work, the Nc_t-product is our most reliable variable for representing oil-in-place.

Analysis of Reservoir Performance—Material Balance.--As Womack Hill Field is presumed to still be producing at pressures above the bubblepoint, we elected to attempt a material balance calculation using the production and pressure data. Our goal was simply to attempt an "initial analysis," if material balance appears viable, we will refine these analyses later to include other potential drive mechanisms. The material balance equation for a slightly compressible liquid in a volumetric reservoir is given by: (Dake, 1977).

$$p_i - \bar{p} = \frac{1}{Nc_t}\frac{B_o}{B_{oi}}N_p \quad \text{.....(1)}$$

On a plot of $\bar{p}$ versus N_p the extrapolation of the straight-line trend to $\bar{p} = 0$ yields the "recoverable" oil, $N_{p,max}$. Figure 88 presents a material balance plot constructed for Womack Hill Field. This plot yields an estimate of $N_{p,max}$ of 76 MMSTB—which appears to be quite high. The slope of the straight-line trend can be used to estimate the original oil-in-place (N), but once again an accurate estimate of c_t is required. This high estimate of recoverable oil suggests that the reservoir pressure is too high for a volumetric model, and may be receiving external energy support. The most logical source of this "external" energy would be an aquifer—whose characteristics should be considered during the construction of the reservoir simulation model. Again, this exercise

Table 7. Summary results for decline type curve analysis — Womack Hill Field.

Well permit	Region	N_p (STB)	Nc_t (STB/psi)	N (STB)	A (acres)	k_o (md)	s
1639	West	977305	183.30	1.02E+07	6688.80	0.1833	-6.401
1655	West	1772155	261.80	1.46E+07	11135.80	0.1235	-7.195
1667	West	1168145	272.80	1.52E+07	12443.70	0.3950	-1.372
1760	East	349215	104.60	5.81E+06	10697.30	0.2792	-6.125
1781	East	1923054	529.90	2.94E+07	48353.80	0.3605	-4.577
1804	East	3217813	1083.00	6.01E+07	80988.80	0.7045	-2.309
1825	East	364831	42.10	2.34E+06	3184.90	0.1854	-5.519
1826	East	981820	304.00	1.69E+07	65494.40	0.2521	-7.542
1847	East	1901848	517.90	2.88E+07	36189.60	0.2190	-7.245
1899	East	152230	32.10	1.78E+06	4096.80	0.0821	-6.695
2109	West	1637015	420.10	2.33E+07	27513.00	0.7026	-5.904
2327	East	421841	71.80	3.99E+06	30376.40	0.6467	-5.954
2341	East	1417137	387.30	2.15E+07	41360.70	0.4650	-7.312
3452	East	481699	141.30	7.85E+06	16665.20	1.2105	-1.518
3657	East	127460	29.10	1.62E+06	8168.80	0.3776	-6.501
1732-B	West	198755	42.40	2.36E+06	2675.70	0.2383	-4.739
2130-B	West	2793767	800.00	4.45E+07	194229.70	0.7249	-10.011
2248-B	West	3177666	1057.00	5.87E+07	41355.40	0.2514	-7.851
2257-B	West	1443996	382.30	2.12E+07	34397.20	0.6226	-7.220
4575-B	West	2280222	829.00	4.61E+07	66367.20	0.5044	-7.549
SWD-1890-83-3	East	106874	26.60	1.48E+06	2221.00	0.0689	-7.775
SWD-2263-85-5	East	352008	104.30	5.79E+06	44128.90	1.2025	-6.834
WI-1573-69	West	105302	294.30	1.64E+07	11621.30	0.1041	-6.677
WI-1591-77-1	West	576835	180.10	1.00E+07	6043.80	0.1648	-3.537
WI-1678-93-8	West	1489082	309.90	1.72E+07	20128.80	0.4208	-4.139
WI-1720-77-2	West	174337	38.10	2.12E+06	1699.30	0.1139	-6.255
WI-1748-92-1	West	909261	247.10	1.37E+07	16818.90	0.3155	-5.658

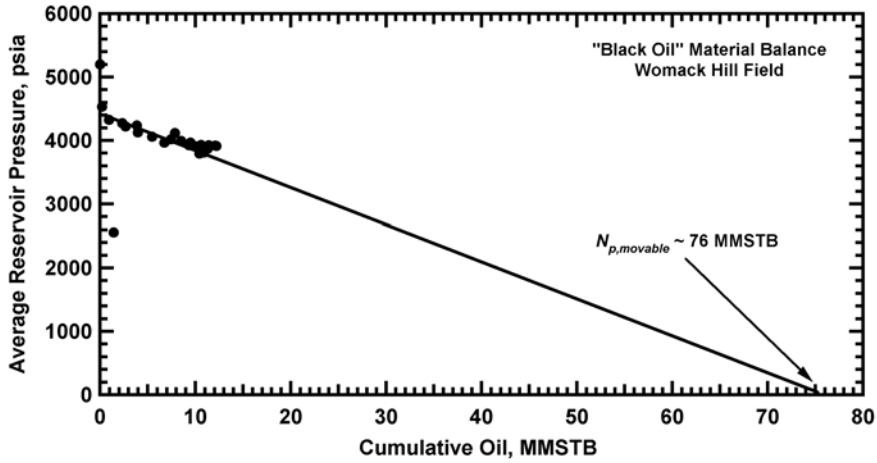

Figure 88. Material balance plot — Womack Hill Field. The straight-line trend produces an estimate of oil-in-place that is presumed to be high due to injection support and possible water influx.

was more for the benefit of confirming the external energy than for estimating the oil-in-place—this work will continue.

Integration of Results.--In this section, we present the integration of the results we obtained from the petrophysical and production data analyses. We utilized contour maps in order to establish spatial relationships of reservoir properties and to compare performance-derived parameters with other data such as geological and petrophysical descriptions. Reservoir structure based on the "top of structure" for the Upper Smackover sequence shows two ridges, one in the Eastern area and another toward the central-Western Unit area. Most of the wells are located on these ridges, the water injection wells are located on the periphery in the Western Unit area of the reservoir. The anhydrite of the Buckner Member is presumed to provide the reservoir seal, and laterally, the reservoir is bounded on the south by a fault and controlled on the west, east, and north by the water-oil contact.

In Figures 89 through 91, we present the porosity distributions generated using the statistical analysis of data for Flow units A, B, and C, respectively. The contours show a homogeneous trend in Flow unit A; however, in Flow unit C there is insufficient data to produce a meaningful map. From Figures 89 to 91, we can conclude that a porosity estimate of 18 percent would serve as a reasonable average value for the entire Smackover sequence (Flow units A, B, and C). Likewise, Figures 92 to 94 present the permeability distributions generated using the statistical analysis on the core data given for Flow units A, B, and C. Again, the shortage of data in Flow unit C prohibits us from making any conclusions. However, in Flow units A and B the contours show a apparent permeability contrast between the Eastern and Western Unit areas.

Permeability reaches a maximum for the field just on the Western Unit ridge area and its minimum on the south of the Eastern ridge area. The pressure data suggest that a flow barrier may exist between both areas, and the permeability distributions (Figs. 92 to 94) tend to confirm this hypothesis. This permeability contrast has to be considered as the "barrier" between the two areas. Using pressure transient tests (production or injection wells), we can attempt to quantify the

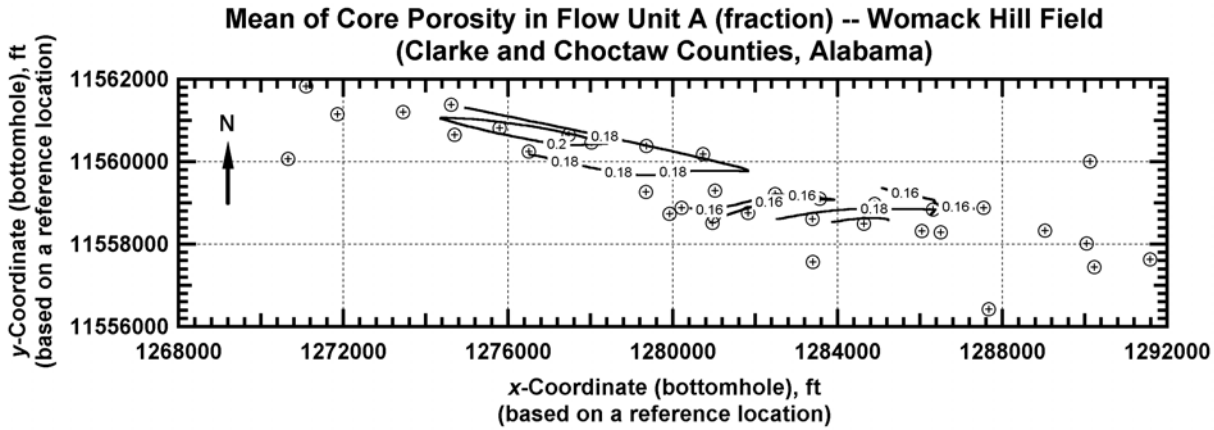

Figure 89. Flow Unit A — Core porosity distribution obtained from statistical analysis (histogram for each well) —the contours tend to indicate a homogeneous reservoir model.

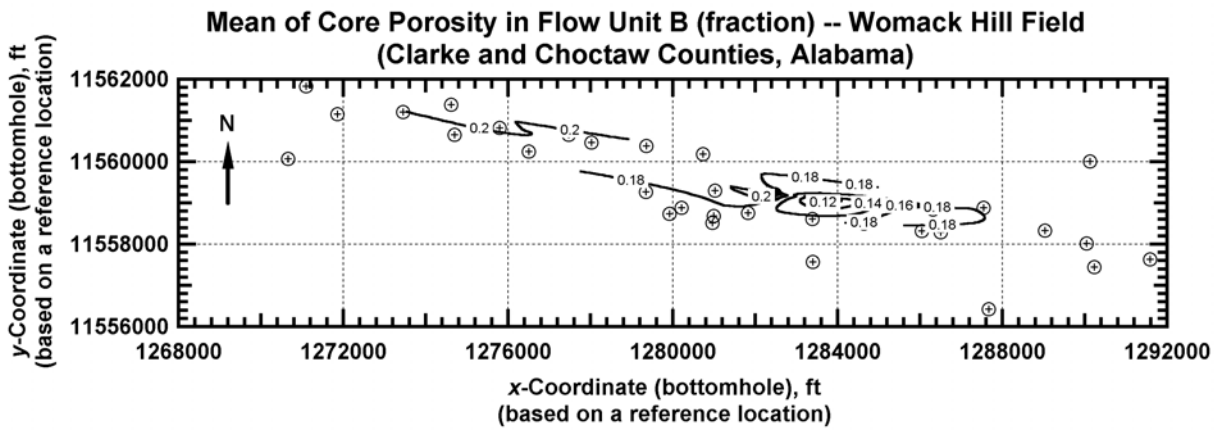

Figure 90. Flow Unit B — Core porosity distribution obtained from statistical analysis (histogram for each well) —the contours tend to indicate a homogeneous reservoir model.

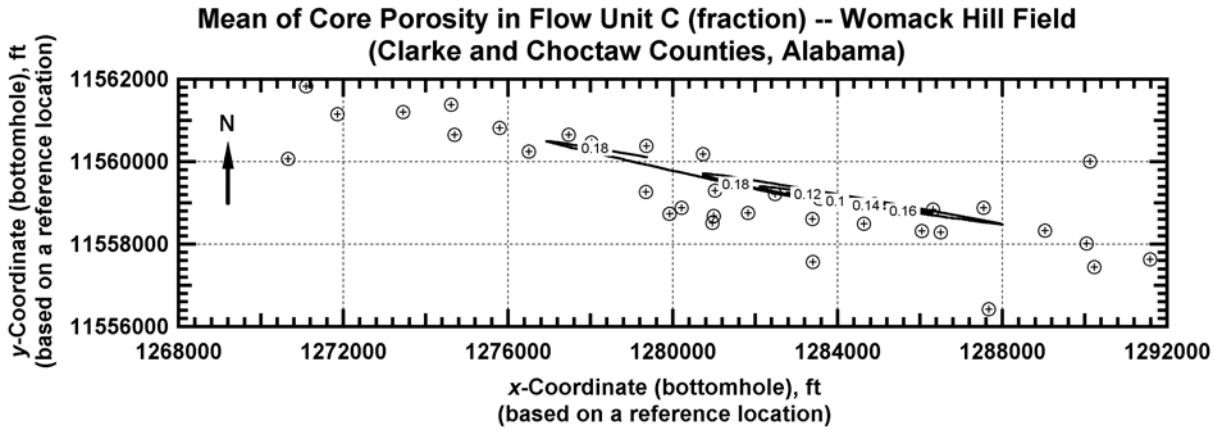

Figure 91. Flow Unit C — Core porosity distribution obtained from statistical analysis (histogram for each well) — insufficient data.

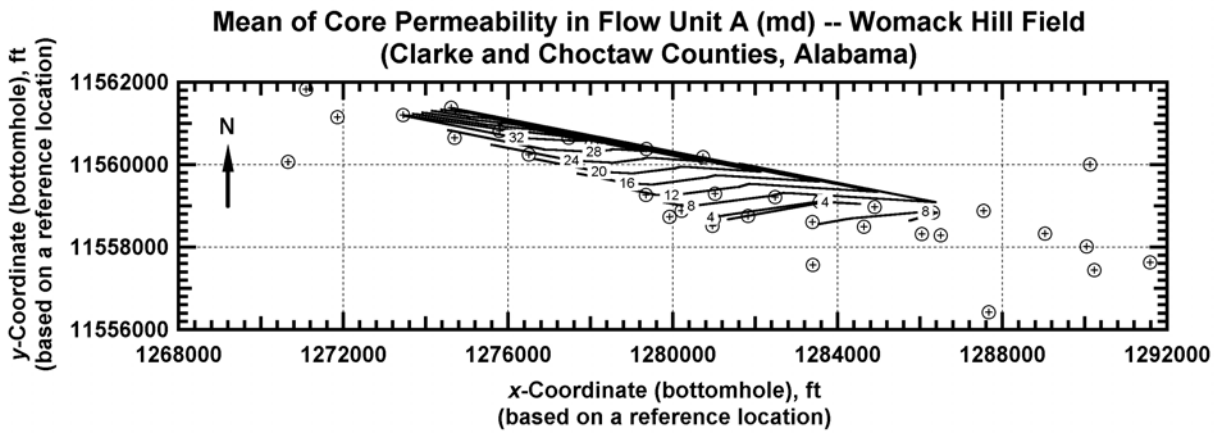

Figure 92. Flow Unit A — Core permeability distribution obtained from statistical analysis (histogram for each well) — a permeability contrast is evident between the Eastern and Western areas.

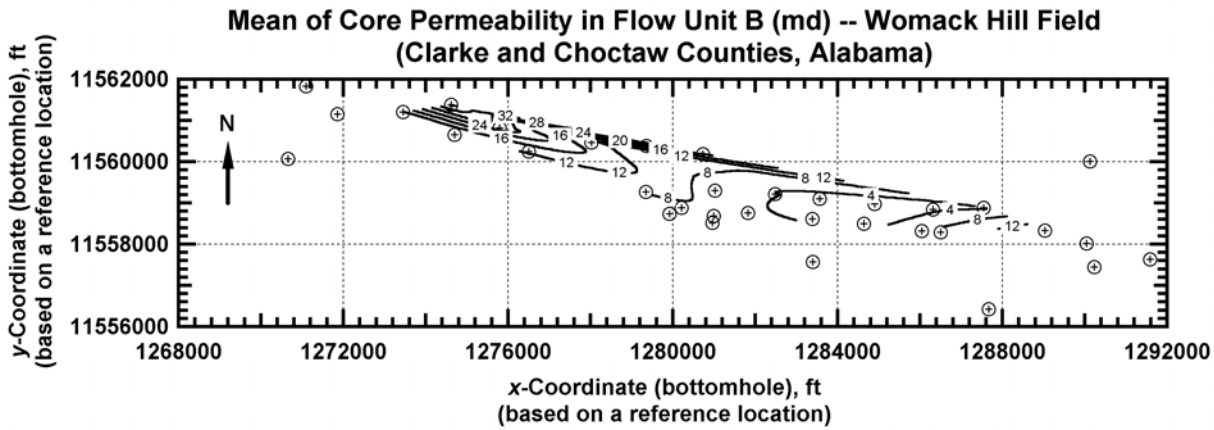

Figure 93. Flow Unit B — Core permeability distribution obtained from statistical analysis (histogram for each well) — a permeability contrast is evident between the Eastern and Western areas.

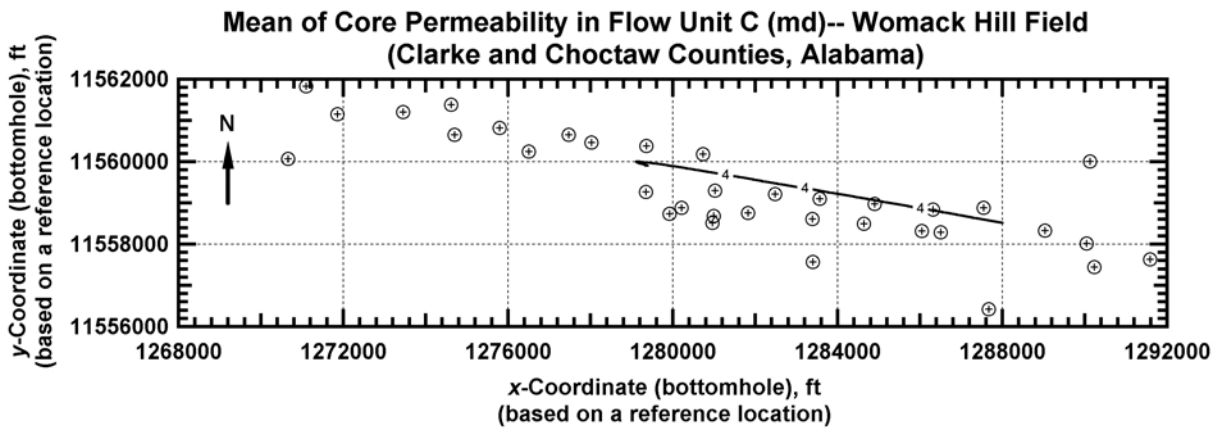

Figure 94. Flow Unit C — Core permeability distribution obtained from statistical analysis (histogram for each well) — insufficient data.

existence/influence of this of this barrier. In summary, the "barrier" could simply be a reduction of permeability that was caused by a change in mesoscopic heterogeneity (depositional facies), a change in microscopic heterogeneity (diagenetic changes), or a combination of the two processes—at this point in time we simply confirm the apparent existence of this flow "contrast."

Figure 95 shows the distribution of the cumulative oil production throughout the field area—this plot shows that the best production is in the Western Unit area (where the formation is thicker and permeabilities are higher). In the Eastern area the oil production is less, presumably as consequence of the lower reservoir quality. Figure 96 shows the 3-month initial oil rate distribution, this variable behaves consistently throughout most of the reservoir area (probably because of regulatory constraints), and only a few values lie out of the average range (350-450 STB/D)—these values are in the margin of the Eastern area, where the gross pay thickness is relatively small.

A map of the *EUR* estimated from the rate versus cumulative production plots is presented on Figure 97; this map revels that the highest recovery is in the vicinity of the Eastern ridge area, reaching a maximum value of 3 MMSTB per well. However, this higher recovery is very localized, and is surrounded by contours of much lower magnitudes. Towards the west, the distribution is more consistent and averages 1.5 MMSTB per well. As we saw earlier, *EUR* and the Nc_t-product correlate quite well—on Figure 98 we can see that the area with higher Nc_t-products generally coincides with the area of higher *EUR*. The distribution reflects the fact that most of the oil-in-place lies in the area associated with the two ridges in the field. Outside of this area, the Nc_t-product is significantly lower. Finally, we note in Figures 98 and 99 evidence of irregular performance behavior at Womack Hill Field as the zone with higher *EUR* and Nc_t-products is in the area of lower permeability and variable reservoir thickness.

Reservoir Modeling (Simulation).--Reservoir simulation efforts have been initiated and have focused on quantifying the sources of reservoir energy. Qualitatively we believe that fluid compressibility, water injection, and aquifer influx provide various components of reservoir energy.

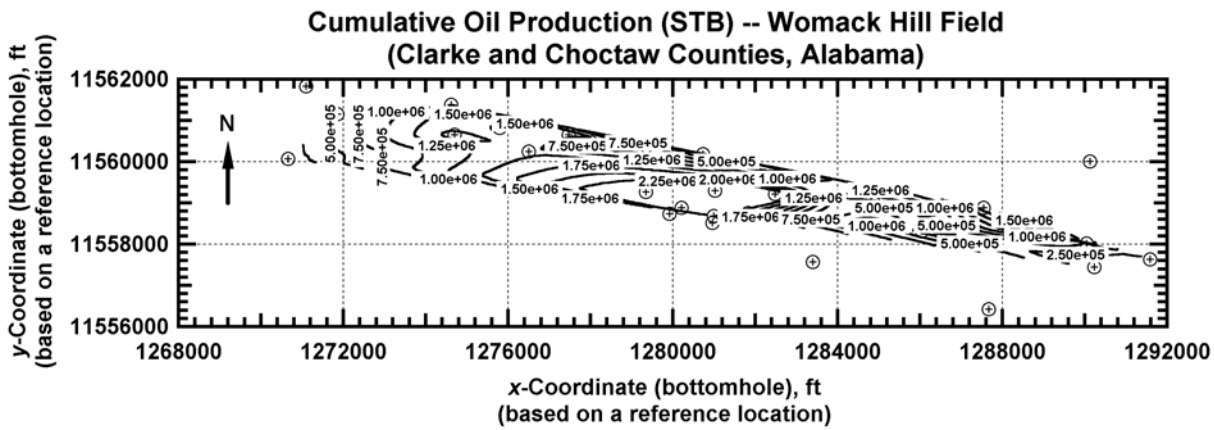

Figure 95. Distribution of cumulative oil production — the best productive area is the Western part of the structure, this area is presumed to have the highest reservoir quality.

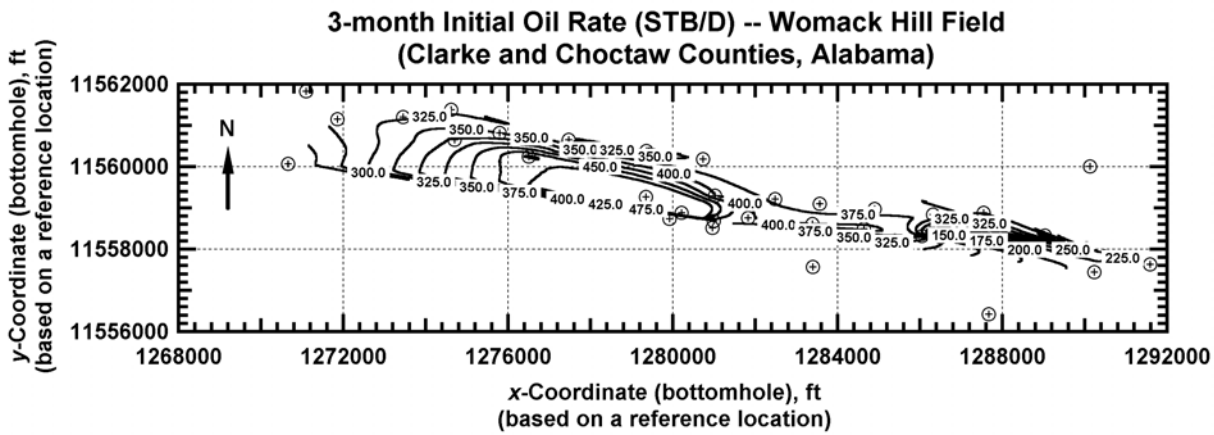

Figure 96. Distribution of the 3-month initial (oil) production (IP) — the trend is consistent throughout most of the field, with the exception of the Eastern edge of the structure.

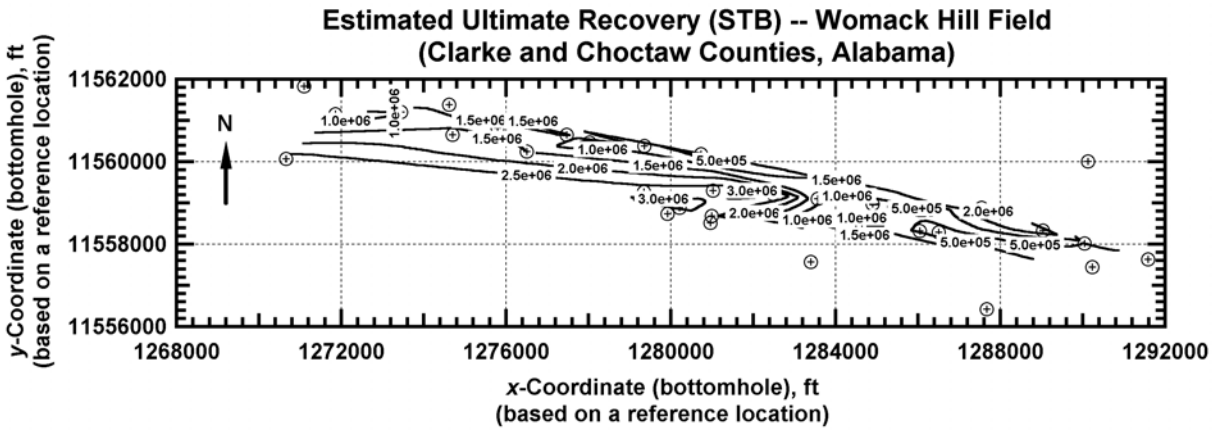

Figure 97. Distribution of estimated ultimate recovery (*EUR*) — note that the zone with the highest *EUR* is around the Eastern ridge of the structure.

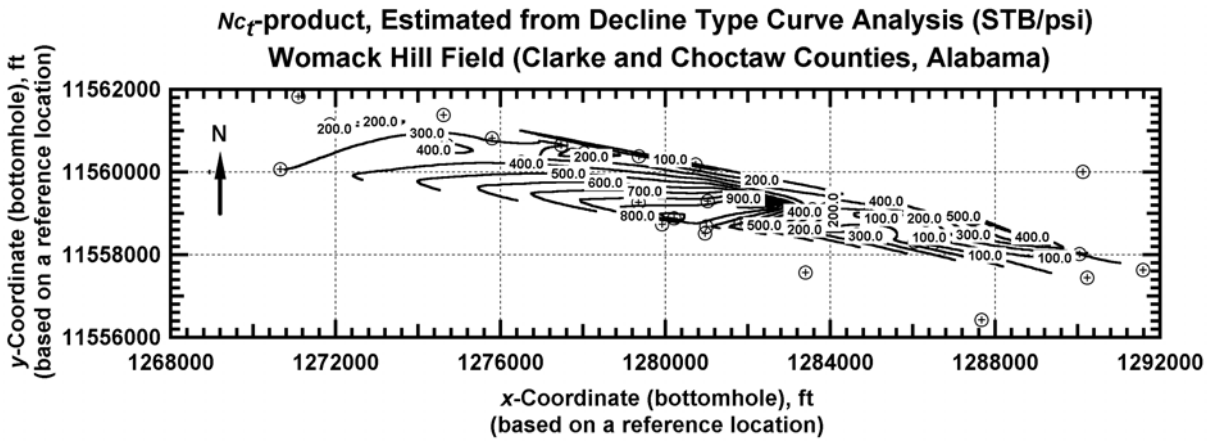

Figure 98. Nc_t-product estimated using decline type curve analysis — Nc_t-product correlates very well with *EUR*.

We are therefore trying to establish the strength and orientation of the aquifer. In simulations made without an aquifer, the average reservoir pressure declines to very low levels (under 1000 psi) which would not have yielded the flow rates we observed in the production wells

The available static bottomhole pressure data suggests that the average reservoir pressure in the model should not drop below about 3000 psia. This is also consistent with the fieldwide gas-oil ratio, which has remained approximately constant over the life of the field. If the average reservoir pressure dropped below the bubblepoint (1938 psi) we would expect an increase in the field gas-oil ratio with time. In the current model, using a strong aquifer causes the model to suffer convergence failures (*i.e.*, the computational scheme is unable to solve the equations modeling fluid flow with sufficient accuracy and a reasonable timestep length).

Based on production data, the distribution of water influx across the reservoir is not believed to be uniform. Water production is highest in a group of wells (Permits #1639, #1655, #1667, #1678 and #2109) in the western portion of the field. This non-uniformity in the distribution of water influx may be due to discontinuities in the nonporous layers between the productive zones. There is insufficient well control to fully characterize the continuity of these reservoir layers, so additional simulations are being performed to assess the effect of the continuity of the nonporous layers on the production history. This continuity issue is also likely to contribute to the convergence failures mentioned above.

We are also trying to ascertain the initial location of the water-oil contact. The performance of the field in terms of water production is very sensitive to this estimate. However, the estimates of the water-oil contact significantly under-predict water production for the field.

Water-oil contact depth, ft	Cumulative water production, MSTB
11340	2603
11360	1210
11380	672

Another problem we face in matching the volumes of produced water is that apparently no water production data are available until after 1982. We know that substantial volumes of water were produced prior to January 1982 as some wells had very high water rates (*e.g.*, Well 1639, q_w = 13,300 STB/D). This means that we can not necessarily "fine-tune" the relative permeability profiles by matching water breakthrough times.

The history matching process in the simulation process has been initiated. Our first target is to match field-wide performance (*i.e.*, cumulative produced oil, water and gas). Once we are satisfied with this match we will then pursue matches of individual well performance.

Task RC-3.--Microbial Characterization

Description of Work.--This task will determine whether *in-situ* micro-organisms are present in the Smackover carbonate reservoir at Womack Hill Field and will determine through laboratory experiments the ability of these microbes to produce a single by-product (acid) by supplying them with only enough nutrients to sustain the cells but not enough to support cell proliferation.

Rationale. Researchers at Mississippi State University have demonstrated the cost-effectiveness of utilizing the growth of indigenous microbes in enhancing the efficiency of an active waterflood for the recovery of incremental oil. The technology involves injecting a regulated stream of nutrients into a sandstone reservoir at a subsea depth of -2,300 ft to stimulate indigenous microbe growth. Cell proliferation by these micro-organisms acts to reduce the flow of injected water in more permeable zones of the reservoir by selective plugging, thereby diverting the water to other areas of the reservoir. This diversion and altering of flow patterns in the reservoir serve to enhance the sweep efficiency of the waterflood. This technology will be expanded upon in this study by using the ability of these microbes to produce a single by-product (acetic acid).

This immobilized enzyme technology will be applied to the carbonates at a depth of 11,300 ft in Womack Hill Field. It is anticipated that the acetic acid will act to break down the Smackover reservoir through dissolution thereby creating enhanced reservoir connectivity.

Microbial Identification and Characterization.--The objectives of this subtask are to characterize the microflora present in the Womack Hill Oil Field in terms of their ability to convert

alcohols to acids and to determine the nutritional requirements to maintain cells in a metabolically active state with minimal replication.

Four water samples from Womack Hill Field Well Turner 13-6 and two cores taken from the Womack Hill Field a number of years ago were analyzed for micro-organisms capable of growing at 90˚C, but none were found in any of the samples. This was not unexpected since the cores had been exposed to the air for years. Likewise, it was not surprising that no micro-organisms capable of growth at 90˚C were found in the water samples since micro-organisms prefer to grow attached to a substrate and consequently may be absent in the water. At the time that these samples were tested, the equipment necessary to maintain an anaerobic environment was inadequate and may have prevented the growth of strict anaerobes. A Coy® Anaerobic Flexible Vinyl Chamber, which efficiently maintains an anaerobic atmosphere, was purchased and resolved the problem.

In order to design the amounts and schedule for the introduction of nutrients into the injection wells for the field demonstration of the immobilized enzyme technology, cultures from the Smackover Formation were required. Attempts to obtain a core from a well being drilled near the Womack Hill Field were unsuccessful for several reasons. As an alternative, cuttings and drilling mud were obtained from Crosby's Creek Oil Field located in Washington County, AL, that is situated near Womack Hill Oil Field.

When attempting to isolate micro-organisms from petroleum reservoirs it is expected that most, if not all, will be in the form of ultramicrobacteria (UMB). They are extremely small in size due to lack of essential nutrients and are metabolically dormant. Specifically, the oil reservoir is deficient in nitrogen- and phosphorus-containing nutrients. Furthermore, UMB's normally cannot be reactivated using conventional strength media and more dilute media must be employed in isolation procedures. Therefore, approximately two g of the cuttings were placed into nine 60 ml volatile organic analysis (VOA) vials containing 20 ml of either $^1/_2$, $^1/_{10}{}^{th}$, or $^1/_{20}{}^{th}$ strength mineral salts broth (MSB). MSB consisted of 1 g KNO_3, 0.38 g K_2HPO_4, 0.20 g $MgSO_4{\cdot}7H_2O$, and 0.05 g $FeCl_3{\cdot}6H_2O$ per liter of distilled water. The pH was adjusted to 7.0 with 10% HCl (vol/vol). Of the nine VOA vials prepared, three contained 20 ml of $^1/_2$-strength mineral salts broth (MSB), three

contained 20 ml of $^{1}/_{10}$-strength MSB, and three contained 20 ml of $^{1}/_{20}$-strength MSB. To each of the VOA vials, ~100 µl of Womack Hill Oil Field crude oil was added. All 9 vials were incubated under stationary conditions at 90˚C.

After 21 days of incubation, growth of micro-organisms was evident in all of the vials. It was next decided to determine if the micro-organisms in these enrichments had the ability to convert the ethanol into acetic acid. Five µl of 95% ethanol was added to each of the nine vials and the vials placed in the 90˚C incubator to allow the ethanol to reach equilibrium between the gas and aqueous phases. The concentration of ethanol in the headspace of the vials was determined using a Varians® Model 3800 Gas Chromatograph equipped with a flame ionization detector. Additionally, carbon dioxide was determined using a Fisher dual column, dual detector, gas partitioner fitted with thermal conductivity detectors.

As shown in Figure 99, the enrichments from all three dilutions of media consumed ethanol. The difference in the amounts of ethanol consumed is probably a reflection of a difference in cell concentration rather than a difference in species of micro-organism. It should be pointed out that after four days of incubation, 6.9 mg of bicarbonate was added to each vial to react with the acids to form carbon dioxide.

Figure 100 shows the amount of carbon dioxide produced by the enrichments cited above. As may be seen, a large quantity of carbon dioxide was produced by the enrichments and was considerably more than could be accounted for by the reaction of acetic acid with the carbonate. This additional carbon dioxide could be derived from utilization of the ethanol or oil. Also, carbon dioxide may have been derived from organic acids produced from the oil directly reacting with the carbonate.

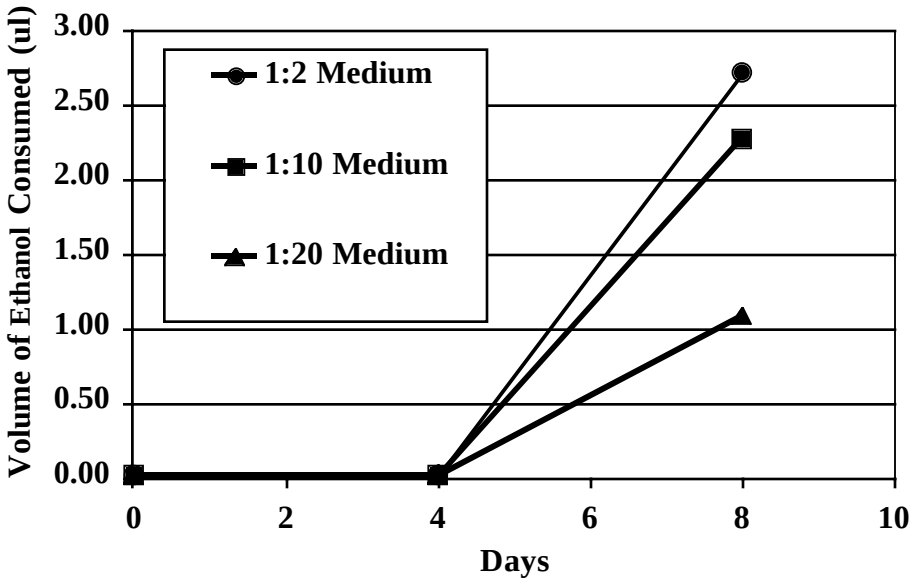

Figure 99. The utilization of ethanol by enrichment cultures.

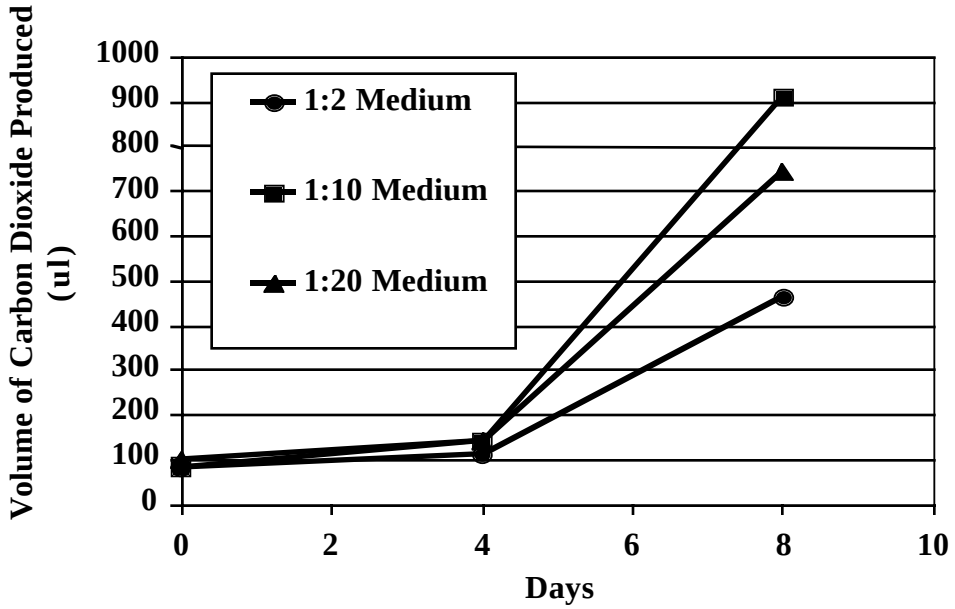

Figure 100. The production of carbon dioxide by enrichment cultures.

These enrichment cultures were subcultured into new medium with oil. Also, the original cultures were again tested for their ability to utilize ethanol and the results are given in Table 8. As may be observed, all of the cultures consumed ethanol.

Table 8. Utilization of Ethanol by Enrichment Cultures Growing at 90˚C Under Anaerobic Conditions

MSM/H2O	Ethanol Utilization in 5 Days	Ethanol Utilization in 9 Days
(Dilution)	(90)	(90)
1:2	75	88
1:10	74	85
1:20	60	82

Samples of these enrichments were examined using a confocal laser-scanning microscope. In transmitted light, the bacteria are visible within menisci of oil as shown in Figure 101. These bacteria auto fluoresce (fluoresce without staining) when stimulated with the laser (see Figure 102). A reverse negative picture of the cells is given in Figure 103.

These findings are highly encouraging and suggest that micro-organisms capable of producing acetic acid from ethanol will be present in the Womack Hill Oil Field reservoir and that they can be induced to grow and be metabolically active at the temperature in the reservoir. Nevertheless, cores from near the Womack Hill Oil Field and/or from the same producing formation are still being sought.

Ultimately, the ability of the microflora to grow and produce acetic acid from ethanol in live cores needs to be determined. Toward this end, a core plug testing system designed to operate at 90˚C has been fabricated and is depicted in Figure 104.

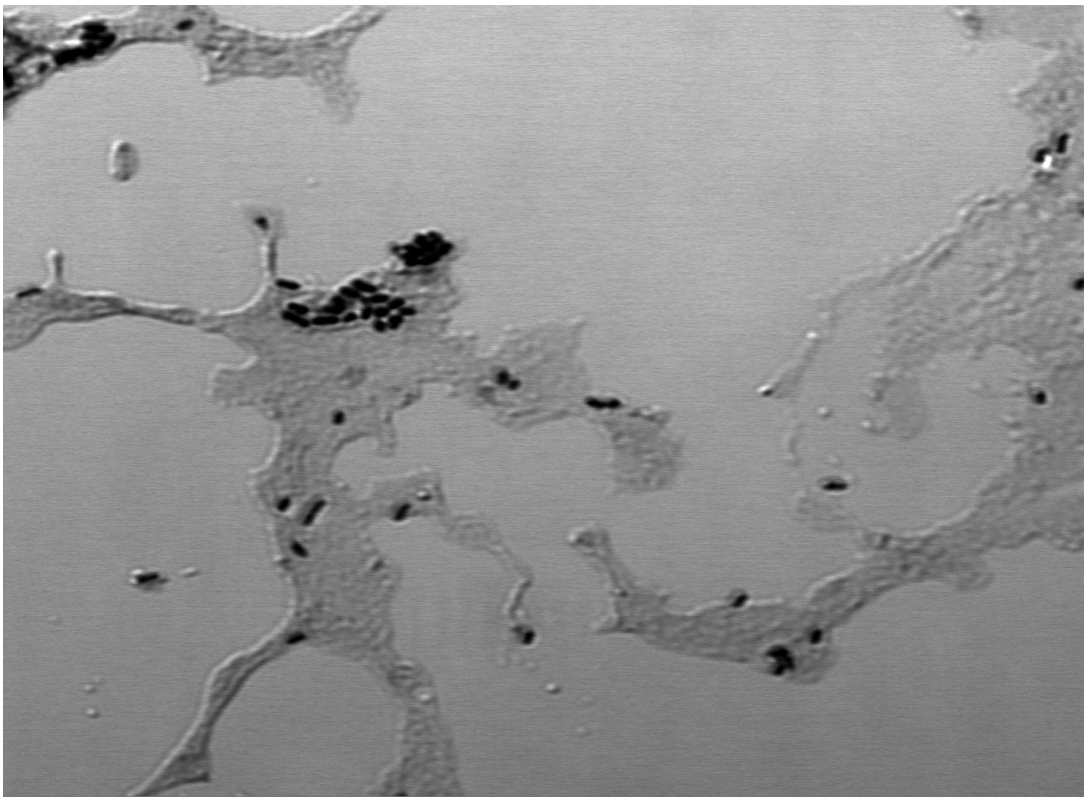

Figure 101. Laser confocal microscope image of oil-degrading grown anaerobically at 90˚C.

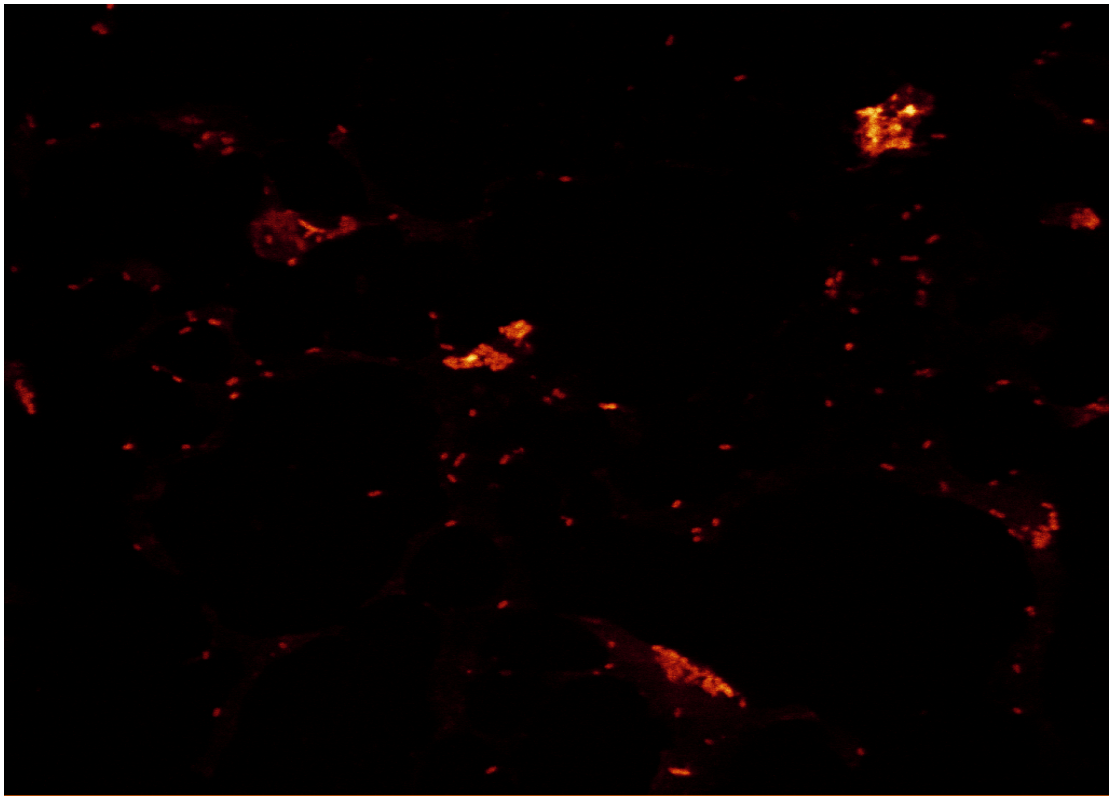

Figure 102. Auto fluorescence of bacteria grown anaerobically at 90˚C when stimulated by laser using a confocal laser-scanning microscope.

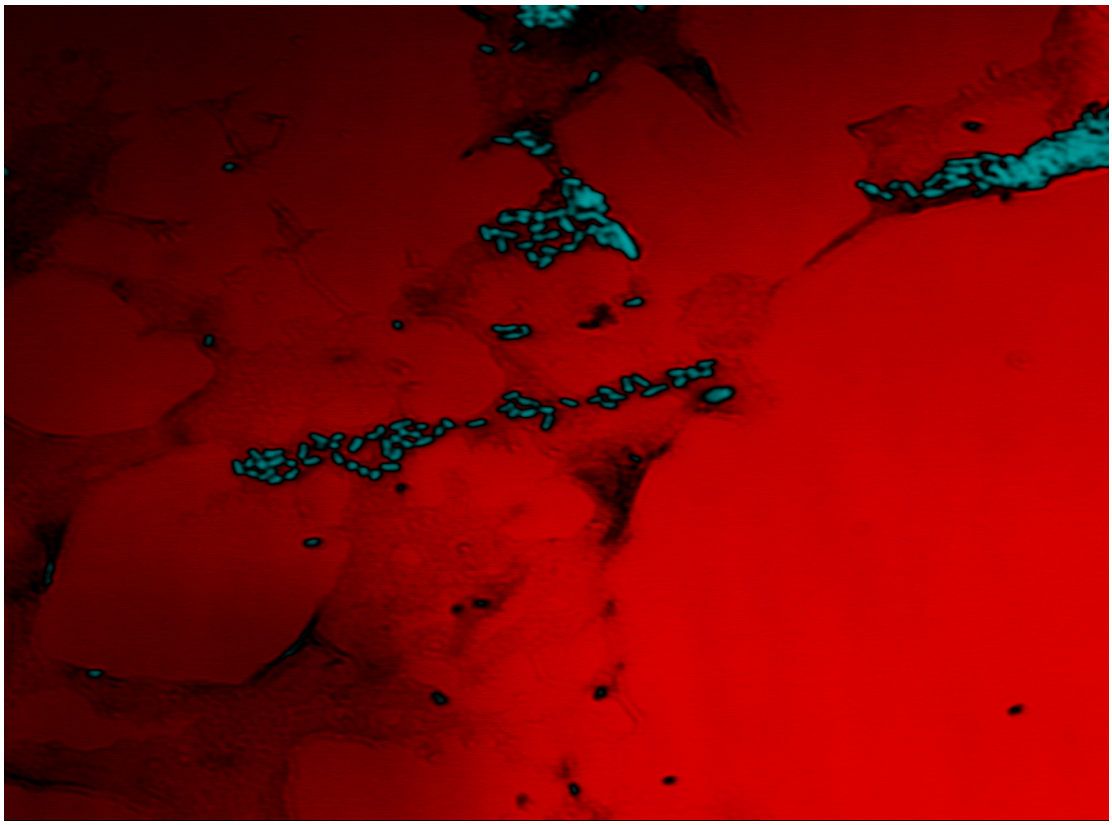

Figure 103. A reverse negative confocal laser-scanning microscope image oil-degrading bacteria grown at 90˚C.

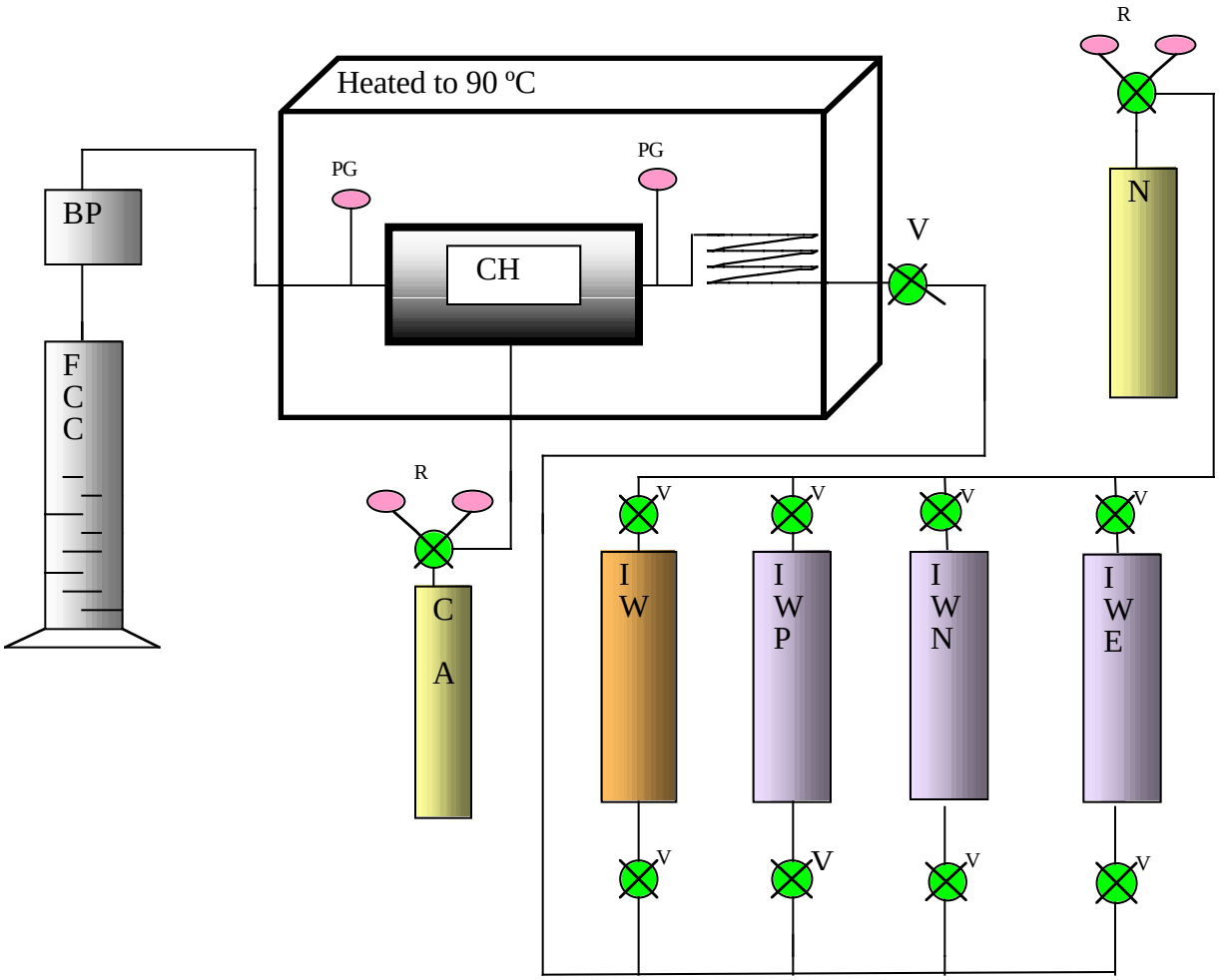

BP: **B**ack **P**ressure regulator
CA: **C**ompressed **A**ir
CH: **C**ore **H**older
FCC: **F**luid **C**ollection **C**ontainer
IW: Injection **W**ater
IWE: Injection **W**ater with **E**thanol
IWN: Injection **W**ater with **NO_3**
IWP: Injection **W**ater with **PO_4**
N: Nitrogen gas
PG: **P**ressure **G**uage
R: **R**egulator

Figure 104. Diagram of the core plug testing system.

As shown, the core holder is enclosed in a 90˚C incubator. All fluids entering the core will be preheated to 90˚C and the effluent from the core will be collected in the Fluid Collection Container where the quantities of oil and water can be measured.

Once cores become available, experiments will be conducted in the core plug testing system shown above at 90˚C to determine the effects of nutrient concentrations on the indigenous micro-organisms and evaluate the ability of these micro-organisms to convert ethanol to acetic acid. Scanning electron microscopy (SEM) will be used to gain some insight into the manner of attachment of cells in the cores and follow their reproduction. This is especially important in the immobilized enzyme technology since the goal is to maximize metabolic activity (conversion of ethanol to acetic acid) rather than cell proliferation. One of the problems in scanning electron microscopic studies of bacteria has been the preservation techniques being employed. Five techniques have been tested thus far, including air-drying, 10% glutaraldehyde fixation, standard ethanol dehydration with hexamethyldisilazane, ethanol dehydration with critical point drying, and ethanol/acetone dehydration with critical point drying.

Ethanol dehydration and critical point drying are the standard preservation procedures used for microbiological studies, and our investigation shows that bacterial cells preserved according to these techniques maintain their vital shape. However, our investigation also has shown that these techniques greatly change the morphology of the polysaccharide capsule. Simple air-drying and glutaraldehyde fixation best preserved the shape of polysaccharide biofilm. It was concluded that an accurate investigation requires two samples, one preserved by glutaraldehyde fixation for characterization of the biofilm, and one by ethanol dehydration for examination of the bacterial cells themselves.

It has been proposed that a third major species of organic material, along with bacteria and humus (or kerogen), is present in soils and rocks. Nannobacteria are 25-300 nm ovoid shapes that are observed during high-magnification SEM research. Because of their general resemblance to eubacterial cocci or bacilli, and because of their tendency to occur in chains or clusters, they have been characterized as nannobacteria. They have been implicated in the formation of mineral deposits

in terrestrial and extraterrestrial samples, and in the development of arterial plaque in the human body (Folk, 1993; McKay *et al.*, 1996; Folk and Lynch, 1997, 1998, 2001; Kirkland *et al.*, 1999; Folk *et al.*, 2001).

It would be difficult to find a more contentious geologic or biologic topic than the existence or non-existence of these nannobacteria. Critical attention from the microbiology community has been focused on the small size of the nannobacteria, which are often 1/1000th the volume of typical bacteria. Nonetheless, confirmation of the biological affinity of some of these features, especially the larger ones, has been made using molecular biology techniques (Spark *et al.*, 2000). However, laboratory experiments have shown that the suspect textures also can be formed by mineral precipitation in an organic-rich, though abiotic, environment (Kirkland *et al.*, 1999). Our current research also shows that textures very similar to the purported nannobacteria can be produced by dehydration of polysaccharide capsule or biofilm (Fratesi and Lynch, 2001). The relationship between the textures, different minerals, and different organic compounds requires further research.

Task RC-4. Integration of Data

Description of Work.--This task will integrate the geological, geophysical, petrophysical and engineering data for the Womack Hill Field into a single comprehensive digital database for reservoir characterization, 3-D geologic and seismic modeling, 3-D reservoir simulation, cost-effective field management, and for making operational decisions in the field.

Rationale. This task serves as a critical effort to the project because the construction of a digital database is an essential tool for the integration of large volumes of data. This task also serves as a means to begin the process of synthesizing concepts. The database also provides a mechanism for quality control in that core and log data can be compared to geophysical, petrophysical and engineering data. These measured and calculated data are utilized in developing predictive algorithms for calculating variable values for interwell areas. The database serves as an archival record that can be updated in the future. The database is built using a spreadsheet approach. The data are accessed, managed, and analyzed by using standard industry software. The goal is to develop a relevant and transportable database.

Data Integration.--All geological, geophysical, petrophysical and engineering data for the Womack Hill Field acquired to date have been integrated into a comprehensive digital database.

Task RTA-1. 3-D Geologic Model

Description of Work.--This task involves using the integrated database which includes the information from the reservoir characterization tasks to build a 3-D stratigraphic and structural model of the Womack Hill reservoir. Previous reservoir models constructed for the Smackover and for the Permian carbonate shoal reservoirs in West Texas and the depositional modeling of modern ooid sand shoals of the Great Bahama Bank are used as analogs in building the 3-D stratigraphic and structural model for the Smackover shoal reservoir at Womack Hill Field.

Rationale. This task provides the framework for the reservoir simulation model. Sequence stratigraphy in association with structural interpretation will form the framework for the model for Womack Hill Field. The model will incorporate data and interpretations from the core and well log analysis, sequence stratigraphic, depositional history and structural studies, petrographic analysis, and diagenetic, pore system, and petrophysical and engineering studies. The purpose of the 3-D stratigraphic and structural model is to provide an interpretation for the interwell distribution of systems tracts, lithofacies, and reservoir-grade rock. This work is designed to improve well-to-well predictability with regard to reservoir parameters, such as primary depositional lithologies, diagenetic features, pore types and systems, porosity and permeability values, and heterogeneity. This layer-based model will be built utilizing data mining and associated neural networks to populate and distribute property and attribute data. Key data include structural features, physical surfaces, depositional sequences, stratigraphic event beds, sedimentary structures, carbonate textures and mineralogy, diagenetic features, pore types and throats, and porosity and permeability. Geologic modeling sets the stage for reservoir simulation and for the recognition of flow units, barriers to flow and flow patterns in the respective fields. The reservoir model and integrated database become effective tools for cost-effective reservoir management for making decisions regarding operations in the field. Accepted industry software, such as Stratamodel, will be used to build the 3-D geologic model.

3-D Geologic Model.--Building a 3-D geologic (stratigraphic and structural) model (Figs. 105 and 106) to illustrate the geometry of the reservoir(s) at Womack Hill Field requires understanding of the stratigraphic framework of the reservoir and the structural framework in the field area (Kerans and Tinker, 1997). The Smackover stratigraphic, sedimentologic and petrophysical information (stratigraphic units, carbonate lithologies, lithofacies, cycles, porosities, and permeabilities) obtained from core, well log and thin section studies and from core analysis are fundamental to the construction of the model for this field. These data and information from the subsurface structure and isopach maps and cross sections are integrated into the model to illustrate Smackover cycle distribution, thickness, and reservoir quality and structural configuration. The 2-D seismic data (Fig. 20) for the field provide an independent confirmation of the location of faults in the Womack Hill Field.

Work Planned in Year 3

The work planned for Year 3 includes the following (Table 9):

Task RTA-2. 3-D Reservoir Simulation

Description of Work.--This task builds a numerical simulation model for the Womack Hill Field that is based on the 3-D geologic model (stratigraphic and structural framework), petrophysical properties, fluid (PVT) properties, fluid-rock properties, and the results of the well performance analysis. The geological/geophysical model will be coupled with the results of the well performance analysis to determine flow units, as well as reservoir-scale barriers to flow. The purpose of this work is to build forecasts for the Womack Hill Field that consider the following scenarios: base case (continue field management as is); optimization of production practices (optimal well completions, including stimulation, injection/production balancing, etc.); active reservoir management (includes replacement and development wells); targeted infill drilling program; and enhanced oil recovery scenarios of gas injection, water/chemical injection, and immobilized enzyme technology.

Rationale. This task is the critical step for any enhanced oil recovery technology. Reservoir simulation is used to forecast expected reservoir performance, to forecast ultimate recovery, and

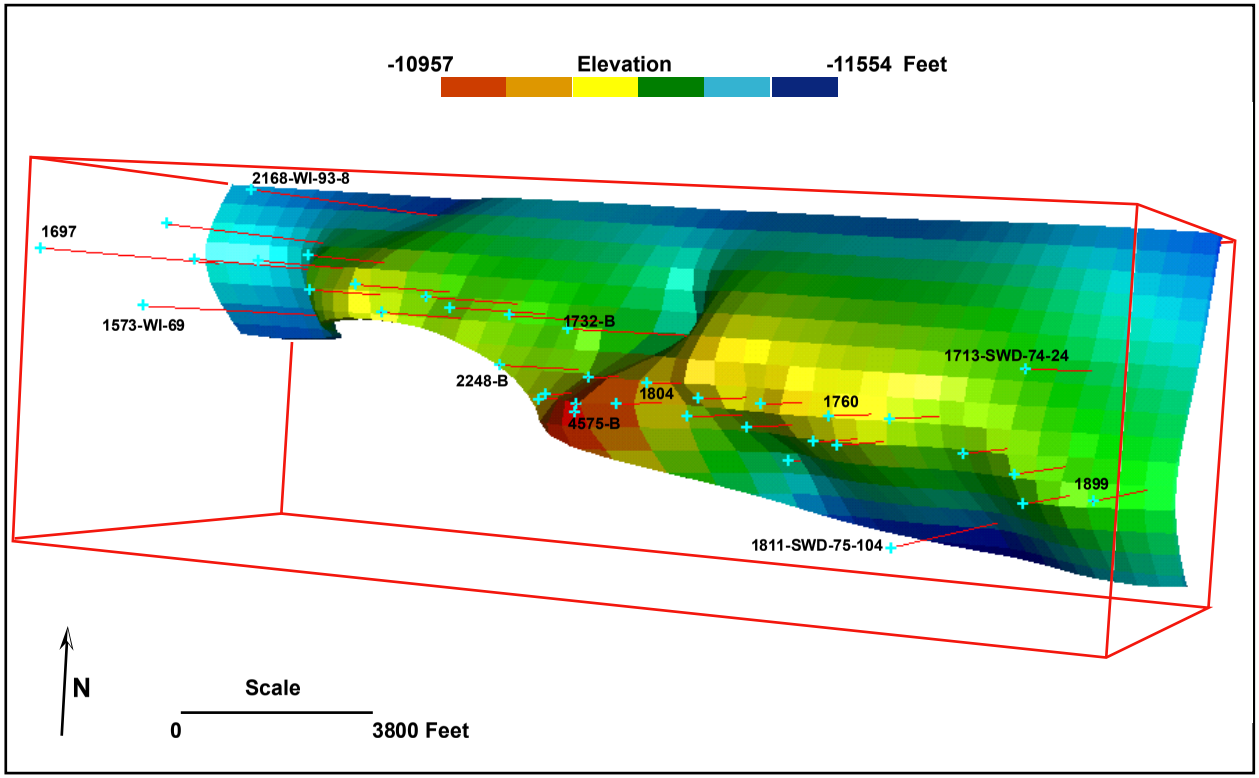

Figure 105. 3-D geologic model of Womack Hill Oil Field. Model depicting elevation of top of Smackover Formation. Model constructed using Stratamodel software. See Figure 8 for location of wells.

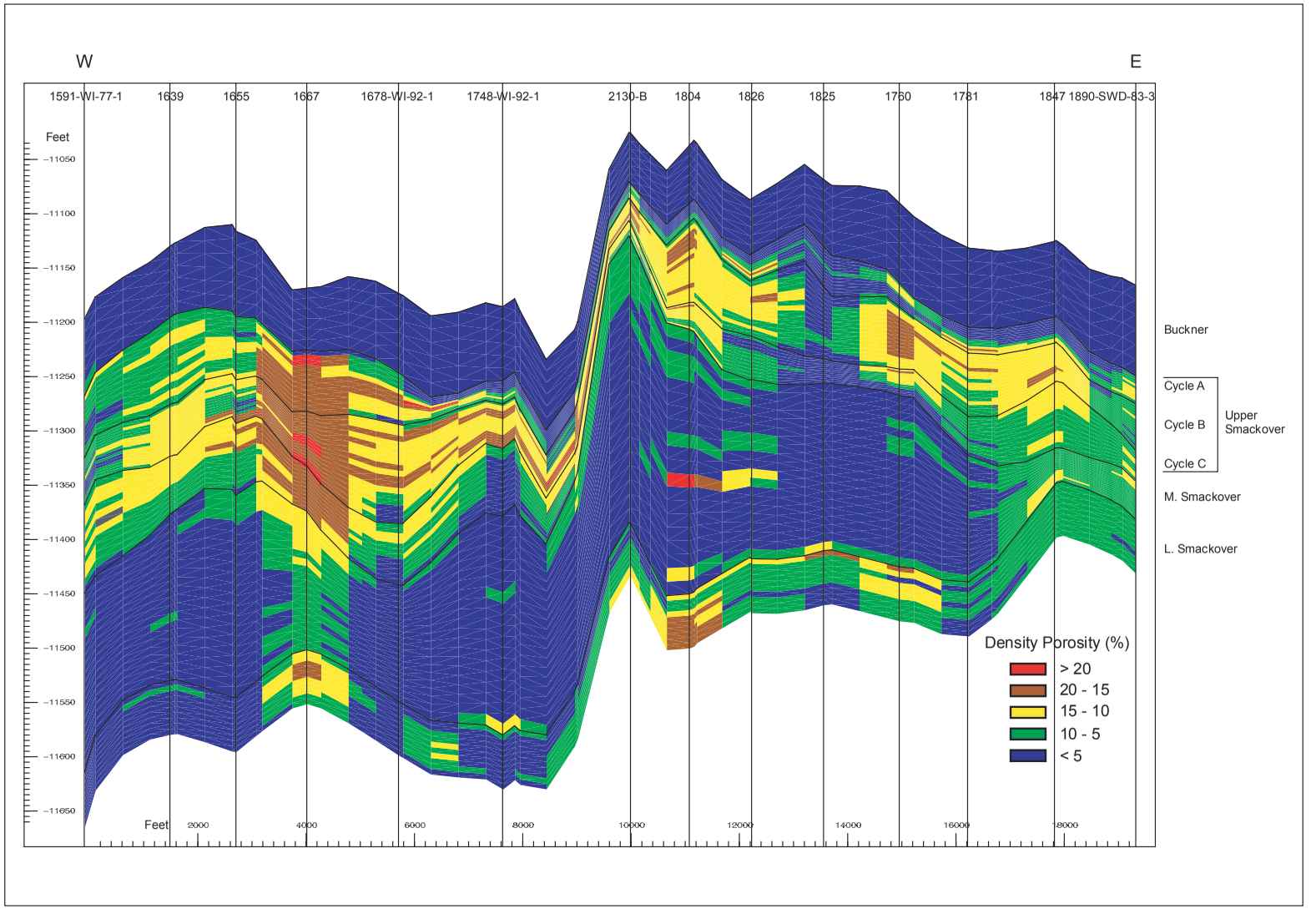

Figure 106. Cross section across Womack Hill Oil Field showing changes in porosity, as determined from density log analysis, in the Smackover Formation, including Cycles A, B, and C. Cross section constructed using Stratamodel software. This cross section corresponds to line of cross section A-A' in Figure 8.

Table 9
Milestone Chart—Year 3

Reservoir Characterization Tasks (Phase I)	M	J	J	A	S	O	N	D	J	F	M	A
Recovery Technology Analysis												
3-D Simulation												
Core Experiments												
Recovery Technology Evaluation												
3-D Seismic												
Pressure Maintenance												
IET Concept												
Decision for Implementation												

Work Planned

evaluate different production development scenarios. In itself, modeling of the current scenario at Womack Hill Field is necessary to establish whether or not the existing efforts in reservoir management (i.e., evaluation of the existing pressure maintenance program) are sufficient, and if not, how could these activities provide optimal performance. Conceptually, it is important to understand (i.e., be able to model) the current behavior at Womack Hill Field prior to initiating any new activities. Probably the most important aspect of the simulation work will be the setup phase. Developing a detailed reservoir model for the Womack Hill Field is essential because this is a geologically complex system, and the long production/injection history has not been evaluated relative to a detailed reservoir description. Much should be learned about the reservoir, including in particular, insight regarding the carbonate reservoir architecture and regarding the inherent heterogeneities in such a complex reservoir system.

Subtask 1 is the setup phase and will be conducted in conjunction with the creation and validation of the integrated reservoir description. However, this work has more specific goals than simply building the simulation data file. Considerable effort will go into the validation of the petrophysical, fluid (PVT), and fluid-rock properties to establish a benchmark case, as well as bounds (uncertainty ranges) on these data. In addition, well performance data will be thoroughly reviewed for accuracy and appropriateness.

Subtask 2 is the history matching phase. In this phase we will continue to refine and adjust data similar to the previous subtask, but in this work the focus will be to establish the most representative numerical model for the Womack Hill Field. Adjustments will undoubtedly be made to all data types, but as a means to ensure appropriateness, these adjustments will be made in consultation and collaboration with the geoscientists on the research team. In this phase, the goal is not to obtain a perfect match of the model and the field data, but rather to scale-up the small-scale information (core, logs, etc.) in order to yield a representative reservoir model. We envision the use of a black oil formulation, but it is conceivable that a compositional model may be incorporated if the black oil formulation is deemed insufficient.

Subtask 3 is the forecasting phase. In this phase, the goals for forecasting are to establish the viability of individual scenarios, where these cases include: a base case (no changes), optimal well practices, continued field development, and enhanced recovery activities (water, gas, or chemical injection). As the project progresses to Phase II, this work will be refined and the focus will be to establish the most viable improved recovery strategy.

Task RTA-3. Core Flood Experiments

Description of Work.--This task involves the maximization of the chemical addition program using core flood experiments. Live cores are anticipated for use in this work. If live cores are not available, artificial cores will be prepared from stratal material from archived cores. The cores will be incorporated into the core flood apparatus. The chemical addition program from Task RC-3 will be employed initially and changes made to maximize acid production while minimizing cell proliferation. All experiments will be conducted under anaerobic conditions at reservoir temperature. In addition to the parameters monitored in Task RC-3, a variety of other parameters will be monitored including oil recovery and petrophysical characteristics. These studies will finalize the chemical addition program to be implemented in the field demonstration project.

Rationale. As stated in Task RC-3, researchers at Mississippi State University have demonstrated the cost-effectiveness of utilizing the growth of indigenous microbes in enhancing the efficiency of an active waterflood for the recovery of incremental oil. This technology expands on the previous study by using the ability of *in-situ* microbes to generate acetic acid as a growth by-product. This IET is applied to a carbonate reservoir at a depth of 11,300 ft. It is anticipated that the acetic acid will act to break down the reservoir through dissolution, thereby increasing porosity and permeability in less permeable zones of the reservoir. This should result in reduced reservoir compartmentalization and more contacted oil, thereby increasing producibility of the reservoir.

Task RTE-1. Evaluation and Acquisition of 3-D Seismic Data

Description of Work.--This task involves the use of the 3-D geologic model to determine whether there are zones in the Womack Hill reservoir where uncontacted oil remains and whether there is attic oil remaining in the field. The task also includes evaluating whether the acquisition of

3-D seismic data is required to confirm the presence of uncontacted oil, including attic oil in the Womack Hill Field Unit. If so, 3-D seismic data will be acquired, processed and interpreted as part of this task to facilitate the implementation of the integrated demonstration project of the Womack Hill Field Unit.

Rationale. Petroleum companies have been extremely successful in the Eastern Gulf Region in exploring for and developing Upper Jurassic Norphlet, Smackover and Haynesville Fields using 3-D seismic data. Utilizing 3-D seismic data, in combination with well logs, has proven to be a powerful tool in imaging Smackover structures and reservoirs in the Eastern Gulf Region. It is anticipated that 3-D seismic imaging of the reservoir structure, in combination with the 3-D geologic model, which incorporates the 3-D structural interpretation of the Womack Hill petroleum trap, generated by using GeoSec software and a series of balanced cross sections for the field, will provide the information required to determine whether uncontacted oil and attic oil remain in the Womack Hill Field Unit. The importance of using petrophysics data and balanced cross sections in combination with 3-D seismic data for reservoir and structure modeling has been shown by a study of the Ellenberger in West Texas. Standard industry software, such as 2d/3d Pak and SeisWorks, will be used to perform this task.

Task RTE-2. Evaluation of the Pressure Maintenance Project

Description of Work.--This task is designed to verify/dispute the effectiveness of the existing pressure maintenance activities being conducted at Womack Hill Field Unit. The reservoir simulation history matches will be used as a mechanism to establish water loss and to provide insight as to large-scale water movement within the unit. The well performance activities will be designed to determine if the water injection program is being effective. Efforts will be made to: evaluate pressure and fluid communication in the field (data analysis, data correlation), review injection/ production behavior on a pattern basis to verify pressure support in a particular area, and review completion and production practices. The short-term goal of this work is to determine if modifications are required for the injection strategy, as well as to determine whether or not an advanced oil recovery technology (such as the introduction of chemicals) should be considered or

discarded. The long-term goal is to establish the practices and procedures for implementing optimal pressure maintenance, regardless of the mechanism (waterflood, chemical injection, etc.).

Rationale. Profitability is currently down at Womack Hill Field Unit because production is declining and the cost of operations is escalating. The operator has cited water loss due to the heterogeneous nature of the Smackover reservoir as a major source of the production decline (i.e., pressure support is insufficient to provide good pressure/fluid communication). It is clear that modification of the existing pressure maintenance project and/or the addition of an advanced oil recovery technology has the potential to extend the life of this reservoir by increasing profitability.

Subtask 1 consists of additional analyses of the production/injection data to establish the state of pressure/fluid communication at Womack Hill Field. In particular, a separate evaluation of the production and injection data on a per-well basis using a multiwell reservoir model will be considered. In theory, it is possible to analyze per-well performance using an analytical solution for a closed multiwell reservoir; but, because of reservoir heterogeneities, it may not be feasible to implement a multiwell solution. Interference and/or injector/producer communication, as well as utilizing the conventional (albeit simplified) analysis of injection well rates and pressure (the Hall and Hearn plots), will be studied.

Subtask 2 will focus on the use of the results from the history-matches obtained in the reservoir simulation tasks. The focus will be to correlate simulated performance with other analysis results to verify pressure/fluid movement in different areas of the field. The work in this subtask will guide the efforts to optimize injection/production behavior, as well as to identify possible target areas for infill drilling and/or enhanced recovery activities (cyclic injection, IET, etc.)

Task RTE-3. Evaluation of the Immobilized Enzyme Technology Project Concept

Description of Work.--This task involves the evaluation of the laboratory results of the proposed IET project at Womack Hill Field Unit to determine whether it is feasible to implement an IET field-scale demonstration project at Womack Hill Field Unit.

Rationale. MEOR technology has been demonstrated to be profitable at North Blowhorn Creek Field Unit, Alabama. The reservoir at this field is a sandstone at a depth of -2,300 ft. The

application of this biological technology to Smackover carbonates at a depth of 11,300 ft has the potential to increase oil production at Womack Hill Field Unit, thereby increasing profitability and saving this endangered mature field from premature abandonment.

Task. Decision to Integrate Demonstration Project

Description of Work.--The project results, to date, will be evaluated by Pruet Production Co. and DOE to determine whether project continuation is justified.

Rationale. This activity represents the decision process on whether it is feasible for Pruet Production Co. to implement the technologies addressed and evaluated in Phase I of this study. The decision may be to implement an enhanced pressure maintenance project, initiate an advanced oil technology application, implement a strategic infill drilling program, and/or initiate an immobilized enzyme technology project at Womack Hill Field Unit. This activity also presents DOE with the opportunity to decide whether DOE will continue to support the project.

RESULTS AND DISCUSSION

The Project Management Team and Project Technical Team are working closely together on this project.

Geoscientific Reservoir Characterization

In the Womack Hill Field, the Smackover Formation ranges in thickness from 220 to 422 feet with an average thickness of 340 feet (Fig. 15) and overlies sandstone beds of the Norphlet Formation. The Norphlet Formation overlies the Jurassic Louann Salt, which in combination with faulting, is responsible for the petroleum trap at the field. The Smackover Formation is overlain by the Buckner Anhydrite Member of the Haynesville Formation. These anhydrite beds form the seal in the field. The Smackover Formation includes lower, middle and upper units in the Womack Hill Field (Fig. 9). The Smackover lower member or unit typically is composed of peloidal packstone and wackestone (Benson, 1988), which has reservoir potential in the field area but generally is not the reservoir in the Womack Hill Field. The middle member or unit includes laminated carbonate mudstone and fossiliferous wackestone and mudstone. The upper member or unit ranges in thickness from 30 to 209 feet with an average thickness of 120 feet (Fig. 16), and consists of a

series of three cycles, Cycle A, Cycle B, and Cycle C (Fig. 9). Porosity is developed in the upper part of the middle Smackover in the central part of the field along the Tombigbee River on the Clarke County side of the river. Cycle A (carbonate shoal) is an upward shoaling cycle composed of lower energy, carbonate mudstone and peloidal wackestone at the base and is capped by higher energy, ooid grainstone. The carbonate mudstone and wackestone have been interpreted as restricted bay and lagoon sediments, and the grainstone has been described as beach shoreface and shoal deposits (McKee, 1990). Although Cycle A is present across the field (Fig. 10), the reservoir quality in this cycle varies. The thickness of Cycle A ranges from 9 to 82 feet with an average thickness of 30 feet (Fig. 17). The grainstone associated with Cycle A is dolomitized (upper dolomitized zone) in much of the field area (Fig. 12), and is the main reservoir perforated in the field. Hydrocarbons have been produced from Cycle A in 21 of the 27 productive wells in the field. Six wells (Permit #1678, #1781, #1826, #2257B, #2327 and #3657) only have been perforated in Cycle A, and the cumulative oil production ranges from 127,000 to 1.9 million bbls for these wells. Porosity and permeability in the more productive wells (Permit #1678) average 16 percent and 11.5 md, respectively, and porosity and permeability in the less productive wells (Permit #2327) average 12 percent and 3 md, respectively (Fig. 51A). The mudstone/wackestone associated with this cycle has the potential to be a barrier to vertical flow in the field. Cycle B and Cycle C also occur across the field (Fig. 10). Cycle B thickness ranges from 8 to 101 feet with an average thickness of 47 feet (Fig. 18), and the thickness of Cycle C ranges from 11 to 86 feet with an average thickness of 40 feet (Fig. 19). These cycles are part of shoal complexes which include lagoonal deposits. The reservoirs associated with these cycles are a result of depositional and diagenetic processes, particularly dolomitization. Dolomitization (lower dolomitized zone) can be pervasive in the shoal grainstone lithofacies and in the lagoon wackestone lithofacies in these cycles (Fig. 12) and the interval immediately below Cycle C. Hydrocarbons have been produced from Cycle B in 17 wells, and oil and gas have been produced from Cycle C in 5 wells in the field. Three wells (Permit #1847, #2248B and #2263) only have been perforated in Cycle B, and the cumulative oil production is 350,000 to 3.2 million bbls for these wells, respectively, One well (Permit #2109) only has been

perforated in Cycle C, and its cumulative oil production is 1.7 million bbls. Porosity and permeability in well Permit #1847 average 17.5 percent and 9 md, respectively (Fig. 51B). The large scatter of the porosity and permeability data for this well illustrates the heterogeneity in Cycle B. Production from the upper part of the middle Smackover interval immediately above Cycle C is from the only two wells perforated in this interval that are located in the central part of the field. Cumulative oil production for well Permit #2130B is 2.8 million, and cumulative oil production for well Permit #4575B is 2.4 million bbls. Porosity and permeability in well Permit #4575B average 19 percent and 15 md, respectively (Fig. 52A). Permeability shows good correlation (0.87) with porosity in this interval probably due to dolomitization of these carbonates. The best producing well (Permit #1804) is perforated in Cycles A, B and C, and the well production is 3.3 million bbls of oil. Porosity and permeability in Cycle C in this well average 20 percent and 4 md, respectively (Fig. 52B). The variability of the porosity and permeability data for this well and wells (Permit #1732B and #4575B) (Fig. 53) illustrates the heterogeneity within and among Cycles A, B and C.

Although the primary control on reservoir architecture in Smackover reservoirs, including Womack Hill Field, is the fabric of the depositional lithofacies, diagenesis plays a significant role in modifying reservoir quality (Benson, 1985). Of the diagenetic events, the multiple dolomitization and dissolution events probably had the greatest influence on the quality in Smackover reservoirs. While the dolomitization created only minor amounts of intercrystalline porosity, it significantly enhanced permeability; it also stabilized the lithology which reduced the potential for later porosity loss due to compaction (Benson, 1985). The dissolution events enlarged primary (interparticle) and early secondary (moldic and intercrystalline) pores (McKee, 1990). Although the dissolution did not create large amounts of new porosity, it did expand existing pore throats and enhanced permeability (Benson, 1985).

Porosity in the shoal grainstone reservoirs at Womack Hill Field is chiefly secondary. The main pore types in the Smackover reservoirs, including the Womack Hill Field area, are solution-enlarged interparticle, intercrystalline dolomite, and grain moldic. Primary interparticle porosity has been reduced in the field due to compaction and cementation. Solution-enlarged interparticle and

grain moldic porosity is produced by early leaching in the vadose zone that dissolved aragonite in the Smackover carbonates (McKee, 1990). Moldic porosity is produced by early, fabric selective dissolution of aragonitic grains and is associated with areas of subaerial exposure (Benson, 1985). Intercrystalline porosity is chiefly a result of mixed-water dolomitization resulting from the mixing of marine and meteoric waters or from the mixing of evaporitic brines with meteoric waters (McKee, 1990). Several phases of dolomitization have been identified in the Smackover carbonates at Womack Hill Field. The upper zone of dolomitization is fabric-destructive and is a result of an early stage diagenetic event that involves downward-moving, evaporitically-concentrated brine, and the lower zone of dolomitization is, in part, fabric-destructive creating large amounts of intercrystalline porosity and permeability and is a result of mixing zone processes. Vuggy porosity of Choquette and Pray (1970), which is common in the field area, is the product of late, non-fabric selective dissolution of calcite or dolomite and is produced by solution enlargement of earlier formed interparticle or intercrystalline pores (Benson, 1985; Benson and Mancini, 1999). Reservoirs characterized by vuggy porosity have good porosity and permeability (Benson and Mancini, 1984). Shelter, intraparticle, and fracture pores are also present in the Smackover reservoirs in the Womack Field area (McKee, 1990).

Pore systems are the building blocks of reservoir architecture. Pore origin, geometry, and spatial distribution determine the amount and kind of reservoir heterogeneity. Pore systems affect not only hydrocarbon storage and flow but also reservoir producibility and flow unit quality and comparative rank within a field. Hydrocarbon recovery efficiency and total recovery volume are determined by the 3-D shape and size of the pores and pore throats (Kopaska-Merkel and Hall, 1993; Ahr and Hammel, 1999). Therefore, the pore systems (pore topology and geometry and pore throat size distribution) of the Womack Hill Field reservoirs are extremely important. Pore throat size distribution is one of the important factors determining permeability because the smallest pore throats are the bottlenecks that determine the rate of which fluids pass through a rock. Permeability has been shown to be directly related to the inherent pore system and degree of heterogeneity in Smackover reservoirs (Carlson *et al.*, 1998; Mancini *et al.*, 2000). Generally, the more

homogeneous (little variability in architecture and pore systems) the reservoir, the greater the hydrocarbon recovery from that reservoir. However, heterogeneity at one scale is not necessarily paralleled by heterogeneity at other scales. For example, the shoal grainstone reservoirs at Womack Hill Field can be dominated by a moldic or intercrystalline pore system and have low mesoscopic-scale heterogeneity but low to high microscopic-scale heterogeneity, depending upon the pore system. The heterogeneity is a function of both depositional and diagenetic processes. The grainstones accumulated in linear shoal environments, which tend to have uniformity of paleoenvironmental condition within a given shoal, but these carbonates can be later subjected to dissolution and dolomitization, such as at Womack Hill Field, to produce dolograinstones and large crystalline dolostones. The moldic pore system is characterized by multi-sized pores that are poorly connected by narrow pore throats. Pore size is dependent on the size of the carbonate grain that was leached. The intercrystalline pore system is characterized by moderate-sized pores that are well-connected by uniform pore throats. The size of the pores is dependent upon the dolomite crystal size. Interparticle porosity of Lucia (1998), which includes intergrain and intercrystal pore types in grainstones, dolograinstones and large crystalline dolostones, provides for high connectivity in carbonate reservoirs and results in high permeability (Lucia, 1998; Jennings and Lucia, 2001).

Petrophysical and Engineering Characterization

Petrophysical and Engineering Characterization is on schedule except for a delay in well downhole pressure testing. Extensive efforts have been made to integrate and correlate the core and well log data for the field. Reservoir permeability has been correlated with core porosity, gamma ray well log response, and resistivity well log response. The petrophysical data have been segregated into flow units prescribed by the geological data, and for the data in these flow units a histogram of core porosity and the logarithm of core permeability. These histograms yield statistical measures, such as the mean and median values, which will be used to develop spatial distributions and to provide data for the numerical simulation model. Evaluation of production, injection and shut-in bottomhole pressure data for the field have been interpreted and analyzed using appropriate

mechanisms, such as decline type curve analysis and estimated ultimate recovery analysis. The volumetric results are relevant as virtually every well yielded an appropriate signature for decline type curve analysis. However, a discrepancy in the estimate of total compressibility for this system has arisen, and the absolute volumetric results will need to be revised. The estimation of flow properties, such as permeability and skin factor has emerged as a problematic issue because little early time data, which are required for this analysis, are available. Therefore, the results of these analyses should be considered qualitative. The correlation of estimated ultimate recovery and the Nc_{+}- product is consistent suggesting that a strong relationship exists between contacted oil-in-place and recovery.

Microbial Characterization

Microbial Characterization is on schedule with the recent acquisition of Smackover core material from south Alabama. Initially water samples and core samples taken from wells in the Womack Hill Field yielded no micro-organisms capable of growing at 90˚C. This result was due to a combination of factors, including the fact that the core samples were exposed to air for decades and the equipment necessary to maintain an anaerobic environment was inadequate. Well cuttings from the Smackover Formation acquired from a field near Womack Hill Field were analyzed for micro-organisms. Growth of micro-organisms was evident in the samples prepared from these well cuttings in association with oil from the Womack Hill Field. These organisms consumed ethanol and are presumed to produce carbon dioxide or the gas was derived from organic acids produced from the oil reacting with carbonate. These findings suggest that micro-organisms capable of producing acetic acid from ethanol have a high probability of being present in Womack Hill Field and of being induced to grow and be metabolically active at the subsurface temperature in the reservoir.

3-D Geologic Model

The 3-D geologic model (Fig. 105), shows that the petroleum trap at Womack Hill Field is more complex than originally interpreted. The 2-D seismic data assists with the location of the major fault to the south of the field (Fig. 13). However, the seismic data are not adequate to

determine if the petroleum trap is a fault trap (bounded on three sides by dip closure and on a fourth side by a fault) or a faulted anticline trap (four-way dip closure). The geologic modeling shows that the trap in the western part of the field is a fault trap with closure to the south against the fault, and that the trap in the central and eastern parts of the field is a faulted anticline trap with four-way dip closure. In addition, the fault salt anticline trap appears to consist of two distinct highs separated by a structural low in the central part of the field (Fig. 105). The 2-D seismic data (west-east line P2635-136, Figs. 20), which is along the northern margin of the field, shows a north-south trending fault in the vicinity of the Choctaw-Clarke County line. If the fault trace is projected south to intersect with the major west-east fault (Fig. 13), the offset in the two structural highs along the southern margin of the field may be attributed to the effects of this north-south trending fault. Also, the pressure difference and well Permit #4575B between wells (Permit #4575B) in the western and central parts of the field (unitized area) and wells (Permit #1804) in the eastern part of the field may be attributed to the flow barrier in the field due to this fault.

The 3-D geologic modeling also shows that the Smackover reservoirs at Womack Hill Field is heterogeneous (Fig. 106). Four reservoir intervals are identified in the field area (Fig. 10). These include Cycle A, Cycle B, Cycle C, and the interval immediately below Cycle C (Fig. 9). Although the Cycle A reservoir is the most productive areally (has been productive in 21 wells), the production from this reservoir is highly variable with cumulative oil production ranging from 127,000 to 1.9 million bbls for wells only perforated in Cycle A. The thickness and lateral and vertical reservoir quality are also variable for the Cycle A reservoir interval. The Cycle B reservoir interval also is heterogeneous in thickness and lateral and vertical reservoir quality; however, the overall porosity as indicated by density log analysis is higher in this interval than the other reservoir intervals. The Cycle C reservoir interval also is heterogeneous in thickness and reservoir quality. Although the total oil production from this interval is not as high as the Cycle A and Cycle B reservoir intervals, production from well Permit #2109, the only well solely perforated in this interval and located in the western part of the field has had a cumulative oil production of 1.7 million bbls. The reservoir interval immediately below Cycle C has only been perforated in two

wells (well Permit #2130B and well Permit #4575B) in the central part of the field. Reservoir quality is high and production is high. The geologic modeling indicates this reservoir interval has the potential for high reservoir quality in the western part of the field in the vicinity of well Permit #1667 and well Permit #2109. The high reservoir quality and productivity in this interval in well Permit #2130B and well Permit #4575B is attributed to mixing zone dolomitization (fresh water lens development in structurally higher areas of the field). The area around well Permit #2109 is in a structurally higher area in the field (Figs. 13 and 105).

A permeability barrier to flow, especially in the Cycle A reservoir interval is present potentially between the western (well Permit #4575B) and eastern (well Permit #1804) parts of the field (Figs. 53 and 106). Communication in the field through the Cycle B reservoir interval appears likely, in comparing the porosity and permeability data between well Permit #1732B and well Permit #1804 (Fig. 53) and in comparing the area of well Permit #2130B with the area of well Permit #1804 (Fig. 106). The improved reservoir communication in the Cycle B interval is probably due to dolomitization. Porosity and permeability data are insufficient in the field to assess the potential of a permeability barrier to flow in the Cycle C reservoir interval and the reservoir interval immediately below Cycle C. Communication between the western part of the field and the area of well Permit #1804 appears likely, but communication between the wells in the western part and the other wells in the eastern part of the field probably is limited.

CONCLUSIONS

Pruet Production Co. and the Center for Sedimentary Basin Studies at the University of Alabama, in cooperation with Texas A&M University, Mississippi State University, University of Mississippi, and Wayne Stafford and Associates are undertaking a focused, comprehensive, integrated and multidisciplinary study of Upper Jurassic Smackover carbonates (Class II Reservoir), involving reservoir characterization and 3-D modeling and an integrated field demonstration project at Womack Hill Oil Field Unit, Choctaw and Clarke Counties, Alabama, Eastern Gulf Coastal Plain.

Phase I (3.0 years) of the proposed research involves characterization of the shoal reservoir at Womack Hill Field to determine reservoir architecture, heterogeneity and producibility in order to increase field productivity and profitability. This work includes core and well log analysis; sequence stratigraphic, depositional history and structure study; petrographic and diagenetic study; and pore system analysis. This information will be integrated with 2-D seismic data and probably 3-D seismic data to produce an integrated 3-D stratigraphic and structural model of the reservoir at Womack Hill Field. The results of the reservoir characterization and modeling will be integrated with petrophysical and engineering data and pressure communication analysis to perform a 3-D reservoir simulation of the field reservoir. The results from the reservoir characterization and modeling will also be used in determining whether undrained oil remains at the crest of the Womack Hill structure (attic oil), in assessing whether it would be economical to conduct strategic infill drilling in the field, and in determining whether the acquisition of 3-D seismic data for the field area would improve recovery from the field and is justified by the financial investment. Parallel to this work, engineers are characterizing the petrophysical and engineering properties of the reservoir, analyzing the drive mechanism and pressure communication (through well performance data), and developing a 3-D reservoir simulation model. Further, the engineering team members will determine what, if any, modifications should be made to the current pressure maintenance program, as well as assess what, if any, other potential advanced oil recovery technologies are applicable to this reservoir to extend the life of the field by increasing and maintaining productivity and profitability. Also, in this phase, researchers are studying the ability of *in-situ* micro-organisms to produce a single by-product (acid) in the laboratory to determine the feasibility of initiating an immobilized enzyme technology project at Womack Hill Field Unit.

The principal problem at Womack Hill Field is productivity and profitability. With time, there has been a decrease in oil production from the field, while operating costs in the field continue to increase. In order to maintain pressure in the reservoir, increasing amounts of water must be injected annually. These problems are related to cost-effective, field-scale reservoir management, to reservoir connectivity due to carbonate rock architecture and heterogeneity, to pressure

communication due to carbonate petrophysical and engineering properties, and to cost-effective operations associated with the oil recovery process.

Improved reservoir producibility will lead to an increase in productivity and profitability. To increase reservoir producibility, a field-scale reservoir management strategy based on a better understanding of reservoir architecture and heterogeneity, of reservoir drive and communication and of the geological, geophysical, petrophysical and engineering properties of the reservoir is required. Also, an increased understanding of these reservoir properties should provide insight into operational problems, such as why the reservoir is requiring increasing amounts of freshwater to maintain the desired reservoir pressure, why the reservoir drive and oil-water contact vary across the field, how the multiple pay zones in the field are vertically and laterally connected and the nature of the communication within a pay zone.

The principal research efforts for Year 2 of the project have been reservoir characterization, which has included three (3) primary tasks: geoscientific reservoir characterization, petrophysical and engineering property characterization, and microbial characterization and recovery technology analysis, which has included 3-D geologic modeling. In the second year, the research focus has primarily been on completion of the geoscientific reservoir characterization and 3-D geologic modeling tasks. This work was scheduled for completion in Year 2.

Geoscientific Reservoir Characterization has been completed. The upper part of the Smackover Formation is productive from carbonate shoal complex reservoirs that occur in vertically stacked heterogeneous porosity cycles (A, B, and C). The cycles typically consist of carbonate mudstone/wackestone at the base and ooid and oncoidal grainstone at the top. The carbonate mudstone/wackestone lithofacies has been interpreted as restricted bay and lagoon sediments, and the grainstone lithofacies has been described as beach shoreface and shoal deposits. Porosity has been enhanced through dissolution and dolomitization. The grainstone associated with Cycle A is dolomitized (upper dolomitized zone) in much of the field area. Although Cycle A is present across the field, its reservoir quality varies laterally. Dolomitization (lower dolomitized zone) can be pervasive in Cycle B, Cycle C and the interval immediately below Cycle C. Cycle B and Cycle C

occur across the field, but they are heterogeneous in depositional texture and diagenetic fabric laterally. Porosity is chiefly solution-enlarged interparticle, grain moldic and dolomite intercrystalline pores with some intraparticle and vuggy pores. Pore systems dominated by intercrystalline pores have the highest porosities. Median pore throat aperture tends to increase with increasing porosity. Probe permeability strongly correlates with median pore throat aperture, and tortuosity increases with increasing median pore throat aperture. Larger tortuosity and median pore throat aperture values are associated with pore systems dominated by intercrystalline pores.

Petrophysical and Engineering Characterization is on schedule except for a delay in well downhole pressure testing. Extensive efforts have been made to integrate and correlate the core and well log data for the field. Reservoir permeability has been correlated with core porosity, gamma ray well log response, and resistivity well log response. The petrophysical data have been segregated into flow units prescribed by the geological data, and for the data in these flow units a histogram of core porosity and the logarithm of core permeability. These histograms yield statistical measures, such as the mean and median values, which will be used to develop spatial distributions and to provide data for the numerical simulation model. Evaluation of production, injection and shut-in bottomhole pressure data for the field have been interpreted and analyzed using appropriate mechanisms, such as decline type curve analysis and estimated ultimate recovery analysis. The volumetric results are relevant as virtually every well yielded an appropriate signature for decline type curve analysis. However, a discrepancy in the estimate of total compressibility for this system has arisen, and the absolute volumetric results will need to be revised. The estimation of flow properties, such as permeability and skin factor has emerged as a problematic issue because little early time data, which are required for this analysis, are available. Therefore, the results of these analyses should be considered qualitative. The correlation of estimated ultimate recovery and the Nc_{+}- product is consistent suggesting that a strong relationship exists between contacted oil-in-place and recovery.

Microbial Characterization is on schedule with the recent acquisition of Smackover core material from south Alabama. Initially water samples and core samples taken from wells in the

Womack Hill Field yielded no micro-organisms capable of growing at 90˚C. This result was due to a combination of factors, including the fact that the core samples were exposed to air for decades and the equipment necessary to maintain an anaerobic environment was inadequate. Well cuttings from the Smackover Formation acquired from a field near Womack Hill Field were analyzed for micro-organisms. Growth of micro-organisms was evident in the samples prepared from these well cuttings in association with oil from the Womack Hill Field. These organisms consumed ethanol and are presumed to produce carbon dioxide or the gas was derived from organic acids produced from the oil reacting with carbonate. These findings suggest that micro-organisms capable of producing acetic acid from ethanol have a high probability of being present in Womack Hill Field and of being induced to grow and be metabolically active at the subsurface temperature in the reservoir.

A 3-D Geologic Model has been constructed for the Womack Hill Field structure and reservoir(s). The 3-D geologic modeling shows that the petroleum trap is more complex than originally interpreted. The geologic modeling indicates that the trap in the western part of the field is a fault trap with closure to the south against the fault, and that the trap in the central and eastern parts of the field is a faulted anticline trap with four-way dip closure. The pressure difference between wells in the western and central parts of the field and wells in the eastern part of the field may be attributed to a flow barrier due to the presence of a north-south trending fault in the field area. The modeling shows that the Smackover reservoirs are heterogeneous. Four reservoir intervals are identified in the field area: Cycle A, Cycle B, Cycle C, and the interval immediately below Cycle C. A permeability barrier to flow is present potentially between the western and eastern parts of the field.

REFERENCES

Ahr, W.M., and Hammel, B., 1999, Identification and mapping flow units in carbonate reservoirs: an example from Spraberry (Permian) field, Garza County, Texas, USA: Energy Exploration and Exploitation, v. 17, p. 311-334.

Bebout, D.G., and Loucks, R.G., 1984, Handbook for logging carbonate rocks: Handbook 5, The University of Texas at Austin, Bureau of Economic Geology, Austin, Texas, 43 p.

Benson, D.J., 1985, Diagenetic controls on reservoir development and quality, Smackover Formation of southwest Alabama: Gulf Coast Association of Geological Societies Transactions, v. 35, p. 317-326.

Benson, D.J., 1988, Depositional history of the Smackover Formation in southwest Alabama: Gulf Coast Association of Geological Societies Transactions, v. 38, p. 197-205.

Benson, D.J., and Mancini, E.A., 1984, Porosity development and reservoir characteristics of the Smackover Formation in southwest Alabama, in Jurassic of the Gulf Rim, Proceedings GCS-SEPMF 3rd Research, p. 1-17.

Benson, D.J., and Mancini, E.A., 1999, Diagenetic influence on reservoir development and quality in the Smackover updip basement ridge play, southwest Alabama: Gulf Coast Association of Geological Society Transactions, v. 99, p. 95-101.

Blasingame, T.A. *et al.*, 1998, "Well Performance Analysis (*WPA*) (software) Vers. 1.8b, Texas A&M U., College Station, Texas (1998).

Breiman, L. and Friedman, J., 1985, Estimating Optimal Transformations for Multiple Regression and Correlation, Journal of the American Statistical Association (September 1985) 80, No. 391, 590.

Carlson, E.C., Benson, D.J., Groshong, R.H., and Mancini, E.A., 1998, Improved oil recovery from heterogeneous carbonate reservoirs associated with paleotopographic basement structures: Appleton Field, Alabama: SPE/DOE Eleventh Symposium on Improved Oil Recovery, p. 99-105.

Carozzi, A.V., 1958, Micro-mechanisms of sedimentation in the epicontinental environment: Journal of Sedimentary Petrology, v. 28, p. 133 – 150.

Choquette, P.W., and Pray, L.C., 1970, Geologic nomenclature and classification of porosity in sedimentary carbonates: American Association of Petroleum Geologists Bulletin, v. 54, p. 207-250.

Dake, L.P., 1977, Fundamentals of Reservoir Engineering, Elsevier, Amsterdam.

Doublet, L.E., and Blasingame, T.A., 1996, Evaluation of injection well performance using decline type curves: paper SPE 35205 presented at the 1996 SPE Permian Basin Oil and Gas Recovery Conference, Midland, TX, March 27-29.

Doublet, L.E., Pande, P.K., McCollum, T.J., and Blasingame, T.A., 1994, Decline curve analysis using type curves—analysis of oil well production data using material balance time: application to field cases: paper SPE 28688 presented at the 1994 Petroleum Conference and Exhibition of Mexico held in Veracrus, Mexico, October 10-13.

Erwin, C.R., Eby, D.E., and Whitesides Jr., V.S., 1979, Clasticity index: a key to correlating depositional and diagenetic environments of Smackover reservoirs, Oaks field, Claiborne Parish, Louisiana: Gulf Coast Association of Geological Societies Transactions, v. 29, p. 52–62.

Fetkovich, M.J., 1980, "Decline Curve Analysis Using Type Curves," JPT (June 1980) 1065.

Folk, R.L., 1993, SEM imaging of bacteria and nannobacteria in carbonate sediments and rocks: Journal of Sedimentary Petrology, v. 63, p. 990-999.

Folk, R.L., and Lynch, F.L., 1997, Nannobacteria are alive on Earth as well as Mars: Proceedings of the International Symposium on Optical Science, Engineering, and Instrumentation (SPIE), v. 3111, p. 406-419.

Folk, R.L., and Lynch, F.L., 1998, Morphology of nannobacterial cells in the Allende carbonaceous chondrite, *in* Hoover, R.B., ed., Instruments, methods, and missions for astrobiology: Proceedings of the Society of Photo-optical Instrumentation Engineers, v. 3441, p. 112-122.

Folk, R.L., and Lynch, F.L., 2001, Organic matter, putative nannobacteria, and the formation of ooids and hardgrounds: Sedimentology, v. 48, p. 215-229.

Folk, R.L., Kirkland, B.L., Rodgers, J.C., Rodgers, G.P., Rasmussen, T.E., Lieske, C., Charlesworth, J.E., Severson, S.R., and Miller, V.M., 2001, Precipitation of minerals in human arterial plaque: the potential role of nannobacteria: Geological Society of America annual meeting, abstracts with programs, p. A-189.

Fratesi, S.E., and Lynch, F.L., 2001, Comparison of organic matter preservation techniques for SEM study of geologic samples: Geological Society of America annual meeting, abstracts with programs, p. A-296

Gregg, J.M., and Sibley, D.F., 1984, Epigenetic dolomitization and the origin of xenotopic dolomite texture: Journal of Sedimentary Petrology, v. 54, n. 3, p. 908–931.

Hopkins, T.L., 2002, Integrated petrographic and petrophysical study of the Smackover Formation, Womack Hill Field, Clarke and Choctaw Counties, Alabama: Texas A&M University, unpublished Masters thesis, 156 p.

Humphrey, J.D., Ransom, K.L., and Matthews, R.K., 1986, Early meteoric control of Upper Smackover production, Oaks field, Louisiana: American Association of Petroleum Geologists Bulletin, v. 70, n. 1, p. 70 – 85.

Jennings, J.W., and Lucia, F.J., 2001, Predicting permeability from well logs in carbonates with a link to geology for interwell permeability mapping: Society of Petroleum Engineers Paper 71336, p. 1-16.

Kerans, C., and Tinker, S.W., 1997, Sequence stratigraphy and characterization of carbonate reservoirs: SEPM Short Course No. 40, 13 p.

Kirkland, B.L., Lynch, F.L., Rahnis, M.A., Folk, R.L., Molineux, I.J., and McLean, R.J.C., 1999, Alternative origins for nannobacteria-like objects in calcite: Geology, v. 27, pp. 347-350.

Kopaska-Merkel, D.C., and Hall, D.R., 1993, Reservoir characterization of the Smackover Formation in southwest Alabama: Geological Survey of Alabama Bulletin 153, 111 p.

Lucia, F.J., 1999, Carbonate reservoir characterization: Springer, New York, 226 p.

Mancini, E.A., Benson, D.J., Hart, B.S., Balch, R.S., Parcell, W.C., and Panetta, B.J., 2000, Appleton field case study (eastern Gulf Coastal Plain): field development model for Upper Jurassic microbial reef reservoirs associated with paleotopographic basement structures: American Association of Petroleum Geologists Bulletin, v. 84, p. 1699-1717.

McKay, D.S., Gibson, E.K., Thomas-Keprta, K.L., Vali, L.H., Romanek, C.S., Clemmett, S.J., Chillier, Z.D.F., Maechling, C.R., and Zare, R.N., 1996, Search for past life on Mars: Possible relic biogenic activity in Martian meteorite ALH84001: Science, v. 273, p. 924.

McKee, D.A., 1990, Structural controls on lithofacies and petroleum geology of the Smackover Formation: eastern Mississippi Interior Salt Basin, Alabama: University of Alabama, unpublished master's thesis, 254 p.

Spark, I., Patey, I., Duncan, B., Hamilton, A., Devine, C., and McGovern-Traa, C., 2000, The effects of indigenous and introduced microbes and deeply buried hydrocarbon reservoirs, North Sea: Clay Minerals, v. 35, p. 5-12.